



IN-TECH Conference
Rijeka 2012

International Conference on Innovative Technologies

IN-TECH2012

RIJEKA, CROATIA 26. - 28.09.2012.



Organized by: **World Association for Innovative Technologies**



**Proceedings of International Conference
on Innovative Technologies IN-TECH**

International Conference on Innovative Technologies

IN-TECH 2012

Rijeka

Proceedings



IN-TECH 2012

Proceedings of International Conference on Innovative Technologies

Editors:

- Zlatan Car – Croatia
- Jan Kudláček – Czech Republic
- Tomaž Pepelnjak – Slovenia

IN-TECH 2012 Organization committee:

- Zlatan Car – Croatia
- Jan Kudláček – Czech Republic
- Tomaž Pepelnjak - Slovenia
- Leon Šikulec – Croatia
- Marko Kršulja – Croatia
- Hrvoje Radelja – Croatia
- Petr Drašnar – Czech Republic
- Vladislava Ostrá – Czech Republic

Publisher: Faculty of Engineering University of Rijeka

Printed by: Grafika Helvetica d.o.o.

Printed in 250 copies.

IN-TECH 2012 International Conference on Innovative Technologies runs from 26.09.2012 to 29.09.2012 in Rijeka, Croatia.

E-mail: info@in-tech.info

URL: <http://www.in-tech.info>

The CIP record is available in the computer catalogue of the University Library Rijeka under No. 121219001.

ISBN 978-953-6326-77-8



Sponsors & supporters

- RIJEKA TOURIST BOARD, <http://www.tz-rijeka.hr>.



Kvarner

RIJEKA

Difference is beautiful

- GRAND HOTEL BONAVIA RIJEKA, <http://www.bonavia.hr>.



- UNIVERSITY OF RIJEKA FOUNDATION,
<http://www.zaklada.uniri.hr>.



- MINISTRY OF SCIENCE, EDUCATION AND SPORTS OF
THE REPUBLIC OF CROATIA, <http://public.mzos.hr>.

- CENTRAL EUROPEAN EXCHANGE PROGRAM FOR
UNIVERSITY STUDIES, NATIONAL CEEPUS OFFICE
CROATIA HR – 108 Network,
<http://www.ceepus.info/default.aspx>.



- Organized in cooperation between:



University of Rijeka Faculty of Engineering

<http://www.riteh.uniri.hr/>



University of Faculty of Mechanical
Engineering, Czech Technical University in
Prague

<http://www3.fs.cvut.cz>





Scientific Committee

- Ali Hashem, O. (Egypt)
- Bozek, P. (Slovakia)
- Brdarević, S. (B & H)
- Burger, W. (Germany)
- Car, Z. (Croatia)
- Carjali, E. (Romania)
- Castilla Roldán, M. V. (Spain)
- Cep, R. (Czech Republic)
- Chen, W. (Netherland)
- Cizek, J. (Singapore)
- Cosic, P. (Croatia)
- Cotetiu, R. (Romania)
- Crisan, L. (Romania)
- Czan, A. (Slovakia)
- Duda, J. (Poland)
- Durakbasa, N. (Austria)
- Frietsch, M. (Germany)
- Elhalabi, M. (Egypt)
- Evin, E. (Slovakia)
- Galinac, T. (Croatia)
- Galvao, J. R. (Portugal)
- Genis, V. (USA)
- Gomez, M. E. (Columbia)
- Greenhut, V. (USA)
- Gyenge, C. (Romania)
- Guarino, S (Italy)
- Hodolič, J. (Serbia)
- Ivanov, K. (Russia)
- Jung, J. (Korea)
- Junkar, M. (Slovenia)
- Yashar, J. (Iran)
- Katalinić, B. (Austria)
- Kiss, I. (Romania)
- Kocov, A. (Macedonia)
- Kozak, D. (Croatia)
- Kreibich, V. (Czech Republic)
- Kudláček, J. (Czech Republic)
- Kundra, J. (Hungary)
- Kuric, I. (Slovakia)
- Kuzman, K. (Slovenia)
- Kuzmanović, S. (Serbia)
- Legutko, S. (Poland)
- Lee, J. H. (Korea)
- Li, M. (China)
- Lukovics, I. (Czech Republic)
- Majstorović, V. (Serbia)
- Makis, V. (Canada)
- Mamuzić, I. (Croatia)
- Marcinčin, J. N. (Slovakia)
- Math, M. (Croatia)
- Matsuda, H. (Japan)
- Miltenovic, V. (Serbia)
- Ohmura, E. (Japan)
- Ohkura, K. (Japan)
- Omran, A (Malaysia)
- Pepelnjak, T. (Slovenia)
- Plančak, M. (Serbia)
- Pop-Iliev, R. (Canada)
- Raos, P. (Croatia)
- Rucki, M. (Poland)
- Sankaranarayananasamy, K. (India)
- Senabre, C. (Spain)
- Sercer, M. (Croatia)
- Serpil, K. (Turkey)
- Sučić, V. (Croatia)
- Suchánek, J. (Czech Republic)
- Szalay, T. (Hungary)
- Tingle, J. (Croatia)
- Tisza, M. (Hungary)
- Tomesani L. (Italy)
- Turkalj, G. (Croatia)
- Turna, M. (Slovakia)
- Udiljak, T. (Croatia)
- Ungureanu, N. (Romania)
- Varga, G. (Hungary)
- Velay X. (Great Britain)
- Wilke, M. (Germany)
- Zivkovic, D. (Serbia)



INVITED PAPERS	
Miroslav Plancak, Dejan Movrin, Zlatan Car, Dragiša Vilotić, Igor Kacmarcik and Marko Kršulja	BI-METALLIC COLD BACKWARD EXTRUSION – NUMERICAL SIMULATION WITH EXPERIMENTAL VERIFICATION
Jan Suchánek and František Černý	INFLUENCE OF IBAD SINX COATINGS ON TRIBOLOGICAL PROPERTIES OF P/M HSS
Tomaž Pepelnjak, Sanja Smoljanič and Robert Zakrajšek	INFLUENCE OF STRAIN RATE ON COLD SHEET METAL FORMING
Joa~o Galva~o, Licinio Moreira, Elson Silva and Mário Neto	POLI ENERGY: EFFICIENCY AND SUSTAINABLE ENERGY FOR INDUSTRY
Mirza Suljic and Lejla Banjanovic-Mehmedovic	MLP NEURAL NETWORK BASED PREDICTION OF COAL QUALITY CATEGORIES
Natalia Okhapkina and Lubov Strogonova	USE OF ONBOARD SHORT ARM HUMAN CENTRIFUGE TO CREATE ARTIFICIAL GRAVITY
Nikita Markov, Paul Fomkin, Alecsandr Ermakov and Lubov Strogonova	THE DYNAMIC COMPONENT OF THE PATTERN RECOGNITION SYSTEM OF MICROORGANISMS UNDER MICROGRAVITY CONDITIONS
Damir Godec, Ines Kramarić and Mladen Šercer	APPLICATION OF REVERSE ENGINEERING IN THE DEVELOPMENT OF POLYMER PRODUCTS
Petar Piljek, Zdenka Keran and Miljenko Math	AN ANALYSIS OF SINGLE-PASS CONVENTIONAL SPINNING PROCESS
N. Bulic, D.Sumina and Z. Car"	DSP-BASED CONTROL SYSTEM FOR EXCITATION CONTROL OF SYNCHRONOUS GENERATOR



CONTENTS

THE PRESENT SITUATION OF THE TPM SYSTEM IN SLOVAK ENTERPRISES	
Juraj Drahňovský	1-4
NACRE DESIGN AS INSPIRATION FOR OPTIMAL DESIGN OF ROOF	
Tina Kegl	5-9
OPTIMIZATION OF A DIESEL FUEL INJECTION SYSTEM USING BIOFUEL	
Marko Kegl, Stanislav Pehan and Breda Kegl	11-15
OPTIMAL DESIGN OF A GASOLINE ENGINE	
Stanislav Pehan, Marko Kegl and Breda Kegl	17-21
CHECKING THE STABILITY OF TIO₂ NANOPARTICLES SIZE BY RESPONSE SURFACE METHOD	
Olivia Giuca	23-27
USING EXPERIMENTAL METHODS FOR CHECKING STABILITY OF TIO₂ NANOPARTICLES SIZE	
Olivia Giuca, Ioan Nicoară and Ioan Grozescu	29-33
UNCONVENTIONAL VARIABLE DISPLACEMENT INTERNAL COMBUSTION ENGINE	
Jovan Dorić, Nebojša Nikolić and Ivan Klinar	35-39
UNCONVENTIONAL RELIABILITY GROWTH MODELS	
Zuzana Krajcuskova, Marek Kukucka and Daniela Durackova	41-44
ENERGY BALANCE OF HYBRID SOLAR HEATING AND COOLING SYSTEM	
Stanisław Gil, Bogusław Gradoń and Wojciech Bialik	45-48
SYNTHESIS OF A FUZZY MODEL FOR THE PLANT PROTECTION SYSTEM IN THE APPLE ORCHARD	
Peter Berk, Denis Stajanko, Miran Lakota, Peter Vindiš and Jurij Rakun	49-52
ROBUST COMMAND FOLLOWING CONTROL IN THE ROBOT JOINT SPACE	
Ján Kardoš	53-57
INFLUENCE OF TEMPERATURE TO THE EFFICIENCY OF VISCOSE TREATMENT USING COPOLYMER CHITOSAN-EUGENOL	
Olivera Sauperl, Julija Volmajer-Valh and Jasna Tompa	59-62
SPEED/POSITION SENSORLESS CONTROL OF TWO-PHASE PMSM DRIVE SYSTEM USING VIRTUAL INJECTION METHOD	
Branislav Dobrucky, Slavomir Kascak, Michal Prazenica and Jan Kassa	63-67
QUALITY ASSESSMENT OF PVD COATING AND TOOL USED AT COLD-FORMING PROCESS	
Pavol Beraxa, Lucia Domovcova and Ľudovít Parilák	69-72
INTRA- AND INTERLAMINAR SHEAR BEHAVIOUR OF TEXTILE COMPOSITES TESTED WITH V-NOTCHED RAIL SHEAR TEST METHOD	
Werner Hufenbach, Robert Schirner and Manuela Andrich	73-77
NOISE ANALYSIS OF THE CROSS WIGNER-VILLE DISTRIBUTION BASED INSTANTANEOUS FREQUENCY ESTIMATION METHOD	
Damir Malnar, Victor Sučić and Srdjan Stanković	79-82
REDUCTION OF CHIP AREA FOR FEED-FORWARD NEURAL NETWORKS WITH USE THE SPECIAL MULTIPLICATION BY AND GATE	
Roman Zalusky, Daniela Durackova and Vladimír Sedlak	83-86
IRREGULAR INFLUENCE OF PLASTIC DEFORMATION OF THIN PACKAGING SHEETS TO THEIR CORROSIVE RESISTANCE	
Janka Majerniková, Emil Spišák, Ľuboš Kaščák and Ján Slota	87-90



RESISTANCE SPOT WELDING OF AHSS STEEL AND HSLA STEEL	
Luboš Kaščák, Emil Spišák, Ján Slota and Janka Majerníková	91-95
MODIFICATION OF THE ICI RULE APPLIED TO SIGNAL DENOISING	
Ivan Volarić, Jonatan Lerga, Viktor Sučić, Irena Orović and Srdjan Stanković	97-101
APPLICATION OF SPACE TELEMEDICINE TECHNOLOGY IN MANAGING EMERGENCIES ON THE GROUND	
Lubov Strogonova and Daria Litvina	103-105
PRELIMINARY STUDY OF ACTIVATED SLUDGE ABILITY TO DEGRADE SELECTED METALWORKING FLUIDS	
Kristína Gerulová, Katarína Fabianová, Tatiana Černeková and Tamara Hubinská	107-111
IMPACT OF VISUALIZATION ON DATA AVAILABILITY	
Ljiljana Popovic, Srdjan Popov, Djordje Cosic and Dusan Sakulski	113-116
PRESENTATION OF ENVIRONMENTAL RISKS FROM THE PERSPECTIVE OF INDUSTRIAL ACCIDENTS	
Jakub Rak and Lucie Jurikova	117-120
MATHEMATICAL METHODS IN ENSURING SECURITY DURING THE LAUNCH OF MANNED SPACECRAFT.	
Elizaveta Davydova and Lubov Strogonova	121-124
INVESTIGATION OF USAGE POSSIBILITIES OF A MEAN VALUE ENGINE MODEL IN SIMULATION OF IC ENGINE INTAKE SYSTEM FAULTS	
Nebojša Nikolić, Tripo Torović, Života Antonić and Jovan Dorić	125-129
SIMULATION SOFTWARE FOR MODELLING AND SIMULATING EMERGENCY EVENTS	
Lucie Jurikova and Jakub Rak	131-134
SCHEMES FOR THE CONSERVATION OF STAINED GLASS IN THE PALACES AND HERITAGE BUILDINGS	
Maher Ismail	135-138
CFD AND THERMAL ANALYSES APPLICATION AT REFLOW OVEN DESIGN IMPROVEMENTS BASED ON VIRTUAL PROTOTYPING TECHNIQUES	
Georgi Todorov, Ivan Dobrev and Konstantin Kamberov	139-143
VALIDATING DOMAIN-SPECIFIC PROPERTIES WITH GRAPH TRANSFORMATIONS	
Laszlo Lengyel and Hassan Charaf	145-148
ELECTRO-MECHANICAL CONTINUOUSLY VARIABLE TRANSMISSIONS FOR AUTOMOTIVE APPLICATIONS	
Kamarul Baharin Tawi, Izhari Izmi Mazali, Nurulakmar Abu Husain and Bambang Supriyo	149-153
NUMERICAL MODELING OF TRACK ROLLER - SHOE INTERACTION AT CRAWLER MACHINES	
Salko Cosic, Mevludin Avdic and Salko Bukvarevic	155-158
MEASUREMENTS OF EPR SPECTRA FOR THE POWDERS USED IN CERAMIC CORES AND FORMS IN THE AEROSPACE INDUSTRY	
Stefaniuk Ireneusz and Potera Piotr	159-162
THE EPR MEASUREMENTS OF THE CERAMICS CORES USED IN AIRCRAFT INDUSTRY OBTAINED BY HIGH PRESSURE INJECTION METHOD	
Ireneusz Stefaniuk, Piotr Potera and Iwona Rogalska	163-166
IMPLEMENTATION OF CONTENT MANAGEMENT SYSTEM FOR INSTITUTION LINUX USERS GROUP USING JOOMLA UNDER UBUNTU LINUX.	
Aditya Mehta and Dr. B. Vijaykumar	167-170
DEVELOPING AN IOS APPLICATION FOR RESTAURANT MENU CARDS	
Aditya Mehta, Dr. D. V. Prasad and Christus Cleetus	171-174



POLI ENERGY: EFFICIENCY AND SUSTAINABLE ENERGY FOR INDUSTRY	
Joa~o Galva~o, Licinio Moreira, Elson Silva and Mario Neto	175-179
CONTEMPORARY INTERIOR DESIGN BETWEEN THE ISLAMIC HERITAGE INSPIRATIONS AND SUSTAINABILITY CONCEPTS	
Eman Badr	181-185
ROBOT CONTROL SYSTEM BASED ON INERTIAL NAVIGATION	
Pavol Bozek	187-190
OPTIMAL MOTION PLANNING FOR CAR BODY-IN-WHITE INDUSTRIAL ROBOT APPLICATIONS	
Kamil Trnka and Pavol Božek	191-193
THE APPLICATION OF SYSTEM MEASUREMENTS IN INDUSTRIAL ENTERPRISES IN SLOVAKIA	
Marta Kucerova and Zdenka Gyurak Babelova	195-197
INCREASING OF THE INTERNAL COMBUSTION ENGINES PERFORMANCES THROUGH THE INTAKE MANIFOLD SYSTEM	
Hiticas Ioan D-Tru, Marin Daniel and Mihon Liviu Nicolae	199-203
SIMULTANEOUS MEASUREMENT OF VELOCITY AND TEMPERATURE FIELD DOWNSTREAM OF A HEATED CYLINDER	
Peter Bencs, Szilard Szabo and Daria Oertel	205-209
APPLICATION OF THERMOGRAPHY TECHNIQUE FOR SURFACE TEMPERATURE VISUALIZATION OF A HEATED CYLINDER	
Szilard Szabo, Peter Bencs and Andras Farkas	211-215
ANALYSIS OF FUZZY CONTROL SYSTEMS USING STABILITY INDEXES – SOME CASE STUDIES	
Ramon P. N~eco, Rafael Puerto, Mara A. Vicente and Cesar Fernandez	217-220
DESIGN AND IMPLEMENTATION OF SEARCH ALGORITHM FOR DNA SEQUENCE DATABASE	
Varunkumar Vijayakumar and Vijayakumar Balakrishnan	221-224
MODEL REFERENCE ADAPTIVE CONTROL OF A DC SERVO MOTOR WITH DIFFERENT INPUT-OUTPUT SAMPLE RATES	
Ramon P. N~eco, Mara Asuncion Vicente, Cesar Fernandez and Rafael Puerto	225-228
THE SEARCH FOR OPTIMAL TRAJECTORIES OF THE WELDING TOOL IN THE AUTOMATIC WELDING LINE USING EVOLUTIONARY COMPUTATION	
Marian Klucik, Ladislav Jurisica, Peter Paszto, Andrej Babinec, Jaroslav Hanzel and Jozef Rodina	229-232
THE INTELLIGENT LIGHTING CONTROL SYSTEMS IN INTERIOR DESIGN FOR HOSPITALITY BUILDINGS	
Reda Mostafa	233-237
EXPERIMENTAL RESEARCH CONCERNING THE POLLUTION OF AN INTERNAL COMBUSTION ENGINE WITH INJECTION OF GASOLINE, IN CONDITIONS OF CHANGING THE FUEL	
Hiticas Ioan D-Tru, Marin Daniel and Mihon Liviu Nicolae	239-243
INNOVATIVE NANOFIBER FILTRATION MATERIALS OF THE BIOPOLYMER ALGINATE FOR SEQUESTRATION OF DISSOLVED LEAD FROM WATER	
Melissa Bradley and Matthew Cathell	245-249
INFORMATION AND COMMUNICATION TECHNOLOGY IN 3PL ORGANIZATIONS	
Saru Saseedharan and Pushkala Muralidharan	251-255
EXTENDED ENTERPRISE MANUFACTURING PROCESS AND QUALITY INTEGRATION	
Juan Ramon Lama Ruiz, Francisco Aguayo Gonzalez, Mariano Marcos and Alejandro Manuel Martın Gomez	257-260



PROCESS DESIGN OF ULTRA-SHORT PULSE LASER ABLATION BY MODERN QUALITY-ORIENTED DESIGN OF EXPERIMENTS	
Claus Emmelmann and Juan Pablo Calderón Urbina	261-264
SUPPRESSION OF FLUTTER OF AN AIRFOIL-FLAP WING USING ACTIVE CONTROL	
Khalid Alsaif, Abdulmohsen Albedah, Faycal Benyahia and Mosaad Foda	265-267
FIRST AND SECOND ORDER IMAGE STATISTICS IN SPECIFIC IMAGE ARTIFACT DETECTION	
Marius Rogobete and Ciprian Racuciu	269-272
MLP NEURAL NETWORK BASED PREDICTION OF COAL QUALITY CATEGORIES	
Mirza Suljic and Lejla Banjanovic-Mehmedovic	273-277
ENERGY DISSIPATION AS A MEASURE OF VIBRATION INDUCED FATIGUE PROCESSES IN ENGINEERING MATERIALS	
Przemyslaw Drozner, Arkadiusz Rychlik, Jerzy Napiórkowski, Piotr Szyglak and Małgorzata Kaczmarek-Jasiulewicz	279-282
A SEMANTIC SEARCH ENGINE IMPLEMENTED WITH OPEN SOURCE	
Sorin-Alexandru Cristescu and Florica Moldoveanu	283-286
MODEL OF THE FERROSILICON MELTING PROCESS IN THE SUBMERGED ARC FURNACE	
Bolesław Machulec and Wojciech Bialik	287-290
PREDICTION OF ONSET OF EPILEPTIC SEIZURE BY ANALYSIS OF PRE-ICTAL STATE OF EEG	
Prasad D. V., Swarnalatha R. and Natasha Giridhar	291-294
TECHNOLOGY PLANNING OF HARD TURNING IN CASE OF ROTATIONAL FEED	
János Kundrák, Károly Gyáni, István Deszpoth and István Sztankovics	295-299
ENVIRONMENTAL LOAD REDUCING IN HARD MACHINING	
Janos Kundrak and Gyula Varga	301-304
COMPARATIVE EXAMINATIONS FOR THE MACHINING OF HARD SURFACES	
Janos Kundrak, Istvan Deszpoth and Viktor Molnar	305-309
DENSITY FUNCTIONAL THEORY STUDY OF ALUMINUM DOPED HEXAGONAL ZINC OXIDE SHEETS	
Hatice Kökten and Sakir Erkoç	311-313
PRELIMINARY CALIBRATION AND FUTURE DEVELOPMENTS OF A MINIATURIZED TENSILE TEST DEVICE BASED ON FLEXURE HINGES	
Luca Dassa and Alessandro Copeta	315-318
USE OF ONBOARD SHORT ARM HUMAN CENTRIFUGE TO CREATE ARTIFICIAL GRAVITY	
Natalia Okhapkina and Lubov Strogonova	319-321
USE THE METHODOLOGY OF USER CENTERED DESIGN FOR LEARNING FURNITURE DESIGN	
Salwa Abdel Bary	323-326
PRELIMINARY PHYSICO-CHEMICAL CHARACTERIZATION OF WASTEWATER FROM THE FARM IN VOJVODINA REGION, SERBIA	
Maja Djogo, Milena Stosic, Dusan Milovanovic, Jelena Radonic, Ivana Mihajlovic and Zoran Cepic	327-330
COLOR SEGMENTATION FOR SEGMENT-BASED STEREO MATCHING	
Martin Beneda and Roman Prokop	331-333
MATHEMATICAL MODELLING OF SURFACE GREASE DEPOSITS	
Jan Kudlacek, Petr Chabera, Tomaz Pepelnjak and Zlatan Car	335-338



INTRODUCTION OF NEW SURFACE TREATMENT TECHNOLOGIES INTO PRACTICE - ZINC BASED COMPOSITE COATING WITH PTFE PARTICLES (ZN-PTFE COATING)	
Petr Drasnar, Jan Kudlacek, Petr Roskanin, Tomaz Pepelnjak, Zlatan Car and Miroslav Vales	339-342
THE DYNAMIC COMPONENT OF THE PATTERN RECOGNITION SYSTEM OF MICROORGANISMS UNDER MICROGRAVITY CONDITIONS	
Nikita Markov, Paul Fomkin, Alecsandr Ermakov and Lubov Strogonova	343-347
A MATHEMATICAL MODEL FOR DETERMINING SOME TRIBOLOGICAL CHARACTERISTICS OF PLAIN JOURNAL BEARING	
Života Antonić, Nebojša Nikolić, Tripo Torović and Jovan Dorić	349-352
INFLUENCE OF IBAD SINX COATINGS ON TRIBOLOGICAL PROPERTIES OF P/M HSS	
Jan Suchánek and František Černý	353-355
ANALYSIS OF BULK METAL FORMING BY UBET – CASE STUDIES	
Igor Kacmarcik, Branko Štrbac and Leon Šikulec	357-360
INVESTIGATION OF THE SUBSURFACE LAYER OF NI3AL-BASED ALLOY AND ITS COMPOSITES INDUCED BY FRICTION	
Karin Gong	361-364
VALUE STREAM MAPPING METHODOLOGY FOR PRE-ASSEMBLY METAL PROCESSES IN SHIPBUILDING	
Damir Kolić, Richard Lee Storch and Nikša Fafandjel	365-368
APPLICATION OF REVERSE ENGINEERING IN THE DEVELOPMENT OF POLYMER PRODUCTS	
Damir Godec, Ines Kramarić and Mladen Šercer	369-372
EXPERIMENTAL INFLUENCE VERIFICATION OF THERMAL AND MECHANICAL SHOCKS ON CUTTING EDGE DURING IRREGULAR INTERRUPTED CUTTING	
Robert Cep, Adam Janasek, Jana Petru, Lenka Cepova and Michal Hatala	373-376
MEAT INDUSTRY WASTEWATER AS POTENTIAL SOURCE OF EMERGING POLLUTANTS IN THE VOJVODINA PROVINCE	
Srđan Kovačević, Maja Turk Sekulić, Jelena Radonić, Ivan Špánik, Mirjana Vojinović Miloradov, Dušan Milovanović and Zoran Čepić	377-379
ANALYSIS OF PD RESPONSE ON DIFFERENT INPUT VOLTAGES AND INCIDENT LIGHT WAVELENGTHS	
Željka Milanović, Ivan Marasović and Vlasta Zanchi	381-385
URBAN ELECTRIC VEHICLE DEVELOPMENT AS PART OF SMART GRID	
Predrag Šaša, Srđan Skok and Vedran Kirinčić	387-390
CHARACTERIZATION OF FUNCTIONALISED MATERIALS BY ATR-FTIR METHOD AND RAMAN SPECTROSCOPY	
Lidija Fras Zemljic, Marko Munda, Simona Strnad, Minka Kovač and Julija Volmajer	391-394
AN ANALYSIS OF SINGLE-PASS CONVENTIONAL SPINNING PROCESS	
Petar Piljek, Zdenka Keran and Miljenko Math	395-399
NUMERICAL MODELING OF PRESSURE VESSEL UNDER CREEP REGIME	
Dominik Pesa and Domagoj Lanc	401-404
FEM SIMULATION OF STRUCTURAL BEHAVIOUR OF LAMINATED COMPOSITE PLATE	
Ivan Sterpin and Domagoj Lanc	405-408
OVERVIEW OF SEARCH-BASED OPTIMIZATION ALGORITHMS USED IN SOFTWARE ENGINEERING	
Goran Mauša, Tihana Galinac Grbac and Bojana Dalbelo Bašić	409-412



THE POTENTIAL OF MANURE UTILIZATION FOR DEVELOPMENT OF SMALL TO MEDIUM SCALE PLANTS FOR BIOGAS PRODUCTION IN VOJVODINA REGION Zoran Čepić, Maja Sremački, Miodrag Živančev, Zoran Đukić, Dejan Ubavin and Mirjana Vojinović-Miloradov	413-416
BI-METALLIC COLD BACKWARD EXTRUSION – NUMERICAL SIMULATION WITH EXPERIMENTAL VERIFICATION Miroslav Plancak, Dejan Movrin, Zlatan Car, Dragiša Vilotić, Igor Kacmarcik and Marko Kršulja	417-420
PROFESSIONAL SOFTWARE FOR HARMONIC ANALYSIS Silviu Darie	421-424
FORCE CONTROLLED GRASPING IN A TWO FINGER ROBOTIC HAND Ottó Botond Lőrinczi, Petra Aradi and Tibor Szalay	425-428
COMPARATIVE ANALYSIS OF THREE MICRO-HOLE MACHINING TECHNOLOGY Vilmos Csala, Sándor Markos and Tibor Szalay	429-433
THE INFLUENCE OF CHITOSAN CHARGE BEHAVIOUR ON ANTIMICROBIAL PROPERTIES Tijana Ristić, Lidija Fras Zemljić, Olivera Šauperl and Andrej Zabret	435-437
PCN2 – CYCLIC LOADING PULSATOR, FOR RESEARCH ON HYDROGEN EMBRITTLEMENT IN SURFACE TREATMENT TECHNOLOGY. Karel Vojkovský, Jan Kudláček, Michal Pakosta and Marko Kršulja	439-442
INVESTIGATION OF COATINGS FRICTION COEFFICIENT USED IN PRODUCTION OF DEEP DRAWN PACKAGING CANS Marko Kršulja, Petr Rožkanin, Jan Kudláček, Loreta Pomenić and Zlatan Car	443-446
AN APPLICATION OF PLANT PATHOGENS, PHYTOPHTHORA SPP. BIOLOGICAL CONTROL BY ANTAGONISTIC BACTERIA IN DURIAN FIELD, UTTARADIT PROVINCE, THAILAND. Kitti Mueangtoom	447-450
LCA AND NEW MATHEMATICAL METHOD FOR THERMIC TREATMENT PROCESSES BY INDUSTRIAL ORGANIC WASTE Viktoria Dr. Mannheim and Zoltan Dr. Simenfalvi	451-454
ADVANCED MEASUREMENTS FOR CONTROL AND PROTECTION OF SMART HYDROPOWER SYSTEMS Razvan Magureanu, Sergiu Ambrosi and Cristina Lupu	455-458
SEASONAL AND SPATIAL VARIATIONS OF PARTICLE-BOUND POLYCYCLIC AROMATIC HYDROCARBONS IN THE CITY OF NOVI SAD, SERBIA Nataša Jovčić, Jelena Radonić, Maja Turk Sekulić, Mirjana Vojinović Miloradov, Srđan Kovačević and Zoran Čepić	459-462
RESEARCH OF MOBILE ROBOT BEHAVIOR WITH EMIR Mladen Crneković, Davor Zorc and Zoran Kunica	463-467
EFFECT OF SINTERING ATMOSPHERE ON SURFACE AND HIGH-TEMPERATURE OXIDATION OF PRESSURE-LESS SINTERED $MOSI_2$-ZRO_2 COMPOSITE Yiming Yao, Erik Ström and Xin-Hai Li	469-473
PHISICAL-CHEMICAL PROPERTIES OF POULTRY FEATHER FIBRES Tatjana Kreže and Simona Strnad	475-479
THE CONVERGENCE OF CROATIA AND SLOVAKIA IN THE FIELD OF R&D FOUNDING TO THE EU 27 AVERAGE Emilia Spišáková and Emil Spišák	481-485
INFLUENCE OF THE CUTTING EDGE RECTIFICATION OF THE CIRCULAR INSERTS FROM CERMET ON THEIR EFFICIENCY Ivana Česáková and Miroslav Zetek	487-490



OBSERVATION OF LASER BEAM HARDENED LAYER HARDNESS USING CUTTING FORCE MEASUREMENT	
Jan Kutlwašer, Josef Sklenička, Eliška Samiecová and Miroslav Zetek	491-494
CONDITIONS FOR DEFINING AND A BRIEF OVERVIEW OF THE TECHNICAL SOLUTIONS FOR DESULPHURIZATION FACILITY AND NITROGEN OXIDES EMISSIONS REDUCTION IN POWER PLANT NIKOLA TESLA	
Branka Nakomčić-Smaragdakis, Zoran Čepić, Tijana Stajić, Maja Turk-Sekulić, Maja Stupavski and Maja Djogo	495-498
MOBILE ROBOT NAVIGATION WITH ANDROID DEVICE USING OPENCV	
Peter Pászto, Marian Klůčik, Martin Smofák, Luboš Chovanec and Peter Hubinský	499-502
EVALUATION AND THE USE OF GPS RECEIVERS FOR SMALL MOBILE ROBOTS IN LOCAL COORDINATE SYSTEM	
Jaroslav Hanzel, Marian Klůčik, František Duchoň and Jozef Rodina	503-506
CREATING A WEB-BASED MODEL FOR FINANCIAL PLANNING AND FORECASTING. USING ENERGY CONVERSION IN A SOLAR GENERATOR	
Aksheta Mehta and Pushkala Muralidharan	507-511
Basel Alsayyed	513-516
IDENTIFICATION OF THE DAMAGE IN THE BEAM-LIKE STRUCTURE ON THE BASIS OF TIMOSHENKO BEAM MODEL	
Sergey Shevtsov, Igor Zhilyaev, Vladimir Akopyan and Arcady Soloviev	517-521
ALUMINA CERAMICS BRAZED USING METALLIC ALLOYS	
Ionelia Voiculescu, Victor Geanta, Radu Stefanoiu, Horia Binchiciu and Dana Daniela Daisa	523-527
EFFECT OF TYPES AND THICKNESS OF LOCAL EVAPORATIVE COOLING PADS INSIDE THE GREENHOUSES IN SUDAN	
Abdelnaser Omran, Egbal Elmsaad and Mohd Rodzi Ismail	529-532
INVESTIGATION TO DISTRIBUTION OF ADDITIVES IN OPEN- AND CLOSED-CELL ALUMINUM FOAM (WORD-FILE)	
Denny Schmidt, Günther Lange and Robert Albrecht	533-537
PROBLEM OF FLOW CONTROL OF PRODUCTION MAKE TO ORDER	
Justyna Trojanowska and Edward Pająk	539-542
RESEARCHES OF THE IMPACT OF INCORRECT DIAGNOSIS CAUSES OF DAMAGE TURBOCHARGER ON THE EFFICIENCY OF THE NEW COMPONENT	
Marek Idzior, Jerzy Markisz, Maciej Bajerlein and Maciej Bieliński	543-546
THE IMPACT OF MODIFIED PISTON TWO STROKE ENGINE ON TOXIC EMISSIONS DETERMINED ON THE BASIS OF RESEARCH CARRIED ON THE CHASSIS DYNAMOMETER	
Jerzy Merkisz, Maciej Bajerlein, Michał Dobrzyński and Łukasz Rymaniak	547-549
METHODS OF RESEARCHES AND EVALUATION OF WEAR INJECTORS USED IN MODERN COMPRESSION IGNITION ENGINES	
Marek Idzior, Jerzy Markisz, Maciej Bajerlein and Paweł Stobnicki	551-554
THE ANALYSIS OF INFLUENCE OF THE EGR VALVE OPENING DEGREE OF ON THE EMISSION OF TOXIC COMBUSTION ENGINES WITH DIRECT INJECTION	
Marek Idzior, Jerzy Merkisz, Maciej Bajerlein and Paweł Daszkiewicz	555-558
INFLUENCE OF STRAIN RATE ON COLD SHEET METAL FORMING	
Tomaž Pepelnjak, Sanja Smoljanič and Robert Zakrajšek	559-562
RESEARCH ON THE INFLUENCE OF ALLOYING ELEMENTS ON THE MICROSTRUCTURE AND MICROHARDNESS OF BIOCOMPATIBLE COBALT-CHROMIUM ALLOYS	
Victor Geanta, Ionelia Voiculescu, Radu Stefanoiu, Dana Daniela Daisa and Emilia Binchiciu	563-566



DSP-BASED CONTROL SYSTEM FOR EXCITATION CONTROL OF SYNCHRONOUS GENERATOR	
N. Bulic, D. Sumina and Z. Car	567-570
NEW TECHNOLOGY FOR VARIABLE PITCH AND VARIABLE	
Cs. Gyenge, L. Oláh and Hodis Andrei	571-574
THE MAIN INVENTORY MANAGEMENT SYSTEMS – THEORY OF INVENTORY, THREE METHODOLOGIES	
H. Pechová, V. Preclík	575-578
VIRTUAL MODEL AND PRODUCTION PLANT SIMULATION FOR OPTIMIZATION OF POWDER COATING PROCESS	
L. Šikulec, D. Hasković and H. Radelja	579-582
INVESTIGATION OF SINGLE POINT INCREMENTAL FORMING PROCESS APPLIED ON THIN SHEET METAL	
Marko Kršulja, Karl Kuzman, Miroslav Plančak, Miljenko Math and Zlatan Car	583-586
ANALYZING USING THE GOLDEN RATIO IN THE ENGINEERING NETWORKS IN THE OLD CIVILIZATIONS (OLD EGYPTIAN – GREEK – ISLAMIC) AND ITS REFLECTION UPON THE CONTEMPORARY DESIGNS	
Ebtesam Khamees	587-590
SYNERGISTIC FORMULATION OF CHITOSAN AND CURCUMIN AS A POTENTIAL ANTIMICROBIAL AND ANTIOXIDANT COATING FOR POLYMERS	
Lidija Fras Zemljic, Tijana Ristić, Matej Bračić and Julija Volmajer	591-594
ICE JET MACHINING: PRESENTATION OF THE PROTOTYPE DEVELOPMENT	
M. Jerman, A. Lebar, H. Orbanic, M. Junkar and A. Suárez	595-598
CFD INVESTIGATION OF THE TURBULENT FLOW IN A ONE-STAGE RADIAL-FLOW BLOWER AGGREGATE	
L. Kalmár, G. Janiga and L. Soltész	599-602



International Conference on Innovative Technologies, IN-TECH 2012,
Rijeka, 26. - 28.09.2012





THE PRESENT SITUATION OF THE TPM SYSTEM IN SLOVAK ENTERPRISES

Juraj Drahňovský¹

¹ Slovak University of Technology in Bratislava, Faculty of Materials Science and Technology in Trnava,
Paulinska 16, Trnava, 917 24, Slovakia, juraj.drahnovsky@stuba.sk

Keywords: TPM, Motivation, Overall Equipment Effectiveness, Equipment Categorization

Abstract. The TPM (Total productive maintenance) is presently one of the basic elements of the successful industrial enterprises. Many of them established the TPM system with a view to the growth of the production effectivity. But often it is not. The goal of the article is to inform about the present situation of the TPM system in Slovak enterprises, about the possible causes of this status and to suggest the proposals for improvement of the TPM implementation which could be a part of the sustainable development in the industrial enterprises.

Introduction

Maintenance is a conducive factor to the production process which creates optimal conditions for its existence. It is necessary to pay attention to this activity in business units, it must be provided organized, based on links within maintenance process as well as links with other company departments or its surroundings.

Presently, Total productive maintenance is a mass implemented solution of the maintenance organization in Slovak enterprises. This trend occurs after foreign investors coming in Slovakia who brought with them not only new technologies but also new insights on various things. However, many times I met a question in the companies if TPM is not just another name for something what is here for a long time and it works.

Total Productive Maintenance

Many large failings occur only because employees often ignore the apparent trifles. In order to make maximum use of equipment, it is necessary to know the ideal conditions for the operation of each machine component, as well as values that represent the peak performance of the machine. If these conditions are known it is a task for employees to maintain them. The device is more complex, the responsibility for compliance with these conditions is greater.

Productive maintenance rule says that „the maintenance, as well as the main production areas, must maximally contribute to raising productivity and become a productive maintenance“. The word *productivity* is then necessarily given to the title of the most modern organizing and maintenance system under the name Total Productive Maintenance. [1]

TPM is oriented on the involvement of all employees in the workplace in activities aimed at the downtime, accidents and rejects minimizing. It is about overcoming of the traditional division of „workers who work on the machine“ and „workers who can repair“. It is considered that even machine operator is able to detect abnormalities in the machine work and possible sources of equipment failures as the first.

Maximum diagnostic and maintenance activities are therefore transferred from the traditional maintenance department directly to production workers – production departments. It usually starts with workplace order improvement, machines cleaning and checking their condition (loose screws, cables, covers, cleaning and lubrication of friction surfaces, etc.). Furthermore, operators learn „to understand their machines“ as an experienced car machine driver knows to establish proper diagnosis and perform appropriate repair in time. The operator also takes over this role, gradually learns to behave like to his „own“ equipment. In addition to maintenance workers and operators in the TPM system also involving other professions, such as the technical preparation of production. [2]

It is a common phenomenon that the maintenance reliability is overlooked in favour of the production reliability and the ability to produce without breakdowns. Production reliability usually increases with backup equipments and focusing on problem symptoms without addressing the real causes. By focusing on reliability of machinery and equipments, we can further improve production reliability and reduce long-term costs associated with the production. Various methods and tools are needed for this step; indicators for maintenance reliability which have been successfully applied to increase the reliability of machinery and equipment.

Calculation of Overall Equipment Effectiveness

In this paper I focus on the proposal to change the OEE calculation only which is one of the basic TPM principles.

Overall Equipment Effectiveness (OEE) is a function of losses due to failures (breaking down), the power losses due to reduced speed and set-up times and also low-quality of the manufactured products. [1] According to S. Nakajima it is primarily the elimination of these six basic types of big machine losses [2, 3]:

1. *Breakdowns* (Down Time Loss),
2. *Setup and Adjustments* (Down Time Loss)
3. *Small Stops* (Speed Loss)
4. *Reduced Speed* (Speed Loss)
5. *Startup Rejects* (Quality Loss)
6. *Production Rejects* (Quality Loss)

T. Suzuki mentions as many as 16 major losses in production, which are summarized in Table 1.

Table 1 Sixteen Major Losses in Production [4]

Category	Loss
Losses that impede equipment efficiency	1. Failure losses - Breakdown loss 2. Setup / adjustment losses 3. Cutting blade loss 4. Start up loss 5. Minor stoppage / Idling loss 6. Speed loss - operating at low speeds 7. Defect / rework loss 8. Scheduled downtime loss
Losses that impede human work efficiency	9. Management loss 10. Operating motion loss 11. Line organization loss 12. Logistic loss 13. Measurement and adjustment loss
Losses that impede effective use of production resources	14. Energy loss 15. Die, jig and tool breakage loss 16. Yield loss

So, the calculation of the OEE is as follows [5]:

$$OEE = A \times P \times Q \quad (1)$$

where:

A – Availability

$$A = \frac{\text{Operating Time}}{\text{Planned Production Time}} \quad (2)$$

P – Performance

$$P = \frac{\text{Ideal Cycle Time}}{\frac{\text{Operating Time}}{\text{Total Pieces}}} \quad (3)$$

Ideal Cycle Time is the minimum cycle time that the process can be expected to achieve in optimal circumstances. It is sometimes called Design Cycle Time, Theoretical Cycle Time or Nameplate Capacity. Since Run Rate is the reciprocal of Cycle Time, Performance can also be calculated as:

$$P = \frac{\frac{\text{Total Pieces}}{\text{Operating Time}}}{\text{Ideal Run Rate}} \quad (4)$$

Performance is capped at 100%, to ensure that if an error is made in specifying the Ideal Cycle Time or Ideal Run Rate the effect on OEE will be limited.

Q – Quality

$$Q = \frac{\text{Good Pieces}}{\text{Total Pieces}} \quad (5)$$

The value of OEE ranges from 30 to 60% in our country. The world class OEE value is around 90%.

Conclusions from Current State Analysis of TPM in Industrial Enterprises in Slovakia

The *first part of the current state analysis* consisted of obtaining an objective view of the TPM implementation and application. After conducting a thorough analysis of technical papers at conferences, in professional journals and other publications, and after comparing the TPM implementation and application in several companies, I came to the conclusion that the implementation methodology and use of this system is largely identical in these enterprises. This is mainly due respect of the same steps in the TPM implementation in any enterprise, according to TPM methodology.

In the *second part of the current state analysis* of TPM implementation and application in industrial enterprises in Slovakia was used a questionnaire survey, it was conducted in 8 enterprises predominantly in the automotive industry.

Conclusions from the questionnaire survey can be summarized as follows:

- ◆ 28% of respondents are dissatisfied with the TPM system,
- ◆ 7% of respondents have never participated in the TPM training,
- ◆ 34% of respondents understood the principles, nature and reasons for the TPM implementation only partly,
- ◆ 28% of respondents said that filled forms are not evaluated at all, or they do not know about that,
- ◆ 42% of respondents do not carry out regularly maintenance activities according to plan,
- ◆ more than a third of respondents said that their direct superiors do not check the equipment status after cleaning,
- ◆ some respondents are working under greater time pressure, which is associated with excessive bureaucracy,
- ◆ some workers ignore TPM system,
- ◆ greater motivation is lacking.

Controlled interviews with the managers were the *third part of the current state analysis*. It was compiled 6 basic questions which were asked all respondents, but were used also subsidiary questions to complement during interviews. Based on responses to the questions, the following conclusions have been formulated:

- ▲ Lack of senior management interest in the challenging problems solving in production and maintenance.
- ▲ Irregularity in carrying out a routine maintenance activities by the operators.
- ▲ Dysfunctional motivation of employees.
- ▲ Poor communication between production and maintenance workers.
- ▲ Too much administration at the expense of maintenance activities.
- ▲ Slovak workers' view on the maintenance – it is still an opinion that the maintenance is in charge of servicemen, not operators.

A vast majority of respondents considers TPM system as very good and beneficial for an enterprise. On the other hand, it is clear from the current state analysis that there are serious shortcomings by the TPM implementation and application.

In a complex sense, these shortcomings were the basis for design solutions to enhance TPM implementation and application in industrial enterprises in Slovakia which I propose:

- ♣ *Lack of senior management interest in the TPM.*
- ♣ *Inconsequence of the TPM activities execution.*
- ♣ *Inconsequence of check of the TPM activities execution.*
- ♣ *Dysfunctional staff motivation.*

The Proposal for Improvement of the TPM Implementation - OEE Calculation

Based on data obtained from the production needed to calculate OEE, they are then daily evaluated for each production equipment. TPM coordinator of each workshop is *responsible* for OEE evaluation. OEE calculation of i-th equipment is as follows:

$$OEE_i^D = A \times P \times Q \quad (5)$$

where:

OEE_i^D – Overall Effectiveness of i-th Equipment in Particular Day.

For *monthly* evaluation is then the following calculation:

$$\Phi OEE_i^M = \frac{\sum_{D=1}^{NOD} OEE_i^D}{NOD} \quad (6)$$

where:

ΦOEE_i^M – Average Overall Effectiveness of i-th Equipment in Particular Month.

NOD – Number of Days when Equipment is In-Service.

However, I propose to divide equipments into several categories so that OEE indicators could be comparable among themselves. Equipment categorization is shown in Table 2. Equipment Complexity Coefficient (ECC) is then assigned into each equipment category, its value shall be determined at the solving teams meetings. Individual equipments shall also be assigned into categories at these meetings. The calculation is then following:

$$OEE_{Ci}^M = \Phi OEE_i^M \times ECC_J \quad (7)$$

where:

OEE_{Ci}^M – Overall Effectiveness of i-th Equipment with Regard to Equipment Complexity Coefficient in Particular Month.

J – Symbol of the Category Which the Equipment Is Assigned to.

Table 2 Criteria for Equipment Categorization [6]

Symbol of the Category „J“	Category	Auxiliary Criteria for Categorization	ECC _J
A	Bottleneck Equipment	- Technology Indispensability - Greater Complexity (8 and more Assembly Groups) - High Working Accuracy	ECC _A
B	Usual Equipment	- Technologically Substitutable Machines - Machines with the Middle Complexity (4-8 Assembly Groups) - Mechanized Machines with the Lower Degree of Automation - Machines in Bigger Numbers	ECC _B
C	Auxiliary Equipment	- Technologically Simple Machines (up to 3 Assembly Groups) - Machines Used only Occasionally - Machines for Auxiliary Operation	ECC _C

It thereby means that $ECC_A > ECC_B > ECC_C$. It is obvious that these categories and criteria for equipment categorization may be altered according to any industrial enterprise. ECC_j value can be given in several ways, e. g. on the basis of rejects statistics; according to duration of use; depending on the last overhaul date; by expert estimates; or other quantitative and qualitative methods.

Thus, the resulting indicator – OEE_{Ci}^M – expresses in percentage the effectiveness and productivity of i -th equipment in particular month. For further needs, it will be also counted the average ratio – ΦOEE_{Cn} – for each production team, by formula:

$$\Phi OEE_{Cn} = \frac{\sum_{i=1}^m OEE_{Ci}^M}{m} \quad (8)$$

where:

ΦOEE_{Cn} – Average Overall Effectiveness of All Equipments with Regard to Equipment Complexity Coefficient within n -th Production Team.
 m – Number of Equipments on Which the OEE_{Ci}^M Is Monitored within n -th Production Team.

The basis of the proposal is to define the sequence of steps in the evaluation of the TPM application, which is based on two obtained parameters:

- ΦOEE_{Cn} – based on the used OEE indicator. The average indicator OEE_{Cn} expresses the efficiency and productivity of all devices in n -th production team.
- F_{TPMn} – this percentage shows the monthly TPM functionality, what is the level of Total Productive Maintenance in n -th production team. It provides on the basis of the proportion of positive responses to the all questions of the form Monthly check of TPM functionality. The more questions are answered, the more objective is an indicator of TPM functionality.

After obtaining these data follows the calculation of the summary indicator, which is marked as OE_{TPMn} and represents the Overall Effectiveness of TPM in n -th Production Team. Its calculation will achieve as a product of the two above-mentioned parameters, i. e.:

$$OE_{TPMn} = \Phi OEE_{Cn} \times F_{TPMn} \quad (9)$$

The calculation resulted in the expression, on how many % the production team meets the sub-indicators, which compose the calculation of OEE (Availability, Performance, Quality), in conjunction with the TPM activities realization, which are checked in terms of the monthly checking.

Conclusion

However, this is just a part of my research and proposals. If you want more information of it, please do not hesitate to email me or visit this link for further information: http://books.google.sk/books/about/TPM_in_Slovakia.html?id=5J4I0xvo61QC&redir_esc=y.

References

- [1] Rakyta, M.: *Ako úspešne začať projekt TPM*. In *Totálne produktívna údržba 2004*. Belušké Slatiny.
- [2] Košťuriak, J., Gregor, M., Mičieta, B., Matuszek, J.: *Projektovanie výrobných systémov pre 21. storočie*. Žilina, ŽU, 2000. ISBN 80-7100-675-0.
- [3] http://www.oeo.com/oeo_six_big_losses.html, available on July 9th, 2012.
- [4] http://www.plant-maintenance.com/articles/tpm_intro.shtml, available on July 9th, 2012.
- [5] http://www.oeo.com/calculating_oeo.html, available on July 9th, 2012.
- [6] Burcl, R., Bestvinová, V.: *Starostlivosť o stroje a zariadenia*. Trnava, AlumniPress, 2007. 1st edn, eTextbook. ISBN 978-80-8096-009-4.
- [7] Drahňovský, J.: *TPM in Slovakia?*. Łódź: KSIEZY MLYN Dom Wydawniczy Michał Kolinski, 2011. 121 pp. ISBN 978-83-7729-113-9

NACRE DESIGN AS INSPIRATION FOR OPTIMAL DESIGN OF A ROOF

T. Kegl¹

¹ II. Gymnasium Maribor, Trg Miloša Zidanška 1, SI-2000 Maribor, Slovenia

Keywords: nacre shell, architecture, roof strength analysis, practical implementation

Abstract. This paper deals with biomimetics, which studies natural solutions to address technical problems. Attention is focused on the usage of biomimetics in architecture, especially on the usage of design of nacre as inspiration for roof design. For this reason, the structural requirements for a roof structure and some properties of the nacre shell are presented. Among the modern methods of architecture design, parametric modeling and optimal design method are used to design a nacre-like roof in order to fulfill the requirements of functionality, economy and ecology. At first, the strength analysis of a flat and wavy roof, calculated with the STAKx research program, is presented. The displacements, the total strain energy and volume of material are compared. An optimal design procedure, using the iGOx research program, is also performed. The design variables are related to the thickness and to the geometry of roof. The constraints are related to maximal displacement and maximal volume of the roof. Meanwhile, the objective function to be minimized is defined as the total strain energy. The obtained optimal design of the roof is a wavy, nacre-shell-like, design which has excellent properties like low mass, high load capacity, low strain energy and low cost. Some practical implementations of this optimal roof design are proposed.

Introduction

The word biomimetics is used to describe the substances, equipment, mechanisms and systems by which humans imitate natural systems and designs. Today, biomimetics finds applications in all areas, including architecture and building. Biological models may be emulated, copied, learnt or taken as starting points for new technologies. Through studies of biological models, new forms, patterns and building materials arise in architecture. Because of their properties, biomimetic materials often outperform conventional materials and constitute future challenges for architecture [1]. A lot of natural systems is studied and imitated in the field of architecture [1,2,3,4,5,6].

Some spider spin webs, Fig. 1, resemble a tarpaulin covering thrown over a bush. The web is borne by stretched threads, attached to the edges of a bush [2,3,4]. The load-bearing system lets the spider spread its web wide, while still making no concessions as to its strength. This marvelous technique has been imitated by man in many structures to cover wide areas. Some of these include the Munich Olympic Stadium, Figure 3, the Sydney National Athletic Stadium, the Jeddah Airport's Pilgrim Terminal, ZOOs in Munich and Canada, Denver Airport in Colorado, and the Schlumberger Cambridge Research Centre building in England.

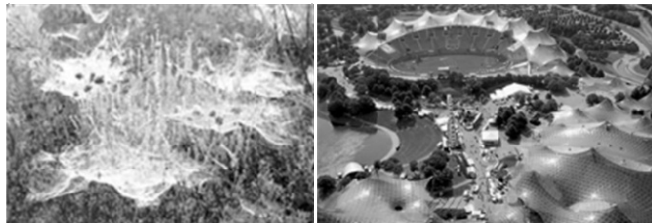


Fig. 1 Spiders spin web (left) and Olympic Stadium in Munich (right) [2,3]

All successful examples show that for imitation of the living beings, at first a really good observation is necessary. Furthermore, frequently some coincidence is necessary, like, for example, for the Velcro. The idea came to George de Maestral, someday, after returning from a hunting trip with his dog in the Alps [3]. He took a close look at the burrs (seeds) of burdock that kept sticking to his clothes and his dog's fur. He examined them under a microscope, and noted their hundreds of "hooks" that caught on anything with a loop, such as clothing, animal fur, or hair. He saw the possibility of binding two materials reversibly in a simple fashion, if he could figure out how to replicate the hooks and loops. In a similar way, one can admire the beautiful shapes of shells at the sea coast. If one steps on a shell, it does not break under your weight. This was one of the reasons to start to investigate the possibility to design roofs of buildings like nacre shells: tinny and unbreakable.

In this paper, at first some properties of nacre shell and some structural requirements for a roof structure are presented. Then, two modern methods of architecture design, the parametric modelling and optimal design method, are presented. This is followed by the strength analysis of a flat and a nacre-like roof, computed with the STAKx research program. The displacements, the total strain energy, and volume of material are compared. An optimal design procedure of 1000 m² pavilion, using the iGOx research program, is also performed and the roof properties like mass, load capacity, strain energy, and cost are analysed. Finally, some practical implementations of this optimal roof design are proposed.

Nacre shell design, roof requirements and optimization

Many researchers have investigated the properties of a nacre shell [6,7,8]. They established that the tensile strength in the direction perpendicular to the layered structure can be explained by the presence of mineral bridges. These bridges, having a diameter of approximately 50 nm, have a tensile strength no longer determined by the critical crack size, but by the theoretical strength. Their number is such that the tensile strength of the tiles is optimized for the tile thickness of 0.5 μm . A higher number of bridges would result in tensile fracture of the tiles with loss of the crack deflection mechanism. The elastic modulus of the shell material is about 100 GPa [6]. Mechanical

tests with loading applied perpendicular to the plane of the organic layers reveal a tensile strength lower than 10 MPa, whereas the compressive strength is approximately 190-550 MPa. All mechanical experiments and analyses of nacre indicate that mineral bridges effectively increase the stiffness, strength and toughness of the organic matrix layers, and demonstrate that the effect of the mineral bridges on the organic layers and wavy design of shell are of significant importance.

Generally, it seems that regarding roof design we can learn a lot from the design of sea shells. This is because a sea shell exhibits all the main properties typically required for a roof structure. However, maybe the most important requirements, related to roof design, are [8]: (i) strength and resistance to external loads, (ii) economic (sparing) use of material, and (iii) aesthetic appearance.

In this paper we concentrate mainly on roof strength, necessary to resist external loads, primarily induced by snow. For buildings being designed in cold regions, local building codes provide guidelines to determine loads attributed to snow accumulations. These guidelines necessarily apply to a range of generic situations that are fairly simple. Model testing and computer analyses, utilizing detailed meteorological histories, have now developed to the point where many variables that affect snow loading can be accounted for, even in complex situations, leading to more accurate loading predictions. The variables affecting snow loading include [9]: building shape; building orientation; building insulation; wind speed; wind direction; precipitation (both snow and rain); temperature (melting, re-freezing); cloud cover; and, solar exposure.

According to Slovenian weather circumstances, especially wind and snow action, analysis has an instrumental role in the design and optimization of roof structures. For that purpose the dead and permanent loads, as well as snow and wind have to be considered for the roof strength analysis. The snow loads for Slovenian circumstances are in the range of about 3000 N/m².

Keeping this in mind it makes a good idea to include the sea shell design into the design process of a roof structure. Of course, this can be made either in a more or less heuristic manner, or one can go one step further and try to enrich this procedure by modern techniques such as computer supported structural analysis and mathematical optimization [10].

In architecture a lot of commercial programs can be used for parametric modelling and structural analysis, e.g., AutoCAD, Abaqus, Ansys, etc. However, these commercial programs are not easily integrated into an optimal design procedure. For this reason, in this work the structural analysis program STAKx has been used, which is easily combined with a gradient-based optimization program iGOx. Both of these research programs were developed at the Faculty of Mechanical Engineering at the University of Maribor. STAKx is actually a finite element program for static analysis of elastic structures. The speciality of this program is its strong orientation into the shape parameterization of structures and the possibility to compute the gradients of response quantities. The employed parameterization is based on the so-called design elements whose shape is determined by the positions of their control points. The program iGOx is actually a gradient-based optimizer which enables interactive optimization by making use of external response analysis programs like STAKx.

The sea shell-like roof structure model

In this paper it is assumed that we want to design sea shell-like roof structure to cover a fixed area of an, for example, exhibition pavilion. The program STAKx is used to define the geometrical model of the roof. The top view of the roof is shown in Figure 6, where the thick blue lines mark the supported edges of the structure. To describe the geometry, 3×11=33 control points are used. Some of the control points will be fixed, while the other the control points will be allowed can move in order to change the shape of the roof. By changing the positions of the movable points adequately, the roof may obtain a se shell-like form.

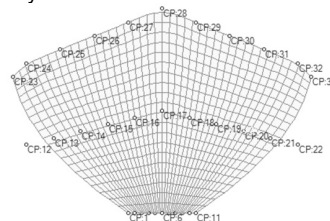


Fig. 2 Top view of the roof and the control points

The span of the roof is 60 m in the x direction and 30 m in the y direction. Its cover area is approximately 1000 m². The roof is vertically supported along all edges, except along the front edge, defined by the control points 23-33.

The roof is assumed to be loaded in the vertical direction. More precisely, the imposed snow load is 3000 N/m². Additionally, the actual weight of the roof was also taken into account. Of course, weight depends on the roof volume and the material chosen. In our case the selected material is concrete. Its modulus of elasticity is 30·10⁹ N/m² and its density is taken as 3000 kg/m³.

Optimal design of the roof

In order to obtain a roof design that is really optimal with respect to specific criteria, it is necessary to enrich the parametric modelling by one of the optimal design methods. In order to use such a method one needs to formulate the problem of optimal design, i.e., to define the objective function and constraints as well as to select the design variables.

The objective function is the quantity that has to be minimized during the optimization process. In our case this could be the strain energy of the roof. Strain energy, here denoted as Π , is the energy that is stored within an elastic body when it is deformed under the influence of external loads. From practical experience we know that good designs exhibit low strain energy when subjected to some given external loads. We can use this fact to formulate the problem in the following sense: find such values of the design variables that the strain energy of the roof under the prescribed loads will be minimal.

On the other hand, we also know from practical experience that the strain energy of the structure can be reduced by keeping the design fixed and just adding material, i.e., in the case of a roof by making the roof thicker. Because it is not our intention to make the roof too thick, we have to impose a constraint on the volume of the used material. If the structural volume is denoted by V and its maximal allowed value equals V_{max} , the constraint can be written as $V \leq V_{max}$.

In addition to the volume constraint, we impose for practical reasons one further requirement: the vertical displacement Δz of the most exposed point of the roof (CP: 28) should be less than the maximal allowed value Δz_{max} . This constraint can be written as $\Delta z \leq \Delta z_{max}$.

In the case of our roof, the selected design variables $b_i, i=1..21$ are related to the roof thickness $d=1+ b_1$ and x, y or z coordinates of some of the 33 control points as follows:

$$\begin{array}{lll} z_{2,4,6,8,10,24,26,28,30,32} = 0.1 + b_2 & z_{13,21} = 1 + 12 \cdot b_7 & x_{13,21} = 16 + 0.4 \cdot b_{17} \\ z_{17} = 1 + 25 \cdot b_3 & y_{17} = 15 + b_8 & x_{27,29} = 5 + 0.4 \cdot b_{18} \\ z_{16,18} = 15 \cdot b_4 & y_{16,18} = 14 + b_9 & x_{26,30} = 10 + 0.4 \cdot b_{19} \\ & & y_{13,21} = 10 + b_{13} \\ & & x_{16,18} = 4 + 0.4 \cdot b_{14} \end{array}$$

$$\begin{aligned} z_{15,19} &= 1 + 20 \cdot b_5 \\ z_{14,20} &= 10 \cdot b_6 \end{aligned}$$

$$\begin{aligned} y_{15,19} &= 13 + b_{10} \\ y_{14,20} &= 12 + b_{11} \end{aligned}$$

$$\begin{aligned} x_{15,19} &= 8 + 0.4 \cdot b_{15} \\ x_{14,20} &= 12 + 0.4 \cdot b_{16} \end{aligned}$$

$$\begin{aligned} x_{25,31} &= 15 + 0.4 \cdot b_{20} \\ x_{24,32} &= 20 + 0.4 \cdot b_{21} \end{aligned}$$

In short, we have 21 design variables that influence the thickness and the shape of the roof. If we summarize the above discussion, the optimal design problem can be defined as follows:

minimize the total strain energy: $\min \Pi$
subject to constraints: $V - V_{\max} \leq 0$ and $\Delta z - \Delta z_{\max} \leq 0$

where, in our case, $V_{\max} = 600 \text{ m}^3$ and $\Delta z_{\max} = 0.2 \text{ m}$. The quantities Π , V , and Δz depend on design variables. They have to be computed by using adequate software, in our case, by the finite element analysis program STAKx.

The initial values of all design variables were zero: $b_i^{\text{ini}} = 0, i = 1 \dots 21$. The corresponding initial thickness and design dependent coordinates of the control points (in meters) were: $[1.00000, 0.10000, 1.00000, 0.00000, 1.00000, 0.00000, 1.00000, 15.00000, 14.0000, 13.0000, 12.0000, 11.0000, 10.00000, 4.0000, 8.0000, 12.0000, 16.0000, 5.00000, 10.00000, 15.00000, 20.0000]^T$. The displacements and distribution of strain energy of the initial roof design are presented in Fig. 3.

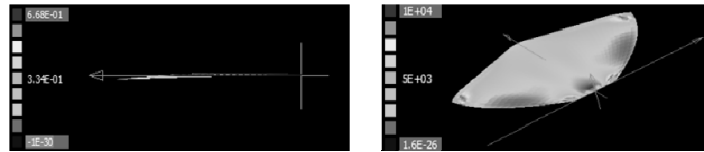


Fig. 3 Displacements and distribution of strain energy of initial roof

Optimization, i.e., the solution process of the above optimal design problem, has been performed by the program iGOx, which can run the program STAKx in order to perform the response and sensitivity analysis of the structure. iGOx is an interactive gradient-based optimization program, which enables continuous monitoring and eventual adjustments during the optimization process, Fig. 4.



Fig. 4 Interactive optimization program iGOx

The optimization process converged nicely after 30 iterations. The final (optimal) values of design variables were as follows:

$$b_i^{\text{opt}} = [-0.55015, 0.04322, 0.99534, 0.78061, 0.64040, 1.00000, 1.00000, -1.00000, 0.568073, -0.05508, 0.51398, 1.00000, 1.00000, 0.43664, 0.40026, 0.69340, 0.23342, -0.97349, -0.24194, -0.00034, 1.00000]^T$$

which corresponds the following optimal values of thickness and design dependent coordinates of the control points:

$$[0.44985, 0.14322, 5.88349, 11.70908, 13.80794, 6.00000, 13.00000, 14.00000, 14.56807, 27.56807, 12.51398, 12.0000, 11.00000, 4.17466, 8.16010, 0.69340, 16.09337, 4.61060, 9.90322, 14.99986, 20.40000]^T$$

The obtained optimal design of the roof, which looks similar to the nacre design, is presented in Fig. 5.

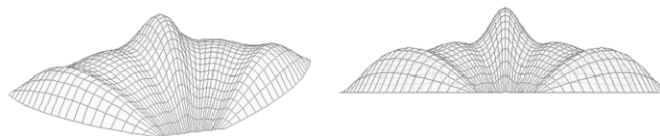


Fig. 5 Optimal design of the roof

The response of the optimal roof, i.e., the displacements and the distribution of the strain energy, are presented in Fig. 6.

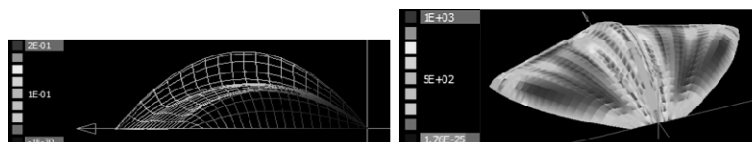


Fig. 6 Displacements and distribution of strain energy of the optimal roof

For comparison, the response and some other parameters of initial and optimal design are presented in Table 1. It is evident that by optimization, both, the strain energy and the volume of the roof, decreased. Furthermore, all constraints have been fulfilled by the optimization process.

Table 1. Properties of initial and optimal roof design

Parameters of response analysis and optimization	Initial roof design	Optimal roof design
Π (Nm)	3 252 607	496 688
Max. constraint violation	0.46774	< 0

Δz (m)	0.668	0.19
V (m ³)	871.47	531.12
Mass (kg)	2 614 417	1 593 361

The obtained optimal roof design is obviously similar to a sea-shell. On the basis of the properties of the optimal roof design, given in Table 1, it is evident that the roof, which imitates the sea shell design, exhibits low mass and better load carrying capabilities.

Experimental verification of optimal roof design

To verify the correctness of the strength analysis and optimal design procedure, models of initial and optimal roof, reduced by a factor of 200, have been manufactured, Fig. 7. For this purpose rapid prototyping technology on the machine EOSINT P800 has been used. The used material is the composite PA 2200 on the basis of polyamide. Its elastic modulus is 1.7 GPa and its density is about 930 kg/m³. The surface load of 300 N/m² has been used for the numerical simulation and for the experiment. For the experiment this load was approximated by a water-filled plastic bag, Fig. 8.



Fig. 7 The manufactured reduced models of initial and optimal roof



Fig. 8 Measurement of maximal displacements of the manufactured model

The measurements and numerically determined displacement of the initial roof model is 7.0 mm and 6.0 mm, respectively. The measurements and numerically determined displacement of optimal roof model is 0.35 and 0.3 mm, respectively. The numerically and experimentally obtained displacements agree quite well. This is especially true, if one takes into account that the experimental loading is quite far from an ideal constant distributed load. Furthermore, for practical reasons the supports in the experiment could not be realized as prescribed in the numerical simulation. Taking only these two quite significant sources of error into account, one can say that the agreement is good enough in order to conclude that the numerical simulation was accurate within reasonable limits.

Practical applicability

The roof obtained by the optimization is in some sense similar to the nacre shell. The supporting in the vertical direction of this roof structure is supposed along all three short edges. Therefore, the face side of the roof can be open, offering free access, e.g., for visitors, logistics and so on. Obviously this nacre shell-like roof could be potentially used, e.g., for: exhibitions pavilion, commercial building, sport stadium, market building and so on. In the case of an exhibitions pavilion, Fig. 9, the front side can be glazed. This would offer various possibilities for light effects, which are very important to attract visitors and potential buyers.



Fig. 9 Usage of nacre shell-like roof for car exhibition pavilion

Conclusions

This paper discusses how to enrich biomimetics by the use of modern methods of architecture in the field of roof design. On the basis of the results obtained in this work, the following conclusions can be made: (i) a sea shell surely represents an interesting draft of a roof design, (ii) some of the most important quantities, related to a free form roof design are strain energy, displacements, mass and volume of material, (ii) parametric modelling and optimal design can offer efficient techniques in architecture where statics and aesthetic aspects has to be taken into account, (iv) optimization of a free form roof design by minimizing the strain energy can yield a light weight but strong roof structure.

Acknowledgements

This investigation was supported by the mentors MSc Stane Kodba and Alenka Prapotnik-Zalar at IInd Gymnasium Maribor and by company CHEMETS, Kranj, d.o.o, Slovenia, where the roof models were manufactured by rapid-prototyping.

References

- [1] M. Zbašnik-Senegačnik, L. Koprivec: Biomimetics in the architecture of tomorrow, *Architecture Research*, Volume 1 (2009), pp. 40-49.
- [2] H. Yahya: Biomimetics: *Technology Imitates Nature*, Global Publishing, Istanbul, 2006.
- [3] T. Kegl: *Z biomimetiko do učinkovite strehe nad glavo*, Research work. II. Gymnasium Maribor, Maribor, 2011.
- [4] A.M.T. Harmer, T.A. Blackledge, J.S. Madin, M.E. Herberstein: High-performance spider webs: Integrating biomechanics, ecology and behavior, *Journal of the Royal Society Interface*, Volume 8 (2011), pp. 457-471.
- [5] J.R. Usherwood, F.O. Lehmann: Phasing of dragonfly wings can improve aerodynamic efficiency by removing swirl, *Journal of the Royal Society Interface*, Volume 5 (2008), pp. 1303-1307.
- [6] T. Kegl: Optimal design of a roof using biomimetics, *Mechanical Testing and Diagnosis*, Volume 1 (2011), pp. 73-81.



-
- [7] M.A. Meyers, A.Y.M. Lin, P.Y. Chen, J. Mucho: Mechanical strength of abalone nacre: Role of the soft organic layer, *Journal of the mechanical behaviour of biomedical materials*, Volume 1 (2008), pp. 76-85.
- [8] R. Nagarajan, S.E.G. Lea, J.D. Goss-Custard: Seasonal variations in mussel, *Mytilus L.* shell thickness and strength and their ecological implications, *Journal of experimental marine biology and ecology*, Volume 339 (2006), pp. 241-250.
- [9] H.A. Baker, C.J. Williams, P.A. Irwin: Experiences with model studies to determine roof snow loading. Proceedings, Annual Conference - Canadian Society for Civil Engineering, Volume 2003 (2003), pp. 1687-1695.
- [10] M. Stavric, O. Marina: Parametric modeling for advanced architecture, *International Journal of Applied Mathematics and informatics*, Volume 5 (2011), pp. 9-16.



International Conference on Innovative Technologies, IN-TECH 2012,
Rijeka, 26. - 28.09.2012



OPTIMIZATION OF A DIESEL FUEL INJECTION SYSTEM USING BIOFUEL

M. Kegl¹, S. Pehan¹, B. Kegl¹

¹ University of Maribor, Faculty of Mechanical Engineering, Smetanova 17, SI-2000 Maribor, Slovenia

Keywords: optimal design, diesel fuel injection system, biodiesel

Abstract. The paper presents an optimization procedure of a fuel injection system of a bus diesel engine. Attention is focused on various results obtained by using two different types of fuel: diesel and biodiesel. The proposed design procedure is based on the assumption that the diesel engine performance, fuel consumption, and harmful emission are significantly influenced by the atomization of the fuel spray. The Sauter mean diameter is utilized as a measure of spray atomization and introduced into the objective function. The design problem is formulated as a multiobjective optimization problem, taking into account the ESC 13 mode test for commercial diesel engines. The design variables of the injection system are related to the shape of the cam profile, to the nozzle geometry, and to the control parameters which influence the injection quantity and timing. The geometrical properties of the cam profile and the injection parameters are kept within acceptable limits by the imposed constraints. The results of optimization using diesel and biodiesel are compared to each other to show the influence of fuel type on final design and performance of the system.

Introduction

In the last decade enormous efforts have been done in order to reduce harmful diesel engine emissions. One of the most important factors is precise control of the fuel injection process [1,2]. The injection system must satisfy the following requirements: (i) high pressure capability, (ii) injection pressure control, (iii) flexible timing control, and (iv) injection rate control. Another factor, influencing the emissions, is the use of alternative fuels. It has already been shown that alternative fuels offer an opportunity to reduce harmful emissions while keeping other engine characteristics within acceptable limits [1,3-5].

High injection pressure generally contributes to decreased fuel droplet size and improved combustion, resulting in reduction of smoke emission. Low injection pressure, on the other hand, is required to reduce noise at idling and in the very low load range. In other words, optimum injection pressure must be determined in accordance with engine load and speed. Regarding the fuel consumption, it was found out that some improvement might be achieved by increasing the injection pressure. More precisely, the fuel should be injected with low pressure at the initial phase of injection and with high pressure in the later phases. According to above requirements, a fuel injection system should have a wide pressure controllability.

Optimization of the injection timing is also important to control nitrogen oxidant (NO_x) and particulate matter (PM) emission simultaneously. Flexible injection timing control, which considers both, engine speed and load, is required. Injection timing is directly related to the initially injected fuel quantity, which in turn influences harmful emissions [1,6]. NO_x-PM trade offs are handled by variation of the injection timing and injection rate history. Besides of NO_x and PM emission, the injection rate history also affects the fuel consumption.

Once the above mentioned injection characteristics are optimally matched to each other, they typically result in a fuel spray with small droplet size (good atomization), long tip penetration and narrow spray angle. These spray characteristics play an important role to improve engine performance, to reduce fuel consumption and to reduce harmful emission. This is especially true for the fuel atomization [7]. For this reason, it seems to be a good idea to involve fuel spray atomization (Sauter mean diameter) into the optimization process of the fuel injection system.

Optimization of a time dependent mechanical system may often be based on a solution process of a non-linear problem P of mathematical programming, written in the following form

$$\min g_0(\mathbf{b}, \mathbf{u}) \quad (1)$$

$$g_i(\mathbf{b}, \mathbf{u}) \leq 0, \quad i = 1, \dots, j \quad (2)$$

$$\dot{\mathbf{u}} = \mathbf{f}(\mathbf{b}, \mathbf{t}, \mathbf{u}), \quad \mathbf{u}|_{t=0} = \mathbf{u}_0 \quad (3)$$

where $\mathbf{b} \in R_n$ denotes the vector of design variables, $\mathbf{u} \in R^m$ is the vector of response variables, and $\dot{\mathbf{u}} \in R^m$ are their time derivatives. The dependency of \mathbf{u} on time t and \mathbf{b} is given by the response equation (3). The scalar functions g_0 and g_i are termed the objective and constraint functions, respectively. The objective function is related to the quality of the design \mathbf{b} , while the constraints (2) reflect mechanical, technological and other limitations. The symbol n denotes the number of design variables, m is the number of response variables and j is the number of constraints.

In order to solve P, different methods have to be applied, depending mainly on the properties of the involved functions and the type of design variables. If the functions g_0 and g_i are at least once differentiable with respect to \mathbf{b} and if the components of \mathbf{b} are continuous variables, P can usually be most efficiently solved by employing one of the gradient-based methods of mathematical programming.

In the last decade, optimal design of diesel engines and diesel injection systems has been quite frequently addressed; as an example, a few of the recent papers are listed in the references [7]. However, in recent years the production and usage of alternative fuels also came into foreground. Because biodiesel may potentially be used on existing diesel engines, it might be quite interesting to see how the usage of biodiesel influences the optimal design of the injection system. The present paper addresses this topic by optimizing the injection system for diesel and biodiesel usage separately. The purpose of this optimization is to see what the needed design differences are, if diesel is replaced by biodiesel. Furthermore, it would be interesting to see if by the optimized injection and fuel spray characteristics the harmful emissions of biodiesel can be expected to be within the range of those of mineral diesel (or even lower).

The outline of the paper is as follows. At first, the tested fuels and the injection system are described. This is followed by a description and experimental verification of the mathematical model for numerical simulation of fuel injection and spray characteristics. In the next

sections, the optimal design problem is formulated and the solution procedure is described briefly. Numerical implementation and results are presented in the last section.

Tested fuels and injection system

The tested fuels are neat diesel fuel D2, conforming to European standard EN 590 and neat biodiesel fuel B100, conforming to European standard EN 14214. Biodiesel, produced from rapeseed by Biogoriva in Slovenia, has kinematic viscosity @ 30 °C about 5.51 mm²/s, surface tension @ 30 °C about 0.028 N/m, calorific value about 38.177 kJ/kg and cetane number more than 51. The tested biodiesel has water content less than 208 mg/kg [21].

The tested injection system is a mechanically controlled fuel injection M system, Figure 1. Fuel injection pump type is Bosch PES 6A 95D 410 LS 2524, the diameter and lift of pump plunger are 9.5 mm and 8 mm, respectively, the length and diameter of high pressure tube are 1024 mm and 1.8 mm, respectively. The one hole nozzle has a hole diameter of 0.68 mm and the maximal needle lift is 0.3 mm. The needle opening pressure is 175 bar and the pump injection timing is 17 °CA BTC.

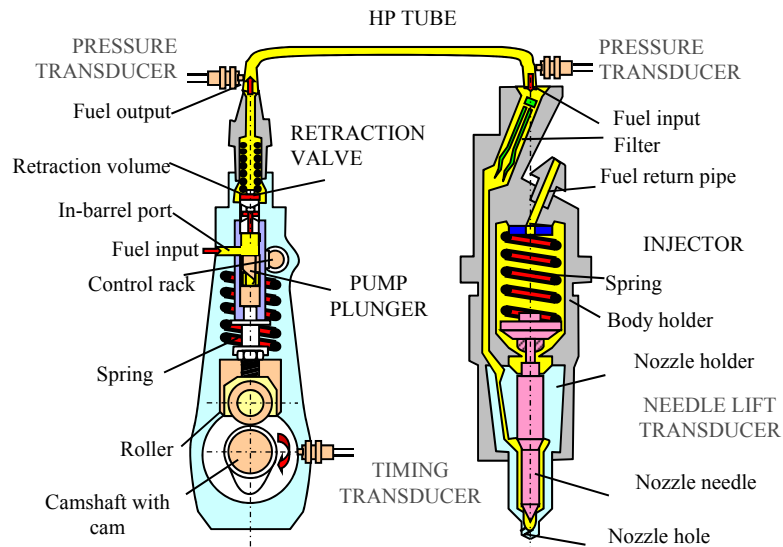


Fig. 1 Schematic diagram of inline fuel injection system

The computations of injection and engine characteristics were performed at the 13 characteristic mode steady-state regimes of the ESC test. The ESC test cycle (also known as OICA/ACEA cycle) for emission certification of diesel engines has been introduced together with the ETC (European Transient Cycle) and ELR (European Load Response) tests in Europe (Directive 1999/96/EC of December 13, 1999). The importance of an individual mode is determined by the corresponding weighting factor [7]. According to the ESC test, the pump speeds to be tested in this paper are: 680 rpm, 850 rpm, 1000 rpm, and at the idle 275 rpm.

To find the optimal design of the system for tested fuels D2 and B100, at first the mathematical model for numerical simulation has to be verified experimentally for both fuels.

Mathematical model for numerical simulation of fuel injection and spray characteristics

The fuel injection characteristics are investigated using our own mathematical model BKIN for numerical simulation of processes [1,7]. In BKIN the fuel transport is modeled as a 1D flow. The whole injection process is described by fifteen quantities: the fuelling; the pressures in the barrel chamber, delivery valve chamber, snubber valve chamber, and in the injector chamber; the lifts and velocities of the delivery valve, snubber valve, and of the needle; the vapor volumes in the delivery valve chamber, snubber valve chamber, HP tube, and injector chamber. These quantities are related to each other and to time by fifteen ordinary differential equations, containing an unknown parameter - the residual pressure. Since this quantity is not known in advance, iterations are needed to solve this system of differential equations. Because two different fuels are considered, the corresponding fuel properties have to be determined properly [7].

The different properties of D2 and B100 lead to different injection characteristics and consequently to different fuel spray. The spray penetration length is calculated by the Lustgarten equation [7]. Figure 2 shows the spray comparison for D2 and B100 at mode 3 of the ESC test. One can see that the biodiesel penetration length is somewhat larger than that of D2. Numerical simulation gives similar results. At mode 3, the numerically obtained spray tip penetration is 176.5 mm for D2 and 186.3 mm for B100 - the average fuel spray penetration of three experiments is 174.2 mm for D2 and 186.1 mm for B100. The experimental and numerical values are compared at the same time moment: 2 ms after fuel spray development.

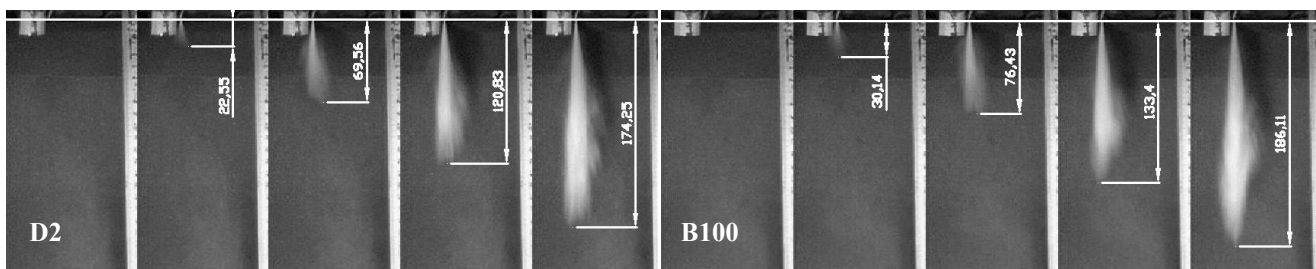


Fig. 2 Fuel spray development of D2 and B100 at mode 3 of ESC test (50 % load and 850 rpm)

Compared to D2, the sprays of B100 were narrower and longer at most tested operating regimes. Some of the most important reasons for that are worse atomization and higher injection pressure of B100. Worse atomization is a consequence of higher surface tension and viscosity of B100, which leads to higher mean droplet size (SMD). Higher injection pressure causes a higher injection rate, which obviously results in higher spray velocity and penetration. Higher injection pressure also annihilates the effect of increased friction between fuel and nozzle surface due to higher viscosity of B100.

Commonly, the Sauter mean diameter d_{32} is taken to be a very important index of atomization. One of the many empirical formulas for the determination of d_{32} (μm) is the very well known Hiroyasu & Kadota formula [7]

$$d_{32} = 2.39 \cdot 10^3 \cdot (p_{inj} - p_{am})^{-0.135} \cdot \rho_a^{0.121} \cdot q^{0.131} \quad (4)$$

where: ρ_a (kg/m^3) is air density, q (m^3/stroke) is fuelling, p_{inj} (Pa), p_{am} (Pa) are injection and ambient pressures.

Generally, one can conclude that numerical simulation agrees quite well with the experiment [7]. Based on this observation, one may assume that the influence of different fuels on the injection and fuel spray characteristics (at various operating regimes) can be determined with reasonable accuracy using this mathematical model only.

Formulation of the optimal design problem

Let the objective be to determine such values of the design variables that the injection characteristics will be optimal in some sense. Let us further assume that the quality of injection is closely related to the average SMD – the SMD averaged over the time of injection.

According to the above arrangement, the objective can be expressed as

$$\min \{d_{32}^{z_1}, d_{32}^{z_2}, \dots, d_{32}^{z_N}\} \quad (5)$$

where: d_{32}^z is the average SMD corresponding to the z -th operating regime and N is the total number of operating regimes under consideration. In other words, the objective is to minimize the average SMD at all N operating regimes.

The design variables $b_i, i = 1, \dots, n$ are related to geometrical and control parameters. The cam profile is related to the cam profile, HP tube and nozzle. The cam profile is defined as a rational Bézier curve $\mathbf{r} = \sum_{i=1}^k B_i^k \psi_i \mathbf{q}_i / \sum_{i=1}^k B_i^k \psi_i$, where B_i^k is the Bernstein blending polynomial of the order $(k-1)$, $\mathbf{q}_i = \mathbf{q}_i(\mathbf{b})$ is the position vector of a control point, $\psi_i = \psi_i(\mathbf{b})$ is a positive weighting factor and k is the number of all control points [7]. The first control point is determined by the angle of zero pump plunger lift $\varphi_0 = \varphi_0(\mathbf{b})$ meanwhile the components of the intermediate control points can be defined in terms of the parameters $c_{ix}(\text{mm}), i = 2, \dots, 5$ and $c_{iy}(\text{mm}), i = 3, 4$ [21,22]. The last two parameters are the high pressure tube length L and the nozzle hole diameter d_m .

The control parameters are related to the pump plunger pre lift h_p and to the geometrical duration of fuel delivery t_d . The pump plunger pre lift influences the injection timing meanwhile the geometrical duration of delivery influences the injection duration, which affects also the fuelling. It should be noted that these two parameters are related to an individual operating regime. Thus, for N operating regimes $2 \cdot N$ of such parameters enter the set of design variables.

In technical applications the design variables can typically not be varied completely unconstrained. In our case, for technological reasons the minimal positive value $\xi^+ = \min(e^+)$ and the maximal negative value $\xi^- = \min(e^-)$ of the local radius of the cam profile should be constrained properly. In the above expressions $e^+ = \{e | e < 0\}$ and $e^- = \{e | e < 0\}$. The local radius e of the cam profile curve can be expressed by $e = \frac{[(h+r_0+r_{rot})^2+v^2]^{1.5}}{(h+r_0+r_{rot})^2+2v^2-(h+r_0+r_{rot})a} - r_{rot}$, where r_0 is the cam basic radius, r_{rot} is the tappet roller radius, h is the pump plunger lift, $v = dh/d\varphi$ is the relative pump plunger velocity, $a = d^2h/d\varphi^2$ is the relative pump plunger acceleration and φ is the camshaft angle. The term "relative" is used to emphasize that the pump plunger lift h is differentiated with respect to the camshaft angle so that v and a are measured in (m/rad) and (m/rad²), respectively.

To avoid torsion torque overloading and loosing contact between the cam and the follower, the minimal, $\zeta = \min_{0 \leq t \leq T}(a)$, and maximal, $\lambda = \max_{0 \leq t \leq T}(a)$, pump plunger acceleration has to be limited also.

Additionally, proper constraints also have to be imposed on the injection timing θ and injection duration ϑ (both quantities are measured in degree of camshaft), on the fuelling q ($\text{mm}^3/\text{stroke}$), and on the maximal injection pressure p_{max} .

Finally, to prevent a technologically unacceptable design, constraints on lower and upper limits of the design variables have to be imposed as well.

All of the above constraints can be written in a normalized form as

$$\begin{aligned} 1 - \frac{\xi^+}{\xi^+L} \leq 0, \quad -\frac{\xi^-}{\xi^-U} + 1 \leq 0, \quad \frac{\lambda}{\lambda U} - 1 \leq 0, \quad \frac{\zeta}{\zeta L} - 1 \leq 0 \\ 1 - \frac{\theta_z}{\theta_z^L} \leq 0, \quad \frac{\theta_z}{\theta_z^U} - 1 \leq 0, \quad 1 - \frac{q_z}{q_z^L} \leq 0, \quad z = 1, \dots, N \\ \frac{q_z}{q_z^U} - 1 \leq 0, \quad 1 - \frac{\vartheta_z}{\vartheta_z^L} \leq 0, \quad \frac{\vartheta_z}{\vartheta_z^U} - 1 \leq 0, \quad z = 1, \dots, N \\ \frac{p_{z,max}}{p_{z,max}^U} - 1 \leq 0, \quad z = 1, \dots, N \\ b_i^L \leq b_i \leq b_i^U, \quad z = 1, \dots, N \end{aligned} \quad (6)$$

where the right superscripts L and U denote the prescribed lower and upper limits.

The objective function (5), the selection of the design variables, the constraints (6), and an appropriate response model (BKIN) define completely the design problem. Unfortunately, this problem does not have the standard form (1)-(3) since it is a multiobjective one. In order to solve it efficiently, we have to transform it into the standard form, i.e., into a form with one objective function.

This transformation can be done in several different ways that typically yield different results; usually, these are the points belonging to the Pareto front. In any case, we have to replace the requirement to minimize N independent functions by minimization of a substitute scalar function. This can be done in a satisfactory manner only if the relative importance (weighting) factors of original objective functions are known. In general, these factors can not be determined easily; in fact, observation of the optimization progress and good intuition are needed to get a satisfactory result. Luckily, in our case the original objectives are related to individual operating regimes, which in turn are already weighted adequately by the ESC test weighting factors χ^z . Therefore, in this work we decided to take the ESC weights to be the factors of the original objective functions. Thus, by multiplying each d_{32}^z by the corresponding χ^z and summing up, one gets a substitute scalar objective function of the form

$$g_0 = \sum_{z=1}^N \chi^z d_{32}^z \quad (7)$$

It is expected that minimization of the above sum will yield a Pareto point, being satisfactory from the engineering point of view.

Optimization procedure

The optimization problem was solved by employing the convex approximation method of mathematical programming [7]. This method belongs to the family of gradient-based methods. Similarly as other methods, it also solves a sequence of approximate subproblems P_i , $i = 0, 1, 2, \dots$. However, to obtain P_i , the method employs a non-linear convex approximation technique with automatically adjustable conservativeness. The automatic adjustment is based on function gradient data, collected during previous optimization cycles.

In each optimization cycle (iteration) this method requires only one evaluation of all involved functions and their design gradients. In this work, the functions have been evaluated by employing the described mathematical model, while the design derivatives have been obtained numerically by using finite differences.

Numerical implementation and results

The considered engine operating regimes are the ones given in the ESC test so that one has $N = 13$. The following geometrical and control parameters are selected to be the design variables [7]: (i) the parameters $\varphi_0, c_{2x}, c_{3x}, c_{3y}, c_{4x}, c_{4y}, c_{5x}$ related to the cam profile, (ii) the weighting factors $\psi_2, \psi_3, \psi_4, \psi_5$ related to the rational Bezier curve representing the cam profile, (iii) the HP tube length L , (iv) the nozzle hole diameter d_m , (v) the control parameters (h_p^z, t_p^z) , $z = 1 \dots N$, related to individual engine operating regimes. Since $N = 13$, we have a total of $n = 39$ design variables. The initial values of the design variables, their lower and upper limits are as follows: $\varphi_0 (^{\circ}\text{CAM}) = (35; 20; 50)$, $c_{2x} = c_{3x} = c_{3y} = c_{4x} = c_{4y} = (0.25; 0.001; 0.5)$, $\psi_2 = \psi_3 = \psi_4 = \psi_5 = (1.0; 0.1; 2.0)$, $d_m (\text{mm}) = (0.68; 0.5; 0.9)$, $L (\text{mm}) = (1000; 500; 1500)$, $h_p^z (\text{mm}) = (1.87; 1.0; 5.0)$ and $t_p^z (\text{mm}) = (0.5, 1.5, 0.5, 1, 0.5, 1, 0.5, 1.5, 0.5, 1.5, 0.5, 1, 0.5; 0.1; 3.0)$, $z = 1, \dots, N$. The following lower and upper limits of the constrained quantities have also been taken to be the same at all operating regimes: $\xi^{+L} = 2\text{mm}$, $\xi^{-U} = -60\text{mm}$, $\zeta^L = -100\text{mm}$, $\zeta^U = 100\text{mm}$. The limits of the maximal injection pressure $p_{z,max}$, fuelling q_z , injection timing θ_z , and injection duration ϑ_z differ for individual operating regimes as described in [7].

Two optimization cases were considered; neat diesel was used in the first case and neat biodiesel in the second case. Both cases have been solved successfully within 8 iterations. The average SMD values $d_{32}^z (\mu\text{m})$ for $z = 1, \dots, N$ at initial and optimal design for diesel and for biodiesel are presented in Figure 3. It can be seen that the improvement at higher pump speeds and higher loads is not significant. However, it must be pointed out, that at these regimes the constraints were not fulfilled at the initial design whereas at optimal design all of the imposed constraints are fulfilled. The weighted sums $\sum_{z=1}^N \chi^z d_{32}^{*z}$ are $29.55 \mu\text{m}$ and $28.59 \mu\text{m}$ at initial and optimal design for diesel and $29.76 \mu\text{m}$ and $29.11 \mu\text{m}$ at initial and optimal design for biodiesel.

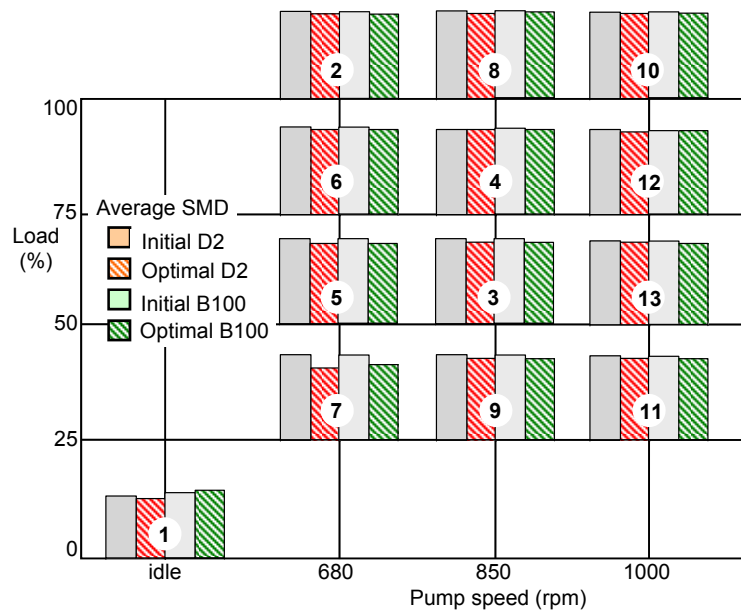


Fig. 3 Average SMD at initial and optimal designs for D2 and B100

As can be seen from Figure 6 the optimized designs offer atomization improvements practically at all engine operating regimes without increasing the maximal injection pressure beyond the prescribed limits. This result might offer a possibility to improve NO_x -PM trade-off.

Conclusions

The paper discusses the optimal design of fuel injection M system of a bus engine MAN D 2566 when D2 and B100 fuels are used. The tested biodiesel (B100) was produced from rapeseed oil. On the basis of the presented results, the following conclusions can be made: (i) Optimization may lead to significant improvements of the injection process regardless of the fuel used. One must note, however, that the optimal design depends significantly on the fuel type. This is true for both, geometrical and control, design variables. (ii) Owing to quite different optimal designs, it seems that a diesel engine, equipped with the injection system under consideration, can not run very efficiently with both tested fuels. It has to be adjusted either to D2 or B100. (iii) From the numerical results it also follows that with both fuels satisfactory performance regarding harmful emissions may be obtained. The calculated numbers (fuelling during needle lifting and needle closing) might even indicate that in that view B100 might perform slightly better than D2.

References

- [1] B. Kegl: Numerical analysis of injection characteristics using biodiesel fuel. *Fuel*, Volume 85 (2006), pp. 2377–2387.
- [2] J.P. Szybist, A.L. Boehman, J.D. Taylor, R.L. McCormick: Evaluation of formulation strategies to eliminate the biodiesel NO_x effect. *Fuel Processing Technology*, Volume 86 (2005), pp.1109–1126.



-
- [3] N. Nabi, S. Akhter, M.Z. Shahadat: Improvement of engine emissions with conventional diesel fuel and diesel – biodiesel blends. *Bioresource Technology*, Volume 97 (2006), pp.372–378.
 - [4] M. Canakci: Combustion characteristics of a turbocharged DI compression ignition engine fueled with petroleum diesel fuels and biodiesel. *Bioresource Technology*, Volume 98 (2007), pp. 1167–1175.
 - [5] B. Kegl: Experimental investigation of optimal timing of the diesel engine injection pump by using biodiesel fuel. *Energy & Fuels*, Volume 20 (2006), pp. 1460–1470.
 - [6] B. Kegl: A procedure for upgrading an electronic control Diesel fuel injection system by considering several engine operating regimes simultaneously. *Journal of mechanical design*, Volume 121 (1999), pp. 159–165.
 - [7] B. Kegl, M. Kegl, S. Pehan: Optimization of a fuel injection system for diesel and biodiesel usage, *Energy & Fuels*, Volume 22 (2008), pp. 1046–1054.



International Conference on Innovative Technologies, IN-TECH 2012,
Rijeka, 26. - 28.09.2012



OPTIMAL DESIGN OF A GASOLINE ENGINE

S. Pehan¹, M. Kegl¹, B. Kegl¹

¹ University of Maribor, Faculty of Mechanical Engineering, Smetanova 17, SI-2000 Maribor, Slovenia

Keywords: internal combustion engine, intake and exhaust systems, optimal design

Abstract. The paper presents a simple and effective approach to improve engine performance of a racing car with special requirements. Attention is focused on optimal design of the intake system, using a gradient-based approximation method of mathematical programming. Since optimization relies on accurate numerical analysis of engine processes, the sub-models and parameters needed in the analysis software are carefully determined by experiment. Subsequently, the influence of various design parameters of intake and exhaust systems on engine performance is investigated numerically. The most influencing parameters are utilized as design variables in the optimization process. In order to improve engine power at several engine speeds, two different forms of the optimal design problem are proposed, solved, and compared in order to identify the most appropriate one. The optimization procedure is implemented by employing the optimization software as a master (driver) program while the analysis software acts as the slave program. The results obtained confirm the usefulness of the presented approach.

Introduction

The optimal design procedure of a mechanical system is usually based on an iterative improvement of the system. It can usually be regarded as a solution process of a standard non-linear problem P of mathematical programming [1]. When considering mechanical systems, P may be often written in the following form

$$\min g_0(\mathbf{b}, \mathbf{u}) \quad (1)$$

subject to constraints

$$g_i(\mathbf{b}, \mathbf{u}) \leq 0, \quad i = 1, \dots, j \quad (2)$$

where \mathbf{b} denotes the vector of design variables – the set of all parameters that can be varied independently in order to search for the best possible design of the system – and \mathbf{u} denotes the response variables of the system. The response \mathbf{u} typically depends on time t and \mathbf{b} ; this dependency is given by the response equation. The scalar functions g_0 and g_i are termed the objective and constraint functions, respectively. The objective function is related to the quality of the design \mathbf{b} , while the constraints reflect mechanical, technological, and other limitations.

To solve P different methods have to be applied, depending mainly on the properties and complexity of the involved functions and on the type of design variables. A gradient-based method starts from some initial design and then proceeds in an iterative fashion. In each iteration, the response and sensitivity analysis has to be done in the first step, while the optimization algorithm has to be called in the second step. This procedure might become somewhat tedious to implement, when considering real-word engineering optimization problems. In the easiest case, the source code of the analysis software is available, making it relatively straightforward to utilize a suitable optimizer [2-5]. The situation becomes more complicated, if commercial black-box software is used to analyze the system. This paper describes such a situation, where black-box analysis software, originally not intended to be used in an optimization process, was employed.

Initial engine set-up and special requirements

The tested engine is gasoline engine from the Honda 600 CBR motorcycle to power the car for the international Formula Student competition with special requirements. The basic requirement is a water-cooled, four-stroke piston engine with a maximal displacement of 610 cm^3 . The fuel tank volume is limited, but the car must run the whole endurance test without refill. Consequently, the brake specific fuel consumption (BSFC) has to be as small as possible. Furthermore, the car is equipped with a muffler in the exhaust system to reduce the noise to an acceptable level (less than 110dBA), measured at the distance of 0.5 m from the end of the exhaust outlet. The engine with intake and exhaust systems must be placed inside the car frame. Furthermore, an important restriction is related to the power capability of the engine. For this reason, a single circular restrictor is required at the intake system between the throttle and the engine. All engine air flow must pass through this restrictor of a diameter of no more than 20 mm.

Keeping this in mind, a modification of the intake and exhaust systems should be the most effective approach to get optimal engine performance. Consequently, the carburetor system was replaced with a multipoint injection system with a programmable open electronic control unit. Subsequently, the input and exhaust systems were redesigned completely, as shown in Figure 1. Using a CFD simulation software [8], this was done so that the distribution of fresh air among the engine's cylinders was uniform and with minimal pressure losses along the pipes. All of the geometrical restrictions, related to the car frame, have been taken into account as well [8].

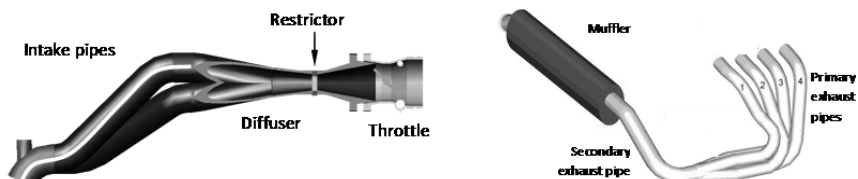


Fig. 1 Initial design of intake and exhaust systems

The intake and exhaust systems were manufactured and tested on the laboratory engine test bed. Due to acceptable performance, this design was considered to be a good initial design for optimization.

Accurate and efficient numerical analysis is the key factor for successful optimization. For the steady state performance prediction of gasoline engines, there are several commercial packages that are widely accepted, rigorously tested, and verified in practical applications. This software typically employs a mathematical model based on the first law of thermodynamics, which can be for an internal combustion piston engine written as

$$\frac{d(m_c u)}{d\alpha} = -p_c \cdot \frac{dV}{d\alpha} + \frac{dQ_f}{d\alpha} - \sum \frac{dQ_w}{d\alpha} - h_{BB} \cdot \frac{dm_{BB}}{d\alpha} \quad (3)$$

Basically, for the high pressure cycle this law states that the change of the internal energy in the cylinder ($\frac{d(m_c u)}{d\alpha}$) is equal to the sum of piston work ($-p_c \cdot \frac{dV}{d\alpha}$), the conversion of chemical energy to the thermal energy ($\frac{dQ_f}{d\alpha}$), heat transfer ($-\sum \frac{dQ_w}{d\alpha}$), and the enthalpy flow due to blow-by ($-h_{BB} \cdot \frac{dm_{BB}}{d\alpha}$). The conversion of chemical energy to the thermal energy represents the heat release. In equation (3) the symbol α denotes the angle of the crankshaft rotation, m_c is the mass of the mixture in the cylinder, u is the specific inner energy, p_c is the pressure inside the cylinder, V is the cylinder volume, Q_f is the fuel energy, Q_w the heat loss on the liner, h_{BB} and m_{BB} is the enthalpy and mass of the mixture that escapes through the gap between the piston and the liner, respectively.

Good agreement between experimentally and numerically obtained results indicates adequate selection of the sub-models, coefficients, and parameters in the simulation software AVL-BOOST. Since the computation time was also acceptable, this simulation model was considered to be a good foundation for the optimization process.

The success of an optimization procedure may depend significantly on the choice of parameters that will be employed as design variables. The best way is to choose only the most significant ones since this reduces potential numerical difficulties. For that purpose, a parametric study was done, using numerical simulation. The aim was to see how the individual parameters influence engine power, engine noise, specific fuel consumption and emissions of NO_x . Those quantities are either limited by the rules of the Formula Student competition, or they can positively influence the scoring, related to ecology.

The investigated parameters of the intake system were related to the joints of the intake system, the length of secondary intake pipes as well as to the diameter and length of the primary intake pipes, Figure 2. The investigated parameters, related to the exhaust system, were the diameter of the primary exhaust pipes as well as the diameter and length of the secondary exhaust pipe, Figure 2.

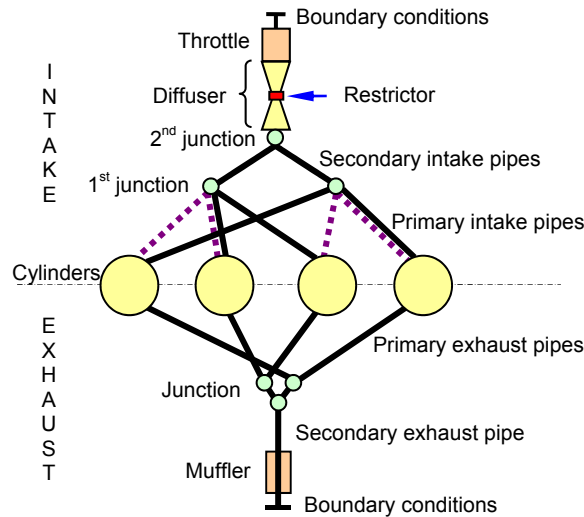


Fig. 2 Initial design of intake and exhaust systems

According to the results of parametric study [8], it seems that the most promising parameters are the diameter and length of the primary intake pipes. Only these two parameters have a decisive influence on all investigated engine performances. One can expect that by optimizing only these two parameters, the initial design of the intake system can be improved significantly. All other intake and exhaust parameters have a rather minor influence. Therefore, they were eliminated from the set of design variables.

Optimal design problem

The purpose of optimization is to maximize the effective engine power P_e at several engine speeds, which are of interest for the competition. This means that one has to deal with a multiobjective optimal design problem. This problem is here converted into its scalar substitute, whose solution will yield a single Pareto optimal point. Two types (cases A and B) of this conversion are considered: the simplest one (case A) where the engine powers are simply multiplied by appropriate weights and summed up to give a scalar objective function, and another one (case B) which is based on the introduction of an artificial design variable.

According to the above discussion, the original vector objective function (to be minimized) is defined as

$$\mathbf{g} = [-P_{e,1}, -P_{e,2}, -P_{e,3}, \dots, -P_{e,N}]^T \quad (4)$$

where: $P_{e,z}$ is the effective power corresponding to the z -th engine speed and N is the total number of engine speeds under consideration. The considered engine operating regimes are selected on the experience from previous competitions and with respect to the acceleration event, skid-pad event, autocross event, and endurance event. For these reasons, in this optimization procedure only the engine full load conditions at nine ($N = 9$) engine speeds $\mathbf{n} = \{7500, 8000, 8500, 9000, 9500, 10000, 10500, 11000, 11500\}^T$ are considered.

According to the parametric study, two design variables are introduced as follows: $b_1 = L_i$, $b_2 = d_i$, where L_i is the length and d_i the diameter of primary intake pipes, Figure 2. The initial values of these design variables as well as their lower and upper limits are as follows: $L_i(\text{mm}) = (340; 300; 400)$ and $d_i(\text{mm}) = (37; 20; 60)$. The initial values correspond to the manufactured initial intake system.

While maximizing the engine power, some constraints related to the specific fuel consumption $g_{e,z} \leq g_{e,max}$, $z = 1, \dots, N$ and to the engine noise $\xi_z \leq \xi_{max}$, $u = 1, \dots, N$ at several engine speeds, have to be taken into account. These two types of constraints are related to

the competition rules. The permissible maximal effective specific fuel consumption is $g_{e,max} = 350$ g/kWh and the permissible maximal value of engine noise is $\xi_{max} = 110$ dBA.

Finally, the minimal intake runner length (together with plenum) L_{min} has to be prescribed because of the intake system installation into the car. From the geometrical requirements, the formula for L_{min} was derived as a function of d_i [8].

Thus, the whole optimization problem can be written as

$$\begin{aligned} & \min g \\ & L_{min} - L_i \leq 0 \\ & g_{e,z} - g_{e,max} \leq 0, \quad z = 1, \dots, N \\ & \xi_z - \xi_{max} \leq 0, \quad z = 1, \dots, N \\ & b_i^l \leq b_i \leq b_i^u, \quad i = 1, 2 \end{aligned} \quad (4)$$

In order to convert this multiobjective optimization problem into a suitable scalar substitute, two approaches are used as already indicated above.

By the first approach (case A) the new scalar objective function is obtained as a weighted sum

$$g_0 = -\sum_{z=1}^N \psi_z P_{e,z} \quad (5)$$

where: the symbols $\psi_z, z = 1, \dots, N$ denote the weighting factors $\psi_1 = \psi_9 = 0.04, \psi_2 = \psi_8 = 0.06$ and $\psi_3 = \psi_4 = \psi_5 = \psi_6 = \psi_7 = 0.16$. These chosen values indicate approximately the relative importance of individual engine regimes. Note that by choosing only one set of these weights, only one Pareto optimal point will be obtained. A systematic search through the Pareto set is beyond the scope of this paper.

By the second approach (case B), an artificial design variable b_3 is introduced and a new scalar objective function is defined as

$$g_0 = -b_3 \quad (6)$$

This objective function is related to engine power by the introduction of new constraints

$$b_3 - \frac{P_{e,z}}{\zeta_z} \leq 0, \quad z = 1, \dots, N \quad (7)$$

which are added to the original constraints (4). The symbols $\zeta_z, z = 1, \dots, N$ denote suitable normalization factors, where $\zeta_1 = \zeta_9 = 40, \zeta_2 = \zeta_8 = 41$ and $\zeta_3 = \zeta_4 = \zeta_5 = \zeta_6 = \zeta_7 = 42$. Note that by minimizing the new objective function, the engine effective power will be maximized simultaneously at all engine speeds. This is in contrast to case A, where theoretically only the power at one engine speed might be increased. As in case A, case B will also yield only one Pareto optimal point.

Optimization procedure

A gradient-based optimizer requires the response and sensitivity analysis to be done in each iteration. Theoretically, the sensitivity analysis can be done in several ways, but in the case of using a commercial black-box and response-analysis-only program one actually does not have much options left. In fact, one has to do the sensitivity analysis using numerical finite (preferably central) differences. At this point it might be worth to note that the sensitivity analysis by using finite differences can be implemented completely in the optimization program – a general program that is always the same, irrespective of the analysis program, actually employed.

By employing a gradient-based optimizer, the solution procedure layout is well known and can be graphically represented as shown in Figure 3.

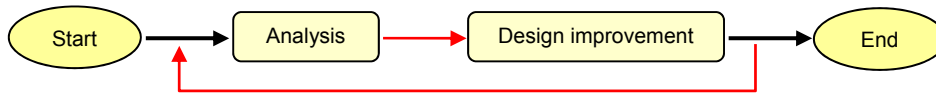


Fig. 3 Iterative solution procedure of problem P

In our case the analysis part (the calculation of functions) has to be done by a black-box program, while the design improvement part will be done by the optimization algorithm based on adaptive convex approximation [6,7]. Of course, in order to run the whole procedure, one additionally needs some driving program that will execute the corresponding processes as needed [7,8], Figure 4.

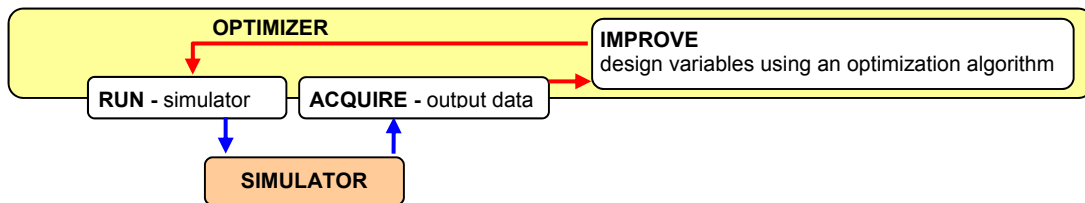


Fig. 4 The optimizer drives the whole procedure and improves the design

In order to fit into the iterative optimization process, the simulator must accept two input files and output an adequate response file, Figure 5. The first input file is termed here the mechanical system data (MSD) file, which is the actual input file of the black-box program. The second input file is the current design variables (CDV) file, which contains current design variable values. This file is written by the optimizer in each iteration, just before the simulator is run.

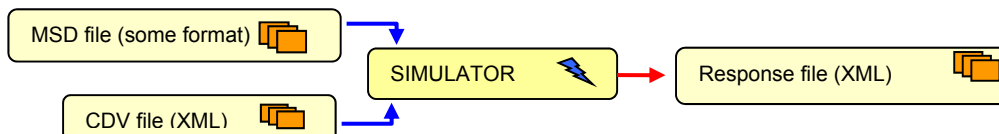


Fig. 5 The expected functionality of the simulator

A commercial black-box program obviously does not exhibit the functionality shown in Figure 5. Thus, in order to circumvent this problem, an attractive solution is to code two (usually rather simple) ad-hoc wrapper programs and to define the simulator as a combination of three stand-alone programs: the input wrapper, the black-box program and the output wrapper, Figure 6.

Although the use of wrapper programs might appear to be somewhat tedious to implement, one should emphasize that the wrappers are usually really simple programs and can be coded very quickly. Especially, if the same black-box program is employed several times, virtually the same wrappers may be employed, containing perhaps only minor changes of the code.

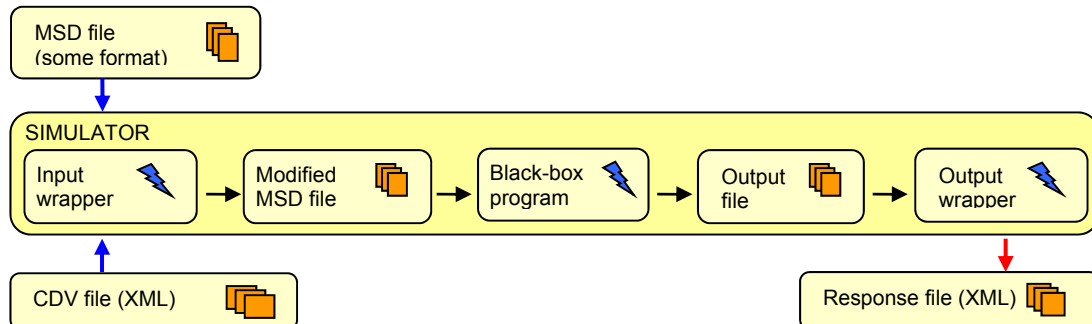


Fig. 6 Getting the expected simulator functionality by employing wrapper programs

Results

The optimization process was run as described in the previous section. The sensitivity analysis was performed using the central differences. Both cases were solved without problems and the number of iterations was 10 in case A and 17 in case B. The optimal values of design variables in case A are $L_i = 310.2$ mm and $d_i = 40.6$ mm, in case B the optimal values are $L_i = 343.8$ mm and $d_i = 49.7$ mm.

Figure 7 shows the differences between the mean effective power P_e , noise ζ and specific fuel consumption g_e at initial and optimal designs A and B. It can be seen that optimization actually increased the effective power. In both cases, all constraints were fulfilled, but the power is higher in case B almost in the whole speed range.

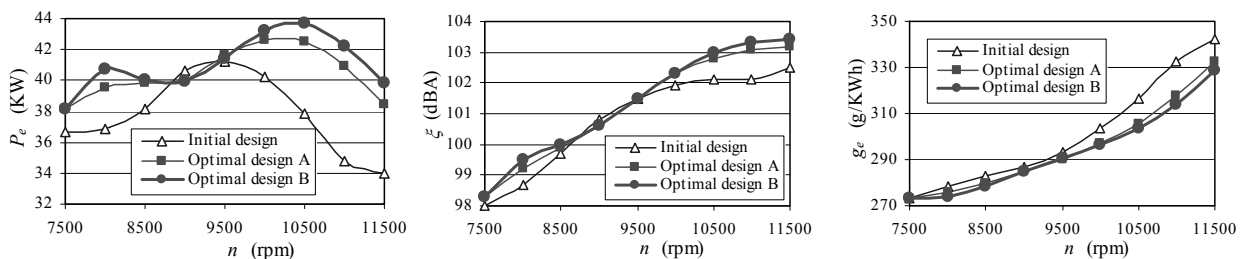


Fig. 7 The effective brake power P_e , noise ζ and specific fuel consumption g_e of the initial and optimal designs A and B of intake system

Around 9000 rpm, the effective engine powers of all three designs are almost the same. However, at lower speeds and especially at speeds above 9500 rpm, the optimized designs give significantly better results. The maximal engine power of 43.7 KW is obtained with optimal design B at 10 500 rpm. This is about 15% higher than the power obtained with the initial design. Evidently, both optimal designs give higher noise values almost at all speeds. However, the noise level is still lower than the allowed limit value. In contrast to the noise, both optimal designs exhibit lower g_e at most engine speeds.

Conclusions

Gradient-based optimization algorithms may be somewhat tedious to implement because of the need to compute the design derivatives of the involved functions. And the situation becomes even trickier, if one employs a commercial black-box program in order to analyze the considered mechanical system. It seems that the proposed solution of using two stand-alone programs – the optimizer and the simulator – works quite well. The optimizer can be coded as a completely independent general-purpose program by agreeing on suitable data exchange protocols.

A careful selection of design variables is very advisable and a study of influencing parameters is always recommended. In this paper, the parameters related to the joints and intake/exhaust pipes were investigated. Due to their influence on engine power, specific fuel consumption as well as noise and NO_x emission, the diameter and length of primary intake pipes have been selected to enter the optimal design procedure.

Since engine power at several speeds had to be optimized, the original optimal design problem was a multiobjective one. In order to transform it into a standard form two approaches were employed. Both gave good results, although the results of case B are slightly better. The effective engine power has been increased practically at the whole operating regime, while the specific fuel consumption and NO_x emission have even been slightly reduced.

References

- [1] G.N. Vanderplaats: *Numerical Optimization Techniques for Engineering Design: With Applications*, McGraw Hill, New York, 1984.
- [2] D. Song, M. El-Sayed: Multi-objective optimization for automotive performance, *International journal of vehicle design*, Volume 30 (2002), pp. 291–308.
- [3] B. Kegl: Optimal design of conventional in line fuel injection equipment, *Proceedings of the Institution of Mechanical Engineers, Part D: Journal of Automobile Engineering*, Volume 209 (1995), pp. 135–141.
- [4] B. Kegl: A procedure for upgrading an electronic control diesel fuel injection system by considering several engine operating regimes simultaneously, *ASME Journal of Mechanical Design*, Volume 121 (1999), pp. 159–165.
- [5] B. Kegl: Injection system design optimization by considering fuel spray characteristics, *ASME Journal of Mechanical Design*, Volume 126 (2004), pp. 703–710.



-
- [6] M. Kegl, M.M. Oblak: Optimization of mechanical systems: on non linear first order approximation with an additive convex term, *Communications in Numerical Methods in Engineering*, Volume 13 (1997), pp. 13–20.
 - [7] M. Kegl, B.J. Butinar, B. Kegl: An efficient gradient-based optimization algorithm for mechanical systems, *Communications in numerical methods in engineering*, Volume 18 (2002), pp. 363–371.
 - [8] B. Kegl, S. Pehan, M. Kegl: Improvement of engine performance using and optimization procedure, *Proceedings of the Institution of Mechanical Engineers, Part D: Journal of Automobile Engineering*, Volume 221 (2007), pp. 1001–1014.



International Conference on Innovative Technologies, IN-TECH 2012,
Rijeka, 26. - 28.09.2012



CHECKING THE STABILITY OF TiO₂ NANOPARTICLES SIZE BY RESPONSE SURFACE METHOD

O. Giuca¹

¹Politehnica University of Timisoara, 2 Piata Victoriei, Timisoara, Romania

Keywords: TiO₂ nanoparticles, response surface, factors, fast hydrothermal, industrial

Abstract. Given the importance of titanium dioxide in areas such as automotive industry, environmental protection, health, and from its properties, synthesis methods have advantages and disadvantage used. For practical applications, from all socio-economic, nonmaterial's with special properties different from macro-scale materials, we provide a broad, new problems to solve theoretical and applied technology related to design their synthesis processes because each application has some well-defined morphostructural features of nanoscale materials. This it is necessary to develop and acquire advanced knowledge by developing appropriate methods of synthesis, to facility control of their size. So you want to check the dimensional stability of nanoparticles, obtained by various methods of synthesis. These nonmaterial's are produced at industrial scale, is important for the manufacturer to obtain nanoparticles of size approximately equal or close to the target. In this sense he must know exactly what factors most influence particle size. The paper checks the size of TiO₂ nanoparticles obtained by fast hydrothermal method, by using a Box Behnken experimental plan, for which were taken into account four factors at three levels. In most RSM, the response function y is usually unknown and to build a fair approximation for y begins with a polynomial of rank 1 and is called function approximation model of order I. If there is some response curve on a surface, you should use a higher degree polynomial. Function approximation for the two variables is called second order model which appear quadratic terms (interactions between factors) and error term. In conclusion, if you want an accurate modeling of the system must take into account the interactions, but if you want only to obtain the target value for the size of nanoparticles when first-order model can be considered satisfactory.

1. Introduction

In practice, from all socio-economic areas, nano-materials with special different properties compared with macro-scale materials, gives us a broad perspective to solve new theoretical, technological and practical problems, related with designing processes of synthesis of them because each application presents a number of morfostructural proprieties well-defined of the material at nanometric scale. Thus, it requires the need for advanced development and acquisition of knowledge by developing appropriate methods of synthesis, to facilitate a strict control of their size. A special interest is granted to obtain generally nano-materials and titanium dioxide (TiO₂) which was used intensive as photocatalysts for solar energy conversion into chemical energy and in environmental applications.

2. Metods

It is important to analyze a large number of influencing but should be a careful planning experiments (in order to reduce them) to take into account the economic aspect and the time for experimentation, to obtain experimental models that approximate as good as possible real systems, which are difficult to obtain when the degree of complexity is high, there are many influencing factors.

The Response Surface Method (RSM) is a conglomerate of statistical-mathematical techniques for the construction of empirical models. By designing experiments it is desirable to optimize response (the output variable - the size of the TiO₂ nano-particles doped with Ag), which is influenced by several independent variables (variables of input doping concentration, autoclaving time, autoclaving temperature, power oven), and the change of the input variables behavior lead to identify the changes in the response variable (output). For example, it is considered the function of response y from the relationship (1) by which it is desired to find out the level input variables x_1 and x_2 for which y is maximum and where ε represents the noise or error observed in it:

$$y = f(x_1, x_2) + \varepsilon \quad (1)$$

The area represented by $f(x_1, x_2)$ is called the response surface. The answer may be graphically represent, either three-dimensional or two-dimensional (contour), for ease viewing response surface shape (Fig. 1). The contours represent constant curves response shown in the plan x_i, x_j , keeping other variables fixed. Each contour corresponds to a specific height of the response surface.

In the majority of the applications RSM, the response function y is unknown and usually to build a correct approximation of y is begins with a polynomial rank 1 degree in a small area. If the answer can be defined by a linear function of independent variables, then the approximation function is called the order I model.

If there is a certain curvature in the response surface, must use a polynomial of higher degree. Generally in RSM's issue is used one of the two models separately or a mixture thereof. In any of the situations above it is necessary that the levels of each factor levels to be independent of other factors. It is also important that the plan of experiments used for data collection is correctly chosen so as to obtain effective results in the polynomials approximation.

Plans of Box-Behnken experiments are a reasonable alternative to complete factorial plans (4 factors at 3 levels = 81 experiments) and plans for CCD experiences for those situations where it is desired a plan with 3 levels and which should be almost rotatable. Plans for CCD experiences with central dots on their faces also have the 3 levels and places the experience points at the corners of testing region.

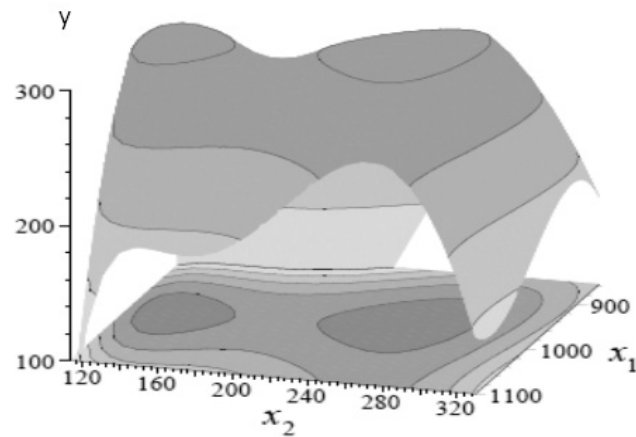


Fig. 1 Tridimensional response surface and contour bidimensional

This option is feasible if that region defines conditions process. But if it starts at a particular combination of the factors and it is desired to obtain better conditions, a more spherical arrangement of the experience points it is more efficient. The plans of the Box-Behnken experiments consist of experiments in which each pair of factors is diverse between the levels of minimum and maximum, while others experimental factors are maintained at middle -level.

3. Applying RSM design for dimensional stability

For this experience plan was chosen 4 factors at 3 levels (concentration doping (2 %, 3 %, 4 %), autoclaving time (15 min, 30 min, 45 min), autoclaving temperature (150°C, 200°C, 250°C) and oven power (800W, 1000W, 1200W)) which is being run in 3 blocks at a total of 27 experiments including 1 central point on the block. The plan is complete randomized; the number of grades of freedom for error is equal to 10. In the table 1 shows the results of the measurements factors and levels for the 27 experiments. It should be noted that for each condition of experimentation have been measured 5 nano-crystals. Target value for the nano-crystals size has been set to 5 nm with a tolerance of ± 0.2 nm.

Table 1 Levels factor and experiments results for Box-Behnken experience plane

Exp.	Bloc	Dopant concentration	Time Autoclaving	Autoclaving temperature	Power oven	Size
		%	min	grade C	W	nm
1	1	2	15	200	1000	4,9
2	1	4	15	200	1000	5,11
3	1	2	45	200	1000	5,21
-	-	-	-	-	-	-
25	3	3	15	200	800	4,82
26	3	4	30	150	1000	5,03
27	3	3	15	200	1200	5,14

Were analyzed primary estimates effects of factors, and the analysis of variance with the ANOVA method that divides the variability of nano-particles size into separate components for each effect, and figure 2 shows factors effects in decreasing order, with a vertical line it is determinate which effects are significant from a statistical point of view (standardised diagram Pareto).

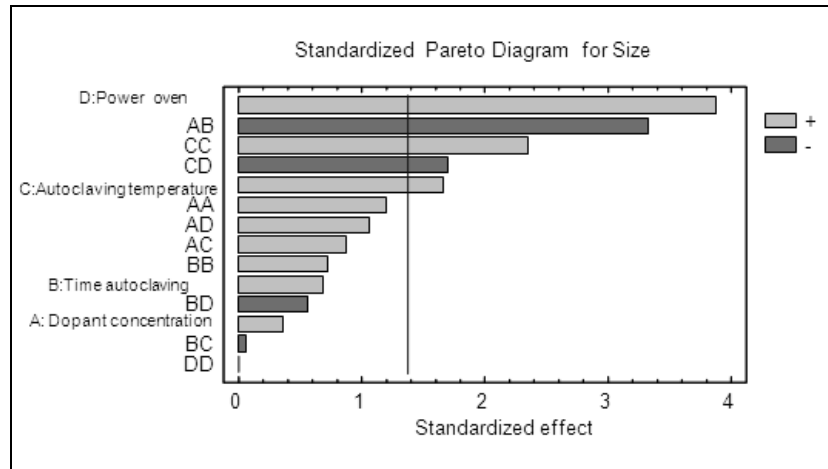


Figure 2 Standardized Pareto Diagram for factor effect

In relationship (2) is shown the regression equation, according to the order II model associated to the Box-Behnken experiments plan, and in which variable values are specified in originals units of measurement:

$$\begin{aligned}
 Size_{nanoparticles} [nm] = & 4,72958 - 0,326667 \cdot Concentration_{dopant} [\%] + \\
 & + 0,0290556 \cdot Time_{autoclaving} [min] - 0,00748333 \cdot Temperature_{autoclaving} [^{\circ}C] + \\
 & + 0,00138333 \cdot Power_{oven} [W] + 0,04125 (Concentration_{dopant} [\%])^2 - \\
 & - 0,00883333 \cdot Concentration_{dopant} [\%] \cdot Time_{autoclaving} [min] + \\
 & + 0,0007 \cdot Concentration_{dopant} [\%] \cdot Temperature_{autoclaving} [^{\circ}C] + \\
 & + 0,0002125 \cdot Concentration_{dopant} [\%] \cdot Power_{oven} [W] + \\
 & + 0,000111111 \cdot (Time_{autoclaving} [min])^2 - \\
 & - 0,00000333333 \cdot Time_{autoclaving} [min] \cdot Temperature_{autoclaving} [^{\circ}C] - \\
 & - 0,0000075 \cdot Time_{autoclaving} [min] \cdot Power_{oven} [W] + \\
 & + 0,00003235 \cdot (Temperature_{autoclaving} [^{\circ}C])^2 - \\
 & - 0,00000675 \cdot Temperature_{autoclaving} [^{\circ}C] \cdot Power_{oven} [W] + \\
 & + 0,0 \cdot (Power_{oven} [W])^2
 \end{aligned}
 \tag{2}$$

Table 2 provide information on the nano-particles size generated on the basis of order II model associated to plan of experiments Box-Behnken namely measured values, the values predicted for them on the basis of the model, the values predicted for environments as well as their limits with a probability of 95% (signification of 5%).

Table 2 Estimation of nano-particles size on the basis of order II model associated to Box-Behnken plan of experiments

No	Measured values	Predicted values	Predicted power limit average P=95%	Predicted upper limit P=95%
1	4.9	4.86181	4.71787	5.00574
2	5.11	5.14347	4.99954	5.28741
3	5.21	5.15847	5.01454	5.30241
4	4.82	4.83847	4.69454	4.98241
5	4.89	4.91014	4.76621	5.05407
6	5.11	5.05014	4.90621	5.19407
7	4.88	4.95222	4.83891	5.06553
8	5.13	5.09347	4.94954	5.23741
9	5.11	5.15181	5.00787	5.29574
10	5.09	5.11014	4.96621	5.25407
11	5.11	5.03847	4.89454	5.18241
12	5.08	5.13347	4.98954	5.27741
13	5.0	5.08347	4.93954	5.22741
14	5.0	4.95222	4.83891	5.06553
15	4.98	4.93847	4.79454	5.08241
16	5.01	5.00181	4.85787	5.14574

17	4,89	4.87014	4.72621	5.01407
18	5,0	5.03181	4.88787	5.17574
19	5,01	5.05306	4.90912	5.19699
20	4,99	5.04639	4.90246	5.19032
21	5,05	5.04306	4.89912	5.18699
22	4,82	4.90972	4.76579	5.05366
23	4,96	4.93556	4.82225	5.04886
24	5,19	5.13972	4.99579	5.28366
25	4,82	4.83306	4.68912	4.97699
26	5,03	4.99306	4.84912	5.13699
27	5,14	5.05639	4.91246	5.20032

For maintaining of the response (size nano-particles) to 5 nm, table 3 presents the optimized combination of factors levels.

Table 3 The optimized combination of factors levels for Box-Behnken plan

Factor	Min	Max	Optimum	Optimum value
Dopant concentration	2.0	4.0	2.49645	5
Autoclaving time	15.0	45.0	31.1997	
Autoclaving temperature	150.0	250.0	212.969	
Oven power	800.0	1200.0	1121.84	

In figures 3 to 4 are shown the estimated surface response and the estimated contours response.

It should be noted that the surface height of represents the values for the size of the TiO₂ nano-particles doped with Ag on a space determined by 2 factors (doping concentration, autoclaving time), the rest of 2 factors (autoclaving temperature, power oven) being maintain to their medium values.

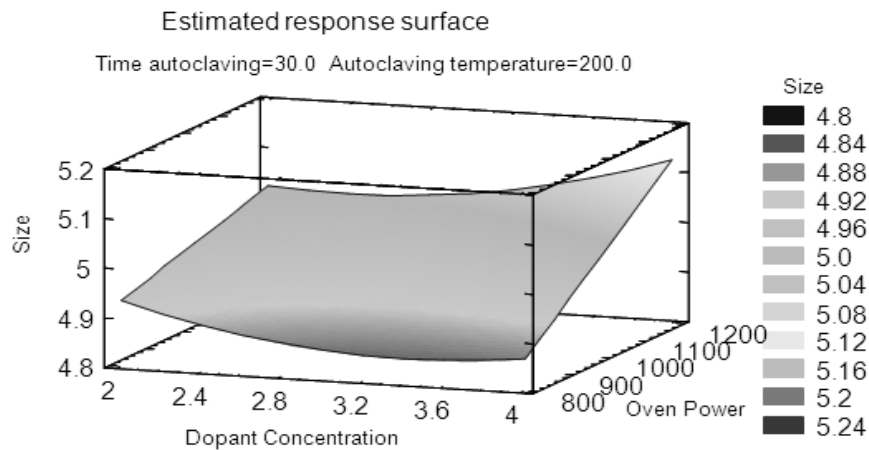


Fig. 3 Estimated response surface (Dopant concentration – oven power)

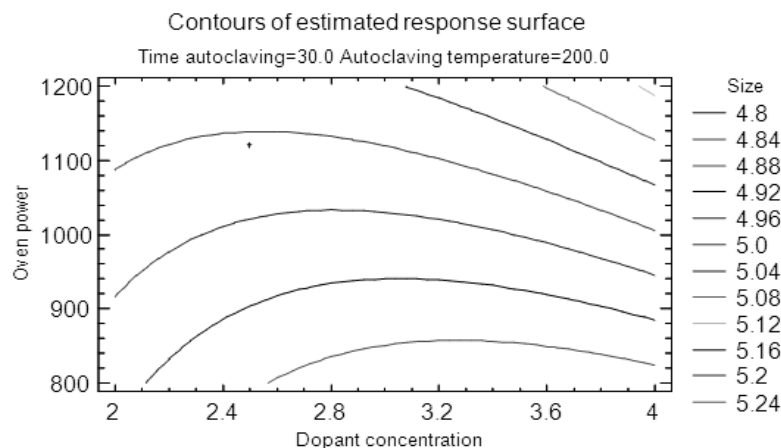


Fig. 4 Contours of estimated response surface ((Dopant concentration – oven power)

4. Conclusion



Using a Box-Behnken plan experience (27 experiences), which represents a reasonable alternative to complete factorial plans (4 factors at 3 levels = 81 experiments) and plans for CCD experiences for those situations where it is desired a plan with 3 levels and which should be almost rotatable, it may be observed that:

- Equation of regression is of 2 degree (taking into account that was taken into account also interactions) and is obtained between the response variable and factors (relationship 2).

- Order II model associated with the order of the experience plan explains 80,5926 % of Box-Behnken variability of nano-particles size (table 2)

- If we don't take into account interactions, then the model associated with Box-Behnken experiments plan is a order I model (linear relationship between the output and factors variability), and explains only 34,5670 % of the particles size variability

In conclusion, if it is desired an exact modelling system it shall be taking into account also interactions, however, if it is desirable to obtain only target value for the nano-particles size then order I model may be considered satisfactory.

References

- [1] J., ALEXIS – Metoda Taguchi în practica industrială – Editura Tehnică, București, 1999.
- [2] C. MINTO - Response Surface Modeling of Drug Interactions. (2006). <http://eurosiva.org/Archive/Vienna/abstracts> (accesat Iulie 17, 2010).
- [3] R.H., MYERS ș.a. – Response Surface alternatives to the Taguchi robust parameter design approach – the American Statistician 46 (2), pp 131-139, 1992.
- [4] R. H., MYERS, A. I., KHURI, W. H., CARTER Jr. (1989). Response surface methodology: 1966-1988. Technometrics 31 (2): 137-153 <http://www.jstor.org/> (accesat Iunie 19, 2011).
- [5] R. H., MYERS, D. C., MONTGOMERY, (1995). Response Surface Methodology: process improvement with steepest ascent, the analysis of response Surfaces, experimental designs for fitting response surfaces, 183-351, New York: John Wiley and Sons, Inc



International Conference on Innovative Technologies, IN-TECH 2012,
Rijeka, 26. - 28.09.2012





USING EXPERIMENTAL METHODS FOR CHECKING STABILITY OF TiO₂ NANOPARTICLES SIZE

O. Giuca¹, I. Nicoara¹ and I. Grozescu²

¹ Politehnica University of Timisoara, 2 Piata Victoriei, Timisoara, Romania.

² National Institute of Electrochemistry and Condensed Mater Timisoara, Plautius Andronescu 1, Timisoara, Romania.

Keywords: nanoparticles, dimension, target value

Abstract. One possibility to increase efficiency and competitiveness of nanomaterials, is introducing scientific design of experiments in the methods of synthesis of nanomaterials. To obtain experimental models to better approximate the actual technology systems must analyze a large number of factors, on the other hand, to reduce the overall volume of testing economic reasons.

Given the importance of using titanium dioxide and industrial properties, is preferable to obtain nanoparticles of size approximately equal or similar to the target. So you want to check the dimensional stability of nanoparticles, obtained by various synthesis methods, the methods of design of experiments.

The paper dimension verify stability of TiO₂ nanoparticles obtained by hydrothermal method in the microwave field by applying a Taguchi experimental plan, for which they took into account seven factors at two levels.

Compared with other antimicrobial agents, TiO₂ attention through good stability offered, but also because it is environmentally friendly, safe, inexpensive, nontoxic, bioactive, etc. Catalytic nanoparticles have great potential, respectively redox active agents for purifying water and air.

Thus, in recent years, nanoparticles of titanium dioxide (TiO₂) proved to be a promising photocatalysts, serving both as oxidant and reductant for organic and inorganic pollutants in the presence of ultraviolet light.

To determine the accuracy of prediction L₈ Taguchi experiment to compare the performance obtained with the optimal conditions required solution, obtained by hydrothermal method in the microwave field. Experimental research conducted with plan L₈ Taguchi experiments showed that the synthesis of TiO₂ is strongly determined by three factors temperature autoclaving, high filling and microwave power.

1. Introduction

Special interest is granted to obtain nano-materials, and the titanium dioxide TiO₂ is used intensively as photocatalyst for converting solar energy into chemical energy, mainly in applications for the protection of the environment.

Compared with other anti-microbial agents, TiO₂ has drawn attention due to his good stability, but also due to the fact that it is friendly to the environment, safe, inexpensive, nontoxic, bioactive etc. Nano-particles have a great catalytic potential and redox active agents for water and air purification. Thus, in the last few years, nano-particles of titanium dioxide (TiO₂) have been shown to be a promising photocatalyst, serving both as oxidant as well as reduction for organic and inorganic pollutants in the presence ultraviolet light. Thus, in order that nano-particles to be able to have a high efficiency in practice, must possess a number of properties such as: high purity, uniform chemical composition, the size of the nano-particles to enroll into uniform, narrow and controllable distribution, the shape and the morphology of nano-particles to be identical. In practice it is quite difficult to be obtained nano-particles that meet all of these features.

2. Using methods

A new procedure for synthesis of nano-particles is the hydrothermal method with heating in the field of microwave, which is based on a series of new physical mechanisms which contribute to reducing the consumption of energy by removing the losses and a much lower synthesis time, as well as a more rigorously control of the thermal field from the synthetic environment by removing the causes of thermal inertia and the possibility for temperature control through the microwave generator [1, 3, 5].

The use of microwave involves a complex process, multidisciplinary from the point of view of equipment and properties of materials, many of them significantly depending on the working temperature. Technical and economic knowledge required, to know how, when, where, and where it is effective to use microwave in synthesis of material. Experimental modeling strategy provides information with respect to direction that research must follow to move toward optimal experimental model obtained through a minimum number of experiments.

Most of the criteria for optimal designing of experiments are associated with the mathematical model of the process. Usually these mathematical models are composed of unknown structural polynomials so that appropriate experiments are designed for each particular case. The type of the chosen experiments has decisive influences on the accuracy of approximation and cost of the experiment [6]. Genichi Taguchi's approach to strategy, (Fig. 1), is based on minimize the impact of harmful factors (factors - noise), acting on experimental check factors by finding the combinations of their values so that the process or product to comply with operational performance and also to be robust with respect to factors - noise [7].

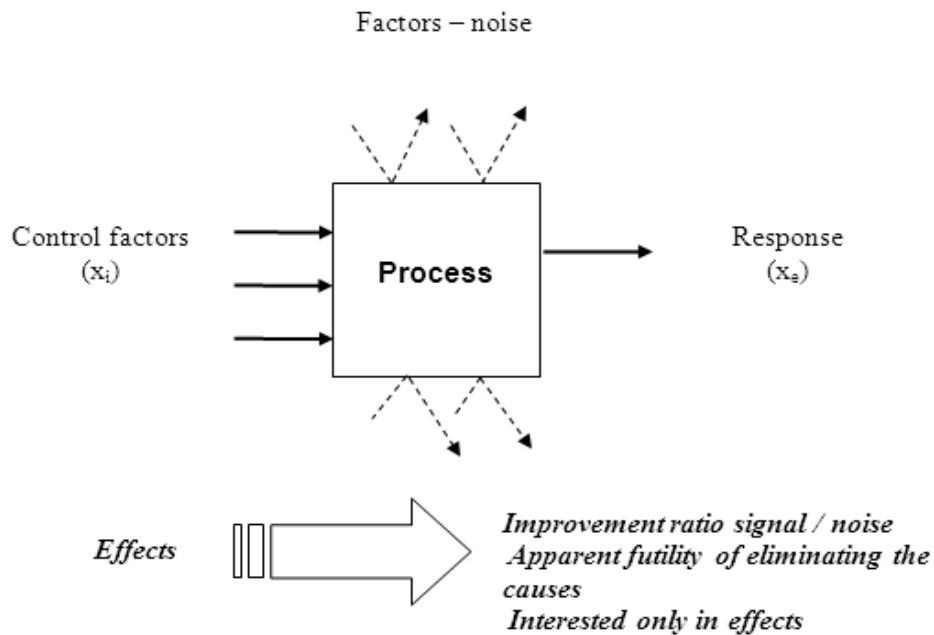


Fig. 1 Genichi Taguchi's approach to strategy is based on minimize the impact of harmful factors - noise

With respect to the design of products, Genichi Taguchi has a new approach (Fig. 2).

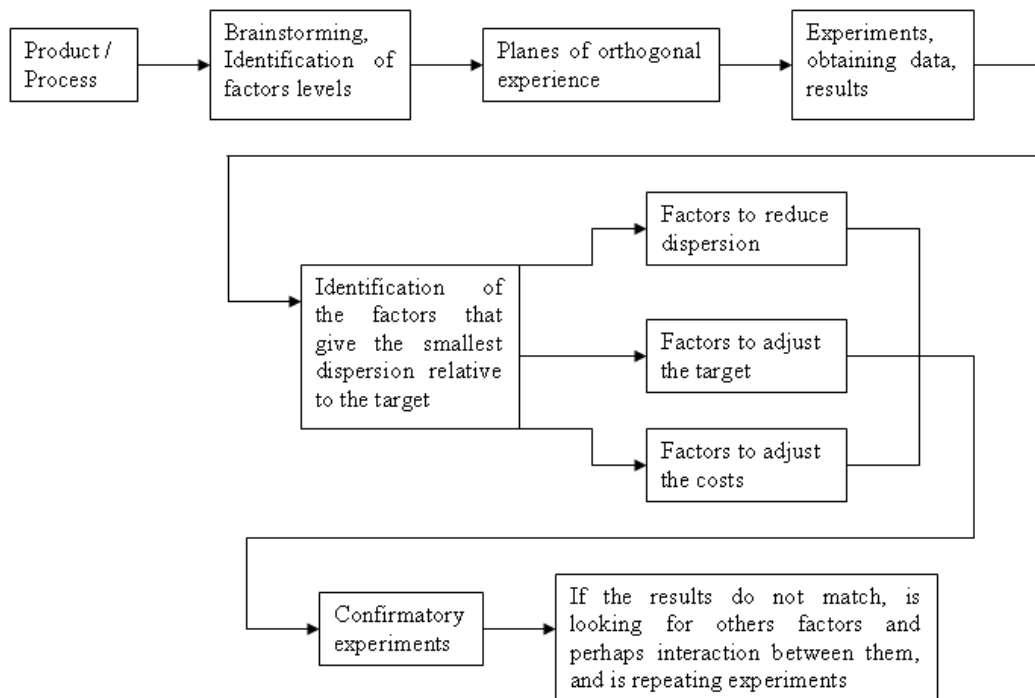


Fig. 2 Genichi Taguchi's approach for the design products

We believe that "Performance" is the "Output" of a system with one or more "Inputs", and when it is desirable to assess performance of a system, should be considered at the time both "desired outputs" (the ones that we want to achieve) and "unwanted outputs" (those that we want to avoid). At the first we refer as "Signals" and at the other as "Noises", by analogy with traditional use of the two concepts of the expression "Signal/Noise Ratio (S/N)" used in the electronic or optoelectronics communications. Unlike conventional approaches (traditional) which treat separately these two components, G. Taguchi uses to assess the quality of the product or process, a synthetic measure of performance with the same designation (signal/noise ratio) which takes into account simultaneously both media as well as dispersion. The plans of the trials consists in carrying out some experiments established before in order to determine with the minimum of testing and maximum precision, the possible influences of the different parameters in such a way as to optimize performance of a system.

Making a plan for split factorial experiments, Taguchi is based on the idea that some possible combinations of tried factors bring more effective information, succeeding such considerable reduction of the number of experiments made.

3. Process-orientated research

In order to achieve the check size stability of TiO₂ nano-crystals doped with Ag within hydrothermal synthesis in the field of microwaves, was applied Taguchi method, in which the output variable is the quality feature of TiO₂ nano-crystals of (nano-particles size), and, for the input variables are taken into consideration seven factors: doping concentration, autoclaving time, temperature autoclave, oven power, nutrient quantity, solution's ph, filling degree, using Qualitek 4 (Automatic Design and analysis of Taguchi Experiments), the objective being optimal determination of the combination of the factors in such a way as to obtain a target value of 10 nm with a tolerance of ± 0.2 Nm for the nano-crystals size. It has chosen a standard Taguchi's matrix L₈ (7 factors at 2 levels each), shown in figure 3. Assigning factors as well as determining their levels has been carried out in accordance with table 1.

	1	2	3	4	5	6	7
1	1	1	1	1	1	1	1
2	1	1	1	2	2	2	2
3	1	2	2	1	1	2	2
4	1	2	2	2	2	1	1
5	2	1	2	1	2	1	2
6	2	1	2	2	1	2	1
7	2	2	1	1	2	2	1
8	2	2	1	2	1	1	2

Fig. 3 Matrix of experiments L₈

Table 1 Control factors and levels

No.	Description of factor	Level 1	Level 2
1	Dopant (Ag) concentration	2 %	3%
2	Autoclaving duration	15 min	30 min
3	Autoclaving temperature	150 °C	200 °C
4	Microwave oven power	800 W	1000 W
5	Nutrient quantity	10 g	20 g
6	Solution pH	2.5	2.8
7	Autoclave filling degree	50 %	60 %

Conditions	Sample# 1	Sample# 2	Sample# 3	Sample# 4	Sample# 5	Sample# 6	S/N Ratio
Trial# 1	9.85	9.79	9.88	9.94	9.85		16.691
Trial# 2	10.11	10.18	9.98	9.96	9.92		19.755
Trial# 3	9.81	9.83	9.82	9.9	9.87		16.044
Trial# 4	10.12	10.18	10.17	10.17	10.11		16.318
Trial# 5	9.94	10.14	10.12	10.19	9.98		18.291
Trial# 6	9.8	9.89	9.87	9.91	9.92		17.772
Trial# 7	10.18	10.12	9.93	9.89	9.86		17.778
Trial# 8	10.12	9.98	10.14	10.12	9.94		19.796

Fig. 4 Experimental results and S/N ratios

Experimental results of the dimension of the TiO₂ nano-crystals doped with Ag obtained by the hydrothermal method in the field of microwaves are shown in figure 4. It should be noted that for each condition of experimentation have been measured 5 nano-particles.

Target value for the size nano-crystals has been set to 10 nm. The values obtained for the 8 experiments are: overall average 9,987 nm, standard deviation 0.132, S/N average 17,806 dB.

Based on analysis of the medium effects of factors on the ratio S/N, optimal condition for checking the stability of the nano-particles size is given by factors positioning at the levels from table 2, respectively from the analysis factor interactions, optimal condition for checking the stability of the nano-particles size is given by factors positioning at the levels from table 2. It should be noted that depending on the type interaction, the period of autoclaving and solution ph are acceptable from this point of view on both levels.

Table 2 Optimal condition based on analysis of the medium effects of factors, respectively factors interaction

Analysis of the medium effects of factors and factors interaction		
Factors	Level (medium effects)	Level (interactions)
Dopant (Ag) concentration	2	2
Autoclaving duration	2	2(1)
Autoclaving temperature	1	1
Microwave oven power	2	2
Nutrient quantity	2	2
Solution PH	2	2(1)
Autoclave filling degree	2	2

To check the stability of nano-particles size, -was made the analysis of variance with ANOVA method and has been found that the factors "PH solution" and "Quantity nutrient" are not significant from a statistical point of view and can be eliminated from the model (can have either of the two levels). As a result of this analysis it was determined the order of importance factors as well as the percentage properly (Table 3).

Table 3 Order of factors importance

Order of importance	Factors	Percentage [%]
1	Autoclave temperature	26.869
2	Autoclave filling degree	24.368
3	Microwave oven power	20.096
4	Dopant (Ag) concentration	20.020
5	Autoclaving duration	5.687
6	Nutrient quantity	2.901
7	Error/other	0.391
TOTAL = 100%		

The table of optimal, presented in table 4 are shows the equation for optimal performance at optimal condition and any other conditions possible. The values calculated and shown in the table are those for optimal condition. Expected performance in the calculation shall be included only significant factors the optimal condition being determined on the basis of the quality feature selected for analysis. It is noted that levels of optimal factors are consistent with those presented in analysis of the medium impact and of the interactions factors listed above.

The fact that the of the "autoclaving time" factor is at level 1 and not 2 (as obtained from analysis of medium impact) is favorable from the economic point of view.

Table 4 The table of optimal

Description of factor	Level description		Contribution
Dopant (Ag) concentration	3 %	2	0.603
Autoclaving duration	15 min	1	0.321
Autoclave temperature	150 °C	1	0.699
Microwave oven power	1000 W	2	0.604
Nutrient quantity	20 g	2	0.229
Autoclave filling degree	60 %	2	0.665

4. Conclusion

After simulating of 128 conditions of experimentation, using the linear generalized equation (1) was revealed the orthogonal matrix L_8 obtained from complete factorial experiment simulation, respectively the maximum and minimum condition.

By comparing the values calculated from complete factorial experiment simulation and the values obtained by measurement, through implementation of the plan of the trials orthogonal Taguchi L_8 , optimum value resulting from complete factorial experiment simulation is: $Y_{opt1}=10,00$ and $Y_{opt2}=10,02$ and the error using an orthogonal matrix L_8 instead of a complete factorial experiment is 0% and 0.02 %. Maximum relative error is approximately - 3.87 % and errors for experimental conditions number 78 and 80 (those who actually provides optimal combination of factors) are 0% and 0.02%, which allows to conclude that the equation of relationship (1), is the correctly analytical solution of a relationship between the characteristic performance (nano-particles size) and factors take into account.

Assuming that the characteristic equation represents behavior of the system, the maximum value obtained from complete factorial experiment combinations, may be regarded as exact solution which it may be compared with the solution in the experiment based on orthogonal matrix L_8 . Also performance at optimum conditions can be compared with the exactly solution in order to be sure with the accuracy prediction of experiment L_8 .

In conclusion this research experiments carried out with the plan of the trials Taguchi L_8 , have revealed that the process of synthesis of TiO_2 is strongly determined by the three factors autoclaving temperature, degree filling and power oven.

References

- [1] J., ALEXIS – Metoda Taguchi în practica industrială – Editura Tehnică, București, 1999.
- [2] B. O., ADUDA, P., RAVIRAJAN, K. L., CHOY, J., NELSON – Effect of morphology on electron drift mobility in porous TiO_2 , International Journal of Photoenergy 6, 141, 2004.



International Conference on Innovative Technologies, IN-TECH 2012,
Rijeka, 26. - 28.09.2012



-
- [3] J., BLANCO, P., FERNANDEZ, S., MALATO – Solar photocatalytic detoxification and disinfection of water: Recent overview. *Journal of Solar Energy Engineering* 129, 4 -15, 2007
 - [4] W., DUNCAN – Total Quality Key Terms. p. 171
 - [5] S., GELOVER, L. A., GÓMEZ, K., REYES, M. T., LEAL – A practical demonstration of water disinfection using TiO₂ films and sunlight, *Water Research*, 40, 17, 3274, 2006
 - [6] AI., ISAIC – MANIU, V. Ch., VODĂ - Proiectarea statistică a experimentelor, *Fundamente și studii de caz*, Ed. Economică, 2006.
 - [7] G., TAGUCHI, ș.a. – *Robust Engineering* –McGraw-Hill, New York, 2000.



International Conference on Innovative Technologies, IN-TECH 2012,
Rijeka, 26. - 28.09.2012



UNCONVENTIONAL VARIABLE DISPLACEMENT INTERNAL COMBUSTION ENGINE

J. Dorić¹, N. Nikolić² and I. Klinař³

¹ Teaching Assistant, Faculty of technical sciences, Serbia, Novi Sad, Trg Dositeja Obradovića 6

² Teaching Assistant, Faculty of technical sciences, Serbia, Novi Sad, Trg Dositeja Obradovića 6

³ Full Professor, Faculty of technical sciences, Serbia, Novi Sad, Trg Dositeja Obradovića 6

Keywords: IC engine, variable displacement, variable compression ratio

Abstract. In this paper was presented one solution for realization of variable displacement internal combustion engine. One of the major disadvantages of today's IC engine is in relation to constant volume displacement. Low efficiency during partial load operation can be avoided with changing piston stroke which will reducing current engine volume. This article presents basic shape of engine parts, also in this paper will be presented some important kinematic results and piston motion law. With this unconventional piston movement it is easy to provide variable compression ratio, variable displacement and combustion during constant volume. These advantages over standard piston mechanism are achieved through synthesis of the two pairs of non-circular gears. Presented mechanism is designed to obtain a specific motion law which provides better fuel consumption of IC engines.

Introduction

During its more than one hundred years long history, a reciprocating four stroke piston internal combustion engine has evolved in a very mature thermal machine which has excluded all the alternatives offered for motor vehicle's drive. The main goal of its further development is to harmonize the growing traffic with environmental and energy consumption. Nowadays, there are a very large number of internal combustion engines, which are applied to various fields of science and technology. In some areas IC engines are so dominant without concurrence of other types of engines. These facts suggest that today's internal combustion engines are at a high technical level. However, construction of conventional internal combustion engines that are now used is based on inefficient thermodynamic and mechanical concept. It can be said that the main characteristics of today's engine is a very small amount of work in relation to used fuel, in other words, today's engines have a very low coefficient of efficiency. Realistically speaking Otto engines today use about 25% of input energy, while Diesel construction about 30% (in some cases can be expected a little more). Approximately 35% in Otto engine and 30% of heat in the diesel engines goes through exhaust gases and around 33% goes for cooling the engine in both versions, other 7% is attributed to friction and radiation. For illustration can be taken into account combustion of one liter of fuel in the classical combustion engines. Combustion of this amount of fuel frees approximately 39 [MJ] of power, the engine output shaft is generated only around 13 [MJ], while the other 26 [MJ] mostly heat the environment.

Methods for increasing efficiency at partial load

Most popular methods for increasing efficiency at partial load are in relation to variable piston motion. Variable displacement and variable compression engines are gaining attention by scientist and automobile manufactures because of their fuel consumption economy advantage. One of the successfully constructed IC engine with variable compression ratio is certainly made by SAAB [1]. In conventional IC engines the load regulation is balanced by throttling the intake mixture. Schematic views of the most used methods for improvement of spark ignition engine efficiency are presented on Fig. 1.

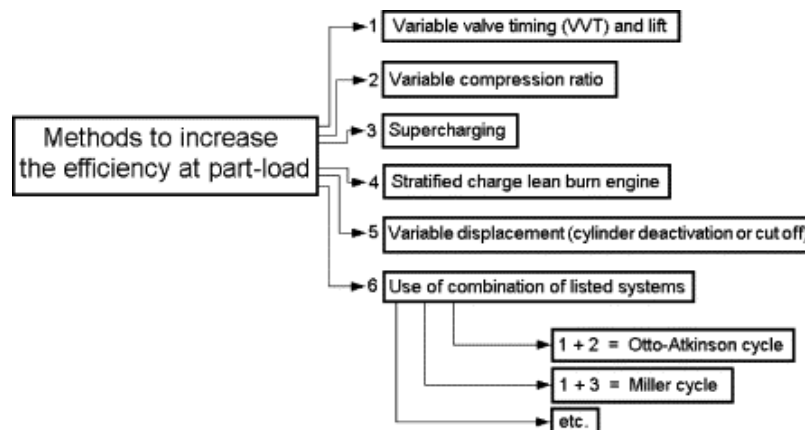


Fig 1. Methods for increasing the efficiency at partial load [2]

Variable displacement SI engine

Variable displacement concepts have been analyzed in many different scientific publications. Siewart [3] reported a fuel economy approaching 20% for variable stroke engines over fixed stroke engines. Also there is a several patents about mechanisms which provides variable stroke, one of them are patented by Freudenstein and Maki [4]. Several authors [5-7] have proposed different complex mechanisms to achieve variable displacement engine. In the paper of Yamin and Dado [8] was investigated the effect of a variable stroke mechanism on the engine performance, the conclusion showed that the engine performance was improved with this novel design. Also Pouliot et al. [9], proposed, constructed and studied a five-cylinder, four-bar linkage engine and Filipi et al. [10] theoretically, investigated the effect of varying the stroke length on a homogeneous charge engine's combustion, heat transfer and efficiency using gasoline as fuel. Wong et al. [11] presented and analyzed a four cylinder engine with Alvar cycle that utilizes secondary pistons and auxiliary chambers

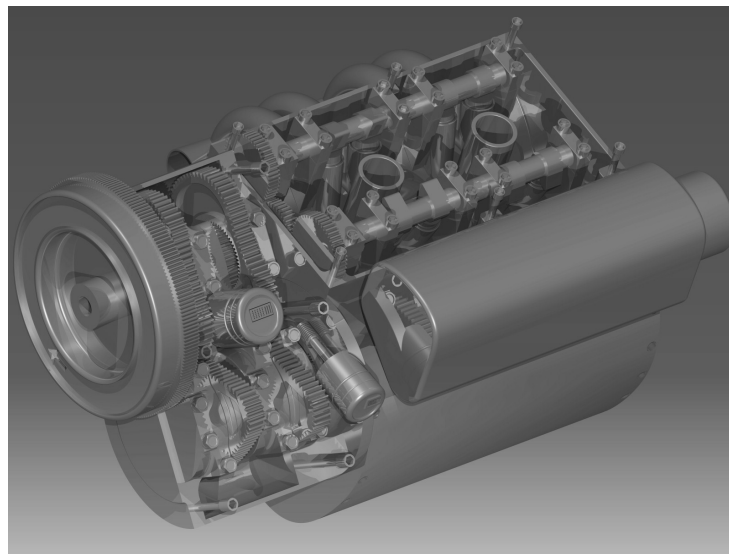


Fig. 2 CAD model of new variable displacement internal combustion engine

In this paper will be only briefly presented basic shape and parts of unconventional variable displacement spark ignition engine concept. In the previous Fig. 2 was presented CAD model of this engine made by CATIA V5 R17. The main idea is to create engine concept that will be able to provide variable compression ratio at partial load and variable displacement for small power requirements.

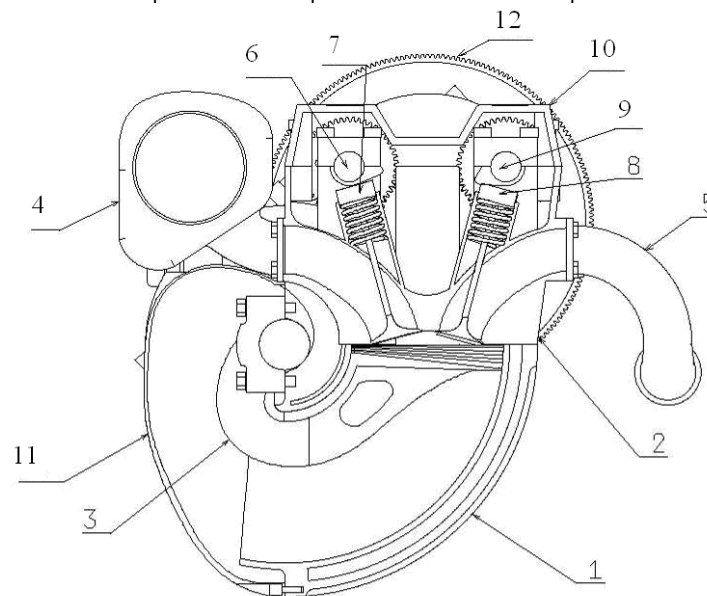


Fig. 3 Cross section of basic engine parts [12]

In the following section will be presented basic parts and shape of a new IC engine concept. Variable piston motion IC engine is presented on the fig. 1. Basic parts of the VPM engine are: 1-engine block, 2-engine head, 3-toroidal piston, 4-intake manifold, 5-exhaust manifold, 6-intake camshaft, 7-intake valve, 8-exhaust valve, 9-exhaust camshaft, 8-valve spring, 9-housing, 10-valve cap, 11-crankcase and 12-flywheel. As can be seen from the described CAD illustration toroidal piston make a movement conditioned by the mechanism consisting of two pairs of non-circular gears. In this article will not be presented detailed description of this concept, since it is not the intention of the authors to propose a kinematic analysis of a new internal combustion engine design but only thermodynamic features and advantages over ordinary spark ignition engines.

Modelling

The analysis of the potentials of aforementioned measures on fuel economy at part load engine conditions has been carried out by engine cycle mathematical simulation. For this purpose the Ricardo/WAVE program for engine working process simulation has been used [5]. Program code WAVE contains so called "preprocessor" which enables the forming of engine calculating scheme, selection of model type for processes and sub processes, specification of all parameters and starting values and boundary conditions etc. The calculating scheme of the engine is formed graphically using offered standard elements such as: cylinders, receivers, pipes, pipe conjunctions, cleaners, injectors etc. For all elements must be specified their geometrical and other characteristics according to real engine conditions, and they are assembled to so called "engine calculation scheme". With Table 1 are presented most important engine specification which are used in simulation.

Table 1. Main engine data

type	oto
stroke	četvorotaktni
number of cylinders	2
number of valves per one cilinder	4
bore	120 [mm]
stroke	30-177 [mm]
intake valve diametar	44 [mm]
exhaust valve diametar	40 [mm]
valve stroke	15 [mm]
EVDUR	235 [°]
IVDUR	230 [deg]
EVMP	253.3-245[deg]
IVMP	479.3-471 [deg]
compression ratio	8-16

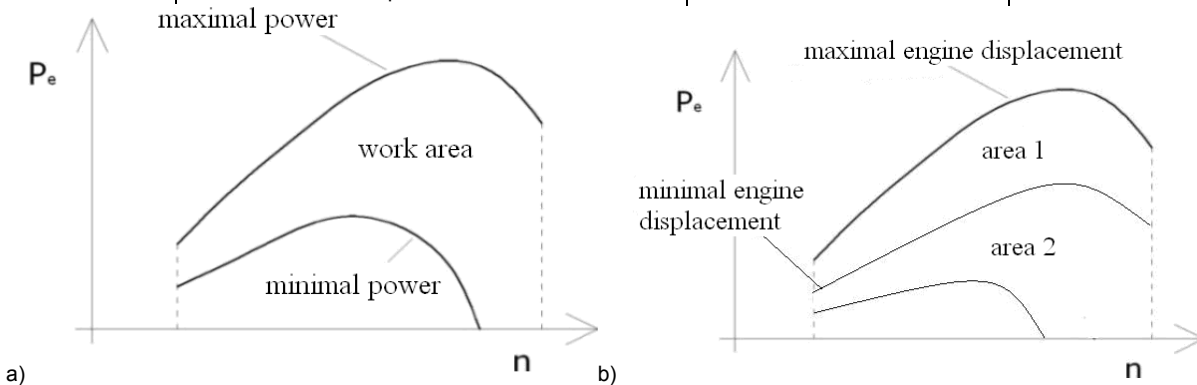


Fig. 4 Comparison of power regulation in ordinary (a) and unconventional (b) internal combustion engine

Results of one dimensional simulation of engine model can be performed in several ways. Focus of the research in this paper is to present engine torque curves for several different S/D ratios. Ratio of piston stroke (S) and bore (D) is very important parameter, this engine concept is able to change this value in order to make constant power with higher efficiency for wide range of engine speed. Such engine torque curves are presented in Fig. 5. From the same figure it is clear that with variable displacement there is a large area when IC engine have constant power, i.e. torque hyperbole.

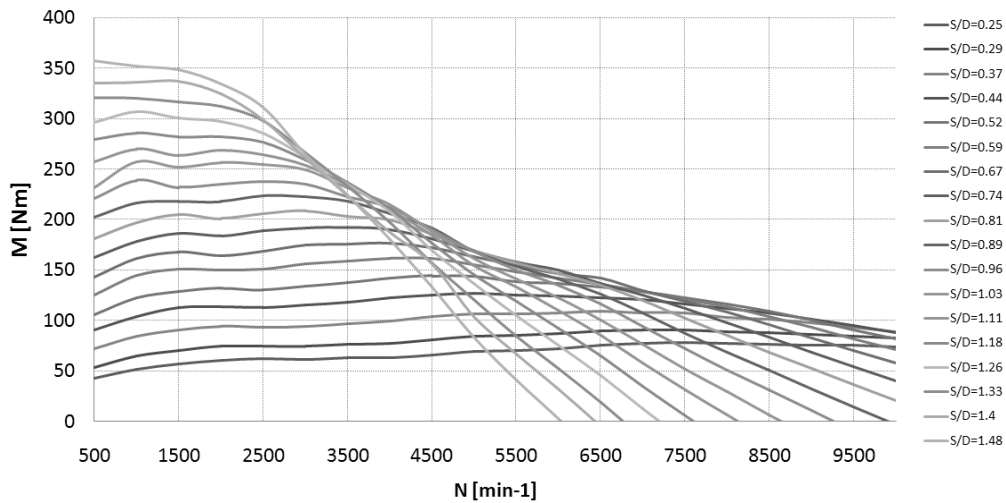


Fig. 5 Engine torque in relation to S/D ratio

With variable displacement engine power curves are different than in conventional engine as is described in Fig.4. Besides higher efficiency which is well known advantages of variable displacement, variable S/D ratio offers the possibility that engine have much larger area of constant power operating points.

Conclusion

In this article was briefly presented basic shape of unconventional spark ignition internal combustion engine with variable displacement. Main aim is to achieve power control without throttle body. Generally speaking, throttling in SI engine have significant effect on efficiency, in other words have negative impact on pumping work and effective compression ratio. These changes in pressure-volume diagrams are shown in the following Fig. 6.

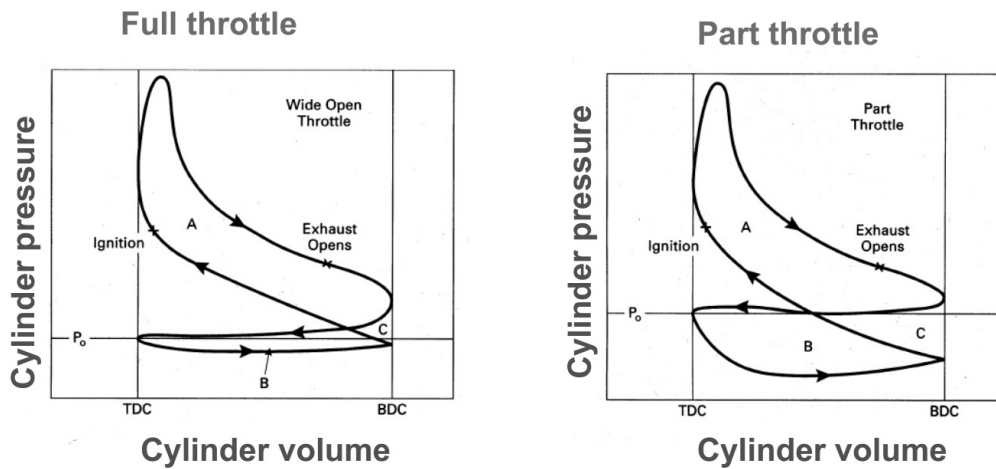


Fig. 6 Impact of conventional power regulation of IC engine on pumping work

With this paper novel four stroke cycle for IC engines was analyzed. Main goal of this unconventional cycle is to increase engine's efficiency. The essential challenges in developing this procedure are the control of the start of combustion, and proper selection of intake and exhaust valves open duration and also intake and exhaust valves open angle. Improvement in efficiency is achieved through unconventional kinematics of piston movement, as a result of more favorable heat input and lower pumping work.

Variable displacement, which is in this concept achieved through variable S/D ratio, opens the way to much easier and better power regulation in IC engine. As can be seen from Fig. 5 such unconventional engine will have hyperbolic curves of engine torque which means that engine will have constant power in a wide range of operating speed. That basically means that motor vehicle with such propulsion system can be made without classic transmission system.

Acknowledgment

This paper is realized in the scope of the Project TR-35041 "Investigation of the Safety of the Vehicle as a part of cybernetic system: Driver-Vehicle-Environment" supported by Ministry of Science and Technological Development of the Republic of Serbia.

References

- [1] H. Ozcan, J.A.A. Yamin: Performance and emission characteristics of LPG powered four stroke SI engine under variable stroke length and compression ratio, *Energy Conversion and Management* Volume 49, (2008), pp. 1193–1201



-
- [2] O.A. Kutlar, H. Arslan, A.T.Calik: Methods to improve efficiency of four stroke, spark ignition engines at part load, *Energy Conversion and Management*, Volume 46, (2005), pp. 3202–3220
 - [3] R.M. Siewert: Engine Combustion at Large Bore-to-Stroke Ratios, *SAE Trans*, Volume 87, (1978), pp. 3637–51
 - [4] F. Freudenstein, E.R. Maki: Variable displacement piston engine, U.S. Patent No 4,270,495, (1981)
 - [5] J. Pierce: Variable Stroke Mechanisms, U.S. Patent No. 1,112,832, (1914)
 - [6] A.E. Biermann: Variable Stroke Piston Engines, U.S. Patent No. 2,909,163, (1959)
 - [7] H.W. Welsh, C.T. Riley: The Variable Displacement Engine, An Advanced Concept Power Plant, SAE Paper 710830, (1971)
 - [8] J.A. Yamin, M.H. Dado: Performance simulation of a four-stroke engine with variable stroke-length and compression ratio, *Applied Energy*, Volume 77, (2004), pp. 447–463
 - [9] H.N. Pouliot, W.R. Delameter, C.W. Robinson: A Variable Displacement Spark Ignition Engine, SAE Paper 770114, (1977)
 - [10] Z.S. Filipi, D.N. Assanis, The effect of the stroke-to-bore ratio on combustion, heat transfer and efficiency of a homogeneous charge spark ignition engine of given displacement. *International Journal of Engine Research*, Volume 2, (2000), pp. 191–208
 - [11] V.W. Wong, M. Stewart, G. Lundholm, A. Hoglund: Increased Power Density via Variable Compression/Displacement And Turbocharging using the Alvar-Cycle Engine, SAE Paper 981027, (1998)
 - [12] J. Dorić: Variable piston motion IC engine, patent application No 2012/0073, Belgrade, Serbia, (2012)



International Conference on Innovative Technologies, IN-TECH 2012,
Rijeka, 26. - 28.09.2012



UNCONVENTIONAL RELIABILITY GROWTH MODELS

Z. Krajcuskova¹, M. Kukucka¹, D. Durackova¹

¹ Institute of Electronics and Photonics, Slovak University of Technology, Ilkovicova 3, 812 19 Bratislava, Slovak Republic

Keywords: Reliability growth model (RGM), Poisson theorem, homogenous and non-homogenous stochastic Poisson process, statistical data processing, homogeneity testing

Abstract. The reliability of electronic circuits, system and devices is one component of their quality. An electronic device has three phases of existence. First phase – the development is very important for reliability growth. In this phase constructor implements three basic components of reliability - reliability, longevity and maintainability in the electronic device. The reliability growth model (RGM) is a very specific tool used during the development phase of electronic devices and software products. New unconventional reliability growth models are based on the homogeneity testing of different Poisson process characteristics. This enables to find the time frame for finishing the technological constructing operations for further reliability growth in the next design of an electronic object. The goal is to find boundary time t_b using statistical methods, from which the Poisson process is homogenous (stationary).

In this paper we review new unconventional reliability growth models – RGM algorithm based on Poisson process homogeneity testing of mean value $m(t)$, RGM algorithm based on Poisson process homogeneity testing of dispersion $D(t)$. We introduce experimental results those obtained by applying these two reliability growth models.

Introduction

Reliability of electronic circuits, systems and devices is one component of quality. An electronic device has three phases of existence. They are development phase, production phase and working phase. The development phase is very important for reliability growth. In this phase the constructor implements three components of reliability – reliability, longevity and maintainability in the electronic device

Reliability Growth Model

It is not very simple to present precise (specific) definition of the reliability growth model. The reliability growth model is the instruction for constructor. The constructor must do construction changes, corrective interventions in the development phase of the electronic device. All changes and interventions have one goal. It is reliability increase of the developed electronic device.

Definition of Reliability Growth Model

Let $X(n)$ be one-parametric discrete stochastic process of reliability increase of the electronic device, where n is for example time, number of failures in time interval, number of experiments,.... Let this stochastic process be asymptotically stationary and ergodic on parameters m_i . Let s_1, s_2, \dots, s_k be assessment statistic dependent on process $X(n)$ for parameters m_1, m_2, \dots, m_k , of function $f(m_1, m_2, \dots, m_k; X)$. Then the function $f(m_1, m_2, \dots, m_k; X)$ is the reliability growth model [1, 2].

Poisson Process

Poisson process is a process representing "full-stochastic occurrence" on event (for example failure creation of a device) in time. This model is a process with continuous time t and discrete values of stochastic process. It is a model with independent step increases [3].

We consider occurrence of events in time interval $t \in (0, \infty)$. For $t > 0$ let $X(t)$ be the number of events, which had results in interval $(0, t)$, open in zero and closed in time moment t . Let $N(t)$ and $N(t+h) - N(t)$, for arbitrary continuous $h > 0$, be integer positive values, meaning 0, 1, 2, 3,.....

Axiomatic definition of Poisson process is [3, 4] :

- Axiom 1 : $X(0) = 0$.
- Axiom 2 : Process $\{X(t), t \geq 0\}$ has independent increases.
- Axiom 3: For arbitrary $t > 0$ $P\{X(t) > 0\} < 1$.
- Axiom 4 : For arbitrary $t \geq 0$

$$\lim_{h \rightarrow \infty} \frac{P\{X(t+h) - X(t) \geq 2\}}{P\{X(t+h) - X(t) = 1\}} = 0.$$

This axiom says, that in a very small interval it is only possible that one event occurs, that means, that it is not possible that two events occur in the same time.

- Axiom 5 : Enumerable process $X(t)$ has stationary increases. It means, that for two time moments $t > s \geq 0$ stochastic variables $X(t) - X(s)$ and $X(t+h) - X(s+h)$ equal distribution function.

Process $\{X(t), t \geq 0\}$, which meets these five axioms is homogenous Poisson process.

If axiom 4 is not met, than it is generalized Poisson process. If axiom 5 is not met, than it is non-homogenous Poisson process. This is a Poisson process with non-stationary increases.

Poisson process homogeneity testing

The principle of reliability growth models, which is based on Poisson process homogeneity testing, is in fact that system is no-stationary or stationary. It means, if there are many early failures, also high intensity inherent failures in the system, the constructor must do construction changes with goal to increase reliability of the system. Poisson process with non-stationary is non-homogenous Poisson process, Poisson process with stationarity is homogenous Poisson process. Reliability growth model is finished in time t_b (boundary time), from time t_b process is statistically stationary.

Generally stochastic process has different types of stationarity with four basic characteristics [3, 4] :

- mean value $m(t)$,
- dispersion $D(t)$,
- correlation function $R(t_1, t_2)$,
- density of probability distribution $f(t)$ in time t .

New unconventional reliability growth models are based on a simple idea of Poisson homogeneity testing in time reliability test of repairable systems. The goal is to find boundary time t_b using statistical methods, from which the Poisson process is homogenous (stationary).

RGM algorithm based on Poisson process homogeneity testing of mean value $\hat{m}(t)$

For homogeneity mean value of Poisson process testing it is necessary to know actual data from the experiment – number of failures in a set up time interval Δt (for example $\Delta t = 20$ hours) in sequence 0-20 h, 20-40 h, 40-60 h, Again we need information if in actual time interval is failure 0, 1, 2, ... ,i-s . Zero failure means no failure in the operating ability of systems.

Estimation of mean value $\hat{m}(t)$

The statistic estimation of mean value $\hat{m}(t)$ in time t_k , $k = 1, 2, 3, \dots$ we calculated using the equation :

$$\hat{m}(t_k) = \frac{\sum_{i=0}^k n_i \cdot i}{N} = \frac{\sum_{i=1}^k n_i \cdot i}{N} \quad (1)$$

N – number of systems in a reliability test.

Estimation of dispersion $\hat{D}(t)$

For homogeneity testing mean value of Poisson process it is necessary to know statistic estimation of dispersion $\hat{D}(t)$ in actual times t_k . We can calculate it using the equation :

$$\hat{D}(t_k) = \frac{\sum_{i=0}^k n_i [i - \hat{m}(t_k)]^2}{N - 1} = \frac{\sum_{i=1}^k n_i [i - \hat{m}(t_k)]^2}{N - 1} \quad (2)$$

In next steps we applied first (fragile) criterion of Poisson process homogeneity testing with mean value $m(t)$, second (strong) criterion with mean value $m(t)$ and third criterion with mean value $m(t)$. We found the boundary time t_b , in which it is possible to finish process RGM.

RGM algorithm based on Poisson process homogeneity testing of dispersion $\hat{D}(t)$

Input data are equal as in previous chapter. We calculated the estimation of dispersion using equation (2) for different values t_k in time range $t_k \in \langle 0, T \rangle$, T is whole time of test. We applied the criterion of Poisson process homogeneity testing with dispersion $D(t)$ and criterions of Poisson process homogeneity testing with dispersion $D(t)$ with help of Fischer-Snedecov test (F-criterion) and we found the boundary time t_b , in which it is possible to finish process RGM.

Experimental results

For verification of RGM algorithm based on the Poisson process homogeneity testing of mean value $\hat{m}(t)$ and GRM based on Poisson process homogeneity testing of dispersion $\hat{D}(t)$ we used data from a real reliability test. In the reliability test were 160 electronic systems, the time of whole test was 1000 hours, the time interval was 20 hours.

Homogeneity of means value $m(t)$

Input data were times of first, second, ..., r-s failure in 20hours time intervals. We calculated number of first n_1 , second n_2 , ..., r-s n_r failures in time moments 20, 40, 60, ... ,1000 hours. Using algorithm from previous chapter we calculated estimations of mean values in time moments $t_k = 20, 40, 60, \dots, 1000$ hours Poisson process . The mean value of Poisson process (statistic estimation) is in Fig.1. The renewal function $H(t)$ is in Fig.2.

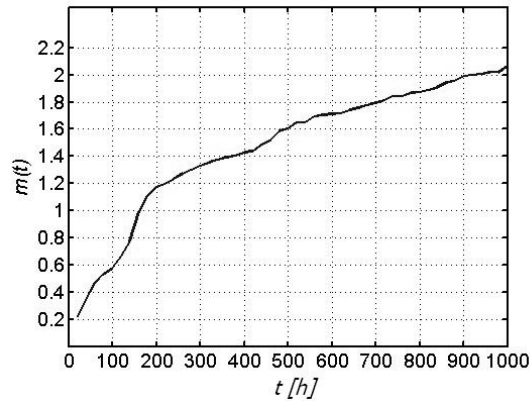


Fig. 1 The mean value of Poisson process (statistic estimation)

We can see, that the first part of the function (from 0 to 220 hours) it is non-linear – non-homogenous Poisson process with non-stationary increases. Second part, in time interval 220 – 1000 hours, better in time interval 500 – 1000 hours is possible to approximate with a line. This is a homogenous Poisson process with stationary increases of failures.

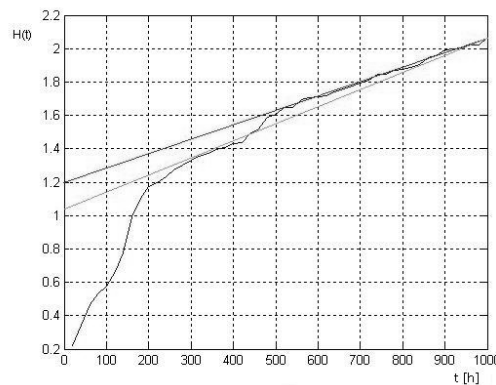


Fig.2 Renewal function $H(t)$ obtained from the experiment
(blue curve), $t \geq 500$ h – red line, $t \geq 200$ h – green line

Homogeneity of dispersion $D(t)$

We used input data from homogeneity testing of mean value $m(t)$.

Estimation of dispersion $D(t)$

We calculated coefficient $\hat{\delta}_D(t)$. The value of this coefficient fluctuated in whole time interval (0, 1000 hours) in range of values $\langle 0,00000, 0,07819 \rangle$. It means the Poisson process realized with the determined experiment is homogenous with dispersion $D(t)$.

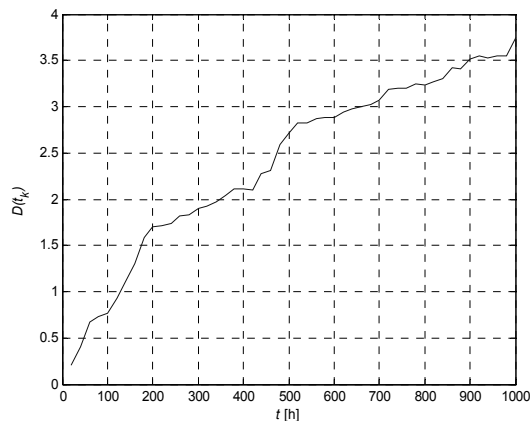


Fig. 3 The dispersion of Poisson process (statistic estimation)

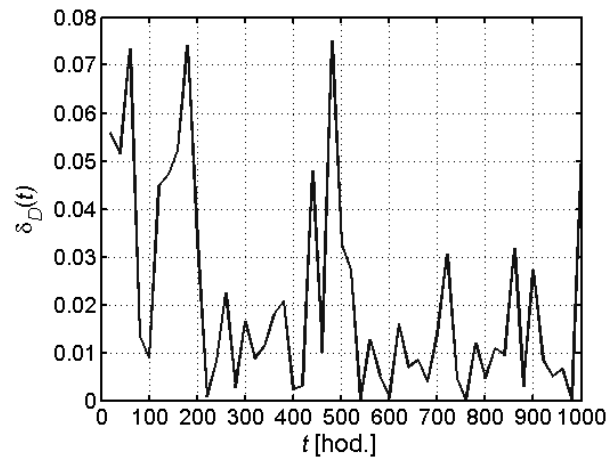


Fig.4 Criterion $\hat{\delta}_D(t)$

Conclusion

Unconventional reliability growth models of electronic devices (hardware) are very specific tools used during development phase. We verify algorithms of new unconventional models on data from a real reliability test of electronic devices.

The advantage of a new reliability growth model is the simplicity of processing the results of an experiment, simple calculation and authentic results if the number of tested electronic devices is sufficient (minimum 30).

In this paper we have published new unconventional reliability growth models of electronic systems for which verification has confirmed their eligibility for use in engineering practice.

We have also results from reliability growth model algorithm based on Poisson process homogeneity testing of density of probability distribution $f(t)$ in time t [1, 2].

However there are some unconventional reliability growth models, which are in the process of further research. At this moment we cannot confirm their accuracy. Specifically, this is the unconventional reliability growth model based on the Poisson process homogeneity testing of the correlation function $R(t_1, t_2)$, and the unconventional reliability growth model based on testing the homogeneity of the Poisson process in its time-frequency representation. [1, 2].

Acknowledgment

The research described in the paper was financially supported by VEGA 1/0987/12 grant. New design approaches for VLSI implementations of neurochips and their use for signal processing in bioapplications and neuroimplants, by the Slovak Ministry of Education.

References

- [1] Z. Krajcuskova : Reliability Growth Models. Work for dissertation exam. SUT, Faculty of Electrical Engineering and Information Technology, Bratislava, 2006.
- [2] Z. Krajcuskova : Unconventional Reliability Growth Models. PhD. Thesis, SUT, Faculty of Electrical Engineering and Information Technology, Bratislava 2008.
- [3] E. Parsen : Stochastic Processes, Holden-Day, San Francisco, 1962
- [4] M. Majzinov supervisor group of authors : Cislennyje metody analiza sluchajnyh proceseiv, izd. Nauka, Moskva 1976
- [5] P.V.N. Prasad, K.R.M. Rao : Reliability Models of Repairable Systems Considering the Effect of Operating Conditions. In Proceedings Annual Reliability and Maintainability Symposium, 2002, pp.503-510.
- [6] Z. Krajcuskova : New Unconventional Reliability Growth Model. In Proc. Of 20th International Czech-Slovak Scientific Conference "RADIOELEKTRONIKA 2010", Brno, Czech Republic, April 2010, p.97-100.

ENERGY BALANCE OF HYBRID SOLAR HEATING AND COOLING SYSTEM

Stanisław Gil¹, Bogusław Gradoń¹, Wojciech Bialik¹

¹Group of Process Energy, Department of Metallurgy,
Silesian University of Technology, 40-019 Katowice, Krasińskiego 8, Poland

Keywords: hybrid solar system, heating, cooling, energy-efficient building.

Abstract. At present, buildings in the European Union countries account for approximately thirty percent of the total primary energy consumption. However, due to the economic development, the energy demand for heating and electricity constantly increases. The need for environmental protection results in searching for new solutions in the use of alternative and renewable energy sources. In the paper, results of the analysis of a hybrid solar-assisted heating and cooling system for buildings in the temperate climate conditions of West and Central Europe are presented. The system consists of an evacuated solar collector coupled with a single-stage NH₃-H₂O absorption chiller. The impact of the main system parameters on its effectiveness was analysed on the basis of the energy balances.

Introduction

Predicted global warming [1] and architectural tendencies reflected in the use of large, glazed surfaces of building front elevations let us expect that the need for both heating and cooling systems will increase in the nearest future. Currently, the most common cooling systems are based on electricity supplies. Depending on climate conditions, it is estimated that 30 to 50% of the global electricity production is used for air conditioning and cooling purposes [2]. The alternatives are thermal technologies. Their advantage is a potential for utilization of waste heat and solar energy sources with the latter one in particular having been intensively analysed and developed in recent years.

Among thermal technologies currently used for cooling purposes, there are generally two primary types [3-9] technologies with a closed circuit and so-called open circuits. In closed circuits, heat is transported via chillers where typically water is cooled and used in further parts of the installation for ventilation air conditioning. There two most commonly used types of chillers: chillers with liquid sorbents operating through dissolution and absorption, chillers with solid sorbents where adsorption phenomena are utilized. In absorption chillers, the following two pairs of working medium/sorbent are normally used: H₂O/LiBr and NH₃/H₂O. The coefficient of performance depends on the temperature of the "driving" heat source and reaches about 0.7 for single-stage cycles (with one desorber) and up to approximately 1.3 for two-stage cycles (with two desorbers) [7]. In adsorption chillers, the most common sorbent is silica gel.

Open circuits are also called dry- evaporative cooling systems with a combination of a cooling process during moisture evaporation and an air drying process through contact with a desiccant. The most frequently used desiccants are solids (silica gel, lithium chloride) placed in a rotating drum. The desiccant is regenerated through contact with ventilation air evacuated from the installation and the heat stream from the solar collector or another 'driving' heat source. Also, the use of liquid desiccants is investigated with regard to some of their advantages: a potential for more extensive air drying at lower regeneration temperatures and the use of sorptive materials for heat storage [7]. The following compounds are taken into account: lithium chloride (LiCl), calcium chloride (CaCl₂), lithium bromide (LiBr) and triethylene glycol [10]. The coefficients of performance for open circuits are 0.6 to 1.2 [11]. Two following concepts are also being investigated [10]: thermomechanical chillers and steam jet ejector chillers.

According to the 2006 data, in the mid-decade there were 70 solar collector systems in Europe – mostly in Germany (about 27) and Spain (about 19) [8, 11]. The total cooling capacity was 6.3 MW, and the total surface area of collectors was about 17500 m². In the majority of installations (59%), closed absorption circuits are used, while the others are [11]: 11% – closed adsorption circuits, 23% – open circuits with a solid dryer, 7% – circuits with liquid desiccants. They are mostly small, often mass-produced installations designed for small residential buildings or selected premises in commercial buildings. There are significantly fewer large installations requiring a specific, individual design [7, 12].

A comprehensive installation operating in the temperate climate should provide controlled heat supplies intended for all-year domestic hot water heating, seasonal central heating and cooling purposes during the hottest summer months. Utilization of solar heat with reasonable collector surface areas is limited in these conditions due to insufficient heat stream values in autumn, winter and spring. A possible coverage of heat demand with regard to thermal installations used for cooling purposes during summer months also needs further investigations. A solution is a hybrid system where heat is gained partially from the solar energy and partially from a conventional heat source, e.g. fossil fuel or biomass combustion processes.

In the paper, the project and results of a preliminary energy performance analysis for an experimental installation containing a solar collector and a single-stage absorption chiller are presented.

Installation

A general scheme of the installation is presented in Fig. 1. It contains three major modules: a heat gain module, a water heating module and an absorption chiller. The key component of the heat gain module is a Vaciosol CPC12/CPC6 vacuum tube collector comprised of ten tubes with the total active surface area of 0.91 m². The heat medium is a 33% (wt.) solution of Henock blue ethylene glycol. The glycol flow rate is 1.67·10⁻⁵ m³/s. Based on the preliminary experiments, the efficiency of solar energy conversion to thermal energy in the collector system is 62%. Due to an adequate valve system, the entire heat can be provided to a selected module or it can be divided. The domestic hot water heating module contains a 0.02 m³ tank with an immersed heat exchanger. The circulation medium in the cooling system is a 35% (wt.) aqueous NH₃ solution. The chiller is used for air cooling with a ventilator-forced flow. A general scheme of the cooling system is shown in Fig. 2.

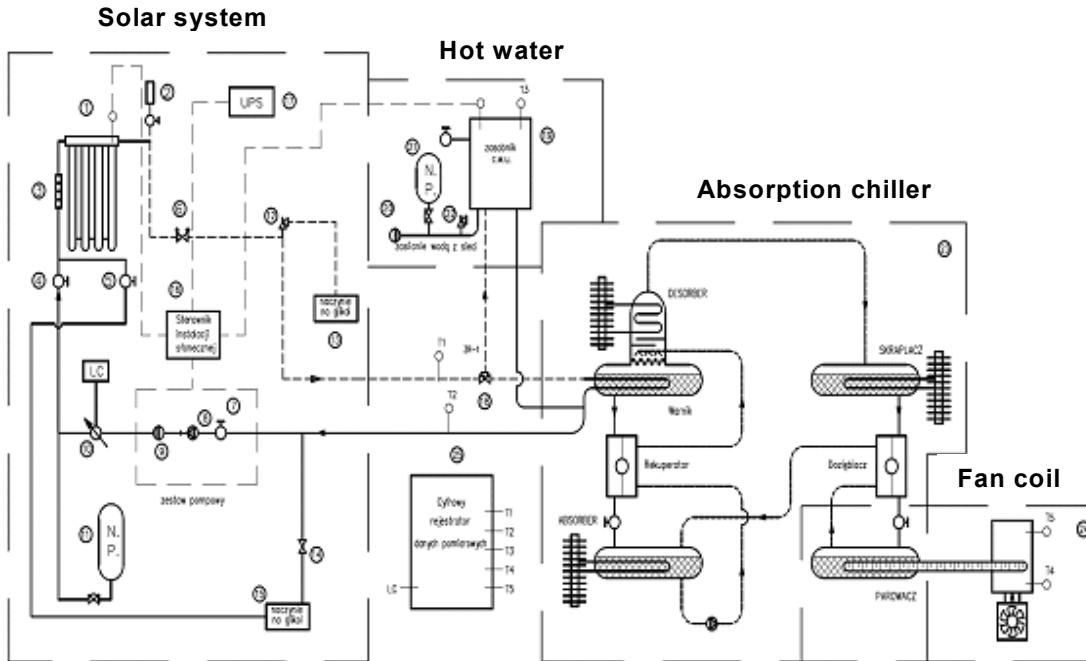


Fig. 1. Scheme of the research installation

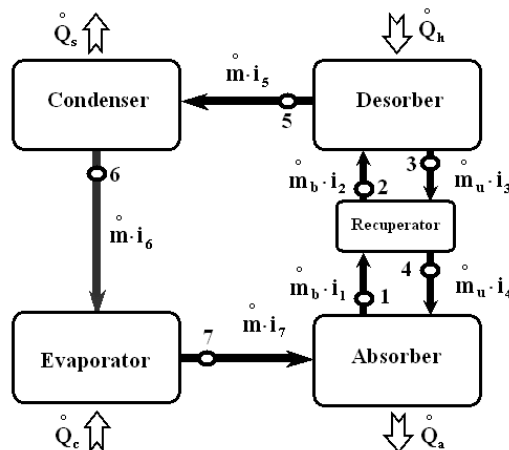


Fig. 2. Scheme of the chiller

Energy analysis

The energy performance analysis was performed based on the energy balances of individual components of the system: the energy balance of the solar energy system

$$\dot{Q}_k = A_k \cdot [\tau \cdot \alpha \cdot \dot{e} - k_1 \cdot (T_{ab} - T_{ot}) - k_2 \cdot (T_{ab} - T_{ot})^2] \quad (1)$$

where: \dot{Q}_k is a heat stream from the collector, A_k is the collector surface area, τ is the coefficient of permeability for the collector cover plate, α is the solar absorption coefficient for the absorption coating, \dot{e} is a solar energy stream, k_1 is a linear heat transfer coefficient, T_{ab} is the temperature of absorber, T_{ot} is the ambient temperature and k_2 is a non-linear heat transfer coefficient; the energy balance of the domestic hot water heating system

$$\eta_w \cdot \dot{Q}_w = \dot{V}_w \cdot \rho_w \cdot c_w \cdot \Delta T_w \quad (2)$$

where η_w is the system performance, \dot{Q}_w is a heat stream supplied to the system, ρ_w is water density, c_w is the specific heat of water and ΔT_w is a value of water temperature rise;

a general energy balance of the cooling system

$$\dot{Q}_h + \dot{Q}_c = \dot{Q}_s + \dot{Q}_a \quad (3)$$

where individual symbols denote the heat streams shown in Fig. 2;

the energy balance of the desorber-recuperator system

$$\dot{Q}_h = \dot{m} \cdot [i_5 + (f-1) \cdot i_4 - f \cdot i_2] \quad (4)$$

where \dot{Q}_h is a heat stream supplied to the desorber from the collector or another heat source, \dot{m} is a mass stream of the working medium (NH_3), f is the multiplicity of the circuit medium recirculation and i_2, i_4, i_5 are specific enthalpies in points presented In Fig. 2;

the energy balance of the absorber

$$\dot{Q}_a = \dot{m} \cdot [i_7 + (f-1) \cdot i_1 - f \cdot i_3] \quad (5)$$

where \dot{Q}_a is a heat stream evacuated from the absorber, \dot{m} is a mass stream of the working medium (NH_3), f is the multiplicity of the circuit agent recirculation and i_1, i_3 are specific enthalpies in points presented In Fig. 2;

the energy balance of the condenser

$$\dot{Q}_s = \dot{m} \cdot (i_5 - i_6) \quad (6)$$

where \dot{Q}_s is a heat stream evacuated from the condenser, \dot{m} is a mass stream of the working medium (NH_3), f is the multiplicity of the circuit agent recirculation and i_5, i_6 are specific enthalpies in points presented In Fig. 2;

the energy balance of the evaporator

$$\dot{Q}_c = \dot{m} \cdot (i_7 - i_6) \quad (7)$$

where \dot{Q}_c is a heat stream collected from the cooled air, \dot{m} is a mass stream of the working medium (NH_3), f is the multiplicity of the circuit agent recirculation and i_6, i_7 are specific enthalpies in points presented In Fig. 2.

The coefficient of the performance with regard to the cooling system is described by the relationship:

$$COP = \dot{Q}_c / \dot{Q}_h \quad (8)$$

In Fig. 3, the values of unitary heat streams gained from a unit of the collector surface area (q_k) during selected months versus the values of unitary solar energy streams (\dot{e}) supplied to the collector are presented. In the Eastern and Central European climate, the best conditions for solar energy gain occur only from May to August (300 W/m^2 on average).

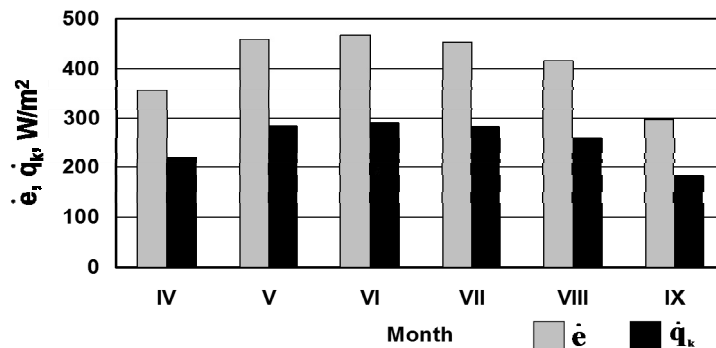


Fig. 3. Unitary solar energy stream (\dot{e}) and heat from the collector (q_k) values

The effect of the air stream size in the cooling system on its outlet temperature rise is presented in Fig. 4. In the calculations, a constant evaporator surface temperature of 253 K was assumed. For the stream change of 0.003 to 0.01 kg/s, the cooling air temperature increased by approximately 12 K.

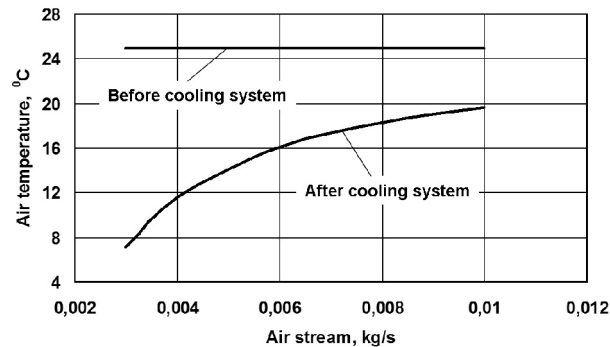


Fig. 4. The effect of the stream size on the cooling air temperature rise

Conclusion

A laboratory installation for heating and cooling purposes was designed and constructed where the thermal cooling technology coupled with a solar collector is used. The preliminary experiments as well as the energy performance analysis were performed based on the balances of the masses and substances of the individual system components. The estimated coefficient of performance with regard to the cooling process was 0.45. Further systematic experimental studies will be conducted.

Acknowledgments

The installation was designed and constructed within the research project PBS 5/RM1/2010 supported by the Polish National Centre for Research and Development.

References

- [1] Fourth Assessment Report. Intergovernmental Panel on Climate Change, 2007.
- [2] Fong K.F., Chow T.T., Lee C.K. Lin Z., Chan L.S.: Comparative study of different solar cooling systems for buildings in subtropical city. *Solar Energy*, 84, (2010), 227-244.
- [3] Balaras C.A., Grossman G., Henning H.M., Infante Ferreira C.A, Podesser E., Wang L., Wiemken E.: Solar air conditioning in Europe – an overview. *Renewable & Sustainable Energy Reviews*, 11, (2007), 299-314.
- [4] Desideri U., Proietti S., Stringola P.: Solar-powered cooling systems: Technical and economic analysis on industrial refrigeration and air-conditioning applications. *Applied Energy*, 86, (2009), 1376-1386.
- [5] Murphy P. (editor): IEA Solar Heating and Cooling Programme, 2010 Annual Report, April 2011.
- [6] Eicker U.: *Solar Technologies for Buildings*. Wiley 2003.
- [7] Henning H.M.: Solar assisted air conditioning of buildings – an overview. *Applied Thermal Engineering*, 27, (2007), 1734-1749.
- [8] Qu M., Yin H., Archer D.A.: A solar thermal cooling and heating system for a building: Experimental and model based performance analysis and design. *Solar Energy*, 84, (2010), 166-182.
- [9] Venegas M., Rodriguez-Hidalgo M.C., Salgado R., Lecuona A., Rodriguez P., Gutiérrez G.: Experimental diagnosis of the influence of operational variables on the performance of a solar absorption cooling system. *Applied Energy*, 88, (2011), 1447-1454.
- [10] IEA, Solar Heating and Cooling Programme, Task 38: Solar Air-Conditioning and Refrigeration, C1: State of the art – Survey on new solar cooling developments, technical report, 31 October 2010.
- [11] Núñez T.: Technology and Literature Review. PolySMART Project, Work Package 1, final report 2010.
- [12] Henning H.M.: Solar Air-Conditioning and Refrigeration. Feature Article in: Murphy P. (editor): IEA Solar Heating and Cooling Programme, 2010 Annual Report, April 2011.

SYNTHESIS OF A FUZZY MODEL FOR THE PLANT PROTECTION SYSTEM IN THE APPLE ORCHARD

P. Berk¹, D. Stajniko¹, M. Lakota¹, P. Vindiš¹, J. Rakun¹

¹ University of Maribor, Faculty of Agriculture and Life Sciences,
Pivola 10, 2311 Hoče, Slovenia

Keywords: automation, fuzzy logic, synthesis, plant protection

Abstract. Application of plant protection products takes place with today's machines in optimal weather conditions, evenly and without a controlled application across the vineyard, orchard or corn field. With increasing use of chemical preservatives (insecticides), that have harmful effects on human health, we can automate the process of coating with the help of different machines which reduce negative impacts. Doses of the plant protection product should be adjusted, depending on the amount of vegetation. Therefore we developed an application of the synthesis of a fuzzy controller coating plant protection system, which works with the help of pulse width modulation and intensity measurements of the ultrasonic echo signals reflected from the tree canopy. Based on the thresholds of the measurements produced by ultrasonic sensors, we control both on and off states of the solenoid valves of the standard fruit – wine dispenser. Synthesis of fuzzy controller was realized with a laptop HP Compaq 6830s NA779ES, Matlab/Simulink 2011b simulation software package, spraying components and target expansion card. Using the simulation program Matlab/Simulink/FIS we simulated the operation of the application process for the coating plant protection on the selected parts of the tree canopy (below, in the middle, above).

Introduction

With development of the chemical industry has developed a range of synthetic products to ensure appropriate protection of plants against pests. Knowledge about the effects of chemical substances on humans and the environment behind the use of, so that the observed temporary and permanent negative impacts on the environment, and even poison the people. General environmental awareness is roused only in the eighties of the 20th century, since then it has changed the uncritical attitude to the use of plant protection (PP, also called pesticides).

The main goal of our project is to develop a modular system for the controlled application of plant protection products on the target surface in a tree orchard space habitat. The system consists of three units, namely the propulsion plant, orchard sprayer and control upgrades [2]. The system will provide the intended application of optimal amounts of plant protection products as a function of distance, size and density of trees of their leaves treated at a single site. This will reduce consumption and removal of plant protection products with equal efficiency. With this will be achieved reducing of an environmental burden (soil, groundwater, air, plants) with plant protection and energy consumption for the implementation of the action (this has also reduced the environmental impact of greenhouse gases). Testing of a modular system will be held at the Faculty of Agriculture and Life Sciences, where we evaluated the reduction of risks and impacts of pesticides on human health and the environment (uncontrolled application of pesticides) and to introduce an integrated production plant, which primarily involves alternative techniques by means of a soft logic system in collaboration with the project team from the Agricultural Institute of Slovenia, Agricultural Engineering Department and Laboratory of Agricultural Engineering, Jable in the Trzin. In the project so far we have made the synthesis of a model applications, providing automated application using fuzzy logic controller, through which we control solenoid valves. The model will serve as a basis for drawing up the final real model. Automated techniques in the field of the PP also meet the following major areas of application which are summarized in the following bullet points.

- One of the key issues in crop protection products to be applied in tree crops is the dose rate adjustment [1]. An inappropriate dose selection could be responsible of the lack of efficacy due to under dosage and a loss in efficiency due to over dosage. Both situations imply economical losses and greater impacts on the environment. A better dose adjustment is possible from a variable rate technology approach [4] by measuring the crown volume and adjusting the dose rate on-the-go according to the variation of the estimated vegetation volume. Tests have been done with a variable rate sprayer prototype and satisfactory results have been achieved.
- Two different application methods were compared in three vine varieties at different crop stages. A conventional spray application with a constant volume rate per unit ground area ($1 \cdot \text{ha}^{-1}$) was compared with a variable rate application method designed to compensate electronically for measured variations in canopy dimensions [3]. An air-blast sprayer with individual multi-nozzle spouts was fitted with three ultrasonic sensors and three electro-valves on one side, in order to modify the emitted flow rate of the nozzles according to the variability of canopy dimensions in real time. The purpose of this prototype was to precisely apply the required amount of spray liquid and avoid over dosing. On average, a 58 % saving in application volume was achieved [3] with the variable rate method, obtaining similar or even better leaf deposits.
- The research aims to demonstrate the basic system elements of a prototype automated orchard sprayer, which can deliver pesticide spray selectively with respect to the characteristics of the targets [2]. The contour of the apple tree canopy was detected by ultra sound sensors Prowave 400EP14D and appropriate electronics. Ultra sound signal was processed by a personal computer and fed in real-time to spraying nozzles which open and close in relation to the canopy structure. The current project focuses on developing the system components for spraying an individual tree [2]. The evaluation was performed in field experiments by detecting deposits on leaves and water sensitive papers (WSP). The demonstrated concept of precise application of pesticide sprays supports a decrease in the amount of delivered spray, thereby reducing both costs and environmental pollution by plant protection products.

Materials and Methods

To build a realistic model that will serve for the automated application of pesticides on selected trees canopy were selected components of the standard fruit growers spray of a vineyard (on the dispenser are installed nozzle type Lechler, labeled TR-80-015C, and TR-80-02C) with the air rectifier (Figure 1) and up to, that it is possible to upgrade the electronic control electromagnetic valves through specific microcontrol target unit LPC1343 (Figure 2), circular route for the simulation of spray passage past the tree (Figure 3), data on the size and leaf surface habitat for the synthesis of fuzzy controller for controlling solenoid valves were obtained through ultrasonic sensors PROWAVE 400EP250 in the form of numeric values in the range of [0-600], which representing the intensity of the reflected signal.

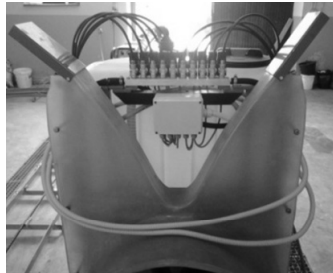


Fig. 1 Vineyard fruit growers sprayer

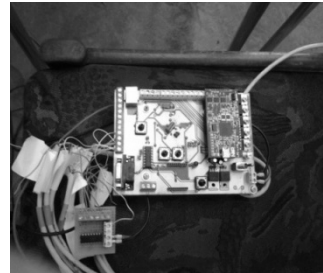


Fig. 2 Target microcontrol unit LPC1343



Fig. 3 Circular route to simulate the sprayer transition



Fig. 4 The system of ultrasonic sensors

Synthesis applications of the pesticides process in a selected parts of the tree canopy (lower, middle, above) in the apple orchard (Figure 5) was made using the fuzzy logic model (Figure 6), which is controlled solenoid valves, through which we are opening and closing of individual nozzles on the fruit- wine sprayer via pulse width modulation. Pulse width modulation for time opening and closing of solenoid valves in the interval of [0-1] second was made by block Subsystem (Figure 6). In the Subsystem block with help of the Simulink block we built logic for pulse width modulation. Interval [0-1] seconds were selected according to the size of canopy trees in our case crown width (Figure 3) was no more than one meter, the speed of simulation of transition and spray was no more than 1 m / s, so we have fixed terms that nozzles can be controlled by the solenoid valves open via a second peak. Maximum nozzle opening occurs in the case of the total intensity of the reflected signal from the ultrasonic sensor, whose numerical value is 600.

Fuzzy logic model, we started so we used the effective fuzzy logic tools in Matlab/Simulink [7], where we first made the synthesis process of the PP with the help of fuzzy logic controller. For input and output fuzzy controller, we chose the same membership functions; M (a little), S (middle), V (a lot), MOV (small open solenoid valve), SMS (medium open solenoid valve) and VOV (large open solenoid valve). We first started with development of the Simulink software package model, which was later used to start the application of pesticides simulation process, on selected parts of the trees canopy. We have drive a software package MATLAB/Simulink and create a new file. In the simulink we started to build the model using the block system shown in Figure 6 below.

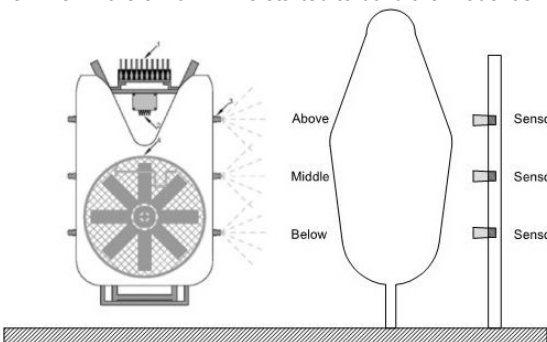


Fig. 5 Application process PP

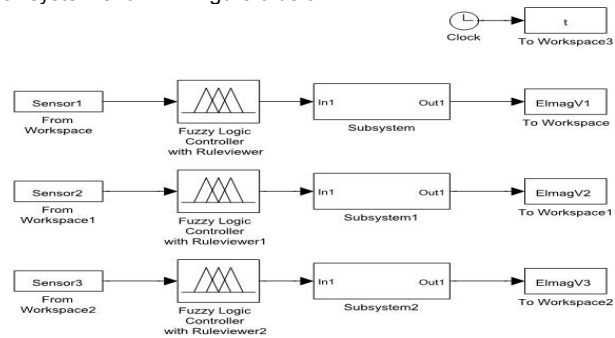


Fig. 6 Application process model of pesticides in the Matlab/Simulink

Once we have identified throughout the process we started to design fuzzy logic controller. Fuzzy logic controller was planned with the help of fuzzy logic inference system (FIS). Therefore, we need to open a new file with the FIS Editor [5], where we entered the programming environment MATLAB code << fuzzy, which represents the fuzzy inference system editor. With the help of FIS editor, we can define input and output membership functions, defined the basic rules and terms of soft operators fuzzy controller.

Default inference system has one input and one output, and uses Mamdani inference. Editor shows the three aspects of fuzzy control: fuzzification, inference and defuzzification, [6]. At the beginning we define membership functions. We have defined the membership functions (Figure 7) of a input variables (Sensor 1, Sensor 2 and Sensor 3), which are characterized by M (a little), S (middle) and V (high). Membership functions had trapezoidal shape, which was selected in the FIS Editor, the shape of membership functions can be arbitrarily selected in the editor of FIS arbitrary function. Reference area can be arbitrarily defined in the editor, where we have defined the reference range input variables that represent the total intensity of the reflected signal via ultrasonic sensors in the range [min: 0 - max: 600]. For membership function which was marked by M is equal to the reference area parameters [0 0 150 200], which gives us a peak. Parameters area membership marked function S is equal to [150 250 350 450] and for membership function marked by V [400 450 600 600]. In the editor for the determination of membership functions we can also define the membership functions (Figure 8) of the output variables EI-MA-V1 (solenoid valve 1), EI-mag-V2 (solenoid valve 2) and EI-MA-V3 (solenoid valve 3) . We define the output variable membership functions (EI-MA-V1, EI-mag-V2, EI-MA-V3), which was marked by MOV (small open solenoid valve), SMS (medium open solenoid valve) and VOV (large open solenoid valve). Membership functions had trapezoidal shape, which was chosen in teh FIS editor, the shape of the membership functions can be arbitrarily selected in the editor FIS during any other function. For membership function which was marked by the MOV, amounted parameters in a reference range [0 0 150 200], which gives us a peak. Parameters area membership marked function SMS is equal to [150 250 350 450] and the membership function VOV [400 450 600 600]. Reference area output variables are defined in the range [0 - 600].

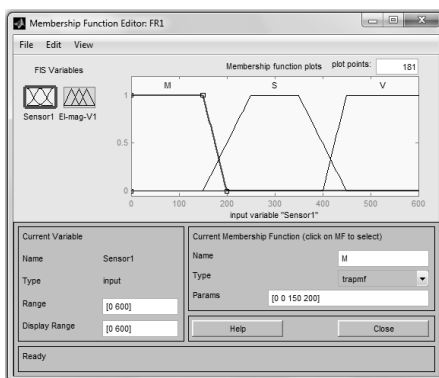


Fig. 7 Membership functions of input variables

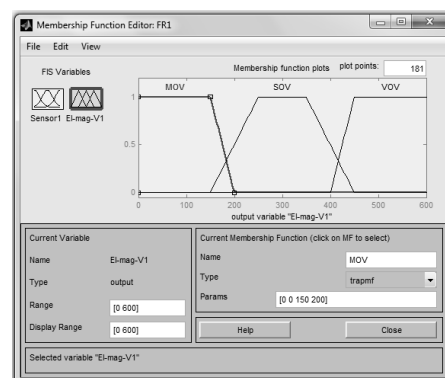


Fig. 8 Output variables membership functions

With the help of FIS were determined the rules (Figure 9). With the help of the rules editor we write the rules of membership linguistic variables. The rules are defined using fuzzy membership functions M, S, V, and MOV, SMS, VOV. For the entry rules we have selected the option of a conditional sentence" if" option" and then". In our system we used for the first three rules of fuzzy controller: 1 If (Sensor1 is M) then (EI-MA-V1 is MOV), 2 If (Sensor1 is S) then (EI-MA-V1 is SOV), 3 If (Sensor1 is V) then (EI-MA-V1 is VOV). For the other two fuzzy controller we chose the same rules. After finishing down the rules we exported the inference system in a Simulink Model. You can then run the simulation in Simulink where Viewer window appears with the rules (Figure 10).

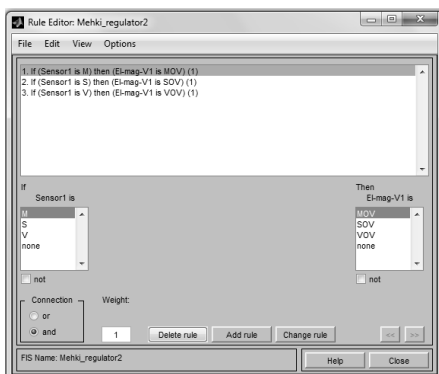


Fig. 9 Editor fuzzy inference rules system

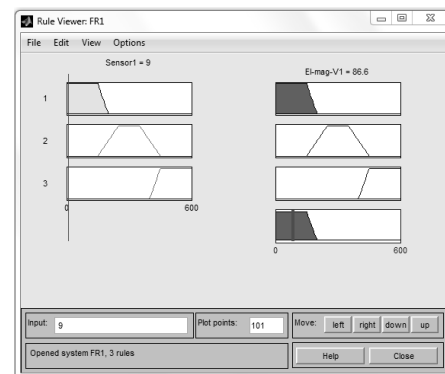


Fig. 10 Display fuzzy inference rules system

The display shows the relevant rules of the input and output membership functions, for each rule. For a given input who be modified by means of inferential membership output function is described by a blue color (Figure 10). This is the result of fuzzification (softening). When the numeric value of the input variables (sensor1) is an active one common rule and membership functions is the same. Default sharpening process (defuzzification) used a centroid method and the red line (Figure 10) indicates where the center of gravity is, which is then illustrates by numeric value of output variables.

Results

In the end we made a comparative analysis between conventional and automated implementation synthesis application of pesticides in selected parts of the tree habitat using fuzzy logic and the ultrasonic sensors through which we get the size of the canopy reflectance intensity of habitat in the form of numeric values. For our example we did an analysis for the case of application of pesticides namely the position of the Above (Figure 5), where we include data from Sensor1 that the actuators nozzle type Lechler, labeled TR-80-015C. We made a synthesis example of application of pesticide in the interval of [0-5] seconds. In this interval we get a sequence of signals from Sensor1 in the form of numeric values (intensity of the echo signals from the habitat canopy), Figure 11.

Based on the sequences obtained from signal Sensor1 we have made the synthesis application process of pesticides on a selected parts of the tree canopy (above) in the apple orchard (Figure 5), through the fuzzy logic model (Figure 6) which is controlled by solenoid valves, to help which will be opened and closed each nozzle on the the vineyard orchards sprayer through pulse width modulation. The graph in Figure 12 shows the pulse width control solenoid valve via fuzzy logic system, for example of pesticide application through the nozzle type Lechler.

In the case of classical synthesis applications of pesticides application on canopy habitat (above), we considered that the type of nozzle Lechler, at intervals of 1 second is constantly opened. Therefore we take a numeric value of 100% for the case where the nozzle is in the interval [0-1] second a constant opened. In the case of synthesis applications of automated application of pesticides (Figure 12) we found that this value is smaller, namely for our sequences characterized by a solenoid valve for an application of pesticides (above) according to the numerical values of input and output variables of a fuzzy controller (Figure 10) in the interval [0-1] seconds, average percentage open 14.43%.

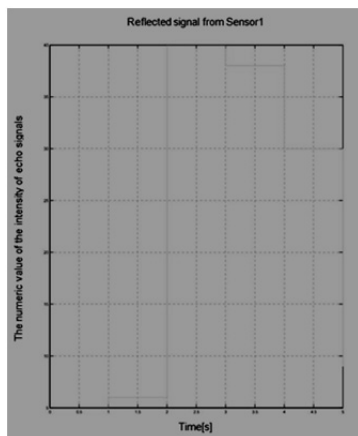


Fig. 11 Reflected signal from Sensor1

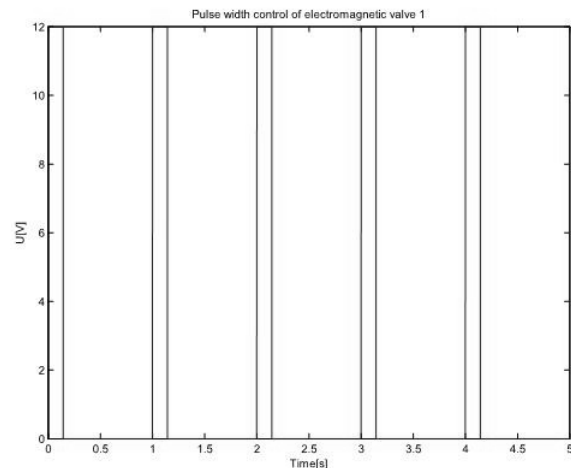


Fig. 12 Pulse width control El-mag-V1

Percentage values in our case varied from 0 to 100% (in the case of maximum intensity of reflection from the canopy of trees). Looking at Figure 3, we can see that we take for example canopy habitat (above), which is not as lush, this result is that the solenoid valve which is controlled by pulse width is not too open.

Conclusion

The results show that fuzzy logic is useful in applications for automated application of pesticides in selected parts of the tree canopy, where usually the classical method of constant direct application not be a satisfactory outcome. Fuzzy logic controller system (FLC) allows the user to use their own knowledge about the problem and transfer it to the appropriate system environment, which is close to the human way of thinking. Since this is a more complex task than just inserting a few control parameters, we used a specific user interface (FIS) for the design of FLC applications. Fuzzy controller is in the control process application of the electromagnetic valve proved to be a very good choice since the FLC design procedure relatively simple and suitable for engineering practice.

Acknowledgment

Modern approach to the implementation of control systems requires the use of development tools for rapid development time (fast prototyping). One such tool is a simulation tool (Matlab/Simulink R2011b) in which we have made the synthesis of application process of pesticides model on selected trees, where we are using target LPC 1343 microcontrol units in performed measurements via ultrasonic sensors. In the near future we will do an automated process control solenoid valves which will run in real time.

When designing fuzzy controller, we take advantage of simulation tools a Matlab and associated tools for analyzing real-time simulation results. If the simulation results were not satisfactory, we process modeling-simulation-analysis repeated until we get the desired response. In the EUREKA project we would like to thank Agricultural Institute of Slovenia, Agricultural Engineering Department and Laboratory of Agricultural Engineering, Jable in the Trzin .

References

- [1] A. Escolà, F. Camp, F. Solanelles, J. Llorens, S. Planas, J.R. Rosell, F. Gràcia, E. Gil and L. Val: Variable dose rate sprayer prototype for dose adjustment in tree crops according to canopy characteristics measured with ultrasonic and laser lidar sensors, "ECPA-6th European Conference on Precision Agriculture", Skiathos: 2007, pp. 563-571.
- [2] V. Jecic, T. Godesa, M. Hocevar, B. Sirok, A. Malneric, A. Strancar, M. Lesnik and D. Stajniko: Design and testing of an ultrasound system for targeted spraying in orchards, *Stroj. vestn.*, Volume 57 (2011), Issues 7-8, p. 587-598.
- [3] J. Llorens, E. Gil, J. Llop and A. Escolà: Variable rate dosing in precision viticulture: use of electronic devices to improve application efficiency, *Crop protection*, Volume 29 (2010), Issue 3, p. 239-248.
- [4] P. Balsari, G. Doruchowski, P. Marucco, M. Tamagnone, J. Van de Zande and M. Wenneker: A System for Adjusting the Spray Application to the Target Characteristics, *Agricultural Engineering International (2008)10*, ISSN 1682-1130, p. 12.
- [5] P. Berk, D. Stajniko, P. Vindis, B. Mursec and M. Lakota: Synthesis water level control by fuzzy logic, *J. Achiev. Mater. Manuf. Eng.*, Volume 45 (2011), Issue 2, p. 204-210.
- [6] D. Dzonlagic: *Basics of the design of fuzzy control systems*, (Faculty of Electrical Engineering and Computer Science, Maribor, second edition, 1995).
- [7] *** (2001), http://courses.washington.edu/css457/matlab/learning_matlab.pdf-The Mathworks, MATLAB student version, Accessed: 2012-01-07

ROBUST COMMAND FOLLOWING CONTROL IN THE ROBOT JOINT SPACE

J. Kardoš¹

¹ Institute of Control and Industrial Informatics, Faculty of Electrical Engineering and Information Technology,
Slovak University of Technology in Bratislava, Ilkovičova 3, 812 19 Bratislava, Slovak Republic

Keywords: variable structure control, reaching law, robot motion control, tracking accuracy

Abstract. The goal of this contribution is the synthesis of a robust, reliable and easily implementable control algorithm for the accurate tracking of a desired trajectory in a robot joint space. Theoretical background of the presented command following control strategy is given by the theory of variable structure control (VSC). The accuracy of the trajectory tracking is assured by the control parameter synthesis in frequency domain. The resulting control algorithm represents a continuous control law taking both the actuating variables boundary and the system's dynamic parameters limitation into account. Matlab simulation on the 3-DOF robot dynamic model verifies the quality and feasibility of the provided control.

Introduction

The accurate tracking of desired joint variables or commands in robotic systems with multiple degrees of freedom represents a complex MIMO control task coping with the significant parametric uncertainty of the system, the strong influence of coupling and external forces, as well as with the requirement of a strictly prescribed motion quality specified by the actual technological task. Robust control techniques, particularly the *variable structure control* one [1], give a promising solution to this problem. An important advantage of the provided approach is the *decoupling* of a MIMO dynamic system to a set of independent SISO systems corresponding with the individual DOFs controllable via a simple and reliable algorithm. Thus, any coupling forces among the DOFs are treated as the external disturbances. Moreover, in robust control algorithm design, only the amplitudes of signal disturbances (e.g. in motion control system the amplitudes of Coriolis, centrifugal, gravitational and coupling forces) and the boundary values of variable parameters (e.g. the boundary values of moment of inertia variation) – i.e. neither the frequency spectra nor the time history of signals or parameters – are utilized, which radically simplifies the process of synthesis.

The tracking capability analysis of the controlled plant can be viewed as a keystone of the command following control design. In this contribution, to establish the tracking capability of the robot under the variable structure control, the phase velocity vector approach [2] has been utilized. The outcome of this original analysis method is the value of the control signal maximal frequency the controlled system subjected to the given dynamic boundary can cope with.

Variable structure control belongs to the discontinuous control algorithms suffering from the undesirable *chattering* (low-frequency oscillation of the system's actuating and state variables) in real control systems applications [3]. Caused by the discontinuous nature of VSC, the chattering arises due to presence of parasitic (unconsidered) non-linearities and dynamics in any real dynamic system. To deal with the chattering phenomenon, the reaching law approach [4, 5] has been applied. This yields the *continuous approximation* of the originally discontinuous control algorithm, and therefore the chattering elimination, without the loss of control robustness and quality. An additional benefit of the reaching law utilization is the applicability of the command following control parameter synthesis in frequency domain ensuring an acceptable tracking accuracy for the given frequency spectra of a reference trajectory.

MIMO system description and decoupling

Mathematical description (based on the Euler-Lagrange formalism) of a multi-DOF robot with n degrees of freedom yields the second order matrix differential equation [6]

$$\mathbf{J}(\mathbf{q})\frac{d^2\mathbf{q}}{dt^2} = \boldsymbol{\tau} - \mathbf{B}\frac{d\mathbf{q}}{dt} - \mathbf{c}\left(\mathbf{q}, \frac{d\mathbf{q}}{dt}\right) - \mathbf{g}(\mathbf{q}), \quad (1)$$

where $\mathbf{q} = \mathbf{q}(t) \in \mathcal{R}^n$ represents the vector of generalized coordinates, $\boldsymbol{\tau} \in \mathcal{R}^n$ denotes the vector of driving torques, $\mathbf{J}(\cdot) \in \mathcal{R}^{n \times n}$ stands for the inertia matrix, $\mathbf{B} \in \mathcal{R}^{n \times n}$ refers to the diagonal matrix of viscous friction, $\mathbf{c}(\cdot) \in \mathcal{R}^n$ stands for the vector of Coriolis and centrifugal forces and $\mathbf{g}(\cdot) \in \mathcal{R}^n$ stands for the vector of gravitational forces. Considering that the vector of driving torques $\boldsymbol{\tau}$ will be generated by a robust control algorithm, the decoupled dynamic model of a single DOF (the i -th DOF, $i = 1, \dots, n$) corresponds to Eq. (2)

$$j_{ii}(\mathbf{q})\frac{d^2q_i}{dt^2} + B_i\frac{dq_i}{dt} = \tau_i - \tau_{Li}, \quad (2)$$

where q_i , τ_i , $j_{ii}(\cdot)$ and B_i match with the elements of related vectors and matrices in Eq. (1), and

$$\tau_{Li} = c_i\left(\mathbf{q}, \frac{d\mathbf{q}}{dt}\right) + g_i(\mathbf{q}) + \sum_{j=1, j \neq i}^n j_{ij}(\mathbf{q})\frac{d^2q_j}{dt^2} \quad (3)$$

stands for the load (signal disturbance) in the i -th DOF. As can be seen, the latter consists of elements of vectors $\mathbf{c}(\cdot)$, $\mathbf{g}(\cdot)$, and the sum of coupling forces given by the third item in Eq. (3). Similarly to the maximal value of the moment of inertia $j_{ii}(\mathbf{q})$, in robust control algorithm design only the maximal value of the load τ_{Li} is utilized.

Let the desired trajectory in the robot joint space be given by the reference vector $\mathbf{q}_d(t) \in R^n$. Denote $\mathbf{e}_i(t) \in R^2$ the phase error vector of the i -th DOF, i.e.

$$\mathbf{e}_i(t) = \begin{pmatrix} e_i \\ de_i/dt \end{pmatrix} = \begin{pmatrix} q_{di} - q_i \\ dq_{di}/dt - dq_i/dt \end{pmatrix}. \quad (4)$$

The aim of a tracking control is to keep the minimal values of both elements of the phase error vector in each degree of freedom for the whole period of robot motion despite the uncertainty of inertia matrix $\mathbf{J}(\mathbf{q})$ and the variability of the load vector τ_L . This requirement is identical with the requirement of keeping any DOF's state in the closest vicinity of the origin (0, 0) in the phase plane ($e_i, de_i/dt$).

Variable structure control

The well-known common formula for the variable structure control is given by the discontinuous switching law [1, 4]

$$\tau_i^* = M_i \operatorname{sgn}(F_i(\mathbf{e}_i)), \quad (5)$$

where the positive constant M_i stands for the driving torque τ_i boundary and $F_i(\cdot)$ represents the *switching function* stemming from the VSC synthesis. Under the variable structure control Eq. (5), satisfying the *sliding mode existence* condition [1, 3]

$$F_i(\mathbf{e}_i) \frac{dF_i(\mathbf{e}_i)}{dt} < 0 \quad (6)$$

despite the presence of parametric uncertainty and signal disturbances, the system's state doesn't leave the switching manifold given by the zero value of the switching function and remains in sliding mode on it. Thus, the *robustness* of the system is assured.

An inherent feature of the motion system's phase trajectory – that is of considerable importance to tracking control – is its perpendicularity to the e -axis of the phase plane ($e, de/dt$). This implies the fulfillment of condition Eq. (6) in the origin of the phase plane for any linear switching manifold

$$F_i(\mathbf{e}_i) = \frac{de_i}{dt} + k_i e_i = 0, \quad (7)$$

where $1/k_i$ stands for the time constant of the exponential solution of the differential equation Eq. (7). The higher is the k_i value, the faster is the system's behavior in sliding mode. Therefore, the value of k_i is responsible for the accuracy of the reference trajectory tracking, and, consequently, it should be the result of the command following control synthesis.

To eliminate the influence of parasitic nonlinearities and dynamics in real VSC systems, let us apply the reaching law [4, 5] rather than the traditional linearization of the discontinuous (relay) element in control algorithm [1]. Reaching law ensures a continuous evolution of the switching function and meets the sliding mode existence condition Eq. (6). The straightforward expression of reaching law has the form

$$\frac{dF_i(\mathbf{e}_i)}{dt} = -k_i F_i(\mathbf{e}_i). \quad (8)$$

Parameter k_i in Eq. (7) has been chosen identical with the parameter in Eq. (8) because the dynamics of the switching function evolution – given by the reaching law – influences the accuracy of the command following control in the same way like the dynamics of sliding mode. Moreover, this simplification reduces the number of control parameters. After some algebra, using the expressions Eq. (2), Eq. (4), Eq. (7) and Eq. (8), considering the dynamically worst case of moment of inertia $J_{i\max}$, we obtain the continuous control law

$$\tau_{i\text{cont}} = \left((2k_i J_{i\max} - B_i) \frac{de_i}{dt} + J_{i\max} k_i^2 e_i \right). \quad (9)$$

The resultant control law satisfying the driving torque τ_i boundary M_i (cf. Eq.(5)) has then the form

$$\tau_i = \begin{cases} \tau_{i\text{cont}} & \text{for } |\tau_{i\text{cont}}| < M_i \\ M_i \operatorname{sgn}(\tau_{i\text{cont}}) & \text{for } |\tau_{i\text{cont}}| \geq M_i \end{cases}. \quad (10)$$

Dynamics of tracking

Due to discontinuity of VSC in sliding mode, conventional methods of the motion dynamics analysis fail. To deal with this problem, an original analysis method – the *phase velocity vector method* – has been provided in [2]. In this chapter, a brief outline of this method is presented.

Let the i -th element $q_{di}(t)$ of the robot reference vector $\mathbf{q}_d(t)$ and its first time derivative $dq_{di}(t)/dt$ form the reference phase position vector $\mathbf{q}_{di}(t) \in R^2$. The evolution of vector $\mathbf{q}_{di}(t)$ represents the desired phase trajectory of the i -th DOF in the phase plane ($q_i, dq_i/dt$). In any point of this trajectory there exists a desired tangential velocity vector

$$\frac{dq_{di}}{dt} = \frac{d}{dt} \begin{pmatrix} q_{di} \\ \frac{dq_{di}}{dt} \end{pmatrix} = \begin{pmatrix} \frac{dq_{di}}{dt} \\ \frac{d^2q_{di}}{dt^2} \end{pmatrix}. \quad (11)$$

Similarly, for the i -th element $q_i(t)$ of the vector of generalized coordinates $\mathbf{q}(t)$, there exists a phase position vector $\mathbf{q}_i(t) \in \mathbb{R}^2$ for any i -th DOF. Due to switching nature of the VSC, there are two values of the actuating variable τ_i^* (cf. Eq (5)), and for that reason there exists a pair of tangential velocity vectors (*phase velocity vectors*) to the phase trajectory of the i -th DOF

$$\left. \frac{dq_i}{dt} \right|_{\tau_i^*=M_i} = \begin{pmatrix} \frac{dq_i}{dt} \\ \frac{d^2q_i}{dt^2} \end{pmatrix} \Bigg|_{\tau_i^*=M_i} \quad \text{and} \quad \left. \frac{dq_i}{dt} \right|_{\tau_i^*=-M_i} = \begin{pmatrix} \frac{dq_i}{dt} \\ \frac{d^2q_i}{dt^2} \end{pmatrix} \Bigg|_{\tau_i^*=-M_i}. \quad (12)$$

Comparing the maximal value of each element of the desired tangential velocity vector Eq. (11) with the corresponding element of the phase velocity vector Eq. (12) under the dynamically worst conditions, we obtain the boundary values of the dynamic parameters in the robot reference vector $\mathbf{q}_d(t)$. Thus, the dynamics of trajectory tracking in sliding mode is determined and limited by these boundary values.

The satisfactory benchmark for the dynamics evaluation in motion control systems is the application of a harmonic type of the reference signal

$$q_{di} = A_i \sin(\omega_i t). \quad (13)$$

Using the expressions Eq. (2), Eq. (11) and Eq. (12), considering the dynamically worst case of moment of inertia $J_{i\max}$ and the worst influence of the maximal load value $\tau_{Li\max}$ with $\text{sgn}(\tau_{Li\max}) = -\text{sgn}(\tau_i)$, the boundary value $\omega_{i\max}$ of the reference signal frequency ω_i for trajectory tracking in the i -th DOF is given by Eq. (14):

$$\omega_{i\max} = B_i \frac{-1 + \sqrt{1 + 4 \frac{M_i - |\tau_{Li\max}|}{A_i J_{ii\max}}}}{2 J_{ii\max}}. \quad (14)$$

The boundary frequency $\omega_{i\max}$ characterizes the tracking capability of the dynamic system given by the expression Eq. (2).

Accuracy of tracking

Dynamic limitation of the reference signal frequency Eq. (14) in previous chapter is entirely valid for the discontinuous control in sliding mode given by Eq. (5) and Eq. (6). Using the continuous control algorithm given by Eq. (9) and Eq. (10), the accuracy of the harmonic reference signal tracking is influenced by the parameter k_i value. To keep the satisfactory tracking accuracy, let us choose the appropriate k_i values minimizing the control error $e_i = q_{di} - q_i$ in every DOF of the motion system. For the system subjected to parametric uncertainty and external disturbances, the frequency domain approach gives a straightforward method for such a control algorithm parameter design.

For the i -th DOF, let $F_{ei}(j\omega)$ and $F_{0i}(j\omega)$ denote the frequency transfer function of the control error and the open loop, respectively, i.e.

$$F_{ei}(j\omega) = \frac{1}{1 + F_{0i}(j\omega)}. \quad (15)$$

Let Δ_i (in % of the reference signal q_{di} amplitude) be the accuracy of command tracking in the i -th DOF. To keep the desired accuracy of tracking, the magnitude of the control error frequency transfer function should meet the following condition

$$|F_{ei}(j\omega)| = \left| \frac{1}{1 + F_{0i}(j\omega)} \right| = \frac{\Delta_i}{100} \ll 1, \quad (16)$$

which implies

$$|F_{0i}(j\omega)| \approx \frac{100}{\Delta_i}. \quad (17)$$

Consequently, the Bode magnitude diagram for the open loop transfer function $F_{0i}(s)$ should satisfy the coordinates

$$\omega = \omega_{i\max} \quad \text{and} \quad 20 \log |F_{0i}(j\omega)| = 20 \log \left(\frac{100}{\Delta_i} \right). \quad (18)$$

Expression (18), which is – due to control algorithm included in $F_{0i}(s)$ – a function of control parameter k_i , represents a straightforward method for the suitable value of parameter k_i design (cf. Eq. (9) and Eq. (10)). Thus, the tracking accuracy Δ_i of the command with the dynamic boundary given by Eq. (14), is assured.

Experimental results

To show the quality of the presented command following control algorithm, the numerical simulation on a dynamic model of a 2-link anthropomorphic robot manipulator with three DOFs in Matlab has been performed (two revolute joints mutually perpendicular in the first link, one revolute joint in the second link). The parameters of the robot manipulator are as follows: the length of the link $l_i = 0.75$ m ($i = 1, 2$), the mass of the link $m_1 = 30$ kg, $m_2 = 40$ kg, the viscous friction matrix element $B_i = 2$ kgms⁻¹ ($i = 1, 2$ and 3). The dynamic limitation of the robot motion is represented by the maximal values of the joint angular velocity $v_{i\max} = \pi/2$ rads⁻¹ and acceleration $a_{i\max} = \pi/2$ rads⁻² in any DOF, which corresponds to the equivalent harmonic signal for the joint angular position q_i with the amplitude $A_i = 1.5708$ rad and frequency $\omega_i = 1$ rads⁻¹. Alternatively, the maximal values $v_{i\max}$ and $a_{i\max}$ define an S-shape type of the angular position reference signal $q_i(t)$.

Considering the maximal dynamic performance of the robot, the maximal load in the i -th joint given by Eq. (3) is $\tau_{L1\max} = 750$ Nm, $\tau_{L2\max} = 1325$ Nm and $\tau_{L3\max} = 540$ Nm. The values of the driving torque boundary M_i have been chosen twice as high as the values of the maximal load, i.e. $M_1 = 1500$ Nm, $M_2 = 2650$ Nm and $M_3 = 1080$ Nm. Consequently, from Eq. (14), the boundary values of the reference signal frequency are $\omega_{1\max} = 2.1019$ rads⁻¹, $\omega_{2\max} = 2.8010$ rads⁻¹ and $\omega_{3\max} = 3.8546$ rads⁻¹. As can be seen, the frequency of the equivalent harmonic signal $\omega_i = 1$ rads⁻¹ doesn't exceed any boundary value $\omega_{i\max}$ ($i = 1, 2$ and 3). Thus, the accurate tracking of the reference angular position signal with the velocity $v_{i\max}$ and the acceleration $a_{i\max}$ limitation is assured.

The control parameter k_i values, in accordance with Eq. (18) and considering the desired tracking accuracy $\Delta_i = 0.1\%$ ($i = 1, 2$ and 3), have been chosen as follows: $k_1 = 100$, $k_2 = 130$ and $k_3 = 170$.

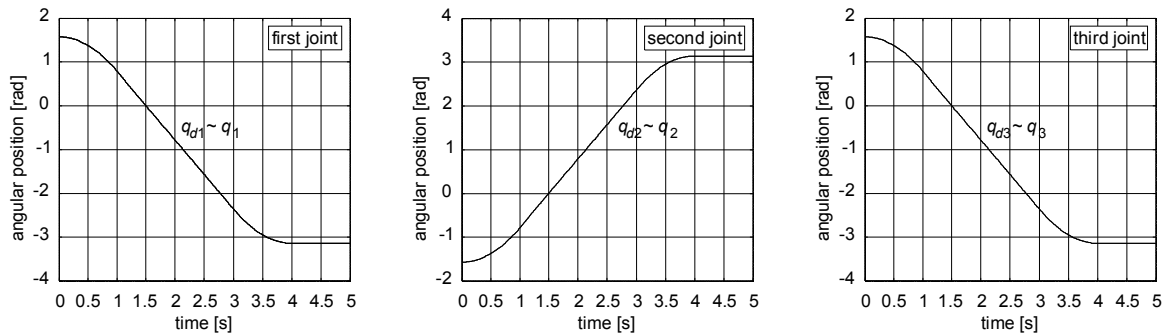


Fig. 1 Robust reference angular position $q_{d,i}$ tracking in the robot joint space

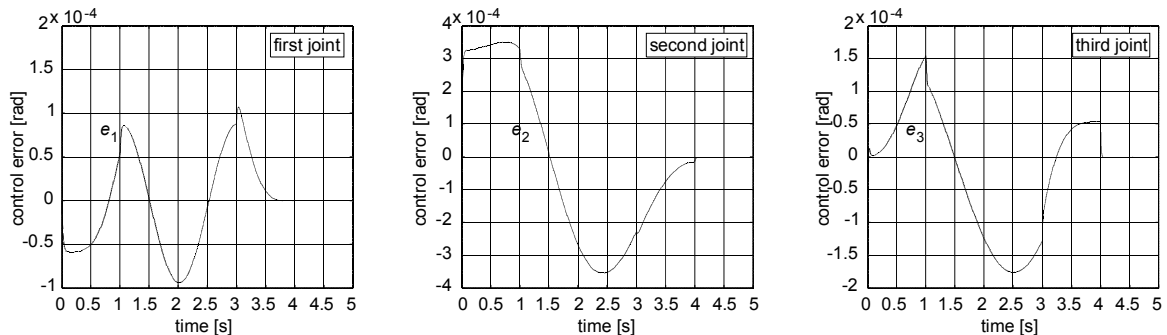


Fig. 2 Control error in reference position tracking

In Fig. 1, both the reference S-curve $q_{d,i}$ and the controlled angular position q_i versus time plots under the given dynamic limitation are depicted for all three joints. The initial conditions correspond with the angular position $q_1(0) = \pi/2$ rad, $q_2(0) = -\pi/2$ rad, $q_3(0) = \pi/2$ rad, and the final position (after the positioning period 4 seconds) is $q_1(4) = -\pi/2$ rad, $q_2(4) = \pi/2$ rad, $q_3(4) = -\pi/2$ rad. It is evident, that the tracking accuracy is better than the desired one, due to reserve in motion dynamics ($\omega_i < \omega_{i\max}$) (cf. the control error e_i plots in Fig. 2).

Conclusion

The aim of this paper has been to give a brief outline of a challenging method of a robust and accurate trajectory tracking control synthesis with a simple control algorithm given by the linear combination of the position and velocity control error in the robot joint space. In spite of the discontinuous character of the original VSC, the presented control law doesn't suffer from the chattering. The dynamic model of the controlled multi-DOF robot takes the real parametric uncertainty as well as the influence of any external and coupling forces into account. Presented Matlab simulation, which is only a part of the extensive set of simulations, shows the effectiveness and perfect quality of the reference trajectory tracking process.

Acknowledgment

This contribution has been supported by the Grant Agency of Ministry of Education and Academy of Slovak Republic VEGA under Grant No. 1/0690/09.

References

- [1] V.I. Utkin: *Sliding Modes in Control and Optimization*, (Springer, Berlin, 1993).



-
- [2] J. Kardoš: The Accuracy of Tracking in Variable Structure Motion Control System, *Proc of International Conference on Innovative Technologies IN-TECH 2011, Bratislava, Slovak Republic*, (2011), pp. 273-276.
 - [3] V.I. Utkin, J. Guldner and J. Dhi: *Sliding Mode Control in Electromechanical Systems*, (Taylor & Francis, London, 1999).
 - [4] J.Y. Hung, W. Gao and J.C. Hung: Variable structure control: A survey, *IEEE Transactions on Industrial Electronics*, Vol. 40, (1993), No. 1, pp. 2-22.
 - [5] J. Kardoš: Reaching Law Modification of the Time Sub-Optimal Variable Structure Control, *International Journal of Mechanics and Control*, Vol. 6, (2005), No. 2, pp. 39-49.
 - [6] J. Kardoš: The Simplified Dynamic Model of a Robot Manipulator, *Proceedings of the 18th International Conference – Technical Computing Bratislava 2010, Bratislava, Slovak Republic*, (2010).



International Conference on Innovative Technologies, IN-TECH 2012,
Rijeka, 26. - 28.09.2012



INFLUENCE OF TEMPERATURE TO THE EFFICIENCY OF VISCOSE TREATMENT USING COPOLYMER CHITOSAN-EUGENOL

O. Šauperl¹, J. Volmajer-Valh¹, and Jasna Tompa¹

¹ University of Maribor, Faculty of Mechanical Engineering, Institute for Engineering Materials and design, Smetanova ulica 17, SI-2000 Maribor, Slovenia

Keywords: chitosan, eugenol, viscose, FT-IR spectroscopy, antimicrobial, acid orange VII.

Abstract. Recently, there has been intense trend of finding and developing new technologies based primarily on the use of alternative natural materials. In the past few decades, chitosan has been enforced mainly because of good anti-microbial properties due to its active amino groups. To achieve optimal anti-microbial treatment of textiles, chitosan sometimes does not provide desired results so it is meaningful to include some other of the natural anti-microbial active compound in the system with chitosan. To this end, it seems suitable natural phenol derivative called eugenol which is an integral part of cloves. For this reason, the synthesis of graft copolymer of chitosan in combination with eugenol and subsequent application to the textile substrate is particularly interesting. Except synthesis of anti-microbial active copolymer and its applications in the textile substrate it is also important to evaluate the effect of temperature on the effectiveness of such treatment. To examine the effectiveness of treatment using copolymer chitosan/eugenol FT-IR spectroscopy and amino group determination is an interesting approach together with an anti-microbial evaluation against different pathogen microorganisms. The results obtained on the basis of tests performed with viscose which was treated by the system chitosan/eugenol afterwards dried at different treatment temperature were compared with the results of the viscose treated only with 1% solution of chitosan. It is concluded that the system chitosan/eugenol resulting in an anti-microbial effect which is comparable to the treatment with chitosan only. The processing method slightly affects the effectiveness in the sense of pathogen microorganisms' reduction.

Introduction

Medical textiles are one of the most interesting areas in terms of textile material functionalization. In the field of the protection of textile materials against micro-organism it is also indispensable to use environment and human-friendly compounds [1-4]. Chitosan is considered to be a very important material for possible biomedical usages because it demonstrates a lot of excellent properties e.g. non-toxicity, biodegradability, bio- and haemo- compatibilities, antimicrobial, hypoallergenic, etc. [5] Owing to its structure being similar to cellulose, chitosan is ideal for cellulose fibres' surface modifications, in order to develop cellulose antimicrobial activity. However, despite of chitosan common and widely spread use and its popularity, it shows drawbacks, especially limited solubility. Due to the nature of its conventional production from animal origin (crustaceous) it is very difficult to produce reproducible material with defined properties. Therefore, to achieve optimal antimicrobial treatment of textiles, chitosan sometimes does not provide desired results so it is meaningful to include some other of the environmentally friendly anti-microbial active compound in the system with chitosan. To this end, it seems suitable natural phenol derivative called eugenol which is an integral part of cloves. For this reason, the synthesis of graft copolymer of chitosan in combination with eugenol and subsequent application to the textile substrate is very interesting approach to create antimicrobial active textiles. For the medicine needs is a very attractive substrate viscose [6]. This is due to its higher purity in comparison with cotton, which contains a significant proportion of waxes, pectins and natural dyes, which means that technological process of cotton pre-treatment is more expensive if compared to the viscose. Viscose functionalization using copolymer eugenol-chitosan could therefore contribute to the creation of a new generation of materials suitable also for medical use. It is anticipated that the temperature of treatment influences the reaction of substrate (viscose) with the treatment agents, thus resulted in different proportions of available amino groups which are responsible for the antibacterial efficiency of the substrate. Therefore, the main purpose of the presented work was to determine the optimal drying temperature after chitosan/eugenol application onto viscose, by which it might be possible to provide a greater efficiency of the antimicrobial activity. The chitosan/eugenol system was evaluated using FT-IR spectroscopy. On the other hand, the proportion of available amino groups was chosen as the important criterion in terms of antimicrobial effectiveness, respectively. The latter was evaluated using the CI Acid Orange VII spectrophotometric method [7], supported by testing against selected pathogen microorganisms. [ASTM E2149-01 test method].

Experimental

Materials

The low molecular weight chitosan ($M_r \sim 150,000$) was purchased from Aldrich, whilst Eugenol (2-methoxy-4-(2-propenyl)-phenol) and ceric ammonium nitrate (CAN) were from Sigma-Aldrich.

The investigations were carried out on 100 % viscose fabric (Lenzing Austria) with a surface mass of 140 g/m^2 , warp density (32 threads / cm), filling density (27 threads / cm) and the weave, (linen).

Methods

Synthesis of Eugenol-chitosan

Fig.1 presents the prepared molecular-scheme for grafting copolymer chitosan-eugenol, according to the used procedure as follows: Chitosan (84 g) and a predetermined amount of eugenol (4×10^{-3} M) were added into a reactor containing 200 mL of 2 % acetic acid, and then stirred for 4 h within a nitrogen atmosphere, heated at 40 °C. The 6×10^{-3} M CAN, dissolved in 100 mL of 1 N HNO_3 , was added into the reactor in order to initiate graft polymerization. The reaction products were precipitated in acetone, filtered [8], and then used for viscose functionalization. The samples were impregnated with the help of foulard (W. Mathis AG, Switzerland, $p = 3$ bar, the rollers' speed rotation = 2 m/min). 80 % wet pick-up was achieved under these conditions. After completing the process of impregnation, the samples were dried for 3 min. at 120 °C, 150 °C and 170 °C, respectively. Then, the samples were rinsed at room temperature until reaching the conductivity of the distilled water ($0.4/(\mu\text{S}/\text{cm})$).

FT-IR spectroscopy

ATR-FTIR spectra were recorded on a Perkin Elmer Spectrum GX spectrometer. The ATR accessory contained a diamond crystal. All spectra (16 scans at 4 cm^{-1} resolution and rationed to the appropriate background spectrum) were recorded at room temperature. Any changes in the chemical structure of the graft can be estimated using FTIR spectroscopic measurements. Molecular-scheme for grafting copolymer chitosan-eugenol is presented in Fig. 1. On the other hand, Fig. 2 shows the spectra for chitosan (a), copolymer chitosan-eugenol (b), and eugenol (c). The FTIR spectrum of the chitosan shows peaks at 1653 and 1598 cm^{-1} . These two wavenumbers are assigned to the carbonyl stretching vibration (amide I), and the N-H bending vibration (amide II) of a primary amino group, respectively. On the other hand Fig. 2 (c) shows characteristic peaks at 3443, 1610, and 1434 cm^{-1} , which can be attributed to the characteristic peaks of -OH attached to the benzene, and the C=C and $\text{CH}_2=$ in the vinyl group, respectively. In the copolymer chitosan-eugenol (Fig. 2 b), the formation of a covalent-linkage between the amino group of chitosan, and eugenol is confirmed by the peak shift of amide II in the chitosan to 1553 cm^{-1} and the disappearance of the free-amino group of chitosan at 1598 cm^{-1} , when compared with chitosan itself. In addition, the characteristic peaks at 1610 cm^{-1} (C=C), 1434 cm^{-1} ($\text{CH}_2=$), and C-H vinyl out-of-plane bending vibrations, observed within the spectrum of the monomer (Fig. 2 (c)), had disappeared in the chitosan-eugenol copolymer (Fig. 2 (b)). The grafting of the eugenol molecules onto the chitosan was confirmed from the FT-IR results.

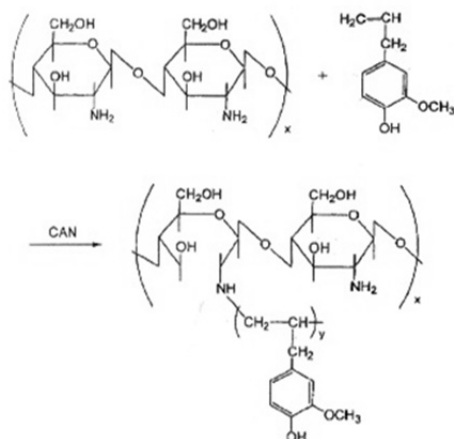


Fig. 1 Molecular-scheme for grafting copolymer eugenol-chitosan

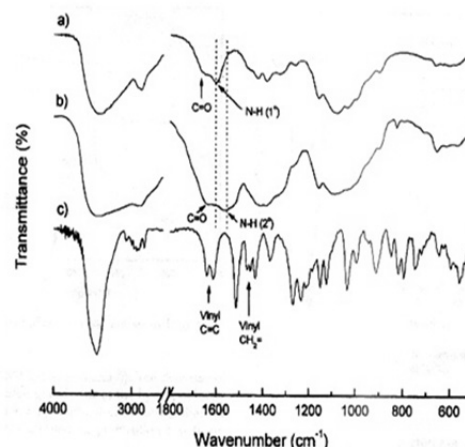


Fig. 2 Spectra for chitosan (a), copolymer eugenol-chitosan (b), and eugenol (c)

Acid Orange VII spectrophotometric method

The accessible amino groups of functionalized fibres were determined using the CI Acid Orange VII spectrophotometric method. This method is based on absorption of the dye CI Acid Orange VII (Fig. 3) by the principle of reducing the dye concentration in the dye bath by following the Lambert-Beer law.

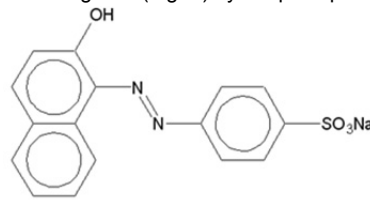


Fig. 3 Chemical structure of Acid Orange VII dye

The initial absorbance at a wavelength of 484 nm, which corresponds to a maximum absorption of the dye Acid Orange VII was measured after adding 2 ml of the dye CI Acid Orange VII ($c = 0.005 \text{ mol/L}$) into 250 ml of water with pH 3.66 (acetic acid). Then 0.25 g of fibres was immersed in the dye solution and stirred for three hours at a constant speed, by a magnetic mixer. After a three hour period, the balance between the concentration of the dye in the dye-bath and the concentration of the dye bound on fibres was established; the final absorbance was measured using a Cary 50 spectrophotometer, Varian (USA). Based on these measurements of initial and final absorbance, the concentration of the dye on fibres was calculated as follows (Eq. 1):

$$A_i = ((A_0 - A_f)V)/(k.l.m_f) \cdot 10^6 \quad (1)$$

Where: A_i – is the amount of amino groups of chitosan bound to the fibers/(mmol/kg), A_0 –initial absorbance, A_f –final absorbance, V – volume of the dye bath/L, k – correction factor/(L/mol cm), l – length of the optical field/cm, m_f – mass of absolutely dry fibres/g

- Antimicrobial test

The antimicrobial properties of the treated samples were evaluated in Institute of Public Health Maribor according to ASTM E2149-01, which is a quantitative antimicrobial test method performed under dynamic contact conditions. *Escherichia coli* and *Candida albicans* were used as test organisms. An incubated test culture in a nutrient broth was diluted using a sterilised 0.3 mM phosphate buffer (KH_2PO_4 ; pH = 6.8), to give a final concentration of $1.5\text{-}3.0 \times 10^5$ colony forming units (CFU)/mL. This solution was used as a working bacterial dilution. Each sample (0.5 to 2 g) was cut into small pieces (1×1 cm) and transferred into a 250 mL Erlenmeyer flask containing 50 mL of the working bacterial dilution. All the flasks were loosely capped, placed in the incubator, and shaken for 1 h at 37°C and 120 rpm, using a Wrist-Action incubator shaker. After a series of dilutions using the buffer solutions, 1 mL of the diluted solution was plated in nutrient agar. The inoculated plates were incubated at 37°C for 24 h and the surviving cells were counted. The average values of the duplicates were converted to CFU/mL in the flasks by multiplying by the dilution factor. The antimicrobial activity was expressed as $R = \%$ (Eq. 2) reduction of the organism after contact with the test specimen, compared to the number of bacterial cells surviving after contact with the control [ASTM E2149-01 test method].

$$R = \frac{A-B}{A} \times 100/\% \quad (2)$$

Where: R – is reduction of microbes/%, A - number of bacterial colonies after 1 min. (time "0"), and B - number of bacterial colonies after 1 hour

Results and discussion

In our experiment, different temperatures of drying (120°C , 150°C and 170°C), were used after the samples had been impregnated by a combination of chitosan/eugenol, and by 1% solution of chitosan, respectively. In our previous studies [6] it was found that a good anti-bacterial effectiveness of cellulose can be achieved by 1 % mass fraction of chitosan with an 85 % degree of de-acetylation, which also ensures the appropriate viscosity of the chitosan solution for its subsequent application onto cellulose. For this reason, 1 % chitosan dissolved at pH=3.6 (acetic acid) was also used for the functionalization of the viscose, in addition to the system chitosan/eugenol. A laboratory drying machine represents the conventional method for textile materials' pad-dry treatment; there the procedure of so called dry treatment is performed over a two-stage heat treatment in the sequences of drying-condensation. By drying at 100°C the impregnated material is dried, at condensation of temperature above 120°C , however, a reaction between substrate and the crosslinking compound takes place. Therefore, the optimal temperature of condensation may affect the more efficient reaction between the substrate and the treatment compound resulted in a large proportion of the available amino groups. For this reason, the proportion of available amino groups was chosen as the most important parameter of this research, because the anti-microbial action of the material depends on the amount and availability of amino groups which are crucial to ensure efficiency regarding micro-organism reduction. The proportion of amino groups, depending on the treatment temperature was determined by the Acid Orange VII method and is presented in (Fig.4). Sulphonic groups (SO_3^-) of the dye form in the acidic medium's ionic bonds in the ratio of 1: 1 with positively-charged amino groups of chitosan (NH_3^+), so amount of dye bound to the fibers corresponds to the amount of accessible amino groups.

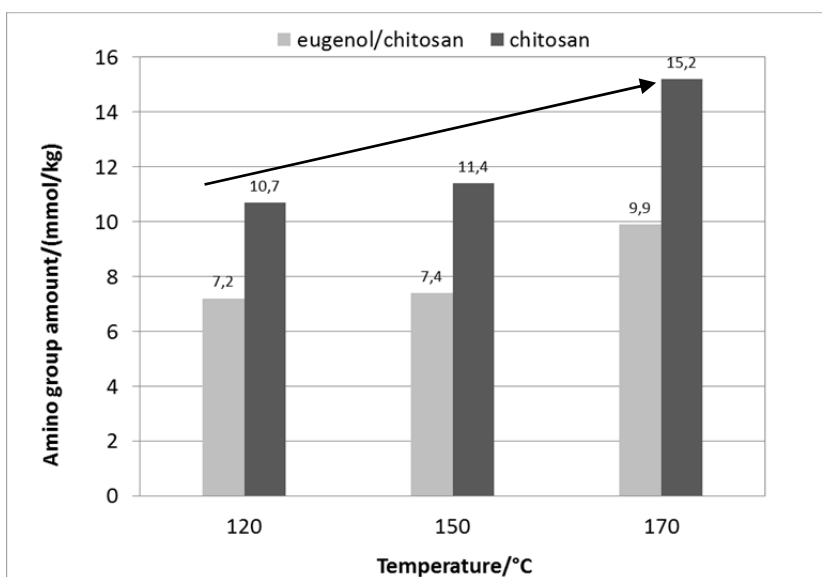


Fig. 4 Amino group amount in dependence of the treatment temperature (the arrow indicates the trend of amino groups' increase)

In this research, the proportion of available amino groups was chosen as the most important parameter, because the anti-microbial action of the material depends on the amount and availability of amino groups which are crucial to ensure efficiency regarding micro-organism

reduction. For this reason, the functionalization of viscose using 1 % solution of chitosan, and a system of chitosan/BTCA was used primarily to increase the proportion of amino groups that could potentially reduce a wide-variety of pathogenic microorganisms. The proportion of amino groups determined by the Acid Orange VI method, depending on the treatment, is shown in Fig. 4.

The results of the individual treatment show that with an increase in the temperature of the treatment the proportion of available amine groups increases (see Fig. 4). The highest increase in the proportion of available amino groups appears after treatment at a temperature of 170 °C. Here, a significantly higher proportion of available amino groups can be seen in the case of treatment using 1 % solution of chitosan than in the case of the samples treated with the system chitosan/eugenol. As is seen from the results presented in Fig. 4 samples treated using 1 % solution of chitosan exceeded the values of samples functionalized using system chitosan/eugenol in all cases of treatment, and is: 3.5 mmol/kg in the example of treatment at 120°C, 4.0 mmol/kg in the case of treatment at 150 °C, and 5.3 mmol/kg available amino groups after treatment at 170 °C, respectively.

Anti-microbial testing was used to examine the impact of the amino group amount on the antimicrobial properties of functionalized viscose. Since the drying at 170 °C in terms of availability of amino groups was the most effective the antimicrobial testing was performed only for these samples. From the results shown in Table 1 a reduction can be seen regarding pathogenic *Staphylococcus aureus* and *Candida albicans*, respectively. These results also demonstrate that the reference, which means the non-functionalized sample, showed a positive reduction in the selected pathogenic microorganisms which was, in both cases, 57 %. The most likely cause for the inhibition of the pathogenic microorganisms of the non-functionalized sample represents the adsorption of the microorganisms onto the textiles. It must be pointed out that the reduction of microorganisms under 60 % by using the ASTM E2149-01 test method, which is a quantitative antimicrobial test method, means a lack of antibacterial effectiveness. Notwithstanding this, the results showed that the adsorption of chitosan onto viscose, irrespective of the chosen type of treatment, contributed to reductions in *Staphylococcus aureus* and *Candida albicans* which is, in the example of 1% chitosan 100 % against both microorganisms used in this research. On the other hand, in the case of the treatment with the system chitosan/eugenol the reductions regarding *Staphylococcus aureus* were 96 % and for *Candida albicans* 97 %, respectively. The results show a very effective reduction regarding selected pathogenic micro-organisms in both cases of functionalization (1 % solution of chitosan as well as the system chitosan/eugenol). Reduction against selected pathogenic micro-organisms is very successful although the reduction of them is slightly more efficient in the case of viscose functionalization using the 1% solution of chitosan.

Table 1: Reductions (R/%) of the microorganisms regarding the non-functionalized viscose, and viscose functionalized with 1% chitosan solution as well as with the system chitosan/eugenol, after drying at 170 °C

Sample	Reduction R/% <i>Staphylococcus aureus</i>	Reduction R/% <i>Candida albicans</i>
Reference	57	57
1% chitosan	100	100
System chitosan/eugenol	96	97

Conclusion

- The grafting of the eugenol molecules onto the chitosan was confirmed from the FT-IR results
- The highest increase in the proportion of available amino groups appears after treatment at a temperature of 170 °C. Here, a significantly higher proportion of available amino groups can be seen in the case of treatment using 1 % solution of chitosan than in the case of the samples treated with the system chitosan/eugenol.
- The results show a very effective reduction regarding selected pathogenic micro-organisms in both cases of functionalization.

References

- [1] M. N. V. Ravi Kumar: A review of chitin and chitosan applications, *Reactive & Functional Polymers*, Volume 46 (2000), p. 1-27.
- [2] D. Severiaon: *Polymeric Biomaterials*, Second Edition, (Marcel Dekker, New York, 2002).
- [3] B. O. Jung, C. H. Kim, K. S. Choi, Y. M. Lee, J. J. Kim: Preparation of amphiphilic chitosan and their antimicrobial activities, *J. App. Polym. Sci.*, Volume 72 (1999), Issue 13, p. 1713–1719.
- [4] D. Laemmermann: New Possibilities for Non-Formaldehyde Finishing of Cellulosic Fibres, *Melliand Textilberichte*, Volume 3 (1992), p. 274-279.
- [5] S. Strnad, O. Šauperl, L. Fras Zemljič, A. Jazbec: Chitosan – universally applicable polymer, *Tekstilec*, Volume 50 (2007), Issues 10-12, p. 243-261.
- [6] L. Fras-Zemljič, O. Šauperl, I. But, A. Zabret, M. Lušicky: Viscose material functionalized by chitosan as a potential treatment in gynecology, *Textile Research Journal*, Volume 81 (2011), Issue 11, p. 1183-1190.
- [7] L. Fras-Zemljič, S. Strnad, O. Šauperl, K. Stana-Kleinschek: Characterization of amino groups for cotton fibers coated with chitosan, *Textile Research Journal*, Volume 79 (2009), Issue 3, p. 219-226.
- [8] J. Byung-Ok, C. Suk-Jin, L. Sang Bong: Preparation and characterization of Eugenol-Grafted Chitosan Hydrogels and Their Antioxidant Activities, *Journal of Applied Polymer Science*, Volume 99 (2006), p. 3500-3506.

SPEED/POSITION SENSORLESS CONTROL OF TWO-PHASE PMSM DRIVE SYSTEM USING VIRTUAL INJECTION METHOD

B. Dobrucky¹, S. Kascak¹, M. Prazenica¹, J. Kassa¹

¹ University of Zilina, Faculty of Electrical Engineering, Department of Mechatronics and Electronics, Univerzitna 1, 010 26 Zilina, Slovakia

Keywords: space vector modulation, virtual high-frequency injection method, FOC control of synchronous machine, VSI inverter

Abstract. The paper deals with speed/position servosystem with 2-phase electrical permanent magnet synchronous motor for robotic applications. The new developed method has been used for speed/position control. The precision of position determination is less than 2.5 °el. in steady-state operation in spite of virtual sensorless method. It needs – for real time control - high computing power for control algorithms and very small time sampling interval. Maximum of motor electromagnetic torque is providing by field oriented control (FOC).

Speed/position control of two-phase permanent magnet synchronous motor using VHFIM

The conception of a FOC controlled two-phase permanent magnet synchronous machine without using a sensor is depicted in Fig. 1. PWM signal generation for 2-phase VSI inverter can be realized as a classical sinusoidal modulation or a space vector modulation [1]. A connections possibility of two-phase inverters will be described later in the text. Virtual high frequency injection method VHFIM is used to determine information about the position and velocity of the rotor [2].

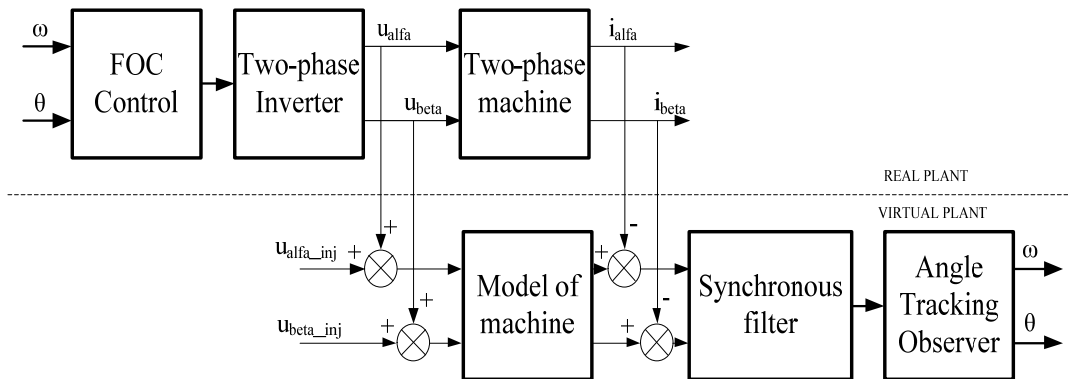


Fig. 1 Speed/position FOC control of two-phase PMSM using VHFIM

The principle of the VHFIM is injection of the high frequency harmonic voltage component to the stator one in the model of the motor. The result is that the current response after subtracting from real stator current the high frequency signal current component comprises the information about position of the rotor. The most important in this method is that the current of machine model and real stator current must be synchronized. Using synchronous filter (Fig. 2) we can determine estimated currents.

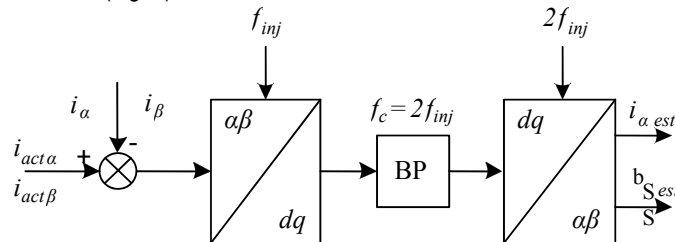


Fig. 2 The block diagram of the synchronous filter

$$i_{\alpha\beta_inj} = i_{\alpha\beta} - i_{\alpha\beta_act} \quad (1)$$

We can obtain the current response $i_{\alpha\beta_inj}$ using bandpass filter instead subtracting block. The current response equation $i_{\alpha\beta_inj}$ in stationary frame is shown in (2). The current consist of two parts: the positive one i_{injPos} and the negative one i_{injNeg} . Only the negative one contains information about position. Since the positive component does not contain useful information, it must be removed. This shall be done in two steps. Firstly, we have to transform the system, which is identical to injected field. We achieve that the positive element after transformation has only the dc component (3) and secondly, it can be removed by using simple band-pass filter. Equation (4) shows the current vector i_{dq_filt} spins of approximately twice the frequency as the frequency of the injected signal in the opposite direction. The last

step is transformation to the system (5), which rotates exactly with twice the frequency of the injected signal in the opposite sense of rotation as the current i_{dq_filt} .

$$i_{\alpha\beta_inj} = I_{injPos} e^{j(\omega_{inj}t)} + I_{injNeg} e^{j(2\theta_{el} - \omega_{inj}t)} \quad (2)$$

$$i_{dq_inj} = I_{injPos} + I_{injNeg} e^{j(2\theta_{el} - \omega_{inj}t)} \quad (3)$$

$$i_{dq_filt} = I_{injNeg} e^{j(2\theta_{el} - 2\omega_{inj}t)} \quad (4)$$

$$i_{\alpha\beta_est} = I_{injNeg} e^{j(2\theta_{el} - 2\omega_{inj}t)} e^{j2\omega_{inj}t} = I_{injNeg} e^{j2\theta_{el}} \quad (5)$$

Information about position and velocity we can find out from the estimated currents by the angle tracking observer (ATO, Fig. 3) or only the information about position using ATAN2 computing block. This information can be used for feedback loop of speed/position FOC control.

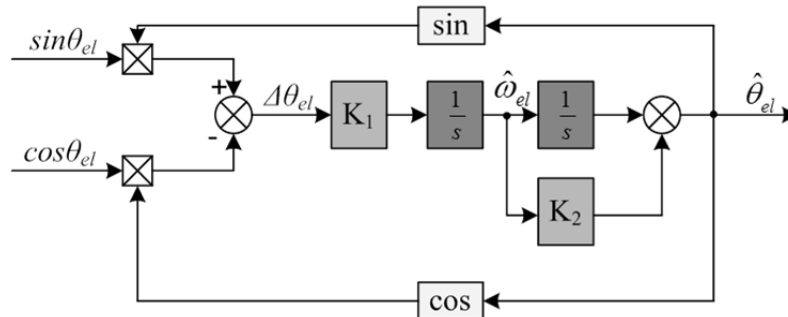


Fig. 3 Angle tracking observer

Method ATO can be used for sensor and sensorless control. The main requirement is to bring the signal with sine and cosine component to the input of the observer. The principle of operation is in comparison input and output estimated signal. Observer error is given by the difference estimated and actual rotor position.

Supply possibilities of two-phase permanent magnet synchronous motor

There is in Fig. 4 shown the two-leg, three-leg and four-leg inverter, which represents separated two full-bridge inverters. In connection with two-leg and three-leg inverter the common points of the phases are connected between two capacitors in first case and between two transistors of the phase in the second case. The common used three-phase inverter drive [3,4], which utilizes six switches or one IGBT intelligent power module (IPM). In third case two full-bridge matrix converters can drive the phases of the motor independently. There is more possibilities how to drive two phase induction motor like half-bridge matrix converter. The half-bridge matrix supply MXC-HB provides less power losses of the converter due to soft switching (in spite of more number of switches) [5,6].

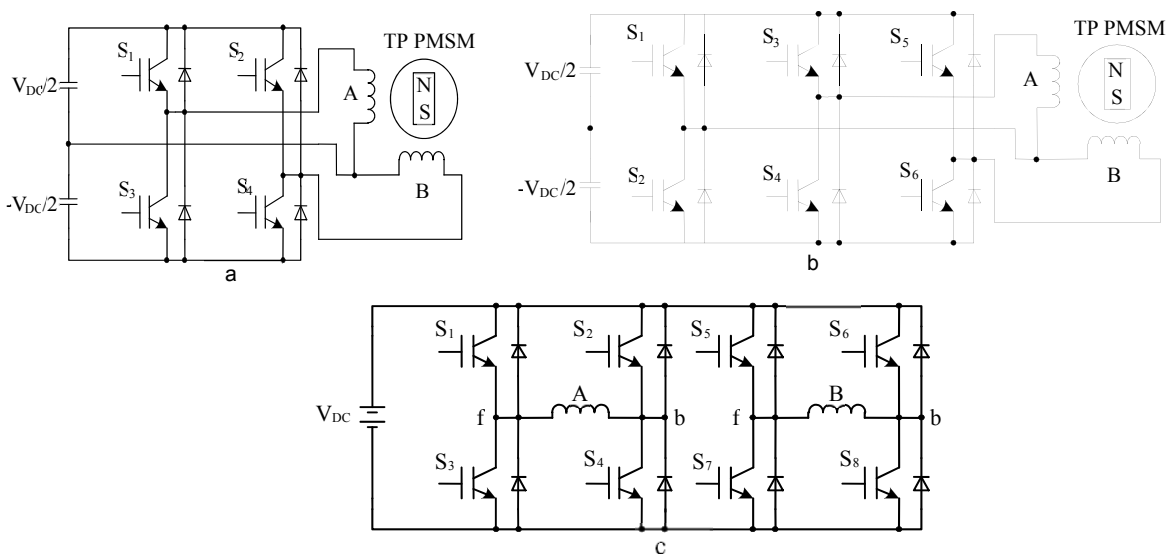


Fig. 4 Two-leg a), three-leg b) and four-leg inverter c) for supplying two-phase induction

Field oriented control of two-phase permanent magnet synchronous machine

Model of Two-Phase Permanent Magnet Synchronous Motor (TP PMSM) and Field Oriented Control is explained in [7,8] and therefore the motor and control algorithm will not be described in great detail in this paper. The control algorithm scheme of Field Oriented Control is depicted on Fig. 5.

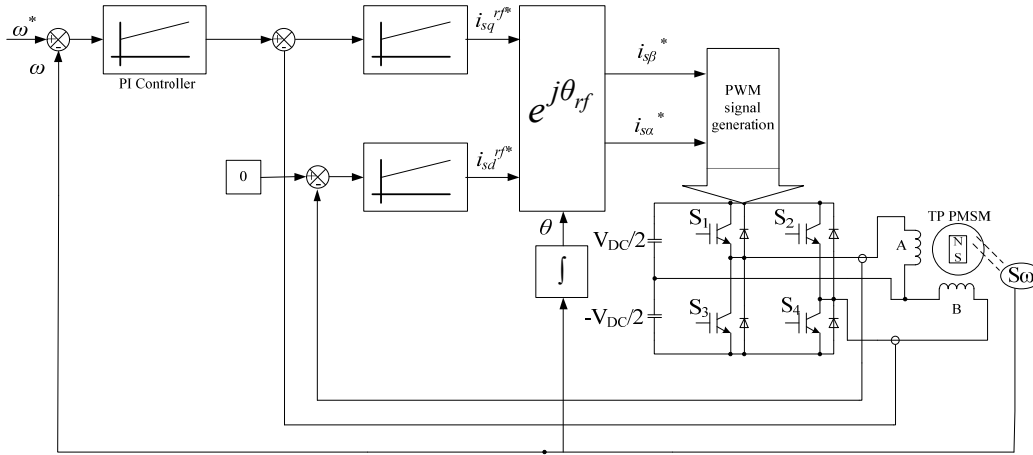


Fig. 5 IFOC control strategy for driving two-phase induction machine

Simulation experiments

The parameters of two-phase PMSM needed for simulation are shown in Table. 1.

Table 1 Parameters of two-phase PMSM

$U_n = 180\text{V}$	$n_n = 1500\text{ min}^{-1}$	$R_s = 1.1\ \Omega$	$J = 1.2 \cdot 10^{-3}\text{ Kg.m}^2$
$L_d = 4.73\text{ mH}$	$L_q = 4.5\text{ mH}$	$\Psi_{pm} = 0.096\text{ Wb}$	

The advantage of ATO opposite to ATAN2 is that the computing algorithm works in feedback loop and accuracy of the first mentioned method should be therefore much better. The simulation results are depicted in Fig. 6, Fig. 7 and Fig. 8.

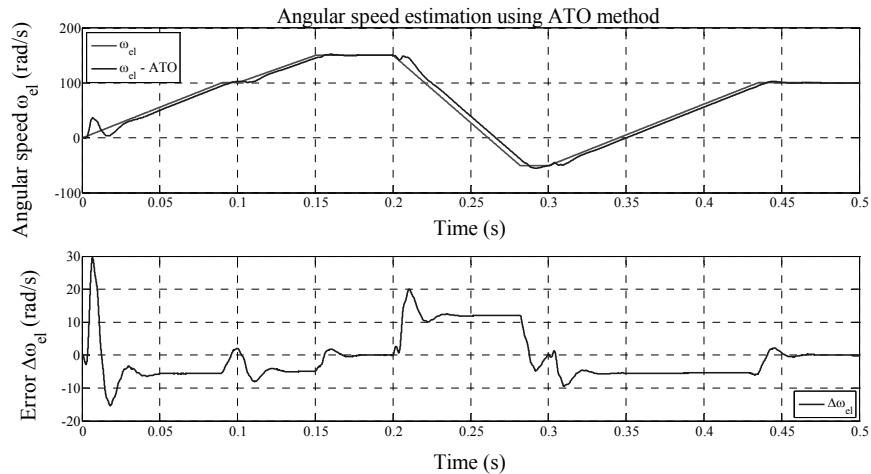


Fig. 6 Actual and estimated angular speed a), error of angular speed b) using ATO

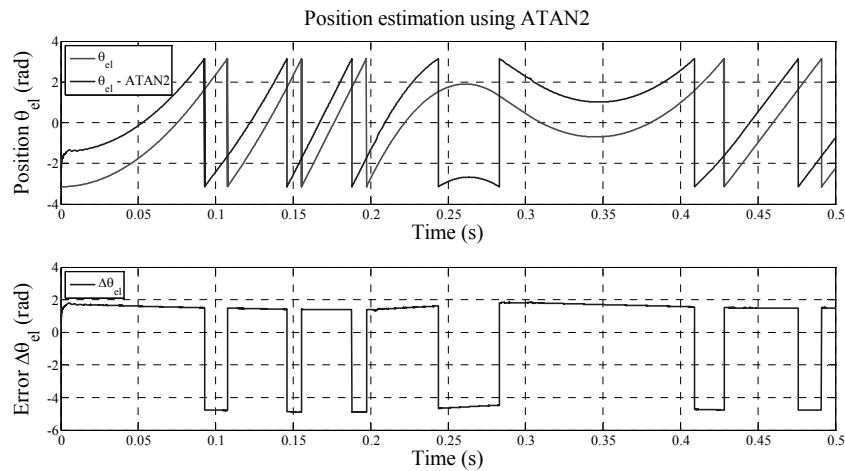


Fig. 7 Actual and estimated position a), error of position b) using ATAN2

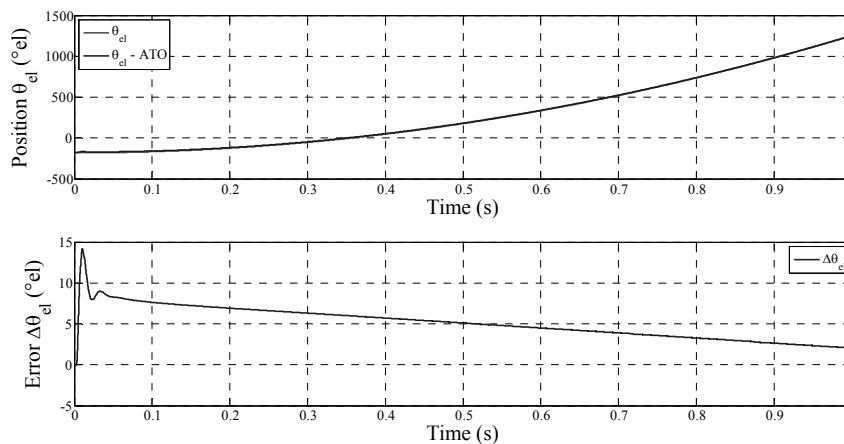


Fig. 8 Actual and estimated position in °el. a), error of position b) using ATO

Conclusion

A speed/position servosystem with 2-phase electrical permanent magnet synchronous motor for robotic applications was introduced and presented. The new developed method has been used for speed/position control. The results of simulation experiments of the using of the VHFIM injection method are good. The precision of position determination is less than 2.5 °el. in steady-state operation (see Fig. 8) in spite of virtual sensorless method. The field oriented control technique provides the maximum of motor electromagnetic torque. The high frequency signal current component comprising the information about position of the rotor needs subtracting of modeled stator current (with HF signal) from real stator current in real time.

Acknowledgement

The authors wish to thank for the financial support to Slovak Research and Development Agency project No. APVV-0138-10 and R&D operational program Centre of excellence of power electronics systems and materials for their components No. OPVaV-2008/2.1/01-SORO, ITMS 26220120046 funded by European regional development fund (ERDF).

References

- [1] L.C. Tomaselli, T.B. Lazzarin, D.C. Martins, I. Barbi: Application of the Vector Modulation in the Symmetrical Two-Phase Induction Machine Drive, *IEEE Power Electronics Specialists Conf.*, 2005, p. 1253 – 1258.
- [2] B. Dobrucky, J. Michalik, P. Spanik and V. Bobek: Virtual HF Injection Method (VHFIM) of a Rotor Position Estimation of PMSM under Field Oriented Control, *IEEE SPEEDAM Int'l Symp. on Power Electronics, Electrical Drives, Automation and Motion*, 2006, p. 28-31.
- [3] F. Blaabjerg et al.: Evaluation of Low-Cost Topologies for Two-Phase IM Drives in Industrial Application. *Record of 37th IEEE IAS Annual Meeting on Industry Application*, Volume 4, p. 2358 - 2365, ISSN 0197-2618.
- [4] M.B.R. Corrêa, C.B. Jacobina, A.M.N. Lima.: Three-leg voltage source inverter for two phase ac motor drive system, *IEEE Trans. on Power Electronics*, Volume 9, No. 4, p. 377-383.
- [5] J. Kassa, P. Sekerak, M. Prazenica.: Design Analysis of Two-Stage Power Electronic Converter for Feeding of 2-Phase PMSM, *9-th European Conference of Young Research and Scientific Workers SECTION 4 TRANSCOM 2011*, 27 – 29 June 2011, p. 65 – 72.



International Conference on Innovative Technologies, IN-TECH 2012,
Rijeka, 26. - 28.09.2012



-
- [6] Kassa, J., Prazenica, M.: New Concept of Two-Stage Two-Phase Orthogonal Converter with Two-Phase Motor, *Proceedings of 17th International Conference on Electrical Drives and Power Electronics*, EDPE 2011, 28 – 30 September 2011, Stará Lesná, The High Tatras, Slovakia, CD-ROM, p. 188-193, ISBN 978-80-553-0734-3.
- [7] V. Bobek, B. Dobrucky, R. Pavlanin, P. Sevcik: VHFIM sensorless control of PMSM, *IEEE Industrial Electronics (ISIE) 2010*, 4-7 July 2010, p. 1536 – 1541, ISBN 978-1-4244-6390-9
- [8] V. Bobek: Determination of rotor position SMPM using the method of virtual injected HF signal, *PhD. Thesis*, Faculty of Electrical Engineering, Zilina



International Conference on Innovative Technologies, IN-TECH 2012,
Rijeka, 26. - 28.09.2012



QUALITY ASSESSMENT OF PVD COATING AND TOOL USED AT COLD-FORMING PROCESS

P. Beraxa^{1,2}, L. Domovcová¹, Ľ. Parilák¹

¹ ŽP VVC s.r.o. (Research and development centre), Kolkáreň 35, Podbrezová, Slovakia

² TUKE - FVT Prešov, Bayerova 1, 080 01 Prešov, Slovakia

Keywords: PVD process, microstructure, microhardness, hardness of PVD coating

Abstract. Along with technologies development rise demands on the technical level of new machinery and equipment and also the reliability and efficiency of tools used in the production processes. One of the options for increasing tool life and wear resistance is the use of tools surface treatment technology called as PVD (Physical Vapor Deposition) process. This process is atomistic deposition process in which material is vaporized from a solid or liquid source in the form of atoms or molecules, transported in the form of a vapor through a vacuum or low pressure gaseous (or plasma) environment to the substrate where it condenses. The paper introduces the possibilities of application of this process for straightening rolls used in operating conditions of Železiarne Podbrezová, a.s. Rolls are evaluated in terms of microstructure and microhardness measurement of the rolls material, thickness and hardness measurement of PVD coating of roll operating surface after PVD process.

1. PVD process

PVD (physical vapor deposition) processes for creation of thin layers are based on spraying or evaporation of solids (chemical element) e.g. titanium, aluminum, to bombard the substrate (forming tool), by a mixture of neutral atoms and ions and condensation of chemical elements or compounds of the metal on the substrate surface under high vacuum 10^{-6} to 10^{-10} Pa [1].

Conditions and properties of formed layers are very diverse. Surface layers are created at a defined pressure in a vacuum chamber which the working gas for example argon or nitrogen are supplied into. In our case, the evaporation method using low-voltage arc was used for coating of straightening rolls.

Low voltage arc is preferred for its high evaporation rate of the electrode material and a high plasma ionization. Process time varies in the order of several hours. The low voltage arch has very convenient parameters, because it burns at the cathode spot at around $10\mu\text{m}$ in diameter, where the temperature reaches about $15\,000\text{ }^\circ\text{C}$ [2].

Under these conditions it is possible to evaporate virtually any electrically conductive material. High plasma ionization, in turn, brings the possibility of preparing coatings and structures that commonly occur in nature. Scheme of arc evaporation device is shown in Fig. 1.

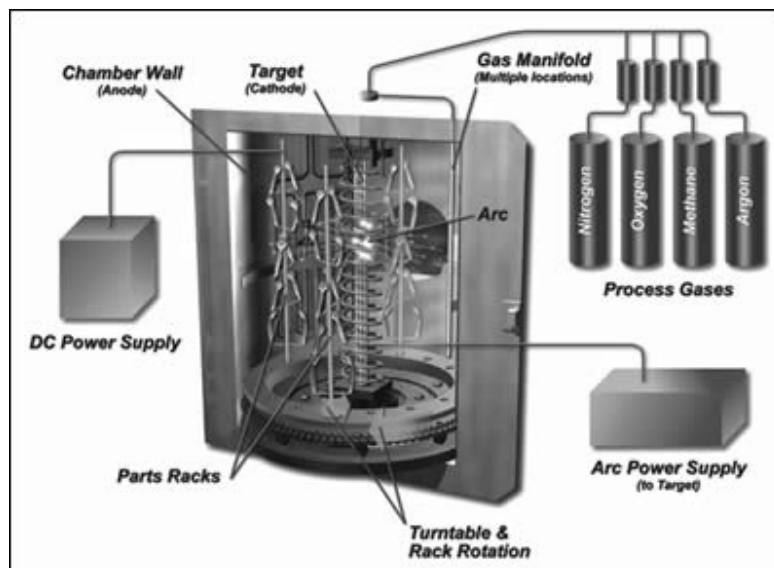


Fig. 1 Scheme of PVD device [3]

2. Tube straightening technology in ŽP, a.s.

Straightening is a technology that is used to remove undesirable distortions. Curvature of the product axis arises as a result of the production technology [4]. Straightening leads to the elimination or reduction of curvature in the metal products using external forces. In practice, the tube runs between the straightening rolls that are rotated to the direction of straightening at an angle (Fig. 2).



Fig. 2 Scheme of the straightening process [5]

The roll's profile is not the tube's radius. The tube rotates as it passes through the straightening machine. While passing through the machine, the tube is subjected to two specific straightening forces:

- 1.) Pressure straightening. Each pair of rolls can be adjusted so that the gap between them is slightly smaller than the outside diameter of the tube. As the tube passes through this restricted gap, it is subjected to pressure which, if sufficient, will cause the tube walls to be strained past their elastic limit, thereby causing some straightening of the tube. If this ability to squeeze the tube is used correctly, the tube will be "rounded up," removing some or all of its ovality.
- 2.) Bend, or offset, straightening. One or more pairs of rolls can be adjusted to cause the tube to follow a curved path through the machine. Bending the tube in this manner is the main straightening action.

The amount of bend must be carefully controlled so that it has enough force to take the tube past its elastic limit to achieve straightness, but not so much that it causes excessive work hardening.

3. Straightening rolls material

The material used for the production of the rolls is a high-chrome, high-carbon tool steel (DIN 17350 - 1.2080, marking X210Cr12) with high through-hardening, high wear resistance by metals and minerals, with a very high compressive strength, significantly low toughness in the transverse direction, with a strong carbide line spacing structure with good dimension stability to heat treatment, suitable for quenching the secondary hardness. Chemical composition of steel according to DIN 17350 is shown in Table 1.

Hardness requirement according to drawings is 57 to 63 HRC and roughness of operating – hyperbolic part of the roll must be less than 0.8 μm .

Table 1. Chemical composition of a high-chrome tool steel

Material	C [%]	Si [%]	Mn [%]	Cr [%]
X210Cr12	1,9 -2,2	0,10-0,60	0,20-0,60	11,0-13,0

4. PVD coating

The coating used to increase rolls service life is a commercial named as ALWIN (fig. 3). It is a nanocomposite CrAlSiN coating with high chromium content, which consists of small monocrystals in the range below 10 nm, that are embedded in an amorphous matrix with a suitable thin intercrystalline boundaries below 1 nm. Grain boundaries serve as an effective barrier against the spread of failure - thus allowing the high hardness of these materials [6]. The structure of the nanocomposite layer is schematically shown in Figure 3.

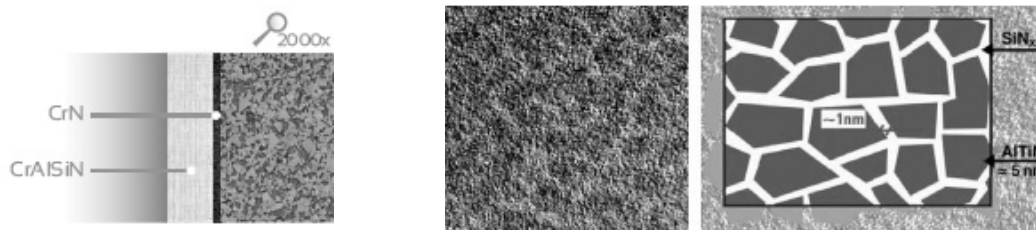


Fig. 3 The ALWIN coating and structure of nanocomposite layer [6]

The coating temperature is adjusted according to the type of tool material in the range of 180 to 600 °C. Temperatures above 500 °C are used for carbide tools, high speed steel with high tempering temperature are coated at temperature to 450 °C. Materials with lower tempering temperature or the requirements to minimize thermal distortion can be coated from the 180 °C.

5. Experiment

Tempering temperature or temperature limits of the material changes – to choose suitable PVD technology or safe maximum temperature of PVD process it is necessary to know these temperatures for different materials from which tools are made [7].

Our straightening rolls were quenched from 1060 °C in oil, tempered at temperature about 490°C and then PVD coated at the temperature close to 500°C. The final structure (fig. 4) consists of tempered martensite in which the carbides of size 44 µm are distributed. The thickness of PVD layer is about 1 to 2 µm.

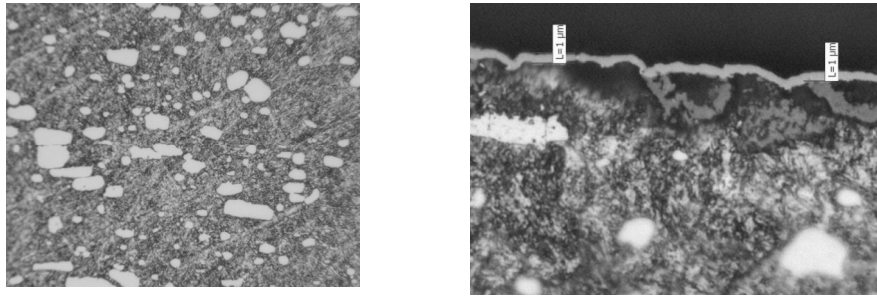


Fig. 4 Final structure of rolls material and thickness of PVD coating

It should be noted that the surface roughness of the rolls working surface has a large impact on life time and quality of coating. The roughness of straightening rolls was measured as the arithmetic mean deviation Ra. The resulting roughness values are shown in Table 2 and the roughness of working surface at roll no. 6 is graphically illustrated in the figure 5.

Table 2. The measured Ra roughness of the rolls working surface

Roll no.	1	2	3	4	5	6
Ra (µm)	0,26	0,27	0,22	0,34	0,19	0,24

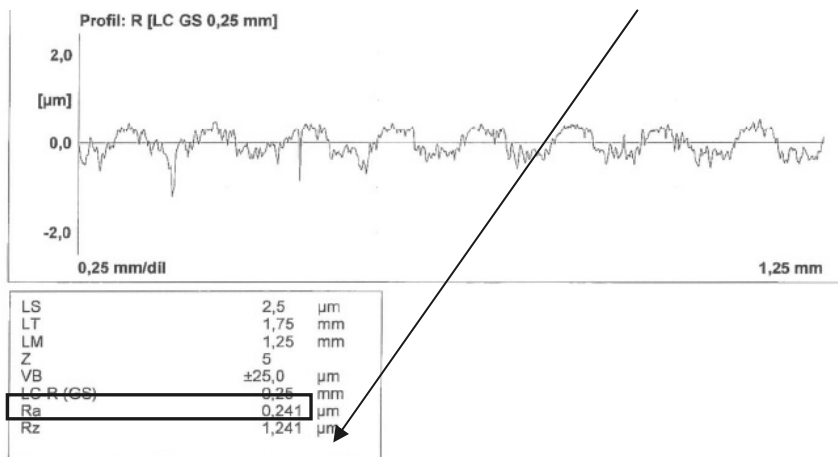


Fig. 5 Roughness measurement on roll no. 6

The measured values of microhardness are shown in table 3 and also graphically shown on figure 5. The hardness of CrAsiN coating was measured at the load 50 g (HV0,05) and is approx. 24.5 GPa.

Table 3. The results of microhardness measurement HV0,05

Description	Measurement no.					
	1	2	3	4	5	6
Rolls material in cross section HV 0,05	652	641	616	632	624	640
PVD coating HV 0,05	2436	2384	2585	2485	2411	2360

We also measured the hardness of the base material (substrate), which is 4 times lower compared to the hardness of the coating. The above measured values are shown at the figure 6, where the red line refers to microhardness of PVD coating and blue line presents the material of rolls.

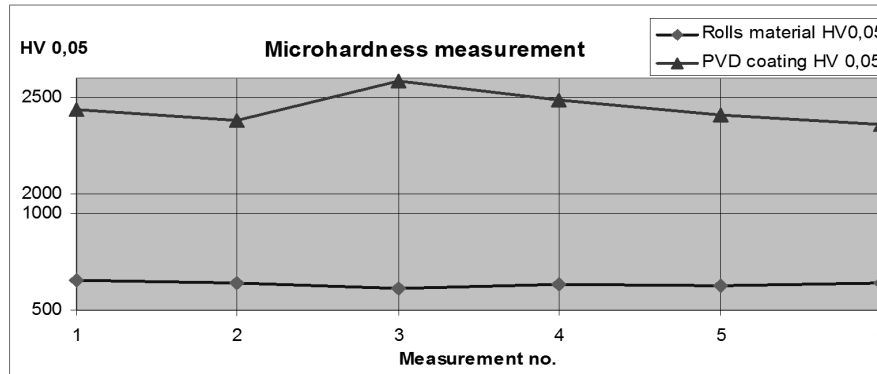


Fig. 6 Results of microhardness HV 0,05 measurement

6. Conclusion

The straightening rolls made of a high-chrome, high-carbon tool steel 14CrNi14 whose structure consists of tempered martensite and carbides of size about 44 μm were deposited by CrAlSiN coating. The coating was evaluated in terms of roughness on rolls operating surface. The roughness ranges from 0.19 to 0.34 μm .

We also focused on the evaluation of coating hardness, we measured the microhardness by using the Dura-scan 20 - micro hardness tester and the resulting value is 24.5 GPa. The results of the above measurements meet the requirements for reliable operation of straightening rolls coated with PVD coating but will need to examine other coating properties such as adhesion and friction properties.

References

- [1] A. Humár: Nové povlaky a povlakovací metody pro řezné nástroje, ITC (2003)
- [2] <http://www.shm-cz.cz/cs/technicke-informace/pvd-technologie-shm>
- [3] K. Brondum, G. Larson: Reinventing Chrome Coatings, Products finishing magazine Vol.12 (2005)
- [4] P. Kostka, J. Lukšič, M. Podolský: Technológia tvármenia, STU Bratislava (1995)
- [5] *The Tube and Pipe Journal* : Rotary straighteners for tube and pipe, October/November (2009)
- [6] M. Růžička, O. Zindulka: ALWIN - nanokompozitní PVD vrstva AlSiCrN, Strojárstvo Vol.4 (2007)
- [7] P. Beraxa, L. Domocová, Ľ. Parilák: The application of PVD coating for tools used at tube straightening, Inżynieria Materialowa , Vol. 4 (2011)

INTRA- AND INTERLAMINAR SHEAR BEHAVIOUR OF TEXTILE COMPOSITES TESTED WITH V-NOTCHED RAIL SHEAR TEST METHOD

W. Hufenbach¹; R. Schirner²; M. Andrich¹

¹ Technische Universität Dresden, Institute of Lightweight Engineering and Polymer Technology (ILK), 01062 Dresden, Germany

² Leichtbau-Zentrum Sachsen GmbH, Marschnerstraße 39, 01307 Dresden, Germany

Keywords: notched rail shear test, composite material, mechanical properties, strain measurement

Abstract. The advanced design of multidirectional fibre-reinforced polymers (FRP) shows an increased need of reliable inter- and intralaminar shear property data. Various test methods have been proposed to determine shear moduli and shear strengths of composite laminates.

It can be shown that the standardised V-notched rail shear test method is best suitable for a reliable material characterisation for intralaminar shear properties. A modified V-notched rail shear test fixture was developed to determine interlaminar shear behaviour of textile-reinforced composites.

In addition, the standardised strain measurement with strain gauges is compared to optical measurement systems. For the optical measurements, a suitable analysis area has to be selected depending on the specimen geometry. The results are compared to finite element analyses.

Introduction

Fibre-reinforced polymers (FRP) are distinguished by anisotropic material properties with high specific stiffness and strength values in fibre direction. These exceptional material properties lead to a wide range of application fields with a need for a large lightweight design potential. In order to utilise the lightweight potential of FRPs, it is necessary to determine their mechanical properties. Therefore, suitable experiments are essential. Dependent on load application and stress distribution within the laminate, the material is exposed to fibre and inter-fibre failure modes. The material properties in fibre direction are remarkable, however, the inter-fibre properties limit maximum load of the material. Inter-fibre strain occurs in almost all applications of multi-axially reinforced or multi-axially loaded laminates.

Focus of this work is the mechanical testing of CFRP by intra- (in-plane) and interlaminar (out-of-plane) shear load. Various standardised test methods were analysed and rated after various eligibility criteria e.g. economic and robust testing as well as stress distribution. A modified rail shear test fixture is introduced and compared to other common test devices. The benefits of an optical shear deformation measurement are analysed and compared to conventional strain gauges as well. Furthermore, experimentally determined shear deformation of a V-notched rail shear (VNRS) specimen is compared to numerical analyses of a finite element model (FEM) of the specimen.

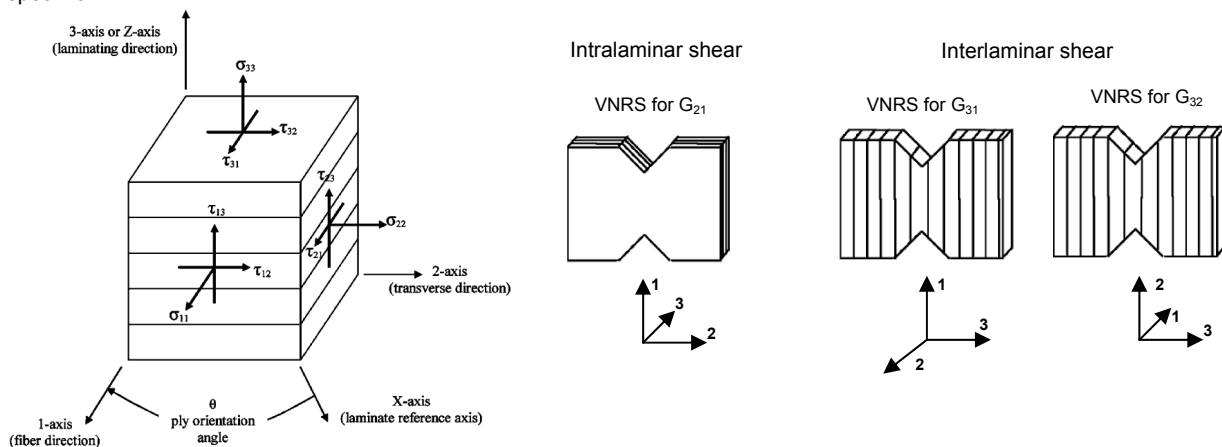


Fig. 1 Standardised definition of fibre orientation in relation to Cartesian coordinate system, single-layer orientation of fabric-reinforced laminates for intra- and interlaminar V-notched rail shear testing [1]

Test devices for determination of shear properties

Various, partially standardised, test methods exist to determine shear property data of unidirectional fibre- and fabric-reinforced polymers. They differ from each other by homogeneity of state of stress, marginal influence, influence of clamping, precision of results, and complexity of specimen as well as costs for specimen preparation, test fixture and testing process. Most common test standards for shear determination are the $\pm 45^\circ$ tension test (ASTM 3518), the V-notched beam test method by Iosipescu (ASTM 5379) and the V-notched rail shear test method (ASTM 7078). Another well-known shear test is the non-standardised torsion tube, by which the shear properties can be determined with a higher precision [2]. Although specimen manufacturing and preparation is sophisticated, the determination of interlaminar shear properties of fabric-reinforced polymers is not possible with torsion tube test. Other test methods, e.g. off-axis or arcan tests, have limitations concerning an increased effort for specimen preparation, homogeneity of state of stress and shear strength or

stiffness evaluation. Therefore, only test methods and results of $\pm 45^\circ$ tension and both V-notched shear tests will be compared to each other. A universal test machine is required for all three standardised tests.

$\pm 45^\circ$ tension test, ASTM 3518 - 2007

The most common, because efficient, testing device is the $\pm 45^\circ$ tension test on flat specimens with end tabs for evaluation of the intralaminar shear modulus of unidirectional fibre- or fabric-reinforced polymers [3]. The specimen dimensions should be 250 mm of length and 25 mm of width, while the thickness depends on the thickness of the textile pre-product but should be at least 2 mm. The testing of interlaminar shear properties is not possible. Requirements for the test fixture as well as the testing process for this test standard are relatively low. However, there is a negative influence on mechanical properties by marginal effects. [4]

V-notched beam test method (Iosipescu), ASTM 5379 - 2005

The V-notched beam test method, also called Iosipescu test, was first established in the 1960s for isotropic materials only. Walrath and Adams optimised the test method for composite materials [5]. Intra- and interlaminar shear properties can be determined on unidirectional and fabric-reinforced polymers, although fabrics with large filament count tows or braided structures should not be tested because of the relatively small test section of the specimen [6]. Because of the symmetrical notches, an approximately homogeneous state of stress can be attained within the test section. Specimen preparation is quite demanding, especially the quality and surface finish of the notches influence the test results. To avoid premature compression failure within the load introduction zone, specimen thickness should be at least 3 or 4 mm, otherwise end tabs should be applied.

Standardised and modified V-notched rail shear test method, ASTM 7078 - 2005

The well-known V-notched rail shear test [1] is a combination of the two rail shear test and the Iosipescu test method. The planar introduction of load, inherited from the two rail shear test, reduces stress peaks near the clamping area and thus the risk of premature failures of the specimen. The failure within the gage section between both symmetrical notches, adapted from the Iosipescu test, is caused without any considerable influences on the load introduction zone [7]. Another difference to the Iosipescu test is the increased gage length between both notches, which allows the testing of textile-reinforced polymers with an increased roving bandwidth or pattern repeat. Intra- and interlaminar shear properties can be determined. According to ASTM 7078 the testing of unidirectional fibre-reinforced composites as well as interlaminar shear initiation are not recommended, since there are no reinforcing fibres between both fixture halves which can lead to a pre-damage of the specimen while mounting.

In order to reduce a possible pre-damage of the specimen and to increase manageability, a modified V-notched rail shear test fixture (Fig. 2) was developed. With it, among others, comes an alignment system with low-friction components for each fixture half, which reduces handling difficulties and allows specimen mounting without dismantling the test fixture from the test machine. Since misalignments of the usually multi-component load strand build-up of the test machine can provoke premature failures, integrated slideways reduce possible inaccuracies.

Additionally, the clamping system of the standardised VNRS test fixture was modified. Originally, each fixture half contains two triple packs of gripping bolts, which fix the specimen with two clamping jaws. Misalignment by means of turning the specimen out of the symmetric plane of the testing device can occur. Furthermore, while fixing the specimen in the second fixture half, a torsional moment can be applied on the specimen. Another handling weakness of the standardised testing device is the positioning of the clamping jaws, since there is no accurate guidance. Inhomogeneous stress distributions and stress interferences can be caused by misalignments of the clamping jaws. A promising simplification is the installation of a fixed clamping jaw at each fixture half. Turning of the clamping jaws around the axle of the load strand is not possible and the number of adjustable bolts is reduced. Different specimen thicknesses can be adjusted by various clamping jaw thicknesses or by inserting spacer plates between the fixed clamping jaw and the fixture half. Due to a large variety of specimen thicknesses from 2 to 5 mm [1], spacer plates with various thicknesses are preferable. In addition, each adjustable clamping jaw is equipped with at least two guide pins for a well-controlled positioning.

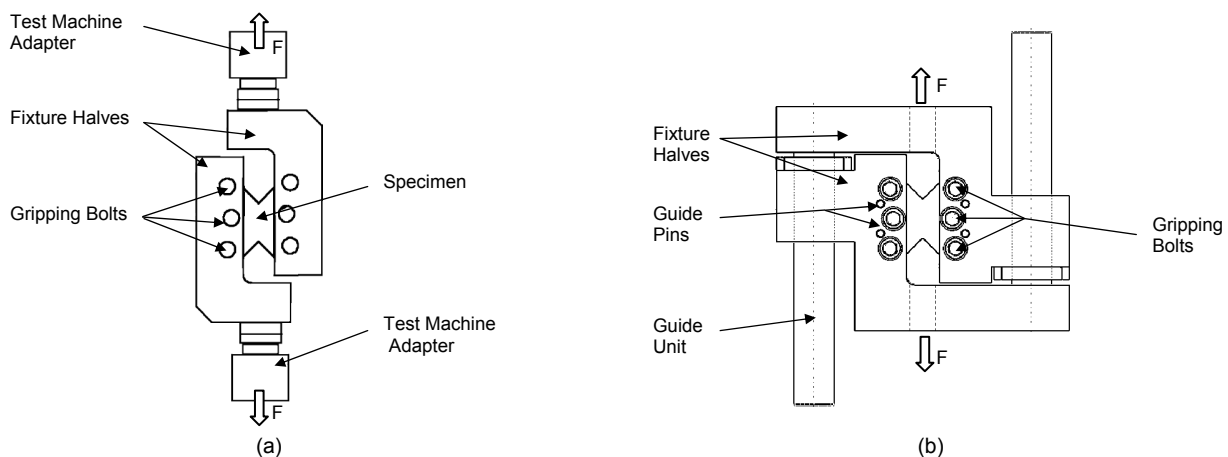


Fig. 2 Standardised V-notched rail shear test fixture (a) and modified V-notched rail shear test fixture (b)

Tested materials and specimen preparation

Two textile-reinforced polymers were investigated which are quite common in industrial applications. The first one is a carbon fibre unidirectional laminate (GV300/RTM6), where the unidirectional reinforcement is a woven UD fabric of high-tenacity PAN-based fibre Grafil 34-700 with additional thermo fixation by glass yarn and thermoplastic. This fixation in weft has the purpose to ensure fibre position and is only 6 % of the weight. The second investigated material was a carbon fabric-reinforced laminate (ECC 452/RTM6). As textile reinforcement a 2/2 twill weave of high-tenacity carbon fibres HTA40, with the same fibre count in warp and weft direction, was used. Both textiles were infused with the mono-component epoxy resin HexFlow[®] RTM6 by advanced resin transfer moulding process. The fibre volume fraction was about 57 %.

Several sample plates with different thicknesses were manufactured for specimen preparation. In addition a laminate block with dimensions of 80 mm x 80 mm x 80 mm was manufactured. In order to ensure the quality of such a thick composite material concerning inhomogeneities or pores, detailed non-destructive analyses were done such as computer tomography analysis and ultrasonic analysis. These investigations proved high material quality.

Specimen preparation was done by machining with diamond saw blades and appropriate milling and grinding tools. A water coolant was used as well. Therefore, it was possible to get tight tolerances and best surface of the samples with a roughness R_z of 10 μm .

Table 1 shows the investigated specimens with characteristic features.

Table 1. Specimen dimensions and specifications

	$\pm 45^\circ$ Tension	Iosipescu	VNRS
specimen main dimensions			
GV300/RTM6 (UD-EP)			
specimen thickness	5 mm	4 mm	4 mm
layup	16 plies in $\pm 45^\circ$ -orientation	14 plies in 0° -orientation	14 plies in 0° orientation
investigated material plane	1-2	1-2	1-2; 1-3; 2-3
ECC452/RTM6			
specimen thickness	3 mm	not tested	2 mm
layup	16 plies in $\pm 45^\circ$ -orientation	not tested	11 plies in $0^\circ/90^\circ$ orientation
investigated material plane	1-2	not tested	1-2; 1-3; 2-3

Strain measurement system

Although test standards recommend strain gauge measurement, an optical measurement system (ARAMIS[®]) was used. A comparison with common strain gauges was realised on a VNRS specimen and was done for verification of the optical measurement system. Therefore, the ARAMIS[®]-Software was used to analyse the area for strain gauge application (Fig. 3).

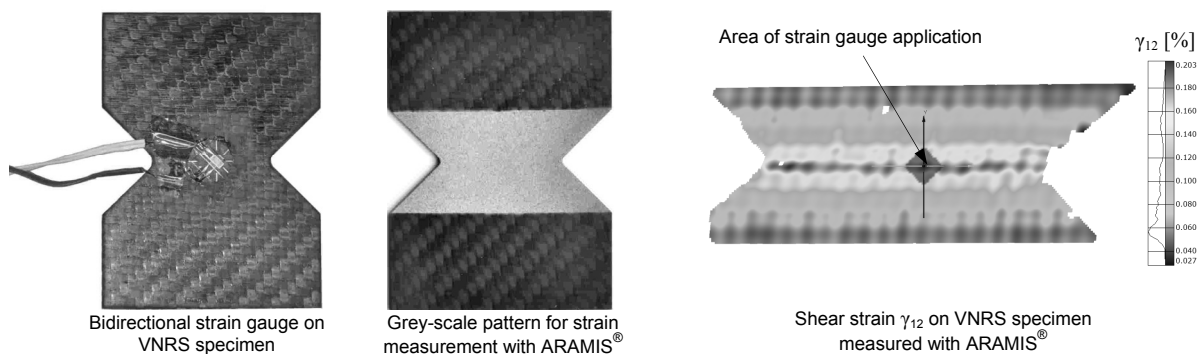


Fig. 3 ARAMIS[®] vs. Strain gauge measurement on VNRS specimen

Results of the comparison show, that the strain values measured with ARAMIS[®] are slightly above the values determined by strain gauge measurement. A possible cause for this variance may be the conversion of the analogue force signal of the universal test machine due to an analogue-digital-transducer added to each measurement system. The signal is impaired by noise interference, thus the recorded data of the ARAMIS[®]-system, respectively strain gauge measurement system, includes an unknown and random disturbance. Nevertheless, both strain results show a sufficient compliance to analytically determined shear strain values. For a suitable evaluation of the strain measurement with ARAMIS[®]-system, the width of the region of interest (ROI) should not exceed the diameter of the V-notches, otherwise the measured strain values will be lower, accompanied by an increased shear stiffness evaluation.

For an efficient analysis of VNRS test data with ARAMIS[®]-software, an application with an automatic evaluation-algorithm was created and utilised. Furthermore, for analysis of multiple specimens in one series of tests, a stacked job processing was implemented within the application. Therefore, an economic, repeatable testing process as well as test evaluation could be achieved.

Test results

Mechanical shear testing was performed to determine absolute values of shear moduli and shear failure strengths as well as standard deviation using VNRS, Iosipescu and $\pm 45^\circ$ tension test methods. All tests were carried out with at least 5 specimens. Testing was performed using a universal test machine. Load and crosshead deflection were recorded as the test was performed at a constant crosshead displacement rate of 2 mm/min. Additionally, specimen gripping capabilities, failure modes, reproducibility of testing and robustness of the test device were analysed. Optical measurement of shear deformation of VNRS specimen was compared to finite element analysis.

Intralaminar shear property data of GV300TFX and ECC452 laminate were determined with VNRS, $\pm 45^\circ$ tension and Iosipescu (GV300TFX only) test methods. Test results of $\pm 45^\circ$ tension test with GV300TFX laminate show the lowest intralaminar shear modulus G_{21} (3020 ± 343 MPa) compared to Iosipescu test (3658 ± 723 MPa) and VNRS test (3943 ± 138 MPa) (Fig. 4). The high shear modulus of VNRS testing is accompanied by a low standard deviation compared to the other test methods. The shear modulus of VNRS testing fits best to previous analytically determined shear modulus of the tested laminate. Similar outcomes show the evaluated shear failure strength data R_{21} . The highest shear failure strength was measured with VNRS test method ($74,4 \pm 2,6$ MPa), whereas Iosipescu and $\pm 45^\circ$ tension

show similar strength data values ($65,4 \pm 7,5$ MPa and $66,5 \pm 0,4$ MPa). As already mentioned, testing of fabric-reinforced polymers with Iosipescu test method is not suitable since the ROI between both notches is too small for fabrics with a large pattern repeat. The shear failure strengths determined with $\pm 45^\circ$ tension test method are also relatively low, which can be caused by the effect of free edges, since ending fibres cannot transfer loads into fibre-parallel direction. [5]

The laminate with ECC452 fabric reinforcement was tested with VNRS and $\pm 45^\circ$ tension test method (Fig. 4). Here as well, the average shear modulus G_{21} tested with VNRS was nearly 20 percent higher (3942 ± 147 MPa) than the shear modulus tested with $\pm 45^\circ$ tension test (3181 ± 318 MPa). The obtained shear failure strength R_{21} for both tests was almost equal (VNRS: $129,1 \pm 2,2$ MPa; $\pm 45^\circ$ tension: $127,2 \pm 3,7$ MPa). The standard deviation for both tests is similar to test results of GV300TFX laminate.

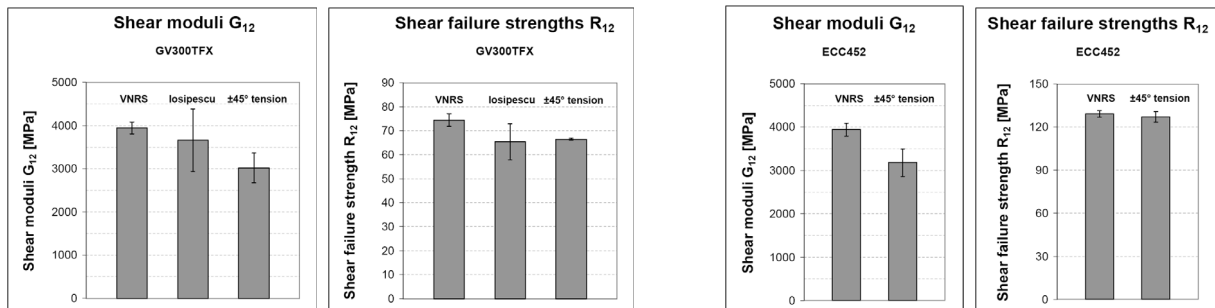


Fig. 4 Intralaminar shear property data of fabric-reinforced polymers GV300TFX (left) and ECC452 (right)

Interlaminar shear property data (G_{31} , G_{32} , R_{31} , R_{32}) was determined by VNRS test method on fabric-reinforced polymers using the modified VNRS test device (Fig. 5). Interlaminar shear modulus determination for GV300TFX and ECC452 reinforced laminate was carried out for 31-plane and 32-plane. Test results for GV300TFX laminate G_{31} ($3860 \pm 100,3$ MPa) show a similar average shear modulus compared to in-plane shear property data ($G_{21, GV300TFX} = 3943$ MPa). However, shear modulus data in 32-plane shows a significantly lower modulus compared to 31-plane of GV300TFX laminate. This effect may be caused by an unfavourable fibre orientation in relation to V-notched specimen geometry. Friction between two layers of fabric material (ECC452) may increase interlaminar shear stiffness of the material. Especially interlaminar shear property data of laminates with thick fabric pre-products, with a strong waviness, may benefit from this effect. Nevertheless, unidirectionally reinforced fabric material like GV300TFX does not have much waviness especially in 32-plane and, therefore, the shear modulus is significantly lower.

Since there is no reinforcement in thickness direction of the laminate, the average interlaminar shear modulus G_{31} or G_{32} (3334 MPa) for ECC452 material is naturally lower compared to in-plane shear property data ($G_{12} = 3942$ MPa).

Interlaminar shear failure strengths for material GV300TFX and ECC452 have been determined as well. Shear failure strengths R_{31} and R_{32} (26,7 MPa and 26,8 MPa) of GV300TFX are lower compared to ECC452 (37,6 MPa). Friction, caused by the waviness effect, may also increase interlaminar shear failure strength R_{31} or R_{32} of fabric material ECC452.

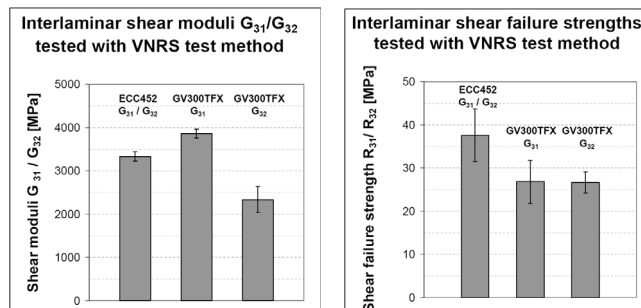


Fig. 5 Interlaminar shear property data of fabric-reinforced polymers GV300TFX and ECC452

Conclusion

Standardised shear test methods were analysed and various tests on textile-reinforced polymers were performed. Shear property data was determined for woven UD fabric GV300TFX and for well-balanced fabric ECC452. Both textiles were infused with the mono-component epoxy resin HexFlow[®] RTM6 by advanced resin-transfer-moulding process. The modified VNRS test fixture is best suitable for intra- and interlaminar shear testing of unidirectional and fabric carbon fibre reinforced polymers and allows a reliable determination of shear property data. The modified VNRS test fixture is equipped with an alignment system as well as guided clamping jaws. It was developed to increase manageability of the test fixture and to simplify specimen mounting as well as to enable a robust and economic intra- and interlaminar shear testing. Standard deviations of the determined shear moduli and strengths were acceptable.

Additionally, it could be shown that an optical strain measurement system is best suitable for strain determination especially for fabric reinforcements with a large pattern repeat of the textile pre-product. Stress-strain-curves can be recorded until specimen failure. Evaluation of strain measurement data was realised with an automatic evaluation-algorithm.

Acknowledgment

The authors gratefully acknowledge the financial support of EU-programme ERDF (European Regional Development Fund) and the support of the German Free State of Saxony.

References

- [1] Standard Test Method for Shear Properties of Composite Materials by the V-Notched Rail Shear Method, ASTM D 7078/D 7078M-05 (2005). American Society for Testing and Materials, West Conshohocken, PA.



International Conference on Innovative Technologies, IN-TECH 2012,
Rijeka, 26. - 28.09.2012



-
- [2] Basan, R.: Untersuchungen der intralaminaren Schubeigenschaften von Faserverbundwerkstoffen mit Epoxydharzmatrix unter Berücksichtigung nichtlinearer Effekte. Dissertation, BAM-Dissertationsreihe, Band 74, Berlin. 2011.
 - [3] Standard Test Method for In-Plane Shear Response of Polymer Matrix Composite Materials by Tensile Test of a $\pm 45^\circ$ Laminate. ASTM D 3518/D 3518M-94 (2007). American Society for Testing and Materials, West Conshohocken, PA.
 - [4] Becker, W.; Kress, G.: Stiffness reduction in laminate coupons due to the free-edge effect. Composites Science and Technology 52 (1994), Nr. 1, S. 109-115.
 - [5] Walrath D.; Adams, D.: The Iosipescu Shear Test as Applied to Composite Materials. Experimental Mechanics, Vol. 23 (1983), P. 105-110.
 - [6] Standard Test Method for Shear Properties of Composite Materials by the V-Notched Beam Method. ASTM D 5379/D 5379M-05. American Society for Testing and Materials, West Conshohocken, PA.
 - [7] Whitney, J. M.; Stansbarger, D.L.; Howell, H.B.: Analysis of the Rail Shear Test-Application and Limitations. Journal of Composite Materials, Vol. 5 (1), 1971, p.: 24-34.



International Conference on Innovative Technologies, IN-TECH 2012,
Rijeka, 26. - 28.09.2012



NOISE ANALYSIS OF THE CROSS WIGNER-VILLE DISTRIBUTION BASED INSTANTANEOUS FREQUENCY ESTIMATION METHOD

D. Malnar¹, V. Sucic¹ and S. Stankovic²

¹ University of Rijeka, Faculty of Engineering, Vukovarska 58, HR-51000
Rijeka, Croatia

² University of Montenegro, Faculty of Electrical Engineering, Džordža Vašingtona bb, 81000
Podgorica, Montenegro

Keywords: time-frequency, instantaneous frequency estimation, cross-terms, noise analysis

Abstract. Noise analysis of the Cross Wigner-Ville distribution (XWVD) based method for the signal components instantaneous frequency (IF) estimation is presented. The utilized method deliberately forms cross-terms in the XWVD between the analyzed signal and a reference signal, and it yields a scaled and time shifted image that closely resembles the IFs of the signal components. Based on the geometrical rules that govern interferences, and by using a reference signal that is well localized in time and frequency, the time-frequency coordinates of the components IF are calculated in an automatic way. The effect of noise on the method's performance is tested for various levels of additive white Gaussian noise. Statistical performance measures are given for multi-component synthetic signals examples.

Introduction

Everyday real life signals which surround us, such as speech, video or animal life or various artificial signals like radio broadcast, sonar or radar, have their information simultaneously present in time and frequency. To be able to fully decode such signals we require joint time-frequency (TF) analysis and processing methods and many such methods have been developed over time. Generally they fall into one of the two categories of time-frequency distributions (TFD); the linear time-frequency distributions and the quadratic (bilinear or energy) TFDs [1].

The key point in TF signal analysis is often revealing how signal's frequency content changes over time, or more precisely, finding the instantaneous frequency (IF) laws of the signal components where component could be, in general, considered an energy continuity in time without abrupt changes in frequency. Therefore, signals can be mono-, or multi-component in nature.

Often the first choice in TF analysis are linear TFDs, such as the short-time Fourier transform (STFT). Rather intuitive and easily understood they lack in TF resolution, whereas the Quadratic class of TFDs has proven to be better but at a price of non-linearity and the associated problems of interference terms [1]. The Wigner-Ville distribution (WVD), being the core representative of the Quadratic class of TFDs possess many useful properties, yet it is corrupted by interferences or cross-terms caused by its bilinear nature whenever the signal under analysis is multi-component. The cross-terms make the interpretation of the TF image more challenging by obscuring signal features.

The majority of work so far, has been directed towards suppression of cross-terms since they are considered as undesirable in general but they do carry valuable information, as it is recognized in [2].

In recent paper, an automatic method that exploits geometrical properties of cross-terms evoked between components of the analyzed signal (AS) and the introduced reference signal (RS) for signal components IF laws estimation has been proposed [3].

This paper briefly outlines the method in [3] and presents noise performance analysis for different classes of multi-component signals in various levels of noise.

The Method Description

Given a real signal $s(t)$, WVD can be calculated according to, [1]:

$$W_z(t, f) = \int_{-\infty}^{\infty} z\left(t + \frac{\tau}{2}\right) z^*\left(t - \frac{\tau}{2}\right) e^{-j2\pi f\tau} d\tau, \quad (1)$$

with $z(t)$ being the analytic associate of $s(t)$ [1]. Considering a mono-component linear frequency modulated signal (LFM), Eq. (1) will yield a perfect localization of signal energy content in the time-frequency plane but a multi-component signal, say, a signal with two components $x(t)$ and $y(t)$, the quadratic superposition principle will take place [1]:

$$W_{x+y}(t, f) = W_x(t, f) + W_y(t, f) + 2\Re\{W_{x,y}(t, f)\}, \quad (2)$$

where

$$W_{x,y}(t, f) = \int_{-\infty}^{\infty} x\left(t + \frac{\tau}{2}\right) y^*\left(t - \frac{\tau}{2}\right) e^{-j2\pi f\tau} d\tau, \quad (3)$$

is the Cross Wigner-Ville distribution (XWVD) of $x(t)$ and $y(t)$ and also the source of cross-terms that obscure the readability of $W_{x+y}(t, f)$.

WVD as the Eq. (2) states, consists of the signal auto-terms (the WVDs of the individual components) and the cross-terms (the XWVD of the components). Any signal component yields an auto-term, and any pair of signal components produces a cross-term [2]. If only the WVD of a signal is presented a clear distinction between the signal terms and the interference terms could not be easily made. As no signal is ever perfectly clear of noise, the TF image becomes even more obscured as noise provides additional cross-terms caused by its interaction with the signal components. However, the position of the cross-terms is not random. They are governed by strict geometrical laws [2], such that they appear half-way on a straight line between any two points in the signal. Therefore, their TF coordinates can be calculated according to [2]:

$$t_i = \frac{1}{2}(t_1 + t_2), \quad (4)$$

$$f_i = \frac{1}{2}(f_1 + f_2). \quad (5)$$

where t_i and f_i are time and frequency coordinates of the cross-term, while (t_1, f_1) and (t_2, f_2) represent the coordinates of the points in the signal that interfere.

Knowing the coordinates of one of the interfering points and the coordinates of the cross-term, it is possible to localize the other signal point utilizing the method in [3], steps of which are as follows:

1. form the RS of length N as a low frequency Gaussian atom. This provides the reference t_1 and f_1 coordinates.
2. if needed, concatenate zero-valued samples at the start of the AS. This insures a clear time reference point, but also shifts the AS forward in time. Accounted for in step 6.
3. Calculate the XWVD of the RS and the AS, as per Eq. (3). A scaled image of the true signal components is revealed.
4. Extract the envelope of each of the time slices of the XWVD. For each time slice of the XWVD, perform peak detection. The detected peaks represent t_i and f_i coordinates in Eqs. (4) and (5), respectively.
5. Link the detected coordinates into individual cross-components by following the criterion of energy continuity in time.
6. Perform the scaling of the cross-terms coordinates according to Eqs. (6) and (7):

$$t_2 = 2 \cdot t_i - t_1, \quad (6)$$

$$f_2 = 2 \cdot f_i - f_1. \quad (7)$$

In Eq. (6), the time shift of step 2 needs to be compensated. The values of t_2 and f_2 , resulting from Eqs. (6) and (7), respectively, represent the estimated time and frequency coordinates of the AS component.

7. Smooth and interpolate the scaled coordinates to obtain the IF estimate of the AS component.

Performance Evaluation

Three multi-component signals of different classes were considered for the performance evaluation of the method in [3] against additive white Gaussian noise of zero mean and variance of 1. The reference signal of 512 time samples for all cases is a Gaussian atom with a time spread of 26 points, centered at time index 32 and frequency 0.05.

The first signal represents a class containing only LFM components of unit amplitude and various rates of frequency change; component 1 is varying in frequency from 0.2 at the time index 35 to 0.35 at the time index 350. Component 2, goes from frequency 0.35 to 0.45 in the time frame [80, 490], while component 3 is varying from frequency 0.1 at the time index 100 to 0.35 at the time index 450.

After numerical simulation, the resulting mean squared errors (MSE) as performance measures, for each of the AS components IFs are provided in Table 1. In Fig. 1, the WVD of the considered signal is presented. Fig. 2 shows the IF estimates overlaid with the true component IFs for the case of 5 [dB] SNR.

Table 1. MSE of the estimated IF laws for the three components of the first considered signal (Fig. 1) for different noise levels.

	$20 \log_{10} \frac{A_{Signal}}{A_{Noise}} \text{ [dB]}$		
	∞	10	5
Component 1	$8.64 \cdot 10^{-5}$	$4.60 \cdot 10^{-4}$	$7.04 \cdot 10^{-4}$
Component 2	$3.07 \cdot 10^{-6}$	$9.01 \cdot 10^{-4}$	$1.69 \cdot 10^{-3}$
Component 3	$2.70 \cdot 10^{-6}$	$3.59 \cdot 10^{-4}$	$8.42 \cdot 10^{-4}$

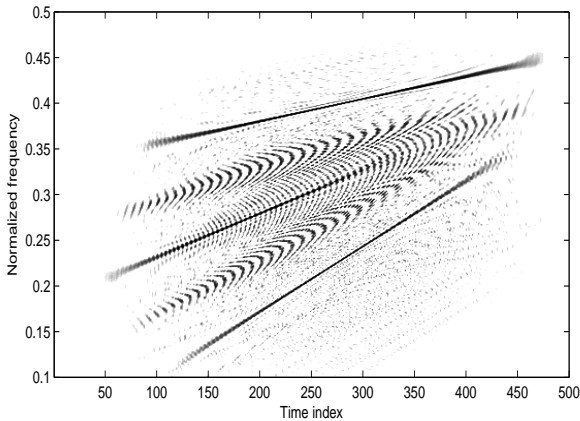


Fig. 1 The WVD of the first considered signal. SNR of 5 [dB].

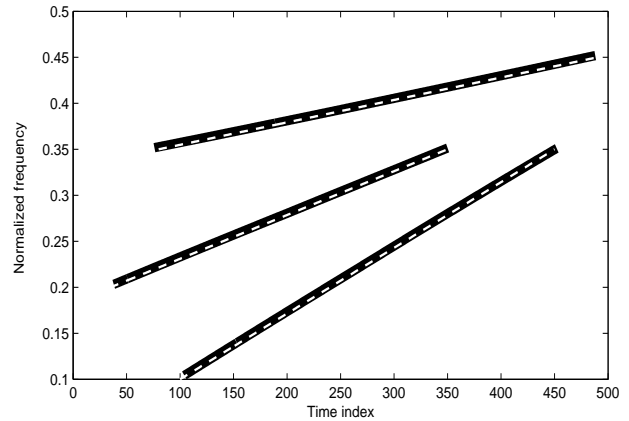


Fig. 2 Estimated IF laws (solid) of the signal in Fig. 1 with the true IF laws (dashed).

The second signal (Fig. 3) is a mixture of two non-linear and one linear FM component:

- a parabolic, unit amplitude FM (PFM), defined by three points: it starts at frequency 0.08, time index 50, peaks at frequency 0.2, time index 250, and ends at frequency 0.1, time index 450,
- a positive slope, unit amplitude LFM, varying in frequency from 0.15 at time index 60 to 0.45 at time index 500, and again,
- a parabolic, unit amplitude FM that starts at frequency 0.25, time index 80, peaks at frequency 0.35, time index 280, and ends at frequency 0.45, time index 380.

Table 2 provides performance values in terms of MSE for three levels of SNR while Figs. 3 and 4, respectively, offer visual comparison of the performance for SNR of 5 [dB].

Table 2. MSE of the estimated IF laws for the three components of the second considered signal (Fig. 3) for different noise levels.

	$20 \log_{10} \frac{A_{\text{Signal}}}{A_{\text{Noise}}} \text{ [dB]}$		
	∞	10	5
Component 1	$3.99 \cdot 10^{-6}$	$3.93 \cdot 10^{-5}$	$5.18 \cdot 10^{-5}$
Component 2	$1.02 \cdot 10^{-4}$	$8.12 \cdot 10^{-4}$	$1.20 \cdot 10^{-3}$
Component 3	$3.82 \cdot 10^{-6}$	$9.61 \cdot 10^{-4}$	$1.50 \cdot 10^{-3}$

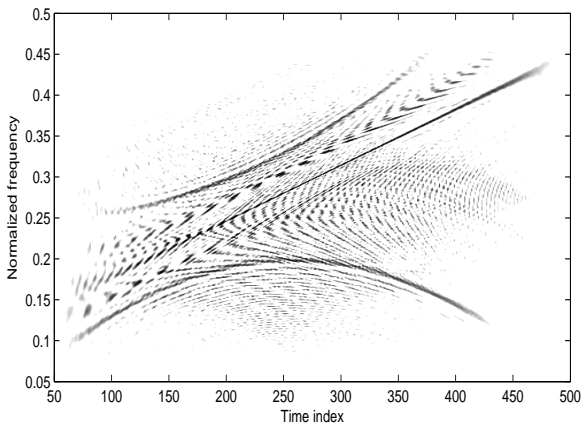


Fig. 3 The WVD of the second considered signal. SNR of 5 [dB].

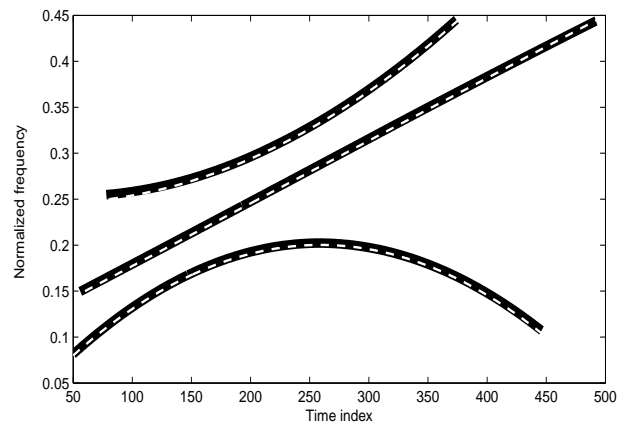


Fig. 4 Estimated IF laws (solid) of the signal in Fig. 3 with the true IF laws (dashed).

As a final measure of performance we considered a signal constituted of a three, relatively closely spaced, slowly varying LFM that can be used to model EEG patterns of epileptic seizures in newborns [4]. The first and the second component of the signal decrease in frequency from 0.15 to 0.14, and from 0.20 to 0.19, respectively, from time index 50 to 500, while the component 3 varies from frequency 0.25 at time index 220 down to 0.24 at time index 400. Again, as in the previous examples, Table 3 and the subsequent Figs. 5 and 6, present performance characteristics of the method for three levels of SNR.

Table 3. MSE of the estimated IF laws for the three components of the third considered signal (Fig. 5) for different noise levels.

	$20 \log_{10} \frac{A_{Signal}}{A_{Noise}} \text{ [dB]}$		
	∞	10	5
Component 1	$8.83 \cdot 10^{-5}$	$1.22 \cdot 10^{-4}$	$1.59 \cdot 10^{-4}$
Component 2	$1.59 \cdot 10^{-4}$	$1.61 \cdot 10^{-4}$	$3.54 \cdot 10^{-4}$
Component 3	$1.45 \cdot 10^{-6}$	$2.69 \cdot 10^{-4}$	$4.85 \cdot 10^{-4}$

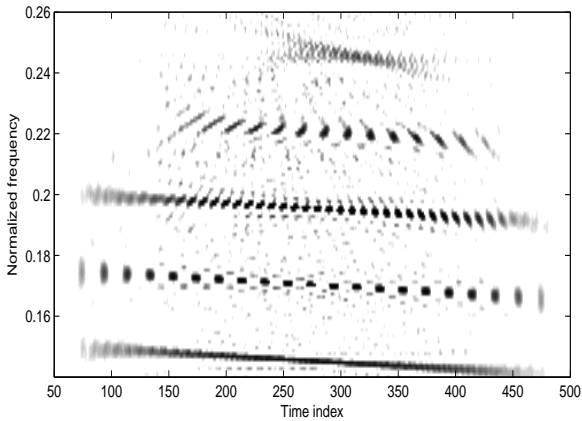


Fig. 5 The WVD of the third considered signal, a model of the EEG seizure patterns in newborns. SNR of 5 [dB].

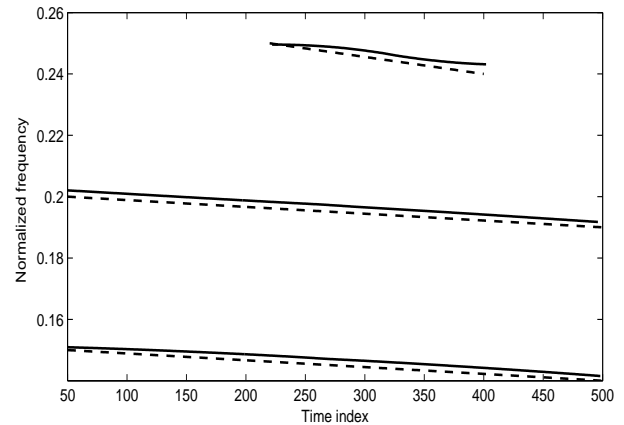


Fig. 6 Estimated IF laws (solid) of the signal in Fig. 5 with the true IF laws (dashed).

Conclusion

In this paper, a simple, yet effective method for signal components IF estimation has been briefly outlined and the results of noise analysis presented. The method was tested with multi-component signals of linear only FMs, and with a class of mixed non-linear and linear FMs. The tests were also performed on a model of an EEG signal. The obtained results, numerical and visual, show the method's capability in dealing with various signal classes and different time durations of signal components as well as its high-performance in low SNR, indicating its potential in practical applications, such as analysis of biomedical signals, where classical approaches based on stationarity assumptions are not appropriate.

Acknowledgment

This work is a part of the research project "Optimization and Design of Time-Frequency Distributions", No. 069-0362214-1575, which is financially supported by the Ministry of Science, Education and Sports of the Republic of Croatia.

References

- [1] B. Boashash: *Time-Frequency Signal Analysis and Processing: A Comprehensive Reference* (Elsevier, 2003).
- [2] F. Hlawatsch: Interference terms in the Wigner distribution, *Digital Signal Processing*, Vol. 84 (1984), pp. 363 - 367.
- [3] D. Malnar, V. Sucic and B. Boashash: A Cross-terms Geometry Based Method for Components Instantaneous Frequency Estimation Using the Cross Wigner-Ville Distribution, *Proc of 11th ISSPA International Conference on Information Sciences, Signal Processing and their Applications*, (2012), pp. 1250 - 1255.
- [4] P. Celka, B. Boashash, and P. Colditz: Preprocessing and time-frequency analysis of newborn EEG seizures, *IEEE Engineering in Medicine & Biology Magazine*, Vol. 20 (2001), pp. 30 - 39.

REDUCTION OF CHIP AREA FOR FEED-FORWARD NEURAL NETWORKS WITH USE THE SPECIAL MULTIPLICATION BY AND GATE

R. Záluský¹, D. Ďuračková¹ and V. Sedlák¹

¹ Slovak University of Technology in Bratislava, Faculty of Electrical Engineering and Information Technology, Ilkovičova 3, 812 19 Bratislava, Slovakia

Keywords: Feed-forward Neural Network, Multiplication, FPGA, chip area overhead

Abstract. This paper deals with the design of a new architecture of digital neurons for use in the feed-forward neural networks and their subsequent implementation in the FPGA chip. The proposed neuron uses a special type of multiplication realized by AND gate. Comparison of usual ways of implementing digital feed-forward neural networks using integers, numbers with floating point and the novel architecture that uses a new special multiplication is presented. Finally, chip area consumption and other features of the feed-forward neural network with the new architecture are compared to standard architectures.

Introduction

Calculation of output activity of huge number of neurons is very demanding on the computer performance, so this implementation leads to a slower neural network compared to a hardware network implemented on the chip. Hardware implementation offers parallel data processing and therefore, the calculation of such a network is very fast. Artificial neuron itself is a complex element, which includes the operations of multiplication, sum and non-linear functions. In the commonly used data formats and standard circuits to implement the basic operations, only a small number of neurons can be feasibly implemented on the chip. Therefore, an effort to design a new neural network architecture that would use neurons working with operations could significantly help to reduce their complexity. This would also ensure less chip area overhead and therefore, much larger number of neurons on the chip could be implemented. The novel NN architecture that uses a new type of serial multiplication employing a simple AND gate is presented, and the achieved results as well as the main advantages are discussed.

Theoretical part

Some systems are very difficult to describe, or are so complex that their description is almost impossible. If we have input data and the required outputs, it is possible to approximate the response of the system. As universal approximators are widely used artificial neural networks that are trained on a given problem. Basic principles of neural networks are referred in [1] – [4].

Neural network work in two modes. The first mode is learning or training. In this phase, it is necessary to train the neural network on a given problem. For training, so called the training data set is used, composed of the inputs and the related expected output values. Learned knowledge is stored in the synaptic weight coefficients w and threshold coefficients ϑ . After the learning period is the run mode. In this mode, the neural network is able to solve the problem that it was trained for. During the run mode, weights and threshold coefficients are constant. The basic element of the neural network is a neuron. A model of the neuron consists of several inputs x_i , potential of the neuron ξ and the activation function $s(\xi)$. The potential is obtained by multiplication of inputs x_i with the corresponding weights w_{ij} and their subsequent summation and addition to the threshold coefficient ϑ_i , as stated in equation 1. The output activity of a neuron is given by processing the neuron potential ξ_i using the activation function $s(\xi_i)$, as stated in equation 2. The activation function has a specific shape and significantly affects the function of the neuron. There are many types of the activation functions referred in [1], [2] and [3]. Type of used activation function depends on the network topology and the particular application. For classification purposes and applications, the most suitable type is the sigmoidal function, described by equation (3), where A and B are maximum and minimum of the sigmoidal function and α is the slope.

$$\xi_i(x, w, \vartheta) = \sum_{j=1}^m w_{ij}x_j + \vartheta_i \quad (1)$$

$$y_i = s(\xi_i) \quad (2)$$

$$s(\xi) = \frac{B + Ae^{-\alpha\xi}}{1 + e^{-\alpha\xi}} \quad (3)$$

By arrangement of neurons in several layers one can obtain the multilayer feed-forward neural network. Layers are divided into the input layer, hidden layers and the output layer. In feed-forward NN, the input data is distributed and processed in only in the direction from input to output. Neurons of one layer are interconnected to the neurons from the next layer. Thus, the outputs activities y_j in the current layer depends only on the output activities of neurons in the previous layer.

The main advantage of neural networks is definitely their ability to learn. This is different from the capabilities of conventional computers that need to have programmed the algorithm for a given task. Computer algorithms can perform exactly the programmed task but can not adapt to changes in the parameters of the task. In contrast to computer algorithms, it is necessary only to learn a neural network to solve the problem. Neural network is then able to classify correctly the objects that are different from standard objects of the task. Another very important feature of neural networks is their parallelism that offers huge computational performance/capacity.

Experimental part

The main disadvantage of neural networks working with integers as well as with floating-point numbers is high complexity of the units performing mathematical operations. Therefore, we developed a new method for serial multiplication using simple AND gates. In the proposed method of serial multiplication, the potential of the neuron is calculated in one step, because the operations of multiplication and summation are performed simultaneously. This brings a significant simplification of the neuron circuitry resulting in less area overhead.

The method of multiplication using AND gate is based on subsequent multiplication of two numbers bit by bit using a simple 2-input AND gate. Numbers are always in the interval $\langle 0; 1 \rangle$, because a given number is part of the specified range. This means that by two 4-bit numbers it is possible to express 16 values. Therefore, a given number will be the n -th of this value. For example, number 5 would be $5/15$. We will refer to the operations of multiplication symbol as \cdot (Eq. 4). Multiplication operation is performed over a time interval called "time window". Length of the time window is defined as the maximum value, which the number can take. To perform the product of n -bit numbers, a and b are the lengths of the time window 2^{n-1} time units. For the proper function of multiplication, it is necessary that coefficients are encoded in time. One number has to be encoded in the time from the beginning of the time window (Fig. 1a). For example, number 5 would have first five units of time (clock cycles) value of 1 and then value of 0. The other number has to be encoded in the time symmetrically around the center of the time window as shown in Fig. 1b). In the multiplication process, it does not matter, which number is encoded one way or another but both numbers must be encoded in different ways. The operation of multiplication is implemented by gating encoded numbers a and b of the individual moments of time window. The product of multiplication is spread over time. The final result of multiplication is count of the ones in the time window. This multiplication has an effect of natural rounding. In order to be able to work also with negative values, it is necessary to extend the numbers a and b with the signs a_s and b_s . Sign of result y_s is then calculated using the logic function XOR.

$$y = a \cdot b \tag{4}$$

$$\xi = \sum_{j=1}^m w_j \cdot x_j + \vartheta \tag{5}$$

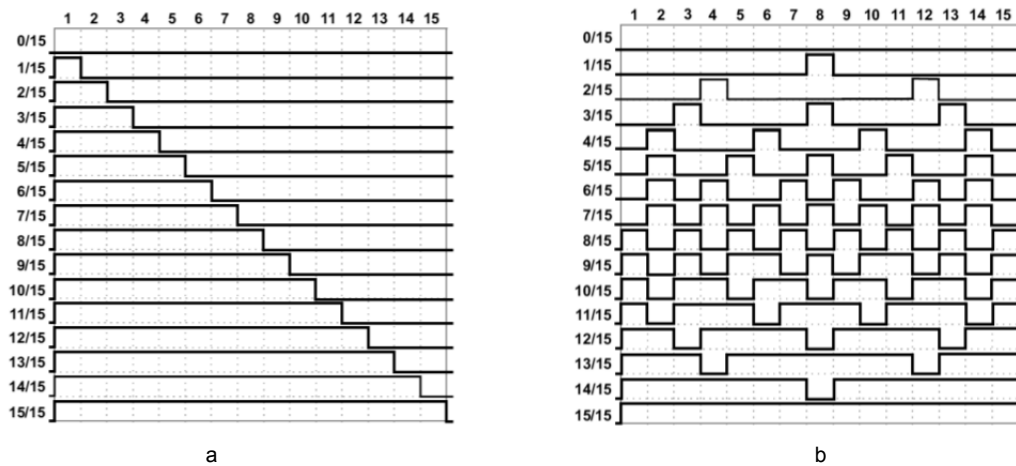


Fig. 1 Encoding the number: a) from the beginning of time window
b) symmetrically around the center of the time window

In architectures working with integers or floating-point numbers, the calculation of the neuron potential is realized in two steps. Firstly, inputs x_n are multiplied with the corresponding weight coefficients w . Then, the products of multiplications are subsequently up by use of multi-input adder. In the proposed novel architecture of a digital neuron using multiplication by AND gate, the multiplication of inputs with weights coefficients is performed simultaneously within the duration of one time window (5). Nonlinear activation function is realized by a table. The proposed architecture uses 4-bit numbers and one bit to store the sign, so we can express 32 values from the interval $\langle -15/15; 15/15 \rangle$. In this case, the ROM memory size is 32×5 bits. Function values are calculated for the following parameters of sigmoidal function: $A = -15$, $B = 15$ and $\alpha = 0.3$.

Fig. 2 shows the schematic of a digital neuron using special multiplication by AND gate. Signals x_n are inputs of neuron encoded in time from beginning of time window (Fig. 1a). Each input x has the corresponding sign x_s . Signal *start* is used to begin the computation of output activity of the neuron. Circuit *sum* computes the potential of the neuron (Eq. 5). The calculation of activation function is realized by circuit *Sigmoid*. Circuit *ConvertX* encodes the number in direct code from the beginning of time window (Fig. 1a), and *PISO* register converts it to serial data. *TW_counter* counts the length of the time window. Weight coefficients w_n and the neuron threshold ϑ are encrypted symmetrically around the center of the time window (Fig. 1b), and are permanently stored in the *SUM* circuit. This neuron can be optimized for use in the output layer of neural network. Neurons in the output layer needs the parallel output. In the optimized output neurons, circuits for encrypting the output activities have been excluded from the optimized neuron structure.

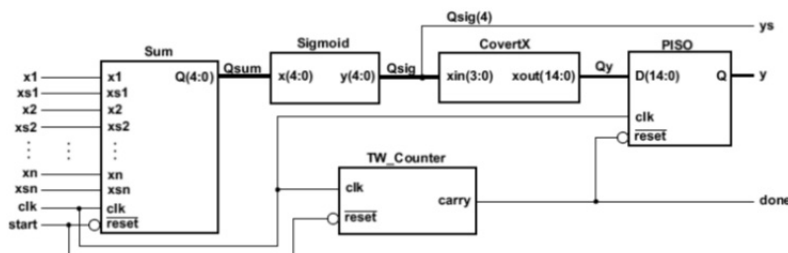


Fig. 2 Schematic diagram of a digital neuron employing special multiplication by AND gate

The feed-forward neural network consists of neurons organized into multiple layers. Computation of output activities of the neural network is sequential, layer by layer, while the output activity of neurons in a given layer are calculated in parallel. End of calculation in the layer is indicated by a high level of signal *done*. Simultaneously, the output activities of the neuron in previous layer are fed serially to inputs of neurons in next layer. The high level of signal *done* triggers the computation of the output activities of neurons in next layer. Entire calculation of the output activities of the whole neural network takes as many time windows as many layers the neural network has. In the optimized neural network, the output layer is composed of the optimized neurons. Thus, non-optimized neural network of the proposed architecture using a special multiplication by AND gate would need circuits for encoding the network inputs and circuits for decoding the output activities of the network. Decoding the network output activities takes one time window, so the total computation of the output activities takes $l+1$ time windows, where l is the number of layers forming the neural network. Output activities in the optimized neural network are represented in the direct code and therefore, no additional circuits for decoding them are needed. This will make the computation of output activities in one time window shorter.

Similar architecture of Stochastic Hopfield Neural Networks (SHNNs) using the same multiplication principle was presented in [5]. However, the architecture proposed there contains only one layer, and to calculate the neural network outputs, lot of cycles are needed. On the other hand, the architecture proposed in this paper, the calculation of the neural network outputs requires only $l*15$ clock cycles, where l is the number of all network layers.

Results

We have designed three usual architectures of FFNN for comparison with then novel architecture. First two architectures works with 8-bits integers and uses serial and parallel multipliers. Another type of usual architecture is based on working with numbers using floating-point. This architecture works with Microfloat format, which takes only 8 bits [6]. All the architectures were described by VHDL language and synthesized for three FPGA chips Xilinx Spartan 3 of different sizes, listed in Table 1. FPGA chip consists of configurable logic blocks (CLB). Each CLB contains four slices, and each slice contains two look-up tables and two flip-flops, multiplexers and logic gates. The chip area is determined mainly by the number of slices needed to implement the circuit.

We compared the chip area of the neuron circuits for increasing number of inputs in the range from 5 to 50 with step of 5. The obtained results for the proposed neural network architectures are shown in Fig. 3. Both types of neurons of the novel architecture need for the implementation to the FPGA chip approximately 7 times less number of slices. Moreover, the digital neuron, which uses the optimized novel architecture consumes 10 slice less than that of the non-optimized architecture. This is because the neuron optimization is performed only on its output and does not affect the calculation of the potential of a neuron.

Table 1. List of used FPGA chips

Type	CLBs	Slices
Xc3s1000	1920	7680
Xc3s1500	3328	13312
Xc3s2000	5120	20480

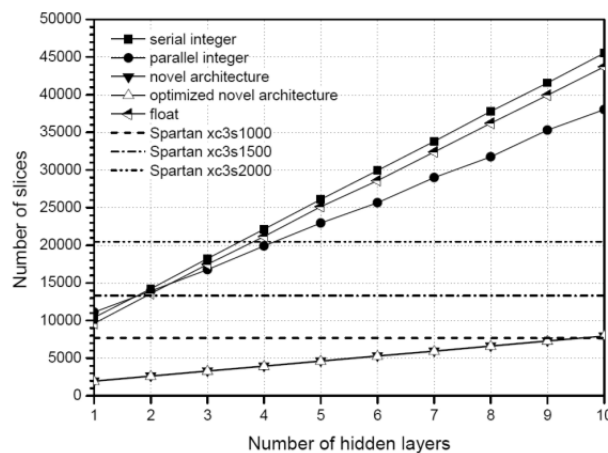


Fig. 3 Comparison of chip area for FFNNs in dependence on the number of hidden layers

Next, the comparison of chip area for feed-forward neural networks versus the number of hidden layers with constant number of hidden neurons has been carried out. The input layer consisted of 20 input neurons, each hidden layer was formed by 10 hidden neurons, and output layer contained 6 output neurons. Number of hidden layers was varied in the range from 1 to 10 with step of 1. Obtained results are shown in Fig. 4a. Dependency of chip area consumption on the number of hidden layers of neural network is linear. This is due to only the increasing number of neurons and connections between neurons, without changing complexity of the neurons. The smallest number of slice blocks needed to implement the neural network in FPGA chip was achieved for both types of the novel architecture, which needed on an average 5 times smaller slice number of blocks than the other three architectures. In the smallest type of FPGA chip Spartan xc3s1000 (dashed line), it can be implemented only a neural network with novel architecture (non-optimized and optimized) of complexity up to 9 hidden layers. To implement the novel architecture of the neural network containing 10 hidden layers it is necessary to choose a larger type of FPGA chip, e.g. Spartan xc3s1500 (dash dot line). On the other hand, none of the other three regular NN architectures can be implemented in the smallest FPGA chip Spartan xc3s1000. Medium size FPGA chip Spartan xc3s1500 would be able to implement a neural network, which contains only one hidden layer. In the largest type of FPGA chip Spartan xc3s2000 (dash dot dot line) it is possible to implement classical neural networks with up to three hidden layers.

For further comparison of the chip area depending on the neural network topology, we varied the number of neurons in hidden layers, while keeping the number of hidden layers constant. Each neural network consisted of two hidden layers. The input layer consisted of 20 input neurons, both hidden layers contained hidden neurons in the range from 5 to 50 with step 5, and the output layer was composed of 6 output neurons. The chip area as a function of the number of neurons in the hidden layers is shown in Fig.4b. The obtained dependences are exponential. This is due to the increasing number of neurons, connections between neurons, and also the enhanced complexity of neurons for the increasing number of inputs (Fig.3). The proposed novel neural network architecture requires on an average of 5 to 6 times less slices to be implemented in an FPGA chip in comparison to the other three architectures. To the smallest FPGA chip Spartan xc3s1000 (dashed line) can be implemented a neural network of the novel architecture with two hidden layers and 25 hidden neurons in each hidden layer. Medium size FPGA chip Spartan xc3s1500 (dash dot line) can implement a neural network of the novel architecture containing two hidden layers with 35 hidden neurons. Finally, into the FPGA type xc3s2000 (dash dot dot line), a neural network of the architecture with two hidden layers and 45 hidden neurons in each hidden layer can be implemented. The other three architectures of neural networks can be implemented into the smallest FPGA chip xc3s1000 only in the complexity containing two hidden layers with 5 hidden neurons in each hidden layer. To the largest type of FPGA chip xc3s2000 can be implemented a neural network with two hidden layers of 10 hidden neurons in each hidden layer. Neural networks working with integers and using serial multipliers take a larger number of slices because they use both combinational and sequential circuits.

Taking this fact into account, the novel neural networks require less chip area compared to architectures using integer or float numbers. This is due to simpler neurons needed for the novel architecture. Other reason is that the new neural network architecture includes 1-bit nets between neurons, through which the signals are distributed serially, while the other NN architectures using multibit signals (8 and 9-bits) work with parallel data transfer.

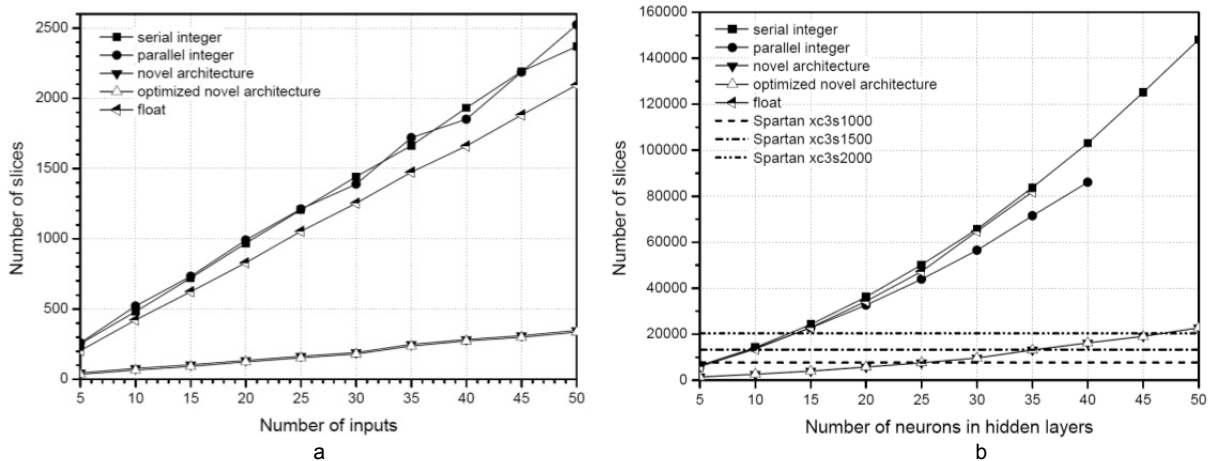


Fig. 4 Chip area for FFNNs as a dependence of the: a) number of hidden layers
b) number of neurons in hidden layers

Conclusion

A novel architecture of a digital neuron, which uses the special multiplication by AND gate has been proposed and designed. The aim was to achieve the smallest chip area consumption in hardware implementation. Consequently, the new architecture of a digital neuron was compared to neurons working with integers and floating-point numbers. In case of neurons working with integers, we realized two different solutions, one working with serial multipliers and the other using parallel multipliers. Neurons working with floating-point numbers use Microfloat format, since it is the simplest FP format. The most complex solution is the architecture of a neuron employing integers and serial multipliers. The architecture employing parallel multipliers takes comparatively the same chip area as the architecture with FP numbers. On the other hand, the novel architecture takes approximately about 2/3 less chip area than the second simplest conventional network architecture. In comparison to the most complex architecture, the proposed novel neuron hardware is roughly 6 times smaller.

Acknowledgment

This work has been supported by the project "Support of the Centre of Excellence for Smart Technology, Systems and Services II", ITMS Code 26 24 01 20 005, and by projects VEGA 1/0987/12 and VEGA 1/0285/09 sponsored by Ministry of Education of the Slovak Republic.

References

- [1] V. Kvasnička, L. Beňušková, I. Farkaš, A. Kráľ, J. Pospíchal and P. Tiňo: Introduction into the neural networks (In Slovak), (*IRIS, Bratislava, 1997*).
- [2] P. Sinčák and G. Andrejková: Neural Networks (The engineering methodology) part 1. (In Slovak), (*Elfa s.r.o., Košice, 1996*).
- [3] C. R. Alavala: Logic and Neural Networks: Basic concepts and applications, (New Age Publications, 2007).
- [4] S. Theodoridis and K. Koutroubas: Pattern Recognition, (Academic Press, Boston, 2009).
- [5] A. Torralba, F. Colodro and L. G. Franquelo: *A mixed parallel-sequential SHNN for large networks*. Lecture Notes in Computer Science, VOL 930/1995, p. 789-793, 1995.
- [6] W. Kahan: *IEEE standard 754 for Binary Floating-Point Arithmetic*. Elect. Eng. and Computer Science, 1997.

THE EFFECT ON NON-UNIFORM PLASTIC DEFORMATION OF THIN TINPLATES ON THEIR CORROSIVE RESISTANCE

E. Spišák¹, J. Majerníková¹, L. Kaščák¹ and J. Slota¹

¹ Technical University of Košice, Mechanical Engineering Faculty, Department of Technologies and Materials, Mäsiarska 74, 040 01 Košice, Slovakia

Keywords: thin tinplates, corrosion, cracking of meat tins

Abstract. Nowadays thin tinplates are processed predominantly by compression moulding. At the production of two-piece tins (lid and cap with flange) various types of stresses and deformations of thin wrapping sheet occur. From the viewpoint of material stress, the least appropriate scheme is the one containing tension stress. In this contribution we have tested the corrosive resistance of thin tinplates after the biaxial tensile test (Bulge test). Corrosive resistance was evaluated after various time spans (corresponding to 3 years). Samples were deformed in three deformation levels (approx. 5%, 10% and after deformation). For the purpose of this test, samples made from continually annealed, batch annealed, once reduced and twice reduced sheets were used.

Introduction

Nowadays thin tinplates belong among the most important production and export goods of the biggest metallurgical companies. Within the last three years the production of these plates in U.S. Steel Košice has boosted to more than twice the quantity before and currently it makes more than 300 thousand tones of thin tinplates per year. In the last years the development of these plates led to a significant reduction of thickness (from thickness of 0,26 mm to 0,14 – 0,18 mm) and considerable reduction of tin coating thickness from the former 11 and more gram/m² (hot-dip tinning) to the current 1 – 2 gram/m² (electrolytic tin coating)[1]. There is a significant change in the treatment of thin tinplates for the production of wrappings [2]. Currently the majority of produced wrappings are of so called two-piece metal wrappings made by drawing round, square, oval, etc. caps and tin lids that are mutually connected by flanging. The current technology of drawing for the purpose of caps production lays extensive demands on the plastic properties of thin tinplates. With this drawing process there are considerable plastic deformations of steel material, as well as tinned layer. These days even prominent manufacturers feel the pressure of quality demands on tinplates. Thicknesses of tinplates need to be reduced while maintaining the required elongation [5]. There are increasing requirements as to the inner and outer cleanness of bands, as to their close dimensional tolerances and ideal planeness. Requirements for surface microgeometry are tightening. In this contribution the intention was to point out the relation between the size of plastic deformation and corrosive resistance of thin tinplates.

Experimental Material

For the experimental research we used materials once reduced continually annealed with marking TH 435CA, thickness 0,24mm and twice reduced batch annealed with marking TS 550 BA, thickness 0,16 mm. Mechanical properties of applied sheets discovered by the uniaxial and biaxial tensile force test are shown in sheet No. 1. Graphic relation between tension and deformation at biaxial tensile force test of tested materials are presented in Fig. No. 1, 2. Once reduced continually annealed sheet showed higher tensibility as well as lower yield value and strength (see Fig. 1) in comparison with twice reduced batch annealed sheet (see Fig. 2).

Table 1. Mechanical properties of examined materials

Material	Tensile test			Biaxial test		
	Re [MPa]	Rm [MPa]	A ₅₀ [%]	Re [MPa]	Rm [MPa]	A _B [%]
TH 435CA ⊥	468	447	28,1	342	506	14,6
TH 435CA	453	448	25,5			
TS 550BA ⊥	525	534	2,6	535	587	6,3
TS 550BA	523	531	3,1			

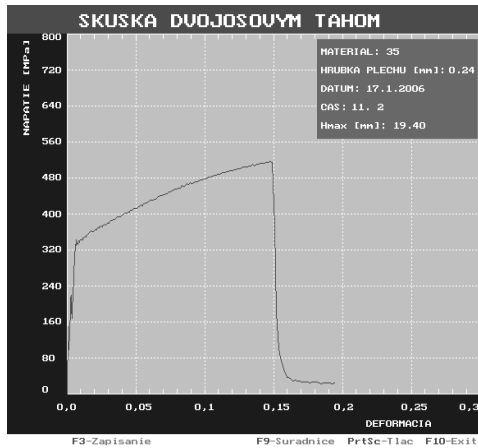


Fig. 1 Dependence stress-strain of sample number 35, material TH 435,CA, thickness 0,24 mm

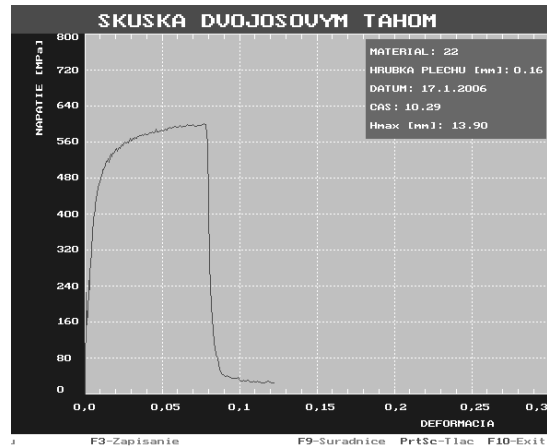


Fig. 2 Dependence stress-strain of sample number 22, material TS 550,BA, thickness 0,16 mm

Evaluation of Corrosive Resistance of Examined Sheets after Biaxial Tensile Test

After approx. 3% (5%) and after 6% (10%) deformation the tested materials were placed into corrosive chamber with salt fog at the temperature 20°C. Action time of the corrosive environment corresponded with the average period of 3 years in real conditions. The corrosive treatment of tested materials was evaluated both visually and metallographically. Figures No. 3, 5, 7 show sheets from steel TS 550BA after 3%, 6% deformation and breakage. Figures No. 4, 6, 8 show sheets from steel TH 435CA after 5%, 10% deformation and breakage.

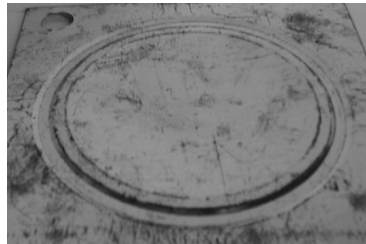


Fig. 3 Sheet TS 550BA after 3% deformation

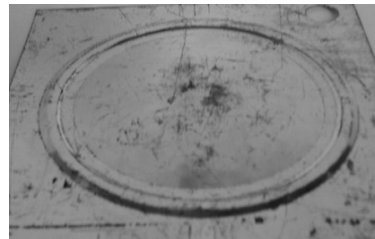


Fig. 4 Sheet TH 435CA after 5% deformation

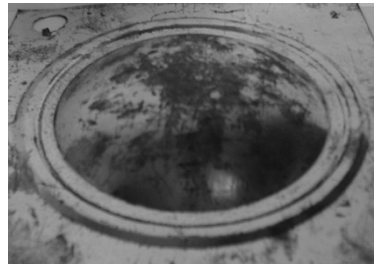


Fig. 5 Sheet TS 550BA after 6% deformation

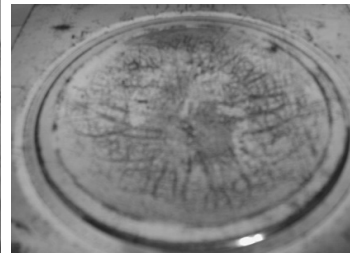


Fig. 6 Sheet TH 435CA after 10% deformation



Fig. 7 Sheet TS 550BA after breakage

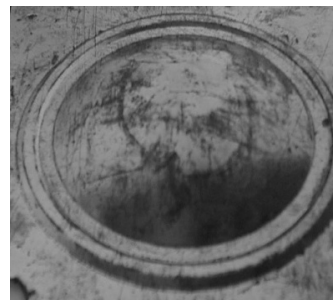


Fig. 8 Sheet TH 435CA after breakage

Sheets from steel TS 550BA were distinguished by a higher yield value, higher breaking strength and lower elongation (rupture occurred at approx. 8% deformation), but the deformation process ran without any significant slip planes in the entire deformed volume. In

case of continually annealed sheet TH 435CA we measured a higher elongation, lower yield value and lower tensile strength, but the sheet deformation showed a considerable inhomogeneity in form of significant slip planes (see Fig. No. 9 and 10).



Fig. 9 Sheet TS 550BA after breakage before corrosion Fig. 10 Sheet TH 435CA after breakage before corrosion

With sheets batch annealed the corrosion became evident on a larger area, though it was more uniform and did not do significant damage to the base material. As with sheet continually annealed, the corrosion collected right on the place of local deformations (slip planes), see Fig. No. 6 and 8. This corrosion damaged the tin protective layer and a rather significant corrosion of base material occurred (see Fig. No. 11 and 12).

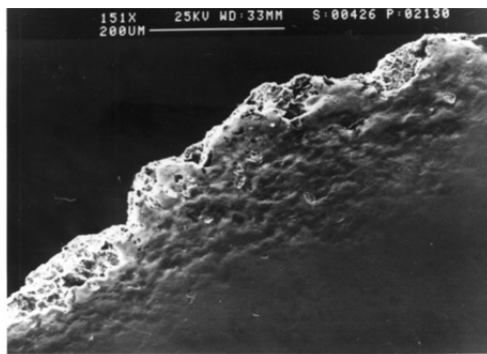


Fig. 11 Sheet corrosion near to material breakage

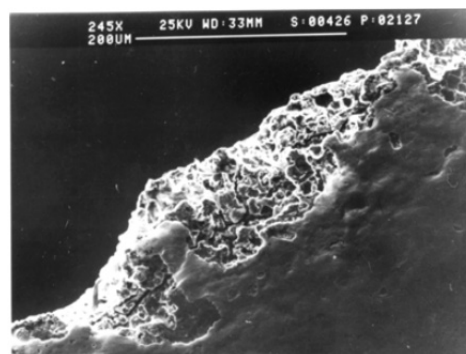


Fig. 12 Secondary corrosion cracks

Influence of Corrosive Resistance in Breaking of Wrapping of Tinned Meat

Teams of experts started to be concerned with the issue of breaking of tinned meat in the sixties of the 20th century. This phenomenon came to be seriously significant with long-term storage of tins and, in fact, has partially persisted to these days. The mentioned problem was even more obscure, as meat and meat products were categorised as the least aggressive filling by all the authors in accordance with the contemporary expert literature. Considerably more works were dedicated to breaking of tinned meat that contained fillings releasing hydrogen sulphide (e.g. green bean). According to these sources, sulphides are rather effective accelerators of hydrogen diffusion in steel [4, 5, 8]. Hydrogen then accelerates the electrolytic corrosion. In particular it is manifested on those places that are concurrently deformed and contain internal tension. It is assumed that the reasons for unsystematic occurrence of FeS are found in steel production faults. The effect of diffused hydrogen on the corrosion process is an especially significant accelerator of non-metallic inclusion and carbide occurrence. As for continually cast steel the effect of hydrogen is significantly lower [6].

In case of tinned meat it is the interaction of wrapping and filling, which are mostly associated only with the occurrence of dark iron sulphides and tin on the inner tin surface. With the case of the above breaking, theoretically two types of corrosive cracking could apply herein:

- a) sulfidic – material embrittlement by diffusing hydrogen released on steel surface, or tin coating by hydrogen sulphide,
- b) stress-corrosion cracking with the mechanism of anodic dissolution of metal, in this case možu hrat' rolu some substances released from meat or additives, above all NH₃, amines and Cl⁻, but also NO₂⁻, carboxyl acids, residues of pesticides, etc.

These facts, however, needed to be unambiguously proven and demonstrate that tinned meat cracking occurring with long-term storage is not caused merely by low-quality sheet, but it is a corrosive-mechanic process, indeed. For the above to apper, only two conditions are necessary and sufficient:

1. specific minimum level of residual tensile stress,
2. specific corrosive environment.

As for tinned meat both the above conditions [4] have been fulfilled. There was significant residual tensile tension on lid and bottom curvature radii and the filling made for long-term storage contained significantly more chlorides. The above mentioned assumptions were proven on several types of tinned meat, which at the time of research were not damaged. The example of such tin cap with apparent corrosion and local thinning in the radius of lid curvature is present in Figure No. 13. Figure No. 14 shows an example where the lid was damaged by corrosion nearly over the entire thickness.

On figure No. 15 it is evident that except for primary corrosive rupture in the lid there are further secondary corrosive ruptures that are being expanded, which in turn could cause material rupture. In Fig. No. 16 there is the part of lid damaged by corrosion which serves as clear evidence of intercrystalline corrosion spreading over the edges of base material grains. The above spreading was further enhanced by

a partial decarburization of the thin steel sheet surface prior to its tinning, where the enlargement of grain in surface layers [6] had occurred.

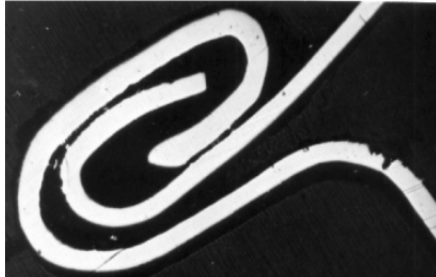


Fig.13 Lid of the tin damaged by corrosion

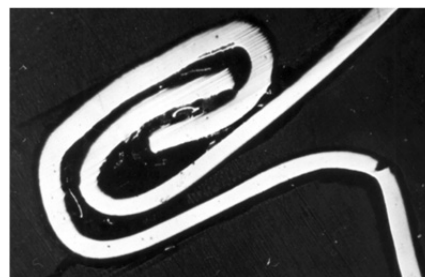


Fig.14 Lid of the tin damaged by corrosion



Fig.15 Missing tin layer in the area of breakage

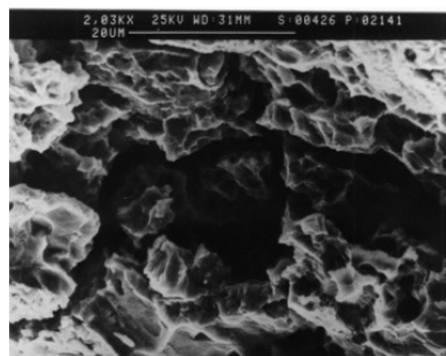


Fig.16 Intercrystalline corrosion of the sheet

Conclusion

On the basis of experiments performed with tested corrosive resistance of plates continually annealed and batch annealed, once or twice reduced, we can observe that as for sheets batch annealed twice reduced even at lower plastic properties and higher yield point and tensile strength there is a uniform plastic deformation, thus also to uniform thinning of protective tin layer. The corrosion was more uniform and did not affect the base material to a large extent. The plates continually annealed were distinguished by lower yield point, lower tensile strength and higher plasticity, yet their deformation with biaxial stress was characterized by inhomogeneity (significant slip bands). In the places of their significant slips there is a considerable thinning of protective tin layer, increase of their porosity, and as a result loss of anti-corrosive effects. If such sheets are used for the production of tin wrappings, the effects of corrosive activity of the tinned meat filling can result in significant corrosion of the tin lid, later even to its damage.

Acknowledgment

This contribution is the result of the project implementation: č.1/0396/11- Research and optimization of evaluation methods of strength and plastic properties of thin tinplates.

References

- [1] E. Spišák: Odkształcalność blach ocynowanych, *Rudy i metale nieżelazne*, Volume 40 (1995), No.11, pp.499-501.
- [2] E. Spišák, F. Greškovič, J. Slota: Evaluation of plastic properties of tinned steel sheets, *Rudy Metale*, Volume 42 (1997), No.11, pp. 510-512.
- [3] E. Spišák, J. Slota: Hodnotenie plastických vlastností tenkých ocelových plechov, *Acta Mechanica Slovaca*, No. 3 (1998), pp.39-44.
- [4] E. Spišák, A. Hrivňák, F. Greškovič: Vlastnosti a podmienky spracovania obalových plechov, *Strojárska výroba*, No.11-12 (1993), pp. 33-35.
- [5] L. Sobotová, E. Spišák: The Influence of Production of Thin Tinplate Steel on its Formability, *Journal of Materials Processing Technology*, Volume 34 (1992), pp. 411-417.
- [6] M. Šlesár, J. Billy, P. Marek, E. Zárubová: Vzťah mikročistoty, technológie valcovania a kvality povrchu tenkých plechov, *Plechovy vyšších technických parametrov*, Stará Lesná, 1994, pp. 6.
- [7] C. Jung: Creasteel – An asset for steel packaging innovation, *Metal bulletin and Tinplate Technology*, 8th International Tinplate Conference, Paris 2004.
- [8] D. Gade: D and I CAN: Tribological behaviour of tinplate during ironing, *Metal bulletin and Tinplate Technology*, 8th International Tinplate Conference, Paris 2004.
- [9] P. Duchemin: The Steel Beverage Can: A Sustainable Development, In: *Metal bulletin and Tinplate Technology*, 8th International Tinplate Conference, Paris 2004.
- [10] J. Majerníková: Medzné deformácie tenkých obalových plechov pri rôznych napätovo-deformačných stavoch, Dizertačná práca, Košice, 2008.
- [11] F. Trebuňa, M. Buršák: *Medzné stavy a lomy*, (ManaCon, Košice, 2002).

RESISTANCE SPOT WELDING OF AHSS STEEL AND HSLA STEEL

L. Kaščák¹, E. Spišák¹, J. Šlota¹ and J. Majerníková¹

¹ Department of Technology and Materials, Faculty of Mechanical Engineering, Technical University of Košice, Mäsiarska 74, 040 01 Košice, Slovakia

Keywords: resistance spot welding, tensile test, metallographic analysis.

Abstract. Advanced high strength steels and high strength low alloy steels are utilized in automotive industry to reduce weight of the vehicle body and consequently lowering the fuel consumption to achieve the lowest possible fuel consumption, high active and passive safety of passengers while decreasing the amount of emission. The contribution deals with the optimization of parameters of resistance spot welding and quality analysis of welded joints made by combination of galvanized steel sheets AHSS (TRIP 40/70+Z100MBO) and HSLA (H220PD). It is an advanced material combination used in designing car body parts. The quality of welded joints was evaluated by destructive tests and non-destructive tests. The shear tensile test according to STN 05 1122 standard was used. The basic mechanical properties of welded joints were evaluated. Some samples were prepared for metallographic analysis, where the influence of the welding parameters on the structure of welded joint as well as the influence of welding parameters on the dimensions of the weld nugget and occurrence of pores in the weld metal caused by evaporation of zinc from the coating was observed.

Introduction

Resistance spot welding is one of the oldest of the electric welding processes in use by industry today. The weld is made by a combination of heat, pressure and time. This technique is commonly used in automotive industry due to its high efficiency in manufacturing thin metal sheets. A wide variety of metal sheets up to 3 mm thickness can be handled by the resistance spot welding method [1,2]. In the last decade a change in body shell mass production has occurred in the automotive industry. In answer to the intensifying energy crisis and in order to meet customer requirements for automobiles such as weight reduction for energy saving and enhancement of passenger safety, new materials, e.g. advanced high strength steels (AHSS) have to be applied [3,4]. These materials are gaining in popularity due to their high strength in combination with good ductility characteristics compared to traditional high strength steels, for example micro-alloyed steels [5]. An important AHSS representative is the so-called TRIP (Transformation Induced Plasticity) steel dominated by a ferrite matrix with retained austenite, bainite and martensite as dispersed phases, offering excellent mechanical properties due to the transformation of retained austenite into martensite during plastic straining [6]. As a result, both strength and uniform strain increase owing to the appearance of a harder phase and to the additional local plastic yielding of the surrounding grains related to the transformation strain [7,8]. The TRIP effect, which is exhibited by such materials, is characterized by the phenomenon known as strain-induced martensitic transformation (SIMT). Due to the onset of plastic straining, the retained austenite undergoes SIMT which enhances the work hardenability of such steels due to the transformation of the austenite phase to the much harder martensite phase. This brings about a resistance to local necking which explains the uniform elongation and enhanced formability observed in such steels [].

The challenge of using the coated AHSS steels in the industry is that they are readily inclined to exhibit expulsion during the spot welding. As well, the presence of the coating results in the accelerated degradation of the welding electrodes, leading to earlier expulsion and frequent replacement or re-dressing of the electrodes [10,11].

HSLA steel is well-known type of steel alloy that provides many benefits over regular steel alloys. In general, HSLA alloys are much stronger and tougher than ordinary plain carbon steels. HSLA steels are so called because they only contain a very small percentage of carbon. A typical HSLA steel may contain 0.15% carbon, 1.65% manganese and low levels (under 0.035%) of phosphorous and sulphur. Most HSLA steels are furnished in the as-hot-rolled condition with ferritic-pearlitic microstructure. The exceptions are the controlled-rolled steels with an acicular ferrite microstructure and the dual-phase steels with martensite dispersed in a matrix of polygonal ferrite. These two types of HSLA steels use the formation of eutectoid structures for strengthening, while the ferritic-pearlitic HSLA steels generally require strengthening of the ferrite. Pearlite is generally an undesirable strengthening agent in structural steels because it reduces impact toughness and requires higher carbon contents. Moreover, yield strength is largely unaffected by a higher pearlite content. The ferrite in HSLA steels is typically strengthened by grain refinement, precipitation hardening, and, to a lesser extent, solid-solution strengthening. Grain refinement is the most desirable strengthening mechanism because it improves not only strength but also toughness [12-14]. Commonly, TRIP steels and HSLA steels are of good weldability.

Spot welding is an inexpensive and effective way to join metal sheets. More cracks and failures tend to occur around welds, in the heat affected zone (HAZ), because the joints are exposed to dynamic and static loads in the automobile structures. After spot welding, important changes occur in mechanical and metallurgical properties of the spot welded areas and heat affected zones [15]. The investigation of these changes is very important for the safety strength of the welded joints. In some parts of the modern automobiles, galvanized AHSS steels sheets and HSLA steels sheets are joined together with resistance spot welding technique. The paper evaluates joints of combined materials made by resistance spot welding the materials utilized in automotive industry in car body production.

Materials and Experiments

The following combination of dissimilar steel sheets were used for resistance spot welding: high strength low alloy steel H220PD with the thickness of 0.8 mm and advanced high strength steel TRIP 40/70+ Z100MBO with the thickness of 0.77 mm. Their basic mechanical properties and chemical composition are shown in Table 1 and Table 2.

Table 1. Basic mechanical properties of used steels

	Rp0.2 [MPa]	Rm [MPa]	A80 [%]	n90
H220PD	238	382	36	0.228
TRIP40/70	450	766	26	0.278

Table 2. Chemical composition (wt%) of used steel sheets

	C	Mn	Si	P	S	Al	Cu	Ni	Cr
H220PD	0.06	0.7	0.5	0.080	0.025	0.020	0.011	0.017	0.310
TRIP40/70	0.204	1.683	0.198	0.018	0.003	1.731	0.028	0.018	0.055
	Ti	V	Nb	Mo	Zr				
H220PD	0.037	0.002	0.026	0.005	0.001				
TRIP40/70	0.009	0.004	0.004	0.008	0.007				

On order to evaluate the properties of the joints, the following tests were performed: tension test, microhardnesses test and a metallographical analysis. The samples with dimensions of 40 x 90 mm and 30 mm lapping according to STN 05 1122 standard were used for the experiments (Fig. 1). Five samples were prepared for every combination of sheets. Resistance spot welding was carried out in laboratory conditions on a pneumatic spot welding-machine BPK 20 made by VTS ELEKTRO Bratislava, as shown in scheme in Fig. 2. CuCr welding electrodes were used according to ON 42 3039.71 standard. The diameter of working area of the electrode was $d = \varnothing 5$ mm. The parameters of resistance spot welding with marked tested samples are shown in Table 3. The samples were prepared by cutting against the direction of rolling. The surfaces of the samples were degreased in concentrated CH_3COCH_3 .

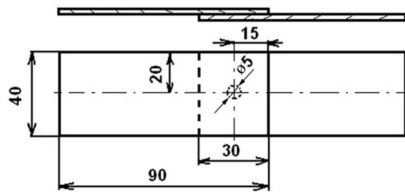


Fig. 1 Dimension of samples for the tensile test

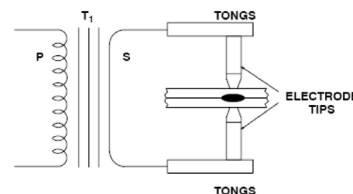


Fig. 2 Scheme of resistance spot welding machine

The welding current is the most important parameter in resistance welding which determines the heat generation by a power of square as shown in the formula [16]. The size of the weld nugget increases rapidly with increasing welding current, but too high current will result in expulsions and electrode deteriorations. The amount of weld current is controlled by two things: first, the setting of the transformer tap switch determines the maximum amount of weld current available; second, the percent of current control determines the percent of the available current to be used for making the weld. Low percent current settings are not normally recommended as this may impair the quality of the weld. The weld current should be kept as low as possible. When determining the current to be used, the current is gradually increased until weld spatter occurs between the metal sheets [1,16].

Table 3. Parameters of resistance spot welding (Fz – pressing force, T – welding time, I – welding current)

Samples	Welding parameters		
	Fz [kN]	T [per.]	I [kN]
A ₅	6	10	5
A ₆	6	10	6
A ₇	6	10	7
A ₈	6	10	8
A ₉	6	10	9

The carrying capacities of the spot welded joints were evaluated according to standard STN 05 1122 – Tension test of spot welded joints. This test was used for measuring the maximum carrying capacities F_{max} of the joints. The test was carried out on the metal strength testing machine TIRAtest 2300 produced by VEB TIW Rauenstein, with the loading speed of 8 mm/min.

Further tests for quality evaluation of spot welded joints included the metallographical analysis. The quality of welded joints was evaluated by light microscopy on metallographical scratch patterns prepared according to ISO 6507-1 and ISO 6507-2 standards on Olympus TH 4-200 microscope.

Results and Discussion

The measured values of carrying capacities F_{max} of resistance spot welded joints are shown in Table 4. Only one type of the joint occurs in all chosen parameters of welding – fusion welded joint. The values of carrying capacity of welded joints were in the range from 5224 N to 7496 N. Measured values of carrying capacities of joints on welding current are shown in Fig. 3.

Dependency of carrying capacity of spot welds F_{max} on welding current I can be expressed:

$$F_{max} = 401.49 \cdot I + 3491; \text{ coefficient of determination } R^2 = 0,8829 \quad (1)$$

Table 4. Carrying capacities of resistance spot welded joints

Fmax [N]				
Samples A ₅	Samples A ₆	Samples A ₇	Samples A ₈	Samples A ₉
5263	5922	6427	6919	6878
5224	5763	6439	6558	7496
5383	5771	6562	6435	6782
5537	6121	6320	7098	6875
5720	6052	6321	6693	7090

Tensile tests were executed under displacement control conditions on the specimen configurations in order to characterise the static behaviour of the joints and to estimate the ultimate tensile strength. The maximum shearing load was the most significant value obtained from the "load-displacement" curves as shown in Fig. 4. The form of the curves indicates the behaviour of the joints under loading, especially capacity for deformation.

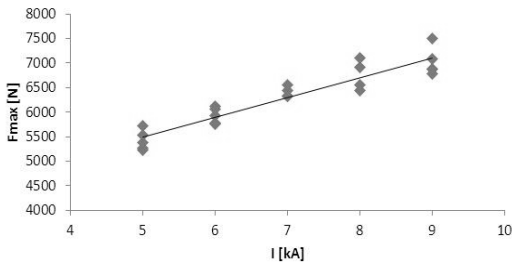


Fig. 3 Dependency of carrying capacities of spot welds Fmax [N] on welding current I [kA]

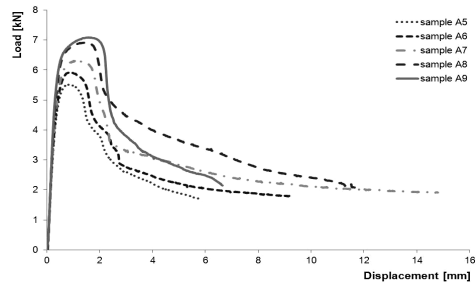


Fig. 4 Load-displacement curves and deformation of spot welded joints after tensile test

In this case the average maximum shearing load was: for sample A₅ around 5500 N with the corresponding displacement about 1.0 mm, for sample A₆ around 5900 N with the corresponding displacement about 1.2 mm, for sample A₇ around 6200 N with the corresponding displacement about 1.7 mm, for sample A₈ around 6900 N with the corresponding displacement about 1.9 mm and for sample A₉ around 7100 N with the corresponding displacement about 2.1 mm.



Fig. 5 Failures of spot welded joints of samples A₅ and A₈

The specimen failed partially through the periphery of the weld and partially through the base metal, which is confirmed in the failure mode of spot welded joints (Fig. 5) together with corresponding characteristic load vs. displacement curves generated in the experiments (Fig. 4). The carrying capacities of the samples are then influenced by the base metal strength.

Figure 6 shows indentations formed by the welding electrodes. Changing the values of welding current influenced the welding electrode indentations on the surfaces of welded materials. The most obvious indentations were observed on the surfaces of samples prepared with the parameters of maximum value of welding current of 9 kA. The least obvious indentations were on the surfaces of both welded steels prepared with the minimum value of welding current of 5 kA.

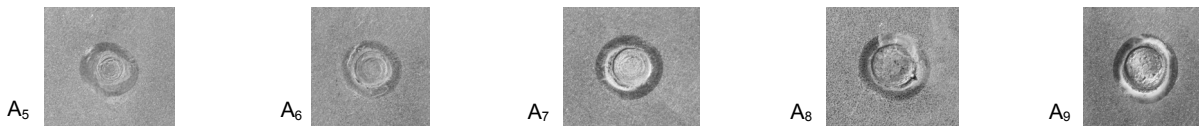
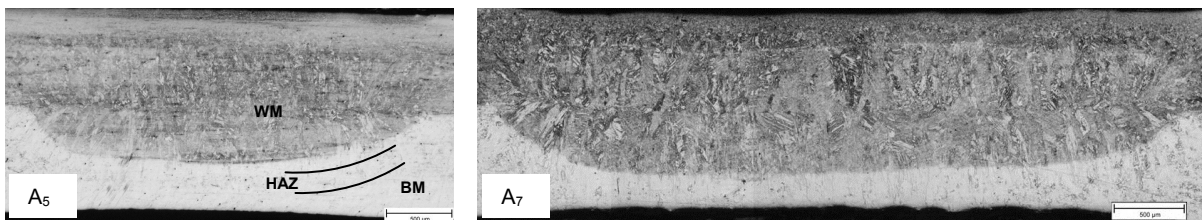


Fig. 6 Welding electrodes indentations of all observed types of samples



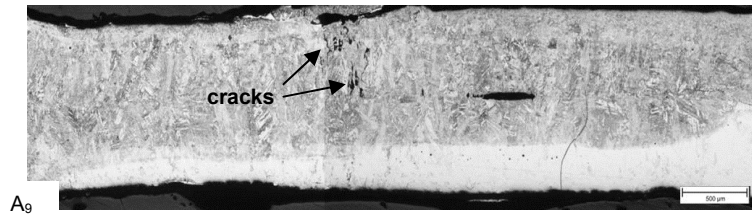


Fig. 7 Microstructures of welded materials of dissimilar combination of TRIP steel and H220PD steel

The metallographical analysis confirmed formation of fusion welded joints with characteristic areas of weld metal (WM), heat affected zone (HAZ) and base material (BM). Figure 7 shows the macrostructures of spot welded joints of samples A_5 , A_7 and A_9 . The size of spot welds increased with increasing values of welding current. The sample A_5 welded with the lowest value of welding current 5 kA shows the smallest weld nugget of all observed samples, with the narrow heat affected zone. The macrostructures of a weld joint show the solidification process of weld metal with a characteristic dendrite structure typical for resistance spot welds. The microscopic observation of macrostructures of the welds shows no pores and cavities occurring in the weld metal. The bigger weld nugget was observed in samples A_7 , welded with the current of 7 kA. No pores and cavities occurring in the weld metal.

The microstructure of weld metal consists of mostly fine-grained martensite arranged in typical lamellar formations from the side of TRIP steel. Such lamellar formations prevent the austenite from transformation; therefore the retained austenite occurs in the microstructure. Besides martensite, also ferrite and both forms of bainite occur in the microstructure of weld metal. The microstructure of H220PD can be characterized as a fine-grained ferrite-pearlite structure. Because of heating in resistance spot welding, continual growth of grains towards the weld metal can be observed. A significant growth of pearlite grains occurs in the heat affected zone.

The sample A_9 welded with the highest values of welding current 9 kA shows the void and solidification cracks inside the biggest weld nugget. The formation of void in a spot weld is the result of nucleation and growth process during solidification of a liquid nugget after the heat source, i.e. electric current is shut off as was described in [16]. The solidification cracking may form under certain condition. The cracks extended from the surface of a weld into its interior with some voids in the nugget. Such cracks may not reduce a joint's strength if they are confined to the centre of the nugget. However, when they extend to the edges of weld nugget they can affect the weld quality.

Conclusion

In this study, resistance spot welds of material combination of galvanized AHSS steels sheets and HSLA steels were evaluated.

On the basis of the conducted experiment, the following conclusions can be formed:

- Fusion weld joints occur with all chosen parameters of resistance spot welding.
- The highest tensile strength was observed in samples made with welding current of 9 kA. The average carrying capacity of samples was 7024 N. The lowest values of carrying capacity were observed in samples made with welding current of 5 kA, where the average value of carrying capacity decreased by 23 % in comparison to samples A_9 .
- Linear dependence of carrying capacities of spot welds F_{max} on welding current I was determined. Increasing values of welding current caused increasing of carrying capacity.
- The metallographical analysis confirms that the chosen combination of advanced high strength steels and high strength low alloy steels is suitable for resistance spot welding. On the basis of the results it can be stated, that welding current has a determining influence on the weld joint. When using the welding current of 5 kA, weld joint was of high quality, fusible and without defects, but the weld nugget had smaller dimensions in comparison with other weld nuggets made with higher values of welding current. Welding current of 9 kA is not suitable for the examined thickness and sheet combination, because cracking was observed in the heat affected zone of multi-phase material of TRIP.

Acknowledgment

Authors are grateful for the support of experimental works by project Center for research of control of technical, environmental and human risks for permanent development of production and products in mechanical engineering (ITMS:26220120060) and the project VEGA No. 1/0396/11- Research and optimization of evaluation methods of strength and plastic properties of thin tinplates.

References

- [1] E. Spišák, L. Kaščák, J. Viňáš: Research into properties of joints of combined materials made by resistance spot welding, *Chemické listy*, Vol. 105 (2011), No. 16, pp. 488-490.
- [2] I. Sevim: Effect of hardness to fracture toughness for spot welded steel sheets, *Material and Design*, Vol. 27 (2006), Iss. 1, pp. 21-30.
- [3] S. Brauser, L.A. Pepke, G. Weber, M. Rethmeier: Deformation behaviour of spot-welded high strength steels for automotive applications, *Materials Science and Engineering*, Vol. 527 (2010), Iss.26, pp. 7099-7108.
- [4] J. Mucha, L. Kaščák, E. Spišák: Joining the car-body sheets using clinching process with various thickness and mechanical property arrangements, *Archives of civil and mechanical engineering*, Vol. 11 (2011), No. 1, pp. 135-148.
- [5] M.D. Tumuluru: Resistance spot welding of coated high-strength dualphase steels, *Welding Journal*, Vol. 85 (2006), No. 8, pp. 31-37.
- [6] G. Lacroix, T. Pardoën, P.J. Jacques: The fracture toughness of TRIP-assisted multiphase steels, *Acta Materialia*, Vol. 56 (2008), Iss. 15, pp. 3711-4124.
- [7] M.H. Saleh, R. Priestner: Retained austenite in dual-phase silicon steels and its effect on mechanical properties, *Journal of Materials Processing Technology*, Vol. 113 (2001), Iss. 1-3, pp. 587-593.
- [8] W. Frącz, F. Stachowicz: Determination of the forming limit diagram of zinc electro-galvanized steel sheets, *Metallurgija*, Vol. 51 (2012), pp. 161-165.
- [9] R. Sierra, J.A. Nemes: Investigation of the mechanical behavior of multi-phase TRIP steels using finite element methods, *International Journal of Mechanical Sciences*, Vol. 50 (2008), pp. 649-665.



-
- [10] C. Ma, D.L. Chen, S.D. Bhole, G. Boudreau: Microstructure and fracture characteristics of spot-welded DP600 steel, *Materials Science and Engineering*, Vol. 485 (2008), Iss. 1-2, pp. 334-346.[11] N.T. Williams, J.D. Parker: Modelling and control of weld nugget formation, *International Material Review*, Vol. 49 (2004), No. 2, pp. 45-75.
- [12] A.A. Gorni, P.R. Mei: Austenite transformation and age hardening of HSLA-80 and ULCB steels, *Journal of Materials Processing Technology*, Vol. 155-156 (2004), pp. 1513-1518.
- [13] J. Fernández, S. Illescas, J.M. Guilemany: Effect of microalloying elements on the austenitic grain growth in low carbon HSLA steel, *Materials Letters*, Vol. 61 (2007), Iss. 11-12, pp. 2389-2392.
- [14] B.K. Show, R. Veerababu, R. Balamuralikrishnan, G. Malakondaiah: Effect of vanadium and titanium modification on the microstructure and mechanical properties of a microalloyed HSLA steel, *Materials Science and Engineering*, Vol. 527 (2010), Iss. 6, pp. 1595-1604.
- [15] M. Vural, A. Akkus: On the resistance spot weldability of galvanized interstitial free steel sheets with austenitic stainless steel sheets, *Journal of Materials Processing Technology*, Vol. 153-154 (2004), pp. 1-6.
- [16] H. Zhang, J. Senkara: *Resistance welding: Fundamentals and Applications*, (Taylor & Francis, New York, 2006).



International Conference on Innovative Technologies, IN-TECH 2012,
Rijeka, 26. - 28.09.2012



MODIFICATION OF THE ICI RULE APPLIED TO SIGNAL DENOISING

I. Volaric¹, J. Lerga¹, V. Sucic¹, I. Orovic² and S. Stankovic²

¹ Department of Automation and Electronics, Faculty of Engineering, University of Rijeka, Vukovarska 58, HR-51000 Rijeka, Croatia

² Faculty of Electrical Engineering, University of Montenegro, Dzordza Vasingtona bb., MN-81000 Podgorica, Montenegro

Keywords: Signal denoising, Intersection of confidence intervals (ICI) method, Adaptive filtering.

Abstract. The paper provides a detailed performance analysis of the modified ICI based denoising method. The original ICI based method has been modified in order to reduce its computational complexity, hence enhancing its execution time. The method is applied to denoising of signals corrupted by additive noise in order to study the methods efficiency in noise suppression for various noise probability density functions (PDF) and noise levels. It is shown that the algorithm execution time is significantly reduced when compared to the original ICI based method.

Introduction

Edge preserving and local adaptivity are prudent for an efficient signal denoising [1], [2]. One of such denoising methods was introduced by Katkovnik *et al* [1], combining local polynomial approximation (LPA) method with intersection of confidence intervals (ICI) rule as tool for filter support size calculation. It was shown that this denoising algorithm is particularly sensitive to signal sudden slope changes [3], [4], [5].

However, the shortcoming of the ICI based method is that the method is time consuming. This modification of the ICI method solves these problems by significantly speeding-up the denoising algorithm, resulting in an algorithm execution time reduction. In this paper, both the original and modified LPA-ICI methods are used to denoise several artificially created signals, originally proposed in [6], all characterized by sudden slope changes with embedded zero mean noise of various probability density functions (PDF), for a range of signal-to-noise ratio (SNR) values.

The paper is organized as follows. Section 2 gives the brief overview of the modified ICI method, while in Section 3 both of algorithms are compared, in terms of mean square error (MSE) reduction and its execution time.

Modification of the ICI rule

Let us assume that the noise-free signal $y(n)$ is corrupted by independent additive white Gaussian noise (AWGN) $\varepsilon(n) \sim N(0, \sigma_\varepsilon^2)$, such that the noisy signal is:

$$x(n) = y(n) + \varepsilon(n). \quad (1)$$

The goal of denoising procedure is to obtain estimated signal $\hat{y}(n)$, with estimation error as small as possible. To achieve this, for each data point, set of growing support windows $H = \{h_1 < h_2 < \dots < h_K\}$ are introduced, with appropriate confidence intervals, of which the upper and lower boundaries are defined as [1]:

$$L_K(n) = \hat{x}_{h_k}(n) - \Gamma \sigma_{h_k}(n), \quad (2)$$

$$U_K(n) = \hat{x}_{h_k}(n) + \Gamma \sigma_{h_k}(n), \quad (3)$$

where $\hat{x}_{h_k}(n)$ is the estimated signal sample (obtained by LPA), Γ is ICI threshold value, and $\sigma_{h_k}(n)$ is the standard deviation of the $\hat{x}_{h_k}(n)$. Optimal window support size calculated with ICI method, h^+ , is then determined as largest one for which following inequality holds true:

$$\bar{L}_K(n) \leq \underline{U}_K(n), \quad (4)$$

where smallest upper $\bar{L}_K(n)$ and largest lower $\underline{U}_K(n)$ confidence intervals boundaries are calculated as:

$$\bar{L}_K(n) = \max_{i=1, \dots, k} L_i(n), \quad (5)$$

$$\underline{U}_K(n) = \min_{i=1, \dots, k} U_i(n), \quad (6)$$

Unlike the original LPA-ICI method, this modification introduces set of growing support windows just for the first sample inside the support window, and it is used for all samples within it, hence results in significantly reduced algorithm execution time.

Performance analysis of the modified LPA- ICI method

The performance of the algorithms are compared in terms of algorithm execution time and mean squared error (MSE) reduction on two synthetic signals named the *Blocks* and *Sineoneoverx*, with number of signal samples $N = 1024$, shown by Fig. 1. Test signals are additionally corrupted with various types of noises, PDFs of which are listed in Table 1, for a range of different SNR values. The threshold value of the ICI method is set to $\Gamma = 4.4$ (as in [1]), and LPA of order $m = 0$ is used. The MSE of the estimated signal $\hat{y}(n)$ is calculated as the mean value of MSE over $M = 20$ different noise realizations, and the obtained error is shown in Fig. 2.

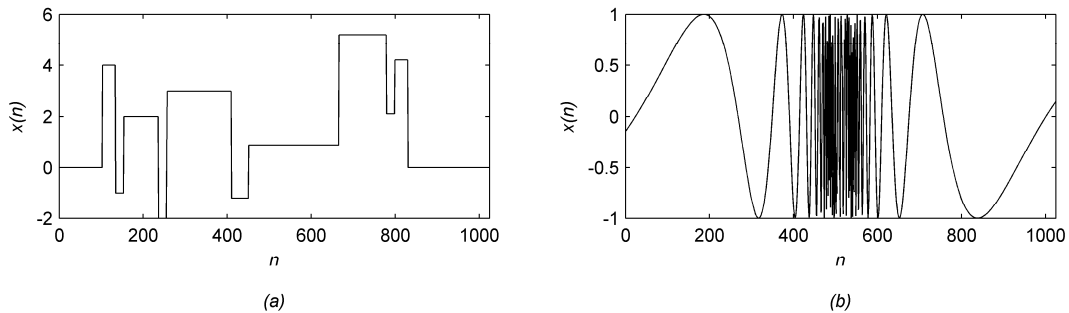


Fig. 1 (a) *Blocks* signal. (b) *Sineoneoverx* signal.

Table 1: Algorithm execution time and MSE for test signals denoised using modified ICI rule. (SNR=5)

Noise PDF	<i>Blocks</i>				<i>Sineoneoverx</i>			
	LPA-ICI		Modified LPA-ICI		LPA-ICI		Modified LPA-ICI	
	MSE	t	MSE	t	MSE	t	MSE	t
Beta	0.1553	1040.8ms	0.9195	5.9ms	0.0761	651.0ms	0.1148	5.8ms
Binomial	0.1520	1035.5ms	0.9114	5.8ms	0.0772	656.3ms	0.1164	5.8ms
Chisquare	0.1574	1033.4ms	0.9032	5.8ms	0.0785	656.4ms	0.1133	5.8ms
Exponential	0.1561	1036.9ms	0.9046	5.8ms	0.0777	651.6ms	0.1130	5.8ms
Extreme Value	0.1543	1037.2ms	0.9175	5.8ms	0.0777	650.0ms	0.1154	5.8ms
F	0.2887	1024.6ms	0.9326	5.8ms	0.0980	666.0ms	0.1147	5.9ms
Gamma	0.1546	1036.6ms	0.9126	5.8ms	0.0770	648.7ms	0.1169	5.8ms
Generalized Extreme Value	0.1542	1034.2ms	0.9113	5.8ms	0.0769	653.9ms	0.1151	5.8ms
Generalized Pareto	0.1526	1036.2ms	0.9005	5.8ms	0.0763	651.6ms	0.1129	5.8ms
Geometric	0.1538	1032.0ms	0.9064	5.8ms	0.0779	653.3ms	0.1163	5.8ms
Hypergeometric	0.1577	1038.2ms	0.9155	5.9ms	0.0774	653.5ms	0.1137	5.8ms
Lognormal	0.1730	1032.8ms	0.9067	5.8ms	0.0792	651.5ms	0.1126	5.8ms
Negative Binomial	0.1554	1037.9ms	0.9035	5.9ms	0.0776	648.5ms	0.1169	5.8ms
Noncentral F	0.2857	1026.9ms	0.9252	5.8ms	0.0981	666.5ms	0.1159	5.8ms
Noncentral t	0.2070	1028.1ms	0.9178	5.8ms	0.0824	655.8ms	0.1155	5.8ms
Noncentral Chi-square	0.1566	1035.4ms	0.9142	5.8ms	0.0771	651.2ms	0.1141	5.8ms
Poisson	0.1582	1036.4ms	0.9176	5.8ms	0.0770	650.7ms	0.1121	5.8ms
Rayleigh	0.1522	1035.5ms	0.9167	5.8ms	0.0768	650.7ms	0.1136	5.8ms
T	0.2161	1028.7ms	0.9024	5.8ms	0.0816	650.5ms	0.1143	5.8ms
Uniform	0.1560	1035.1ms	0.9151	5.9ms	0.0767	648.2ms	0.1134	5.8ms
Discrete Uniform	0.1555	1033.1ms	0.9149	5.9ms	0.0757	649.6ms	0.1161	5.8ms
Weibull	0.1535	1032.2ms	0.9141	6.6ms	0.0773	651.3ms	0.1127	6.2ms

Table 2: Algorithm execution time and MSE for test signals corrupted by zero-mean AWGN denoised for a range of SNR values using modified ICI rule.

SNR	<i>Blocks</i>				<i>Sineoneoverx</i>			
	LPA-ICI		LPA-FICI		LPA-ICI		LPA-FICI	
	MSE	t	MSE	T	MSE	T	MSE	t
0.2	0.8665	1361.4ms	1.8125	5.9ms	0.3741	5288.5ms	0.4006	6.9ms
0.4	0.8603	1349.9ms	1.3499	5.9ms	0.3812	5327.6ms	0.4031	7.0ms
0.6	0.7884	1331.3ms	1.7766	5.9ms	0.3779	5084.6ms	0.4093	7.0ms
0.8	0.7804	1318.8ms	1.7557	5.9ms	0.3724	5037.4ms	0.4067	6.8ms
1	0.7436	1304.6ms	1.7230	5.9ms	0.3698	4712.6ms	0.4091	6.7ms
2	0.6036	1229.7ms	1.6278	5.9ms	0.3549	4107.1ms	0.3972	6.6ms
4	0.4250	1125.1ms	1.4424	5.9ms	0.3271	2983.4ms	0.3782	6.3ms
6	0.2800	1071.1ms	1.1788	5.9ms	0.3009	2308.9ms	0.3557	6.1ms
8	0.1643	1037.9ms	0.9367	5.9ms	0.2539	1762.5ms	0.3089	6.0ms
10	0.0997	1016.0ms	0.7412	5.9ms	0.2073	1349.2ms	0.2557	5.9ms
20	0.0049	964.8ms	0.1962	5.9ms	0.0395	539.4ms	0.0741	5.9ms

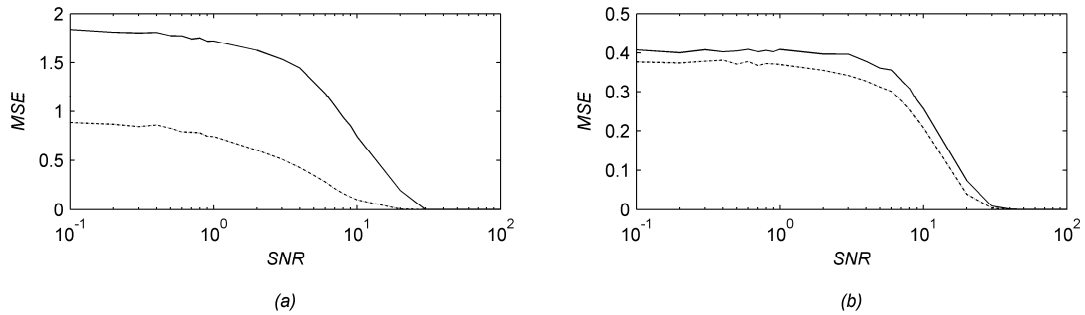


Fig. 2 MSE as a function of SNR for signals denoised using LPA-ICI method (dotted) and its modification. (a) *Blocks* signal. (b) *Sineoneoverx* signal

Table 1 compares the algorithm execution time and obtained MSE values for both of methods for various PDFs. It can be seen that modified LPA-ICI method outperforms the original LPA-ICI method in algorithm execution time. Algorithm execution time of the modified LPA-ICI method is relatively constant and over 175 times faster for *Blocks* signal and over 110 times faster for *Sineoneoverx* signal when compared to the original LPA-ICI method. The same conclusion can be drawn from Table 2 where both of methods are compared on signals corrupted by AWGN of various levels. The reduction of algorithm execution time is even larger for smaller values of SNR (e.g. for $SNR = 0.2$, the modified LPA-ICI algorithm is 230 times faster for *Block* signal and 766 times faster for *Sineoneoverxs* signal). However, the shortcoming of the reduction of algorithm execution time is in the obtained error, which is larger for the case of the modified LPA-ICI method.

Fig. 3 shows the *Blocks* signal corrupted with Exponential noise with $\lambda=1$ (Fig. 3(a), Poisson noise $\lambda=1$ (Fig. 3(d)), and the Student's T noise with $\nu=2$ (Fig. 3(g)). Each signal was denoised using both the original and modified LPA-ICI method, and obtained results are shown in Figs. 3(b), 3(e), and 3(h), respectively, while the estimation errors are given in Figs 3(c), 3(f), and 3(i), respectively. Fig. 4 shows the results for *Sineoneoverx* signal.

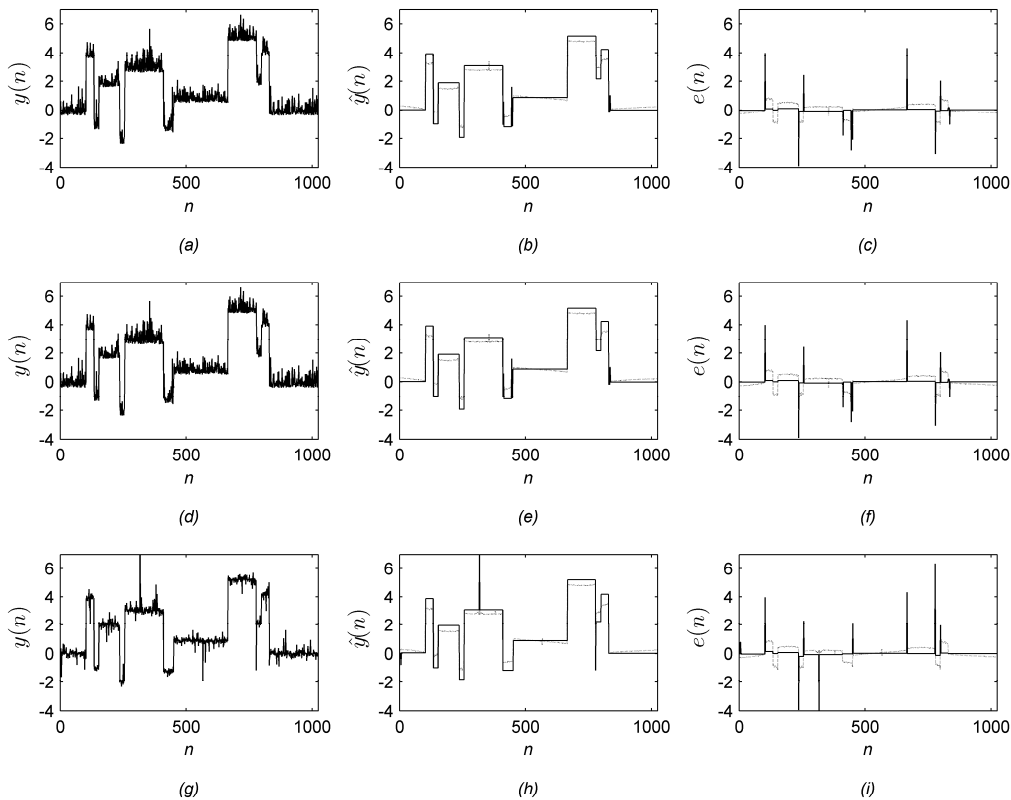


Fig. 3 *Blocks* signal. (a) Signal in exponential noise. (b) Signal denoised using the LPA-ICI (dotted) and the modified LPA-ICI rule. (c) Estimation error for the LPA-ICI (dotted) and the modified LPA-ICI rule. (d) Signal in Poisson noise. (e) Signal denoised using the LPA-ICI (dotted) and the modified LPA-ICI rule. (f) Estimation error for the LPA-ICI (dotted) and the modified LPA-ICI rule. (g) Signal in T noise. (h) Signal denoised using the LPA-ICI (dotted) and the modified LPA-ICI rule. (i) Estimation error for the LPA-ICI (dotted) and the modified LPA-ICI rule.

Signal denoised using the LPA-ICI (dotted) and the modified LPA-ICI rule. (i) Estimation error for the LPA-ICI (dotted) and the modified LPA-ICI rule.

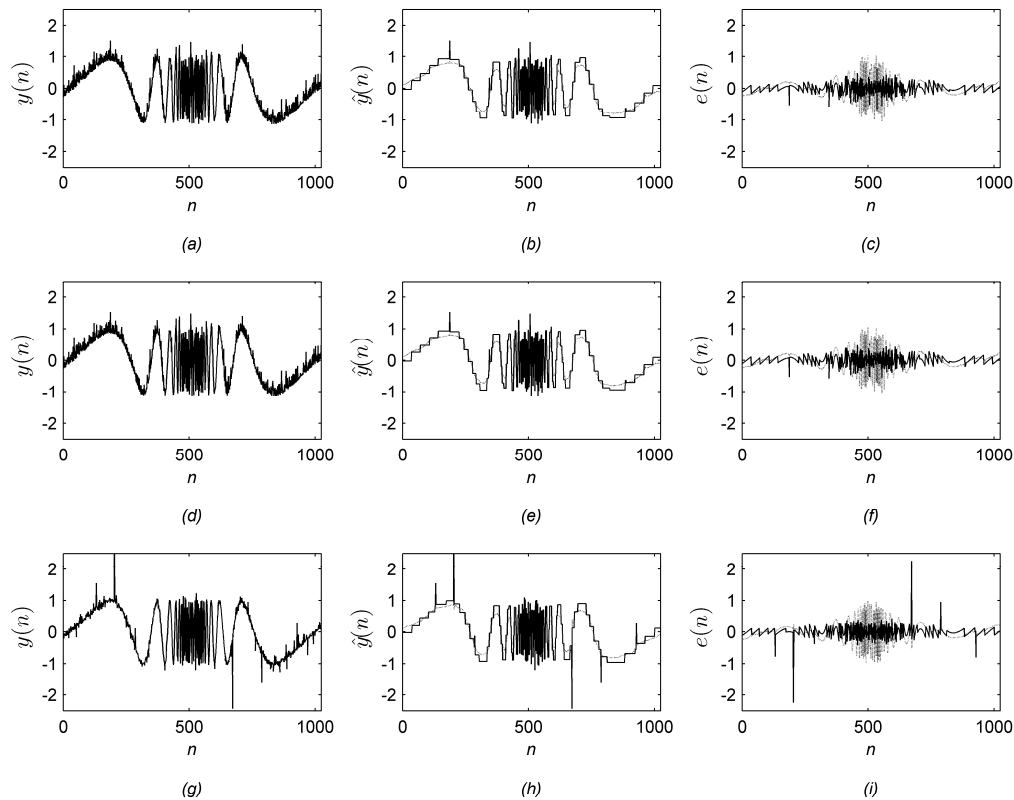


Fig. 4 *Sineoneoverx* signal. (a) Signal in exponential noise. (b) Signal denoised using the LPA-ICI (dotted) and the modified LPA-ICI rule. (c) Estimation error for the LPA-ICI (dotted) and the modified LPA-ICI rule. (d) Signal in Poisson noise. (e) Signal denoised using the LPA-ICI (dotted) and the modified LPA-ICI rule. (f) Estimation error for the LPA-ICI (dotted) and the modified LPA-ICI rule. (g) Signal in T noise. (h) Signal denoised using the LPA-ICI (dotted) and the modified LPA-ICI rule. (i) Estimation error for the LPA-ICI (dotted) and the modified LPA-ICI rule.

Conclusion

In this paper, the performance of the modified method which combines local polynomial approximation (LPA) and intersection of the confidence intervals (ICI) rule has been analyzed in details for a range of noise probability density functions (PDF) and signal-to-noise ratio values (SNR). The mean squared error (MSE) of signal estimates and the algorithm execution time obtained using both the original and the modified LPA-ICI are compared. It has been shown that for all of noise types and SNRs, for the considered synthetic signals, the modified LPA-ICI algorithm significantly outperforms the original in terms of algorithm execution time. This feature of the algorithm is specially suited for applications where denoising algorithms are rerun numerous times (e.g. image and video denoising). The shortcoming of the algorithm is a larger noise level in the estimated signal, which can be compensated for by introducing additional requirements when finding the optimal window size.

Acknowledgment

This work is a part of the research project "Optimization and Design of Time-Frequency Distributions" (number 069-0362214-1575), which is financially supported by the Ministry of Science, Education and Sports of the Republic of Croatia.

References

- [1] V. Katkovnik: A new method for varying adaptive bandwidth selection, *IEEE Trans. Signal Process*, Vol. 47 (1999), No. 9, pp. 2567 - 2571.
- [2] M. Tomic, D. Sersic and M. Vrankic: Edge-preserving adaptive wavelet denoising using ICI rule, *Electronics Letters*, Vol. 44 (2008), No. 11, pp 698-699.
- [3] V. Katkovnik and I. Shmulevich: Nonparametric density estimation with adaptive varying window size, *Proc. SPIE Image and Signal Process for Remote Sensing*, Vol. 6 (2001), pp. 141-150.
- [4] V. Katkovnik and I. Shmulevich: Kernel density estimation with varying data-driven bandwidths, *Pattern Recognition Letters*, Vol. 23 (2002), pp. 1641 - 1648.



-
- [5] Lj. Stankovic: Performance analysis of the adaptive algorithm for bias-to-variance tradeoff, *IEEE Transactions on Signal Processing*, Vol. 52 (2001) No. 5, pp. 1228-1234.
 - [6] D. Donoho and I.M. Johnstone: Adapting to unknown smoothness via wavelet shrinkage, *JASA*, Vol. 90 (1995), No. 432, pp 1200-1224



International Conference on Innovative Technologies, IN-TECH 2012,
Rijeka, 26. - 28.09.2012



APPLICATION OF SPACE TELEMEDICINE TECHNOLOGY IN MANAGING EMERGENCIES ON THE GROUND

D. Litvina¹, L. Strogonova²

¹ 125993, Moscow, GSP-3, A-80, Volokolamskoe Shosse, 4
Russia

² 125993, Moscow, GSP-3, A-80, Volokolamskoe Shosse, 4
Russia

Keywords: telemedicine, aerospace, emergency.

Abstract. Under spaceflight conditions the astronaut's body is subjected to a variety of adverse health and cognitive risks. One of the most detrimental factors is microgravity which has harmful effects on all aspects of the human organism. Without an appropriate and timely diagnosis there is a high probability of the subject developing physical illness and cognitive degradation, which inevitably leads to incidents or unpredicted situations on the spacecraft. Atypically functioning internal organs and biological structures inside the body cause lack of concentration and consequently, increased possibility of inadequate judgement while making important decisions or operating the ship's machinery. This endangers the overall security of the manned spaceflight. A system of regular medical examinations has been created in order to minimize such risks and ensure the safety of the flight. Nevertheless despite constant evolution and modification of medical control in space there still exists a degree of uncertainty regarding the precise psychophysical condition of the astronaut in space. A potential course of action is to introduce continuous monitoring of the astronaut's psychophysical indicators. The medical data can be transferred by means of telemetry. Over the last decades, telemedicine in extreme conditions (catastrophes) was being developed on the basis of cosmic medical controls. Both explore telecommunicating medical results in digital form and medical consultation in online and offline modes. There are however significant differences such as overabundance of requests from victims and otherwise affected. In particular, this article examines the overflow of emergency calls to the centre of telemedicine services, typical in extreme situations.

Introduction

Currently increasing volume of medical information received in flight complicates the decision making process of the on-board physician. Hence the decisions are often made by the medical personnel at the mission control centre on the ground. With the inevitable increase in the duration and the distance of space flights a question of improvement and development of on-board tools and techniques of medical monitoring and diagnostics rises more sharply.

Safety of space flight is directly linked with the analysis of data obtained by performing the following:

- Ongoing monitoring of the health of the crew;
- Diagnosis of adverse health conditions developing during the space flight;
- Assessment of physical and mental fitness of astronauts;
- Forecasting capability of flight continuation.

Influence of Microgravity on Humans

Analysis of data obtained from space missions and simulation experiments allowed defining the basic mechanisms of the effects of microgravity on the human body.

Table 1. The response of the human body to the state weightlessness

Functions	Symptoms
Sensory system	Reduced activity of the proprioceptive input; reduced static and increased dynamic sensitivity of the vestibular receptors; interruption of the interaction of sensory systems; illusions; development of space motion sickness.
Motor	Atony of the antigravity muscles, atrophy, changes in contractile properties of antigravity muscles. Disruption of control systems.
Bone	Osteopenia of the core bones (lumbar spine, pelvis and thighs). Reduced bone mineral density.
Cardio-vascular	The tendency for cardiac arrhythmias during stress. Reduced postural and physical stability.
Fluid and electrolyte	Hydropenia. The decrease in blood plasma and interstitial fluid. The negative balance of some minerals, including calcium.
Blood system	Functional erythropenia, the development of morphological and metabolic changes in red blood cells.
Metabolism	The prevalence of decay processes over synthesis processes, a negative nitrogen balance.
Immune system	Reduced activity of T-cell immune system and antiviral immunity.

Medical Support of Space Flight

The safety of space flight depends on the reliability of technology and on the effectiveness of the medical support of manned flight.

A range of functional disorders, acute illnesses and injuries that are most likely to occur at different stages of space missions, produced at the SSC RF Institute for Biomedical Problems of RAS serves as the basis for the creation and improvement of on-board systems of care and prevention.

General principles of medical care of the expedition are:

- Establishment of an autonomous on-board medical center;
- The inclusion of highly skilled physician and an assistant (paramedic), medical training for other members of the crew;
- Ability to self-diagnosis, prevention and care;
- Participation of experts from the Mission Control Center (MCC) in telemedicine consultations.
- Use of the latest advances in medicine, biology and nanotechnology in developing methods of diagnosis, prevention and treatment;
- Application of expert systems for analysis and management of the astronauts' condition;
- Minimizing the time of diagnostic and preventive treatments.

Medical Control

Medical control in space flight is linked to the following key tasks:

- Ongoing monitoring of the health of the crew;
- Diagnosis of adverse health conditions, developing during the space flight;
- Assessment of physical and mental fitness of astronauts;
- Assessment the possibility of adjusting prevention;
- Forecasting capability of flight continuation.

An important condition for solving these problems is the ability to automate full medical monitoring and diagnostics directly during the flight. Therefore a set of medical devices for collecting and analyzing health data directly on board the spacecraft has been developed. Along with the development of these instruments, information-retrieval systems were set up. Such systems are essential for accumulating and processing data collected in a variety of flight experiments, starting with the initial flights. The transmission of telemetric data to Earth to support decision-making process in emergency situations on board seems outdated, and in some cases - impossible. Therefore arises an issue of creating a flexible approach to decision making, allowing the on-board doctor to perform continuous medical monitoring of the overall health of crew members aboard.

Telemedicine Technology

As follows from the above, it is necessary to carry out medical control for virtually all systems of the human body. In Russia, telemedicine is based on the knowledge and achievements in the field of space medicine. Advances in information and telecommunication technologies have created a fundamentally new direction for the organization and delivery of medical care - telemedicine.

Telemedicine can undoubtedly have a significant positive impact on medical and preventive care systems and efficiency of actions undertaken in emergency situations. Telemedicine network in Russia is built as a decentralized system based on the functional standardization principles.

Medical databases are important components of information technologies that provide the intellectual support of the healing process. Medical databases allow storing the collected data. During the observation of patients, the data from inspection, consultation and surveys is recorded in the databases.

Medical knowledge database is a system of diagnostic algorithms, formulas and procedures, including rules for combining sections of active directories and dictionaries. They provide the ability to form medical conclusions and recommendations, based on the incorporated system of decision-making algorithms. In addition, medical knowledge databases contain templates for patient health history and other medical documents, which are automatically populated on the basis of data collected about the patient.

The size of Russian territory presents an issue of remote consultation where the patient and the physician may be hundreds or thousands of kilometers away from each other.

Medical systems developers now offer more universal algorithms for introduction of IT into the medical diagnostic process. This would provide support for making medical decisions and the collection of primary health statistical information. The main areas of information support of the physician are shown in Fig. 1.

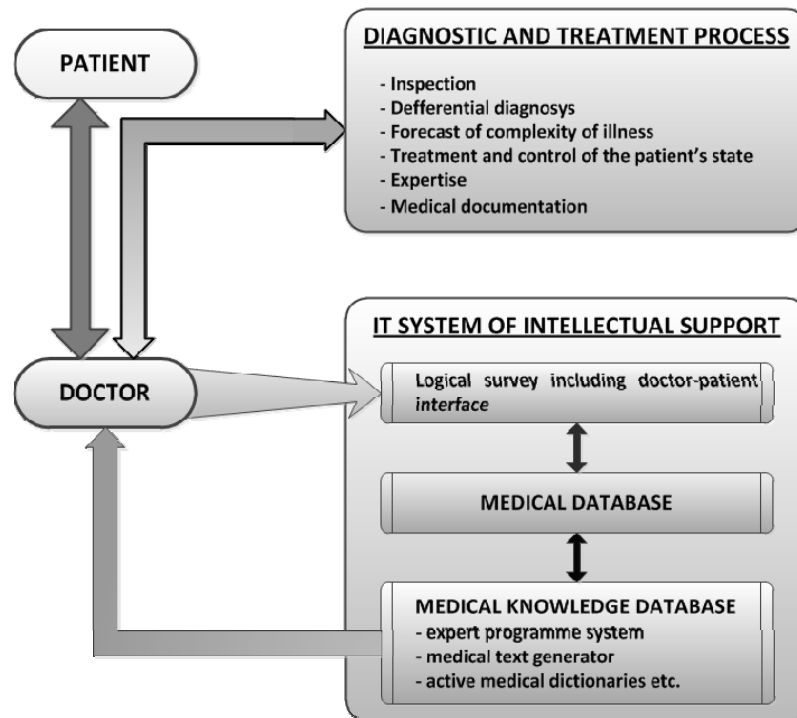


Fig. 1 The main areas of information support of the physician

Effective medical information and diagnostic system must provide the following functions:

- Automation of record keeping;
- Creating medical data and knowledge databases;
- Automation of the diagnostic and treatment process;
- Telemedicine technology;
- Providing high-tech medical care;
- Application of IT in medical education.

Prospective Directions of Telemedicine

Prospective areas of telemedicine include telesurgery and telemonitoring. Active influence on the patient's body from a remote destination is essential. Currently this is being developed in two directions: remote control of medical diagnostic equipment and remote medical influences such as surgery using remote-controlled robotics. Undoubtedly, the latter direction has the most demanding requirements for all the elements of telemedicine complex, especially for reliability and quality of telecommunications. Telesurgery assumes utilization of telerobotics and remote control over them directly during the operations (management of a scalpel, laser, etc.).

The prospects of telemedicine are linked with the further miniaturization of control and measuring devices, the introduction of smart technologies, robotics and the latest achievements of information science and nanotechnology.

Conclusion

Currently a variety of data from experiments in space telemedicine has been accumulated. This experience will promote creation of a network of ground-based telemedicine centers in Russia. With its help an opportunity to effectively eliminate the consequences of emergencies will be realized.

Contacts

Litvina Daria, +7 (963) 765-43-38, queen71@mail.ru

References

- [1] Strogonova L., Makarova S., Terentiev M.: Realization of permanent 24-hour medical control of psychophysiological state and registration of spatial coordinates, International Conference on Innovative Technologies IN-TECH 2011 proceeding, Slovakia, P542-545, G. p.
- [2] Strogonova L., Makarova S., Stolyrchuk V.: Pilot project "Habitability of a manned lunar station problems and methods of solution", GLUC 2010 Paper
- [3] Litvina D., Strogonova L.: Health control of liquid biological media during a manned space flight, Moscow Youth Scientific Conference of Innovation in aviation and aerospace - 2012, Russia, P 197-198.



International Conference on Innovative Technologies, IN-TECH 2012,
Rijeka, 26. - 28.09.2012



PRELIMINARY STUDY OF ACTIVATED SLUDGE ABILITY TO DEGRADE SELECTED METALWORKING FLUIDS

K. Gerulová¹, K. Fabianová¹, T. Černeková¹ and T. Hubinská¹

¹ Department of Environmental Engineering, Institute of Safety and Environmental Engineering,
Faculty of Materials Science and Technology in Trnava, Slovak Technical University in Bratislava,
Paulínska 16, 917 24 Trnava, Slovakia

Keywords: Degradability, Ecotoxicity, Metalworking Fluids

Abstract. The main aim of this study was to evaluate the ability of the activated sludge to degrade a part of the 10 selected metalworking fluids according to OECD 302B (with different addition of activated sludge – 0.25 g l⁻¹, 0.50 g l⁻¹ and 1.00 g l⁻¹ SS), and also to evaluate toxicity (50% inhibition of the respiration) to the same bacterial consortium of activated sludge according to OECD 209. The degradability test showed that, after the first 3 hours of cultivating, adsorption grew with the increasing amount of inoculums. The lowest adsorption rates showed Akvol B and Zubora TXS, where were also observed the lag phase (adaptation of the bacteria's to the carbon source). If occur adsorption rate more than 20% it is probably impossible to distinguish biological degradation of organic matter from abiotic elimination from the suspension. To differentiate it there were realized some more experiments with inhibiting of consortia's activity by HgCl₂ addition. The addition in preliminary study of Mobilcut 222 and Adrana D2420 showed decrease of adsorption rate after first 3 hours of cultivating deeply below 20%. It can be stated that, according to the test basic conditions, all the tested MWFs (excepted Zubora TXS) have a potential to ultimate degradation. According to OECD 209 toxicity test were Cimstar 597 and Emulzin H evaluated as the lowest toxic MWF's (none of tested concentrations achieved EC₅₀); followed by Zubora TXS, Aquamet LAK-E, Mobilcut 222, Adrana D407, Hocut 3380 and finally Adrana D 2420, which was evaluated as the most toxic from the list.

Introduction

Clean and safe machining is one of the industry's important topics. Both economic and environmental factors contribute to the recent increase in applications of machining under dry or minimal lubrication conditions. Manufacturers are looking for ways of reducing production costs and, at the same time, of avoiding the environmental problems associated with the use of metalworking fluids – MWFs [1]. Future lubricants have to be more environmentally adapted, have a higher level of performance, and lower total life cycle cost - LCC than presently used lubricants [2]. The use of rapidly biodegradable lubricants could significantly reduce environmental pollution. Environmental friendly alternatives are available for a large variety of mineral oil based lubricants [3]. The most interesting group for formulation of environmentally adapted lubricants is base fluids such as vegetable oils and synthetic fluids [2, 3, 4, 5]. These oils can offer significant environmental advantages thanks to resource renewability, biodegradability and nontoxicity [3].

Methods of Biodegradability Assessment

Degradation processes can be both abiotic (e.g. photochemical reactions and hydrolysis) and biotic [6]. Biodegradation by natural populations of microorganisms is the major route by which oil products are removed from soil and water compartments [7]. During these ultimate biodegradation processes the organic matter is converted into CO₂, H₂O, inorganic salts, microbial biomass and organic metabolites [8]. Methods for measuring biodegradability can be divided into two principal groups: direct measurement of parent compound concentrations and indirect measurement of parent compound bioconversion, such as CO₂ production, decrease in DOC, cumulative oxygen consumption (BOD), and decrease in COD (chemical oxygen demand). The indirect measurement of biodegradation by using summary parameters, such as BOD, COD or DOC is often easy and can be automated but it may be necessary to determine physical chemical elimination processes, such as adsorption to biomass or stripping processes, to differentiate biodegradation from abiotic elimination. The use only one indirect biodegradation parameter for biodegradation may be misleading [9].

By EPA OPPTS 835.3110 and OECD 301 A-F primary biodegradation is the alteration in the chemical structure of a substance, brought by biological action, resulting in the loss of a specific property of that substance. Ultimate biodegradation (aerobic) is the level of degradation achieved when the test compound is totally utilized by microorganisms resulting in the production of CO₂, H₂O, mineral salts and new microbial cellular constituents (biomass). Readily biodegradable is an arbitrary classification of chemicals which have passed certain specified screening tests for ultimate biodegradability; these tests are so stringent that it is assumed that such compounds will rapidly and completely biodegrade in aquatic environments under aerobic conditions. Inherently biodegradable is classification of chemicals for which there is unequivocal evidence of biodegradation (primary or ultimate) in any test of biodegradability [10, 11]. Ready biodegradability test were designed for quickly selecting "soft" chemicals in order to avoid time and money consuming further research. Inherently biodegradable tests were designed to demonstrate the potential degradability of a compound and finally simulation test were designed to measure the rate of biodegradation in a specified environmental compartment [6]. A chemical (or a waste water) may not be degraded or removed in the simulation test and may even have an inhibitory effect on the sludge micro-organisms. Other chemicals are biodegraded at low concentrations but are inhibitory at higher concentration. Inhibitory effects may have been revealed at an earlier stage or may be determined by applying a toxicity test, using an inoculums similar to or identical with that used in the simulation test. Such methods measure inhibition of oxygen uptake such as OECD Guideline 209 and ISO Standard 8192 or inhibition of growth of sludge organisms (ISO 15 522). Screening tests for ready biodegradability (OECD 301 A-F) indicates if a compound is degradable under natural conditions without any problem [12]. The biodegradation is monitored as the degree of mineralization, by means of summary parameters

such as O₂ uptake, CO₂ production or elimination of DOC. Without employing ¹⁴C techniques this is only possible if the test compound is the sole carbon and energy source for microorganisms. The test duration is 28 days, allowing some adaptation of the microorganisms to the compound but mineralization as a test criterion adds some extra stringency as it prevents chemicals to pass the test which are only converted into persistent products [6]. These informative tests basically discriminate readily biodegradable compounds from others, but they often underestimate the potentiality of degradation in environmental systems. Therefore when the result is negative, inherent (potential) biodegradability tests are required [12].

The estimation of biodegradation rates is an important source of uncertainty in chemical risk assessment mandated by new EU legislation. The existing OECD tests for ready biodegradability have been developed to devise screening methods to determine whether a chemical is potentially easily biodegradable, rather than to predict the actual rate, of biodegradation in the environment. However, risk assessment needs degradation rates. In practice these rates are often estimated (default values) from ready biodegradability tests - RBTs. These tests have many compromising arbitrary features compared to the situation in the real environment. One important difference is the concentration of the chemical. In wastewater treatment or in the environment many chemicals are present at ng l⁻¹ to µg l⁻¹ levels whereas in the tests the concentrations exceed 10 – 400 mg l⁻¹ of C. These different concentrations of the chemical will lead to different growth kinetics and hence different biodegradation rates. At high concentrations the chemical, if it is degradable, can serve as a primary substrate and competent microorganisms will grow exponentially, resulting in a sigmoid biodegradation curve. At low environmental concentrations the chemical does not serve as a primary substrate, and therefore does not support significant growth of the degraders, and the substrate has a linear biodegradation rate [13]. When assessing the biodegradabilities of lubricants, procedures have to be used which will increase bioavailability (by increasing surface area and hence the solubilisation rate) and facilitate accurate dosing. Commonly used techniques include: emulsification in a poorly biodegradable surfactant, ultrasonic dispersion, the use of a carrier solvent and/or a solid support [11]. RBTs based on the measurement of CO₂ evolution or O₂ uptake are useful methods for assessing the ultimate biodegradability of lubricants, provided special procedures are used to present the insoluble, hydrophobic test substance to the microbial inoculums. Tests which measure CO₂ production (e.g. OECD 301 B, ISO 14 593) are preferred as they give an unequivocal measure of biodegradation and only the organic carbon content of the lubricant needs to be known in order to calculate the extent of biodegradation. The 10 - day window pass criterion is inappropriate and in many cases incubation may need to be continued beyond 28 days before biodegradation reaches a plateau [11]. Biodegradability of lubricant industry recognized the following test OECD 301 B – Modified Sturm test, ASTM D 5864 [10]. In 2011/381/EU on establishing the ecological criteria for the award of the EU Eco label to lubricants the biodegradability shall be determined for each constituent substance in the lubricant separately by test methods specifies as OECD 306, OECD 310 for ultimately biodegradable substance. And for inherent biodegradable substance is a used OECD 302 C. Possible are also OECD 301 F for readily biodegradation [2] (according ISO 9408:1999). Many lubricants, particularly those based on mineral oils, are not readily biodegradable and data on their inherent biodegradability is perhaps more useful when assessing their likely environmental impact. However, two of these tests (OECD 302 A and B) measure biodegradation as the loss of DOC and are therefore unsuitable for testing lubricants which usually have a very low solubility in water (however, in OECD 302 B biodegradation can be realized also with COD, or COD according to the comparable ISO standard). The third test measures biodegradation as O₂ uptake and could therefore be applied to insoluble substances. However, with the exception of Japan, the OECD 302 C is reported to have fallen into disuse, and has technical limitations concerning the need for a ThOD value and a (needlessly) complex inoculum [11]. OECD 302 C is suitable for inherently biodegradable substance. Others newest are ASTM D6731 – 01/2011, ASTM D 6139 – 11 and ASTM D 5864 – 11 which were final release in 2011 especially for lubricant testing.

The Zahn-Wellens test according to OECD 302 B, C.9 or ISO 14593 is the most important of the existing standardized method for testing inherent biodegradability. The biodegradation process is monitored by determination of DOC (or COD, newly TOC) in filtered samples taken at daily or other time intervals. The ratio of eliminated DOC (or COD), corrected for the blank, after each time interval, to the initial DOC value is expressed as the percentage biodegradation at the sampling time. The percentage biodegradation is plotted against time to give the biodegradation curve. However, this method is not suitable for testing substances that are poorly soluble, volatile or adsorb to activated sludge, since the DOC or COD analysis it encompasses does not allow a clear differentiation between biodegradation and elimination by abiotic processes. Modification of the Zahn-Wellens test by continuous measurement of O₂ consumption (pressure measurement) and CO₂ (conductivity measurement) production was discussed in [14]. It is a closed test system consisting of a culture flask, a carbon dioxide adsorption flask, a pump as well as integrated measuring and control instruments. The air circulating within the test system causes the carbon dioxide present in the test solution to be stripped out completely and directly absorbed by the adsorption solution. This new test system also facilitates to test poorly soluble, adsorbing and volatile substances for inherent biodegradability and constitutes an appropriate complement to the standardized Zahn-Wellens test [14]. The biodegradability of oil products was usually assessed use in the CEC L 33-A-93 test, which was developed for two-stroke outboard engine lubricants only; it was widely used to test formulated lubricants, base fluids and additives [15,16] wheatear soluble or insoluble in water. In this test the loss of lubricant (containing CH₂ methylene groups - Absorbance can be measured in 2956 cm⁻¹ Methyl C-H bond stretch and 2926 cm⁻¹ for C-H Methylene bond stretch) due to microbial degradation is assessed by measuring the infrared absorbance after extracting in 1,1,2-trichloro-1,1,2-trifluoroethane at [6,10,17]. Because the CEC extraction solvent is an ozone-depleting chemical, its supply and use are restricted by the Montreal Protocol [16]. Unfortunately this test is not now supported by a CEC Working Group and will not be updated. In [17] there was used as solvent for analysis perchlorethylene (PCE) and in [16] was used and the analytical grade CCl₄ as an extraction solvent.

Materials and Methods

Fresh activated sludge from sewage treatment of the Jaslovské Bohunice plant was used as inoculums for the both tests (preliminary toxicity test and degradability test) the same day as the experiment started. In each of degradability tests, used were 0.25, 0.50 and 1.00 g of dry matter per liter in the final volume and 0.10 g of dry matter per liter in the final volume for toxicity evaluation. The degradability of MWFs was evaluated by OECD 302 B, while the toxic effect caused by inhibition of respiration was evaluated by OECD 209. Measurement of COD was realized spectrophotometrically by the Merck spectroquant SQ 118, TOC measurement was realized by the TOC V-CPN Shimadzu Scientific Instruments.

Results and Discussion

Toxicity to aquatic organisms is generally used to reveal potentially adverse environmental effects of a compound or product. According to OECD 302B test, there is a presumption with appropriate methods that no inhibition of sludge occurs at the chosen concentration of the test substance if this is not already known. If an inhibitory effect is found, it is needed to reduce the concentration of the

test substance to a level which is unlikely to be inhibitory. The test of activated sludge inhibition of respiration is recommended also when OECD 301A-F for primary biodegradation is realized. Compounds with an EC_{50} value greater than 300 mg l^{-1} are not likely to have toxic effects in ready biodegradability testing. Toxic impact can affect different responses, particularly the inhibition of respiration measured from the oxygen consumption in a closed bottle according to the OECD 209. Results from the test of 8 selected MWFs are discussed in the Table 1. The lowest toxic MWF's were Cimstar 597 and Emulzin H (the highest tested concentration was below EC_{50}), then Zubora TXS ($EC_{50} - 8\,449 \text{ mg l}^{-1}$), Aquamet LAK-E ($EC_{50} - 5\,600 \text{ mg l}^{-1}$), Adrana D 407 ($EC_{50} - 4\,354 \text{ mg l}^{-1}$), Mobilcut 222 ($EC_{50} - 3\,122 \text{ mg l}^{-1}$) followed, and finally, Hocut 3380 ($EC_{50} - 2\,828 \text{ mg l}^{-1}$) and Adrana D2420 ($EC_{50} - 1\,754 \text{ mg l}^{-1}$) were assessed as the most toxic. Important note of this test was the fact that all tested MWFs had effective concentration much higher than it was used in the degradability test, so no inhibition of the inoculum was considered.

Table 1. EC_{50} - Inhibition of respiration of activated sludge bacteria according to OECD 209.

Type of MWFs	R ²	EC ₂₀ [mg l ⁻¹]	95 % confidence interval	EC ₅₀ [mg l ⁻¹]	95 % confidence interval	EC ₈₀ [mg l ⁻¹]	95 % confidence interval
Cimstar 597	-	4 726	4 808 – 4 890	-	-	-	-
Emulzin H	-	2 539	2 625 – 2 719	-	-	-	-
Zubora TXS	0.9730	2 196	2 166 – 2 228	8 449	8 309 - 8587	-	-
Aquamet LAK-E	0.9640	-	-	5 600	5 567 – 5 658	-	-
Adrana D 407	0.9935	1 643	1 633 - 1654	4 354	4 304 – 4 405	-	-
Mobilcut 222	0.9880	1 653	1 570 – 1 727	3 122	3 099 – 3 144	6 189	5 884 – 6 629
Hocut 3380	0.9730	-	-	2 828	2 741 - 2912	8 828	7 759 - 9060
Adrana D 2420	0.9890	-	-	1 754	1 518 – 1 966	5 012	4 622 – 5 547

Important in this test (OECD) is that the starting concentration of the tested substance must not decrease below 20% after 3 hours of cultivating. After that, it is impossible to distinguish biological degradation of organic matter from abiotic elimination from the suspension through adsorption. Tested were 11 MWFs of similar concentration and different addition of activated sludge (AS) – 0.25 g l^{-1} , 0.50 g l^{-1} and 1.00 g l^{-1} . In the Fig. 1 are summarized results of adsorption rates from the degradability testing.

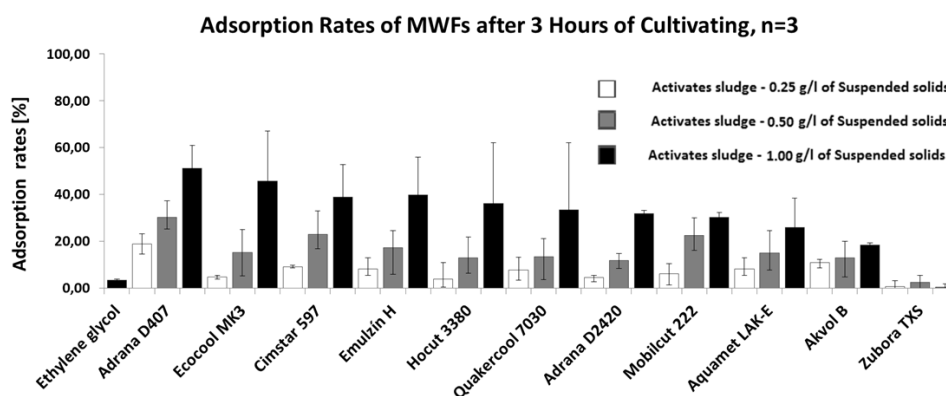


Fig. 1 Adsorption rates of tested MWFs in different addition of activated sludge.

As it was shown in the Fig. 1 in many cases the adsorption rates exceeded the 20% recommended value mostly in the AS addition – 1.00 g l^{-1} . Instead of Adrana D 407, Cimstar 597 and Mobilcut 222 - AS addition 0.50 g l^{-1} were all others in the limit. Because of achieving higher adsorption rates it was realized test to differentiation the potential sorption with the inhibitor HgCl_2 at the same test conditions for Adrana D2420 and Mobilcut 222. It was assumed that used inhibitor stopped all biological activity of the inoculum. For Adrana D2420 was achieved for AS addition 1.00 g l^{-1} decrease from 34% to 15%, and in the case of AS addition 0.50 g l^{-1} decrease from 14% to 6%. For Mobilcut 222 was achieved for AS addition 1.00 g l^{-1} decrease from 33% to 5%, and in the case of AS addition 0.50 g l^{-1} decrease from 28% to 12%. It is important point which indicates that around one half in Adrana D2420 and only one sixth in Mobilcut 222 may be eliminated by the abiotic processes. The study of the differentiation the biotic degradation and abiotic elimination is more complex and needs to be study in followed experiments. In the Fig. 2 and 3 there are shown selected results for Zubora TXS and Mobilcut 222.

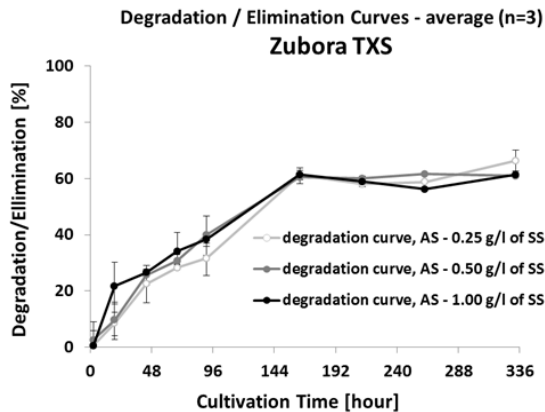


Fig. 2 – Degradation curves of Zubora TXS.

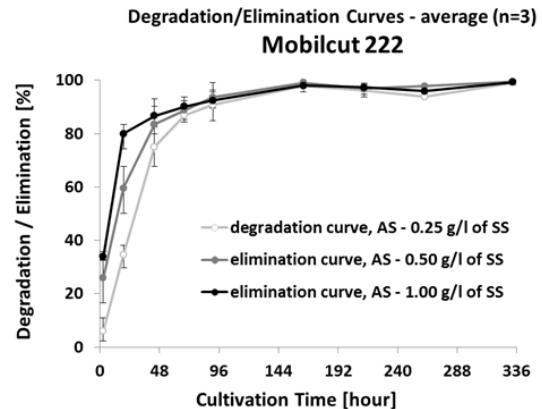


Fig. 3 – Degradation/elimination curves of Mobilcut 222.

As it is shown in the Fig 3 similar trend of the curves as it is shown in the case of mobilcut 222 had all tested MWFs (Adrana D407, Eccocool MK3, Cimstar 597, Emulzin H, Hocut 3380, Quakercool 7030, Adrana D2420 and Aquamet LAK-E) instead Akvol B, which has trend as Zubora TXS. The decrease of measured parameter COD (or TOC) was faster than it is expected in biotic degradation. In all cases absent the log phase, this could mean the no adaptation of the inoculum or that abiotic elimination may play an important role in whole elimination of the substance from the solution.

Conclusion

In our preliminary experiments, we measured the rate of elimination of 11 MWFs under the terms of the OECD 302 B (or ISO 9 888). The tests used a variety of allowances activated sludge (0.25 g l^{-1} , 0.50 g l^{-1} and 1.00 g l^{-1} of Suspended Solids). The rate of adsorption (after the first three hours of testing) were increased with increasing addition of activate sludge. To distinguish abiotic elimination of substances from solution was carried out follow-up experiment by the monitor of organic matter kinetics in the presence of microorganisms' activity inhibitor (HgCl_2). It was achieved a decrease in adsorption rate of more than 50% compared to conditions where the inhibitor was not used. Given that the most commonly used test for monitoring degradability of lubricants CEC-L-33-A-93 test which used an ozone-depleting substance and this test was cancelled, in the future we will focus on the modification of existing methods for determining biodegradability of substances by on-line recording of both parameters oxygen consumption and carbon dioxide production in closed system with possibility of simultaneously sampling.

Acknowledgment



Supporting research activities in Slovakia/
Projects is co-financed by European Community



The article has been realized under the research and development (50%-50%):

OP for project Centre of Excellence of Five axis Machining Experimental Base for High Tech Research ITMS 26220120045. Co-financed by European Funds for Regional Development.

Promoting young researchers 2012
(Slovak University of Technology in Bratislava)

References

- [1] J. RECH, J., BATTAGLIA, L., MOISAN: Thermal influence of cutting tool coatings, *Journal of Materials Processing Technology*, volume 159 (2005), p. 119–124.
- [2] A., PETERSSON: High-performance base fluids for environmentally adapted lubricants, *Tribology International*, Volume 40 (2007), p. 638–645.
- [3] K. VERCAMMEN, J. BARRIGA, A. ARNSEK: Annex 4: deliverable 11- summary of results, combining biolubricants and low friction coatings.
- [4] L. DE CHIFFRE, F. TOSELLO, M. PÍŠKA, P. MÜLLER: Investigation on capability of the reaming process using minimal quantity lubrication. *CIRP Journal of Manufacturing Science and Technology*, No. 2 (2009), p. 47-54.
- [5] L. Ö. EKENGREN, I. NIEMINEN, R. BERGSTRÖM: Environmentally acceptable metalworking processes, IVL SWEDISH ENVIRONMENTAL VTT RESEARCH INSTITUTE, 2002-01-18, A96291.
- [6] J. STRUIJS, R. VAN DEN BERG: Standardized biodegradability tests: extrapolation to aerobic environments. *Wat. Res.* Vol. 29, (1995), No. 1, p. 255-262.
- [7] H. FREDERIQUE, J. GERMAN, G. A. JUNTER: Primary biodegradability of mineral base oil in relation to their chemical and physical characteristics, *Chemosphere*, Vol. 45 (2001), p. 983-990.
- [8] P. REUSCHENBACH, U. PAGGAA, U. STROTMAN: A critical comparison of respirometric biodegradation tests based on OECD 301 and related test methods, *Water Research* 37, 2003, p. 1571–1582.
- [9] U. STROTMANN, R. REUSCHENBACH, H. SCHWARZ: Development and Evaluation of an Online CO_2 Evolution Test and a Multicomponent Biodegradation Test System, *Applied and environmental microbiology*, Vol. 70 (2004), No. 8, p. 4621–4628.
- [10] Engineering and Design: Lubricants and Hydraulic Fluids, Department of the army, U.S. Army Corps of Engineers, Washington, DC 20314-1000, 31 July 2006, Manual No. 1110-2-1424.
- [11] N. S. BATTERSBY: The biodegradability and microbial toxicity testing of lubricants - some recommendations, *Chemosphere*, No. 41 (2000), p.1011-1027.
- [12] M. E. LAPERTOT, C. PULGARIN: Biodegradability assessment of several priority hazardous substances: Choice, application and relevance regarding toxicity and bacterial activity, *Chemosphere*, vol. 65 (2006), p. 682–690.



-
- [13] J. AHTIAINEN, M. AALTO, P. PESSALA: Biodegradation of chemicals in a standardized test and in environmental conditions, *Chemosphere*, No. 51 (2003), p. 529–537.
 - [14] NORR, C., MEINECKE, S., BRACKEMANN, H., Modification of the Zahn-Wellens test: determination of the biodegradability of poorly soluble, adsorbing and volatile substances by measurement of oxygen consumption and carbon dioxide production. In: *Chemosphere*, No. 44, 2001, p. 553 – 559.
 - [15] N. S. BATTERSBY, D. CICCOGNANI, M. R. EVANS, D. KING: An inherent biodegradability test for oil products: description and results of an international ring test, *Chemosphere*, Vol. 38 (1999), No. 14., p. 3219-3235.
 - [16] YOUNG, L., ZHU, Y., FAN, G., at al. Test on Evaluation Method for Biodegradability of Lubricants. In Tianjin University and springer-Verlag 2008, No. 14, p. 61 – 65
 - [17] A. T. SIMPSON: Comparison of Methods for the Measurement of Mist and Vapor from Light Mineral Oil–Based Metalworking Fluids, *Applied Occupational and Environmental Hygiene*, No. 18 (2003), p. 865–876.



International Conference on Innovative Technologies, IN-TECH 2012,
Rijeka, 26. - 28.09.2012



IMPACT OF VISUALIZATION ON DATA AVAILABILITY

Lj. Kikinđanin¹, S. Popov², Đ. Čosić³, and D. Sakulski⁴

^{1,2,3,4} Faculty of Technical Science, University of Novi Sad, Trg Dositeja Obradovića 6, Novi Sad, Serbia

Keywords: data representation, disaster risk management, information seeking, visualization

Abstract. Data representation, as well as the appropriate information distribution and sharing is very important in Disaster Risk Management. Not only scientific communities, but general public too, needed adequate ways to visualize the huge data masses that are generating nowadays, through different distribution channels. Visualization, as field of a computer science, has been appeared as solution, a tool, for data analysis, using human visual system that can detect connections and patterns among data.

This paper highlights the importance of visualization in the representation of natural or man induced hazards data. Realizations of these hazards could have catastrophic consequences on population and environment. Transparency of these data proved to be a problem, hidden behind inadequately represented data.

Deficiencies of a data representation are identified during the pilot study. The vast amount of this data type is available via Internet, but it shows to be a problem for the user. The user is not able to find ones that are needed, during the shortest, most reasonable time period, especially during an emergency. Implementation of data representation methods and models that are used in other areas such as commercial sites, or social networks, could neutralize negative aspects of inadequately represented data. It could increase their availability to the user.

Introduction

Modern society is facing data redundancy problem these days. Never before, in the history of mankind, such amount of data has not been generated, as it is done today. Pieces of information are collected through sensors, by simulation, via systems used for tracking and monitoring and by using a supercomputer. This contributed significantly to reduce the time that elapses between major scientific discoveries. Total growth of knowledge, that used to be linear, now became exponential, which is amazing. The use of Internet and web browsers for scientific purposes became inevitable. Only two centuries ago, people needed to cross long distances in search of data and information relevant for their research. Today, on the contrary, it is possible to obtain the necessary information without leaving the laboratory or office.

However, at the same time, we become overwhelmed with an abundance of data that create new problems regarding scientific work. Research and analysis of such amount of data has become increasingly difficult in terms of recognition of the necessary from unnecessary data. Finding the needed information and obtaining the necessary information is a major challenge for the scientific community. If there is no adequate method to search and display the data, gathered because of potential benefit they can have, the data becomes useless as some sort of "data dump".

Term of visualization

The human brain is a "machine" that continuously processes a large amount of data and information. Thanks to the ability of visual perception, human beings understand (perceive) images and graphics better and more quickly in relation to the text and numeric data and can process them much easier and simpler (Fig. 1). The term visualization is used for such display of data and it represents a set of methods used to display large sets of data in the simplest and most visible way.

Visualization is viewed as transformation of data from symbolic representation into contextual geometry. Using visual representation of data, it can be very easy to find extreme values of these data, or to notice interesting connections between data or trends. It is also easier to find information that might otherwise remain hidden in data. The purpose of visualization techniques is to shorten the time needed to find information, to interrelate data and present them to the user, in such way that he can easily understand. In other words, purpose is to simplify something that, at first glance, seems very difficult, to bring the data into context and create information.

The *Figure 1* presents the population density of Belgrade. In order to assess where is the greatest population density by only looking at the table, we have to read each numerical value, remember it while we read it and then compare each value separately to the other values, in order to decide which value is less and which one is higher. Looking at the map, the information is processed through our visual perception, which recognizes various colors, and by looking at the map legend we can easily conclude which one of the regions is the one with the highest population density.

Process of visualizing data is a cognitive activity with which people build mental models of data, or rather an internal representation of the world around them, from which they manage to expand on and understand such data. [1] Today, computers can make the process of visualization much easier if we use some of the visualization tools, but actual visualization is indeed activity which happens in our mind, and it is essential for understanding the data. The process of understanding as a "continuum of understanding" [2] is a continuity that generates information from data. The information can then be transformed into knowledge and knowledge finally into wisdom. In this process, the visualization is located between data and information. Different combinations of the same data can give different information. The visual context functions in the same way, different visual contexts may lead to the formation of different information.

In order for visualization to be effective, it has to have purpose, and it has to be efficient and effective. From a pragmatic standpoint, we can immediately say that visual representation is considered "good quality" when it fully satisfies the communication and analytic requirements of those for whom it was intended and created. [3] Users' motives may range from fact-finding to browsing, professional to casual, or serious to playful. [4] Visualization should be different depending on whether its creator is company, non-profit organization or academic institution. However, regardless of the actual motives for visualization of the data, the speed which the user reaches the needed information or data is that what makes a significant difference between the services that deliver information nowadays.



1. Укупно пописана лица, укупан број становника према Пописима 2011. и 2002. и укупан број домаћинстава и станова
Total enumerated persons, total number of population according to the Censuses 2011 and 2002 and total number of households and dwellings

	Укупно пописана лица Total enumerated persons	Укупан број становника Total number of population		Апсолутни пораст-пад 2011-2002 Absolute increase-decrease 2011-2002	Индекс 2002 = 100 Index 2002=100	Укупан број домаћинстава Total number of households	Укупан број станова Total number of dwellings	
		2011	2002					
РЕПУБЛИКА СРБИЈА	7 565 761	7 120 666	7 498 001	-377 335	95,0	2 497 187	3 243 587	REPUBLIC OF SERBIA
СРБИЈА – СЕВЕР	3 727 104	3 556 010	3 608 116	-52 106	98,6	1 301 571	1 591 859	SERBIA – NORTH
Београдски регион	1 731 425	1 639 121	1 576 124	62 997	104,0	604 134	739 630	City of Belgrade
Београдска област	1 731 425	1 639 121	1 576 124	62 997	104,0	604 134	739 630	Area of Belgrade
Београд – Барајево	28 000	27 036	24 641	2 395	109,7	9 004	15 239	Belgrade – Barajevo
Београд – Вождовац	166 575	157 152	151 768	5 384	103,5	60 363	73 242	Belgrade – Voždovac
Београд – Вршац	61 085	55 463	58 386	-2 923	95,0	24 168	31 832	Belgrade – Vršac
Београд – Гроцка	87 649	83 398	75 466	7 932	110,5	27 882	38 299	Belgrade – Grocka
Београд – Звездара	160 076	148 014	132 621	15 393	111,6	55 704	69 380	Belgrade – Zvezdara
Београд – Земун	172 530	166 292	152 950	13 342	108,7	58 034	65 365	Belgrade – Zemun
Београд – Лазаревац	59 742	58 224	58 511	-287	99,5	18 801	23 996	Belgrade – Lazarevac
Београд – Младеновац	54 749	53 050	52 490	560	101,1	17 656	22 211	Belgrade – Mladenovac
Београд – Нови Београд	226 832	212 104	217 773	-5 669	97,4	81 064	91 708	Belgrade – Novi Beograd
Београд – Обреновац	74 460	71 419	70 975	444	100,6	23 611	33 745	Belgrade – Obrenovac
Београд – Палилула	181 346	170 593	155 902	14 691	109,4	64 795	75 690	Belgrade – Palilula
Београд – Раковица	111 724	108 413	99 000	9 413	109,5	39 984	43 796	Belgrade – Rakovica
Београд – Савски венац	41 557	38 660	42 505	-3 845	91,0	16 454	21 191	Belgrade – Savski venac
Београд – Сокоп	21 501	20 199	20 390	-191	99,1	7 013	14 136	Belgrade – Sokop
Београд – Стари град	51 967	48 061	55 543	-7 482	86,5	21 601	28 590	Belgrade – Stari grad
Београд – Сурчин	44 635	42 012	38 695	3 317	108,6	12 445	15 147	Belgrade – Surcin
Београд – Чукарица	186 997	179 031	168 508	10 523	106,2	65 555	75 763	Belgrade – Čukarica

Fig. 1 Data visualization on example of density of the Belgrade city [5]

Visualization of natural hazards data

When it comes to services that deal with environmental issues and distribute this type of data, visualization of hazard data must be designed in such way to primarily provide quick access to the requested information in order to make decisions in emergency situations. In this field the process of visualization can be defined as the symbolic representation of geographical information in the form of visual images, an externalization of internal (mental) representations for the purpose of communication. [6]

The term hazard implies the occurrence of a condition or phenomenon, which threatens disasters to anthropogenic spheres of interest in a defined space and time. [7] In general, a hazard is a natural, technical or social process or event that is a potential damage source. Usually when it is referring to hazards, it is deemed to the natural hazards that can be defined as “An interaction of people and nature governed by the co-existent state of adjustment of the human use system and the state of nature in the natural events system” [8] It is a physical event which makes an impact on human beings and their environment by causing disaster.

The data that are available on mentioned services, such as spatial and temporal indicators, are essential for monitoring hazardous events (floods, droughts, fires, earthquakes, etc.), preventively and correctively. The availability of this data is extremely important because they allow assessment of the nature and population vulnerability to the hazardous events. They also, indicate the possible outcomes of risk realization and raise global awareness about this issue. Thus, the visualization that should follow this type of data differs from the one used for commercial purposes (which is used to boost sales). Visual representation of this data is extremely important, because the data must be, above all, interoperable, structured and presented in such way that they can be quickly and easily found and used.

Visualization of data and visualization in general can have many different goals that differ from the needs. The goal of commercial visualization is to attract more consumers and keep them attracted as long as possible. For that purpose, the companies are using visualization as marketing “trick” in order to achieve that goal. On the other hand, there are scientific and abstract visualization [3, 9], whose goal is to transform the data into information as soon as possible.

For services that address the environment and provide information about natural phenomena and hazards, the objectives are consistent with both of these groups. These services must be carefully designed that, in case of emergency, they can provide the necessary information easily and quickly. The data should be represented in such way that user can easily and quickly find the necessary information, in both emergency situation and recovery periods. However, these services should promote and raise awareness about serious issues such as climate change and disasters that occur as consequences of climate change. Thus they have an educational character which should be close to as many users as possible.

With the aim of identifying high-quality solutions in the field and their further propagation, we analyzed how and in which way the data are represented in the institutions and at the services that are collecting and placing data which are important for decision making in hazardous situations.

Research

We analyzed 12 websites (regional websites and sites of leading institutions in the area of interest globally) (Annex 1) The analysis involved people who were between 25-30 years of age and who are highly educated in different professions that are not directly associated with the field. The reason for this is that the content of analyzed sites should be accessible and clear to everyone regardless of their interest. Application of these data is multidisciplinary.

The respondents were asked to choose four sites from above mentioned (one from each interest group: drought, hydrology, seismology and meteorology). Annex 2 shows a questionnaire that respondents completed. Sites were evaluated according to two leading criteria:

- design and navigation possibilities and
- depth and variety of content

First, the authors wanted to know whether there is a correlation between the sites that were most frequently chosen, and which sites were positively or negatively evaluated by respondents. On the basis of quantitative analysis it was concluded that the most commonly chosen sites were not and highly graded sites. It turned out that, the sites that the respondents were reluctant to choose got better reviews:

- sites 1, 3 and 6 received positive reviews;
- however, the most chosen were sites 1 and 7;
- site under the number 1 was the most frequently chosen because of good visibility, easy navigation on the site and multilingualism;
- website number 7 was the second most frequent choice for finding information; the reason for the choice of this site was attractive home page; respondents believe that the site was comprehensive, but for most of them very messy, difficult to navigate, and the search was time-consuming. That is why this website it was badly accepted by respondents.
- the other sites got negative reviews or respondents ended their search without the required information.

After that, a detailed qualitative analysis was conducted. It was analyzed what the reasons for positive or negative criticism were, and why only 3 of 12 offered sites were evaluated positively. The most important observations are the following:

- The choice of a website that will be the first used to start a search, was highly influenced by the look, appeal and attraction of its Home page.
- Visibility of the site content and organization of content in menus and submenus significantly affects not only the search for information but also the speed of finding the information (visibility was essential for a positive assessment of the site).
- For more complicated web site structures, use of „search“ and/or „index“ tools were of great assistance for quick access of needed data or information; however, they were not available on each website, or they were undetected by the user (they are imperceptible).
- There has been often language barriers or the site was monolingual which made the site repulsive for the user.
- The formats in which data are available are PNG, GIF or JPEG.
- Spatial data (in formats KMZ, GML, etc.) are usually not available (except for the site number 6) or their availability is very limited, and often reduced to the purchase (website 7).
- The data are usually represented through reports and publications.
- Graphical views are of great help to facilitate understanding of the presented data, but most of them are available only as informative, but not as interactive maps.
- The explanations of terms from the field are mostly left out or insufficient for understanding the presented content.

Discussion

Derived from observations of the respondents there are numerous conclusions on how visualization affects the availability of data for above mentioned services.

The attractiveness of the site and its design affect the decision of the user to opt for a certain site. Sites that were analyzed have tradition of government agency websites and are often with unattractive design. If you add to that the large amount of data that is regularly and irregularly updated, users get the chaotic impression and then they choose another service. Those services that adopt modern principles of graphical modeling the websites and that look like commercial sites are commonly used as an initial source of the search.

Due to large amounts of data stored by these services, the visibility is often neglected. But, visibility is precisely what affects the speed of information retrieval. Site structure should be simplified to the maximum for content to be visible, and this is what bothers the user at first. It can be said that the lack of visibility is a common problem among these services at the moment. Site structure and easy overview affect the formation of user's attitude about the site, because „readability and the attraction of the proper amount of attention to the right elements are crucial and when these issues are addressed in a proper way, an attractive design will result“. [10]

For the services that have a large database, certain tools are required, so they can be searched efficiently and effectively. Tools like „search“ and „index“ have proved to be very successful in commercial sites and library services, and they should be available also in services in this field of research, which is not the case at the moment.

Speaking of the visualization of data, it is necessary to emphasize that the graphics like charts or maps are highly represented in these services. They contribute significantly to the user so he can obtain needed information quickly and easily. However, although the data are presented to the user, their further use is limited because of the format in which they are represented. As these services provide the geo-spatial data, their use in emergency situations is essential for mapping the terrain and to locate the affected regions, as well as for decisions making based on past events. In order to apply the data to the GPS devices or some software which displays the geo-referenced data (GIS, Google Earth, etc.) they must be stored as a binary or textual file. Therefore, the data represented in reports, tables (as PNG, GIF or JPEG format) are practically useless in the required time. For some services, however there are data in adequate data formats that could be further applied, but there is limit too. Represented in needed form, the data can be accessed only with special permission, or can be purchased (only a limited amount of data can be downloaded free of charge, as a sample, to display what the user can purchase).

The graphical representation, which, on the one side, is good for understanding and producing the information, can however, be a significant limitation. Data visualization through graphical representations only „apparently“ provides access to all data, because in fact it only displays the information that service wants to show. The data is placed in a certain context and their visualization creates certain information, while the original data remain „trapped“ behind the graphical display. This prevents the application of the same data for gathering any other information, by putting data in a different context or by different visual representation.

Conclusion

The use of computers and the Internet has led to an explosion of data, but their search has become a problem. On the other hand, computers have many tools for finding, sorting, filtering, and finally, presentation of data. However, the presentation of data through visualization should not be the ultimate goal, it should serve as a tool for achieving higher goals.

As the visualization of data varies depending on the field in which it applies, it has its peculiarities also in the field of Disaster Risk Management. First of all, visualization is essential for the rapid creation of the necessary information, but its application in this area affects on the availability of the data. Services that provide data are mainly governmental agency services and they only „formally satisfy“ the public by providing data and information through reports and publications, or just by a simple graphics on the site, but in formats that are inadequate for further use. This prevents their use in emergency situations, and use of data for further research, because access to the original data is disabled.

The design of the sites from this field is unattractive, immense, one word – repellent, and their structure is very complicated. Multilingualism is almost nonexistent, which means that the application of data is reduced for local and regional areas.

To ensure the successful implementation of data on right time it is necessary that:

- sites of this type follow the trends that are used in the design of commercial sites;
- site structure is simple and easy to navigate;



- sites are multilingual, and that, in addition to the parent language, provide content in any of the official world languages (English, Spanish, French etc.);
- data are visually represented, but also available in appropriate formats for further use and visualization.

Only by adoption of these recommendations, services that provide data and information from the test area can be purposeful and effective, and the response of all participants in emergency situations prompt and satisfactory.

Acknowledgment

This work was supported by the Ministry of Education and Science of the Republic of Serbia within the project "Development of methods, sensors and systems for monitoring water quality, air and soil" (No. III 43008)

References

- [1] R. Jacobson: *Information Design* (MIT Press, Cambridge, 1999).
- [2] R. Spence: *Information Visualisation* (Addison-Wesley, Harlow, 2001).
- [3] R. Mazza: *Introduction to Information Visualization* (Springer, London, 2009).
- [4] B. Sneiderman et al: *Designing the User Interface: Strategies for Effective Human-Computer Interaction* (Addison-Wesley, Instock, 2010).
- [5] *2011 Census of Population, Households and Dwellings in the Republic of Serbia*, ISSN 0354-3641.
- [6] A.L.H. Pang: The Educational Effectiveness of Dynamic and Interactive Data Visualization and Exploration in Geographical Education, *Proc of International conference on Redesigning Pedagogy: Research, Policy, Practice*, (2005).
- [7] S. Fuchs: Probabilities and uncertainties in natural hazard risk assessment, *Proc of 4th International Probabilistic Symposium*, (2006), pp. 189–204.
- [8] G.F. White: *Natural Hazards Research* (Methuen Publishing, London, 1973).
- [9] M.C.F de Oliveira and H. Levko: From Visual Data Exploration to Visual Data Mining: A Survey, *IEEE Transactions on Visualization and Computer Graphics*, Vol. 9 (2003), No. 3, pp. 378-394.
- [10] J.J. van Wijk: Views on Visualization, *IEEE Transactions on Visualization and Computer Graphics*, Vol. 12 (2006), No. 4, pp. 421-432.

Annex I

Analyzed websites:

1. <http://www.bafu.admin.ch/>
2. <http://www.dwd.de/>
3. <http://www.seismo.ethz.ch/index>
4. <http://www.jma.go.jp/jma/indexe.html>
5. <http://drought.unl.edu/>
6. <http://www.dmcsee.eu/>
7. <http://www.noaa.gov/>
8. <http://www.met.hu/>
9. <http://meteo.hr/index.php>
10. http://www.hidmet.gov.rs/index_lat.php
11. <http://www.arso.si/>
12. <http://www.meteo.bg/>

Annex II

Questionary:

1. Why did you decide for choosing this site precisely?
2. Did you find the required information?
3. How much time did you need to find requested information and do you consider that time acceptable to you?
4. Did you use the tool "search" or "index" during a search?
5. What is the first impression about the website and its Home page? Explain.
6. Do you like the website design? Explain.
7. What is the visibility of the website in your opinion?
8. What is the website structure in your opinion?
9. Did you find some other information in addition to those who you are looking for, that would be useful to you?
10. Do you consider that presented information could be useful to a different customer profile from yours? Explain.
11. Did you understand the content presented on the site?
12. Were there adequate explanations of terms from the field?
13. Have information and content on the site adjusted for each website visitor?
14. Are you satisfied with the representation of data and information on the site? Explain.
15. Do you understand graphs that represent data sets?
16. Are data available for further use? Explain.
17. Will you returning in the future to this site and using data and information that could be found there? Explain.
18. Suggest if there is something that needed to be improved on the website and that could make its content more operable for the user.

A PRESENTATION OF ENVIRONMENTAL RISKS FROM THE PERSPECTIVE OF INDUSTRIAL ACCIDENTS

J. Rak¹, and L. Jurikova²

¹ Faculty of Applied Informatics, Tomas Bata University in Zlín, Nad Stráněmi 4511, 760 05 Zlín,
jrak@fai.utb.cz, Czech Republic

² Faculty of Applied Informatics, Tomas Bata University in Zlín, Nad Stráněmi 4511, 760 05 Zlín,
ljurikova@fai.utb.cz, Czech Republic

Keywords: Industrial accidents, geographic information systems, environment protection, emergency management, population protection.

Abstract. This article describes the methods and use of information support in the field of the management of emergencies in the Czech Republic. Specifically, it deals with the use of specialized software and geographic information systems in the planning and preparation for assessing industrial disasters in relation to environmental risks. The introduction of this article is focused on the ways of determining emergency planning zones together with their graphic representation for the needs of prevention of damage to the environment, life and public health. Furthermore, it analyses issues from the perspective of the municipalities with extended powers as well as the regional authorities which are primarily responsible for population and environment protection in the Czech Republic.

Supporting documentation for the determination of emergency zones and their explanation are based on the legislation that is valid in the Czech Republic. Nevertheless, this presentation can also serve as an example for the solution of the given issues in other countries.

The results presented were obtained by means of the analysis and synthesis of current methods for the implementation of emergency planning. The method of analysis and synthesis was primarily used in the graphical part and the presentation. The data acquired was consequently evaluated. The desired output emerging from the comparison enables the determination of the key points for the whole process.

Thus, the main objective of the research is the creation of a map of risks affecting the environment of the municipalities with extended powers, which would increase the preparedness of the authorities responsible for the implementation of safety measures in case of industrial disasters and other events threatening the environmental security.

Introduction

Along with the development of human society and the increase in industrial production come the related hazards and risks. These hazards include, for instance, dangerous leakage of chemical substances, explosions of production facilities, etc. Generally, these hazards are referred to as industrial accidents. Not only do the industrial accidents threaten lives, health and the property of the population but they also threaten the environment. These hazards are, for example, contamination of water streams and groundwater, fire, contamination of soil and air, etc. Such accidents can then cause irreversible damage to the environment. The removal of these damages and all consequences requires considerable funding and extensive use of human resources and technologies. Renewal and revitalization of the environment to its original condition also requires a substantial amount of time. In some cases the renewal may take decades.

With respect to these facts, the prevention of industrial accidents represents the primary element of the protection. In the Czech Republic as well as in many other countries considerable attention is being paid to the prevention of industrial accidents. However, the full security in the field of prevention can never be guaranteed and it is therefore necessary to make preparations to cover possible industrial accidents. Mapping of the affected area, method of evacuation of persons and animals and other activities form part of this preparation. The use of geographic information system (GIS) and other specialized software within this process enables a significant reduction in costs and time required. Together with this it also contributes to the visualization and presentation of data, such as emergency zones, evacuation routes, affected areas, etc.

Preparation for industrial accidents in the Czech Republic

In the Czech Republic industrial accidents are regulated by Act No. 59/2006 Coll. along with implementing regulations No. 256/2006, Coll. and No. 103/2006, Coll. These documents contain basic responsibilities for manufacturing companies and other entities handling excessive amounts of dangerous chemical substances; furthermore, these regulations stipulate the execution of security measures and compliance with the procedures for the safe handling and safe use of dangerous substances. Moreover, these documents specify the procedures and activities of the authorities that are responsible for controlling and ensuring compliance with these procedures as well as a description of security documentation (specifically external emergency plans) and identification of zones of emergency planning. Nevertheless, a more extensive description of these documents is beyond the capacity of this article. Documents are listed in the bibliography (1, 2 and 3). For the purposes of the research, a method for the identification of emergency zones is particularly significant – these are areas, which are supposed to be affected due to industrial accidents. The zone for emergency planning is an area around a building or a facility in which the regional authority, in whose territory the object or facility is located, applies the requirements on emergency planning by means of the external emergency plan.

Methods for the determination of emergency zones

Methods for defining zones of emergency planning are regulated by Decree No. 103/2006 Coll. Of the primary significance is the determination of an R parameter which represents the minimum radius for the determination of initial boundaries. Methods for calculating the parameter R are listed in the Decree. For a more detailed study Document 3 in the bibliography is recommended. For the purposes of this article the means for the presentation of these methods and searching of points of interest in the zones are important.

Supplementary tools for the determination of zones at risk

Specialized software tools can be especially useful for calculations related to the affected area, calculations of the extent of contamination or similar values. In the Czech Republic the most frequently used tool is "TEREX" software. Terex offers several basic modules used for the determination of areas at risk or affected areas.

"TEREX" software

Terex is a simple tool that allows the quick determination of areas at risk. It contains several modules by means of which it is possible to determine the effects of dangerous substance leakages, explosive systems and toxic agents. The acquired results can also be displayed as circular zones in base maps of the particular areas, which enables the visual evaluation of objects in the area at risk. The basic modules are, as follow:

a) Dangerous chemical substances – evaluation:

- models of type TOXI – reach and shape of a cloud according to concentration of toxic substance.
- models of type UVCE – effects of an air shock wave causing detonations of a mixture of the substance and the air
- model PLUME – prolonged release of the gas into a cloud, boiling liquid leakage with rapid evaporation into a cloud, slow evaporation of the liquid from a pool into a cloud
- model PUFF – one-shot release of the gas into a cloud, boiling liquid leakage with rapid evaporation into a cloud
- models of type FLASH FIRE – size of the space in which persons are at risk by a flame zone (Flash Fire, Jet Fire and Pool Fire effects)

b) Explosive systems – evaluation:

- model of type TEROR – possible effects of detonations of explosive systems based on the condensed phase, used with the aim of exposure of the surroundings of the detonation to danger

c) Toxic agents – evaluation:

- model POISON – spread of a cloud formed by dispersion of the toxic agent to a particular territory (according to the size of the territory, kind of the agent, means of dispersion and secondary evaporation)
- model ATP-45C – dependence of results on the way the substance is applied and on the strength of the wind. The model ATP-45C proves to be very rough for the evaluation of terrorist use of toxic agents and is more suitable for military use.

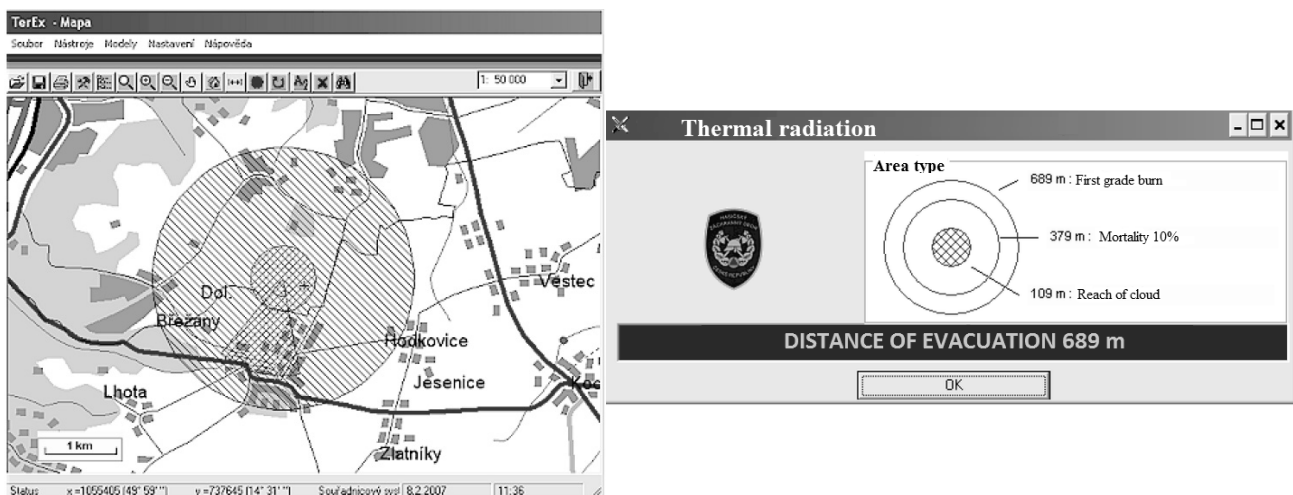


Fig. 1 Examples of "TEREX" software [4]

The use of a geographic information system – the creation of a map of risks

The GIS is a computer based information system for acquisition, storage, analysis and visualization of data which has a spatial relationship to the Earth's surface. Geographical data with which the GIS operates is defined by the geometry, topology, attributes and dynamics.

The geographical information system enables the creation of models of the Earth's surface using available software and hardware resources. This model can then be used for Land Registry records, weather forecasting, identifying flood zones of rivers, selection of a suitable location for a waste treatment plant, planning of roads, etc. [1]. Rudiments for creating maps of interest are spatial analyses and queries.

The use of the GIS extends the possibilities for the presentation and display of zones of emergency planning. It also makes it possible for the data created during the determination of emergency planning zones to be used in emergency planning and management, or other activities, such as planning of transportation of dangerous substances, etc. Within the framework of territorial units (municipalities, regions) this data serves for the creation of maps of risks, vulnerability and hazard. As a result of this, it is possible to create comprehensive maps of risks in any given territory which can be used for various purposes. In addition, it can be used for the creation of a map of environmental risks. Provided such a map is supplemented by additional information (risks of different nature – mining of mineral resources, road transport, transport of dangerous substances, etc.) it is possible for the given territory to create a map of primary environmental risks.

The fact that the GIS is capable of providing geographic information is one of its major advantages, which enables the use of spatial and other analyses. By means of these analyses it is, for instance, possible to locate rivers at risk within the zones of emergency planning, or to plan the transport of dangerous substances, including the identification of areas at risk and many others.

Spatial analyses in the GIS

Spatial analyses are sets of techniques for analysis and modelling of localized objects where results depend on the arrangement of these objects and their properties. Spatial analyses represent sets of analytical methods that require the attribute data of the studied objects, as well as their locations to be obtained.

Spatial data analyses are associated with the study of the spatial data arrangement. Specifically, they deal with a search for new relations between arrangement and objects' attributes or features within the studied area and with the modelling of these relationships in order to achieve a better understanding and predicting of progression in the area [2].

The analyses of the spatial data can be divided into several categories. Primarily, these are [2]:

a) Used procedures of applied techniques

- Spatial statistics;
- Map analysis – in the sense of map algebra;
- Overlay operations;
- Methods of mathematical modelling;
- Interpolation methods;
- Location and allocation methods;
- Network analyses;
- Other analyses of the area and their connections.

b) Method of data processing

- Visualization methods: they focus on visualization of spatial data without modification of graphical elements of data;
- Research methods: do not show the original data but use spatially modified data;
- Methods of modelling: their objective is to create an appropriate model and to verify its appropriateness for the intended purpose.

An example of the use of GIS for determination of the area at risk during the transport of dangerous substance

For the purposes of this article, locating of the area at risk during the transport of dangerous chemical substance serves as an illustrative example of the use of spatial analyses in determination of environmental risks. In the said area the transport of dangerous chemical substance from point A to point B is to be accomplished. The task is to determine possible environmental risks related to this transport.

- 1) The selection of a route and determination of the area at risk (based on the range of possible accidents gained by a calculation in "Terex" software) + the location of the rivers in the zones that can be affected, together with consequent contamination of lower sections of these rivers.

Fig. 2. depicts points A and B together with the transport route of the dangerous chemical substance. The figure further shows the location of the zones near the transport route which could be affected by DCS; the zones are located by means of the spatial analysis in Terex software, using the knowledge of a damage radius of the leakage or explosion of dangerous chemical substance. Another part of the figure represents the location of rivers that are likely to be affected. The sections of the rivers that would be directly affected by dangerous chemical substance leakage are highlighted, together with their lower sections.

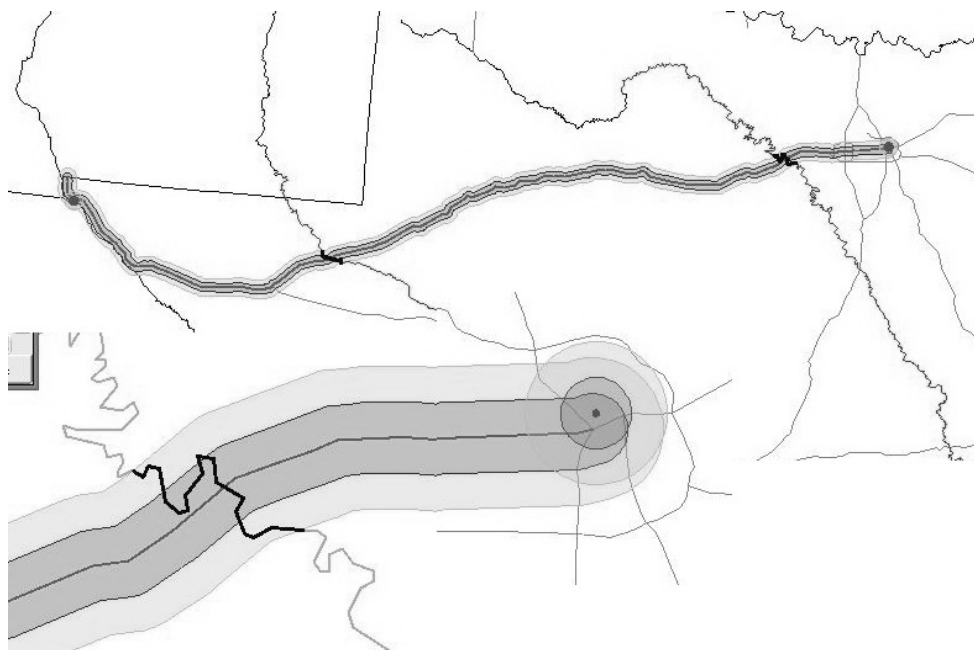


Fig. 2 Determination of areas and rivers at risk during transportation of dangerous chemical substance

1) The creation of the map of environmental risks.

Fig. 3 depicts the final map of environmental risks connected to the transportation of DCS. The presentations of risks in the form of a map can considerably increase the efficiency and transparency of risk visualization.

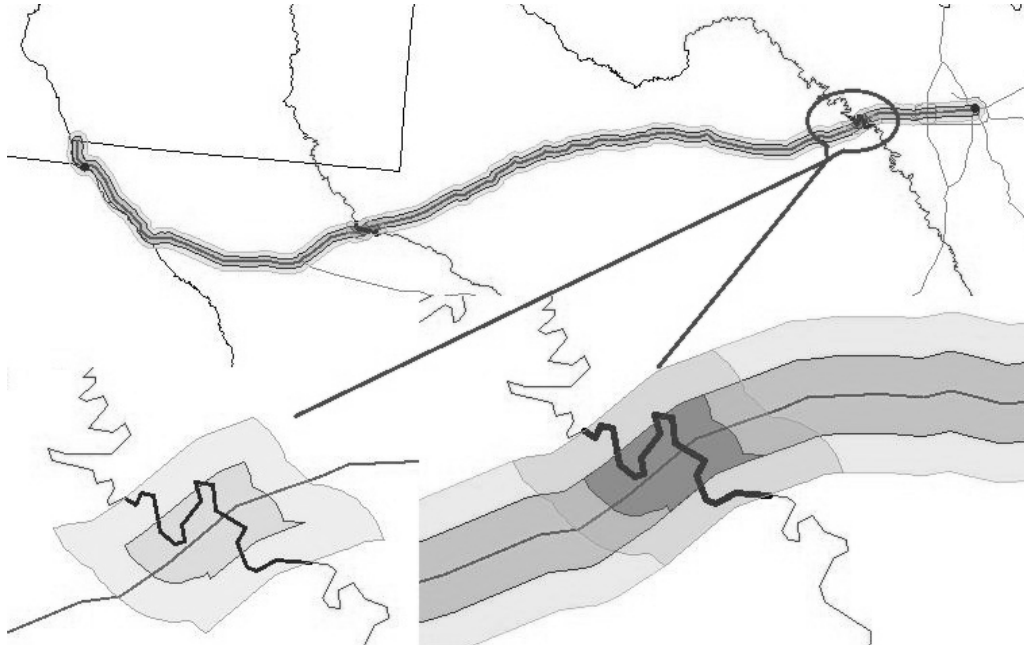


Fig. 3 The map of environmental risks connected to the transportation of dangerous chemical substance

Based on the creation of the map of environmental risks it is possible to adjust the security measures in order to ensure a higher degree of security during the transport of the dangerous chemical substance. For rivers at risk it is possible, for example, to reduce the speed of a vehicle in the area at risk, etc. Therefore, such information helps to streamline the work of the security forces and eventually reduce the costs if the system is employed. Maps of environmental risks makes it possible to present in quite a simple way a large amount of information, which is a great advantage compared to conventional methods (tables, calculations and text).

Conclusion

The use of the GIS in determining and presenting environmental risks is an effective solution. The creation of maps of risks allows the reduction in the time spent in the evaluation of risks and it also simplifies the whole process. Owing to these qualities it seems to be the optimal solution. One undeniable advantage of the GIS is the possibility of the use of spatial analyses and the visual presentation of the acquired results. However, there are also certain disadvantages related to the GIS. It is, for instance, the requirement for large amounts of data in a particular format to be provided. Such data is not always available and it must often be modified or even created. Another crucial condition is knowledge of information technologies by the staff responsible for the emergency management and security. In the Czech Republic the wider use of information technologies is often rejected. However, in the course of time the trend for increasing computer literacy of the staff together with the growth in digital data required for the needs of the GIS are anticipated. From the perspective of the GIS, in particular, there is a space for development of spatial analyses and its interconnection with modelling methods. Thanks to this interconnection it will be possible to map risks with greater accuracy and in a superior quality. As an example of modelling in the GIS, flood prediction using modelling of the flow of rainwater based on the knowledge of slope of the terrain can be mentioned as well as direction and size of a cloud of dangerous chemical substance based on the knowledge of concentration of the substance together with direction and strength of wind and other variables. Not only do these activities predispose the GIS for the extensive use of environmental security but it is also generally of use in the field of emergency management and other related areas.

Acknowledgment

This paper is supported by the Internal Grant Agency at TBU in Zlin, project No. IGA/FAI/2012/028, IGA/FAI/2012/054 and by the European Regional Development Fund under the project CEBIA-Tech No. CZ.1.05/2.1.00/03.0089.

References

- [1] *Geographical information systems*: Wikipedia open encyclopedia, online: 20.06.2012, http://cs.wikipedia.org/wiki/Geografický_informační_systém
- [2] J. Pecina; *Principle of spatial data analysis*, Pilsen: University of west bohemia, Faculty of Applied Sciences 2005. p. 84
- [3] J. Rak, L. Jurikova, M. Beneda; Possible solutions to the civil protection by the concealment under the Czech republic conditions, *Proceedings of the International Conference on Military Technologies 2011, ICMT'11*, Brno : University of Defence, 2011, p. 1147-1152, ISBN 978-80-7231-787-5.
- [4] *Terex – terrorist expert*. Website of T-soft, online: 17.06.2012, <http://www.tsoft.cz/terex>
- [5] T.J. Cova.: GIS in emergency management, *Geographical Information Systems: Principles, Techniques, Applications, and Management*, USA - New York, 1999. p. 845-858.

MATHEMATICAL METHODS IN THE ISSUE OF SAFETY DURING THE START OF MANNED SPACESHIP

L. Strogonova¹, E. Davydova²

¹ 125993, Moscow, A-80, GSP-3, Volokolamsk Highway, 4 Russia

² 125993, Moscow, A-80, GSP-3, Volokolamsk Highway, 4 Russia

Keywords: wireless sensor network, space, an emergency.

Abstract. Practice of manned space flight shows that the problem of crew safety on manned space vehicles is becoming increasingly important and difficult implemented in practice. The main problem of safety is to ensure that no increase in redundant systems circuits, no increase in the number of test events, no increase in resource systems does not lead to an increase in security work at the launch complex. Some share of the safety measures are making the administration and methods instruction personnel, of training condition the occurrence as well as emergency relief at the start, this causes both the appearance and emergency situation at the start. Taking into account high cost of development and exploitation of manned spacecraft, the cost of losses in case of accidents and failures of rocket, engineering of promising new generation of manned spacecraft and the construction of the Far East new Russian cosmodrome "East", a new approach to ensuring the safety of people at the launch complex.

The main task in the way of solving this problem is the introduction into the practicespace of principally new methods of remote monitoring of psycho-physiological condition and health of astronauts in space during actuation system of emergency rescue. For these purposes, is proposed to create a node wireless sensor network "Salvation." The node wireless sensor network "Salvation" are sensors that record physiological parameters (heart rate, respiration rate), the spatial position sensors, the coordinator, which includes a microcontroller, flash memory, a transceiver, an autonomous power supply and antenna.

In addition to the development of wireless sensor network node "Salvation" is necessary to pose the problem of mathematical research. This will allow, based on a matrix of unknown parameters purposes, assume the possible states of the astronaut, but as a consequence, the nature of the rescue and resuscitation.

For licensing and certification of a new method of monitoring the state of the astronaut need ground model experiment simulating the system response time of emergency rescue. In the event of a positive outcome of the experiment, the wireless sensor network will be applied at the time of the launch of the spacecraft and allow in the event of an emergency rescue operation to provide proper emergency care to victims, as well as make proper evacuation of the crew of the capsule. At this stage in time, we are preparing for this model experiment, despite its high cost, which is much lower, its scientific significance. There is still a lot of work, but the solution above mentioned problems in the complex will necessarily lead us to the goal.

Introduction

Continuous medical monitoring and tracking of the spatial position of the astronaut in the volume of Launch Escape System (LES) will:

- A. Will collect health information at the time of activation LES, at the time of the strongest shock overload;
- B. The principal novelty of this type of medical information is determined by the need to improve safety;
- C. Mission control centre, using the received data on the coordinates of the astronauts with their physiological state at the time of operation of LES can more quickly and accurately make decisions on the provision of necessary medical intensive care, and conduct regular evacuation of the LES.

The impact of shock overload on the body

At the time of activation of the emergency rescue, and when the capsule hit the ground on, the astronaut operating the strongest shock overload, which can sometimes lead to loss of life astronaut, or to other border states.

Table 1 - Effects of shock overload on the body

Effect of shock overload on the physiological systems of the astronaut	
System:	The physiological response:
1. Cardiovascular system	Impeded the flow of blood through the veins, reduced cardiac output, the possibility of anemia of the brain (\pm Gz). Poor circulation in small blood vessels, increase heart rate (\pm Gx). Sinus tachycardia, shortening of the electrocardiogram waves: PQ, QT, RP. Poor circulation in the small circle ($+G_x$), as a consequence of hypoxia, increased blood pressure.
2. Breathing system	The increase in respiratory rate, changes in biomechanics of the respiratory act, reducing lung capacity.
3. Visual analyzer	The blood pressure in the central retinal artery is increased in comparison with the intraocular pressure, therefore, reduced visual acuity, field of view, increasing the dead zone, a red or a black shroud.
4. Central nervous system	Shortened the latent periods of conditioned reflexes, it is possible fainting, coma, and death. There are changes in the endocrine glands
5. Circulatory system	Hyperglycemia, decreased number of red blood cells, hemoglobin, there is a segmentary leukocytosis. The volume of each red blood cell. Increased anticoagulant properties of blood.
6. Gastrointestinal tract	Changing the motor function of the gastrointestinal tract, decreasing the selection of juices, and products of metabolism increases, so maybe poisoning food exchange, it becomes possible emetic response.
7. Urinary system	The appearance of red blood cells in urine, increased urine output, hemodynamic changes and increased glomerular filtration.
8. Overall health	The efficiency drops, attention and reaction speed is dulled, made possible failures in the system "man-technical complex."

The main advantages of wireless sensor networks

Wireless sensor network (WSN) - a wireless system, which is a distributed, self-organizing and resilient to failures of individual elements of the network computing device with autonomous power supply. The nodes of such a system broadcast messages through each other, providing a large area of network coverage for low-power transmitter.

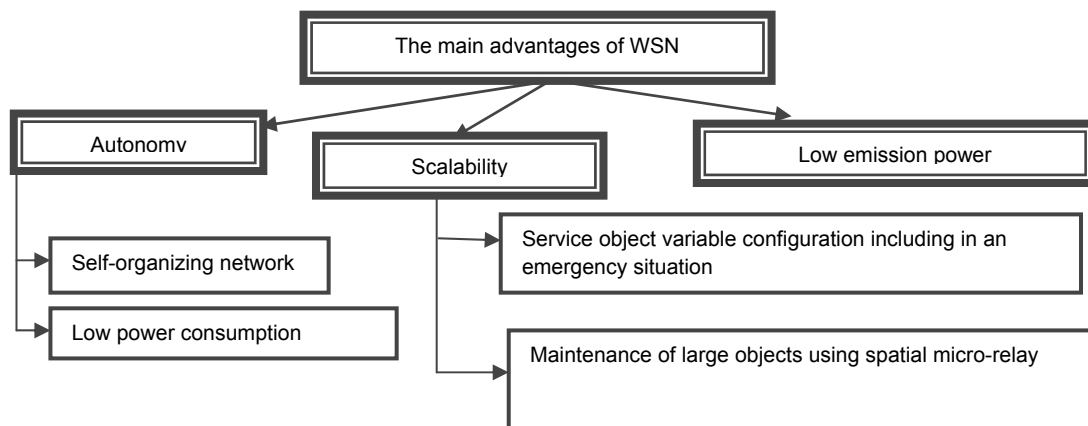
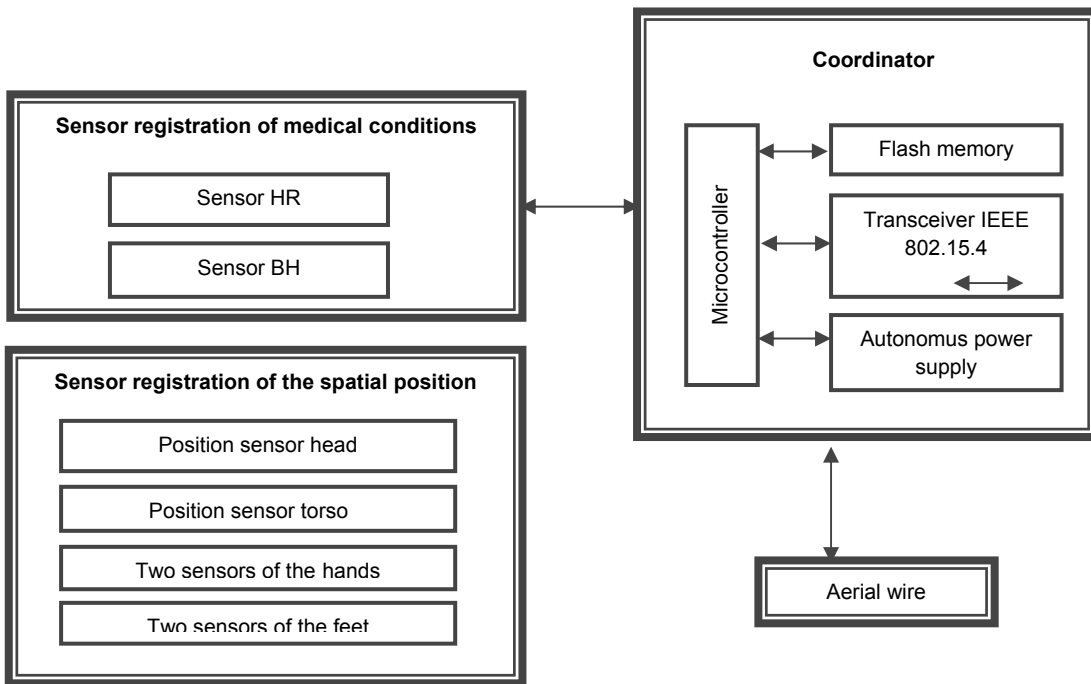


Figure 1 - The main advantages of the WSN

Wireless sensor networks consist of tiny computational and communication devices - sensors. The sensor is a charge size of 2.5 cm³. Sensors HR, RR, and spatial position are connected via both digital and analog connectors. Power sensor carried by a small battery. Sensors are used only for the collection, primary processing and transmission of sensor data. The main functional processing of the data collected by sensors is carried out on site, which is a fairly powerful computer, called a microcontroller. In order to process the data, they must be obtained for this antenna is equipped with a coordinator.

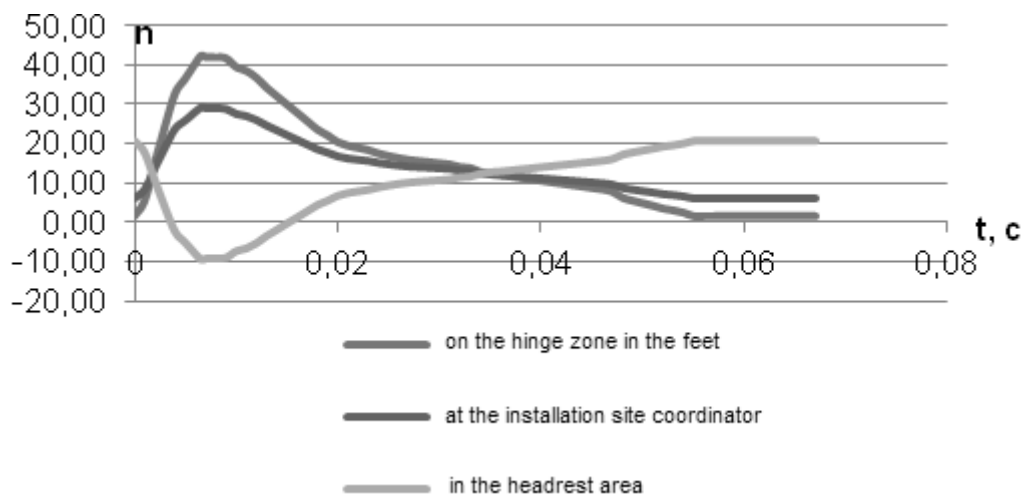
The microcontroller does not receive information from each sensor. The sensors can communicate with each other information with transceivers operating at radio frequencies. Firstly, sensory information is read by the sensors, and secondly, the information on the status of devices and the results of the data transfer process. The information is transferred from one sensor to another chain, and eventually coming to the controller sensors shed it all the accumulated information. If part of the sensor fails, the work of the sensor network after reconfiguration, which is automatically set to continue.

Functional diagram of the node WSN "Salvation":



Over-allocation schedule with a hinged seat suspension

One of the factors that influence the work of WNS are overloads. We know that you are using at the moment of medical monitoring devices do not support the transfer of medical signal in their effects. Calculations show that the WNS may sustain overload, but the functionality of full-scale tests are needed. To successfully test the system developed a mathematical decision-making under uncertainty of the event.





Findings

For the first time become possible diagnostics of the astronaut at the time of activation of the emergency rescue, continuously transmitted in the centers of flight data to help coordinate the work of resuscitation correctly, which leaves a chance for the preservation of life and health of astronauts. Tracking the spatial position and its visualization, helps to coordinate the work of rescue services, thereby to produce the right amount of capsule evacuation from the LES.

Conclusion

Davydova Elizaveta, +7 (963) 961-93-96, elizaveta_2710@mail.ru.

Literature

1. Mathematics methods and equipment applied for medical and physiological control and support system for groups of people involved into extremely dangerous technological processes, ISTIC Scientific Advisory Committee, London, UK, 2008, pp. 106-130.
2. Elements of medical and biological safety of the crew manned transport spacecraft of new generation in preparation for launch, Innovations in aviation and aerospace, Moscow, Russia, 2012.
3. Issues of safety of the crew in preparation for launch, taking into account the "human factor", Innovations in aviation and aerospace, Moscow, Russia, 2011.

INVESTIGATION OF USAGE POSSIBILITIES OF A MEAN VALUE ENGINE MODEL IN SIMULATION OF IC ENGINE INTAKE SYSTEM FAULTS

N.Nikolić¹, T. Torović¹, Ž. Antonić¹, and J. Dorić¹

¹ Faculty of Technical Sciences, Trg Dositeja Obradovića 6, 21000 Novi Sad, Serbia

Keywords: IC engine, model, fault, simulation

Abstract. Due to ever stringent requirements of environmental legislation, on-board diagnosis of automotive internal combustion engines is becoming increasingly important. It is estimated that up to 50% of the engine management system is dedicated to the diagnosis at the present time. One of big problems in the development of internal combustion engine diagnostics is a necessity to intentionally cause malfunctions on the engine during its operation, and then explore how these can be detected and identified using the diagnostic system. It is clear that such a research is very expensive and impractical, so it would be very convenient if all this could be done without destroying engine components. The solution is a fault simulation with the help of a mathematical model of the entire engine or the engine subsystem concerned. In this paper the focus is on the intake system of internal combustion engines and malfunctions that can occur in this system. A well-known mean value engine model (MVEM) is used to simulate possible faults in the intake system of an engine. To achieve this, some components of the model are rebuilt and adapted to the new purpose of the model. This is illustrated by a few examples showing the simulation results of some malfunctions that can occur in the intake system, compared with the no-fault state.

Introduction

Mean value engine model (MVEM) is a mathematical model that is simpler than large cycle simulation models but more complicated than transfer function based models of IC engines [1]. It predicts time development of mean values of some important engine variables such as engine speed, intake pressure, intake temperature etc. The essence of a mean value engine modeling is to isolate a dominant physical influence in an engine or a subsystem of the engine, and not to describe all the details of engine operation.

Possibility to describe dynamic behaviour of an engine, relative simplicity and quite good accuracy of mean value engine models enable the models to be incorporated in engine control microprocessors. In addition to MVEMs application in design and analysis of engine control systems, there is a great potential in their application in development of engine diagnostics systems.

In the 80's of the last century some researchers [2,3,4] developed the engine models that could be classified as *mean value engine models* although that term had not yet existed at that time. In addition to these pioneering models, describing engine in its entirety, a number of mean value models was created, considering not an engine as a whole, but the subsystems dealing with fuel and air flow dynamics in the engine [4,5,6]. However, the term *mean value engine model* was introduced by Hendricks [7] in 1989. Later on, the originally developed model was upgraded and improved [8,9,10] and finally got its generic form [11].

The Hendricks' generic mean value engine model was utilized here to explore the possibility of its application in an initial phase of engine diagnostics system development. The aim is to modify the existing Hendricks' model in such a way that some faults appearing in an engine intake system could be simulated by means of it.

In the first section of the paper, the Hendricks' mean value engine model was presented briefly. The second section describes some intake system faults that are not easy detectable. The third section contains the description of the modified Hendricks' mean value engine model and the way the fault simulations are performed. The simulation results are given in the fourth section and the conclusion in the last one.

The Hendricks' Mean Value Engine Model

The Hendricks' mean value engine model consists of three important subsystems describing: fuel mass flow, intake manifold filling dynamics and crankshaft acceleration. For the model application, it is very important that the only input variable is the throttle angle, and the output variables are the intake manifold pressure and temperature and the engine speed. Detailed derivation of the model with the submodels can be found in [8,9,10], so only the most important equations are given here.

Fuel Flow/Evaporation Dynamic Submodel

The dynamics of fuel flow in intake ports of spark ignition engines was investigated at the Danish Technical University and it was found that it can be successfully described by the equations:

$$\ddot{m}_{ff} = \frac{1}{\tau_f} (-\dot{m}_{ff} + X_f \dot{m}_{fi}) \quad (1)$$

$$\ddot{m}_{fv} = (1 - X_f) \dot{m}_{fi} \quad (1a)$$

$$\ddot{m}_f = \dot{m}_{fv} + \dot{m}_{ff} \quad (1b)$$

where: \dot{m}_{fi} is the injected fuel mass flow, \dot{m}_f is the engine port fuel mass flow, \dot{m}_{ff} is the fuel film mass flow, \dot{m}_{fv} is the fuel vapor mass flow, τ_f is the fuel evaporation time constant and X_f is the proportion of injected fuel deposited on intake manifold.

Intake Manifold Filling Dynamics

The intake manifold filling dynamics submodel is based on an assumption that the process is adiabatic and that the ideal gas law is valid. It is also assumed that the intake manifold temperature is accurately (instantaneously) known. The submodel is composed of two equations describing the time development of the intake manifold pressure and temperature. Both equations are derived from the energy conservation law. The pressure time development equation has the form:

$$\dot{p}_i = \frac{\kappa R}{V_i} (\dot{m}_{at} T_a + \dot{m}_{EGR} T_{EGR} - \dot{m}_{ap} T_i), \quad (2)$$

where p_i is the manifold absolute pressure, \dot{m}_{at} is the air mass flow past throttle plate, \dot{m}_{ap} is the air mass flow into intake port, \dot{m}_{EGR} is the EGR mass flow, T_i is the intake manifold temperature, V_i is the overall manifold and port passages volume, R is the gas constant and κ is the ratio of the specific heats. The temperature time development equation can be written as follows:

$$\dot{T}_i = \frac{RT_i}{p_i V_i} [\dot{m}_{at} (\kappa T_a - T_i) + \dot{m}_{EGR} (\kappa T_{EGR} - T_i) - \dot{m}_{ap} (\kappa - 1) T_i]. \quad (3)$$

Crankshaft Speed State Equation

The final submodel of the mean value engine model describes the crankshaft dynamics. It is derived using conservation of rotational energy on the crankshaft and can be expressed as:

$$\dot{n} = -\frac{1}{I n} (P_f(p_i, n) + P_p(p_i, n) + P_b(n)) + \frac{1}{I n} H_u \eta_i(p_i, n, \lambda) \dot{m}_f(t - \Delta \tau_d), \quad (4)$$

where I is the scaled moment of inertia of the engine and its load, P_f is the friction power, P_p is the pumping power, P_b is the load power, H_u is the fuel lower heating value, η_i is the indicated efficiency, λ is the excess air factor and $\Delta \tau_d$ is the mean injection/torque time delay.

On Some Faults in Engine Intake System

Intake system of an IC engine contains many components and sensors, the faults of which can lead to deterioration of the engine performance and, if not detected in time, to more serious problems. Some of hardly detectable intake system faults with possible negative consequences are considered here: air leakage in the intake manifold, inaccurate reading of the pressure sensor, inaccurate reading of the temperature sensor and the EGR valve stuck up.

Intake manifold air leakage can cause negative consequences, especially in an engine with the air flow meter. If there is an orifice allowing the air to flow in or flow out from the intake manifold, the air flow meter will send the wrong air flow data to the electronic control unit (ECU). Therefore, the air-fuel ratio will deviate from the desired one, causing deterioration of the exhaust emission. Besides, misfiring can appear due to too lean or too rich mixture, decreasing the engine power output and the driveability of the vehicle.

Inaccurate reading of an intake manifold temperature sensor can be caused by the dirt at the sensor tip or the ageing of the sensor. The result may be a lean or rich fuel mixture that causes drivability symptoms such as poor idle quality when cold, stumble on cold acceleration, and surging when the engine is warm.

Intake manifold pressure sensor sends the information on the engine load to the ECU. The ECU uses this information to adjust ignition timing and fuel enrichment. However, sensor ageing, dirty and clogged hoses between the sensor and the intake manifold can cause inaccurate reading of the sensor. This can result in poorer fuel economy, higher air pollution and higher risk of engine knock.

As far as the EGR valve concerned, it should be closed when the engine is idling and stay closed until the engine is warmed up. The EGR valve should also be closed when the engine is operating at wide open throttle. When the engine is warmed up and is operating in a wide range of medium loads, the EGR valve should be open, in general. As long as the EGR valve is operating properly, it does not affect the engine performance noticeably. But, if it gets stuck for dirt or for any other reason and can not close/open completely, some problems can occur in the engine operation including engine knock, rough idling or even engine stalling, hard starting, higher levels of NOx and even HC emission.

Simulation of Faults Using Modified Hendricks' Model

Simulations of IC engine faults considerably facilitate research in the field of diagnostics since causing the real malfunctions is quite expensive. In addition, such experiments are also time consuming. Previously described Hendricks' mean value engine model, with certain modifications, could serve as a basis for residual generation. A residual is a signal that responds to an inconsistency between a faulty process and the same process without faults. When no faults exist, the residual should be close to zero and when a fault appears the residual should be noticeably different from zero, if it is sensitive to that specific fault.

The faults, mentioned in the previous section, can be simulated using modified Hendricks' mean value engine model in a way described below.

Intake manifold air leakage is simulated by introducing a new variable, \dot{m}_{leak} , representing the air mass flow through the leakage orifice. This flow can be modeled as a flow of an ideal incompressible gas through an aperture [12], with satisfactory accuracy for the purpose of fault simulation. Mathematically, it is expressed as follows:

$$\dot{m}_{leak} = \mu A \sqrt{2\rho(p_i - p_a)}, \quad (5)$$

where μ is the discharge coefficient for the aperture, A is the cross-sectional area of the orifice, ρ is the air density and p_a is the atmospheric pressure.

Further, the fault, when the EGR valve is stuck in a position preventing the EGR flow to be that large as calculated by ECU, is simulated by a coefficient k_{EGR} multiplying the EGR mass flow \dot{m}_{EGR} . Taking this into account, and applying the energy and mass conservation laws, Eqs. (2) and (3) become:

$$\dot{p}_i = \frac{\kappa R}{V_i} \left(\dot{m}_{at} T_a + k_{EGR} \dot{m}_{EGR} T_{EGR} - \dot{m}_{ap} T_i + \dot{m}_{leak} T_a \right) \quad (6)$$

$$\dot{T}_i = \frac{RT_i}{\rho_i V_i} \left[\dot{m}_{at} (\kappa T_a - T_i) + k_{EGR} \dot{m}_{EGR} (\kappa T_{EGR} - T_i) - \dot{m}_{ap} (\kappa - 1) T_i + \dot{m}_{leak} (\kappa T_a - T_i) \right]. \quad (7)$$

In Eqs. (6) and (7) the variable \dot{m}_{leak} is with a positive sign since the Hendricks' model is derived for a naturally aspirated engine, meaning that the pressure inside the intake manifold is lower than the pressure outside. Therefore, the leak air flow direction will always be from the outside into the intake manifold. By implementing Eqs. (5), (6) and (7) in the original Matlab/Simulink Hendricks' MVEM, a new, modified model has been obtained, the most important parts of which are shown in Figs. 1 and 2.

Similarly, intake manifold pressure and temperature sensors faults are simulated using the values k_p i k_T . By introducing the coefficients k_p i k_T , simulation of different fault intensities is made possible. Values of the coefficients k_p i k_T that are higher than 1 denote the high reading of the corresponding sensor, and the values less than 1, denote the low reading of the sensor, compared to the real values of the pressure/temperature.

Using this model, a large number of variants of the aforementioned faults can be simulated. These are various intensities of various faults, at different throttle angles, in stationary and in transient regimes. However, for brevity, only few examples are shown here to illustrate the application of the modified Hendricks' model.

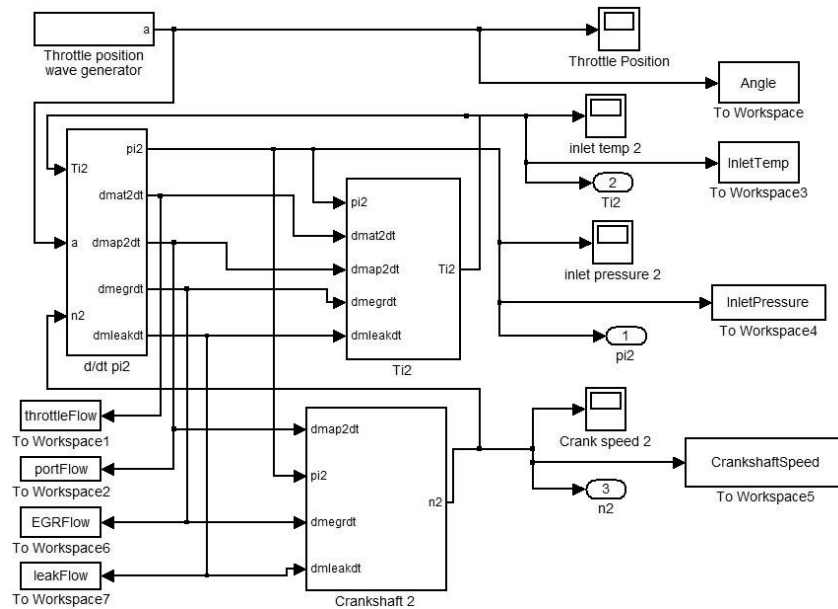


Fig. 1. The upper level of the fault simulation model

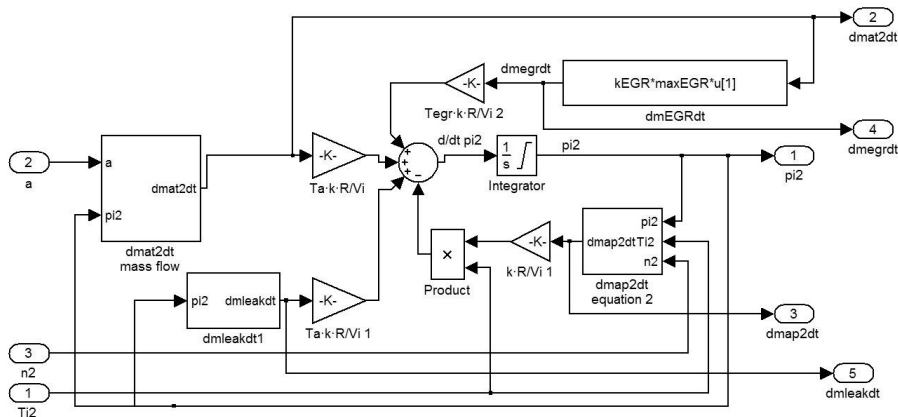


Fig. 2. The submodel for the intake manifold pressure calculation

Simulation Results

Simulations of several faults are shown here, with stationary and transient regimes applied. The load change is represented in the form of the time dependency of the throttle angle α during 12 seconds, which was the duration time of each simulation. Such a change of throttle angle has been chosen to include stationary engine operation as well as fast tip-in and tip-outs (Fig. 3a). The time dependencies of the intake manifold pressure, the engine speed and the intake manifold temperature in the course of the simulations are given in Fig. 3b, 3c and 3d, respectively. Each diagram shows the variables in the no-fault case and in all the fault cases considered. The simulations are performed for medium loads with the EGR active, which are the most frequent regimes during the engine lifetime.

The figure clearly shows that the simulation results can be used in identification of the faults considered. This is because each fault causes at least one of the considered engine variables to differ noticeably in comparison with the no-fault case.

For example, in Fig. 3b it is seen that the intake manifold air leakage decreases the engine speed. Moreover, the larger the leakage orifice the lower the engine speed, which completely coincides with real engine operation. In contrast to the engine speed, the intake pressure is increased at the same time (Fig. 3c). This is natural since a new air flows into the manifold. The air flowing through the leakage orifice reduces the proportion of the recirculated exhaust gases in the intake manifold thus lowering the intake temperature (Fig. 3d).

Further, reduced EGR flow due to the EGR valve stuck up lowers the intake pressure and temperature (Fig. 3b and 3d, respectively) and increases the engine speed (Fig. 3c). Lower intake pressure is due to the decrease of the overall gas flow through the intake manifold and the intake temperature drop is caused by smaller proportion of the EGR flow in the overall intake manifold gas flow. The engine speed increases owing to the higher quality of cylinder charge.

Simulations of inaccurate pressure and temperature sensor readings are clearly visible in Fig. 3b and 3d, respectively.

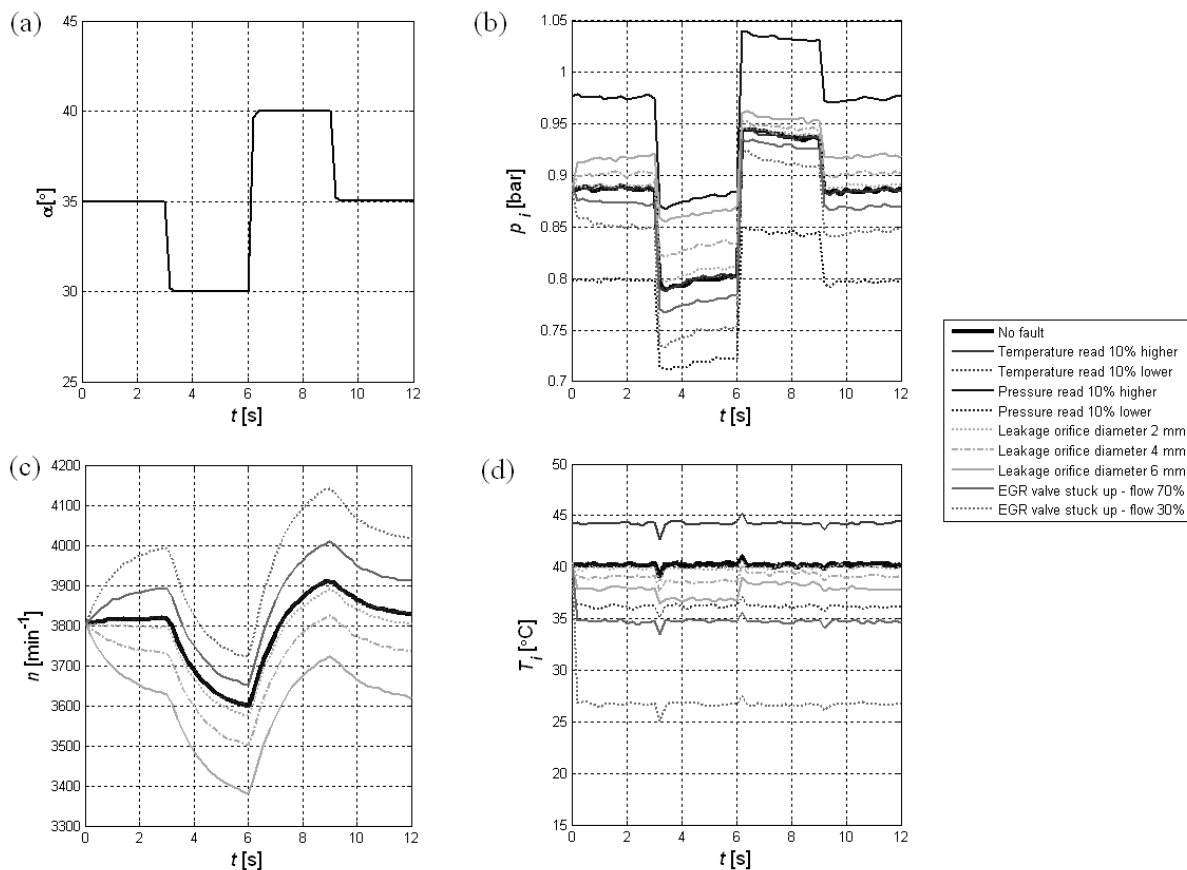


Fig. 3. Engine variables during simulations: (a) Throttle angle, (b) Intake pressure, (c) Engine speed, (d) Intake temperature.

Conclusion

To simulate faults in a system, it is necessary to have a good enough model describing the behaviour of the system. It is shown here that there are quite good possibilities to simulate a number of intake system faults by utilizing a modified Hendricks' mean value engine model. In this way, approximate values of some important engine variables are predicted when the engine operates with a fault. Various sorts and intensities of faults are possible to simulate, which is very important in the development of engine diagnostics systems. Great savings are thus achieved in technical and human resources since the need for expensive and time consuming experiments is reduced.

References

- [1] R. Rajamani: *Vehicle Dynamics and Control*, (Springer, New York, 2012).
- [2] J. D. Dobner: A Mathematical Engine Model for Development of Dynamic Engine Control, *SAE Technical Paper No. 800054*, (1980).
- [3] J. J. Moskwa: *Automotive Engine Modelling for Real Time Control*, Ph.D. Thesis, Dept. of Mechanical Engineering, MIT, (1988).
- [4] H. Wu, C. F. Aquino, and G.L. Chou: A 1.6 Liter Engine and Intake Manifold Dynamic Model, *ASME Paper No. 83-WA/DSC-39*, (1983).



-
- [5] C. F. Aquino: Transient A/F Control Characteristics of the 5 Liter Central Fuel Injection Engine, *SAE Technical Paper* No. 810494, 1981.
 - [6] D. J. Boam, I. C. Finlay and G. S. Fairhead: The optimization of fuel enrichment patterns with throttle body injection, *Proceedings of the Institution of Mechanical Engineers, Part D: Journal of Automobile Engineering*, 202 (1988), pp. 9-20.
 - [7] I. C. Finlay, D. J. Boam and J. J. G. Martins: A Model for Predicting Engine Torque Response during Rapid Throttle Transients in Port-Injected Spark-Ignition Engines, *SAE Technical Paper* No. 890565, (1989).
 - [8] E. Hendricks and S. C. Sorenson: Mean Value Modelling of Spark Ignition Engines, *SAE Paper* No. 900616, (1990).
 - [9] E. Hendricks, A. Chevalier, M. Jensen, S. C. Sorenson, J. Asik and D. Trumpy: Modelling of the Intake Manifold Filling Dynamics, *SAE Technical Paper* No. 960037, (1996).
 - [10] E. Hendricks, T. Vesterholm, P. Kaidantzis, P.B. Rasmussen and M. Jensen: Nonlinear Transient Fuel Film Compensation, *SAE Technical Paper* No. 930767, (1993).
 - [11] E. Hendricks, D. Engler and M. Fam: A Generic Mean Value Engine Model for Spark Ignition Engines, *Proceedings on 41st Simulation Conference, SIMS 2000*, Lyngby, Denmark, September 18-19, (2000).
 - [12] F. M. White: *Fluid Mechanics*, 4th Edition, (McGraw-Hill, New York, 2001).



International Conference on Innovative Technologies, IN-TECH 2012,
Rijeka, 26. - 28.09.2012



SIMULATION SOFTWARE FOR MODELLING AND SIMULATION EMERGENCY EVENTS

L. Jurikova ¹, J. Rak ²,

¹ Tomas Bata University in Zlín, Faculty of Applied Informatics, Nad Stráněmi 4511, 760 05 Zlín, Czech Republic, ljurikova@fai.utb.cz

² Tomas Bata University in Zlín, Faculty of Applied Informatics, Nad Stráněmi 4511, 760 05 Zlín, Czech Republic, jrak@fai.utb.cz

Keywords: Chemical substances, extraordinary and emergency situations, modelling, simulation, analysis, filtered ventilation.

Abstract. This contribution focuses on dangerous chemical substances, mainly from the perspective of possible leakages and extraordinary or emergency situations. It identifies the chosen chemical substances in defined areas, especially in factories handling these substances where there is a risk of leakage to the atmosphere causing danger to the population in the neighbourhood. The article describes the specific types of dangerous chemical substances, including their analysis together with an analysis of their influence on humans, both in the short and long term. Another part of the contribution deals with the analysis of suitable software for the simulation of the spread of the dangerous chemical substances. The simulation predicts the spread of these substances from the place of origin to the contaminated areas where persons are sheltered in the improvised shelters, equipped with a filtered ventilation unit. These shelters are to be reviewed from the perspective of their segmentation, their distance from the location of the incident, their construction together with building materials and weather conditions, etc. A further objective of the article is to highlight the existing filtered ventilation in the shelters. For the modelling and simulation of airflow there exist various kinds of software which differ in extent, time requirements, applicability during a design process, relations to the law, norms, customs as well as in processing the results. The analysis is to be focused on software that enables modelling of airflow, transport of contaminants, indoor air distribution, distribution of temperature and humidity and other factors. The objective of this analysis is to choose the most suitable software to be applied to the specific simulation of the emergency situation including the leakage of dangerous chemical substances.

Introduction

The research is, in particular, focused on the population protection (PP) by sheltering. It points out extraordinary or emergency situation (ExS or EmS) and risks related to them. This contribution describes possible risks originating from these situations, mainly when it relates to the leakage of dangerous chemical substances (DCS). Within the outlined area of the region the areas at risk and specifically plants handling DCS have been mapped because there is a potential risk of leakage of these substances and where the ExS or EmS could arise. The objective of this contribution is to outline a procedure for dealing with the leakage of these substances employing modelling and simulation software. In other words, this contribution aims to select the most suitable software for the simulation of the leakage of chemical substances.

The risk of ExS or EmS occurrence in the chosen area

By the chosen area is meant the Zlín region; the areas at risk are depicted in the Fig. 1. In the Zlín region there are lots of companies (entrepreneurs) handling DCS; nevertheless, for this research 3 of the closest areas to the town of Zlín have been chosen. These areas are located in the town of Otrokovice. One of the main reasons for this choice is the research of the PP in the town of Zlín.

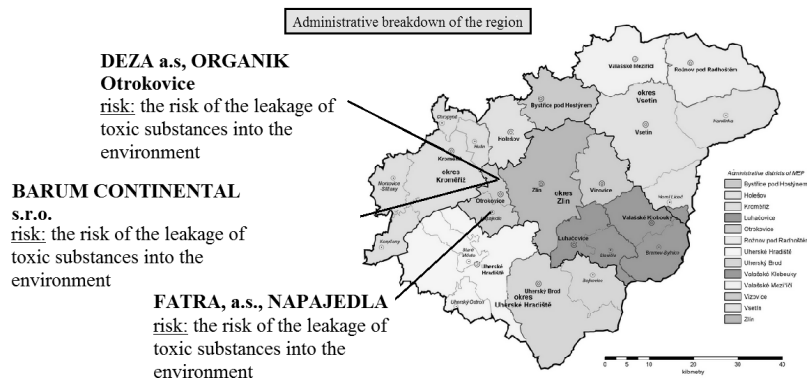


Fig. 1 The chosen areas of possible DCS leakage [7]

Chemical accident

A chemical accident is an extraordinary, partly or wholly uncontrollable, time and space-bounded event. It is, for instance, serious leakage, fire or explosion, that emerged or whose emergence is imminent in connection with the use of an object or facility in which the dangerous substance is produced, processed, used, transported or stored. A chemical accident is such an event that results in serious exposure to danger or seriously impacts lives and the health of people, livestock and the environment, or when it causes damage to property. A chemical accident can occur during road or train accidents but it is most often in the vicinity of a chemical plant. Prevention and observing the laws plays a crucial role in the field of PP.

Risk of chemical substances in the given area

Toxicity – a significant term related to chemical substances – the ability of substances, given by their physical and chemical characteristics, to harm organisms. Within the chosen area there are factories that handle various substances, such as phenol, cresol, phthalanhydride, benzene, fluorinated hydrocarbons, and other DCS. Any of these substances can escape into the air during an accident and adversely affect not only the environment but also humans.

The analysis of chemical substances and their effects on humans

The above mentioned chemicals, such as phenol, cresol and benzene are highly flammable, toxic, corrosive and harmful. For instance, phenol is commonly found in nature; it is a substance contained in leaves of plants that serves as a protection against browsing by herbivores. In the industry it is produced by partial oxidation of benzene or during the oxidation of coal. Nevertheless, thanks to its antiseptic effects it is used in the health service and it is further used in production of pharmaceuticals and in cosmetics for suntan creams, hair dyes or skin whitening products.

However, chemical substances have negative effects on the human body. For instance, phenol is corrosive and it quickly absorbs into the body in various ways. High concentrations of phenols may affect the ability of blood to transport oxygen, which causes headache and nausea while legs and lips turn blue. It can lead to difficulties in breathing, collapse and death. Repeated exposures can cause liver, kidney and central nervous system damage. Moreover, phenols have mutagenic effects and can also cause erratic heartbeat (cardiac arrhythmia). The previously mentioned chemicals have irreversible negative effects on the human body; therefore, it is necessary to be aware of the spread of these substances if it comes to their leakage. It is possible to simulate the spread of DCS from the place of the accident or their penetration into the shelter using the following software. [6]

Modelling and simulation software in the field of PP

The software listed in the Table 1 represents a part of the chosen simulation and modelling software to be tested for emergency or extraordinary situations. Above all, the research is focused on the simulation of contaminants, especially the chemical substances and their spread from the place of accident to the shelter. As evident from the table, the software CONTAM and AUTODESK SIMULATION have been tested. Out of these two softwares, AUTODESK proves to be more suitable. By means of this software the simulation of airflow in the shelter with certain parameters was made.

Table 1 Description of the simulation software to be used in the field of PP (T/U - tested/untested)

Tool	Description of capabilities of the tool	T/U
AIRPAK	Modelling of the airflow, transport of contaminants, air distribution in a room, distribution of temperature and humidity, thermal comfort and CFD	U
COMIS	Multi-zone airflow, transport of contaminants	U
CONTAM	Analysis of the airflow, ventilation, concentration of contaminants, indoor air quality, multi-zone analysis, regulation	T
PHOENICS	CFD, contaminants in the air, including smoke; airflow	U
AUTODESK SIMULATION	Nonlinear static and dynamic analyses; it simulates rigid and flexible body motions, and fluid flow (including fluid dynamics), hydrostatic pressure; it further calculates combined voltage, electrostatics and it also combines analyses with multiphysical simulations	T
ANSYS	Nonlinear, multiphysical software including structural and thermodynamic analysis, continuum flow analysis, analysis of electrostatic and electromagnetic fields and acoustic analyses	U
SOLIDWORKS FLOW SIMULATION	SolidWorks Flow Simulation takes the complexity out of computational fluid dynamics to quickly and easily simulate fluid flow, heat transfer, and fluid forces critical to a design.	U

Program Autodesk Simulation

The application Autodesk Simulation CFD (Computational Fluid Dynamics) analyses and simulates the behaviour of a product at an early stage of design. It employs the method of "computational fluid dynamics". This advanced computational method generally simulates the fluid flow and heat transfer inside or around a digital prototype by means of mathematical laws. It offers a range of advanced functions, various models of heat transfer, laminar and turbulent flows, networking, calculations and the presentation of results.

Autodesk Simulation software accomplishes nonlinear static and dynamic analyses, simulates rigid and flexible body motions, and fluid flow (including fluid dynamics) and hydrostatic pressure; it further calculates combined voltage, electrostatics and it also combines analyses with multiphysical simulations. [1]

An example of simulation using Autodesk Simulation software

By means of the Autodesk Simulation software the airflow in the imaginary shelter has been tested, based on chosen parameters. The following figures depict the simulation of the air flow inside the imaginary shelter with clearly defined parameters. The imaginary shelter created for the purposes of simulation is a building with 5 sections and without window openings in the basement of the building. Every section is equipped with an air inlet unit. In the back of the building there is an air outlet system. The possible inadequate performance of the computer had to be taken into consideration when creating a construction design of the imaginary shelter. Selected parameters for simulation:

- Input temperature of air = 19°C;
- Output temperature of air = 22°C;
- Velocity normal = 35km/h;
- Standard Velocity Magnitude = cca 20000m/s;
- Rotation = 3580 per/min.

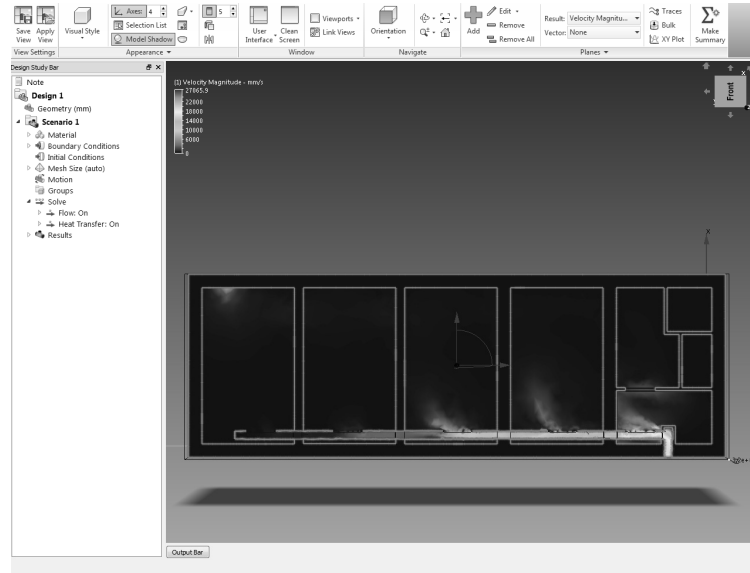


Fig. 2 The design of the imaginary shelter transferred into Autodesk Simulation CFD (depicting the time period of the air flow velocity into the interior of the shelter; the values of the air flow velocity ranged from ones to tens of m/s).

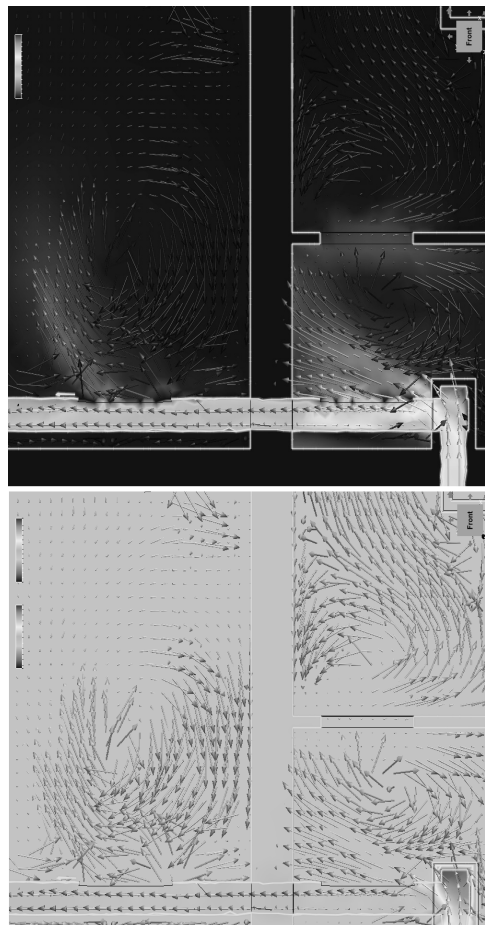


Fig.3 Vector air flow from the inlet of the shelter; the upper figure depicts the velocity of the air flow, the

bottom one depicts the air flow under dynamic pressure in the shelter.

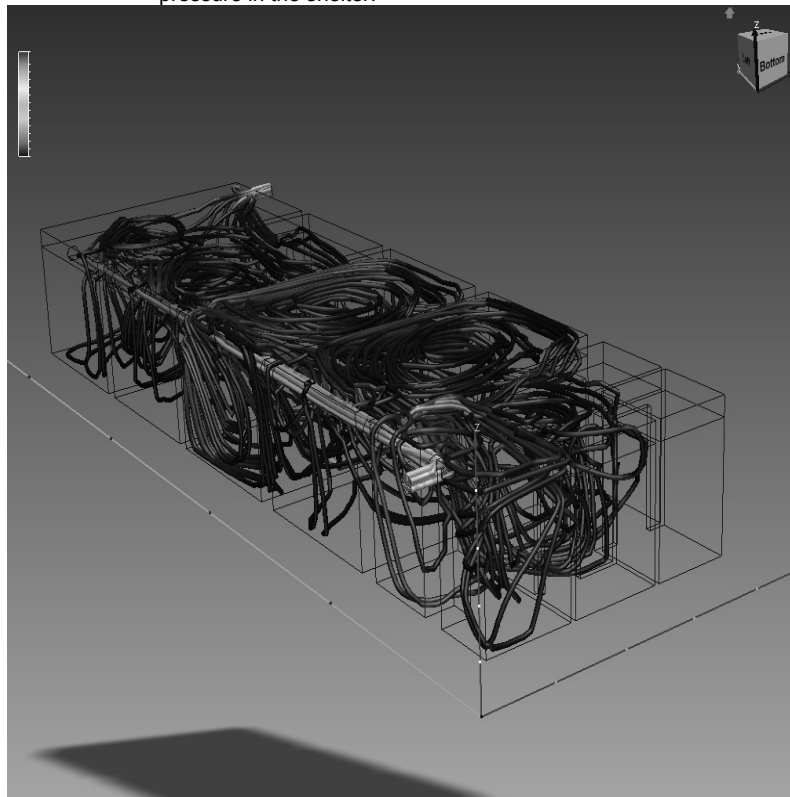


Fig. 4 The view of the simulated flow in the improvised shelter (yellow streamlines indicate the direction of air into the inlet and into the outlet in the back part; the yellow colour of flow indicates a higher velocity of air on entry into ventilation, while the blue colour shows direction and velocity of the air flow in individual sections).

Conclusion

The aim of the contribution is to point out software that proves to be the most suitable in the field of population protection by sheltering. Through careful analysis the most suitable software for extraordinary or emergency situations will be chosen. These situations include, for instance, chemical accidents during which residents of the place of origin of the accident are particularly at risk. The result of the research is to be the creation of a simulation model, which is to define the spread of DCS from the place of accident to premises where people are sheltered. This model will then enable competent personnel to act more efficiently in extraordinary situations and at the same time it will provide a visualization of the DCS spread, e.g. during chemical accidents.

Acknowledgment

This article has been supported by grant of IGA University of Thomas Bata in Zlin, Faculty of Applied informatics, number IGA/FAI/2012/054, IGA/FAI/2012/028 and by the European Regional Development Fund under the project CEBIA-Tech No. CZ.1.05/2.1.00/03.0089.

References

- [1] Autodesk: *Autodesk Simulation CFD*, Copyright 2012 Autodesk, online: 27.06.2012, <http://usa.autodesk.com/adsk/servlet/pc/index?id=17141897&siteID=123112>
- [2] Fořt P., Kletečka J., Autodesk Inventor: Functional design in industrial practice, Brno: Computer Press, 2007, 318 p., ISBN 978-80-251-1773-6.
- [3] Jurikova, L., Rak, J. Proposal for technology of improvised shelters design in conditions of the Czech republic, *Annals of DAAAM for 2010 & Proceedings of the 21 st International DAAAM Symposium*, Austria - Vienna: DAAAM International 2010., 1337 p., ISBN 978-3-901509-73-5.
- [4] Jurikova L., Rak J., Adamek M., Suggestion of improvised shelter design, *13th WSEAS International Conference on AUTOMATIC*, Canary Islands, Spain, 2011. ISBN: 978-1-61804-004.
- [5] L. Jurikova, J. Rak, M. Adamek, The Population Protection by Sheltering – A Design of the Chosen Shelters under the Auspices of a Municipality, *NAUN: International Journal of Mathematical models and methods in applied Sciences*, www.naun.org, 2011, p. 1380-1387. ISSN: 1998-0140.
- [6] Matoušek J., Linhart P., CBRN: Chemical weapons, Ostrava: Association fire and security of engineering, 2005, 151 p., ISBN 80-86634-71-X.
- [7] *Statistical yearbook of region Zlin: Czech statistical authority*, 2012, online: 22.06.2012, <http://www.zlin.cz/so/csu/2010edicniplan.nsf/krajkapitola/721011-10-2010-30>.



SCHEMES FOR THE CONSERVATION OF STAINED GLASS IN THE PALACES AND HERITAGE BUILDINGS

M. Ismail¹

¹ Maher Ibrahim Mohamed Ismail, Associate Professor, Department of Glass, Faculty of Applied Arts, Helwan University, Egypt.

Keywords: Conservation, Stained Glass, Heritage Buildings.

Abstract. The world has many heritage buildings such as mosques, temples, and cathedrals, containing many works of art including the teachings and religious stories. These works have appeared in cathedrals since the beginning of the ninth century AD. They call for communicating between the teachings and stories of religious and human beings, after that painters excelled in painting fictional religious on glass windows of churches in the Renaissance.

Introduction

Egypt has many churches, palaces and heritage installations that contain a variety of stained glass which should be preserved from damaging environmental hazards and human behavior. It is necessary to coordinate efforts by specialists and officials and to exchange experiences for the conservation and restoration of this cultural heritage.

Research problem: the lack of maintenance and preservation to all buildings and palaces, unconscious behaviors of governments and individuals as using these buildings as administrative institutions which considered as art works.

Objectives

Preservation of these palaces and buildings of damaging factors and the unjust human behavior. There are many heritage buildings in Egypt, such as the cathedrals and palaces, which contain many works of art reflect the Religious beliefs in a lot of drawings and paintings.

Research importance

There is no diversity in drawing and painting topics including the mural painting, Frescoes and the stained glass on the windows, which was affect the environment, drawing and painting in Churches Architecture.

The topics Aims to further enrich the knowledge of visitors to that churches, so teachings religious that should be followed by topics of religious pictures on the walls and windows.

The period between the fifth century and the fifteenth in Europe (middle Ages) was a period of dark ages, it was a separation between Classical and Renaissance prosperous, when the civilization and the arts returned to prosperity again.

Section Headings

Distinguish those periods beginning of the fifth century until the period of modern art into three main periods which represent the basic features of the disparities in the art of drawing and painting through the ages as follows:

- The old period: it was the middle Ages from the 5 century to 15 century.
- The intermediate period: it was the Renaissance from the beginning of the 15 century to the late of 19 century.
- The modern period: the beginning of modern art in the early twentieth century.

Characteristics of art's works in each period:

- **The old period:**
 1. Focus on issues of religion and belief
 2. Caring for portraying Christ and the Virgin Mary and the saints as, and sometimes as subjects religious Emperors
 3. Flatness in terms of image looks two-dimensional and the dimension of realism was the people seem to be rigid, and devoid of life.
 4. The main techniques used and the raw materials: Painting, Frescoes, Icons, Mosaic and stained glass.
- **Phase of the Renaissance:** The most important characteristic of drawing and painting:
 1. Focus on the element of movement in the painting.
 2. Highlight the emotions and feelings in human subjects of religious and life.
 3. The Paintings was like the architectural work by divided it into spaces, mass and lines in the relations of aesthetic.
 4. Highlight the third dimension in the paintings and shows that through excellence in detail and demonstrate the use of perspective in painting as well as show the opposite relationship between shadow and light
 5. Expression of the artist and his own vision as well as the freedom to choose the subject of work.
- **The modern period:** After the French Revolution in 1898, through the art schools:
 1. The New Classics: featuring the court lines and dark colors with a focus on issues free of emotions.
 2. The Romance: drawing and painting subjects with an exaggerated drama to highlight the movement, the violence and brutality to gain access to the excitement of full.
 3. The Realism: deal with the problems of the poor and the oppressed and their subjects were characterized by building an arbitrator in terms of composition and distribution of the blocks and the rhythm of the line.

4. The Influential: focused on the color spaces with the neglect of the line to register a sense of visual snap to light and use the theories of analysis the lights and use of its components in the effects to the re-emergence of light compound in a natural way with the effects of rapid brush and opposite of colors manner coherent to look like the paintings more elegant and beautiful.
5. Abstract: It is the modern arts more linked with the architecture of Churches because its properties were consistent with spirit of the times, and there are two directions in the abstract: Abstract expressionism, Abstract geometric.

The historical study of the pattern of imaging in the churches in Egypt is characterized by the following:

- All subjects reflect on the art is subject to the environmental effects of the environment, which is an apt description of the life of Egyptian art, which makes it popular.
- The topics away from the representation of graphics and idolatry, and to return to the human self rather than the glorification of the gods and rulers.
- The symbolism topics and lack of attention to detail with non-compliance the scales of Humanitarian standards.

The methods of implementing the works of art:

1. Frescoes: a method of painting on plaster colors, mixed with water or egg whites installed with a layer of wax or glue.
2. Icons: an extension of the method Frescoes but on a small piece of wood.
3. Drawing and painting on wood and cloth
4. Mosaic
5. Stained glass: Windows consists of stained glass and painted.

Figure 1 shows the most important topics of art:

1. Escape to Egypt, the gospel, the resurrection, Christ's entry, Jerusalem and Last Supper
2. Drawing the saints and angels, monks on the icons in particular
3. Topics of interest in daily life and character of the comic spirit of fun
4. Topics related to traditions of Egyptian funerary old such as the Fayoum's Faces.



Fig. 1 The most important topics of art

Steps to the conservation of stained glass:

1. Register and characterization of the case of the stained glass.
2. Stages of examination and study of the glass panels.
3. Stages of restoration the stained glass.

Table 1. Schemes for the Conservation of Stained Glass

Installation	Conservation	restoration	Work Drawings	Design
Handling	Strengthening	Implementation	Scale 1:1	Model of the fillings
Carrying	Protection	Cut glass	Details of Charges	
fitting		The application of coatings	Cutting lines	
		Leading up	Colors of stained	
		Finishing		
The manifestations of deterioration				
Buckling	Curves	Sagging	Loading	Cracking
-----%	-----%	-----%	-----%	-----%
				Corrosion
				missing
				-----%

Table 1 contains the data sets serve as a basis to carefully selected samples is used to apply the schemes for the conservation the stained glass works in the palaces and heritage buildings to analyses the effect of different preprocessing techniques is studied as well.

Samples of the manifestations of deterioration the Palaces in Egypt:

Figure 2 shows the first model: Palace of "Ismail Pasha Muhammad" at Zamalik in Cairo.

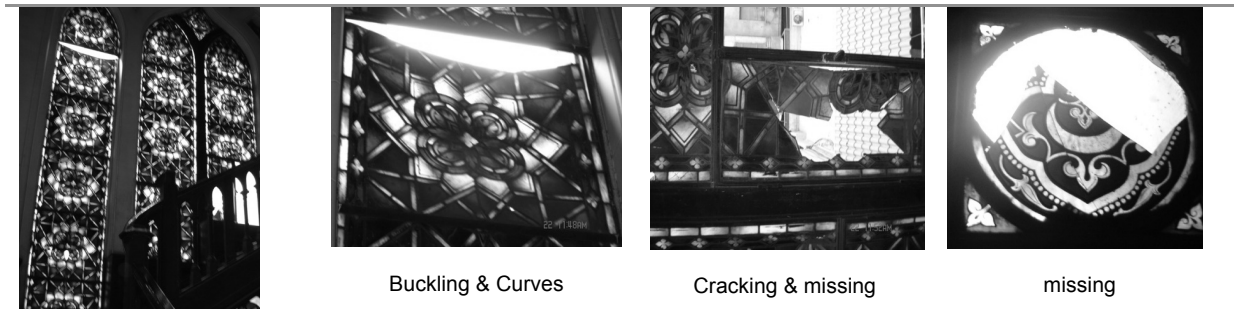


Fig. 2 Stained Glass Palace of "Ismail Pasha Muhammad"

Figure 3 shows the second model: Palace of "Habib Basha" Al- Sakakini in Cairo.

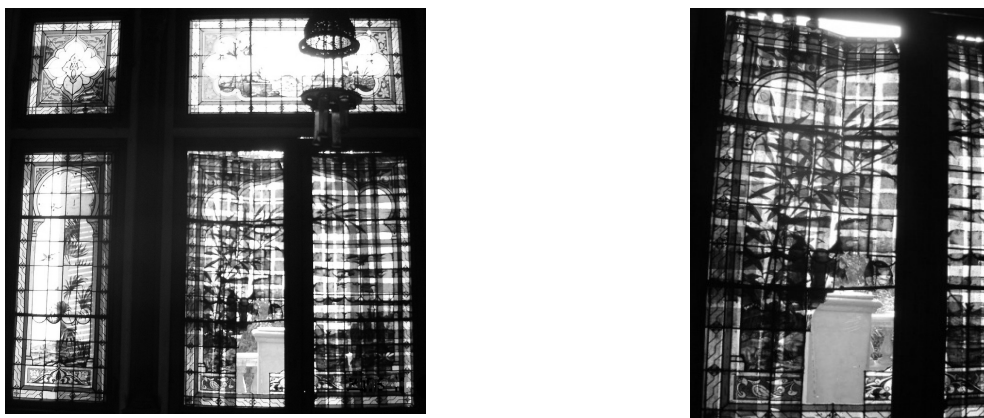


Fig. 3 Cracking, missing, Buckling and Curves in Palace of "Habib Basha"

Table 2 show analytical scheme for the conservation of stained glass

N o		the schemes for the conservation	Palace of "Ismail Pasha Muhammad"
1	Description of the artwork	Consists of three architectural openings separated by commas stone as well as the presence of four small upper openings complementary to the architectural form of contracts for architectural. The panes show divided into parts using metal of iron. -The right pane is divided into three horizontal parts, and ends with a small moving window. -The middle pane is divided into 4 parts horizontal, and the bottom is a window moving. -The right pane is divided into 6 horizontal parts, and all parts of fixed.	
2	Artistic style & Technique	The work belongs to the decorative architectural style, so the pieces of glass divided to geometric shapes. The method depended on the colors of the glass with little use of glass coatings and colors.	
3	The Storyboard	Decorative and geometric	
4	The Composition	The art work divided to geometric shapes almost equal parts.	
5	The Shape	Contains several geometric elements square, rectangle, triangle, half-circles, rhombus and some elements of plants	
6	Colors	Use black color to layout, glass paints and pigments and silver stain.	
7	Metal design	It was simple so as not to affect the work of art, but show its details.	
8	glass Kinds	colored glass (red, yellow, orange, light green & dark -green bluish, violet light and dark, dark & light blue, white transparent...	
9	materials	- Metal of iron and lead a variety of sectors starting from ¼ inch to 3 / 16 inch. - Tin was used for welding by 60% of lead. - Wood bars to install glass units in the sector Metal of iron.	
10	Description & Percentage of damage	Cracking, buckling and sagging in most of the glass panels. - The right pane shows buckling, bending and the lower part is missing. The proportion of damage 40% . -The middle pane shows buckling and contraction and detachment of the glass. The proportion of damage 30%. - The right pane shows separation from metal of iron implemented to 10 cm, while the third part of the curved and dented the top of the outside. The penultimate section shows some pieces missing.	
11	Causes damage	The artwork area was divided into specific parts, making them the ability to resist environmental factors, but the damage was the result of the behavior of a human has to break a small part of it and the loss of large areas completely as a result of the lack of necessary maintenance and failure to maintain it.	
12	The requirements of conservation	The best ways to save this work is to put part of the transparent glass out of the slot architecture of a protective effect of various environmental factors.	

Table 3 show analytical scheme for the conservation of stained glass

the schemes for the conservation		Palace of " Habib Basha" Al- Sakakini"
Description of the artwork	The door is 3 parts (right - Middle - left) surmounted by a fixed 3 slots, and doors from the inside is divided into 3 parts horizontal sector of iron 2 mm.	
Artistic style & Technique	The art work belongs to the academic school of photography in the Renaissance, where the doors and vents used of stained glass and photography, with the transfer and the simulation of nature by use of some elements of decoration and marked by the multiplicity of color realism.	
The Storyboard	Decorative Photo	
The Composition	Division of perspective and divided the space to the line of the earth and the sky.	
The Shape	Show elements such as trees, palms, hills, water, plants and birds of the sky background. As well as the presence of the three pyramids and Sphinx, with the use of some floral, geometric, mosques and houses.	
Colors	- Black color to determine the plant motifs and shadows. - Multiple layers of light brown to dark, green from light to dark, turquoise, violet, light yellow and orange.	
Metal design	Three slots are divided horizontally into three parts, while the upper stator is divided into three parts vertically to highlight the aesthetics of the artwork.	
glass Kinds	Stained glass transparent light blue, Turquoise blue, pale blue, translucent white, red orange, violet light, and light green.	
materials	Iron metal rods of 2 cm, and sectors of lead $\frac{1}{4} \frac{3}{16} \frac{3}{8}$ inches, as well as the tin is used for welding process and the percentage of lead 60%. The panels of wood to fixed glass units in the steel sector.	
Description & Percentage of damage	Break some parts of the work and missing of other parts, sagging and bulging, with some cracks and separation of parts of the glass for the lead. The proportion of damage 40%	
Causes damage	The artwork is divided into parts within the borders to endure various environmental factors, but the damage occurs as a result of a human behavior that cause cracking and the missing of parts of the artwork because the doors moving.	
The requirements of conservation	The best ways to save the upper part of work is to put part of the transparent glass out of the slot architecture of a protective effect of various environmental factors. For moving doors must to strengthen saddle bar of iron that separates the component parts of the glass units to withstand the vertical pressure, and prevent sagging and buckling the artwork. Use toothpaste with the flexibility and high hardness is not affected by environment factors to work on strengthening the cohesion of lead and glass.	

Recommendations

Egypt has many churches, palaces and heritage installations that contain a variety of stained glass which should be preserved from damaging environmental hazards and human behavior. It is necessary to coordinate efforts by specialists and officials and to exchange experiences for the conservation and restoration of this cultural heritage.

The best ways to save the artwork is to put part of the transparent glass in the front of it for protective from effect of various environmental factors.

References

- [1] Albinas Elskus, "The Art of Painting on Glass Techniques and Designs for Stained Glass", (1980).
- [2] Roy Newton, Sandra Davison, "Conservation of Glass" (1989).
- [3] Shirin Ahsan Shirzad, "Principles of Art and Architecture" National Library, Baghdad, (1985).
- [4] Nemat Ismail Allam, "Arts West in the Middle Ages and the Renaissance and Baroque" Dar El-Maraf, Egypt, (1982).
- [5] Dr. Mohamed Abdel-Hadi Mohammed, "the principles and the restoration and maintenance of monuments non-organic" renaissance of the Middle Library, Cairo, (1996).

CFD AND THERMAL ANALYSES APPLICATION AT REFLOW OVEN DESIGN IMPROVEMENTS BASED ON VIRTUAL PROTOTYPING TECHNIQUES

G. Todorov¹, I. Dobrev² and K. Kamberov³

¹ Laboratory "CAD/CAM/CAE in Industry", MTF, Technical University - Sofia,
8 "Kl. Ohridski" Blvd., Sofia, BULGARIA

² Laboratoire de Mécanique des Fluides, Ecole Nationale Supérieure d'Arts et Métiers,
151, boulevard de l'Hôpital, 75013 Paris, FRANCE

³ Laboratory "CAD/CAM/CAE in Industry", MTF, Technical University - Sofia,
8 "Kl. Ohridski" Blvd., Sofia, BULGARIA

Keywords: Virtual Prototyping, CFD, Thermal, Analysis

Abstract. The presented paper aims to show the possibilities for modeling in detail the thermo fluid behavior of a complex technological module using contemporary numerical techniques. Application of virtual prototype techniques allows to explore in detail the nature of ongoing physical processes. This enables to evaluate various technology and design parameters and to improve product's overall performance. The subject of current survey is a particular heating convection module – an important component of thermal equipment – oven for microelectronics surface mounted device operations. The extremely high requirements about the thermal parameters of the equipment – dynamic profile and homogeneity of heating – definitively need to apply simulations in order to evaluate its parameters and to improve them. Two main groups of parameters are explored and quantified – fluid flow (velocities, pressures) and thermal (temperature distributions over time). Design modifications are examined as to reach better product performance. This industrially applied case is a good illustration of the possibilities for time shortening to market and money-saving by high technologies application.

Introduction

Current situation at world global market requires to go for application of high technologies or reaching low affordable production price. Industrial production and services globalisation, the complex of technical and commercial operations, the need for customised and sustainable products and the increased importance of managing knowledge assets make the use of high-level product development tools an imperative for companies. More and more small and medium enterprises (SMEs) are searching for and using such tools to develop their products. This process is growing with the development of Virtual Prototyping (VP) technology. Virtual Prototyping has emerged as a significant enabler for cost effective management of complex products over their lifecycle. The VPs, or digital mock-up (DMA), usually is defined as a computer simulation of a physical product that can be presented, analyzed and tested from concerned life-cycle aspects such as design/engineering, manufacturing, service, and recycling as if on a real physical model. It also include possibilities for simulating and visualizing its 3D motion behavior under real-world operating conditions, and refining/optimizing the design through iterative design studies prior to building the first physical prototype. [1, 2, 3]

This study specific focus is set on reflow oven as a product which is developed very dynamically and is influenced by the globalisation of the world market. As a part of the microelectronics technology line, which performs the soldering process between the Printed Circuit Board (PCB) and placed over it components, reflow oven has a lot of requirements for its output parameters. During the reflow phase the temperature is risen to melt the solder paste alloy and then form the solder joints. The most commonly used reflow oven today is the forced convection type. Hot air is forced into the processing chamber through a high number of holes or nozzles (impinging jets) and onto the PCBs passing on the conveyor system. The air then heats the PCBs. Although air is a relatively poor heat transfer media, the benefit of this type of system is that the delta T measured on a PCB is quite low. Heating ability, which is fundamental to the performance of reflow ovens can be estimated by the accuracy with which it conforms to the required temperature profile. [4, 5]

Conventional ovens are more or less well studied and developed as design and parameters. The major problem rises for specific equipment, where additional study is required as to prevent failures at late development stage. Virtual Prototyping and especially – application of thermal and Computational Fluid Dynamics (CFD) techniques – are very suitable for such cases. Additional complexity comes from the need of simulating time-dependent thermo-fluid process. This complexity is because of the bi-directional connection between the fluid flow parameters as velocities and pressures and the thermal coefficients as convection coefficients.

Studied problem description

The design of the second section of reflow oven is examined at the stage of its design development to improve its parameters – homogeneity (+/-3°C temperature difference) and – highest heating velocity. The design of the convection module and treated product are shown on figure 1 below. The processed product major parameters are included in table 1. Two rows of six components are placed on single carrier. 70 carriers are processed at one module at once (or 840 products at same time). This convection module process a closed volume of fluid, which recirculates thanks to the positioned on the top turbine. It drives the fluid in horizontal direction and the guiding channel turns the direction down and redistributes the flow by deflectors to a plate with impinging jets on it. These jets are blowing between the rows of carriers. The fluid is heated by resistance, placed at the entry of the turbine, which compensates the energy transferred to the carriers.

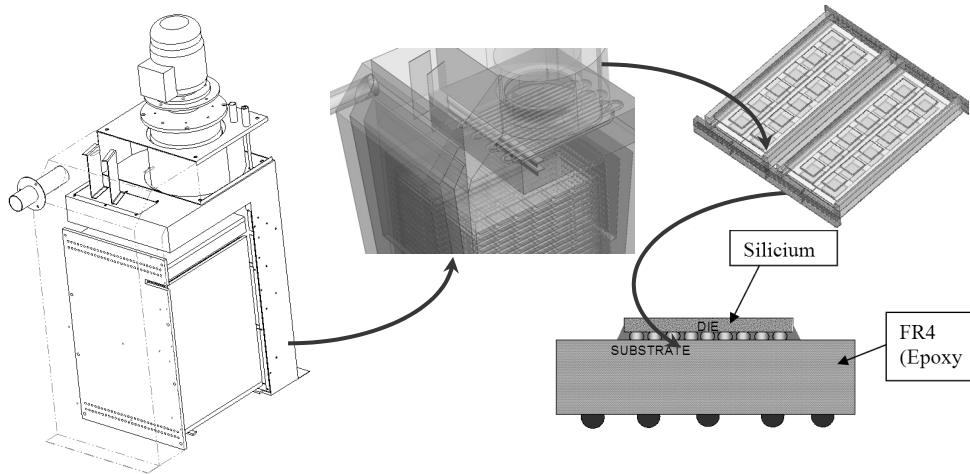


Fig. 1 Examined convection module and processed product

Table 1. Title of the Table used for Exemplification

Product/Carrier Information	Target
Packages/platform covered	FCPGA
Substrate Outline Dimension	35x 35 mm
Metal Carrier Dimension (width x length x height)	150x323x10 mm (5.9x12.7x0.4 in)
Metal Carrier Weight (fully loaded)	1.8 lbs
Parts per Metal Carrier	12

Developed simulation model. Methodology

The thermal CFD model is built according to the design geometry files. Supplied models are geometrically simplified by removing some details that do not have influence upon the work process – geometry clean-up. The built geometric model contains the entire fluid zone as solid including the plates on the entry and on the exit as separate volumes. A mesh model is generated that contains about elements and nodes – enough detailed mesh for the analysis. The CFD numerical model is shown on fig.2. This figure also shows the applied boundary conditions on the simulation model. They represent a standard work cycle for the examined equipment: initially, inside fluid (air) is heated at 175°C and the entering carriers are at preheated temperature of 140°C. Processing time is 700sec. Turbine characteristics are aluminum for the impinging jets plates, structural steel for the deflectors and casings.

Examined physics nature is complex, because the fluid parameters are influenced by the temperature and vice versa. Transient process is highly nonlinear, additionally influenced by temperature dependent material and fluid properties. These preconditions require proper methodology for performance optimisation to be carried out. Thus, two steps are introduced, separating the problematics in more simple tasks:

- ◆ examining and optimising fluid flow parameters by a steady-state modelisation;
- ◆ transient thermal analysis for heating exploration and possible optimisation.

Main optimisation process will be performed in the first step, as to improve fluid flow parameters, especially in order to reach homogeneous feed at each carrier. Transient thermal analysis will be used mainly to study the results of performed design optimisations on the previous step, and, to perform slight changes if it is required.

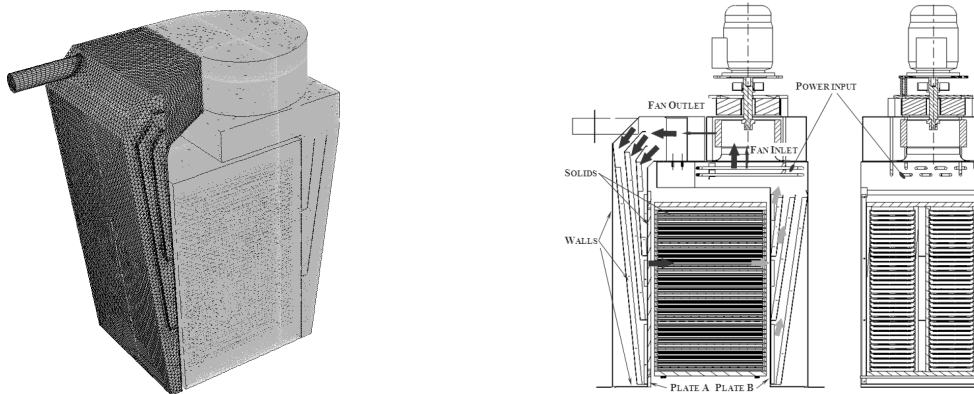


Fig. 2 Generated simulation model and applied boundary conditions

Fluid flow parameters optimisation

Prepared simulation CFD model is solved under uniform temperature of 175°C, starting with initial design geometry. Several results are shown on figure 3 below – a section, parallel to the feeding impinging jets plate (to review the homogeneity at the entrance inside the rack), and, perpendicular section through the fan axis (showing again the nature of fluid feeding). It is well seen that there are a gradient between the separate vertical areas of the carriers, caused by the “shadow” of the angled deflectors.

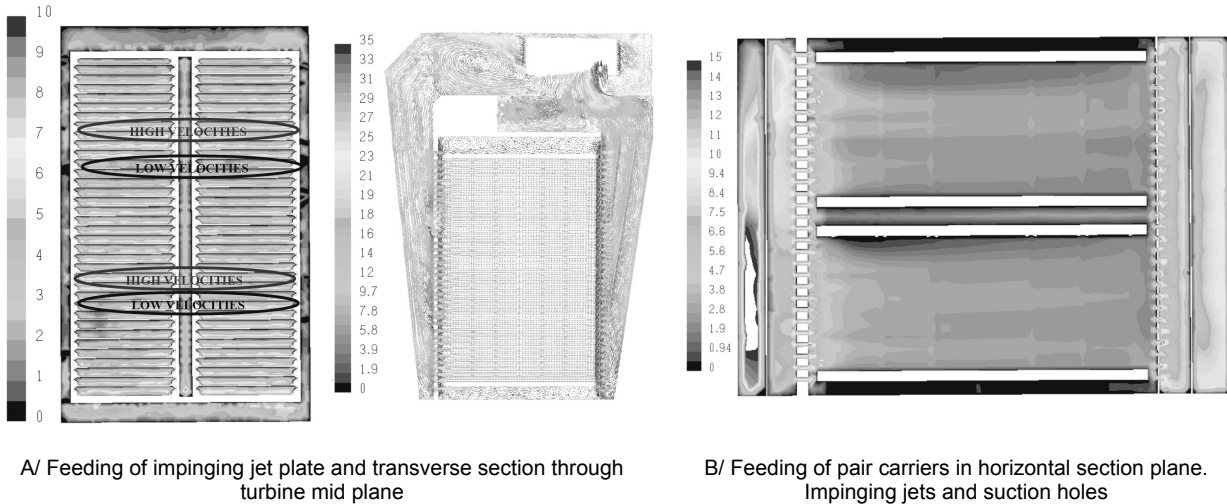


Fig. 3

The highest velocities are on the lowest placed carrier on each subsection of the channels and the maximal velocity difference, if compare for longitudinal PCB areas, is about 3 m/s. Average velocity value for a carrier section is 2.7 m/s, while the maximum mean value is 3.8 m/s (as it is marked by HIGHEST VELOCITIES on fig.3 A/) and the minimum mean value is 1.5 m/s (for zones marked as LOW VELOCITIES). The section in transverse direction shows zones of recirculation, just after the turbine exit and, zones of high velocities (losses) at its entrance. The poor uniformity of outgoing flow leads also to uneven feeding in horizontal plane section, which is illustrated on figure 3 B/ as well. The source of this poor uniformity is recognized at the turbine exit chamber. The number of the nozzles, diameter and their placement are not of great importance for the fluid flow through the rack as it is, because the flow is parallel.

Review of the results shows two main problematic design zones:

- ◆ Turbine exit chamber deflectors are ineffective;
- ◆ Vertical deflectors for feeding impinging jets plate are not optimal.

Thus, four modified design models are examined to explore and optimise these problematic design zones:

- ◆ **Variant A:** enlarged and relocated deflectors near the turbine;
- ◆ **Variant B:** removed deflectors near the turbine;
- ◆ **Variant C:** initial deflectors near the turbine and removed horizontal parts of the vertical deflectors in “outlet to plate” zone.
- ◆ **Variant D:** initial deflectors near the turbine and removed at half horizontal parts of the vertical deflectors in “outlet to plate” zone.

Part of results are presented on the figure 4 below to illustrate the output parameters for examined variants – in a horizontal section through the mid turbine plane for its exit chamber. Results analysis shows several conclusions. The best results are for the variant WITHOUT DEFLECTORS (variant B). In fact, asymmetric placement of the turbine and the included SPIRAL CAMERA does not need deflectors. The flow is partially uniform, but with big gradient of the velocity between the upper rows of holes on the impinging jets plate and the lower. The optimised design is developed with removed deflectors near the turbine and shortened horizontal parts of the vertical deflectors.

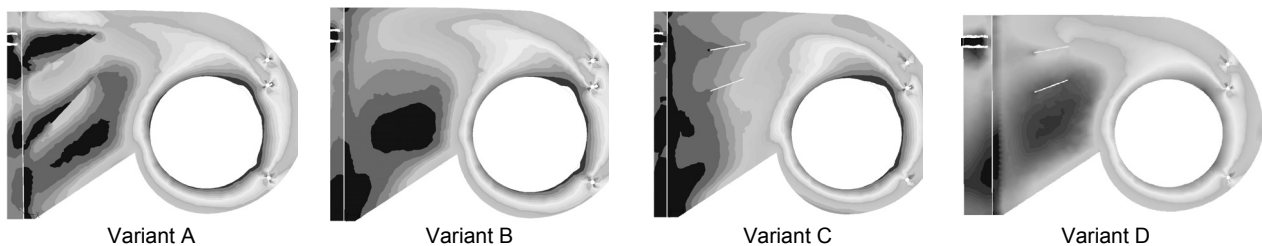


Fig. 4 Horizontal plane section for the turbine exit chamber

Transient thermal CFD analysis

The entire model is analyzed under unsteady, transient thermal CFD solution. The entire rack of carriers is patched at 140°C, presuming uniform heated products. The results are initially illustrated by temperature fields on a half carrier over time on figure 5 below. The scale is common for better understanding. It is seen that the products are unevenly heated, which is predefined by the design

conception. The main question is whether all the six components reach temperature uniformity at the end of the process. The volume average temperature for each separate product, as a function of time, is shown on figure 6, together with the change of the maximal temperature difference for the components in time.

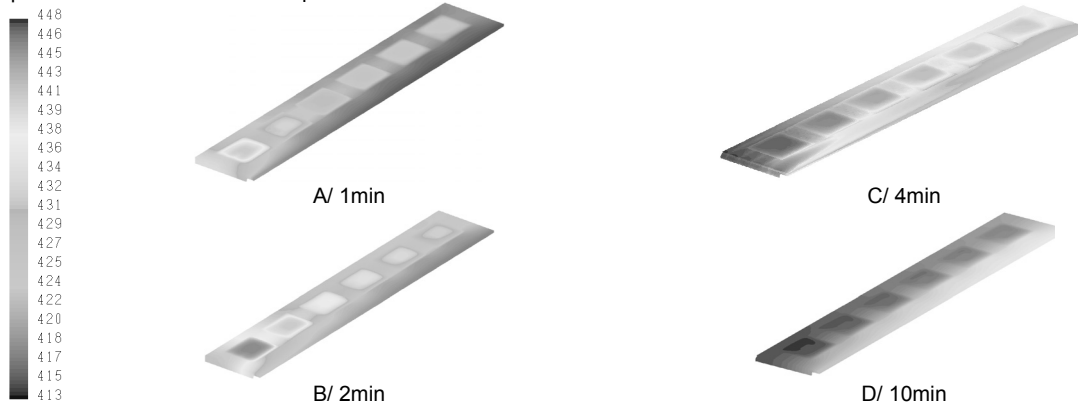


Fig. 5 Temperature distributions over a half carrier at different heating times

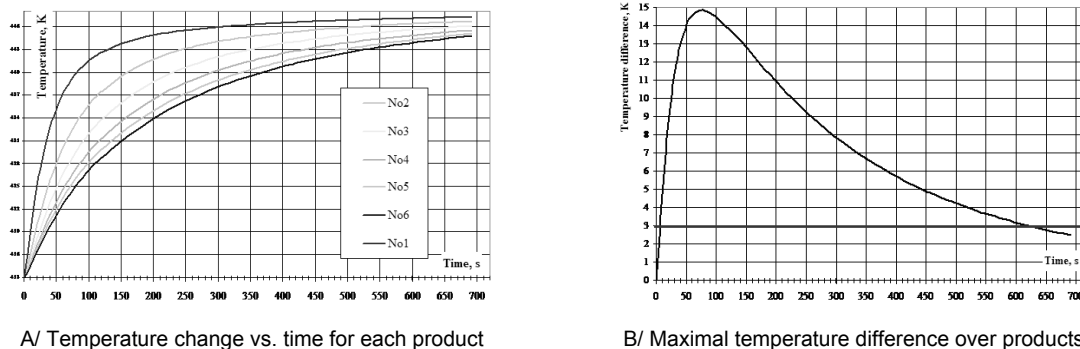


Fig. 6 Temperature volume averaged profiles over time

The maximal temperature difference between the first and the last products is reached out at the 76 sec after the heating is started and its value is of 14,8°C. This is due to the type of the fluid stream which one is “ a stream in a channel”. During its way, the fluid transmits thermal energy to the front components and loses its initial temperature and the maximal velocity values near the components’ surfaces decrease. This causes the first component to be heated rapidly, while the last one – relatively slow. After reaching the maximal difference between the 1 and last components, the difference decrease slow. The maximal temperature difference (between component No 1 and component No 6) decreases less than 3°C at 10min heating time, which corresponds to the main requirement for uniform heating. The process heating speed in beginning is not more then 0.7°C/s, which is an acceptable value as well.

Conclusion

Several general conclusions could be formed, based on performed fluid optimisation and next transient thermal CFD analysis:

- ◆ The CFD analysis results show that the general geometry shape and parameters are well designed – i.e. gives relatively good velocity distribution – the mean velocity fields for section varies from 1,5 – 3.8 m/s;
- ◆ Optimised design is achieved, based on removed turbine exit deflectors and shortened horizontal deflectors which is a good basis for subsequent temperature uniformity (predefines good distribution via heated components in process cameras);
- ◆ Output products are heated uniformly, with max temperature difference under required 3 °C – for the predefined total process time for the examined chamber;
- ◆ Thus, an improved design is obtained at the early stage of its development, based on virtual prototyping technology implementation. Major advantage for applying computational techniques is the ability to review in detail various parameters (velocity of the fluid flow, pressure, distributions) of the ongoing physical processes and to perform corrective actions;
- ◆ This approach requires powerful computational resources and knowledge database, but results in effective evaluation and improvement of the design at the early stage which gives an important advantage on the global market.

Acknowledgment

This research study is performed by the support of project DUNK-01/03 “University Scientific and Research Complex” of National Science Fund, Ministry of Education, Youth and Science, Bulgaria.

References

- [1] I. Horvath: Collaborative Virtual Prototyping Environments – a big soup of new technologies?, *Computer-based Design: Engineering Design Conference* (2002), pp.134-141.
- [2] M.M.Tseng, J.Jiao, Ch.Su: Virtual Prototyping for Customized Product Development, *Integrated Manufacturing Systems*, vol. 9, no. 6 (1998), pp.334-343.
- [3] A. Connel: The Rise and Rise of Virtual Prototyping, *Time-Compression Technologies*, Vol.12, (2004), Issue 3, pp.44-49.



International Conference on Innovative Technologies, IN-TECH 2012,
Rijeka, 26. - 28.09.2012



-
- [4] M.Yamane, N.Orita, K.Miyazaki, W.Zhou: Development of New Model Reflow Oven for Lead-Free Soldering, *Furukawa Review*, No26 (2004), pp.31-36.
- [5] E.Iwasaki, K.Nakao, Development of High-Speed Pb-Free Reflow Ovens, *Furukawa Review*, No27(2005), pp.40-46.



International Conference on Innovative Technologies, IN-TECH 2012,
Rijeka, 26. - 28.09.2012



VALIDATING DOMAIN-SPECIFIC PROPERTIES WITH GRAPH TRANSFORMATIONS

László Lengyel¹ and Hassan Charaf¹

¹ Budapest University of Technology and Economics, Hungary
{lengyel, hassan}@aut.bme.hu

Keywords: Verification and validation of graph transformation, Graph rewriting, Domain-specific properties.

Abstract. The two key points in application development are evergreen: make the development as effective as possible and provide high quality software artifacts. Model-driven approaches address both of these issues. With the increasing need of reliable systems, the verification and validation of model transformation-based approaches becomes an emerging research field. Verification/validation means determining the correctness of a model transformation in the sense that the output models of the transformation satisfy certain conditions. We assume Domain-Specific Modeling Languages (DSMLs) as input and output languages and concentrate on graph rewriting-based model transformations. Based on the current capabilities of the model transformation approaches and tools, in this paper, we compile and investigate some open issues that are verification/validation-related challenges of the next years: (i) Verification/validation of global properties, (ii) Supporting the verification/validation of domain-specific properties and behavior, (iii) High-level languages/methods to define verification/validation properties, and (iv) Industrial applicability of the existing verification/validation approaches. We believe that providing solutions for these issues will significantly improve the usability and availability of model transformation-based approaches.

Introduction

Model transformations are important in software engineering for a number of applications, such as transforming artifacts from a source domain to a different target domain, code generation, consistency checking, and refactoring. With model transformation being more widely applied, ensuring properties such as syntactic and semantic correctness, equivalence, termination, and global determinism of model transformations becomes an important issue for the software engineer designing transformations.

The verification/validation (V&V) of a model transformation is the process of checking that the transformation definition meets specifications and that it fulfills its intended purpose. Based on [1], we use the following definitions. *Verification* is the process of evaluating transformation definition to determine whether the transformation fulfills the imposed specification. *Validation* is the process of evaluating transformation during or at the end of the transformation execution to determine whether it satisfies the end-user requirements. In other words, validation is intended to answer the question "Is this the system that we are supposed to develop from the user's point of view?", i.e., is the product specified according to the user's actual needs? Verification is about to answer the question "Is the system in accordance with the design?", i.e., does the product conform to the specifications?

During the analysis of a transformation, our goal is to prove that certain properties hold for the output model if the input model is valid, or to provide the criteria that need to be satisfied by the input model to guarantee the desired properties for the output models. The analysis of a transformation is said to be *static* when the implementation of the transformation and the language definition of the input and output models are used during the analysis process, but we do not take concrete input models into account. In the case of *dynamic* approach, we analyze the transformation for a specific input model, and then we check whether certain properties hold for the output model during or after the successful application of the transformation. The static technique is the more general and poses the more complex challenges. The goal of the static analysis is to determine if the transformation itself meets some requirements.

Developing systems using models and model transformations facilitates their formal analysis and validation. In general, if we write program code only to describe a piece of software, V&V are a more complex challenge, and sometimes they are completely impossible.

In our context, model transformations are specified by graph transformations [2] that provide a powerful specification formalism combining a visual appearance with a formal semantics and facilities for V&V. In this paper, we introduce some open issues that are verification/validation-related challenges. We concentrate on the verification/validation of domain-specific properties and behavior.

Contribution

It is crucial to realize that not only software artifacts, e.g. models or source code, but model transformations themselves can be erroneous. Therefore, we need solutions to make model transformations free of conceptual errors. Assume that we transform our system models into a formal domain with the goal to assess some important system properties (such as functional correctness, dependability or timeliness). We want model properties important for the assessment to be transformed correctly into the output domain. During the design of such a transformation and later during the application of this transformation we face the following questions. What ensures that the transformation process to the output domain is correct? What type of properties can a transformation preserve? The rest of this paper introduces domain-specific modeling and investigates different aspects of the previous questions, such as V&V of domain-specific model properties, or V&V of global properties.

Domain-specific modeling and model processing

Domain-specific languages (DSLs) provide a means for narrowing the communication gap between users and developers [3, 4]. The main benefits of domain-specific modeling (DSM): increase in productivity and quality as well as use of expertise to share the knowledge within the development team.

Throughout the history of software development, developers have always sought to improve productivity by improving abstraction. The new level of abstraction has then been automatically transformed to the earlier ones.

DSM raises the level of abstraction beyond current programming languages by specifying the solution directly using problem domain concepts. The final products are then generated from these high level specifications. This automation is possible because both the language and generators need fit the requirements of only one domain.

We define a domain as an area of interest to a particular development effort. Domains can be a horizontal, technical domain, such as persistency, user interface, communication, or transactions, or a vertical, functional, business domain, such as telecommunication, banking, robot control, insurance, or retail. In practice, each DSM solution focuses on even smaller domains because the narrower focus enables better possibilities for automation and they are also easier to define.

Developers generally differentiate between modeling and coding. Models are used for designing systems, understanding them better, specifying required functionality, and creating documentation. Code is then written to implement the designs. Debugging, testing, and maintenance are done on the code level. Quite often these two different representations are unnecessarily seen as being rather disconnected, although there are also different ways to connect code and models.

In model-driven development, we use models as the primary artifacts in the development process: we have source models instead of source code. As a result we raise the level of abstraction and hide complexity.

Truly model-driven development uses automated transformations in a manner similar to the way a pure coding approach uses compilers. Once models are created, target code can be generated and then compiled or interpreted for execution. From a modeler's perspective, generated code is complete and it does not need to be modified after generation. This means, however, that the knowhow is not just in the models but in the code generator and underlying framework. Otherwise, there would be no raise in the level of abstraction.

We have to realize that model-driven development is domain-specific: to raise the level of abstraction in model-driven development, both the modeling language and the generator need to be domain-specific, that is, restricted to developing only certain kinds of applications.

Focusing on a narrow area of interest makes it possible to map a language closer to the actual problem and makes full code generation available.

If we look at industrial cases and different application areas where models are used effectively as the primary development artifact, we recognize that the modeling languages applied were not general purpose but domain-specific. Some well-known examples are languages for user interface development and database design.

The following list summarizes the facts and suggestions of domain-specific modeling and model processing:

- i. Knowledge is not general, it is based on domains. → We have to develop and use domain-specific environments.
- ii. Each domain has its experts. → We have to provide domain-specific environments for experts and apply domain rules during the modeling.
- iii. Experts are usually not software developers. → We have to use the notation of the domain during modeling.
- iv. Information presentation is important. → We have to use intuitive (graphical) environments.
- v. Models are not the final product. → We have to generate applications, reports, etc. from models, that requires to apply domain-specific generators to improve efficiency.

Graph rewriting-based model transformation

Graph rewriting-based transformation is a widely used technique for model transformation [5]. Graph transformation has its roots in classical approaches to rewriting, such as Chomsky grammars and term rewriting [6]. Although, there are several representations, in essence, a rewriting rule is composed of a left-hand side (LHS) pattern and a right-hand side (RHS) pattern. Operationally, a graph transformation from a graph G to a graph H follows these main steps:

- i. Choose a rewriting rule.
- ii. Find an occurrence of the LHS in G satisfying the application conditions of the rule.
- iii. Finally, replace the subgraph matched in G by the RHS.

Rewriting rules can be made more relevant to software engineering models if the transformation specifications allow assigning validation constraints to the transformation rules.

An example transformation rule that generates database tables from UML classes is depicted in Fig. 1. Constraints propagated to the transformation rule nodes are also presented: *Cons_C1*, *Cons_C2*, *Cons_H1*, *Cons_T1*, and *Cons_T2*. With the help of these constraints, we can require the transformation rule to meet certain properties, and we can make them validated [7].

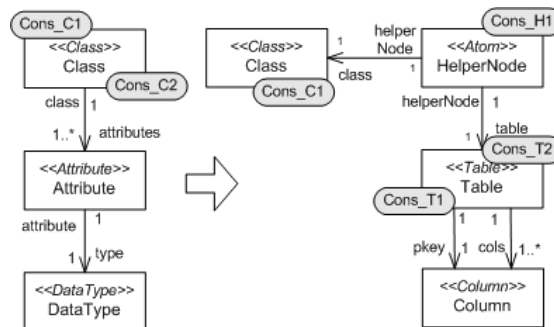


Fig. 1 Example transformation rule: *ClassToTable*

```
context Class inv NonAbstract:
not self.abstract
```

The constraint *NonAbstract* (*Cons_C1*), assigned to the node *Class* of the rule *ClassToTable*, is a precondition for the rule and requires the rule to process only non-abstract classes.

```
context Table inv PrimaryKey:
```

```
self.columns->exists(c | c.datatype = 'int' and c.is_primary_key)
```

The constraint *PrimaryKey (Cons_T1)* is a postcondition of the rule *ClassToTable*, it is assigned to the node *Table*. This constraint requires the rule that all created table has a primary key of type *int*.

```
context Atom inv ClassAttrsAndTableCols:  
self.class.attribute->forAll( self.table.column-> exists(c| (c.columnName = class.attribute.name))
```

The constraint *ClassAttrsAndTableCols (Cons_H1)* is propagated to the node *TableHelperNode*, it requires that each class attribute should have a created column with the same name in the resultant table.

The constraints assigned to the transformation rule guarantee our requirements. After a successful rule execution, the conditions hold and the output is valid. The fact that the successful execution of the rule guarantees the valid output cannot be achieved without these validation constraints.

Based on the current capabilities of the model transformation approaches and tools, we identified the following open issues as the V&V-related challenges of the next years.

Verification/validation of global properties

The scope of a V&V property can be local or global. One of the main limitations of the current model transformation approaches and tools is the local nature of their transformation rules. The local nature of a V&V property means that if we want to specify a constraint for an element, it must be included in the context of a transformation rule, or it must be referenced by a traversal expressions assigned to a rule element. Elements not appearing in a rule cannot be included in the V&V expressions. Therefore, this method does not provide an easy way to check constraints of global nature (e.g. deadlock examination). Of course there are numerous cases, for example, source code generation from statechart model, user interface generation from resource model, or projecting a source model into a different domain, where the whole right side is generated, thus, all the output model elements are included in transformation rules.

We need approaches that support the V&V of global properties in the processed models.

Supporting the verification/validation of domain-specific properties and behavior

Transformation methods should be provided that are able to verify/validate domain-specific properties with model transformations. These are output model-related requirements that model transformations should support. In several cases model transformation rules do not contain certain node or edge types that we are about to include into our V&V requirements. These requirements may relate to the temporary (during the model processing) or final (after the model processing) state of the processed or generated models. There are different directions that can be followed; e.g. we can state additional requirements against the input and output models (metamodel constraints), or the model transformations can be automatically extended with appropriate testing and validating transformation rules.

Dynamic model transformation validation covers the attribute value and interval validation. These properties can be expressed in first-order logic extended with traversing capabilities. Example languages currently applied for defining attribute value and interval conditions are Object Constraint Language (OCL) [8], C, Java, and Python.

Besides structural conditions, several approaches apply constraint languages to define the execution conditions and requirements related to the result. These conditions and requirements are pre- and postconditions of a transformation rule.

A *precondition* assigned to a transformation rule is a Boolean expression that must be true at the moment when the transformation rule is fired. A *postcondition* assigned to a transformation rule is a Boolean expression that must be true after the completion of a transformation rule. If a precondition of a transformation rule is not true, then the transformation rule fails without being fired. If a postcondition of a transformation rule is not true after the execution of the transformation rule, the transformation rule fails.

With pre- and postconditions the execution of a transformation rule is as follows:

- i. Finding the match according to the structure of the LHS.
- ii. Validating the constraints defined in LHS on the matched parts of the input model.
- iii. If a match satisfies the constraints (preconditions), then firing the transformation rule, otherwise the rule fails.
- iv. Validating the constraints defined in RHS on the modified/generated model. If the result of the transformation satisfies the postconditions, then the rule was successful, otherwise the rule fails.

A direct corollary is that an expression in LHS is a precondition to the transformation rule, and an expression in RHS is a postcondition to the transformation rule. A transformation rule can be fired if and only if all conditions enlisted in LHS are true. Also, if a transformation rule finished successfully, then all conditions enlisted in RHS must be true [7].

This method can be followed in Fig. 1. Finding the structural match the preconditions (*Cons_C* and *Cons_C2*) are validated, and after performing the rewriting postconditions (*Cons_C1*, *Cons_H1*, *Cons_T1*, and *Cons_T2*) are validated. Both of the validation should be successful in order to the whole transformation rule be successful.

With this method the required domain-specific properties can be defined on low-level, on the level of the transformation rules. A valid requirement is to support high-level constraints that are on the level of transformations, therefore, they are closer to the normal human thinking. Examples for such constraints: the transformation *ClassToRDBMS* (Class diagram to Relational Database Management System diagram) guarantees that each class has its corresponding table, each table has an appropriate primary key, the primary key columns do not allow NULL values, and so on. To be able to use this type of high-level constraints we need high-level languages to define them and methods to translate them to the level of rewriting rules. Next section introduces this topic.

High-level languages/methods to define verification/validation properties

Generating source code from software models is a wide-spread method to make system development more effective. While generating model artifacts we can require quite usable quality factors, but in the case of source code generation, really usable and complex source code properties still cannot be defined. There are approaches, e.g. [9, 10, 11, 12], that facilitate source code generation, but they are either to language-specific (they can process only few type of source languages) [9], or the V&V opportunities of such transformations are on too low-level [10, 12]. Low-level V&V capabilities mean that because even a short source code requires a quite big model, e.g. an abstract syntax tree model, therefore, the transformation designer must be familiar with all of the details regarding to the generated source code in order to be able to define its quality requirements. On the other hand the goal is to involve a wider user group to be able to provide their quality-related V&V properties.

High-level, easy-to-use languages should be provided that facilitate defining V&V requirements against the model transformation.

Currently the most user friendly languages are OCL and similar languages that we can use to define our requirements. The research should identify the appropriate, first-order logic, second-order logic, or other formalism. These languages should be general purpose languages and easy-to-use even for non-experts.

Industrial applicability of the existing verification/validation approaches

The applicability of the already existing approaches and tools should be shown within industrial environments: experiments should be performed on larger (industrial size) transformations and models. According to the current state of the art these open issues are hard. Each of them requires further research and development. Some of the model transformation approaches or tools partly address one or two of these open issues, but most of the tools are used only within academic research groups. Therefore, the most important challenge is to achieve that current V&V approaches become applicable within industrial environments.

Conclusion

Domain-specific languages have been a part of the computing landscape since the appearance of programming languages. Domain-specific modeling fundamentally raises the level of abstraction while at the same time narrowing down the design space, often to a single range of products for a single company. The final products are automatically generated from the high-level specifications with domain-specific transformations. With DSM, there is no need to make error-prone mappings from domain concepts to design concepts and on to programming language concepts. In this sense, DSM follows the same recipe that made programming languages successful in the past: offer a higher level of abstraction and make an automated mapping from the higher level concepts to the lower-level concepts known and used earlier.

In this sense model transformations have a significant relevance in model-driven development. These transformations have to be verified/validated. In this paper we have highlighted the importance of domain-specific model processors and their validation. Furthermore, we have identified the open issues in the field of V&V of model transformations. The overall goal is to prepare the existing modeling, model processing, and V&V approaches to support the V&V of domain-specific properties and to be applicable within industrial environments.

Acknowledgment

This work is connected to the scientific program of the "Development of quality-oriented and harmonized R+D+I strategy and functional model at BME" project. This project is supported by the New Széchenyi Plan (Project ID: TÁMOP-4.2.1/B-09/1/KMR-2010-0002).

References

- [1] IEEE Standard Glossary of Software Engineering Terminology, 610.12-1990 (1990)
- [2] Corradini, A., Montanari, U., Rossi, F., Ehrig, H., Heckel, R., Lowe, M.: Algebraic approaches to graph transformation part I: basic concepts and double pushout approach, *In Handbook of Graph Grammars and Computing by Graph Transformation*, Vol. 1: Foundations (1997), World Scientific, Singapore, 163-245.
- [3] Fowler, M.: *Domain-Specific Languages*, (Addison-Wesley Professional, 2010)
- [4] Kelly, S., Tolvanen, J.P.: *Domain Specific Modeling*, (Wiley, 2008)
- [5] Taentzer, G., Ehrig, K., Guerra, E., de Lara, J., Lengyel, L., Levendovszky, T., Prange, U., Varró D., Varró-Gyapay, Sz.: *Model Transformation by Graph Transformation: A Comparative Study*, *ACM/IEEE 8th International Conference on Model Driven Engineering Languages and Systems*, (2005), Montego Bay, Jamaica
- [6] Rozenberg, G. (ed.): *Handbook on Graph Grammars and Computing by Graph Transformation: Foundations*, Vol. 1: Foundations (1997), World Scientific, Singapore
- [7] Lengyel, L.: *Online Validation of Visual Model Transformations*, PhD thesis, Budapest University of Technology and Economics, Department of Automation and Applied Informatics (2006)
- [8] OMG Object Constraint Language (OCL) Specification, Version 2.2, OMG document formal/2010-02-01, 2010, <http://www.omg.org/>
- [9] Fujaba Tool Suite website, <http://www.fujaba.de/>
- [10] GReAT: Graph Rewriting and Transformation website, <http://www.isis.vanderbilt.edu/tools/GReAT>
- [11] VIATRA2 (Visual Automated model TRAnsformations) framework website, <http://eclipse.org/gmt/VIATRA2>
- [12] VMTS: Visual Modeling and Transformation System website, <http://www.vmts.aut.bme.hu>

ELECTRO-MECHANICAL CONTINUOUSLY VARIABLE TRANSMISSIONS FOR AUTOMOTIVE APPLICATIONS

Kamarul Baharin Tawi¹, Izhari Izmi Mazali¹, Nurulakmar Abu Husain¹, Bambang Supriyo¹
and Mohd Salman Che Kob¹

¹ Faculty of Mechanical Engineering, Universiti Teknologi Malaysia, 81310 Johor Bahru, Malaysia

Keywords: Continuously variable transmission (CVT), electro-mechanical CVT, transmission, automotive, environmentally friendly

Abstract. Producing an efficient transmission for automotive applications has always been a significant challenge for transmission manufacturers, carmakers and research institutions alike, with many different options and ideas to be considered. Electro-mechanical continuously variable transmission (EM CVT) is an innovative idea that has been studied in recent years by researchers from certain research organizations worldwide as a possible solution for an efficient transmission in a passenger car. In this paper, the concept of EM CVT and its potential benefits will be reviewed. Firstly, the working principle of EM CVT will be introduced and compared with the working principle of the existing conventional CVT with electro-hydro-actuation (EHM) system currently used for automotive applications. Consequently, the potential benefits and advantages that can be gained in term of efficiency, practicality and environmental impact by applying EM CVT in a passenger car will be described. Finally, the possible limitations that lie ahead before this new idea of EM CVT can be introduced for the automotive market worldwide will be briefly discussed.

Introduction

Recently, many researchers have started the studies to produce an efficient continuously variable transmission (CVT) for applications in automotive fields. There are many types of CVT used currently for automotive applications, and one of the most common types is the pulley-based CVT with metal pushing V-belt. Generally, all types of CVT, unlike conventional transmissions for automotive applications, do not have discrete gears. In the pulley-based CVT with metal pushing V-belt, the transmission ratio is changed by simultaneously varying the radius of metal pushing V-belt on primary pulley, which is connected to the internal combustion engine (ICE), and secondary pulley, which is connected to the vehicle's wheels. This type of CVT normally uses electro-hydro-mechanical (EHM) system to actuate the process of changing CVT ratios.

The main advantage of the existing pulley-based CVT with EHM system (EHM CVT) is its wider transmission ratio as compared to conventional automotive transmissions with discrete gears. According to Klaassen [1], with this advantage, ICE can be operated at a more economical operating range, hence potentially improves the fuel efficiency of the vehicles. Another important advantage of this CVT is the possibility to change the ratio steplessly. This feature, according to Lang [2], increases the durability of the vehicle's powertrain system, while at the same time makes the process of shifting the CVT ratio smoother. Besides, the mentioned advantage also allows the CVT to be used not only in the conventional vehicles but also in alternatively-powered vehicles like hybrid cars and fully-electric cars.

However, the existing EHM CVT still has major disadvantages in term of high power consumption and significant power loss [1, 3, 4, 5]. The first disadvantage is inevitable during the event of constant CVT ratio. In order to maintain constant CVT ratio, continuous sufficient hydraulic pressure is required to retain the position of primary and secondary pulleys, and to achieve this, the ICE will have to provide extra power continuously to the hydraulic pump of the EHM CVT. The second disadvantage, meanwhile, is caused by the inaccurate clamping force exerted to metal belt for maintaining the desired CVT ratio. Excessive clamping force leads the metal belt to overstress, while insufficient clamping force results in the slipping of the metal belt itself. Both cases will cause significant power loss between primary pulley and secondary pulley of the CVT. In EHM CVT, the clamping force is controlled through the additional hydraulic control system. Because of this extra control system, the process to effectively control sufficient clamping force becomes very complicated.

In order to overcome these disadvantages, researchers from Universiti Teknologi Malaysia (UTM) have recently come out with the new concept of CVT with electro-mechanical system (EM CVT). In this paper, the working principle of EM CVT, together with its potential benefits and limitations will be described.

Background of Electro-Mechanical CVT

In the conventional EHM CVT, CVT ratio is shifted by simultaneously changing the radius of metal belt on both primary and secondary pulleys. This is achieved by axially moving the movable sheaves of primary pulley and secondary pulley, and in EHM CVT, it is done with the EHM system. The mathematical function to relate the axial distant of movable sheave of the pulley, X_{pulley} , and the radius of metal belt on the pulley, R_{pulley} , is explained in Eq. (1). Next, the relationship between CVT ratio, r_{CVT} , and the radius of both primary pulley, R_p , as well as secondary pulley, R_s , is shown in Eq. (2). The parameters from both Eq. (1) and Eq. (2) are illustrated in Fig. 1 and Fig. 2, on the other hand, shows the example of EHM CVT in low ratio, medium ratio and overdrive ratio [1].

$$X_{pulley} = (R_{pulley} - R_{pulley0}) \tan \alpha, \quad (1)$$

where: X_{pulley} is the axial distant of the movable sheave of the pulley (primary or secondary), R_{pulley} is the radius of metal belt on the pulley (primary or secondary), $R_{pulley0}$ is the initial radius of metal belt on the pulley (primary or secondary) and α is the angle of the pulley.

$$r_{CVT} = R_s / R_p$$

(2)

where: r_{CVT} is the CVT ratio, R_s is the radius of the secondary pulley and R_p is the radius of the primary pulley.

The EM CVT, unlike conventional EHM CVT, uses no hydraulic pump as part of its actuation system. Instead, the concept of moving screw is applied here, where the fix gear with inner thread will transfer torque to the moving screw to move it axially. The sufficient torque to actuate the movement of the moving screw is provided by an electric motor for each primary pulley and secondary pulley. Then, the axial movement of the moving screw will cause the movable sheave of the pulley to move axially, hence varying the radius of the metal belt on the pulley accordingly. Once the desired CVT ratio is achieved, the position of the pulleys will be retained through the thread design of the moving screw itself. The simplified sketch of the EHM CVT and EM CVT systems are shown in Fig. 3 and Fig. 4 respectively.

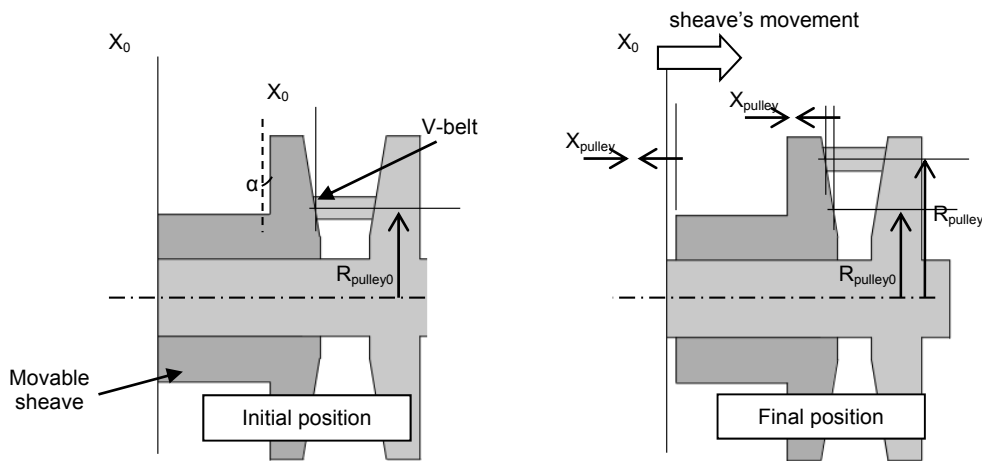


Fig. 1 Important parameters to determine the CVT ratio.

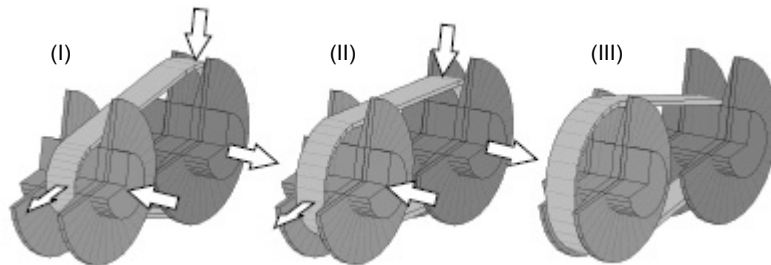


Fig. 2 Shifting from low ratio (I) to medium ratio (II) and overdrive ratio (III) in conventional EHM CVT [1].

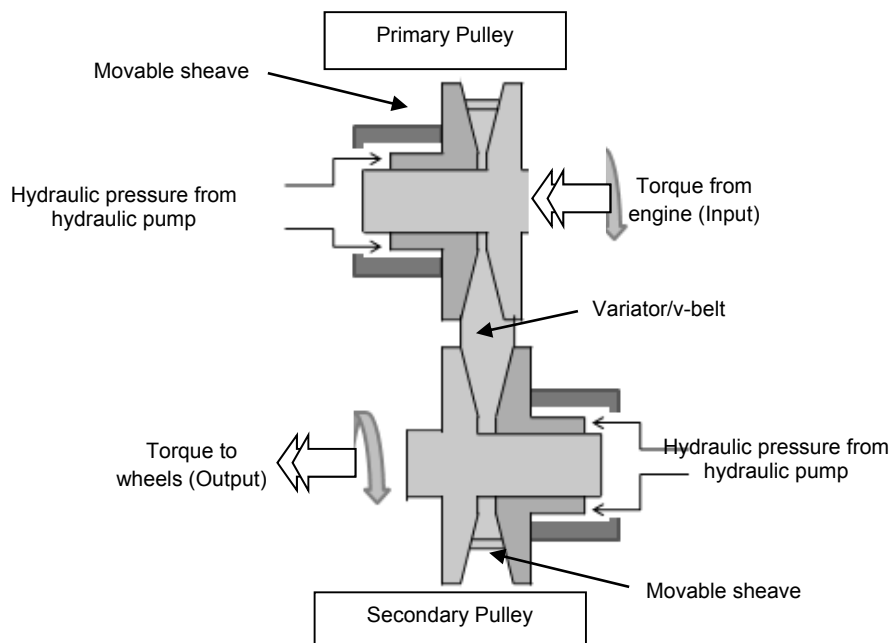


Fig. 3 The conventional EHM CVT.

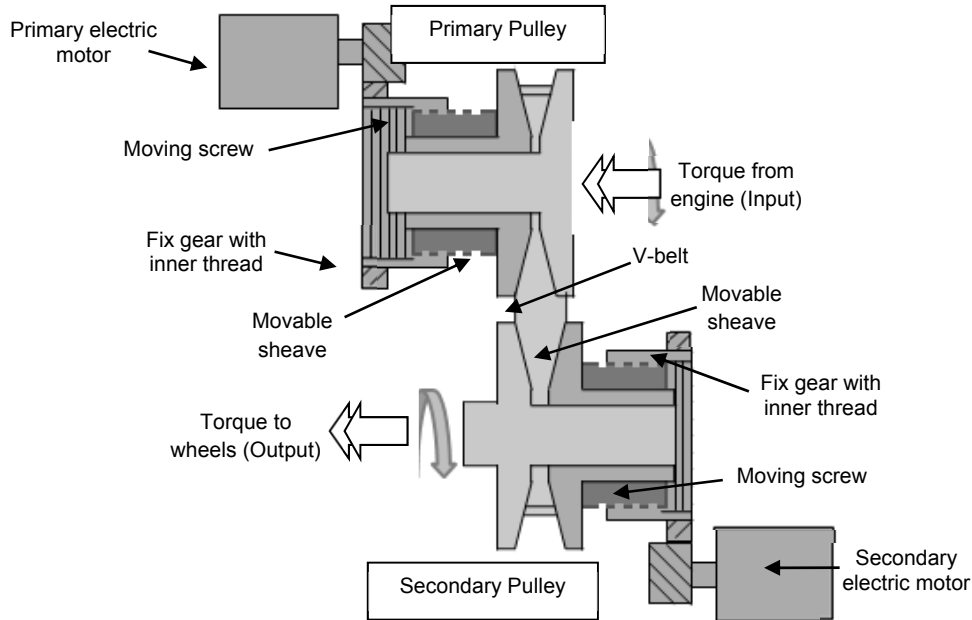


Fig. 4 The proposed concept of EM CVT.

Potential Benefits from Electro-Mechanical CVT

Minimize Loss in Actuation System

Based on the research by Klaassen [1], conventional EHM CVT suffers about 11% of transmission losses as compared to about 3% in normal manual transmission (Fig. 5), and these losses mostly caused by the hydraulic pump during the event of constant CVT ratio. This is because of the continuous hydraulic pressure required to maintain the desired CVT ratio, which results in a very high amount of power consumption from ICE. On the contrary, in EM CVT, no continuous hydraulic pressure is required to maintain constant CVT ratio, since it uses thread of the moving screw to retain the position of the primary pulley and secondary pulley, thus maintaining the desired CVT ratio accordingly. Therefore, with EM CVT, the high power consumption required for maintaining the desired CVT ratio can be avoided, hence reduces the amount of transmission losses suffered in the conventional EHM CVT.

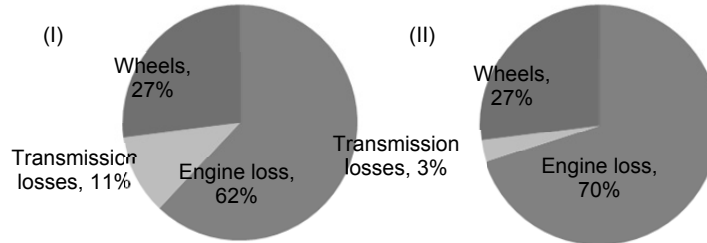


Fig. 5 The efficiency of engine with conventional CVT (I) and engine with normal manual transmission (II) at car's speed of 120km/h from Klaassen's thesis in [1].

Efficient Control of Clamping Force on the V-belt

In the pulley-based CVT with metal belt, the clamping force is exerted on the metal belt through secondary pulley. For the conventional EHM CVT, sufficient clamping force on the V-belt is controlled through hydraulic pressure from the hydraulic pump. This system major weakness is the compressibility of hydraulic oil, which increases as the pressure decreases. Because of this, the required hydraulic pressure for maintaining the desired CVT ratio and at the same time providing sufficient clamping force cannot be realized. In order to overcome this, an additional hydraulic control system is required, and this makes the process to control sufficient clamping force very complicated.

With EM CVT, sufficient clamping force is controlled through the axial displacement of the spring, which depends on the axial position of the moving screw. The process to control the axial position of the moving screw is easier since it is actuated by an electric motor, and no extra measurement must be taken on sensitive parameters like compressibility of the hydraulic oil. As a result, sufficient clamping force on V-belt can be controlled more efficiently and effectively, and this leads to an improvement in efficiency of the CVT.

No Unplanned Leakage in the Hydraulic System

Generally, there are two types of unplanned leakage that could happen within hydraulic pump; namely external leakage and internal leakage. The external leakage in hydraulic pump means that the hydraulic oil leaks out from the hydraulic system. The internal leakage, on the other hand, means that the hydraulic oil leaks out from one component to other component unintentionally within the hydraulic system. These leakages reduce the efficiency of hydraulic system since it causes a significant drop in hydraulic pressure [6].

The existing EHM CVT uses hydraulic pump as part of its actuation system, therefore makes it vulnerable to these issues. However, the proposed concept of EM CVT applies EM system as its actuation system without the usage of hydraulic pump. Consequently, the issues of unplanned leakage in the hydraulic system can be avoided entirely.

Better Environmental Impact

The concentration of CO₂ in atmosphere is a major concern currently since it contributes directly to the global warming. In general, the level of CO₂ emissions of a passenger car is proportional to its fuel consumption. With the application of EM CVT in conventional passenger cars, the ICE will be allowed to operate within its optimum operating line [1]. Furthermore, EM CVT also improves the issues of high power consumption and significant power loss suffered in the conventional EHM CVT. All these factors contribute to an improvement in fuel consumption of the cars, and consequently help in minimizing the threat of global warming by reducing the emissions of CO₂ into atmosphere.

Additionally, the existing CVT technologies, including EHM CVT, have already been used widely for alternatively-powered vehicles like hybrid and fully-electric cars. For example, the papers from Modak and Sane [7] as well as Hofman et al. [8] describe the application of CVTs for such cars. Thus, it will definitely be possible to apply EM CVT for applications in this area. Moreover, with EM CVT, because of its aforementioned potential benefits, the efficiency of these cars can potentially be further increased as well. Eventually, with the efficient usage of fuel in these cars, the total production of fuel from crude petroleum can be reduced significantly, hence lessen the impacts of pollution from this industry to environment.

Possible Limitations of Electro-Mechanical CVT

Potential Significant Lag during Shifting the CVT Ratio

The hydraulic pump used in EHM CVT has the ability to exert large hydraulic pressure in a very short time, thus shorten the time taken to shift the CVT ratio. However, in the concept of EM CVT, the duration of time to change the CVT ratio will be longer because of the rotation of gears and their frictions. This will eventually cause the feeling of sluggish during the process of changing CVT ratio. In order to improve this aspect, a more powerful electric motor can be used, though this ultimately might adversely affects the CVT's efficiency.

Belt Misalignment

Issue of belt misalignment is relevant for all pulley-based CVTs with metal belt. Hence, this weakness actually affects both existing EHM CVT and the concept of EM CVT. Excessive belt misalignment in CVTs will cause extra scratch between metal belt and pulleys. This will not only increase the amount of transmission losses in CVTs, but it will also reduce the lifespan of metal belt and pulleys [5, 9,10]. This issue can be overcome by using dual-acting pulley mechanism, which allows both sheaves of primary pulley as well as secondary pulley to be moved axially during the changing of CVT ratio. In recent years, researchers from Universiti Teknologi Malaysia have started an extensive work to produce EM CVT that applies this mechanism.

Conclusion

As a conclusion, the concept of EM CVT apparently offers enormous potentials for improving the efficiency of CVT technology that can be used for automotive applications. Nevertheless, there are still numerous concerns that could potentially diminish the gains from this concept. Therefore, it makes a lot of sense for research institutions and companies from relevant industries to jointly spend more efforts to perform further researches on this concept so that it can be optimized and eventually prepared for possible commercialization in future.

Acknowledgement

The authors would like to thank all persons from Drivetrain Research Group of Universiti Teknologi Malaysia who have involved in providing comments and suggestion for improving and completing this paper as well as Malaysia's Ministry of Science and Technology for providing Technofund to fund this project.

References

- [1] T. W. G. L. Klaassen: *The Impact CVT; Dynamics and Control of an Electromechanically Actuated CVT*, (Library Eindhoven University of Technology, Eindhoven, 2007)
- [2] K. R. Lang: *Continuously Variable Transmissions; An Overview of CVT Research Past, Present and Future*, (21W. 732, 2000)
- [3] E. Kirchner: *Leistungsübertragung in Fahrzeuggetrieben; Grundlagen der Auslegung, Entwicklung und Validierung von Fahrzeuggetrieben und deren Komponenten*, (Springer, Heidelberg, 2007)
- [4] G. Vogelaar: VT2+; Further improving the fuel economy of the VT2 transmission, *Proc. 6th Int. Conf. Continuously Variable Hybrid Transmissions CVT2010*, Maastricht, The Netherlands (2010), pp. 105–109.
- [5] S. Akehurst: *An Investigation into the Loss Mechanisms Associated With a Pushing Metal v-belt Continuously Variable Transmission*, (University of Bath, Bath, 2001)
- [6] M. A. Kulkarni: *Application of Fuzzy Logic to Detection of Internal Leakage Fault in Hydraulic System*, (Digital Conservancy University of Minnesota, 2011)
- [7] G. S. Modak, S. S. Sane: Mechanical Continuously Variable Transmission (CVT) for Parallel Hybrid vehicle, *IEEE Conference on Electric and Hybrid Vehicles ICEHV*, (2006), pp. 1-4.
- [8] T. Hofman, M. Steinbuch, R. v. Druuten, A. F. A. Serrarens: Design of CVT-Based Hybrid Passenger Cars, *IEEE Transaction on Vehicular Technology*, Volume 58 (2009), No. 2, pp. 572-587.
- [9] F. Zang: Simulation research of the electro-hydraulic control system of CVT metal v-belt's axial misalignment, *IEEE International Technology and Innovation Conference ITIC*, (2009), pp. 1-5.
- [10] K. B. Tawi: *Investigation of Belt Misalignment Effect on Metal Pushing V-Belt Continuously Variable Transmission*, (Cranfield University, Cranfield, 1997)



- [11] B. Supriyo, K. B. Tawi, H. Jamaluddin, S. Ariyono: Position control for pulley axial movement of electro-mechanical dual acting pulley continuously variable transmission system, *Jurnal Mekanikal Universiti Teknologi Malaysia*, No. 22 (2006), pp. 89-102.
- [12] A. A. Shafie, M. H. Ali: Development of an Efficient CVT using Electromechanical System, *World Academy of Science, Engineering and Technology*, Issue 32 (2009), pp. 555-558.
- [13] Y. Xinhua, C. Naishi, L. Zhaohui: Electro-Mechanical Control Devices for Continuously Variable Transmissions, *SAE International Powertrains, Fuels and Lubricants Congress*, Shanghai, China (2008).
- [14] N. Cholis, S. Ariyono, A. A. Kadir: A review on control strategy for electro-mechanical rubber belt continuously variable transmissions (CVT), *2nd National Conference in Mechanical Engineering Research and Postgraduate Studies NCMER* (2010), pp. 804-813.
- [15] T. W. G. L. Klaassen, B. G. Vroemen, M. Steinbuch: *Dynamic Analysis of the Impact CVT; Ratio and slip dependent, non-minimum phase dynamics*, (Conference Proceeding, Library Eindhoven University of Technology, Eindhoven, 2005)
- [16] B. Bensen: *Efficiency optimization of the push-belt CVT by variator slip control*, (Library Eindhoven University of Technology, Eindhoven, 2006)
- [17] S. Ariyono: *Intelligent electromechanical continuously variable transmission ratio controller*, (Library of Universiti Teknologi Malaysia, Johor Bahru, 2009)
- [18] K. G. O. v. d. Meerakker, P. C. J. N. Rosielle, B. Bensen, T. W. G. L. Klaassen: Design of an Electromechanical Ratio and Clamping Force Actuator for a Metal V-belt Type CVT, *International Continuously Variable and Hybrid Transmissions CVT2004*, Davis, USA (2004).
- [19] P. A. Vaanhuizen, B. Bensen, T. W. G. L. Klaassen, P. H. W. N. Albers, C. Changenet, S. Poncy: Pushbelt CVT Efficiency Improvement Potential of Servo-Electromechanical Actuation and Slip Control, *International Continuously Variable and Hybrid Transmissions CVT2004*, Davis, USA (2004).
- [20] P. A. Vaanhuizen, B. Bensen, T. W. G. L. Klaassen, K. G. O. v. d. Meerakker, F. E. Veldpaus: Variator loading and control in a V-belt type geared neutral transmission in and around the geared neutral point, *International Continuously Variable and Hybrid Transmissions CVT2002*, München, Germany (2002).
- [21] K. v. Berkel, T. Fujii, T. Hofman, M. Steinbuch: Belt-Pulley Friction Estimation for the Continuously Variable Transmission, *IEEE 50th Conference on Decision and Control and European Control Conference (CDC-ECC)*, (2011), pp. 6672-6677.
- [22] V. Miltenovic, M. Velimirovic, J. Stefanovic-Marinovic, M. Banic: Differential Planetary Transmission of Wind Turbine Continuously Variable Transmission, *Journal of Faculty of Technical Sciences Machine Design*, Volume 2 (2010), pp. 123-128.
- [23] Y. Fu, W. Zhang: The Deadband Control of the Electro-hydraulic Actuator of the Motor-pump Coordinated Control, *IEEE International Conference on Mechatronics and Automation*, (2010), pp. 1239-1244.
- [24] L. Yongming, J. Youshi, Y. Fensheng, G. Yang: A New Analytical Model of Pressure Performance in Water Injection Well and Its Application, *IEEE International Conference on Computational and Information Sciences*, (2011), pp. 598-601.
- [25] Z. Sun, K. Hebbale: Challenges and Opportunities in Automotive Transmission Control, *American Control Conference*, (2005), pp. 3284-3289.
- [26] Volkswagen AG: DSG: Das neue DQ500, Info Center (Themes), <http://www.volkswagenag.com>, Wolfsburg, 2010.
- [27] ZF Friedrichshafen AG: ZF Develops 9-Speed Automatic for Passenger Cars, Press Information, <http://www.zf.com>, Friedrichshafen, 2011.
- [28] GETRAG Corporate Group: GETRAG Powershift Getriebe 6/7HDT451 Mild-Hybrid, Product Highlights in International Motor Show, <http://www.getrag.com>, Untergruppenbach, 2011.



International Conference on Innovative Technologies, IN-TECH 2012,
Rijeka, 26. - 28.09.2012



NUMERICAL MODELING OF TRACK ROLLER - SHOE INTERACTION AT CRAWLER MACHINES

S. Cosic¹, M. Avdic², S. Bukvarevic³

¹ University of Tuzla, Faculty of Mechanical Engineering, Univerzitetska 4, 75000 Tuzla, BiH

² University of Tuzla, Faculty of Mining and Civil Engineering, Univerzitetska 1, 75000 Tuzla, BiH

³ University of Tuzla, Faculty of Mining and Civil Engineering, Univerzitetska 1, 75000 Tuzla, BiH

Keywords: numerical modeling, finite elements analysis, contact, elastic-plastic deformation

Abstract. In this paper we describe numerical analysis of inelastic contact problem between roller and link at crawler machines. Upon generating of 3D model, it is discretized by the finite elements and resolved as non-linear contact problem. We determine external load that initiate plastic deformation of the link member material and analyse possibilities of protection by depositing of hardfacing layer for appropriate characteristics of material, its geometry and loads.

Introduction

Mining shovels, military vehicles and other heavy-duty equipment use endless track shoe belt to distribute loads to the ground. Huge construction, large mass, work in abrasive and corrosive environment, non-uniform distribution of load on carrying elements due to uneven or non-homogenous terrain, dynamic forces, structural vibrations and other brings loads that are much greater than nominal. Elements for horizontal movement are in the most unfavourable position taking into account all of constructional modules of the crawler machines. Gear transmissions, driving sprocket, bearing wheels (rollers) and track pads (shoes, links) are exposed to considerable contact stresses whose values and directions are stochastic variables. Magnitudes of stress in mentioned components are often over the stress values that components can endure. These leads to appearing of plastic deformations and cracks along with intensive wear of some surfaces.

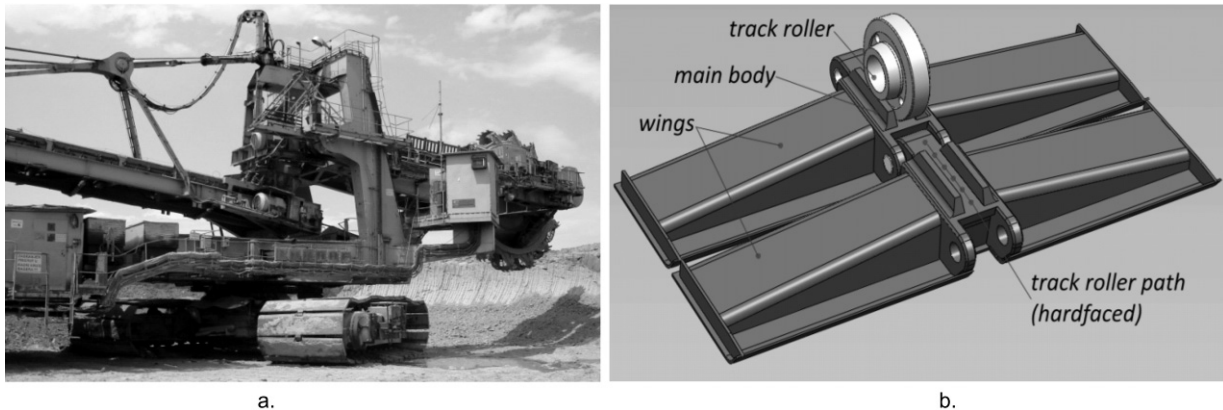


Fig. 1 BW Excavator (a) and 3D CAD model of the BWE track shoe (b)

Plastic deformation of the track roller path at the shoe is an occurrence noticed at all types of crawling vehicles especially observable in the bucket wheel excavator (BWE) due to its weight (Fig. 1). Due to plastic deformation the roller path geometry is being distorted which cause rolling difficulties and that is why the tension force in crawling chain is being increased, as well as the stresses at driving sprocket. Plastic deformation of all link members in the chain bring about cumulative increase of the crawling chain perimeter causing changes in contact conditions at driving sprockets. The common case in practice is to use contact surfaces improved or repaired by hardfacing. Upon possibility of crawling chain stretching is being exhausted, it is necessary to repair crawler pad geometry, which is done by depositing hardfacing layer. In order to predict mechanical behaviour and load bearing capacity of layered contact pair with respect to material and geometrical properties we conduct numerical simulation and analysis of inelastic layered contact problem for the case of bucket wheel excavator, Fig.1 (a). The model geometry is shown in Fig.1 (b).

FEM analysis of inelastic contact problem

Realistic 3D CAD model of the track shoe is generated for the bucket wheel excavator SRs 402, using 3D modeling software and then it is "imported" into the application which executes the nonlinear FEM analysis. Geometry of the model is based on original technical documentation. Characteristic position in which real loads are especially unfavourable may be determined despite the fact that these loads are of stochastic character. Due to movement of the crawling chain, besides high level of the contact stresses, there are tension and bending stresses caused by chain stretching and it's twisting around driving sprocket. Mentioned stresses are being added to the contact stress which brings link member to complex and extremely unfavourable stress-strain condition. For couple of characteristic load cases (one of which is presented in Fig. 3a) a numerical simulation has been performed. Model domain was discretized in tetrahedral and hexahedral finite elements. For the case of small radius, abrupt changes of cross sections, thin or small parts of the construction, mesh generator is forced to generate smaller elements that can follow change of geometry. In such conditions, it may appear huge increase of DOF number, as the track pad dimensions are great, and number of the nodal points is being increased to several hundred thousand.

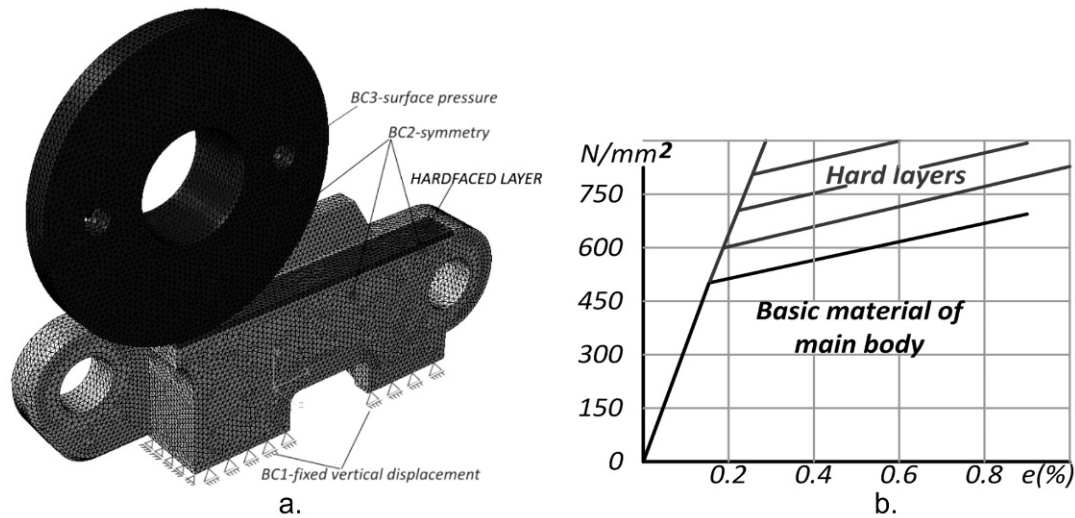


Fig.2 Discretised symmetrical model with boundary conditions (a), bi-linear material model properties (b)

Problem is additionally complicated due to existence of contact on small surface of several square millimetres. In order to obtain the contact pressure and deformation distribution, it is necessary to have several elements within the contact zone.

Material, loading and boundary conditions

According to manufacturer specification, material of the main body part of track shoe is manganese steel GS-40MnCrSi3V. Modulus of elasticity for this material $E=2.1 \cdot 10^{11}$ Pa, and yield stress is taken as 470 MPa. The hardfacing layer is modelled with 3-10 mm thickness and yield strength 600-1200 MPa, Fig 2 (b). In this series of simulations, we use the same elastic material parameters (E, ν) for the hard layer and substrate. Hardening behaviour of steel is described by linear isotropic law

$$\sigma_Y = \sigma_{Y_0} + H_{iso} \epsilon^{pl} \quad (1)$$

where σ_{Y_0} and H_{iso} are initial yield stress and isotropic hardening modulus for given material, determined experimentally. The ϵ^{pl} is equivalent or accumulated plastic strain. For roller material we assumed a little bit larger values of mechanical properties, regarding basic material of the track shoe main body. Analysis was performed for several characteristic (the most unfavourable) cases and one of results is presented in Fig. 3 (a) where loaded roller is rolling along horizontal crawler link member (entrance, mid-point and exit). The aim was to establish magnitude and influence of hardface layer thickness and mechanical properties on stress-strain state. Lower surface of the segment is considered to be fixed in vertical direction, and certain number of nodes is fixed in all direction due to elimination of "rigid body movement". Specified boundary conditions provide stable and statically completely determined model, Fig. 2 (a).

Contact interaction modeling

There are several methods for resolving contact problem, but the most frequently applied are "penalty" and Lagrange-multiplier procedures. The "penalty" method is much simpler for numerical implementation, but the solution is sensitive to the penalty factor magnitude, i.e. existence of certain penetration is unavoidable. The bigger penalty parameter increases the accuracy, but may bring to the numerical instability. The second (LM) procedure provides exact solution, but includes series of numerical difficulties during implementation. As the number of contact elements change with the load increment, format of system matrices change too. Augmented Lagrange-multiplier method is, in some sense, combination of both mentioned methods. It was applied in the analysis, as it is more robust and in numerical sense more effective. Although we use small strain assumption, the problem is nonlinear due to plastic deformation and the contact. The main discrete equations system is given by:

$$\begin{aligned} F_{INT}(U) &= F_{EXT} + F_{CONT}(U) \quad \text{or} \\ R(U) &= F_{INT}(U) - F_{EXT} - F_{CONT}(U) = 0 \end{aligned} \quad (2)$$

where F_{INT} and F_{EXT} are internal and external force vectors. First of them nonlinearly depend on nodal displacement vector "U". Contact force contribution is included by F_{CONT} . Nonlinear system of equations (2) is solved by NR procedure. Newton-Raphson procedure was chosen due to quadratic convergence, and effectively implemented algorithm in commercial FEM codes. Convergence, according to the energy criteria, was realized after 3-6 iterations in average in each load increment. Contact analysis was performed for five loading cases. Due to fact that elastic parameters (E, μ) of hardfacing layer, roller and track main body are almost the same, while load is in elastic range, stress components and deformation can be approximately calculated by Hertz contact theory. The peak contact stress is given by:

$$p_{MAX} = \sqrt{\frac{E^* F_{EXT}}{\pi LR}} \quad (3)$$

$$\frac{1}{R} = \frac{1}{R_1} + \frac{1}{R_2}; \quad \frac{1}{E^*} = \frac{1-\mu_1^2}{E_1} + \frac{1-\mu_2^2}{E_2}$$

where E_1 , E_2 , μ_1, μ_2 , R_1 and R_2 are material and geometric properties of contact pairs respectively. Results obtained numerically are compared and find to be in good agreement with analytical Hertz contact theory (in elastic range). When stress excide yield limit there is no analytical solution to be compared with, so experimental results is the only way to validate numerical simulation. All deformation tensor components in this problem are relatively small values, and that is why the effect of geometrical nonlinearity may be neglected without substantial loss of accuracy, i.e. the model is considered geometrically linear.

Simulation results

The main post-processing variables are stress and plastic strain components. As secondary variables, they have a little bit reduced degree of accuracy in relation to the primary ones (displacements). As the most relevant, the value of equivalent (vMises) stress and equivalent (accumulated) plastic strain are being accepted. Distribution the former in longitudinal cross section is shown in Fig.3 (a).

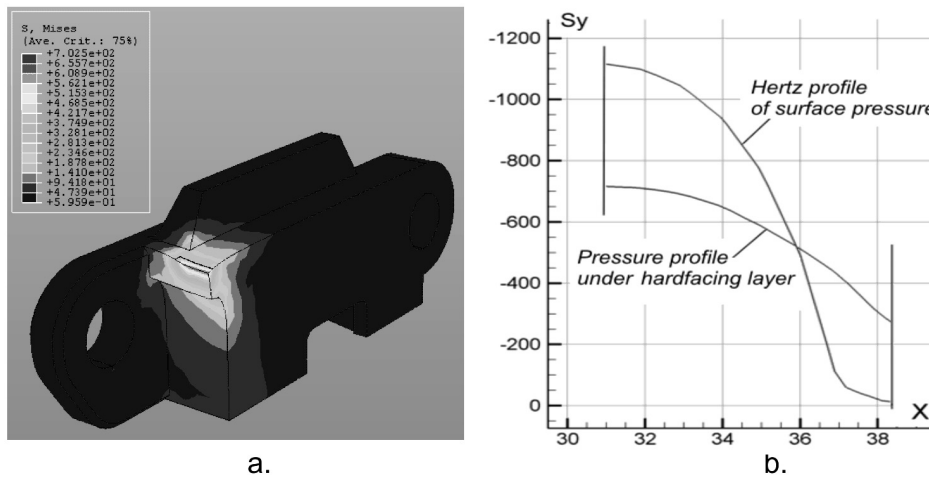


Fig.3 vMises stress distribution (a) and protecting effect of hardface layer (b)

Beside of 3D model, the stress–strain analysis in contact zone was also performed through series of 2D numerical simulations, varying the key parameters: thickness of surface layer, yield stress of surface layer material and yield stress of basic (substrate) material. By numerical simulation we get information about external load level necessary to induce plastic deformations in contact zone, depth of point where first yield occur and influence of surface layer thickness and material properties on these values. Protective effect of hardfacing layer is clearly shown in Fig.3 (b). The maximum contact pressure on the upper surface of hard layer is transmitted to basic material below. Stress level under hardface layer is significantly lower than contact stress at upper surface. Also, it is interesting to see the way of the plastic zone spreading as load increase. Equivalent (accumulated) plastic strain is variable the most favourable for this purpose. For presented data, plastic deformation appears for load of 600 kN at depth of 6 mm, i.e. at transition from hard layer to the basic material. After initial plastic deformation, material properties of basic material and hard layer are changed (deformation induced hardening). This is very characteristic for manganese steel. Due to influence of cyclic loading, the shakedown effect takes place. Actual stress state results from superposition of working stresses and residual stresses due to permanent (plastic) deformation. In Fig.4 (b) we can see residual stress distribution (vMises equivalent stress) for load cycle given at Fig.4 (a). According to shakedown theorem (Melan), residual stresses are in this case protective and it reduces working stresses. Also, it reveals possibility of improving contact stress resistance by controlled plastic pre-deformation of roller path.

It could be very useful in practice to have a possibility for the preliminary determination of layered contact pair load capacity without numerical simulation. For that purpose, we develop mathematical model based on the data obtained by numerical simulation (meta-model). The model should include three parameters: thickness of surface layer (h), yield stress of surface layer material σ_{y0}^{lay} and yield stress of main body material σ_{y0}^{basic} . We assume geometric parameters are known in advance. In mathematical sense, it is necessary to establish relation between external load level that causes plastic deformation (F_{max}), layer thickness and material properties. The relation could be in the form: $F_{max} = f(\sigma_{y0}^{basic}, \sigma_{y0}^{lay}, h_{lay})$. For the given geometry, we have performed series of numerical simulations consisting of $4 \cdot 4 \cdot 4 = 64$ individual simulation. The obtained database is used for multidimensional polynomial approximation based on last square fit. The quadratic polynomial model with three variables requires a lot of parameters C_i to be computed. From the practical point of view, it is not suitable so we choose to develop model based on 2 variables, considering the value of yield stress of basic material as constant for the given model. In that case, the quadratic model can be defined as:

$$F_{max} = f(\sigma_{y0}^{lay}, h_{lay}) = C_0 + C_1 \cdot \sigma_{y0}^{lay} + C_2 \cdot h_{lay} + C_3 \cdot (\sigma_{y0}^{lay})^2 + C_4 \cdot (h_{lay})^2 + C_5 \cdot \sigma_{y0}^{lay} \cdot h_{lay} \quad (4)$$

where σ and h are corresponding layer yield stress and thickness. It is easy to determine coefficients C_0 - C_5 for the given data set.

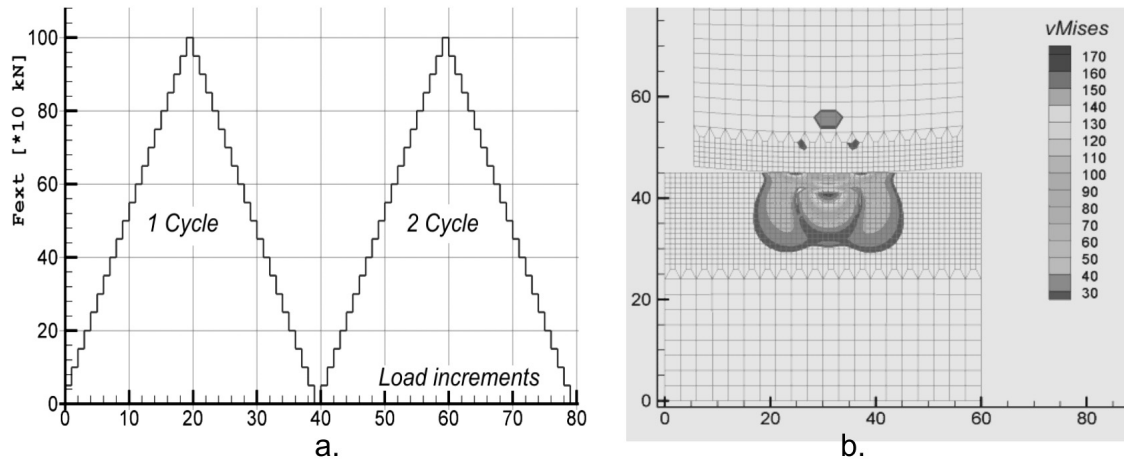


Fig. 4 Load cycles (a) and distribution of residual stresses (b)

Conclusions

Upon performed simulations for critical load cases, appropriate set of results is obtained, based on which it is possible to draw the following conclusions:

- Contact stresses have much more influence than stresses caused by tension force and bending moments in crawler shoe.
- Along with the loading increase, critical point in which initial plastic flow starts is being moved into the depth of basic material. When equivalent stress reaches value of the yield stress, plastic flow starts, and plastic zone develops laterally and towards down.
- With further loading increase, plastic zone propagates up, and for some level of loading may come out to the free surface causing large surface deformations.
- Deformations close to the contact surface remain within the small limits, despite the initialization and spreading of plastic zone, as it is surrounded with elastically deformed material. Plastic and elastic deformations are of the same order.
- Appearance of plastic deformations in depth does not influence on decreasing the contact pressure that further increases with the loading increase. Dimensions of contact surface also do not change considerably in the initial plastic flow phase. Only on higher degree of plastic deformations, redistribution of the contact pressure becomes noticeable due to enlargement of the contact surface.
- By increase of the yield stress of hard layer, there is no any effect of protection against the plastic deformation, until layer thickness reaches appropriate value. For the case of hard, but not enough thick layers, plastic flow appears within the basic material below the hard layer which can lead to the brittle failure of thin hard layer.
- Mathematical model (4) is well suited for practical, preliminary determination of load bearing capacity for the given geometry and the given range of thickness/material properties. The extrapolation of data out of numerical simulation scope should be done with special attention.

References

- [1] Arnell, R.D. and Djabella, H., "Two-dimensional finite element analysis of elastic stresses in double layer systems under combined surface normal and tangential loads", *Thin Solid Films*, No.226, 1993., pp 65-73.
- [2] Chen W.T., "Computation of stresses and displacements in a layered elastic medium", *Int. J. Eng.Sci.*, No.9, 1971., pp 775-800.
- [3] Chen W.T. and Engel, P.A., "Impact and contact stress analysis in multi-layered media", *Int. J. Solids Structures*.,No.8, 1972, pp 1257-1281.
- [4] Cosic S., Maneski T., "Contact Analysis of Crawler Pads", TMT 2006, Barcelona, Spain 2006.
- [5] Cosic S., Maneski T., Jurkovic M.: Numerical simulation of elastic-plastic contact of layered bodies, 11th International Research/Expert Conference "Trends in the Development of Machinery and Associated Technology" TMT 2007, Hammamet Tunisia, 2007
- [6] Elsharkaway, A.A. and Hamrock, B.J., "Numerical solution for dry sliding line contact of multi-layered elastic bodies", *ASME J. Tribology*, No.115, 1993., pp 237-245.
- [7] Gupta P.K. and Walowit, J.A., "Contact stresses between an elastic cylinder and a layered elastic solid", *ASME J. Lub. Tech.*, No.96, 1974., pp 259-257.
- [8] Johnson, K.L., "Contact Mechanics", Cambridge University Press, 1985.
- [9] J.C. Simo, T.J.R. Hughes, "Computational Inelasticity", Springer-Verlag, New York 1998.
- [10] Komvopoulos, K., "Finite element analysis of a layered elastic solid in normal contact with a rigid surface", *Trans. ASME J. Trib.*, No.110, 1988., pp 477-485.
- [11] Komvopoulos, K. (1989), "Elastic-plastic finite element analysis of indented layered media", *Trans ASME J. Trib.*, No.111, 1989., pp 430.
- [12] Pfister, Eberhard, "Frictional contact of flexible and rigid bodies", Springer-Verlag, 2002.
- [13] Tian, H. and Saka, N., "Finite element analysis of an elastic-plastic two-layer half-space; normal contact", *Wear*, No.148, 1991., pp 47-68.
- [14] Wriggers P., "Computational Contact Mechanics", John Wiley and Sons, Ltd, 2002.

MEASUREMENTS OF EPR SPECTRA FOR THE POWDERS USED IN CERAMIC CORES AND FORMS IN THE AEROSPACE INDUSTRY

Ireneusz Stefaniuk¹ and Piotr Potera¹

¹ Institute of Physics, University of Rzeszow, Rejtana 16a, 35-310 Rzeszow, Poland

Keywords: ceramic cores and forms, Al₂O₃, ZrO₂, electron paramagnetic resonance (EPR)

Abstract. In this work the results of measurements of electron paramagnetic resonance (EPR) spectra for Al₂O₃ and ZrO₂ powders of mullites of different grain sizes were presented. The measurements were performed at room temperature and in the temperature range from 140 K up to 380 K.

The purpose of this study is demonstrate the applicability of EPR methods for the assessment of impurities of Cr and Fe ions in the materials used as ceramic cores and forms in the aviation industry. The analysis of EPR spectra were obtained and the characteristic lines were selected to rating the level of impurities. The results for selected powders were compared with the X-ray phase analysis.

Introduction

Powders used in ceramic cores and forms in the aerospace industry are widely studied by different methods. The basic powder is Al₂O₃ which comes as part of the of mullites. Corundum (Al₂O₃) doped with transition-metal ions (Fe, Cr, Ti, Cu, etc.) has been proved to be an important ceramic and laser crystal material [1–5]. The micro-structural distortion of local lattice where transition-metal ion locates in the crystal has been discussed in many works and different viewpoints have been proposed. The ceramic nano-powders are widely used in various industries, including aerospace industry. The polymer nanocomposites stiffened by ceramic nano-filling are characterized by very high hardness and resistance for abrasion in comparison with composites in micrometric scale [6]. The annealing of Al₂O₃ powders in temperatures 350, 600, 900°C do not influence the size of particles of the investigated powders. The heating in temperature 1200° C leads to the 30% growth of the average size of grains (due to the fritting processes) and at the same time the growth of crystallinity degree of alumina and the phase transition $\delta, \gamma, \eta, \epsilon - \text{Al}_2\text{O}_3 \rightarrow \alpha - \text{Al}_2\text{O}_3$ take place [7]. The conditions of synthesis of the precursor as well as usage of its modifier significantly influence the Al₂O₃ morphology [8]. Also important is the reaction of environment in which the homogenization of both Al₂O₃ and nanometric ZrO₂ powders take place. The environment, in which particles of both powders have the same electric charge signs, leads to the forming of the mechanically resistant agglomerates. This is detrimental for the condensation of material during fritting. In the sintering process, the cracks with sizes about of hundreds of micrometers as well as inhomogeneity of packing in individual micrometers scale are created [9].

The purpose of this study is to demonstrate the applicability of EPR methods for the assessment of impurities of Cr and Fe ions in the materials used in ceramic cores and forms in the aerospace industry. In the end of research will be done to improve the quality of the ceramic cores and forms as well affect the quality of the final product for direct use in the aerospace industry.

Experimental details

For the experiment the samples of corundum (Al₂O₃) and ZrO₂ with different size and incorporating a second phase were used. [10,11]. The Al₂O₃ powders from different batches from different suppliers with a grain # 200th has been studied by EPR method [12]. from each batch of 4 samples weighing 0.02 g in order to detect heterogeneity of the material have been selected.

For the EPR measurements the standard X-band (~ 9 GHz) spectrometer, produced in Wroclaw Technical Univeristy, with digital registration of the spectra was used. The temperature measurements were done using the digital temperature control system (BRUKER ER 4131VT), which allows the temperature range from 100K to 500K.

Results and discussion

Selected EPR spectra are shown in Fig. 1 to 3. The composition of Al₂O₃ sample were measured by X-ray diffraction method and the results of the analysis are presented in Table 1

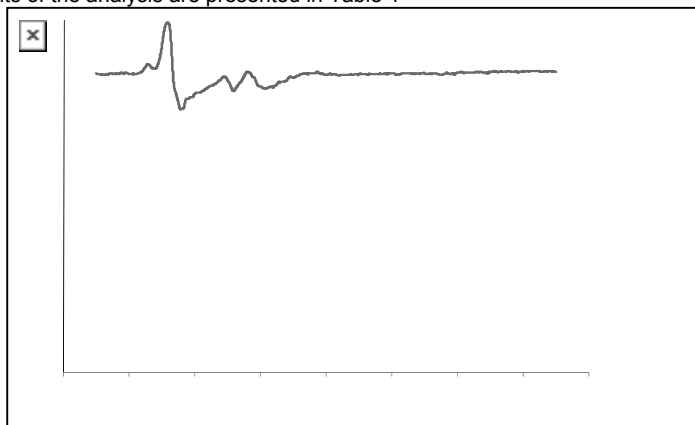


Fig. 1. EPR spectra for selected samples from the investigated materials
Table 1. Chemical composition XRF of Al₂O₃#200

	Content of main and trace roots, % Loss of roasting in 1025°C		SiO ₂	Al ₂ O ₃	Fe ₂ O ₃	CaO	MgO	K ₂ O	Na ₂ O
	Treibacher Al ₂ O ₃ -200 [%]	0,17		0,23	99,33	0,03	0,02	0,01	-
	TiO ₂	Zn	Bi	Co	Ni	Mn	Pb	Cr	Cu
Treibacher Al ₂ O ₃ -200 [%]	0,02	0,000	0,002	0,000	0,023	0,000	0,001	0,06	0,002

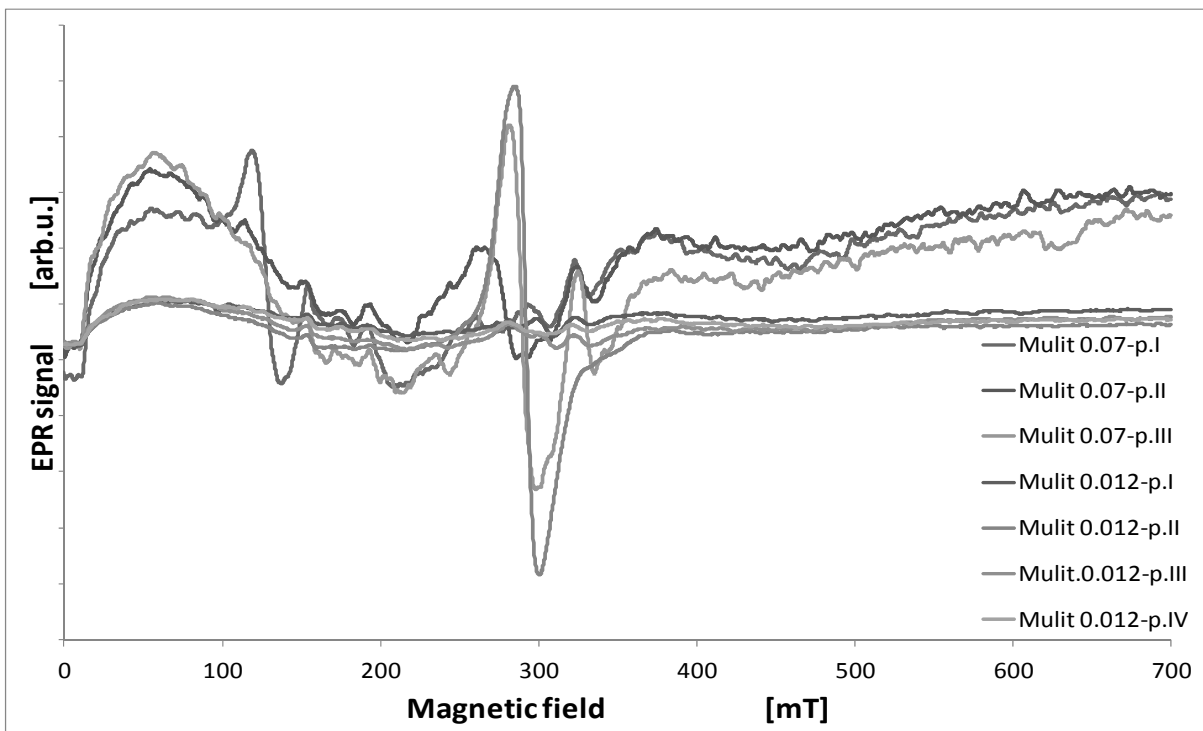


Fig. 2 . EPR spectra for mullite samples.

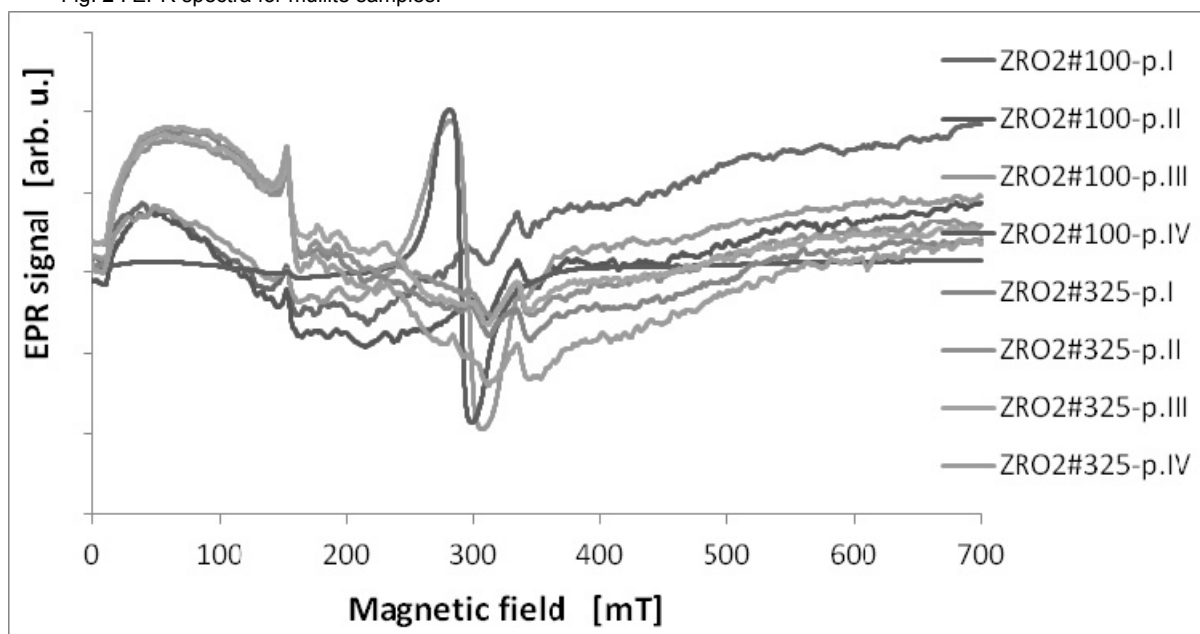


Fig. 3 . EPR spectra for ZrO₂ samples.

For samples Al_2O_3 #200 no. 1 and 2 the spectral analysis were performed in our early work [10]. As the results of analysis the Fe^{3+} and Cr^{3+} ions were detected in all sample of corundum.

For the Al_2O_3 sample the calculated g_{eff} -factor values for each line are as follows: $g_{\text{eff}}=5,6$, $g_{\text{eff}}=4,29$, $g_{\text{eff}}=3,36$, $g_{\text{eff}}=2,57$, $g_{\text{eff}}=2,26$, $g_{\text{eff}}=2,00$, $g_{\text{eff}}=1,97$, $g_{\text{eff}}=1,69$. However, for the mullgrain sample we obtain the values: $g_{\text{eff}}=4,28$, $g_{\text{eff}}=2,33$, $g_{\text{eff}}=2,23$, $g_{\text{eff}}=1,97$. The estimated experimental uncertainty of the g -values is $\pm 0,02$. For mullites samples the calculated g_{eff} -factors for each line are: $g_{\text{eff}}=5,6$, $g_{\text{eff}}=4,29$ and $g_{\text{eff}}=2,06$, $g_{\text{eff}}=1,97$.

For the ZrO_2 #100 sample the calculated g_{eff} -factor values for each line are as follows: $g_{\text{eff}}=6,84$; $g_{\text{eff}}=4,23$; $g_{\text{eff}}=2,54$, $g_{\text{eff}}=2,24$, $g_{\text{eff}}=2,37$; $g_{\text{eff}}=1,88$.

The analysis of the line positions suggest that the lines with $g_{\text{eff}}=4,28$ $g_{\text{eff}}\approx 2,00$ may be attributed to Fe^{3+} ($S=5/2$) ions, because they present a typical spectrum for so called disordered systems [13] present in a glassy hosts [14]. The line intensities decrease progressively showing the evolution of the relative line shapes and the intensities at $g = 4,3$ from isolated ions in local tetrahedral (and eventually octahedral) sites [14]. The line with $g_{\text{eff}}=1,98$ may be attributed to Cr^{3+} ($S=3/2$) ions in the slightly distorted octahedral sites [15].

The temperature dependence of gyromagnetic factor (g) of ZrO_2 sample is presented in Fig. 4

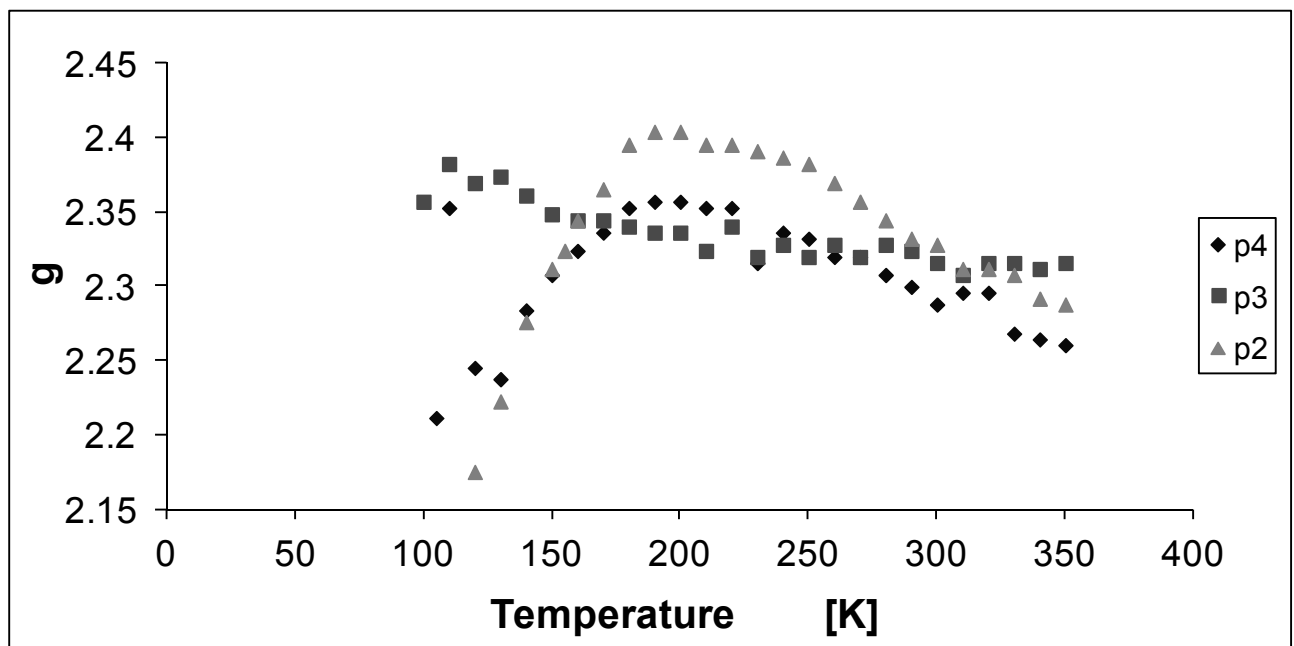


Fig. 4 Temperature dependence of gyromagnetic factor (g) of ZrO_2 sample

For ZrO_2 sample are observed characteristic temperature around of 200K which is a change the of all EPR line parameters, such as: peak-to-peak line width (H_{pp}), the intensity (I) as well as the gyromagnetic factor (g).

For the samples Al_2O_3 #200 no 3 and 4 high differences in EPR spectrum was observed, as due to appearing of new line near 270 mT. This line is probably as results of presence of Cr^{3+} ($S=3/2$) ions in different size Cr_2O_3 nanoparticles [16]. The analysis of the line positions suggest that the lines with $g_{\text{eff}}=4,23$ may be attributed to Fe^{3+} ($S=5/2$) ions, analogously then for Al_2O_3 sample. EPR spectrum of the sample Al_2O_3 with the low chromium loading shows a weak broad line centred at $g = 1,97$ with the line width $H_{\text{pp}} = 80$ mT indicating a strong dipolar interaction among the Cr^{3+} ions. Superimposed on it there is a sharp signal around $g = 1,9$. This signal is composed of two narrow isotropic lines with $g = 1,983$ and $g = 1,971$. In agreement with previous paper [17,18] the sharp axially symmetric signals are usually attributed to isolated, mononuclear Cr^{5+} ($3d^1$, $S = 1=2$) species and are interpreted as due to a pseudotetrahedral CrO_3 species [17].

In the studied materials differences in ion content of Cr^{3+} and Fe^{3+} were observed and heterogeneity have been linked as a possible source of cracking if the core components have not been good mixed. [19]

Comparing the results obtained by the EPR and XRF we notice discrepancies. For XRF analysis of CrO_3 phase was not detected, whereas for the EPR method, this phase has been observed for parts of the samples. It is worth mentioning a large sensitivity of the EPR method which makes it possible to detect subtle changes in content of doping as well as detecting other phases or impurities.

Conclusions

Identification of the paramagnetic complex and its surroundings based on the analysis of the EPR line shapes as well as the line positions in magnetic field was performed. The EPR lines with $g_{\text{eff}}\approx 2,0$ and $g_{\text{eff}}\approx 4,3$ in the spectra of the glass samples studied may be due the impurity Fe^{3+} ions substituted at octahedral sites.

Similarly, the EPR lines $g_{\text{eff}}\approx 1,97$ may be due to the impurity Cr^{3+} ions substituted at slightly distorted octahedral sites. Whereas for line $g_{\text{eff}}\approx 1,9$ the Cr^{5+} have been assigned. EPR spectra showed the presence of two different chromium species e.g. Cr^{3+} species in the $\text{Al}_2\text{O}_3/\text{Cr}$ sample and dispersed Cr^{5+} species.

For Al_2O_3 powders from different parts of the same size of grain different EPR spectra was obtained. As a result of the analysis the identification of existing complexes of paramagnetic ions were performed, where nanoparticles Cr_2O_3 in addition to chromium and iron were detected. Cr_2O_3 phase occurs only in the II part of Al_2O_3 powder with a particle size #200, and a small amount in mullite powder.

The EPR line near $H = 300$ mT ($g_{\text{eff}} = 3,4$) for sample #200 may possibly be related to the change the iron valence from Fe^{3+} to Fe^{2+} .



In this work high efficiency of detecting of subtle differences in the presence of certain phases in the material of the same chemical composition by the EPR method was shown. These differences have a high influence on the processes of cracking and the durability of molds.

Acknowledgements

Financial support of Structural Funds in the Operational Programme – Innovative Economy (IE OP) financed from the European Regional Development Found –Project “Modern material technologies in aerospace industry”, Nr POIG.01.01.02-00-015/08-00 is gratefully acknowledged.

References

- [1] R.M. Macfarlane: Perturbation Methods in the Calculation of Zeeman Interactions and Magnetic Dipole Line Strengths for d^3 Trigonal-Crystal Spectra, *Phys. Rev. B*, Volume 1 (1970), Issue 3, pp. 989-1004.
- [2] M.G. Zhao, J.A. Xu, G.R. Bai, H.S. Xie: d-orbital theory and high-pressure effects upon the EPR spectrum of ruby, *Phys. Rev. B*, Volume 27 (1983), Issue 3, pp. 1516-1522.
- [3] X.Y. Kuang: Analysis of the electron paramagnetic resonance zero-field splitting for Fe^{3+} in sapphire, *Phys. Rev. B*, Volume 36 (1987), Issue 1, pp. 712 -714.
- [4] D.S. McClure: Comparison of the Crystal Fields and Optical Spectra of Cr_2O_3 and Ruby, *J. Chem. Phys.*, Volume 38 (1963), Issue 9, pp. 2289-2294.
- [5] J.Y. Buzare, G. Silly, J. Klein, G. Scholz, R. Stosser, M. Nofz: Elektron paramagnetic resonance investigations of $\alpha-Al_2O_3$ powders doped with Fe^{3+} ions: experiments and simulations *J. Phys. Cond. Mater*, Volume 14 (2002), Issue 43, pp. 10331.
- [6] M.Jurczyk, J.Jakubowicz: *Nanomateriały ceramiczne*, (Wyd. Politechniki Poznańskiej, Poznań, 2004).
- [7] A.Zawada, A.Boczkowska, W.Ziemkowska, A.Kunicki, A.Pietrzykowski, A.Olszyna: Preparatyka nanocząstek Al_2O_3 do otrzymywania nanokompozytów poliuretanowych, *COMPOSITES*, Volume 6, (2006), pp. 79-84.
- [8] A.Solgała, A.Kunicki, A.Olszyna: Wpływ modyfi katora prekursora tlenku glinu na morfologię otrzymanego nanoproszku Al_2O_3 , *Ceramic Materials*, Volume 60, (2008), pp. 262-265.
- [9] Ł.Zych, K.Haberko, M.M.Bućko, P.Rutkowski, B.Trybalska, J.Piekarczyk, R.Lach: Wpływ nanometrycznych cząstek tlenku cyrkonu na mikrostrukturę i właściwości mechaniczne spieków tlenku glinu, *Ceramic Materials*, Volume 60 (2008), Issue 4, pp. 254-257.
- [10] I.Stefaniuk, P.Potera, J.Cebulski The EPR measurements of Al_2O_3 powders and mullites used in aerospace industry for cores and shapes, *Current Topics in Biophysics 2010*, vol. 33 (suppl A), 227-230
- [11] I.Stefaniuk, P.Potera, The EPR measurements of Al_2O_3 and ZrO_2 powders used in aerospace industry; IN-TECH 2011; Bratysława 1-4.09.2011, Conference Proceedings, p.516-519
- [12] A.Abraham, B.Bleaney, *Electron Paramagnetic Resonance of Transition Ions*, Clarendon Press, Oxford 1970. Reprinted in 1986.
- [13] D.L.Griscom: Electron Spin Resonance in glasses, *J. Non-Cryst. Solids*, Volume 40, (1980), pp. 211-272.
- [14] R. Berger, J.Kliava, E.M.Yahiaoui, J.C.Bissey, P.K.Zinsou, P.Béziade: Diluted and non-diluted ferric ions in borate glasses studied by electron paramagnetic resonance. *J. Non-Cryst. Solids*, Volume 180, (1995), pp. 151-163.
- [15] S.Simion, A.van der Pol, E.J.Reijerse, A. P. M.Kentgens, G. J. van Moorsel and E. de Boer: Magnetic Resonance Studies on Porous Alumina doped with Iron and Chromium, *J. Chem. Soc. Faraday Trans.*, Volume 91, (1995), Issue 10, pp. 1519-1522.
- [16] D. Tobia, E. Winkler, R. D. Zysler, M. Granada, and H. E. Troiani: Size dependence of the magnetic properties of antiferromagnetic Cr_2O_3 nanoparticles *Phys. Rev. B*, Volume 78, (2008) pp. 104412.
- [17] D. Cordischi, M.C. Campa, V. Indovina, M. Occhiuzzi, Exchange coupled CrV and MoV ions on the surface of $CrOx/ZrO_2$ and $MoOx /ZrO_2$, as investigated by ESR spectroscopy *J. Chem. Soc. Faraday Trans.* 90, 207 (1994).
- [18] Z. Zhu, M. Hartmann, E.M. Maes, R.S. Czernuszewicz, L. Kevan, Physicochemical Characterization of Chromium Oxides Immobilized at Surface Titanium Centers of Titanosilicate Mesoporous TiMCM-41 Molecular Sieves" *J. Phys. Chem. B*, 104, 4690 (2000).
- [19] I. Stefaniuk, I. Rogalska, P. Potera, D. Wrobel, The EPR measurements of the ceramics cores used in aircraft industry, II FORUM EMR-PL, Częstochowa –Hucisko 16-18 05.2012, Conference Proceedings, p.37

THE EPR MEASUREMENTS OF THE CERAMICS CORES USED IN AIRCRAFT INDUSTRY OBTAINED BY HIGH PRESSURE INJECTION METHOD

I. Stefaniuk¹, P. Potera¹, I. Rogalska¹

¹ Institute of Physics, University of Rzeszow, Rejtana 16a, 35-310 Rzeszow, Poland

Keywords: ceramic cores, electron paramagnetic resonance (EPR),

Abstract. In this work the electron paramagnetic resonance (EPR) spectra of the ceramics cores were measured. The measurements were performed at room temperature and in the temperature range from 140 K up to 380 K. The main purpose of this work was to investigate the possible relationships between EPR spectra and the size of powder grains as well as the identification of EPR spectra in view of potential application of EPR technique as a fingerprinting method. In this work, materials originate from different manufacturer were investigated. The main purpose of this work is demonstrate of relationships between impurities and cracking of cores.

Introduction

In the ceramic forms, there are several quite different from one another and having a completely different purpose coatings:

a) the first coat- this layer acts as a facing sand layer, its task is the most accurate representation of the shape model of the wax and the combating of the reaction liquid metal - ceramic form,

b) a second coat - This layer is a layer of transition between the first and back coatings

c) coating back - the main act as of these coatings is to produce mechanical strength of a form, resistance should be high enough to enable the form has not been damaged in the flooding, and yet flexible enough to ensure that during crystallization are not generated too much stress, which cause cracks in the castings. In particular very sensitive to such defects is the first coat.[1,2,3]

The problem of cracking of composite materials has been studied in detail in various works, for example in [4] describes how to produce Al_2O_3 -Fe composites by casting of ceramic masses of successive, developed for the improvement of fracture toughness. In [5] ceramics based on alumina and mullite takes into account chemical reactions have been studied and highlights the problem of cracking.

In work [6] authors presents the results of numerical calculations of temperature distribution and thermal stresses induced in the various layers and zones of samples (ceramic coating- interlayer- creep-resisting alloy) annealing in the temperature range from 200 to 1200 ° C, annealing isothermally and cooled in air, which is results allowed us to deepen the analysis of the destruction of ceramic coatings during cyclic changes of temperature.

The aim of this work is to investigate by EPR methods the role of cores and shapes of basic Al_2O_3 materials used for industrial applications.

The motivation for this study comes from the need to solve the problem of fractures of shape. In work [7] using shape criterion, the classifications of inclusions in regular composites ZrO_2 - Al_2O_3 on convex and about variable the curvature both positive, as and negative were made. The probable mechanisms responsible for appearing of inclusions with classified shape m.in. connected with shape of particles of initial Al_2O_3 powder, were showed. For the evaluations of influence of inclusions shape on evolution of crack the thermal stresses called out the maladjustment of thermal expansion coefficient of the zirconium warp and corundum inclusions the method of rank elements (MES) was used.

Experimental details

For the experiment the samples of mullgrain with different size were used. The ceramic core prepared materials by high-pressure injection method, we also studied (Table 1). For the EPR measurements the standard X-band (~ 9 GHz) spectrometer, produced in Wroclaw Technical Univeristy, with digital registration of the spectra was used. The temperature measurements were done using the digital temperature control system (BRUKER ER 4131VT), which allows the temperature range from 100K to 500K.

Table 1. The specification of the corundum samples.

Sample	Ceramic core 1	Ceramic core 2	Ceramic core 3
Qualitative analysis of phase composition by X-ray diffraction methods	SiO_2 (120 mesh) – 37,5 % mas.	SiO_2 (120 mesh) – 40 % mas.	SiO_2 (120 mesh) – 72 % mas.
	SiO_2 (milled) – 37,5 % mas.	SiO_2 (milled) – 40 % mas.	Boron glass – 3 % mas.
	$ZrSiO_4$ (300 mesh) – 13 % mas.	$ZrSiO_4$ (300 mesh) – 10 % mas.	$ZrSiO_4$ (300 mesh) -- 13 % mas.
	Al_2O_3 (325 mesh) – 12 % mas.	Al_2O_3 (325 mesh) – 10 % mas.	Al_2O_3 (325 mesh) – 12 % mas.
	SILIPLAST HO - 25 % mas.	SILIPLAST HO - 20 % mas.	SILIPLAST HO – 20 % mas.

Results and discussion

EPR spectra obtained for the ceramic cores are shown in Figs 1 and 2. In Figure 1 shows the effect of sample size influence on the obtained EPR spectrum. While in Figure 2 EPR spectra are presented for three different ceramic cores.

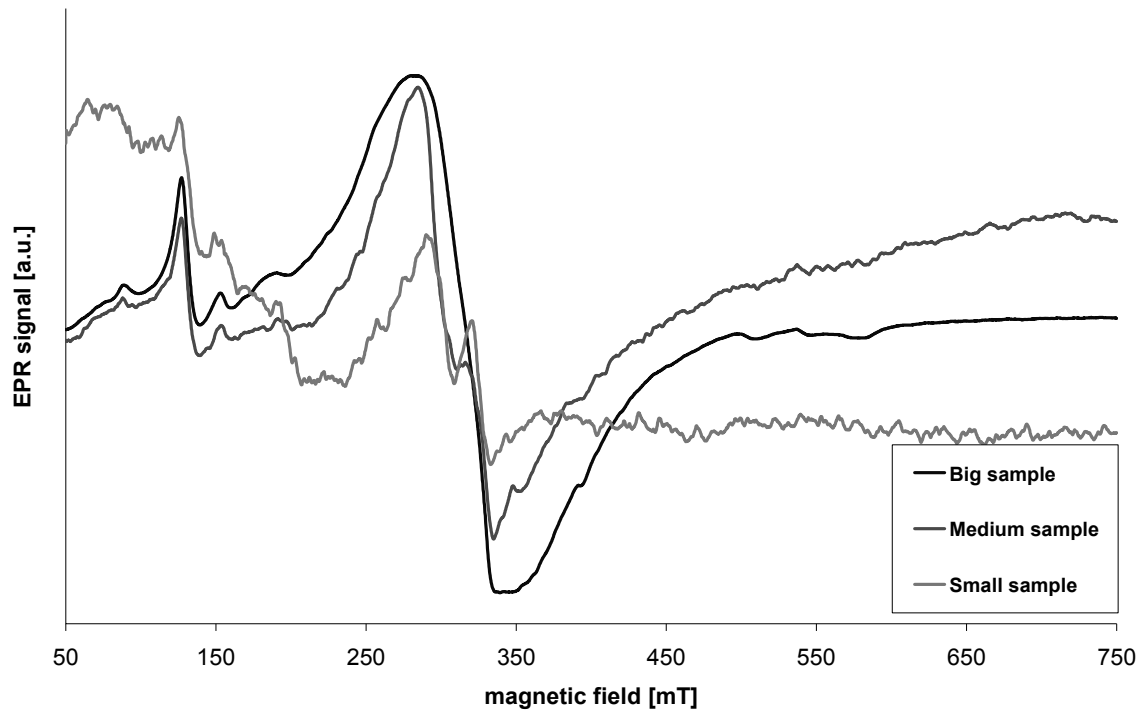


Fig.1. The dependence obtained for different size ceramic core no.1.

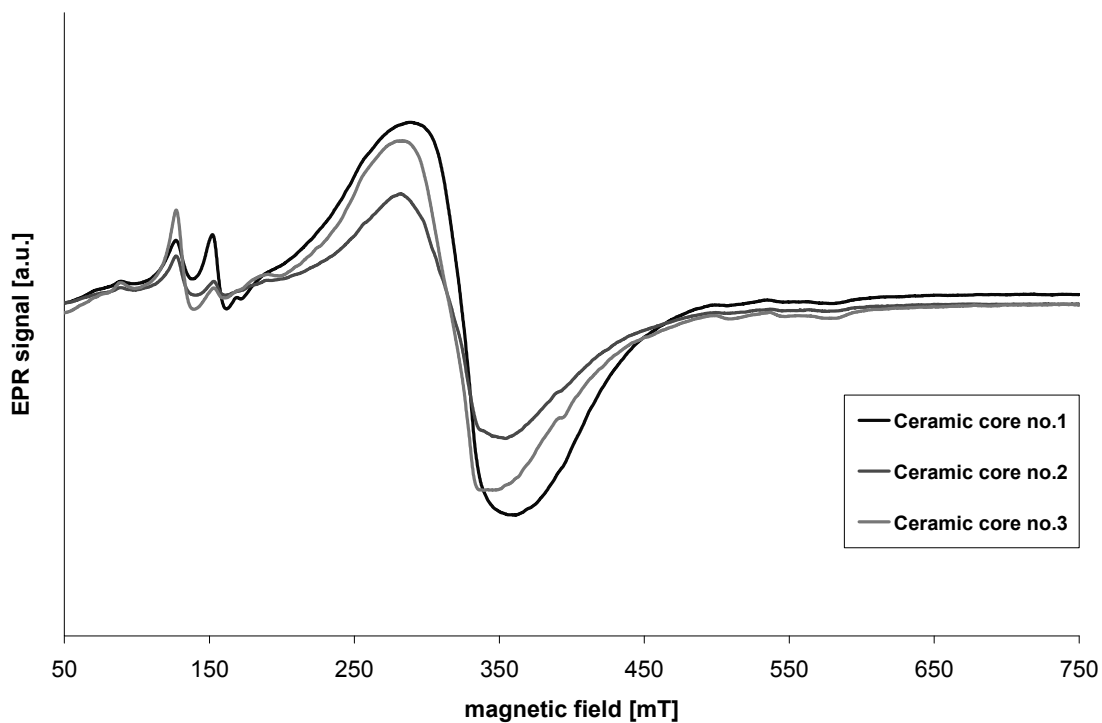


Fig.2. The dependence obtained for ceramics cores

On the Fig.1 marked lines using to the identification paramagnetic centers by arrows. The wide line near 300 mT consists of a minimum two components. They can be used for the analysis of changes in ion concentration and indirectly the component materials.

The g factor and line width with EPR spectra obtained for all the cores were measured

The analysis of the line positions suggest that the lines with $g_{\text{eff}} = 4.28$, $g_{\text{eff}} = 2.00$ may be attributed to Fe^{3+} ($S=5/2$) ions, because they present a typical spectrum for so called disordered systems [8,9], present in the glassy hosts [10]. The line with $g_{\text{eff}} = 1.98$ may be attributed to Cr^{3+} ($S=3/2$) ions in the slightly distorted octahedral sites [11].

The parameters of the line EPR, ie g factor and the width of line were obtained from temperature dependence of EPR spectra for the ceramic core. In Figure 3 shows selected EPR spectrum for the core No. 3

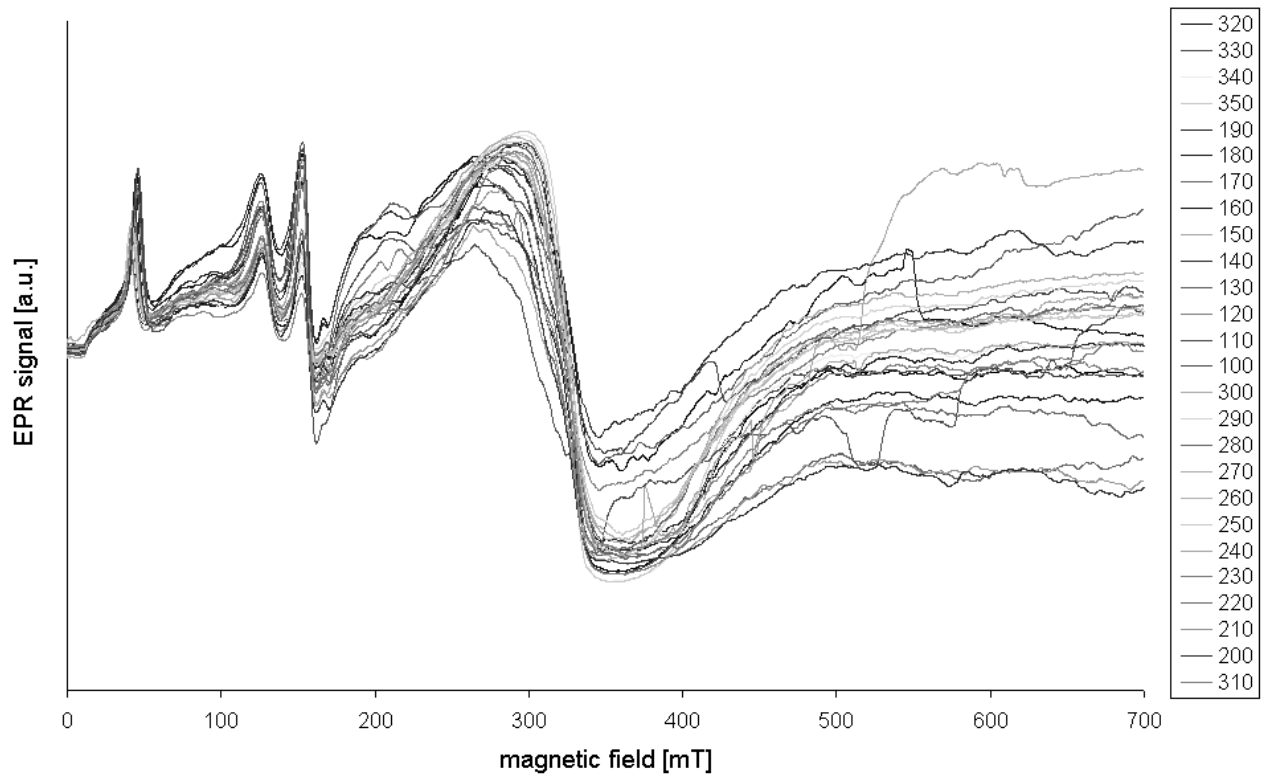


Fig.3. The temperature dependence for ceramic core no. 3.

From obtained values of the width peak to peak of the line relaxation time calculations were performed.

The estimation of the spin-lattice relaxation time T_1 can be made using the conventional method of line broadening, using the expression:

$$T_1^{-1} = 2.8 \times 10^{10} \pi g \Delta B \quad (1)$$

In the temperature range 140 – 370 K the relaxation time T_1 is governed by the Orbach process:

$$T_1^{-1} = A \left(\exp\left(\frac{\delta}{k_B T}\right) - 1 \right)^{-1} \quad (2)$$

where δ represents the energy splitting between the ground paramagnetic centers state and the first excited state, whereas A is a constant characteristic of the Orbach process (in s^{-1}).

In Figure 4 the Orbach model fit for the selected core samples have been showed. However, Table 2 shows the parameters achieving a the best fit.

Table2. Parameters obtained from model of Orbach.

Sample	A	delta
Ceramic core 1	1,19E+12	2,75E-22
Ceramic core 2	1,4E+12	2,75E-22
Ceramic core 3	1,9E+12	2,75E-22

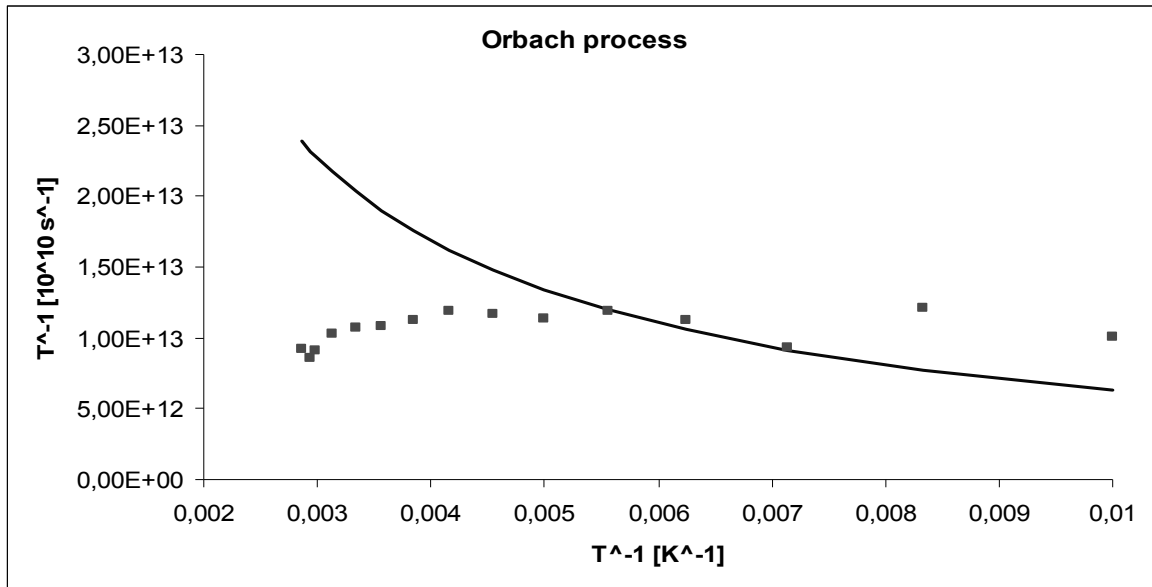


Fig.4. Temperature dependence of the spin-lattice relaxation time T_1 , of the ceramic core no.2. The solid curve is an exponential fit to the obtained data by the equation.

As shown in Figure 4 experimental points are not matched in the whole temperature range, as observed for other samples. However, for input materials (eg. mullite) for building the core were found very good agreement with the model of Orbach and is presented in our previous work [12]. While no match for the cores is associated with a combination of two EPR lines which are mutually compensate by giving no dependence on the temperature. Taking this into account it can be assumed that such compensation has a positive effect on the quality of the core, and increases its resistance to cracking.

Conclusions

Identification of the paramagnetic centers present in the examined materials having position and shape of the EPR lines have been performed.

The temperature dependence of the EPR line of the peak-to-peak (B_{pp}) line widths were also measured. From these measurement, the values of the broadening (ΔB) of the EPR line width, can be determined.

The analysis of the temperature dependence for the EPR line width in ceramic cores was performed with of Orbach process. Parameters obtained from the model of Orbach presented in Table 2. In the case of a ceramic core only part of the experimental points is related to the Orbach process.

This inconsistency with the model of Orbach is results from the deposit lines. These effects in some way may be excluded. Some overlapping sum up, others will subtract. For the mullite adjustment is consistent with the Orbach process.

Acknowledgements

Financial support of Structural Funds in the Operational Programme – Innovative Economy (IE OP) financed from the European Regional Development Found –Project “Modern material technologies in aerospace industry”, Nr POIG.01.01.02-00-015/08-00 is gratefully acknowledged.

References

- [1] D. A. Woodford, D.F Mowbray, Effect of material characteristics and test variables on thermal fatigue of cast superalloys. A review, *Materials Science and Engineering*, 1/2, (1974), 5-43
- [2] P.G. Bailey, W. H Schweikert.: HIP Improves Castings, *USArmy ManTechJournal* Vol. 5,(1980),28-32
- [3] L.A. Dobrzanski - Podstawy nauki o materialach i metaloznawstwo.(WNT, Warszawa, 2002)
- [4] A.Oziebło, K.Konopka, K. J.Kurzydłowski, M.Szafran, E.Bobryk, Odpornosc na peknie kompozytow Al_2O_3 -Fe otrzymanych metoda odlwania z ceramicznych mas lejnych, *Kompozyty*, 3, (2003), 7.
- [5] J. Stjernberg, M.-L. Antti, J. C. Ion and B. Lindblom, Lab Scale Study of the Depletion of Mullite/Corundum-Based Refractories Trough Reaction with Scaffold Materials, *IOP Conf. Ser.: Mater. Sci. Eng.* 18, (2011), 222004
- [6] K. Kobylanska-Szkaradek, J.Gryczynska, Thermal stresses in the ZrO_2 - Y_2O_3 ceramic coating Deposited by plasma spraying method on the nickel Base super –allom, *Inżynieria Materiałowa*, 3-4, (2007), 179-182.
- [7] M.M. Bucko, W. Pyda, G. Grabowski, Z. Pedzich: Wplyw kształtu wtracien na naprezenia cieplne w kompozycie regularnym ZrO_2 - Al_2O_3 , *Kompozyty (Composites)*, Volume 6,(2006), pp. 3
- [8] A.Solgała, A.Kunicki, A.Olszyna, Wplyw modyfikatora prekursora tlenu glinu na morfologie otrzymanego nanoproshku Al_2O_3 . *Ceramic Materials*, 60, (2008), 262-265.
- [9] A. Zawada, A.Boczkowska W.Ziemkowska, A.Kunicki, A. Pietrzykowski, A. Olszyna, Preparatyka nanocząstek Al_2O_3 do otrzymywania nanokompozytow poliuretanowych. *COMPOSITES* 6, (2006), 79-84.
- [10] L.Zych, K. Haberko, M.Bucko, P.Rutkowski, B.Trybalska, J.Piekarczyk, R.Lach, Wplyw nanometrycznych cząstek tlenu cyrkonu na mikrostrukture i wlasciwosci mechaniczne spiekow tlenu glinu. *Ceramic Materials*, 60, (2008), 4, 254-257.
- [11] I.Stefaniuk, P.Potera, J.Cebulski The EPR measurements of Al_2O_3 powders and mullites used in aerospace industry for cores and shapes, *Current Topics in Biophysics*, vol. 33 (suppl A), (2010),227-230
- [12] I. Stefaniuk, I. Rogalska, P. Potera, D. Wrobel, The EPR measurements of the ceramics cores used in aircraft industry, II FORUM EMR-PL, Częstochowa –Hucisko, Conference Proceedings 16-18 05.(2012), p.37



IMPLEMENTATION OF CONTENT MANAGEMENT SYSTEM FOR INSTITUTION LINUX USERS GROUP USING JOOMLA UNDER UBUNTU LINUX:

A. Mehta¹, B. Vijaykumar²

¹ Final Year CS Student, BITS Pilani, Dubai Campus, Dubai, UAE. Email: adi101010@gmail.com

² Associate Professor, CS Dept., BITS Pilani, Dubai Campus, Dubai, UAE. Email: vijay@bits-dubai.ac.ae

Keywords: Joomla, Ubuntu, Linux, website, users, group.

Abstract. The functions discussed in this paper will assist web users in the design and development of a website using the widely used Content Management System (Joomla) to host reference material for the Institution Linux Users Group. It also deals with the steps to host instructions and updates related to Linux for new and regular users. This website can be very beneficial for Institution Linux Users Group as it will be a Centre for all the information regarding the activities in university and also around the world. This will make the group more connected and popular among regular and new users. This will drastically reduce the work done earlier by its members to stay connected and to share information and ideas. This can help the user to improve skills in LINUX application development, utilize the low cost, reliability and expandability of LINUX, provide guidance for setting up LINUX Systems and to get upgraded with LINUX Technologies. It will facilitate and focus knowledge regarding not just Linux but also about Free and Open Source software and other things of equal interest. An user friendly and interactive website can improve awareness among all students within the university as well as within the region.

The paper describes the main features, important concepts and basic components of Joomla and how they can be used to create a website for the institute Linux users group in the Ubuntu-Linux environment. Further the customization of the template is also discussed.

Introduction

Linux Users Group

A Linux Users Group (LUG) or GNU/Linux Users Group (GLUG) is non-profit organization that provides information, support and educates both regular and inexperienced Linux Users. Such a group can be within an organization that meets at regular intervals or in form of online support groups spread over a wide area. The main agenda of these meetings/discussions is to discuss Linux and other open source technologies.

To give just one indication of how LUGs differ from traditional user groups: Traditional groups must closely monitor what software users redistribute at meetings. While illegal copying of restricted proprietary software certainly occurred, it was officially discouraged -- for good reason. At LUG meetings, however, that entire mindset simply does not apply: Far from being forbidden, unrestricted copying of GNU/Linux should be among a LUG's primary goals. In fact, there is anecdotal evidence of traditional user groups having difficulty adapting to GNU/Linux's ability to be lawfully copied at will. [1]

Install fests are organized by many LUGs so that the novice users can get help and guidance from experienced users in installing and configuring Linux Systems.

A LUG website will generally have the following sections: About Us, News, Events, Links, and About Linux.

Joomla

Joomla is a widely used content management system (CMS), which enables the user to build Web sites and powerful online applications. Many aspects, including its ease-of-use and extensibility have made Joomla the most popular Content Management System available. Best of all, Joomla is an open source solution that is freely available to everyone.

Joomla is designed to be easy to install and set up even for new users. Many Web hosting services offer a single-click install, which helps the user to get the site running in just a few minutes. Then, with a minimal amount of instruction, clients can be empowered to easily manage their own sites. If the clients need specialized functionality, Joomla is highly extensible and thousands of extensions (most for free under the GPL license) are available in the Joomla Extensions Directory. [2]

Features of Joomla

Joomla has a back-end administrator panel which helps in managing the front-end website. The features it offers display the power of Joomla. Following are some of the main features of Joomla that prove its extensibility; all of these can be accessed by the Joomla administrator Panel.

1. *User Manager:* Joomla has a registration system that allows users to configure personal options. There are nine user groups with various types of permissions on what users are allowed to access, edit, publish and administrate. Authentication is an important part of user management and Joomla support multiple protocols, including LDAP, OpenID, and even Gmail. This allows users to use their existing account information to streamline the registration process. [3]
2. *Language Manager:* Helps in managing the language of the website as well as the administrator panel. Also, both of them can be used in different languages.
3. *Media Manager:* Helps in uploading and organizing media files.

4. *Menu Manager*: Helps in creating of the menus and sub-menus needed by the user. The user can define the menu hierarchy according to the requirements.
5. *Article Manager*: Helps to add and manage all of the articles of the website. It also includes a WYSIWYG Content Editor for editing articles just like editing articles in a word processor.
6. *Category Manager*: It shows a list of categories defined on a website.
7. *Extension Manager*: Manages all the third party extensions that can be put on the website for example, hotel reservation extension, search engine optimization tools, file management etc.
8. *Template Manager*: Helps in assigning and modifying the template of the website as well as the administrator panel.

Web Design Process in Joomla

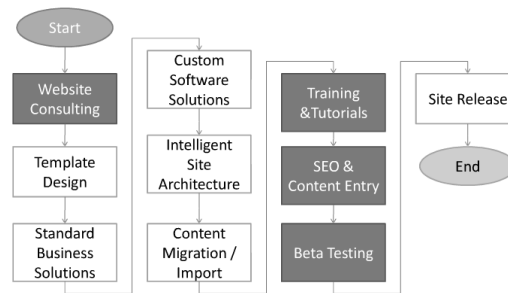


Fig. 1 Joomla Design Process Phases [4]

The Web Design Process in Joomla starts by *Website consulting* phase, in which the full project stages are defined and explained. The next phase is *Template Design* in which the template of the site is designed according to the images that have been approved; the *Standard Business Solution* phase involves installation, configuration and personalization of the Joomla, its extensions and its components. *Custom Software Solutions* Phase involves adding extensions that were specifically created for this website. The *intelligent site architecture* phase helps in building the site outline and organizes its content.

Content Migration Phase involves porting the customer database into the website from a spreadsheet or other CMS's. Next the *Training and tutorial* phase deals with training the customer about the working of the website, *SEO and Content Entry* optimizes the site for search engines like Google, bing etc., and finally *Beta testing* is done before releasing the site.

LAMP Stack

To run a Joomla website on Linux we need something called as a LAMP Stack. LAMP is an acronym for a solution stack of free, open source software, referring to the first letters of Linux (operating system), Apache HTTP Server, MySQL (database software) and PHP (or sometimes Python), principal components to build a viable general purpose web server. [5]

Website Development

Installing a Template

After downloading the template from a source, it needs to be installed in the Joomla website.

Step 1: Go to the siteaddress/administrator

Step 2: Enter the User Name and Password in the Joomla Administration Login Screen

Step 3: From the Control Panel go to the Extension Manager and in the Upload Package file area select the template file (.7z or .rar) to be installed.

Step 4: After Template is installed go to Template Manager and make the newly installed template default by clicking on the star next to it or the make default button on top.

Creating a Category

The next step would be to create category in which the articles can be placed and distinguished.

Step 5: Go to Category Manager -> Add new Category

Here we can create new categories.

Create and article

In this step we will create an article.

Step 6: Go to Article Manager-> Add new Article

Now we get a new screen as in Figure 2, in this we simple enter the title, category that we created in previous step, then we can either compose the article with the editor given below or use the html editor.

Creating a Menu

After creating an article, we will create the menu item in which it has to be displayed.

Step 7: Menu Manager -> Add New Menu

Step 8: After creating a new menu we will create Menu Items.

The menu items can be of a varied nature like:

Contacts - list all contact categories, list contacts in a category, single contact, featured contacts.

Search - search, search form or search results

Web links - list all web link categories, list web links in a category, submit a web link

Articles - archived articles, single article, list all categories, category blog, category list, featured articles, create article

Newsfeeds - list all news feed categories, list all news feeds in a category, single news feed

Users Manager - login form, user profile, edit user profile, registration form, username reminder request, password reset

Wrapper – iframe wrapper

System Links – external URL, Menu item alias, text separator

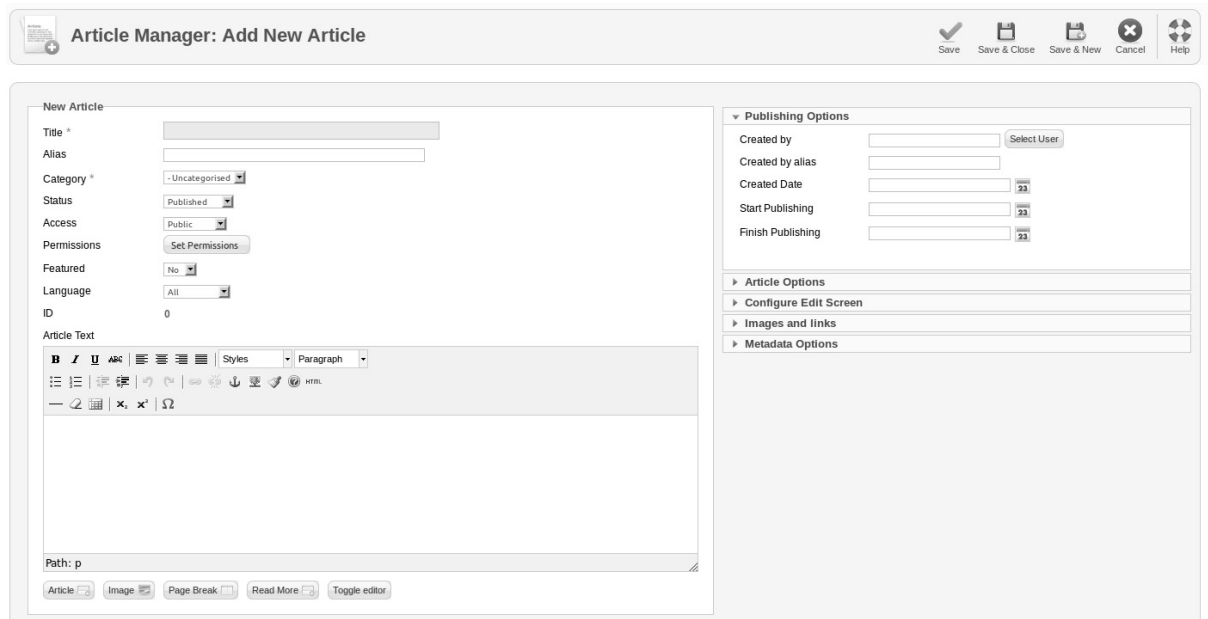


Fig. 2 Article Manager: Add New Article

Creating a Module

In this step we will create a module.

Step 9: Go to Module Manager-> Add New Module and select the type

Following are the default module options:

Archived articles, articles category, articles - related articles, breadcrumbs, feed display, language switcher, latest users, menu, random image, search, statistics, web links, wrapper, articles category, articles - newflash, banners custom HTML, footer, latest news, login, most read content, smart search module, syndication feeds and Who's online.

Apart from these default modules if any custom or third party modules were installed they will also be shown in the list. After selecting the type of module we can customize the module in any which way we want.

Template

One of the following methods can be used to create a Template.

1. Starting with one of the default templates that come with Joomla
2. Choosing a template that looks similar to what is desired and then tweaking it with custom logo and colors.
3. Starting with a skeleton template that has all the mechanisms but no formatting – easily available on the Internet.
4. Starting from the scratch and building a totally custom template, this would consume more time but the desired result will be what was needed.

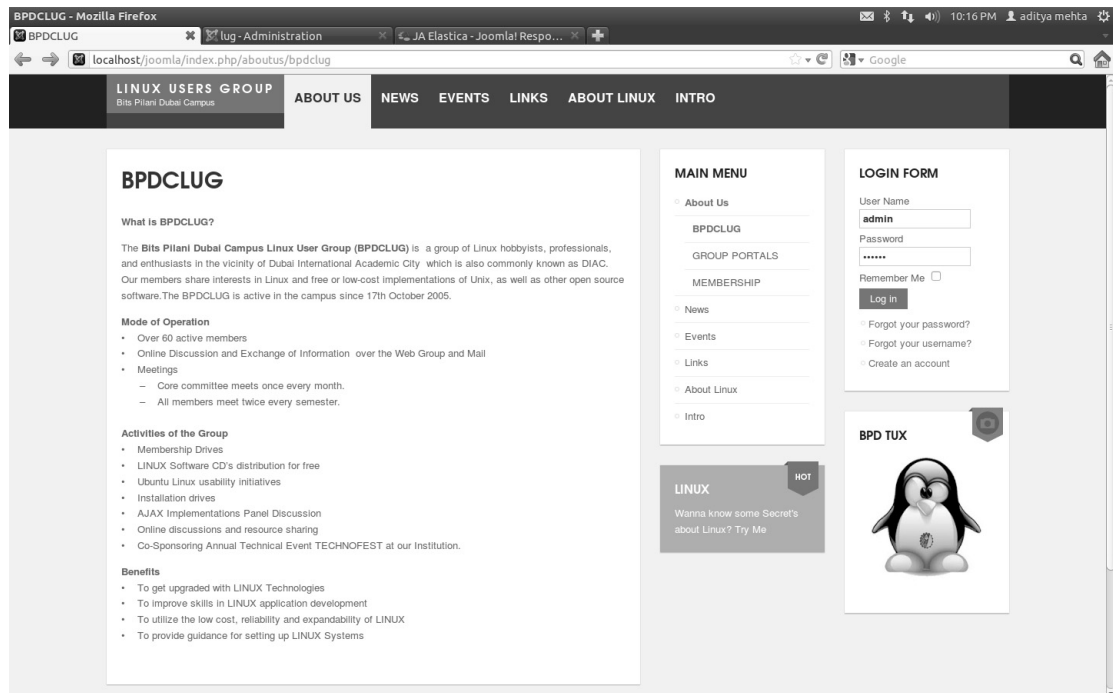


Fig. 3 Template – JA ELASTICA for Institution Linux Users Group

Figure 3 shows the final Joomla Website created for my institution. This template shows on the left hand side the big text box, on the right hand side we can see four different modules and on the top is the main menu bar. The website is built using a template called JA ELASTICA. Built upon JA's robust JAT3 2 Framework and jQuery Masonry script, JA Elastica works well and fits well on all the web enabled devices and mobile browsers [6].

Conclusion

This website will definitely benefit the institution Linux Users Group in creating awareness about Linux and its benefits easily and securely. Using Joomla for this project will help maintenance and modification of the website easy for the administrator. This website will help in centralizing all the information related to the LUG, and help the members work more effectively and efficiently. This website will facilitate resource sharing which can be very useful for Linux Users.

Linux in itself is a very powerful, customizable and secure Operating System. It is developer friendly as a lot of discussions and forums already exist and since it is open source, getting the resources is easy and free.

Acknowledgment

The authors are grateful to the IN-TECH 2012 reviewers and organizers for their valuable suggestions in improving this Paper.

References

- [1] Linux User Group HOWTO, "A guide to founding, maintaining, and growing a Linux User Group", <http://tldp.org/HOWTO/User-Group-HOWTO-2.html>, June 2010 [June 24, 2012]
- [2] Joomla, About Joomla, *What is Joomla?*, <http://www.joomla.org/about-joomla.html>, [June 24, 2012]
- [3] Joomla, About Joomla, *Features Overview*, <http://www.joomla.org/core-features.html>, [June 25, 2012]
- [4] O. Nikolic: *Joomla Design Process Phases*, <http://www.slideshare.net/ogosen/ten-steps-of-a-modern-joomla-web-design-process>, [June 25, 2012].
- [5] J. Lee, B. Ware: *Open Source Web Development with LAMP: Using Linux, Apache, MySQL, Perl, and PHP* (Pearson Education, Boston, 2003).
- [6] E. Andrea: *Responsive Design and Joomla Templates*, <http://www.ostraining.com/blog/joomla/mobile-ready-joomla-templates>, February 2, 2012 [June 25, 2012].



DEVELOPING AN IOS APPLICATION FOR RESTAURANT MENU CARDS:

A. Mehta¹, D.V. Prasad² and C. Cleetus³

¹ Final Year CS Student, BITS Pilani, Dubai Campus, Dubai, UAE. Email: adi101010@gmail.com

² Associate Professor, EIE Dept., BITS Pilani, Dubai Campus, Dubai, UAE. Email: prasad@bits-dubai.ac.ae

³ Founder and CTO, Xuslimits Technologies Pvt. Ltd., Kerala, India

Keywords: restaurant, mobile, application, iOS, menu card, view

Abstract. Application Development for mobile devices is an area that is developing at an exponential rate. Every regular or a new developer is focusing on application development as the use of mobile devices is increasing day by day. As, the mobile devices, phones or tablets, are dubbed, to be the future of technology, mobile application development becomes a necessity for a developer.

An Apple iOS application “Let’s Order” was developed which to provide the takeaway menu cards for the entire restaurant within a region or location. “Let’s Order” will change the way a user orders food. Before the user orders the food he will have a clear picture of what he is ordering. It has been designed with utmost simplicity keeping in mind the user and what the user really wants from a Menu Card Application. It has been made with an aim of replacing the takeaway menu cards with this easy to use application and gives the phrase “Let’s Order” a totally different meaning. The paper describes the application development process, the User Interface Elements of Xcode (Apple Integrated Development Environment), application structure and the application views with the header and implementation files. Further the interface development is also discussed.

Introduction

Apple’s mobile devices have been a huge success since the time when they were launched in 2007 with iPhone to now with the recent launch of the new iPad. Their mobile operating system has also come into its sixth generation with the recent launch of iOS 6. With the evolution of the iOS there have been a lot of new features over time that have created a loyal line of developers dedicated to building iOS applications. Also, it has become easier for the new and novice application developers to adapt to apple development process and environment. Since apple is growing day-by-day so are its users and so are its developers.

Let’s Order is an app that basically provides the takeaway menu cards for the entire restaurant within a region. The user can either select the region of which he wants the menu to be shown or directly search for a particular restaurant within a region. This app gives detail information about the Restaurant and also gives detail information about *each* and *every* item on its menu card. It is even better than ordering when in a restaurant as the printed restaurant Menu Cards don’t necessarily show the picture of the menu item whereas Let’s Order shows the user exactly what he is ordering.

Some of the features of the app include: easy to use interface, big wide buttons for the ease of touch; no clutter on the screen: simple and easy transition from one screen to another; since the App has a multiple drill down structure, it has been provided with a home tab bar option to directly take the user to the first screen to start all over again; in-app calling feature; *around me*: a special feature which gives the user a random suggestion around their location.

Literature Review

Pilone and Pilone in this book has described clearly the process of iPhone development inform of adequate examples like the drink mixer app and many more. It uses simple language, simple examples and good analogies. So, the book has been written for simple and new user may or may not have coding experience. The way of explaining the user with such amazing graphics and real tie examples makes this book one of its kind.

The iOS apprentice tutorials have been specifically designed to help start people learn about the new iOS 5 and work with features like storyboards. The examples explained in these tutorials are adequate and help the user understand iPhone and iPad development for iOS 5. Hollemans has explained the new features extensively with examples. The full process is explained with the help of apps, starting from the most basic hello world app to apps involving GPS (Global Positioning System).

iOS vs. Other Platforms

One of the big questions is why develop for iOS when there are other platforms such as *Android*, *blackberry OS*, *Symbian*, *Windows Phone* etc.

The reason is *Apple*. Apple products are no doubt the best products maybe not price-wise but quality wise. The user enjoys using apple products because of the smooth touch, amazing software and the quality of the content in it. Also Apple is always developing its products i.e. hardware as well as software. The *quality* is the main reason why apple products work.

In comparison to Android, Android has some advantages over iOS like there is no approval process anybody can put up an app on Android Market, which makes it easier for the developers, but as a result the quality of the Market goes down which directly affects the User. If the user is not happy with the product/ quality of apps then he might want to shift to other platforms. Although Apple has some set of restrictive rules but those rules are what make the products stand-out. Still android is the biggest competitor for apple iOS but when it comes to quality apple iOS stands-out.



Methodology

The App Development Process

Building an app for the app store is basically divided into 4 steps, which help the developer or a developing organization to branch out there development process. With these steps the development of an apple app can be made easier for the developer.

Preparing the Development Team

One-person signs up as a team agent and in the process create a new development team. Then, the team agent can invite other people to join the team and set their access privileges. Finally, the team sets up signing certificates and other resources necessary for developers on the team to sign apps. [1]

Configure the Project

The next step is to create a new Xcode project for the app. Then choosing an Xcode template that most closely corresponds to the kind of app wanted and customizes the initial settings for the app. Also, other items required to sign and publish the app should be created.

Depending on the design of the app and the services planned to be used in it, other kinds of app configuration must be set up. Some Apple technologies require a combination of written code and data configured to operate properly. For example, Apple Push Notification Service requires to create special certificates used to authenticate the server to the push notification service. If push notification is to be used in the app, then these push notification certificates should be created during this step. [1]

Develop the App

Designing user interfaces and functionality, implementing those ideas in code, and testing the resulting app to ensure it works correctly. While a lot of this work is programming, this step also includes other important tasks, such as creating data assets used by the app. These assets, including but not limited to icons, sound files, and artwork, are used directly by the app or by the operating system on the app's behalf. Many assets need to be localized into other languages or locales; an important part of designing the app is planning for the assets to be created and knowing which assets should be localized. [1]

Publish the App in the App Store

Publishing an app on the App Store requires a few administrative tasks. The development team provides the information displayed for the app by the App Store. Then the app should be submitted to Apple for approval. Once the app is approved, the date the app should appear for sale in the App Store should be set. Then, Apple's tools are used to monitor the sales of the app, customer reviews, and crash reports. These data can be useful to prepare bug fixes and decide on what improvements to make in a major revision to the app. When there is a bug fix or a major revision ready to ship, it should be sent for approval and a publication date should be set, just as was done for the initial release. [1]

Each of the following described views has a header and an implementation file. The header file describes the interface for the classes in the project and the implementation file has the basic implementation files of the app. [2]

Emirate Selection View - ① (Fig. 1)

Creating a Single *Table View Controller* containing the four options that is the four emirates of United Arab Emirates that are Sharjah, Dubai, Ajman and Abu Dhabi started the app development stage of "Let's Order".

The basic function of this view is to let the user select the emirate in which he tends to order. Each row has been customized so that it fills up the view. The arrow in each tab is called a disclosure indicator, which shows that there is a right to left transition of the view when the row is tapped.

The three tab bar buttons at the bottom are Home, Theme and About Us options. The Home button brings the user to the emirate selection view from anywhere in the App. The About Us button takes the user to the About Us view and the theme button takes us to the Theme View.

At the top is the status bar of iOS, which displays the time, battery and carrier. Below the status bar is the Navigation Bar, which displays the name of the App.

The Menu Options View - ② (Fig. 1)

This View/Screen/nib gives the user three options: a menu option that will take the user to the area nib, a search option with which the user can search among the restaurants within the selected emirate and *around me* is a unique feature of this app that leaves the selection of the restaurant to the app i.e. it gives a random restaurant suggestion.

As the previous view this view /nib also contains a status bar, navigation bar. But on the navigation bar there is a back button this time, this back button helps the user to go back to the emirate selection view.

Area View - ③ (Fig. 1)

This is a simple table view that lets the user select the region within the selected emirate. The User Interface in this view consists of the previously mentioned Navigation Bar, the Back Button, Table View and the three tab bar buttons.

Restaurant List View - ④ (Fig. 1)

This view lets the user select a restaurant of choice, whose detail view will be displayed on selection.

The row of this table comprises of four components that is a picture, a subtitle, a title and a disclosure indicator. It also has a Search Bar in black that is governed by an algorithm, which helps in character-by-character search just like the Google search.

Restaurant Detail View - ⑤ (Fig. 1)

This view shows the details of the restaurant. The detail like the *address*, *timings* and it also has a special button to display the *in app calling feature* via an *actionsheet*.

It has two text boxes: one for address and one for timings. Four text labels: *title*, *subtitle*, *address*, and *timings*. It has two buttons one is "Menu" which takes the user to the menu categories and the other being Call, which gives an actionsheet displaying all the numbers of that restaurant. The actionsheet incorporates the in-app calling feature. In addition to these elements it also has the elements from the previous views i.e. navigation bar, tab bar, status bar.

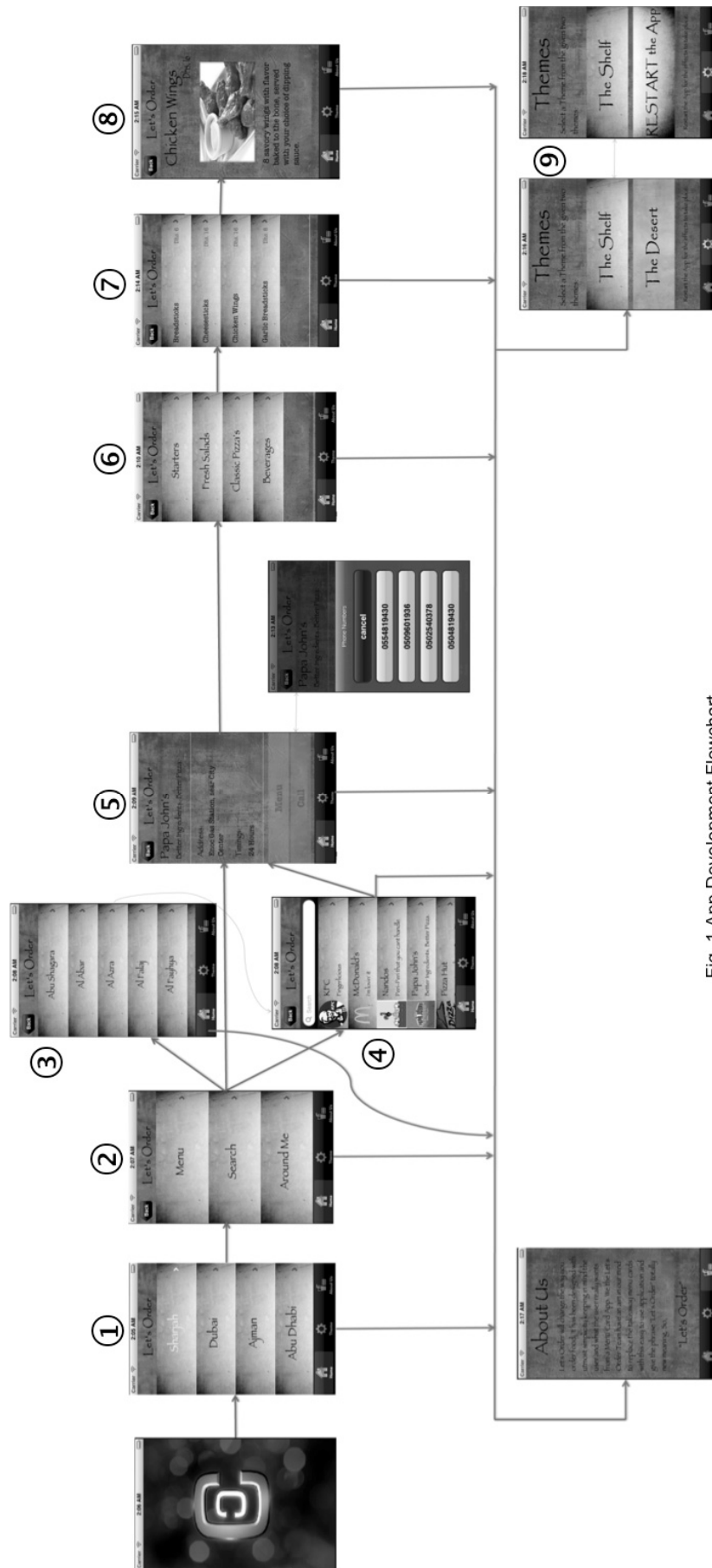


Fig. 1 App Development Flowchart



Menu Category ⑥, List ⑦ and Item Detail Views ⑧ (Fig. 1)

The *Menu category view* is just a simple table view which has been already been discussed earlier, so is the *Menu List view* but just with a small difference that is the right detail in the row which displays the price. The *Item Detail view* displays the item details with a picture, details and description of the item. The *Item Detail view* has a UIImage Element and a UITextView element and two labels.

Theme View ⑨ (Fig. 1)

The Theme view has a text label and has two buttons one for each theme and the user gets to select which theme he wants to use. As soon as a button is tapped *Restart the App* text is shown. Since the theme is a major change in the interface, it will only be applied once the app is completely shut down and started again.

Main Storyboard: The Nib Structure

A storyboard is a visual representation of the user interface of an iOS application, showing screens of content and the connections between those screens. A storyboard is composed of a sequence of scenes, each of which represents a view controller and its views; scenes are connected by segue objects, which represent a transition between two view controllers. [3]

Besides the View Controllers (explained above) there are two other controllers called the Navigation Controller and the Tab Bar Controller.

Navigation Controller

UINavigationController is a specialized view controller that manages the navigation of hierarchical data. It creates and manages a UINavigationController, and it manages view controllers using a navigation stack. You add view controllers to the stack by pushing a view controller onto the stack. Pushing the view controller will cause its view to display since it is the top view controller on the stack. When you pop a view controller from the stack, the topmost view controller is removed and the new topmost view controller is displayed. You can programmatically pop view controllers from the stack, or UINavigationController will do it for you when the user taps the left (back) button on the navigation bar. [4]

Tab Bar Controller

Applications use tab bar controllers to manage multiple distinct interfaces, each of which consists of any number of custom views and view controllers. For many applications the UITabBarController is used to provide all of the views the user sees. As in our application there are three buttons on the tab bar i.e. home, Theme and About Us. [5]

Conclusion

Objective C is a very advanced and a very unorthodox computer language. The learning curve for Objective C is much greater than any other language as the syntax and interaction with the objects is totally different from other languages. But once understood it can be a very lethal language as it is very powerful. Also most of the syntax resembles normal English language. Development for an iOS device is not hard when the elements are understood properly. Let's Order is a commercial app, which will provide all the restaurant menu cards at one place, replacing a drawer full of menu cards.

This app makes us learn the application development process, how mistakes are corrected, the designing process and also the made us understand that languages may differ but the logic behind everything is same. The world is moving towards app development be it any platform. All the big companies are now giving more effort in app development like Google has a chrome web store, android has a market, apple has app store, blackberry has an App World, Nokia has a Ovi Store etc.

So App development is the new field people should look up to, as everything in the coming future will be controlled by apps.

Acknowledgment

I would like to express my heartfelt gratitude to Dr. R.K Mittal, Director Bits Pilani, Dubai who has given us an opportunity and platform to conduct my research. The authors are also grateful to the IN-TECH 2012 reviewers and organizers for their valuable suggestions in improving this Paper.

References

- [1] OSX developer Library, "Building an app for the app store", <http://developer.apple.com/library/mac/-documentation/General/Conceptual/ApplicationDevelopmentOverview/BuildinganApplicationfortheAppStore/BuildinganApplicationfortheAppStore.html>, January 9, 2012 [June 24, 2012]
- [2] D. Pilone, T. Pilone: *Head First iPhone Development* (O'Reilly Media, California, 2009).
- [3] OSX developer Library, "Storyboard", <http://developer.apple.com/library/mac/-documentation/General/Conceptual/Devpedia-CocoaApp/Storyboard.html>, October 3, 2011 [June 24, 2012]
- [4] K. Turner, T. Harrington: *Learning iPad Programming: A Hands-On Guide to Building iPad Apps with iOS 5* (Pearson Education, Michigan, 2012).
- [5] OSX developer Library, "Tab Bar Controllers", <http://developer.apple.com/library/ios/-DOCUMENTATION/WindowsViews/Conceptual/ViewControllerCatalog/Chapters/TabBarController.html>, February 16, 2012 [June 25, 2012]
- [6] M. Hollemans, *The iOS Apprentice: Learn iPhone and iPad Programming via Tutorials!*, [November 2011]

POLI_ENERGY: EFFICIENCY AND SUSTAINABLE ENERGY FOR INDUSTRY

J. Galvão (PhD)^{1,2}, L. Moreira (MSc)¹, E. Silva (BSc)¹, M. Neto (BSc)¹

¹ Electrical Engineering Department, ESTG, Polytechnic Institute of Leiria, Portugal

² INESC Coimbra, Delegation in Polytechnic Institute of Leiria, Portugal

Keywords: rationalization, environmental impact, energy efficiency, installation audit

Abstract. Energy efficiency can be defined as a set of actions that lead to the optimization of energy consumption needs, while maintaining the level of customer satisfaction. This involves a more rational use of energy and the adoption of best practices in various sectors: transport, industry, commerce, buildings (services and residential), and other municipalities [1]. Moreover, energy efficiency can involve the use of cleaner energy sources for the environment compared with other that many countries use intensively nowadays!...

Energy efficiency is not confined to demand management of energy it can be applied to the production, transport and distribution of energy. Thus the Directive 2002/91/EC on the EU (European Union) Energy Performance of Buildings is a document that demands the member states for energy certification systems in buildings and, therefore, determining their energy class [2]. It is also a key document for the development of energy efficiency activities of the EU in order to achieve the goals of the Kyoto Protocol.

The main objective of this work is to develop an energy model for a small export plastics industry (case study) that may lead to further rationalization of consumptions, with environmental advantages (less greenhouse gas emissions). This may grant access to eco - sustainable certifications/awards, as a factor of competitiveness, as well as economic benefits. The methodology followed in designing the new energy model, started from an energy audit to characterize the existing consumptions and use of energy.

Introduction

The Poli_ENERGY project aims to raise standards of energy efficiency of a case study and develop a methodology for applying the principles of the policy governing this issue, transverse to different sectors: housing and industrial buildings and the activities inside. Also intended to be a model for other similar industries, to meet European legislation and best practice environmentally sustainable energy. A significant part of this project and which has been proposed to the company management is the production of electrical energy for supply the lighting part by means of a photovoltaic system, due to the amounts involved are relatively low, in relation to the total energy consumption involved in this industrial activity [3], [4]. On the other hand, the availability of radiation of the case study geography place has capacity of solar radiation, which makes viable, in medium term the investment on this system.

Energy Policies and Measures

With this research it is also intended that the national program which implements these requirements for greater energy efficiency that is the 20/20/20 Plan is more easily assimilated by the various economic and industrial players. This 20/20/20 Plan provides for the EU by the year 2020 one cut in GHG emissions of 20%, a share of 20% of energy from renewable sources and a 20% increase in efficiency energy [5], [6], [7].

This objective result in Portugal the program ENE 2020 (National Strategy for Energy, with the 2020) which serves as a guide in implementing the European policy, to lead to the execution of these actions and has the main ideas to accomplish are the following:

- Being an agenda for competitiveness, growth and energy independence and financial; Investing in renewable energy, promote energy efficiency, ensure security of supply; Sustainable Energy Strategy for the purpose of achieving some of the following goals;
- Reduce energy dependence to the outside of Portugal to 74% in 2020, producing, on this date, from indigenous resources, equivalent to 31% of final energy;
- Implement commitments taken by Portugal in the context of European policies to combat climate change, allowing, in 2020, 60% of electricity produced from renewable sources has and final energy consumption is reduced by 20%;
- Promote sustainable development by creating conditions for achieving the emissions reduction targets assumed by Portugal in the European context.

With this number of shares present and the emerging importance of this area is of high potential.

Research Developed Methodology

The energy audit plays a key role in defining and establishing the plan of action, which gives a deep knowledge of the facility analyzed, in order to detect, quantify, and try to correct the existing energy losses [8].

The audit procedures depend on the scope thereof, as well as the size and type of the audit facilities. In general one can consider the following steps: Planning; Fieldwork; Data processing; Preparation of Report.

Briefly, an energy audit to a facility energy consumer has the following objectives: Quantify the consumption and costs by type of energy; Examine how energy is used at the facility; Relating energy consumption to production, an indicator determining energy of great relevance, the specific energy consumption; Determine the energy consumption by sector, process or equipment; Examine in detail how energy is used; Identify situations of wasted energy; Propose corrective measures and analyze the technical and economical viability of the proposed measures; Propose, if not yet exist, an organized energy management system.

Features of Case Study

The TECTIL, Ltd company (case study) produces and sells retractable and non retractable plastic films, leaf, open and closed sleeves and bags, of several measures, mainly under direct order of the customer. This company has clients in many different industries and countries. It has customers in the beverage industry, soft drinks, coating, electrical equipment and retailers. It is located in one industrial area and occupies a covered space of 2800 m². The facilities consist of the production areas, storage and administration offices. The production is made by several machines (several extruders, one co-extruder, cutting machines and the compressed air system). The production process is a continuous cycle, ie, the company starts operating on Monday morning and shuts the production on Friday afternoon.

In 2005 obtained certification under ISO 9001 "Conception and Development, Production and Marketing of Film, Polyethylene Bags and Sleeves".

Electrical Installation

The company owns a LV costumer substation that is fed by an aerial 30 kV line. The substation has a transformer of 630kVA - 30/0.4kV, which will supply the LV main switchboard located inside the company, more precisely within the industrial building.

From this switchboard, the energy is distributed to other partial switchboards spread by the facilities. In the main switchboard is guaranteed differential and over current protection of each electrical circuit. These switchboards are one for each machine in production area, compressors and pumps and administrative area. In addition, the main switchboard includes the illumination of the industrial building and general use outlets (single and three phase).

Partial switchboards for each machine, ie, the six extruders, one co-extruder and three cutting machines, in addition to the electrical feeders and respective protection, contain all types of instrumentation and automation associated with each machine. Electrical switchboard installed in administrative area, allows the control of lighting and outlets for general use areas of administration, boardroom, accounting, dining room and other facilities.

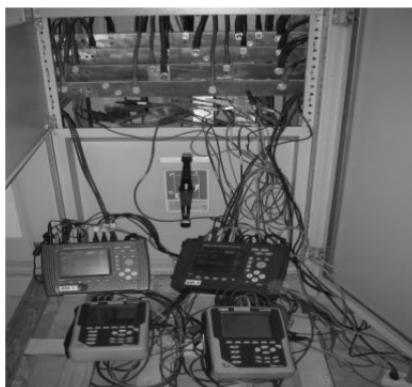
The electrical switchboard feeds two compressors, a dryer (for compressed air), two air pumps for raw material suction and distribution for production machines and single phase and three phase outlets for general use.

Energy Audit for Energy Consumption Characterization

The characterization and understanding of the energy in a variable energy consumer installation is based on energy audit [9], [10]. This consists of several aspects that will allow us to identify critical parts of this facility and should be improved in order to achieve a higher level of performance. In this context, the energy facilities and activities associated with him were characterized. Every energy consumption was analyzed, discriminated by energy source. Electricity is the sole form of used energy. Besides energy use, the extrusion machines present in the production area, the building structure and materials (walls, roof, warehouse and office) were also analyzed. The energy audit of all sectors and all forms of energy, and its realization requires knowledge in the following areas: electrical, mechanical and environmental of the building.

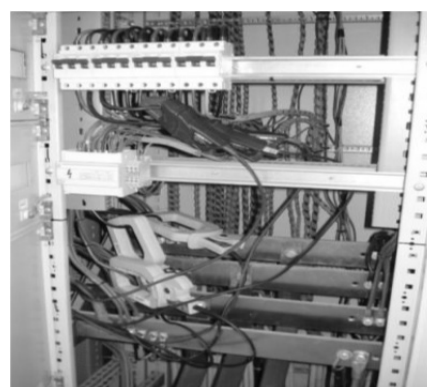
Thus, energy audits allow you to provide specific information and identify the actual energy savings, consisting primarily of an examination critical of how energy is used based on the records as much as possible stringent consumption and costs.

There will be an energy analysis in the context of an audit case study, leading to the characterization of energy consumption in recent years, through the values of existing energy bills from the utility and notably in 2011 and 2012 with various monitoring and data records using several energy analyzers shown in Fig. 1 a), b). Data recording campaigns were carried out over one week in December 2011 (winter period) and another week in May 2012 (almost summer period). The data collected (by energy analyzers and energy bill analysis) was thoroughly analysed, leading to a remarkable information volume. Some relevant information is depicted in the following Figures. Fig. 2.b) shows the consumptions disaggregated by fares (peak hours; half-peak hours; normal off-peak hours and super off-peak hours) and Fig. 2.a) shows the recorded daily consumptions. The Fig. 3.a) and b) depict the specific energy consumption of the process and Fig.3.a) shows the electricity use per unit of production (kWh of electricity per kg of plastic produced). Later, some measures were proposed in order to increase efficiency and reduce energy bills.



a)

Fig. 1 a) The four energy analyzers connected to the electrical entry box of case study industry.



b)

b) The clamps connection detail of analyzers for electric currents measures.

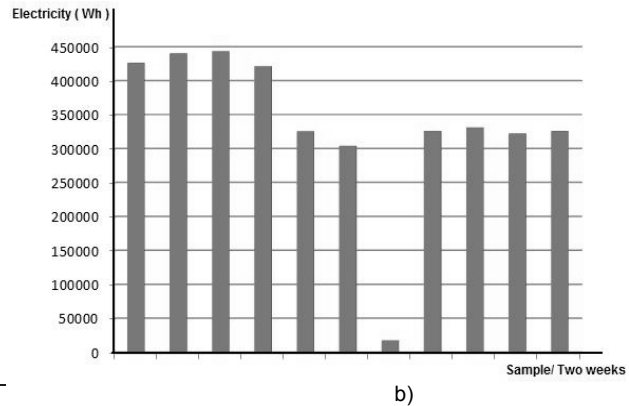
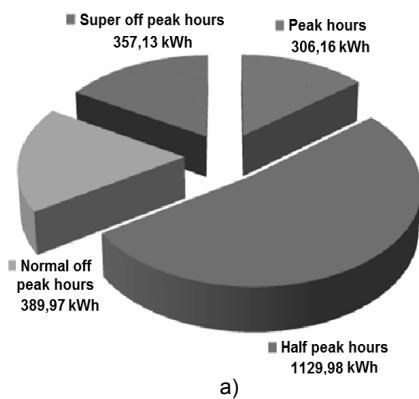


Fig. 2 a) Distribution of total energy; b) Maximum power measures in the general business (Wh) over two weeks (winter period).

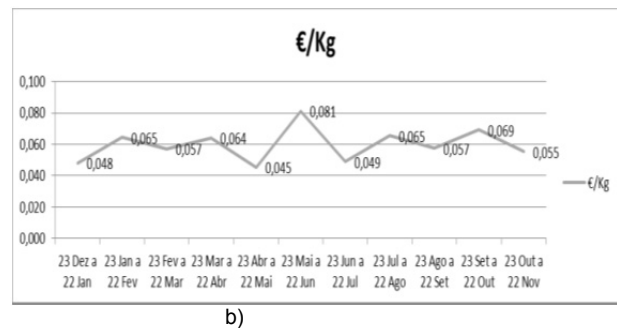
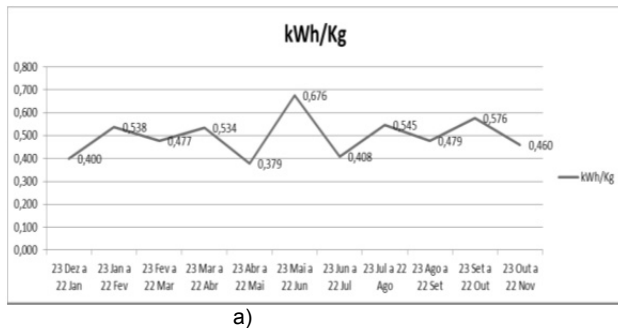


Fig. 3 a) Electricity use per each kilogram produced in several months; b) Cost of electricity per kilogram produced.

Actions to Improve Efficiency

Various solutions were proposed, particularly in terms of power factor correction (reactive power compensation), motion and presence detectors in the corridors and offices and energy consumption monitoring at a distance (web, phone) for a more effective control of consumption. Advantages, limitations, design and financial return for each proposed measure were studied... But the main focus of the analysis was centred on the lighting and compressors, because the potential savings were the highest. We also analyzed the feasibility of a 20 kW photovoltaic power plant since the company provides optimal coverage for solar use.

We decided to propose the implementation of a photovoltaic solar plant, for the lighting area of the company, as well as illuminate more effectively the production area of the cutting machine and control the consumption of the compressors, taking into account the costs of these actions not conditioned or stop the remaining work in production plant.

For the conception of small photovoltaic production, it has been taken into account, the needs of the company and the national legislation [11]. The photovoltaic system is to be projected to sell the produced energy to the utility under a sponsored rate of 0.215 €/ kWh during the first 15 years. In the case of a technical/legislative impossibility to sell the energy, the energy produced could be consumed by the company, suppressing the energy needs of the manufacturing area illumination and administrative area. A system with more than 20 kW would imply the need to auction the energy sell rate, implying a lower rate.

To evaluate energy and projection of the installation program was used Sunny Design since it is reliable and a program with a comprehensive database. The study uses photovoltaic panels Sunpower SPR-327NE-WHT-D, which have a nominal power of 327 Wp, efficiency of 20.05%, comprising the installation of 63 panels for a total of 20.60 kWp [12]. For interconnection of the central to the utility grid inverters must be used, in this case are two inverters STP 10000TL-10 with a nominal power of 10 kW and maximum efficiency of 98.1%. The investment should be around 52 000 € and, considering a discount rate of 5%, the net present value (NPV) of the project over 15 years is estimated in 18 500 €. The estimated internal rate of revenue (IRR) is 9.9% and the estimated return on the investment (ROI) is 35.7%. Fig. 4 resumes the NPV analysis of the photovoltaic installation, considering that the energy produced will be sold to the company that manages the national electrical grid.

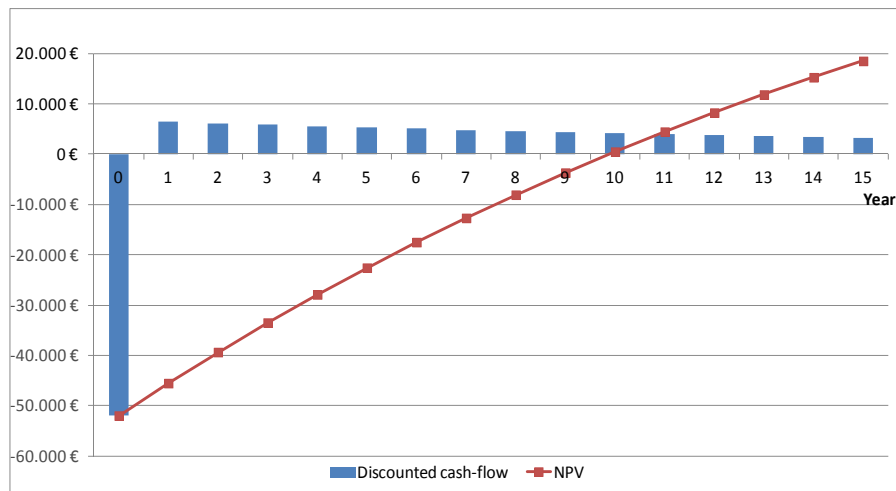


Fig. 4 – Net Present Value analysis for the implementation of an 20 kW photovoltaic system.

Since the NPV is positive and the IRR assumes an interesting figure, the project should be seriously considered by decision makers (company owners) [13].

Another set of actions that lead to greater energy efficiency are interventions at the level of power factor correction, install a system for reactive power compensation and motion and presence detectors. The study of the advantages, limitations, design constrains and financial return of these systems was carried out. Although the placement of electric motors, in particular the high-performance motors associated with control by variable speed drives (VSDs). It is intended to be a replacement for conventional equipment by state-of-the-art production and control of driving force. Thorough analysis was not conducted due to the major investments and the need to shut down the manufacturing for a considerable period for technological adjustments.

With an area of 2800 m² of covered space, there is a large need of lighting. During the day (even with bright sky), it is estimated that 60% of the area requires artificial lighting, since only the administrative area and part of the extruders have sufficient natural lighting. So one of the proposed measures was to increase natural lighting, with the replacement of some opaque roof panels with translucent roof panels. The estimated area for roof panel substitution was 42 m². Considering a cost of around 45€/m² (including installation cost) the investment is estimated 1890€. Several artificial lighting reduction scenarios were analyzed, being the most realistic the reduction of 50% of electricity consumption to lit the referred area during daytime (from 9h to 17h during winter and from 8h to 20h during daylight saving time). Besides the energy savings, the natural light shall improve the lighting quality of some workplaces that have insufficient illumination levels. The estimated savings for this scenario are 950 €/year, which leads to a simple payback time of approximately two years. The installation of a time switch to be control the lighting in industrial building would also be a solution for ensuring energy saving, leaving it less dependable on user behaviour.

Finally, the monitoring process of energy consumption on-line or by phone (at distance) are actions to be taken into account for better control of all consumptions. The isolation of the exterior walls of the offices area with new types of materials is an energy factor of rationalization inexpensive and relevant to the climate inside these compartments, having as a consequence the diminution on the consumption for heating and cooling indoor air [14].

Conclusion

The energy audit is a viable and essential tool for the disaggregation of the types energy consumed in this industry. After completion of the audit, the most relevant findings relate to energy efficiency improvement, with moderate investment, by acting on the roof, ensuring a greater use of natural light, and also install a small photovoltaic system.

It is found that there was a concern for the projection of the electrical installation and that there is no phase overloaded and that each phase is 1/3 of the maximum load. With the measures presented here is expected that the case study has a reduction in power consumption and energy costs, without compromising the company proper functioning. The use of translucent roof panels will allow the use of natural lighting and better lighting quality in the storage area and cutting machines.

Field work resulting from the collection of data analyzers was essential, for detection energy problems and propose a reformulation of the parameters of the power contract with energy supply company.

The increase in the cost of primary energy, including fossil fuels, will pass on the costs of producing electricity ultimately worsen the price per kWh, aggravating the economy of the industries in which energy is an important production factor. So energy efficiency is of most relevance as a way to boost the level of competitiveness of the industry.

Finally it is intended that energy efficiency is a catalyst for sustainable development.

Acknowledgment

Our thanks to the company's management (TECTIL – Plásticos Retrátéis/Retractil Plastics Ltd, Leiria - Portugal; info@tectil.pt or http://www.tectil.pt) for all the collaboration in the development of this research.

References

- [1] Directive on Energy Efficiency (proposal) and repealing Directives 2004/8/EC and 2006/32/EC; see http://ec.europa.eu/energy/efficiency/eed/eed_en.htm; access June 2012
- [2] European Commission Energy: Directive 2002/91/EC, *On the Energy Performance of Buildings*; see http://ec.europa.eu/energy/demand/legislation/buildings_en.htm, access May 2012.



- [3] National Law - DL n.º 34/2011 de 8 de March, *Electricity Production by Small Unities*
- [4] National Law - DL n.º 58, 26 Fev. 1982, *RGCE - Regulamento da Gestão do Consumo de Energia*, year 1982.
- [5] P. Wilde, D. Coley; *The Implications of Changing Climate for Buildings, Building and Environment* Vol. 55, Elsevier (2012), doi:10.1016/j.buildenv.2012.03.014
- [6] R. Critchley, J. Gilbertson, M. Grimsley, G. Green; *Living in Cold Homes Heat. Improvements: Evidence from Warm-Front, England's H. E. Efficiency Scheme*, Applied Energy Vol. 84, pp.147-158 (2007).
- [7] J. Galvão, S. Leitão, S. Malheiro, T. Gaio, *Biofuel for the Energy Efficiency on a Building with Small CCHP*, In Proceedings of IEEE/International Conference Clean Electrical Power, Italy, doi: <http://dx.doi.org/10.1109/ICCEP.2009.5212076>, year 2009.
- [8] João Galvão, Sérgio Leitão, Salvador Malheiro, Tiago Gaio; Chapter: *Hybrid Model for the Energy Efficiency of Building Services of Book: Energy Efficiency: Methods, Limitations and Challenges*, Nova Science Publishers, Inc. ISBN: 978-1-62081-817-6; see: https://www.novapublishers.com/catalog/product_info.php?products_id=30968, access June 2012.
- [9] R. Martinez, F. Javier, V. Eloy, *Eficiencia Energetica en Edificios: Certificacion y Audit. Energéticas*, Thomson Paraninfo (2006).
- [10] B. Bellosio, L. Giaccone, A. Guerrisi, P. Lazzeroni, M. Martino, M. Tartaglia, *Energy Networks in Sustainable Cities: Towards a Full Integration of Renewable Systems in Urban Area*, DIE, Politecnico di Torino, Italy, 2011.
- [11] S. Ransome, *A Summary of Outdoor Testing and Modelling of PV Systems*, BPSolar/3rd Photovoltaic Science, Applications and Technology Conference (PVSAT-3), Durham University, UK (2007).
- [12] Solar Desing Tool –Corporation; see <http://www.solardesigntool.com/components/module-panel-solar/Sunpower/>, July 2012.
- [13] S. Baker, *Economics Interactive Tutorials*, University of South Carolina, USA (2006).
- [14] P. Drasnar, J. Kudlacek, V. Kreibich, Vojtech Kracmar, Miroslav Vales, *The Porperities of Electrolytically Deposite Composite ZN-PTFE Coatings*, published: MM Science Journal, Czech Technical University in Prague, Czech Republic, year 2011.



International Conference on Innovative Technologies, IN-TECH 2012,
Rijeka, 26. - 28.09.2012



CONTEMPORARY INTERIOR DESIGN BETWEEN THE ISLAMIC HERITAGE INSPIRATIONS AND SUSTAINABILITY CONCEPTS

Dr. Eman Ibrahim Badr Surkn¹

¹ Assistant professor of interior design, King of Abdul Aziz University, Saudi Arabia

Keywords: Islamic Heritage - creative Values - Originality- Contemporary – Inspiration - Dual Language – Morphological- Chaotic systems- the Constants - the variables - the identity

Abstract. The interior design is a field that does not deviate from the human search for the heritage identity in the time of accelerating the contemporary challenges to achieve uniqueness and creativity.

based on this concept the Arabian designer seeks in how to expression the dimensions of his own historical and cultural unique heritage, And especially after the border opened and spaces expanded to become Necessary to confirm the identity, and he must Aware that the greatest target is as the openness to ideas World design, as more he need to uphold with the heritage identity, the theorist and critic Architectural Charles Jencks Says: " we are now witnessing the end of geography no secluded place where independent homeland, or culture is immune"- So it was incumbent on the interior designer to understand the philosophical dimensions of the sustainability concepts in heritage and deepen its sense in his own soul,

The concepts of sustainability in interior design

- Depend on create a double-dimensional heritage language in interior design, which integrate between all the advantages of Originality and contemporary and not individually.
 - Depend on create a unique design language in interior design, which based on the reformulation of heritage vocabulary with a concept of modern and contemporary.
 - Depend on dealing with interior design philosophy as a matching of Constants and variables
- Considerations group

And through this concept, the creative values of interior design can be realized, and this consequently leads to provide a permanent source of heritage inspiration for all the next interior design generations. This paper research about interactive the sustainability intellectual Ideology in interior design by inspiration from the Islamic heritage, and how to dealing with the features of heritage identity Depending on its intellectual features, not as elements or an vocabulary of heritage rigid.

Introduction

The call to establish the deep-rooted Islamic heritage values in interior design and architecture is growing, day after day, as a part of create a new Islamic Arabian designers Generation, a movement is emerging in response to the imminent danger of losing these special qualities through the destruction and mutilation of buildings of value. The revival of the Islamic architectural heritage has become a universal concern which can be shared by critics, architects, interior designers etc. to emphasize the great and effective role of revitalization in the contemporary architecture and the sustainable development. Within this intellectual framework, cultural heritage in its concept and meaning is considered functional and a must for the human existence and also functionally and aesthetically in artistic works represented in the interior design and architecture.

Cultural identity represents the sum of our past creativity, and the results of creativity are what keep society going and moving forward [1]. The language of architecture represents an integral part of manifesting a society's image of itself, and architects are both the custodians of our heritage of architectural and interior design forms and spaces, as well as the creators of tomorrow's heritage [2], as the language of architecture is more than a form; it evokes the past, prefigures the future and articulates the present for all people. Community and humanity are the ultimate goals of most much human activity, professionals with their specialized knowledge and through their dedicated service work together to serve humanity.

Islamic Heritage and interior design:

The history and heritage of Islamic architecture and to some extent, those of the entire Arab region, its size, splendor, power and functions have been a reflection of the fact of interest for the past centuries [3] and the survival of the Islamic architectural heritage has become a universal concern which can be shared by all the actors involved in the urban development process. Islamic architecture reflects a strong aesthetic value, manifested in the facades and gateways of buildings, the colorful designs, the different arches and geometric shapes, the beautifully carved stones and pillars. The respective regional style of Islamic architecture shows inner affinities which are clearly based on related traditions, patterns of use and corresponding structuring principles [4].

The rise and spread of Islamic culture from the seventh century onward has provided us with one of history's great artistic and decorative traditions. In a broad swath of Islamic rule, at one time extending across Europe, Africa, and Asia, we find artistic treasures of unrivaled beauty, Islamic art encompasses great achievements in calligraphy, stylized floral designs, architecture, and abstract geometric patterns.

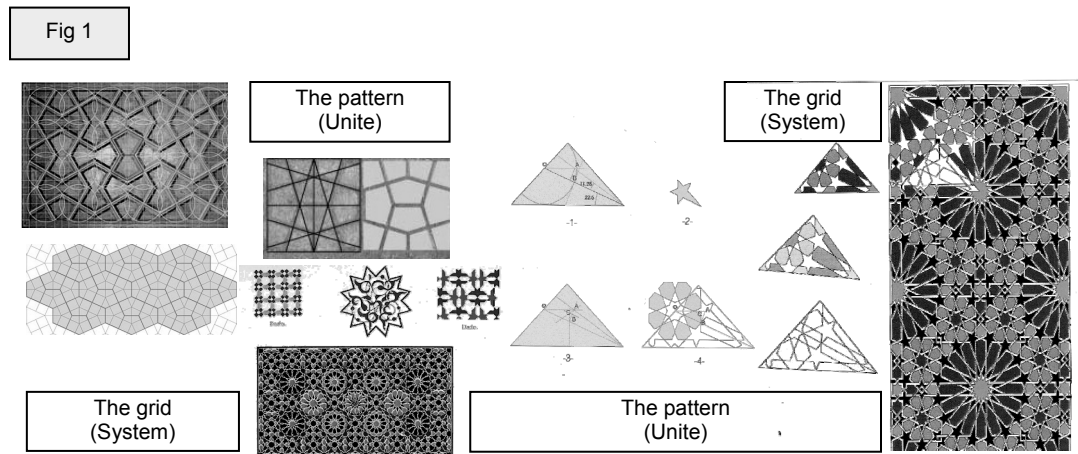
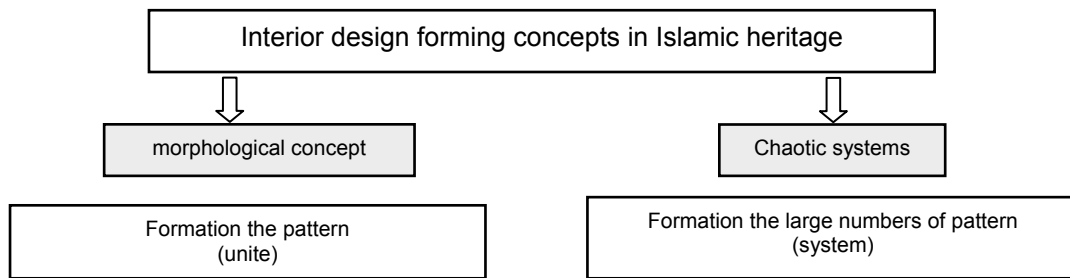
Aesthetic and functional values of the Islamic heritage in Interior Design

Traditional islamic pattern designs consist of motifs which are combined using geometrical transformations to fill the spaces. The different ways of combining these transformations and, therefore, all possible symmetries of the design pattern, are limited and have been

described in the theory of symmetry groups [5]. The different motifs together with their plane symmetry group (design structure) provide all the information of the design pattern.

Ancient Islamic design constitute a historical heritage consisting of pattern that were manufactured using many types techniques. Pattern design recovery and image processing are of great importance for different purposes in interior design , like Treatment and the formation the different levels of walls, floors and ceilings ,Design and treatment of elements and architectural slots, Design and the formation of furniture and lighting units, the creative Values of This pattern depend on tow types of design concept :

- 1) The morphological concept which forming and configurationally the shape of the unite in the hole system , this forming Simulated the formalism systems, which living in different environments as plants or animals – and also this simulated shape can be based on geometric abstraction process in anther types of forming the unite shape.
- 2) The Chaotic systems design, which forming the Systems with large numbers of elements or pattern that seems like chaotic form but in fact they really ranked by complex relationships.



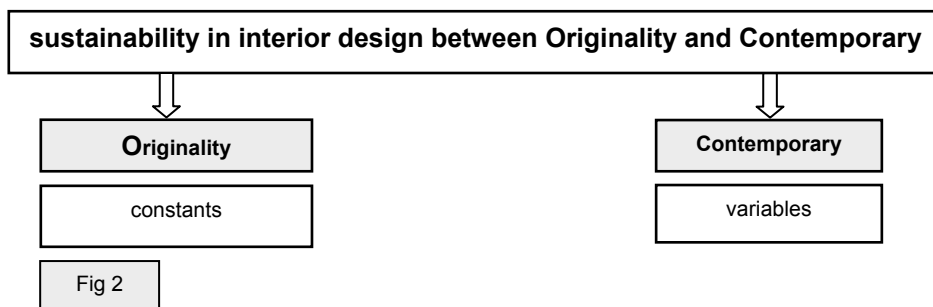
The concept of sustainability in interior design

the concept of Contemporary interior design between the Islamic heritage inspirations and sustainability has grown out of the concept of sustainable development (SD), which defined SD as:

development which meets the interior design needs of the present with dealing with the features of heritage identity Depending on its intellectual features, not as elements or an vocabulary of heritage rigid [6] ,and that will create a very rich source and creative Values of design thoughts and unique solutions for Consistent with the ability of future generations and to meet their own needs [7].

interior design sustainability between Originality and Contemporary

Contemporary interior design need formulations of Dual Language to conform with the requirements of present intellectual and technological methods, but at the same time it need to adhere to the traditional identity which represents the concept of Originality - and this concept can only be achieved through the activation of sustainability concepts that rely on intellectual dealing with traditional elements as a set of constants and variables.



When dealing with elements of Islamic heriitage we can activate the concept of sustainability intellectual through analysis of the elements of unity in the overall system in the islamic geomtric grid- and use these items after analysis in a modern networked systems such as

Chaos system ,molecular system , fractal system , nano design system, deconstruction system.and also the design process in this level can be used the basics of interior design, such as deletion and addition and repetition, displacement, and zoom in and out
Dealing with islamic heritage as Originality sources (constants) need Fully aware of the complementary relationship between the field of interior design and the geometrical theory, geometrical Sciences and Philosophy of the physical output of the heritage. This creates design solutions are characterized by uniqueness, originality, and bear the features of the formal expression of contemporary as(variables).

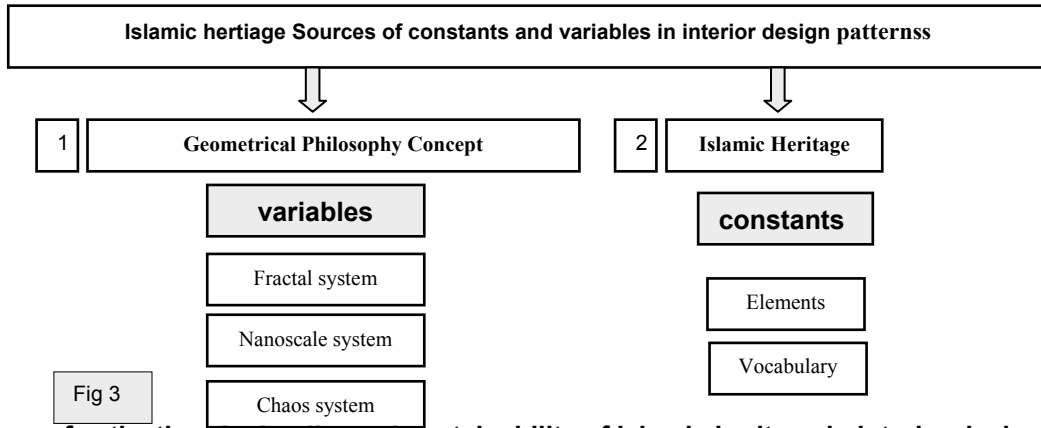


Fig 3

Methodology of activation the intellectual sustainability of islamic heritage in interior design

In this chapter can be illustrated a set of contemporary network design based on pattern (unite) decorative elements which depending on the activation of the intellectual sustainability concepts in interior design , through the selection of one of the the Islamic heritage elements as a source of Originality (constants) and then re-drafting of this unit the contemporary network and also through the using design Basics , which will create a a contemporary intereior design structure grids (variables)- that can be used in design walls, floors and ceilings ,Design and treatment of elements and architectural slots, Design and the formation of furniture and lighting units.....etc.
Activation the sustainability intellectual Ideology in interior design by inspiration from the Islamic heritage, and dealing with the features of heritage identity Depending on its intellectual features, not as elements or an vocabulary of heritage rigid ,This proposed methodology can be formed for the languages and design formulations original and contemporary at the same time, and stick to identity

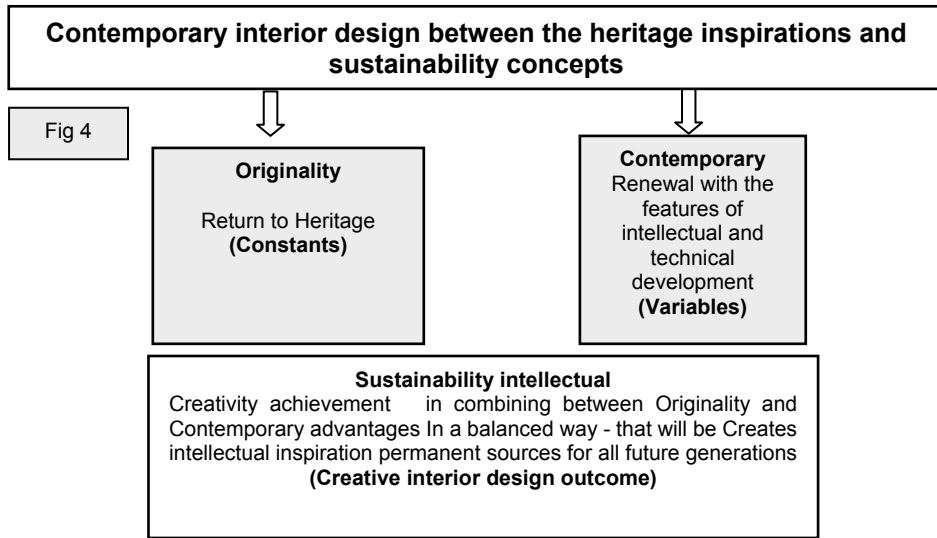
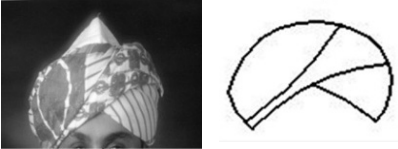
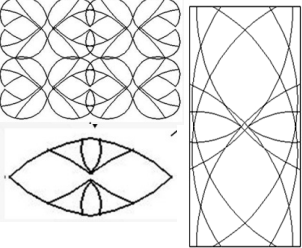
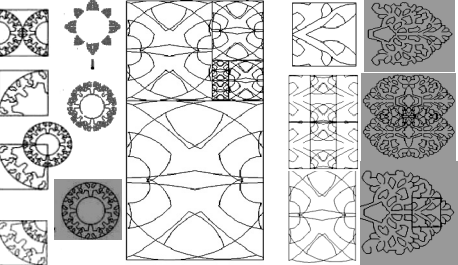
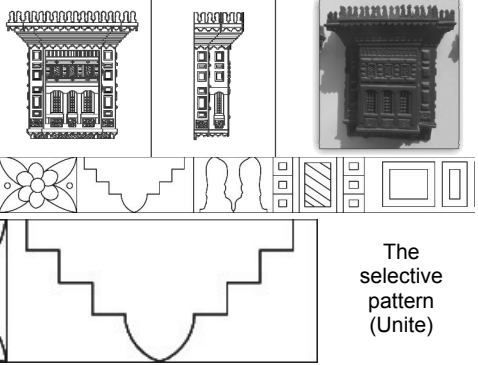
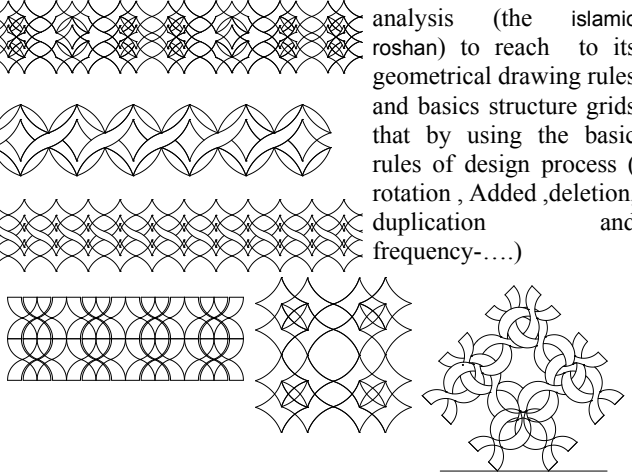


Fig 4

Methodology of activation the intellectual sustainability of islamic heritage in interior design		
Sr.	Islamic heritage pattern	the intellectual sustainability
	Originality (constants)	Contemporary (variables)
1	<p>(the islamic mafruka) which was a geometrical Arabian elements used in decorating windows and doors .</p>	<p>analysis (the mafruka)to reach to its geometrical drawing rules and basics structure grids- that by using the basic rules of design process (rotation , Added ,deletion, duplication and frequency-....)</p>

Table Methodology of activation the intellectual sustainability of islamic heritage in interior design

2		
Sr.	Islamic heritage pattern Originality (constants)	the intellectual sustainability Contemporary (variables)
2	 <p>the second model take (the islamic Turban) which like a headband and it still have a great value for arabian men</p>	 <p>the design process adopted on inspiration from the lines of the turban, then analyzed and stripped these lines in the form of chaos system grid</p>
3	 <p>the third model take (the islamic mekhalh) which was a tool Arabian women used in making up her eye</p>	 <p>analysis (the mekhalh) to reach to its geometrical drawing rules and basics structure grids that by using the basic rules of design process (rotation , Added ,deletion, duplication and frequency-....)</p>
4	 <p>The selective pattern (Unite)</p> <p>the fourth model take (the islamic roshan) which as a window</p>	 <p>analysis (the islamic roshan) to reach to its geometrical drawing rules and basics structure grids that by using the basic rules of design process (rotation , Added ,deletion, duplication and frequency-....)</p>

Results

1. The intellectual sustainability of Islamic heritage in interior design Depend on create a double-dimensional heritage language in interior design, which integrate between all the advantages of Originality and contemporary and not individually.
2. The intellectual sustainability of Islamic heritage in interior design Depend on dealing with interior design philosophy as a matching of Constants and variables Considerations group.

Acknowledgment

I deeply thank my senior grade students in king of Abdul Aziz University, interior design department, those who answered all my directions to activate the concepts of intellectual sustainability of the Arab and Islamic heritage to solve the interior design problems in a values of originality way, and a contemporary outcome forming .

References

- [1] Landry, C.2000. The Creative City, A Toolkit For Urban Innovators , Earthscan , U.K. , p.6. (2003), Issues 1-3, p. 111-119.
- [2] Davidson, C.Serag Eldin, I. 1995. Architecture Beyond Architecture, The AgaKhan Award For Architecture, Academy editions, (2008), Great Britain, p. 76.
- [3] Saqqaf, A.1987. The Middle East City, Ancient Traditions Confront A Modern World, Paragon House, (2003), p.7-8- 209
- [4] Bianca, S.2000. Urban Form In the Arab World, Past And Present , Thames &Hudson, (2004) , England, p.10- 56.
- [5] J. Bourgoin, Les Ele` ments de l'Art Arabe: Le Trait des Entrelacs,Firmin-Didot, 1879. Plates reprinted in Arabic Geometric Pattern and Design, Dover Publications, 1973, p.53- 59.
- [6] Dan Bucsescu , Michael Eng,"Looking Beyond the Structure: Critical Thinking for Designers & Architects"- Fairchild Pubns- New York, (2009),pp.122:124
- [7] J. Bonner, 'Three traditions of self-similarity in fourteenth and fifteenth century Islamic geometric ornament', Proc. ISAMA/Bridges:



International Conference on Innovative Technologies, IN-TECH 2012,
Rijeka, 26. - 28.09.2012



Mathematical Connections in Art, Music and Science, Granada, (2003), pp. 1–12.



International Conference on Innovative Technologies, IN-TECH 2012,
Rijeka, 26. - 28.09.2012



ROBOT CONTROL SYSTEM BASED ON INERTIAL NAVIGATION

P. Božek¹

¹ Slovak University of Technology, Faculty of Materials Science and Technology, Institute of Applied Informatics, Automation and Mathematics, Hajdóczyho 1, 917 24 Trnava, Slovakia
pavol.bozek@stuba.sk

Keywords: Inertial system, micromechanical sensor, calibration, industrial robot

Abstract. The paper deals with constructing the inertial navigation system (hereafter INS) which will be utilized for the calibration of a robotic workplace. The calibration is necessary for adapting the simulation of a production device model to real geometric conditions. The goal is to verify experimentally the proposed inertial navigation system in real conditions of the industrial robot operation.

Introduction

The aim of the research is to investigate and develop a new combined inertial navigation system based on electronic gyroscopes, magnetic and barometric sensors. The crucial activity is focused on three basic fields:

- The first goal is to analyze accelerometer and gyroscopic sensors and their possibilities of utilization for inertial navigation. The simulation of the effect of sensors with different metrological parameters and their effect on the properties of the proposed combined navigation system.
- The second goal is to optimize a specialized processor system for processing the data from the defined sensors in connection with controlling items of an industrial robot [3]. The proposal of an algorithm of combined navigation with respect to the used processor system.
- The third goal is to verify experimentally the proposed inertial navigation system in real conditions of the industrial robot operation.

Characteristic of the issue

The inertial navigation system consists of a measurement unit containing accelerometers and gyroscopes and from a navigation computer which evaluates the data from measuring devices. In contrast to all the other navigation systems inertial navigation is completely autonomous, self-sustaining and independent of the surrounding environment, i.e. the system is resistant to outside influences such as magnetic disturbances, electronic interference and signal distortion. Computing operations in the inertial navigation system are based on Newton's law of motion.

For the purpose of navigation in a coordinate system it is necessary to keep the direction of motion in the direction of acceleration. This is not practically possible, and therefore sensors – gyroscopes are used for detecting the rotary motion. Seeing that each free object in space has six degrees of freedom (internally mutually independent variables) the inertial navigation system usually consists of three gyroscopes and three accelerometers where each pair (gyroscope, accelerometer) is able to record the rotation or acceleration in the direction of one axis which is perpendicular to the others. Of the six degrees it is three linear degrees of freedom, the translation in the X-axis, Y-axis and Z-axis which indicate the position of the object and three degrees of freedom of rotation which indicate rotating around the X-axis, Y-axis, and Z-axis.

The inertial measurement unit (IMU) is an essential item of each INS. Sensors, whose output is influenced by the motion of the object on which the IMU is placed, are regarded as primary sensors of the IMU. Primary sensors in inertial navigation are sensors of angular velocity, whose output signals after integration are used for determining the orientation in space, and accelerometers whose output signals after precise compensation of gravitational acceleration and the Coriolis force can be integrated onto the speed and position. Such an inertial measurement unit has six degrees of freedom. This means it enables to measure translational and rotary motion in three orthogonal axes. The accuracy of inertial sensors plays a key role in autonomous navigation. Errors of current inertial sensors have the approximate value of 0.01°/hour for gyroscopes and 100 µg for accelerometers [2]. The mentioned errors are integrated in time and cause the error of determining the position which is expressed by the non-accuracy of measuring per hour, which is, however, minimal. Such high-power IMU are implemented only into the inertial navigation systems for special use.

ADVANTAGES OF INS CONTROL SySTEMS

At the current space requirements and efficient use of space the robot is often forced to work in cramped conditions. The movement of the tool or handling of parts requires high accuracy. This implies great demands on the correct calibration of robotic devices. Using the INS the calibration is considerably simplified. The benefits of verification and measurement, such as to prevent accidental collisions of robots, will be significant.

3.1 Theory of basic principle

The methodology is based on the 1st and 2nd Newton's law, which reflects the change in motion and acceleration vectors for the action of external forces F on mass m (1st NL).

The speed is proportional by direction and size to the vector of external forces (2nd NL):

$$\mathbf{F} = m \cdot \mathbf{a} \quad 1$$

then it is possible to obtain the instantaneous speed and to determine the trajectory by integrating over time:

$$\mathbf{v}(t) = \mathbf{v}_0 + \int_0^t \mathbf{a}(t) dt \quad 2$$

$$s(t) = v_0 + \int_0^t a(t) dt$$

3

Because the acceleration vector is needed to capture acceleration in three mutually perpendicular axes, allowing the positioning in XYZ Cartesian coordinate system. At the movement the acceleration of gravity also operates on the object and, so it must be eliminated from the measurement.

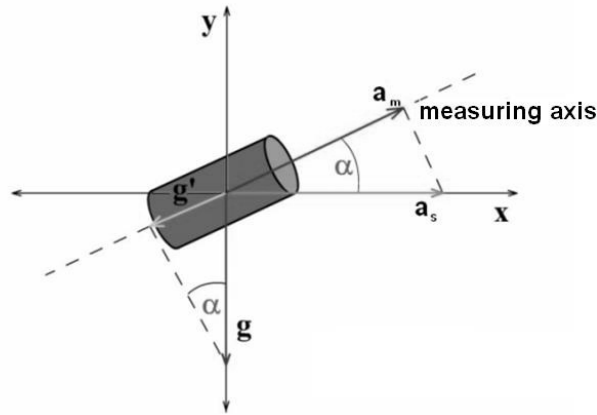


Fig. 2. The effect of gravitational acceleration to measurement

If the navigation axis (measurement axis of the accelerometer) is identified with the horizontal axis ($\alpha \neq 0$) then:

$$a_m = a_g \cdot \cos \alpha$$

4

$$g^r = g \cdot \sin \alpha \cong g \cdot \alpha \text{ for } \alpha \rightarrow 0, \text{ where } g \text{ is gravitational acceleration}$$

5

Relationship (5) also defines a single measurement error, which accumulates without compensation by applying relations (2) and (3). It is therefore necessary to measure the actual angle α by gyro sensor. The requirement of eliminating of the gravitational acceleration is possible to solve by stabilized base, or by using gyroscopes – by so called inertial navigation systems without shaft.

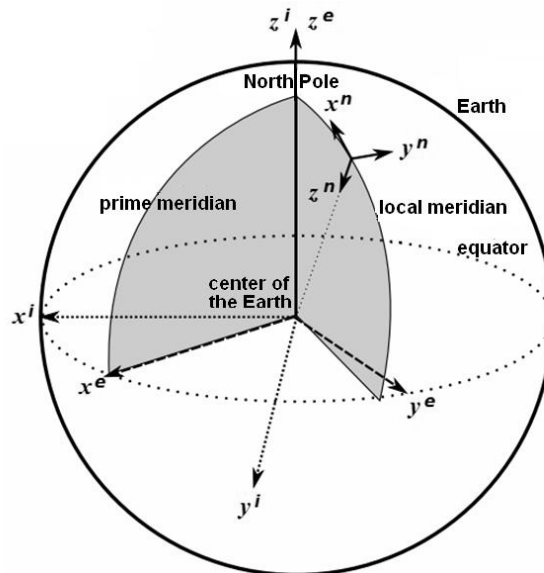


Fig. 3. Coordinate systems: inertial (i), Earth (e) and navigational (n)

Besides the coordinate system shown in Figure 3 also moving body has its own coordinate system (x^b, y^b, z^b), which angular orientation is measured by the gyroscopes and acceleration by the accelerometers. At the inertial navigation is therefore necessary to carry out conversions between coordinate systems. There are several useful mathematical methods, eg.: direction cosine matrix, Euler angles or by using the quaternions.

At the orientation of the body it is suitable the compliance with the established guidelines of navigation, which are shown in Fig. 4.

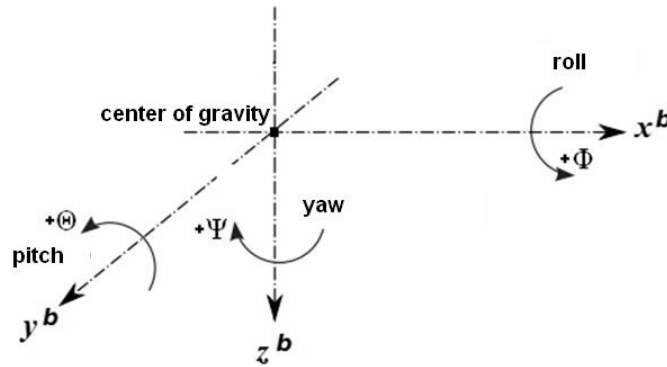


Fig. 4. Body coordination system

It is then possible to express general rotation R_n^b with three partial rotations R_x, R_y, R_z around axis x^b, y^b, z^b , which is a method of Euler angles:

$R_n^b = R_x R_y R_z$

$$R_y = \begin{bmatrix} \cos \theta & 0 & -\sin \theta \\ 0 & 1 & 0 \\ \sin \theta & 0 & \cos \theta \end{bmatrix} \quad R_z = \begin{bmatrix} \cos \psi & \sin \psi & 0 \\ -\sin \psi & \cos \psi & 0 \\ 0 & 0 & 1 \end{bmatrix}$$

6

$$R_n^b = R_x R_y R_z$$

Equations (6) represent the conversion from the navigation system (n) to the body coordinates (b). The conversion of coordinates of the body to the navigation system is carried out according to equation (7).

$$R_n^b = R_n^b{}^T = R_x^T R_y^T R_z^T$$

7

In addition to basic errors resulting from measurement methods it is necessary in the process of navigation to eliminate errors resulting from measuring accelerometers and gyroscopes and particularly distortion (bias), change the scale and noise. These errors vary depending on the quality (cost) of sensors.

Noise of measurement sensors is a serious error to be eliminated in the process of navigation. The theoretical and practical work of navigation presents the download of the application of Kalman filter (Fig. 5) to eliminate this deficiency before processing.

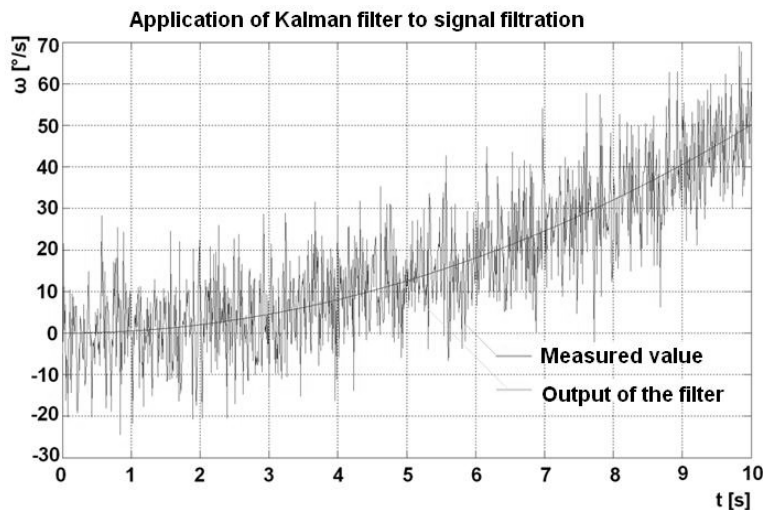


Fig. 5. Kalman filter signal filtration

The core of the inertial navigation system, navigation computer, which processes the measured values of the measuring unit, preprocesses them, transforms them into the reference system and carries out the elimination of gravity and the Coriolis acceleration. It also calculates (equation (2) and (3)) based on the initial parameters (position, speed) the position of the navigated object. Contribution to the navigation of the Coriolis acceleration, as a result of the Earth's rotation, is reflected at the long navigation. Although the process of the inertial navigation seems simple in principle, it implies solving three differential equations.

Benefits of solution



In contemporary space requirements and the effective utilization of space the robot often has to work in confined conditions. Moving a tool or manipulating with parts requires great accuracy. The enormous demands for the correct calibration of a robot device result from this. The calibration will fundamentally be simplified by using the INS in the field of calibration. The contribution in the field of control and measurement, for example, preventing the accidental collisions of robots, will be significant.

It is possible to expect the next contribution in the original proposal of the algorithm of combined navigation with respect to the used processor system and its optimization in connection to the use in robotics and connection to the operation of robots mainly on their safety and economics. Description of used methodological procedures - modern methods, analyses and simulations with the use of modern software tools such as OrCAD, Matlab, Multisim will be used in mentioned fields [5]. The shape of stationary magnetic fields will be investigated on an experimental laboratory model which uses an area positioning system. Possibilities of using the magnetoresistance sensors and barometric sensors will be verified in the sensor system [4]. The original own algorithms will be utilized in the course of processing the data from the sensors. The solution implements planned experimental verification of the navigation system first on a model robot, and later, in real operation conditions of a robot device with evaluating the uncertainties.

The output is the original construction of the navigation system utilizable in the operation of robots – the elaboration of the study with the possibility of implementation of inertial navigation for the calibration of robotic workplaces, the system of control with a possibility of avoiding collisions during the operation.

Conclusion

The possibilities of utilizing the inertial systems are directly proportional to the advance in their development. The ability of precise measuring the position of the robot mainly in necessarily regularly repetitive calibration is increased by this. The implemented INS is able to measure accelerating and slewing the watched point of the arm and to use it for determining the position of the robotic arm in space [1].

References

- [1] J. Hromada, P. Bubenik and M. Hradnansky: Simulation as a supporting tool for the election management system, *19th International Workshop*. Ostrava: MARQ (1997), pp.283-288. ISBN 80-85988-20-8
- [2] A. King: *Inertial Navigation / Forty Years of Evolution*, (2009).
- [3] M. Sotak et al.: *Integration of navigation systems*, Košice (2006).
- [4] J. Suchánek, V. Kreibich, J. Kudláček et al.: *Technology forum 2011*, Praha: ČVUT, Faculty of Mechanical Engineering (2011), 168 pp. ISBN 978-80-01-04852-8
- [5] I. Zolotova, J. Flochova and E. Ocelikova: Database Technology and Real Time Industrial Transaction Techniques in Control, *Journal of Cybernetics and Informatics*, Volume 5, Slovakia, Bratislava (2005), ISSN 1336-4774. pp. 18-23 <http://www.sski.sk/journal/index.php>

OPTIMAL MOTION PLANNING FOR CAR BODY-IN-WHITE INDUSTRIAL ROBOT APPLICATIONS

P. Božek¹, K. Trnka²

¹ Slovak University of Technology, Faculty of Materials Science and Technology, Institute of Applied Informatics, Automation and Mathematics Hajdóczyho 1, 917 24 Trnava, Slovakia
pavol.bozek@stuba.sk

² Slovak University of Technology, Faculty of Materials Science and Technology, Institute of Applied Informatics, Automation and Mathematics Hajdóczyho 1, 917 24 Trnava, Slovakia
kamil.trnka@stuba.sk

Keywords: Trajectory planning, off-line programming, robotic simulation, body-in-white, motion optimization

Abstract. This paper discusses the problem of effective motion planning for industrial robots. The first part dealt with current method for off-line motion planning. In the second part is presented the work done with one of the simulation system with automatic trajectory generation and off-line programming capability. An spot welding process is involved. The practical application of this step strongly depends on the method for robot path optimization with high accuracy, thus, transform the path into a time and energy optimal robot program for the real world, which is discussed in the third step.

Introduction

In the past, and even today the technology of automotive industry operations are in a certain amount performed by man. The advantage and disadvantage is also that the speed of the work of man depends on his skills. Today spot welding is an important technology used in the production of body in white in the automotive industry. With the increase in competition, this technology is increasingly required in automated or robotic form. For its application in practice by current demands must often use computer aided technology. Modern virtual technologies are examined and applied in various sectors of development and production. Body in white consists of more than 300 smaller different shaped parts connected by many welding points (over 4000) [1]. Therefore, the high demands for precise positioning of welding points, the optimal trajectory planning of robot motion and perfect synchronization of robotic workstations cells.

Off-line programming robots and manufacturing facilities represent a significant technological and time advantage not only in introducing new products, but also to change the existing production applications. Emulated environment allows program the robot without stopping production well in advance to prepare robot programs, which increases overall productivity. We are able to create realistic simulations using real robot programs and configuration files identical to those used in production. Although currently used simulation tools, such as Robcad, IGRIP or Catia, are unable to solve the problem of optimal robot motion planning [2]. Planning spot welding robot trajectories requires much more experience and subjective decision-making, leading to a continued need for on-line correction of robot programs. The speed of the machine work depends not only on its parameters, but mainly on the ability of humans to learn this machine to work quickly.

Basic principle of trajectory planning

Traditional robot trajectory planning problem can be described as a task in the initial and target configuration q , create in the final time between them a continuous sequence of valid configurations or evaluate an error if no such sequence. Robot configuration is valid if its construction does not intersect any obstacles or herself. The set of all valid configurations defines the topology of continuous motion.[3,4]

The trajectory planning of industrial robots are used the principle of interpolation in the configuration, or Cartesian space. The simplest and quickest method of interpolation is the point interpolation. Point interpolation guides the robots end effector from one point to another, regardless of the trajectory between goal points. To avoid collision with obstacles between the goal points via points are defined.[6]

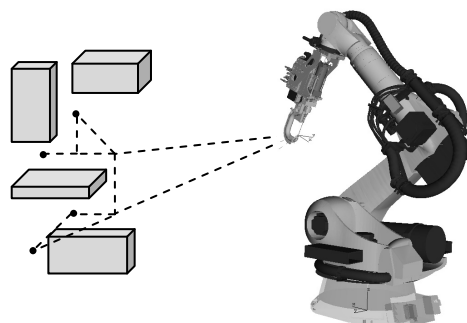


Fig. 1 Searching collision-free path between the goal configurations

Most of the off-line motion planners are based on an explicit representation of the free C-space. The free C-space computation consists of the obstacle transformation into the C-space and the construction of a free-space representation [4]. Both tasks are very time and memory consuming, and their calculation effort increases with the robots DOF. In order to avoid these time consuming obstacle transformations, one can search in an implicitly represented C-space and detect collisions in the workspace. This strategy enables the planner to cope with on-line provided environments, moving obstacles and grasped objects. For searching in the implicit C-space, we apply variation of the A*-search algorithm shown in figure 1. The main task of the A*-algorithm consists of the expansion and the processing of configurations, which are C-free. In the first step, the algorithm search for collision free path between the goal configurations. The next step is to connect the starting location of the trajectory to the nearest node path between goal configurations. Obstacles are circumvented along the perpendicular vector from actual location toward the next goal location.

Design and analysis of case study

The first prerequisite for solving the trajectory planning of robotic spot welding is the existence of N different target configurations q_i where $i = [1 \dots N]$. These configurations are the solution of inverse kinematics for a set of welding points. Based on the location of welding points we can create a different model situations. One such is shown in figure below. The next step is to try to create collision-free path between goal points. To move the robot we use PTP interpolation using via points for avoiding collisions.

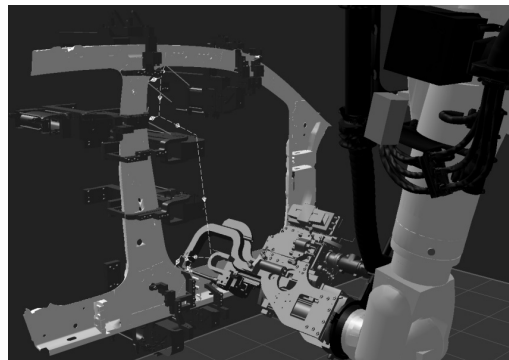


Fig. 2 Case Study of Robot spot welding (Robcad)

To circumvent the obstacles we choose the path along approach vector from that point toward the next goal point. If we are always connected nearest goal points with a straight line and all points of the lines belong to the set C-free, we choose the shortest direction around the obstacles. In this case we arrived the goal point at the direction of the approach vector in perpendicular angle (figure 3). Passing to the next goal point we use the previous via point from which we came to the current destination.

In practice welding points are almost always concentrated in groups due to technological requirements [5]. Looking at the trajectory under consideration in the previous procedure, we find that it is divided into segments by which we can move between any two goal points. Goal points can be grouped into sets of nearest neighbors and for each set we can test the fastest sequence always from one destination point. This testing can be divided into subsets and so accelerate the process of finding the optimal sequence.

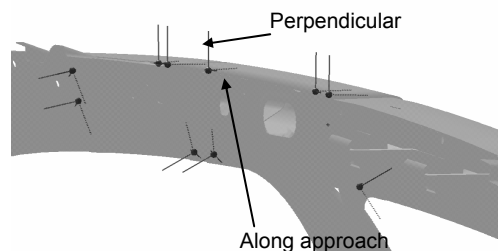


Fig. 3 Welding points projection

Movement optimization

Trajectory planning examined only the kinematics of the robots. In the following optimal velocity profiles must be computed, necessary for a time and energy optimal path execution. Therefore, several robot constraints like maximal joint velocities, maximal joint accelerations, admissible motor- and gear moments etc. have to be considered. In the body in white welding line mostly of welding or placement operations are implemented by point to point (PTP) movement. At PTP movement all axes starts moving in the same time and also stops simultaneously after a time frame that is necessary by the axis that requires the most time to reach the target angle. Since most placement operations expectation a specific trajectory only in a matter that any collisions are avoided, there is an open space for trajectory optimization.

A. Point approximation

Most of robot controllers allow to fly-by the programmed locations of TCP within the predefined range and without stopping there. This effect is called point approximation and is used by movement between work locations using the so-called via location. It creates the movement smoother, often shorter and therefore quicker. An example of approximation between two TCP linear movements is shown in figure 4. The actual optimization possibilities are dependent on initial robot's program. The disadvantage at large approximation distance is the deviation from the original path. However, 100% approximation does not mean that the TCP will always be going to fly-by the via location in the same distance as far as the deviation does not lead to any collisions it is a practical approach to save up 20% of movement costs.

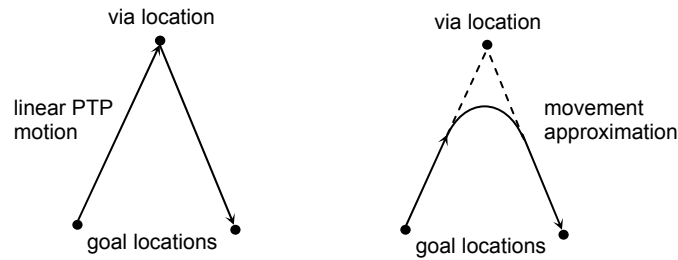


Fig. 4 Principle of point approximation

B. Speed and acceleration

Another point of optimization is to evaluate movement profile in correlation between tasks cycle time and the potential energy savings. Running the robot at lower speed, the total consumption decreases, running a robot at constant speed and decreasing the acceleration, the consumption decreases as well. From the figure 5 may derive conclusion that if there is a spare time to do the task slower, it is worth to do so. For example, if it takes 10 seconds to do the pick the component and place somewhere else, and just after that the robot is waiting another 5 seconds for some external signal, there is actually 50% extra time to complete this movement, and by moving slower it may be saved 20% of energy per this cycle time.

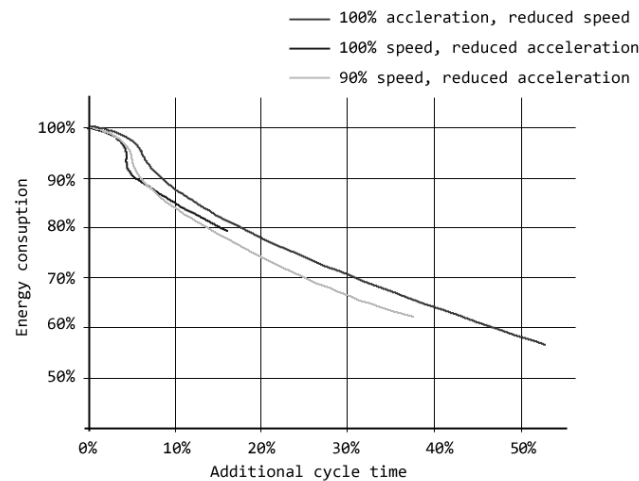


Fig. 5 Cycle time and energy saving comparison

Conclusion

Optimal motion planning of robots using different methods and algorithms is in great attention of planning theory, however due to the computational complexity many solutions are rarely used in practice. Often solution accuracy depends more on the actual experience of the programmer. In the case of robotic spot welding the aim is to achieve a reasonable compromise between finding a long path that can be execute faster and short trajectory, which requires movement of the lower speed. Using one algorithm is obviously impossible to achieve the desired result and combination of several methods can be time and hardware consuming. Based on the requirements of the car body welding line, we can say that it is necessary to deal with so much precision solutions to achieving a sufficiently rapid trajectory in a relatively short time.

The aim of this article was trajectory planning and optimization of robot welding path according to effective energy consumption and cycle time exploitation. Our proposal is based on the Robcad simulation model and therefore we don't present a proposal of real robotic workcell. Because of the fact that the actual savings are hardly application dependent and one method may as rise as decrease the influence of others, so only the statistic averages are estimated. Future research work will involve studying the optimization effect of the several planning algorithms.

References

- [1] Z. Wang et al.: Off-line programming of Spot-Weld Robot for Car-Body in White Based on Robcad, *International Conference on Mechatronics and Automation*, China (2007).
- [2] R. Dillmann et al.: *Robotik in Deutschland - Lehre, Forschung und Entwicklung*, Shaker (1998), pp. 9 – 1. ISBN 3826531868
- [3] J. N. Pires: *Industrial Robots Programming: Building Applications for the Factories of the Future*, Springer (2007). ISBN 038-72-33-253
- [4] S. M. Lavalle: *Planning Algorithms*, Cambridge University Press (2006), viewed January 6 2012, <http://planning.cs.uiuc.edu/>
- [5] Holeček, P., Kudláček, J.: *Simulation of production conditions rivet holes in aircraft structures made of aluminum alloy material Al-Cu-Mg*. Praha: České vysoké učení technické v Praze, 2010, ISBN 978-80-01-04586-2.
- [6] Leonardo da Vinci Programme: *Automatizační a robotická technika*, SjF Košice (2011), viewed January 15 2012, http://www.sjf.tuke.sk/vitralab/files/vystupy/prirucka_cz_final.pdf



International Conference on Innovative Technologies, IN-TECH 2012,
Rijeka, 26. - 28.09.2012



THE APPLICATION OF SYSTEM MEASUREMENTS IN INDUSTRIAL ENTERPRISES IN SLOVAKIA

M. Kučerová¹, Z. Gyurák Babel'ová²

¹ Institute of Industrial Engineering, Management and Quality, Faculty of Materials Science and Technology in Trnava, Slovak University of Technology Bratislava, Slovakia

² Institute of Industrial Engineering, Management and Quality, Faculty of Materials Science and Technology in Trnava, Slovak University of Technology Bratislava, Slovakia

Keywords: Quality, quality management, system measurement, improvement, management review, self-assessment, audit.

Abstract. System approach belongs to the eight basic principles of quality management, underlying the comprehensive quality management and normative documents for building quality systems. In accordance with system approach is currently required the application of new processes of measurement, which do not have the nature of technical measurements, but are referred as system measurements in quality management. In the framework of project focused on the development perspectives of quality management was examined the application of the basic principles of quality management in business practice. In the article are specified significant aspects regarding the system approach with emphasis on the system measurements and their application in business practice in Slovakia.

Introduction

Quality management systems and the level of their real effectiveness depend mainly on the quality of information obtained from different measurements. Recent requirements on the quality management systems require also application of new measurement processes, which are not characterised as technical measurements, but the system measurements as well. The organisation shall define, plane and introduce measurement and monitoring activities necessary in providing for the compliance and in achieving of improvements. Any measurements executed in the organisation have no sense, if the managing employees will not systematically deal with achieved results in the frame of their strategic and operative decisions. Right understanding of the system measurements may be an important aspect of success of the whole quality management system.

System measurement characteristics

System approach in very close connection with the process management is based on a principle of management and mutual interaction of all company processes, so that they would meet assigned purposes. Continuous control of relations among particular processes, as well as the control of the processes combinations and interactions is an advantage of such approach. According to the process management, it is necessary to provide for permanent monitoring, measurement and analysing not only the processes, but the measurement and monitoring of the quality management system effectiveness as well. From this point of view, there can be defined two basic groups of measurement in the quality management:

- a) *Technical measurements* with the purpose to determine a value of such parameter, which relates only to the processes material outputs, i.e. products, whereas the measurements are important particularly because their results are necessary for measurements of the second group.
- b) *System measurements* with common characteristics of enabling to learn and to define the organisational system behaviour, i.e. the organisation quality management whereas the measurement results are the key inputs for decision making at the different levels of management.

In the past, stress used to be laid on the products technical parameters measurements to declare the product compliance with requirements. Recently, there has been stressed necessity of the system measurements execution important mainly for the quality system effectiveness increase. These are especially following measurements: [1, 2]

- Measurement of satisfaction of customers, employees, and other involved parties;
- Measurement of performance of processes, quality management system performance, and an organisation performance;
- Measurement of contractors performance;
- Measurement of costs related to the quality;
- Measurement of a training effectiveness;
- Quality audits;
- Self-assessment.

For the organisation performance increase it is useful to establish the indicator system, which would inform of the organisation performance as the whole. It is essential to understand interaction between the processes performance indicators and the performance key results, i.e. economic indicators.

Executed survey results

Within the scope of the survey task, we have executed a survey focused on the assessment of the actual status of application of the quality management basic principles in different industrial establishments in Slovakia. The survey has been executed in form of questionnaire, in which 124 organisations from different industrial sectors have taken part in (35 % automobile industry, 35 % engineering and 30 % other sectors of industry). [2]

Among the survey results in connection with the system approach application, there will be presented some of the most important survey results namely related to system measurements.

On the ground of the process management and the system approach, the organisation effective operation has to be provided for the measurement and monitoring of the quality management system performance. According to the executed survey, the examined organisations have been providing for this system measurement primarily on the ground of the internal audit results and they almost never apply other methods.

Effective management and processes provision shall be supported by systematic process data gathering, but it is also necessary to check-up the gathered information in term of objectivity and reliability. The survey has revealed that the data from all processes are achieved only by approximately half of the all examined organisations with established quality system. From the satisfied customer's point of view it is necessary, so that all processes, which run within the organisation, were managed distinctly and effectively and were properly secured. It may be achieved only if there exists a measurement and monitoring of data and particular process data are objective and reliable.

With respect to the survey of the data objectivity and reliability, such activities have been executed in only about 50 % of examined organisations, including automobile industry establishments.

A lot of the measurement and monitoring, which are executed in the establishment practice, have only formal character and data achieved are not always used effectively in the frame of the quality management. Several organisations have stated in the survey that they have not used any methods for the system measurement and monitoring of the process performance, what may signalise there have been executed no measurement, or there have not been paid appropriate attention to it. Only about 50 % of the questioned organisations with the quality system have been using the data analysis results as details for the management examination, what is not very positive situation. About 70 % of examined organisations use the data for the process improvement, what may be assessed positively. [2]

In the course of finding, what is considered by the organisation as the main contribution of measurements and monitoring, the most frequent answer was – *to improve efficiency and effectiveness of the organisation* (more than 80 % of all reviewed organisations; in the automobile industry it has been stated only by 74 % of respondents). Favourable are also results, improved communication (what has been stated by about 50 % of the organisations) and confidence and motivation creating conditions for increased productivity (about 40 % of organisations).

Topics for the system measurement application improvement

Following the executed survey it can be stated that right *the system measurements and methods used by system measurement* are the considerable problem in connection with the system approach in the quality management in the factory practices in Slovakia.

To improve the negative conditions in the factory practices in connection with the system measurement application it is essential that the competent employees were more extensively informed of the quality management system measurement methods. For the organisations, the process performance measurements represent activities, which shall provide with objective and accurate information on the progress of particular processes, so that the process owners were able to control them continuously, i.e. operatively to meet all requirements imposed to the processes. To increase of effectiveness and efficiency of the quality management system, in the frame of the system measurement we recommend the organisations to pay more attention to methods of *the management review and self-assessment*.

1. Management review

Any measurement, executed within an organisation, has no sense, if the managing employees will not systematically deal with achieved results in the scope of their strategic and operative decisions. Indeed, the organisations carry out system review by management, but in many cases it is only formal approach, i.e. management meetings take place to discuss quality reports for certain period, corrective actions are approved and all that is being recorded, but this information is not used in full extent, or appropriately on all levels of the organisation respectively. Correct comprehension and realisation of the concept of management review may be an important aspect of success of the whole quality management system.

Management review are actions executed to find out suitability, accuracy, effectiveness and efficiency of the review by achieving goals. [3]

On the ground of the management principles the management review shall be practically understood as the only control instrument for the quality management system senior management, which has the following tasks:

- to find out, whether the quality management system allows and supports achieving quality goals of the company;
- to monitor the quality management system ability to meet basic functions, i.e. to maximize satisfaction of external customers and other involved parties, and to minimize the costs associated therewith.

Thank to these two functions, any company quality management system may contribute for fulfilment of every organisation main function – to create and to increase the profit. The management review should represent one of the most powerful quality management instruments in all types of organisations and it shall be understand as the real process with itemized definition of inputs, e.g. results of internal and external quality audits, measurement results of satisfaction of customers and all involved parties, process performance measurement results, benchmarking, etc.

In the practise it means that the senior management shall require information of such type from appropriate company units. The units shall introduce and make use of the system measurement processes, for which the senior management will be the main customer. Data analyses shall be a part of these processes, particularly in the field of trend detection. The quality reports submitted to the management should unconditionally reflect that information inputs.

Just like the inputs, also the management review outputs are defined, which shall represent e.g. decisions on proposals of the continuous improvement projects, recommendation on adoption of adequate corrective and preventive actions, decisions on future quality audit fields, decisions on the risk management, etc.

The management review should be understood as systematic process, therefore every input shall have particular supplier and each output shall have particular customer. Every process shall have an owner, who may be a physical person or a legal entity, who shall be responsible for the output quality and the process effective progress. In case of management review, the process owner is the senior management, who is, at the same time, the customer of the system measurement processes.

The management review is undoubtedly a key process and a limiting factor of the performance of the company quality management system (QMS). Following actions may be recommended for all types of organisation:

- the senior management should take part in a special training to understand importance of the management review;
- an organisation should appoint the management representative, who shall be responsible for submitting of quality reports;
- it is recommended to perform the management review once every three months in initial phases, and once a year in case of more advanced QMS;
- the management review shall be in form of the senior management special consultations and meetings and all top management members, including the company director, shall take part in it;
- reports on the quality development should include all QMS processes, as well as achieved results;
- the management review shall be recorded in detailed reports, which shall include all relevant decisions on next activities and related aspects;
- to lay stress especially on the process improvement in decision making regarding further QMS development.

2. Self-assessment

In the company practice in Slovakia, the organisations only rarely apply the self-assessment method in frame of the measurement and monitoring of the quality management system performance.

The self-assessment is defined as a complex, systematic, and regular process of examination of the organisation activities and its results on the basis of a Model of exceptionality. [3]

The self-assessment process shall include all activities, without any exception, and all aspects for achieving the particular organisation economic and non-financial results. It shall be an obvious part of the organisation management system, requiring systematic work with the self-assessment process findings. The self-assessment process success depends on readiness for spending resources for its execution and on the chosen self-assessment process method.

The basic goal of the self-assessment is to find the company strong aspects, but especially to reveal opportunities for improvement. A customer for the self-assessment shall always and exclusively be the organisation senior management, which may find out, at the same time, where the organisation stays at the road to excellence and prosperity from the self-assessment.

Application of the self-assessment methods represents for the organisation the following advantages:

- it is an assessment based on facts – it is the examination and evaluation of proofs with subsequent quantification of the QMS advance;
- it is very effective form of learning of people within the organisation, it leads the employees to reveal strong and weak aspects;
- it is a strong instrument for revealing and detection of weak spots;
- it provides with quantifying results and it forces the organisation to introduction and systematic use of different measurements;
- it allows to participate in the quality management for wide spectrum of employees;
- it allows continuous assessment of the achieved excellence status also in comparison with other organisations;

There exist several methods of the self-assessment process execution, which have common basic algorithm. The last step of this algorithm is the output that should be a comprehensive list of weak aspects, i.e. opportunities for improvement. The list shall serve as an input for decisions on courses for further improvement, as it has been stated in the management review as well.

Conclusion

Quality management is a very dynamic category and in connection with ongoing society development in changing conditions goes into new meaning. Currently is not enough, if organization provides quality products, which meet requirements of customers, but also must take into account the interests of all interested parties and accept the requirements of the environment. In this meaning, the quality management obtains still broader content and there have to be involved also limiting conditions involving the quality of all activities involved in providing the site, interests and aspirations of human needs into understanding of quality of products and services.

In the accordance with systematic approach is in the present in the quality management required application of the no measurement processes, which don not have features of technical measurements and they are called systematic measurements. Measuring process is enhanced for measuring and monitoring, which is linked for example with quality management performance system, performance of processes, satisfaction of customers, satisfaction of employees and other involved parts, costs related to the quality etc. These measurements are not only for mining of information, they are the base for further analysis and consecutively improvement. Application of the consecutively improvement is requirement for the success of the organization and however for the sustainably development.

This paper was supported by the Slovak Research and Development Agency under the contract No. LPP-0384-09: "Concept HCS model 3E vs. Concept Corporate Social Responsibility (CSR)." The paper is also a part of submitted KEGA project No. 037STU-4/2012 "Implementation of the subject "Corporate Social Responsibility Entrepreneurship" into the study programme Industrial management in the second degree at MTF STU Trnava".

References

- [1] STN EN ISO 9004:2009: *Manažérstvo trvalého úspechu organizácie. Prístup na základe manažérstva kvality*
- [2] STN EN ISO 9001:2009: *Systémy manažérstva kvality. Požiadavky.*
- [3] I. Paulová a kol.: *Perspektívy rozvoja manažérstva kvality v súvislosti s požiadavkami trhu Slovenskej republiky*. Trnava: AlumniPress, 2010. ISBN 978-80-8096-129-9
- [4] J. Nenadál: *Měření v systémech manažmentu jakosti*. Praha: Management Press, 2001. ISBN 80-7261-054-6
- [5] H. Fidlerová: *Návrh procesného modelu environmentálne orientovanej logistiky priemyselného podniku*. Trnava, AlumniPress, 2008. ISBN 978-80-8096-070-4
- [6] K. Teplická: *Základná charakteristika procesov v oblasti manažérstva kvality*. Košice: TU. Dostupné na internete < <http://katedry.fmmi.vsb.cz>>



International Conference on Innovative Technologies, IN-TECH 2012,
Rijeka, 26. - 28.09.2012



INCREASING OF THE INTERNAL COMBUSTION ENGINES PERFORMANCES THROUGH THE INTAKE MANIFOLD SYSTEM

I. Hiticas¹, D. Marin² and L. Mihon¹

¹ Politehnica University of Timisoara, P-ta Victoriei, nr.2, RO-300006, Timisoara, Romania,

² Hautes Etudes d'Ingenieur, 13 rue de Toul, F-59046, Lille Cedex, France

¹ Politehnica University of Timisoara, P-ta Victoriei, nr.2, RO-300006, Timisoara, Romania

Keywords: intake manifold system, CFD simulation, engine performances.

Abstract. Nowadays the vehicles are not used just for transportation, but to offer safety and comfort. Designers and engineers have continually analyzed and redesign new solutions and systems for vehicles that offer high performance at lowest costs. The air filter is one of these systems. Electronic command and control systems have found applications in automotive area, the experimental tests conducted in laboratory in real time (like hardware in the loop simulation), are able to eliminate many errors. In this paper it was studied the air flow inside the filter housing, using the CFD (Computational Fluid Dynamics) simulation software, resulting the important influence of the air filter system on vehicle performance. This paper presents studies, research and experimental tests performed on air intake system of today's road vehicles, being mentioned the importance of the simulation when we have a goal to achieve, and our purpose is to obtain a higher performances of the internal combustion engine.

Introduction

Increasing demands on improving vehicles performances, the complexity processes of the internal combustion engines, the reduction of fuel consumption, the reduction of the CO₂ emission [1], had made the today's engineers and researchers from area, to reanalyse the systems which until now have been left on the second plane. The intake manifold is one of these systems [2]. Our studies are regarding the theoretical studies and experimental research about the role of the intake manifold in formation and distribution of the fuel mixture of the internal combustion engine.

The intake manifold system is one of the most important systems concerning the functioning of the vehicle. For thermal engine it is impossible the functioning without O₂, which is a component of the earth atmosphere [4] (which involves several elements, the main elements are N₂ – 78.1%, O₂ – 20.9%, Ar – 0.9%, CO₂ – 0.035% and others – 0.065%).

A part of intake manifold tasks are:

- Separation of solid particles from intake air to avoid their penetration inside the cylinder
- Improving performance of the engine through optimal location in relation to the intake manifold
- Preventing absorption of water to not affect the life of the filter and air flow meter
- Preheat the intake air to help optimize the engine torque and for lower fuel consumption.

But today's vehicles require more from an intake manifold system, like:

- Resistance at temperature from – 40 ° C to 100° C, resistance to thermal shock and aging
- Chemical resistance to the engine oil, to fuel vapours and crankcase gases
- Range as high maintenance, up to 120,000 km;

Taking into account these basic functions [5, 6] the intake manifold has and another important place on increasing the performances of the engine thought the supercharging effect due to the shape of the intake. The controlled movement of air currents, with some new valves installed specifically for this purpose, it could be improved the fuel mixture formation and the combustion process. These lead us to a reduction of the fuel consumption, and thus reducing the exhaust.

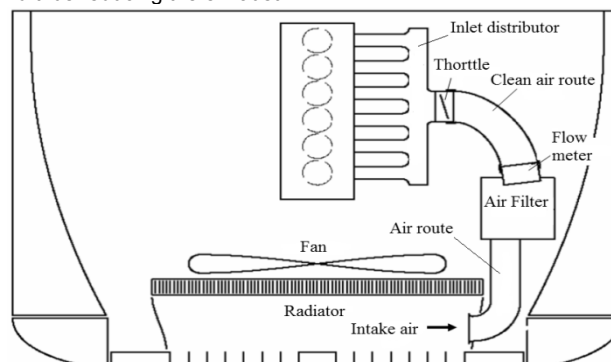


Figure 1 – Constructive scheme of filter system

Technical Data

The internal combustion engine, as we know, transforms the heat produced by the fuel burning inside the combustion chamber, in mechanical work. Four-stroke engine is running a complete cycle in four races, which involves two rotations of the crankshaft. To achieve an engine cycle [7], it is necessary to be introduced a fresh fluid, process called intake, and here it comes the intake manifold system. The exhaust process must evacuate, from the cylinder, the combustion gases and the intake manifold must introduce a huge quantity of fresh air to resume the motor cycle. Calculation of A_r – air requirements, for an engine with spark ignition and 4-stroke is given by equation:

$$A_r = \frac{D \times S \times E_f}{2}, \quad (1)$$

were,

- D – displacement [mc]
- S – speed [rpm]
- E_f – the filling efficiency

Proportional dependence of air flow reaching the engine and power indicated, at constant speed, is shown in the equation:

$$P_i = \eta_i \frac{\dot{m}_a}{\lambda L_{min}} Q_i, \quad (2)$$

were,

- P_i – power indicated [W]
- η_i – indicated efficiency
- ṁ_a – airflow rate [kg/sec]
- λ – excess air coefficient
- L_{min} – minimum air necessary for combustion [kg_{air}/kg_{fuel}]
- Q_i – lower calorific power of fuel [J/kg].

The main purpose of the gas exchange system is to introduce and to keep inside the cylinder the maximum amount of air necessary for combustion. This exchange involves the intake and exhaust processes.

The mathematical model used for calculation the intake process is taking into consideration the following:

- Pressure is constant during the intake stroke
- Intake begins in TDC and the period of simultaneous opening of valves is null
- Fresh fluid is heated by the walls of the intake path
- In the beginning of intake process, inside the cylinder are residual gases
- At the end, but during the intake process, inside the cylinder is a homogeneous mixture of combustion gases and fresh fluid
- Variable parameters, such as speed inside the intake manifold (w_{ga}), the flow velocity beside the valves (w_{sa}), are considered constant throughout the intake process.

To have, the thermal engine, a normal function, it must be solved the problems which appears along the air intake process. It is know that the air is not a perfect fluid, and for this reason we accepted the previous points. We have to mention and other elements, which are presented along this process, like hydraulic resistance of intake route, air compressibility, and different values for pressure and for temperature [8].

The followed equations are used to calculate different parameters for air intake process:

- Mass conservation:

$$\frac{d\rho}{\rho} + \frac{dw}{w} = 0, \quad (3)$$

were,

- ρ – fluid density [kg/m³]
- w – speed of the flow [m/s]

- Impulse conservation:

$$dp + \frac{4 \cdot t_p \cdot dx}{D} + \rho \cdot w \cdot dw = 0, \quad (4)$$

were,

- p – static pressure [Pa]
- t_p – peripheral tension given by the friction between fluid and walls [Pa]
- x – length of the pipe [m]
- D – diameter of the pipe [m]

- Energy conservation:

$$c_p \cdot dT + w \cdot dw = 0, \quad (5)$$

were,

- c_p – specific heat of fluid [J/kg]
- T – fluid temperature [°K]

- thermodynamic equation state:

$$\frac{dp}{d} = \frac{d\rho}{\rho} + \frac{dT}{T}, \quad (6)$$

and

- tension definition:

$$T_p = \frac{1}{8} \cdot f \cdot \rho \cdot w^2, \quad (7)$$

were,

- f – local coefficient of friction, Darcy.

Along the route of intake air, are presented the hydraulic resistances, which are calculated with different equation, like next equation for the throttle, one of the important hydraulic resistances:

$$\zeta_{sf} = \frac{120}{Re} \cdot \frac{1 + \frac{1}{2}(1 + \sin\delta)}{(1 - \sin\delta_i)^2} + \left(1 - \frac{50}{Re}\right) \cdot \left(\frac{1.56}{1 - \sin\delta} - 1\right)^2, \quad (8)$$

Were,

ζ_{sf} – hydraulic resistance coefficient of the throttle

δ – angle of throttle position, toward the axis of air flow.

Another important hydraulic resistance is produced by the conical valve:

$$\zeta_{cv} = 2.7 - \frac{0.8}{\frac{h}{d_{0a}}} + \frac{0.14}{\left(\frac{h}{d_{0a}}\right)^2}, \quad (9)$$

were,

ζ_{cv} – hydraulic resistance of the conical valve

h – pumping valve [m]

d_{0a} – channel's diameter of the cylinder head [m]

Pressures waves it is another phenomenon which is presented in the intake air process. Is produced by the opening and closing the waves and also, by the movement of the cylinder in the intake process. Pressure wave propagation in gas column of inlet path are made on speed of sound, so by providing the route length, with pressure oscillation wave length, it can be obtained significant improvements of the degree of filling, even a dynamic boost.

At the end of the calculation, are resulted the engine fluid status.

Experimental research

The experimental research was conducted inside of Mahle Timisoara testing laboratory. The first stage of the experiments was to create the model by CFD simulation [9, 10]. The advantages of the CFD simulation are made up by difficult areas which cannot be studied by experimental research, and also the boundary conditions cannot be properly controlled during the experimental analysis. Another advantage of these simulation are the cost, because the errors or the problems during the simulation process can be easily solved, compared by the experimental research situation.

The simulations are made on an inhomogeneous fluid, with uneven flow to take into account the sequential opening of the intake valves. The purpose of this simulation is to determine the pressure distribution on each intake channel for each cylinder, during four cycles and analysis of flow uniformity on the surface of separation between intake manifold and cylinder head. After the simulation process, where it was created the air flow model and after the optimisation of 3D model, we build the intake manifold which was subjected to experimental tests to determine the accuracy of the values from simulation.

For testing we choose the intake manifold from the engine BMW N52, with ne following dates:

- Year of manufacturing – 2004
- Fuel – Petrol
- Capacity – 2996 cm³
- Mass – 1580 kg
- Number of cylinder – 6 (in line)
- Power – 189.2 kW at 6600 rpm
- Torque – 300 Nm at 2500 – 4000 rpm
- CO₂ emission – 226 g/km
- Compression ration – 10.7:1

The simulation process started with difference between individual intake routes, called dispersion, D , calculated with relation:

$$D = \frac{(M-m)}{p}, \quad (10)$$

Were,

M – maximum pressure drop

m – minimum pressure drop

p – average pressure drop

The pressure drop, PL , is given by the relation:

$$PL = \frac{P_o}{P_i}, \quad (11)$$

Were,

P_o – outlet pressure

P_i – inlet pressure

The next figure shows the 3D model of CFD simulation with the discretized model (a) and the distribution of the velocity (b)

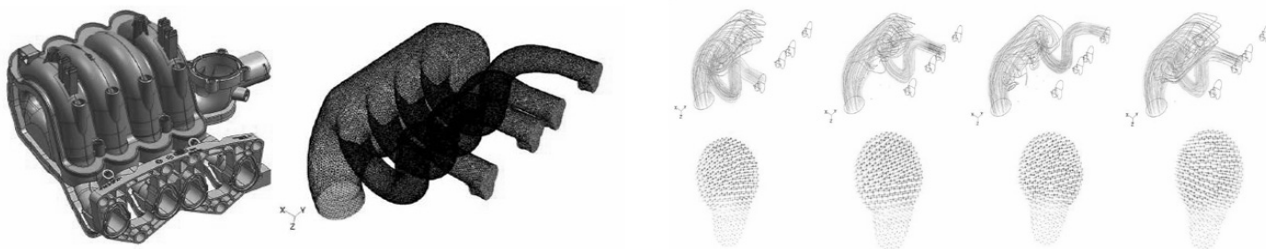


Fig. 2 a) 3D model and discretized model of CFD simulation

b) Velocity distribution inside the collector

The imposed condition during the simulation was [11, 12]: pressure set out in individual channels -50 mBar, and the frequency of applying the pressure to the output channel -1250 cycles per minute. This figure 2 b) presents us the velocity vectors inside the intake manifold, with red colour are the vectors for high speed (200 m/s), and with blue colour are the vectors for low speed (50 m/s). It can be observed the reduction of the speed after the entry in distributor, also the speed increase to the outlet from the individual channels. There were two attempts to compare results obtained from optimizations made and the resulted are presented below:

Table 1 – Simulation values

Individual channel	Pressure drop				D (%)
	1	2	3	4	
First simulation	8.30	8.60	8.40	9.20	10
Second simulation	8.60	8.90	8.75	8.75	3.4

There were made two tests to compare the results obtained from optimizations. It can be seen subtracted the value of dispersion, uniform velocities of individual channels.

To determine individual flow values of the inlet channels [13], we take the BMW N52 intake manifold model. To correlate the data with experimental tests, the gallery is subjected to testing performed on a bench, built specifically for measuring pressure differences, thus deducting the debts secured by individual galleries.

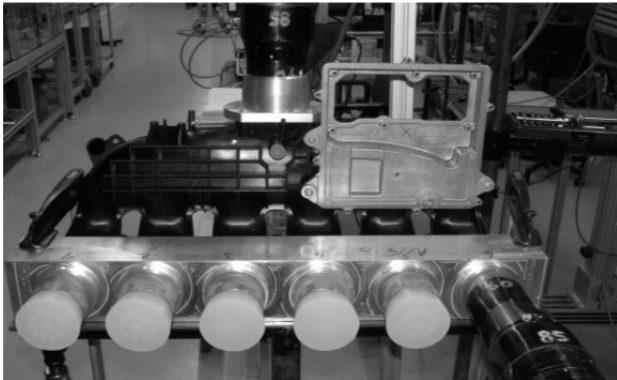


Fig. 3 – Functional scheme of the bench test

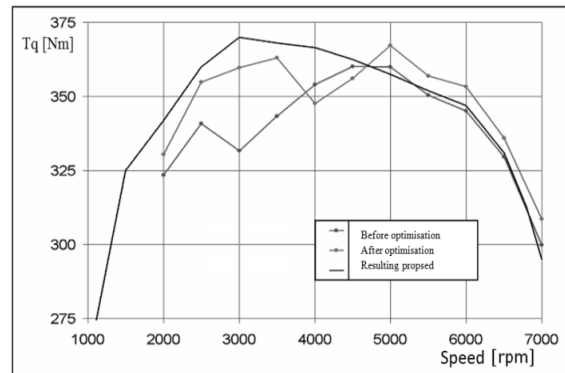


Fig. 4 – Influence of simulation and optimization on engine performances

Conclusion

Analysing the influence of the intake manifold concerning the performances of today vehicle, after our research we can affirm that the today's engine are able to offer high power and torque because all the systems and elements have been reanalyzed and redesigned for this purpose and the intake manifold is one of this system. In our simulation with CFD software, we made a model chose from a vehicle from our days, the BMW N52, E63 engine, and we calculated the influences of the pressure, the hydraulic resistance, the wave phenomenon and other several elements across the simulation, followed by the experimental testing made in a laboratory specially designed for this purpose. Analysing the experimental research we observe that the curve of the simulation bring us close to the proposed target. In figure 8 is easily to observe the advantage of the simulation, concerning the torque of the engine, compared with the purposed result.

As future research, another phenomenon that we mentioned and which comes with the intake process is the phenomena of wave. It is a phenomenon that can improve a fresh flow air inside the cylinders, which creates a dynamic supercharging without additional blower installation, situation what must be analyzed and proved the benefits.

Acknowledgment

This work was partially supported by the strategic grant POSDRU/88/1.5/S/50783, Project ID 50783 (2009) co-financed by the European Social Fund – Investing in People, within the sectorial Operational Programme Human Resources Development 2007-2013. This work was partially supported by the strategic grant POSDRU/21/1.5/G/13798, inside POSDRU Romania 2007-2013, co-financed by the European Social Fund – Investing in People.

References

- [1] S. Moazzem, M.G. Rasul, M.M.K. Khan: An Evaluation of CO₂ Emission Reduction through Carbonation Technology, *Power and Energy Engineering Conference (APPEEC)*, 2011 Asia-Pacific, Wuhan, 2011, pp. 1 – 5.
- [2] A.Algeri, S. Bova, C. de Bartolo, F. Fortunato: Numerical analysis of the flow field in the filter housing of a four-cylinder spark ignition engine, *1st International Conference on Motor Vehicle and Transportation MVT 2006*, Timisoara.
- [3] A. Algeri, S. Bova: Influence of valve-wall distance on the intake flow in high performance I.C.E., *SAE International*, 2004.
- [4] J.C. Gervin, C.R. McClain, F.G. Hall, P.S. Caruso: A comprehensive plan for studying the carbon cycle from space, *Aerospace Conference 2003*, Proceedings 2003 IEEE, vol.1, pp. 1 - 172.
- [5] R.Bosch Gmbh: Gasoline-Engine Management, Handbook, 2nd Edition, Germany, 2004.
- [6] R. D. Atkins: An Introduction to Engine Testing and Development, Handbook, *SAE International*, 2009.
- [7] S.Ratiu, Liviu Mihon: Motoare cu ardere internă pentru autovehicule rutiere –procese și caracteristici, *Editura Mirton*, Timișoara, 2008.



International Conference on Innovative Technologies, IN-TECH 2012,
Rijeka, 26. - 28.09.2012



- [8] R.Hentiu: Studii si cercetari privind influenta sistemului de admisie asupra performantelor motoarelor cu aprindere prin scanteie si injectie indirect de combustibil, *Editura Politehnica*, Timisoara, 2011.
- [9] T. K. Sengupta: Fundamentals of Computational Fluid Dynamics, *Universities Press*, Hyderabad, (India), 2004.
- [10] E. S. Oran, J.P. Boris: Numerical simulation of reactive flow. 2nd edition, *Cambridge University Press*, New-York, 2001.
- [11] L. Xie, H. Ogai, Y. Inoue: Engine intake manifold modeling and high speed solving for predictive control, *International Conference on Control Applications*, 2006 IEEE, Munich, pp. 515 – 520.
- [12] A. Al-Sarkhi, F. W. Chambers: Optimization technique for design of automotive air filter housings with improved fluid dynamic performance and filtration, *Particulate Science and Technology*, Vol. 22, 2004, pp 235-252.
- [13] J. Deur, D. Hrovat, J. Asgari: Analysis of mean value engine model with emphasis on intake manifold thermal effects, *Control Applications 2003, CCA 2003*, Proceedings of 2003 IEEE, vol.1, 2003, pp. 161 – 166.

Address for correspondences: I.Hiticas – ihiticas@yahoo.com, D.Marin – marindaniel1@yahoo.com, L.Mihon – liviu.mihon@mec.upt.ro



International Conference on Innovative Technologies, IN-TECH 2012,
Rijeka, 26. - 28.09.2012



SIMULTANEOUS MEASUREMENT OF VELOCITY AND TEMPERATURE FIELD DOWNSTREAM OF A HEATED CYLINDER

P. BENCS¹, Sz. SZABÓ², D. OERTEL³

^{1,2} Department of Fluid and Heat Engineering, University of Miskolc. H-3515 Miskolc-Egyetemváros.
Tel.: +36 46 565 154, Fax: +36 46 565 471, E-mail: arambp@uni-miskolc.hu, Hungary

³ Laboratory of Fluid Dynamics and Technical Flows, University of Magdeburg "Otto von Guericke".
D-39106 Universitätsplatz 2. Magdeburg.

Tel.: +49 0 391 67 18654, Fax: +49 0 391 67 12840, E-mail: dariaoertel@lavabit.com, Germany

Keywords: heated cylinder, Schlieren, PIV, experiment, velocity field, temperature field

Abstract. The flow around heated cylinders has already been investigated by many researchers. Object of the present examination is an electrically heated circular cylinder placed in a parallel flow in a wind tunnel. The experimental tests were carried out at low Reynolds numbers ($Re < 200$), thus the flow field was approximately two dimensional (same flow in every normal plan of the heated circular cylinder). The relationship between the vortices and the heat transfer was determined by relevant numerical simulations. Experimental results showed that vortices are shed with a frequency almost identical to that of the heat transfer from the cylinder. This transfer takes place in 'heat packages'. Validation of numerical simulations (in case of velocity field) was done with the help of PIV (Particle Image Velocimetry). The main objective of the present experimental investigation is validating the temperature field results of numerical simulations. Two dimensional flow and the principle of Schlieren measurement technique were used to visualize the temperature field. The Z-type Schlieren technique was applied to measure the temperature distribution. The experiments were carried out at forced convection in a $500 \times 500 \text{ mm}$ cross-section wind tunnel. The measurement technique and results were shown at different levels of forced convection.

Introduction

Bluff bodies placed in a flow often have a different temperature compared to that of the surroundings, e.g. in case of heat exchangers. The structure of the flow around bluff bodies has been already examined in many studies [1-6]. The observed Kármán vortex street has been the subject of numerous experimental and numerical investigations.

Nevertheless, it is still unclear how this vortex street might be modified in the case of a heated body. What is the possible influence of heating on the frequency of the detaching vortices, on the structure of those vortices and on the location of the detachment? A further important issue is the heat loss associated with the vortex structures and the forced convection. The objective of the present work is to present first development steps for a measurement method allowing a quantitative investigation of these issues.

The development and validation of this method requires a well-defined flow. Therefore, a low Reynolds number flow ($Re < 200$) is first considered. Such a flow is mostly two-dimensional, i.e. the flow does not change considerably along the axis of the cylinder. The experiments are carried out in an open wind tunnel with a measurement cross-section of $500 \times 500 \text{ mm}$. The employed bluff body is an electrically heated cylinder of 10 mm diameter. The wake of the cylinder is investigated when placed in an air flow with 0.3 m/s mean velocity and 28°C temperature and with imposed cylinder temperatures of 100 , 200 and 300°C .

The main innovation of the developed method is the simultaneous and quantitative determination of the velocity and temperature fields. For this purpose, the Z-type Schlieren method is employed to measure temperature together with Particle Image Velocimetry (PIV) for velocity. All recorded images from both methods are processed by the commercial software from TSI® and Matlab®.

Experimental setup

In the following the measuring setup is introduced by describing the wind tunnel, the heated cylinder, the PIV/BOS methods and the triggering, which was important for the connection between the velocity and temperature field of the flow behind the cylinder.

The flow behind a heated cylinder was investigated in an open wind tunnel. The cross-section of the measurement area had the dimensions of $500 \times 500 \text{ mm}$. The mean flow velocity was set to 0.3 m/s , since this was the minimum stable velocity of the wind tunnel in this configuration. This led to a flow Reynolds number of $Re = 9,460$, calculated from the mean flow velocity in the test section, the hydraulic diameter and the viscosity of the air at ambient temperature.

Two transparent windows were mounted on both sides of the measurement section, with a hole in the middle, used to mount the heated cylinder transversally to the main flow direction (see Fig. 1). The cylinder with a diameter of 10 mm was electrically heated by an adjustable transformer. The mean temperature of the cylinder was measured by a thermocouple and the power of the transformer was adjusted according to the desired value. The cylinder Reynolds number was $Re = 100$, calculated with the mean flow velocity, the diameter of the cylinder and the viscosity of the air at the reference temperature [6] of $T_r = 0.5 \cdot (298 + 573) [\text{K}]$ ($\nu = 2.984 \cdot 10^{-6} \text{ m}^2/\text{s}$). The predicted frequency of the vortex shedding was $f_s = 4.8 \text{ Hz}$, calculated from a Strouhal number of $St = 0.16$ [6].

The main objective of the measurements discussed in this publication was to investigate the relation between the velocity and temperature field behind this heated cylinder in a low Re-number (cylinder reference) flow. The system used for the present measurements was a regular 2D-PIV system and a Z-type Schlieren system, consisting of the components listed in Table 1.

The applied software for the acquisition and evaluation was commercial PIV software (INSIGHT3G™ from TSI), used for the PIV measurements. The PIV and Z-type Schlieren measurements are only briefly discussed here, since there are numerous publications describing the principals of PIV (e.g., [7]). Two different cameras were used to PIV and Schlieren measurements. The PIV camera was

calibrated with the help of a calibration plate to set the pix/mm factor and to eliminate possible distortion. The camera optics was focused on the calibration plate and the f -number was set to 4.

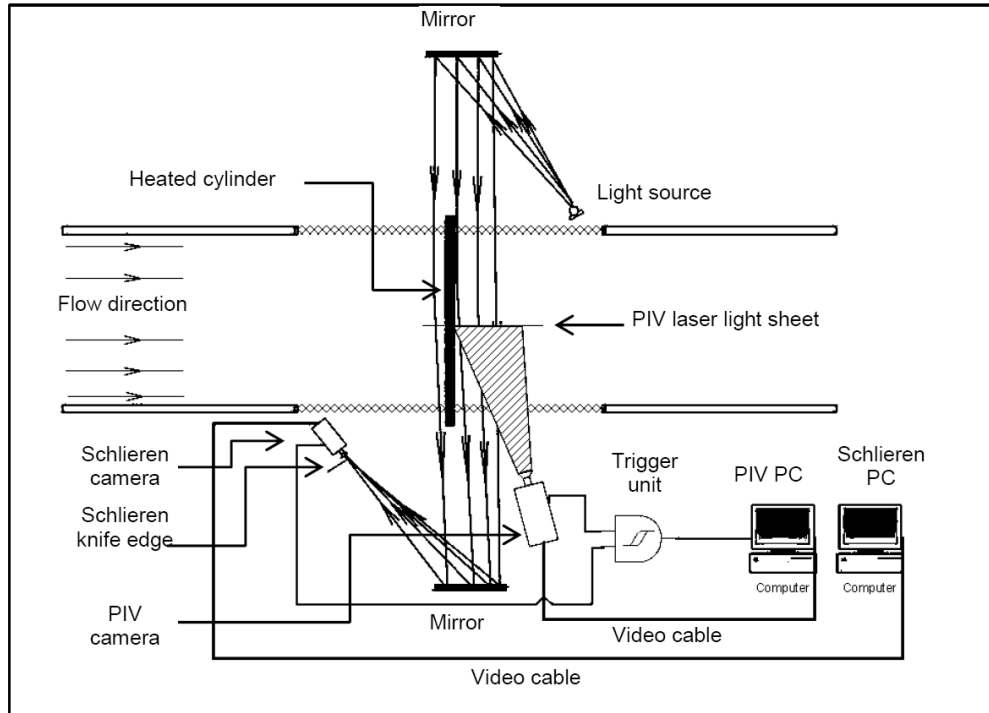


Fig. 1 Schematic of experiment setup

Table1. Description of the PIV and Z-type Schlieren system

Component	Remarks	Manufacturer
PIV system		
Double frame CCD camera	PowerView™ Plus 4MP PIV camera with 12bit resolution, recording freq.: 15Hz	TSI
Objective	AF Nikkor 50mm f/1.8D; f -number: 4 and focus set to 500mm	Nikon
Double pulse Nd-YAG laser	Power: 2x135mJ at 532nm, max. frequency: 15Hz	Litron
Trigger box	Synchronization of PIV camera and laser timing and trigger signals of the Schlieren camera	TSI
PC with a frame grabber card and PIV software	For image data acquisition and for the processing of the acquired data	TSI
Z-type Schlieren system		
CCD camera	AVT Stingray F-033C CCD camera with 16bit resolution	Allied Vision Technologies
Objective	75mm Focusable Double Gauss Lens; f -number: 4 and focus set to 2000mm	TECHSPEC®
PC with a firewire 1394b card and software	AVT SmartView v1.13.1, For image data acquisition and for the processing of the acquired data	Allied Vision Technologies
Schlieren light source	Super Bright White LED, 530XW8C, 8000mcd	-
Schlieren mirrors	Mirror thickness: 25% of the diameter; Optical quality of the mirror: $\lambda/8$; Offset angle: $\theta=3^\circ$; Power of lens: $f/10$; Distance between the mirrors: 4500mm.	ANCHOR Optics

The sensitivity of a measuring instrument is one of its basic characteristics, relating the output of the instrument and the input received. In the case of the here considered Schlieren optics, the output is a 2-D image in x and y – coordinates. More specifically, it is an array of picture elements characterized by their amplitude or grayscale contrast variations.

In a Schlieren system, the blockage of light by a knife-edge placed at the exit focal plane is due to the deviation of light by an inhomogeneous medium. This blockage can be similarly obtained in a homogeneous medium by a knife-edge which is allowed to be

translated laterally by a quantity Δx . By considering this, we can establish a relationship between the light levels at the observation plane (the exit focal plane) to the corresponding transverse knife-edge position. This transverse position may cover the conditions from no cutoff of light (maximum intensity) to full cutoff of light (minimum intensity). Relationship between Δx and light intensity was determined by 3-axis stage (see in Fig. 2).

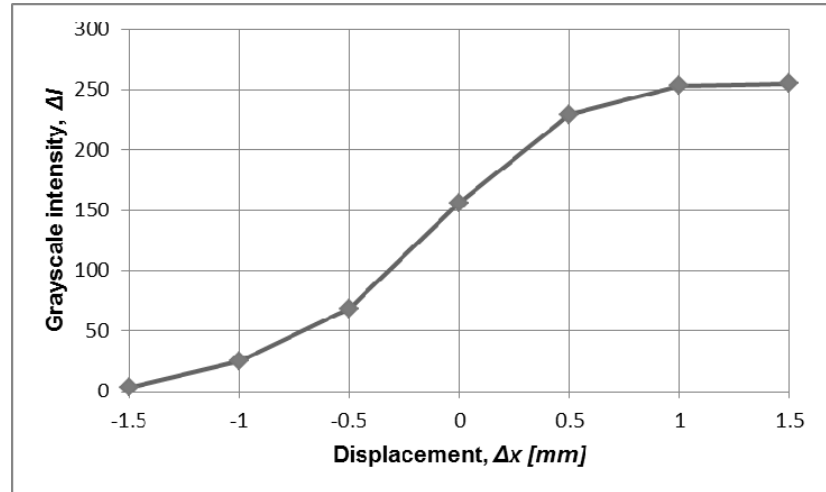
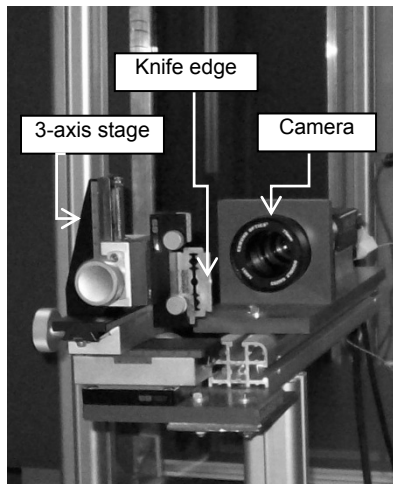


Fig. 2 Knife edge with 3 axis stage and calibration curve

Measurement results

The raw PIV (laser lighting) and Z-type Schlieren (LED lighting) recordings are shown in Fig. 3. The vortex shed can be seen in the PIV picture (left image). The diffraction, caused by the air density change near the heated cylinder, can slightly be seen in the Schlieren picture.

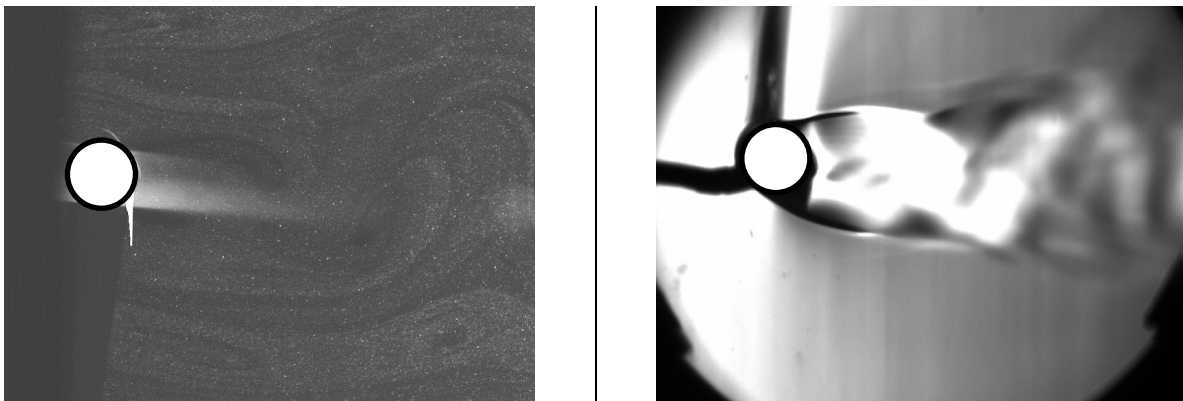


Fig. 3 PIV and Schlieren raw picture (heated cylinder surface temperature: 300°C and mean velocity: 0.3m/s)

The resulting velocity field (PIV method) and temperature field (Schlieren method) are shown in Fig. 4. More details about PIV and Schlieren method can be found in the references [7-9]. The periodicity of the vortex and temperature detachment can be seen in Fig. 4 (velocity vector field and temperature field).

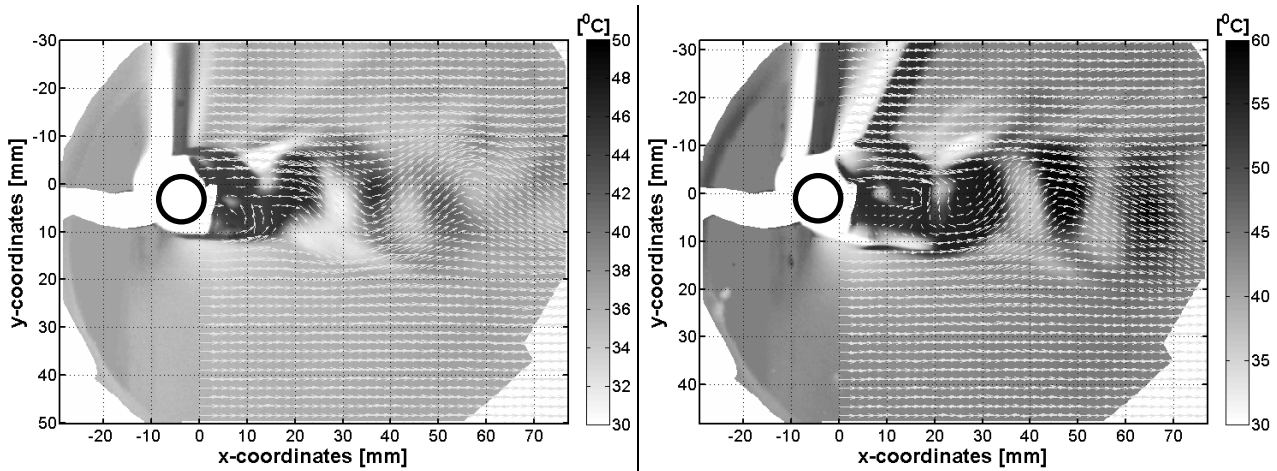


Fig. 4 Temperature- and vector field (100°C (left) and 200°C (right))

The results of temperature field only visualized the average value of the 3D flow (because the principle of Schlieren measurement technique). Both end of the heated cylinder was outside the wind-tunnel; so the free convection (outside the wind tunnel) can be seen in Fig. 4-5 (vertical temperature distribution over the heated cylinder).

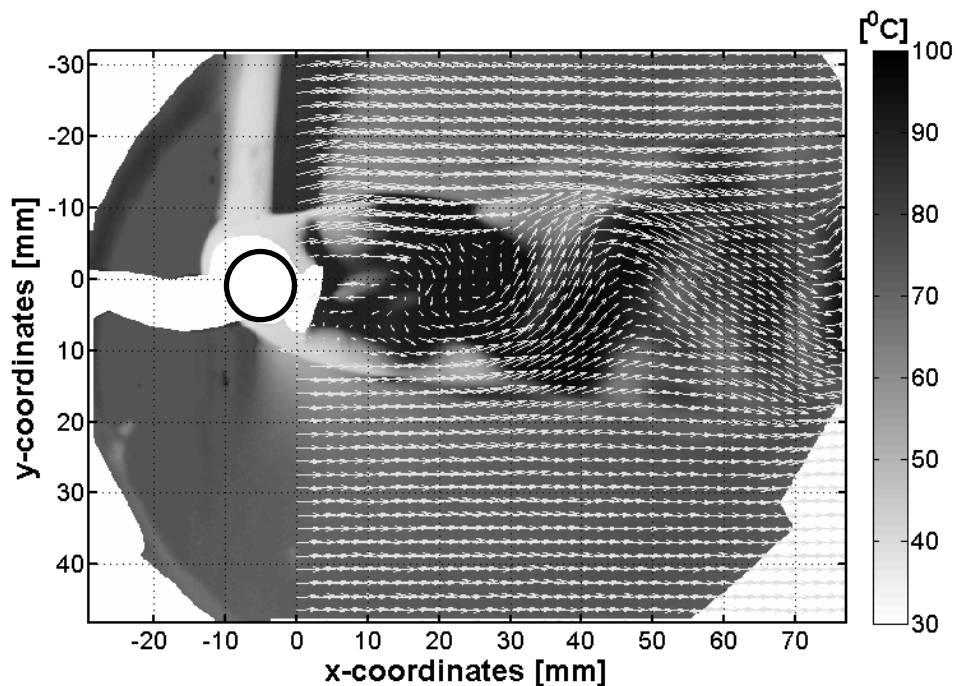


Fig. 5 Temperature- and vector field (heated cylinder surface temperature: 300°C and mean velocity: 0.3m/s)

Conclusions and future plans

The measurements results presented in this work confirm that the Z-type Schlieren system is in principle suitable to visualize and quantitative analyze the temperature field in a wind tunnel. However, considerable improvement (such as precision color filter) is still required in the existing system to make more precise and really accurate measurements. In order to analyze the images in a further step, the recording quality must be increased to get more meaningful images. These temperature field results will be good to validate our results of numerical simulations (numerical simulations are made by own code and commercial software). The developed Matlab® script was successfully applied to the calculation of the temperature field from the measured deflection, resulting from the density variations in the flow. Thank to the employed triggering mechanism, the temperature and velocity measurements could be reasonably synchronized and finally presented simultaneously. A further validation possibility should also be found to check the measured temperature values in the aim to detect the differences in vortex shading due to the temperature of the cylinder.

Acknowledgements

The authors are grateful to OTKA (76085), NKTH-OTKA (68207) and to the Hungarian-German Intergovernmental S&T cooperation programs P-MÖB/386 for the financial support of this research.

The described work was carried out as part of the TÁMOP-4.2.1.B-10/2/KONV-2010-0001 project in the framework of the New Hungarian Development Plan. The realization of this project is supported by the European Union, co-financed by the European Social Fund.



References

- [1] Williamson, C.H.K. Vortex dynamics in the cylinder wake. *Annual Review of Fluid Mechanics*, 1996. 28(1): p. 477-539.
- [2] Wang, A.B. and Tr vn ek, Z. On the linear heat transfer correlation of a heated circular cylinder in laminar crossflow using a new representative temperature concept. *International Journal of Heat and Mass Transfer*, 2001. 44(24): p. 4635-4647.
- [3] Baranyi, L., Szabó, S., Bolló, B., and Bordás, R. Analysis of Flow Around a Heated Circular Cylinder. in *The 7th JSME-KSME Thermal and Fluids Engineering Conference*. 2008. Sapporo, Japan: on a CD ROM (No. 08-201.), A 115. p. 1-4.
- [4] Bencs, P., Szabó, Sz.: Temperature field visualization around a heated circular cylinder by Schlieren technique. *Proc. MicroCAD '10 International Computer Science Conference*, Section F, Miskolc, Hungary (2010), pp. 61-66.
- [5] Bolló, B., Baranyi, L., Bordás, R., Tolvaj, B., Bencs, P., Daróczy, L., and Szabó, S. Numerical and experimental investigation of momentum and heat transfer from a heated circular cylinder. in *microCAD'08 International Scientific Conference*. 2008. Miskolc, Hungary. 978-963-661-816-2 p. 1-8.
- [6] Baranyi, L., Szabó, S., Bolló, B., and Bordás, R. Analysis of Flow Around a Heated Circular Cylinder. *Journal of Mechanical Science and Technology* 2009. 23: p. 1829-1834.
- [7] Adrian, R.J. Particle-Imaging Techniques for Experimental Fluid Mechanics. *Annual Reviews in Fluid Mechanics*, 1991. 23(1): p. 261-304.
- [8] Hargather, M.J., Settles, G.S. A comparison of three quantitative schlieren techniques. *Optics and Lasers in Engineering*, 2012. 50(1): p. 8-17.
- [9] Bencs, P., Szabó, Sz.: Application of Z-type Schlieren technique for Flow Visualization around Heated Cylinder. *Proc. 14th International Symposium on Flow Visualization*, Daegu, Korea (2010) pp. 1-7.



International Conference on Innovative Technologies, IN-TECH 2012,
Rijeka, 26. - 28.09.2012



APPLICATION OF THERMOGRAPHY TECHNIQUE FOR SURFACE TEMPERATURE VISUALIZATION OF A HEATED CYLINDER

Sz. SZABÓ¹, P. BENCS², A. FARKAS³

^{1,2,3} Department of Fluid and Heat Engineering, University of Miskolc. H-3515 Miskolc-Egyetemváros.
Tel.: +36 46 565 154, Fax: +36 46 565 471, E-mail: arambp@uni-miskolc.hu, Hungary

Keywords: heated cylinder, surface temperature distribution, thermographic camera

Abstract. The experiment of the flow around rod has been searched by many researchers. The object of this study to analyze the flow around a $\varnothing d=10\text{mm}$ diameter heated rod that was placed in low speed flow (mainly laminar flow). The wall temperature T_w , widely found in the literature, is generally considered to be constant, because experimental measurements are carried out using mostly small diameter (max. $\sim 2\text{mm}$) electrically heated rods [1,2]. In our case the diameter of the rod is $\varnothing d=10\text{mm}$, raising the question to whether the temperature distribution of the cylindrical surface depends on the flow direction at the angle measured. To answer this question we set up experimental equipment to measure cylinder surface temperature [3]. The surface temperature of a horizontally placed heated cylinder in a wind tunnel was measured by thermographic camera. The cross surface temperature was examined at different air speeds and different intensity of cylinder heating. The temperature distribution of cylinder surface can not be discarded and it was showed well definable characteristics. The measurements were carried out by a heated cylinder (a steel tube in a ceramics-coating electrical filament).

Introduction

The characteristic of heated cylinder experiments was described by dimensionless quantities and the number of similar such as other basic researching. The measurements were carried out in environment temperature and unheated cylinder (rod and air/water temperature was similar to the environment temperature), therefore it was not problem with temperature depend material properties. In case of the heated cylinder measurements were difficult to determine the correct temperature for the temperature depend material properties (particularly, if the temperature of the heated cylinder was higher than the environment temperature). The main question is, which is the correct temperature to calculate the temperature depend material properties (Reynolds number – kinematics viscosity, Nusselt number – thermal conductivity). In the basic case the environment temperature T_∞ was used for the calculation of the properties of material. Afterwards the T_f film temperature was established [4,5]:

$$T_f = \frac{1}{2} \cdot (T_\infty + T_w) = T_\infty + 0.5 \cdot (T_w - T_\infty). \quad (1)$$

The temperatures in the Eq. (1) were treated as constant. Afterwards from the measurements got the similar expression than the Eq. (1). This expression was suitable for the number of similar. The difference between the two expressions were only the 0.5 multiplier, because in the new expression was a C coefficient (it is different from 0.5). The temperature definition and number of similar was evolved from the experiment results. Effective temperature form was defined:

$$T_{eff} = T_\infty + C_{eff} \cdot (T_w - T_\infty), \quad (2)$$

where in the laminar flow case $C_{eff}=0.28$ value was acceptable. This equation was used to determine the $St(Re)$ correlation of similar [1].

Other definition was used by Wang and Trávníček [8] for calculation the Nusselt number by effective temperature and Reynolds number was calculated by represent temperature $Nu_f(Re_{rep}^{0.5})$:

$$T_{rep} = T_\infty + C_{rep} \cdot (T_w - T_\infty), \quad (3)$$

where $C_{rep}=0.36$. In every case the temperature depend material properties was calculated from only one heated cylinder temperature. Was the surface temperature of the bigger diameter of a heated cylinder constant in the reality? The main question is how depend on the surface temperature of the heated cylinder what was in flow (force convection)? How much is the integrated surface average temperature of the heated cylinder? The equation for small diameter wire (only one surface temperature) is suitable for the bigger diameter heated cylinder? To answer these questions we show step by step the experimental process. We successfully set up the experimental equipment to measure cylinder surface temperature, but the complexity and number of measurements are not still enough. The level and profile of the temperature distribution of the cylinder surface $T_w(\alpha)$ depending on the angle measured α was proved. The future work will be to analyze the effects of this relationship.

Experimental setup

The surface temperature of a horizontally placed heated cylinder in a wind tunnel was measured by thermographic camera. The images were taken from different directions along the framework and then assembled to form one image. The measuring apparatus is

shown in Fig. 1 as it is assembled in the wind tunnel test section. The heated cylinder is placed in the middle section of the test area and the same axis acts as both the cylinder axis and the framework, with the thermographic camera fixed to for the top cross bar of the framework. Based on the angular scale fixed on the framework we changed the angle of camera to observe the cylinder from $\beta=33^\circ$ to 144° . The test cylinder was placed in the test area with transparent side walls. In order to prevent recording error, we cut a longitudinal hole into the test area cover to provide direct sight to the heated surface of the measuring cylinder for the camera. The gap left free is just enough for angular positions of the camera to view the cylinder surface.

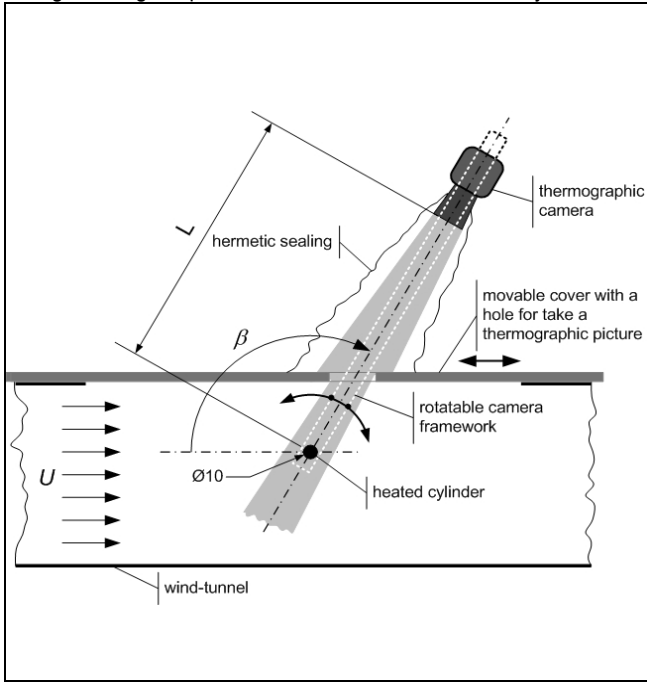


Fig. 1 Schematics of the experimental setup

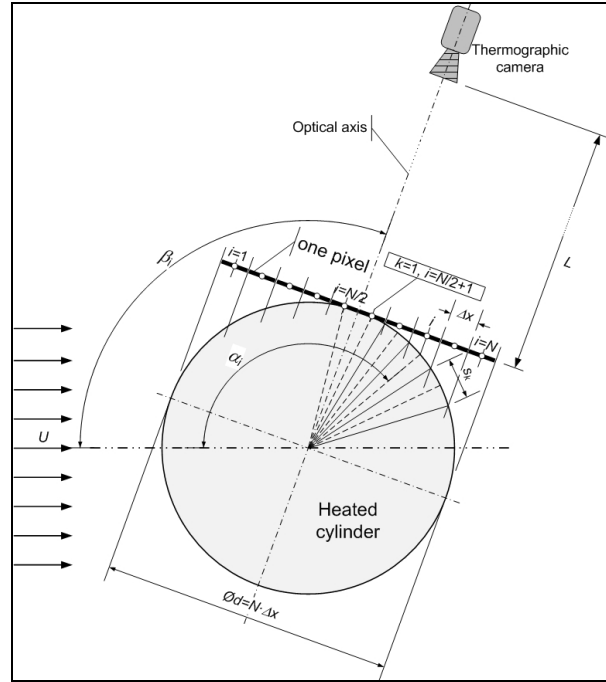


Fig. 2 Symbols of thermographic measurement

The space between the camera and this hole was separated by a flexible piping system from the environment in order to prevent the air leaving the channel. Thus, the air tightness of the test area was always ensured, despite the fact that the camera was located outside the channel. The distance between the camera lens and the heated cylinder (L) was chosen to be as small as possible in order to be able to view the cylinder cross section $\text{Ø}d=10\text{mm}$ with as many pixels as possible. The direction angles of thermal recordings are determined so that a cylinder point can be recorded from as many directions as possible. This ensures the accurate assembly of images and verifies the reliability of measurements.

The high resolution thermographic camera (Jenoptik VarioCAM hr 680) was chosen for its significant geometrical resolution (640×480 pixels) and fine resolution: $<50\text{mK}$ (30°C) the measurement for these reasons. The application of the maximum temperature range (max. 300°C) at approximately 2°C accuracy is quite good and definitely corresponds to the target for the implementation of the measurement tasks. The images are made by thermographic camera; each pixel of the camera-processing software assigns a temperature value to each pixel, which is provided in table form for the users. The temperature value of each pixel belongs to different angle values on the cylinder surface.

See in Fig. 2 for the determination of these angle values. The number of pixels falling on the cylinder perpendicular to the heated cylinder axis from the thermographic camera images is N . We assume that N is an even, whole number of pixels. Thus, the length of the pixels perpendicular to the axis of the cylinder length is $\Delta x=d/N$, where d is the diameter of the cylinder. The distance between the cylinder and the thermographic camera is L . In our study this distance was $L=400\text{mm}$, in this case the number of pixels is $N=36$. Based on the literature [3] we can state the center max. 17 pixels have nearly the same arc length.

Let β_i ($i=1, 2, \dots, 12$) be the angle between the flow direction and the camera's set optical axis: $33^\circ, 45^\circ, 60^\circ, 80^\circ, 85^\circ, 90^\circ, 95^\circ, 100^\circ, 105^\circ, 120^\circ, 135^\circ$, and 144° . The minimum and maximum angle of framework was limited by the wind tunnel geometric.

Measurement results

The viability of the method is shown in this part of the study. The measurement parameters are shown in the Table 1. The (Re) value was calculated by the environment temperature and the (Re_{eff}) value was determined by the Equation 2. and use the effective temperature.

Table1. The variation of the measurements

$t_{nominal} [^\circ\text{C}]$	100	200	300	100	200	300
U [m/s]	Re			Re_{eff}		
0.1	67	67	67	58	50	44
0.3	200	200	200	175	150	131
0.9	599	599	599	525	451	393

The typical measurement result is shown in Fig. 3, when the flow velocity is $U=0.9\text{m/s}$ and the heated cylinder nominal temperature is $t_{\text{nominal}}=300^\circ\text{C}$. The dimensionless $T_w(a)/T_{w,\text{mean}}$ absolute temperature is shown in Fig. 3. The plot data is only the center 17 pixel from every measurement data.

Fig. 3 shows, that every measurement data is overlapped. The important part of the plot is the $\alpha \approx 90^\circ$ point, because there is the maximum velocity speed around the cylinder (temperature decreasing). The other important part of the plot is the $\alpha \approx 100^\circ\text{-}110^\circ$ range, because there is the vortex shedding place.

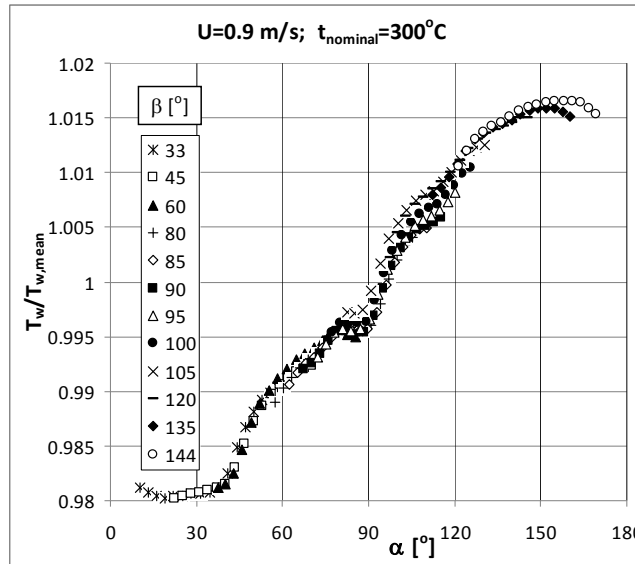


Fig. 3 Temperature distribution in the measurement points

This is the reason of the big standard deviation in the every measurement data. In the same place the temperature is decreased. The place of the vortex shedding [3] was analyzed in this measurement process. We try to find the relationship between this uncertain temperature part of the plot and the frequency of the vortex shedding. The results do not show this effect in spite of the fact that the camera frequency is 7 times faster, than the frequency of the vortex shedding. One of the reasons of this effect is that the accuracy of the camera is similar to this effect. These phenomena are independent from the flow velocity and temperature of the heated cylinder. The following figures will confirm this effect.

The surface temperature distribution is shown in Fig. 4, where velocity speed is $U=0.9\text{m/s}$ and the nominal temperatures of the heated cylinder are ($t_{\text{nominal}}=100^\circ\text{C}$, 200°C , 300°C). The temperature mean value was used for good arrangement to show the surface temperature distribution of the heated cylinder. The wall temperature of the heated cylinder was particularly changes around the heated cylinder surface (in the measurement points). The difference between the minimum and maximum value is depend on the nominal temperature of the heated cylinder. When the nominal temperature of the heated cylinder was 300°C , the difference is reaching 4% ($\sim 21^\circ\text{C}$). The difference between the minimum and maximum temperature is decreased in common with decreasing the nominal temperature of the heated cylinder.

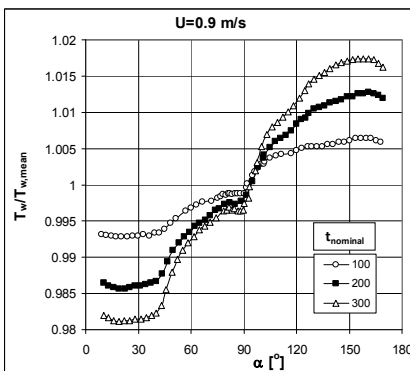


Fig. 4 Temperature distribution $U=0.9\text{m/s}$

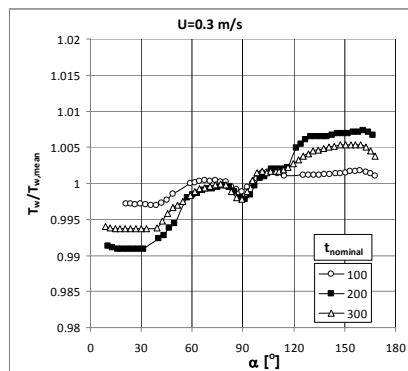


Fig. 5 Temperature distribution $U=0.3\text{m/s}$

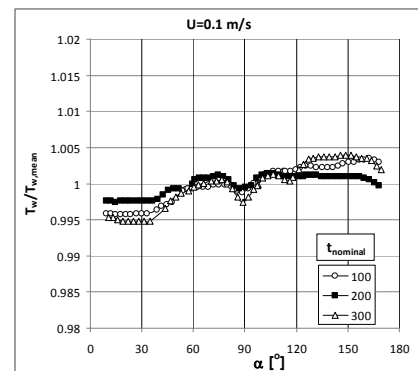


Fig. 6 Temperature distribution $U=0.1\text{m/s}$

The surface temperature distribution of the heated cylinder is shown in Fig. 5 and Fig. 6 (the nominal temperatures are similar and the velocity speed is $U=0.3\text{m/s}$, and $U=0.1\text{m/s}$). The temperature difference is also decreasing by the flow speed decreasing. The measurement result is shown is the same axis scaling for the good comparison. The uncertainty of measurement is increasing by the smaller temperature difference. The sequence of the temperature series is not same in the three cases. In case of the smaller temperature difference, the temperature series is not in ascending sequence.

The wall temperature is reached the nominal temperature value in the $\alpha=95^\circ$ and in every case. This effect was experienced in low speed cases and different angles (before and after the $\alpha=90^\circ$). In every case were experienced the cooling effect in the $\alpha=90^\circ$ and the decreasing temperature at $\alpha=100^\circ$ - 110° , which we attached to the vortex shedding effect.

Fig. 7 shows the temperature temporal variation in three surface point of heated cylinder. The results were obtained based on the video recording; the camera frequency was 50Hz, whereas in the case at one side of vortex detachment frequency was $\sim 18\text{Hz}$. Since the camera recording frequency was about seven times higher than the vortex detachment frequency, possible cyclic changes we should have been detected. The Fig. 7 showed that the vortex detachment and the accompanying heat transfer frequency are so strong that it can not follow a periodic cooling and warming of the cylinder surface. A stationary temperature distribution (thermal equilibrium) is formed that angel range, i.e. the temperature of the test points is practically constant.

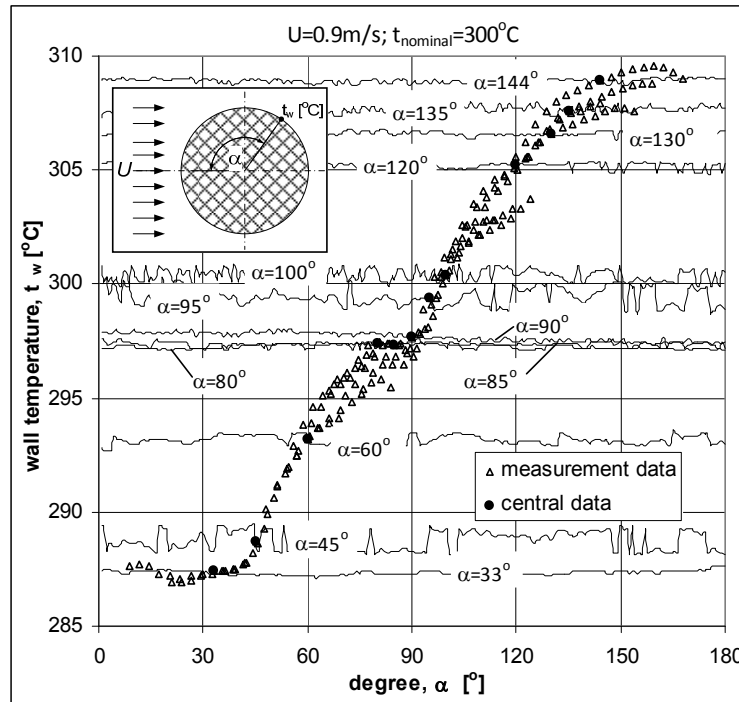


Fig. 7 Time variation of temperature in three point of the cylinder surface

Conclusions and future plans

The following statement was confirmed by our experiment: the surface temperature distribution of the heated cylinder was not neglectable especially in high flow velocity and high nominal temperature case. The main properties of the temperature distribution were shown around the cylinder perimeter.

The measurement results in high velocity and nominal temperature of cylinder case show the following statement: question arises as to how to consider the single surface temperature given in the literature of the dimensionless number of similar, and whether to give an average value for thermal characterization of the heat transfer.

Further processing of the results of numerous measurements is needed, yielding data from which we can draw further conclusion. The accuracy of the measurement will be increase and new temperature and velocity combination will be analyzed to quantify the experienced effects.

The experimental wind tunnel will be changed to the measurement will be done in the total angle range $\alpha=0^\circ$ - 180° .

Acknowledgements

The authors are grateful to OTKA (76085), NKTH-OTKA (68207) and to the Hungarian-German Intergovernmental S&T cooperation programs P-MÖB/386 for the financial support of this research.

The described work was carried out as part of the TÁMOP-4.2.1.B-10/2/KONV-2010-0001 project in the framework of the New Hungarian Development Plan. The realization of this project is supported by the European Union, co-financed by the European Social Fund.

References

- [1] A.-B. Wang, Z. Trávníček, K.-C. Chia: On the relationship of effective Reynolds number and Strouhal number for the laminar vortex shedding of a heated circular cylinder, *Physics of Fluids*, 12 (6), (2000), pp.1401–1410.
- [2] J. C. Lecordier, L. Hamma, P. Paranthoën: The control of vortex shedding behind heated circular cylinders at low Reynolds number, *Experiments in Fluids*, 10, (1991), pp. 224–229.
- [3] P. Bencs, Sz. Szabó, A. Farkas: Improvement of Thermovision Measurement Method for Analysis of Surface Temperature Distribution of a Body in Flow, *Proc. of Micro CAD International Computer Science Conference*, No. N, Miskolc (2012), Hungary, pp. 1-6.
- [4] M. N. Özisik: *Heat Transfer*, (McGraw Hill, New York, 1985).
- [5] Bejan: *Heat Transfer*, (John Wiley & Sons, New York, 1993).



-
- [6] Norberg,: Flow around a circular cylinder: Aspects of fluctuating lift, *Journal of Fluids and Structures*, 15, (2001), pp. 459-469.
 - [7] M.-H. Wu, A.-B. Wang: On the transitional wake behind a heated circular cylinder, *Physics of Fluids*, 19 (8), (2007), 084102-1–084102-9.
 - [8] A.-B. Wang, Z. Trávníček: On the linear heat transfer correlation of heated circular cylinder in laminar crossflow using new representative temperature concept, *International Journal of Heat and Mass Transfer*, 44, (2001), pp. 4635-4647.



International Conference on Innovative Technologies, IN-TECH 2012,
Rijeka, 26. - 28.09.2012



ANALYSIS OF FUZZY CONTROL SYSTEMS USING STABILITY INDEXES – SOME CASE STUDIES

R. P. Neco¹, R. Puerto¹, M.A. Vicente¹, C. Fernández¹

¹ Miguel Hernandez University, Av. de la Universidad s/n, 03202 – Elche (Alicante), Spain

Keywords: Artificial and Computational Intelligence, Control Systems, Fuzzy Control

Abstract. In this paper, we show some non-linear methods for stability analysis of fuzzy controllers. In the literature we can find a variety of stability analysis methods, but most of these methods are difficult to apply in practical engineering applications. In this paper we show how to use some of the bifurcation-based stability analysis methods which are common for the study of non-linear systems. The main conclusion of the paper is that the described analysis methods are valid for complex systems and, in addition, we have obtained some practical rules to adapt the conclusions obtained in the analysis to ensure the stability of the controlled systems.

Introduction

In this paper, we show the application of some non-linear stability analysis methods to the particular case of fuzzy controllers. Although these controllers have, in general, a satisfactory behavior for the control of complex non-linear systems, one of its main disadvantages is the lack of a simple method to ensure the stability of the controlled system, which is the main reason these controllers are not used for some critical applications. In the literature we can find a variety of stability analysis methods [1, 2]. In this paper we show how to use some of the bifurcation-based stability analysis methods which are common for the study of non-linear systems. In particular, we use two stability indexes (static bifurcation index and Hopf bifurcation index [1]) and show that they can be applied successfully to the analysis of some practical real-time fuzzy control systems.

As a result, we have obtained some practical rules to adapt the conclusions obtained in the analysis to ensure the stability of the controlled systems. In the experiments and examples studied in the paper we compute, using the described analysis methods, specific values for the parameters of the controller for which the closed-loop system should be stable. Then, we show that these *theoretical* values are very close to the *experimental* values obtained by simulation and real-time control. The practical use of the analysis methods implies the inclusion of a security margin, which depends on the static gain of the system, according to our experiments. In general, we have shown that this security margin should be about 10% of the gain of the system in order to ensure global closed-loop stability.

Fuzzy Controllers are knowledge-based or rule based-controllers in which there is a knowledge-base consisting on the so-called fuzzy if-then control rules [3, 4]. The fuzzy if-then control rules are statements that are expressed in terms of “natural language” rules, which are then quantified using continuous membership functions.

The starting point of the design of a fuzzy controller is to obtain the collection of fuzzy if-then control rules from human experts or from some knowledge database. The next step is to combine and quantify these rules into a controller which can be implemented. Different fuzzy controllers use different principles and parameters for this combination. For a detailed description of the structure of a fuzzy controller see, for example, [3].

Design and Analysis of the Controllers

In the experiments described in the next section we have designed fuzzy controllers using a combination of three groups of methods. These methods are the following:

- (1) Direct design. This is a knowledge-based trial and error method which obtains the control rules from an expert or from the analysis of the dynamics of the system.
- (2) Data-based design. In this method, the rules are obtained from input-output pairs of data which represent the desired behaviour of the controller.
- (3) Control rules to satisfy design requirements (settling time, overshoot, etc.).

Stability Analysis

The analysis of fuzzy controllers is quite complex because they are strongly non-linear systems. Therefore, non-linear analysis techniques should be applied. In this section we present the stability analysis using bifurcation-based methods which are used in the analysis of nonlinear dynamic systems. The description that follows is made using two-order systems, and can be easily extended to systems of order n (see, for example, [1]).

The model of a two-state system can be expressed as

$$\begin{cases} \frac{dx}{dt} = f(x) + bu \\ u = \phi(x) \end{cases} \quad (1)$$

where $x \in \mathbb{R}^2$ is the state vector, $u \in \mathbb{R}$ is the input to the system (control signal), f is a function modelling the dynamics of the system, $b \in \mathbb{R}$ is the input gain, and ϕ is a non-linear function representing the fuzzy controller. The state equations of the system can be written as

$$\dot{x}_1 = f_1(x_1, x_2) + b_1\phi(x_1, x_2), \quad \dot{x}_2 = f_2(x_1, x_2) + b_2\phi(x_1, x_2) \quad (2)$$

where f_1 and f_2 are the state functions corresponding to the state variables x_1 and x_2 , respectively, and b_1 and b_2 are the input gains corresponding to the state variables x_1 and x_2 , respectively. To simplify the notation, equation (2) can be written as

$$\dot{x}_1 = f_{1T}(x_1, x_2), \quad \dot{x}_2 = f_{2T}(x_1, x_2) \quad (3)$$

where $f_{1T}(x_1, x_2) = f_1(x_1, x_2) + b_1\phi(x_1, x_2)$ and $f_{2T}(x_1, x_2) = f_2(x_1, x_2) + b_2\phi(x_1, x_2)$. If we linearize the system around the origin, we obtain

$$\begin{bmatrix} \dot{x}_1 \\ \dot{x}_2 \end{bmatrix} = \begin{bmatrix} a_{11} & a_{12} \\ a_{21} & a_{22} \end{bmatrix} \begin{bmatrix} x_1 \\ x_2 \end{bmatrix} + \begin{bmatrix} b_1 \\ b_2 \end{bmatrix} \phi(x_1, x_2) \quad (4)$$

We assume that the origin is a stable equilibrium point, and if the system is linearized around the origin it will have two poles with negative real part. If we obtain the Jacobian matrix of $f(x)$ as

$$J = \begin{bmatrix} \frac{\partial f_{1T}}{\partial x_1} & \frac{\partial f_{1T}}{\partial x_2} \\ \frac{\partial f_{2T}}{\partial x_1} & \frac{\partial f_{2T}}{\partial x_2} \end{bmatrix} = \begin{bmatrix} a_{11} & a_{12} \\ a_{21} & a_{22} \end{bmatrix} \quad (5)$$

then we can define two stability indexes as follows

- The **static bifurcation index** gives the loss of stability of the system when a *real* pole crosses the imaginary axis and becomes positive, and it can be obtained as $I_1 = \det(J)$. The controlled system will be stable if $I_1 > 0$.
- The **Hopf bifurcation index** gives the loss of stability when a pair of *complex* conjugate poles with negative real part crosses the imaginary axis and has positive real parts. It can be obtained as $I_2 = -\text{tr}(J)$, where $\text{tr}(J)$ is the trace of J . The controlled system will be stable if $I_2 > 0$.

It should be noted that, although we have linearized the system around the origin, the input to the system is the control signal $u = \phi(x)$, where ϕ is a non-linear function representing the controller. For this reason, non-linear analysis methods are still needed.

Practical Cases

In this section we consider some systems for which a fuzzy controller is designed and the static and Hopf bifurcation indexes are computed. Then, we check if the stability conditions obtained are valid for the controlled system. We have used a number of systems in order to find general conclusions for the practical application of this analysis method. As an example, we give in this section some details for two different systems: an inverted pendulum and a magnetic levitation system (in [5] a more detailed description can be found).

Inverted Pendulum

In this section we consider an inverted pendulum as the one shown in Fig. 1.

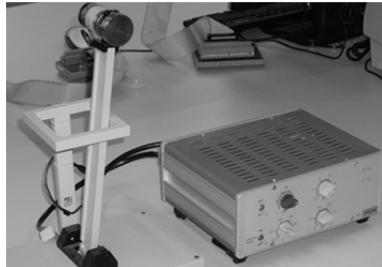


Fig. 1. Inverted pendulum used in the experiments.

The model of the system is given by the equation

$$\frac{d^2\theta(t)}{dt^2} = -2.85 \frac{d\theta(t)}{dt} + 74.63 \cdot \text{sen}\theta(t) + 111.76 \cdot u(t), \quad (6)$$

where θ is the measured output of the system (angle of the pendulum with respect to the vertical) and u is the control signal (voltage applied).

In order to control the system, a fuzzy controller is designed and connected to it using the closed loop shown in Fig. 2. In this figure, the inputs of the controller are the error (e) and the derivative of the error (\dot{e}) (which in our case corresponds to θ and its derivative, respectively, because we have used the reference $r = 0$ which represents the vertical position of the pendulum). The output of the controller (u) is multiplied by a gain $K > 0$, which is used to satisfy the stability conditions given by the stability indexes.

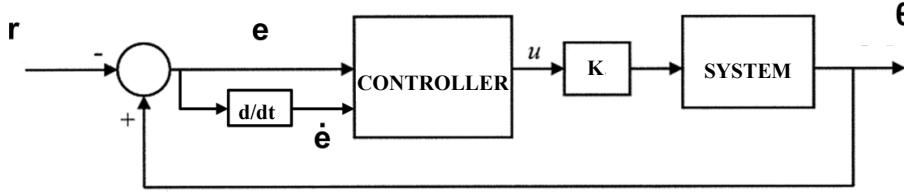


Fig. 2. Closed loop system with controller.

We then obtain the conditions to achieve the following indexes inequalities: (1) $I_1 > 10$ (Static bifurcation index), and (2) $I_2 > 10$ (Hopf bifurcation index). The required values of the indexes are greater than 0 in order to obtain an adequate margin of stability (the stability limit is $I_1, I_2 = 0$). The model of the system with the controller can be written as

$$\begin{bmatrix} \dot{x}_1 \\ \dot{x}_2 \end{bmatrix} = \begin{bmatrix} 0 & 1 \\ 74,63 & -2,28 \end{bmatrix} \cdot \begin{bmatrix} x_1 \\ x_2 \end{bmatrix} + \begin{bmatrix} 0 \\ 111,76 \end{bmatrix} \cdot K \cdot \phi(x_1, x_2) = \begin{bmatrix} x_2 \\ 74,63 \cdot x_1 - 2,28 \cdot x_2 + 111,76 \cdot K \cdot \phi(x_1, x_2) \end{bmatrix} \quad (7)$$

The Jacobian matrix of this expression can be computed as

$$J = \begin{bmatrix} \frac{\partial x_1}{\partial x_1} & \frac{\partial x_1}{\partial x_2} \\ \frac{\partial x_2}{\partial x_1} & \frac{\partial x_2}{\partial x_2} \end{bmatrix} = \begin{bmatrix} 0 & 1 \\ 74,63 + 111,76 \cdot K \cdot \frac{\partial \phi(x_1, x_2)}{\partial x_1} & -2,28 + 111,76 \cdot K \cdot \frac{\partial \phi(x_1, x_2)}{\partial x_2} \end{bmatrix} \quad (8)$$

From the desired index margins conditions, we obtain the inequalities

$$I_2 > 10 \Rightarrow \frac{\partial \phi(x_1, x_2)}{\partial x_2} < \frac{-0,069}{K} \quad (9)$$

$$I_1 > 1 \Rightarrow \frac{\partial \phi(x_1, x_2)}{\partial x_1} < \frac{-0,75}{K} \quad (10)$$

Given the fuzzy controller for this system, the derivatives $\phi_{x_1} = \frac{\partial \phi(x_1, x_2)}{\partial x_1}$, and $\phi_{x_2} = \frac{\partial \phi(x_1, x_2)}{\partial x_2}$ can be obtained as an approximation, considering an interval around the origin. In this example, the approximations of the derivatives are computed considering the intervals $[-0.1, 0.1]$ for x_1 and $[-1, 1]$ for x_2 . The values obtained are $\phi_{x_1} = \frac{\partial \phi(x_1, x_2)}{\partial x_1} = \frac{\Delta u}{\Delta x_1} = -5$ and $\phi_{x_2} = \frac{\partial \phi(x_1, x_2)}{\partial x_2} = \frac{\Delta u}{\Delta x_2} = -0.5$. Substituting these values in equations (9) and (10), we obtain that the stability conditions are $K > 0,0026$ from the inequality corresponding to ϕ_{x_1} and $K > 0,0024$ from the inequality corresponding to ϕ_{x_2} .

From these two conditions we take the more restrictive, $K > 0,0026$. We have simulated the system with the fuzzy controller and the minimum value of K for stability resulted to be $K = 0,0033$, so the practical condition for stability is $K > 0,0033$, which is very close to the condition obtained by the bifurcation theory. As a conclusion, we can say that the condition obtained with the described analysis method is valid in this case, although we should take a small security margin to ensure that the system is stable.

Magnetic Levitation System

In this case a magnetic levitation system with a fuzzy controller is modeled and analyzed (Fig.3). The objective is to control the position of a magnet suspended above the electromagnet, assuming that the magnet can only be moved vertically. The dynamics of the system can be expressed as:

$$\frac{d^2 y(t)}{dt^2} = -g + \frac{\alpha}{m} i(t) - \frac{\beta}{m} \frac{dy(t)}{dt} \quad (11)$$

where y is the distance between the magnet and the electromagnet, $i(t)$ is the current applied to the electromagnet, m is the magnet mass, $g = 9,8 \frac{m}{s^2}$ is the gravity force, $\beta = 12$ is viscous friction coefficient of the medium in which the magnet moves, and $\alpha = 15$ is a field constant which is determined by the strength of the magnet. In order to control the system a fuzzy controller is designed and connected in closed loop, using the same architecture as in the previous example (Fig. 2).



Fig. 3. Magnetic levitation system.

For this system, we establish the following stability conditions: $I_1 > 0$ (Static bifurcation index) and $I_2 > 0$ (Hopf bifurcation index). The state-space model of the system, including the controller, can be obtained as

$$\begin{bmatrix} \dot{x}_1 \\ \dot{x}_2 \end{bmatrix} = \begin{bmatrix} 0 & 1 \\ 0 & -4 \end{bmatrix} \cdot \begin{bmatrix} x_1 \\ x_2 \end{bmatrix} + \begin{bmatrix} 0 \\ 5 \end{bmatrix} \cdot K \cdot \phi(x_1, x_2) + \begin{bmatrix} 0 \\ -9,8 \end{bmatrix} = \begin{bmatrix} x_2 \\ -4 \cdot x_2 + 5 \cdot K \cdot \phi(x_1, x_2) - 9,8 \end{bmatrix} \quad (12)$$

The Jacobian matrix of the linearized system is

$$J = \begin{bmatrix} \frac{\partial x_1}{\partial x_1} & \frac{\partial x_1}{\partial x_2} \\ \frac{\partial x_2}{\partial x_1} & \frac{\partial x_2}{\partial x_2} \end{bmatrix} = \begin{bmatrix} 0 & 1 \\ 5 \cdot K \cdot \frac{\partial \phi(x_1, x_2)}{\partial x_1} & -4 + 5 \cdot K \cdot \frac{\partial \phi(x_1, x_2)}{\partial x_2} \end{bmatrix} \quad (13)$$

From this model, we can express the stability conditions in function of the derivatives of the control signal as $\phi_{x_2} < \frac{4}{5K}$ and $\phi_{x_1} < 0$. The next step is to obtain the range of values of K where the stability conditions I_1 and I_2 are met. To compute the derivatives ϕ_{x_1} and ϕ_{x_2} we use a linear approximation in the interval $[-1, 1]$ for the two input variables (the error e and for the error derivative \dot{e} , see Fig. 2). Taking into account the structure and characteristics of the fuzzy controller designed for this system, we obtain the following conditions for the values of the gain K :

- $K > 0$ (for $\phi_{x_1} < 0$), and
 - $K > -0,8$ (for $\phi_{x_2} < \frac{4}{5K}$).
- (14)

From these two conditions, we obtain that the overall stability condition is the most restrictive solution; therefore the system is stable with: $[K > 0]$. This is our *theoretical stability condition* (for $I_1 > 0$ and $I_2 > 0$) and the condition obtained after making *real* experiments is $K > 0.7$, which is relatively close to the theoretical value considering the values of the gains in this particular system.

In order to obtain the experimental limits of K for stability, we implement Simulink diagrams including the designed fuzzy controller. An example of a Simulink diagram used for the inverted pendulum example is shown in Fig. 4. Then, using different initial conditions, we simulate the system for different values of K and obtain the minimum and maximum value for which the system output reach the desired reference.

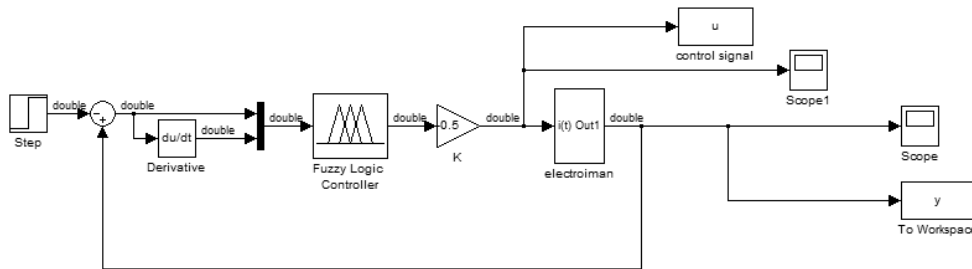


Fig. 4. Example of Simulink diagram used in the experiments.

Using this method we have designed fuzzy controllers for other complex systems, and then we have obtained the theoretical stability conditions and the practical stability conditions (some of these experiments are described in [5]). The results obtained are very similar to the results for the cases described in this section. For example, another system considered in the experiments is the control of the level of the liquid contained in an industrial tank where, considering again the restrictions $I_1 > 0$ and $I_2 > 0$, we have obtained the condition $K > 0$ using the stability analysis and in the experiments (in this case we have found no difference between the theoretical results and the results obtained in the experiments [5]).

Conclusion

In the work presented in this paper we have described a theoretical method used to obtain stability conditions for fuzzy controllers and then we have proved that this method is feasible for practical applications. In the experiments and examples studied we have shown that the values obtained by the theoretical stability analysis are very close to the actual values obtained by simulation. The practical use of the method implies the inclusion of a security margin, which depends on the static gain of the system. In our experiments we have shown that this security margin should be about 15% of the gain.

We are now extending the application of the analysis method to multi-rate fuzzy control systems. In these systems there exist more than one sample time in the close loop. This fact adds more complexity to the design and stability analysis, but has the advantage of being more efficient than control systems with one sample time in specific situations. We hope that the bifurcation-based analysis method described in this paper, with some variations, will be useful for the stability analysis of these systems.

Acknowledgment

This work has been supported by the Spanish Government (*Ministerio de Ciencia e Innovación*) through project TIN2010-17513 and by the Local Government (*Conselleria de Educaci3n, Generalitat Valenciana*) through project ACOMP/2012/148.

References

- [1] J. Aracil, F. Gordillo and T. Álamo. Global Stability Analysis of Second Order Fuzzy Control Systems, in *Palm, Driankov and Hellen-Doorn, Eds. Advances in Fuzzy Control* (1998), Springer-Verlag, pp. 11-31.
- [2] F. Cuesta, E. Ponce, Aracil, J. Local and Global Bifurcations in Simple Takagi-Sugeno Fuzzy Systems. *IEEE Transactions on Fuzzy Systems*, Vol. 9, No. 2, April (2001), pp. 355-368.
- [3] L.X. Wang: *A Course In Fuzzy Systems and Control*, (Prentice Hall, NJ, 1997).
- [4] D. Driankov, H. Hellendoorn and M. Reinfrank: *An Introduction to Fuzzy Control*, (Springer, NY, 1996).
- [5] G. Berenguer: *Design and Stability Analysis of Fuzzy Controllers Applied to Non Linear Systems*, (Master Thesis, Miguel Hernández University, 2012).



DESIGN AND IMPLEMENTATION OF SEARCH ALGORITHM FOR DNA SEQUENCE DATABASE

V. Varunkumar¹, B. Vijaykumar²

¹ Student, Grade 12, Emirates National School, Sharjah, UAE Email:uma_vvk_66@yahoo.co.in

² Associate Professor, Dept. of CS, BITS Pilani, Dubai Campus, Dubai, UAE Email: vijay@bits-dubai.ac.ae

Keywords: DNA Sequence, Database, Probe Sequence, Search Algorithm, EGREP.

Abstract. A DNA sequence database stores information about nucleic acid patterns in molecular biology. The database is created from the archival databanks of biological information. The user can perform search over the DNA sequence database using one or more input probe sequences. The input probe sequences can be complete or partial. The search algorithm looks for similar sequences in the database and outputs the matching sequences along with their locations in the database. The present work helps in identification of specific gene sequences associated with the diseases. The paper is organized into six sections. Section 1 gives an introduction to nucleic acid sequences. Section 2 deals with Objectives and Motivation. Section 3 describes the steps in data collection and experimental setup. Section 4 presents Implementation. Section 5 presents Test Scenario and observed results. Section 6 deals with Conclusion and Future Work. The References are listed at the end.

Introduction

DNA is basically a long molecule that contains coded instructions for the cells [1]. Everything the cells do is coded somehow in DNA - which cells should grow and when, which cells should die and when, which cells should make hair and what color it should be. Our DNA is inherited from our parents. We resemble our parents simply because our bodies were formed using DNA to guide the process - the DNA we inherited from them. We may resemble our parents, but we are never exactly like them. This is because each child gets only some of the DNA each parent carries. Thus, siblings may have the same parents, but they usually do not have exactly the same DNA (except for identical twins). DNA is a long molecule, like a chain, where the links of the chain are pieces called nucleotides (sometimes also called 'bases'). There are four different types of nucleotides in DNA : 'A', 'G', 'C' and 'T' (Adenine, Guanine, Cytosine and Thymine). These four are all that's necessary to write a code that describes our entire body plan [1]. A DNA sequence database stores information about DNA sequence from one or more organisms. The current work considers archival information for DNA sequence corresponding to Homo_sapiens (human) as mentioned in Ensembl Website [2, 3].

Objectives and Motivation

The present work is intended to meet the following objectives:

- **Read** a DNA sequence or fragment of a sequence from an user.
- **Find** the sequences and their locations in the database that are similar to the user input.

Searching DNA sequences against a DNA database is very useful for sequence analysis. Information relating to the effects of variation of DNA among individuals can be useful in diagnosing, treating and preventing a number of diseases that affects the human beings. The present work helps in identification of specific gene sequences associated with the diseases. It also facilitates a good analysis of biological relationships.

Data Collection and Experimental Setup

The primary database in text format is created from Ensembl Website [3]. The experimental setup involves the software tool **egrep** (Extended Global Regular Expressions Print: pattern matching tool) [4] under LINUX operating System installed in a personal computer. grep/egrep has been created by Ken Thompson as a standalone application, in 1973 . It is based on the regular expression parser.

Implementation

This section deals with the unix shell scripts **run1**, **run2** and **run3**. The **chmod** command assigns execute permission to these scripts. These scripts can be run at the shell prompt (**\$**). The search algorithm has been implemented using the unix tool **egrep** [4]. The database is stored as a text file. The input pattern(s) corresponding to probe sequences(s) is/are stored in separate file(s). **run1** corresponds to search involving a single pattern for three different input database sizes. **run2** corresponds to search involving two patterns for three different input database sizes. **run3** corresponds to search involving three patterns for three different input database sizes.

```
// Shell Script and related documentation for searching one or more input patterns in an input DNA sequence database.  
// each script file is created using text editor vi.  
// assign execute permission to each script file using chmod command.
```



```
// execute each script file in the batch mode and redirect the output ( output redirection symbol > )
// to a separate text file.
// the time command displays the execution time in (milli)seconds for each script.
// the command egrep (pattern matching tool in unix) can search for one or more patterns from an input database.
// The input database is stored in text format (h1.txt, h2.txt, h3.txt, h4.txt).
// The patterns are stored in text files: pat1, pat2, pat3.
// The -f option of egrep refers to a file where the pattern(s) are stored. The -n option displays line numbers.
// The matched results (output) are stored in the files
// pat1h1out, pat1h2out, pat1h3out, pat1h4out
// pat2h1out, pat2h2out, pat2h3out, pat2h4out
// pat3h1out, pat3h2out, pat3h3out, pat3h4out.
The script (run1 or run2 or run3) is executed, the output is saved and the observed execution time for each script is noted.
/* ----- */
$vi run1
$chmod +x run1
$run1
/* ----- */

/* ----- */
$vi run2
$chmod +x run2
$run2
/* ----- */
/* ----- */
$vi run3
$chmod +x run3
$run3
/* ----- */
/* contents of the script: run1 */

time egrep -n -f pat1 h1.txt > pat1h1out
time egrep -n -f pat1 h2.txt > pat1h2out
time egrep -n -f pat1 h3.txt > pat1h3out
/* ----- */

/* contents of the script: run2 */
time egrep -n -f pat2 h1.txt > pat2h1out
time egrep -n -f pat2 h2.txt > pat2h2out
time egrep -n -f pat2 h3.txt > pat2h3out

/* ----- */

/* contents of the script: run3 */
time egrep -n -f pat3 h1.txt > pat3h1out
time egrep -n -f pat3 h2.txt > pat3h2out
time egrep -n -f pat3 h3.txt > pat3h3out

/* ----- */

// contents of the patterns file: pat1
AACCCCGTCTC

// contents of the patterns file: pat2
AACCCCGTCTC
GTCCTGGCCA

// contents of the patterns file: pat3
AACCCCGTCTC
GTCCTGGCCA
ATAGTGCCCA
```

// end of source code and related documentation.

Test Scenario and Observed Results

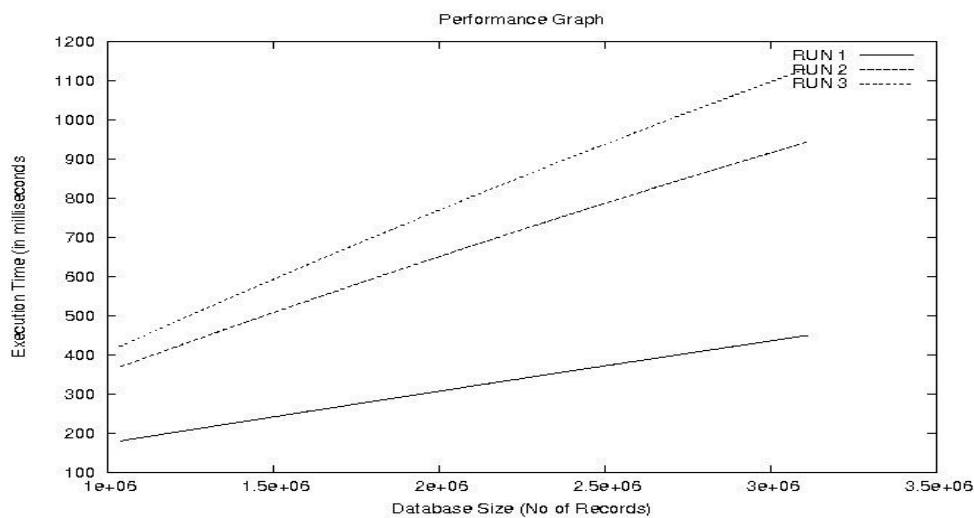
This section presents the test scenario for **run1** involving a typical DNA sequence database in text format, the input pattern and the corresponding output. For brevity, only few records are shown here, although the actual database and output are quite large in terms of number of records.

```
// Contents of a typical input DNA sequence database in text format
// only a few records are shown
// -----
```


The matched patterns are highlighted in the input database and its output. The observed results are shown in **Table 1** and **Figure 1**; It is observed that there is a linear relationship between **Database Size** and **Execution Time**.

Table 1: Observed Results

INPUT DATABASE SIZE (NO OF RECORDS)	RUN 1			RUN 2			RUN 3		
	OUTPUT (NO OF RECORDS)	Hit Ratio (% Match)	Execution Time in milliseconds	OUTPUT (NO OF RECORDS)	Hit Ratio (% Match)	Execution Time in milliseconds	OUTPUT (NO OF RECORDS)	Hit Ratio (% Match)	Execution Time in milliseconds
1038545 (h1.txt)	2372 (pat1h1out)	.2284	180	2504 (pat2h1out)	0.2411	369	2527 (pat3h1out)	0.2433	421
2077090 (h2.txt)	3435 (pat1h2out)	.1654	319	3633 (pat2h2out)	0.1749	687	3696 (pat3h2out)	0.1779	815
3115635 (h3.txt)	4557 (pat1h3out)	.1462	450	4815 (pat2h3out)	0.1545	944	4910 (pat3h3out)	0.1576	1132



Conclusion

The search algorithm for a DNA sequence database has been dealt with in this paper. The present work has potential applications in Bioinformatics and related areas. The experimental work can be extended to heterogeneous databases stored at geographically dispersed locations. Data Mining techniques such as classification and clustering can be applied over these DNA sequence databases and interestingness measures can be computed.

Acknowledgment

The authors are grateful to the IN-TECH 2012 reviewers and organizers for their valuable suggestions in improving this paper.

References

- [1] The Univ. Of Michigan, "DNA Sequencing Core", <http://seqcore.brcf.med.umich.edu/doc/educ/dnapr/pg1.htmls> [accessed:01/07/12].
- [2] Arthur M Lesk, "Introduction to Bioinformatics", Oxford University Press, 3rd edition, 2008, pp. 108.
- [3] Ensembl website, "Human genome information", <http://www.ensembl.org> [accessed:01/07/12].
- [4] Sumitabha Das, "Unix Concepts and Applications", Tata McGraw-Hill pub., 2005.

MODEL REFERENCE ADAPTIVE CONTROL OF A DC SERVO MOTOR WITH DIFFERENT INPUT-OUTPUT SAMPLE RATES

R. P. Neco¹, M.A. Vicente¹, C. Fernández¹, R. Puerto¹

¹ Miguel Hernandez University, Av. de la Universidad s/n, 03202 – Elche (Alicante), Spain

Keywords: Automatic Control, Real-Time Systems, Simulation and Identification of Systems, Learning and Adaptive Systems

Abstract. In this paper we present the design and implementation of Model Reference Adaptive Controllers (MRAC) for a DC servo motor using two different sample rates at the input and output of the controlled system. In the experiments described in the paper we have used two classical design methods for model reference adaptive controllers: (1) the gradient method and (2) design based on Lyapunov stability theory. We have shown the advantages and disadvantages of both methods for the dual-rate control of the DC servomotor: (1) the design based on the gradient computation is easier, but some controllers does not perform well enough for practical use; and (2) the design based on Lyapunov stability theory is more difficult and theoretically tedious, but it obtains controllers for which closed-loop stability is ensured.

Introduction

In this paper we present the design and implementation of Model Reference Adaptive Controllers (MRAC) [1, 2, 3] for a DC servo motor using two different sample rates at the input and output of the controlled system. We assume that there are two different sample rates involved:

- A slow sample rate which corresponds to the acquisition of the signals from the servo motor sensors (speed or position), and
- A high sample rate, which corresponds to the computations needed to obtain the control signal (input to the system).

If we had to use just one sample rate, then we would use the slow sample rate and the whole system would be slowed down by the acquisition rate of the sensors signals. In the controllers described in this paper, we use some dual-rate control techniques combined with the adaptive controllers to achieve a better performance than using one sample rate.

In the experiments described in the paper we have used two classical design methods for model reference adaptive controllers:

- (1) The gradient method, and
- (2) The design based on Lyapunov stability theory.

We have shown the advantages and disadvantages of both methods for the dual-rate control of the DC servomotor:

- (1) The design based on the gradient computation is easier, but some controllers does not perform well enough for practical use; and
- (2) the design based on Lyapunov stability theory is more difficult and theoretically tedious, but it obtains controllers for which closed-loop stability is ensured.

Moreover, the use of two different sample rates in the experiments shows that the designed controllers are suitable for industrial environments in which the system sensors are slow or the controlled system is located in a remote area and the data acquisition is much slower than the computation of the control signals.

Model Reference Adaptive Controllers

An Adaptive Controller is a controller that must adapt its behavior to a controlled system with parameters which change, or are initially indeterminate. For example, as an aircraft flies, its mass will slowly decrease as a result of fuel consumption; a control law is needed that adapts itself to such changing conditions.

Basically, there are two kinds of adaptive controllers: Self-Tuning Regulators (STR) and Model-Reference Adaptive Controllers (MRAC). In this paper we only give the simulation tasks and tools that we have use for MRAC controllers. The results presented in this paper are expected to be similar when using Self-Tuning Regulators.

Gradient Method

The gradient method consists on the minimization of the difference (model error) between de output of the system and the output of the model [1,3]. In our experiments we have used the typical error function to minimize:

$$J(\theta) = \frac{1}{2} \cdot e^2 \quad (1)$$

where e is the model error. The parameters of the controller are updated according to the gradient:

$$\frac{d\theta}{dt} = -\gamma \cdot \frac{\partial J}{\partial \theta} = -\gamma \cdot e \cdot \frac{\partial e}{\partial \theta} \quad (2)$$

where γ is the adaptation gain. In our experiments we have used an RST controller as the non-adaptive module.

Lyapunov Stability Method

The Lyapunov stability method is based on the second Lyapunov stability method [1, 3]. This theorem establishes that, given a system

$$\dot{x} = f(x, t) ; f(0, t) = 0 \tag{3}$$

where x is the state vector (n -dimensional), then if we can find a real function $V(x, t)$ (Lyapunov function), such as (1) $V(0, t) = 0$; (2) V is differentiable with respect to x and t ; (3) V is positive-definite, then a sufficient condition for the asymptotic stability in the equilibrium point ($x=0$) is that $\dot{V}(x, t)$ is negative-definite. Using this theorem, and assuming that the state vector x is the model error, e , which we want to minimize, it is possible to design adaptive controllers which are stable.

Model Reference Adaptive Control of a DC Motor

Using the methods outlined in the previous section, we have designed adaptive controllers for a DC motors, using two different sampling rates for the input and output of the system (dual-rate controller). The system used in the experiment and the data acquisition card used in the experiments are shown in Fig. 1.

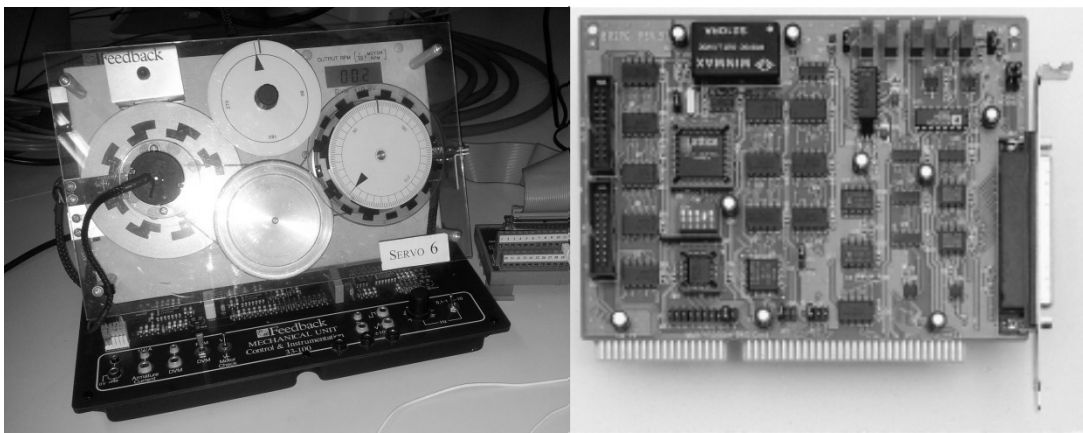


Fig. 1 Servomotor (Feedback) and data acquisition card use in the experiments.

Figure 2 shows the adaptive control scheme used to control the system (gradient descent, using Simulink [4]). In this scheme we have simulate two different sampling rates at the input and output using two different samples in the Simulink model. We have used three different first-order models in all the experiments: G_1 , which is different to the system and has its pole at the left of the pole of the system; G_2 , which is similar to the system; and G_3 , which is different to the system and has its pole at the right of the pole of the system.

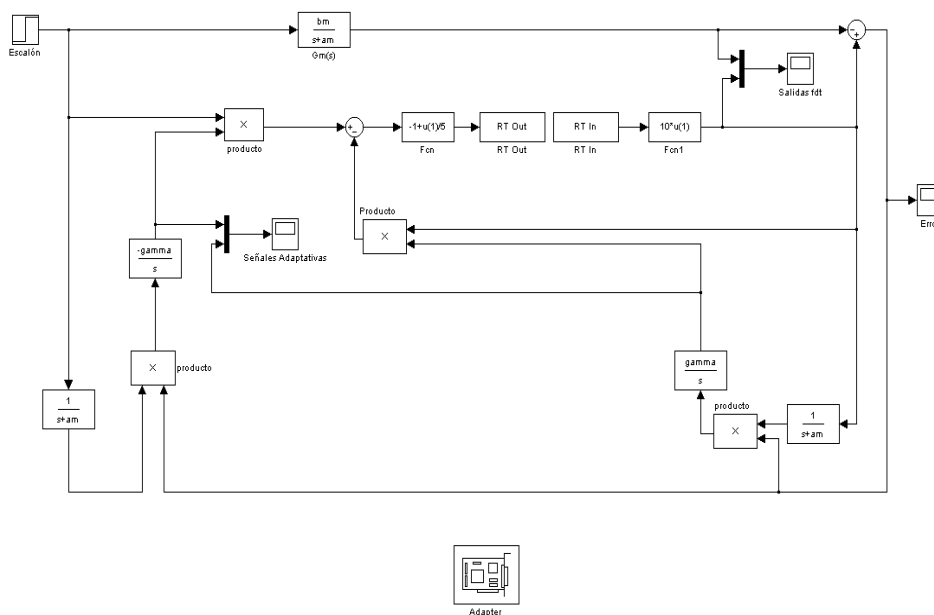


Fig. 2 Adaptive control scheme used in the experiments

Tables 1 and 2 show the settling time (in seconds) of the model error signal, for the gradient method and the Lyapunov method, respectively. This settling time represents the time needed by the system to adapt to the model output. We can see that for small adaptation gains, the settling time increases, but the adaptation is more precise. On the other hand, if the adaptation gain increases, then the system needs less time to adapt its behavior to the model, but the adaptation is less precise. In the results presented in these tables, the relation between the two different sample rates is $T_1 = N \cdot T_2$, where T_1 is the input sample rate and T_2 is the output sample rate.

Table 1. Time needed to adapt the system output to the model, gradient method (seconds).

Gamma	G _{m1}	G _{m2}
Step		
Gamma = 0.5	4.5	4
Gamma = 0.09	15	10
Ramp		
Gamma = 0.5	14	12
Gamma = 0.09	22	20
Sine		
Gamma = 0.5	1	4
Gamma = 0.09	4	7

Table 2. Time needed to adapt the system output to the model, Lyapunov method (seconds).

Gamma	G _{m1}	G _{m2}
Step		
Gamma = 0.5	3	3.5
Gamma = 0.09	4	4
Ramp		
Gamma = 0.5	10	8
Gamma = 0.09	15	14
Sine		
Gamma = 0.5	3	4
Gamma = 0.09	2	3

Figure 3 shows an example of the adaptation process for a sinusoidal reference input for the system and the model. In this figure we can see that, in this case (Lyapunov method), the time needed by the system to adapt its output to the output of the model is 5 seconds and the system remains stable and properly adapted even if the adaptation mechanism is turned off.

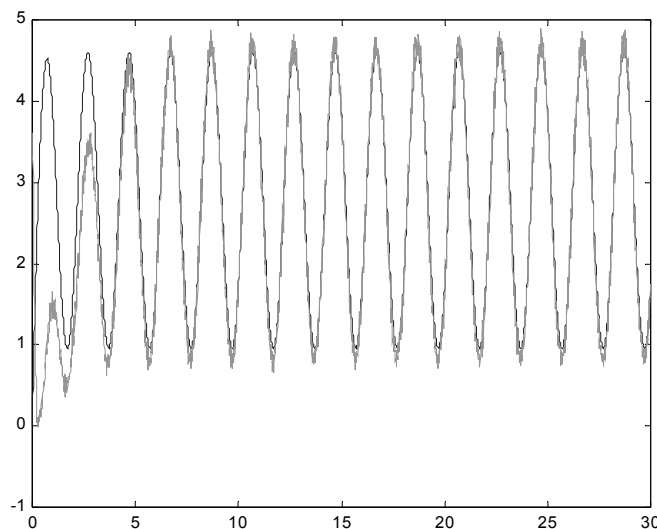


Fig. 3 Example of adaptation for the servomotor: the output of the system and the output of the model (the periodic signal).



Conclusion

In this paper we have shown some experiments designed to show the behavior of two typical model reference adaptive controllers when two different sample rates are present. We have shown the advantages and disadvantages of two classical adaptive methods for the dual-rate control of the DC servomotor: the gradient descent method and a method based on the Lyapunov stability theory. The conclusions obtain for each method are the following: (1) The design based on the gradient computation is easier, but some controllers does not perform well enough for practical use; and (2) the design based on Lyapunov stability theory is more difficult and theoretically tedious, but it obtains controllers for which closed-loop stability is ensured. The use of two different sample rates in the experiments shows that the designed controllers are suitable for industrial environments in which the system sensors are slow or the controlled system is located in a remote area and the data acquisition is much slower than the computation of the control signals.

Acknowledgment

This work has been supported by the Spanish Government (*Ministerio de Ciencia e Innovación*) through project TIN2010-17513 and by the Local Government (*Consellería de Educación, Generalitat Valenciana*) through project ACOMP/2012/148.

References

- [1] K.J. Astrom, K.J. and B. Wittenmark: Adaptive Control, (Addison-Wesley, 1994).
- [2] G. Tao: Adaptive control design and analysis, (Hoboken, N.J. : Wiley-Interscience, 2003).
- [3] K. Ogata: Discrete-Time Control Systems, (Prentice-Hall, 1996).
- [4] N. Aliane: A Matlab/Simulink-Based Interactive Module for Servo Systems Learning. IEEE Transactions on Education, 53(2): 265 – 271, 2012.

THE SEARCH FOR OPTIMAL TRAJECTORIES OF THE WELDING TOOL IN THE AUTOMATIC WELDING LINE USING EVOLUTIONARY COMPUTATION

M. Ključik¹, P. Paszto¹, A. Babinec¹, L. Jurišica¹, J. Hanzel¹ and J. Rodina¹

¹ Institute of Control and Information Technology, Faculty of Electrical Engineering and Information Technology, Slovak University of Technology, Ilkovičova 3, 812 19 Bratislava, Slovakia

Keywords: trajectory planning, optimization, evolutionary computing, modeling, virtual model, ADAMS/View

Abstract. The main objective in the planning of the welding trajectories is to keep this process without interrupts and to keep speed of this process in predefined range. Also the direction and the distance of the welding tool must be kept in these predefined parameters. The more precise are kept these technology requirements the higher quality of the welding process we get. There are various problems in welding of the large-capacity tanks and pipes – such as the problem of the positioning of the welding tool on greater distances, the problem of directing of the welding tool to guarantee the quality of the weld and also the welding time should be minimized. The positioning of the tool over the point of the welding can be done in several ways. It can be done by moving of the workpiece in different directions and/or it is possible by positioning of the tool itself. The aim of this article is to present some special welding situations that may occur in the welding process of high-capacity tanks. One way to solve this problem is to optimize the positioning of the welding tool with using of the evolutionary computing and with using of the virtual model of the welding machine. In this article are presented the criteria, with which is evaluated each solution, generated by the evolutionary computing. The basic environment for testing of the kinematic behavior of welding machine in various situations is the ADAMS/View environment, and as an optimization tool is used application developed in our department. In conclusion, this paper outlines the possibility of improvement of welding processes with additional equipment and procedures.

Introduction

The welding of large tanks and pipes brings new additional technical problems compared to the welding of smaller units. Tanks or boilers with big size are characterized by the fact that to these units are cut holes with various dimensions and to which are pipes to be welded. Tanks are usually cylindrical in shape, causing that the attachment edge of additional pipes has non-trivial weld trajectory. Example of such a trajectory is on fig. 1. The shape of such a trajectory then causes problems with learning of the welding robot and problems with the robot motion planning. It is necessary to create such trajectory where are met the parameters of used technology – the desired direction of the welding tool and movement of the tool over the welding trajectory at desired speed. The welding technology creates the necessary requirements such as the welding speed by concurrent tracking of the trajectory and the direction of the welding tool. These requirements can be secured in several ways:

- with positioning of the welding tool,
- with positioning of the workpiece itself,
- concurrent positioning of the workpiece and the welding tool

Most number of the welding robots have five or more degrees of freedom. The positioning device of the workpiece usually has also at least two degrees of freedom. With such configuration arise many possibilities to create the welding trajectories. If are counted in possible beginnings and ends of welding trajectories (it is possible to divide some trajectories into several continuous sections), the number of options increases even more. The situation may be complicated by the nature of the workpiece - at some points the welding tool can't reach desired position - just for lack of space (for example fig. 1 – space between the smaller pipes). Often is by the welding process required, that the welding trajectory can not be divided (or at least the count of trajectory interruptions is minimal), and at the same time it is necessary to avoid the singular points (the unreachable positions). The following subsection shows the different models of machines for welding or cutting.

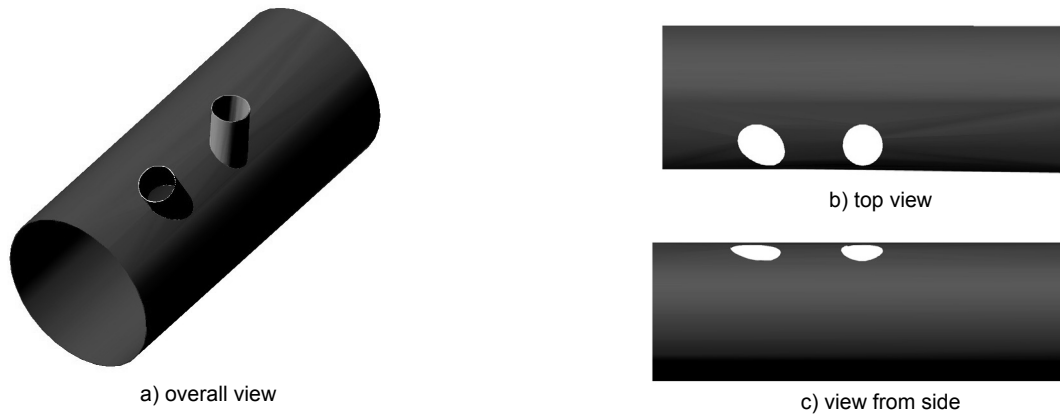


Fig. 1 Example of the workpiece

Possible configurations of welding machines

Some possible configurations of welding/cutting machines are shown in fig. 2. All models are presented as models in ADAMS/View environment. Concept no. 5 is a classic orthogonal welding machine, with a rotating welding tool. It has five degrees of freedom - three linear and two rotary. Concept no. 1 is a classic welding robot with five degrees of freedom. Concept no. 2 is a concept no. 1 supplemented with the positioning system of the workpiece. The robot and the positioning system together have seven degrees of freedom. Concept no. 3 is a somewhat exotic model of welding machine. Inside the blue circle is placed manipulator with six degrees of freedom. The blue ring is possible to turn a full circle and with the portal can move a linear movement along the entire length of the machine. This concept can reach any place outside of the workpiece. This concept has in total eight degrees of freedom. For purposes of this article has been analyzed the concept of no. 2 with three simple trajectories.

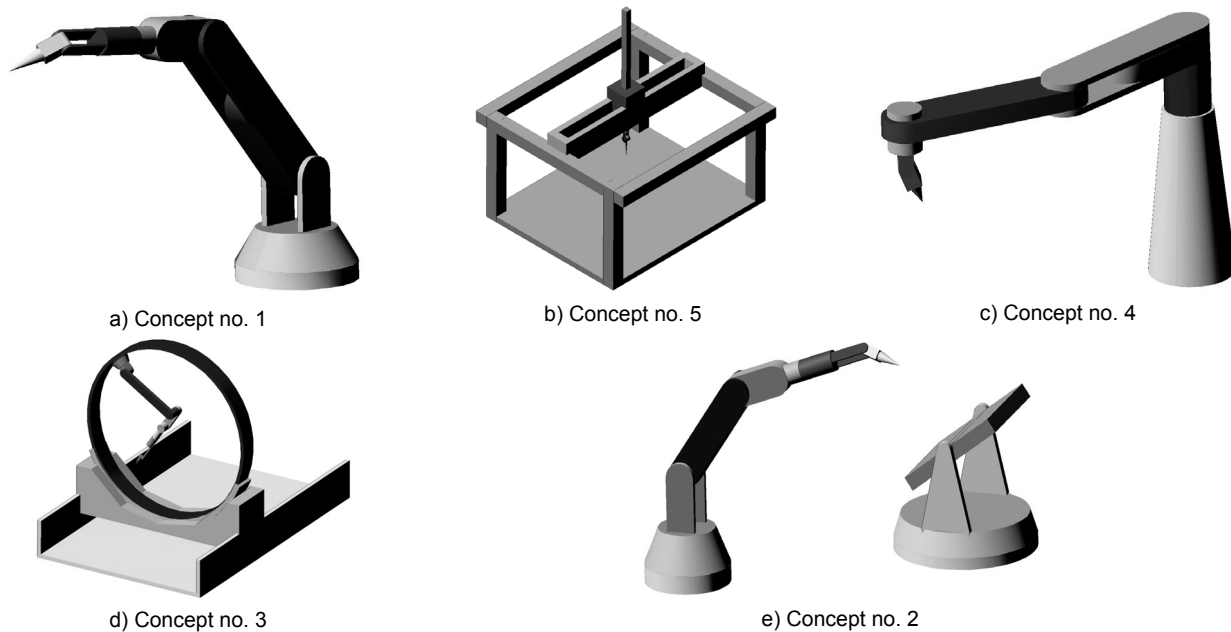


Fig. 2 Configurations of welding/cutting machines

Mathematical model of the machine

The used system has seven degrees of freedom. As the basic position of the machine configuration was determined fully outstretched arm upward and the basic position of the positioner is horizontal. There were determined transformation matrices between the coordinate systems of the arm (gradually from system S_5 to coordinate system S). In the case of the positioner, there were determined transformation matrices from coordinate system S to system S_{12} . The origin of the global coordinate system S is placed in the beginning of the S_0 and orientation of the axes of the system S is shown in fig. no. 3 top right.

The coordinate system S_0 is associated with a rotating base of the robotic arm. The rotation of the basis can be determined by the angle α_0 . The range of the angle rotation α_0 is $\langle -\pi, \pi \rangle$ radians. The coordinate system S_1 is connected to the main arm. The coordinate system S_1 is rotated with respect to the system S_0 about axis z_1 and the rotation itself is expressed by the angle α_1 . The range of rotation is from $\langle -\pi/2, 0 \rangle$. The coordinate system S_2 is connected to the secondary arm (forearm). The coordinate system S_2 is shifted from S_1 and can be rotated about the axis z_2 . The rotation of the coordinate system is expressed by the angle α_2 and has the range is $\langle -3\pi/4, 3\pi/4 \rangle$ radians.

The coordinate system S_3 is associated with the rotating wrist of robot. The origin of the coordinate system S_3 is shifted with regard to the system S_2 distance a_2 . The coordinate system is rotated with respect to S_2 and the rotation can be expressed by the rotational angle α_3 with the range $\langle -\pi, \pi \rangle$ radians.

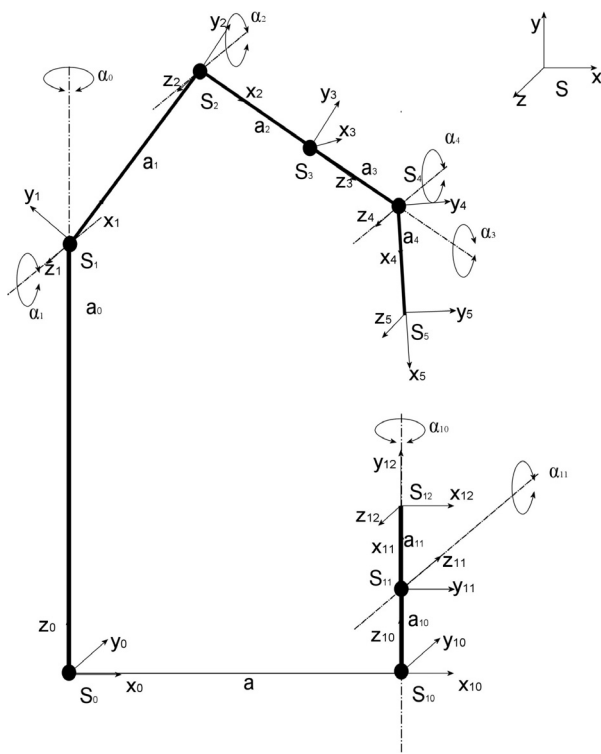


Fig. 3 The coordinate systems of concept no. 2

The coordinate system S_4 is connected to the second part of the wrist. To this system is mounted the welding tool. The origin of the coordinate system S_4 , compared to the beginning of the coordinate system S_3 is moved by a distance of a_3 . The coordinate system S_4 can be rotated, the rotation axis is the axis z_4 . The rotation is expressed by the angle α_4 with range $\langle -3\pi/4, 3\pi/4 \rangle$ radians.

The origin of the coordinate system S_5 is the position of the working point of the welding tool. The coordinate system beginning is shifted from S_4 over to distance a_4 .

The coordinate system S_{10} is a coordinate system of the positioner. This system is shifted compared to the beginning of the system S in distance a in the direction of the x axis. The coordinate system S_{10} is rotated about the axis z_{10} , and the rotation angle is expressed by α_{10} with the range $\langle -\pi, \pi \rangle$ radians. This coordinate system expresses the rotation of the workpiece in a horizontal plane.

The coordinate system S_{11} is a coordinate system of the table itself. This coordinate system is rotated about the axis of z_{11} . The rotation angle is expressed by α_{11} with range $\langle -\pi/2, \pi/2 \rangle$ radians.

The last coordinate system S_{12} is the coordinate system of the workpiece. This coordinate system is tight connected to the workpiece and it doesn't moving to the respect of previous coordinate system S_{11} .

Based on these definitions and fig. 3 were determined the transformation matrices between the coordinate systems and also the inverse problem was solved. The basis for solving the inverse task was to calculate the movement of the wrist to the desired trajectory (calculation of the required positions of S_4 in the global coordinate system with help of transformations matrices of the positioner).

The rest of the task was then divided into three parts - α_0 calculate the desired angle to the planar position of S_4 , then were calculated the angles α_1 and α_2 based on a determined plane with positioning systems S_1, S_2 and S_4 . The third part is the determination of angles α_3 and α_4 with help of the supporting plane S_3, S_4 and S_5 .

Trajectories used in optimization process

In the welding process of large-scale boilers and pipes can possibly occur various situations (for example small space between components that are to be welded, welding from inside of workpiece). In the case of jobbing contracts (small number series) can really occur any situation. This article is aimed to analyze some simple situations that may occur during welding process (or cutting process), and to verify the possibility to optimize trajectory planning of more complex systems. For this reason were outlined simple circle trajectory in three variants: trajectory no. 1 - the welding tool direction is always perpendicular, trajectory no. 2 - welding tool changes his directions from perpendicular to 45 degrees and back (outside of the circle oriented) and trajectory no. 3 the welding tool changes his direction from perpendicular to 45 degrees and back (inside oriented - example is in fig. 4 – lines represent direction of welding tool). All three trajectories represents the requirement for the positioning of the welding tool. For each point of the trajectory is determined the direction of welding tool. The situations present only simple variations, which can be used to optimization of joint angle trajectories for machine learning in the particular cases.

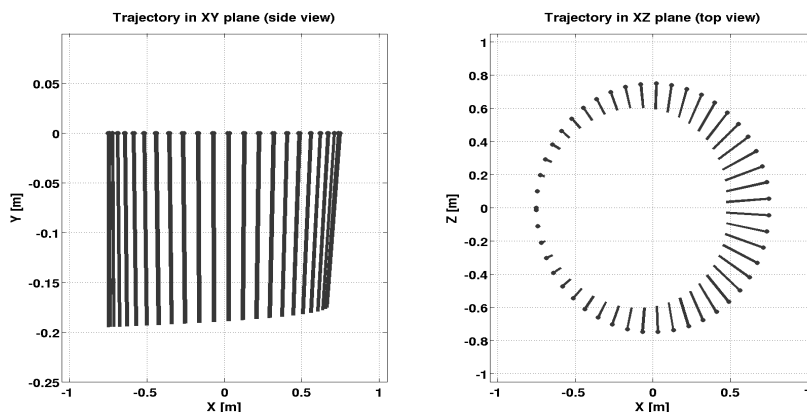


Fig. 4 Example of trajectory used in optimization process

The optimization process – inputs, criterion and results

As optimization tool was used genetic algorithm, implemented in a application and developed in our department. The optimization strategy was determined as follows: for the specified trajectory (such as in figure 4, it is in principle the requirement of the welding technology) is randomly determined initial welding point and direction of motion. Each of the three tested relatively simple trajectories were composed from about 50,000 points, eg. the starting point could be any of them. The direction of motion could be clockwise or counterclockwise. By experiments was also randomly determined the movement of the positioner of the workpiece. The movement or

position of the positioner was generated with various methods:

- constant angle α_{10} and α_{11} , (they were randomly generated in range of each joint),
- constant angle velocity for α_{10} and α_{11} , (the acceleration was not under consideration, but the range of velocities was relatively low)
- angles α_{10} and α_{11} were generated as angle function of time (for example - sin, cos. Also other functions have been considered, of course, with the parameters derived from the desired trajectory).
- combinations of previous methods.

These parameters are components of genetic string in the process of optimization with genetic algorithms. With these parameters is calculated the inverse task for the manipulation robot with welding tool. The reason is, that it makes no sense to generate random angles in the joint variables, when the clear position of the robotic arm can be calculated.

If it is successfully calculated for the whole trajectory, the evaluation process continues with evaluation in the ADAMS/View environment, where is analyzed the reachability for the points of the trajectory (for example whether any unwanted contact with the material arises). In the ADAMS/View environment are also analyzed the torques, and the traveled angles in each joint of the machine. The tool ADAMS/View is a simpler option for evaluating the proposed trajectories, especially in terms of multicriteria optimization. The calculated angles α_0 , α_1 , α_2 , α_3 and α_4 and generated waveforms or fixed positions for angles α_{10} and α_{11} (angles of the positioner of workpiece) were used as inputs to model in ADAMS/View environment. From the performance in the ADAMS/View is calculated the fitness of an individual. After number of generations are obtained results of the optimization – initial point for welding, required movements in each joint of the machine. The results of optimization can also be used as a guide for the operation of the machine in particular case or for automatic import of data in the required language. In the optimization process is used the next criterion to evaluate the success of set of parameters:

$$J(\bar{\alpha}(t)) = \sum_{i=0}^n w_i \int \left| \frac{d}{dt} \alpha_i(t) \right| dt$$

where w_i – weight of criterion in joint i , α_i – angle in joint i , n - number of joints

In this case it is a very simple test which can be obtained using the results from the inverse transformation. But by testing only with the results of the inverse task it is not possible to assess conflict situations, torques and forces of the mechanism. Weight for the assessment were determined by the peak torques in the joints of the machine. If the inverse problem has no solution or conflict situation occurred during the simulation in ADAMS/View, the individual is excluded from further optimization. The optimization was used standard structure of evolution, as for the example [5,6,7]. The optimization process was performed with a 100 of individuals and the number of generations was set at 200. A total of 60 experiments were carried out - 20 for each trajectory. The time of the calculation with computer with four processor cores and one evolution was approximately one hour.

As the result of the optimization, it was found that in all three cases was the positioner and the arm set to initial position, and then began the tracing using the manipulator, while the positioner was fixed. The obtained results are summarized in tab. 1. The final direction of motion of the gripper is missing, because in this case it does not matter in which direction will it go - it is a circular trajectory and value criteria is the same for both directions, whether clockwise or counterclockwise.

Table 1. Results of optimization

Traj. nr.	Initial point	Angle α_{10}	Angle α_{11}	Crit. value
1	The furthest point from manipulator	0 degrees, not moving	29 degrees, not moving	1.4433
2	The furthest point from manipulator	0 degrees, not moving	24 degrees, not moving	1.3226
3	The nearest point from manipulator	0 degrees, not moving	25 degrees, not moving	1.6133

Conclusion

As seen from the end of the previous chapter and from tab. 1, the results are relatively simple instructions, on how to plan the movement of the machine, when it is necessary to realize the trajectory from fig. 4. It should also be noted, that the movements of the machine optimization was performed only for simple trajectories, but this experiments also show, that it is possible to perform more complex trajectories, only it is needed to assume a higher computational complexity of the process. In the near future, will be the main effort to obtain results of the optimization of the complex product as shown in fig. 1. and with concept from fig. 2e). During the project is the main task to reduce the computational complexity of the optimization process (by reducing the number of points of trajectories).

Acknowledgment

This work has been supported by Autoweldlink (ITMS 26240220033).

References

- [1] M. Klučik, T. Sedlar: Mechatronical Device for Training of the Service Dogs 2, *Metalurgija*, Vol. 49, (2010), No. 2, pp. 337-340
- [2] V. Goga, T. Jediny, V. Kralovič, M. Klučik: Mechatronic Model of Anti-Lock Braking System (ABS), In R. Jablonski, T. Březina - *Mechatronics: Recent Technological and Scientific Advances*, (Springer Verlag, Berlin, 2011), pp. 63-70
- [3] M. Klučik, F. Duchoň, L. Jurišica, A. Vitko, A. Babinec: Detekcia miest zvaru pre automatizované zvarovanie veľkokapacitných nadrží a potrubí, *Zvárač*, Vol. 8, (2011), No. 4, pp. 12-15.
- [4] W. Weber: Industrieroboter (HANSER, Munchen, 2009)
- [5] J. Koza: *Genetic Programming* (MIT Press, Massachusetts, 1992)
- [6] C. Leger: *An Evolutionary Approach to Automated Design for Robotics* (Kluwer Academic Publishers, Boston, 2000)
- [7] I. Sekaj: *Evolučné výpočty a ich využitie v praxi*, (Iris, Bratislava, 2005).



THE INTELLIGENT LIGHTING CONTROL SYSTEMS IN INTERIOR DESIGN FOR HOSPITALITY BUILDINGS.

Dr. Reda Bahy-Eldin Mustafa Youssef¹

¹ Associate Professor of interior design, Faculty of Applied Arts - Helwan University – Egypt

Keywords: Intelligent lighting - control systems – Hospitality - LED Lighting – human factor – luminaries – story board - Optical Control.

Abstract. The purpose of this research is to explore the cognitive mechanisms involved in intelligent lighting control systems in interior design for Hospitality.

Hospitality, by definition, is “the quality or disposition of receiving and treating guests and strangers in a warm, friendly, generous way.” Lighting plays a significant role in setting the mood and atmosphere in an establishment. There is no single formula to abide by or a “one size fits all” approach. It is important to create a careful balance between style, simplicity, functionality, and energy efficiency. LED Lighting- “light emitting diodes”- is exceptionally qualified to fulfill all guests lighting needs. With an unsurpassed selection of track systems, curve able and flexible track systems, both line and low voltage, as well as recessed down lighting. Intelligent lighting control systems are becoming standard in the hotel industry where guest comforts and services are essential. An intelligent lighting control system, correctly specified, installed and maintained, provides programmable control of all interior design lighting, and creates an atmosphere which attracts repeat guests for dining, entertainment and accommodation.

Lighting Control Systems enhance the visual impact of every hospitality experience. Great lighting delivers the immediate impression of style, quality and sophistication tuned to the changing needs of each type of space throughout the day - The advantages of using Lighting Control Systems

- Mix light sources. LED, fluorescent HID under one seamless control system.
- Set the perfect mood for each space according to time and activity
- Control lighting effortlessly with manual, automatic and time clock programs
- Make a statement: highlighting interior design and exterior features and finishes
- Guests can relax in control of their luxurious surroundings
- Built in energy management with extend lamp life, reduced maintenance and lower energy costs.
- Integrate lighting with site-wide systems including, Security & Emergency Systems.

Introduction.

As the international hotel industry continues to re-invent itself in keeping with the latest evolutions of lifestyle, fashion and leisure, intelligent lighting control systems increasingly offer multiple benefits to developers and operators of quality hotel projects worldwide. These days the focus in hotel management is on attracting additional market share by appealing to a far more diverse clientele, including younger travellers and tourists interested in health and well-being. Hotel operational lighting requirements include ‘front-of-house’, food-and beverage, guest accommodation, entertainment venues, function / conference / seminar facilities, and architectural lighting. Multi-point programming/switching and the ability to operate with all types of standard and specialised lamps – as well as operational reliability, ease of maintenance and superb product support – are of paramount importance for any system controlling lighting for an industry which never closes and is expected to provide seamless 24-hour/365-day service to a discerning clientele.

Intelligent Lighting Controls for Hospitality buildings.

Intelligent lighting control systems are becoming standard in the hotel industry where guest comforts and services are essential. An intelligent lighting control system, correctly specified, installed and maintained, provides programmable control of all exterior and interior lighting, and creates an atmosphere which attracts repeat guests for dining, entertainment and accommodation. The recommended solution for quality hotels is installation of a complete-building lighting control system for controlling lights in all public and commercial areas, augmented by stand-alone or networked dimmers in guest rooms.

Lighting to Enhance Visual Environment

This will depend on the quantity and quality of light as well as surface characteristics and reflection factors. To enhance an interior, light will normally be varied in color, level and source. Variations of luminance and accentuation of certain areas or objects may be desirable. Experience and judgment will replace calculation and science in this type of design. Co-ordination with the architect or interior designer is very important here. The selection of strong colors for large parts of the interior would be better suited to a direct lighting scheme than an indirect one. Indirect lighting reflected from bright coloured interiors would become color distorted. Notwithstanding this, small areas of strong color are often necessary to provide visual stimulation in indirect lighting schemes. These areas should not be used to reflect light to the interior [1].

The State of LED Technology in interior design

LEDs are solid-state semi-conductor devices that produce light. Because of the way they are constructed, the light they produce is highly directional. As with any light source, LEDs have certain characteristics and limitations which need to be understood from the interior designer before the technology can be utilized to its maximum potential [2].

LEDs have some significant characteristics making them excellent general lighting sources: high source efficacy, optical control, extremely long operating lives and exceptional delivered lumens when used in a properly designed lighting system. In addition, LEDs also have a number of other favorable attributes. However, there are important technical limitations that must be understood in order to properly utilize these marvelous light sources in luminaries.

LED Technology & Optical Control

Most light sources, when utilized in luminaries, produce uncontrolled light – resulting in “hot spots” and other discontinuities in the illumination. The elimination of uncontrolled light results in incredible uniformity. Beta LED luminaries are designed with patented Nano-Optic product technology, which controls the photometric distribution of the LED luminaries. Nano-Optic product technology uses precision, injection molded acrylic plastic covers over the LED package. Beta LED luminaries closely match the light distribution achieved with traditional reflectors and with the other light sources in use today. The increased uniformity allows the lighting designer to specify lower average light levels in a layout while maintaining or improving the minimums [3].

The result: Increased energy savings and a better quality of lighting design.

Types of lighting and lighting technology

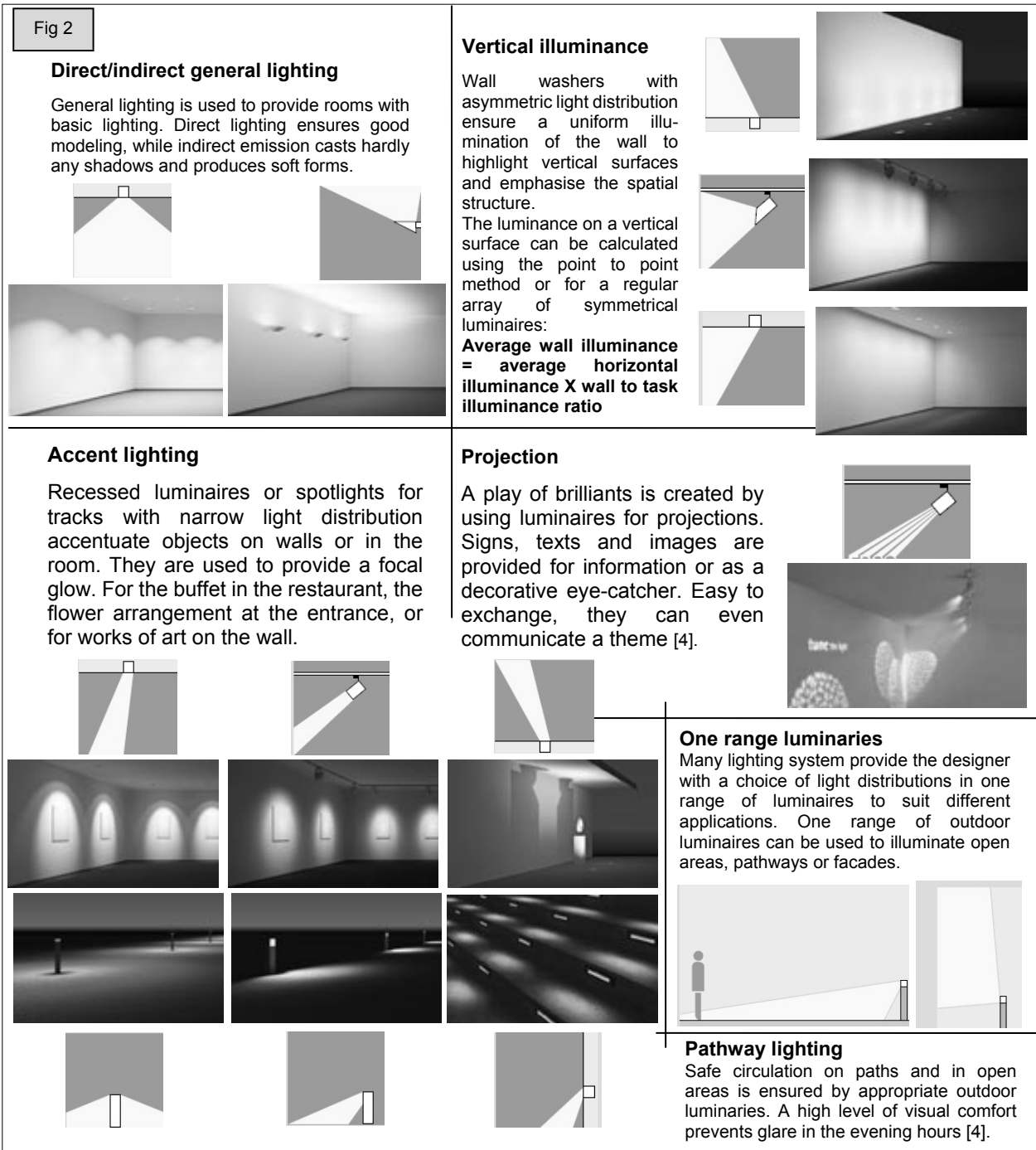


Fig 1

Without
Nano-Optic
Product
Technology



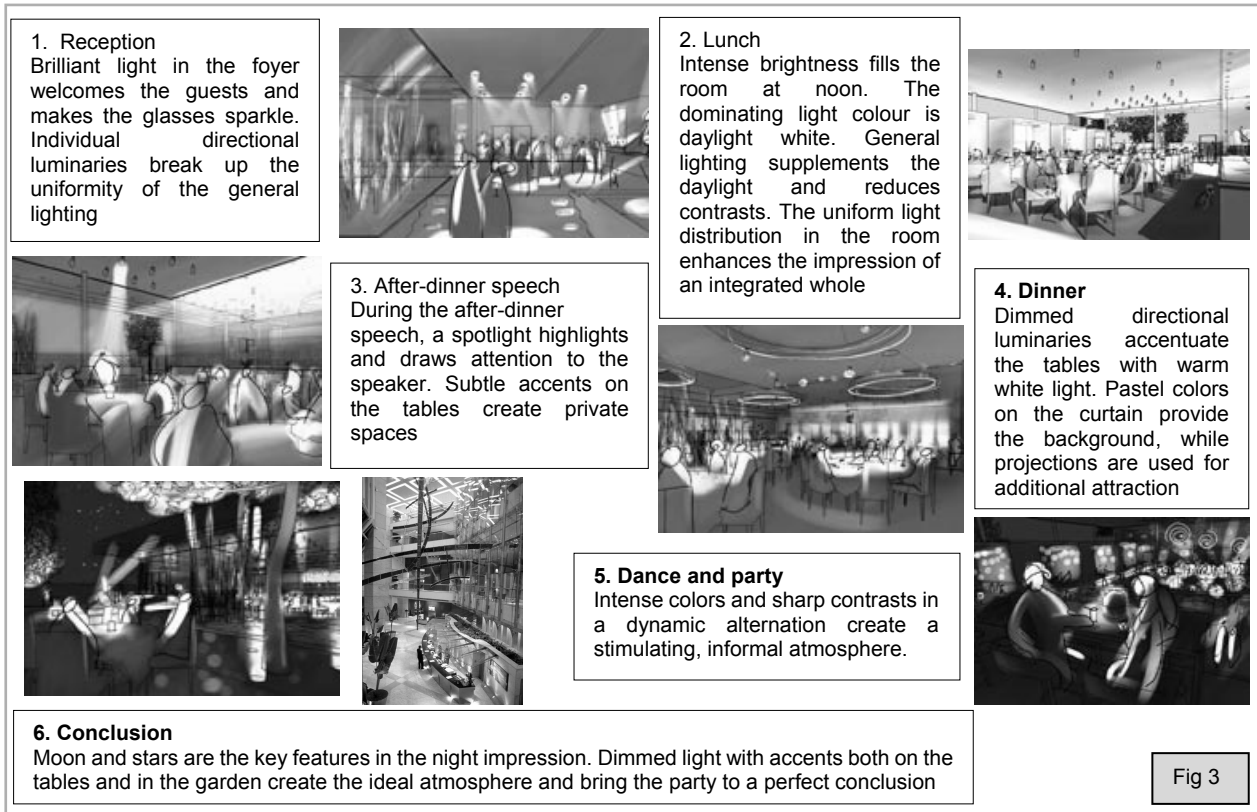
With
Nano-Optic
Product
Technology



Dynamic lighting and planning techniques in interior design for Hospitality buildings.

From reception through to ordering, to the courses and onto payment: even a simple restaurant visit follows a fixed sequence. Stenographic light can support and interpret such progressions and enhance them to create an atmospheric lighting experience. The story board here proves a useful tool in the visual planning of these progressions [5].

The basics of this method have already been introduced in the "Light and scenography" brochure. The key aspect on which to focus for a hotel or restaurant is to set up and complete an effective progression for the visit or event. The story board can be used to outline the movements of the guest in the room and along the timeline and to visualize the plot: the sophisticated lighting concept for the façade or the foyer should not suffer a loss in quality when the guest enters the next room. The light sequence is also influenced by the change in daylight conditions – even down to the light colors, the daylight white light of noon, for example, is perceived as inappropriate at night. Thus, the story board not only reflects the lighting concept with light quantity and contrasts of light and dark. It also reproduces parameters such as light colors and colored light. The dynamic effect of the light for evening scenes can be captured in a short series of images. The scenography of the light can be stored and is easily recalled for unique but specific events such as weddings, family parties, or theme nights. This gives the culinary experience a suitable atmospheric setting.



The benefits of interior design Lighting Controls

The interior design Lighting Control Systems enable to not only create and enhance the overall experience, but reduce maintenance and energy costs as well [6].

1. Enhance visual effects by highlighting • architecture or finishes
2. Create different moods in different spaces • during different times of day
3. Manage energy costs better with real-time • energy metering
4. Extend lamp life by dimming to reduce expenses •
5. Dim or turn lights OFF with time clock/sensors in • non-crucial spaces

An application Matrix guide to interior design Lighting Controls for restaurant projects. (Case study)

Table 1	Handheld Remotes	Occupancy or Daylight Sensor	BMS Integration	Scene Control	Zone Control	Timeclock	A/V Integration	DMX	Shade Integration
Entry				✓		✓			✓
Bar				✓	✓			✓	
Dining				✓	✓				
Event Room	✓			✓	✓		✓	✓	✓
Restroom		✓							
Exterior		✓	✓	✓		✓			

Working methods and interior planning techniques.

In restaurant planning, consideration must be given to different situations involving a variety of visual tasks and a different atmosphere and interior design. The characteristics of these can be recorded separately and assigned to specific zones [7].

A key element in the design process is to understand the functional criteria of a visual task – such as the perception of size and contrast of details: the lighting in the kitchen or at the buffet must be of higher quality than in traffic zones. Further important factors include the color and surface structure to perceive subtle nuances of the food on the plate. Another component to be considered in the project analysis is the psychological requirements: should the restaurant be perceived as a whole or are private areas required in a larger room. In order to give guests the feeling of privacy, the lighting designer could base his concept on small zones for each table instead of using uniform-general lighting. In terms of architecture & interior design, the creation of zones can boost the perception of spatial order. The question of room shapes, modules, rhythms, and materials is used here as a starting point from which to design light and luminaries so as to provide a structure that enhances the appearance of the architecture. The lighting design develops different light moods for the individual zones, the dynamics of which in terms of brightness and light colors can tell independent stories or be combined to fit into an

overall theme. The scenography can also change in the course of an evening, with dynamic progressions of light colors initially limited to the bar and later on extending over the entire room and out into the garden. To set up and recall light scenes for a specific zone, lighting control software with an easy to- use user interface is helpful. Through software control, the light scenes and operating devices can be flexibly assigned and adapted to meet new requirements as they arise [8].

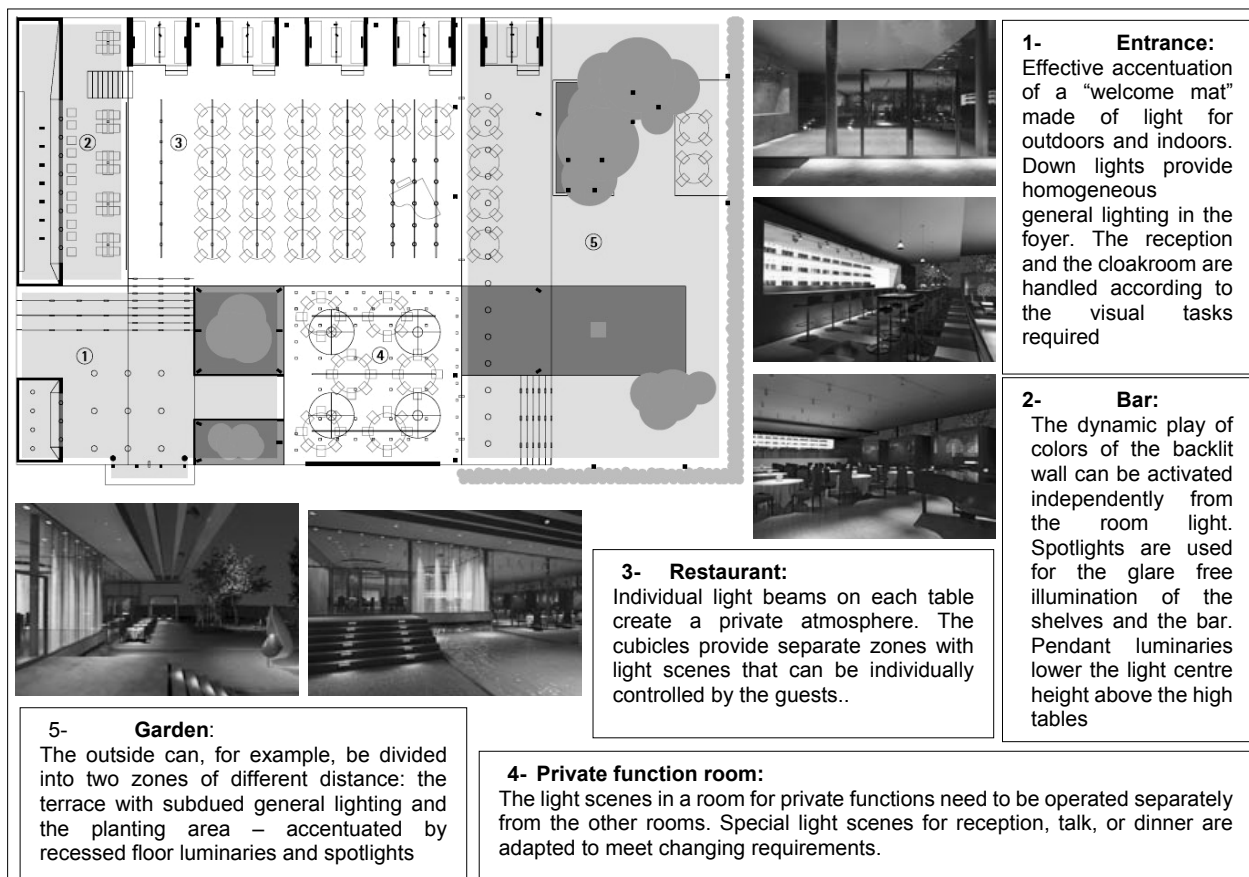


Fig 4

Results

1. Lighting Control Systems enhance the visual impact of every hospitality experience by using an application Matrix guide to interior design Lighting Controls for Hospitality buildings.
2. It is important to work experience (the story board) during the design of lighting in interior design for Hospitality buildings. As well as take advantage of modern technologies in the field of lighting in line with the preservation of the environment

Acknowledgment

I deeply thank Alexandria Library and its staff by helping me to finish the research through the appropriate information.

References

- [1] Rea, M.S (Ed.) The IESNA Lighting Handbook, (9th ed.), Illuminating Engineering Society of North America, New York, 2000 , p103 - 108
- [2] Patrick Mottier , LED for Lighting Applications , Wiley-ISTE , 2009 , p 87 - 95
- [3] Ron Lenk & Carol Lenk, Practical Lighting Design with LEDs, Wiley-IEEE Press, 2011, p172 - 176
- [4] Futronix , INTELLIGENT LIGHTING FOR HOTELS v17 , Hotel Lighting the Smart Way , Intelligent lighting controls for hotels , 04/03/2006 , www.futronix.com/
- [5] Figueiro, M.G., Research Matters. The Bright Side of Night-lighting, Lighting Design and Application, 2005, p 94 - 96
- [6] Philips Color Kinetics, Philips Solid-State Lighting Solutions, Inc , Burlington, Massachusetts 01803 USA, 2010 , www.colorkinetics.com.
- [7] Boyce, Peter, Human Factors in Lighting. New York: Taylor & Francis, 2003 - page number 56 - 61.
- [8] Bob Ponzini, LED Lighting Systems: Applications and Case Studies, Program Manager, Retail LED Business Unit OSRAM SYLVANIA, EEI National Key Accounts Workshop October 2010, p 146 - 153



International Conference on Innovative Technologies, IN-TECH 2012,
Rijeka, 26. - 28.09.2012



EXPERIMENTAL RESEARCH CONCERNING THE POLLUTION OF AN INTERNAL COMBUSTION ENGINE WITH INJECTION OF GASOLINE, IN CONDITIONS OF CHANGING THE FUEL

I. Hiticas¹, D. Marin² and L. Mihon¹

¹ Politehnica University of Timisoara, P-ta Victoriei, nr.2, RO-300006, Timisoara, Romania

² Hautes Etudes d'Ingenieur, 13 rue de Toul, F-59046, Lille Cedex, France

¹ Politehnica University of Timisoara, P-ta Victoriei, nr.2, RO-300006, Timisoara, Romania

Keywords: air pollution, gases, internal combustion engine, isobutene, pollution, pollutant measurement.

Abstract. This paper presents the experimental tests performed on a road vehicle, in dynamic laboratory in University Politehnica of Timisoara, Faculty of Mechanical Engineering, concerning the pollution of an internal combustion engine in its operation with fuel mixture composed by gasoline + isobutene alcohol (IP – from *2-methyl-1-propanol*), with percentages of 50% gasoline + 50 % isobutene, at full load and at partial load. The experimental results lead us to conclude that the concentration of CO₂ in the exhaust gases is relatively high, both the IP50 engine operation and the operation of gasoline, but there are also advantages of using mixture IP50. We mentioned about the CO₂ element because he is responsible for the greenhouse effect, air pollution and also for global warming effect, one of the most important problem what we have it today, and must be solved quickly.

Introduction

The road vehicles present advantages and disadvantages [1, 2] pollution by exhaust is the biggest problem when talking about cars. In this paper are presented the advantages offered by using an alternative fuels as energy source compared to the classics fuels. The reasons for which we considered alternatives fuel for internal combustion engine were those related to the nature of exhaust gases, global warming problems caused by the greenhouse effect – the air pollution in the whole world – the effect of carbon dioxide has a high level, as real is possible, the consequences of the rules becoming stricter on regulating the amount of CO₂ discharged by road vehicles, and alternative options proposed and applied on the energy sources used to obtain mechanical work, pay attention to the engineer on the field [3, 16].

Technical data and experiments research

Isobutene, which in nomenclature is called *2-methyl-1-propanol*, with the molecular formula C₄H₁₀O, was chosen as an alternative energy source for the internal combustion engine [4, 5], the table 1 presenting, compared with gasoline, two of these fuel characteristics. The first attempts to use alcohol as energy sources for heat engines were during the '70s, the first oil crisis, the advantages are low cost and availability of this new solution. Compared with gasoline, isobutene is superior to gasoline, as fuel, and thermal efficiency values are higher, being a very good solution for high compression engines due to high octane. The advantage of higher octane combutibil is that it allows certain engine parameters, such as compression ratio, be modified, the consequences are high power and low power consumption [6]. Below are presented, compared, two characteristics of fuels used in our experienta research.

Table1. Comparative characteristics of fuels used in experiments

	Gasoline	Isobutene	Gasoline + Isobutene 50% + 50%
Q _i [kJ / kg]	43500	30447	36936
ρ _{fuel} [kg/m ³]	760	780	770

One of the method to obtain the isobutene alcohol is the combination of water at high pressure with active catalysts, and to separate alcohol from water, it resort to distilling. Isobutene is widely useful as an additive to prevent freezing of water in the tank or on the pipeline. The experimental research was conducted in Automotive Dynamics Laboratory of the Faculty of Mechanical Engineering, University Politehnica of Timisoara. Pollutant measurements were made in order to see the benefits afforded by the alternative fuel used, concerning the nature of components by exhaust, like CO, CO₂, NO_x, HC and O₂. The vehicle tested bearing the Opel Omega A, vehicle is equipped with an internal combustion engine, fuelled with multipoint injection system Bosch Motronic. As experimental attempts to be close to real engine running conditions, were kept all auxiliary systems which equipped the car and no major changes was made. Table 2 shows the characteristics of the vehicle.

Table2. Features test car, opel omega A

Maximum Power [kW]	Maximum Torque [Nm]	Displacement [cm ³]	Reaming x Stroke [mm]	Compression ratio	
85 at 5200 rpm	170 at 260 rpm	1998	86 x86	9.2	
Maximum speed[rpm]	Supply	Fuel pressure [bar]	Firing order	Exhaust control	
6400	Bosch Motronic 1.5 Injection	2.5 – 3 on the ramp injector	1-3-4-2	Oxygen probe, catalytic convertor	
Distribution	Valves dimension [mm]	Advance at opening	Delay in closing	Maximum lift height	
One camshaft in the piston head	AD	EV	AD	EV	6.67
	41.8	36.5	23	60	
			AD	EV	
			71	35	

The experimental test stand was a Dyno Maha LPS 3000, consisting of: user interface, a remote control that can be activated in-vehicle, and roller, that are coupled to the eddy brake. Stand for power measurements can provide measurements for powers up to 520 kW with a maximum running speed of 250 km / h. The stand also features two more auxiliary modules, one for simulating air flow, to simulate the vehicle running on the road, and another module that monitors temperature, pressure and relative humidity environment. For measurements of pollution [7, 8], we used the program running at constant speed for speeds of 50 km / h and 100 km / h. Table 3 is presented the characteristics of Maha Dyno.

Table3. Maha roller stand characteristics

Maximum axle load [kg]	Diameter rollers [mm]	Distance between the roller axis [mm]	Speed range [rpm]
2500	318	540	0...10000
Maximum power at wheel [kW]	Maximum speed at wheel [km/h]	Maximum wheel traction [kN]	Precision [%]
260	250	6	± 2from measured values

AVL DiCom 4000 gas analyser allows the measurement of pollutant species found in the exhaust gases (CO, CO₂, NO_x, HC), and calculating the excess air ratio, λ, based on measured values of these pollutant species.

As we know, the amount of air aspirated by the engine is based on throttle opening and engine rotation mode. These quantities are difficult to keep under control therefore the amount of gasoline, in our case IP50 mixture, will be that it should be adjusted depending on the amount of air.

To determine the main parameters of the intake process is necessary, in advance, we have to calculate or to adopt some sizes, like:

1. Theoretical density of the fluid fresh, ρ_{off} – for this engine, thermal engine, and the density of the fresh fluid is different from the air density, because the intake fresh fluid is a mixture between air and fuel. In this case, the equation for theoretical density is:

$$\rho_{off} = f_{\rho} \cdot \rho_{0a} \quad (1)$$

Were f_{ρ} calculated with equation

$$f_{\rho} = \frac{1 + \lambda G_{a \min} \frac{R_f}{R_a}}{\lambda G_{a \min} + R_a} \quad (2)$$

Were

f_{ρ} – density correction factor

ρ_{0a} = 1,185 kg/m³ – air density at ambient temperature T_0 = 298 K and at ambient pressure p_0 = 0.1 MPa

λ – excess air coefficient

$G_{a \min}$ ≈ 15 kg air/kg fuel - minimum quantity of air required for a complete combustion of 1 kg fuel

R_f = 73 J/kg·K and R_a = 287 J/kg·K - the constant characteristic for fuel and for air

2. Ambient pressure, p_0 – reference pressure of ambient is p_0 = 99kPa ≈ 0.1MPa

3. The initial temperature, T_0 (the temperature of the air in the engine compartment from where the aspiration is made) – T_0 = 298K

4. Heating degree of fresh fluid, θ - it take into consideration that the fresh fluid heats from the walls during the intake process influencing the density (decreasing the density), and it can be calculated with the formula:

$$\theta = \frac{(T_0 + \Delta T)}{T_0} \quad (3)$$

Were,

ΔT – temperature variation of the fresh fluid as a consequence of the heat received from the walls. Usually are used θ = (1.06...1.15).

5. Adiabatic component of fresh fluid, k_a – is adopted – for spark ignition engine is k_a = (1.33...1.35)

6. Speed of sound in fresh fluid, a_{ff} - is adopted – for spark ignition engine is a_{ff} = (310...315)m/s

Much more element is adopted or calculates, including: after filling coefficient (φ_{af}), flow weighted average coefficient (μ_{sa}), section litres of throttle (s_t), supercharging pressure (p_s), global coefficient of resistance of the route of intake (ζ_a). After calculation or adopting these parameters, we can go forward for calculating the elements required for the intake process.

The filling coefficient of the cylinder, η_v , with fresh air is an equation which can be solved by experimental research or by graphics.

$$\frac{press \cdot \eta_v \theta k_a (\varepsilon - 1) (1 - \varphi_{af}) + p_{gk}}{press - 5 \cdot 10^{-7} (1 + \zeta_a) \rho_{off} \left(\frac{1}{d_{ra}^2} \cdot \frac{180}{\Delta \alpha a} \overline{w_p} \eta_v \right)^2} = [1 + k_a (\varepsilon - 1)] \cdot \left[1 - 1.8 \cdot 10^3 (k_a - 1) \left(\frac{\eta_v n_p}{a_{ff} \mu_{sa} \Delta \alpha s_t} \right)^2 \right]^{k_a - 1} \quad (4)$$

If the engine is with inlet natural, that $p_{gk} = p_{ge} = (0.105...0.120)$ MPa, and $press = p_0 = 0.1$ MPa, but if the engine is supercharged, the relation for p_{gk} is:

$$p_{gk} = p_0 \eta_v (\varepsilon - 1) \gamma_r \frac{T_{ge}}{T_0} \quad (5)$$

A solution of this equation is presented in the following graph. The equation has two parts: the left side (Lt) and the right side (Rt). To solve the equation means is to find, by testing, the filling coefficient η_v for which $Lt = Rt$ to at least the second decimal place. Testing is made for different filling factors in the range $\eta_v = 0.70 \dots 0.92$.

Another element which must be calculated is manifold gas pressure, p_{gm} .

$$p_{gm} = press - 5 \cdot 10^{-7} (1 + \zeta_a) \rho_{off} \left(\frac{1}{d_{ra}^2} \cdot \frac{180}{\Delta \alpha a} \overline{w_p} \eta_v \right)^2 \quad (6)$$

Were $press = p_0 = 0.1$ MPa

The coefficient of waste gases γ_r must be adopted, if the intake is supercharged, or calculated, if the intake is natural, with the formula:

$$\gamma_r = \frac{p_{gk} \cdot T_0}{p_0 \cdot T_{ge}} \cdot \frac{1}{\eta_v (\varepsilon - 1)}$$

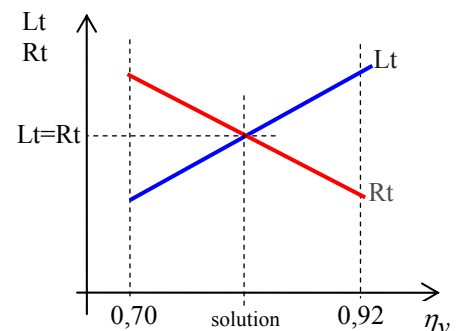


Fig. 1 The graphic solution for η_v

(7)

Also it must be calculated the followed elements: fresh gas pressure at the end of intake process (p_i), fresh gas temperature at the end of intake process (T_i), the average speed of gas in the gallery and under the intake valve (\bar{w}_{gg} and \bar{w}_{ig}), the amounts of air ($G_{a\ min}$ and $G_{a\ r}=\lambda \cdot G_{a\ min}$), constant characteristic of fresh fluid ($R_{\#}$), the theoretical and real consumption of fresh fluid ($C_{0\#}$), real consumption of air and fuel of the entire engine (c_a , c_f and c_e), fuel consumption per 100km (c_c), consumption per cycle and per cylinder (theoretical mass, real mass and total mass).

Pollutant measurements were performed for two cases, namely partial load and full load, [9, 10, 11]. The graphs shows the curves associated to engine adaptation for the operation with isobutene, also for operation with fuel mixture and the reference position was taken the operation with 100% gasoline. Since the catalytic converter is programmed to run at maximum efficiency, the injection system of the vehicle will keep the mixture in the $0.98 < \lambda < 1.002$. This mode is provided to reduce nitrogen oxides, [12, 13], and unburned HC and CO oxidation. In the following, we present the graphs derived from measurements:

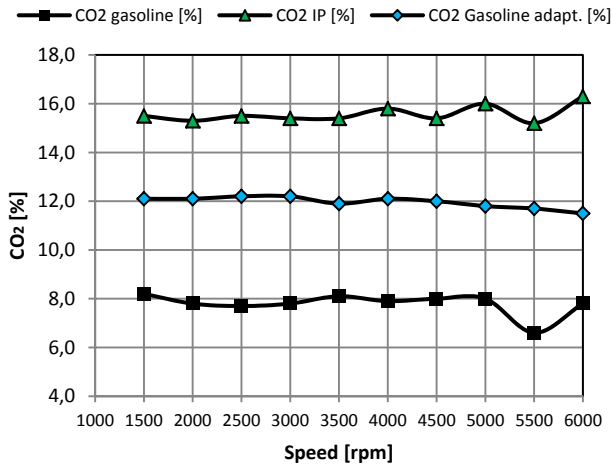


Fig. 2 CO₂ concentration in the exhaust gases at full loads

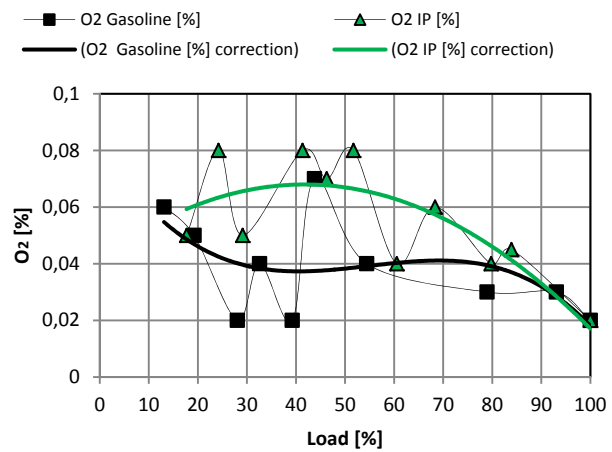


Fig. 3 O₂ concentration in exhaust gases from partial load

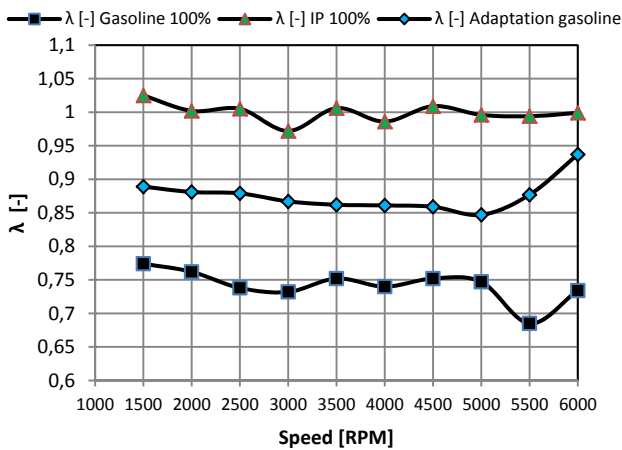


Fig. 4 Evolution of excess air ratio λ at full loads

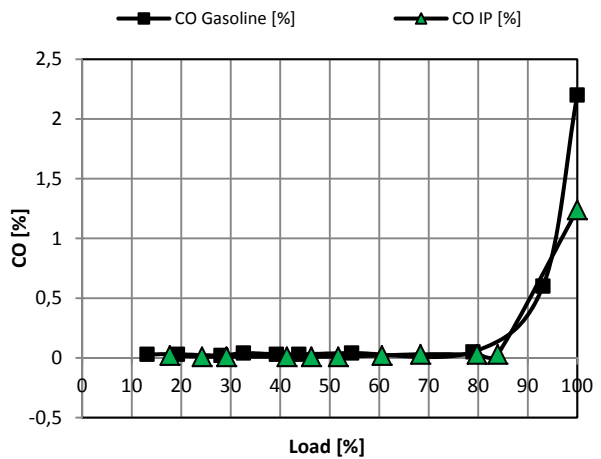


Fig. 5 Concentration of CO in exhaust gases at partial load

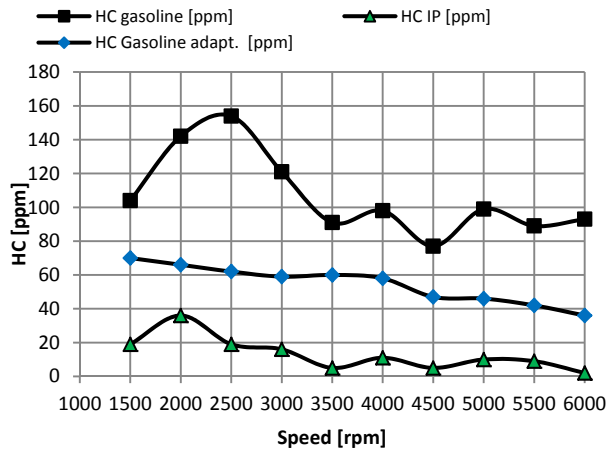


Fig. 6 HC concentration in exhaust gases at full load

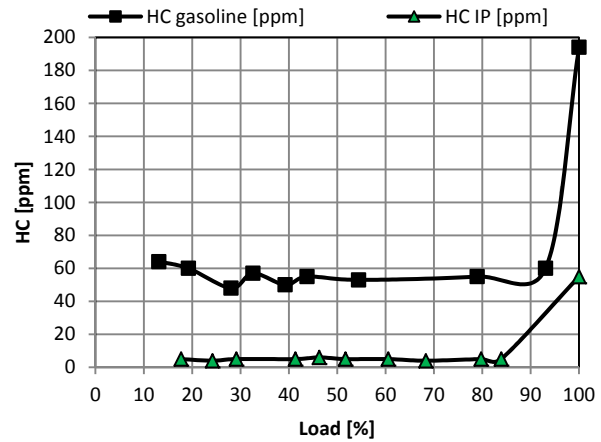


Fig. 7 HC concentration in exhaust gases at partial load

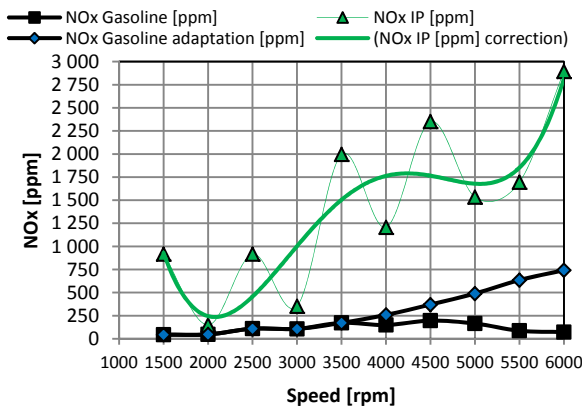


Fig. 8 The concentration of NO_x in exhaust gases at full load

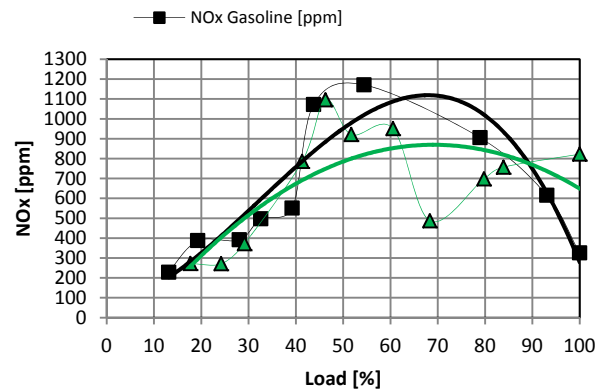


Fig. 9 The concentration of NO_x in exhaust gases at partial load

Conclusion

The pollution problem must be solved today, that's why we made these pollutant measurement and we used an alternative solution for fuel. The two fuel, gasoline and isobutene, are from different sources, but the nature of the exhaust gas, can be observed that the differences are not very big, of course, but both have the advantages and disadvantages when are compared. Analysing one by one each element of exhaust gases, we note that the concentration of CO₂ in the exhaust gases is relatively high, both the engine operation IP50 and the operation of gasoline. Gasoline stations, commercial gasoline, have a carbon content of 85-88% and 12-15% hydrogen, which may be reason to concentrations of 12% of CO₂ for gasoline. Regarding the oxygen, through the excess air ratio, λ values are relatively the same as for gasoline and still slightly higher. In the carbon monoxide case, the vehicle disposes less CO, quantitatively, for IP50, especially at full load, and this is an advantage for isobutene. Unburned hydrocarbons are very few quantitative on this case IP50, both at full load and partial load, on the graphics can be observed the differences, and also the functioning vehicle advantage with the mixture IP50, for this case of HC. But the NO_x concentrations are not within the acceptable limits, running at full load doubling or even tripling the quantitative values emitted by motor operation with IP50 mixture. The final conclusion at the end of experimental research, concerning the quality of engine exhaust gases on Opel Omega A in its operation with petrol + isobutene mixture in concentration of 50% + 50%, are: the car behaves normally kept in its operation parameters acceptable performance, the major advantage of this fuel is the hydrocarbons case, where the quantities emitted are much lower than for gasoline operation. Note that, have not been made major functional changes to the motor vehicle, thus the behaviour of the engine operation with mixture IP50 proves to be advantageous on exhaust gas quality. The alternative fuels will soon find the place for vehicles, taking into account any adjustments to increase performance and reduce vehicle exhaust gas quantity to run these vehicles with alternative fuels, one of them being the IP50. Today's scientists are searching solutions to reduce the CO₂ from the atmosphere [14, 15], concerning the human health and nature health, and all the alternative solution for thermal engine, as sources energy, is a new chance for a better life.

Acknowledgment

This work was partially supported by the strategic grant POSDRU/88/1.5/S/50783, Project ID 50783 (2009) co-financed by the European Social Fund – Investing in People, within the sectorial Operational Programme Human Resources Development 2007-2013. This work was partially supported by the strategic grant POSDRU/21/1.5/G/13798, inside POSDRU Romania 2007-2013, co-financed by the European Social Fund – Investing in People.



References

- [1] R.Bosch Gmbh, Gasoline-Engine Management, Handbook, 2nd Edition, Germany, 2004.
- [2] S.Ratiu, L. Mihon: Motoare cu ardere internă pentru autovehicule rutiere – procese și caracteristici, *Editura Mirton*, Timișoara, 2008.
- [3] J.A. F.K. Akinbami: Analysis on the energy pricing strategy with CO₂ tax and its effect on mitigation of CO₂ emission in total energy systems, *Power Engineering Society Winter Meeting*, IEEE, 2001.
- [4] M. Guatam, D.W. Martin: Combustion Characteristics of Higher Alcohol/Gasoline Blends, *US Department of Energy*, 2010.
- [5] G. Najafi and all: Performance and exhaust emissions of a gasoline engine with ethanol blended gasoline fuels using artificial neural network, *Applied Energy*, 2009.
- [6] A.Demirbas: Social, Economic, Environmental and Policy Aspect of Biofuels, *Energy, Education and Technology*, 2009.
- [7] R.D.Atkins: An Introduction to Engine Testing and Development, *SAE International*, 2009.
- [8] A. P. Stoicesc: Proiectarea performanțelor de tracțiune și de consum ale automobilelor, *Editura Tehnică*, București, 2007.
- [9] H. Balat: Prospect of biofuels for a sustainable energy future: a critical assessment, *Energy, Education and Technology*, 2009.
- [10] G.P.Blair: Design and Simulation of Four-Stroke Engines, *SAE International*, USA, 1999.
- [11] R.Hentiu: Studii si cercetari privind influenta sistemului de admisie asupra performantelor motoarelor cu aprindere prin scanteie si injective indirecte de combustibil, *Editura Politehnica*, Timisoara, 2011.
- [12] A.Irimescu: Cercetări privind influența stării amestecului carburant și a naturii combustibilului asupra performanțelor și gradului de poluare al unui motor cu aprindere prin scânteie cu injecție în poarta supapei, *Editura Politehnica*, Timisoara, 2010.
- [13] I. Hiticaș, D. Iorga, L.Mihon, E. Resiga and N. Uricanu, Studies and experimental research concerning the performances of the internal combustion engine, controlled over the powertrain control module, *Fiability & Durability Journal*, 2012, Romania, pp. 23-28.
- [14] L.Xu: Control of exhaust pollutants from gasoline engine of vehicle, Conference Publication, *ICCASM, China*, IEEE, 2010.
- [15] T. Yusaf, D. Buttsworth, G. Najafi: Theoretical and experimental investigation of SI engine performance and exhaust emissions using ethanol-gasoline blended fuels, *Energy and Environment*, 2009, 3rd International Conference on ICEE 2009, Malacca – Malaysia, pp. 195 - 201.
- [16] I. Hiticaș, D.Marin, L.Mihon, E. Resiga and D. Iorga, Parameters Control of a Spark Ignition Engine through Programmable ECU for Specific Regimes, *SACI 2012, 7th IEEE International Symposium on Applied Computational Intelligence and Informatics*, PROCEEDING, Timisoara, Romania, pp. 399-404.

Addresses for correspondence: I.Hiticas – ihiticas@yahoo.com, D.Marin – marindaniel1@yahoo.com, L.Mihon – liviu.mihon@mec.upt.ro



INNOVATIVE NANOFIBER FILTRATION MATERIALS OF THE BIOPOLYMER ALGINATE FOR SEQUESTRATION OF DISSOLVED LEAD FROM WATER

Melissa Bradley¹, Matthew D. Cathell¹

¹ The College of New Jersey. Department of Technological Studies, School of Engineering. 2000 Pennington Road, Ewing, New Jersey. United States of America.

Keywords: water remediation, alginate, biopolymers, electrospinning, nanofibers, metal sequestration, biosorption

Abstract. We have created nanofibers of the biopolymer alginate and have investigated their ability to sequester the toxic metal lead from aqueous solutions. The noted capacity of alginate to biosorb metals makes it a compelling candidate material for biological purification of metal-contaminated drinking water. Nanofibers were produced by electrospinning aqueous solutions of alginate and polyethylene oxide in a high voltage electric field, producing fibers with diameters ranging from 100–500 nm. Calcium ions were used to crosslink the alginate component of the fibrous product to render it water-insoluble; the uncrosslinked polyethylene oxide was removed by rinsing with water. Nanofibers were characterized using electron microscopy and infrared spectroscopy. UV-Visible spectroscopy, with a colorimetric indicator, was used to quantify sequestration of Pb²⁺ ions from aqueous solutions using mats of alginate nanofibers.

Introduction

Alginate

The biopolymer alginate (alginic acid) is an unbranched polysaccharide composed of (1–4) linked β -D-mannuronic acid (M) and α -L-guluronic acid (G) subunits, arranged in various sequences (Figure 1a). Alginate is produced naturally with varying amounts of M and G subunits in brown algae, as well as in bacterial species such as *Azotobacter vinelandii* and *Pseudomonas aeruginosa*. Alginate is used in a variety of industries because of many desirable properties; it is biocompatible, biodegradable, non-toxic, and is classified “generally regarded as safe” (GRAS) by the U.S. Food and Drug Administration. Alginate is used for medical applications in dental impressions, wound dressings, and drug delivery technologies. In the food and cosmetics industry, it is commonly used as a thickener and binding agent. Alginate is also used in various industrial products including lubricants, sealants, and pastes [1].

When dissolved in water, sodium alginate salts dissociate into anionic polymer chains and form viscous syrups. Dissolved alginate can be converted into an insoluble hydrogel through crosslinking, either via binding with metal ions or by covalent bonding. Alginate associates with multivalent metal cations through a variety of mechanisms, including functional group interactions, ion exchange, and coordination. This property makes alginate an ideal candidate for biosorption and removal of metals from aqueous solutions [2-4].

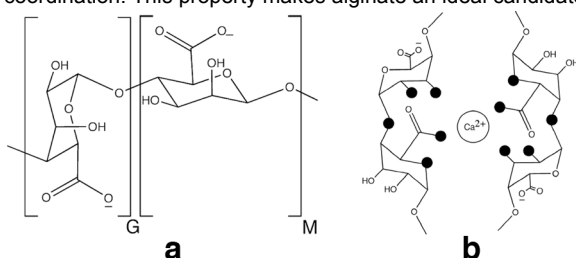


Figure 1. The structure of alginate (a) consists of both guluronic acid (G) and mannuronic acid (M) subunits. In the presence of multivalent cations, such as Ca²⁺, guluronic acid subunits form a coordination sphere (b), crosslinking the polymer to form a hydrogel. Darkened circles represent oxygen atoms participating in coordination.

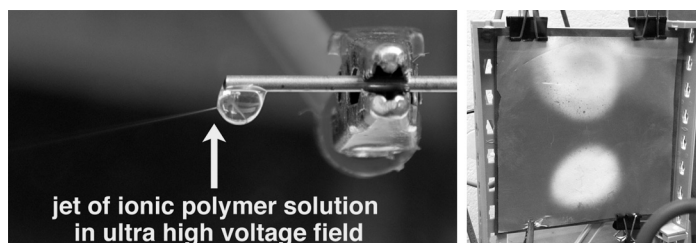
Investigations have focused on alginate sequestration of a wide variety of metals, including gold, cadmium, chromium, cobalt, copper, iron, nickel, lead, uranium, and others [3, 5, 6]. Metal cations readily associate with alginate, particularly within regions of the polymer chain rich in the guluronic acid subunit [7, 8]. The negatively charged carboxylate groups are key to metal-binding, but are not the only titratable sites. Metal binding occurs via a coordination sphere involving carboxyl and hydroxyl oxygen atoms, as well as oxygen atoms within the ring and glycosidic linkage [9, 10]. Blocks of guluronic acid residues present more favorable coordination geometries, compared with less favorable mannuronic acid blocks. Alginate–metal complexes are frequently represented by the “egg-box” model illustrated in Figure 1b, in which divalent calcium ions (or other cations) are coordinated within the guluronic-rich regions of the alginate chain, similarly to the packing of eggs in a carton (Figure 1b). In this study, we have processed alginate into nanofibers using a technique known as electrospinning, and subsequently crosslinked the fibers with Ca²⁺.

Electrospinning

Electrospinning is a process that uses a high voltage electric field to transform a liquid polymer solution into incredibly thin fibers, often hundreds or thousands of times thinner than human hairs. Electrospun fibers, made from both natural and synthetic polymers, are

currently investigated for applications ranging from the production of pharmaceutical-laden bandages to biodegradable insect-resistant nets for crops. The principle of electrospinning is relatively simple, requiring basic equipment and little expense. A high voltage power supply is used to accelerate a stream of ionically-charged polymer solution from the needle of a syringe (Figure 2, left) to a metallic "target" object. During the split-second transit from needle to target, the solvent in the polymer solution flash evaporates and leaves behind a nanoscale polymer fiber to impact and collect on the target. A fibrous mat is generated on the target surface, appearing as a visible deposition to the unaided eye (Figure 2, right). Because of their minute diameters, electrospun fibers possess very high surface area-to-volume ratios. The high surface area of alginate fibers, coupled with the material's intrinsically high binding affinity for metals, give these structures significant potential for biosorption and water remediation applications.

Figure 2. An electrospun fiber forms from the polymer solution droplet within the high voltage electric field (left). The electrospinning target is shown (right) with multiple fiber deposition sites.



Sequestration of Dissolved Lead

A key motivation underlying this investigation is the development of novel biosorption technologies for the removal of the toxic metal lead from water. Lead is commercially used in a wide variety of industries. It is found in lead-acid batteries and electronics solder, and is a component metal of many alloys [11]. Lead finds its way into the environment through emissions from mining and metalworking industries, as well as the burning of fossil fuels. Lead contamination of drinking water can also arise from corrosion of plumbing and by erosion of natural deposits [12]. Household exposure can occur from dust, soil, and older lead-based paints.

The human consequences of lead contamination can be dire. The U.S. Environmental Protection Agency (EPA) recognizes lead as a contributor to developmental delays in infants and children, causing attention deficit conditions and learning disabilities. Lead exposure in adults can lead to a variety of health ailments, including kidney problems, high blood pressure, disrupted metabolism, suppressed heme synthesis, and neurotransmitter interference [13]. Lead is arguably the most consequential neurotoxic element. It causes measurable declines in cognitive function at blood concentrations of less than 100 µg/L; each additional increase of 100 µg/L is correlated with a drop in IQ of 4.6 on the Stanford-Binet Intelligence Scale [13]. According to World Health Organization guidelines, up to 0.01 mg/L of lead is allowable in drinking water [11]. The U.S. EPA maintains a Treatment Technique action level of 0.015 mg/L for lead; corrective actions must be taken if more than 10% of samples from a water supply test above this level [12]. Contamination of water with lead and other heavy metals is a pressing issue in the United States and around the world.

Experimental

Materials

Chemical reagents were obtained from Sigma-Aldrich (St. Louis, MO). Low viscosity alginate (alginic acid sodium salt from brown algae) had a molecular weight range of 12–80 kDa and consisted of approximately 61% mannuronic acid and 39% guluronic acid subunits, as reported by the supplier. Polyethylene oxide (PEO) had an average viscosity molecular weight of 600 kDa. Triton X-100 surfactant was used to improve fiber uniformity. Crosslinking was achieved using solutions of calcium chloride (≥99% purity) in an ethanol–water solution. The metal-binding study was conducted using aqueous solutions of lead(II) nitrate (>99% purity). Pb²⁺ ions were measured using 1,5-diphenylcarbazone dissolved in ethanol. All aqueous solutions were made with Type 1 ultrapure water (18.2 MΩ-cm resistivity at 25 °C) from a purification system (Millipore, Billerica, MA).

Nanofiber Preparation

Aqueous solutions of sodium alginate and PEO, with total solute concentrations ranging from 2.0–3.0% (w/v), were prepared separately from one another. Solutions were stirred and agitated for periods ranging from 1–3 days until solutes were completely dissolved. The solutions were then combined at various ratios ranging from 50:50 to 80:20 (alginate:PEO). Triton X-100 was added to the solutions at a concentration of 1 wt. %. The electrospinning apparatus consisted of a 10 W high voltage DC power supply (Gamma High Voltage Research, Ormond Beach, FL) with a positive polarity. A syringe pump (Smith Medical, Kent, UK) was used to advance polymer solutions through tubing to a negatively charged and grounded blunt-tipped needle. A positively charged copper plate, mounted on a motorized platform, served as the target. Nanofiber specimens were collected on sheets of aluminum foil or copper mesh clamped to the target. The target and needle were enclosed in a poly(methyl methacrylate) box, with an approximate internal volume of 0.06 m³. Fibers were produced at voltages ranging approximately 15–20 kV, with needle-to-target distances of 10–15 cm. Typical environmental conditions inside the electrospinning enclosure were temperatures of 20–22 °C and relative humidity values of 55–65%. After electrospinning, the fiber products were crosslinked with Ca²⁺ ions. Fiber mats were immersed in a 2% (w/v) solution of calcium chloride dissolved in ethanol:water (5:1). After 30 seconds of exposure, with gentle agitation, the fiber mats were removed from the CaCl₂ solution, rinsed in pure water, and allowed to dry.

Nanofiber Characterization

Micrograph images of nanofibers were obtained using a scanning electron microscope (Hitachi High-Technologies Corp., Tokyo). Specimens were sputter coated with AuPd prior to imaging. SEM micrographs were typically taken with a working distance of 5 mm and an accelerating voltage of 5–15 kV. Images were captured in RAW format using digital SLR camera mounted to the SEM. Infrared spectra were obtained using an FT-IR spectrometer (PerkinElmer, Waltham, Massachusetts). Bulk powdered starting materials, as well as fiber specimens, were ground with potassium bromide powder and pressed into pellets for IR analysis.

Lead(II) Ion Testing

Colorimetric testing was used to quantify Pb²⁺ ion sorption by the polymer fibers. An indicator solution was prepared by dissolving 0.5 g of diphenylcarbazone in 100 mL of anhydrous ethanol. The diphenylcarbazone solution (50 µL) was pipetted into a cuvette along with 1 mL of Pb²⁺ solution. The cuvettes were gently agitated on an orbital mixer stage for 15 min before absorbance measurements were made using a UV-Visible spectrophotometer (Beckman Coulter, Brea, CA). The presence of Pb²⁺ ions caused a transition in solution color from a pale yellow to a distinct pink–red. Pb²⁺ concentrations were quantified by absorbance at 530 nm. To generate a concentration curve, a series of neutral lead(II) nitrate solutions, ranging in concentration from 2.5E-1 to 1.5E+3 parts-per-million (ppm), were prepared using

serial dilution from a stock solution. The tested concentrations (in ppm) were 1500, 1250, 1000, 750, 500, 250, 100, 75, 50, 25, 5, 1, 0.5 and 0.25. Ultrapure water served as a 0 ppm control. After treatment with diphenylcarbazone, three averaged replicate absorbance measurements were made of each solution. The absorbance data at 530 nm were fitted to a sigmoidal curve. A series of crosslinked alginate nanofiber mats were peeled from aluminum foil and weighed with an analytical balance. Each fiber mat was immersed for 10 min in a known volume of neutral 100 ppm Pb^{2+} solutions. The concentrations of lead in these solutions were analyzed before and after immersion of the nanofiber mats, using the previously generated calibration curve. The difference in Pb^{2+} concentration between the two sets of measurements was attributed to binding and sequestration of lead ions by the alginate nanofibers.

Results and Discussion

Nanofiber Production and Crosslinking

Early attempts to produce fiber mats resulted in electro spray and splatter of the liquid polymer. After adjusting of a number of experimental factors, including applied voltage and target distance, fibers mats were produced. Typical successful parameters included a syringe-to-target distance of approximately 10 cm, a voltage of 18–20 kV, and a solution infusion rate of 0.25 mL/h. Attempts were made to produce fibers with a positively charged needle and a negatively charged grounded target — however, this configuration led to the rapid growth of unwanted three-dimensional dendritic structures emanating from the target plate, rather than flat fibrous mat structures.

Fiber specimens were submerged in a solution of $CaCl_2$ dissolved in an ethanol–water solution; the ethanol minimizes polymer dissolution and aggregation upon initial submersion [14, 15]. In this process, the alginate material was crosslinked and converted into a water-insoluble hydrogel. At the same time, PEO dissolved and was extracted into the solution, leaving behind only crosslinked alginate fibers. The removal of PEO material was confirmed with IR spectroscopy. Although the nanofiber mats lost some of their structure with the removal of PEO, it was possible to generate specimens, with high alginate/PEO ratios, that remained largely intact throughout the crosslinking process. This Ca^{2+} crosslinking method can be aided by additional covalent crosslinking of specimens using glutaraldehyde or similar agents.

Nanofiber Characterization

Nanofibers were characterized using infrared spectroscopy (**Chyba! Nenalezen zdroj odkazů.**). Spectra of the bulk powdered PEO and alginate starting materials were obtained for comparison to spectra of fibrous specimens. Characteristic spectral signals for both PEO and alginate are highlighted in **Chyba! Nenalezen zdroj odkazů.**. The infrared spectrum of alginate features a number of characteristic bands (highlighted with light gray bars). The prominent bands centered near 1615 cm^{-1} and 1425 cm^{-1} are the result of asymmetric and symmetric stretches of the COO^- group. There are also strong signals ranging from approximately $1150\text{--}1000\text{ cm}^{-1}$, which are the result of C–C and C–O stretching. The IR spectrum of PEO contains its own distinct bands (highlighted with dark gray bars) that differentiate it from alginate. The signals highlighted in **Chyba! Nenalezen zdroj odkazů.** include bands associated with CH_2 asymmetric bending (1466 cm^{-1}), wagging (1344 cm^{-1}), twisting (1284 and 1244 cm^{-1}) and rocking (845 cm^{-1}). The spectrum also features a broad asymmetric C–O–C stretching signal (1105 cm^{-1}) that overlaps with similar signals in the alginate spectrum [16, 17]. As expected, the spectrum of alginate+PEO fibers features spectral bands from both polymers. This combination of signals indicates that the nanofiber specimens, when initially spun, are comprised of a blend of PEO and alginate. After the crosslinking process, PEO signals disappear, resulting in a spectrum that looks quite similar to that of the alginate (bulk) starting material. This evidence suggests that PEO was successfully extracted from the fibrous mats, while alginate remained behind. The signal at approximately 1090 cm^{-1} is correlated with carboxyl C–O stretching, and is strengthened in the alginate fiber spectrum because of increased C–O stretching associated with coordination around the crosslinking Ca^{2+} ion.

Electron micrographs of typical fibers are shown in Figure 4. These images depict distinct but highly branched and networked fibers with generally uniform diameters. Early specimens contained only a few non-uniform fibril structures, and were mostly composed of granular textured surfaces. Fiber quality was improved by adjusting the percent of dissolved polymer and ratio of alginate:PEO. The most successful fibers were produced from a 2.5% solution using a 70:30 alginate:PEO blend. The addition of a surfactant, at a concentration of 1 wt. %, reduced the formation of bead structures and resulted in more uniform fibers. Fiber diameters, measured at 100 random points per specimen, ranged from approximately 100–500 nm, depending on specific electrospinning and solution parameters.

Figure 3. UV-Visible spectroscopy was used to generate a Pb^{2+} calibration curve (a) using lead solutions of known concentrations. The zoomed view (b) illustrates the change in Pb^{2+} concentration of a 100 ppm solution before and after exposure to alginate nanofibers.

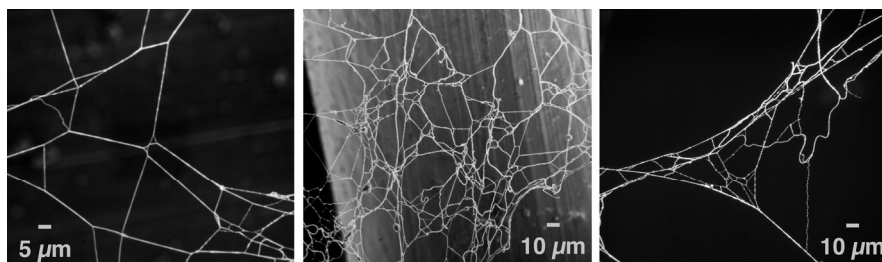
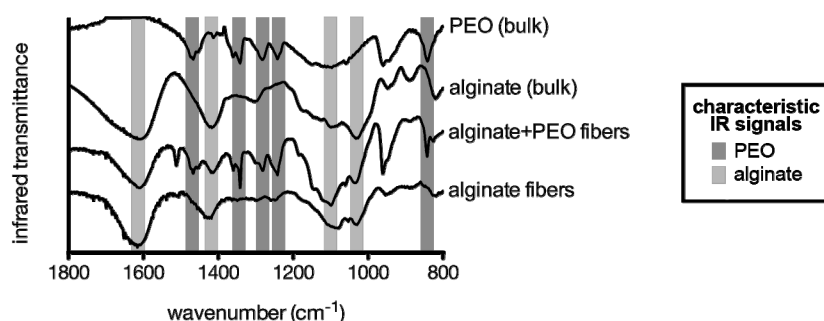
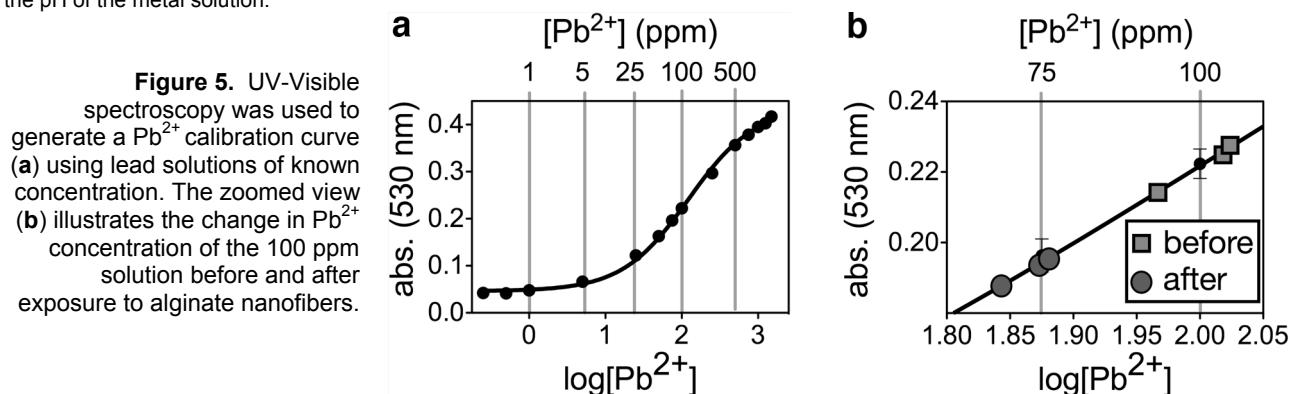


Figure 4. Electron micrograph images of electrospun nanofibers, electrospun from a 2.5% solution of alginate:PEO (70:30 ratio).

Lead(II) Ion Testing

Figure 5a shows the sigmoidal concentration curve generated from lead(II) nitrate solutions of known concentrations. The lower detection limit is near 5 ppm. The response from 25–250 ppm is essentially linear, following the Beer–Lambert law. We chose to conduct metal ion studies of the alginate nanofibers using 100 ppm Pb^{2+} , in the middle of this Beer–Lambert region (Figure 5b). This concentration was also chosen to so that there would be excess Pb^{2+} ions in solution to ensure that all available alginate binding sites became occupied, corresponding to the maximal uptake level in the Langmuir isotherm model [3].

Three replicate absorbance measurements of 100 ppm Pb^{2+} solution were taken and compared with our previously measured calibration data, in order to validate the calibration curve and ensure repeatability. This validation test resulted in an average measurement of 100.9 ± 4.3 ppm for our 100 ppm solution. After 10 min of alginate nanofiber mat immersion, the Pb^{2+} concentrations were again assessed and found to be 77.2 ± 2.5 ppm. Based on the masses of the fiber mats, these results correlate to a mass uptake of approximately 81 mg Pb^{2+} per 1 g alginate, and a molar uptake of approximately 0.39 mmol Pb^{2+} per 1 g alginate. Using the molecular weight of 159.12 g/mol for each alginate subunit, we calculate that a Pb^{2+} ion is associating with approximately one of every 6–7 alginate subunits; we assume that most of these binding sites are among blocks of guluronic acid [8]. The uptake levels for our alginate nanofibers are in agreement with general ranges reported by others for bulk alginate hydrogels. Mass uptake of metals by polymers, including alginate and other similar polysaccharides, are frequently reported on the order of tens or hundreds mg metal per g polymer [3-5, 18, 19]. It should be noted that uptake levels depend on a variety of factors, including the specific source organism of the biological material and the pH of the metal solution.



Conclusion

Alginate and PEO have been electrospun together to form nanoscale fibrous mats. Through the calcium crosslinking process, the alginate fibers were rendered insoluble and separated from PEO, which dissolved from the specimens. Our lead binding experiment indicates that these nanofibers can be used to bind and sequester lead ions, suggesting significant potential for water remediation applications. This study serves as a proof-of-concept for the viability of alginate nanofiber filtration media, which is capable of reducing concentrations of harmful metallic contaminants in water. Ongoing and planned investigations focus on studying the effects of additional covalent fiber crosslinking methods, as well as binding studies between alginate and additional heavy metals.

Acknowledgment

This work was made possible by support from Academic Affairs at The College of New Jersey, through the Mentored Undergraduate Summer Experience, from the New Jersey Space Grant Consortium, and from TCNJ Dept. of Technological Studies.

References

- [1] D.J. McHugh: Production and Utilization of Products from Commercial Seaweeds (Food and Agriculture Organization of the United Nations, Rome, 1987).
- [2] M.D. Cathell and C.L. Schauer: Structurally Colored Thin Films of Ca^{2+} -Cross-Linked Alginate, *Biomacromolecules*, 8 (2007), 1, pp. 33-41.
- [3] T. Davis, B. Volesky, and A. Mucci: A Review of the Biochemistry of Heavy Metal Biosorption by Brown Algae, *Water Research*, 37 (2003), pp. 4311-4330.
- [4] Z.R. Holan and B. Volesky: Biosorption of Lead and Nickel by Biomass of Marine Algae, *Biotechnology And Bioengineering*, 43 (1994), 11, pp. 1001-1009.
- [5] J.P. Ibanez and Y. Umetsu: Uptake of Trivalent Chromium from Aqueous Solutions Using Protonated Dry Alginate Beads, *Hydrometallurgy*, 72 (2004), pp. 327-334.
- [6] A. Haug and O. Smidsrod: Strontium, Calcium and Magnesium in Brown Algae, *Nature*, 215 (1967), pp. 1167-1168.
- [7] M.D. Cathell, J.C. Szewczyk, and C.L. Schauer: Organic Modification of the Polysaccharide Alginate, *Mini-Reviews In Organic Chemistry*, 7 (2010), 1, pp. 61-67.
- [8] T.A. Davis, F. Llanes, B. Volesky, and A. Mucci: Metal Selectivity of Sargassum spp. and Their Alginates in Relation to Their Alpha-L-Guluronic Acid Content and Conformation, *Environmental Science & Technology*, 37 (2003), pp. 261-267.
- [9] R. Schweiger: Acetylation of Alginic Acid. I. Preparation and Viscosities of Algin Acetates, *The Journal of Organic Chemistry*, 27 (1962), pp. 1786-1789.
- [10] R. Schweiger: Acetylation of Alginic Acid. II. Reaction of Algin Acetates with Calcium and Other Divalent Ions, *The Journal of Organic Chemistry*, 27 (1962), pp. 1789-1791.
- [11] M. Shaw and P. Haddad: The Determination of Trace Metal Pollutants in Environmental Matrices Using Ion Chromatography, *Environment International*, 30 (2004), pp. 403-431.
- [12] United States Environmental Protection Agency: National Primary Drinking Water Standards (Office of Water, Washington, DC, 2003).
- [13] T.W. Clarkson: Metal Toxicity in the Central Nervous System, *Environmental Health Perspectives*, 75 (1987), pp. 59-64.



-
- [14] S.I. Jeong, M.D. Krebs, C.A. Bonino, S.A. Khan, and E. Alsberg: Electrospun Alginate Nanofibers with Controlled Cell Adhesion for Tissue Engineering, *Macromolecular Bioscience*, 10 (2010), 8, pp. 934-943.
- [15] C.A. Bonino, M.D. Krebs, C.D. Saquing, S.I. Jeong, K.L. Shearer, E. Alsberg, and S.A. Khan: Electrospinning Alginate-Based Nanofibers: From Blends to Crosslinked Low Molecular Weight Alginate-Only Systems, *Carbohydrate Polymers*, 85 (2011), 1, pp. 111-119.
- [16] T. Yoshihara, H. Tadokoro, and S. Murahashi: Normal Vibrations of the Polymer Molecules of Helical Conformation. Iv. Polyethylene Oxide and Polyethylene-D4 Oxide, *Journal Of Chemical Physics*, 41 (1964), 9, pp. 2902-2911.
- [17] S.J. Wen, T.J. Richardson, D.I. Ghantous, K.A. Striebel, P.N. Ross, and E.J. Cairns: FTIR Characterization of PEO+ LiN(CF₃SO₂)₂ Electrolytes, *Journal of Electroanalytical Chemistry*, 408 (1996), 1, pp. 113-118.
- [18] J. Ibanez and Y. Umetsu: Potential of Protonated Alginate Beads for Heavy Metals Uptake, *Hydrometallurgy*, 64 (2002), pp. 89-99.
- [19] B. Volesky and Z.R. Holan: Biosorption of Heavy Metals, *Biotechnology Progress*, 11 (1995), 3, pp. 235-250.



International Conference on Innovative Technologies, IN-TECH 2012,
Rijeka, 26. - 28.09.2012





INFORMATION AND COMMUNICATION TECHNOLOGY IN THIRD PARTY LOGISTICS

S. Saseedharan ¹, P. Muralidharan ²

¹ Red Orange, P O Box 84791, Dubai, United Arab Emirates

² BITS Pilani, Dubai Campus, P O Box 345055, Dubai, United Arab Emirates

Keywords: 3PL, Logistics, Supply Chain Management, Warehouse Management System, ICT, Outsourcing

Abstract. With the advent of globalization, the scene of international trade has been changing drastically. Trade across the boundaries gives more value and profitability to organizations which are under pressure to reduce costs and compete on a global level. Logistics & Supply Chain Management needs to be fine tuned so that businesses and their customers are connected efficiently and to meet the customer requirements of a faster lead time, quick turnaround, reduced costs, better customer service and quality. Information and Communication Technology should give the customers end-to-end real time visibility on the status of their orders such as movement schedules, shipment details, costs, performance measures, reporting. Setting up own logistics services may distract the organizations from concentrating on their core competencies and blunt their competitive advantage. For this reason, businesses outsource activities such as outbound transportation, warehousing, inbound transportation, customs brokerage, freight forwarding, and customs clearance to third party logistics (3PL) companies. This paper aims to identify the key performance indicators of 3PL organizations and to investigate the different supply chain challenges arising in 3PL organizations. Efficient communication practices and advanced technologies in information and communication technology (ICT) that can be developed for the use in Warehouse Management have been identified to offer competitive advantage in a global market. A survey has been conducted among 35 different organizations which has warehouses to find out what kind of ICT they are using in their warehouses, how this is benefitting the organization in terms of cost effectiveness, enhancing efficiency, the challenges that they are facing on a daily basis.

Introduction

Warehousing holds an important role in logistics and needs to be handled strategically in order to bring about efficient and cost effective solutions for the organization in the supply chain. Warehouses help in reducing cycle times, bringing down inventory levels, reducing costs, and giving a better customer service perspective. Information and communication technology is being used extensively in warehouses in order to achieve order-processing and cost goals and are being relocated to strategic locations so as to achieve overall supply chain customer service goals in warehouses and third party logistics.

Literature Review

3PL organizations provide outsourcing services to organizations like inventory management, freightforwarding, etc so that organizations can concentrate on their core competencies and help in reduction of costs(Lieb, Millen and Wassenhove, 1993). The last couple of decades, organizations have been building up strategies, which would help them design products for a global market and which also helps organizations to source globally (Cooper, 1993). Such processes has helped in developing complicated supply chain and logistics processes across the boundaries and some organizations have no idea about administrative processes such as customs, tax regulations, and infrastructure of other countries - this is where 3PLs add in their value while allowing organizations to focus on their core competencies (Byrne, 1993; Foster & Muller, 1990; Trunick, 1989). One of the biggest ways that effectiveness and efficiency is being improved within the 3PL organizations is by Information and Communication Technology (ICT) and this can even help gain competitive advantage (Porter and Millar 1985). Baker, 2004, says that a large proportion of warehouses offer a same-day or next-day lead time to customers from inventory and to do this reliably, they would need to do this with high tolerances of speed, accuracy and lack of damage.

Key Performance Indicators (KPIs) of 3PLs

A third party logistics (3PL) organization can be defined as an external supplier that performs all or part of a company's logistics functions. The KPIs of different 3PL organizations vary based on the clientele who can bring about varying degrees of complexity and can have different needs and business models. These need to be measurable and relevant as well as consistent over a period of time and could include on time delivery, order accuracy, inventory accuracy, Customer service, reliability, responsiveness, real time information system. ^[1] The 3PLs should have a way to obtain, maintain and validate the data that is collected from end to end and should also be accountable, responsible, reliable and communicate efficiently with the clients giving them real time status of their shipments. Clients look at 3PL providers who can be aligned to the competitive advantage, provide on time and on place delivery, convenience and cost savings. With the information that is collected, the 3PL organizations should be able to give reports to their customers which would help them decide on their supply chain strategies in the long term and would help them decide on the kind of transportation network that they want to follow. The 3PL organizations should be able to give different delivery modes to the customers to help reduce transportation costs further and in turn give reduces and flexible transit times.

Improvement in the performance of logistics

The use of ICT has improved the exchange of supply chain information, leading to the development of integrated production and logistics management systems and has thereby improved supply chain performance in many ways. Electronic Data Interchange (EDI) use

computer links instead of hard-copy paper which required extensive time to transfer and often contained errors. The advantages of these ICT-supported information exchange systems include: increased speed, reliability, storage capacity, worldwide coverage, transparency, and reduced transaction costs. Goods and vehicle tracking as well as real-time vehicle routing and scheduling systems have transformed logistics management. Lead-time has been reduced by the introduction of EDI, mechanisation, automation and optimal vehicle routing systems, leading to potentially lower levels of stock surplus. The development of the Internet provides a convenient way of gathering, organising and distributing information on products, services and trade regulations at a global level. Major freight transport service providers have resorted to creating Web pages on the Internet to provide information on their services, schedules and rates that can be easily accessed around the clock by the global market. More advanced freight transport suppliers already provide the possibility for interactive responses to cargo-tracking inquiries made by shippers and forwarders. Customized ERP are employed many major corporations for their day to day functioning. One of the major components of ERP is a ware house management system which is used for inventory monitoring and maintenance and also to deal with complex storage and distribution needs thus facilitating improvement in efficiency of the entire supply chain of the organization. Warehouse Management System can allow various important statistics to be monitored and develop comprehensive strategies for optimizing the systems in use from these indicators. The core of a WMS supports the basic processes in an organizations warehouse such as receiving, storage, warehouse management, picking, retrieval, shipping, inventory and forms management. The more complex functions that can be performed by a WMS include batch/serial management of returns etc. the other extra modules can connect self-contained software packages like RFID software or pick-by-voice /pick-by-light systems.

Analysis

For the purpose of this study, a questionnaire was prepared and sent to 160 different organizations with warehouses to find out what kind of ICT they are using in their warehouses, the benefits in terms of cost effectiveness, enhancing efficiency, the challenges that they are facing on a daily basis etc. Out of the 160 surveys sent out, a total of 35 responses were received- (21% response level). The category of organizations selected are of different types – Manufacturers, Retail Organizations, Logistics Companies, MEP with warehouses, Equipment Rentals, etc. The first part of the analysis is being directed towards seeing how manual practices prove to be time consuming for warehouses in terms of inventory management, preparation of documents, real time tracking of information on shipments etc. Then the analysis shifts to the different technologies being used within warehouses. The perceived challenges in implementing and using these technologies are further analyzed followed by the perceived benefits of using these technologies. The different activities being outsourced is being analyzed and finding out important factors to be considered while selecting a logistics services provider and what the perceived challenges with outsourcing activities are. The features of this questionnaire are : (a)Purely logistics companies are being included (b) Other retail/manufacturers/rentals organizations with warehouses are included (c) The cost factor which can be effectively and efficiently reduced with the help of ICT has been considered.

Summary of Findings

The survey was prepared in discussion with the warehouse manager of Red Orange General Trading (www.redorange.com). The population considered was vendors and logistics partners used by Red Orange General Trading, who have warehouses. The main objectives of carrying this survey out can be listed as : (a)To analyze how costs can be reduced using ICT in warehouse management (b)To analyze how time consuming and repetitive tasks can be minimized and duplication of work be avoided by the use of ICT (c) To identify the challenges and benefits of using ICT in warehouse management (d) To see the how different technologies can eventually be implemented at Red Orange General Trading to upgrade the ICT being used there.

The comprehensibility and suitability of the survey was tested on a small sample of 5 companies. The feedback received from these organizations helped in further refining the questionnaire.

Main Results

Out of the 35 responses received, several organizations used more than one method for managing their supply chain functions such as Just-in-Time supply, Outsourcing, 3PL, holding safety stock, e-procurement and Subcontracting. A good portion of organizations also keeps stock of their popular products based on customer demand.32 of them have their own warehouses and 3 of them outsourced their warehousing activities outside. 23 of the organizations holds safety stock. Counting of inventory : 24 organizations does this on a daily basis. 7 of them every week and 4 every month. Documents such as invoices, packing lists, etc.is done manually by 9 organizations. And such organizations take on an average 1-8 working hours on a daily basis to do this work. It was found that 22 organizations use ICT technologies such as warehouse management systems, global positioning system, online order and tracking systems and tracking provided by 3PL organizations to receive real time information of their shipments to coordinate the information between the different departments within their organizations and externally as well. The time taken for organizations who do not have any sort of ICT to centrally track the system real time is between 15 min to upto 2 days.The different ICTs being used by organizations was evaluated and the most common ones being used are JIT, ERP, and Warehouse Management System. (Figure 1)

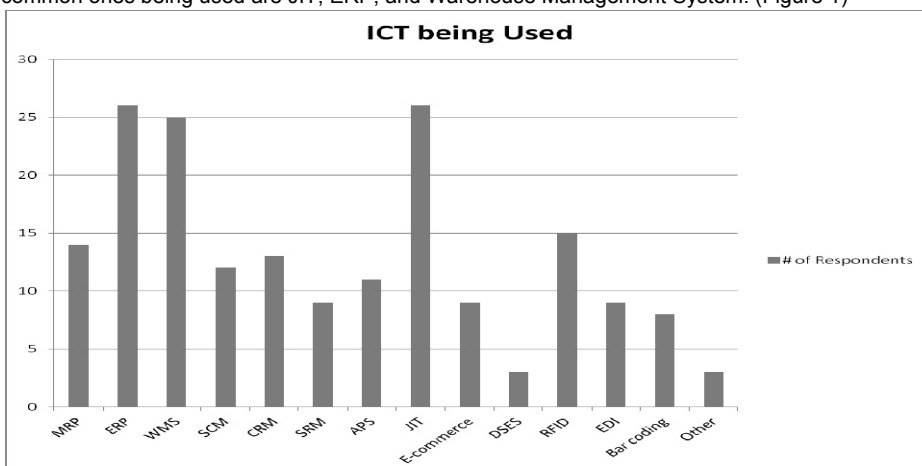


Figure 1 : ICT being used by different organizations

Challenges faced by organizations while implementing ICT- Resources shortage takes the highest ranking that clients perceive as the biggest challenge to implementing ICT to their organizations. This was ranked as major challenge by 18%. The next on the list is insufficient vendor support – those who assists in implementing the ICT may not always be helpful in post-sales support. (Figure 2)

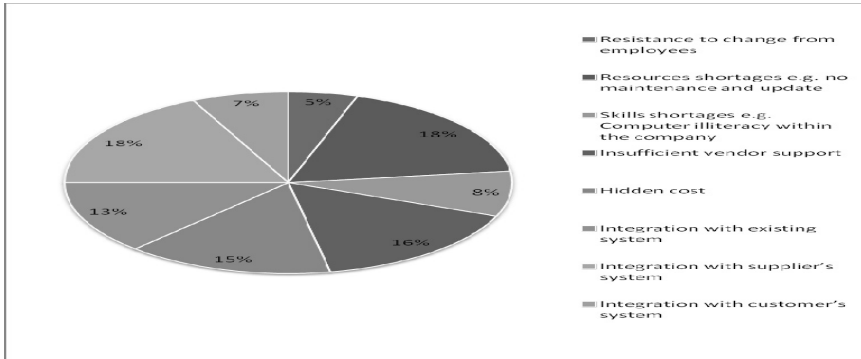


Figure 2 : Challenges faced by organizations while implementing ICT

Out of the 14 options given as benefits of implementing ICT in their organizations in warehouse management, the biggest benefit perceived by the customers is increased coordination with customers (Figure 3) – 14% ranked this as the highest benefit. 13% perceived a better coordination between departments and 12% perceived better coordination with the suppliers.

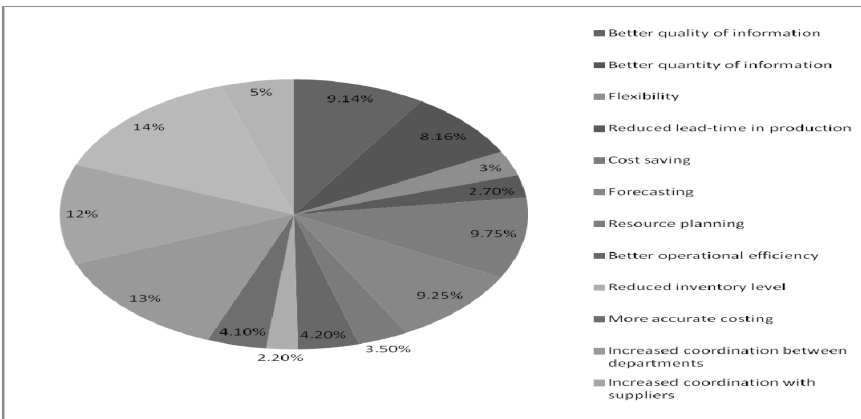


Figure 3 : Perceived Benefits of Implementing ICT

Coming to Part 2 of the survey, Out of the outsourcing activities, most organizations go to outsource international Transportation and Customs Clearance. This would probably be because they do not have presence in the other countries to do this on their own. The 3rd most commonly outsourced activity is Domestic Transportation. The reason as to why Outsourcing is not used commonly is mainly attributed to the reason that the costs are not reduced as is expected (Figure 4)

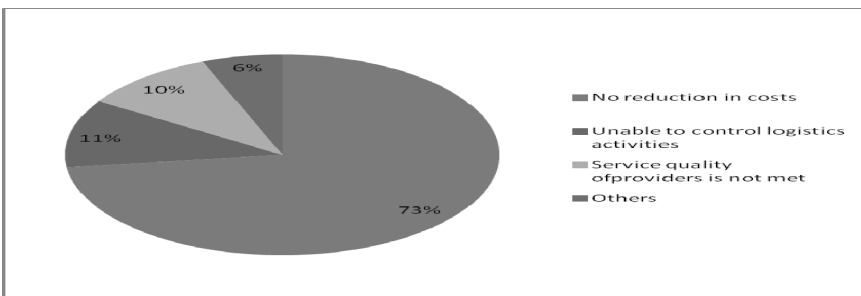


Figure 4 : Reasons as to why outsourcing is not used

On the question as to whether outsourcing is considered to be used in the future, 86% said no. It was seen that after price and quality, the most important feature that clients look while selecting a logistics provider is that the logistics provider has a suitable IT system that caters to their requirements (Figure 5). And figure 6 shows that amongst the biggest challenges faced by the clients with their existing logistics providers is that their IT system is not met as required. It was also found that the expenditure on ICT as part of overall operational costs is minimum for most organizations and will be under 2% of total costs for most companies.

Factors Important for Selecting Logistics Provider

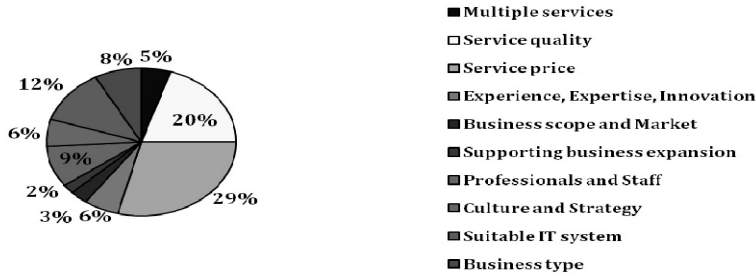


Figure 5 : Important Factors for Selecting Logistics Provider

Challenges in Selecting Logistics Provider

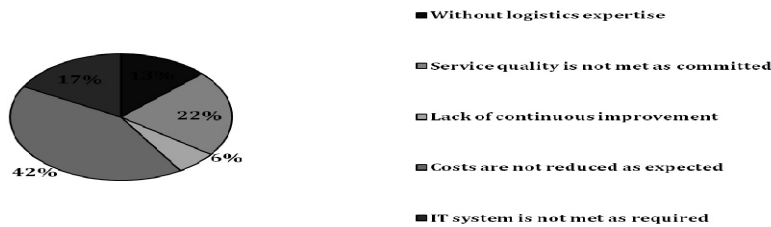


Figure 6: Challenges in Selecting Logistics Providers

Scope for Future Work

For future research, the different ways to reduce Carbon Emission through Green ICT needs to be considered. The biggest concern of the day is how climate changes can be slowed down by reducing carbon emissions into the environment and the ICT sector in logistics needs to take the initiative in reducing its own carbon footprint intensity and achieving sustainable growth. Logistics Operations can be optimized with respect to fossil fuel consumption through the use of supply chain execution systems such as CAD, WMS, etc coupled with technologies such as RFID, GPS and wireless networks. The other way that GHG Emissions can be reduced by this sector is by the use of new technologies of vehicles such as Hybrid and Electric ones. Dematerialization, which is the substitution of carbon intensive activities with alternates of the digital world. Face to face meetings can be substituted by tele-conferencing and video-conferencing. Working from home instead of commuting to have physical presence at work will also help reduce the emissions.^[2,3] The other route where the research can be directed to is the relationship between cloud computing and warehouse management systems. Cloud computing in Warehouse Management Systems will offers reduced costs and lesser risks in activities.^[4] The WMS vendor can host software application and hardware infrastructure centrally which can help the warehouses access data centrally on-demand. The costs of WMS Technology administration, Hardware purchases, Patches and Upgrades, Implementation, etc is reduced. There will be no or negligible up-front costs and IT drain. A web browser will be all that is required to access the WMS.

Recommendations

The below recommendations are proposed for the use at Red Orange General Trading LLC where all warehouse and distribution centre processes are done manually and through human inputs. Warehouse management systems is aimed at making management of warehouse space highly efficient as well as maximizing the storage life of items. Real time information through wireless networks can help join the warehouses as well as the equipments in such a way that they can be used to coordinate picking, receiving, storage etc. Through the help of such wireless technologies, order management can be made much more efficient with quicker turnaround times and accuracy than that can be done through manual procedures. Errors caused by humans can be greatly reduced and avoided to the maximum with the help of ICT. Another point that needs to be taken care of is that all the systems are integrated well and seamlessly with each other. There are many instances where different systems may not use effective communication or have weak databases plus the connectivity may be weak. This may cause applications to be poorly connected and would not be able to work together. Different software solutions such as the ERP would need to be used in such a way that otherwise independent solutions be connected seamlessly. Sharing of information and Communication is made a whole lot stronger and tied up together in such a way that the flow of goods is continuous and seamless. In the case that an employee no longer works at the organization, Knowledge Transfer can be made a lot easier since there is a Central Information System. For the purpose of Supply Chain Management, the integration of processes and functions not only needs to be done internally, but also to the suppliers and Clients as well who are external to the company and yet needs such critical information to proceed further. The next recommendation will be the use of Radio Frequency Identification tags on shipments. Through RFID, all the information will be stored within the RFID chip which can be used to give real time information of the product and inventory as well.



Conclusion

In order to efficiently and effectively manage trade across borders as well as within countries, a flawless Information & Communication Technology is becoming inevitable in the strategies of businesses. So as to not become too focused on logistics, organizations would be outsourcing their tasks to 3PLs. This can help the organizations making use of this revolutionary process by helping them focus on their core competencies and utilization of resources. However, there are several barriers to effective communication such as the resistance to change by suppliers, partners, customers as well as internally within organizations, the complexity of customizing applications for supply chain processes within organizations, the unavailability of skilled personnel to operation ICT systems. Its very essential that an organization have skilled workers who can implement and work on ICT systems with ease since it is necessary to utilize the ICT optimally and plan out the schedule and modes of implementation. The implementation of ICT allows 3PL to have real time information that can be tracked by logistics partners as well as help make the quality of customer service as high.

Authors : Saru Saseedharan, saru.s@redorange.com, sars229@gmail.com, +971555207377
Pushkala Muralidharan, pushkala@bits-dubai.ac.ae, +971506562687

Acknowledgment

Firstly, I would like to thank the Director of BITS Pilani, Dubai Campus, Dr. R.K. Mittal, for giving me an opportunity to do this dissertation at BITS Pilani, Dubai Campus Without the support of the CEO of Red Orange - Lalith Paulus, Strategic Director - Prem Nair, Head of Logistics – Sam Philip, this paper would be rendered incomplete. I am very obligated to Ms. Pushkala Muralidharan for her encouragement and guidance and I would also like to thank my family & friends (especially Seetha Sujit and Sangeeta Shiv Ram) or being my pillars of strength.

References

- [1] R. V. Delaney, R. Wilson : 11th Annual State of Logistics Report, Cass Information Systems and ProLogis (2000), 12
- [2] A. McKinnon, et.al. :Green Logistics,Improving the Environmental Sustainability of Logistics, Kogan Page Limited, London, pp. 3 – 30. (2010A)
- [3] Supply Chain Decarbonization, The Role of Logistics and Transport in Reducing Supply Chain Carbon Emissions [Online], Available at: <http://www.weforum.org/pdf/ip/SupplyChainDecarbonization.pdf>
- [4] M. Sengbusch , G. Neights : Where is cloud computing the best fit?, Supply chain Digital (2012)



International Conference on Innovative Technologies, IN-TECH 2012,
Rijeka, 26. - 28.09.2012



Development of Extended Enterprise Model

The lack of integration of quality management system over all design and manufacturing process of the product causes many problems in manufacturing projects in the EE [7]. Among the main causes of these problems are the design errors, triggered not only by the lack of integration, but also by the pressures in the calendar, leading to an increase of rework and/or design changes. The control of information flows among enterprises that work together for the assurance of lack failure in the information transmission and the processing of the updated information to the shared through data in real time, is also a major problem in this type of project. Another problem is the relationship among several partner of the EE, focusing on the degree of cooperation between agents and the ability of each one to predict the impact in their decisions [8]. All these causes reflect negatively affecting the three vertices of the triangle that supports the base of the manufacturing project management: the level of quality, the lead time and the project costs.

To corroborate this statement, and after reviewing the management literature concerning this subject, it develops the causal diagram showed in Fig 1, where the model Quality Management System of a company dedicated to the design and manufacturing of electronic products is developed. The model consists of a set of feedback loops, whose interplay determines both the structure as the overall system behaviour to different situations and to the existence of suitable mechanisms that facilitate the integration, in order to identify the effects that these mechanisms can occur in the system.

The first step in the realization of the model is to identify the parts of the system to model [6]. For the realization of the model was taken as a reference standard UNE-EN-ISO 9001:2008, in order to identify the processes, relationships and quality information that flows between them.

The next step in the modelled process is the construction of causal diagrams [6]. Which notes the importance of the variables from the point of view of the proposed analysis, usually appreciate a strong influence on other variables to the other ones and the formation of feedback loops both negative and positive [9].

In the causal model of the system, Fig. 1, can be observed different links representing quality system processes and their control on the main variables. Customer satisfaction, for example, is defined by several loops, since the level of satisfaction depends mainly on the late delivery [6] [10], causing a temporary negative effect, and in the level of product quality [7], which effect has a greater impact over time. The level of satisfaction differs between the customer has and that the company perceives. The UNE-EN-ISO 10004:2010 establishes that the perceived satisfaction, which are measurable data do not correspond to real data, thereby determining mechanisms for their estimation. The standard indicates the advantages with respect to the transmission time information and its validity, in function of the tool is used for sampling. For the proposed application case, the system is based on the implementation of an integrated environment using Distributed Intelligent Agents, which is responsible for collecting and managing information on warranties, complaints, questionnaires, etc.

Defective products derived from both those produced internally and those coming from other parts of the supply chain. In any case defective products are generated, among other causes, as a consequence of the existence of troubles in the development of the same by the existence of errors in the requirements and specifications. The use of a reference standard for quality management, allows the proper definition of the processes, establishing its inputs and outputs, as well as the skills necessary to manage the processes. On the other hand, work procedures and the technology used by organizations have to be updated from time to time, being present the introduction of these advances in the manufacture of specific products. This means an average increase in the number of potentially defective products due to the introduction of errors in the process until the adaptation of these developments [11], see Fig 1. Similarly, shown in the causal model, the correction of defective products increases the number of potentially defective products due to the generation of new errors during the correction phase [12].

Another important loop is the one that includes the level of quality, which is negatively affected by the number of defective products that are not detected during the inspection process, and which are either taken to a second phase, which can be used as basis for other products, or go directly to the customer [12]. This escape of defective products is determined, as shown in Fig. 1, for the detection capacity of the system and the existence of defective products that could be detected [13]. Being this capacity depended mainly on the adequacy of inspection procedures to the process [7]. Each product includes the development and approval of a specific inspection plan, which may imply the occurrence of errors in procedures, thus allowing the escape of defective products.

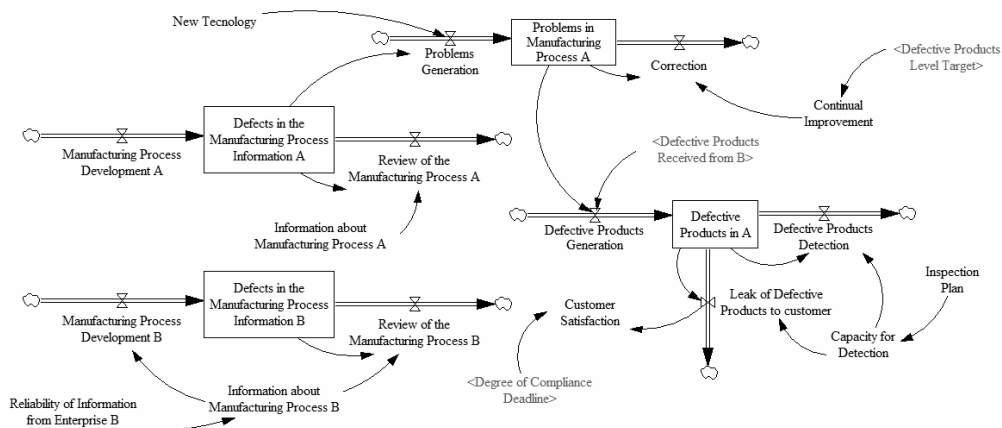


Fig. 2 Partial Forrester Diagram information flows

Being identified the dynamic of the system and the main variables that define the model, a Forrester diagram of system quality management has been developed, including different parts of the system: order management, customer satisfaction, inspections management, design and process development, process improvement, human resources, purchasing, non-compliance, audits and document control. In Fig. 2 shows some parts of this Forrester diagram, specifically the one that models the processes of development of requirements and specifications of product, process manufacturing, control and inspection.

Defined the model, the set of inputs and outputs that affect the dynamics of quality management has been identified, showing as main inputs the implementation of a new technology, the development of manufacturing process information, the introduction of a new inspection plan and procedures (all expressed as problems per week) and the demand (expressed as product per week), and the main

outputs [10] are the level of quality, the perceived customer satisfaction and the percentage of defective products manufactured (all expressed in percentages) [12].

Finally, the interface of quality management system among the participating companies in the EE of manufacturing is designed. The interface models the flows that contain the information necessary to meet their interactions and through the use of rates, models the degree of system integration on the reliability and the delays in the transmission of the information.

Integration Requirements

The advantages of integration in the EE are supported by a number of factors. First using an information protocol, such as information exchange standard ISO 10303, which as adapted STEP-AP-CAL allows the system the exchange and sharing of quality information among enterprises, ensuring the quality of transmitted information [14]. Second, the protocol is supported by an information platform based on Distributed Intelligent Agents, enabling the transfer of data between heterogeneous and dispersed systems [15], such as those in companies that configure the EE, avoiding the problems arising from the presence of islands of information. Finally, ease of access by enterprises to communications networks, and the possibility of connection points in virtually any location, allowing the management of updated information at any location.

Using this type of platform provides the system integration improvements, as they provide flexibility, scalability and agility, enabling the system to adapt to changing market conditions [16].

This integration framework can help reduce errors and delays that occur both in the transference and in the conversion of data among companies. Standing, evidently arisen from human factors [17].

Case of Study

This section describes the considerations and the starting hypothesis for the simulation of quality management system of a group of companies that design and manufacture of electronic products, considering that work together to achieve a common goal. The stated enterprise model consists of two companies: one dealing with the design and manufacturing (Partnership A) and the second dealing with to the manufacture of specific parts of the product (Partnership B), which will be subsequently incorporated into the production process of the first enterprise. Again, the idea is to simulate and measure the performance of a greater or lesser quality system integration of both enterprises. The model only includes the partner network formed by the two companies, limiting the model in regard to the network interaction with other stakeholders such as suppliers and distributors.

The starting hypothesis considers that the production capacity of all the companies will be 1000 products per week. The model considers the flow of information relating to quality and material flows. The system has been simulated for a period of ten years, 520 weeks, using the well know simulation tool of dynamical systems VENSIM®.

Simulation and Key

In this application case is submitted the comparison of model quality management for the scenarios of EE integration and another one without integration. Both models have undergone the same pattern of inputs, which have an increasing and decreasing sigmoid way, resembling the behaviour that has the appearance of defects in the life cycle of a project [13]. In this type of function, Eq. 1, the variable $x(t)$ starts from an initial value $x_0=x(0)$, then grows exponentially until there is a turning point at time tm , and thereafter evolves asymptotically to a final value $x_f=x(\infty)$. In this case using two opposite sigmoid curves to represent each entry, so that reaching the maximum value the function back down into the initial value, like the descent that shows the number of defects in the ending phase of a project.

$$x(t) = x_f/1 + e^{-k(t-tm)}, \tag{1}$$

The growth expressed by the above function is well defined if it sets the initial value x_0 , the final value x_f and the time tm which has to produce the turning point $x_f/2$. The parameter k is defining the rate of growth, so it is known as growth rate, and is related to the three parameters x_0 , x_f and tm according to the expression defined in Eq. 2.

$$k = 1/tm \cdot \ln((x_f - x_0)/x_0), \tag{2}$$

Using these expressions the model inputs are modelled. These being: the implementation of a new technology (NT) [11], the development of manufacturing process information (MPI) [13] and the introduction of a new inspection plan and procedures (IP) [10].

Results

Subjected the model to a sequence of inputs described above, the response of the model in both scenarios is shown, as it is shown in Fig. 3

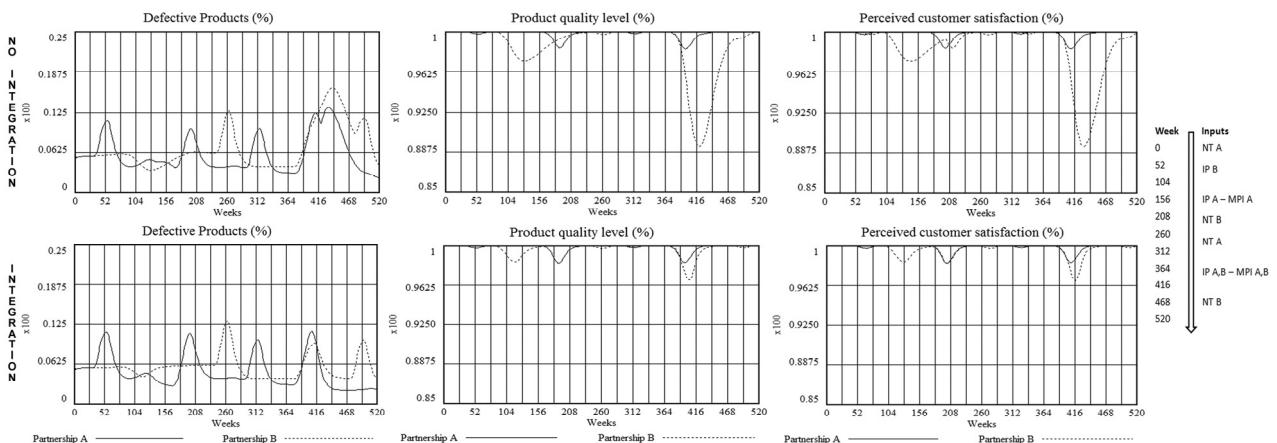


Fig 3. Comparative between both extended enterprise model

No integration Scenario

In the extended enterprise model without integration, the interface between enterprises is considered to have a delay of 3 weeks in the transmission of information and a reliability of the information transmitted of 70%. This will cause that in the quality system appears delays in the information transmission and failure by unreliability.

First, the inadequacy of quality procedures to process causes a decrease of defective products that are detected. The input IP B at week 78 causes in Partnership B this effect with a decreased level of quality to 97.25% for 140 weeks, and therefore a lower level of satisfaction. The next two inputs, MPI A and IP A at week 156, cause a decline in the level of quality in Partnership A to 98.39%, and therefore a decline in customer satisfaction, showing a delay in the transmission of this information from Partnership A to Partnership B around the 208 week, Fig 3. Finally, errors in the manufacturing process and in product requirements and inspection plans of both enterprises are inserted by inputs MPI A, MPI B, IP A and IP B at week 364, causing oscillations at the level of defective products in the Partnership A due to Partnership B. Reflecting these results in a decrease in Partnership B of the values of the quality level to 89.27% for 104 weeks and the level of defective products to 16.29% at an interval of 130 weeks.

Integration Scenario

In this scenario a system integration quality management is considered, particularly through the implementation of the holonic paradigm in its design and implementation of an information system using Distributed Intelligent Agents and support information through STEP-AP-CAL, operating in a network of high-speed communications. This implies a reduction in delays and errors due to lack of reliability of the information. It is considered, therefore, that in the interface there is a delay of 1 day in the information transmission and a reliability of information transmitted of 95%. That is, only considering the delays and errors caused by human causes. Then the model with integration is subjected into the same input sequence as for the previous stage and new results are obtained, as to amplitude and duration is concerned.

First, the input IP B at week 78 rebounds in a decreased level of quality in Partnership B to 98.50% for 78 weeks. Then the inputs MPI A and IP A at week 156 have the same effect as in the above scenario, unless seeing that the curves of customer satisfaction of both enterprises are jointly and severally. Finally, the inputs applied at week 364 cause a more controlled than in the preceding case. With respect to Partnership B the value of the quality level drops to 96.74% for 78 weeks and the level of defective products increases to 12.95% in an interval of 56 weeks, as show in Fig. 3.

Conclusions

From the results of simulation experiments based on system dynamics can be corroborated, with reservations for model validation [18], that the main problems arising from the existence of errors in the information (quality plans, procedures, requirements, etc.), as well as errors and delays in the transmission and conversion of information among Extended Enterprise manufacturing are: cost overruns, delays in delivery and quality losses in the early stages, they reappear thereafter according these tasks are used to develop further interventions. Simulation has shown that proper use of models of integration provides a reduction in unwanted situations that have been found. It can be concluded that the proposed integration framework allows a better response to the changes occurring throughout the product lifecycle in the Extended Enterprise manufacturing, reducing the risk of quality deviations and cost overruns. These variables are controlled by appropriate models that are being applied in the new paradigms of quality management, including integration with FRABIHO, and the use of appropriate technologies that support the implementation of these models, such as Distributed Intelligent Agents Systems and application support information standards such as STEP.

References

- [1] A.A. Pereira, et. all: Managing distributed business processes in the virtual enterprise, *Journal of Intelligent Manufacturing*, Volume 12 (2001), pp. 185-197.
- [2] R.N. Nagel: Performance Capabilities Of The Next Generation Manufacturing Enterprise, *Thirteenth IEEE/CHMT Intl. Elect. Manuf. Technology Symposium*. (1992), pp. 21-324.
- [3] M. Marcos, et all: Toward the Next Generation of Manufacturing Systems. FRABIHO: A synthesis model for distributed manufacturing, *Intell. Prod. Machines and Systems: First I*PROMS V. C.*, (2005).
- [4] D. Kotak: Agent-based holonic design and operations environment for distributed manufacturing, *Computers in Industry*, Volume 108 (2003), pp. 52:95.
- [5] H. Hvolby. Challenges in business systems integration, *Computers in Industry*, Volume 61(2010), pp. 808-812.
- [6] J. Sterman: *Bussiness Dynamics, Systems Thinking and Modeling for a Complex World*, (McGraw-Hill, USA, 2000).
- [7] J.H. Dyer: *Collaborative Advantage Winning Through Their Extended Enterprise Supplier Networks*, (Oxford University Press, USA, 2000).
- [8] N. Pardo: Cooperative subcontracting relationship within a project supply chain: A simulation approach. *Simulation Modeling Practice and Theory*, Volume 15 (2007), pp. 137-152.
- [9] T.T. Burton, et all: *The Lean Extended Enterprise Moving Beyond the Four Walls to Value Stream Excellence*, (J. Ross Pub, USA, 2003).
- [10] M. Ozbayrak: Systems dynamics modelling of a manufacturing supply chain system, *Simulation Modelling Practice and Theory*, Volume 15 (2007), pp. 1338-1355.0
- [11] N.P. Repenning y J. Sterman: Getting quality the old-fashioned way: self conforming attributions in the dynamics of process, *Sloan School of Management, Massachusetts Institute of Technology*, (1997), pp. 53-56.
- [12] H. Rahmandad: Modeling the rework cycle, capturing multiple defects per task. *System Dynamics Review*, (2010), pp. 59-68.
- [13] T.K.A. Hamid y S.E. Madnick: *Software Project Dynamics: An Integrated Approach*, (Prentice-Hall, 1991).
- [14] F. Tanaka. STEP-based quality diagnosis of shape data of product models for collaborative e-engineering, *Computers in Industry*, Volume 57(2006), pp. 245-260.
- [15] Y. Xue. Web services-based and Multi-Agent information platform, *Proceedings of the Ninth International Conference on Machine Learning and Cybernetics*, (2010).
- [16] D. Zhengwen. An agent-based approach for e- manufacturing and supply chain integration, *Computers and Industrial Engineering*, Volume 51 (2006), pp. 343-360.
- [17] B. Caldwell. Delays and user performance in human-computer-network interaction tasks, *The Journal of the Human Factors and Ergonomics Society*, Volume 51 (2009), pp. 813-830.
- [18] R.G. Sargent: Verification and validation of simulation models, *In Proceedings of the 2009 Winter Simulation Conference (WSC)*, (2009), pp. 162-176.

PROCESS DESIGN OF ULTRA-SHORT PULSE LASER ABLATION BY MODERN QUALITY-ORIENTED DESIGN OF EXPERIMENTS

J. P. Calderón Urbina¹ and C. Emmelmann¹

¹ Institute of Laser and System Technologies (iLAS) Hamburg University of Technology (TUHH),
Denickestraße 17, 21073, Hamburg, Germany

Keywords: ultra-short pulse laser; picosecond laser; laser ablation; quality; design of experiments; Shainin; process design

Abstract. The penetration of photonic technologies into the manufacturing processes has made wider the perspective of industrial applications since its introduction. Moreover, the development of ultra-short pulse lasers, like picosecond laser (ps), has brought quality and productivity in terms of ablation rate (mm/s) and surface roughness (R_a) to fine manufacturing activities in diverse industries, such as tool production, medical implant fabrication and injection molds manufacture, among others. The design of the laser ablation process might offer competitive advantages when compared to traditional technologies, e.g., grinding, but it has to consider prior research where experimental work with new materials and applications has to be done. Furthermore, the identification of the adequate parameters in the ablation process can result costly and time demanding, due to test and error or long full factorial experimental designs. Therefore, the use of modern quality-oriented design of experiments (DoE) accelerates the investigation phases by identifying the factors with the highest influence on the objectives of the ablation process. This paper describes the design of the ultra-short pulse laser ablation process in its early experimental phases by using the Ishikawa Diagram, Shainin's Variables Search, and the quantification of relevant parameter impact. In addition, it can be mentioned, from this experimental work, that laser power P , and pulse and track overlap O are the most influencing variables in the minimization of surface roughness R_a when ablating steel, e.g. R_a from 6 μm to approximately 1.5 μm . In short, the use of modern quality-oriented design of experiments in ultra-short pulse laser ablation processes makes faster the identification of the controllable factors making simpler, faster, economic and robust the design of the process and the introduction to new applications and materials.

1. Introduction

The photonic activities in manufacturing started with laser material processing mainly in the automobile industry in the 1970's. Processes such as cutting, ablation and welding meant an increase in the productivity of products through the time [1]. More examples of laser processing applications that have got mature are material making, polymer cutting, steel hardening, aluminum welding, laser additive manufacturing and organic tissue cutting among others [1]. Parallely, the development of lasers and laser systems has made wider the application perspective. Laser ablation, thanks to this development, has been able to achieve better results in terms of ablation rate and surface quality by the reduction of the pulse length of the laser source (from nanosecond ns to picosecond ps and femtosecond fs) [2]. Nowadays, laser ablation, defined in general terms as the solid, liquid or vapor separation of material from a solid by laser beam exposure and its related optical energy induced processes [2, 3], represents an attractive innovative alternative for the processing of metals, ceramics, diamonds and its composites, carbon fiber composites, and plastics, many of this already difficult for its traditional processing, e.g., polycrystalline diamond by grinding (very hard material).

When compared to short-pulses (e.g. ns regime), ultra-short pulses (see figure 1) allow a short interaction (e.g., in ps regime) of high power density (W / cm^2) with the material that considerably reduces the side-effects like plasma formation, crack origination, thermal damages and non-desired rough textures [2, 4, 5].

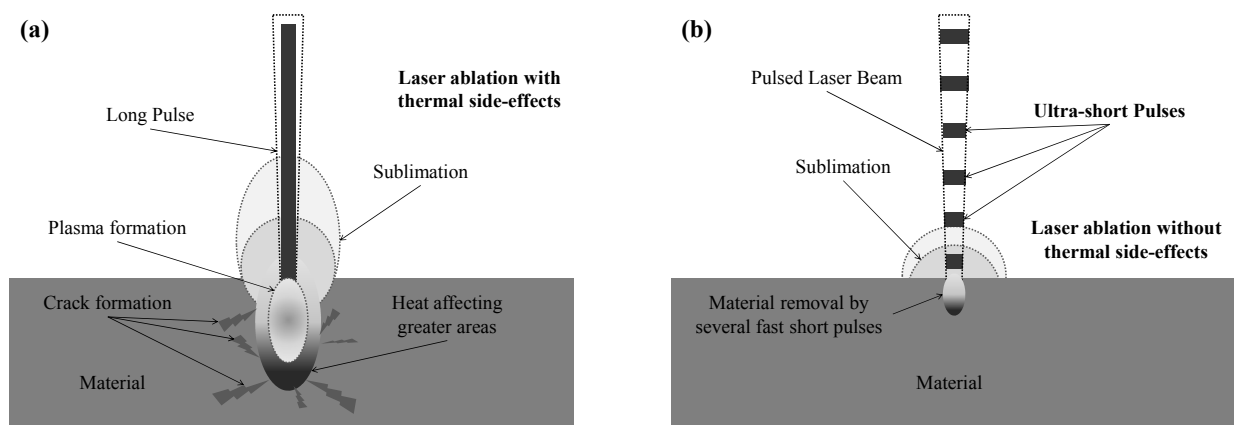


Fig. 1: (a) Laser ablation with long pulses; (b) Laser ablation with ultra-short pulses

2. Modern quality-oriented tools

Based on the author's experience, the innovativeness of a technology is indirectly proportional to the know-how quantity of its applications and interactions. Therefore, the use of quality-oriented tools in its early phases is necessary. Moreover, the complete quality-oriented process design might include a systematic optimization that can be assured by the implementation of common bodies of quality management: planning, control and improvement [6]. The first part, planning, has to include the definition of the specifications and demands, the definition of the objectives, the activities and resources planning. The second part has to understand the system input and output, establish a quantification procedure for the objectives, and measure the variability. Finally, the third part must accumulate the knowledge to use it in a cyclical manner to assure continuous improvement [6, 7]. Therefore, ultra-short pulse laser ablation, as a relatively new technology, requires of a knowledge collection that might be costly and time demanding, especially with new materials, applications and customized uses. For this reason, quality oriented design of experiments (DoE's) targets the simplification of the experimentation by maximizing the information output [8]. Likewise, the number of experiments is reduced, and as a consequence, the experimentation time and costs.

The modern quality-oriented tools and DoE's, used in this study for the process design of ultra-short pulse laser ablation, were the cause-effect diagram (Ishikawa diagram), variables search (Shainin) and parameter impact. In detail, the cause-effect diagram offers a detailed overview of the system inputs and its general output; additionally, Shainin variable search looks for the parameter in the ablation process that contains the highest influence on surface roughness (R_a). Subsequently, the parameter impact can be quantified to select the relevant parameters, which are to analyze by means of targeted full or partial factorial designs [6, 9].

3. Process design of ultra-short pulse laser ablation by modern quality-oriented design of experiments

The approach to understand the behavior of ultra-short pulse laser ablation with new materials and/or applications consists of four phases, as illustrated in figure 2. It is important to mention that process costs and times are part of process design and a very relevant decision factor [10]; however, this work only concentrates on the scope of the ablation process. The first, definition of the specifications and demands, describes the technical and functional requirements that are needed for the applications and processing of the material; for example, a specific angle, structure or functional form. Moreover, during this part the objective of the investigation are set; for this case, the minimization of the surface quality (roughness R_a) but also possible for the maximization of the ablation rate (mm/s). In second phase, the identification of the relevant parameters is targeted. This is done by making use of the cause-effect diagram, which encloses all the direct and indirect influencing parameters that can be as well, intern and extern. The diagram groups the causes and offers a wider view of the system. For laser ablation, there are five groups: beam guidance, laser source, environment, material and processing strategy, and each of these groups have, as well, particular causes, e.g., laser source (picosecond laser) include pulse length, power, frequency, burst-mode (partition of pulse in micro-pulses), wavelength, among others. Furthermore, in phase II, the application of design of experiments is done. Variable search and factorial studies are executed to identify the factors with the greatest influence on the objectives. Once these factors with the greatest influence on the objective (for this case, improvement of the surface roughness) are identified, the processing of the part is done by means of laser ablation. This phase can start from an experimental work to an industrial order. Finally, quality has to be assured, and it is for this reason that phase IV, metrology and quality, points to measure and control the qualitative aspects of the part and process. This is achieved by the used of metrology instrumentation, such as 3D confocal microscopes, coordinates tables, and image analyzing tools. This paper only covers phase I and II of the process chain of ultra-short pulse laser ablation with the objective of showing the high value of quality-oriented tools in the process design.

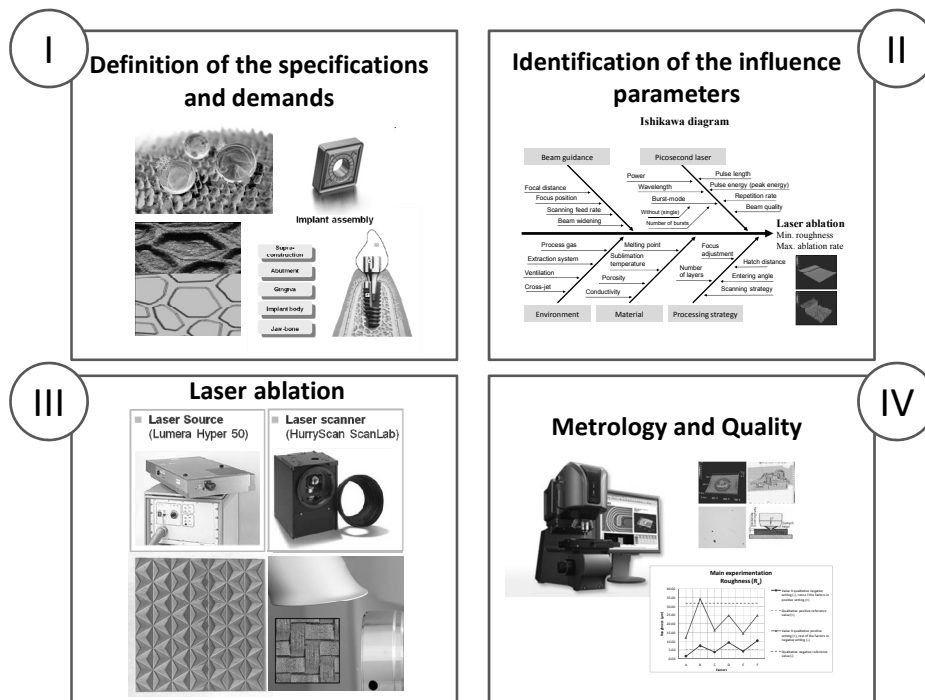


Fig. 2: Process chain of ultra-short pulse laser ablation

Experimental procedure

After setting the pursued objective for the experimentation, minimization of the surface roughness (R_a), a delimitation of the system variables was achieved (as shown in figure 2, phase II – Ishikawa, i.e., cause-effect diagram).

The result was the selection of the parameters of beam guidance, processing strategy and laser source that are controllable: laser power, frequency, burst-mode, scanning speed, scanning strategy, hatch distance, focal distance, incidence angle and number of layers. Similarly, and based on experience, some variables were kept constant and some other (related among them) formed a cluster called overlap (based on DIN V 32540) [3]. Table 1 shows the parameters include in the variables search DoE.

Table 1. Variable search – Choice of the parameters

Factors			Settings	
			Q+	Q-
A	Laser power (P)	[W]	25	50
B	Burst-mode (n)	[-]	1*	5
C	Pulse and track overlap** (O)	[%]	50	90
D	Scanning processing strategy (s)	[-]	bidirectional	meandering

* Single pulse
 ** According to DIN 32540, which includes the factors laser frequency (f), scanner speed (v_s) and hatch distance (h). For O = 50 %: $f = 400$ kHz, $v_s = 7500$ mm/s and $h = 0.01875$ mm, respectively; and for O = 90%: $f = 400$ kHz, $v_s = 3500$ mm/s and $h = 0.0035$ mm, respectively.

The laser source was a Lumera Hyper 50 generating pulses of a pulse length $\tau = 10$ ps at a wavelength of $\lambda = 1064$ nm. The average power was of $P = 50$ W and working from $f = 400$ to 1000 kHz. The marking and positioning speed of the scanner were of $v_s = 3.5$ m/s and $v_s = 15$ m/s, respectively. The diameter of the focus had a value of $d_w = 38 \mu\text{m}$ on the focus. All experiments were performed on a stainless steel (316L – 1.4404, according to AISI norm) plate, ablating a $2 \times 2 \text{ mm}^2$ area, as seen in figure 2. Stainless steel is a common material for tool's and medical instrumentation's fabrication, which also can be manufactured by Laser Additive Manufacturing (LAM). LAM parts represent an opportunity field for surface optimization by laser ablation [11, 12].

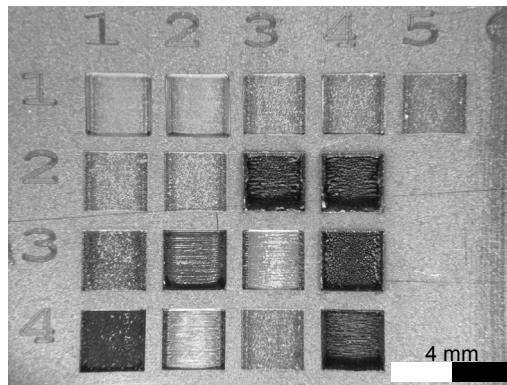


Fig. 2: Ablated samples with ultra-short pulse laser (50W picosecond laser)

The goal of the variable search methodology is to identify the factors with the greatest influence with a small number of experiments [9]. The objective of this experimentation is to identify the factors with the greatest influence on surface quality (R_a). The variable search methodology starts with two preliminary experiments V+ and V- (reference) where all the factors are fixed in the setting where it is thought to release positive results Q+ (minimization of the surface roughness) and where all the factors are thought to release negative results Q-. These help to determine the variation and contrast of each variable. After that, the main experimentation is done. Here, each of the factors is set, first, in its negative setting against the rest of the factors in their positive setting. Then, the factor is set to its positive level and the rest in their negative. This experiment is repeated with each of the parameters. Finally, the reaction to the factors and setting is quantified, and consequently, its impact is measured. Based on the level of impact, the factors with the greatest influence are identified. The measurements were done with a confocal laser scanning microscope (Keyence, VK 8710 Color 3D laser scanning microscope).

4. Results and discussion

The preliminary experiments V+ and V- were of $6.01 \mu\text{m}$ and $15.18 \mu\text{m}$, respectively. These values help to set the limit of the contrast with each of the factors. Table 2 shows the results of the main experimentation, the analysis of the measurements, the variation average and the conclusion. The variation average resulted from the comparison of the particular result versus the corresponding V value, determining its change ratio and then its percentage. The conclusion shows the ranking from high to low variation average (impact).

Table 2. Variable search – Main experimentation and results

Main experimentation					Analysis		
Roughness R_a [μm]							
Factors	Combination	Results	V ₊	V ₋	%	Variation Average (%)	Conclusion
		[μm]	[μm]	[μm]			
A Laser power	A.R.	12.37	6.01		106	98	1°
	A.R.	1.53		15.18	90		
B Burst-mode	B.R.	1.57	6.01		74	75	3°
	B.R.	26.60		15.18	75		

C Pulse overlap and track overlap	C.R.	12.43	6.01	107	96	2°
	C.R.	2.38	15.18	84		
D Scanning processing strategy	D.R.	6.81	6.01	13	17	Less relevant
	D.R.	12.08	15.18	20		

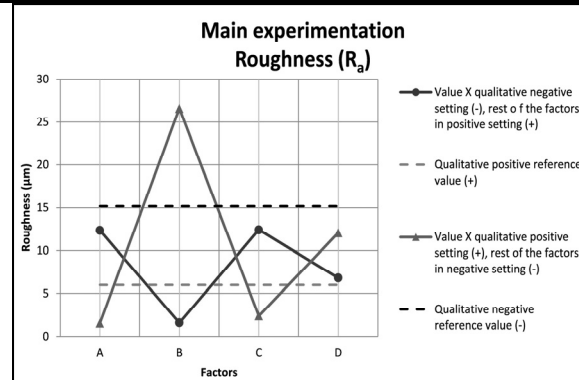


Fig. 3: Results of the main experimentation

As it can be seen in table 2 and figure 3, laser power (factor A), pulse overlap and track overlap (factor C) and burst-mode (factor B) are the factor with the greatest influence on surface roughness. Mainly, factor A and C have a great influence of almost 100% of impact (laser power 98% and pulse overlap and track overlap 96%). Factor B shows an interesting behaviour, when the positive setting is chosen, the surface roughness got worse from 15.18 µm to 26.60, and when its negative setting was selected, the roughness got better, from 6.01 µm to 1.57 µm. This implies that the settings were inverted, i.e., the positive settings should be the negative setting, and inversely. Factor D, scanning processing strategy, resulted less relevant for the surface quality.

5. Conclusions

The use of photonic technologies, i.e., ultra-short pulse laser technologies is a reality in material processing and manufacturing. For this reason, its inclusion in the experimental and industrial process design is necessary. Nevertheless, the use of this innovative technology can result time consuming and costly when used with new materials, applications and products. Therefore, the support of quality-oriented tools and DoE's, such as cause-effect diagram, variable search and impact quantification, accelerate its effective application by saving time and cost with the reduction of the number of experiments. This paper presented a four-phases approach (process chain), based on quality philosophies, to understand the behavior of ultra-short pulse laser ablation with new materials and/or applications in a systematic, efficient and competitive manner; additionally, it was executed an investigation, following phase I and II of the presented approach, to identify the parameters with the greatest influence on surface roughness of stainless steel. The results showed that laser power (factor A) and pulse overlap and track overlap (factor C) are the most influential factors on surface roughness (R_a) with almost an influence of 100%. Moreover, factor B, burst-mode, presents a moderate influence that is subject for further investigation. In short, the use of modern quality-oriented design of experiments helps to speed up the industrial application of innovative technologies, such as ultra-short pulse laser ablation, by being a substantial part of a four-phases process chain that incorporates the definition of the specifications and demands, the identification of the influence factors, the process of laser ablation and the account of metrology and quality.

6. Acknowledgment

This research was supported by CONACYT (Consejo Nacional de Ciencia y Tecnología – National Council on Science and Technology, México) under its Ph.D. Scholarship program, and also, it was supported by Laser Zentrum Nord LZN.

7. References

- [1] J. C. Ion: *Laser processing of engineering materials - Principles, procedures and industrial application*, (Elsevier Butterworth-Heinemann, Oxford, 2005)
- [2] J. Meijer, K. Du, A. Gillner, D. Hoffmann, V. S. Kovalenko, T. Masuzawa, et al.: *Laser machining by short and ultrashort pulses, state of the art and new opportunities in the age of photons. Proceedings of CIRP Annals – Manufacturing technology*, Vol. 51 (2002), pp. 531 - 550
- [3] DIN V 32540: *Laser beam removing – Thermal removing with laser beam – Definitions, influence factors, procedures*. (Beuth, Berlin, 1997-07)
- [4] M. Dirscherl: *Ultrakurzpulslaser, Grundlagen und Anwendungen*, Vol. 2 (Bayerisches Laserzentrum GmbH, Erlangen, 2005)
- [5] K.-H. Leitz, B. Redlingshöfer, Y. Reg, et Al.: *Metal ablation with short and ultrashort laser pulses. Proceedings of Lasers in Manufacturing 2011, Part 2* (2011), pp.231 – 238
- [6] T. Pfeifer: *Quality management – Strategies, methods, techniques*, (Hanser, Aachen, 2002)
- [7] R. H. Lochner, J. E. Matar: *Designing for quality – An introduction to the best of Taguchi and western methods of statistical experimental design*, (ASQC Quality Press, New York, 1990)
- [8] W. Kleppmann: *Versuchsplanung – Produkte und Prozesse optimieren*, (Hanser, Aalen, 2011)
- [9] K. R. Bhole, A. K. Bhole: *World class quality – Using design of experiments to make it happen*, (Amacom, New York, 2000)
- [10] S. Grewal: *Manufacturing process design and costing- An integrated approach*, (Springer, Sydney, 2011)
- [11] C. Emmelmann, J. P. Calderón Urbina: *Analysis of the influence of burst-mode laser ablation by modern quality tools. Proceedings of Lasers in Manufacturing 2011, Part 2* (2011), pp.173 – 181
- [12] MTT Technologies Group: *SLM Materials – Non ferrous metals, tool steel, stainless steel and light alloys*, (www.mtt-group.com)

SUPPRESSION OF FLUTTER OF AN AIRFOIL - FLAP WING USING ACTIVE CONTROL

K.A. Alsaif¹, A. Albedah¹, F. BenYahia¹ and M. A. Foda¹

¹ Mechanical Engineering Department, College of Engineering, King Saud University, Riyadh, Saudi Arabia, Email: mfoda@ksu.edu.sa

Keywords: Flutter suppression, airfoil, Falp, Aeroelastic response, Aactive control.

Abstract. Aeroelastic response control of airfoil-flap wing exposed to loads in an incompressible subsonic flow field is addressed. The aerodynamic model is featuring plunging-pitching-flapping coupled motion. Linear Quadratic Regulator theory is used to design a full state feedback controller in state-space. The control law is implemented through the flap torque to suppress flutter instability and enhance the aeroelastic response. Comparisons of the uncontrolled response with the controlled one are presented. The goal is to suppress flutter and to maintain stability of the closed loop system. The uncontrolled and controlled models are numerically simulated using MATLAB.

Introduction

Flutter is the most important dynamic instability in aeroelasticity and it is mostly encountered in airborne structures subjected to large lateral aerodynamic loads of lift type. The structure presents a self-sustained oscillatory behavior at a certain critical airspeed, called the critical flutter speed. In general, coupling of several degrees of freedom is essential for flutter to occur, and the oscillation that occurs at the critical flutter speed is harmonic. Above that critical speed oscillations are divergent. Nowadays, demand for high maneuverable and high speed aircraft has increased. Active control techniques for suppression of flutter are used to eliminate flutter at low speeds and to increase flutter critical speeds. Marretta and Marino [1] proposed a control law based on a single input-single output controller to suppress flutter. Kargarnovin and Mamandi [2] investigated the effects of sharp edge gust on the response of an airfoil and analyzed its flutter. Lee et al [3] studied flutter as well as the open- and closed loop responses of wing-flap system using sliding mode control. Chen et al [4] used state feedback sliding mode control method in which the trailing-edge flap is utilized for flutter control.

Structural and Aerodynamic Modeling

Applying the Lagrange's equations on the 2-D cross-section of a typical airfoil shown in Fig. 1, the following governing equations are derived [5]

$$m\ddot{h} + S_\theta\ddot{\theta} + S_\beta\ddot{\beta} + 2\xi_h m \omega_h^2 / \omega \dot{\beta} + k_h h = \pi \rho b^2 (L_{nc} + L_c), \quad (1)$$

$$S_\theta\ddot{h} + I_\theta\ddot{\theta} + [(c-a)bS_\beta + I_\beta]\ddot{\beta} + 2\xi_\theta I_\theta \omega_\theta^2 / \omega \dot{\theta} + k_\theta \theta = \pi \rho b^2 (M_{nc} + M_c), \quad (2)$$

$$S_\beta\ddot{h} + [(c-a)bS_\beta + I_\beta]\ddot{\theta} + I_\beta\ddot{\beta} + 2\xi_\beta I_\beta \omega_\beta^2 / \omega \dot{\beta} + k_\beta \beta = \pi \rho b^2 (T_{nc} + T_c) + T_s, \quad (3)$$

where

$$L_{nc} = -\dot{h} + ba\ddot{\theta} + [T_1 + (c-e)\varphi_3]b\ddot{\beta} / \pi - V\dot{\theta} + T_4V\dot{\beta} / \pi, \quad (4)$$

$$M_{nc} = ba\ddot{h} - (1/8 + a^2)b^2\ddot{\theta} + [T_7 + (c-e)\varphi_6 / 4 - (c-e)(1/2 + a)\varphi_3]b^2\ddot{\beta} / \pi \\ + (a-1/2)bV\dot{\theta} + [2P - (a-1/2)T_4 + (c-e)\varphi_5]bV\dot{\beta} / \pi - (T_4 + T_{10})V^2\beta / \pi, \quad (5)$$

$$T_{nc} = [T_1 + (c-e)\varphi_3]b\ddot{h} / \pi + [T_7 + (e-a)\varphi_6 / 4 - (c-e)(1/2 + a)\varphi_3]b^2\ddot{\theta} / \pi \\ [T_3 + (c-e)\varphi_{37} - (c-e)^2\varphi_{17}]b^2\ddot{\beta} / \pi^2 + [(c-e)\varphi_{32} - P + T_1 + T_4 / 2]bV\dot{\theta} / \pi^2 \quad (6)$$

$$+ [T_4T_{11} / 4 + (c-e)(\varphi_{10} + \varphi_{36}) - (c-e)^2]bV\dot{\beta} / \pi^2 + [T_4T_{10} - T_5 + (c-e)\varphi_{35}]V^2\beta / \pi^2 \\ L_c = C(k)\{-2V\dot{h} / b + 2(a-1/2)V\dot{\theta} - [T_{11} - 2(c-e)\varphi_1]V\dot{\beta} - 2V^2\theta / b - 2T_{10}V^2\beta / b\}, \quad (7)$$

$$M_c = C(k)(1/2 + a)\{2V\dot{h} + 2(1/2 - a)bV\dot{\theta} - [T_{11} - 2(c-e)\varphi_1]bV\dot{\beta} / \pi - 2V^2\theta / b \\ + 2T_{10}V^2\beta / \pi\}, \quad (8)$$

$$\begin{aligned}
 T_c = C(k) \{ & [2(c-e)\varphi_{31} - T_{12}]V\dot{h}/\pi - (1/2-a)[T_{12} - 2(c-e)\varphi_{31}]bV\dot{\theta}/\pi \\
 & - [T_{11}T_{12}/2 - (c-e)(\varphi_2\varphi_{31} + \varphi_1\varphi_8) - 2(c-e)^2\varphi_1\varphi_{31}]bV\dot{\beta}/\pi^2 \\
 & + [2(c-e)\varphi_{32} - T_{12}]V^2\theta/\pi - [T_{10}T_{12} - 2(c-e)\varphi_1\varphi_{31}]V^2\beta/\pi^2 \}
 \end{aligned} \quad (9)$$

Where b is the airfoil half-chord, c is the distance between airfoil mid-chord and the flap hinge line, e is the distance between airfoil mid-chord and the flap leading edge, h is the bending deflection of the rotation point, θ is the pitch angle, β is the flap angle, S_θ is the static moment of the pitch angle, S_β is the static moment of the flap angle, I_θ is the moment of inertia of the pitch angle, I_β is the moment of inertia of the flap angle, k is the reduced frequency, k_h is the stiffness of the plunge, k_θ is the rotational stiffness of the pitch, k_β is the rotational stiffness of the flap spring, m is the mass of the wing, $L_{nc} + L_c$ is the lift force, $M_{nc} + M_c$ is the aerodynamic moment, $T_{nc} + T_c$ is the flap aerodynamic torque, T_s is the control torque, $C(k)$ is Theodorsen's function, V is the air speed, ρ is the air density, T_s are Theodorsen's constants, and φ 's are Wagner's constants.

The function $C(k)$ is a characteristic of circulation terms and is expressed as a linear combination of rational terms, which are function of the reduced frequency k ($k = b\omega/V$, ω is the frequency of oscillation) as follows:

$$C(k) = 1 - \alpha_1 ik / (ik + \lambda_1) - \alpha_2 ik / (ik + \lambda_2), \quad (10)$$

Where $\alpha_1=0.165$, $\alpha_2=0.335$, $\lambda_1=0.0455$, $\lambda_2=0.31$.

The circulatory terms are transformed to Fourier domain by replacing k by $b\omega/V$, and then transformed to Laplace domain assuming analytic continuation. Next six aerodynamic lag states

$\mathbf{x}_a(t) = \{x_{a1}(t) \ x_{b1}(t) \ x_{a2}(t) \ x_{b2}(t) \ x_{a3}(t) \ x_{b3}(t)\}^T$ are introduced such that

$$\begin{aligned}
 L_c(t) &= Q_1(t) - x_{a1}(t) - x_{b1}(t), \\
 M_c(t) &= Q_2(t) - x_{a2}(t) - x_{b2}(t), \\
 T_c(t) &= Q_3(t) - x_{a3}(t) - x_{b3}(t).
 \end{aligned} \quad (11)$$

The six aerodynamic states x_{a1} , x_{b1} , x_{a2} , x_{b2} , x_{a3} and x_{b3} satisfy

$$\begin{aligned}
 \dot{x}_{a1}(t) &= -(\lambda_1 V/b)x_{a1}(t) + \dot{Q}_1(t), \quad \dot{x}_{b1}(t) = -(\lambda_2 V/b)x_{b1}(t) + \dot{Q}_1(t), \\
 \dot{x}_{a2}(t) &= -(\lambda_1 V/b)x_{a2}(t) + \dot{Q}_2(t), \quad \dot{x}_{b2}(t) = -(\lambda_2 V/b)x_{b2}(t) + \dot{Q}_2(t) \\
 \dot{x}_{a3}(t) &= -(\lambda_1 V/b)x_{a3}(t) + \dot{Q}_3(t), \quad \dot{x}_{b3}(t) = -(\lambda_2 V/b)x_{b3}(t) + \dot{Q}_3(t),
 \end{aligned} \quad (12)$$

Where

$$\begin{aligned}
 Q_1(t) &= -2V\dot{h}/b + 2(a-1/2)V\dot{\theta} - [T_{11} - 2(c-e)\varphi_1]V\dot{\beta} - 2V^2\theta/b - 2T_{10}V^2\beta/b, \\
 Q_2(t) &= (1/2+a)\{2V\dot{h} + 2(1/2-a)bV\dot{\theta} - [T_{11} - 2(c-e)\varphi_1]bV\dot{\beta}/\pi - 2V^2\theta/b \\
 &+ 2T_{10}V^2\beta/\pi\}, \\
 Q_3(t) &= [2(c-e)\varphi_{31} - T_{12}]V\dot{h}/\pi - (1/2-a)[T_{12} - 2(c-e)\varphi_{31}]bV\dot{\theta}/\pi \\
 &- [T_{11}T_{12}/2 - (c-e)(\varphi_2\varphi_{31} + \varphi_1\varphi_8) - 2(c-e)^2\varphi_1\varphi_{31}]bV\dot{\beta}/\pi^2 \\
 &+ [2(c-e)\varphi_{32} - T_{12}]V^2\theta/\pi - [T_{10}T_{12} - 2(c-e)\varphi_1\varphi_{31}]V^2\beta/\pi^2
 \end{aligned} \quad (13)$$

Therefore, the second order dynamical system is transformed into a state space form as follows

$$\begin{aligned}
 \dot{\mathbf{x}}(t) &= \mathbf{A}\mathbf{x}(t) + \mathbf{B}\mathbf{u}(t), \\
 \mathbf{y}(t) &= \mathbf{C}\mathbf{x}(t),
 \end{aligned} \quad (14)$$

Where \mathbf{A} is dynamic matrix, \mathbf{B} is input control matrix, \mathbf{C} is output control matrix, $\mathbf{u}(t)$ is input control vector which represent the control torque to the flap, and $\mathbf{x}(t)$ is the state vector which is given as

$$\mathbf{x}(t) = \{\dot{q}_s(t) \ q_s(t) \ x_a(t)\}^T, \quad \mathbf{q}_s(t) = \{h(t)/b \ \theta(t) \ \beta(t)\}^T, \quad (15)$$

$$\mathbf{B} = (1/I_\beta) \{M_s^{-1} \{0 \ 0 \ 1\}^T \ 0 \ 0 \ 0 \ 0 \ 0 \ 0 \ 0\}^T, \quad (16)$$

where \mathbf{M}_s is the structural mass matrix.

The optimal Linear Quadratic Regulator control is applied to suppress flutter. The state feedback control $\mathbf{u} = -\mathbf{K}_c\mathbf{x}$ is chosen such that the closed loop system $\dot{\mathbf{x}} = [\mathbf{A} - \mathbf{B}\mathbf{K}_c]\mathbf{x}$ is exponentially stable. The design of \mathbf{K}_c is a tradeoff between the transient response and the control effort. The optimal control approach to this design tradeoff is to define the performance index (cost functional)

$$J = \int_0^\infty [\mathbf{x}^T(t)\mathbf{Q}\mathbf{x}(t) + \mathbf{u}^T(t)\mathbf{R}\mathbf{u}(t)]dt, \quad (17)$$

Next, the control law is obtained by solving the algebraic Riccati equation

$$\mathbf{PA} + \mathbf{A}^T \mathbf{P} + \mathbf{Q} - \mathbf{PBR}^{-1} \mathbf{B}^T \mathbf{P} = \mathbf{0}, \quad (18)$$

Hence the control gain is

$$\mathbf{K}_c = \mathbf{R}^{-1} \mathbf{B}^T \mathbf{P}, \quad (19)$$

Numerical Simulation

The system parameters [1] are $a=0$, $b=0.2032$ m, $c=0.1016$, $e=0.1016$, $m=88.73$ kg, $S_\alpha=0.8873$ kgm, $S_\beta=0.0128$ kgm, $k_h=39199$ N/m, $k_\alpha=4067$ Nm, $k_\beta=220.7$ Nm, $I_\alpha=3.796$ kgm², $I_\beta=8.3e-4$ kgm², $L_w=0.8$ m, $L_f=0.24$ m, $\rho=0.53$ kg/m³. The open loop system ($\mathbf{B}=\mathbf{0}$) in Eq. (14) is simulated using air velocities of $V=160$ m/sec, 174.15 m/sec, and 180 m/sec; respectively. The velocity $V_f=174.15$ m/sec is the flutter speed. The flutter speed is the speed at which the open loop system becomes marginally stable. The simulations time interval is 5 second using the following initial state vector \mathbf{x}_0 .

$$\mathbf{x}_0 = \{0.5 \quad -0.01 \quad 0.005 \quad -0.1 \quad 0.001 \quad -0.001 \quad 0 \quad 0 \quad 0 \quad 0 \quad 0\}.$$

At $V=160$ m/sec, the plunge, pitch and flap angles asymptotically approach zero as shown in Fig. 2. At $V=V_f=174.25$ m/sec, the plunge, pitch and flap angles settle into harmonic oscillations as shown in Fig.3 and flutter occurs. The flutter frequency $\omega_f=24.19$ rad/s. After about 0.5 seconds, the dimensionless plunge oscillates between -0.006 and 0.006 and the pitch oscillates between -0.00172 and 0.00172 radians. The flap angle settles into oscillations between -0.0009 and 0.0009 radians. This means that the plunge, pitch and flap angles oscillate at this constant rate as long as the airplane is flown at this speed. At $V=180$ m/sec, a velocity above the flutter speed, the plunge, pitch and flap angles, and their respective velocities continue to grow without bound with increasing time as shown in Figs. 4 and 5. After about 4 seconds, the dimensionless plunge of the wing reaches amplitude of about 0.058. The pitch grows to amplitude of about 0.015 radians and the flap angle has amplitude of about 0.007 radians. Clearly, the model is no longer valid and the airfoil would have become unstable. This leads to separation of the wing. The closed loop system for $V=180$ m/s are shown in Figs. 6 and 7. The plunge, pitch and flap angles, and their respective velocities do asymptotically approach zero. Therefore the closed loop system is asymptotically stable. Much better performance is obtained using the LQR, as shown in Fig. 6,7 since the pitch, the plunge, and the flap angle asymptotically approach zero by 1.5 seconds. The velocities of the pitch, the plunge, and the flap angle and the aerodynamic lag states also asymptotically approach zero and the system is stabilized in about 1.5 seconds.

Acknowledgements

This work presented herein has been supported by the Deanship of Scientific Research at King Saud University, Saudi Arabia. These supports are greatly appreciated.

References

- [1] R. M. A. Marretta and F. Marino: Wing flutter suppression enhancement using a well-suited active control model, Proc. IMechE, 221 Part G, *J. Aerospace Engineering*, (2007), pp.441- 452.
- [2] K. H. Kargarnovin and A. Mamandi: Aeroelastic response for pure plunging motion of a typical section due to sharp edged gust, using Jones approximation aerodynamics, *World Academy of Science, Engineering and Technology* 6, (2007), pp.154-161.
- [3] B-H. Lee, J-H. Na, P. Marzocca and L. Libreseu, Sliding mode robust control of supersonic three degrees-of-freedom airfoils, *International Journal of control, Automation, and System* 8, (2010), pp.279-288.
- [4] S. Chen, W.U. Zhigang and Y. Chao, Active Flutter Suppression of a Two-Dimensional Airfoil Based on Sliding Mode Control Method, *IEEE* (2011), pp. 1146-1150.
- [5] R.H. Scanlan and R. Rosenbaum, *Introduction to the Study of Aircraft Vibration and Flutter*, (Macmillan, New York, 1951).



International Conference on Innovative Technologies, IN-TECH 2012,
Rijeka, 26. - 28.09.2012



FIRST AND SECOND ORDER IMAGE STATISTICS IN SPECIFIC IMAGE ARTIFACT DETECTION

M. Rogobete¹, C. Răcuciu²

¹ Senior Image/Video Software Engineer, Pentalog HIGH-TECH, Bucharest, Romania

² Prof. Eng., PhD, Titu Maiorescu University, Bucharest, Romania

Keywords: First order gradient, second order gradient, optical artifact, artifact detection, real time image processing

Abstract. An algorithm to recognize a specific image artifact that appears on video frames, randomly, during video capture with professional camera, was developed and implemented. The first and second image statistics are used into an original function, able to detect specific artifact.

The artifact is laying as a blurring area, with a vertical border, on the left or on the right side of it and the blurred area is not homogenous.

Based on an analytical representation of the image statistics, the artifact was defined in terms of absolute range values of these parameters.

The left or right artifact position against the vertical border is classified when the detected rows number is over the count threshold and the proportion between rows number of the sides is over position threshold value.

Because the detection is referred to the rows of image matrix, it was necessary to check the artifact homogeneity from the rows congruency point of view using a threshold value under that the rows are classified as non artifact.

1. Introduction

A professional video camera, already on the market, was reported to embed in the image frame specific optic artifact when apparently some scenic parameters values are satisfied (e.g. light intensity, incidence angle, contrast). Anyway, the exactly optical condition for which the artifact arises is not the subject for this study.

The requested targets were to detect:

- the frames with the artifact embedded
- the artifact position along to the frames vertical symmetry axis
- if the artifact is located on the right or on the left side of the symmetry axe.

Finally, the artifact shall be compensated and thus the affected frames to appear clear and free of any noise. The artifact compensation algorithm is not the subject for presented work.

2. Artifact description

The artifact is optical defined as blurred areas, geometrical bordered by the vertical axe of the frame image (Fig. 1). These regions are looking like dusty spots aligned on the right or left side of vertical border. The classification process is able to recognize the artifact and to locate it in terms of image coordinates.

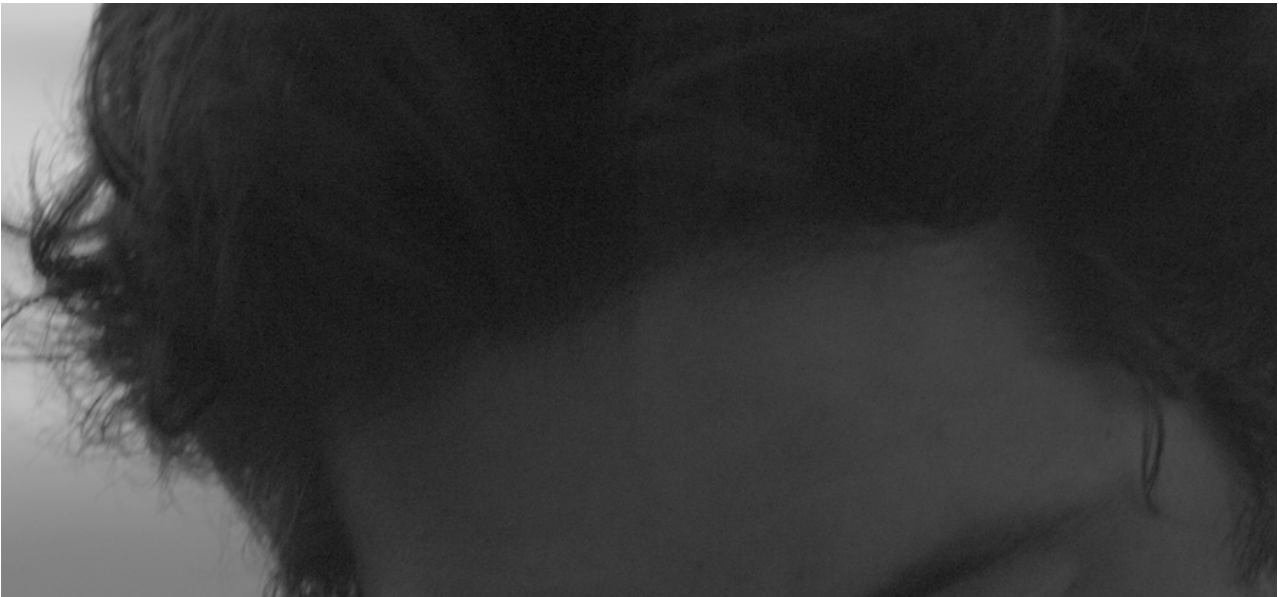


Fig. 1 Part of the image frame that contains specific artifact

2.1 Preliminary analyze

As the artifact typology is looking like a dusty one is possible to try the methods described by C.Zhou and S.Lin [1]. But the artifact is homogenous for the sensor dust case and non homogenous for the studied case (where the artifact has diffraction reason), in conclusion the method has serious limitation.

On the other hand the image statistics complex corroboration could offer a real solution for artifact recognition.

3. Methodology

Overlapping the graphics of several image statistics (Fig.2), synchronized with the artifact apparition, was able to identify the correlation between the image statistics parameters and artifact existence. The statistical parameters for an image without artifact are presented in fig.3.

The computed statistics image parameters are:

1. The RGB average on the left border side
2. The RGB average on the right border side
3. The total RGB average
4. RED – first order vertical gradient
5. GREEN – first order vertical gradient
6. BLUE – first order vertical gradient
7. Horizontal RGB gradient
8. RGB second order gradient
9. Vertical RGB gradient

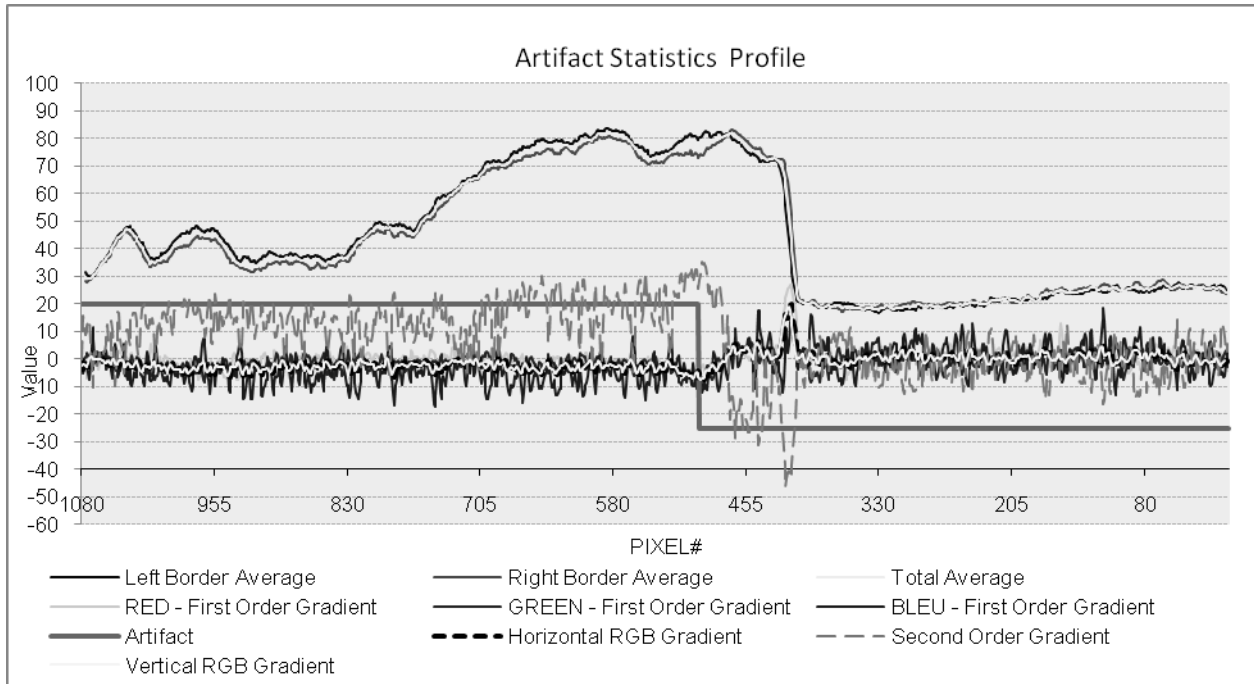


Fig. 2 The image statistics parameters for the image with artifact

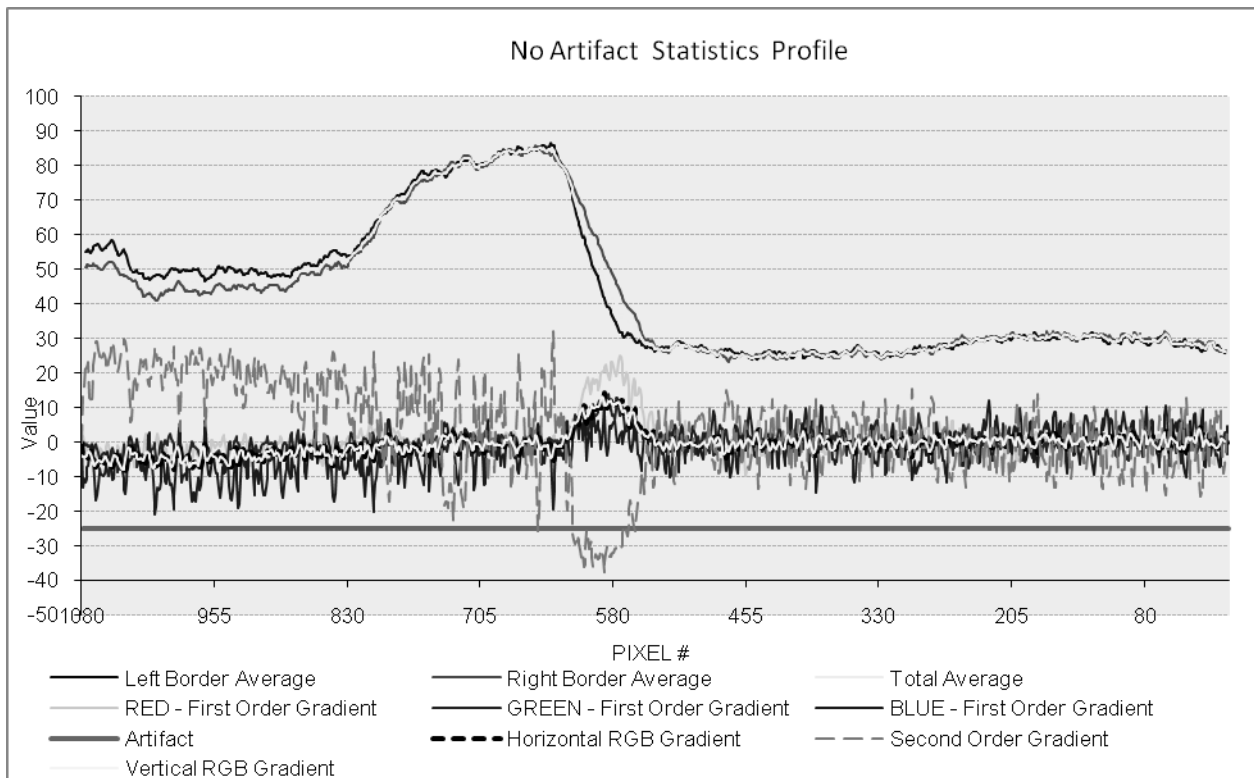


Fig. 3 The image statistics parameters for the image without artifact

4. Classification decision

The classification decision algorithm has the following steps:

1. It is tested the total RGB average values: is in range of $[0,7]$ for right side or $[-7,0]$ for left side. If the one of them is detected the classification process continues.
2. The vertical RGB gradient value is tested, $< =0$ for right side or >0 for left side, if the detection is fitting the process continues.

3. If the line is tested for right side, the vertical gradient differences between left and right side has to be in range $[0,8]$ and then the line could be classified as "right artifact". If the line is tested for left side, the difference has to be in range $[-8,0]$ and then the line could be classified as "left artifact". The RGB second order gradient is correlated for both cases.
 4. The left and right classified lines are now counted and compared with the "count threshold", if no one is over it there is no artifact, otherwise the report between the lines sides counters is compared with the "position threshold" value, if it is over, the image has an artifact on the side with the bigger lines counter.
 5. The detected artifact homogeneity is tested and, if the number of adjacent classified lines is under the threshold value, the lines are eliminated from the artifact classification.
- The detected artifact limit is presented in fig.4.

5. Conclusion

Using an experimental methodology it was defined an algorithm, implemented on embedded professional camera platform, able to detect specific artifact in video frame image. To finalize the task, another algorithm that eliminates the optical artifact was developed (it is not intended to be presented into this study). Both of the real time software modules are running properly and are used with success instead the optical system modifications, which is very expensive

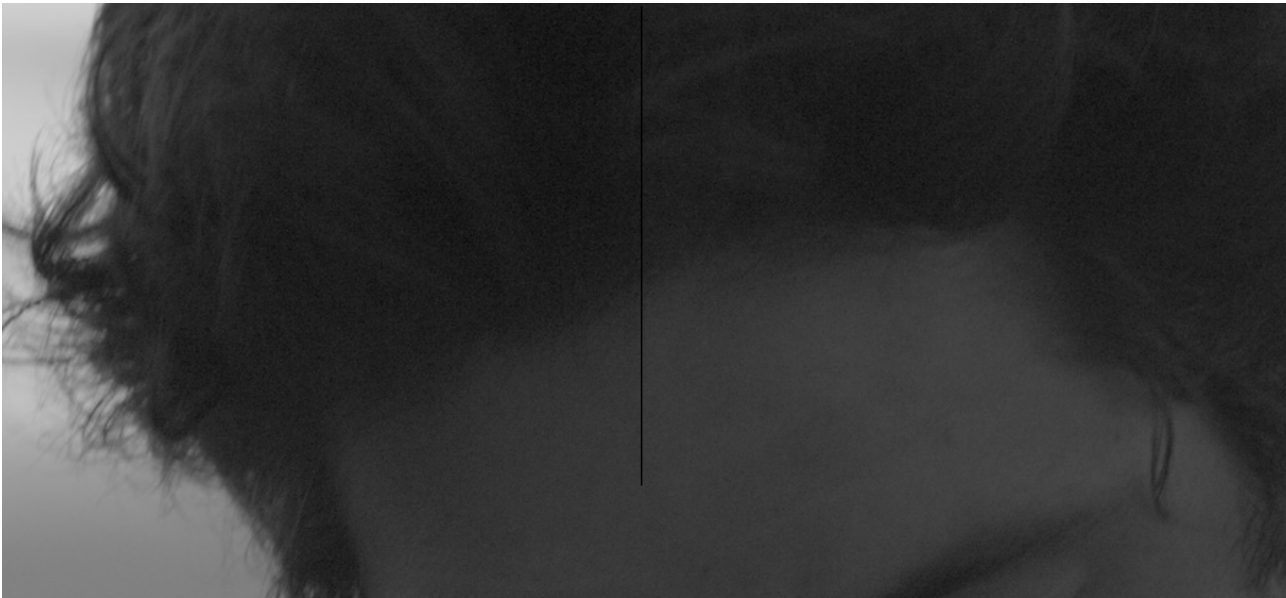


Fig. 4 The image with artifact border down after artifact recognition

6. References

- [1] C. Zhou, S. Lin" Removal of Image Artifacts Due to Sensor Dust, *Association for Computing Machinery, Inc.*, 2007.
- [2] T R. G. Willson, M. W. Maimone, A. E. Johnson, and L. M. Scherr. An optical model for image artifacts produced by dust particles on lenses. *Proc. ISAIRAS*, 2005.
- [3] A. Levin, A. Zomet, and Y. Weiss. Learning how to inpaint from global image statistics. In *Proc. IEEE International Conference on Computer Vision*, pages 305–312, 2003.
- [4] N. Komodakis and G. Tziritas. Image completion using global optimization. In *Proc. IEEE Computer Vision and Pattern Recognition*, pages 442–452, 2006.

MLP NEURAL NETWORK BASED PREDICTION OF COAL QUALITY CATEGORIES

M. Suljic¹, and L. Banjanovic-Mehmedovic²

¹JP Elektroprivreda BiH d.d. – Sarajevo, ZD Rudnici "Kreka" d.o.o.-Tuzla,
Bosnia and Herzegovina

²Faculty of Electrical Engineering, University of Tuzla
Bosnia and Herzegovina

Keywords: coal quality, coal calorific value, neural network prediction.

Abstract. The significant coal deposits which represent the primary source of energy could be found on the territory of Bosnia and Herzegovina, Tuzla region especially. Therefore, the prediction of energy values is the most important task aiming to secure the optimal usage of coal energy value. The coal quality is an important property that depends on its chemical composition and points at useful energy value in coal. It is described with gross calorific value (GCV) and net calorific value (NCV). There are different methods for prediction the gross calorific value (GCV) of a coal sample based upon its proximate and/or ultimate analyses. One of intelligent method is neural network (ANN)-based method for prediction of the coal quality class. It is shown in this paper, that multi-layer perceptron (MLP)-based model based on coal and other data from technical control department of Coal mines "Kreka", achieved good reasonable prediction accuracy in prediction categories of coal (net calorific value, NCV).

Introduction

The coal has been major factor in intensive economic development of Europe as well as Bosnia and Herzegovina (BiH) during the last 40 years. Many regions have achieved their economic and industrial development thank to coal as a source of energy. According the statistics data, coal as a source of fossil energy secure about 30% of total energy production in the EU and around 59% in Bosnia and Herzegovina respectively [1,2]. It is well-proved fact that despite introduction of new renewable sources of energy, coal stays irreplaceable in energy supply of many countries as well as in Bosnia and Herzegovina.

According to the structure and natural characteristics of Bosnia and Herzegovina (BiH), it is a complicated natural complex with significant wealth in coal. Total geological coal reserves are estimated at $5,5 \times 10^9$ tons of which $3,2 \times 10^9$ have proven reserves based on Law on geological reserves [3]. These reserves represent significant basis for electricity production by using either conventional (traditional) technologies or new combustion ones. The largest coal deposits are located in Tuzla region and they are excavated by a group of coal mines called "Kreka" Coal Mine Company with their headquarters located in city Tuzla. Lignite deposits are of pliocene age and they are divided into two synclines (Northern and Southern) with coal layers oriented in the direction northwest-southwest shown in Fig. 1.

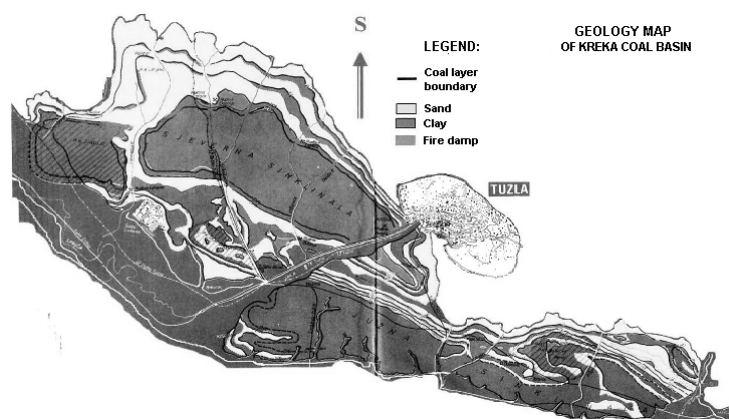


Fig. 1 Kreka lignite basin

Four coal layers seem to be present in the major part of the basin and they are called: floor, main, I intermediate and II roof layer. Thickness of coal layers varies from 8 to 25 m with dip angle ranging from small up to steep one. The depth of the layers is about 1250m below the surface, but only the layers which lay at the shallow part have been excavated by using open-pit and underground-pit methods. There are four mines operating within the Kreka Mines Company, as follows: Šikulje (open pit mine), Dubrave (open pit mine), Mramor (underground pit mine) and Bukinje (underground pit mine).

The measure of the amount of energy that a given quantity of coal will produce when burned is known as calorific value or heating value. Heating value is a rank parameter and a complex function of the elemental composition of the coal, but it is also dependent on the maceral and mineral composition.

The coal quality predicting is the application of science and technology to predict the energy value in coal. Therefore, the prediction of energy value is the task of enormous importance, which should ensure optimal utilization of coal with aim to increase energy efficiency. The coal quality is an important property that depends on its chemical composition and points at useful energy value in coal, so we use two measures for describing it: gross calorific value (GCV) and net calorific value (NCV). At present there are two methods for determination of these values [4]: proximate analysis and ultimate analysis.

The objective of proximate analysis is to determine the relative amounts of moisture, ash, volatile matter and fixed carbon content of the coal. On the other hand, the objective of coal ultimate analysis is to determine the constituent of coal, in a form of its basic chemical elements: carbon (C), hydrogen (H), oxygen (O), sulfur (S) and other elements within the coal sample. The ultimate analysis is performed in a properly equipped laboratory by a skilled chemist, while proximate analysis can be determined with a simple apparatus [4].

Different researchers have proposed different equations for prediction the gross calorific value (GCV) of a coal sample based upon its proximate and/or ultimate analyses [5,6,7,8]. These correlations are mainly linear in character although there are indications that the relationship between the GCV and a few constituents of the proximate and ultimate analyses could be nonlinear.

In recent years a researcher looking for simpler and cheaper methods for prediction the coal calorific value has begun to use nonlinear models such as artificial neural network [8,10,11]. Neural networks are powerful tools that have the abilities to identify nonlinear patterns between input and output values and can solve complex problems. Owing to their wide range of applicability and their ability to learn complex and non-linear relationships – including noisy or less precise information – ANNs are very well suited to solving problems in particularly towards the analysis of predicting of energy value in coal.

Patel et al. (2007) developed seven nonlinear models for prediction of GCV with a special focus on Indian coals, using neural network analyses based on coal properties. It has been found that the performances of the ANN models are much better than those of their linear counterparts. Mesroghli et al. (2009) investigated the relationships of ultimate analysis and proximate analysis with GCV of U.S. coal samples by regression analysis and artificial neural network methods. Three set of inputs were used for the prediction of GCV values and the satisfactory prediction was obtained. Additionally, ANN concept is being successfully applied in solving wide variety of prediction [12,13], estimation and controlling issues that are encountered in power-plant.

The objective of the present work is to develop ANN-based model by using coal and other data from technical control department of Coal mines "Kreka", for the predicting the categories of net calorific value (NCV).

Data settings

Data used in this paper to predict NCV have been taken from the technical control department of Coal mines "Kreka", which are achieved in laboratory conditions during the period 2005-2010. The samples with more than 50% ash, were excluded from the database. Analysis results for a total of 33256 coal samples were used. The number of samples and range of NCV for four operations within the Coal mines "Kreka" are shown in Table 1.

Table 1. Range of NCV (as-received) for different Coal mines "Kreka"

Mine	Number of samples	Range of NCV (kJ/kg)
Bukinje	949	5327 – 15019
Dubrave	14163	5657 – 13776
Mramor	5843	7056 – 15379
Šikulje	12298	7112 – 12323

The part of data which has been measured on sample of every 300 t was shown in Table 2.

Table 2. Coal variables

No.	Coal variables in the every 300t frame	Range of values
1	NRudnik (Mine)	A, B, C, D
2	Eksplo (Type of excavation)	0, 1
3	Sinklin (Syncline)	J, S
4	NAsortiman (Commercial grade of coal)	M, O, S
5	Dan (Day)	1-7
6	BrVagona (Number of waggons)	1-15
7	GVlaga (Free moisture quantity)	13.4 – 52.4
8	HVlaga (Hydroscopic moisture quantity)	0-33.1
9	Pepeo (Ash)	1-50.2

The selected subset of data contains ten attributes of which the nine are conditional and one attribute is predicting. Rows with Null values are omitted because it is extremely difficult to recover missing values. The attribute that predicts the Coal quality can belong to one of seven classes: A, B, C, D, E, F and G.

Cross-validation methods are commonly used in examining the robustness of classifiers. In this study, a 10-fold cross validation was used: we split data set randomly into 10 subsets of equal size. Eight subsets were used for training, one subset for cross validating and one for measuring the predictive accuracy of the final constructed network. This procedure was performed 10 times so that each subset was tested once. Test results were averaged over 10 tenfold cross-validation runs. Data splitting was done without sampling stratification. One of the data set was used for testing MLP, while the remaining was used for training. The training and test sets consisted of 33256 samples.

Neural networks

Neural Network (NN) represents a new generation of systems of information processing that shows characteristics of learning, memorizing and generalizations based on data trained. They are very efficient in tasks such as classification, function

approximation, optimisation and data clustering. Great popularity and success of neural network methods are result of their features that help us to solve complex tasks with high accuracy. The basis of neural networking is usage of the principles on which human brain functions and their application in resolving different tasks. Artificial neural networks (ANN) are connected with environment in two ways: first through inputs that have certain impact on the networks and secondly through output network which in turn affects the environment. It consists of potentially great number of processing elements, normally appearing in layers. Each element is connected with elements in the previous layers by means of adaptable strength or weight. The adaptation of these weights is performed by learning algorithm and this adaptation process improves the learning capability of the system, thereby enabling it to generalize for new situation. The ANN model in our paper is based on one of the neural network architecture, named multi-layer perceptron [14].

Multi-Layer Perceptron (MLP)

This is maybe the most popular network architecture in use today. Each of its units performs biased weight sum of their inputs and passes this activation level through a transfer function to produce their output, and the units are arranged in a layered feed forward topology. The network thus have a simple interpretation as a form of input-output model, with the weights and thresholds (biases) the free parameters of the model. Such networks can model functions of almost arbitrary complexity with the number of layers and the number of units in each layer, determining the function complexity. Important issues of Multi-layer perceptron design take into account specification of hidden layers and the number of units in these layers. Once the number of hidden layers and number of units in each layers have been selected, the network's weight and the threshold must be set so as to minimize the prediction error made by the network. This is the role of the training algorithms. The best known example of a neural network training algorithm is back propagation [15].

Evolving MLP Structures

With this background we designed and trained this network as below. The three-layer network with sigmoid transfer function for hidden layer and linear transfer function for output layer can represent any functional relationship between inputs and outputs, if the sigmoid layer has enough neurons [14], so we selected this three layer structure. MLP had 14 input and 7 output neurons. The gradient based back-propagation learning rule was used to determine the optimal MLP structure: learning rate ([0 ... 0,9] with step 0,1), learning momentum ([0 ... 0,9] with step 0,1) and hidden unit number ([1 ... 45] with step 1). Initial value of parameters MLP before optimization are: number of epochs is 300, the learning rate is 0.3, the learning momentum is 0.2 and hidden unit number is 9.

The accuracy of training and test steps according to learning rate and learning momentum are shown in Fig. 2 and 3, respectively. The best result of training and test steps were obtained when the learning rate was 0.2 and learning momentum was chosen as 0.1.

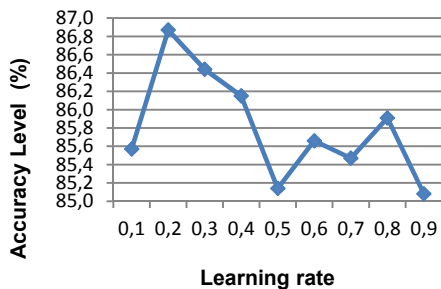


Fig. 2 The classification accuracy of training step according to Learning rate



Fig. 3 The classification accuracy of training step according to Learning momentum

Initial value of parameters MLP before optimization has been as following: number of epoch was 300, the learning rate was 0.2 and the learning momentum was 0.1. The unit number in the hidden layer has been increased from 1 to 45 (incremented by 1). The performance of MLP depends heavily on initial conditions. Hence, the training and testing processes were repeated 45 times. The results were obtained by averaging experimental results of 10-fold cross validation dataset. The accuracy of training and test steps according to hidden unit numbers (H) is shown in Fig. 4.

The best result of training and test steps were obtained when the hidden unit number (H) was chosen as 24. Besides, the root means square error (RMSE) for training and test steps according to hidden unit numbers are given in Fig. 7. As shown in Fig. 5, the minimum MSE errors for training and test processes were acquired when the hidden unit number (H) was 25 and 24, respectively.

The best result of training and test processes are shown while the hidden units are 24. Then, the optimal MLP structure is 14-24-7 for the input, hidden and output layer respectively, the learning rate is 0.2 and the momentum of learning 0.1.

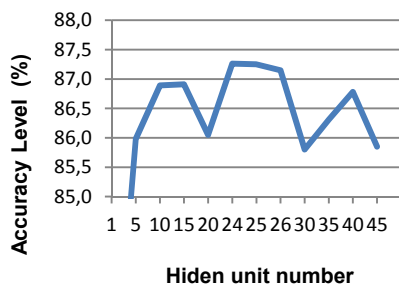


Fig. 4 The classification accuracy according to hidden unit number

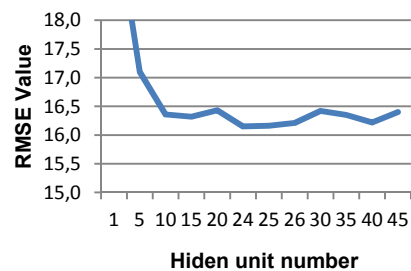


Fig. 5 The RMSC according to hidden unit number

Result and discussion

With a preliminary analysis we have developed the optimal MLP neural network that give the best results. Testing optimal MLP neural network was carried out with the 1000 new samples. The exact and predicted values for each unseen sample by MLP network is shown in Table 3 and Fig. 6.

Table 3. The results of prediction for each quality class

MLP neural network	TP Rate	FP Rate	Precision	Recall	Class
<ul style="list-style-type: none"> • training time: 100 • learning rate:0.2 • learningmomentum:0.1 • hidden unit number: 24 	95.00	1.00	91.40	95.00	A
	86.10	1.40	87.90	86.10	B
	87.20	1.30	90.30	88.70	C
	94.90	5.60	92.00	94.90	D
	87.60	2.20	92.50	87.60	E
	93.80	0.40	88.20	93.80	F
	0	0	0	0	G
	91.30	3.20	91.30	91.30	AVG

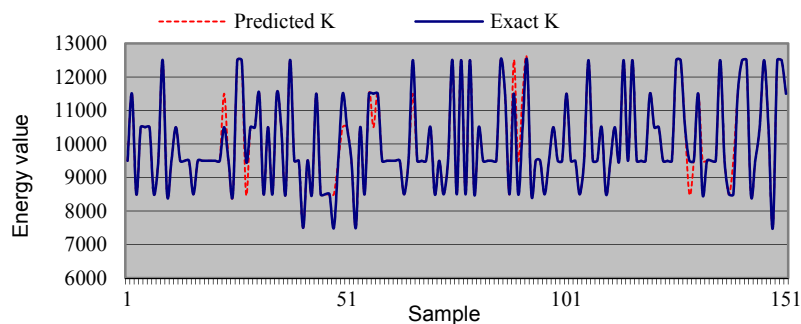


Fig. 6 Comparison between exact and predicted values

Therefore the proposed ANN model with the developed structure shown in Table 3 can perform good predicting the categories of coal quality in Coal Company "Kreka".

Conclusion

The results of MLP neural network model used for predicting categories of coal in Coal Mine Company "Kreka" have shown that MLP neural network was achieved good performance and reasonable prediction accuracy for this model. The results suggest that this neural network could be an important tool in predicting coal quality.

For future work, the experiment can be extended with more distinctive attributes from geological database to get more accurate results useful in improving the outcome. Also, experiments could be done by using other algorithms in order to get more accurate energy value of coal.

References

- [1] European Association for Coal and Lignite. (2012, January) EURACOAL - European Association for Coal and Lignite. [Online]. <http://www.euracoal.be/pages/home.php?idpage=1>.
- [2] Plan Bleu. (2012, January) Plan Bleu - Regional Activity Center. [Online]. http://www.planbleu.org/publications/atelier_energie/BA_Summary.pdf
- [3] Vlada Federacije Bosne i Hercegovine. (2012, January) Strateski plan i program razvoja energetskog sektora FBiH. [Online]. <http://www.fbihvlada.gov.ba/bosanski/izdvajamo/SPP-sept-08-PRIJEDLOG.pdf>
- [4] B.G. Miller, *Coal Energy Systems*. London, United Kingdom: Elsevier Academic Press, 2005.
- [5] P.H. Given, D. Weldon, and J.H. Zoeller, "Calculation of calorific values of coals from ultimate analyses: theoretical basis and geochemical implications," *Fuel*, vol. 65, pp. 849–854, 1986.
- [6] D.M. Mason and K.N. Gandhi, "Formulas for calculating the calorific value of coal and coal chars: Development, tests, and uses," *Fuel Processing Technology*, vol. 7, pp. 11-22, 1983.
- [7] T. Cordero, F. Marquez, J. Rodriguez-Mirasol, and J.J. Rodriguez, "Predicting heating values of lignocellulosic and carbonaceous materials from proximate analysis," *Fuel*, vol. 80, pp. 1567–1571, 2001.
- [8] Sh. Mesroghli, E. Jorjani, and S. Chehreh Chelgani, "Estimation of gross calorific value based on coal analysis using regression and artificial neural networks," *International Journal of Coal Geology*, vol. 79, pp. 49–54, 2009.
- [9] S.U. Patel et al., "Estimation of gross calorific value of coals using artificial neural networks, Volume 86, Issue 3,," *Fuel*, vol. 86, no. 3, pp. 334-344, 2007.
- [10] S. Chehreh Chelgani, J.C. Hower, E. Jorjani, Sh. Mesroghli, and A.H. Bagherieh, "Prediction of coal grindability based on petrography, proximate and ultimate analysis using multiple regression and artificial neural network models," *Fuel Processing Technology*, vol. 89, no. 1, pp. 13-20, 2008.
- [11] H. Salehfar and S. A. Benson, "Neural Network Based Power Plant Coal Quality Analysis," in *IEEE, 29th Annual North American Power*



International Conference on Innovative Technologies, IN-TECH 2012,
Rijeka, 26. - 28.09.2012



Symposium, Laramie, 1997.

- [12] Y. Ozel, I. Guney, and E. Arca, "Application of Neural Network to the Cogeneration System by Using Coal," *INTERNATIONAL JOURNAL OF ENERGY*, vol. 4, no. 1, 2007.
- [13] M.T. Hagan, H.B. Demuth, and M.H. Beale, *Neural Network Design*. Boston, Massachusetts: PWS Publishing, 1996.
- [14] S. Haykin, *Neural Networks: A Comprehensive Foundation*. New York: Macmillan College Publishing, 1994.



ENERGY DISSIPATION AS A MEASURE OF VIBRATION INDUCED FATIGUE PROCESSES IN ENGINEERING MATERIALS

P. Drożyner¹, A. Rychlik¹, J. Napiórkowski¹, P. Szczyglak¹ and M. Kaczmarek-Jasiulewicz²

¹ University of Warmia and Mazury in Olsztyn, Poland

² Poznan University of Technology, Poland

Keywords: fatigue, vibration, energy dissipation

Abstract. This article proposes a method and a laboratory setup for testing the fatigue strength of materials with the use of vibration signals and a neodymium fatigue testing machine. The machine supports non-contact fatigue testing of construction materials; it can also be used to evaluate sample deformation by registering amplitude, RMS deviation from equilibrium-calculated values, temperature of sample notch, deflections along the length of the sample, stress at the cross-section of the notch and load applied at the terminal section of the sample. In the paper there will be also presented a mathematical model of the energy of the process of fatigue-induced vibrations. It is assumed that the force that causes fatigue process is represented by the force of inertia (mass) of an object and a its movement is a function of vibration amplitude, frequency excitations and responses, and number of cycles to destruction. The results discussion will be carried out on the energy potential of the fatigue process and the possibility of its identification in the context of its use in the rational exploitation of technical objects.

Introduction

The starting point of most structural fatigue calculations is the Wöhler diagram, which enables determination of the maximum stress values (i.e. fatigue resistance) in which a sample made of a particular material can work for unlimited number of cycles. Engineers designing devices take into account both the expected load and - among others - fatigue strength of the material which the device is made of by assuming the appropriate safety factors.

Meanwhile, machinery and equipment should be treated as working systems transforming energy into useful one (such as a desired product or working process) and externally dissipated energy (vibration, temperature, noise) and internally, which is accumulated in the object as a result of various wear processes including fatigue wear.

The theory of machines as the power processor of a finite potential of destruction (i.e., storage of internally dissipated energy), implies the possibility of prognosis of the technical state but provided there is a quantitative description of the destruction, both in terms of "initial capacity" of this potential and its current status.

Neodymium fatigue testing machine NMZ-1

The fatigue wear of construction materials is evaluated with the involvement of methods and test stands characterized by various functional solutions [1, 2, 4, 6]. Depending on the type of produced stress, they can be classified into the following categories: a) bending machines, b) tensile-compression machines, c) rotating-bending machines, d) machines for testing samples subjected to complex stress. The above fatigue testing machines come into mechanical contact with the analyzed sample. In this type of contact, the sample cannot be tested at high cycle frequency and low amplitude of material displacement.

This study proposes a method for evaluating the fatigue strength of materials with the use of vibration signals and a neodymium fatigue testing machine. The NMZ-1 neodymium machine has been designed for non-contact fatigue testing of construction materials. All mechanisms and assemblies of the NMZ-1 fatigue testing machine (Fig. 1 and 2) are mounted to a self-supporting frame. NMZ-1 is equipped with three independent measurement sections, two of which have double heads, whereas the central section (No. 3) has a single head. In each section, samples are placed in grip jaws which are attached to the frame with sliding brackets. The machine is controlled by a PLC unit in a panel cabinet. The sample is placed in a grip jaw between two discs on the motor shaft. Alternate neodymium magnets are symmetrically arranged on the discs. Neodymium magnets mounted on rotating discs act upon the sample and cause its displacement from the equilibrium position. The force acting upon the sample is a combination of the distance between the discs, the strength of neodymium magnets and the length of the analyzed sample. The frequency of changes in the amplitude of sample displacement is determined by the rotational frequency of the engine shaft which is controlled by the PLC unit via an inverter. The values of fatigue process parameters, such as the number of fatigue cycles, sample displacement (amplitude) and the temperature of the sample's contraflexure region, are registered by the control unit. The measuring and registering system of the NMZ-1 machine is controlled by the PLC unit with original process management software. Measurement sensors supply the PLC controller with data.

Sample characteristics

The analyzed samples were flat strips of corrugated sheet metal which could be fitted into the applied grip jaws. The notch on the sample determined the place of deformation, and it supported the identification of measured and calculated values (Fig. 3). Preliminary tests were performed using samples of DC01 steel.

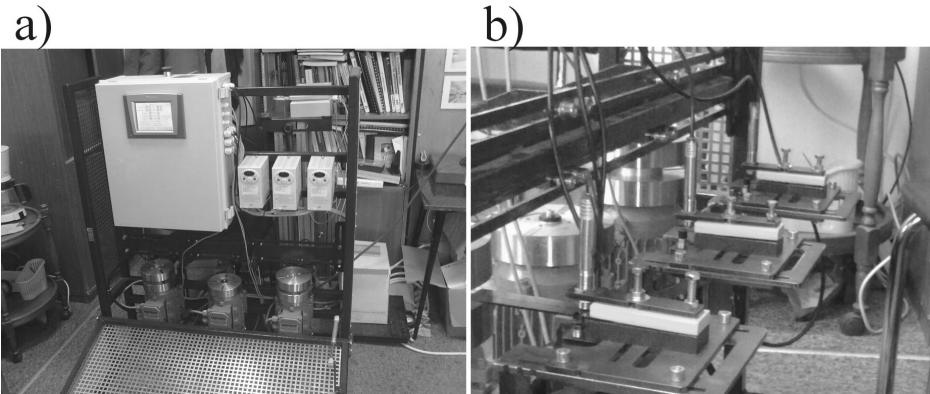


Fig. 1. NMZ-1 Neodymium Fatigue Testing Machine, a) – general view; b) view of clamp section and measurement sensors

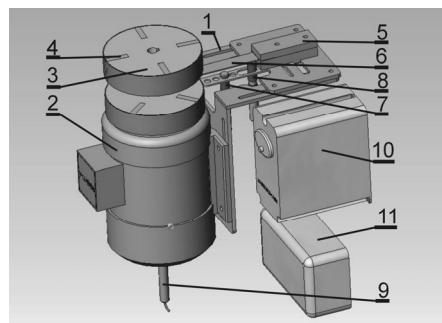


Fig. 2. View of the measurement section with a double head for the identification of selected parameters of the fatigue testing process, 1 – base; 2 – electric motor; 3 – double disc; 4 – neodymium magnets; 5 – sample grip; 6 – analyzed sample; 7 – displacement sensor; 8 – temperature sensor; 9 – cycle meter; 10 – inverter; 11 – PLC controller

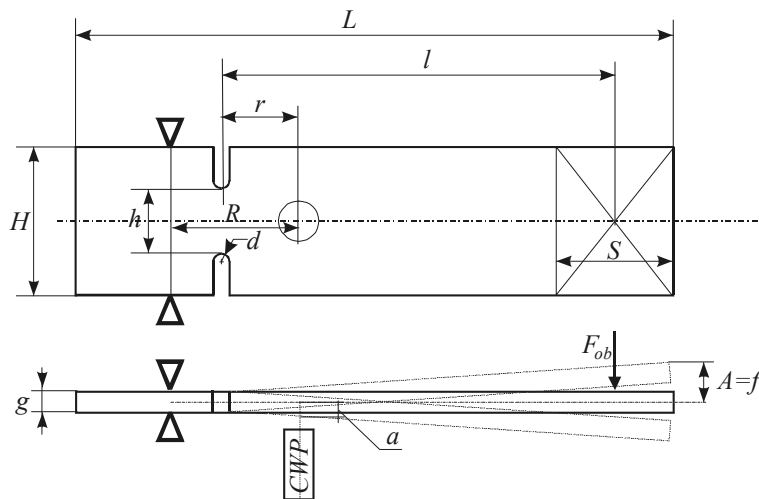


Fig. 3. Principal dimensions of the analyzed sample: L – sample length; l – active face of sample; H – sample width; h – width of sample notch; g – sample thickness; R – distance between the eddy current sensor (ECS) and grip jaws; r – distance between the ECS and sample notch; d – notch radius; S – length of magnetic field acting on the sample; F_{ob} – computed (magnetic) force acting on sample; a – amplitude of the sample's deflection from a state of equilibrium caused by force F_{ob} ; A – displacement amplitude of the sample's terminal section; CWP – eddy current sensor (CW-10) for the determination of sample displacement

Stress values at the cross-section of the notch in samples with a constant thickness are determined by the sample's active face (l), its width (H), notch width (h) and the length of magnetic field acting on the surface of the sample (S).

Load model

Modulus of cross-section bending strength at the notch:

$$W = \frac{h \cdot g^2}{6} [m^3], \quad (1)$$

The moment of inertia relative to the neutral axis was calculated using the following formula:

$$I = \frac{h \cdot g^3}{12} [m^4], \quad (2)$$

The displacement of a material point along the sample's active face caused by the neodymium magnet was determined with the below equation:

$$f = \frac{a \cdot l}{r} [m], \quad (3)$$

The load applied to the active face of the sample was calculated as follows:

$$F_{ob} = \frac{3 \cdot E \cdot I \cdot f}{l^3} [N], \quad (4)$$

Bending stress at the notch of the sample is defined by the below formula:

$$\delta = \frac{F_{ob} \cdot l}{W} [MPa], \quad (5)$$

Displacement of the sample's material point in a magnetic field

The deformation of a sample from a state of equilibrium is determined by the force exerted by neodymium magnets attached to the discs. Examples of sample deformation for double disc and for symmetrical cycles are presented in Figures 4.

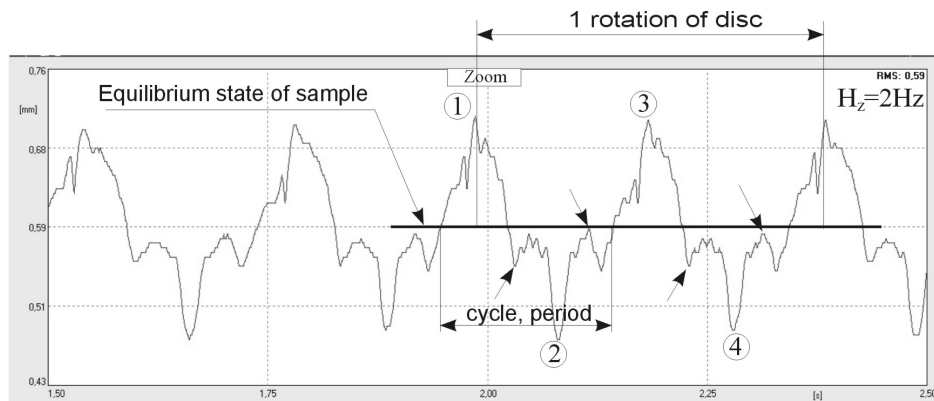


Fig. 4. Displacement range of a material point in the sample induced by neodymium magnets on a double disc, Hz=2Hz

Description of the mathematical elastic-damping model

An important factor which characterises fatigue processes is susceptibility of construction material. The relationship between load and material deflection is a very complex issue and may only be solved in the rough. The theory of ideal mediums allows the creation of a models with a significant simplification while maintaining high precision mapping reality. Nature of the changes of load and deformation can be described by so called ties susceptible [5]. The figure 5 presents model describing susceptibility of bending sample with load not exceeding border elastic. The model takes into account energy dissipation caused by internal friction.

Equations 6 and 7 describe adopted mathematical elastic-damping model of bending of the sample.

Experimental researches were necessary to identify stiffness and suppression in the accepted model. During the tests time course of load and induced by the load deflection were recorded. Obtaining time courses has undergone frequency filtration with use of programme MatLab using a Czebyszew filter. The rigidity and suppression of the model was determined usig MatLab (function "fmins") and optimisation method usung recorded time course of load and induced by the load deflection. The value of stiffness was 18.19 N/mm, and the damping 0,0422 N*s/mm. Designated by the model energy value dispersed for one bending cycle was equal to 0,001555 N*mm.

Knowing the energy in one bending cycle it is possible to calculate energy for the whole process of sample fatigue destruction, irrespective of the amplitude and frequency of vibrations causing deflection. The theory of machines as the power processor of a finite potential of destruction (i.e., storage of internally dissipated energy), implies the possibility of prognosis of the technical state and treating the value of this energy as a measure of the progress of the construction material fatigue damage is possible to predict its durability.

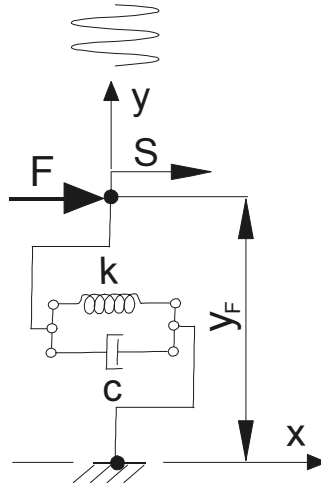


Fig. 5 A simplified model of bending of the sample

$$c \cdot \dot{s}(t) + k \cdot s(t) - F(t) = 0 \quad (6)$$

$$E = \sum_{i=1}^n c \cdot \frac{\dot{s}(t_i) + \dot{s}(t_{i+1})}{2} \cdot (s(t_{i+1}) - s(t_i)) \quad (7)$$

where: s - strain, F - load, E - energy dissipated, k – stiffness (constant), c – damping (constant).

Conclusions

A wide range of methods for analyzing material fatigue with the use of different signals have been discussed in literature [2, 6, 7 8]. This study proposes an original method for analyzing the wear of construction materials using a neodymium fatigue testing machine. Sample vibrations are induced by neodymium magnets mounted on rotating discs. The presented machine was used in preliminary research to determine the correlations between fatigue strength and vibration signals generated by samples. Machinery and equipment should be treated as working systems transforming energy into useful one and dissipated, which is accumulated in the object as a result of various wear processes. The theory of machines as the power processor of a finite potential of destruction (i.e., storage of internally dissipated energy), implies the possibility of prognosis of the technical state but provided there is a quantitative description of the destruction, both in terms of "initial capacity" of this potential and its current status.

A patent application has been submitted to the Patent Office for the discussed machine, described as "Device for non-contact fatigue testing of construction materials", application No. P393316 of 16 December 2010.

Acknowledgment

This study was performed as part of research project N N504 087238 financed by the Ministry of Science and Higher Education.

References

- [1] C. Cempel, *Holistic models of degradation processes in mechanical systems – an outline*, DIAGNOSTYKA'29, 2010.
- [2] G. Franco, G. Marannano, A. Pasta and G. Virzi Mariotti, *Design and use of a Fatigue Test Machine in Plane Bending for Composite Specimens and Bonded Joints*, Advances in Composite Materials - Ecodesign and Analysis, March 2011.
- [3] M. Leonowicz, J. Wysocki, *Współczesne magnesy. Technologie, mechanizmy koercji, zastosowania*, Wydawnictwa Naukowo-Techniczne 2011.
- [4] J. Szala, D. Boroński, *Ocena stanu zmęczenia materiału w diagnostyce maszyn i urządzeń*, Wydawnictwo Instytutu Technologii Eksploatacji – PIB, Bydgoszcz 2008.
- [5] W. Borkowski, S. Konopka, L. Prochowski, *Dynamika maszyn roboczych*. Wydawnictwo Naukowo-Techniczne. Warszawa 1996.
- [6] Ch. Lalanne, *Fatigue Damage: Mechanical Vibration and Shock Analysis*, Volume 4, Second Edition, Published Online: 27 JAN 2010.
- [7] R. C. McCLUNG, *A literature survey on the stability and significance of residual stresses during fatigue*, Fatigue & Fracture of Engineering Materials & Structures, Volume 30, Issue 3, pages 173–205, March 2007.
- [8] Xue H.Q. a,d, Bayraktar E., *Torsional fatigue behaviour in gigacycle regime and damage mechanism of the perlitic steel*, Journal of Achievements in Materials and Manufacturing Engineering, VOLUME 31 ISSUE 2, December, 2008.

A SEMANTIC SEARCH ENGINE IMPLEMENTED WITH OPEN SOURCE

S.A. Cristescu¹, F. Moldoveanu²

¹ Leeuwenstraat 43, 5645 BA, Eindhoven, Netherlands

² Splaiul Independentei 313, Sector 6, Bucharest, Romania

Keywords: semantic web, ontology, semantic search engine

Abstract. The sheer amount of information online makes it difficult to bring any structure and semantics to it. The Semantic Web initiative deals with such issues, but it is still far from producing concrete results. In the area of web services there is some progress, consisting mostly in annotating the WSDL descriptions of the services with semantic concepts. This paper proposes a semantic search engine as a tool able to register (index) annotated web services and semantically search them based on properties such as inputs, outputs, preconditions and effects. We describe the main building blocks of such a semantic search engine and also propose to use open source tools to implement it.

Introduction

SAWSDL [1] is a standard for annotating web services with semantic information. The research [2] in the area of *semantic* registration of services focuses on UDDI [3] extensions based on SAWSDL annotations, with the purpose to make the services discoverable, in order to be consumed by their clients. However, UDDI lost its support from the companies that created the standard in the first place. Thus, it's time for something new, which addresses the limitations of UDDI, namely:

- overwhelming complexity
- ignoring security
- lack of good tooling

The authors of this paper propose a *semantic search engine* as a tool able to index the semantic web services, that is, register the services (thus replacing UDDI), while at the same time enabling true semantic discoverability of the services. Such a semantic search engine is not supposed to be used directly by humans (as opposed to the Google search engine, for example), even though extensions to make it usable for such a purpose are possible. The scenarios we consider here are those in which other web services, software agents or other software clients use the semantic search engine in order to semantically look up a service and invoke it. This orchestration of services based on their meaning (semantics) rather than syntax opens up true interconnectivity among institutions in various domains, such as the medical domain, with the ultimate goal of improving the quality of the medical act.

Let's take as an example the following use case: a person is on holidays in a foreign country and suffers a heart attack. He is unconscious and unable to alert the medical service and there are no people in his immediate proximity. However, he wears an intelligent watch with an embedded *software agent* that recognizes the patient's medical condition and autonomously alerts the local *emergency service*. This service is implemented as a *semantic web service*, as opposed to a regular, syntax-based, service. This enables the service to express its operations with their inputs and outputs linked to certain well-defined ontologies, in order to be able to communicate meaning rather than text to its clients. For example, the patient's agent will send the patient's symptoms expressed in an ontology based on HL7 RIM [4] and the patient's geographical coordinates based on another, well known, geographic ontology. The semantic web service then understands these ontologies or is able to translate the concepts to well-understood ontologies (process called *ontology matching or mapping*) and answers appropriately to the patient's agent, i.e. by sending an ambulance to the patient's location with a defibrillator prepared to resuscitate the patient.

In such scenarios, searching web services based on semantics rather than on plain text is critical in finding the right information and properly orchestrating workflows of interactions among web services and other pieces of software.

Requirements

In this section we refer to the requirements for such a semantic search engine. The essential characteristics of our search engine should be:

1. simplicity – it should offer a simple, clear to use interface through which either a user or a program can search and find the desired services
2. it should offer a secure way to access a web service
3. it should offer APIs to be able to register and discover (semantic) web services
4. it should be scalable to millions of simultaneous users and yet answer within a few hundred milliseconds – like the Google search engine behaves nowadays

Semantic search means looking for registered concepts (the *“advertised profile”*) that can be matched semantically to some given concepts (the *“requested profile”*). Typically we want more than just matching within the same ontology. We are looking for matching across ontologies, i.e. ontology mapping. Restricting ourselves to the same ontology is too drastic and it means rejecting many potential matches. However, in this paper we'll not detail the ontology mapping, but rather describe generically the architecture and the algorithm of the semantic search engine.

Software components (e.g. agents or other services) search semantic web services in order to consume them. These services are deployed on their respective websites, as usual. We consider only the semantically annotated services, namely those that have their inputs, outputs (potentially also preconditions and effects) annotated with ontology information, based on the SAWSDL standard [1]. The more service attributes are annotated with semantic information, the better will be the semantic match.

A semantic search engine needs to fetch the semantic web services' descriptions and index them. The semantic search engine should answer queries with a list of matching services, in the decreasing order of matching degree. This implies that a measure for semantic matching has to be defined, so that the results are sorted properly. Basically, matching services means matching their respective

inputs and outputs (potentially also their preconditions and effects), as defined by the WSDL descriptions. Here we'll use a three-fold semantic distance definition:

1. textual match, where the input/output concept in the requested profile is textually identical to a concept offered by the service (i.e. in an advertised profile), e.g.:
<http://www.w3.org/2002/ws/sawsdl/spec/ontology/purchaseorder#OrderRequest> (both the namespace and the concept name are identical)
2. semantic match based on the *covariance* principle: if the requested profile's *input* is a subclass of the advertised service's input, they match; intuitively this means that if an advertised service can deal with a certain concept, it can also deal with its derived concepts, since they are just restrictions of the original concept; conversely, for outputs we apply the *contravariance* principle: if an advertised service outputs a certain concept, we can never require a more restrictive version (i.e. a subclass) of that; only a superclass of that concept will match
3. semantic match based on the *Tversky semantic similarity* [5]; roughly speaking, the Tversky semantic similarity between two concepts A and B is defined as the number of common properties divided by the total number of properties of concept B; the result is a number between 0 (completely different concepts) and 1 (identical concepts); interestingly, the Tversky similarity also works for concepts from different ontologies

The semantic search engine proposed in this paper needs to be scalable, fault-tolerant, available, reliable, maintainable, etc. In short, it needs to have all the abilities of a traditional, openly used search engine. Also, the speed of reaction (the performance measure of the search engine) is expected to be comparable to the current non-semantic search engines.

Search Engine Design

Fig. 1 shows the building blocks of the proposed semantic search engine. The three main functions of a search engine are covered by the blocks Crawler, Indexer and Searcher.

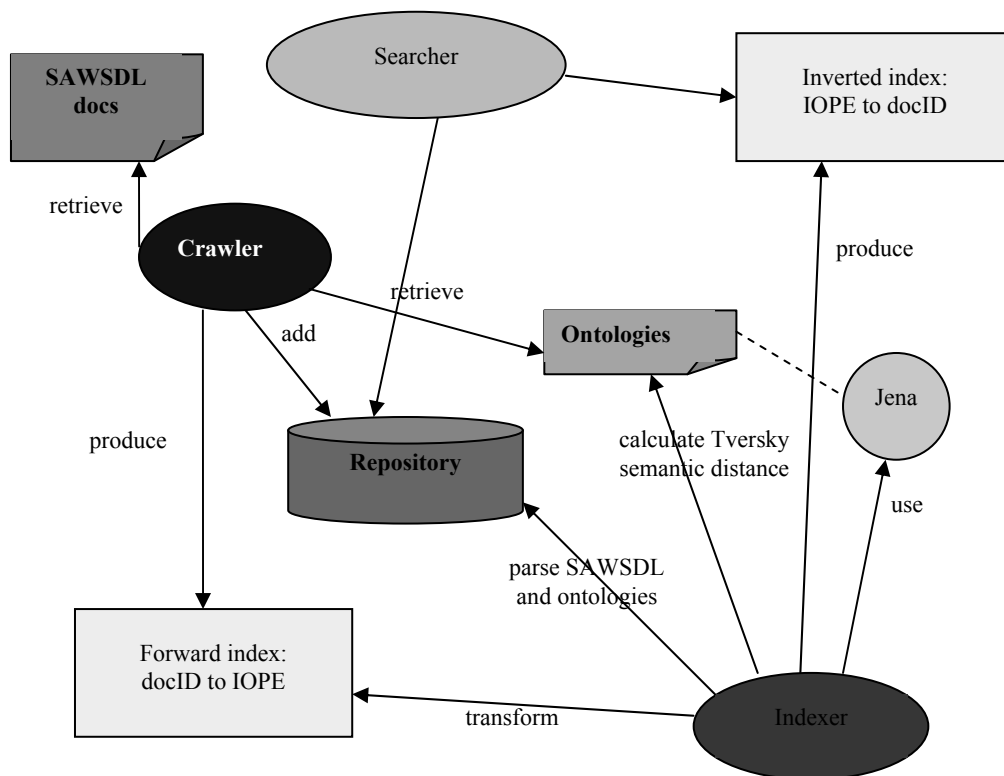


Fig. 1 The building blocks of the semantic search engine

Crawlers

We've implemented our prototype using Crawler4j [6], a Java open source implementation of crawlers. We've programmed our crawlers to retrieve WSDLs from various websites, such as <http://www.service-repository.com>. However, note that most of the service repositories online don't contain annotated WSDL (such as SAWSDL). Thus, we feed the crawlers manually with SAWSDL files. Note also that the SAWSDL pages typically don't have links to other SAWSDL pages (as it is the case with regular web pages). However, the crawlers parse the SAWSDL pages looking for ontologies, pointed to by *sawsdl:modelReference* attributes. Then they also retrieve the ontology pages. Every file retrieved by a crawler is persisted to a repository.

For parsing SAWSDL, originally we used SAWSDL4J [7]; it can parse WSDL 1.1 files, but it doesn't seem to parse *wSDL:types*, so we dropped it for Apache Woden [8] combined with some extensions for SAWSDL. With this we can parse WSDL 2.0 files, which is good enough for demonstration purposes. However, in the real world we need to be able to parse both WSDL 1.1 and 2.0. Luckily, one of the latest Woden versions comes with a convertor from WSDL 1.1 to 2.0, which we use in our prototype.

The alternative is to write an own parser from scratch, potentially using C with yacc and flex for performance reasons. This is one of the future steps.

Notably, the crawlers perform an important step that is in fact typical for indexers: since they need to parse the WSDL documents, they also extract the SAWSDL annotations for inputs, outputs, preconditions and effects (IOPEs) of the services and store them in the repository. A SAWSDL annotation of an input might look like this:

```
<xsd:complexType base="xsd:string" minOccurs="1" use="optional">  
  <value>http://www.hl7.org/spec /ontology/rim#Patient</value>  
</xsd:complexType>
```

The crawlers also gather the ontology files referred to by the SAWSDL annotations (e.g. the file at <http://www.hl7.org/spec/ontology/rim> in the example above) and store them in the repository. The next section describes the organization of data in the repository.

Repository

The *forward index*, containing the mapping between the WSDL files (expressed as unique document IDs) and the IOPEs is built by the crawler and persisted to the repository.

For our prototype implementation, our initial intention was to use Apache Hadoop – in fact the so-called HDFS (Hadoop Distributed File System) – as repository. Among the remarkable features of HDFS, *data distribution and replication* on nodes in a cluster would be very helpful for a full-blown search engine. Namely, using replication in a cluster of distributed machines increases the availability and the scalability of the data store, two of the most important characteristics of a search engine repository.

However, because of immature tooling and too little support, we've dropped Hadoop in favor of InfinityDB. The engine of the InfinityDB is based on an advanced *B-tree* data structure, which allows fast, reliable, memory-efficient data storage. In fact the very purpose of a B-tree is to implement indexes in a repository, such as to *minimize the disk access*, basically the bottleneck in read/write operations with the repository. The issue with InfinityDB was that we couldn't even get a trial version, since we've got not answer to our request from the InfinityDB team. However, the B-tree data structure stays as the basis for our design too.

Finally, we've chosen BerkeleyDB [9] for our prototype implementation of the repository and indexes. BerkeleyDB is an Oracle product that can be used for free for non-commercial purposes. Its architecture is based on storing (*key, value*) pairs in efficient data structures (e.g. B-trees), providing high concurrency and speed along with simplicity in programming. It supports ACID transactions and offers support for *replication*, enhancing thus the availability and scalability of the data store. These characteristics make it a good candidate for implementing the repository and the indexes in a search engine system.

The WSDL files and the ontology files they point to (either RDF or OWL files) are all persisted to repository in a compressed format (zlib, which offers a good tradeoff between performance and compressed size).

Indexers

The WSDL pages are already parsed by the crawler and their IOPE annotations stored in the repository, so the work of the indexer becomes substantially easier.

The indexer needs to build the following indexes:

- one for the ontologies: we need to find each ontology file fast
- one for the inputs of the services: the inputs need to be matched efficiently
- similarly, we need one index for the outputs, one for the preconditions and one for the effects

The indexer takes the forward index (created by the crawler) and creates the four inverted indexes for inputs, outputs, preconditions and effects. The indexer also performs a task that speeds up the searcher: for each Input/Output, it creates a list with the concepts from the same ontology as the current Input/Output, ordered decreasingly by the Tversky semantic similarity to this Input/Output.

All these data structures are stored in our BerkeleyDB repository, as tuples, e.g. $\langle \text{Input1}, \langle \text{list of document IDs where it occurs} \rangle \rangle$. Internally, BerkeleyDB uses highly efficient B-trees to represent the indexes.

Searcher

Given a certain *requested profile* (IOPEs), the searcher tries to find the best match among the advertised services. In order to perform its algorithm, the searcher first accesses the in-memory indexes created by BerkeleyDB, which are stored as B-trees. By using the in-memory B-trees, the disk accesses are minimized. This is utterly important for the searcher, the component for which performance is the single most important characteristic. Note also that the searcher uses the pre-computed Tversky similarity to optimize the selection of the best-matching service.

The search algorithm is based on the three-fold semantic distance definition we gave above. In the first instance, a textual match of the inputs, outputs (preconditions and effects too, if they exist) is performed. If there is a match, the algorithm stops. If not, a match based on the covariance principle (for inputs) and contravariance principle (for outputs) is performed. If there is no match, the algorithm tries a match based on the Tversky similarity between the concepts and it stops when it finds a match with a score above a certain, predefined threshold. The match finds the document IDs (of the WSDL files) that correspond to the searched inputs, outputs, preconditions and effects, respectively. Then the searcher intersects these lists of document IDs in order to find those advertised WSDLs that correspond to the required profile.

The performance of the search algorithm is exceptionally important for any real-world application. While the crawling or indexing steps are running behind the scenes and are not accessed real-time by clients, the search step is the "face to the client", thus its complexity is extremely important.

The search algorithm has a few driving forces:

- the lookup steps: looking up outputs and inputs in the indexes; since the indexes are B-trees, the complexity of a lookup step is $O(\log_M(N))$, where M is the degree of the tree and N is the number of indexed inputs/outputs
- there are two nested lookup steps: one where we test all subclasses/superclasses of outputs/inputs and the other where we test all other classes in the same ontology (using the Tversky semantic similarity); this means the total complexity of the nested lookups is $O(P * \log_M(N))$, where P is the ontology (where the inputs/outputs are found) size in terms of number of concepts



Conclusion

In this paper we argue that instead of using UDDI for service registration and extending it such that it is able to work with semantic information, we propose the design and implementation of a search engine able to register and retrieve semantic web services.

As with a regular search engine, a semantic one involves crawlers for retrieving the semantically annotated services, an efficient repository for storing them, an indexer to index the services and a searcher which retrieves the matching services using the indexes.

There are a few assumptions made by the design of our semantic search engine:

- we only consider SAWSDL files that describe web services; SAWSDL is a standard that extends the WSDL descriptions with semantic information
- matching web services means matching of their inputs, outputs, preconditions and effects (IOPes)

We have implemented a prototype based on open source tools that illustrates the semantic search engine with its components: crawlers, repository, indexer and searcher. The single most important bottleneck is the disk access necessary for the searcher to match the required profile. However, with the highly efficient BerkeleyDB implementation of the repository, based on B-trees, retrieving a record out of 100000 is a matter of 20-30 milliseconds. On the same machine, a classic SQL select operation from a relational database of similar size takes an order of magnitude longer.

References

- [1] SAWSDL – Semantic Annotations for WSDL and XML Schema, <http://www.w3.org/TR/sawSDL/>
- [2] D. Kourtisis, I. Paraskakis: Combining SAWSDL, OWL-DL and UDDI for semantically enhanced web service discovery, *ESWC'08 Proceedings of the 5th European semantic web conference on the semantic web: research and applications*, p. 614-628
- [3] UDDI Version 3.0.2 - http://uddi.org/pubs/uddi_v3.htm
- [4] HL7 – Health Level 7, <http://www.hl7.org/>
- [5] J. Cardoso, J. A. Miller, S. Emani: Web Services Discovery Utilizing Semantically Annotated WSDL, *Reasoning Web LNCS 5224*, C.Baroglio et al, Springer Berlin / Heidelberg, Volume 5224/2008, p. 240-268
- [6] Crawler4J, an open source crawler: <http://code.google.com/p/crawler4j/>
- [7] SAWSDL4J, <http://lsdis.cs.uga.edu/projects/meteor-s/opensource/sawSDL4j/>
- [8] Apache Woden, <http://ws.apache.org/woden/>
- [9] BerkeleyDB, <http://www.oracle.com/technetwork/products/berkeleydb/overview/index.html>

MODEL OF THE FERROSILICON MELTING PROCESS IN THE SUBMERGED ARC FURNACE

B. Machulec¹, W. Bialik²

¹ Silesian University of Technology, 40-019 Katowice, Krasińskiego 8, Faculty of Material Science and Metallurgy, Poland,

² Silesian University of Technology, 40-019 Katowice, Krasińskiego 8, Faculty of Material Science and Metallurgy, Poland,

Keywords: Ferrosilicon Process, FeSi75, Submerged Arc Furnace, Model, Gibbs Minimization Method

Abstract. Based on the minimum Gibbs Free Enthalpy algorithm (FEM), a model of the reaction zones located around electrode tips in the ferrosilicon submerged arc furnace has been presented. In the calculations, new opportunities created by the HSC software package which enables the use of a thermochemical database and equilibrium calculations directly in the Excel spreadsheet have been utilized. The model of the ferrosilicon process in the submerged arc furnace is a system of two closed isothermal reactors: an upper one with a lower temperature T_1 , and a lower one with a higher temperature T_2 . Between the reactors and the environment as well as between the reactors inside the system, a periodical exchange of mass occurs at the moments when the equilibrium state is reached. The condensed products of chemical reactions move from the top to the bottom, and the gas phase components move in the opposite direction. It can be assumed that in the model, the reactor 1 corresponds to the charge zone of submerged arc furnace where heat is released as a result of resistive heating, and the reactor 2 corresponds to the zones of the furnace where heat is produced by electric arc. Based on the model, the balances of heat and mass as well as the relations between temperature conditions of the reactors and the efficiency of the ferrosilicon process have been determined. Using the model, technical and economic indices of the ferrosilicon process have been identified and a good agreement with the industrial data has been obtained.

Introduction

For a fixed composition of the initial reaction mixture and set conditions of temperature and pressure ($T, P = \text{const}$), the equilibrium composition of the system is the most stable and corresponds to the minimum Gibbs Free Enthalpy. The non-stoichiometric algorithm of the Gibbs Free Energy Minimization Method (FEM) is obtained through solving the nonlinear optimization problem with limitations resulting from the mass balances of individual elements that constitute the system in which the objective function is:

$$\min_n \frac{G(T, P, \mathbf{n})}{RT} \quad (1)$$

where:

$G(T, P, \mathbf{n})$ – Gibbs free enthalpy function,

$\mathbf{n} = (n^1, n^2, \dots, n^f)$,

$\mathbf{n}^r = (n_{1r}^r, n_{2r}^r, \dots, n_{kr}^r)$

\mathbf{n}^r - vectors whose elements are numbers of moles of the various phase r components ,

$r = 1, 2, \dots, f$,

f – a number of phases constituting the system,

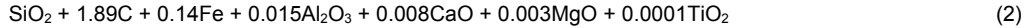
R - gas const.

This algorithm requires delivery of input data of the initial reaction mixture composition, parameters of the process (T, P) and a list of components that may appear in the equilibrium composition of the specific reaction system phases. This approach does not specify the chemical reactions or stoichiometric equations. The analysis of thermodynamic carbon reduction of silica with the use of the FEM algorithm was a subject of many publications [3]-[4], but new opportunities have emerged due to inclusion of an appendix to the HSC 6.1 thermochemical software that allows for the use of a thermochemical database and solution of the FEM problems directly in the Excel spreadsheet.

Model of the Ferrosilicon Process

Based on the FEM algorithm, a model of the reaction zones located around electrode tips in the ferrosilicon submerged arc furnace was presented. The model is an extension of earlier models and concepts described in the publications [1] - [4]. It is a system of two closed isothermal reactors: an upper one with a lower temperature T_1 , and a lower one with a higher temperature T_2 (Fig. 1). Between

the reactors and the environment as well as between the reactors inside the system, a periodical exchange of mass occurs at the moments when the equilibrium state is reached in the reactors. In each cycle, a reaction mixture with the molar composition corresponding approximately to the batch mixture of raw materials for the ferrosilicon smelting process is fed into the upper reactor:



At the same time, the condensed products of chemical reactions move from the top to the bottom, and the gas phase components move in the opposite direction. Simulation of the continuous ferrosilicon smelting process was implemented recursively.

In Cycle 1, a portion of the mixture (2) is fed into the upper reactor where the reactions take place until the equilibrium state at the temperature T_1 is reached. Then, the gas-phase products leave the reactor 1 and after cooling to the temperature $T_w = 850^\circ\text{C}$, they do not participate in the further process. Simultaneously, the products of condensed phases of the reactor 1 flow down and are introduced into the reactor 2 where they react with each other until the equilibrium at the temperature T_2 is reached. Then, the condensed phase products leave the reactor 2 and, after cooling to the temperature T_1 , form a metallic and slag phase and do not participate in the further process. The gas phase products with the equilibrium composition leave the reactor 2 and, after cooling to temperature T_1 , they are introduced back into the reactor 1 where they react to reach the equilibrium state again at the temperature T_1 . Once the reactor 1 reaches the equilibrium, the gas phase products leave the reactor and after cooling to temperature T_w , they do not participate in the further process. The products of condensed phases remain in the reactor 1 and take part in the reactions of the next cycle. Cycle 2 and each next cycle of the reaction system start with an introduction of a new portion of the reactants (2) to the reactor 1. They react together with the other condensed components of the previous cycle until the equilibrium is reached at the temperature T_1 . In the subsequent cycles, the process is the same as in Cycle 1. In the real ferrosilicon process, the temperature T_w corresponds to the temperature of gases that are byproducts of the silica reduction process measured immediately after leaving the furnace charge surface.

Using the HSC 6.1 thermochemical database, it was found that within the temperature range of 1500 to 2500 $^\circ\text{C}$, five phases in the Fe-Si-O-C-Al-Ca-Mg-Ti system with 192 components might occur. Due to a large number of components, Table 1 presents only 53 components of specific phases limited to the Fe-Si-O-C system.

Table 1. The components of specific phases of the Fe-Si-O-C system

Phase1	C(g)	C ₂ (g)	C ₃ (g)	C ₄ (g)	C ₅ (g)	C ₆ O(g)	CO(g)
	CO ₂ (g)	C ₃ O ₂ (g)	Fe(g)	Fe ₂ (g)	Fe(CO) ₅ (g)	FeO(g)	FeO ₂ (g)
	O(g)	O ₂ (g)	C ₂ O(g)	O ₃ (g)	Si(g)	Si ₂ (g)	Si ₃ (g)
	Si ₄ (g)	SiC(g)	SiC ₂ (g)	Si ₂ C(g)	SiO(g)	SiO ₂ (g)	Si ₂ O ₂ (g)
Phase2	FeCO ₃	Fe(CO) ₅	Fe ₂ (CO) ₉	Fe ₃ (CO) ₁₂	Fe _{0.945} O	Fe _{0.947} O	FeO
	FeO _{1.056}	Fe ₂ O ₃	Fe ₃ O ₄	Fe ₃ O ₄	FeO*SiO ₂	2FeO*SiO ₂	FeSiO ₃
	SiO ₂						
Phase3	C						
Phase4	SiC						
Phase5	Fe ₃ C	Fe	FeSi	FeSi ₂	FeSi _{2.33}	FeSi _{2.43}	Fe ₃ Si
	Fe ₅ Si ₃	Si					

It can be assumed that in the model, the reactor 1 corresponds to the charge zone of submerged arc furnace where heat is released as a result of resistive heating, and the reactor 2 corresponds to the zones of the furnace where heat is produced by electric arc. Using the macros developed independently in the Excel Visual Basic, a series of simulation calculations in a spreadsheet was performed. For each cycle, the equilibrium composition of phases of the reaction system as well as the mass and energy balances were determined. The heat balance of the process includes the following components:

$$Q_w = \Delta H_{298}^{T_1} + \Delta H_{T_1}^{R_1} + \Delta H_{T_1}^{T_2}(m_1) + \Delta H_{T_1}^{T_w}(g_1) + \Delta H_{T_2}^{T_1}(g_2) + \Delta H_{T_1}^{R_1}(g_2) + \Delta H_{T_1}^{T_w}(g_2) \quad (3)$$

$$Q_{arc} = \Delta H_{T_2}^{R_2} + \Delta H_{T_2}^{T_1}(m_2) \quad (4)$$

$$Q = Q_w + Q_{arc} \quad (5)$$

where:

$\Delta H_{298}^{T_1}$ – enthalpy change of the substrates (2) during heating from the ambient temperature to the temperature T_1 , (kJ/mol),

$\Delta H_{T_1}^{R_1}, \Delta H_{T_2}^{R_2}$ – thermal effect of reactions in the reactor 1 and 2, respectively, (kJ/mol),

$\Delta H_{T_1}^{T_2}(m_1)$ – enthalpy change of the condensed phases during heating while passing from the reactor 1 to the reactor 2, (kJ/mol),

$\Delta H_{T_2}^{T_1}(g_2) + \Delta H_{T_1}^{R_1}(g_2)$ - enthalpy change of the gas phase during cooling while passing from the reactor 2 to the reactor 1 and the thermal effect of the condensation reactions in the reactor 1, (kJ/mol),

$\Delta H_{T_1}^{T_w}(g_1), \Delta H_{T_1}^{T_w}(g_2)$ - enthalpy change of the gas phase products after leaving the reactor 1 and cooling to the temperature T_w , (kJ/mol)

$\Delta H_{T_2}^{T_1}(m_2)$ – enthalpy change of condensed phases after leaving the reactor 2 and cooling from the temperature T_2 to T_1 , (kJ/mol)

The components Q_w , Q_{arc} of the heat balance characterize distribution of heat in the reaction zones of the ferrosilicon submerged arc furnace. The component Q_w corresponds to the charge zones where heat release results from resistive heating and the Q_{arc} corresponds to gas chambers localized around the electrode tips where heat is released as a result of arc heating. The distribution of heat in the ferrosilicon process can be characterized by percentages Q_1 , Q_2 related to Q_w and Q_{arc} as follows:

$$Q_1 = 100 \cdot \frac{Q_w}{Q}, \quad Q_2 = 100 \cdot \frac{Q_{arc}}{Q}, \quad \% \quad (6)$$

Based on the mass and energy balances of the process, the theoretical Si yield and the specific energy consumption rate E were determined:

$$E = \frac{1000 \cdot Q}{3.6 \cdot \eta \cdot m} \quad , kWh/t \quad (7)$$

where:

- m – weight of the metallic phase leaving the reactor 2, $\frac{kg}{kmol} SiO_2$
- η – factor related to the thermal efficiency of the furnace, $\eta \approx 0.88$
- 3.6 – energy unit converter, $1kWh = 3.6MJ$

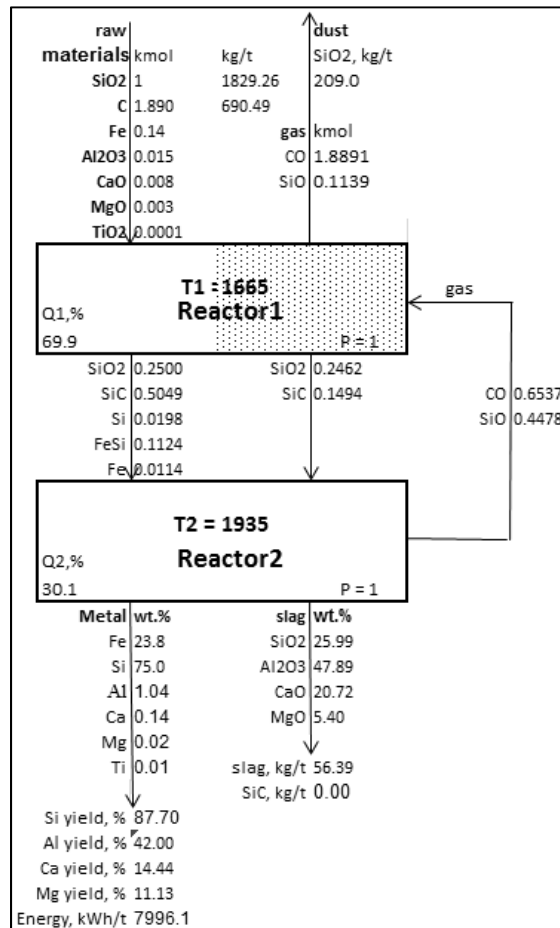


Fig. 1 The results of calculations for a physicochemical model of the ferrosilicon process with two isothermal reactors after 50 cycles. The system Fe-Si-O-C-Al-Ca-Mg-Ti, the reaction mixture (2), $T_1 = 1665 \text{ }^\circ\text{C}$, $T_2 = 1935 \text{ }^\circ\text{C}$, $P = 1$ bar.

The model shows that the most favorable conditions for the silica reduction process with the reaction mixture (2) are as follows: $T_1 = 1665 \text{ }^\circ\text{C}$, $T_2 = 1935 \text{ }^\circ\text{C}$, and the heat percentage $Q_1 = 69.9\%$. Under such conditions, the Si yield in the metallic phase of the reactor 2 stabilizes after about 20 cycles and the reaction system reaches a steady state (Fig. 2). The results of calculations for a model simulating the smelting ferrosilicon process are shown in Fig. 1.

The reactor 2 temperature ($T_2 = 1935 \text{ }^\circ\text{C}$) is the temperature at which the Si yield of the reduction silica process is the maximum for the given temperature $T_1 = 1665 \text{ }^\circ\text{C}$. In the reactor 1, processes of SiC formation through a reaction of silica with carbon and condensation reactions of SiO gas oxide to SiC mainly occur. In the reactor 2, processes of SiO gas generation and silicon metal production through reduction of silica with SiC carbide take place. Table 2 shows the heat balance of the process. According to the relationships (2-6), the components of energy demand Q_w , Q_{arc} in the reactors 1 and 2 as well as the percentages Q_1 , Q_2 that

characterize the distribution of the heat flux in different zones of the reaction system were calculated and the specific energy consumption E was determined.

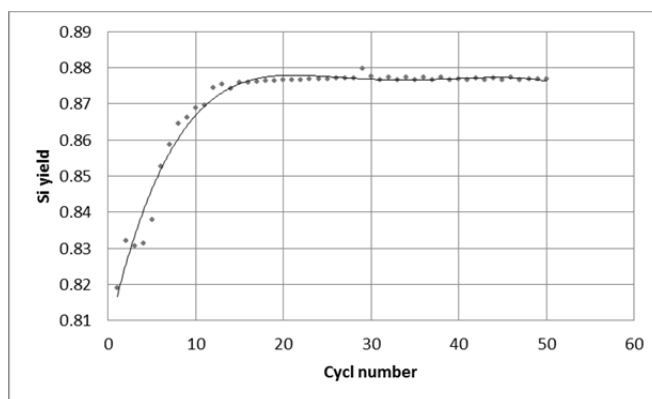


Fig. 2 The Si yield in the metallic phase of the reactor 2 in subsequent cycles of the process, the reaction mixture (2), $T_1 = 1665\text{ }^\circ\text{C}$, $T_2 = 1935\text{ }^\circ\text{C}$ $P = 1\text{ bar}$

$T_1 =$

Table 2.

The heat balance of the process after 50 cycles, $T_1 = 1665\text{ }^\circ\text{C}$, $T_2 = 1935\text{ }^\circ\text{C}$, $P = 1\text{ bar}$, the reaction mixture (2)

No.	The component of the heat balance	kcal/mol	MJ/kmol	kWh/kmol	kWh/t	Part, %
1	Heating to a temp. T_1 and the thermal efekt of the reactions in the reactor 1	152.68	638.83	177.452	5402.52	Q_1
2	Cooling of gas leaving the reactor 1 to a temperature of $850\text{ }^\circ\text{C}$	-13.77	-57.62	-16.006		
Summary heat efect (3), Q_w		138.91	581.21	161.45	4915.21	69.85
6	Heating from temp. T_1 to T_2 and thermal efect of the reactions in the reactor 2	114.47	478.94	133.04		Q_2
7	Cooling of gas leaving the reactor 2 and its condensation in the reactor 1	-52.28	-218.74	-60.76		
8	Cooling of metal and slag phase from the temperature T_2 to T_1	-2.2366	-9.36	-2.60		
Summary heat efect (4), Q_{arc}		59.95	250.85	69.68	2121.39	30.15
Summary energy consumption (5), $Q = Q_w + Q_{arc}$		198.87	832.05	231.13	7036.61	100
Specific energy consumption, $E = Q/\eta$, $\eta = 0.88$					7996.15	

Conclusion

The model allows for the explanation of many characteristic states of the ferrosilicon smelting process in the submerged arc furnace. It also allows for the determination of the effects of temperature conditions in charge zones and arc zones of the furnace on the electro-thermal silica reduction process. The calculation results for the Si yield and the specific energy consumption show a good agreement of the model and the industrial data for the ferrosilicon FeSi75 process [5].

Acknowledgment

This work has been financially supported by Polish MNiSW, project No 4688/B/T02/2009/36 of 2009-03-09.

References

- [1] Schei A., Tuset J.Kr., Tveit H.: Production of High Silicon Alloys, Trondheim, 1998 r., ISBN 82-519-1317-9,
- [2] Batra N.K.: Modelling of ferrosilicon smelting in submerged arc furnace, Iron and Steelmaking, 2003, Vol.39, nr 5, s.399-404,
- [3] Eriksson G., Johansson T.: Thermodynamic Studies of Chemical and Thermal Equilibrium Calculations for a Quantitative Discription of a Non-Isothermal Reactor with Application to the Silicon Arc Furnace, Scandinavian Journal of Metallurgy, 1978, Nr 7, s.264-270
- [4] Machulec B.: Teoretyczne podstawy procesu elektrotermicznego wytopu żelazokrzemu oraz krzemu technicznie czystego, Politechnika Śląska, Zeszyty Naukowe, Nr 1589, Gliwice, 2003
- [5] Dhananjaya Senapati, E.V.S Uma Maheswar, C.R. Ray: Ferro silicon operation at IMFA – a critical analysis, INFACON XI, Proceedings of the International Conference, New Delhi, India, 18-21 February 2007, s.371-380

PREDICTION OF ONSET OF EPILEPTIC SEIZURE BY ANALYSIS OF PRE-ICTAL STATE OF EEG

D.V.PRASAD¹, R.SWARNALATHA², and NATASHA GIRIDHAR³

¹ Associate Professor, BITS PILANI Dubai Campus, International Academic City, Dubai, UAE

² Assistant Professor, BITS PILANI Dubai Campus, International Academic City, Dubai, UAE

³ B.E (Hons), BITS PILANI Dubai Campus, International Academic City, Dubai, UAE

Keywords: Epilepsy, Ictal, Pre Ictal, Seizure and Entropy.

Abstract. Epilepsy is a neurological condition, which affects the nervous system. It is usually diagnosed after a person has had at least two seizures that were not caused by some known medical condition like alcohol withdrawal or extremely low blood sugar. The seizures in epilepsy may be related to a brain injury or a family tendency, but most of the time the cause is unknown. This paper explores the possibility of predicting onset of epilepsy analysing the pre Ictal state of EEG. Epilepsy can be understood as a series of unprovoked synchronous activities occurring in the brain. During epileptic attack all the synchronous activities are occurring together at the same time. Thus the signal will be more organized. During the normal state the signal will be a little more chaotic as compared to Ictal state. It was seen that during the Pre-Ictal state the brain activity is seen to be calmer and less chaotic. This shows increase in entropy. This was tested and confirmed in this paper. Prediction of epilepsy can be done on a small time window occurring before and epileptic seizure. This state called the Pre-Ictal State. The signal was tested for parameters like standard deviation, variance, power and entropy. These parameters have high values in pre Ictal state compared to Normal State and Ictal state. Thus by observing this kind of state we can predict the onset of epileptic seizure.

Introduction

The brain is the centre of all neuronal activities occurring in the body. It has neurons which carry impulses from one part to the other. When these impulses are unprovoked impulses they result in seizure. Thus epilepsy is nothing but a series of unprovoked synchronous activity occurring in the brain. Epilepsy is one of the most common of the neurological disorders, with a prevalence of about 1% of the population or 50 million persons worldwide [1]. Long-term EEG (LTEEG) monitoring is used to closely monitor patients over extended periods who have relatively infrequent but recurring atypical turns or seizures. LTEEG monitoring comprises continuous 19-channel EEG and video recordings over several days. The ability to detect seizures automatically in the EEG will substantially reduce the loss of valuable data due to the manual observation. A seizure is not primarily an electrographic pattern of characteristic morphology, but rather a behavioral event [2, 3]. This wide ranging electrographic morphology and, lack of clear EEG manifestations, can make some seizures very difficult to detect reliably. Visual analysis of EEG signals has some drawbacks. It is a time-consuming and subjective task. Furthermore, it is error-prone due to fatigue, etc. Therefore, automation of the detection of the underlying brain dynamics in EEG signals is significant in order to obtain fast and objective EEG analysis. Thus it is very important to predict the preictal state of the epileptic seizure. Evrim et al differentiated between seizure and non-seizure periods by representing multi-channel EEG signals using a set of features from both time and frequency domains. They evaluated the performance of our model considering both sensitivity and specificity. During epileptic attack all the synchronous activities are occurring together at the same time. Thus the signal will be more organized. During the normal state the signal will be a little more chaotic as compared to Ictal state. It was seen in a research that during the Pre-Ictal state the brain activities are calmer. Hence different activities will take place at different instant indicating an increase in entropy. This is tested in this research paper.

Methodology

The hypothesis of this work is that there exists a zone of significantly calm activity just before the onset of an epileptic seizure. If such a zone is identified then we can predict the onset of the seizure. The signal obtained was first tested at different intervals to detect the Normal State, Pre-Ictal State and Ictal State. In order to predict epilepsy we divided 18,432 samples into sample sizes of 200 and 500 and found out linear as well as non linear parameters like standard deviation, variance, power and entropy[1]. We have chosen one non linear (entropy)[2] and other linear parameters to get a more conclusive test. These values were plotted and 5 different categories were obtained: (1)Pre-Ictal values Highest ,(2) Pre-Ictal value lower than Normal but higher than Ictal (3) Pre-Ictal values lowest (4) Pre-Ictal values higher than Normal but lower than Ictal (5) Pre-Ictal value same as Ictal value. Then a group was made and 500 values before and after this sample. These were then also tested for the above mentioned parameters. The result were then stored in both tabular format and graphs both showing a difference in all the three states. The plots of the *highest entropy* of the Pre-Ictal state as compared to the other 2 states are shown in Fig.

The table for *sample size 500* is given below

Table 1 . Linear and Nonlinear Parameters of Sample Size 500

State	Std	Variance	Power	Entropy	Sample
Normal	15.52397	240.993653	47.622914	0.999928	5405:5905
Pre-Ictal	64.160763	4116.603497	72.277541	0.999974	8311:8811
Ictal	82.076457	6736.544822	76.551768	0.997904	11030:11530

Table2. Linear and Nonlinear Parameters of Sample Size 500

State	Std	Variance	Power	Entropy	Sample
Normal	16.520391	272.923329	48.717536	0.994173	6405:6905
Pre-Ictal	35.947369	1292.213373	62.22066	0.999974	9311:9811
Ictal	144.31255	20826.11244	86.354818	0.998203	12030:12530

Table3. Linear and Nonlinear Parameters of Sample Size 200

State	Std	Variance	Power	Entropy	Sample
Normal	13.687816	187.356318	45.487064	0.998553	6805:7005
Pre-Ictal	38.276447	1465.086418	63.280632	0.999125	9711:9911
Ictal	217.194065	47173.26199	93.431297	0.990534	12430:12630

Table4. Linear and Nonlinear Parameters of Sample Size 500 - Low

State	Std	Variance	Power	Entropy	Sample
Normal	16.586416	275.109206	48.773089	0.999974	5905:6405
Pre-Ictal	39.652312	1572.305868	63.915331	0.999997	8811:9311
Ictal	83.508824	6973.723713	76.851971	0.998479	11530:12030

Table 5: Linear and Nonlinear Parameters of Sample Size 500 - High

<u>State</u>	<u>Std</u>	<u>Variance</u>	<u>Power</u>	<u>Entropy</u>	<u>Sample</u>
Normal	13.328701	177.654283	44.976785	0.993089	6605:7105
Pre-Ictal	35.821715	1283.195289	62.156435	0.998732	9511:10011
Ictal	205.313934	42153.8116	92.479597	0.995164	12230:12730

Figure 1. Comparison of 500 samples of Normal, Pre-Ictal & Ictal

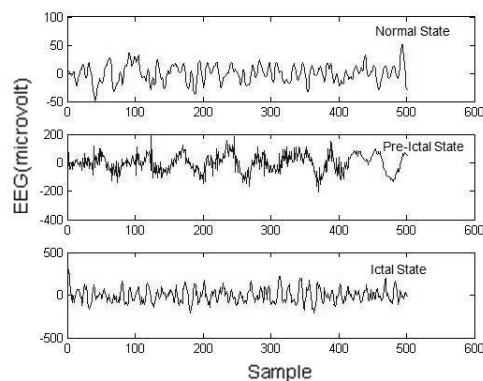


Figure 2: Comparison of 500 samples of Normal, Pre-Ictal & Ictal states

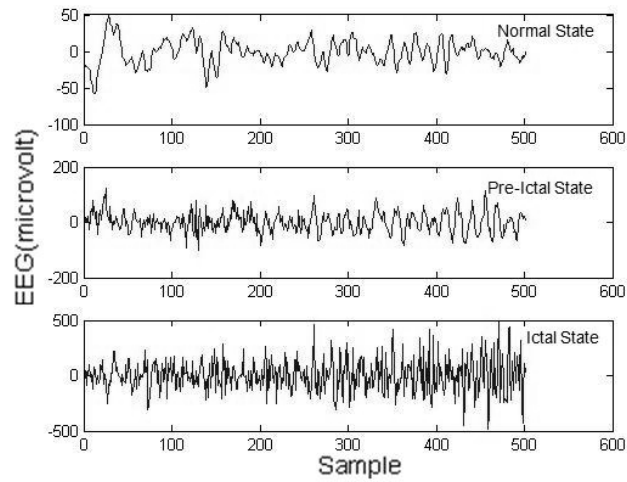


Figure 3: Comparison of 200 samples of Normal, Pre-Ictal & Ictal states

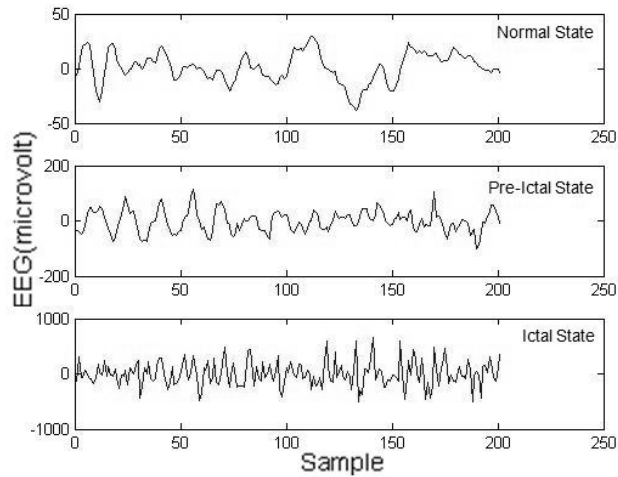


Figure 4: Comparison of 500 before and after samples of the 3 states - Low

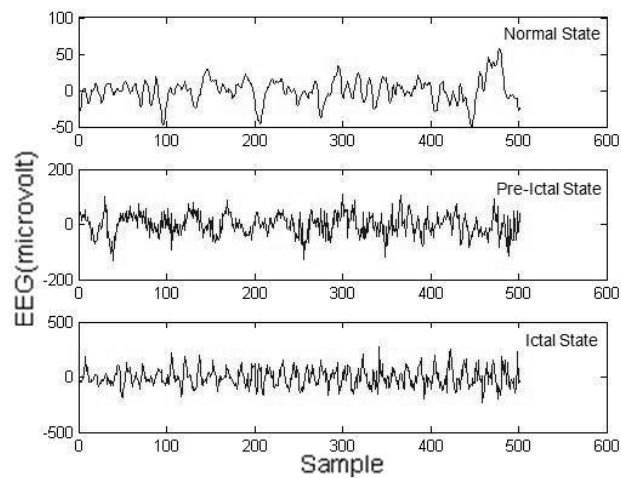
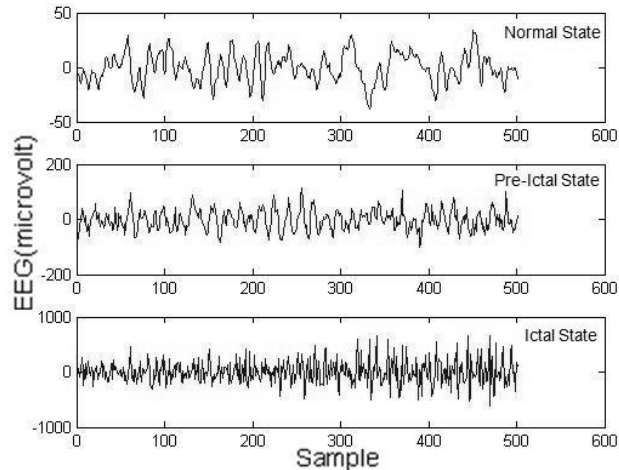


Figure 5. Comparison of 500 before and after samples of the 3 states - High



Conclusion

When the tables for sample size 500 were plotted it was seen that the values of Standard Deviation, Variance, and Power and Entropy of Pre-Ictal state showed a significant high in 4 of the 5 cases as compared to the Normal State. In the fifth case the value of the Pre-Ictal state was lower than that of Normal state but higher than that of the Ictal State. Further when the tables for sample size 200 were plotted it was seen that the values of the parameters varied differently. Out of 13 samples, 5 samples showed a significant high in Pre-Ictal state values as compared to Normal State. 5 samples showed the lowest values of Pre-Ictal State. 2 samples showed a Pre-Ictal value higher than Normal State but lower as compared to Ictal State and 1 sample showed that the value of the Pre-Ictal state was lower than that of Normal state but higher than that of the Ictal State.

To get a more perfect result the values of the same category were combined and 500 samples before this sample and 500 values after the sample were put in a table. A more conclusive result was obtained here. It was seen that out of 18 values, 10 values showed that the values of the Pre-Ictal State were high as compared to that of the Normal State. A few showed the rest of the categories. When the graphs for these samples were plotted it was seen that these values showed significant difference in the Normal, Pre-Ictal and Ictal state which can be seen. These results when put together proved that there a small sample size just before seizure where the signal shows some changes as compared to the Normal state. This change is abrupt. Since the values go relatively higher it can be proved that the signal undergoes a complete transition. During seizure the value of entropy is low because all the activities are occurring at the same time. During Pre-Ictal state the brain is suppose to be calmer as compared to the Normal state. This means that different activities are occurring at different a time which indicates a much a higher entropy. The values prove the same. Hence entropy can be used as a sure test to predict epilepsy. It could be conclusively seen that there was some significant change in the values just prior to the onset of epilepsy. This window though small can be hence used to predict the onset of epilepsy. The patient can thus be given necessary treatment well prior to epileptic seizure.

Acknowledgment

We are thankful to our Director, Prof. R.K.Mittal for providing me with all the facilities in pursuing this work.

References

- [1] Jozef Jansky, EEG: Basic Technology, Hungary, University of Pecs, Department of Neurology
- [2] L.A.Geddes and L.E.Baker, Principles of Applied Biomedical Instrumentation
- [3] Baowei Liu, Lanfeng Yan, Lan Li, Wei Wang, Comparing Study of Nonlinear Model for Epileptic Pre-Ictal Prediction.
- [4] .Laxman Tawade, Hemant Warpe , Detection of Epilepsy Disorder Using Discrete Wavelet Transforms Using MATLABs, International Journal of Advanced Science and Technology ,Vol. 28, March, 2011 17.
- [5] Atef Al-Mashakbeh, Analysis of electroencephalogram to detect epilepsy, International Journal of Academic Research Vol. 2. No.3. May 2010.
- [6] Maarten-Jan Hoeve et al, Automated Detection of Epileptic Seizures in the EEG,
- [7] Erika Molteni, Paolo Perego, Nicolette Zanotta, Gianluigi Reni, Entropy analysis on EEG signal in a case study of focal myoclonus, 30th Annual International IEEE EMBS Conference, August 20-24, 2008
- [8] R J Porter, "Classification of epileptic seizures and epileptic syndromes", A Text Book Of Epilepsy, \$th Ed, Churchill Livingstone, 1993.

TECHNOLOGY PLANNING OF HARD TURNING IN CASE OF ROTATIONAL FEED

J. Kunderák¹, K. Gyáni¹, I. Deszpoth and I. Sztankovics¹

¹ University of Miskolc, Department of Production Engineering; H-3515 Miskolc Egyetemváros

Keywords: hard turning, rotational turning

Abstract: Rotational turning is a subsequent variant of hard turning. Its abilities are not different from former hard turning; however it does not generate orderly periodical topography which is exceptionable in some cases of hard turned surfaces. Rotational turning cut with a long, oblique placed cutting edge contrary to the traditionally single-point cutting tools of turning. The skiving-like material removal is carried out with the slow rotation on a large diameter of the cutting edge and feed marks will not remain on the surface. The rotation angles of the initial-, the constant- and the running out phases must be known for the calculation of productivity and machining times. In our paper we define the rotation angles with exact solutions based on the geometrical conditions. After the geometrical assay was done we deduce the formulas of the exact solutions and we present on examples their main applications. After these the construction of the used tool, the applicable technological parameters, the expectable outgoing parameters of the process and the quality parameters of the workpieces are introduced. Finally we point out the unusual high productivity which is the highest among the other methods of hard turning and grinding.

1. Introduction

However hard turning is a young, not long-used method, there is a lot of experience accumulated about its great economical advantage and disadvantageous characteristics. A meaningful disadvantage is the generated surface topography which is not acceptable in certain cases. Intrinsically there are 3–4 sort of surface where the generated topography is disadvantageous in case of single-point tools: surfaces that are carrying sealings; the active internal and external surfaces of needle roller bearings; surfaces of synchronization cones in transmission and joint surfaces in free-running gears. In precision finishing of those surfaces technologists had to return to grinding because the grinded (so-called random) topography is acceptable in these applications. The return of grinding is disadvantageous in point of expenses even if it is done at high level. Intrinsically the importance of rotational turning is that the return to grinding is unnecessary because the rotational method makes a random grinding-like topography [1, 2, 3]. New machine tools are not necessary for the application of rotational turning because the needed tools can be hold in the turrets of hard turning lathes. The advantages of the method show up in machining external cylindrical surfaces (shafts) because that type of surface must be machined with rotational turning unlike other types of surfaces which can be machined with standard tools. This is because the use of the rotational method is practical only in this case due to the special designed and expensive tool. Since the same objective can be reached with various hard machining methods, the optimal selection among those is important which is suitable for the given case. These methods must be compared according to their productivity and cost-efficiency. In rotational turning the rotation angle of the tool must be known accurately for the calculation of machine times.

2. Cutting with rotational feed method

The material removal in rotational turning is caused by the chip formation movement of the long cutting edge which section is linear in a laid-out plane but in reality it is on a helical curve on a cylinder surface with d_s diameter. In Figure 1 the cutting edge can be seen in plane so it creates a line which line and the axis of the workpiece are skewed. In that can be found the PV distance which is in cut momentarily and generates the chip. In geometrical view the skewed position means that the radius of the generated workpiece (with d_w diameter) is equal to the normal transversal of the lines (in Figure 1 that is the OP distance). The explanation of the symbols in Figure 1 are the followings: $d_{w,z}$ – raw diameter of the workpiece (contains radial direction allowance, z); n_w – angular frequency of the workpiece; v_c – cutting speed; v_s – the speed vector of the rotation of the workpiece; a_p – depth of cut; λ – skewness angle of the cutting edge.

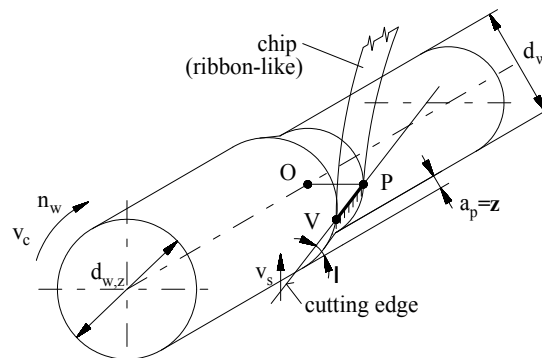


Fig. 1: Material removal principle in rotational turning

Figure 1 also demonstrates that the complete surface of the workpiece is machined by a long section of the cutting edge whereby the tool life of the cutting edge will be longer. Furthermore it can be seen that there is no need of feed from the machine because the axial component of the speed vector (v_c) works as "feed" during machining.

The needed angle of the rotation of the workpiece can be understood in Figure 2. The cut begins when the **P** point of the cutting edge reaches the workpiece. This is the first specific position of the tool. As the tool is rotating further with ϑ_{in} angle the **P** point gets into the **P'** point. This is the second specific position. As the rotation continues with ϑ_a angle the **V** point of the tool gets into the **U** point. This is the third specific position. From here the running-out phase begins while the **V** point gets into the **U'** point with the needed ϑ_{out} angle. This is the fourth specific position of the cutting edge.

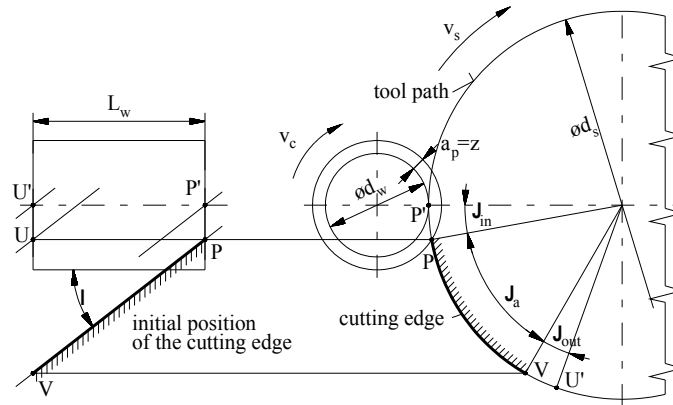


Fig. 2: Specific positions of the cutting edge with the determinative rotation angles

3. Determination of the rotation of the tool

We pointed up the three phases of the cutting edge's movement in connection with Figure 2 however in case of rotational turning the rotation angles (made by the tool) of each phases must be known. The parameters are indicated in Figure 2 which are necessary for the calculation of rotational arches and angles. The knowledge of the length (\bar{PP}') of arch is needed for the calculation of ϑ_{in} . Because of the symmetry the value of ϑ_{out} is the same. Since the depth of cut (a_p), which is also the radial allowance, is very low (around 0.1 mm) we applied the following: in the calculation the arch is approximated to a chord. In this way:

$$\bar{PP}' = \left(a_p \cdot \frac{d_s \cdot d_w}{d_s + d_w} \right)^{1/2}, \quad (1)$$

on the other hand the following proportion is given:

$$\bar{PP}' : d_s \cdot \pi = \vartheta_{in} : 360^\circ, \quad (2)$$

on the basis of the two equation we get the following:

$$\vartheta_{in} = \vartheta_{out} = \frac{360 \cdot \bar{PP}'}{d_s \cdot \pi}. \quad (3)$$

The pitch (p) of the curve of the cutting edge must be known for the calculation of ϑ_a which is the determinant parameter for the second and third specific edge position. We get it with a well-known geometrical equation [4]:

$$p = d_s \cdot \pi \cdot \tan(90^\circ - \lambda), \quad (4)$$

whereby the needed rotation is the following [4]:

$$\vartheta_a = \frac{L_w}{p} \cdot 360. \quad (5)$$

4. The practical use of rotational turning

Rotational turning is capable of machining not only external cylindrical surfaces but also bore-holes and flat surfaces. There is also no limitation for machining interrupted surfaces. The advantages of the use of rotational turning contrary to grinding:

- shorter machining times
- coolant is not needed
- lower investment costs
- greater process stability [2]

The method and the needed machine tool is based on the patent announcement of J. G. Weisser Werkzeugmaschinenfabrik. The manufacturer of the tools is MAAS GmbH. The following results are obtainable [5]:

- | | |
|-------------------------------------|-------------------------------------|
| • roundness tolerance: <0.003 mm | • diameter: IT5...IT6 |
| • straightness tolerance: <0.003 mm | • roughness: Ra<0.02 μm; Rz<1.00 μm |

- concentricity: <math><0.004\text{ mm}</math>
- topography: twist free, random

The cutting is performed with a special tool with a PCBN cutting edge which can be held in the turret of the lathe (Figure 3). The tool life is long because not only one point of the edge works but the whole length of the edge whose size can be around 30 mm. The edge is made of boron-nitride with middle CBN content, TiN binder, and around $2\text{ }\mu\text{m}$ grain size. Its relative high shock resistance enables the cutting of interrupted surfaces. It can be seen In Figure 3 that only a thin, lath-like insert is made of CBN in the tool hence the costs remain on a moderate level. Unusual by careful preparation of the edge is needed: both the rake- and the flank surfaces are lapped multiple times. In Figure 4 the tool can be seen during machining.

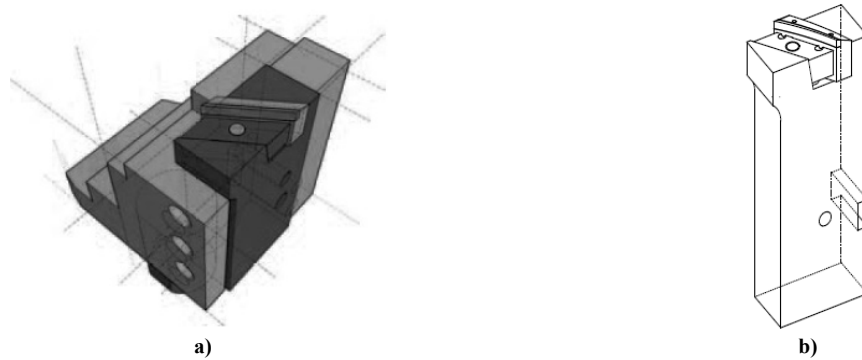


Fig. 3: Rotational turning tool mountable into a turret of a lathe: a) 3D view of the tool, b) design of the tool [5]

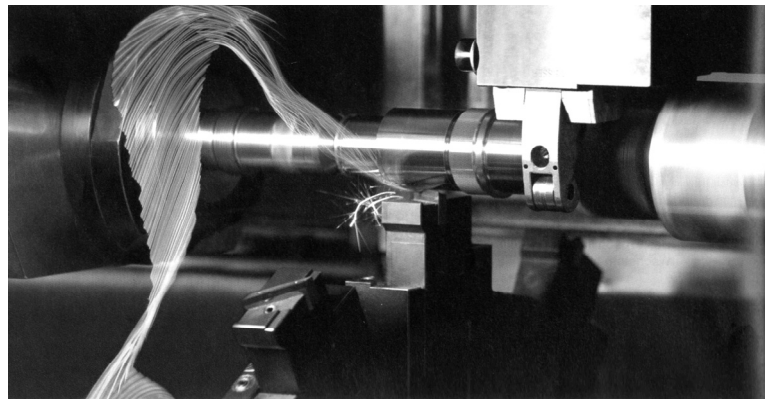


Fig. 4: Rotational turning tool in work [6]

The thin ($h=0.01\dots0.02\text{ mm}$) and wide, red glowing chip is cut down continuously by a ribbon-like way in the cutting zone. The cutting speed is very high: $160\dots240\text{ m/min}$ (which is typical of CBN tools); for the tangential feed (or rotational feed) $0.14\dots0.18\text{ mm/workpiece revolution}$ are (f_t) recommended by the manufacturers [1, 2, 5]. The allowance in diameter is: $z\leq 0.02\text{ mm}$.

Sketch	Condition	Alteration of the chip width
<p>①</p>	$L_w \ll PV \cdot \cos\lambda$	<p>without constant phase</p>
<p>②</p>	$L_w \leq PV \cdot \cos\lambda$	<p>constant phase</p>

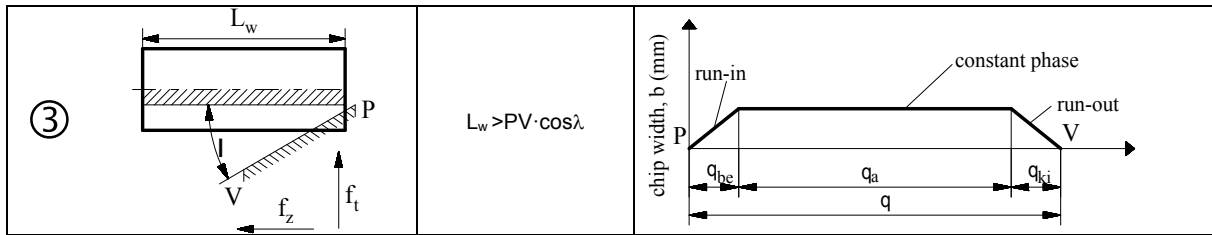


Fig. 5: Three typical cases of rotational turning

5. Technology planning of rotational turning

The first phase of technology planning contains the comparison of the length of the surface to be machined (L_w) and the length of the cutting edge ($\overline{PP'}$). As the data given by the manufacturer the maximum length of the cutting edge is 30 mm. This length is long enough for the majority of the cases to cover the L_w length because the lengths of sealing carrier surfaces of shafts are short. However that case should not be excluded if the L_w length is much longer than the length of the cutting edge; or if the length of the workpiece's surface is much shorter than the projection of the edge. The three possible initial relations can be seen on Figure 4. In the first part we encountered with that case when the so-called constant phase is not observable.

While the chip thickness is growing then it began to decrease after reaching the maximum value, without the constant phase occurring. In the second part the projection of the cutting edge is equal or slightly higher than the L_w length of the workpiece. In this case the constant phase comes into existence thus there will be a section of the rotation during the slow rotation of the tool where the active length of the cutting edge is constant. In this section the chip width is also constant.

In the third part of Figure 4 the projection of the cutting edge is lower than the L_w length of the workpiece. In this case there must be an additional feed component in direction of the Z axis besides the feed component from the rotation of the tool. Attention must be paid that the sum of the two feed components should not be higher than the values in the recommendations.

Lastly we prepared a simple example for the explanation of the equations above on the application of rotational turning.

The parameters of the workpiece:

- material: 20MnCr5, 62 HRC
- diameter: $d_w=60h5$
- length: $L_w=20$ mm
- radial allowance: $z=0.1$ mm
- prescribed roughness: $Rz=3 \mu\text{m}$
- number of passes: 1

Given parameters based on recommendations and experience:

- cutting speed: $v_c=180$ m/min,
- tangential feed: $f_t=0.18$ mm/wp. rev.
- diameter of the tool: $d_s=200$ mm
- skewness angle of the edge: $\lambda=30^\circ$
- length of the cutting edge: $L_s=30$ mm

The equations can be solved on the basis of the given parameters.

a) Angular frequency of the workpiece:

$$n_w = \frac{1000 \cdot v_c}{d_w \cdot \pi} = \frac{1000 \cdot 180}{60 \cdot \pi} = 955 \frac{1}{\text{min}}$$

b) Axial feed (in mm/wp. rev.):

$$f_a = \frac{f_t}{\tan \lambda} = \frac{0.18}{\tan 30^\circ} = 0.312 \frac{\text{mm}}{\text{wp.rev.}}$$

c) Axial feed (in mm/min):

$$v_{f,a} = n_w \cdot f_a = 955 \cdot 0.312 = 298 \frac{\text{mm}}{\text{min}}$$

d) Machining time (with approx. 1+1 mm engage/retract length):

$$t_g = \frac{L_w + 2}{v_{f,a}} = \frac{22}{298} = 0.074 \text{ min} = 4.43 \text{ s}$$

e) Tangential feed (in mm/min)

$$v_{f,t} = n_w \cdot f_t = 955 \cdot 0.18 = 171.9 \frac{\text{mm}}{\text{min}}$$

f) Angular frequency of the tool:

$$n_s = \frac{v_{f,t}}{d_s \cdot \pi} = \frac{171.9}{200 \cdot \pi} = 0.2736 \frac{1}{\text{min}}$$

g) Angular speed of the tool:

$$\omega_s = \frac{2\pi \cdot n_s}{60} = \frac{2\pi \cdot 0.2736}{60} = 0.0286 \frac{\text{rad}}{\text{s}} = 1.642 \frac{\text{grad}}{\text{s}}$$

h) The angle of the engage/retract:

$$\vartheta_{in} = \vartheta_{out} = \frac{360 \cdot \overline{PP'}}{d_s \cdot \pi} = \frac{360 \cdot 2.148}{200 \cdot \pi} = 1.231 \text{ grad}$$

$$\overline{PP'} = \left(a_p \cdot \frac{d_s \cdot d_w}{d_s + d_w} \right)^{1/2} = \left(0.1 \cdot \frac{200 \cdot 60}{200 + 60} \right)^{1/2} = 2.148 \text{ mm}$$

i) Rotation during the constant phase:

$$\vartheta_{a1} = \frac{L_w}{p} \cdot 360 = \frac{20}{1088.3} \cdot 360 = 6.616 \text{ grad}$$

$$p = d_s \cdot \pi \cdot \tan(90^\circ - \lambda) = 200 \cdot \pi \cdot 1.732 = 1088.3 \text{ mm}$$

j) Total rotation of the tool:

$$\vartheta = 1.231 + 6.616 + 1.231 = 9.078 \text{ grad}$$

k) Machining time from the angular speed:

$$t_g = \frac{\vartheta}{\omega_s} = \frac{9.078}{1.642} = 5.53 \text{ s}$$

Summary

The complex chip-geometrical characteristics of the rotational turning make the calculation of machining times seemingly difficult. Therefore the easiest way to achieve the above is the calculation of the needed rotation done by the slowly rotating tool. Each angle of the specific phases (initial, constant, running out) can be calculated simply. The machining time is calculated on the basis of the determined angles and the angular speed. These values can be used for the comparison of the rotational turning to other hard turning methods. The presented example demonstrates that the productivity of rotational turning is very high. Bearing seats or sealing surfaces can be machined under several seconds and the quality of the surface is the same like in grinding. It seems there are some cases when the rotational turning



method can be more an economical solution than the investment of a new grinding machine. Furthermore we are certain that the topography limitations can be prevented which are present without doubt in ordinary hard turning.

Acknowledgment

The research work has been realised as part of project TÁMOP-4.2.1.B-10/2/KONV-2010-0001 – in the frame of New Hungary Development Plan –, by the support of European Union, with the co-finance of European Social Found. This paper was prepared by the support of the Hungarian Scientific Research Found, which the authors highly appreciate. The number of assignment is: OTKA K-78482.

References

- [1] Weisser J.G.: Patent von Werkzeugmaschinenfabrik, St. Georgen, Schwarzwald, Deutschland, 2004
- [2] W. Klingsauf: Drehen ohne Drall, *Fertigung*, Jan/Febr. 2005, pp.16-18
- [3] N. Kummer, B. Voght: Drallfreies Drehen ersetzt Schleifprozesse, *IDR* 4/2004, pp.2-5
- [4] S. Szabó: A rotációs előtolással történő esztergálás vizsgálata, *Manuscript*, Miskolci Egyetem, 2009.
- [5] http://www.mas-tools.de/de/pdf/MAS_Rotationsdrehen.pdf
- [6] J.G. Weisser Söhne GmbH & Co.: Schnelleres Spänemachen, *Werkstatt und Betrieb* 9/2011. pp.120-121



International Conference on Innovative Technologies, IN-TECH 2012,
Rijeka, 26. - 28.09.2012



ENVIRONMENTAL LOAD REDUCING IN HARD MACHINING

J. Kundrak¹, G. Varga¹

¹ University of Miskolc, Department of Production Engineering, H-3515, Miskolc, Egyetemváros, Hungary

Keywords: hard machining, alternative procedures, coolants and lubricants, environmentally conscious machining.

Abstract. For today that is a social demand and technical possibility in every way of life that when manufacturing new engineering products the environmental aspect should predominate better and better. One of the possibilities for that is to decrease the amount of coolants and lubricants (CL) applied in metal machining procedures. The application of CL considerably contributed to the increase of the efficiency of material removal in metal machining procedures. A highlighted task of production technologists' is to increase efficiency while decreasing these auxiliary materials or even eliminate them. In this article we focus on how the CL can be decreased in the alternative procedures of hard turning. Through comparative examinations we sought to ascertain whether a given production task – namely the machining of hard surface – can be fulfilled with the same accuracy and economic efficiency if using less CL.

Introduction

In high productivity cutting of steels the cutting zone heats to high temperature. This type of high temperature increases the dimension difference of cutting tool and its premature failure. It damages the surface integrity of the product by causing tensile residual stress and the formation of micro-cracking on the surface and near surface layers, furthermore, by quick oxidation and corrosion [1]. In high speed cutting the use of coolants and lubricants for conventional cutting is unsuccessful, as the coolants and lubricants cannot reach the contact of chip - cutting tool, so it cannot take away the heat [2]. When EP additives are given to the coolants and lubricants that does not assure their getting to the contact of chip - cutting tool, that is the cooling and lubrication [3]. Lately the advantages of the use of coolants and lubricants were questioned because of their numerous negative effects they cause. When coolants and lubricants are not treated properly they can seriously damage the soil, water resources, and the environment. That is why, because of the protection of the environment, they have to satisfy strict rules. A further disadvantage of their application is that they can have injurious effect on the engine operators causing them skin and respiratory problems [4].

In companies the cost of coolants and lubricants amounts to most of the entire machining cost. Many researchers state that the cost of coolants and lubricants is frequently higher than the costs related to cutting tools [5]. As a consequence the abandonment of coolants and lubricants, if that is possible, can cause a meaningful economic motivation.

In the present manufacturing environment the end users of coolants and lubricants take care of reducing the costs and increasing productivity.

The volume of used soluble oil from the whole manufacturing processes of the German industries were around 60% of the volume of CL used in 1992 which was about 1 151 000 tons, [6]. That means a huge amount of money, varying 7.5%÷17% of the manufacturing costs per part. This cost is higher than the costs in connection with tooling [7], [8].

In the work of Canter [9] it can be read that the estimated cost of coolants and lubricants is 16% of the whole cost for a general end-user which is shown in Fig. 1. [9]

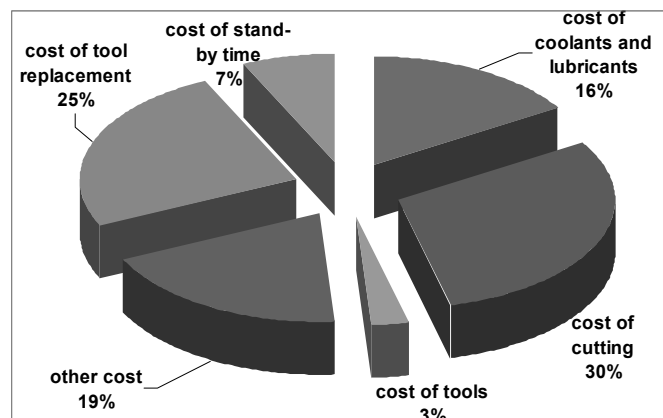


Fig. 1, Typical End-User Manufacturing Costs [9]

According to other estimations the costs of CL took 0.9% of the total production costs in 2001 [9]. This is shown well by the amount of the used CL as well. According to a value from 1998, approximately 2.3×10^9 litres of coolants and lubricants were used to manufacturing operations and their cost value was around $\$2.75 \times 10^9$ [10]. In 2002 in the USA the total amount of coolants and lubricants which help metal working was estimated at 246.6 million gallons, out of which, 117.2 million gallons were metal removal fluids (straight oils, 27.3 million

gallons; soluble oils, 49.3 million gallons; semi-synthetics, 21.7 million gallons; synthetics, 18.9 million gallons) [11]. According to the Association of European Lubricant Manufacturers in 2005 the amount of liquid which helps metal working was about 270 000 tons (84 million gallons) in the European Union [12]. Some alternatives were looked for in order to reduce or avoid the use of coolants and lubricants in machining procedures. Nowadays there is a big interest in dry cutting and really they can be used successfully in the field of environmentally friendly cutting [13]. In reality, however, they are not so effective when the requirements are better manufacturing efficiency, better machined surface and sever cutting conditions. For these cases the use of minimum volume coolants and lubricants is advantageous, which really play a significant role in numerous practical uses [14].

Dry Machining

The substitution of roles of coolants and lubricants in dry machining is really a big challenge, because coolants and lubricants solve several tasks at the same time. Among them is the lubrication of the workpiece and cutting tool, the reduction of the heat in the cutting zone, corrosion prevention of the workpiece, cleaning the workpiece, and washing away chips from the place of cutting. The effectiveness of coolants and lubricants depends on the given operation, the material of the workpiece and the cutting tool and the technological parameters to a great extent.

The missing of coolants and lubricants can lead to negative effects as well. The absence of cooling and lubrication can increase friction and that can increase temperature. That is why the cutting tool can wear more rapidly, built up edge can occur on the cutting tool which can have an effect on the workpiece as well. Its surface roughness can deteriorate; its residual stress can increase [21]. The absence of active removal of chips from the cutting zone can lead to the increase in temperature, hack of tool, or even tool breakage.

In dry cutting special tooling was developed for the substitution of the missing lubrication and the chips washing away. Carbide, cubic boron nitride cutting tools are applied with silicon nitride and diamond coating in dry cutting. These tool materials have good hot hardness and good wear resistance. Individual tooling can be made by further developed tool geometry which can realize functions of chip guiding and chip breaking when there are no coolants and lubricants helping the chip clear away function. Vacuum and compressed air systems can take away chips from the cutting environment in case of no use of coolants and lubricants too. The operational conditions and materials producing short chip, small cutting force and low temperature are the most suitable for dry machining with single point cutting tools. However, dry grinding, honing and lapping mean great challenge [15].

Machining with Minimum Quantity Lubrication

The name of minimum quantity lubrication refers to the case when the coolants and lubricants are used in minimum volume. Their volume is 50-500 ml/h in practice which value is smaller by three or four order of magnitude than the conventionally used so called flood cooling volume. The concept of minimum volume of coolants and lubricants, which is called near dry or micro-lubrication and used only occasionally [6], has been suggested for about twenty years [16]. The reduction of the volume of coolants and lubricants can lead to economic advantages as well by saving the cost of coolants and lubricants and by the reduction of the cleaning cycle time of the workpiece, the cutting tool and machine tool.

The minimum quantity lubrication is defined as coolant and lubricant liquid is sprayed directly to the cutting zone with optimum flow speed at small volume [17]. These fluids contain e.g. hydrocarbons, sulphur, chlorine, emulsive additives and biocides. The environment damaging effect of coolants and lubricants can be reduced by handling coolants and lubricants, but the potential danger cannot be eliminated totally [17]. It can be remarked that the cost of purchasing, maintenance, handling, recirculating, and annihilation is significant, so it requires careful choice.

The minimum quantity lubrication offers the following advantages:

- the volume of coolants and lubricants is reduced [19],
- cost is decreased compared to flood cooling,
- there is the possibility of the application of favourable fluids (e.g. vegetable oil), and the
- productivity is improving compared to dry machining [18].

The minimum quantity lubrication does not spread quickly because of the following:

- its cost is not known exactly,
- chip washing problem can occur,
- combustibility problem of metal powder can emerge.

It can be seen on the base of literature survey that in certain machining there are many advantages. The aim of present work is to show the change of environmental load of the hole of a socket at different machining.

Experimental Conditions

The experiments were made for a hole of a socket of IT7 accuracy when surface roughness $R_z=10 \mu\text{m}$ was to be provided. Table 1 summarizes the signs and descriptions of the procedures investigated and Fig. 2 shows the draft of the workpiece. On the part the hole diameter 26.07mm was machined only in the length of 36.5mm with the examined procedures.

The data of the workpiece were as follows: material: 16MnCr5; hardness: 61+63 HRC; diameter: $d=26.07\text{mm}$; accuracy: IT 7; length of bore: 36.5mm; l/d relationship: 1.4; allowance: 0.3mm; sequence size: $n=200$. From 0.15 mm allowance 0.1 mm were removed by roughing, 0.05 mm by smoothing.

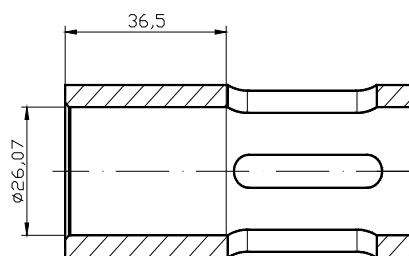


Fig. 2, Draft of the workpiece

The technological parameters were chosen so that the prescribed roughness $Rz=10\ \mu\text{m}$ and accuracy IT7 were to be ensured for all procedures.

Applied procedures:

A – grinding,

B1, B2 – hard boring,

C1, C2 – combined procedures.

In hard boring we used two inserts which were signed by „insert 1” (4NC –CNGA120408TA2) and „insert 2” (4NC-CNGA120408GSW2) and the sign of hard borings executed by them are B1 or B2.

In the combined procedure, the indicated two procedures differ by the applied cutting inserts, similarly to hard turning. The roughing in procedure C1 is done by insert 1, in procedure C2 by insert 2 (Table 1). The smoothing is done by the same grinding wheel in both cases (Corundum wheel: 40x20x16-9A80-K7V22).

Table 1. Hard boring procedures applied in the experiments

Process		Internal traverse grinding	Hard boring		Combined procedure		
	Sign	A	B1	B2		C1	C2
Procedure	Roughing	Corundum wheel	Insert 1	Insert 2	Hard boring	Insert 1	Insert 2
	Smoothing			Insert 1	Internal traverse grinding	Corundum wheel	
Machine tool		SI-4/A	PITTLER PVSL-2			EMAG VSC 400 DS	

Environmental Load Characterised by the Amount of CL Consumption

In metal machining the extent of environmental load is decisively determined by the amount of CL consumption in each procedure. In the hard machining procedures the amount of used up coolants and lubricants are determined by the CL demand of grinding and hard turning since all the other procedures are the combination of these two.

In grinding the removal of the allowance requires high quantity of coolants and lubricants. For that reason this procedure pollutes the environment to a great extent, damages the workers' health, and the used up auxiliary materials increase the expenditure of the procedure.

In hard turning the application of CL is not needed to remove the chips efficiently. Besides, the side products created during cutting are less polluting for the environment and they are easily recycled. Therefore, from the point of view of ecology hard turning is a most beneficial version of hard machining. In a combined procedure the proportion of times spent on turning and grinding provides the extent of CL consumption. The reason for that is that in a combined procedure the roughing is done dry (turning), while the smoothing (grinding) is done with coolants and lubricants. In a combined procedure a hybrid machine tool is used on which parts are machined with one clamping.

First we examined that different companies, machining with cutting parameters that produce components with the same accuracy and surface roughness, how much coolants and lubricants consumed. As described before, the consumption of coolants and lubricants is proportional with the time spent on grinding. The procedure entirely demanding coolants and lubricants (grinding) is 100%, cutting done dry is 0%. In the other machining versions we demonstrate what the proportion of grinding is in each procedure within the operation time.

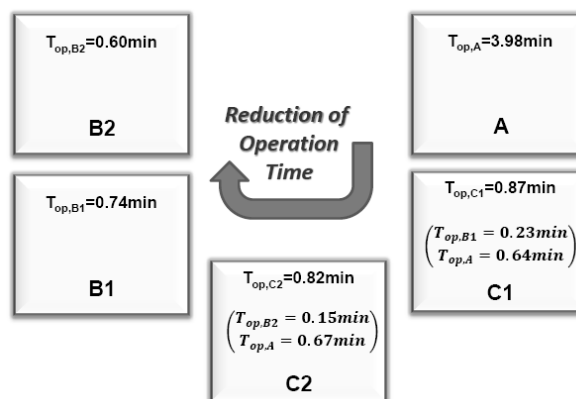


Fig. 3. Operation times in different procedures (Denominations according to Table 1)

In Figure 3 it can be seen that the value of operation time significantly decreases compared to grinding, when applying the other procedures the sequence of which is C', C2, B1, B2 with the decrease of time. The operation time of operation B2 is already only 15.08% of grinding. Figure 4 demonstrates what percentage of CL is used in the different procedures projected on the operation time needed for machining of a hole. The real consumption, however, is provided by Figure 5, because – as mentioned before – in the examined procedures the operation times are not the same, but they significantly differ. Taking this into account, too, it can be seen that the production of a surface with the same accuracy and quality by turned profile is possible with the consumption of CL is 16-17% as compared to the traditional (longitudinal) grinding.

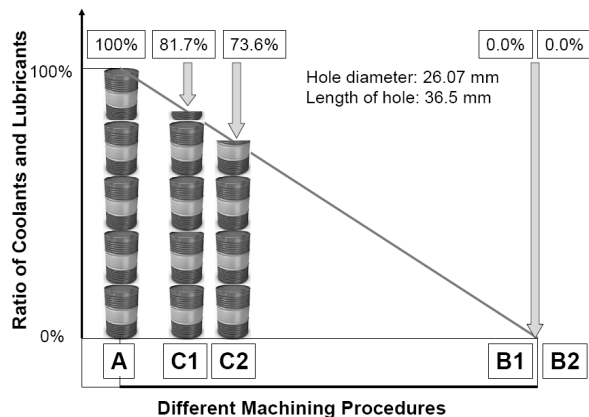


Fig. 4. The proportion of the use of coolants and lubricants in operation time in the different procedures (Denominations according to Table 1)

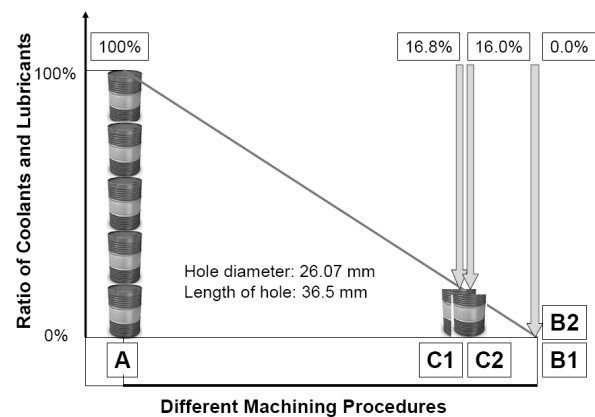


Fig. 5. The proportion of environmental load in different procedures related to grinding (Denominations according to Table 1)

Conclusions

Instead of grinding generally applied before, the application of the other examined procedures can be suggested for finishing the bore holes of disc-type components. Because of the significantly higher material removal rate and the shorter machining time, hard turning is a remarkably more productive and economic procedure. Applying hard turning the rare technical-engineering condition is provided that the environmental load can be decreased while gaining economic benefits.

At present, in most cases, the technical and technological conditions are provided for hard turning to substitute grinding. There are, however, components for which the operational conditions demand ground topography. In such a case the application of the so called combined (hybrid) machining is suggested. Our examinations prove that by a procedure containing hard turning besides grinding, almost the same operation time can be reached as in hard turning and the economic efficiency is similar, too, while with the examined geometrical parameters the CL proportion decrease to its one sixth as compared to grinding.

Acknowledgment

"The described work was carried out as part of the TÁMOP-4.2.1.B-10/2/KONV-2010-0001 project in the framework of the New Hungarian Development Plan. The realization of this project is supported by the European Union, co-financed by the European Social Fund." This publication was also made in the frame of Hungarian – Polish Intergovernmental S&T Cooperation Programme marked PL-7/2009 (Contract number: TÉT_10-1-2011-0016), financially supported by NDA and its foreign contractual partner.

References

- [1] H.K. Tonshoff, E. Brinksmeier, Determination of the mechanical and thermal influences on machined surface by microhardness and residual stress analysis, *Ann. CIRP* 29 (2) (1986) pp.: 519–532.
- [2] S. Paul, N.R. Dhar, A.B. Chattopadhyay: Beneficial effects of cryogenic cooling over dry and wet machining effects on tool wear and surface finish in turning AISI 1060 steel, in: *Proceedings of the ICAMT-2000*, UTM, Malaysia, 2000, pp.: 209–214.
- [3] C. Cassin, G. Boothroyd: Lubrication action of cutting fluids, *J. Mech. Eng. Sci.* 7 (1) (1965) pp.: 67–81.
- [4] M. Sokovic, K. Mijanovic: Ecological aspects of the cutting fluids and its influence on quantifiable parameters of the cutting processes, *JMPT* 109 (1–2) (2001) pp.: 181–189.
- [5] F. Klocke, G. Eisenblatter: Dry cutting, *Ann. CIRP* 46 (2) (1997) pp.: 519–526.
- [6] W. F. Sales, A. E. Diniz, Á. R. Machado: Application of Cutting Fluids in Machining Processes, *Journal of the Brazilian Society of Mechanical Sciences*, Vol. 23 no. 2 Rio de Janeiro, 2001, ISSN 0100-7386, <http://dx.doi.org/10.1590/S0100-73862001000200009>
- [7] Heisel, U.; Lutz, M.; Spath, D.; Wassmer, R.; Walter, U.: *The Minimum Quantity of Fluid Technique and its Application to Metal Cutting*, Máquinas e Metais, Aranda Publisher, February, (1998), pp.: 22 – 38 (In Portuguese).
- [8] F.S. Wisley, E.D. Anselmo, R.M. Álisson: Application of Cutting Fluids in Machining Processes, *Journal of the Brazilian Society of Mechanical Sciences*, (2001), vol.23 no.2 Rio de Janeiro
- [9] N. Canter: The Possibilities and Limitations of Dry Machining, *Tribology & Lubrication Technology*, March 2009, pp.: 40–44,
- [10] T.F. Glenn, F. van Antwerpen: Opportunities and market trends in metalworking fluids, *Lubrication Engineering* 54 (1998) pp.:31-37
- [11] http://www.ilma.org/about/ntp_comments.pdf (May 30, 2011)
- [12] K. Suuronen: Metalworking fluids – allergens, exposure, and skin and respiratory effects, PhD Thesis, Finnish Institute of Occupational Health, Helsinki, Finland; University of Kuopio, Kuopio, Finland, 2009
- [13] F. Klocke, G. Eisenblatter, Coated tools for metal cutting-features and applications, *Ann. CIRP* 48 (2) (1999) 515–525.
- [14] J.W. Sutherland, et al., An experimental investigation of air quality in wet and dry turning, *Ann. CIRP* 49 (1) (2000) 61–64.
- [15] K. Weinert, I. Inasaki, J.W. Sutherland, T. Wakabayashi: Dry machining and minimum quantity lubrication, *Ann. of CIRP*, (2004), 53 (2), pp.: 1-28
- [16] T.F. McClure, R. Adams, M.D. Gugger: *Comparison of flood vs. microlubrication on machining performance*, Internet: <http://www.unist.com/techsolve.html>.
- [17] D.M. Hands, J. Sheehan, B. Wong, H.B. Lick: Comparison of Metalworking Fluid Mist Exposures from Machining with Different Levels of Machine Enclosure, *American Industrial Hygiene Association Journal*, (1996), 57/12:173-1178
- [18] H.K. Tonshoff, W. Spintig: *Machining of holes developments in drilling technology*, *Ann. CIRP* (1994) 551–561.
- [19] F. Szigeti, L. Péter, A. Százvai: Application of Environmentally Friendly Technology, *Gépgyártás*, (2007) Vol.: XLVII, N.: 2-3., pp.: 35-39., (In Hungarian)
- [20] M.N. Morgan, A.R. Jackson, V. Baines-Jones, A. Batako, H. Wu, W.B. Rowe: 'Fluid Delivery In Grinding', *Ann. of the CIRP*, (2008), Vol 57/1 pp 363-366, DOI : 10.1016/j.cirp.2008.03.090,

COMPARATIVE EXAMINATIONS FOR THE MACHINING OF HARD SURFACES

J. Kundrak¹, I. Deszpoth¹, V. Molnar¹

¹ University of Miskolc, Department of Production Engineering, H-3515 Miskolc-Egyetemvaros

Keywords: hard machining, operation time, material removal rate, surface rate

Abstract. When planning hard machining procedures, similar to other types of machining, several factors referring to the component, e.g. geometrical dimensions; have to be considered in order to make the correct technological decisions. In this paper we demonstrate the effect of the geometrical dimensions of the bore on the machining time, surface rate and material removal rate. In the investigations the experimental data of the hard machining procedures were compared. The comparison was performed on the basis of the conventional (traverse) grinding.

1. Introduction

New procedures and methods are appearing more and more often in the finishing procedures of hardened surfaces which have been machined with abrasive procedures, first of all with grinding for a long time. Before the introduction and application of the new procedures, comparative investigations are performed in every case, in which the formerly applied procedures are compared to the new ones. That is why several comparative investigations were performed referring to the hardened surfaces too. The aspects and criteria of these show a large variety and the common characteristic of them is that the conventional grinding is the basis of the comparison.

To prove the applicability of hard turning, the surface roughness and the machining time of it were compared to the same factors of grinding [1, 2, 3, 4, 5]. As a result of these, the researchers gained a favourable experience. Later the whole surface quality was analyzed [6, 7, 8, 9]. It emerged that hard turning had several advantages [10, 11, 12] compared it to grinding. But there are cases in which the regular, so-called periodic topography is not advantageous considering the function of the components. Accordingly such a solution was looked for, in which the material removal was done by grinding as finishing operation after hard turning [13, 14]. These solutions are defined by combined procedures.

The above detailed steps of the development are well traceable in the machining of disc-featured components. The greatest challenge in the production of these components is the machining accordant to the accuracy and quality specifications of the bore.

We investigated how the productivity is influenced in the different procedure versions by the bore dimensions (bore length and diameter) in machining hardened surface bores. We demonstrate how the operation time, the material removal rate and the surface rate change in grinding, hard turning and combined procedure with different bore dimensions.

2. Description of the comparative investigations

The aim of the investigations was the analysis of the effect of bore diameter and bore length on the efficiency of material removal. The technological conditions used in grinding, hard turning and combined procedure facilitate the same accuracy and roughness of the machined surface.

2.1. Method of the investigation

Comparative investigation of five different procedure versions was performed into different bore dimensions. Among the machining times, the operation time was the basis of the comparison (T_{op}).

The efficiency of the procedures was qualified on the basis of the value of material removal rate ($MRR - Q_w$, mm^3/s) and surface rate ($SR - A_w$, mm^2/s) too. The comparison of the efficiency of the different procedures is performed with the use of the practical values of material removal rate (Q_{wp}) and surface rate (A_{wp}) [15, 16]. The calculation of the practical value of the Q_{wp} material removal parameter: the material volume of the allowance is divided by the time consumption of the removal:

$$Q_{wp} = \frac{d \cdot \pi \cdot L \cdot Z}{t_x \cdot 60} \quad (mm^3/s), \quad (1)$$

where d – bore diameter (mm), L – bore length (mm), Z – radial allowance (mm), t_x – a certain economical time, in this case operation time (t_{op}). The calculation of the practical value of the A_{wp} material removal parameter: the size of the surface to be machined is divided by the time consumption of the removal:

$$A_{wp} = \frac{d \cdot \pi \cdot L}{t_x \cdot 60} \quad (mm^2/s). \quad (2)$$

2.2. Material and geometry of the workpieces

The material of them is gear-wheel steel (20MnCr5) which can be case hardened. The hardness of them is 62 ± 2 HRC after hardening. The bores had five different diameters ($d=35, 50, 65, 80, 95$ and $L=30$) and five different lengths ($L=20, 25, 30, 35, 40$ and $d=50$). The difference between lengths L' and L is the overrun of the tools having one cutting edge. The value of it is 1 plus 1 mm.

2.3. The investigated procedures and cutting data

In Figure 1 the specific cutting data and the drafts of the five procedure versions can be seen.

Procedure version **A** is the conventional bore grinding. It is characterized by the traverse feed, the alternating pass in one double stroke.

Procedure version **B** is the conventional hard turning with ISO-standard PCBN insert. The machining with this insert is usually contains one roughing and one smoothing grade.

Procedure version **C** is hard turning with wiper insert.

Procedure version **D** is combined: roughing with standard insert and smoothing with high speed infeed grinding.
 Procedure version **E** is combined: roughing with wiper insert, smoothing with high speed infeed grinding.

Procedure version A				Procedure versions B and C				Grinding for procedure versions D and E			
v_c	30 m/s	v_w	18 m/min	v_c	180 m/s	f (B)	R_{St} : 0,15 mm/rev. S_{St} : 0,08 mm/rev.	v_c	45 m/s	sp.	6 s
$v_{f,L}$	N: 2200 mm/min S: 2000 mm/min	sp.	8 strokes			f (C)	R_w : 0,24 mm/rev. S_{St} : 0,12 mm/rev.	$v_{f,R}$	R: 0,0050 mm/s S1: 0,0033 mm/s S2: 0,0016 mm/s	$v_{f,R,L}$	0,108 mm/s
a_e	N: 0,02 mm/db. st. S: 0,001 mm/ db. st.	Z	R: 0,10 mm S: 0,05 mm	a_p	R: 0,10 mm S: 0,05 mm	Z	R: 0,10 mm S: 0,05 mm	v_w	55 m/min	Z	R: 0,095 mm S1: 0,010 mm S2: 0,005 mm

Figure 1 Drafts and technological conditions of the procedure versions

3. Operation times in hard machining procedures

Figure 2 illustrates the time consumptions of a version, where $d=50$ mm and $L=30$ mm. The diagram demonstrates that the further procedures applied along the grinding; facilitate the reduction of operation time. The accuracy and surface quality reachable with grinding can be provided by these procedures too. The operation times were calculated to all considered cases and thereafter the times were correlated with the grinding as the basis machining.

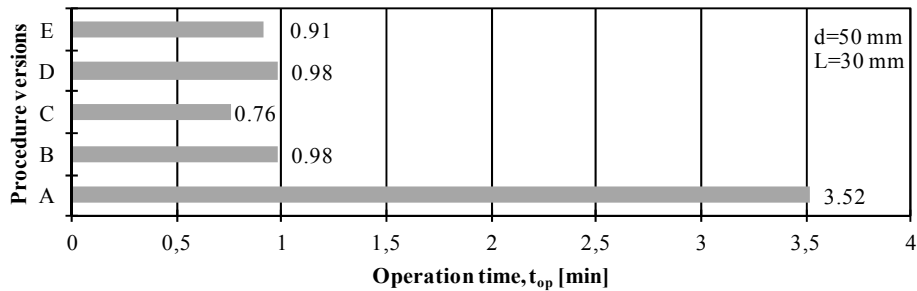


Figure 2 Operation times of the five procedure versions by $d=50$ mm bore diameter and $L=30$ bore length

3.1. Effect of bore length on the operation time

Having accomplished the experiments with different bore lengths and determined the operation times, the results of calculations are represented as the function of the bore length (Figure 3a). The rates of operation times are represented in the figure as the basis of them is the operation time of grinding. Thus the value of grinding is 100% or 1. The effects of bore length on the different procedure versions are the following:

- Since the time of traverse grinding and the hard turning (procedure versions **B** and **C**) increase about in the same extent as the bore length, the relative rates of the two times do not change significantly.
- In the infeed grinding procedure the operation time of it reduces comparing to the traverse grinding procedure. Furthermore the rate of it reduces with the increase of the bore length (procedure versions **D** and **E**).

Since the effect of bore length shows different intensity, the ranges and/or limits (bore lengths) can be designated, at which the surface can be machined in the shortest time with a given procedure. In Figure 3a the rates of operation time were represented as the function of the L bore length comparing to the procedure version **A** by $b=50$ mm bore diameter. The rate of the procedure version **A** is $A/A=1$. This was not recorded in the figure, because the time of conventional grinding was the largest by every combinations of data.

Considering the operation time as a basis the next statement is apparent: the use of wiper insert is recommendable up to length of 50 mm in hard turning (**C**) and beyond that the combined procedure (Figure 3a).

We introduce the limits of bore lengths (concerning any two procedure versions), at which the change of procedure version is worthy to be considered in order to reach shorter machining times. On the other hand we specify which procedures are recommended to apply if it is possible to apply all of them with standard or wiper insert. In Figure 3a it can be seen that at $L=26$ mm the change over from the procedure version **B** to the **E**, at $L=30$ mm to the **D**, at $L=52$ mm from the **C** to the **E** and at $L=79$ mm from the **C** to the **D** is recommended if the choice of a more productive procedure version is preferable. In Figure 3a at $L>40$ mm the limits of bore lengths are theoretical, they were determined by trend curves.

3.2. Effect of bore diameter on the operation time

In Figure 3b the rates of operation time were represented as the function of the d bore diameter at $L=30$ mm bore length. The effects of bore diameter on the different procedure versions are the following:

- The operation time of the traverse grinding is independent of the bore length.
- The operation time increases linearly in the other procedure versions. The extent of increasing is larger in the procedure versions **B** and **C** than in **D** and **E**.

As the basis of the minimization of the operation time at $d=43$ mm the change over from procedure version **B** to the **E**, at $d=50$ mm to the **D**, at $d=75$ mm from the **C** to the **E** and finally at $d=99$ mm from the **C** to the **D** is recommended, if the choice of a more productive procedure version is preferable. In Figure 3b at $d>95$ mm the limits of bore diameters are theoretical, they were determined by trend curves.

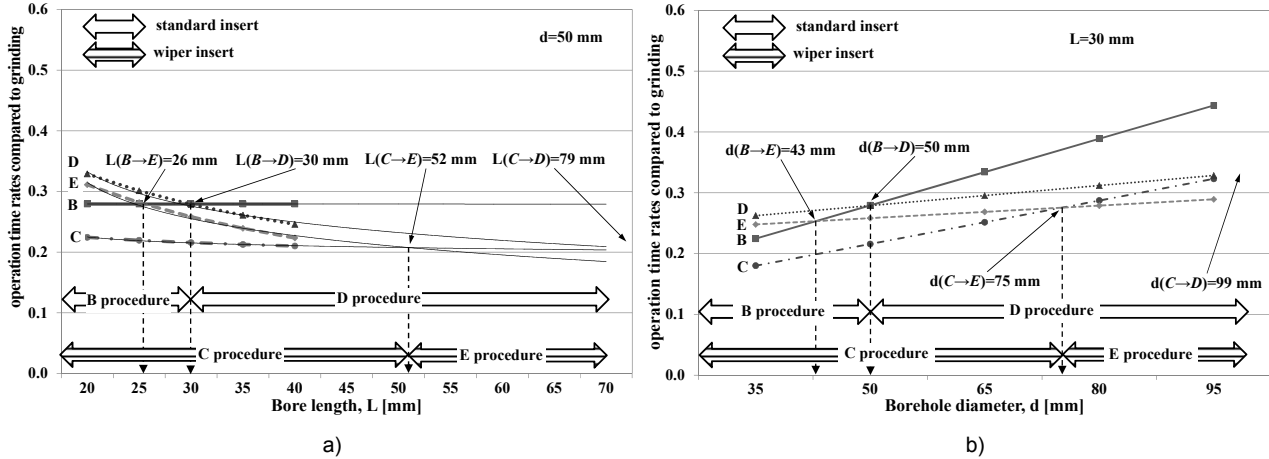


Figure 3 Limits of bore length (a) and bore diameter (b) on the basis of operation time changes

4. The change of material removal rate and surface rate as the function of the bore geometry

The investigations of MRR and SR were performed on the basis of their practical values. The different theoretical values, first of all with using the different possible cutting data of one procedure. However, the theoretical values give only approximate solution when comparing the different procedures [15, 16]. Accordingly the comparison of the efficiency of the different procedures is performed with the use of the practical values of material removal rate (Q_{wp}) and surface rate (A_{wp}).

The comparison of the efficiency of the different procedures is performed with the use of the practical values of material removal rate (Q_{wp}) and surface rate (A_{wp}).

4.1. The effect of bore length on the MRR and SR

The results are demonstrated at five different bore lengths (Figure 4). It can be seen that the A_{wp} and Q_{wp} values of the grinding are the lowest at every diameter.

At the smallest bore length the hard turning has the most favourable value referring to the A_{wp} (B: 67; C: 83.4). These values are 3.6-times and 4.5-times higher than in grinding (Figure 4a). At the largest investigated bore length the rank of the A_{wp} values is: **C**, **E**, **D** and **B**. The rates of these to the grinding are: 4.8; 4.5; 4.1 and 3.6.

Values and rates of the Q_{wp} show similar tendency than the values and rates of A_{wp} (Figure 4b).

4.2. The effect of bore diameter on the MRR and SR

At every diameter, the values are more favourable in the other procedure versions than in grinding (Figure 5). Actually both in hard turning and in combined procedure the material removal is more efficient when wiper insert is used. The lowest increment of the surface rate at the smallest diameter is $A_{wpD}/A_{wpA}=3.8$, while at the largest diameter $A_{wpC}/A_{wpA}=5.6$ (Figure 5a). At the largest diameter the lowest increment is $A_{wpB}/A_{wpA}=2.3$ and at the largest diameter $A_{wpE}/A_{wpA}=3.5$.

Having accomplished the analysis, the MRR reaches favourable values in similar rate compared to grinding considered as a basis (Figure 5b).

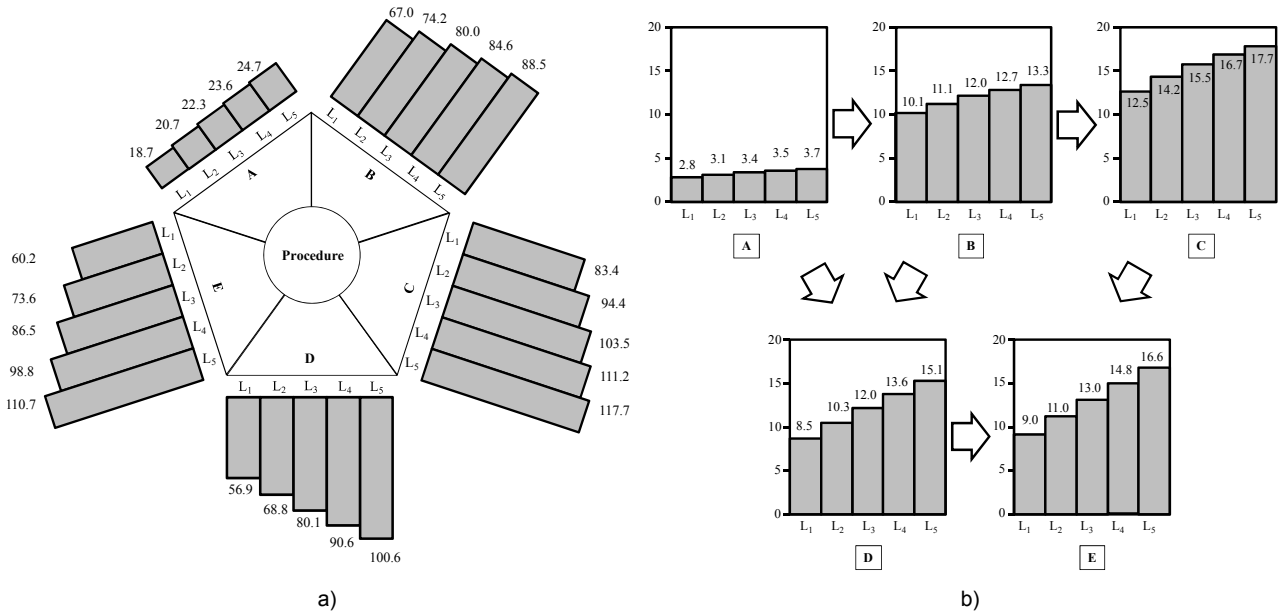


Figure 4 Effect of bore length on the SR (a) and MRR (b) at d=50 constant bore diameter

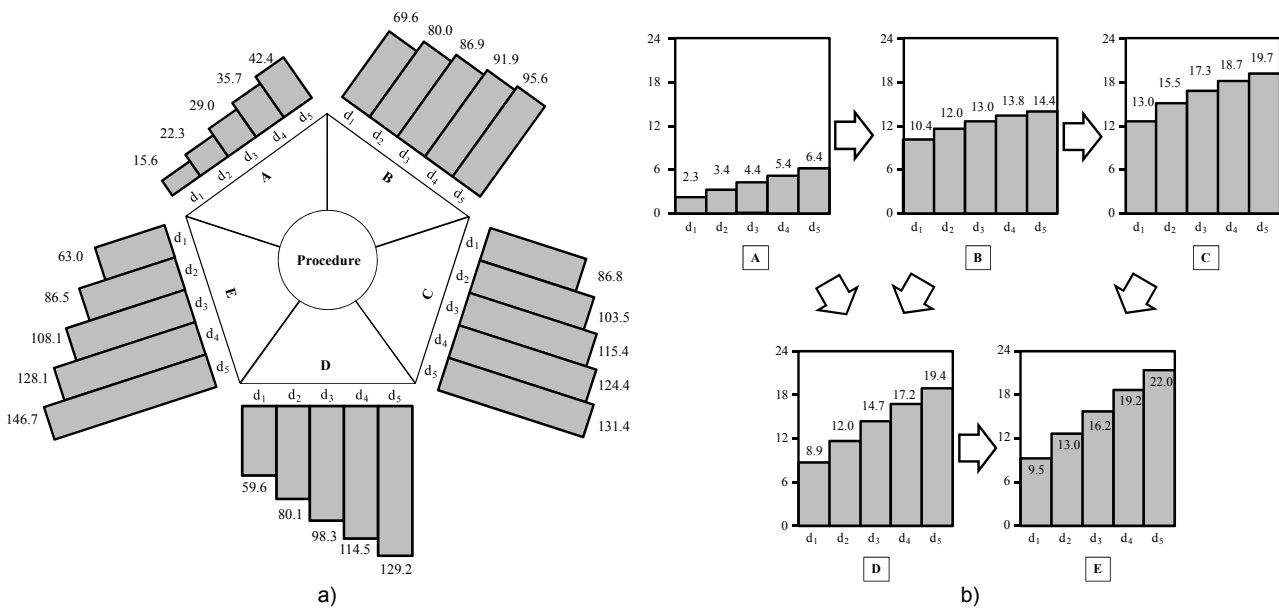


Figure 5 Effect of bore diameter on the SR (a) and MRR (b) at L=30 constant bore length

5. Summary

As a result of the investigation of the rank among the procedures it can be stated that hard turning and combined procedures are significantly more effective procedures than grinding on the basis of the SR and MRR in the range of the investigated bore length and bore diameter.

It also can be stated that applying standard insert with the increase of the bore length hard turning is more effective at the lower lengths and at larger lengths it continuously falls behind the efficiency of the combined procedure. In turn, applying wiper insert the combined procedure continuously approaches the efficiency of hard turning. With the increase of the bore diameter, applying both standard and wiper inserts, hard turning is more efficient at smaller diameters and at larger diameters it continuously falls behind the efficiency of the combined procedure.

Acknowledgment

The described work was carried out as part of the TÁMOP-4.2.1.B-10/2/KONV-2010-0001 project in the framework of the New Hungarian Development Plan. The realization of this project is supported by the European Union, co-financed by the European Social Fund. The presented work was supported by the DAAD Research Project No.29735 (2012-2013).



References

- [1] König W., Klinger M., Link R.: Machining hard materials with geometrically defined cutting edges, fields of applications and limitations, Annals of the CIRP Vol.39/1/1990 pp.61-64
- [2] Kaiser M.: Hartfeinbearbeitung von einsatzgehärteter Stahl mit PKB Werkzeugen, IDR (1992) 1. pp.24-33
- [3] Tönshoff H. K., Arendt C., Ben Amor R.: Cutting of Hardened Steel. Annals of the CIRP Vol. 49/2, 2000, pp. 547-566.
- [4] Fridrik L., Kundrák J., Grey K.: Nachschliff von Werkzeugen aus Elbor-R (Komposit 01) Wiss. Z. Techn. Hochsch. Magdeburg 29. Heft 8 pp.45-47., 1985.
- [5] Kundrák J., Zubar V.P.: Sherokhovatost poverkhnosti pri obrabotke vnutrennikh cilindricheskikh poverkhnostej. Rezanie i instrument, No. 34, pp.59-62., 1985.
- [6] Kundrák J.: Kachestvo poverkhnosti pri tochenii i rastachivanii zakalennykh stalej rezcami iz PSTM na osnove nitrida bora. Rezanie i instrument, No. 49, pp.23-27, 1994.
- [7] Klocke F., Brinkmeier E., Weinert K.: Capability Profile of Hard Cutting and Grinding Process, Annals of the CIRP Vol.54/2/2005 pp.22-54
- [8] Rech J, Moison A.: Surface integrity in finish hard turning of case hardened steels, Int. Journal of Machine Tools and Manufacture 43 (2003) pp.543-550
- [9] Sahin Y., Motorcu AR.: Surface roughness model in machining hardened steel with cubic boron nitride cutting tool, Int. Journal of Refractory Metals and Hard Materials 26 (2008) pp.84-90
- [10] Kundrák J.: Mamalis AG., Markopulos A.: Finishing of hardened boreholes: Grinding or Hard Cutting?, Materials and Manufacturing Processes 19/6/2004 pp.979-993
- [11] Kundrák J., Bana V.: Comparison of Surface Roughness of Hard Turned and Ground Surfaces Rezanie i instrument v technologicheskikh sistemax (Cutting and tools in manufacturing systems), No 56. 2000. pp.103-108
- [12] Fleming M., Wickman A.: PCBN in the Automotive Industry, IDR 2/2006 pp.26-31
- [13] Weinert K., Johlen G.: Kombinierte Bearbeitung durch Hartdrehen und Schleifen, IDR Archiv 1/2003
- [14] Johlen G.: Kombinierte Bearbeitung von Futterteilen durch Hartdrehen und Schleifen, IDR Archiv 1/2004
- [15] Tóth T; Kundrák J; Gyáni K: The removal rate as a parameter of qualification for hard turning and grinding Tools And Methods Of Competitive Engineering Vol. 1 and 2, Apr. 13-17, 2004 Lausanne Switzerland, pp.629-639, 2004
- [16] Kundrák J., Tóth T., Gyáni K.: How to make a choice of machining methods on the basis of economy: comparison between hard turning and grinding The Eleventh International Conference on Machine Design and Production, Conf. proc. 13-15 October 2004, Antalya, Turkey, Matimaren, pp.31-45



DENSITY FUNCTIONAL THEORY STUDY OF ALUMINUM DOPED HEXAGONAL ZINC OXIDE SHEETS

H. Kokten¹, S. Erkoç¹

¹ Department of Physics, Middle East Technical University, 06800 Ankara, Turkey

Keywords: h-ZnO monolayer, density functional theory, formation energy.

Abstract. We systematically investigated the structural and energetic properties of both the relaxed and the unrelaxed cases of Al atom doped in the hexagonal ZnO sheets using density functional theory calculations. Al atom has been substituted in a neutral charge state on both the Zn and the O site in the system as impurities. A systematic study has been performed to see the effect of cell size on the calculated quantities, such as formation energy, charge and bond length. Although it is found that the formation energies of Al on both Zn and O sites are both low in the hexagonal ZnO sheet, the Al atom on the Zn site is more favorable due to the fact that its formation energy is comparably lower than that of the O site.

Introduction

Zinc oxide (ZnO) is an important II-VI compound semiconductor with potential applications in electronics and optoelectronics because of its wide bandgap [1]. The electrical properties and magnetic behavior of materials can be modified by doping. The impurities such as B, Al, Ga, C, N etc. can modify the electronic structure and optical properties of the intrinsic ZnO. Al doped ZnO can be used as a transparent conductive oxides (TCOs). The other commercial applications are the front contact for solar cells and the front contact of liquid crystal displays [2-4].

In recent years, Graphene-like hexagonal ZnO (h-ZnO) is a two dimensional (2D) monolayer of ZnO structure with a direct wide band gap [5,6]. The formation of planar sheets of ZnO observed experimentally by Tusche et al. [7] There is some theoretical and experimental studies about the pristine and doping of atoms in a h-ZnO sheet [8-14].

Al, as a Group III element, is mostly used as a dopant for technological applications of ZnO [15-17]. We have performed a systematic study Al-doped ZnO monolayer to see the effect of cell size on charge, bond length, and formation energy.

Computational Methods

The calculations in the present work are performed by using the CRYSTAL03 package program [18], in which the density functional theory (DFT) type of calculations are implemented. CRYSTAL03 uses the localized Gaussian-type basis sets: 86-411d31G basis set was used for Zn atom, 8-411G was used for O atom, and 8-511G* was used for Al atom. Experimental values of bulk lattice parameters ($a=3.245$ Å and $c=5.207$ Å) were used [19]. CRYSTAL03 computes the matrix elements of the coulomb and exchange terms by direct summation of infinite periodic lattice. The reciprocal space integration was performed by sampling the Brillouin zone of the unit cells with the $8 \times 8 \times 1$ and $8 \times 16 \times 1$ Monkhorst-Pack net [20] that provides the balanced summation in direct and reciprocal space [21]. The numerical thresholds used to ensure the numerical convergence of the self-consistent-field procedure was set to 10^{-9} a.u. for the total energy.

The Al doped h-ZnO monolayer has been investigated by DFT and the calculations have been performed by using the B3LYP hybrid functional. The full geometry optimization and the energetic calculations have been carried out. One Zn or O atom is replaced with one Al to create the doping atom (Al_{Zn} , Al_O). To evaluate the relative stability of Al doping in h-ZnO monolayer with respect to the perfect h-ZnO monolayer, the formation energies have been obtained from the relation,

$$E_f(X) = E_d + E(\text{Zn or O}) - E_p - E(X) \quad (1)$$

where E_d is the energy of the defective system, E_p is the energy of the perfect system and $E(\text{Zn or O})$ is the energy of the isolated zinc or oxygen atom, whereas $E(X)$ is the energy of the isolated dopant atom (Al). To be able to see the size effect on the calculated quantities, different unit cell sizes have been considered, such as 4×4 , 5×5 , 6×6 , 7×7 , and 8×8 . The corresponding total number of atoms for these models are 32, 50, 72, 98, and 128, respectively.

Results and Discussions

We have tried several working cell sizes to see the convergency in the calculated quantities, which are tabulated in Tables 1 and 2 with respect to working cell size. A sample picture for optimized Al substituted for Zn model (Al_{Zn}) generated from 7×7 working cell is displayed in Fig. 1. Some of the calculated quantities show a smooth convergency, however some of them show slight fluctuations. Bond lengths show both behavior depending on dopant position. On the other hand excess charges show a size independent character. Furthermore, the calculated energies also show both behavior. However, we should note that the fluctuations seen in Table 2 are very small.

The structural changes caused by the substitution atoms are significant. The optimized bond length of $d(\text{Zn-O}) = 1.874$ Å for the pristine structure is in good agreement with experimental value of $d(\text{Zn-O}) = 1.92$ Å [7] and theoretical values of $d(\text{Zn-O}) = 1.852$ Å by Tu and Hu [8], 1.895 Å by Topsakal et al. [5], 1.853 Å by Tu [6], 1.85 Å by Wang [9]. The bond lengths of the doped h-ZnO and the charge transfers from

Al atom to h-ZnO layer are given in Table 1. The charge transfer from the substituent atom to the h-ZnO sheet shows an interesting feature. As seen from Table 1, in the Al substituted Zn case $d(\text{Al}_{\text{Zn}})$ bond reduces about %9.8 with respect to the pristine case, on the other hand, in the Al substituted O case $d(\text{Al}_{\text{O}})$ bond increases about %17.1 (for 4x4) and about %18.8 (for 8x8 cell) with respect to the pristine case. We should note that bond length change does not depend on cell size in Al_{Zn} case, but it shows a size dependence in Al_{O} case. Comparing the formation energies and the bond lengths the trend seen in the calculated quantities look meaningful.

From Table 2 one can see that the largest deviation in the formation energy of the relaxed case between the calculated values of the 4x4 model and the 8x8 model is about 0.36 eV for Al_{O} , whereas the difference is about 0.12 eV for Al_{Zn} . The formation energies of Al substitutional defects (Al_{Zn} and Al_{O}) were calculated in Wurtzite ZnO by Li et al. [22], the corresponding values are -9.71 eV and -2.91 eV, respectively. As stated in [22] "The low formation energies mean a high solubility of Al donor and thus high concentrations of electrons in the crystal". According to the present calculations Al_{Zn} is the most favorable case. It is interesting to note that the differences in formation energies between unrelaxed and relaxed cases show dopant site dependence; Al_{O} model has larger difference than Al_{Zn} model.

Table 1. Al doped h-ZnO monolayer: the bond length (d , in Å) and charge transfer (e).

Model	$d(\text{Al}_{\text{Zn}})$	$d(\text{Al}_{\text{O}})$	Charge(Al_{Zn})	Charge(Al_{O})
4x4	1.699	2.194	0.212	0.252
5x5	1.698	2.210	0.212	0.252
6x6	1.698	2.219	0.212	0.252
7x7	1.698	2.225	0.211	0.252
8x8	1.698	2.227	0.211	0.251

Table 2. Defect formation energies (in eV) of h-ZnO monolayer (relaxed E_f , and unrelaxed E_{f0}).

Model	Atomic % of doping	$E_f(\text{Al}_{\text{Zn}})$	$E_f(\text{Al}_{\text{O}})$	$E_{f0}(\text{Al}_{\text{Zn}})$	$E_{f0}(\text{Al}_{\text{O}})$
4x4	3.125	-16.067	-9.660	-14.841	-5.797
5x5	2.000	-16.375	-10.779	-14.795	-5.752
6x6	1.388	-15.984	-9.924	-14.772	-5.739
7x7	1.020	-15.984	-10.234	-14.758	-5.734
8x8	0.781	-16.187	-10.019	-14.983	-5.733

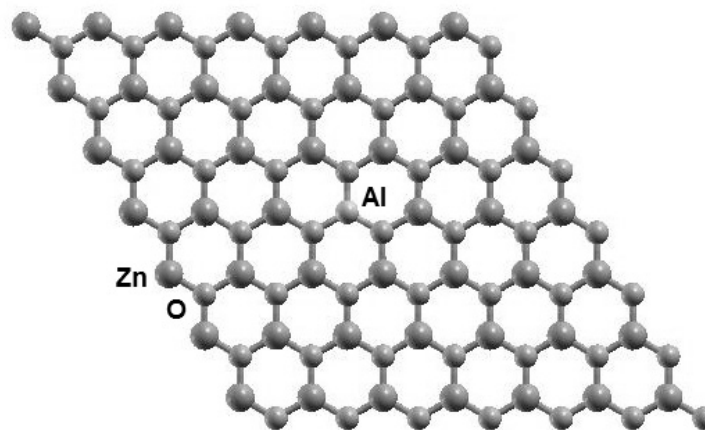


Fig. 1 Optimized 7x7 h-ZnO monolayer working cell for Al substituted (Al_{Zn}) model.

Acknowledgment

One of the authors (HK) would like to thank METU for providing support to attend the IN-TECH-2012.



References

- [1] O.Ozgur, Y.I. Liu, A.Teke, M.A. S. Dogan, V. Avrutin, S. –J.Cho, H. Morkoc: A comprehensive review of ZnO materials and devices, *Journal of Applied Physics*, Volume 98, Issue 4, p. 041301-103.
- [2] C. Klingshirn: ZnO:Material, Physics and Applications, *ChemPhysChem*, Volume 8 (2007), p. 783-803.
- [3] A. De Sio, K. Chakanga, O. Sergeev, K. von Maydell, J. Parisi, E. von Hauff: *Solar Energy Materials and Solar Cells*, Volume 98 (2012), p. 52-56.
- [4] J. Perrenoud, L. Kranz, S. Buecheler, F. Pianezzi, A.N. Tiwari: The use of aluminum doped ZnO as transparent conductive oxide for CdS/CdTe solar cells, *Thin Solid Films*, Volume 519 (2011), p. 7444-7448.
- [5] M. Topsakal, S. Cahangirov, E. Bekaroglu, S. Ciraci: First-principles study of zinc oxide honeycomb structures, *Physical Review B*, Volume 80(2009) p. 235119-14.
- [6] Z.C. Tu : First-Principles Study on Physical Properties of a Single ZnO Monolayer with Graphene-Like Structure, *Journal of Computational and Theoretical Nanoscience*, Volume 7 (2010), p. 1182-1186.
- [7] C. Tusche, H.L. Meyerheim, J. Kirschner: Observation of Depolarized ZnO(0001) Monolayers: Formation of Unreconstructed Planar Sheets, *Physical Review Letters*, Volume 99 (2007) , p. 026102-4.
- [8] Z.C. Tu, X. Hu: Elasticity and piezoelectricity of zinc oxide crystals, single layers, and possible single-walled, *Physical Review B*, 74(2006) p. 035434.
- [9] Y. Wang, Y. Ding, J. Ni, S. Shi, C. Li, and J. Shi: Electronic structures of fully fluorinated and semifluorinated zinc oxide sheets, *Applied Physics Letters*, Volume 96 (2010), p. 213117-3.
- [10] T.M. Schmidt, R.H. Miwa, and A.Fazzio: Ferromagnetic coupling in a Co-doped graphenelike ZnO sheet, *Physical Review B* Volume 81 (2010), p.195413-4.
- [11] F. Wang, R. Liu, A. Pan, L. Cao, K. Cheng, B. Xue, G. Wang, Q. Meng, J. Li, Q. Li, Y. Wang, T. Wang, B. Zou: The optical Propertie of ZnO sheet electrodeposited on ITO glass, *Materials Letters*, Volume 61 (2007), p. 2000-2003.
- [12] I. Demiroglu, D. Stradi, F. retical study of a ZnO graphene analogue: adsorption on Ag(111) and hydrogen transport, *Journal of Physics Condensed Matter*, Volume 23 (2011), p. 334215-6.
- [13] C. Liu, D. Meng, X. Wu, Y. Wang, X. Yu, Z. Zhang, X.Liu: Synthesis, characterization and optical properties of sheet-like ZnO, *Materials Research Bulletin*, 46(2011) p. 1414-1416.
- [14] Q. Chen, J. Wang, L. Zhu, S. Wang, and F. Ding: Fluorination induced half metallicity in two-dimensional few zinc oxide layers, *The Journal of Chemical Physics*, Volume 132 (2010), p. 204703-6.
- [15] R.G. Dhere, M. Bonnet-Eymard, E. Charlet, E. Peter, J.N. Duenow, J.V. Li, D. Kuciauskas , T.A. Gessert: CdTe solar cell with Industrial Al:ZnO on soda-lime glass, *Thin Solid Films*, Volume 519 (2011), p. 7142-7145.
- [16] J.F. Chang, H.H. Kuo, I.C. Leu, M.H. Hon : The effects of thickness ond operation temperature on ZnO:Al thin film CO gas sensor, *Sensors and Actuators B*, Volume 84 (2002), p. 258-264.
- [17] A. Crossay, S. Buecheler, L. Kranz, J. Perrenoud, C.M. Fella, Y.E. Romanyuk, A.N. Tiwari: Spray-deposited Al-doped ZnO Transparent contacts for CdTe solar cells, *Solar Energy Materials and Solar Cells*, Volume 101 (2012), p. 283-288.
- [18] V.R. Saunders, R. Dovesi, C. Roetti, C.M. Zicovich-Wilson, and N.M. Harrison, *CRYSTAL03 User's Manual*, Universita di Torino, Torino, 2003: www.crystal.unito.it.
- [19] X Chen. X. Zhang, Z. Zhang, J. Liu, Y. Qian: A precursor-growth-pyrolysis approach to two-dimensional ZnO micro-platelets with Hexagonal morphologies, *Journal of Crystal Growth*, Volume 280 (2005), p. 244-249.
- [20] H.J. Monkhorst, J.D. Pack: Special points for Brillouin-zone integrations, *Physical Review B*, Volume 13 (1976) p. 5188-5192.
- [21] T. Bredow, R.A. Evarestov, K. Jug: Implementation of the cyclic cluste model in Hartree-Fock LCAO calculations of crystalline systems, *Phys. Stat. Solidi(b)*, Volume 222 (2000) p. 495-516.
- [22] P. Li, Sh.H. Deng, Y.B. Li, J. Huang, G.H. Liu, L. Zhang: Aluminum and nitrogen impurities in Wurtzite ZnO: first-principles studies, *Physica B*, 406(2011) p. 3125-3129.



International Conference on Innovative Technologies, IN-TECH 2012,
Rijeka, 26. - 28.09.2012



PRELIMINARY CALIBRATION AND FUTURE DEVELOPMENTS OF A MINIATURIZED TENSILE TEST DEVICE BASED ON FLEXURE HINGES

A. Copeta¹, L. Dassa¹

¹ Mechanical and Industrial Engineering Department, University of Brescia, via Branze 38, Brescia, Italy

Keywords: compliant mechanism, flexure hinge, miniaturized tensile test device

Abstract. A high precision tensile test device has been designed and built to equip a commercial X-Ray micro-diffractometer in order to carry out tests on plastic specimens in its narrow active area. The device main feature is that the linear motion is performed not by way of standard slides but with a compliant mechanism based on flexure hinges in order to avoid backlash and slip stick phenomena which are common in standard slides. In the first part of this paper we report the results of some preliminary calibration of the device, carried out with a laser displacement sensor: the goal was to verify the parasitic transversal motion of the moving parts. In the second part we carry out a detailed analysis of the DOFs of this device, based on different approaches to the study of a mechanism with flexure hinges: the standard approach and the Henein's innovative approach. The comparison between the different solutions developed has been based on a finite element analysis. The results of such analysis have led the authors to catch the enormous importance of the guidelines suggested by the Henein's point of view. The consequence has been the redesign of the same device with an improvement in terms of transversal stiffness and displacement accuracy.

Introduction

The Chemistry Laboratory of the University of Brescia needed a custom traction device capable of performing tensile actions on a small polymeric specimen within a commercial X-Ray micro-diffractometer. The device is made of flexure joints in order to reduce as much as possible backlash and slip stick phenomena. The slide, suitable for ± 2 mm of stroke, is a fully compliant mechanism manufactured by way of EDM on 7075 aluminum alloy plates. The design process has been fully described in a dedicated paper [1]. In Fig. 1 it is possible to see the device - named Bydlo - installed into the active area of the micro-diffractometer.

In order to check the performance of the device some preliminary calibration tests have been carried out and the results are showed in the first part of this paper. The tests have been performed without the specimen in order to verify the performance of the linear slide without load influence.

During the test period we have been in contact with one of the most important expert in the flexure mechanism field, Mr. S. Henein [2], who suggested to us to study this compliant mechanism with his innovative approach. The innovation brought by the Henein's approach lies in the way it discards the traditional correspondence among the rigid bodies and the flexure mechanisms. The attention is focused on the DOFs of each single flexure joint instead of on the DOFs of a possible corresponding device with rigid bodies. This leads to a different way to analyze the flexure devices. This different approach has led us to a new design of the linear slide of the traction device, with a considerable improvement of the performance as shown by FE analyses.

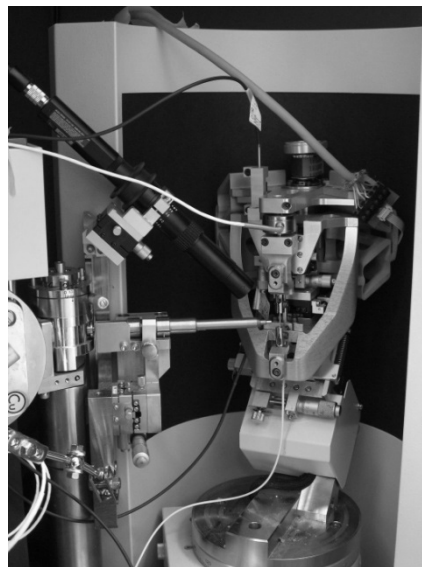


Fig. 1 The traction device installed into the micro-diffractometer

Part 1: performance tests

Test on vertical performances

The first test was performed in order to verify the relationship between the device displacement sensor (DVRT sensor) and the real displacement of the mobile link of the device. The test set is compound by a laser sensor (Lmi3D LTS 15/1) that provides the following performance: resolution 0.25 μm , accuracy $\pm 1 \mu\text{m}$, working range 1 mm, linearity 1 μm . The laser sensor is mounted on a vertical linear stage (PI M521.5i) with the following performance: resolution 0.1 μm , accuracy in the working range 2 μm . The target of the laser beam is the top of the device that is the mobile link of the tensile test device (see Fig. 2). The device has a stroke of $\pm 2 \text{ mm}$ but the test were carried out only in the central part of the stroke, that is $\pm 0.5 \text{ mm}$, according with the laser sensor working range. The difference between the DVRT reading and the laser sensor reading for the vertical test is shown in Fig. 3. The maximum absolute deviation found is equivalent to 33 μm , while the average absolute deviation is 14.5 μm . It has to be noticed that the absolute deviation is bigger at the wings of the working range and close to zero in the middle. This may be due to the laser sensor calibration (polynomial instead of linear); further investigations and tests are planned to verify this aspect.

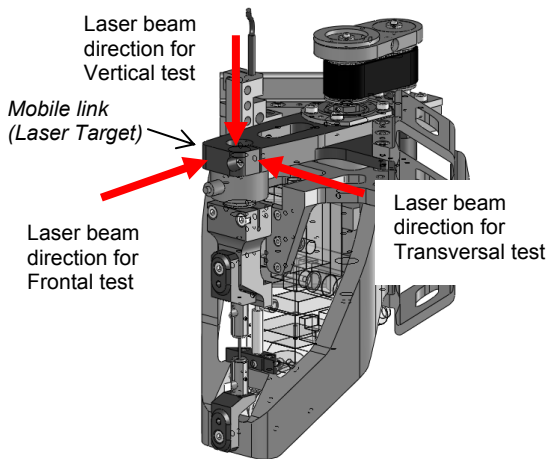


Fig. 2 laser direction for different tests

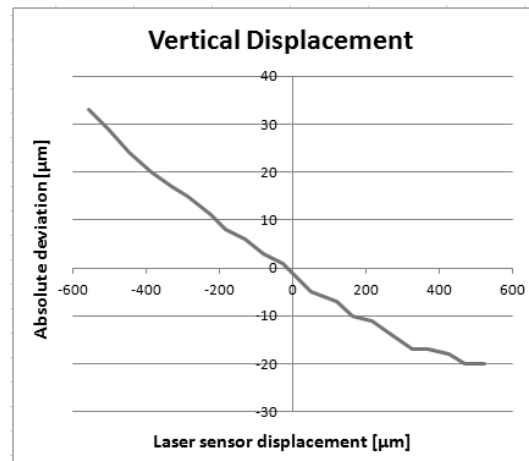


Fig. 3 Vertical test

Test on transversal performances

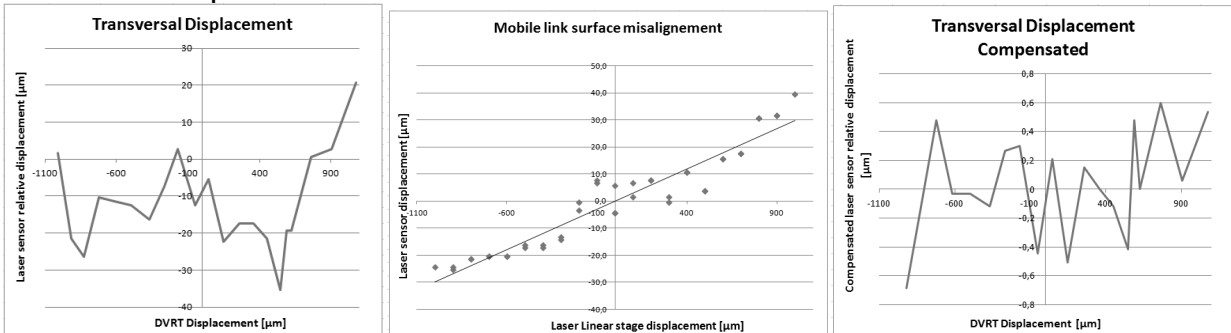


Fig. 4 transversal test

In this case the laser beam points to the mobile link of the device in an orthogonal direction to the device vertical axis, as you can see in Fig. 2. The test goal was to evaluate the transversal slide error in order to verify the entity of the parasite motion of the mobile link with respect of the theoretical straight line. The first analysis has been carried out moving up and down the mobile link of the device. The measurements are shown in Fig. 4a. The performances seem very poor ($\pm 30 \mu\text{m}$ over a $\pm 1 \text{ mm}$ range) but this measurement have to be correct taking into account the device misalignment with respect to the laser axis. The error due to the misalignment of the device with respect to the laser has been evaluated (see Fig. 4b) and then the first analysis has been corrected. The results are shown in Fig. 4c, where it is possible to see that the effective transversal error is below the accuracy of the laser, so below $\pm 1 \mu\text{m}$ over a $\pm 1 \text{ mm}$ range of motion.

Test on frontal performances

This test has been performed as for the transversal test, with the laser placed as shown in Fig. 2. The results are the same as the transversal motion, that is the frontal parasitic motion is not measurable, since it is lower than the laser precision.

Part 2: device improvement

Analysis of the DOFs of the actual design

In order to approach a possible improvement of the performance of the device, a deep analysis has been performed on the frame geometry. As said before, the device frame acts as a linear slide thanks to the presence of flexure hinges. The actual version has been designed at the beginning of our knowledge in flexure hinges, exploiting a 2D approach (see Lobontiu [3] and Howell [4]) and translating it to a 3D mechanism with proper modifications. The two arms of the device have been individually analyzed (replacing each flexure hinge with an ideal hinge) and then the two arms have been analyzed together. With this approach it has been obtained that each arm has 2

DOFs (see [2]) while the contemporary presence of two chains generates the undesired DOF of each arm and enable only the vertical translation. More information can be found in [5].

The review of the project following the Henein's approach [2] has led us to consider all the circular flexure hinges not as a single DOF connection but as a 3 DOFs connection: this has a strong impact on the kinematics analysis of the compliant devices.

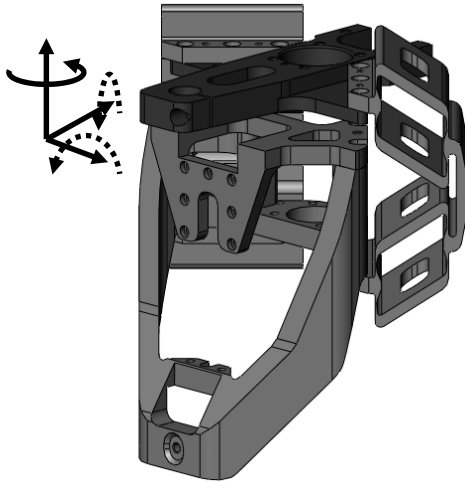


Fig. 5: Current frame of the traction device

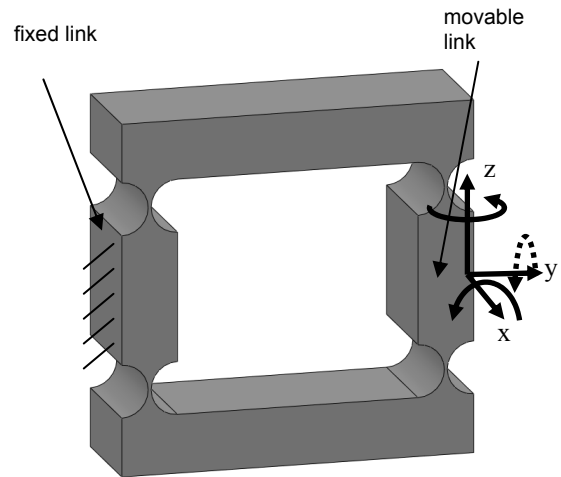


Fig. 6: Single component of the Bydlo current frame

In Fig. 5 it is shown the linear guide of the device as it is now. The lower part is the fixed link whereas the upper dark plate is the mobile link. To simplify the DOFs analysis only the system in Fig. 6 is considered. We discovered that there are 2 internal DOFs (linear displacement of the 2 horizontal intermediate links not locked) and that the mobile link has 5 DOFs (continuous line: free DOF / dotted line: locked DOF): only its rotation around the y axis is locked, and it is locked twice. In traction device kinematics, every chain is composed by two elements such as the four-bars linkage in Fig. 6: the DOFs at the end of each arm are the same as the single element. In the end, composing the 2 chains with 5 DOFs it is possible to analyze the DOFs of the mobile link: the composition is simple because the two chains are orthogonal. We obtain that the mobile link has 4 DOFs: only two rotations are locked, the other DOFs are free. So it is possible to conclude that the designed linear stage is not a linear bearing with respect to the Henein guidelines. Translating this argument in "stiffness" aspects, it means that the stiffness corresponding to a free DOF will be much lower than the stiffness corresponding to a locked DOF. In our case we see that all the linear stiffness are in the same order of magnitude, while we would have the transversal and the frontal stiffness higher than the vertical one.

Suggested improvements on the design (design B and C)

Following the Henein's approach it is possible to outline two possible solutions. In the first one, each kinematics chain composing the "arms" of the 'Sarrus mechanism' can be replaced with a series of two 4-prismatic-hinges guides, as shown in Fig. 7. Each 4-prismatic-hinges slide has only 1 DOF: so each kinematics chain has 2 DOFs (according to the Henein analysis) and the coupling of the two arms provides a device with only one external DOF. Henein provides also the possibility to evaluate the internal DOFs and the over-constraint degree: in this case there are a lot of internal DOFs (each 4-prismatic-hinges bearing has 6 internal DOFs) and some over-constraint degrees too (for instance both the kinematics chains lock all the rotations). In this case we are not interested to evaluate this features, but it is important to remind that the solution is over-constrained because of the problems that this condition can cause. In this application the internal DOFs are less important because the device does not work in high frequencies domain.

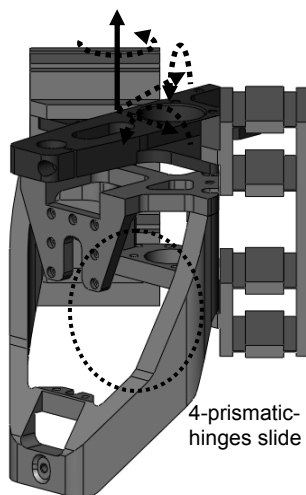


Fig. 7: design B for the Bydlo frame

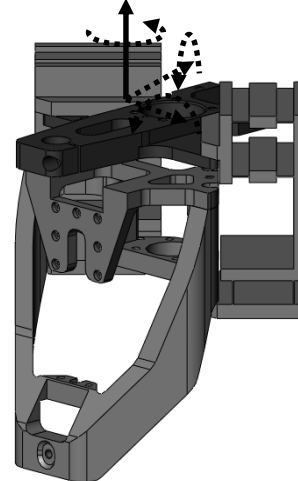


Fig. 8: design C: the Sarrus/Henein mechanism in the Bydlo frame

The second possibility is to use the Sarrus/Henein mechanism, that is a single-DOF linear bearing. Henein ([2] page 154) presents his personal vision of Sarrus' linear guide. In fact, he uses the three-dimensional coupling of two kinematics chains to have a perfect linear displacement. In Fig. 8 it is shown the integration of the Sarrus/Henein kinematics in our device. We have added a small modification with respect to the original idea in order to have equal kinematics chains; so it is possible to manufacture two planar equal pieces to be assembled later. The slide becomes more over-constrained but with respect to the functionality of the device, there is no difference. Let us focus on a single arm: the idea at the basis of this design starts from a 4-prismatic-hinges slide : to compensate the parasitic transversal motion Henein introduces another 2-parallel-blades guide in an orthogonal direction. At this moment each arm has 2 DOFs: the same 2 DOFs of each arm in the solution B. So again combining the two chains the mobile link will have a perfect linear motion and a single DOF. One of the advantages with respect to the first solution is that this mechanism has a lower number of internal DOFs. The other one is that it is less over-constrained: this could seem a minor remark, but we should take into account that every over-constraints can be amplified during machining and can decrease the device performance.

Comparison between different possibilities

To choose the new solution it will not be sufficient to verify the kinematics but it will be mandatory to verify the stiffness of the new solutions, comparing these one with the current device. Due to the complexity of the device, this analysis has been performed with FE analysis.

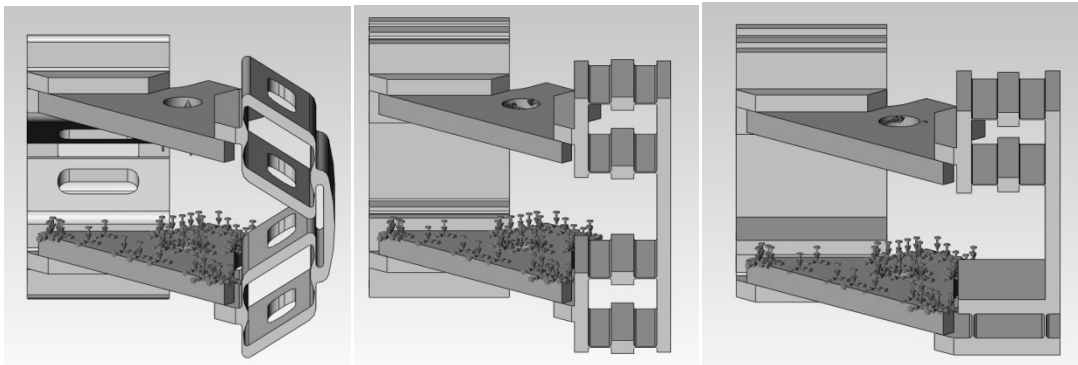


Fig. 9: the 3 different load cases

For all the different designs the common feature are the following: the material is aluminum 7075 T6, the maximum displacement of the complete device is 2 mm, the thickness of each flexure has been selected in order to have the same maximum stress on all the solutions. The other flexure dimensions have been chosen following the Henein's guidelines. The comparison have been done considering the three linear stiffnesses of the device. As shown in picture 9, the different loads have been applied on the mobile link. The performance of the 3 solutions are summarized in table 1. It is possible to observe that the vertical stiffness is in the same order of magnitude, where the solution 3 is the more yielding. This was foreseen since during vertical motion, only 4 blades are deformed instead of 8. Then we observe that the solution 2 and solution 3 are stiffer than solution 1 in transversal and frontal direction. In fact one of the weak points of the solution 1 are the transversal and the frontal stiffness: as derived from the DOFs analysis with the Henein approach the DOFs corresponding to the transversal and frontal motion are not locked, that is are in the same order of magnitude as the vertical stiffness. This is what we exactly wanted. In fact the solution 1 weak point is exactly the ratio between transversal and vertical stiffness and the ration between frontal and vertical stiffness. The other solutions improve the performance and are comparable in term of performance. The solution 3 should be preferable since there is a lower blade number, so it is cheaper. In addition we don't need small thickness for the vertical blades.

Table 1. Comparison

	Design A	Design B	Design C
Kvert [N/mm]	37.9	46.7	13.6
Ktrasv [N/mm]	113	1138	943
Kfront [N/mm]	377	1174	1314

In order to complete the analysis we will check the 3 other stiffness: in fact to fully characterize the device it is necessary to evaluate the 3 angular stiffness of the device. This will be done in the next future.

Conclusion

The tests performed on the manufactured device have shown a good performance without applied load. This is the first fundamental step in order to calibrate the device. Further tests will be carried out with the device under load in order to verify the device performances under standard conditions. In addition other tests will be done in order to verify the friction behavior of the flexure vertical slide.

About the new solutions for the compliant slide, we have found new solutions that improve the device performance and that are easy to install, since the arms are interchangeable.

References

- [1] L. Dassa, V. Villa, Design and testing of a mechanical device able to make possible XRD stress analysis, *Proc of Congreso Internacional Conjunto XXI Ingegraf - XVII ADM*, Lugo, Spain, 9th-13th June 2009
- [2] Henein S., *Conception des guidages flexibles*, Henein S., Conception des Guidages Flexibles, (Presse Polytechniques et Universitaires Romandes, Lausanne, 2004).
- [3] Lobontiu N., *Compliant Mechanisms: Design of Flexure Hinges*, (CRC Press, 2002)
- [4] Howell L. L., *Compliant Mechanisms*, (John Wiley & Sons, New York, NY, 2001)
- [5] Dassa L., *Mechanisms based on flexure articulations*, PhD thesis, Università di Brescia, dottorato di Ricerca in Meccanica Applicata, Ciclo XXI

USE OF ONBOARD SHORT ARM HUMAN CENTRIFUGE TO CREATE ARTIFICIAL GRAVITY

N. Okhapkina¹, L. Strogonova²

¹ Moscow Aviation Institute, Moscow, GSP-3, A-80 Volokolamskoe Shosse,4, 125993, Russian Federation

² Moscow Aviation Institute, Moscow, GSP-3, A-80 Volokolamskoe Shosse,4, 125993, Russian Federation

Keywords: artificial gravity, onboard short-arm human centrifuge, terrestrial readapting, mechanical specifications, countermeasure, conditional standard gravity equivalent.

Abstract. Nowadays with the opportunity of manned flight to Mars the definition of engineering and medical aspects of space missions is kept. Among the aspects are health care and performance assurance of crew members during the long zero-g effect. Zero gravity results in harmful effects on various body systems. Among these are body fluid redistribution, muscle weakness, performance impairment, blood volume and red blood cell count reduction, calcium and phosphate loss, bone mass reduction, vestibular readjustment, sensory motor performance alteration. These physiologic impairments make operator's performance difficult and in addition complicate terrestrial readapting.

Ground and Space based researches have shown that the creation of conditional standard gravity equivalent on the spacecraft would be the best way to reserve harmful weightlessness effects. There are several methods for artificial gravity creation. However the most effective is the use of onboard short-arm centrifuge that allows producing short-term but terminal artificial gravity loads. Onboard short-arm centrifuge produces gravitational action on human body that would make countermeasures to most harmful microgravity effects possible. Onboard short-arm centrifuge could also be used for additional long-term training. Current short-arm centrifuge design projects need to be polished. This study was designed to observe optimum mechanical specifications, vibration and noise reduction devices, centrifuge equipment, optimum mode of exposure to acceleration.

Short-arm human centrifuge aboard of manned space stations and interplanetary spacecrafts could become a valid part of countermeasures focused on astronaut's health care and performance assurance during space flight and terrestrial readapting easement.

Introduction

Nowadays with the opportunity of manned flight to Mars the definition of engineering and medical aspects of space missions is kept. [1]. Among the aspects are health care and performance assurance of crew members during the long zero-g effect. In the interplanetary flight, the astronauts will have to adapt to a wide variety of different levels of gravity.

The flight from Earth to Mars will take from 6 to 9 months, during which the crew will be in a state of weightlessness. Stay on Mars will require adaptation to the conditions of gravity, equal to 0.38 g, followed by a period of weightlessness effects after spacecraft returns to Earth.

One of the harmful microgravity effects control methods is the use of traditional countermeasures which are developed in relation to orbital flights.

However, despite the measures used, the phenomenon of detraining develop on various organs and body systems and persist for 1.5-2 months after returning to Earth, even when using complex of therapeutic measures. Changes in bone tissue persist up to 2-3 years [2].

The main reason for insufficient effectiveness of traditional countermeasures is that it can not completely fill the absence of such gravity stimulus as: the disappearance of the hydrostatic blood pressure, the weight load on the musculoskeletal system and changes in the afferent systems functioning.

One of the possible problem solution under extended interplanetary flight would be the space-borne artificial gravity creation with onboard short-arm centrifuge. When creating artificial gravity it could only be spoken about conditional standard gravity equivalent.

The use of short-arm human centrifuge aboard the Mars spacecraft is the most drastic security measure of harmful microgravity effect.

When onboard short-arm centrifuge had been tested in Mars 500 program a number of design and methodological defects were identified and they are currently undergoing a comprehensive analysis. There are several technical difficulties in creating and testing the onboard short-arm human centrifuge.

The design requirements to the short-arm human centrifuge.

Currently the main emphasis of the studies is on human physiology and technical problems remain unconsidered. The following aspects haven't been resolved: design solution, energy issues, vibration isolation and noise isolation, the conjunction of short-arm centrifuge with spacecraft, methodological and ergonomic issues of the astronaut's placement.

Advantages and disadvantages were identified after analyzing the structures of various centrifuges.

List of researched centrifuges:

- IMBP, Russia, 1973-1979;
- Baylor College, USA, 1990 -1997;
- NASDA, Japan, 2002;
- NASA, USA, 2004;

- ESA, Europe, 2006;
- IMBP, Russia, 2007.

The advantages include the presence of veloergometer (IMBP, Baylor College, NASDA), the ability to change the lodgment relative to arm, and thus the distribution of overload (NASA, ESA, IMBP), the possibility of sitting and lying position (IMBP, NASDA, ESA), the presence of opaque igloo over man's head (IMBP, ESA), emergency stop button (ESA, IMBP).

The disadvantages include inconvenience in placing and removing the person (Baylor College, NASDA, ESA, IMBP), uncomfortable design of headrest and a striker (ESA, IMBP). With regard to IMBP centrifuge it is necessary to work on a system of placement and mounting, brake design, taking into account the smooth emergency braking, a balancing system, the ability to install additional wind deflector.

A number of design requirements were made based on this analysis.

Onboard short-arm human centrifuge consists of a base, an electromechanical actuator, frame of the centrifuge, fixed frame, lodgment and a cope. An external view of short-arm human centrifuge is shown on Fig.1.

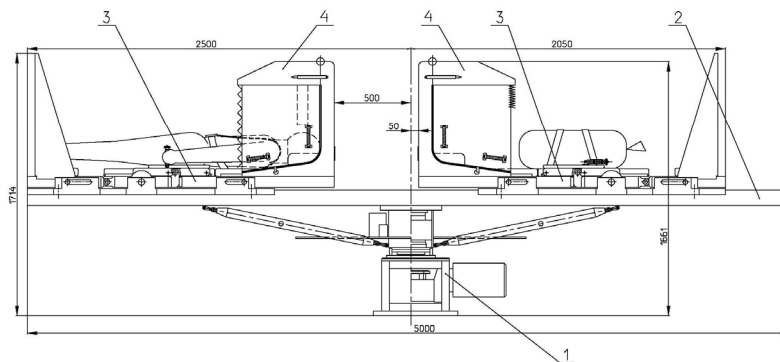


Fig.1. An external view of short-arm human centrifuge.

Where: 1 – a base, 2 – frame, 3 – lodgment, 4 – igloo.

Onboard short-arm human centrifuge has 2 arms. One arm is used to place a man on lodgment. Counterweights and equipment are based on the other arm. The arms have to have reinforced plain framing made of light metal profiles. The arm with the lodgment must withstand without bending, deflections and other deformations a person's weight up to 100 kg at the maximum overload.

Since the optimal human position during overload exposure and optimal head position relative to the axis of rotation haven't been found yet it is proposed to make a transformed lodgment. Lodgment is a three-link mechanism, each link consists of a flat frame. Back frame, seat frame and calves frame are interconnected with axes. Lodgement transforms from a horizontal position to the upright position. The lodgement seats must be made according to the human anthropometric parameters. To minimize the additional head movements during rotation, a special headrest should be installed.

While placing the person the lodgment is covered by two igloos to prevent optokinetic stimulus and cooling the body during long-term rotation because of the airflow. One igloo is only opaque from the outside and is located above the human head. Another igloo (hinged or movable) is situated above the man's body and legs. This cap should not hinder man's activities on the veloergometer. Igloos should have a semi-cylindrical shape, be light and permit rapid evacuation of person from the centrifuge in case emergency medical care is necessary.

Short-arm human centrifuge equipment.

To ensure optimal working conditions during testing and monitoring of the human condition following devices should be installed:

- color video monitoring system for the astronaut's face;
- two-way light and sound alarm system from a doctor (the commander) to the astronaut and conversely;
- duplex intercommunication loudspeaker system with physician's remote;
- "Perimeter" device to determine the changes in the field of vision;
- time rotation indicator.
- Astronaut's face should be light with the non-directional light to provide visual and TV monitoring. This lighting should not hinder the work with "Perimeter".
- The space under the igloo should have natural and forced ventilation systems.
- The system of natural ventilation should be provided by air intakes while rotating.
- Forced ventilation of the face should be carried out by a fan with an adjustable air exchange.

The list of recorded physiological parameters during the rotation on short-arm centrifuge:

- ECG;
- pulsogram of the earlobe vessels;
- toe pulsogram;
- blood pressure in the earlobe vessels;
- electrooculogram;
- tetrapolar rheography;
- blood pressure in the arm and lower leg;
- pneumogram;
- myogram.

The negative effects of gravity loads on the short-arm centrifuge and possible measures to prevent them.

Almost all of the negative effects of rotation on the short-arm centrifuge are related to the influence of two factors: the direct influence of the longitudinal-directed overloads and reactions associated with staying in a rotating system.



The main symptoms that limit the portability of + Gz g-exposure, that is used to create artificial gravity loads on the short-arm centrifuge, were marked by the cardiovascular system (sudden drop in blood pressure, the occurrence of visual disturbances and the appearance of other symptoms of presyncope) and were due to the effects of blood redistribution from head to the feet. It was found that for the prevention of these symptoms of the optimal g-exposure regimes which are well tolerated by man must be defined [3].

The other symptoms that may limit the portability of overloads could be motion sickness symptoms, as the unusual stimulation of the vestibular apparatus during rotation in the centrifuge of any radius can occur during active movements surveyed by the appearance of precessional acceleration and Coriolis acceleration. However, experimental studies' results have shown that accompanied by maintenance (head fixation and optokinetic stimulation exceptions by rotation in a darkened room) the emergence of motion sickness symptoms can be prevented.

While the idea of AG to prevent cardiovascular deconditioning is not new (White et al. 1966), the ideal combination of artificial gravity magnitude, frequency, and duration needed, perhaps in combination with exercise, is yet to be determined; multiple permutations of these variables have been tested in previous studies with varying levels of success [4].

Conclusion

Short-arm centrifuge on board of orbiting space stations and interplanetary spacecraft can be a significant element in the complex of countermeasures aimed at maintaining optimal health and performance of astronauts during flight, and - to ease readaptation to Earth's gravity conditions.

Before the short-arm centrifuge will be used as a countermeasure of negative microgravity effects, a large amount of studies to determine optimal regimes of rotation has to be done. One aspect of this problem is to minimize the time spent on countermeasures in space flight. The solution of this problem may require the creation of large magnitude but short duration overloads.

minussorok@mail.ru, buksan@list.ru

Acknowledgment

The authors gratefully acknowledge the support of the IMBP team and faculty of Moscow Aviation Institute.

References

- [1] A.S. Koroteev: Manned missions to Mars, (Moscow, 2006), p. 320.
- [2] A.R. Kotovskaya: Problems of artificial gravity: condition and perspectives, *Aerospace and ecological medicine*, 2008, v. 42, № 6, p. 74-83.
- [3] A.R. Kotovskaya, A. A. Shipov: Bio-medical problems in creation of artificial gravity, (Moscow, 1996), p. 204.
- [4] M. B. Stenger, J. M. Evans, C. F. Knapp: Artificial gravity training reduces bed rest-induced cardiovascular deconditioning, *Eur J Appl Physiol*, 2012, pp 605–616, 606.
- [5] K. Iwasaki, T. Sasaki, K. Hirayanagi: Usefulness of daily +2Gz load as a countermeasure against physiological problems during weightlessness. *Acta Astronaut*, (2001), pp227–235
- [6] L.B. Strogonova, N. Okhapkina: Use of onboard human short-arm centrifuge, *Aviation and Aerospace Innovations-2012*, p. 206
- [7] L.B. Strogonova, V. Stolyrchuk, S. Makarova: Habitability of a manned lunar stations: problems and methods of solution, *GLUC 2012 paper*

Currently the main emphasis of the studies is on human physiology and technical problems remain unconsidered. The following aspects haven't been resolved: design solution, energy issues, vibration isolation and noise isolation, the conjunction of short-arm centrifuge with spacecraft, methodological and ergonomic issues of the astronaut's placement.



International Conference on Innovative Technologies, IN-TECH 2012,
Rijeka, 26. - 28.09.2012



USE THE METHODOLOGY OF USER CENTERED DESIGN FOR LEARNING FURNITURE DESIGN

Abdel Bary, Salwa Yousef ¹

¹ Department of Interior Design and Furniture, *Faculty of Applied Arts*, Helwan University, Egypt

Keywords: Furniture Design, Furniture Design Learning, Methodology, User-Centered Design, UCD, UCD Process, Usability, virtual learning environment and context.

Abstract. The paper objective is demonstrating a new perspective in learning of furniture design courses, which follows the modern methods and methodologies in product design such as User-Centered Design (UCD).

User-Centered Design (UCD) methodology attempts to improve the quality of furniture design education to be useful, by increasing and upgrade student's practical skills, experience and mental communication skills. It may also help train students deal with the real users and how to involve them in design, and enable students dealing with marketing. The student will be interested and excited with this type of learning, because it uses simulation and virtual learning environment. The paper offers a methodology of user-centered design for furniture and how I integrated it into the curriculum and the syllabus. The curriculum depends on the iterative design process as User-Centered Design, so it was a combination of in-class lecture, demonstration, and hands-on activities in creativity. The material was presented in the same order as the User Centered Design Process itself –which chosen to emphasize the steps and activities at each stage in the UCD process with exposure to the process inputs (context in use), and outputs (usability, as an outcome of UCD practices, and sustainability).

Introduction

User-Centered Design evolved in the field of human-computer interaction, though the process can be applied to any product with end users. The term user-centered design places the focus on the users throughout planning, design, and development, and so has become more widely used [6]. More recently, the term Human Centered Design was introduced to denote a multi-disciplinary activity, which incorporates human factors and ergonomics knowledge and techniques, and advances an approach to interactive system development that focuses specifically on making systems usable [ISO,1997b] [5]. Although the benefit of UCD, Usability describes how well a product can be used for its intended purpose by its target users with efficiency, effectiveness, and satisfaction, also taking into account the requirements from its context of use [10].

Research problem and its importance:

1. Requirement of UCD methodology for design learning, and lack of people with UCD skills and experience.
2. Furniture design learning for students is limited in studios or classrooms faraway of context in use.
3. Few subjects of furniture study are linked with the actual needs of institutions or industry.
4. UCD skills and experience lead to innovation.

Goals, aims

1. Advance a new perspective in teaching and learning of furniture design courses.
2. Develop furniture design methodology, for learning, following the methods and methodologies in product design such as UCD.
3. Providing students with UCD skills and experience, and training students to deal with the real users and how to involve them in design.
4. Increase the rate of acceptance of UCD in industry especially furniture.
5. The pursuit of a better understanding of furniture design and improvement in the quality of furniture design education.
6. Using simulation and virtual learning environment in learning methodology.

Hypotheses

1. UCD methodology will improve the quality of furniture design education.
2. Using virtual learning environment and simulation helps to recognize the behavior patterns of users, and develop the students' skills of creative thinking.
3. Providing a real user /customer, design tools and suitable learning environment may be help the student to innovate.

Themes:

1. UCD and Usability
2. The User-Centered Design Process as a curriculum
3. User-centered design Principles and benefits

1- UCD and Usability

UCD is a methodology and philosophy for creating products, makes users and their goals the primary driver in development. However, several challenges must be surmounted in order to increase the rate of acceptance of UCD in industry [8]. Through UCD we can find out, who are users? Why they buy this furniture? Where and how they use furniture (context, environment)?

Furniture UCD is a methodology that puts the intended users of furniture at the centre of its design and puts their needs as the driving force in design development. By dealing directly with the user at key points in the design to make sure the furniture will verify their requirements.

Usability has quite a simple definition, it means that people can use a product easily and efficiently to accomplish their own tasks, making sure that the people who will use the product or can use it to achieve their needs and goals productively, suitable with their own physical and social environments [10].

2- The User-Centered Design Process- as a curriculum

User-Centered Design is represented as an iterative four stages cycle of Understanding& specifying, Design & Concept, Prototyping, and Evaluation, as illustrated in Fig. 1.

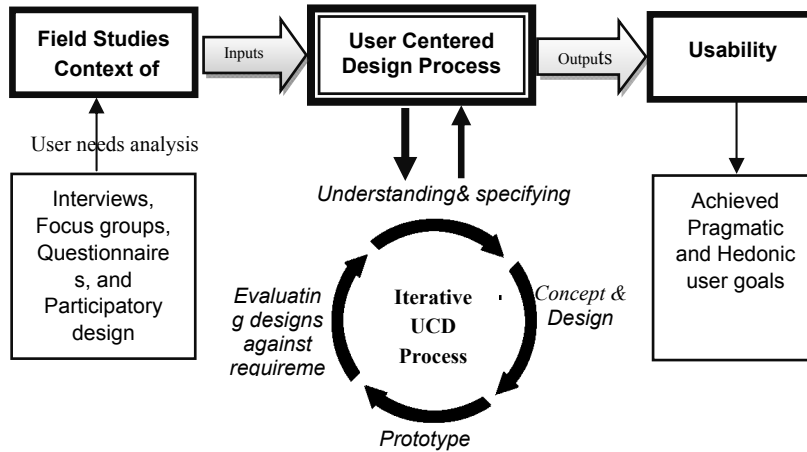


Fig. 1 The User-Centered Design Process- methodology of learning

2-1 Process Inputs (Field Studies)

User and task observations, where observing users at their jobs, identifying their typical work tasks and procedures, analyzing their work processes, and understanding people in the context of their work. Interviews (interview process has 6 phases, shown in fig. 2, Focus groups, Questionnaires, Participatory design (designing with users), and Benchmarking and competitive analysis. Sometimes using recordings, photos, etc to finding out about user's preferences, experiences, and needs. [1, 13].

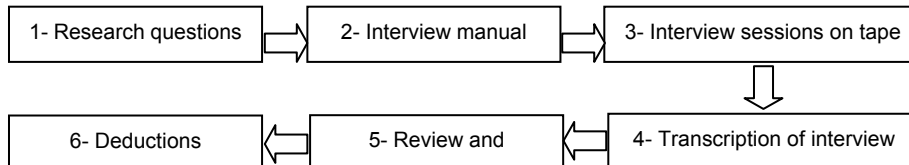


Fig. 2.The phases of the interview process [4].

How one manages field study data? Field Studies discussed several tools to manage field study data. Scenarios, storyboards, task analysis, and personas were the main methods presented [6].

Scenarios—Scenarios are narratives that describe the story of the user and the activity or function – “what people do and experience as they try to use furniture”. This can be the story of what is happening right now (describing) new possibilities for what will happen with the furniture under development. Scenarios make the process come alive for the students. This method of presenting data is more engaging than a bulleted list of steps in an activity – it makes the user more real and looks like virtual environment.

Storyboards – Are scenarios in comic-book form – quick sketches that represent the steps of an activity.

Task analysis—Task analysis is the structured breakdown of the activities a user engages in to reach a goal.

Personas– Is a fictional user created to represent a user group [2, 3]. The students' team creates this user as an aggregate of the real users they have observed and interviewed. A persona is a profile of super typical user with a name, photo, likes and dislikes, habits, background and expectations, and any other information that will help the students' team identify with the user. By using simulation to analyze the patterns of user behavior.

2-2 Iterative Process

Understanding and specifying the context of use—In UCD Process the emphasis is on understanding users through behavior patterns.

Understanding produces empathy for users in the team of students, and creates a foundation for a project that meets real needs instead of functionality added mainly for feature-list comparisons. It consists of (understanding and specifying the function, the user "Echoes, social & economic environment", context of use, Identify important usability factors and students' team tasks).

It is important to study and analyze the cultural environment, as it is related to how people live, and what is their behavior in a particular manner. Then the cultural factor is the one which reflects the thinking of the consumer and purchase behavior. It should be noted that the religion is part of the social and cultural environment, which affects the behavior patterns and consumption. There is no doubt that religious considerations are important in the lives of individuals. When the designers work their designs, they must put religious considerations in mind with regard to the markets they target. There are four basic concepts of culture, customs / traditions / religion / patterns or ways of life,

these four concepts are found in society at three levels, according to their importance and degree of practice by members of the community: generalization, privacy, alternatives or variables or new developments [9].

To exemplify, the function of sitting varies according to the previous three levels as follows:

A - *Generalization* (chair in the garden and waiting chair in a bank)

B - *Privacy* (sitting in Japanese dining room, the Saudis high sitting - Alkrawita – and dining in the Egyptian countryside)

C - *New developments* (Arabian sitting in some touristic places in Egypt. It is inspired by the Gulf States).

The following is a table of analysis distributed to the students at the beginning of the course with of acquainting them with the UCD methodology. Students were requested to fill the table in an attempt to help them realize the importance of the input and how it helps in producing the desired output.

This table helps to specify, in a systematic manner, the function, the characteristics of the users, the tasks they will carry out and the circumstances of use. It also provides a system- focused approach which leads to a shared view among the student team.

Table 1. Analyzing table:

function	user		Context of Use	usability	students' team
Describe the function	Identify users "User behavior pattern"		Describe the Context of Use "Physical Environment"	Identify important usability factors	TASKS
	Echoes	Social Environment			
What is the function?	<i>Culture</i> customs / traditions / religion /A patterns of life		Where does the furniture use?	<i>pragmatic user goals</i> Ergonomics: -Experience of use -Easy to use -Efficient to use -Comfortable	<i>Field Studies</i> the activities undertaken to achieve a goal
How is it work?	<i>By three levels:</i> Generalization /privacy / new developments		When does the furniture use?		Interviews
Why to use?	<i>economic</i>		How does the furniture use?	<i>hedonic goals</i> <i>Semantics / usability / communication</i>	Focus groups
When to use?	Who is the user? Gender (male– female) / Age / Function / Income				Questionnaires
How long to use?	<i>User Goals</i> Viability of purchasing /Quality /Fulfill desires			-Visually pleasing -Easy to remember	Participatory design
Document potential requirements					Benchmarking and competitive analysis

Concept & Design -- are reflecting the philosophy underlying the design, which stems from the motive, determined by the designer; it is a pragmatic philosophy. Design for x reflects the great diversity in the methodology of the design process and its objectives and functioning, beginning of the design concepts for the community or for the needs and access to design for fashionand so on.

Prototyping-- A prototype is-like a mock-up- a full size model; yet it is made as accurately and perfectly as possible, including all materials and finishes that will be used for the final product [8].

Evaluating designs against requirements (ISO, 1997b) -- Evaluation works with a prototype to see how well it meets the user experience requirements from the Understanding phase. Evaluation is usually focused on usability evaluation – how usable is the product? Evaluation can also include broader measures of subjective satisfaction and user response [6].

The UCD Process continues, with the product becoming more and more refined with each iteration. The process is ideally complete when

a project meets all user experience requirements. Even in that case, the UCD process produces better results than if the team designs a product without consideration of the intended user.

2-3 Process Output (usability)

In the end, furniture must be a useable product; three approaches to usability are identified as follows [7]:

1. Process System Usability: Meeting organizational goals for user performance, safety and satisfaction resulting from interaction.
2. User Experience (satisfaction): Meeting user pragmatic and hedonic goals related to the experience and outcomes of interaction.
 - The pragmatic user goals are: Acceptable perceived experience of use (pragmatic aspects including efficiency), results of use (including effectiveness) and consequences of use (including safety).
 - The hedonic goals or the esthetic pleasure: This pleasurable is an emotional reaction to the product. Questionnaires would appear to be the most reliable way to measure the achievement of hedonic goals.
3. Product usability: providing product attributes to support system usability and the user experience.

A typical definition of user experience is "Every aspect of the user's interaction with a product, service, or company that makes up the user's perceptions of the whole" [12]. So in order to encompass the overall user experience, UX needs to be concerned with satisfying both pragmatic and hedonic user goals. A useable product means more satisfied customers and a better reputation for the product [1].



3- User-centered design principles and benefits

For a good UCD design, some principles should be always followed, such as: Setting the business goals, Understanding the user, Assessing competitiveness, Designing the total user experience, Evaluating the design, Active involvement of users, Iterations of design solutions and [11].

Some specific benefits to the organization include [6]:

- Increased sales and customer satisfaction.
- Advertising advantages and better notices in the media.
- Improved productivity and operational efficiency.
- A competitive edge over competitors who do not take usability as seriously.
- Reduced development and maintenance costs.
- Reduced training costs and lower technical support costs. .

Conclusion

UCD provides pragmatic processes and techniques that students can incorporate into existing development efforts. This methodology teaches practical ways for understanding the (function, users and the context of use), determine tasks and manage field study with "scenarios, storyboards, task analysis, and personas ", rapidly exploring design alternatives, making prototype and evaluating design options through observing real users, to obtain usability as a result of the process.

Providing education to create a skill base of UCD practitioners is an important part of implementing of UCD. The students will have a better appreciation for the skills they learn with an understanding of the source of the techniques.

Going forward the practices outlined in this paper will give rise to new methods and techniques suited for the social environment and the own culture of any society and recognize the behavior patterns of users by using virtual learning environment and simulation.

Therefore, UCD is based on these important aspects which are not or are barely available in other furniture design approaches:

1. Know the users and the context of use. By using Interviews, Focus groups, Questionnaires, and Participatory design.
2. Understanding the tasks the user is trying to accomplish.
3. Involving the user in iterative design process, not only in the first or in the last of design process (it is the difference between traditional design process and UCD process).
4. Practicing usability testing and evaluation throughout the development process.

All the above-mentioned qualifies the student through theoretical and practical studies to become furniture designers with the ability to compete locally and internationally as they become more experienced and skillful which results from dealing with a real project and users. However, many organizations still don't use UCD. So I tried to use it in my teaching process.

Discussion:

Field Studies tools involve the user in all the phases of the development unlike conventional methods which gather the users' feedback when the furniture is delivered. Real user involvement allows the team of students to make decisions based on information from real users.

Results

- 1- User-Centered Design is one of the single greatest investments a product developer can make today.
- 2- The use of UCD bridges the gap between the designer and client because it attempts to produce output that meeting the needs.
- 3-The design slogan of UCD becomes "Design by people for people".
- 4- UCD suits the changing environmental conditions, social and economic, Whenever it is a development of products, to suit the new needs and changing.
- 5- The outcome of UCD methodology application in learning is having students with competence and experience in furniture design.

Recommendation

- 1- Expand the application of UCD in education, and promote individual and groups working among students.
- 3- It is incorrect to describe a product as ergonomic or usable without also describing the context of use.
- 4- Encourage the use of virtual learning environment and simulation to identify the user behavior pattern whether in the local or global environment.

References

- [1] Abras, C., Maloney-Krichmar, D., Preece, J: User-Centered Design, In Bainbridge, W. Encyclopedia of Human-Computer Interaction. Thousand Oaks: Sage Publications. (in press), (2004).pdf.p.5.
- [2] Cooper, A: The Inmates Are Running the Asylum, Why High Tech Products Drive Us Crazy and How To Restore The Sanity, SAMS: Indianapolis, IN, (1999).
- [3] Goodwin, K.: Taking Control Back From the Inmates, in User Interface 2000 Proceedings, User Interface Engineering: Boston, MA, (2000).
- [4] El Ansary, Alaa: An Approach to Support the Design Process considering Technological Possibilities- Referring to the Example of Furniture, PHD, University of Duisburg-Essen, Germany, (2006), pp .47.
- [5] ISO, Draft International Standard (DIS) 9241-11 (1997a): Ergonomic Requirements for office work with visual display terminals, Part 11, Guidance on Usability, International Standards Organization, Geneva, Switzerland.
http://www.usabilitynet.org/tools/r_international.htm#9126-1
- [6] Mc Mullin, Jess: User-Centered Origins, An outline of the User-Centered Design Process and the sources of current industry practices, ucd_class.pdf, Grant Mac Ewan College, (2001).pdf, pp. 5, 3, 7, 4 www.findtoyou.com/ebook/view.php?id=4263734
- [7] Nigel, Bevan: UX, Usability and ISO Standards, Professional Usability Services, London, pdf. mail@nigelbevan.com pdf, p.1.
- [8] Pile, J.: Modern Furniture, John Wiley and Sons, New York, (1990).
- [9] <http://www.ahewar.org/debat/show.art.asp?aid=24704>
- [10] http://en.wikipedia.org/wiki/User_interface#Usability
- [11] http://www.nada.kth.se/cid/pdf/cid_40.pdf
- [12] <http://www.usabilitybok.org/glossary>
- [13] <http://www.webcredible.co.uk/user-friendly-resources/web-usability/user-centered-design.shtml>

PRELIMINARY PHYSICO-CHEMICAL CHARACTERIZATION OF WASTEWATER FROM THE FARM IN VOJVODINA REGION, SERBIA

M. Djogo¹, M. Stosic¹, D. Milovanovic¹, J. Radonic¹, I. Mihajlovic¹, Z. Cepic¹

¹Faculty of Technical Sciences, University of Novi Sad, Department for environmental engineering and occupational safety and health, Trg Dositeja Obradovica 6, 21000 Novi Sad, Serbia, e-mail: majadjogo@uns.ac.rs

Keywords: wastewater, farm, physico-chemical characterization, microbiological characterization

Abstract. Farms represent a serious environmental problem in terms of potential water contamination and soil degradation because they produce large amount of animal waste. As a result of increasing number of animals on the farms, the pollution has remained high and farm waste remains a major problem. In some countries about half of all serious water pollution incidents are from manure runoff from farms. Farms have the potential for generating large quantities of solid waste and wastewater. Water quality is threatened by phosphorus and nitrogen, two nutrients present in animal waste. In excessive amounts, nutrients often cause an explosion of algae that robs water of oxygen, killing aquatic life. Manure can also contain traces of salt and heavy metals, which can end up in bodies of water and accumulate in the sediment, concentrating as they move up the food chain. As there is a lack of data regarding the farm wastewater characteristics in Vojvodina region, Serbia, the preliminary physico-chemical characterization of wastewater from the selected farm in Vojvodina region was conducted. This investigation was just one part of the initial phase of National project of the Ministry of Education and Science: Improvement and development of hygienic and technological procedures in production of animal originating foodstuffs with the aim of producing high-quality and safe products competitive on the global market, managed by the Institute of Meat Hygiene and Technology in Belgrade, Serbia. Laboratory analysis were conducted in accredited Laboratory for monitoring of landfills, wastewater and air, Department of environmental engineering and occupational safety and health, Faculty of Technical Sciences, University of Novi Sad and in Microbiological laboratory, Department of biology and ecology, Faculty of Sciences, University of Novi Sad.

Introduction

All dairy farms have to dispose wastewater, which can contaminate both surface and groundwater, from their milking centers. When milking center wastewater enters surface waters, it can damage aquatic communities. Groundwater contamination can adversely affect drinking water quality and create health hazards to humans. The volume of wastewater produced and the concentration of pollutants vary greatly. Milking center wastewater is contaminated with organic matter, nutrients, chemicals and microorganisms [1]. Poorly designed or mismanaged waste disposal systems can contaminate water with ammonia, nitrate, phosphorus, detergents and disease-causing organisms. If not managed properly, these contaminants can be carried directly to a well or cause groundwater or surface water contamination. Surface water can also be affected by manure, milk solids, ammonia, phosphorus and detergents. The composition, quantity, and pollution strength of milking center wastewater can vary dramatically among farms and even on the same farm over time. Several factors can influence wastewater characteristics, including number of cows milked, type of milking facility, length of time cows are confined in holding areas or parlors, feed access in parlors, waste milk management, floor/gutter cleanup method, and operator management throughout the milking cycle [2].

Solids in milking center wastewater come from waste milk, cleaning agents, waste feed, manure, and hoof dirt. Ammonia originates from manure, urine and decomposed milk proteins. Since contamination of milking center wastewater with milk creates an anaerobic environment, the greatest contributor to the BOD₅ of milking center wastewater is waste milk. Cleaning chemicals, especially detergents and acid rinses, milk, feed and manure contribute phosphorus to milking center wastewater [3]. Phosphorus in milking center wastewater is delivered largely in soluble, reactive form, and effectively promotes eutrophication. The COD concentration varies depending on wastewater management, climate, operation conditions, and types of flushing. The high COD concentration is due to waste milk which is produced by washing milking equipment, detergents, manure, and waste feeds. Microbiological characteristics, in addition to physico-chemical characteristics, are a significant and valid indicator of the quality of aquatic ecosystems. Numerous microbiological parameters can show the character and the degree of water pollution which can not be evaluated only on the basis of their physical and chemical properties.

In Vojvodina region, Serbia, there is a lack of data regarding the wastewater characteristics from the farm processes [4]. As the part of the initial phase of National project, the preliminary physico-chemical and microbiological characterization of wastewater from the selected farm in Vojvodina region was conducted.

Methodology

Sampling campaigns of wastewater from the farm in Vojvodina region has been conducted during two periods: winter, in February 2011 and summer, in June 2011. The samples of wastewater were collected from the cow milking parlor of the farm in the vicinity of Novi Sad, where the majority of wastewater is produced on the farm. Water samples were collected in sealed 1 liter plastic bottles, stored in hand refrigerator at 4 °C and transported to the laboratory. The samples were analyzed immediately. Samples that were used for determination of BOD₅ and COD were collected in special sealed glass containers.

Measurements of pH value, dissolved oxygen and temperature were performed in the field with the portable Multi 340i WISSENSCHAFTLICH-TECHNISCHE WERKSTATTEN GMBH device. Chemical and biological oxygen demand were determined using the reagent test tubes in HACH DR5000 spectrophotometer and BOD Trak HACH device, respectively. Ammonium and total phosphorus were determined using standard EPA methods and HACH DR5000 spectrophotometer device. All other chemical parameters were determined in subcontracted accredited laboratory in Novi Sad. The samples for microbiological characterization were analyzed by standard MPN method for microbiological parameters.

Laboratory analysis of wastewater samples was performed in accredited Laboratory for monitoring of landfills, wastewater and air, Department of environmental engineering and occupational safety and health, Faculty of Technical Sciences, University of Novi Sad and in Microbiological laboratory, Department of biology and ecology, Faculty of Sciences, University of Novi Sad.

Results and Discussion

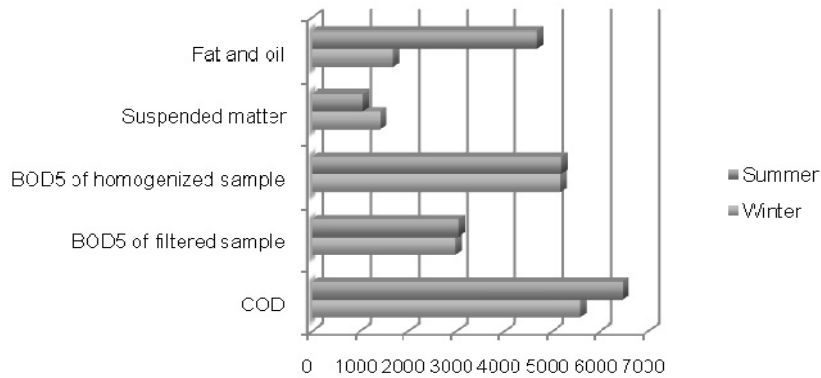
The samples have been analyzed on the parameters defined according to the actual *Regulation on minimum number and type of the sample taking process* at the time of sampling which includes: pH value, dissolved oxygen, nitrates, ammonium, total phosphorus, COD, BOD₅, TSS, total nitrogen, fat and oil, detergents, total coliform, fecal coliform and *Escherichia coli*. The results of physico-chemical and microbiological parameters of the water samples from the two sampling campaigns (winter and summer) are presented in Table 1. All parameters were above maximum allowed values prescribed by Serbian regulations as well as EU regulation and wastewater could not be discharged into the surface water before treatment. Figures 1, 2, and 3 show seasonal variability of the analyzed parameters

Wastewater physical chemical characteristics observed at selected dairy farm are quite variable. High levels of BOD₅, ammonium, TSS, COD, total phosphorus and total nitrogen were found in the samples collected in both campaigns. From the obtained data gathered, it is evident that wastewater contains levels of contaminants that could be toxic to fish and aquatic communities if discharged to surface waters.

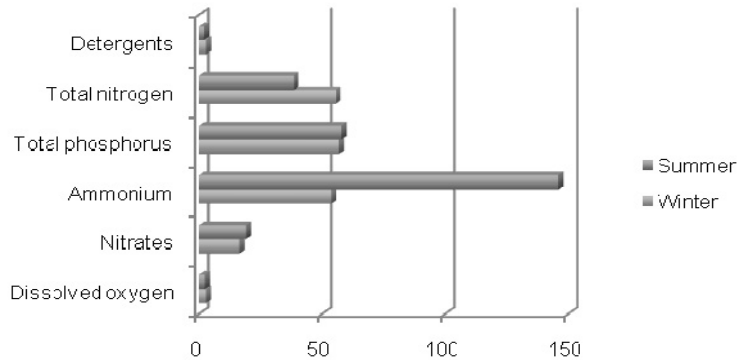
The obtained values of microbiological parameters indicate that the examined water in both sampling campaigns contain large number of total coliform bacteria, as well as the other two bacterial groups which are indicators of fecal pollution. According to the number of present bacteria and on the basis of regulations on wastewater quality and methods of discharging in the public sewage and natural recipient in neighboring countries, analyzed water is with high or maximum contamination and should not be discharged into natural recipients without the prior treatment. This is especially valid in the case of fecal streptococci whose number is several times greater than the maximum allowed value prescribed by regulations. Also, a high proportion of fecal coliforms in the total coliform number in the water from second sampling campaign ($FC/TC = 0,89$) clearly show that water is heavily influenced by fecal contamination and presents a potentially high risk to the human health.

Table 1: Physico-chemical properties of farm wastewater from two sampling campaigns

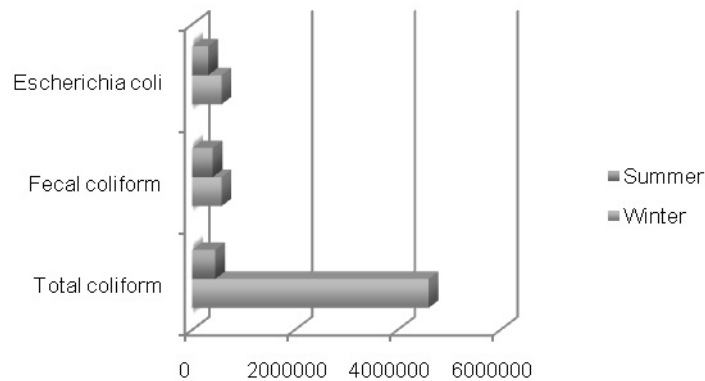
No.	Parameters	Unit	Results	
			February 2011	June 2011
1.	Water temperature	°C	8,4	16.12
2.	Air temperature	°C	4,5	23.20
3.	pH value	-	6,07	5.42
4.	Dissolved oxygen	mg/l	2,69	2.27
5.	Nitrates	mg/l	16,4	19
6.	Ammonium	mg/l	53,7	146
7.	Total phosphorus	mg/l	57,1	58.1
8.	COD	mg/l	5593	6466
9.	BOD ₅ of filtered sample	mg/l	2990	3050
10.	BOD ₅ of homogenized sample	mg/l	5180	5200
11.	Total suspended solids	mg/l	1423	1067
12.	Total nitrogen	mg/l	55,63	38.52
13.	Fat and oil	mg/l	1681,5	4694
14.	Detergents	mg/l	2,75	1.92
15.	Total coliform	CFU/100 ml	4 600 000	450 000
16.	Fecal coliform	CFU/100 ml	570 000	400 000
17.	<i>Escherichia coli</i>	CFU/100 ml	570 000	310 000



Graph 1. Seasonal variability of fat and oil, suspended matter, BOD₅ and COD



Graph 2. Seasonal variability of detergents, total nitrogen, total phosphorus, ammonium, nitrates and dissolved oxygen



Graph 3. Seasonal variability of microbiological parameters

Conclusions

Environmental problems associated with animal manure and wastewaters are contamination of surface and groundwater, as well as soil quality degradation. As there is a lack of data regarding the wastewater characteristics from the farm processes in Vojvodina region, Serbia, the preliminary physical-chemical and microbiological characterization of wastewater from the selected farm in the vicinity of Novi Sad, Vojvodina, Serbia, was conducted within the National project.

Sampling campaigns of wastewater have been carried out during the two periods in 2011. The samples have been analyzed on the parameters: pH value, dissolved oxygen, nitrates, ammonium, total phosphorus, COD, BOD₅, TSS, total nitrogen, fat and oil, detergents, total coliform, fecal coliform and *escherichia coli*. All parameters were above maximum allowed values prescribed by the Serbian, as well as EU regulations. Also there is an evident difference between levels of few parameters in these two sampling periods. Fat and oils and ammonia are the parameters that are higher in summer period and total coliform are higher in winter period.



Obtained data has clearly highlighted the need for waste and wastewater sustainable and cost effective treatment systems within dairy farms and milk production. Also, the monitoring of the final effluent for parameters discussed in the paper should be carried out at least once per month, or more frequently if the flows vary significantly.

Acknowledgement

This research was financially supported by the Ministry of Education and Science, Republic of Serbia, within the Project III46009.

References

- [1] D. Payer: Milking. Center Wastewater and Source Control-bulletins draft, Outreach University of Wisconsin Madison, Agricultural Engineering Department, 1993.
- [2] R. E. Graves: Milking. Center Wastewater Disposal, Pennsylvania Department of Environmental Resources, 1986.
- [3] B. J. Holmes, S. Struss: Milking center wastewater guidelines, A Companion Document to Wisconsin NRCS Standard 629, Wisconsin Natural Resources Conservation Service.
- [4] D. Milovanovic, M. Djogo, M. Miloradov, D. Adamovic, S. Kovacevic, M. Vojinovic Miloradov, Cadstre of polluters from the meat industry in Autonomous Province of Vojvodina, Proceedings, TOP 2011, Casta Papiernicka, Slovak Republic, june 2011, pp 289 – 294.

COLOR SEGMENTATION FOR SEGMENT-BASED STEREO MATCHING

M. Beneda¹, R. Prokop²

¹ Department of Automation and Control Engineering, Faculty of Applied Informatics, Tomas Bata University in Zlín, Nad Stráněmi 4511, 760 05 Zlín, Czech Republic

² Department of Automation and Control Engineering, Faculty of Applied Informatics, Tomas Bata University in Zlín, Nad Stráněmi 4511, 760 05 Zlín, Czech Republic

Keywords: Computer Vision, Segment-based Stereo Matching, Color Segmentation

Abstract. The correspondence problem in the field of stereo vision has been attracting a lot of efforts amongst computer scientists recently. Although the epipolar geometry simplified the search for corresponding pixels in stereo images considerably, many challenging difficulties are still left. In this paper it is proposed the novel image segmentation technique designated for consequent exploitation by segment-based stereo matching algorithm. Segment-based methods arise from assumption that the scene can be divided into segments having homogenous color where each segment from one stereo image coincide with correspondent segment in the other image. In comparison with correlation-based and feature-based methods it tends to have better performance in textureless regions, while dense disparity map is being produced. The new approach is based on the use of standard inter-pixel Euclidean distance utilization, which is enhanced by hue similarity and minimal size of segments criteria. All three conditions can be applied to both 4-connected and 8-connected pixel neighborhood, nevertheless only latter mentioned is used in this article. Segmentation results are shown in some standard stereo image sets, where the accuracy and robustness of proposed algorithm is presented. Finally, the discussion about some significant pros and cons is led and the direction of consequent research is outlined.

Introduction

Correspondence problem is very important and frequently discussed topic in computer vision. Basically, when there are two images of the same scene taken from slightly different position, the challenge is to determine which pixels in these images are projections of the same point on the scene. Generally, the epipolar geometry is utilized to simplify this search considerably. It produces rectified stereo images where corresponding pixels are aligned horizontally thus the following search is constrained, ideally, to the 1D only (along the corresponding image row).

Currently, for the stereo matching there are three main approaches. The correlation-based approach uses a window of fixed size centered at each pixel in one image and searches its corresponding pixel in the other image where the correlation-measure is maximal. Contrariwise, in the feature-based approach some significant features as edges, lines or corners are extracted and, based on similarity measure, the correspondences are searched. Correlation-based local algorithms produce accurate disparity in highly textured regions, but tend to have significant erroneous performance in textureless regions, disparity discontinuous boundaries or occluded areas. In these challenging image regions the feature-based global algorithms are advantageous; however, they normally give rise to sparse depth map only [Hong04]. Finally, the segment-based approach has been attracting a lot of attention recently. It can be considered as a special case of feature-based approach, so it shares good performance on handling boundaries and textureless regions. Segment-based methods arise from assumption that the scene can be divided into segments having homogenous color where each segment from one stereo image coincide with correspondent segment in the other image. Hence, the scene structure can be approximated by a set of non-overlapping planes in the disparity space [Borisagar2011].

The paper is organized as follows. In the next section, we do a short related-literature survey and then explain our novel segmentation algorithm in detail. In following section, we present achieved results in a number of standard rectified stereo data sets. Finally, there is conclusion and outline of a future work.

Segmentation algorithm

We assume that purely pixel-based methods are insufficient to express information of the image. The human identifies the objects by analyzing features of the objects such as color, texture and shape [2], therefore segment-based stereo matching algorithm should be used.

Most of the color segmentation techniques apply Mean shift [3, 4, 5, 7]; less frequently there is Graph cut [6], Hill climbing, Greedy or another algorithm utilized. The algorithm we created is founded on the work of Zitnick at al. [8], but improved considerably in a way described further.

As well as in [1] our approach is built upon the assumption that large disparity discontinuities only occur on the boundaries of homogeneous color segments and segments itself have smooth disparity. Produced segments should be as large as possible in order to minimize computational time. The rapid disparity changes via single segment, occurring in very slanted surfaces, shall be taken into account by matching algorithm. The segmentation process consists of several steps. Firstly, as an input we can use rectified images from calibrated stereo camera; however, for testing purposes, standard Middlebury and Tsukuba stereo data sets are more suitable. Secondly, as a preprocessing step, bilateral edge-preserving and noise reducing blurring filter is applied to both left and right images. This generally helps to create more consistent segments, while thin segments along intensity edges are suppressed [8]. After smoothing, the algorithm goes through the image line by line and assigns new segment to a current pixel if it is not assigned yet. Every two 8-connected neighboring pixels are then merged into single segment (as well as two segments they are part of) if two conditions are valid:

1. The Euclidean distance between their (average) colors is less than requested constant (c. 6-15). For all experiments the value 10 appeared to be the best choice.
2. Their color hue (see Fig. 1) must be the same. This constraint assumes that two apparently very different colors can have quite small Euclidean distance and thus some erroneous segments could be produced.

Ordering	Hue Region
$R \geq G \geq B$	Red-Yellow
$G > R \geq B$	Yellow-Green
$G \geq B > R$	Green-Cyan
$B > G > R$	Cyan-Blue
$B > R \geq G$	Blue-Magenta
$R \geq B > G$	Magenta-Red

Fig. 1: Computing hue from RGB color space

Although the preprocessing significantly reduced the amount of small segments created during the merging procedure, some of them still left. As mentioned above, they occur mainly along intensity edges and in highly textured areas. With a view to decrease the computational expensiveness and simultaneously increase the precision of consecutive matching process, the minimal-size-of-segment constraint is incorporated. Hence, when all pixels are labeled as a part of one from various segments, the second round of merging is performed. This time, two neighboring segments are merged together (based on the same two conditions) until the resulting segment size is bigger than predefined constant.

Results

The proposed algorithm was implemented in MS VCE 2010 and tested on various rectified stereo images, such as Tsukuba and Middlebury datasets (<http://vision.middlebury.edu/stereo/data/>) or stereo images captured by Minoru3D stereo camera. Four examples are shown in Fig. 2. The algorithm's parameters were set as follows: Euclidean distance – 10; Minimal size of segments – 9. This configuration tends to produce very precise results in most tested images; however, in some cases there is needlessly too many small segments or, contrariwise, big loss of details depending on the scene structure and illumination.

Computation cost on Intel(R) Core(TM) i3 CPU U 380 @ 1.33GHz (4 CPUs) laptop for Tsukuba (384x288) is about 11 seconds, but it raises exponentially with increasing image size up to approximately 75 seconds in case of Cones (450x375).



Fig. 2: Cones, Tsukuba, Venus and Map; top row – original (left) images, resulting segmented images at the bottom

Conclusion

In this paper we proposed a new segmentation method, which good performance is presented in four different testing images. Our algorithm utilizes three constraints: Euclidean distance, Hue similarity and Minimal size of segments that can be applied to either 4-connected or 8-connected pixel's neighborhood. Based on subjective evaluation we assume that the resulting segmented images are very precise, however, at the expense of the computation time. Considering that, the content of our future work consists of optimizing current algorithm and implement stereo matching part in order to gain disparity maps.



Acknowledgment

This paper has been supported by the Internal Grant Agency at Tomas Bata University in Zlín, Faculty of Applied Informatics, project No. IGA/FAI/2012/047 and by the European Regional Development Fund under the Project CEBIA-Tech No. CZ.1.05/2.1.00/03.0089.

References

- [1] L. Hong and G. Chen. Segment-based Stereo Matching Using Graph Cuts. In *CVPR*, 2004, vol. 1, pp. 74–81.
- [2] V. Borisagar and M. Zaveri. A Novel Segment-based Stereo Matching Algorithm for Disparity Map Generation. *International Conference on Computer and Software Modeling IPCSIT*, 2011, vol. 14, IACSIT Press, Singapore 2011.
- [3] D. Comanicu and P. Meer. Mean Shift: A Robust Approach Toward Feature Space Analysis. In *IEEE Transactions on PAMI*, vol. 24, no. 5, pp. 603-619, 2002.
- [4] Y. Wei, M Lhuillier and L Quan. Fast Segmentation-based Dense Stereo from Quasi-dense Matching. In *Proceedings of the Asian Conf. on Computer Vision*, Jeju, Korea, 2004.
- [5] A. Klaus, M. Sormann and K. Karner. Segment-based Stereo Matching Using Belief Propagation and a Self-adapting Dissimilarity Measure. In *18th ICPR*, 2006, pages 15-18.
- [6] Y. Boykov, O. Veksler, and R. Zabih. Fast Approximate Energy Minimization Via Graph Cuts. In *IEEE Trans. Pattern Analysis and Machine Intelligence*, vol. 23, pp. 1222-1239, 2001.
- [7] Q. Yang, L. Wang, R. Yang, H. Stewenius and D. Nister. Stereo Matching with Color-Weighted Correlation, Hierarchical Belief Propagation and Occlusion Handling. In *CVPR*, vol. 2, pages 2347-2354, 2006.
- [8] L. Zitnick, S. Kang, M. Uyttendaele, S. Winder, R. Szeliski. High-quality Video View Interpolation Using a Layered Representation. In *ACM Trans. Graph.*, vol. 23, pp. 600-608, 2004.
- [9] Wikipedia contributors. Hue. *Wikipedia, The Free Encyclopedia*, <http://en.wikipedia.org/wiki/Hue> (accessed January 27, 2012).



International Conference on Innovative Technologies, IN-TECH 2012,
Rijeka, 26. - 28.09.2012



MATHEMATICAL MODELLING OF SURFACE GREASE DEPOSITS

J. Kudlacek¹, P. Chabera¹, T. Pepelnjak² and Z. Car³

¹ CTU in Prague, Faculty of Mechanical Engineering, Technicka 4, 166 07, Prague, Czech Republic

² University of Ljubljana, Faculty of Mechanical Engineering, Askerceva 6, SI-1000, Ljubljana, Slovenia

³ University of Rijeka, Faculty of Engineering, Vukovarska 58, 51000, Rijeka, Croatia

Keywords: surface cleanliness; grease detection; degreasing

Abstract. This study deals with a modern way of detecting surface grease pollution. It explains, how to calculate the amount of oil pollution – how to find out the thickness of the oil layer and the related parameters.

Introduction

In the industrial practice, technological processes are often accompanied by defects caused by oil deposits on the surface of products, resulting in system failure or a high rejection rate in production. [7] In particular, grease has a significant effect on the properties of the final coating of the products (its functionality, appearance, adhesion). This is generally caused by poor surface pre-treatment (degreasing) prior to the actual processes of surface treatment. Unspecified grease deposits on the surface of machine parts can affect not only surface treatment, but also many other technological processes such as welding, soldering and adhesive bonding. On the other hand, it may be necessary to know specified surface grease deposits in some cases, such as for the purposes of temporary corrosion protection and preservation. [1]

The possibility to check the degree of surface cleanliness of machine parts is highly time-consuming and there is currently no effective – simple and fast – method for the qualification and quantification of surface cleanliness (grease deposits). [6]

Monitoring of surface cleanliness for the purposes of subsequent surface treatment and the possible reduction of the rejection rate in production is given special attention by the Department of Manufacturing Technology (DMT) within the research into surface conditions and possibilities of suitable methods for the detection of surface cleanliness. In cooperation with TechTest Company, DMT has developed and modified a non-contact device enabling fast tests for residual impurities (grease), called “*Recognoil*”. With this equipment and the relevant software, it is possible to quantitatively and qualitatively assess how much contaminated the measured area is. [3]

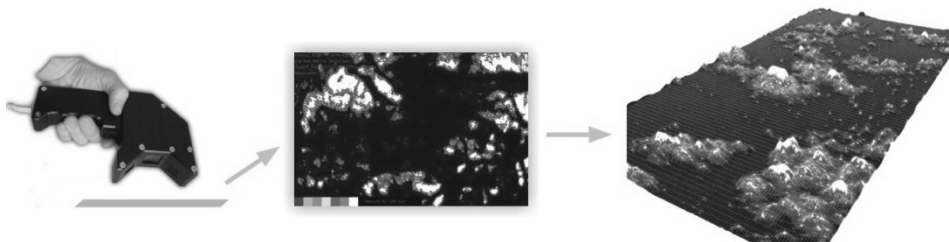


Fig. 1 Diagram of a modern method for fast and efficient measurement of greasy impurities

Detection of oil and grease by *Recognoil*

“*Recognoil*” works on the principle of measuring the luminescence produced by greasy impurities; the optical output is a “map” of the intensity of luminescence emitted by grease deposits.

The aim of this article is to describe how to use this “map” of luminescence intensity to calculate the degree of grease contamination (thickness, concentration of grease deposits).

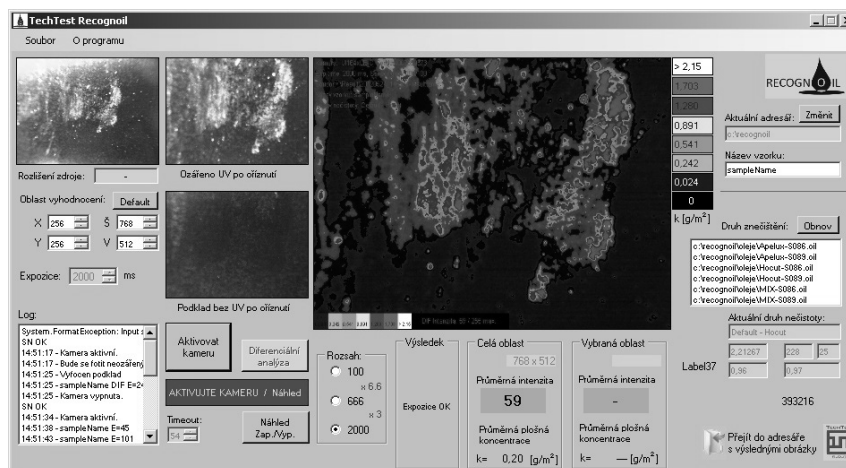


Fig. 2 *Recognoil* Software for evaluation of grease contamination

“Calibration” methods

The mathematical representation of the “map” of grease luminescence intensity and its conversion into the thickness of the layer is based on the numerical representation of luminescence of the measured surface at various, predefined degrees of grease contamination. In subsequent exposures, the software uses mathematical methods to calculate the resulting thickness of the layer based on the parameters of specific contaminants. [2]

First, approximately eight samples were prepared with different amounts of grease (from the smallest possible contamination to the maximum detectable). [1] These eight scanned samples were used to derive a curve correlating luminescence intensity with layer thickness. However, this approach has its limitations - the samples must contain a homogeneous layer of oil film, which can only be achieved if the solubility of oil in the used solvent is 100%. More often, however, industrial processes deal with various emulsions, whole sampling (see above) is impossible using this method.

For this reason, we have developed a reverse method to determine the degree of grease contamination of components directly during the degreasing process. In the process, one sample is prepared and a layer of grease applied to it. Then, the test sample is repeatedly immersed into several degreasing baths in several time intervals and the intensity of luminescence is measured and the sample weighed on accurate analytical scales after each time interval. .

For each type of contamination, we get the values shown in the following diagram:

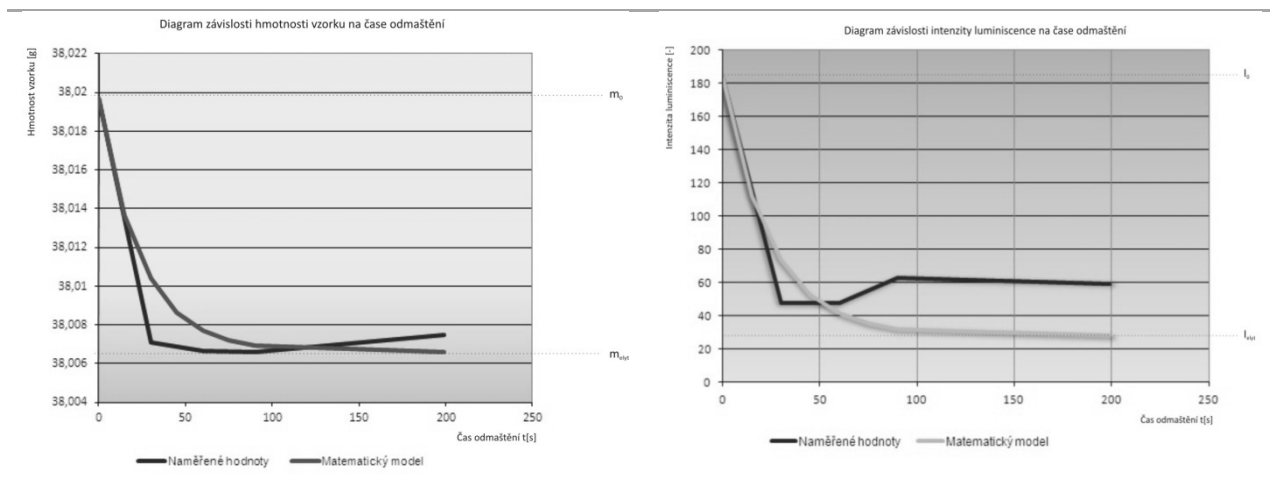


Fig. 1 Example of measured values and corresponding mathematical models

If the interdependencies are known, the device software can, based on the “map” of luminescence intensity and weight loss, calculate immediately the surface concentration k [g.m⁻²] for each specific oily contamination.

Calculation method

The way the “map” of intensity is converted to surface concentration:

- Development of a mathematical model for the change in sample weights in relation to the degreasing time
- Development of a mathematical model for the change in luminescence intensity in relation to the degreasing time
- Mathematical expression of parameter t (time) from the curve of luminescence intensity and its putting into the formula for change in sample weight

The curves of mathematical models correspond to the power function of the parameter p . [5]

$$y = a + b \cdot p^x \quad (1)$$

The formula of the curve of the mathematical model for the change in sample weight:

$$m = m_{cle} + \Delta m \cdot p_k^t, \quad \text{where } \Delta m = m_0 - m_{cle} \quad (2)$$

The formula of the curve of the mathematical model for the change in luminescence intensity:

$$I = I_{cle} + \Delta I \cdot p_l^t, \quad \text{where } \Delta I = I_0 - I_{cle} \quad (3)$$

After the mathematical expression of t and substituting into the formula, after the conversion to surface concentration using the surface S we obtain the final relationship:

$$k = \frac{m_0 - m_{cle}}{S} \cdot p_k^{\frac{\log \frac{I - I_{cle}}{I_0 - I_{cle}}}{\log p_i}} \quad , \text{ where} \quad (4)$$

<i>k</i>	... the resulting surface concentration of oily contamination	<i>[g.m⁻²]</i>
<i>m₀</i>	... weight of contaminated sample	<i>[g]</i>
<i>m_{cle}</i>	... weight of clean sample	<i>[g]</i>
<i>S</i>	... area of the specimen from both sides, neglecting the thickness	<i>[m²]</i>
<i>p_k</i>	... curve share parameter – math. model of surface concentration	<i>[-]</i>
<i>p_i</i>	... curve share parameter – math. model of luminescence intensity	<i>[-]</i>
<i>I</i>	... substituted current value of the luminescence	<i>[-]</i>
<i>I_{cle}</i>	... value of the luminescence of clean sample	<i>[-]</i>
<i>a</i>	... constant for surface concentration	<i>[g.m⁻²]</i>

For simplicity, we introduce the constant of surface concentration **a**:

$$a = \frac{m_0 - m_{cle}}{S} \quad [g.m^{-2}] \quad (5)$$

Contamination can therefore be parameterized by five measured parameters **a**, **I₀**, **I_{cle}**, **p_k** and **p_i**. [4]

After entering these parameters into the software, it automatically converts the intensity of luminescence to surface concentration **k**.

Table 1 Example of contaminant parameters

a	I₀	I_{cle}	p_k	p_i	Contaminant
2,21267	228	25	0,96	0,97	<i>HoCut machining emulsion</i>

This way it is possible to develop a simple database of oil contaminants and select the relevant type of contamination as required.

The output of the software is a numeric value of the average surface concentration on the scanned area. Using "Recognoil", the dimensions of the scanned area are approximately 40 x 30 mm.

The software can convert numerical information into colour coded layers where each layer corresponds to one level of surface concentration. Fluorescence intensity maps, including the conversion to surface concentration with an approximate estimate of thickness can be represented in 3D graphics.

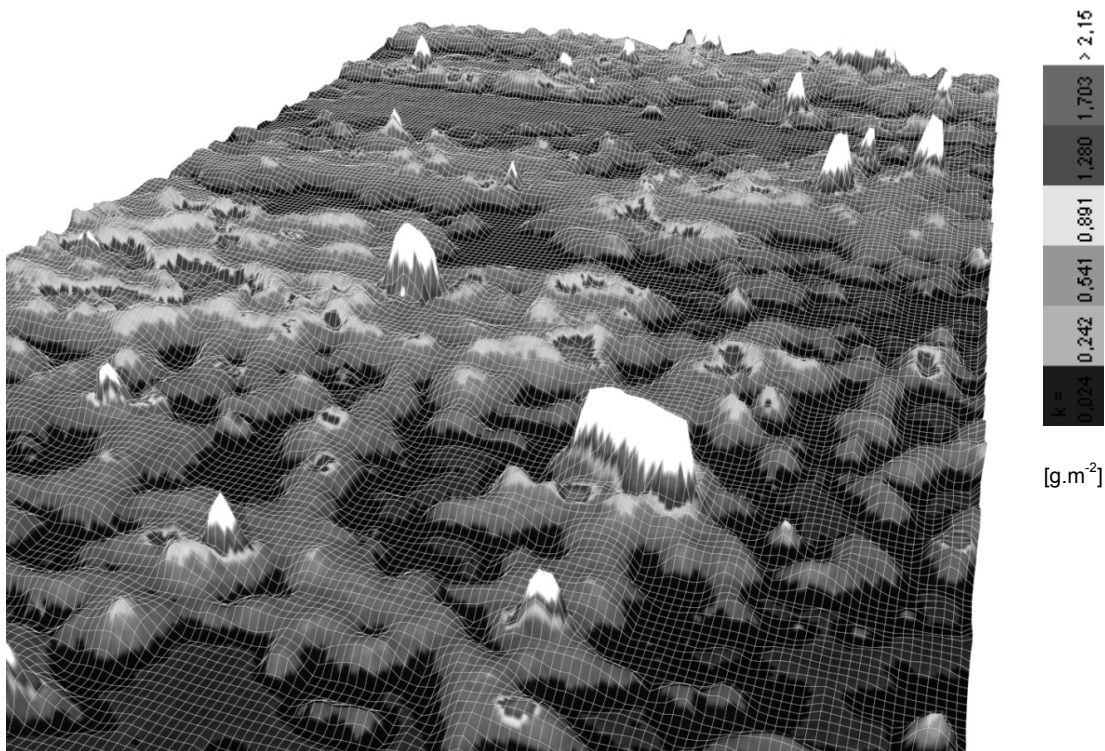


Fig. 1 3D visualization of the nature of grease on the surface of product during degreasing

Conclusion

The "Recognoil" device for detecting oil contamination provides two possible ways to evaluate the condition of the surface of inspected components. In some plants it is necessary to know the numerical values, while others will be more satisfied with illustrative graphical representation. Knowledge of the distribution of residual oil contamination in the degreasing process through graphical evaluation helps to optimize, streamline and generally improve the process of product degreasing before the final surface treatment. Further research into this issue will help to improve the monitoring of surface and thereby prevent substantial rejection in the manufacturing process caused by oil contamination.

Acknowledgment

This article has been prepared in the framework of the CEEPUS HR -108 international exchange program and was supported by the SGS10/259/OHK2/3T/12 project.

References

- [1] Pacák, L. Kudláček, J.: Detekce mastných nečistot v praxi, In: www.povrchari.cz [online], 1-2012, p. 10-13. ISSN 1802-9833.
- [2] Kudláček, J. - Chábera, P. - Barisic, B.: New possibilities of degreasing process evaluation, In: Proceedings of International Conference on Innovative Technologies IN-TECH. Jaroměř: Centrum pro povrchové úpravy, 2010, p. 624-627. ISBN 978-80-904502-2-6.
- [3] Kudláček, J. - Chábera, P. - Pacák, L.: Posouzení odmašťovací schopnosti, [Výzkumná zpráva]. Praha: ČVUT, Fakulta strojní, Ú 12133, 2010. U12133/2010/001. 8 s.
- [4] Kudláček, J. - Pacák, L.: Nové možnosti vyhodnocování procesu odmašťování, In: Sborník příspěvků konference Technologické fórum 2010 [CD-ROM]. Praha: České vysoké učení technické v Praze, 2010, ISBN 978-80-01-04586-2.
- [5] Kuznetsov, A. P. - Božek, P.: Aplikácia matematického vyjadrenia spoľahlivosti technických systémov, - 1. vyd. - Trnava : Tripsoft, 2009. - 73 s. - ISBN 978-80-89291-27-4
- [6] Pacák, L. - Kudláček, J.: The Calibration of a Device Used for the Detection of Surface Cleanliness, In: CO-MAT-TECH 2005. Bratislava: Vydavateľstvo STU, 2005, p. 133. ISBN 80-227-2286-3.
- [7] Božek, P. - Mihok, J. - Barborák, O. - Lahučký, D. - Vaňová, J.: New strategies of virtuality in programming of production technology, In: Annals of DAAAM and Proceedings of DAAAM Symposium. - ISSN 1726-9679. - Vol. 20, No. 1 Annals of DAAAM for 2009 & Proceedings of the 20th international DAAAM symposium "Intelligent manufacturing & automation: Focus on theory, practice and education" 25 - 28th November 2009, Vienna, Austria. - Vienna : DAAAM International Vienna, 2009. - ISBN 978-3-901509-70-4, s. 0403-0404
- [8] Chábera, P. - Kudláček, J. - Pepelnjak, T.: Matematické modelování povrchového zamaštění, In: Technologické Fórum 2012, Praha: ČVUT v Praze, 2012, p.18-21 ISBN 987-80-01-05076-7.

INTRODUCTION OF NEW SURFACE TREATMENT TECHNOLOGIES INTO PRACTICE - ZINC BASED COMPOSITE COATING WITH PTFE PARTICLES (Zn-PTFE COATING)

P. Drasnar¹, J. Kudlacek¹, P. Roskanin¹, T. Pepelnjak², Z. Car³ and M. Vales⁴

¹ CTU in Prague, Faculty of Mechanical Engineering, Technicka 4, 166 07, Prague, Czech Republic

² University of Ljubljana, Faculty of Mechanical Engineering, Askerceva 6, SI-1000, Ljubljana, Slovenia

³ University of Rijeka, Faculty of Engineering, Vukovarska 58, 51000, Rijeka, Croatia

⁴ Aerospace Research and Test Establishment, Beranovych 130, 199 05, Praha – Letnany, Czech Republic

Keywords: electroplating, composite coating, technological process, galvanizing line, Zn-PTFE

Abstract. Paper deals with the description of the implementation of innovative Zn-PTFE coating into industrial production. Zn-PTFE composite coating is presumed to be used primarily on (high-strength) bolts. This coating offers excellent anticorrosive properties together with low friction coefficient. The article summarizes the technological production process of coating which was optimized to ensure homogeneous distribution of PTFE (polytetrafluoroethylene) particles in the coating and also to achieve optimal tribological parameters. The article mainly aims to present the structure of the industrial plating line and the general description of the technical conditions that need to be resolved in order to ensure this electroplating process to function properly.

1. Introduction [1]

Composite materials must generally contain at least two or more chemically and physically different phases. The primary – continuous – phase (zinc) is referred to as a matrix (binder) and allows the distribution of voltage, separates the particles of the discontinuous phase from each other and also determines the shape of the coating. Discontinuous particles, or the secondary phase (PTFE), are usually with different properties (for example different hardness, lubricate function, etc.). The synergistic effects of using such components results in a coating that provides cathodic protection to the steel substrate and the required sliding properties. The properties of the zinc matrix include ductility, electrical conductivity, thermal conductivity, corrosion resistance. The property of discontinuous polymer PTFE phase is primarily acceptable sliding properties.

The functional composite electrolytically deposited Zn-PTFE coating is thus a representative of innovative solutions in the area of electrodeposited coatings and can be included in the group "filled composites" specified as "polymer filled metal".

The aim of this study is to describe the introduction of this coating into industrial production, including a description of basic technical difficulties that needs to be addressed in order to ensure proper operation of the new galvanizing line at CVP Galvanika s.r.o. (leader in the Czech Republic in the area of zinc galvanizing and zinc-nickel plating).

2. The experimental part

The samples for infrared (IR) analysis were prepared by pattern of technological process shown in table 1.

Table 1. Electroplating technological process used in CVP Galvanika s.r.o., Pribram - Zn-PTFE – rack

Operation No	Operation	T [°C]	pH	I [A. dm ⁻²]	t [min]
01	(Chemical degreasing)	80 ± 5	12	-	5
02	Two-stage cascade rinsing	20 ± 3	-	-	1
03	(Pickling)	20 ± 3	-	-	2
04	Two-stage cascade rinsing	20 ± 3	-	-	1
05	Electrolytic degreasing	55 ± 2	12	10	2
06	Two-stage cascade rinsing	20 ± 3	-	-	1
07	Activation (pickling)	20 ± 3	-	-	1
08	Two-stage cascade rinsing	20 ± 3	-	-	1
09	Zn-PTFE electroplating – rack	22 ± 1	5 – 5.5	1.5	30
10	Economical rinsing	20 ± 3	-	-	1
11	Two-stage cascade rinsing	20 ± 3	-	-	1
12	Chemical polishing	20 ± 3	-	-	0.5
13	Passivation	60 ± 3	-	-	1
14	Two-stage cascade rinsing	20 ± 3	-	-	1
15	Drying	80 ± 5	-	-	10

2.1 Technological conditions and prerequisites [2, 3, 4]

- Results of previous studies revealed that weak acid baths (pH 4.8 to 5.5) are the most convenient and suitable in terms of economics, ecology and quality of the process.
- It was also revealed that coatings deposited at lower current density show optimal tribological parameters
- It was experimentally observed that the addition of brighteners to the bath does not influence the deposition of PTFE particles in the coating. The degree of brightness is dependent on the amount of the brightener added into the bath. It is therefore possible to use a bath with brighteners to create Zn-PTFE composite coatings with good visual properties.
- The content of individual components of the bath is reduced in the course of the galvanisation process by being removed together with finished products and by electrochemical consumption. Due to the imbalance of the current yield, anodes melt more zinc than deposited on the cathode so it is not necessary to replenish any zinc chloride. Potassium chloride and boric acid are replenished based on analysis.
- The pH of the bath changes due to the changes in the concentration of PTFE. It is therefore necessary to check and adjust the required pH accordingly.
- PTFE particles tend to deposit on the bottom of the bath tank, so mixing must be provided during the whole process of metal-plating.
- PTFE dispersion has to be mixed well before being added into the bath. However, the dispersion should not be shaken as it foams really easily. When being poured into the bath it is necessary to turn off the mixing in order to eliminate foaming. The foam must not be removed as it contains PTFE particles. Its removal would change the concentration of PTFE in the bath.
- Low-foaming surface-active tensides and dispergators are used to deposit homogenous coatings with the defined surface.

2.2 Optimization of the mixing process – laboratory tank

Prior to the preparation of the test samples, the electroplating tank had to be adjusted to suit the composite Zn-PTFE coatings. The density of the PTFE particles differ from the galvanizing bath and PTFE particles tend to settle on the bottom of electroplating tank. It is necessary to ensure proper mixing of the bath to achieve a homogeneous distribution of PTFE particles in the bath. Proper mixing of the galvanizing bath will also ensure homogenous distribution of PTFE particles in the zinc matrix.

The bath solution is mixed using a pump. For easier control of the mixing process, it is appropriate to fit the system with ball valves in the intake and displacement lines of the pump, which would be part of the tank. These valves could be closed and the pump disconnected from the system whenever needed, e.g. when replacing the bath, in case of pump failure or for flow control.

The last improvement of this electroplating tank was turning the suction elbow in the area of the bath upwards. Whenever the mixing cycle gets interrupted, PTFE particles settle on the bottom, and when the pump is switched on again, it pump draws in almost pure PTFE, which clogs the pump. This may occur especially at high concentrations of PTFE in the bath.

The first model of laboratory tank is shown in Fig. 1. The final draft design of the laboratory tank is shown in Fig. 2. The concept of the laboratory tank can thus be used for the construction of industrial electroplating lines.

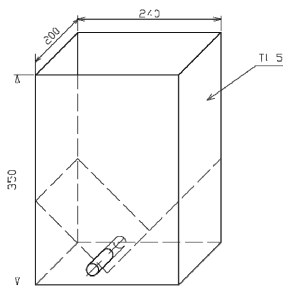


Fig. 1 3D model of laboratory tank

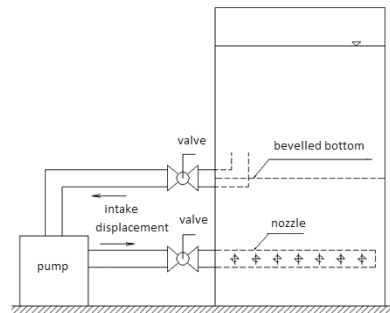


Fig. 2 The final design of the electroplating tank

2.3 Implementation of industrial galvanizing line

CVP Galvanika s.r.o. has built a new line for Zn-PTFE composite coating (Fig. 3), technology of composite Zn-PTFE coating have been transferred into production level.



Fig. 3 The new galvanizing line for Zn-PTFE composite coating..... Fig. 4 Galvanizing bath with 5% PTFE concentration. (Photos - author)

Description of the galvanizing line (Fig. 3)

- 1) The first row (closest to the wall) contains polypropylene tanks for zinc coating and economical rinsing of the parts.
- 2) The second row features a system of tanks for Zn-PTFE composite coating.
- 3) In the third row, there are tanks for passivation of the coatings.

Temperature control and cooling system

The largest investment was made into the equipment needed for cooling the Zn-PTFE bath. The working temperature of the bath with composite coating is automatically adjusted to the desired value. The bath is heated using a powerful heater located in the bath area. When the temperature reaches a certain level, the cooling system turns on automatically and the coolant begins to flow through a set of polypropylene tubes. The process of temperature control is fully automatic.

Bath foaming

Fig. 4 shows bath foaming which occurs when adding polytetrafluoroethylene to the bath. The amount of foam can be reduced by an anti-foam agent that is being applied in Fig. 5.

PTFE dispersion has to be mixed well before being added into the bath. However, the dispersion should not be shaken as it foams really easily. When being poured into the bath it is necessary to turn off the mixing in order to eliminate foaming. The foam must not be removed as it contains PTFE particles. Its removal would change the concentration of PTFE in the bath.

Fig. 6 shows movement of the cathode rod ensured by the conversion of the circular motion of the electromotor into the reciprocating motion of the rod.



Fig. 5 Plating drum for bulk coating.



Fig. 6 Technological layout of Zn-PTFE electroplating tank. (Photos - author)

Visual properties

In Fig. 7 and 8, the difference between the pure zinc coating and Zn-PTFE composite coating is almost unrecognizable to the naked eye. Blue passivation (chromating) adds a nice decorative look and is one of the most common conversion layers applied to bolts.

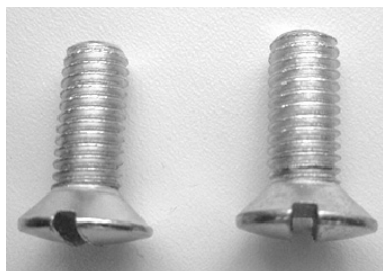


Fig. 7 Zn and Zn-PTFE coating with passivation



Fig. 8 Zn-PTFE without passivation. (Photos - author)

3. IR analysis of the Zn-PTFE coating [5, 6]

The material was analyzed using the infrared microspectroscopy. Infrared spectroscopy is an absorption spectroscopy. Each chemical bond between the atoms in the sample absorbs the incident infrared radiation depending on the energy of their vibrational motion. The energy absorbed from the incident radiation is reflected in the spectrum as an absorption band, whose position on the X axis (i.e. position on the axis of wavenumber) is specific to the particular type of the chemical bond, i.e. the chemical composition of the sample. This measuring method can be used to identify the chemical composition of the sample based on the evaluation of the IR spectra, i.e. the position of absorption bands within the spectrum. Infrared spectroscopy is a comparative method, i.e. the IR spectrum is evaluated by comparing the measured spectra with the standard spectra stored in the spectral library. The measured IR spectrum is a superposition of the spectra of all components of the analyzed mixture. In this case, the identification is based on the evaluation of the positions of the absorption bands using a spectral library, difference spectra or derivative spectra as well as the chemist's – analyst's experience.

The samples were placed under the lens of an infrared micro-spectroscope and analyzed. With respect to the sample character, the beamwidth was adjusted to a small diameter of $3 \times 3 \mu\text{m}$, and the number of spectra accumulations was increased to 1024 proportionally to the beamwidth.

The analysis was carried out using the FTIR spectrometer Nicolet 6700 (Thermo-Nicolet, USA) together with the Continuum microscope, reflectance measurements, MCT detector, parameters of the measurements: spectrum range $4000 - 650 \text{ cm}^{-1}$, resolution 8 cm^{-1} , number of spectra accumulations 128, Happ-Genzelapodization. Gained spectra were evaluated using the Omnic 7.3 (Nicolet Instruments Co., USA) software and identified using the spectral library of The Institute of Chemical Technology, Prague (ICT).

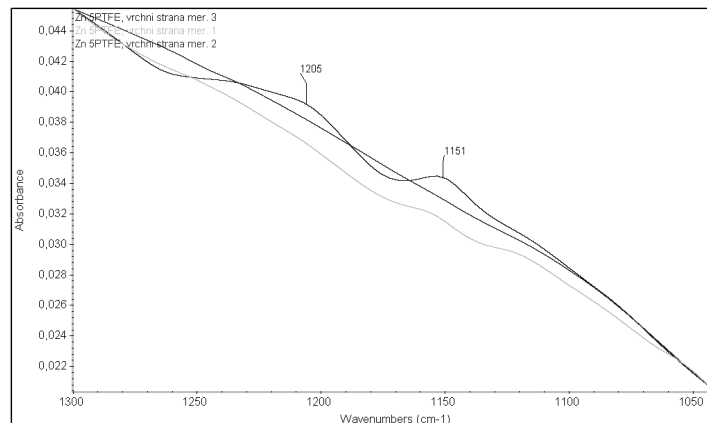


Fig. 9 IR spectra of the Zn-PTFE composite coating with 5% PTFE [5]

In a sample with 5% PTFE in the electroplating bath, PTFE has been identified by the characteristic spectra. The measured spectra are shown in Fig. 9.

4. Conclusions

The aim of this experiment was to build a professional pilot industrial galvanic line, which will be used for example for serial electroplating of bolts with Zn-PTFE according to technological conditions set out in Tab 1. The concept of the technology has been developed in the laboratory conditions of the Faculty of Mechanical Engineering, Czech Technical University in Prague, and technology was transferred to the premises of CVP Galvanika s.r.o.. A new operation (No. 13 – chromating) was added to the technological process of Zn-PTFE coating in order to ensure the desired visual and functional properties of the bolts.

5. Acknowledgements

This paper is part of research work within the project of MPO ČR TIP No FR-TI1/047. The authors thank the CEEPUS programme for making them possible to be mobile within the network CII-HR-0108.

6. References

- [1] J. Kudlacek, V Kreibich, P. Drasnar, J. Cerveny, J. Paitai, et al.: *Technology of Zn-PTFE electroplating*, [Certified technology]. Owner: CTU in Prague, Faculty of mechanical engineering, 2011.
- [2] P. Drasnar, J. Kudlacek, V. Kreibich, V. Kracmar and M. Vales: The properties of electrolytically deposited composite Zn-PTFE coatings, *MM Science Journal*, July, 2011, pp. 248-249, ISSN 1803-1269.
- [3] P. Roskanin: Tribological properties of composite electrolytic coatings Zn-PTFE, *Proceedings of Student's Conference – STC*, CTU in Prague, Prague, 2011, pp. 12-15, ISBN 978-80-01-04796-5
- [4] P. Drasnar, J. Kudlacek, V. Kreibich, P. Roskanin, M. Pakosta and M. Vales, Z. Car: The tribological properties of Zn-PTFE composite coating. *Proceedings of INTECH Conference on Innovative Technology in Design, Manufacturing and Production*, 2011, Bratislava.
- [5] Novotna, M., Miskova, L.: *Analysis of polymer surfaces on steel plates*, Laboratory of molecular spectroscopy, ICT Prague, Prague, 2012.
- [6] P. Drasnar, J. Kudlacek, P. Roskanin and V. Kracmar: Composition analysis and tribological properties of Zn-PTFE coating. *Proceedings of Technologické Forum 2011*. CTU in Prague/Kouty, 2011, pp. 10-16. ISBN 978-80-01-04852-8.

THE DYNAMIC COMPONENT OF THE PATTERN RECOGNITION SYSTEM OF MICROORGANISMS UNDER MICROGRAVITY CONDITIONS.

M. Nikita¹, L. Strogonova², P. Fomkin³, A. Ermakov⁴

¹ Moscow Aviation Institute, Moscow, GSP-3, A-80 Volokolamskoe Shosse,4,125993,Russia

² Moscow Aviation Institute, Moscow, GSP-3, A-80 Volokolamskoe Shosse,4,125993,Russia

³ Moscow Aviation Institute, Moscow, GSP-3, A-80 Volokolamskoe Shosse,4,125993,Russia

⁴ Moscow Aviation Institute, Moscow, GSP-3, A-80 Volokolamskoe Shosse,4,125993,Russia

Keywords: Capillary electrophoresis, electro-osmosis, microgravity conditions.

Abstract. Microbiological risk to manned and unmanned aircraft and space stations, is the combination of medical, technical, technological risks. Scientific researches have shown that the value of risk increases. Risks can influence on flight safety and function reliability of space technique. The processes of microbiological contamination of the environment and living module equipments proceed with high intensity when continuous delivery of various equipment, consumables, etc. Moscow Aviation Institute experts proposed. However, as the complexity of the mathematical description these methods don't always allow to give a definite answer what type of organism was found. The choice of mathematical model for the recognition of the microorganism is rather revolutionary handling of the microbiological control problem. However, from a variety of recognition method and their mathematical description only those method are selected that can be adapted to the conditions of space flight, and those that register diversity of microorganisms and their evolution under microgravity conditions. It is suggested to add the dynamic component to the static model of microorganism recognition. It is assumed that one of the options for solving this problem is to use a method which is based on electrophoresis.

Capillary electrophoresis is well-known method for the analysis of complex mixtures that uses electro kinetic phenomena such as electromigration of ions and other charged particles and electro-osmosis. If the process occurs in a thin capillary, such as quartz, then imposed along the capillary electric field produces the motion of charged particles and the liquid passive flow. As a result, as electromigration parameters are specific for each type of charged particles which are different microbiological agent the sample is separated into individual components. The choice of the dynamic method such as capillary electrophoresis is not random. In this case, the disturbing factors such as diffusion, convection and gravity, are greatly weakened or absent. That results in effective separation particularly under microgravity conditions.

The problem of microbiological sample delivery to the proposed electrophoretic plant under microgravity conditions is observed.

Introduction

While studying the problem of recognition of microorganisms a number of problems could be identified:

- 1) to select a method for detecting microorganisms,
- 2) to adapt mathematical model to the conditions of microgravity.

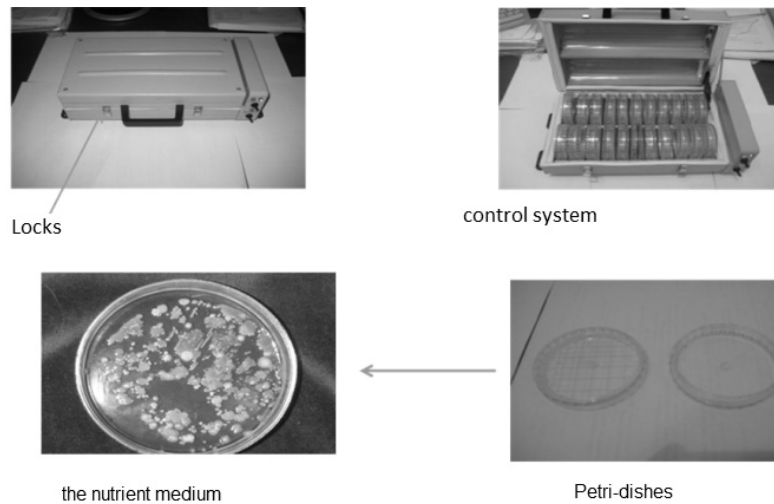
The solution of these problems will result in the decision of purpose which is to recognize micro-organisms and relate them to a certain type and class.

In order to solve the first problem, it was decided to split this item into two stages:

- 1) the dynamic component of the pattern recognition system of microorganisms under microgravity conditions,
- 2) the static component of the pattern recognition system of microorganisms under microgravity conditions.

The static component of the pattern recognition system of microorganisms under microgravity conditions.

The first thing that had been done was to find the way of obtaining the samples for the further exploration. For these purposes IMBP together with scientific research Institute of Cosmic Instrument making (Russian Federal Space Agency) made the special device - the experimental device for express diagnostics of microflora-structure which allows incubating colonies of microorganisms in the conditions of real space flight ("Microflora"). It represents the thermostat in the form of a convenient and compact small suitcase with lock and element of control that switches the thermostat between two operating modes - 28°C and 37°C. Petri-dishes are placed in the thermostat in individual cells with a nutrient medium where an incubation takes place.



The transition to dynamic component of the pattern recognition system of microorganisms under microgravity conditions.

With the aid of Active appearance models (that can be transferred as “active models of exterior view”) it is possible to simulate the images of the objects, subjected both down rigid (rigid) and nonrigid (non-rigid) deformation. Rigid deformation - any deformation, which can be presented in the form to the composition of transfer, turning and scaling. AAM consists of the set of the parameters, part from which controls the form of object, rest assign its texture. The parameters of model are selected automatically, on the basis of the most characteristic deformations of form and changes in the texture, which are present before the training collection of the images of object. The active model of the exterior view of microorganisms assigns changes in the form of microorganisms and its characteristic features, and also possible changes in the texture of microorganisms. For the solution of the problem of detecting the microorganisms on the image, is made the attempt to find the parameters (arrangement, form and texture) OF AAM, which assign image closest down that observed. The degree of the proximity of the exterior view of model before the optimum configuration to the observed image gives the possibility to estimate we see we microorganism or not.

The lecture: «The static component of the pattern recognition system of microorganisms under microgravity conditions» was produced on conference in Slovakia

The dynamic component of the pattern recognition system of microorganisms under microgravity conditions.

Table 1. Methods for recognition microorganisms

1	Coloration microorganisms
1.1	Coloration by Gram
1.2	Coloration by the method of Ziehl-Nelson
1.3	The method of Gins
1.4	The method of Aujeszky's
1.5	The method of Neisseria
1.6	The method Feylgena
2	Fluorimetry
3	Spectroscopy
3.1	Method of ultraviolet spectroscopy
3.2	Methot of infrared spectroscopy
4	ЯМР
5	Method of cgomotography
5.1	Method of thin-layer chromatography
5.2	Method of liquid chromatography
6	Microbiological methods
7	Biochemical methods
8	Microscopy
8.1	Light microscopy
8.2	Electron microscopy
9	Polarimetry
10	Thermometric methods
11	Calorimetry
12	Electrochemical method
12.1	Potentiometry
12.2	Method of voltamperometry
12.3	Capillary electrophoresis

From a variety of recognition method and their mathematical description only those method are selected that can be adapted to the conditions of space flight, and those that register diversity of microorganisms and their evolution under microgravity conditions. It is suggested to add the dynamic component to the static model of microorganism recognition. It is assumed that one of the options for solving this problem is to use a method which is based on electrophoresis.

Capillary electrophoresis is well-known method for the analysis of complex mixtures that uses electro kinetic phenomena such as electromigration of ions and other charged particles and electro-osmosis. (fig.1)

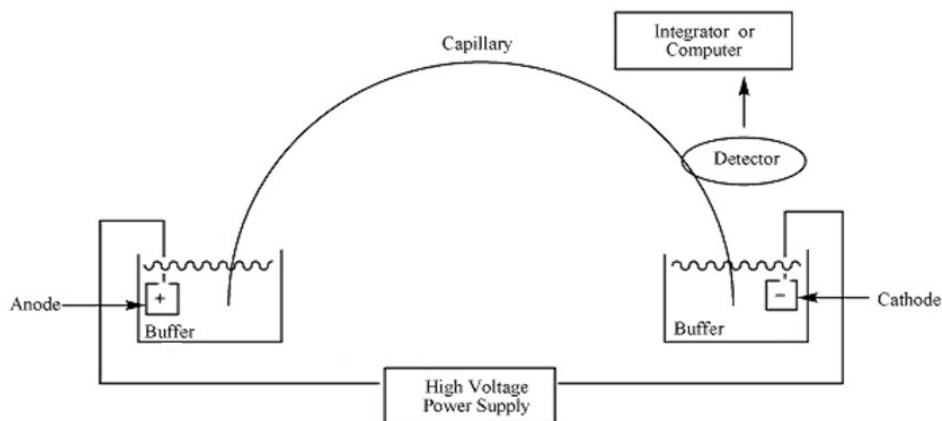


Fig.1 Plan of capillary electrophoresis

If the process occurs in a thin capillary, such as quartz, then imposed along the capillary electric field produces the motion of charged particles and the liquid passive flow. As a result, as electromigration parameters are specific for each type of charged particles which are different microbiological agent the sample is separated into individual components. (fig.2)

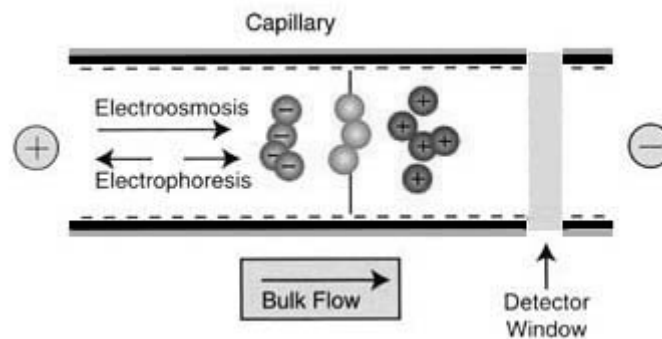


Fig. 2 The motion of charged particles and the liquid passive flow.

The choice of the dynamic method such as capillary electrophoresis is not random. In this case, the disturbing factors such as diffusion, convection and gravity, are greatly weakened or absent. That results in effective separation particularly under microgravity conditions.

The problems associated with the use of this method on the ISS

One problem is that the method requires a high voltage 25-30 kV, and on board the ISS, we have 25V. Consequently, we must raise the initial voltage to a desired, the method which we have proposed is shown in Figure 3.

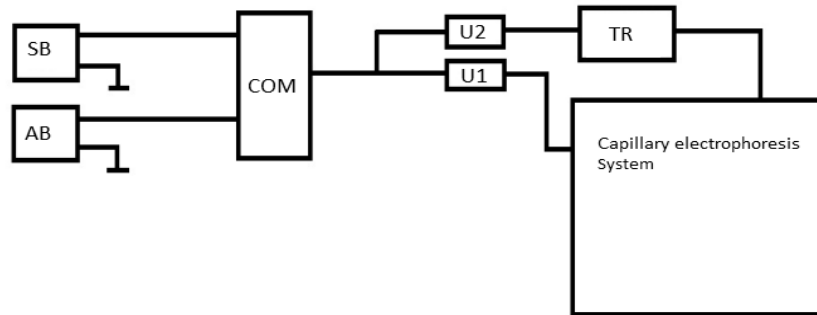


Fig.3 The scheme of voltage raising.

Where: SB-solar battery, AB-battery, Com. – commutator, U1-voltage, which is not transformed, U2-voltage, which will be raised to 30 kV 25, TR - transformer

mathematical model

Methods for separation of particles

The velocity (U_p) separated the molecules in field with respect to the electrode of opposite charge:

$$U_a = \mu_a E \quad (1)$$

where: μ_a is the electrophoretic mobility, E is the force of the electric field

$$\mu_a = z / 6 \pi \eta r \quad (2)$$

where: z is the specific charge, r is Stokes radius of the molecule

$$r = K_B T / 6 \eta \pi D \quad (3)$$

where: K_B is the Boltzmann's constant, T is the temperature, D is the diffusion constant.

μ_a - can be determined experimentally from the time of the molecule in an electric field

$$\mu_a = (L / t_x) (L_x / V) \quad (4)$$

L is the distance from the starting point to the point of detection, t_x is the time spent by a analyzed molecule to reach the detection point, V is the voltage of the electric field, L_x is the total length of the capillary. Since the electric field acts only on the charged molecules, uncharged molecules are separated by capillary electrophoresis weak.

$$U_o = \mu_o E \quad (5)$$

where μ_o is the electroosmotic mobility

$$\mu_o = \epsilon \zeta / \eta \quad (6)$$

where: ζ is the potential of the walls of the capillary, ϵ is the relative dielectric permeability.

The speed of movement (U) of the analyzed molecules in electric field:

$$U = U_a + U_o = E(\mu_a + \mu_o) \quad (7)$$

The detecting of microorganisms

the detecting will be come true with the help of infrared radiation, which will go through the capillary with buffer and the substance. The intensity of radiation after going through the substance will change so as particle differently absorbs and transmits it. After going through the infrared radiation are analyzed and the result is a spectrum, which will be compared with known spectra.

The capillary is made of plastic, which has the property of transparency to infrared radiation, that allows to not take into account the reflection of light from the walls.

In order to calculate the intensity at the exit of the capillary using the law of Bouguer-Lambert-Beer

$$I = I_o e^{-k_a L} \quad (8)$$

Where: k_a - is the absorbance, L - layer thickness of substance.



References

- [1] R. Siegel, John R. Howeeel – Thermal radiation heat transfer, 1972
- [2] A. Lee Smith - Infrared spectroscopy, 1982
- [3] Strogonova L.B., Fomkin P.A. Aspects of microbiological control during longtime space expeditions // IAC 2009 Paper
- [4] Voloshuk A.M. – A guide to the capillary electrophoresis, 1996.



International Conference on Innovative Technologies, IN-TECH 2012,
Rijeka, 26. - 28.09.2012



A MATHEMATICAL MODEL FOR DETERMINING SOME TRIBOLOGICAL CHARACTERISTICS OF PLAIN JOURNAL BEARING

Ž. Antičić¹, N. Nikolić¹, T. Torović¹ and J. Dorić¹

¹ Faculty of Technical Sciences, Trg Dositeja Obradovića 6, 21000 Novi Sad, Serbia

Keywords: Tribology, Reynolds equation, Energy equation, temperature field, pressure field

Abstract. Tribology is the science of friction, wear and lubrication. Bearing as a paradigm of a tribological system is one of the most significant objects investigated in tribology research. Because of their performance, bearings are used in many rotating machines such as turbines, compressors and internal combustion engines. In internal combustion engines, bearings are used to support and lead the crankshaft, connecting rods and camshafts. Bearings in internal combustion engines generally operate under conditions of thermohydrodynamic lubrication. The Couette approximation method for obtaining temperature distribution in oil film of main journal bearing is used in the paper. A conjunction between the Reynolds equation and the adiabatic Energy equation is ruptured by this method enabling the two equations to be solved independently. By solving the adiabatic Energy equation, the temperature field in oil film of journal bearing is determined under different journal speed and load conditions. Relative journal position with respect to the bearing (eccentricity ratio) has been proposed as a measure of load. The exponential viscosity temperature relationship has been incorporated into the Energy equation. By solving the Reynolds equation, the pressure field in oil film under extreme conditions (maximum speed and load – minimum speed and load) has been determined in accordance with adiabatic and isoviscous theory for oil SAE40.

Introduction

Tribology is the science of friction, wear and lubrication. Bearing as a fundamental tribological system generates heat due to internal friction in the oil film. This heat in most cases can not be ignored since it significantly affects bearing performance. Preliminary studies on thermal effects in lubrication were undertaken in the forties of the XX century. In fact, thermal effects had been analyzed much earlier by G. Hirn (1854), O. Reynolds (1886) and N. Petrov (1900). However, a greater awareness of the importance of these effects arose thanks to the Kingsbury (1933), who carried out an experimental and theoretical study in which he concluded that thermal effects were responsible for the large discrepancies between the experimental observation and the theoretical predictions for load capacity of hydrodynamic bearings [1]. According to Colynuck and Medley this heat can reduce the bearing load capacity for two or more times [2,3].

Different methods have been developed considering thermal phenomena in the theory of hydrodynamic lubrication. Among these methods, adiabatic methods take an important place for their simplicity. Dowson and Hudson (1960), introduced the concept of thermohydrodynamical lubrication [4].

The adiabatic methods are focused on the oil film which is assumed to be surrounded by adiabatic surfaces and there are no interaction with other structures of the bearing. Therefore, all the heat, generated in the bearing by the viscous friction, is removed by the lubricant. By neglecting the conduction heat transfer through the bearing surface, a slightly higher oil film temperature is obtained in comparison to its real value. This allows a more reliable assessment of plain bearings characteristics and a choice of appropriate bearing materials [5].

Depending on the mathematical description of the oil film behavior, different adiabatic methods are developed. The first one is the method of the effective viscosity [2,4-9], or so-called global thermal method by Swift (1937) [1]. In this simplified theory, the lubricant is isoviscous. Based on the energy balance equation for the global oil film and the corresponding equations for a variable viscosity, the effective temperature and the effective viscosity are determined. These parameters define the thermal state of the oil film and they are crucial for the determination of the bearing performance. This method is still attractive and gives acceptable results in a limited range of the plain bearing operating conditions [1,5,6].

In contrast to the global methods, local thermal methods are general but more complex category of adiabatic methods. These methods are based on the fundamental differential equations of the adiabatic oil film, the viscosity of which is changed locally in accordance with an equation for the variable viscosity (e.g. Reynolds equation and Vogel equation). The first of the local thermal methods is the adiabatic Cope method (1949) [1,4,10,11]. Cope introduces the adiabatic energy equation that is in fact the general energy equation adapted to the adiabatic oil film in the bearing. This equation is governing the temperature field in the oil film. Another fundamental equation in this method is the Reynolds partial differential equation governing the pressure field in the oil film. In the energy equation the pressure and the temperature gradients along the height of the oil film are neglected. By simultaneously solving these partial differential equations including the appropriate boundary conditions, the temperature and the pressure fields are determined. This demands iterative or other computational procedures which make the process laborious.

To simplify the solving of the Reynolds equation and the adiabatic energy equation, McCallion et al. [4] formulated the so-called Couette method ignoring the pressure gradient in the energy equation. A new energy equation, easy to solve independently of the Reynolds equation, is thus obtained. By integrating the new energy equation, the temperature field is determined. The temperature field is described by the angle θ , the relative eccentricity ε , the temperature-viscosity coefficient α and the adiabatic constant for plain bearing E .

In this paper, the so called direct approach is presented, which is basically a classic approach for models of this type. In this approach, the shaft eccentricity and the attitude angle are prescribed to calculate the other parameters of plain bearings. In contrast to the direct approach, the inverse approach requires knowledge of the shaft load by use of which, the position of the journal in the bearing i.e. the shaft eccentricity is determined. Thus, in the direct approach, the shaft eccentricity is a measure of its load.

Mathematical Model

The Reynolds equation and the adiabatic energy equation can be written in dimensionless form as follows [4]

$$\frac{\partial}{\partial \theta} \left(H^3 \frac{\partial P}{\partial \theta} \right) + \frac{1}{\lambda^2} \frac{\partial}{\partial Z} \left(H^3 \frac{\partial P}{\partial Z} \right) = \frac{\partial H}{\partial \theta}, \quad (1)$$

$$\left(1 - H^2 \frac{\partial P}{\partial \theta} \right) \frac{\partial \bar{T}}{\partial \theta} - \frac{H^2}{\lambda^2} \frac{\partial P}{\partial Z} \frac{\partial \bar{T}}{\partial Z} = 2 \frac{(R/c)^2}{H^2} + 6(R/c)^2 H^2 \left[\left(\frac{\partial P}{\partial \theta} \right)^2 + \frac{1}{\lambda^2} \left(\frac{\partial P}{\partial Z} \right)^2 \right] \quad (2)$$

The dimensionless variables are introduced as written below

$$H = 1 + \varepsilon \cos \theta, \quad \varepsilon = \frac{e}{c}, \quad \lambda = \frac{L}{2R}, \quad Z = \frac{z}{L/2}, \quad P = \rho \frac{(c/R)^2}{6\eta\omega}, \quad \bar{T} = T \frac{\rho c_p}{\eta\omega} \quad (3)$$

where H is the dimensionless oil film thickness, ε is the shaft eccentricity, θ is the angular coordinate, λ is the bearing slenderness or $L/2R$ ratio, Z is the dimensionless axial coordinate along the axis of the bearing measured from the center of the bearing, P is the dimensionless pressure, ρ is the pressure in the oil film, η is the lubricant viscosity, ρ is the density of the lubricant, c_p is the specific heat of the lubricant ω is the angular velocity of the shaft, \bar{T} is the dimensionless temperature and T is the actual temperature.

By neglecting the pressure gradients, the energy equation becomes

$$\frac{\partial \bar{T}}{\partial \theta} = 2 \frac{(R/c)^2}{(1 + \varepsilon \cos \theta)^2}. \quad (4)$$

By using Eq. (3), Eq. (4) is converted into the dimensional form

$$\frac{\partial T}{\partial \theta} = 2 \frac{\eta\omega}{\rho c_p} \frac{(R/c)^2}{(1 + \varepsilon \cos \theta)^2}. \quad (5)$$

Taking into account the boundary condition

$$T(0) = T_0 \quad (6)$$

and Reynolds relationship for the viscosity [4]

$$\eta = \eta_0 e^{-\alpha(T-T_0)} \quad (7)$$

where η_0 is the supply viscosity and α is the temperature-viscosity coefficient, Eq. (5) after integration gets the form

$$T = T_0 + \frac{1}{\alpha} \ln \left(1 + 2 \frac{\eta_0 \omega \alpha}{\rho c_p} \frac{(R/c)^2}{(1 - \varepsilon^2)} \left(\frac{1}{(1 - \varepsilon^2)^{3/2}} \arccos \left(\frac{\varepsilon + \cos \theta}{1 + \varepsilon \cos \theta} \right) - \frac{\varepsilon \sin \theta}{1 + \varepsilon \cos \theta} \right) \right), \quad (8)$$

or

$$\Delta T = \frac{1}{\alpha} \ln \left(1 + \frac{E}{(1 - \varepsilon^2)} \left(\frac{1}{(1 - \varepsilon^2)^{3/2}} \arccos \left(\frac{\varepsilon + \cos \theta}{1 + \varepsilon \cos \theta} \right) - \frac{\varepsilon \sin \theta}{1 + \varepsilon \cos \theta} \right) \right). \quad (8a)$$

Comparing Eq. (8) and Eq. (8a), it is clear that

$$E = 2 \frac{\eta_0 \omega \alpha}{\rho c_p} (R/c)^2, \quad (9)$$

where E is the adiabatic constant that has the universal meaning and refers to the bearing as a whole. McCallion and others have shown that the Couette method is valid for all the values of constants $E < 0.4$ (see the Table 1 – valid results are above the tick line in the table), while ε may take different values depending on the slenderness of the bearing [4]. For a short bearing of the slenderness $\lambda = 1/2$, ε can take values up to 0.8 [4,7,12].

The maximum temperature increase is in the area of the minimum oil thickness, i.e. $\theta = \pi$,

$$(\Delta T)_{\max} = \frac{1}{\alpha} \ln \left(1 + \frac{E\pi}{(1-\varepsilon^2)^{3/2}} \right). \quad (10)$$

For short bearing Eq. (1) becomes [12].

$$\frac{1}{\lambda^2} \frac{\partial}{\partial Z} \left(H^3 \frac{\partial P}{\partial Z} \right) = \frac{\partial H}{\partial \theta}, \quad (11)$$

with the boundary condition

$$p(\theta, Z = +1) = 0, \quad p(\theta, Z = -1) = 0. \quad (12)$$

After integration Eq. (11), taking into account the boundary conditions, the pressure distribution in the oil film will have the form

$$P = \frac{\lambda^2}{2} \frac{\varepsilon \sin \theta}{(1 + \varepsilon \cos \theta)^3} (1 - Z^2). \quad (13)$$

Taking into account Eq. (3), Eq. (13) is converted into the dimensional form,

$$p = 3\lambda^2 \eta \omega (R/c)^2 \frac{\varepsilon \sin \theta}{(1 + \varepsilon \cos \theta)^3} (1 - Z^2). \quad (14)$$

Combining Eq. (7) and Eq. (14), the pressure distribution in the oil layer of variable viscosity becomes

$$p = 3\lambda^2 \eta_0 \omega (R/c)^2 \frac{\varepsilon \sin \theta}{(1 + \varepsilon \cos \theta)^3} (1 - Z^2) e^{-\alpha h T}. \quad (15)$$

Results and Discussion

A number of parameters and dimensionless groupings are present in the analysis of heat problems. In this analysis, the parameters determining the rheological and physical properties of the oil film, such as viscosity, temperature-viscosity coefficient, specific heat and density, are very important. There are various expressions that describe functional dependencies of these parameters on the temperature and the pressure [2,4,8]. It is assumed in the paper that the viscosity, η , is a function of the temperature only. The inlet viscosity was determined by using the Vogel equation for the initial temperature $T_0 = 70^\circ\text{C}$. The parameters ρ and c_p are assumed to be constant and their values are given in the heading of the Table 1. The parameter α is obtained as a mean value of the temperature-viscosity coefficient by using the Reynolds and the Vogel equations [13].

The values of the parameter E, defined by Eq. (8a) are given in the Table 1 for oils SAE10 to SAE60.

Fig. 1 shows the distribution of temperature in the oil film in circumferential direction of the bearing for the oil SAE40 and different values of the eccentricity ratio and three different shaft speeds.

Fig. 2 shows the pressure distribution in the film of oil SAE40 under extreme conditions according to isoviscous and adiabatic theory. The results obtained in this paper are, to a great extent, in accordance with the numerical and experimental results from [14,15,16].

Table 1. The values of constant E for different oil types and shaft speeds

$E = 2 \frac{\eta_0 \omega \alpha (R/c)^2}{\rho c_p}, (R/c) = 10^3, \rho = 880 [\text{Kg}/\text{m}^3], c_p = 1.88 [\text{kJ}/\text{kg } ^\circ\text{C}]$						
the type of oil	$10^3 \eta_0$ [Pas]	$10^2 \alpha$ [1/°C]	$10^2 E$ $n = 1000$ [o/min]	$10^2 E$ $n = 2000$ [o/min]	$10^2 E$ $n = 3000$ [o/min]	$10^2 E$ $n = 4000$ [o/min]
SAE 10	10.322	2.825	3.692	7.383	11.075	14.767
SAE 20	14.094	3.112	5.552	11.104	16.666	22.207
SAE 30	20.967	3.336	8.854	17.708	26.562	35.415
SAE 40	28.472	3.621	13.050	26.101	39.150	52.202
SAE 50	46.121	3.709	21.656	43.310	64.967	86.624
SAE 60	63.217	3.846	30.776	61.551	92.327	123.10

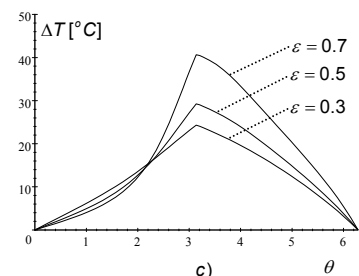
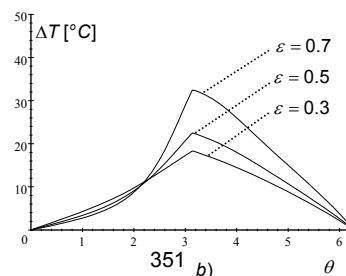
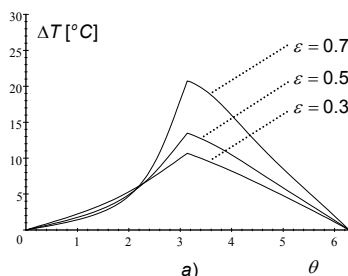


Fig. 1. ΔT versus θ for various values of ε for oil SAE40 under different shaft speed conditions:
a) $n=1000$ rpm, b) $n=2000$ rpm, c) $n=3000$ rpm

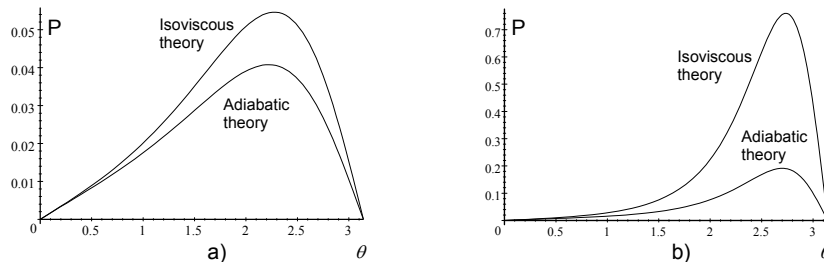


Fig. 2. Pressure distribution in the film of oil SAE40 under extreme conditions, according to the isoviscous and adiabatic theory:
a) $\varepsilon = 0.2$, $n=1000$ rpm, b) $\varepsilon = 0.7$, $n=3000$ rpm

Conclusion

The results can be summarized as follows:

- The temperature gradient increases progressively along the oil film in the direction of the shaft speed for all the values of ε in the convergent part of the bearing. This phenomenon is more pronounced at the higher values of ε , especially in the areas of the smaller oil film thickness. The maximum temperature occurs in the area of the minimum oil film thickness.
- Increasing the shaft speed, the temperature of the oil film is also increased.
- The presence of thermal effects in the oil film significantly reduces the pressure in the oil film and at the same time its load capacity.

Acknowledgment

This research is a part of the project TR-31046 "Improvement of the Quality of Tractors and Mobile Systems with the Aim of Increasing Competitiveness and Preserving Soil and Environment" supported by Ministry of Science and Technological Development of the Republic of Serbia.

References

- [1] F. P. Brito: *Thermohydrodynamic Performance of Twin Groove Journal Bearings Considering Realistic Lubricant Supply Conditions: A Theoretical and Experimental Study*, PhD Thesis, Universidade do Minho, 2009.
- [2] G. W. Stachowiak and A. W. Batchelor: *Engineering Tribology*, (Butterworth-Heinemann, Woburn, 2001).
- [3] A. J. Colynuck and J. B. Medley: Comparison of Two Finite Difference Methods for the Numerical Analysis of Thermohydrodynamic Lubrication, *Tribology Transactions*, Vol. 32 (1989), pp. 346-356.
- [4] O. Pinkus: *Thermal Aspects of Fluid Film Tribology*, (ASME Press, New York, 1990).
- [5] A. Hamoy: *Bearing Design in Machinery - Engineering Tribology and Lubrication*, (Marcel Dekker, Inc., New York, 2003).
- [6] A. Z. Szeri: *Fluid Film - Theory and Design*, (Cambridge University Press, Cambridge, 1998).
- [7] J. Frene, D. Nicols, B. Degueurce, D. Berthe and M. Godet: *Hydrodynamic Lubrication - Bearings and Thrust Bearings*, (Elsevier, Amsterdam, 1997).
- [8] A. Cameron: *Basic Lubrication Theory*, (John Wiley & Sons, Inc., New York, 1976).
- [9] Ž. Antonic, N. Nikolić and T. Torović: Effective Viscosity Method in Hydrodynamic Lubrication Theory, *PSU-UNS International Conference on Engineering and Environment ICEE*, Phuket, Thailand, 2007
- [10] W. F. Cope: The hydrodynamical theory of film lubrication, *Mathematical and Physical Sciences*, Vol. 197 (1949), No. 1049, pp. 201-217.
- [11] D. Dowson: *History of Tribology*, (Longman, London, 1979).
- [12] Ž. Antonic, N. Nikolić and T. Torović: Radne karakteristike kratkog kliznog radijalnog ležišta, *Traktori i Pogonske Mašine*, Vol.10 (2005), No.4, pp. 68-73.
- [13] J. E. Shigley and C.R. Mischke: *Mechanical Engineering Design*, (8th edn. McGraw Hill., 2001)
- [14] S. S. Banwait and H.N. Chandrawat: Study of thermal boundary conditions for a plain journal bearing, *Tribology International* 31 (1998), pp. 289-296.
- [15] J. A. Moreno, F. C. Gomez and F. Alhama: Solution of temperature fields in hydrodynamics bearings by the numerical network method, *Tribology International* 40 (2007), pp. 139-145.
- [16] M. Fillon, J. Frene and R. Boncompain: Historical aspects and present development on thermal effecting hydrodynamic bearings, In *Proceedings of the 13th Leeds-Lyon Symposium on Tribology*, Leeds-Lyon, 1987, pp. 27-47.

INFLUENCE OF IBAD SiN_x COATINGS ON TRIBOLOGICAL PROPERTIES OF P/M HSS

J. Suchánek¹, F. Černý¹

¹ CTU in Prague, Faculty of Mechanical Engineering, Technická 4, 166 07, Prague, Czech Republic

Keywords: IBAD, SiN_x , P/M HSS, RBS, tribology, friction coefficient

Abstract. Polycrystalline silicon nitride is characterized by high chemical stability and excellent tribological properties. Ion-beam-assisted deposition (IBAD) SiN_x is used for preparation of silicon nitride coatings. Amorphous IBAD SiN_x coatings on the hardened HSS have bad tribological properties.

Introduction.

Hard brittle coatings can be damaged rapidly if plastic deformation initiates in the substrate near the coating-substrate interface as a result of high loading. The plastic deformation owing to mechanical and thermal activity at the contact area does not initiate in the coating until a large plastic zone has been developed in the substrate [1]. The load bearing capacity of coating-substrate system increases with improved substrate properties. After material deformability has been depleted, some defects arise here and spread till the cracking and separating of a coating occurs. The damage accumulation process is the most intensive at the area of maximum shear stress.

Silicon nitride is characterized by high chemical stability and good dielectric and mechanical properties. Polycrystalline silicon nitride has excellent tribological properties. Therefore, silicon nitride is a candidate material for use as a wear-resisting coating for metals. Ion-beam-assisted deposition (IBAD) is used for surface properties modification of materials. The irradiation of surface layers by energetic ion beam of Ni^{+1} during Si deposition on the steel changes drastically the film density, structure, crystal-amorphous state, grain size, orientation and defect density, the chemistry and the type produced SiN_x coating. Among the most significant advantages of the IBAD method ranks the fact that it is a relatively low temperature process, and that concentration profiles of a different shape may be constructed by means of this method. Furthermore, the thin films prepared by the high energy IBAD method are of a significantly increased adhesion due to a large area of ion beam mixing at the interface between the film and substrate as a result of the high ion energy. Gradient high energy IBAD SiN_x thin films with predicted type of the shape of nitrogen concentration profile have been prepared. The required course of the value of the variable followed in the coating may sometimes be performed by depositing of the sandwich film, i.e. a coating composed of partial coatings of various materials.

Experimental Details

Tested materials and their surface treatment

The P/M high-speed steels MASTER CUT 1 and ASP 23 have been used as substrate in our experimental programme with high energy IBAD SiN_x . Polished silicon wafers with IBAD SiN_x coatings have been used for analysis of concentration profiles. The substrates were prepared in the form of square silicon monocrystalline wafers of a side approximately equal to $1 \cdot 10^{-2}$ m and of the thickness approximately equal to $2 \cdot 10^{-4}$ m. One square basis of each wafer intended for the IBAD film formation has been polished. Before inserted into the vacuum chamber, the substrates had been cleaned in organic solvents in an ultrasonic bath. There are the interactions of the atoms of a solid material with the nitrogen atoms of two different initial energy values, one of which is a half of the other. In our case 1/7 of the nitrogen atoms has the 90 keV energy and 6/7 have the 45 keV energy. The resulting concentration profile will thus be a superposition of the concentration profiles corresponding the nitrogen atoms of the two different energies.

Resulting nitrogen concentration profiles were measured by RBS method. For this method alpha particles accelerated by van de Graaf accelerator were used. For the adhesive wear tests were prepared homogeneous coatings (200 nm) and gradient coatings (500 nm). Accelerating voltage in our experimental arrangement is 90 kV and the maximum flux density of the nitrogen atoms is approximately $4 \cdot 10^{17} \text{ m}^{-2} \text{ s}^{-1}$. The process of SiN_x films preparation was carried out in three steps. In the first step, only the deposition was carried out. In the second step, the value of the process parameter was $I = 0.22$. For the set maximum flux value of the nitrogen atoms $3.9 \cdot 10^{17} \text{ m}^{-2} \text{ s}^{-1}$, the corresponding flux density of the silicon atoms $\varphi_2 = 1.8 \cdot 10^{18} \text{ m}^{-2} \text{ s}^{-1}$ was then necessary to be set. The third step was carried out with the $\varphi_1 = 3.9 \cdot 10^{17} \text{ m}^{-2} \text{ s}^{-1}$ and $\varphi_2 = 9 \cdot 10^{17} \text{ m}^{-2} \text{ s}^{-1}$ flux densities.

Testing of tribological characteristics

Tribological characteristics are tested experimentally on the HEF tribometer with linear contact. The sliding velocity was 0,001 m/s, normal force – 25, 50, 100 and 150 N, without lubricant. Hardened and low-tempered chromium steel 14109 (= DIN W3) having the hardness 62-64 HRC is used as the second member of the sliding pair.

Results

Concentration profiles of IBAD SiN_x coatings

The measurement of the resulting concentration profiles was carried out by RBS (Rutherford Backscattering Spectroscopy) method. To facilitate the RBS method application for our analyses, two problems were, however, necessary to be solved. The first one rested on the fact that an analysis of a lighter component in a thin film on a heavier component substrate was required. In such a case, the relatively weak signal of the lighter component is superimposed on the strong signal of the heavier component, forming an inaccurately deductible background. The second problem was connected with the fact that current evaluation procedure of the measured energy spectra of the scattered alpha particles for the determination of the concentration profiles does not respect the change of the stopping power of the

investigated film in the calculation of energy losses of alpha particles in their passage through this film. That is why, an correction of the RBS method was carried out for the measurement of the concentration profiles of lighter components in inhomogeneous binary films [2].

For measurement of the nitrogen concentration profiles by the RBS method, the alpha particles were used of the 2180 keV energy. The particles beam had a diameter $1 \cdot 10^{-3}$ m on the surface of the sample. The laboratory scattering angle was 170° and the particles scattered were registered by a Si (Au) detector. The resulting gradient concentration profile deduced from the RBS spectrum of the film on the basis of the paper [3] is in Fig. 1. In Fig. 2, it is compared with the corresponding mathematical model.

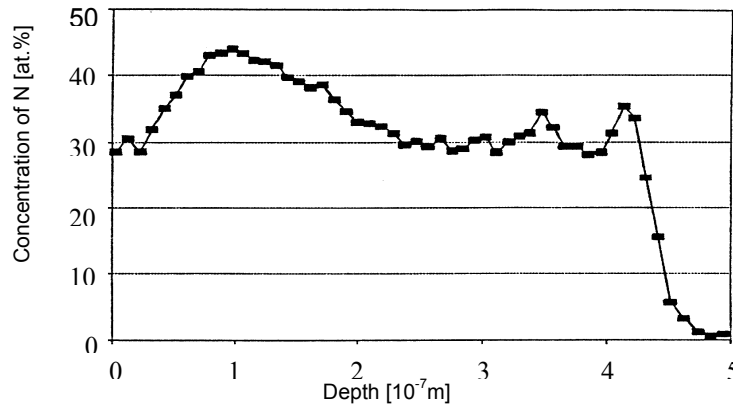


Fig. 1. The resulting gradient nitrogen concentration profile in the SiN_x film.

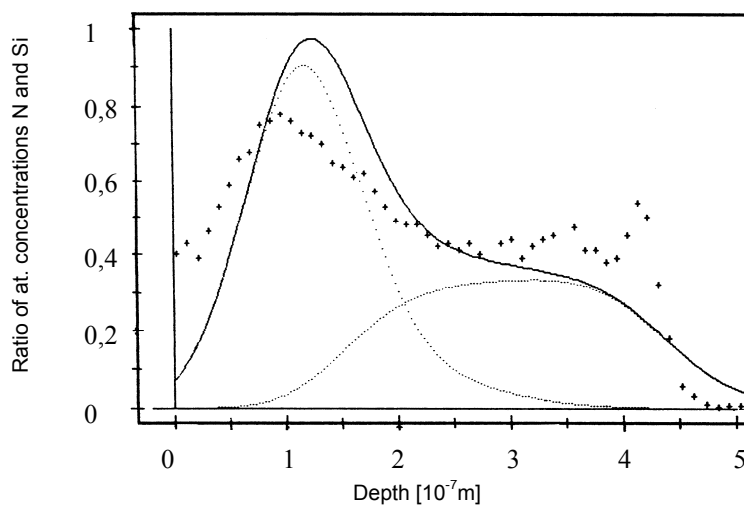


Fig. 2. Comparison of the measured concentration profile with the mathematical model

Friction coefficient

At the beginning of the friction tests of sliding pair - hardened AISI 52100 x thin IBAD SiN_x coatings (about 200 nm) deposited on hardened P/M HSS – started peeling off the coating. The deterioration of IBAD SiN_x coatings started at the minimum load (see tab.1). There is no difference among understoichiometric (Var.1) and stoichiometric coatings (Var.2) from the point of view of friction coefficient. The unsatisfactory adhesion of the IBAD SiN_x coatings was probably influenced by nitrogen oversaturation of the substrate surface layers during IBAD process. Owing to a very low deposition rate of Si nitrogen ions during the implantation penetrated into surface layers of substrate materials and at the end of ion implantation the surface layers contained more than 2×10^{18} ions cm^{-2} . These layers became very brittle and they failed during mechanical loading. The gradient amorphous IBAD SiN_x coatings with 500 nm thickness had improved adhesion, but the adhesion was unsatisfactory for cutting and forming tools. During our experiments on the tribometer HEF with sliding pair IBAD SiN_x coating - hardened bearing steel it was discovered that the SiN_x coating was destroyed after 2500 m path.

Tab. 1 Friction coefficient of sliding pair (IBAD SiN_x coating - hardened bearing steel) as a function of load



Load	25 N	50 N	100 N	150 N
Var. 1	0.934	1.142	1.310	1.231
Var. 2	0.816	0.966	1.344	1.206

Conclusion

Based on concentration profile measured by RBS method and a mathematical model, the gradient concentration profile of nitrogen in the SiN_x coating was constructed. The discrepancy between the profile measured by the RBS method and the mathematical model in the surface area may be explained by the radiation stimulated diffusion in this area.

Amorphous IBAD SiN_x coatings on the hardened HSS have bad tribological properties.

References

- [1] T. Bell.: Realising the potential of duplex surface engineering. In Hutchings, I. M.(ed.): New Directions in Tribology, MEP, London, 1997, 121-133
- [2] V. Hnatowicz et al.: Nucl. Instr. and Meth., B86 (1994) 366
- [3] F. Černý, J. Suchánek, V. Hnatowicz: IBAD $\text{SiN}(x)$ coating: preparation and tribological properties. Thin Solid Films 317 (1998) Issue 1-2, pp. 490-492



International Conference on Innovative Technologies, IN-TECH 2012,
Rijeka, 26. - 28.09.2012



ANALYSIS OF BULK METAL FORMING BY UBET – CASE STUDIES

I. Kačmarčik¹, B. Štrbac¹ and L. Šikulec²

¹ Faculty of Technical Science, University of Novi Sad, Trg Dositeja Obradovića 6,
21000 Novi Sad, Serbia

² University of Rijeka Faculty of Engineering, Vukovarska 58, 51 000 Rijeka, Croatia.

Keywords: Upper Bound, UBET, upsetting, hobbing, open-die forging

Abstract. The most important and in practice most frequently applied bulk metal forming processes are: forging, rolling, extrusion, drawing, upsetting and hobbing. One of the main steps in preparation and performing of bulk metal forming process is determination of optimal input parameters. Efficient way to do this is process of pre-analysis and simulation. Current paper elaborates analysis of different bulk metal forming operation by using UBET simulation: free upsetting, hobbing and open-die forging. Deformation load is determined and analysis and discussion of the results are performed. At the end, results obtained by simulation are compared to theoretical calculations.

Introduction

Modern global market requires cost-efficient manufacturing and low production times. Therefore, in order to optimize manufacturing processes, analysis and simulations are essential. In metal forming, all relevant process parameters (forming load, pressures, material flow...) ought to be approximately foreseen prior to experimental trials. Pre-analysis and simulations are performed to reduce experimental costs and avoid eventual machine hazards. For the analysis of metal forming processes several methods can be applied:

Finite element method is nowadays the most used as it is able to provide the most complex analysis. In this method, deformation zone is divided into small finite elements which are connected at nodal points. By introducing complex equations which act on the elements, the most important process parameters (material flow, pressures, contact areas, friction...) can be determined. The smaller the finite elements, the more precise calculation is possible. However, smaller elements result in more consumption of computer resources and therefore longer simulation times. Based upon this method a number of different software packages have been developed (Simufact, Deform, Abaqus, Forge...).

Slab method is based upon the selection of one particular element in the workpiece and identification of normal and frictional stresses that act on that element. These analyses give final results by introducing several assumptions and simplifications of the process.

Slip line method is restricted to only plane-strain conditions. In this method a set of so called slip-lines are drawn. These lines correspond to the directions of the yield stress of the material in shear. Major drawback of this method is the possibility to analyse only plane-strain processes.

Visioplasticity method uses the inscribed network of lines at the meridian surface of the divided workpiece. This network is observed in the incremental manner, starting with the non-deformed state. Deformed grid is compared after each increment with previous one and in that manner velocity field at the meridian plane can be obtained.

Pin load technique is an experimental method for measurement of contact stresses at the die/workpiece interface. The main element of the measuring device is a small pin which is fixed into the die body. During forming process material of the workpiece presses the die surface as well as the pin head. The force at the pin head is then measured by strain gauges which are located at the pin holder. This force is then transformed into the electrical signal.

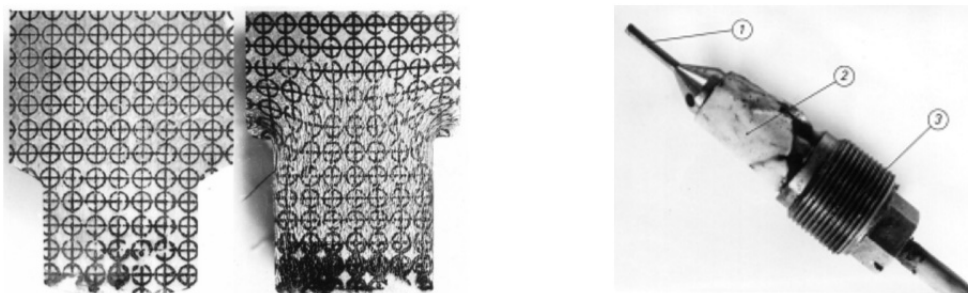


Fig. 1 a) Grid at the meridian plane of the workpiece in visioplasticity method and b) Pin load cell [1]

Upper Bound theory is applied in axisymmetric processes. This theory is based upon the division of the deformation zone into the small elements with constant velocity. It states that: "The power consumed during plastic work is less than or equal to the sum of internal power dissipated within the deforming region and the power dissipated due to friction on its boundaries" [2], [3]. Therefore, the velocity field that minimizes the total power is considered as actual one and it is used in further analysis. Mathematical expression (1) of this theorem is:

$$L \leq L_1 + L_2 + L_3 = \frac{2 \cdot \sigma_e}{\sqrt{3}} \cdot \int_V \sqrt{\frac{1}{2} \cdot \dot{\epsilon}_{ij} \cdot \dot{\epsilon}_{ij}} \cdot dV + \int_A \tau(dV) dA + \int_A \sigma_i \cdot V_i \cdot dA \quad (1)$$

where:

L – total load of deformation,

- L_1 – internal dissipation power,
- L_2 – friction and discontinuity power,
- L_3 – power dissipated due to external forces,
- ϵ_{ij} – strain rate,
- dV – relative velocity at boundaries of discontinuity,
- τ – tangential stress,
- σ – effective stress.

More about Upper Bound theory and about solving practical problems by this method can be found elsewhere: [4], [5], [6].

UBET Software and simulation

UBET stands for Upper Bound Element Technique and it is based on Upper Bound theory. Osman and Bramley developed UBET software used in this paper for estimating forging parameters on axi-symmetric parts [6], [7]. In UBET, the main principle is in the division of deformation zone into a number of regions where parallel velocity fields exist. These regions are afterwards analysed separately. Flow and friction data, as well as velocity field and velocity discontinuities enable estimation of relevant process parameters such as forming load and material flow. UBET program is primarily concerned with the calculation of forging load, but beside that, it can also determine material flow throughout the workpiece. The main input data in the software are workpiece, die and punch geometry, material stress-strain curve, friction, tooling and workpiece temperature and punch velocity. The subdivision of the workpiece is carried out automatically, however the size of the elements can be increased or decreased manually. More details on UBET can be found in [6], [7].

In further text two different case studies are presented in order to illustrate possibilities and limitations of UBET technique.

1) Case study 1 – Free upsetting and free hobbing

Free upsetting and hobbing are elementary operations which are usually applied in order to obtain a proper billet shape for main forming or machining operation. In free upsetting, billet is compressed by two flat parallel plates. Free hobbing produces cup-shaped billets by using a punch with smaller diameter than the billets'. Schematics of free upsetting and hobbing are given in Fig. 2 and 3.

Simulation of free upsetting by UBET simulation was performed on cylindrical $\varnothing 30 \times 30$ mm billet. Final stroke of 10 mm was performed in total of 5 simulation increments, 2 mm each. For these 5 intervals load – stroke diagram was drawn and presented in Fig. 2.

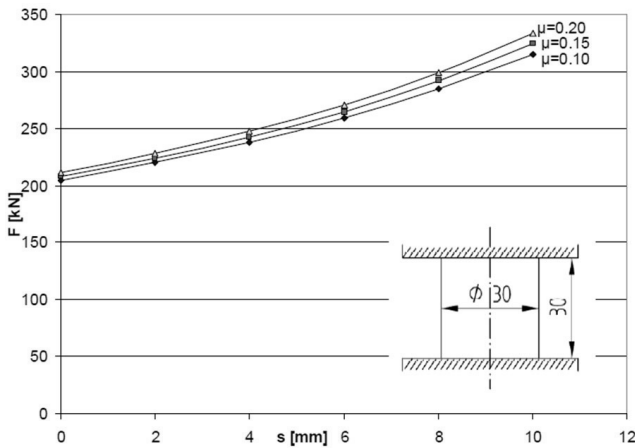


Fig. 2 Load – stroke diagram for free upsetting of $\varnothing 30 \times 30$ mm cylinder in UBET

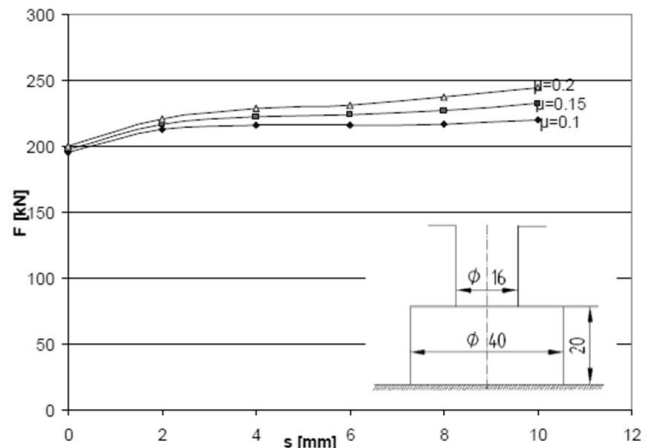


Fig. 3 Load – stroke diagram for free hobbing of $\varnothing 40 \times 20$ mm cylinder in UBET

In order to observe the influence of friction factor in free upsetting, three different friction coefficient in UBET simulation were taken into consideration. As it can be seen from Fig. 2, simulation shows that higher friction values result in higher forming load.

Free hobbing of $\varnothing 40 \times 20$ mm cylinder was also simulated in UBET. A cylindrical $\varnothing 16$ mm punch with 10 mm of total stroke was used. This process is also analysed incrementally, in 5 increments. Load – stroke curve as well as geometry of the workpiece and punch is shown in Fig. 3. Total of three friction coefficients were varied as well, with higher friction resulting in slightly higher forming load.

2) Case study 2 – Open-die forging

Forging is very important in modern industry as many vital components produced by this technology are widely used in vehicles, airplanes, ships, machines, tools, instruments etc. The main reasons for wide application of forging is the high quality of workpieces, excellent mechanical properties and high part complexity that can be made in very short time [3], [8]. In order to fully optimize the forging process, the influence of input parameters and final product quality and process characteristics is a necessity.

This case study presents investigation of close-die forging with flash by using UBET technique. Geometry of the initial billet as well as the flash and land geometry have been varied in order to determine their influence on forging load and die-filling.

As billet material steel C45 was used with forging temperature of 900°C . Flow stress curve for this steel at elevated temperature can be found in [9]. In order to fully optimize the forging process of workpiece shown in Fig. 4, three different initial billet geometries were taken into account (billet A – $\varnothing 100 \times 47$ mm, B – $\varnothing 95 \times 52$ mm and C – $\varnothing 90 \times 58$ mm). Volumes of the initial billets were calculated based upon the volume of the forged part increased by 15%. This increment due to the material loss resulted from burning during heating and due to material which flows into the flash gutter.

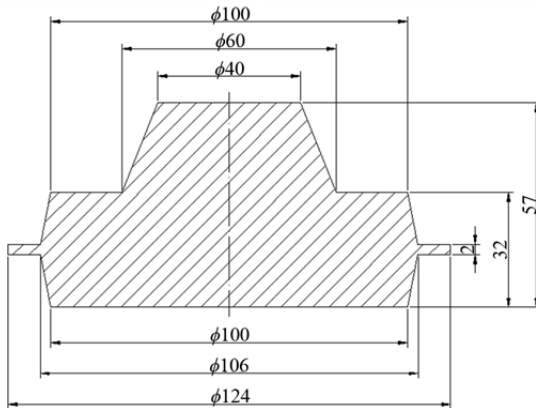


Fig. 4 Geometry of the workpiece

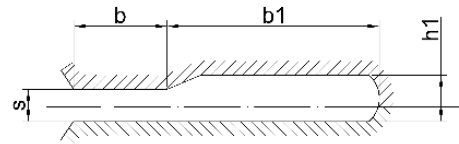


Fig. 5 Flash land and flash cavity geometry

The main task of this case study was to determine optimal flash and initial billet geometry. Flash geometry (Fig. 5) represents a very important factor in open-die forging. If flash land thickness (s) is more narrow and flash land length (b) is longer, than flash has a restrictive geometry. More restrictive flash geometry enables easier cavity filling, but however increases forming load. Less restrictive flash geometry makes material flow less repelling, but on the other hand might not insure full cavity filling. In order to simplify analysis, flash land length (b) was kept constant ($b = 9 \text{ mm}$), while flash land thickness (s) was varied.

Fig. 6 and 7 provide load – stroke diagrams obtained by UBET for forging of the part shown in Fig. 4 by using different initial billet geometries (A, B and C). As initial billet type A is the shortest and the widest it requires the smallest punch stroke (15 mm).

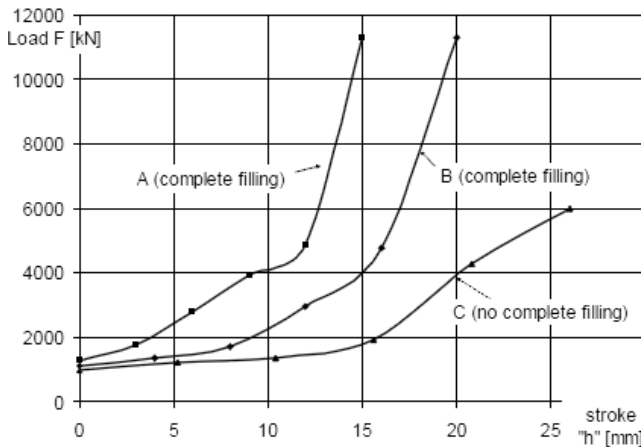


Fig. 6 Load – stroke diagram for different initial billet types and flash thickness $s = 2 \text{ mm}$

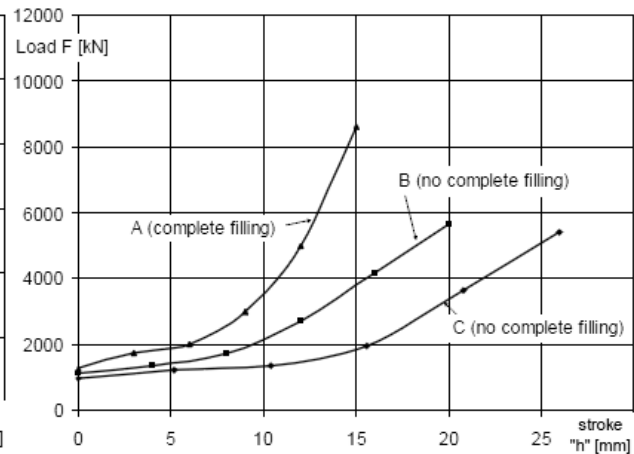


Fig. 7 Load – stroke diagram for different initial billet types and flash thickness $s = 4 \text{ mm}$

Fig. 8 shows dependence of flash thickness on final cavity filling during forging for A-type initial billet. It can be seen that incomplete cavity filling occurs when flash thickness is higher than 4 mm. Final forming load decreases from 11308 kN to 8608 kN when flash thickness is increased from 2 to 4 mm.

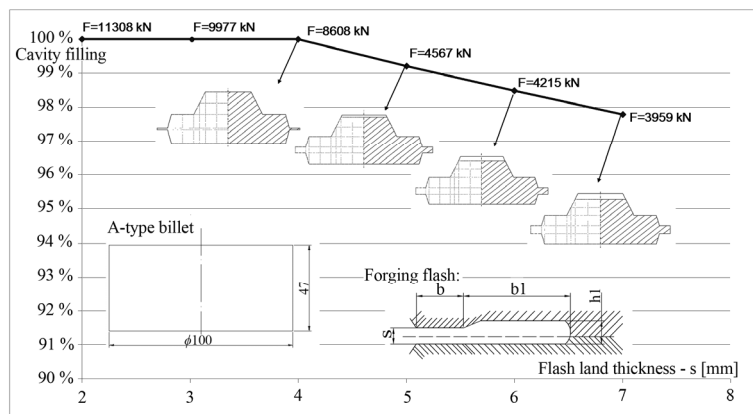


Fig. 8 Cavity filling of A-type billet for different flash land thicknesses

Theoretical approach

Theoretical approach was used to verify results obtained by UBET simulation. According to [10], final forming load for open-die forging can be calculated from following expression (2):

$$F = \sigma \cdot \left[\left(1.5 + \frac{b}{2 \cdot s} \right) \cdot A_p + \left(1.5 + \frac{b}{s} + 0.08 \cdot \frac{2 \cdot b}{s} \right) \cdot A_g \right] \quad (2)$$

Where:

$\sigma = K$ – effective stress,

b – flash land length,

s – flash land thickness,

A_p – projected surface area of complete forging part (without flash),

A_g – projected surface area of the flash.

In Table 1. results obtained by theoretical calculations and UBET simulation depending on the flash thickness (s) are given. Theoretical approach does not take into account if condition of full cavity filling has been met. In case of C-type billet, UBET simulation shows that no full cavity filling is possible when flash thickness is larger than 1.5 mm.

Table 1. Comparison between UBET simulation and theoretical approach

s [mm]	type A billet			type B billet			type C billet		
	2	3	4	1	2	3	1	2	3
UBET [kN]	11308	9977	8608	15402	11302	9962	15174	cavity not filled	cavity not filled
Theory [kN]	10983	8529	7302	17866	10708	8315	17427	10433	8102

Conclusion

Current paper evaluates possibilities of UBET software in simulation of bulk metal forming operations. In first case study, operations of free upsetting and free hobbing were analyzed. Three different load – stroke curves for each operations were obtained for specific workpiece and tooling geometries, based upon three different friction conditions. As expected, higher friction conditions resulted in higher forming loads.

In second case study, three different initial billet geometries and several flash land thicknesses were varied in order to obtain optimized forging process. All initial billets had identical volume, but different diameter/height ratio, with A-type being the widest and the shortest. The goal was to determine optimal solution for forging a specific part with full cavity filling and minimal energy requirements. Type A billet proved to be the most convenient as it required the least restrictive flash geometry. Full cavity filling for A-type billet is possible with flash land thickness is lower than $s \leq 4$ mm. B- and C-type billets require more restrictive flash geometry as full cavity occurs when $s \leq 3.5$ mm and $s \leq 1.5$ mm, retrospectively.

Fig. 6 and 7. show that when A-type billet is employed, lower forming load is necessary for less restrictive flash geometry ($s = 4$ mm compared to $s = 2$ mm.) – 8500 kN compared to 11308 kN. Fig. 8 provides the influence of flash land thickness on cavity filling for A-type billet. Similar dependences can also be drawn for B- and C-type billets. Theoretical calculation of forging load was also calculated. Results from UBET simulation and theoretical calculation show reasonable correspondence.

Finally, based upon UBET results, optimal combination of forging a particular part shown in Fig. 4 is A-type initial billet with 4 mm flash thickness, as it ensures complete cavity filling with minimum load requirements.

Due to its simplicity, UBET proved to be a very useful tool for fast process optimization, although it might not be suitable for more sophisticated analysis. Further investigations would include experimental verification and finite element modelling.

Acknowledgement

This paper is a part of the investigation within the project CEEPUS HR-108 as well as a part of the research realized in the framework of the project "Research and development of modelling methods and approaches in manufacturing of dental recoveries with the application of modern technologies and computer aided systems" – TR 035020, financed by the Ministry of Science and Technological Development of the Republic of Serbia. Authors are very grateful for the financial support.

References

- [1] M. Plancak: Investigation of stress-strain state in the process of cold extrusion of steel, PhD thesis (1984), Novi Sad.
- [2] Avitzur: Metal Forming: Processes and Analysis, McGraw-Hill, (1986).
- [3] K. Lange: Handbook of Metal Forming, Mc Graw- Hill Book, Copmany New York (1985).
- [4] T. Altan: Cold and Hot Forging – Fundamentals and Applications, The Materials Information Society, Ohio, 2005.
- [5] J. Vickerz, J. Managham: An upper-bound analysis of a forging-extrusion process, *J. of Materials Processing Technology* 55 (1995) p. 103-110.
- [6] A.N. Bramley: Computer aided forging design, *Ann. CiPP* 36 (1987), p. 135-138.
- [7] F. Osman: Computerized simulation of forging process, PhD-Thesis, University Leeds (1981).
- [8] Metals Handbook, 8th edition, American Society for Metals (1973).
- [9] M. Plancak, V. Vilotić : Tehnologija plastičnog deformisanja, FTN, Novi Sad (2004).
- [10] M. Plancak, V. Vujović, D. Vilotić: Load prediction in closed-die forging, *International Journal Metallurgy and New Materials Researches*, Vol. II, No. 1 – 2 (1994), Bucharest, Romania, p. 97-104.

INVESTIGATION ON SUBSURFACE LAYER OF Ni₃Al-ALLOY AND ITS COMPOSITES INDUCED BY FRICTION

Karin Gong^{1,*}, Lin Zhi², Tian Zhiling³ and Changhai Li¹

¹ Department of Materials and Manufacturing Technology, Chalmers University of Technology, Sweden

² State Key Laboratories for Advanced Metals and Materials, University of Science and Technology Beijing, China

³ China Iron and Steel Research Institute Group, (CISRI) Beijing 10081, China

Keywords: Nickel aluminides, Wear mechanism; Nanoindentation; Intermetallic matrix composite; Friction.

Abstract. Friction coefficient and specific wear rate of a Ni₃Al-based NAC-alloy and its composites, with 6 vol.% Cr₃C₂- and MnS-particle additions respectively, were studied by pin-on-disk tribological test. Then, the worn surfaces of the tested materials were characterized by using nanoindentation method. It was recognized that the wear properties of the investigated materials are conducted to their strain hardening effect induced by friction. Nanoindentation outlined thickness of the strained subsurface layer and distribution of Nano-hardness in the layers. The added hard Cr₃C₂-particles reduced the thickness of the subsurface layer, but kept a near-same peak-hardness of the friction surface as the monolithic NAC-alloy. A steep negative slope of hardness in the subsurface layer of NAC-alloy/Cr₃C₂ composite may relate to a lower specific wear rate of the composite. MnS-particles were functioned as a solid lubricant in a NAC-alloy/MnS composite. An ineffective strain hardening effect may lead to a less protected surface layer against wearing, resulted in a less improved specific wear rate of the studied composite.

1. Introduction

One of the most attractive engineering properties of Ni₃Al alloys is their increasing yield strength with increasing temperature up to about 650°C. Therefore, the alloys are considered promising in high-temperature construction applications and have been attracting great interest for many years [1-5]. This type of unique strength behaviour also suggested that the Ni₃Al-based intermetallic alloys may have good wear properties in the peak-strength temperature range. Consequently, investigations of their sliding friction and wear behaviour have been initiated [6-8]. The works indicated that the greater the proportional improvement in yield strength with temperature is, the greater the improvement in wear becomes. But so far, the studies on the sliding friction and wear for Ni-aluminides were mostly limited on the laboratory investigation. Further work aimed to industrial applications is needed.

The objective of our previous work [9] is to improve the understanding of the service process behaviour of Ni₃Al-based materials in the engine running system in comparison to commercial vermicular graphite cast iron. The results revealed that a selected single phase Ni₃Al alloy showed friction coefficient and specific wear rate are similar to that of wear-resistant graphite cast iron under the same loading condition. Unfortunately, the single-phase Ni₃Al alloy exhibited weaker performance and caused serious wear of grey cast iron counterpart. Added hard Cr₃C₂ particles in the Ni₃Al-matrix composite reduced wear on both sides of friction pair obviously. Addition of soft MnS particles in the composite functioned as a solid lubricant, resulted in a low friction coefficient and a low wear rate on its counterpart. Therefore, it was recognized that the monolithic Ni₃Al-alloy may not be suitable and applied to a certain wearing condition, but may work well as a matrix material to develop high-temperature and high-strength wear resistant composites, tailored with hard or soft particles, according to specified applications.

In general, Ni₃Al-based materials were worn in a manner typical of that of many metals exhibiting severe metallic wear when unlubricated, which related to the structure and thickness of the most heavily deformed and fragmented subsurface layer. Therefore, nanoindentation was applied on the worn specimens in this study to characterise the distribution profiles of nanohardness in the subsurface layer induced by friction. A further understanding of the wear behaviour of the studied Ni₃Al-based materials and relevant knowledge concerning the alloys development are expected.

2. Experimental methods and results

2.1 Test materials and preparation

A Fe-alloyed Ni₃Al (NAC-alloy) was selected in the work. Composition of the alloy is Ni-18.8Al-10.7Fe-0.5Mn-0.5Ti-0.2B (at. %). The monolithic NAC-alloy and its composites, with addition of 6 vol. %Cr₃C₂ and 6 vol. %MnS particles respectively, were produced by hot isostatic pressing (HIP) process, see Table 1. The powders of NAC-alloy for HIP process were prepared by using Plasma Rotating Electrode Process (PREP). The HIP process bulk specimens are in dimension of Ø70 mm x 150mm. The powder sizes of the NAC-alloy, Cr₃C₂ and MnS applied in the process were in a range of 45-120 µm. The densities of the NAC-alloy, Cr₃C₂ and MnS used to calculate the compositions of the composites in volume percentage are 7.25 g/cm³, 6.68 g/cm³ and 3.99 g/cm³, respectively. The HIP process was applied at a heating temperature of 1130 -1160°C under 140 MPa for three hours.

2.2 Pin-on-Disk test

A conventional pin-on-disk tribometer was used to evaluate the friction coefficient of the friction pair and specific wear rate of the test materials. A grey cast iron with a composition of Fe-3.2C-1.1Si-0.8Mn-0.2P-0.1S-0.02B-1.0Cu-0.22V (wt. %) was utilized as the counterpart disk material in testing, which is usually used as a liner material in ship engines. Dimensions of the pin and disk are Ø3 mm x 16 mm and Ø30 mm x 4 mm, respectively. The applied normalising pressures were 2.83 MPa for determining the friction coefficient and

5.66 MPa, for measuring the specific wear rate. The measured wear rates of the tested specimens are reported in terms of Archard's specific wear rate ($\text{mm}^3/\text{N}\cdot\text{m}$). In the case, wear volumes of the pin samples were calculated from the weight lost during testing by assuming a density of 7.25 g/cm^3 for the monolithic alloy (pin #1) and 7.23 g/cm^3 and 7.12 g/cm^3 for composite pin #2 and #3, respectively. The collected friction coefficients and specific wear rates are given in Table 2.

2.3 Nanoindentation measurement

The nanohardness of the worn specimens was measured after pin-on-disk testing to investigate the hardness variation of the Ni_3Al matrix in the subsurface layer due to friction. The indentations were performed on the Ni_3Al matrix in the studied microstructure. Therefore, longitudinal cross-sections of the tested pins, which are perpendicular to their friction surfaces, were prepared for nanohardness testing.

Nanoindentation test was carried out with a fully calibrated Nanoindenter XP (Agilent) equipped with a standard Berkovich indenter. The applied load is 300 mN, resulted in an indentation depth of less than $1.8 \mu\text{m}$. The first indentation was located on the Ni_3Al matrix at a distance of $10 \mu\text{m}$ from the friction surface. Then the specimen stage was removed by moving the X- and Y-coordinates (see labelled directions in Figure. 1) by $30 \mu\text{m}$ and $50 \mu\text{m}$ for the second indent, respectively. Therefore, the surface distance of the next indentation was increased by $30 \mu\text{m}$. The operation was repeated until the serial sixth indentation was performed at a perpendicular distance of $160 \mu\text{m}$ from the friction surface. In this case, the spacing between two neighbouring indents is greater than $50 \mu\text{m}$ to reduce interference from the nearest indentation. Thus, the interval scale was maintained at $50 \mu\text{m}$ for the seventh to tenth serial indents by moving the specimen stage only along the X-axis. The spacing was increased to $100 \mu\text{m}$ for the eleventh to fourteenth indents. Finally, the nano-hardness was measured on the unaffected substrate at a distance of $1,500 \mu\text{m}$ from the worn surface. Four series of nanoindentation measurements were carried out on tested specimen pins #1, #2 and #3, respectively. Therefore, four indents were applied for each specified surface distance to obtain a statistical value. A map of indents on Pin #2 as an example was given in Figure 1. The collected experimental results of nano-hardness are illustrated in Figure 2.

Clearly, the subsurface layers were formed in the worn samples. The nano-hardness of all three tested samples decreased as the surface distance increased, though with different negative slopes. The estimated thickness of the subsurface layer was in the ranges of $400 \mu\text{m}$, $100 \mu\text{m}$ and $200 \mu\text{m}$ for pin #1, pin #2 and pin #3, respectively. The hardness values at a surface distance of $10 \mu\text{m}$ in the three specimens varied; higher values were observed for pin #1 (5.63 GPa) and pin #2 (5.61 GPa) than for pin #3 (3.98 GPa). It was also recognized that the unaffected substrates of pin #1 and pin #3 have nearly same nano-hardness values of 3.60 GPa and 3.32 GPa, respectively; however a high hardness value of 4.40 GPa was obtained from pin #2. It may relate to the dissolution of Cr_3C_2 particles in pin #2 by the HIP process, which resulted in an additional content of Cr (1.28 at %) in the matrix [10].

3. Discussion

From our previous investigations, it was recognized that the monolithic NAC-alloy is comparable to the commercial vermicular graphite cast iron on wear properties. The graphite cast iron has an optimised phase constitution and microstructure to against wearing. In the case, the hard cementite phase Fe_3C in the pearlite microstructure protected mostly against wearing and was assisted by graphite as a solid lubricant. In contrast, the studied monolithic NAC-alloy has a single Ni_3Al phase in its microstructure. Therefore, it is reasonable to consider that the wear mechanism of Ni_3Al -based materials differs from that of traditional multi-phase metallic alloys, and the wear of the NAC-alloy was mainly conducted to plastic deformation and intrinsic strain hardenability, which resulted in the formation of a wear-resistant subsurface layer. In fact, the researchers [11-17] have studied the subsurface layer by means of analytical electron microscopy, and indicated that large plastic strains and large rotation angles in the layer are achieved after very short sliding distances. It was determined that the thickness of the subsurface layer under normal conditions of friction is on the order of micrometres.

Intermetallic compounds like Ni_3Al possess superdislocations due to their long-range ordered crystalline structure represented by a large Burgers vector. And, the deformation mechanism of superdislocation motion in long-range-ordered alloys leads to higher strain hardenability than in disordered alloys. In this work, it can be seen that a strong strain hardening effect induced a high hardness of 5.63 GPa on the surface layer of Ni_3Al -matrix in pin #1. 50% increased hardness on the friction surface may use to explain the measured specific wear rate of the single phase Ni_3Al -alloy, which is even comparable to the multi-phase graphite cast iron.

The addition of Cr_3C_2 particles reduced the thickness of the subsurface layer to $100 \mu\text{m}$ but maintained the same peak hardness of the friction surface as that of the monolithic NAC-alloy, which revealed that the hard Cr_3C_2 asperities effectively protected the friction surface and formed a thin subsurface layer. Thus, a deeper negative slope of hardness at the friction surface compared to the monolithic NAC-alloy was obtained. A steep negative slope of the hardness at the friction surface indicates that the hardening effect vanished rapidly with increasing surface distance in pin #2, resulting in relatively small wear debris particles. Therefore, low specific wear rates of this composite were observed.

As a soft solid lubricant, MnS particles reduced friction coefficient of the friction pair to 0.45. A lower stress induced by the friction force caused ineffective strain hardening on the friction surface of this composite. Therefore, a peak hardness of 3.98 GPa and $200 \mu\text{m}$ thickness of the subsurface layer of the NAC-alloy/MnS composite were observed, which may relate to a less protected subsurface layer to against wearing.

4. Conclusion

1. The wear properties of the Ni_3Al -alloy are attributed to its strain-hardening effect. High peak hardness on the friction surface of the selected single-phase Ni_3Al -alloy was identified. Gradual strain-hardening subsurface layer was recognized, and may use to understand the wear mechanism of the studied Ni_3Al -based alloy.
2. The intermetallic matrix of composite reinforced by the Cr_3C_2 -particles also showed high peak hardness on the friction surface, but a less thickness of the subsurface layer. A steep negative slope of the hardness at the friction surface may relate to an improved specific wear rate of the composite.
3. The soft MnS particles functioned as a solid lubricant, and decreased both the thickness of the subsurface layer and the peak hardness on the friction surface. An ineffective strain-hardening ability on the friction surface of this composite led to a low friction coefficient, but not a less specific wear rate of the tested composite.

Acknowledgements

The authors wish to acknowledge the Swedish Governmental Agency for Innovation Systems (VINNOVA) and the Ministry of Science and Technology of China (MOST) for the financial support by the Swedish projects (P32737-1 and P32737-2) and the related projects in China. Appreciation is also expressed to the Department of Mechanical and Biomedical Engineering, City University of Hong Kong, University of Science and Technology Beijing, Advanced Technology & Materials Co., Ltd. and China Iron and Steel Research Institute Group for allowing the use of their facilities.

Table 1. Designations of the tested material

Designation	Composition	Process
1#	NAC-alloy	HIP
2#	NAC-alloy+ 6 vol. % Cr ₃ C ₂	HIP
3#	NAC-alloy+ 6 vol. % MnS	HIP

Table 2. The tribologically data of the tested materials from pin-on-disk tests

Sample	Friction Coefficient (20N)	Specific Wear Rate (x10 ⁻⁵ mm ³ /N·m) (40N)
1#	0.55 ± 0.02	1.38
2#	0.68 ± 0.02	0.76
3#	0.45 ± 0.02	1.54

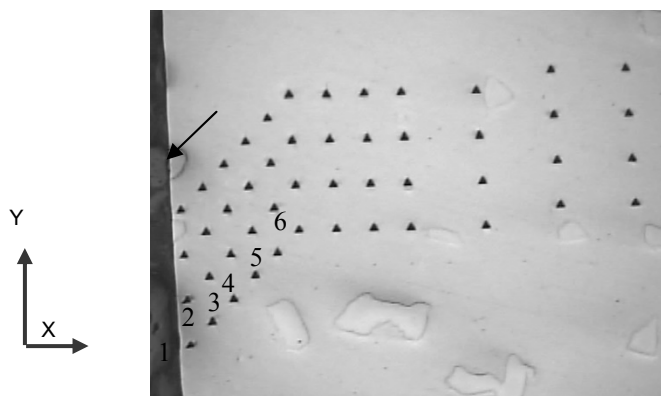


Fig.1 A map of the indents in the subsurface layer of pin 2#. An arrow indicated the worn surface.

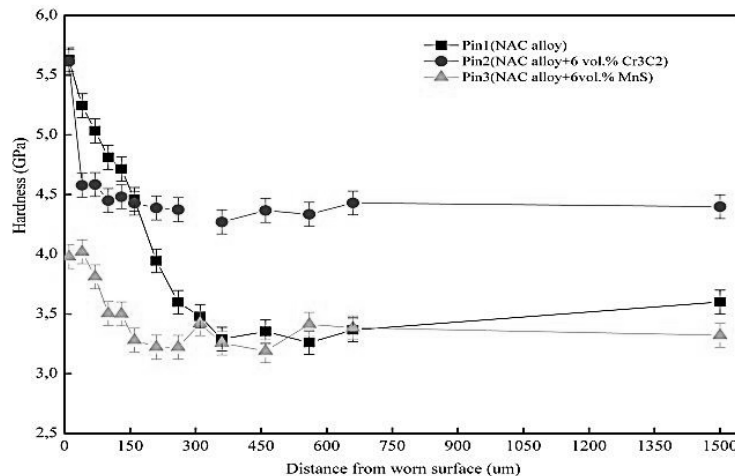


Fig.2 Nano-hardness versus surface distance in the subsurface layer of pin 1#, pin 2# and pin 3#.



5. References

- [1] K. Aoki, O. Izumi, "Flow Stress and Work Hardening in Ni₃(AlTi) Single Crystals " *Acta Metallurgical* Vol. 26 pp.1257-1263.
- [2] J.H. Westbrook, "Dislocations in Solids", Chapter 48 Superalloys (Ni-base) and Dislocations - an Introduction, Vol.10, 1996, pp. 1-26.
- [3] M.H. Yoo, S.L. Sass, C.L. Fu, M.J. Mills, D.M. Dimiduk, E.P. George, "Deformation and fracture of intermetallics", *Acta Metall. Mater.*, Vol.41 (1993) p. 987-1002.
- [4] A. Ishikawa, K. Aoki, T. Masumoto (Eds.), "Material Research Society Symposium on High Temperature Ordered Intermetallic Alloys" VI, 1995, p. 837-842.
- [5] R.W. Cahn, "Load-bearing ordered intermetallic compounds-a historical view", *MRS Bull.* (1991) pp. 18-22.
- [6] Blau P.J, and DeVote C.E. "Sliding behaviour of alumina/nickel and alumina/nickel aluminide couple at room and elevated temperature", *J. Tribology*, Vol. 110, Issue 4, (1988) pp. 646-652.
- [7] Blau P.J. and DeVote C.E. "Sliding behaviour of alumina/nickel and aluminide couple at room and elevated temperature", *Joint ASME/STLE Tribology Conference Baltimore, MD, October 1988.*
- [8] P.J. Blau and C.E. DeVote., "Temperature effects on the break-in of nickel aluminide alloys" *Proc. ASME conference on Wear of Materials*, April 1989, American Society of Mechanical Engineers, New York. pp.305-312.
- [9] Karin Gong, Zhifeng Zhou, P.W. Shum, Heli Luo, Zhiling Tian, Changhai Li, "Tribological evaluation on Ni₃Al-based alloy and its composites under unlubricated wear condition", *Wear* 270 (2011). pp. 195 – 203.
- [10] Karin Gong, Heli Luo, Di Feng and Changhai Li, "Wear of Ni₃Al-based materials and its chromium-carbide reinforced composites", *J. Wear* 265 (2008), pp. 1751-1755.
- [11] I.V. Kragel'skiy, "Friction and Wear", *M: Mashinostroenie* (1968) pp. 480.
- [12] S.Yu. Tarasov, A.V. Kolubaev, "Effect of friction on subsurface layer microstructure in austenitic and martensitic steels", *Wear* 231/232 (1999) pp. 228-234.
- [13] I.I. Garbar and J.V. Skorinin, "Metal surface layer structure formation under sliding friction", *Wear* 51 (1978), pp. 327-336.
- [14] P. Heilmann, W.A.T. Clark and D.A. Rigney, "Orientation Determination of Subsurface Cells Generated by Sliding", *Acta metal.* Vol. 31, No. 8, 1983. pp. 1293-1305.
- [15] S. Yu. Tarasov, A.V. Kolubaev, A.G. Lipnickii, "Application of fractals to the analysis of friction processes", *Tech. Phys. Lett.* 25 (2) (1999) p. 119-121.
- [16] V. Panin, A. Kolubaev, S. Tarasov, V. Popov, "Subsurface layer formation during sliding friction", *Wear* 249 (2002) pp. 860-867.
- [17] N.A. Koneva, E.V. Kozlov, "Physical nature of stages in plastic deformation", *Sov. Phys. J.*33 (2) (1990) pp. 165-179.

VALUE STREAM MAPPING METHODOLOGY FOR PRE-ASSEMBLY STEEL PROCESSES IN SHIPBUILDING

D. Kolich¹, R.L. Storch² and³ N. Fafandjel

¹ University of Rijeka, Faculty of Engineering, Vukovarska 58, 51000, Rijeka, Croatia

² University of Washington, College of Engineering, Mech. Eng. Bldg., Seattle, Washington, 98195-2650, USA

³ University of Rijeka, Faculty of Engineering, Vukovarska 58, 51000, Rijeka, Croatia

Keywords: value stream mapping, lean manufacturing, shipbuilding, steel processing

Abstract. Value stream mapping is used to identify the wastes in industrial processes of many industries such as the automotive and aerospace. In order to remain competitive in the shipbuilding industry it is necessary to continually work on reducing waste in production processes. A clear-cut methodology for shipbuilding is lacking. Since steel makes up the most significant weight composition of commercial ships, shipyard steel processing is analyzed in this paper. A methodology for value stream mapping the current state and a future improved state is presented through a case study of an actual shipyard. The man-hour savings are demonstrated as 33% in the future improved state.

Introduction

The value stream mapping method is actively used in many industries such as the automobile and aerospace industries in order to make production more efficient by reducing unnecessary waste which results in dramatic savings for the companies involved [1], [2]. Since steel makes a significant portion of building commercial ships, making the starting processes related to steel storage and processing efficient as possible is very important. Making the steel processes lean is necessary for the logical downstream flow of materials leading to the assembly processes. Whereas there is treatment of lean manufacturing in the shipbuilding industry, analysis of the pre-assembly steel processes from a lean perspective is lacking. This paper analyzes the pre-assembly steel processes of an actual shipyard. Then the processes are mapped utilizing a value stream mapping methodology. These mapping techniques include analysis of the manufacturing flow of the current state in the shipyard and allow for the mapping of a future improved state.

Background

The ideas of lean manufacturing exist for over two decades since its introduction by Womack, Jones and Roos to the West in their book *The Machine That Changed The World*. The five main principles of lean manufacturing include specifying value from the customer's point of view, identifying the value stream, creating flow in all processes, pull, and perfection or acceptable quality. Value stream mapping is a clear-cut method for implementing all of these five principles. Another integral aspect of value stream mapping is the elimination of waste. The seven wastes are overproduction, transport, waiting, inventory, defects, over processing and excessive movement. Likewise creating a Just in Time (JIT) flow of interim products throughout the manufacturing process, with built in quality, will enable and enhance the flow and create a value stream which eliminates non-value added activities as much as possible.

The treatment of lean manufacturing in shipbuilding was first prominently covered by (Storch, 1999) and (Liker, Lamb, 2002) [3], [4]. Other works include the development of a lean manufacturing methodology in shipbuilding in the panel and built-up panel assembly lines where the lean concepts of one piece flow, Just in Time and built in quality are integrated in order for a lean transformation to occur [5]. Likewise 5S which includes sustaining, sorting, straightening, shining and standardizing leads well to improving flow. In addition to constantly analyzing how to reduce and eliminate waste, kaizen another important principle of lean manufacturing is in compliance with producing future improved value stream maps since it forces management to analyze how to constantly improve the production process.

Case Study

There is much theoretical treatment on lean manufacturing and value stream mapping. A practical way of understanding how to implement the method in a real manufacturing setting is necessary for shipyard lean transformation. The pre-assembly steel processes in a shipyard are analyzed in this case study. The pre-assembly processes include receiving of steel plates, whereby the steel is removed by magnetic cranes and stacked in an interim storage area. Then the steel plates are sorted, labeled and sent to leveling processes. Afterwards, the steel is sent through the processes of heating, grit-blasting and primer coating. Then the steel is ready for cutting and forming prior to being assembled on panel and micro-panel assembly lines.

Steel Stockyard Activities

Steel plates and profiles arrive at the shipyard often in wagons transported by train. They are unloaded from the wagons by use of cranes onto large temporary piles since there are time constraints on the wagons. Afterwards the steel plates are sorted and labeled into other piles depending on whether they will undergo leveling or not. Steel plates arrive from the factory labeled with the shipyard name, the new building number, the classification society that certified the steel, steel plant initials, grade of steel, the batch number and dimensions [6]. Once the shipyard workers start the sorting process, then each plate is again labeled manually with the group number, and the technological phase.

For this case study the processing of 40 steel plates is analyzed as a realistic number of steel plates which could be processed by the shipyard downstream processes on a daily basis. The unloading of the steel from the wagons and stacking in new positions in the interim storage 1 (ISP1) takes 4 minutes per plate for a total of 160 minutes. Then the steel is sorted and labeled manually onto new technological positions in interim storage 3 (ISP3) for a total of 200 minutes [7].

Leveling, Heating, Grit blasting and Primer Coating Activities

Steel plates that were deformed during transport and movement need to be leveled. Usually steel plates that are thinner than 8 mm are the ones that need to be leveled at the shipyard. Approximately 4 plates or about ten percent of the steel plates undergo the leveling process and are stored in interim storage of plates 2 (ISP2) by the magnetic crane. Then the transverse transporter 1 (TT1) moves the deformed plates to longitudinal transporter 4 (LT4) which takes 5 minutes per plate or a total 20 minutes. The actual leveling process lasts 7 minutes per plate or 28 minutes. The leveled steel plates then leave by way of the longitudinal transporter 5 (LT5) back to longitudinal transporter 4 (LT4) and then to interim storage 3 (ISP3) with the other steel plates that did not need to be leveled. The entire cycle of the leveling of 4 steel plates from ISP2 to leveling and to ISP3 lasts about 48 minutes.

Steel needs to be grit blasted in order to prepare the surface for primer application according to the standard Swedish SA standards. Prior to grit blasting it is necessary for information about each steel plate to be inputted into the automated system which takes 5 minutes per plate. Each steel plate is first heated to around 50 degrees Celsius. The pre-heating of the steel is required in order to shorten the drying time upon primer application. Grit-blasting is performed in order to remove rust and impurities on the surface of the steel. Centrifugal blasters are frequently used as is the case of the shipyard analyzed.

The shop primer is applied afterwards in order to protect the steel from corroding during the upcoming assembly processes. Common shop primers include epoxy based or zinc-silicate based primers. Anti-corrosion protection and the weld-ability of the steel are necessary to be compliant to the downstream welding activities that still wait. This process of heating, grit-blasting and primer coating are well automated processes which last 5 minutes per plate. Afterwards the steel plates are again labeled which takes about 1.25 minutes per plate, and then sent to interim storage of plates 4 (ISP4) [7].

Steel Cutting and Forming for Assembly

After the steel plates have been sorted, leveled, heated, grit-blasted and coated with shop primer, the next downstream processes include steel cutting and forming. Various technologies exist for cutting steel plates. This includes oxygen-acetylene flame cutting which is most commonly used due to its flexibility for edge preparation, plasma cutting which is limited to 20 mm steel plate thicknesses, and laser cutting. Mechanical shearing is used for cutting thinner plates. Forming and bending of steel is performed by workers integrating the use of wooden molds and mechanical G and H presses, and bending machines. After these processes are completed, the steel is finally ready for being fed to the automated panel and micro-panel assembly lines.

Value Stream Mapping

The above information is necessary in order to map the pre-assembly steel processes of the present state. The future state can be mapped upon analysis of the present state and integrating lean tools. The use of value stream mapping symbols using Microsoft Visio 2007 is practical. Likewise, the authors used new symbols not available in the program to make the map more adaptable for shipbuilding (See Figure 1).

Current State

Value stream mapping the present state is shown in Figure 2. Every map is read from the left to the right. At the top left is the supplier of steel plates. The steel plates are shipped by wagons to the shipyard, where they are moved to interim storage (ISP1). Afterwards the steel is again moved to other interim storage ISP2 and ISP3 depending on whether it needs to be leveled or not. Then the steel that is sorted and labeled in ISP3 gets transported again to the steel plate reader for grit blasting and then to the automated steel heating, grit blasting and primer coating process. Finally the steel is again transported to another intermediate storage area ISP4. The value stream map illustrates that the steel is pushed between each process. Likewise there is much intermediate inventory, represented by the yellow triangles, as well as excessive movement. During the steel movement process, there are many non value-added processes represented by the processes in black boxes. The total duration time which is represented by adding up the timeline segments (160 +200 + 200 + 200 + 50) = 810 minutes as in Eq. (1) are calculated by the "conventional process method" [8]. The man-hours are calculated by multiplying the duration time of each process with the number of operators: (2.7hrs x 2 operators)+(3.33 hrs x 2 operators)+(3.33 hrs x 2 operators)+(.833 hrs x 2 operators) = 27 man-hours. See Eq. (2).

$$DT_{Total} = DT_1 + DT_2 + DT_3 + DT_4 + DT_5 \tag{1}$$

$$Man-hours_{Total} = DT_1 \times O_1 + DT_2 \times O_2 + DT_3 \times O_3 + DT_4 \times O_4 + DT_5 \times O_5 \tag{2}$$

where: DT_{Total} is the total duration time., $DT_{1,2,3,4,5}$ are the individual process duration times and $O_{1,2,3,4,5}$ are the number of operators.

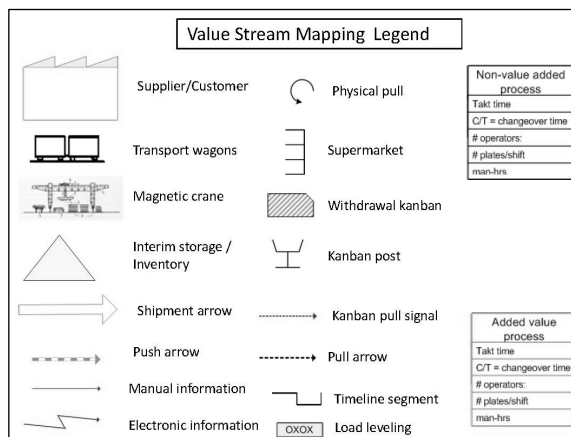


Fig. 1 Value Stream Mapping Legend of Steel Processing [6], [9], [10]

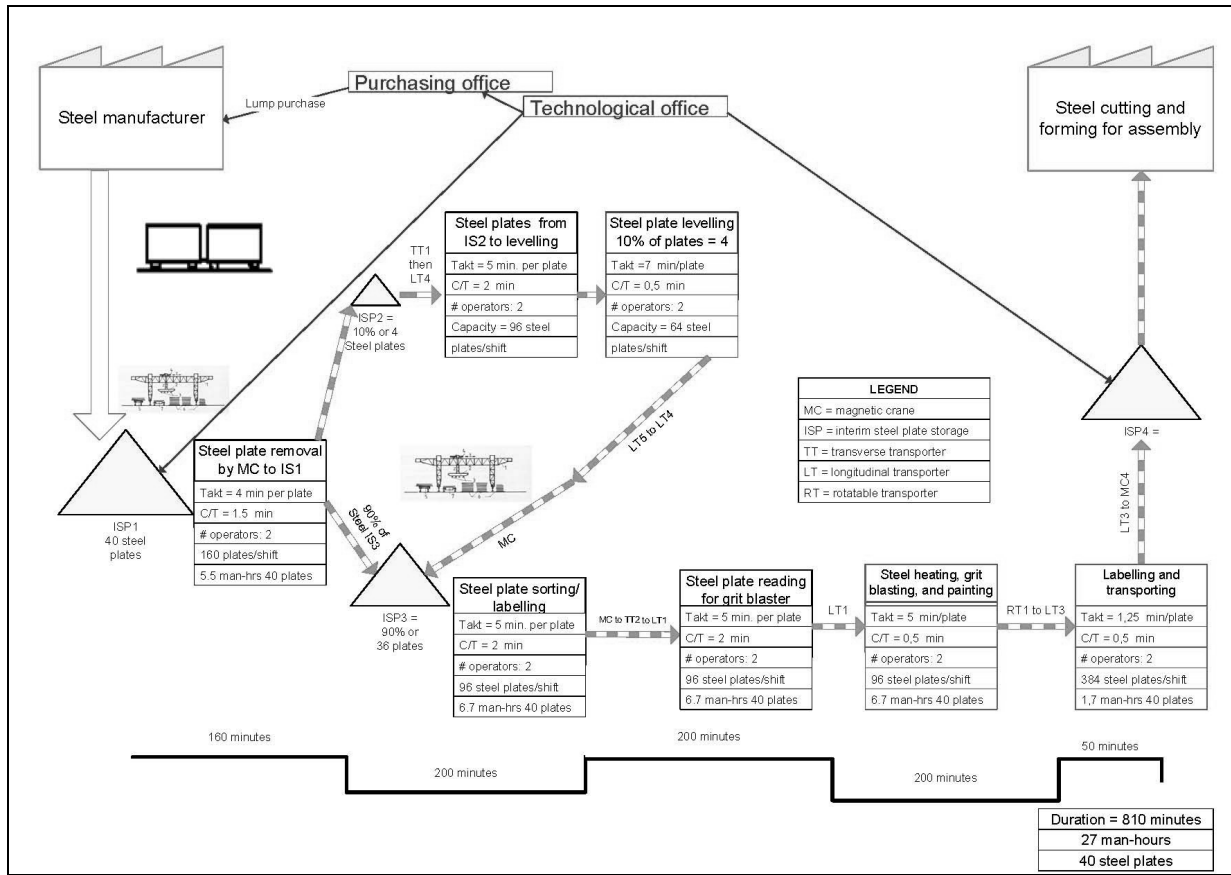


Fig. 2 Current State Value Stream Map of Steel Processing

Future Improved State

For moving to the future improved state, it is necessary to improve flow and eliminate the waste of inventory (yellow triangles) and have the steel pulled from the steel supplier to the steel cutting and forming for assembly. This is done by having production control forecast requirements to the steel manufacturer, who would no longer deliver steel in one big lump shipment, but instead create a kanban supermarket like system, where the steel is delivered incrementally as needed (See Figure 3). The local shipyards in Croatia could make contracts with one steel manufacturer and have milestone payments as well as intermediate batch deliveries which will result in regular steel deliveries which will decrease the storage space necessary. Likewise the steel dimensions should be standardized according to design for production principles in order to simplify the handling of the steel further. This will be more economical for the shipyard and is also compliant with the steel manufacturer because in this way there will be constant steel production for all the four major shipyards as well as regular milestone payments to the steel manufacturer. In addition, the quality of steel will be better maintained, because steel plates usually get deformed and start to rust when there are large inventories lying around on the open for long periods of time.

The kanban post in conjunction with the withdrawal kanban and the kanban pull signal represent the situation where the worker in the shipyard steel stockyard signals to the steel manufacturer who has set up intermediate storage in a practical industrial area close to the shipyard for the next batch of steel to be delivered once the previous batch is on its way to completion (See Figure 3). Likewise the steel is no longer unloaded onto big stacks of steel plates but is instead immediately sorted into few smaller batches and is immediately sent on to further treatment with minimal storage. The OXOX represents load leveling or balanced flow, which is necessary in order to follow an equal takt time with the downstream processes. Steel plate reading for the grit blaster; steel heating, grit blasting and painting; and labeling and transporting to the kanban post all follow an equal takt time of 5 minutes.

The duration time is calculated using the group technology method [8]. The number of processes has been decreased from five to four. Likewise the takt time is set at 5 minutes per plate. The first plate takes $(5 + 5 + 5 + 5) = 20$ minutes time to process, Eq. (3). The rest of the 39 plates take $(39 \times 5) = 195$ minutes to process, Eq. (4). Therefore the total duration time for all forty plates calculated by the "group process method" is 215 minutes, Eq. (5) which is a 73 percent improvement over the conventional process method which pushes material instead of pulling. Likewise the man-hours are 3.58 hours \times 5 operators = 17,91 or about 18 man-hours Eq. (6) which is a 33 percent improvement over the current state.

$$DT_{PLATE 1} = T \times P \quad (3)$$

$$DT_{PLATES 2-40} = NP-1 \times T \quad (4)$$

$$DT_{PLATES 1-40} = (T \times P) + ((NP-1) \times T) \quad (5)$$

$$Man\text{-}hours_{Total} = DT_{PLATES\ 1-40} \times O_{TOTAL}$$

(6)

where: T is takt time, P is the number of processes, NP is total number of plates, DT is duration time and O is number of operators.

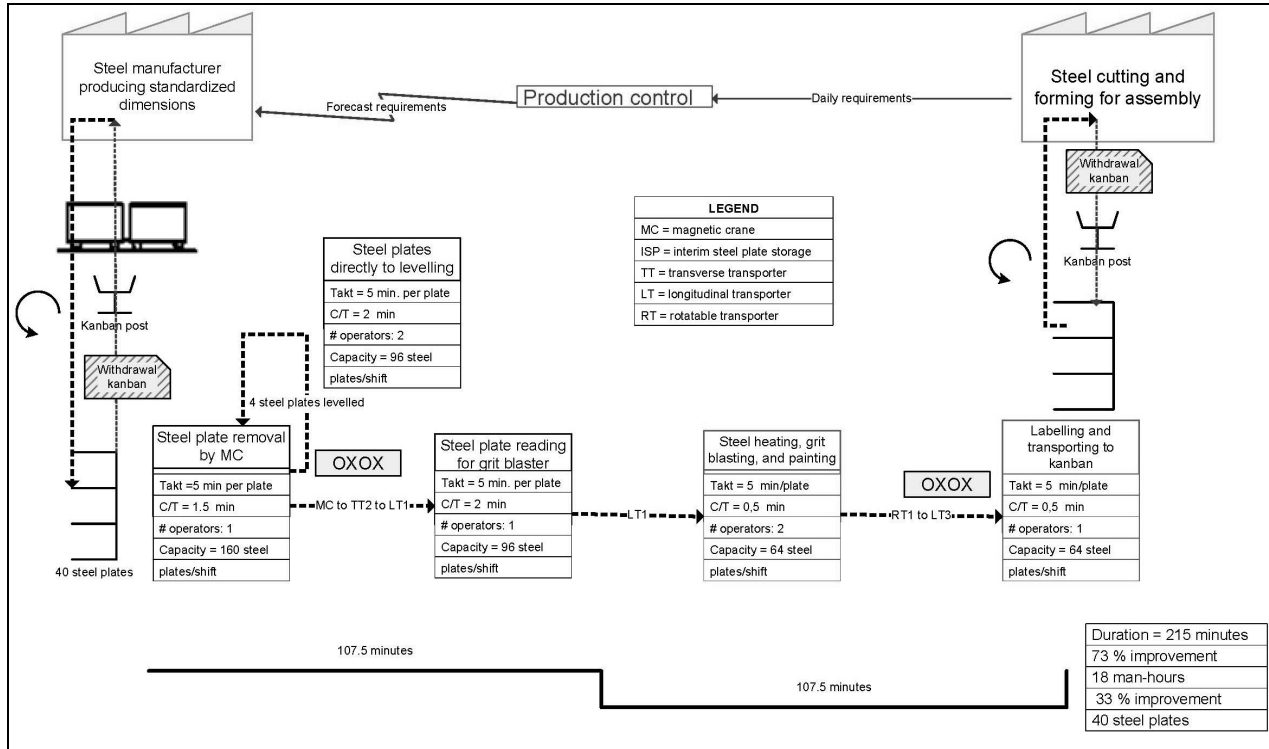


Fig. 4 Future Improved Value Stream Map of Steel Processing

Conclusion

The value stream mapping methodology for the pre-assembly steel processes requires performing a case study and identifying all processes, their duration times, and number of operators per process. Then a value stream map using lean symbols and terminology can be created. Keeping in mind the lean principles of flow, pull and perfection, as well the wastes of excessive transport, movement, and inventory which leads to defections, should allow for a new improved map to be created. With the new map there is no need to change the infrastructure of the shipyard. The key differences are that steel should not be piled up as is done in the current state, but should be brought to the shipyard in batches as requested by the kanban post between the supplier of steel and the shipyard stockyard which results in minimal inventories at manageable levels. Finally, the application of group technology is compliant with lean manufacturing and creating future improved value stream maps which decrease man hours and duration times significantly.

For a future case study and value stream mapping analysis, the authors recommend value stream mapping the rest of the downstream processes which includes steel cutting and forming, panel assembly, outfitting and block assembly, and in determining the optimal takt time between all shipyard processes. The integration of the IHOP concept (integrated hull construction, outfitting, and painting) with lean manufacturing and group technology principles will be pertinent in making dramatic savings in both man-hours and duration times, which results in competitive shipyards.

References

- [1] R. Roy, R. Evans, D.K. Williams, Addressing the impact of high levels of product variety on complexity in design and manufacture, *Proceedings of the Institution of Mechanical Engineers, Part B: Journal of Engineering Manufacture*, Vol. 225 (2011), pp. 1939-1950.
- [2] R.K. Singh et al.: A fuzzy-based decision support system for the selection of lean tools: A case study for the steel industry, *Proceedings of the Institution of Mechanical Engineers, Part B: Journal of Engineering Manufacture*, Vol. 220 (2006), pp. 1735-1749.
- [3] R.L. Storch, S. Lim: Improving flow to achieve lean manufacturing in shipbuilding, *Production Planning and Control*, Vol. 10, No.2 (1999), pp. 127-137.
- [4] J.K. Liker, T. Lamb: What is Lean Construction and Repair?, *Journal of Ship Production*, Vol. 18, No. 3, (2002) pp. 121-142.
- [5] D. Kolich, R.L. Storch, N. Fafandjel: Lean Manufacturing in Shipbuilding with Monte Carlo Simulation, *International Conference on Computer Applications in Shipbuilding*, Vol. 3 (2011), pp. 159-167.
- [6] Z. Furlan, N. Lučin, A. Pavelić: *Tehnologija gradnje brodskog trupa*, (Školska knjiga, Zagreb, 1986).
- [7] 3. Maj. Shipyard archives, 2011.
- [8] R. L. Storch et al.: *Ship Production*, (Society of Naval Architects and Marine Engineers, New Jersey, 1995).
- [9] J. Bicheno, M. Holweg: *The Lean Toolbox*, (PICSIE, Buckingham, 2009).
- [10] Microsoft Office Visio, 2007

APPLICATION OF REVERSE ENGINEERING IN THE DEVELOPMENT OF POLYMER PRODUCTS

D. Godec ¹, I. Kramarić ², M. Šerčer ¹

¹ Univesity of Zagreb, Faculty of Mechanical Engineering and Naval Architecture,
Ivana Lučića 5, 10000 Zagreb, Croatia

² EAG Centar d.o.o., Oreškovićeve 6c, 10000 Zagreb

Keywords: reverse engineering, polymer product development

Abstract. The paper presents systematisation of existing 3D scanning methods, and some basic characteristics of active 3D digitalisation processes used for reverse engineering. Second part of the paper deals with practical 3D scanning of the measuring object - polymer product by measuring system Atos. Further processing and analysis of the digital data of measuring object and comparison with reference 3D CAD model was performed with computer program Gom Inspect V7 RS2.

Introduction

Reverse engineering is the process of reconstruction of the finished product into a form that can be used to create new products, development tools, or can be applied to product or tool modification. In conjunction with other techniques, reverse engineering helps to reduce costs and time required to develop and manufacture products, and improves the quality of the final product, that are extremely important factors in market competition. Reverse engineering can also be used in the preparation of technical documents of the products or systems that are inaccurate, incomplete or simply nonexistent. [1-5]

The paper defines the relationship between the measurement object - thermoplastic moulded part and the reference 3D CAD models with the aid of measurement process, data processing and analysis of the shape and dimensions. 3D digitalization of the measuring object is performed on the projection of a structured system of incoherent light ATOS II SO. Digitized measuring object is processed in a computer environment Gom Inspect V7-RS2, and as such it is compared with the existing 3D CAD model in order to gain insight into deviations from the original model of the STL model obtained by 3D scanning. [5]

Reverse engineering

Reverse engineering is the process of taking an existing physical model and reproducing its surface geometry into three-dimensional data file. Reverse engineering has the purpose of reducing possible design choices until the final product design is reached, with little or without knowledge about necessary technological processes for production of original. It can be also used for generation of technical documentation of old products or systems that is inaccurate, incomplete or simply does not exist. [1-6]

Reverse engineering process is realised through two phases. First is digitalisation or 3D scanning, which presents a process of sampling data round three-dimensional object and its presentation in digital format. Second phase is 3D modelling of the object based on collected data from 3D digitalisation. Devices for 3D digitalisation are faced with demands that are capable to give an accurate as possible scan in satisfactory resolution in shortest possible time. Number, arrangement and density of the recorded points are adjustable parameters in planning and optimisation of scanning. The quality of further processing and application of scanned data depends on their quantity and quality. [1,4-6]

Based on comparison of existing methods for determination of shape and dimensions of free bodies, regarding the way of determination of measuring point, active and passive methods can be distinguished (Fig. 1).

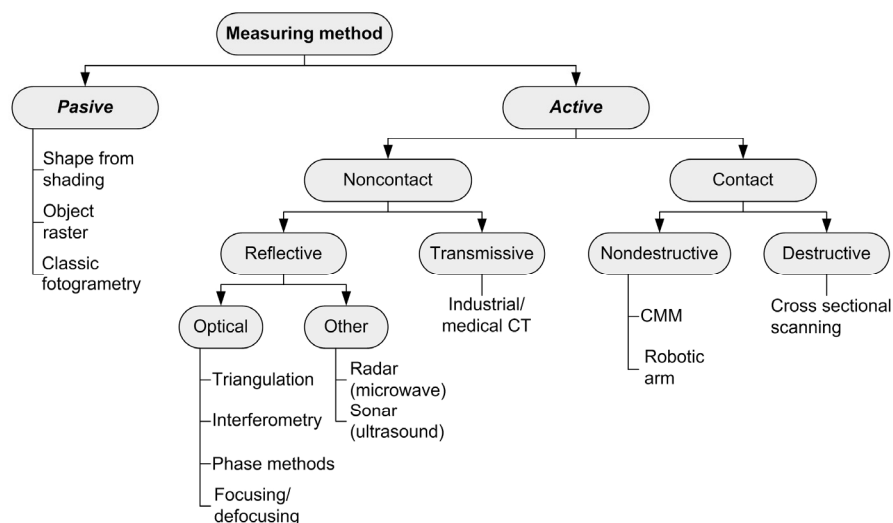


Fig. 1 Systematisation of measuring methods [1]

Characterisation of active measuring methods [1-7]

Active measuring methods get the information on the position of the object's measured points relatively to coordinate position of measuring sensor. Active measuring methods can be divided to contact, where there is a direct contact between contact probe and measuring object and noncontact, where some kind of energy must be projected on the surface of measuring object, and return signal has to be analysed. Active measuring methods also use triangulation for calculation of space coordinates of measured point. Active methods offer online analysis or calculation of position of measured points in real time.

Coordinate Measuring Machines (CMM) can define position of measured points through position of the contact probe in the moment of contact with measuring object. This means that digitalisation of each further point requires movement of measuring probe to the new contact point. Inevitable conclusion is that this method requires noticeable amount of time for data collection on measured points, and number of these points determines the resolution of digitalised object. Experience of the measuring operator, as well as the time necessary for calibration and preparation of the measuring system and measuring object, are very influential on the speed of measuring process. Because of the direct physical contact, this method is not acceptable for measuring very sensitive materials regarding contact such as rubber, silicone, organic tissue or historical valuable artefacts, because of the forming of local deformations on measuring object surface. Limited precondition when using CMM systems is measuring volume, which has to be in the range of measuring head of the CMM. Lower limits of dimension and shape of the measuring object depends on the contact probe.

Active noncontact measuring devices work on the principles of optical projection methods, i.e. emission of a sort of structural light (coded incoherent or laser) towards object as well as catching the reflection. Based on the reflection, spatial positions of object measured points are calculated. The number of measured points can be ranged to several hundred thousand per one scanning process, depending on the resolution of used camera and the way of definition of the measured points. Structures of the projected light can be a point, one line or more lines by the coherent sources, and different sorts of object oriented raster for phase analysis by the incoherent sources.

Because of their noncontact character, without existing of any direct contact of the measuring sensor with measuring object surface, they enable measuring even those measuring objects whose geometry will be impossible to determine with contact methods because of the surface properties of the objects. Noncontact measuring methods are determined by measuring volume and visual field of measuring sensor. Total geometry of the measuring object, similar to passive measuring systems, is described by merging the partial measuring volumes (Fig. 2). Merging of partial measuring volumes is automatically aided with appropriate computer support, which during scanning of the first measuring volume defines global coordinate system which is a reference for positioning and connection of each of next measuring volumes.

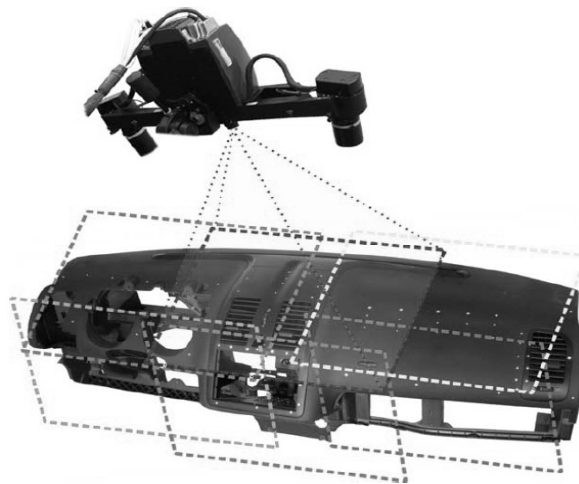


Fig. 2 Non contact measuring system Atos – partial volumes [5]

Systematisation of projection active measuring devices

Projection measuring sensors according to the type of projected light can be divided to the systems that use source of coherent and incoherent light, and according to the definition of the point on the measuring object position relatively to the measuring sensor on interferometric, triangulation and amplitude- or phase- modulated *Time-of-flight* (TOF) systems (laser systems). Interferometric methods (devices) are used for measuring with the smallest distance from measuring object – within 1 mm up to 100 m, and can achieve relative measuring resolution within limits 10^{-7} do 10^{-4} . *Time-of-flight* methods are used for measuring with the largest distances from measuring object – within 10 cm up to 10 km, and can achieve relative measuring resolution within limits 10^{-5} do 10^{-2} . Triangulation measuring methods are spaced between interferometric and TOF methods with measuring range less than 10 cm and above 100 m, and achievable relative measuring resolution within range of 10^{-6} do 10^{-3} . [1,3-6]

Practical application of reverse engineering

In scope of this paper, a 3D digitalisation of the measuring object (thin-walled polymer packaging) was performed by projection system with incoherent structured light Atos II SO. Digitalised measuring object is further processed with computer program Gom Inspect V7-RS2, and compared with existing 3D CAD model in order to get a clear insight into deviations of STL model obtained by 3D scanning process from original 3D CAD model. [5]

Material and geometry of measuring object satisfy basic demands of application of projection method: insensitiveness on surface treatment with colour, thermal stability in conditions of laboratory measuring and possibility of digitalisation of measuring volume.

Projection system Atos enables fast measuring of objects in high resolution. Atos system works on the principle of triangulation and projection of raster sample of lines by using incoherent source of light. System consists of stereo arrangement of convergent cameras that enable constant tracing of sensor, getting information on displacement and visualisation both of measuring volume in real time and central positioned projector of phase displacement. [8]

Measuring procedure

Measuring procedure consists of four steps: measuring sensor calibration, preparation and positioning of measuring object, digitalisation and polygonisation and processing of digitalised data.

Calibration of the measuring sensor is a process of measuring with calibration object (panels or crosses) which enables accuracy and repeatability of the measuring system. Measuring object is made of polypropylene by injection moulding process and has relatively uniform mat surface colour. Further preparation of the measuring object implies gluing of referent points over the measuring object surfaces (Fig. 3). By positioning of the measuring object on the holder, a clear insight into a necessary position of the referent points around measuring object is acquired.



Fig. 3 Referent points placed on measuring object – polymer packaging [5]

Measuring procedure is performed in two phases, i.e. as a scanning of bulged surfaces, and then concave side of the measuring object. Assembling of obtained results is solved automatically by the correct positioning of the measuring points at the measuring object and its holder. Recognition of the identical points from both scanning and thus of local coordinate systems, is solved with computer program by unifying on global coordinate system. Limited factor is the influence of surface geometry, because geometry of the polymer packaging with its edges, inconsistent areas, shadows and slots, demands additional 26 scanning. Measuring system is by hand positioned in each of 26 positions while the measuring desk together with measuring object is remaining in the same position. Thanks to the program support, visualisation of the measuring object is possible in real time, as well as the position of the measuring system in relation to measuring object, which makes orientation significantly easier. The next step is a process of measuring of surface geometry by projection of structured raster. Time required for complete measuring depend a lot on operator's experience and for the complete scanning of polymer packaging, it lasted around 90 minutes.

After finishing of digitalisation of whole volume of measuring object, obtained measured points have to be transformed into a polygonal mesh. That means that the points cloud has to be converted into a mesh of triangles. Depending on geometrical characteristics of digitalised surface, mesh will have different density at some of its regions. Regions of aliasing can be automatically deleted, and open edges are connected. Result of performed polygonisation of the measuring object in this case is a mesh with 667233 points and 179 of discontinuities (Fig. 4). Such record is not usable and needs to be further processed.

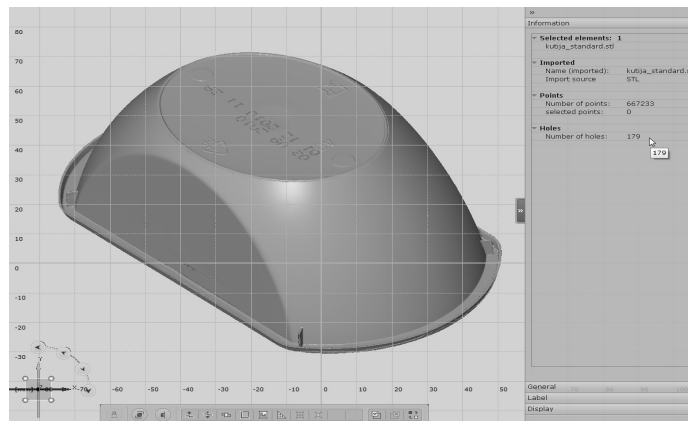


Fig. 6 Polygonised measuring object [5]

Further processing of existing digital record is performed in software GOM Inspect V7 RS2. Appearance of discontinuities in material structure on the surface, dust, damages, etc. will cause local discontinuities in polygonal mesh. Mentioned software package is very efficient in their removal from the mesh. Options such as: smoothing, reducing mesh density and reconstruction have as a consequence reduction of total number of points, and at the same time reduction of the accuracy of definition of the surface near of the area of removing discontinuity. Experience of the operator is very important in this phase of the reverse engineering process.

Analysing procedure

Digitalised measuring object with processed geometry was compared with existing referent 3D CAD model of polymer packaging. Comparison was made in computer software GOM Inspect V7 RS2. To make the comparison possible, it was necessary to reduce a

coordinate system of the digitalised measuring object to an existing coordinate system of 3D CAD model. Method of matching that was used is *best-fit* method. This method assures that points cloud and 3D CAD model match between each other with condition of maximum percentage of matching surfaces. At the same time, a coordinate system of 3D scan is generated related to coordinate system of the 3D CAD model.

Further processing encompasses analysis of deviations of 3D scan from the referent 3D CAD model. Fig. 7 presents topological display of deviations of 3D scan. The biggest deviations are noticed in the area of the ribs below the upper surface of the packaging aimed for packaging cover. These deviations are results of additional reconstruction of mould for injection moulding of packaging, but in general analysis of results obtained with 3D digitalisation, it can be concluded, that they are in good correlation with starting 3D CAD model of polymer product.

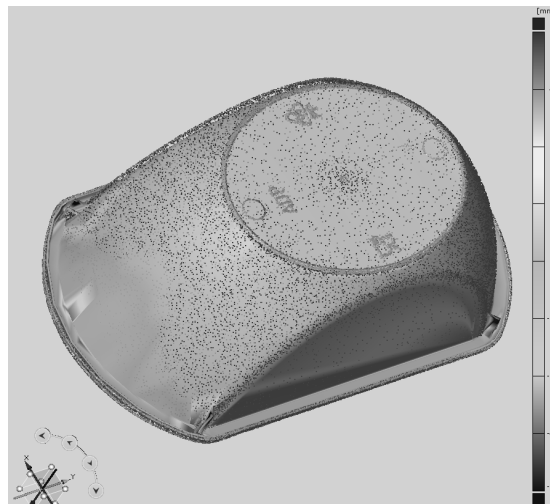


Fig. 7 Deviations of 3D scan from referent 3D CAD model of polymer product [5]

Conclusions

Modern measuring methods for determination of shape, dimensions and deformations found their applications in all areas of human life, including mechanical engineering. Reverse engineering has found its application in manufacturing, scientific research, geological research, archaeology, medicine, etc. But there is always a question which method and under what conditions is the best for specific measuring task with goal to achieve demands regarding accuracy of definition of measured point and the density of the points cloud in measuring volume. 3D digitalisation and reverse engineering as its application can not stand alone, they are a part of a measuring, reconstruction and analysis process.

In this paper, through measuring process, data processing and analysis of shape and dimensions, a correlation between measuring object and referent 3D CAD model has been made. Respecting that they are in direct correlation, digitalised 3D model can be used for further mould manufacturing or reparation. From achieved digital record (STL) it is possible to produce a copy of measuring object by application of Rapid Prototyping or by application of machine tools. For manufacturing a model, i.e. for further processing of existing records to the level of 3D CAD model, it is necessary to geometrically determine conditional and characteristic cross sections, link the points from those cross sections to the splines, and at the end, converts linked splines into a surface. The result is surface 3D CAD model, and by closing obtained surfaces, a solid 3D CAD model of the measuring object can be generated.

Acknowledgment

This work is part of the research included in project ***Increasing Efficiency in Polymeric Products and Processing Development and Advanced Technologies of Direct Manufacturing of Polymeric Products*** that are included in program ***Rapid Production – From Idea to Reality*** supported by the Ministry of Science, Education and Sports of the Republic of Croatia. The authors would like to thank the Ministry for the financing of this project.

References

- [1] R. Noorani: *Rapid Prototyping - principles and applications*, (John Wiley & Sons, New York, 2006)
- [2] A. Gebhardt: *Rapid Prototyping*, (Carl Hanser Verlag, München, 2003)
- [3] N. Drvar: *Usporedba metoda za određivanje oblika i deformacija mehaničkih konstrukcija*, Master of science thesis, (University of Zagreb, Faculty of Mechanical Engineering and Naval Architecture, Zagreb, 2004)
- [4] M. Gomerčić, T. Hercigonja: *3D digitization – a step toward a success in the international market*, *Proc of conference 4th DAAAM International Conference on Advanced Technologies for Developing Countries*, (2005), pp. 49-54
- [5] I. Kramarić: *Primjena 3D skeniranja pri razvoju polimernih proizvoda i alata za njihovu proizvodnju*, Diploma paper, (Polytechnic of Zagreb, Zagreb, 2010)
- [6] N. Drvar: *Optički postupak digitalizacije oblika projiciranog kodiranog svjetla*, Doctoral thesis, (University of Zagreb, Faculty of Mechanical Engineering and Naval Architecture, Zagreb, 2007)
- [7] D. Tvrtković, Z. Baršić, T. Hercigonja: *Primjena fotogrametrije u revitalizaciji hidroenergetskih postrojenja*, *Proc of conference MATEST 2004, NDT Competence & Safety*, (2004), pp. 79-89.
- [8] N.N.: *Atos-User Manual- Software V6.2*, (2009)

EXPERIMENTAL INFLUENCE VERIFICATION OF THERMAL AND MECHANICAL SHOCKS ON CUTTING EDGE DURING IRREGULAR INTERRUPTED CUTTING

R. Čep¹, A. Janásek¹, L. Čepová¹, J. Petruš¹, M. Hatala²

¹ Department of Machining and Assembly, Faculty of Mechanical Engineering, VSB - Technical University of Ostrava, 17. listopadu 15/2172, 708 33 Ostrava - Poruba, Czech Republic

² Department of Manufacturing Technologies, Faculty of Manufacturing Technologies with seat in Presov, Technical University in Kosice, Sturova 31, 080 01 Presov, Slovakia

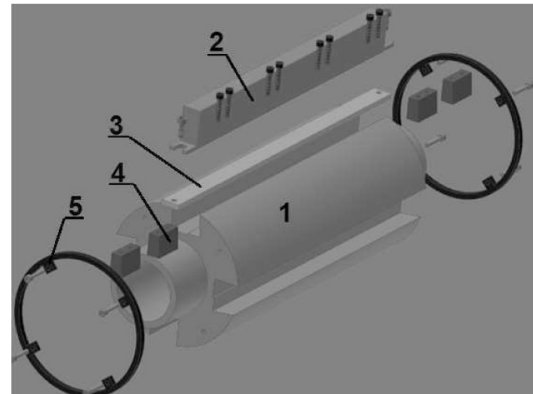
Keywords: Indexable Cutting Inserts; Irregular Shocks; Tool-life; Time Delay

Abstract. The article is interested in tool-life testing of new indexable cutting inserts at irregular shocks by experimental method. Properties of inserts determine not only tool-life and cutting power as well as accuracy and surface quality. The cause of cyclic stress is the cutting phase which involves heating of the cutting edge and its subsequent cooling at the finishing of the cut process. Currently, all tests are performed on the simulator equipped by four slats. The indexable cutting inserts are loaded by the constant shocks and it always beats four times during one revolution. The main aim will be to prove the impact of the time delays between shocks. We can prove this evaluation at a different number of slats fastened in the simulator. These irregular shocks will lead to the different time delays which will have an effect on the thermal shocks.

Introduction

Through the centuries, producers of ceramic cutting tools have taken big steps forward. Namely, increasing durability in maintaining high levels of strength and hardness lend a big advantage [1, 2]. Some producers of these materials advise cutting inserts for the interrupted machining as a path to be followed at the present time. Turning tests are focused on the machining by smoothly cutting at constant or variable depth of the cut [3]. In this work one of the developed tests has been used. It is longitudinal turning, so-called „slat test“. The experiments which are to be conducted require the special preparation (Fig. 1), constructed at Department of Machining and Assembly, VSB – Technical University of Ostrava [4].

If the tool is not in constant cutting process, we can talk about the interrupted cut. The cause of cyclic stress is the cutting phase which involves heating of cutting edge and its subsequent cooling at the finishing of the cut process. The inserts are testing by four types of test. It is a variant of the four, three, two and one shock per one revolution. Usually, we can talk about cyclic stress. The measured number of shocks to tool wear determines the tool life or lifetime period of ceramic cutting insert. Nowadays, these tests are an essential part of the development of the new tools, evaluating their lifetime period and cutting power.



1-Preparation's body; 2-Testing slats; 3-Demarcation pads; 4-Clamping wedges; 5-Circlips
Fig. 1 Constructed preparation

Longitudinal Turning Test at Cyclic Stress

Mechanical or thermal shocks can cause the damage of the insert. The ability to withstand the load of the ceramic cutting edge by thermal and mechanical shocks is very important. Generally, the ceramic materials are characterized by high hardness, low toughness, constant bending strength at high temperatures, chemical stability and wear resistance.

Cyclic stress causes a damage of edge, fracture or abrase. This phenomenon can be studied not only at interrupted cutting but also at uninterrupted. The continuous cutting leads to fluctuate of the main cutting force. In this case, the frequency depends primarily on the chip's character. The larger amplitude of the main cutting force increases the risk of fatigue fracture. [5]

Firstly, the preparation should be clamped to the turning lathe. It is fastened to the turning lathe chuck and buttresses with the tip established in tailstock sleeve. Slats are gradually put in the preparation, which are clamped with wedge-shaped jaws. In order to achieve a constant depth and to avoid vibration, it is necessary to cut off the first layer of chips before measurements can be initiated.

Indexable Cutting Inserts

Ceramic testing cutting tools were supplied by Greenleaf Company. We have tested one type, Greenleaf HSN 100. The article described two testing at the one cutting insert, for this reason, we distinguish as ● HSN 100 and ●● HSN 100.

Greenleaf HSN 100 (SNGN – 454 T2A)

L = 12.7 mm
T = 7.9 mm
R = 1.59 mm
i.C (A) = 12.7 mm

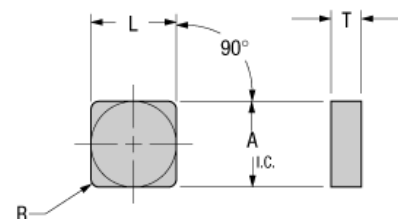


Fig. 2 Technical dimension of the cutting insert [6]

HSN-100 is the latest in engineered silicon nitride-based cutting tools. Advanced materials combined with unique processing techniques give HSN-100 superior toughness and high cutting speed capability. HSN-100 is well suited for the turning and milling of all classes of cast iron. It is an outstanding performer in ductile, malleable, nodular and other difficult to machine irons. [6]

Testing – Slat Material

We chose steels Steel C45 (material No. 1.0503, DIN C45, AISI 1045) as work-piece material. C45 is a medium carbon steel is used when greater strength and hardness is desired than in the "as rolled" condition. Extreme size accuracy, straightness and concentricity combine to minimize wear in high speed applications. Turned, ground and polished. Quenched and subsequently tempered steel for screws, forgings, wheel tyres, shafts, sickles, axes, knives, wood working drills, hammers, etc.

Table 1. Mechanical properties in normalized condition steel C45

Mechanical properties	Proof stress Rp 0,2 [MPa]	Tensile strength Rm [MPa]	Elongation A5 [%]	Hardness [HB]	Elastic modulus E [GPa]
C45	325	630 - 780	17	207 - 255	211

Turning Machine Tool

All tests were performed on a powerful turning lathe, namely Tos Trenčín, type SN 55. Performance of electric machines is 7.5 kW and reaches at the most 1440 rpm. The machine is located in University of Žilina, Faculty of Mechanical Engineering, where we could carry out our measurement. The tests were performed at a constant temperature of 20°C. This turning-lathe is convenient for this type of the experiments.



Fig. 3 Used machine tool - Tos Trenčín, type SN 55

Cutting Parameters

We have chosen these parameters with regard to manufacturer's recommendation of cutting ceramics and experience of the resolver. The following cutting conditions were chosen for testing these types of cutting materials:

Table 2. Used cutting parameters

Cutting Parameters		
Revolution n [rev]	520	360
Cutting speed v _c [m.min ⁻¹]	425	294
Feed f [mm]	0,20	
Axial depth of cut a _p [mm]	1	

The main criterion for measuring of the tool life may be tool wear and tool fracture. This moment was noticed, while changing the cutting sound, sparking or worsening of surface roughness. The limit value of 6000 shocks was determined on the basis of previous experience in terms of time and material demands. If indexable cutting inserts withstand this value, the experiment can be successfully conducted, and cutting insert will be described as satisfactory.

Measured Data – Four Slats Variant

Table 3. Measured values for 4 slats

Greenleaf HSN 100 n = 520 [rpm], v _c = 425 [m.min ⁻¹], a _p = 1 [mm], f = 0.2 [mm]								
4 Slats	●				●●			
No.	l [mm]	Ra [μm]	Rz [μm]	R [-]	l [mm]	Ra [μm]	Rz [μm]	R [-]
1	222	1.26	6.1	4440	189	1.18	5.5	3780
2	234	1.24	5.9	4680	179	1.22	5.8	3580
3	220	1.34	5.7	4400	205	1.18	6	4100
4	220	1.28	5.8	4400	212	1.28	5.9	4240
5	248	1.24	5.9	4960	196	1.26	5.6	3920
Diameter	228.8	1.27	5.88	4576	196.2	1.22	5.76	3924
u _A	5.4626	0.0186	0.0663	110	5.8086	0.0204	0.0928	117

Measured Data – Three Slats Variant

This method had to be adjusted cutting parameters because the preparation had unbalanced cutting process and huge loads on the machine. If we wanted to maintain the same cutting parameters, as for four and two slats, there sprung up the shaking and vibration. For safety reasons and the risk of machine's damage was necessary to reduce the revolution from n = 520 rev to n = 360 rev.

Table 4. Measured values for 3 slats

Greenleaf HSN 100 n = 360 [rpm], v _c = 294 [m.min ⁻¹], a _p = 1 [mm], f = 0.2 [mm]								
3 Slats	●				●●			
No.	l [mm]	Ra [μm]	Rz [μm]	R [-]	l [mm]	Ra [μm]	Rz [μm]	R [-]
1	400	1.29	6.2	6000	400	1.36	6.4	6000

2	400	1.37	6.8	6000	400	1.35	6.4	6000
3	400	1.34	6.4	6000	400	1.29	6.1	6000
4	400	1.36	6.3	6000	400	1.31	6.3	6000
5	400	1.42	6.9	6000	400	1.34	6.5	6000
Diameter	400	1.36	6.52	6000	400	1.33	6.34	6000
u_A	0	0.02112	0.13928	0	0	0.01304	0.06782	0

Measured Data – Two Slats Variant

The preparation is evenly balanced at two slats variant, so there is no increasing shaking or vibration. It could be used a higher revolution = 520 rpm and cutting speed $v_c = 425 \text{ m}\cdot\text{min}^{-1}$.

Table 5. Measured values for 2 slats

Greenleaf HSN 100 n = 520 [rpm], $v_c = 425 \text{ [m}\cdot\text{min}^{-1}]$, $a_p = 1 \text{ [mm]}$, $f = 0.2 \text{ [mm]}$								
2 Slats					• •			
No.	<i>l</i> [mm]	Ra [μm]	Rz [μm]	R [-]	<i>l</i> [mm]	Ra [μm]	Rz [μm]	R [-]
1	198	1.24	6.2	1980	380	1.28	6.4	3800
2	218	1.28	6.4	2180	276	1.29	6.6	2760
3	298	1.3	6.3	2980	321	1.24	6.2	3210
4	354	1.26	6.2	3540	265	1.26	6.4	2650
5	268	1.27	6.1	2680	289	1.25	6.3	2890
Diameter	267.2	1.27	6.24	2672	306.2	1.26	6.38	3062
u_A	28.0114	0.0100	0.0510	281	20.7012	0.0093	0.0663	208

Measured Data – One Slat Variant

As a Three Slats Variant method had to be adjusted cutting parameters because the preparation had unbalanced cutting process and huge load on the machine. During vibrations, the bearings were excessively heated up at tailstock tip and spindle. For safety reasons and the risk of machine's damage was necessary to reduce revolution from $n = 520 \text{ rev}$ to $n = 360 \text{ rev}$.

Table 6. Measured values for 1 slat

Greenleaf HSN 100 n = 360 [rpm], $v_c = 294 \text{ [m}\cdot\text{min}^{-1}]$, $a_p = 1 \text{ [mm]}$, $f = 0.2 \text{ [mm]}$								
1 Slats					• •			
No.	<i>l</i> [mm]	Ra [μm]	Rz [μm]	R [-]	<i>l</i> [mm]	Ra [μm]	Rz [μm]	R [-]
1	1200	1.42	6.7	6000	1200	1.34	6.6	6000
2	1200	1.39	6.5	6000	1200	1.36	6.5	6000
3	1200	1.4	6.6	6000	1200	1.35	6.5	6000
4	1200	1.38	6.5	6000	1200	1.28	6.4	6000
5	1200	1.37	6.6	6000	1200	1.31	6.5	6000
Diameter	1200	1.39	6.58	6000	1200	1.33	6.50	6000
u_A	0	0.0086	0.0374	0	0	0.0146	0.0316	0

Tool Wear – Photographs of Individual Tested Variants

The tables, see below, are shown the tool wear for the tool face and the tool flank. The photographs are at 4-fold magnification. These pictures are only a sample of the entire series of measurements.

Table 7. Four and two slats variant - sample of tool wear for tool face and tool flank (showed only first side of insert) [7]

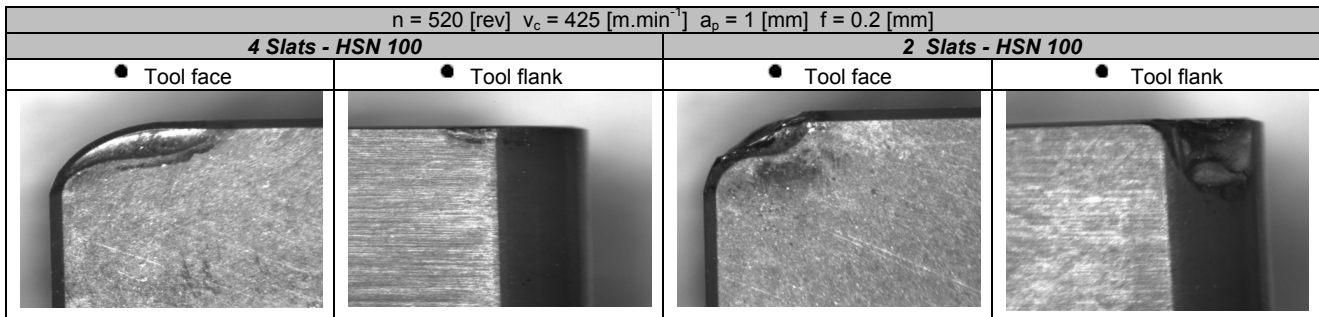
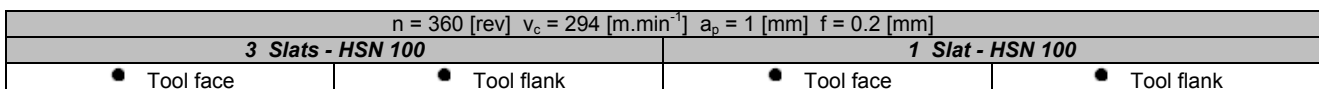
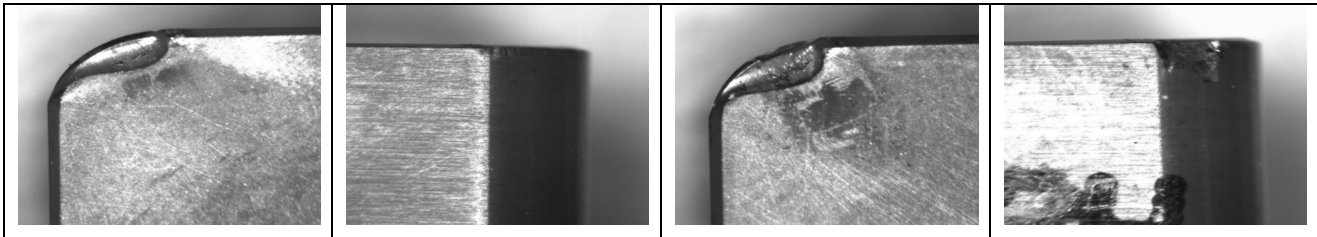


Table 8. Three and one slats variant - sample of tool wear for tool face and tool flank (showed only first side of insert) [7]





Comparison for Different Number of Slats

At four and two slats method, we can talk about "Balanced method" and is able to use a high revolution and the cutting speed. At the four slats method, inserts are exposed to four shocks per revolution and there is not such a large thermal and mechanical shocks as two slats method, where is cooling phase, between mesh and therefore creates the thermal shock.

Greenleaf type HSN 100, which withstood no more than 3062 shocks for two slats method and 4576 shocks for the four slats method, suggests that is not suitable for interrupted cutting under given cutting conditions.

At three and one slats method, we can talk about "Unbalanced method". It was necessary to change the cutting parameters, which was reduced revolution and cutting speed. When you try to maintain the same cutting parameters as "Balanced method", was created a large tremble and vibration, could be a huge risk of machine damage.

During the one slat method, the insert gets on shock per one revolution so there should be a high thermal and mechanical load, for the reason of cooling gaps between shocks. We could not to evaluate due to small revolution and cutting speed, inserts withstood the maximal number of shocks.

This phenomenon is the cause of relatively small cutting parameters for ceramic material. Unfortunately, the technical limitation of the machine have not allowed to test at higher cutting parameters. Thanks to the results showed below we can say the inserts are suitable for interrupted cutting at these parameters $n = 360$ [rev], $v_c = 294$ [m.min⁻¹], $a_p = 1$ [mm], $f = 0.2$ [mm].

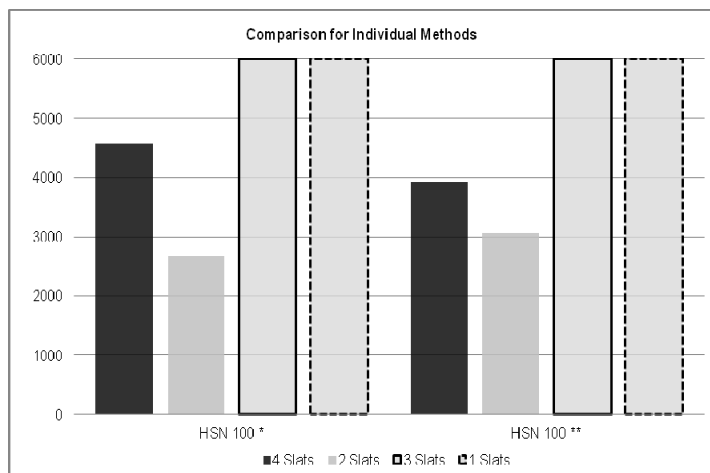


Fig. 4 Comparison – total number of shocks and individual testing methods

Conclusion

Through the centuries, producers of ceramic cutting tools have taken big steps forward. Properties have improved resistance to mechanical stress and tool wear, high temperature resistance, high accuracy, high quality finished surfaces and a wide range from finishing to the light cutting. The main aim was to test ceramic cutting inserts for the use during interrupted cutting.

The measurements showed us the performance of ceramic inserts and suitability for interrupted cutting under given cutting conditions. The main monitored parameter was the number of shocks (R), which was converted from a machined length, others monitored parameters as surface roughness parameters - Ra and Rz.

As the first, the inserts were tested at four shocks per one revolution, which coated inserts did not achieve the limit number of shocks (6000 shocks). Inserts reached the value 3924 and 4576 shocks. On the other hand, the insert had better surface integrity of the machined surfaces.

At the second method, plates were tested at three shocks per one revolution. We could notice changes in the machine's performance as shaking and vibration. For this reason we had to reduce the cutting parameters. The inserts withstood the limit number of shocks, and we can say, that can be used at interrupted cutting conditions.

At the third method, plates were tested at two shocks. We did not register shaking or vibration, but total number of shocks was lower, that with four slats method, at same cutting conditions.

At the last method which has only one shock per revolution. We had to reduce the cutting parameters. The inserts reached the limit number of shocks and had better surface integrity of the machined surfaces.

References

- [1] Bilik, O.; Vleck, M. *Testování nástrojových materiálů s vyšší křehkostí v podmínkách přerušovaného řezu* : Internal report about grant project 2000. Ostrava: FS VŠB – TU Ostrava, 2000. p. 22.
- [2] Čep, Robert; Neslušán, Miroslav; Barišić, Branimir. Chip Formation Analysis During Hard Turning. *Strojárstvo*, 2008, vol 50, No. 6, pp. 337 – 345. ISSN 0562 – 1887.
- [3] Jurko, J., Panda, A., Gajdoš, M.: Accompanying phenomena in the cutting zone machinability during turning of stainless steels. *International Journal Machining and Machinability of Materials*, 2009, vol 5, No. 4, pp. 383-400. ISSN 1748-572X.
- [4] Čep, Robert. *Návrh a ověření metodiky testování řezných nástrojů při přerušovaném řezu*. Ostrava, 2010. p. 119. Habilitation thesis. VŠB - Technical University of Ostrava.
- [5] Houdek, Josef; Kouril, Karel. *Odolnost sliutých karbidů proti teplotním a mechanickým rázům*. *MM Průmyslové spektrum*. 2004. [online]. [cit. 2012-05-06]. Available from: <http://www.mmspektrum.com/clanek/odolnost-sliutych-karbidu-protiteplotnim-a-mechanickym-razum>
- [6] Greenleaf global Support. GREENLEAF CORPORATION. [online]. [cit. 2012-07-08]. Available from: <http://www.greenleafglobalsupport.com/wcsstore/Greenleaf/upload/docs/CeramicGrades.pdf>
- [7] Zalesak, Marek. *Influence of Thermal and Mechanical Shocks on Edge Condition at Interrupted Machining*. Ostrava, 2012. Diploma thesis. Department of Machining and Assembly 346, Faculty of Mechanical Engineering, Technical University of Ostrava. Head: Robert Cep.

MEAT INDUSTRY WASTEWATER AS POTENTIAL SOURCE OF EMERGING POLLUTANTS IN THE VOJVODINA

S. Kovačević¹, M. Turk-Sekulić¹, J. Radonić¹, I. Španik², M. Vojinović-Miloradov¹, D. Milovanović¹ and Zoran Čepić¹

¹ University of Novi Sad, Faculty of Technical Sciences, Department of Environmental Engineering and Occupational Safety and Health

² Slovak University of Technology, Faculty of Chemical and Food Technology

Keywords: Meat production, emerging substances.

Abstract. The meat industry is one of the most developed food industries with the rapid development trend. Throughout the Province of Vojvodina there is a number of centralized slaughterhouses where animals are handled during the production process within emerging contaminants are generated. The treatment of meat industry wastewater is one of the main sources of the dominant environmental problems related to intensive meat production. Wastewater generated in slaughterhouses is usually non treated or deposited in the lagoons. In order to reduce environmental pollution and provide long-term sustainable growth we need to improve and enhance treatment options as well as storage and disposal of slaughterhouse wastes. Wastewater from the meat industry is a source of emerging substances. The emerging substances are contaminants that have been recently recognized especially in the environment due to their constant input in the environment, pseudo persistence and increased use in industrial, veterinary and humanity activities. This paper describes the first phase of monitoring and current state inventory of the meat industry wastewater treatment in the province of Vojvodina, as well as preliminary data on the monitoring and occurrence of potential emerging substances in meat industry wastewater. Natural organic compounds and variety of manufactured substances such as pharmaceuticals are often associated with wastewaters and they have been detected in the vicinity of slaughterhouse wastewater discharges. To provide new data and insights for environmental presence of the emerging pollutants in groundwater sources in the Vojvodina Province, targeted sites were sampled and analyzed for 10 selected analytes with sub-parts per billion detection capabilities. These data will help determination, fate, transport, and health-effects research for subsets of these pharmaceuticals and their degradation products so we can prioritize and suggest how to reduce and minimize the input in the receiving surface water in Vojvodina Province.

Introduction

The meat industry sector emerges as one of top two or three most significant contributors to the most serious environmental problems, from local to global scale. The meat industry is a key player in increasing water use, accounting over 8 percent of global human water use, including irrigation of feed crops.

Wastewater will be generated whenever food in any form is handled, processed packaged and stored. But in wastewater handling, water flushes organic and inorganic matter to the sewer. Wastewater treatment is basically a processing system system to separate the organic and inorganic matter from the water that collected it [1].

The final step of the manufacturing process is the purification of wastewater from different sources. Wastewater treatment should be applied once you have used all known options to prevent the occurrence of waste flows, or after application of an integrated process of operations, which minimize power consumption and water contamination

Intensive development of meat industry in the twentieth century has opened many problems which are affecting environmental status. Meat and other industry, were developed on the principle of achieving the maximum profit with minimal or no investment in environmental protection. Problem analysis and resolving provides processing of large amounts of waste streams that require significant financial resources, and does not solve the problem fundamentally. The requirements in terms of quality of wastewater are in constant daily grow, so today's practice in Republic of Serbia is based only on the deposition of suspended particles and the separation of oils and fats, which is not acceptable [1].

Basic characteristics of the meat industry output waste streams are:

- The high content of organic matter
- High degradation,
- The presence of suspended solids and dissolved organic matter,
- Specific pollutants (blood, excretion, etc.).
- Nutrients (N, P)
- Oils and fats
- Sand, feathers, solid particles

The current state of wastewater management industry include:

- No prior treatment, wastewater is discharged directly into drains leading to the central sewage system

- Fractional treatment on-site, and then discharging into the sewer system.
- Secondary meat industry wastewater treatment.

Methodology

The research within the National project of the Ministry of Education and Science: Improvement and development of hygienic and technological procedures in production of animal originating foodstuffs with the aim of producing high-quality and safe products competitive on the global market included the first phase of monitoring and current state inventory of the meat industry wastewater treatment in the province of Vojvodina, as well as preliminary data on the monitoring and occurrence of potential emerging substances in meat industry wastewater.

Data collection was conducted in two phases. The first phase included preparation, visits to the identified polluters. The first stage resulted in elimination of the subjects that have terminated the company and collection of GIS data of each polluter on the territory of the Autonomous Province of Vojvodina, taking photos of the location.

Second phase included prioritization of emerging substances to be analyzed, sample collection and preliminary results. This research, within project has been conducted in the period from June-September 2011- first phase and second phase from January 2012 – present [2].

Results

Based on the collection data, 59 significant polluters have been identified on the territory of the Autonomous Province of Vojvodina. Small and unregistered farms have not been included in the research. This research included the collection of numerous entries, but this paper will present only results of the number of the selected facilities with wastewater treatment.

Since Serbia is still in the process of EU integration, it is still possible to have the situation where some water polluters have not yet installed and implemented the wastewater facilities. Results showed that almost 30% of identified meat industry polluters still do not treat the wastewater and therefore significantly influence the pollution of the water sources, directly jeopardizing human health.

The second phase of the research included identification of the priority pharmaceuticals, for which the analysis will be performed at selected sites. The following table provides an overview of selected pharmaceuticals that are most commonly used in meat industry.

Table 1. List of the selected pharmaceuticals

No.	Name
1	Ciprofloxacin
2	Tiamulin
3	Sulfamethoxazole
4	Trimetoprim
5	Streptomycin
6	Flortetraciklin
7	Amoxicillin
8	Enalapril
9	Chloramphenicol
10	Cephalexin

Samples for the second phase of the project were taken from wastewater outflows in spring 2012 on selected locations like it is shown in the following picture. At these locations wastewater samples are taken and analysed. Meat processing facilities are marked with the letters A, B, C, schematically and data processing is still ongoing and there are represented selected preliminary results.

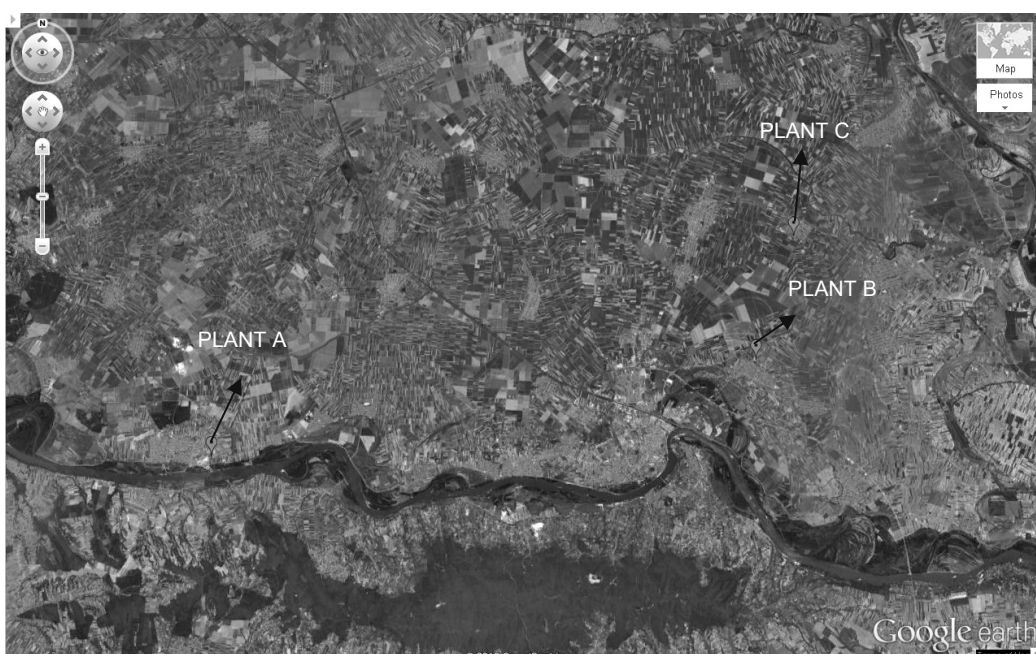


Fig. 1 Locations of selected meat industry plants A, B, C

After sampling and analyzing the first results are obtained. Results show that some of the above mentioned pharmaceuticals were detected. List of detected pharmaceutical with corresponding concentration is shown in table 2. For the second phase of research it is planned to analyse 10 pharmaceuticals, but since the project is still in progress, in this moment there are only the results for five selected pharmaceuticals [3].

Table 2. Concentrations of analysed pharmaceuticals

No.	Name	Concentration ng ^L
1	Sulfamethoxazole	215
2	Trimetoprim	145
3	Hlortetraciklin	n.d
4	Amoxicillin	n.d
5	Enalapril	543

The data relating to cadaster, as a major point for identifying and monitoring of pollution sources, as well as preliminary results of an analysis of selected pharmaceuticals are the first studies on this subject conducted in Vojvodina Region. The results show that there are a number of identified entities that represent a potential source of water pollution. It is therefore necessary to conduct additional research in order to complete the data and identify critical points for monitoring in order to give a proposal how to use the best available technologies and systems for reducing environmental pollution.

Conclusions

Without clean and safe water it is impossible to produce quality food products, including the highest standards of hygiene and food safety and systematic approach to controlling the use and consumption of water. The meat industry during the manufacturing process generates large amounts of wastewater burdened with high concentrations of organic matter. In order to discharge wastewater into the recipient, it is necessary to implement adequate measures for the reduction, treatment and disposal of wastewater. Past practice in the Vojvodina Region is based only on the deposition of suspended particles and separation of oils and fats. In most cases, insufficiently treated or completely untreated wastewater was discharged into the recipient and thus seriously disturbed the ecological status of the environment. The process of joining the European Union includes compliance with legal regulations related to wastewater treatment implemented through national water quality standards in accordance with the high criteria of hygiene and food safety.

Acknowledgement

This research has been supported by the Ministry of Education and Science of the Republic of Serbia within the project: Improvement and development of hygienic and technological procedures in production of animal originating foodstuffs with the aim of producing high-quality and safe products competitive on the global market (III 46009)

References

- [1] Technical Development Document for the Final Effluent Limitations Guidelines and Standards for the Meat and Poultry Products Point Source Category (40 CFR 432), WASTEWATER TREATMENT TECHNOLOGIES AND POLLUTION PREVENTION PRACTICES.
- [2] M. Đogo, D. Milovanović, M. Vojinović-Miloradov and S. Kovačević, Preliminary Results of the Cadastre of Meat Industry Polluters in Vojvodina Region, Serbia, TOP 2012, Čista Papiernicka, Slovak Republic, jn 2012. Pp 93-101.
- [3] J. Čolić, A. Petković, T. Mitrović, Prisustvo lekova u otpadnim vodama, 41. Konferencija o korišćenju i zaštiti voda, jun 2012. Divčibare, Republika Srbija.



International Conference on Innovative Technologies, IN-TECH 2012,
Rijeka, 26. - 28.09.2012



ANALYSIS OF PD RESPONSE ON DIFFERENT INPUT VOLTAGES AND INCIDENT LIGHT WAVELENGTHS

Ž. Milanović¹, I. Marasović², V. Zanchi²

¹ Faculty of Engineering, University of Rijeka, Croatia

² Faculty of Electrical Engineering, Mechanical Engineering and Naval Architecture, University of Split, Croatia

Keywords: Waveform analysis, semiconductor response, local derivative dependence, wavelength distinction.

Abstract. In this paper photodiode response to different excitations, and square, sine and triangular input waveforms is analyzed. Excitations are obtained with single wavelength LE Diode with pulse voltage applied (10kHz – 100kHz). Results for different input pulses have been analyzed. Silicon PD used for measurements has spectral range from 430 nm to 900 nm with high signal to noise ratio. Measurement results show dependence on input signal waveform as well as incident lights wavelength. Significant dependence of PD voltage responses local derivative on incident wavelength has also been assessed. Difference in local derivative could be used to differentiate between incident wavelengths. Current density can be calculated for each incident wavelength as well as I-V, V-t and I-t characteristics in order to find distinguishing features of each wavelength response.

Introduction

Conventional methods of fabricating solid state light sensors are based on applying dyed filters on active sensor area in order to distinguish incident lights wavelengths. Different ways of differentiating role of each sensor element have been proposed [1-4]. Most sensors are based on three different active areas with filters used to differentiate between basic light wavelengths representing three basic colors of visible spectrum. In modern photo sensors 4 active elements are used to feed information to one photo pixel, usually two photodiodes sensitive to green light and one photodiode for blue and one for red light sensing. Photodiodes sensitivity to wavelength is not used as is, so dyed filters are needed, which let only light of particular wavelength through. More up to date sensors have used stacked photodiodes which constitute one color element that gives colorimetric information [1] meaning one sensor pixel takes up surface as big as one photodiode. PD are made of semiconductor material such that light of different wavelengths can penetrate material to different depths, feature that can possibly be used in order to distinguish wavelengths using only one sensor element, as opposed to three commonly used in sensor manufacturing. Since photodiode response to different incident lights gives results that are not distinguishable enough, it is necessary to find a way to use the PD response to correctly determine incident lights wavelength. One probable way of obtaining distinct results is by switching between reverse and forward voltages applied on LED or PD under light stimulus [5-9]. Experiments have shown that PD photocurrent is different depending on light color as well as photo voltage amplitude and shape. In this paper, dependence of local derivative of PD response on different incident wavelengths has been assessed as well as response energy distribution in frequency domain.

Experiment setup

In order to obtain local derivative of PD response, circuit shown in fig. 1. has been designed, consisting of differentiator of first order and circuitry for obtaining PD response to incident light wavelength. Output from photodiode is directly transferred to differentiator over a capacitance C1 in order to get local derivative of response as the output voltage of operational amplifier.

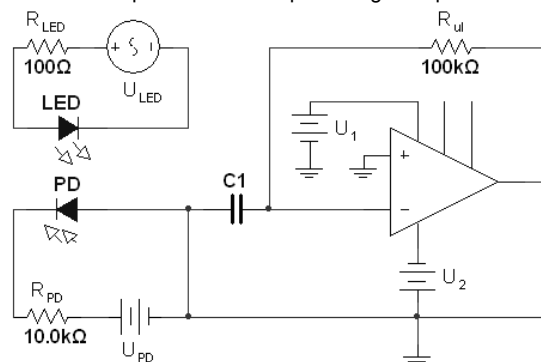


Fig. 1 Experiment setup.

Light emitting diode used in experiment is *Kingbright* full color clear RGB diode with double blue diode and peak wavelengths 627 nm, 565 nm and 430 nm for red, green and blue light respectively. Further characteristics of used light emitting diode are given in table 1. In this experiment single color responses have been analyzed as well as some color combinations with LED current set to 20 mA at most. Detector used in previous setup is *Centronic* photodiode suited for low light level applications throughout the spectral range of 430 nm to 900 nm with high signal-to-noise ratio. It is operated in reverse mode to achieve lower capacitance and therefore higher sensitivity to incident light with $-2V$ voltage applied.

Further characteristics of used detector and operational amplifier are given in table 2. Operational amplifier used in differentiator is integrated general purpose LM741 amplifier.

Table 1. Light emitting diode factory characteristics.

Parameter	Red	Green	Blue
Capacitance	15 [pF]	15 [pF]	65 [pF]
Forward Voltage	2 [V]	2,2 [V]	4 [V]
DC Forward Current	30 [mA]	25 [mA]	30 [mA]
Reverse Voltage	5 [V]	5 [V]	5 [V]
Reverse Current	10 [μA]	10 [μA]	10 [μA]
Power Dissipation	105 [mW]	105 [mW]	105 [mW]

Table 2. Detector and OpAmp factory characteristics.

	Parameter	Max. Rating
P.D	DC Reverse Voltage	15 [pF]
	Peak Pulse Current	200 [mA]
	Peak DC Current	10 [mA]
OpAmp	Supply Voltage	22 [V]
	Differential Input Voltage	30 [V]
	Input Voltage	15 [V]
	Input Bias Current	80 [nA]
	Input Resistance	2 [MΩ]

Results

Analysis of results obtained from differentiator has shown potential for distinguishing incident light color if local maximum is observed, fig 2. The biggest change in local derivative can be observed for blue incident light and smallest change for green light. Also, blue light in this particular measurement has local derivative maximum always above 0.028.

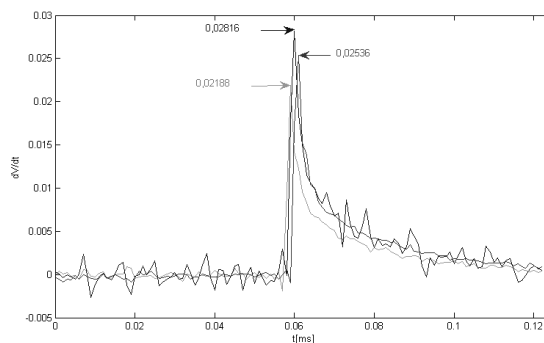


Fig. 2. Incident lights first derivative distinction. Small interval around local maximum is shown.

If unique value occurring at local maximum of first derivative of signal can be determined it would be possible to identify the incident light color. Experiments have shown that local extremes of first derivative of blue light display characteristic values that can be used to confidently differentiate this color from other wavelengths, fig. 3.

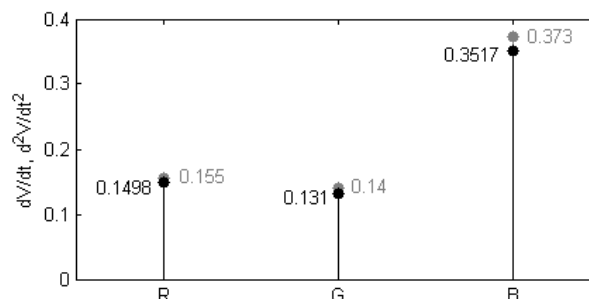


Fig. 3. Incident lights first (gray) and second (black) derivative distinction. Blue light can be easily distinguished.

As shown in fig. 3. local maximum of first or second derivative of detector response for blue light is 0.3 of higher and red or green light response first derivative local maximum is smaller than 0.2 for this particular measurement. Further experiment will include distinguishing local maximums depending on different input signal frequency as well as distinguishing green and red responses.

Square waveform

For square input signal it has been noted that red light response has local maximum, when derived, larger than green light response maximum about two times or more. For example red light response for 100 kHz frequency and 0V constant voltage applied to detector has local maximum of 0.24 and green light in same conditions 0.014, fig. 4 (b).

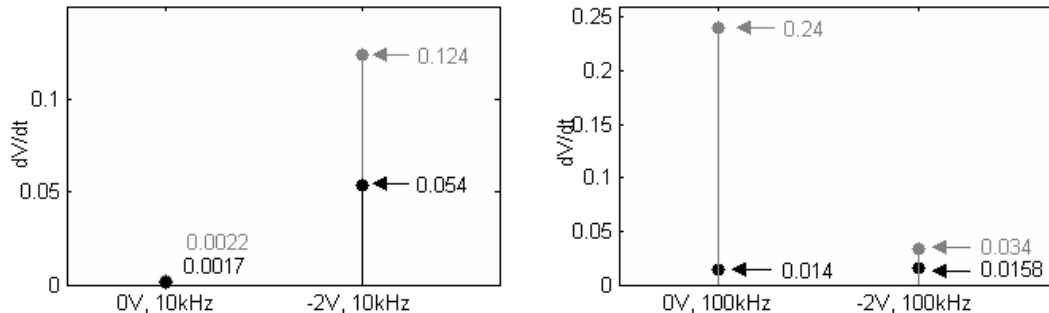


Fig. 4. Local derivative for red and green response with 100 kHz (a) and 10 kHz (b) input signal frequency and 0V/-2V applied to detector.

If frequency of 10 kHz is applied to input signal results show a smaller difference between light color responses as shown in fig. 5 (a). Distinct difference between red and green light can be observed from spectrogram as shown in figure 6. It can be seen that highest energy distribution exists between frequency 5 and 125 Hz for red light and around 80 to 125 Hz for green light.

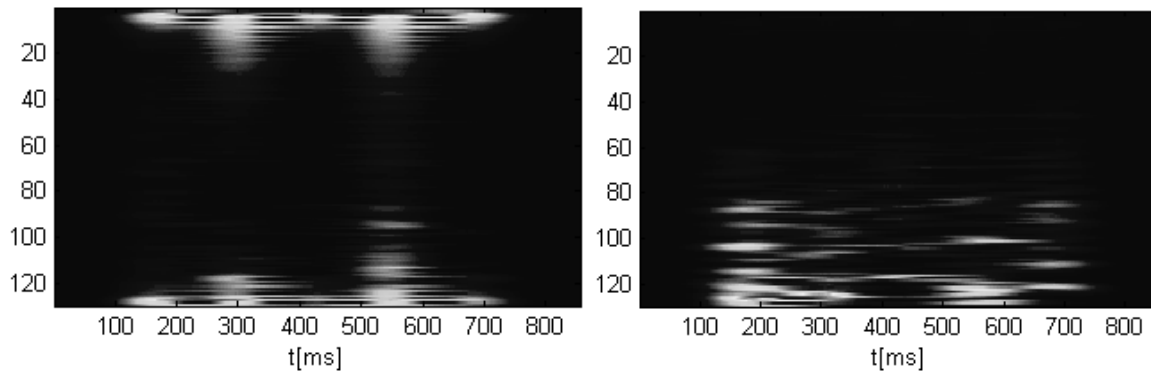


Fig. 5. Spectrogram for red (a) and green (b) incident light and square input signal (first derivative), showing distinct energy distributions. Input frequency is 10 kHz and 0V is applied on detector.

When entire signal of 600 points is observed it can be seen that every local maximum for red light response occurs at much higher level than for green light as can be seen in fig. 6. Also difference is noticeable for 10 kHz and 100 kHz frequency of input signal.

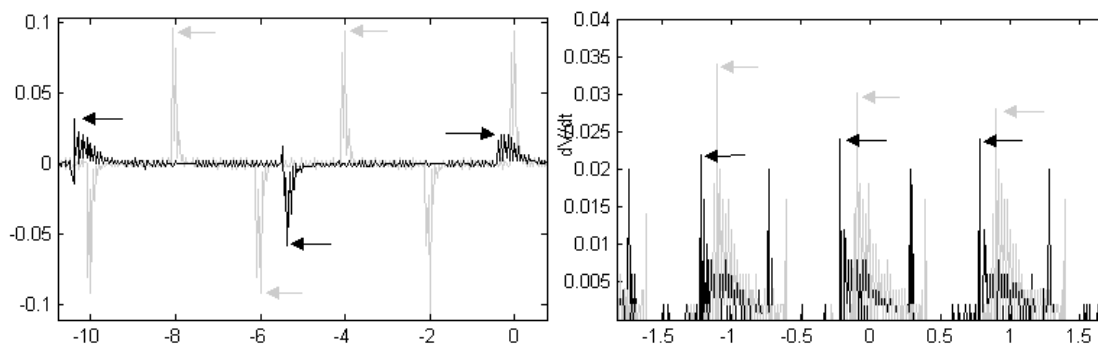


Fig 6. Local derivative maximums of input signal for frequencies 10 kHz (a) and 100 kHz (b). Red light (gray) local maximum is higher than green light (black). On x axis is time $[s] \times 10^{-5}$ and on y axis first derivative (dV/dt).

There is a difference in derived response for different input signal frequency as well as if different voltage is applied to detector.

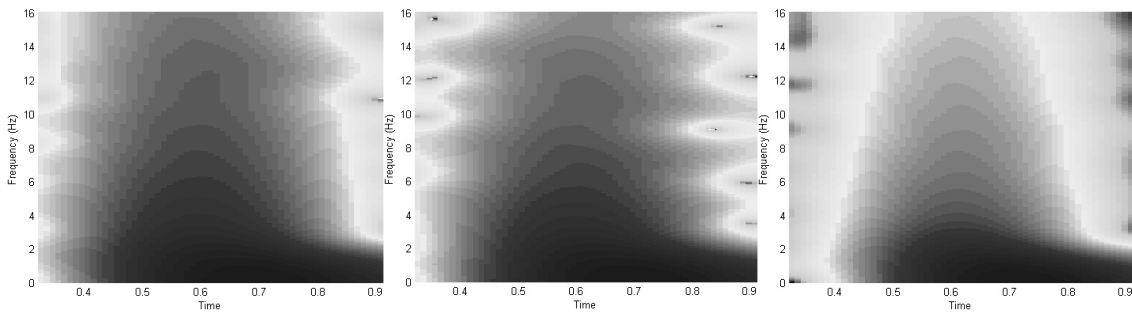


Fig. 7 Spectrogram for wavelengths 495nm, 550nm, 620nm.

Spectrogram of all three light colors show difference when Hamming window of $n/4$ is used as shown in fig. 7. It can be seen that smallest energy distribution exists for red incident light and the largest for blue light.

Triangle and sine waveform

When triangle and sine waveforms are applied there is a difference present between local maximums of red and green responses, similar to those when square waveform is used. Figure 8. shows the difference between maximums when response is derived for sine and triangle waveform.

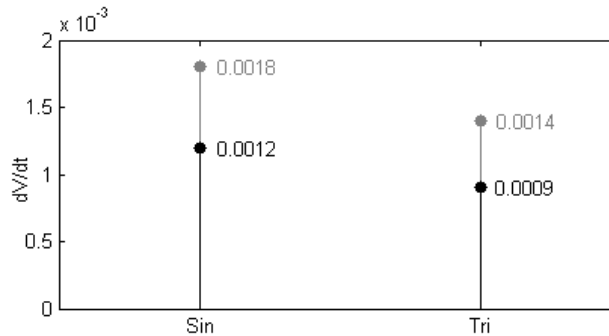


Fig. 8. Sine and triangular input waveform for red (gray) and green (black) detector response.

If spectrogram is constructed from first derivative of sine input signal it can be seen that energy distribution is distinctly different for red and green light, fig. 9, which can eventually be used towards distinguishing incident light color.

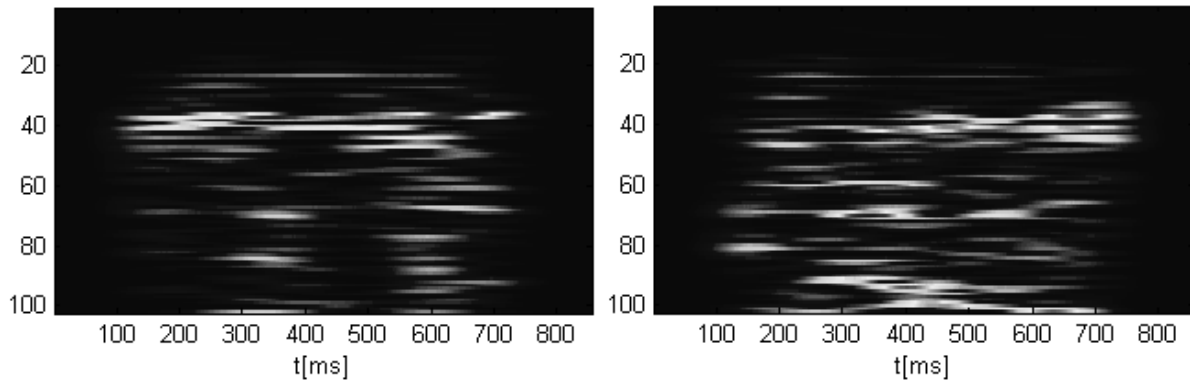


Fig. 9. Spectrogram for red (a) and green (b) incident light and sine input signal (first derivative), showing distinct energy distributions. Input frequency is 10 kHz and 0V is applied on detector.

Conclusion

In order to obtain information about color of incident light without using color filters [1] a circuit with differentiator of first order can be constructed. If comparator is used it can trigger when local maximum of derived signal response exceeds particular value (to be determined for used electronic elements and setup) showing this way that particular wavelength has fallen onto the detectors active surface. Future work should include analyzing color combinations and attempting to place them within results obtained in this paper.

References

- [1] R. F. Wolffenbuttel, E. J. Blaauw, M. R. Wolffenbuttel, G. de Graaf: Tri-Colorimetric Detector in Silicon with One Photodiode, IEEE Transactions on Electron Devices. Vol. 38 (1991), pp. 2697-2697.
- [2] M. Okamura, K. Kimura, S. Shirai, N. Yamauchi: A Light-Transmitting Two-Dimensional Photodetector Array Using a-Si pin Photodiodes and Poly-Si TFT's Integrated on a Transparent Substrate, IEEE Transactions on Electron Devices, Vol. 41(1994), pp. 180-185.



-
- [3] K.-I. Sugimoto, K. Nakajima, Y. Mizushima: Band-Edge-Emphasizing Photodetector Response, IEEE Transactions on Electron Devices, Vol. 37(1990), pp. 2298-2302.
 - [4] R. F. Wolffenbuttel: Integrated All-Silicon Color Filtering Element with an Enhanced Wavelength Tunability, IEEE Electron Device Letters, Vol. 9(1988), pp.337-339.
 - [6] R. F. Wolffenbuttel: Color Filters Integrated with the Detector in Silicon, IEEE Electron Device Letters, Vol. 8(1988), pp.337-339.
 - [7] H. W. Choi: Vertical Integration of Light-emitting Diode Chips, IEEE, 2011.
 - [8] S. Chandrasekhar, J. C. Campbell, A. G. Dentai, C. H. Joyner, G. J. Qua, W. W. Snell: Integrated Waveguide p-i-n Photodetector by MOVPE Regrowth, IEEE Electron Device Letters, Vol. 8(1987), pp.512-514.
 - [9] A. Majumdar, K. K. Choi, J. L. Reno: Voltage tunable two-color infrared detection using semiconductor superlattices, Applied Physics Letters, Vol. 83(2003), pp. 5130-5132.



International Conference on Innovative Technologies, IN-TECH 2012,
Rijeka, 26. - 28.09.2012



URBAN ELECTRIC VEHICLE DEVELOPMENT AS PART OF SMART GRID

P. Sasa¹, S. Skok¹ and V. Kirincic¹

¹ The University of Rijeka, Faculty of Engineering, Department of Power Systems,
Vukovarska 58, 51000, Rijeka, Croatia

Keywords: electric vehicle, Smart Grid, renewable energy sources

Abstract This paper presents a plan of technical solutions and design approach as well as the independent development of electric vehicle by converting the existing vehicle powered by internal combustion engine. Novelty in electric vehicles technology is the idea of using a photovoltaic film on the roof of the vehicle, whereby the produced energy would be used to extend the autonomy of the less demanding power supply systems of the vehicle. A special attention is paid to the development of a charging system as a distributed source of electrical energy.

Introduction

Considering the role of transportation in everyday life along with growing rates of fossil fuels, the number of vehicles with electric power drive is constantly increasing. In order to mitigate climate changes and global warming effects, the intention is to reduce greenhouse gasses emissions, to integrate renewable energy sources and to increase overall energy efficiency [1, 2]. Energy utilities all over the world are collaborating with many R&D teams to develop technologies, concepts and solutions that will gradually evaluate the electric energy power system into a vision usually known as a Smart Grid. Part of the solution and an important area of interest is the automotive sector [3], as a significant factor in overall consumption and pollution.

The development of electric vehicles (EV) leads to three main types: a hybrid electric vehicle (HEV), a plug-in hybrid electric vehicle (PHEV) and a battery electric vehicle (BEV). The HEV and PHEV combine an internal combustion engine with an electric propulsion system. In the HEV charge of the batteries is maintained through the normal operation of the vehicle. The PHEV incorporates a separate battery system, which is charged from an external power source. As the BEV does not have a combustion engine, it relies solely on a battery system so it must be plugged into a charging source [4]. Majority of the EVs are PHEVs, which diminishes the motivation for further development of the BEVs as well as the related infrastructure such as charging stations. The batteries in the EVs have relatively short life expectancy, which renders them non-competitive in comparison with the conventional vehicles. On the other hand, increased use of the BEV has positive effect on the environment due to reduced CO₂ emissions. In urban areas, along with the need to reduce harmful emissions and noise, the lack of parking space is very pronounced. A solution is to offer a small urban electric vehicle (UEV) with sufficient autonomy for urban purposes.

The project described in this paper includes the conversion of the conventional vehicle to the BEV and the development of the charging system, as a part of an overall trend of the Smart Grid development. In the project a group of students and researchers from The Department of Power Systems, University of Rijeka - Faculty of Engineering, is involved.

The urban electric vehicle project overview

The idea of the project is development and deployment of technical solutions for conversion of the conventional vehicle with the internal combustion engine into the BEV. Also, the design, development and implementation of the charging system is planned. Novelty of the project is an innovative application of renewable energy sources (RES). A photovoltaic film on the roof of the vehicle would be an additional power source that can be used for less demanding power systems on the vehicle. The project is consistent with trends of reduced exploitation of the primary energy sources, increase of the energy efficiency and reducing the greenhouse gas emissions. The idea of development of the EV supports the EU goals to reduce the greenhouse gas emissions by 20 %, to increase the energy efficiency by 20 % and to increase the share of RES to 20 %, by 2020.

An important aspect of the project that is offers an opportunity for the students to take part in a research area in which many manufacturers direct their research and pilot projects. On the other hand, presentation of the results of the project to the subjects from industry opens a possibility of closer collaboration between experts from the real sector and researchers from the academia.

The development of a charging system for the UEV, as a distributed source of electrical energy, is in line with the Smart Grid trends. Therefore the project is appropriate for application to the EU funds. In this way the funding sources could be assured for future generations of students to work on the EV topic.

A long term goal of the project is to establish an interdisciplinary team including experts from industry and researchers from the academia, capable of prolonged research, development and implementation of new and innovative technologies for modern vehicles with electric power drive.

Project organisational structure

The students involved in the project are grouped in several interconnected teams, as follows:

- 1) Electric drive team - regarding a chosen vehicle it is necessary to determine the rated output and the placement of the electric drive. The main criterion is total mass of the vehicle and its desired performances.
- 2) Batteries team - it is necessary to collect as many information as possible about available batteries for EVs and then, based on the collected data, the batteries should be selected. The criteria are type of the electric drive, weight and capacity of the batteries, their charge rate and maximum number of charging cycles.

- 3) Charging system team - it has to find the optimal solution for the batteries recharging and solving the accompanying mechanical problems. The criteria for charging system are the batteries voltage and current during charging and electrical and mechanical protection.
- 4) Regulation and control team - an optimal regulation of the chosen electric drive and the batteries in order to achieve the most efficient torque control has to be designed. It is necessary to choose the type of microcontrollers, to review programming characteristics as well as to examine the connection possibilities in order to monitor the parameters and diagnose failures.
- 5) Mechanical team - this group must accomplish safe and secure connection of all the components according to current technical directives and standards.

Organisational structure of the UEV project is given in Fig. 1, which presents the interconnections between the teams.

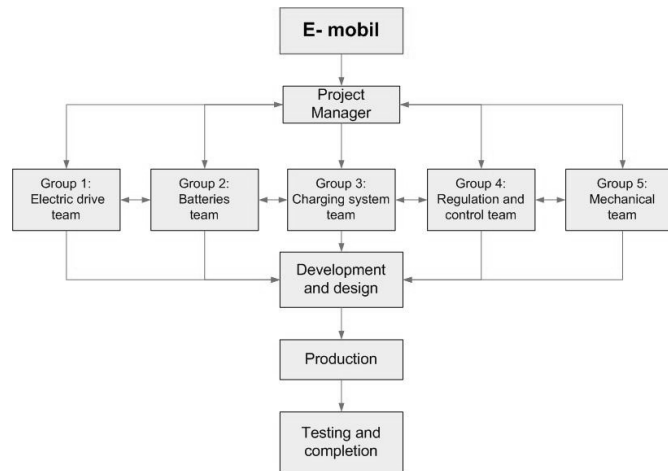


Fig. 1. Organizational structure of the project teams

The project plan is divided into several phases, as given in Fig. 2.

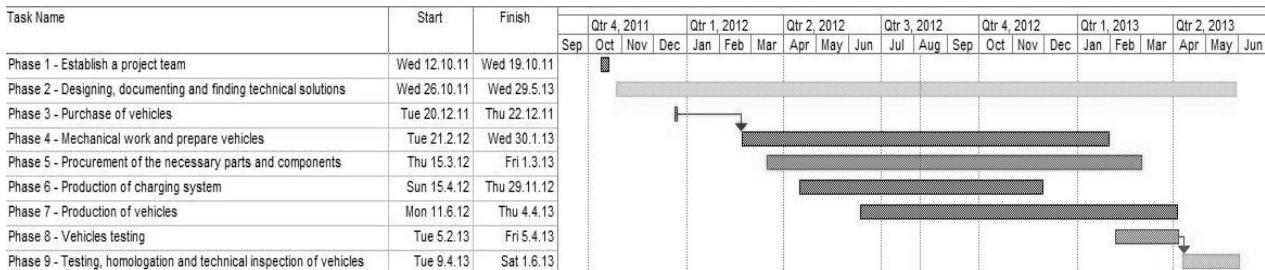


Fig. 2. The Gantt chart of the UEV project

Technical solutions

Selection of the vehicle model

Choosing a conventional vehicle for conversion into a vehicle with electric power drive is one of the starting points of the project. As the project is based mainly on the urban vehicle development, its dimensions and mass are some of the most important factors. The mass of the vehicle affects selection of the rated output of the electric motor, capacity and weight of the battery, and the selection of the control system, all of which are important factors influencing the vehicle's performance and its driving autonomy. Furthermore, it is necessary to define available space for electric propulsion system as well as to eliminate unnecessary parts and components of existing propulsion system with internal combustion engine. The power consumers that remain on the vehicle should be adjusted to the new system by making them as economical as possible in order to reduce the power consumption. As the optimal vehicle for the given UEV project, the model "Smart" is chosen. Fig. 3 illustrates possible placement of key parts of the new propulsion system [5].

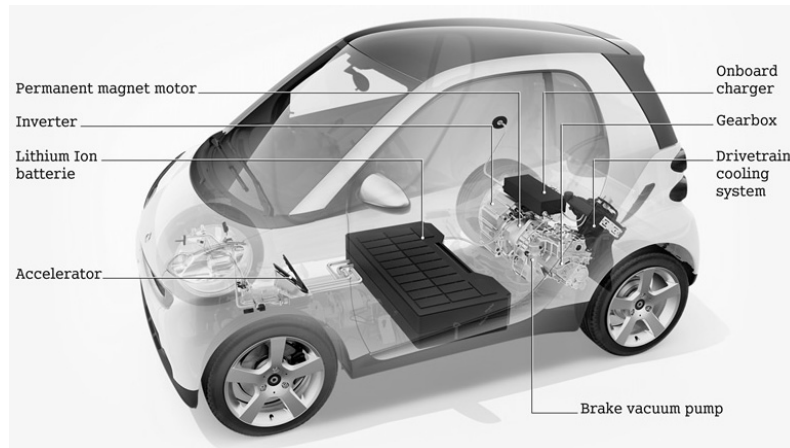


Fig. 3. Possible placements of key parts of the new drive circuit

Propulsion system

In conversion of the conventional vehicle into the electric one, several types of drive circuits are possible. Differences between the types may be regarding the type of electric motor (DC, induction motor, synchronous motor with permanent magnets) or type and recharging of the batteries or the control system (depending on the type of controllers). Also, the financial plan and the purpose of the electric vehicle should be taken into account. Type of the selected electric motor is TEMA SPM132-1, which is a synchronous motor with permanent magnets. Rated power of the motor is 19 kW power with torque of 70 Nm.

After preliminary actions of removing the internal combustion engine and accompanied equipment (fuel tank, exhaust system, cooling circuit), it is important to find an optimal solution for the electric motor placement along with all other components that are necessary for continuous drive. Fig. 4 presents the overall drive circuit.

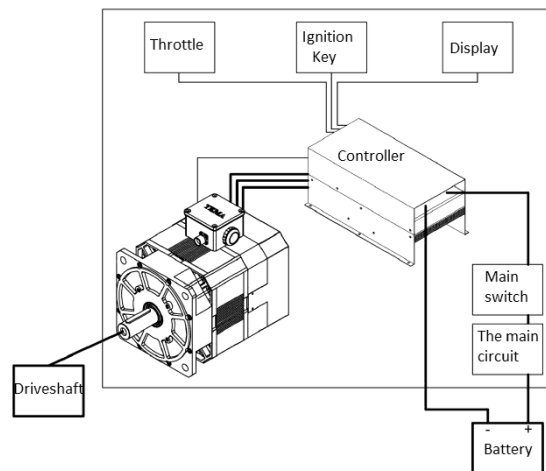


Fig. 4. The overall drive circuit

Special attention must be paid to the construction of the electric motor's drive shaft with gearbox that stays incorporated in the vehicle owing to simplicity of the deployment. The project also includes complete system wiring, correct placement of the controllers and its cooling system, all according to the technical directives and standards. Apart from the drive circuit, it is important to mention the electric energy storage system. The major research in EV industry is aimed towards energy storage systems and in EV technology batteries have an important role. The battery weight per unit of stored energy is still large and creates additional problems for the EV industry. In the UEV project the batteries are placed in lower central part of the vehicle, which assures optimal weight distribution, correct mechanical protection and air flow that is necessary for cooling. The project will use the LiFePo batteries and expected autonomy is 90 km.

Charging system

Regarding the charging of the EVs, there are two basic concepts. The first approach, which is chosen for this project, is to build an infrastructure for charging/recharging the EV, while the second one supposes stations for the battery replacement, which has not become very popular owing to large investment costs.

A technological concept of e-mobility, shown in Fig. 5. includes the following components: the EV, the EV supply equipment (EVSE), the charging station and the charging station control centre (CSCC).

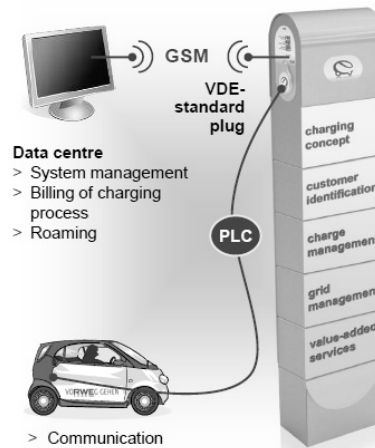


Fig. 5. Technological concept of e-mobility

Different EV manufacturers may specify different charging protocols for their EVs such as Mode 1, Mode 2, Mode 3 or Mode 4 charging. A summary of different modes of charging according to IEC 61851-1 is given as follows [4]:

- Mode 1 charging relates to the connection of the EV to the a.c. supply network utilizing standardized socket-outlets not exceeding 16 A and not exceeding 250 V a.c. single-phase or 480 V a.c. three-phase, at the supply side, and using power and protective earth conductors.
- Mode 2 charging relates to the connection of the EV to the a.c. supply network not exceeding 32 A and not exceeding 250 V a.c. single-phase or 480 V a.c. three-phase using standard sockets. In addition to power conductors and protective earth, these sockets add a control pilot function.
- Mode 3 charging relates connection of the EV to the a.c. supply network utilizing the dedicated EVSE where the control pilot function extends to control equipment in the EVSE, permanently connected to the a.c. supply.
- Mode 4 charging relates to the connection of the EV to the a.c. supply network utilizing an offboard charger where the control pilot function extends to equipment permanently connected to the a.c. supply.

The Mode 1 and 2 charging are also known as standard, normal or slow charging. These modes are suitable for longer period of charging such as home or office charging. The Mode 3 supports slow and fast charging (depending on rated current) and it supposes the use of the special EVSE. The Mode 4 represents fast charging and it is chosen for the UEV project. Disadvantage of this mode is the fact that the vehicle can be charged only at the charging station. In order to alleviate the mentioned drawback, the idea is to implement the charging system into the vehicle. The chosen charging strategy supposes charging of the vehicle during the night when the power system load is at its minimum so the EV has the lowest impact on the distribution network. The advantages of the proposed concept are possibility of the network control, reduction of investments into the distribution network, optimal dispatching and minimization of charging time [6].

Integration of the renewable energy source

The educational goal of this project is to support students in innovative thinking, especially in area of the RES. For this part of the project, the novelty is application of a photovoltaic film on the roof of the vehicle as an additional power source. The rated power and efficiency of the photovoltaic system would not be enough for recharging the batteries needed for the drive circuit. Therefore the system would be used as the secondary power supply system for the less demanding equipment such as the navigation system.

Conclusions

The automotive industry significantly contributes to the overall energy consumption. Regarding the rising trend of prices of the fossil fuels price and the activities to reduce greenhouse gasses emissions and pollution; there is an open challenge in development of the EVs. The paper proposes a small urban vehicle with the electric drive. The project overview and description of the proposed technical solutions can be a good starting point for research groups from academia to get involved in similar projects.

In order to avoid dependency of the charging infrastructure, the charging system embedded with the vehicle is proposed. Novelty in the EV solution is the application of the RES in a form of the photovoltaic film on the roof of the vehicle. The photovoltaic system would be used as the additional power source for part of the equipment.

References

- [1] D. Radulovic; S. Skok; V. Kirincic; "Energy efficiency public lighting management in the cities," Energy, Elsevier, vol. 36, no. 4, pp. 1908-1915, 2011.
- [2] D. Radulovic; S. Skok; V. Kirincic; "Cogeneration – investment dilemma," Energy, Elsevier, accepted for publication, July 2012.
- [3] Larminie, J., Lowry, J. : *Electric Vehicle Technology Explained*, John Wiley & Sons Ltd., West Sussex, England, 2003.
- [4] T. Jakasa, S. Susic: "Electric vehicles charging infrastructure," 10th Symposium HRO CIGRE, Cavtat, November 2011.
- [5] Online <http://nenmore.blogspot.com/2010/12/rent-ev-from-hertz.html> (July, 2012)
- [6] Enel: E-mobility in Italy&G4V and Green eMotion Projects, September, 2010. Online <http://www.enel.com> (July, 2012)

CHARACTERIZATION OF FUNCTIONALISED MATERIALS BY ATR-FTIR METHOD AND RAMAN SPECTROSCOPY

Lidija Fras Zemljič¹, Marko Munda¹, Simona Strnad¹, Minka Kovač²
and Julija Volmajer Valh¹

¹ University of Maribor, Faculty of Mechanical Engineering, Institute for Engineering Materials and Design, Smetanova 17, 2000 Maribor, Slovenia

² Omega d.o.o., Dolinškova 8, 1000 Ljubljana, Slovenia

Keywords: fibre-forming polymers, polysaccharides, functionalization, elemental analysis, ATR-FTIR, Raman spectroscopy

Abstract. The paper discusses the implementation of bioactive functionalization by chitosan of two fibre-forming polymers (a natural polymer: cellulose, a synthetic polymer: polyethylene terephthalate) which are most commonly used in most advanced sectors, such as packaging of food products, development of new medical materials and implants, etc.

Chitosan was used for material functionalization, namely in the form of thin surface layers, by which new functional groups were integrated into the fibres. Most of these groups are responsible for fibre biological activity. Therefore, it is of vital importance to use the techniques which enable the analysis of superficial elementary composition (new functional groups) of functionalized materials.

The purpose of this paper is to examine the surfaces of functionalized fibre-forming materials by using the spectroscopic method ATR-FTIR and complementary Raman spectrophotometrics. Both techniques are useful for qualitative analysis of fibre functional groups.

Until now both techniques have not received enough attention and therefore are examined in details and streamlined for the use of fibre formation polymers with different structure and chemistry which are further functionalized by bioactive chitosan.

The analysis of functionalized PET foils has shown that the chitosan film attaches to the underlying material only mechanically and/or by means of physical adsorption; on the other hand, no chitosan was detected on the cellulose fibres by both of the mentioned techniques. The reasons for the latest were discussed.

Introduction

Natural substances are very attractive for functionalization of polymers in order to introduce high added value properties such as special bioactive properties.

A special attention is paid to amino polysaccharides, including chitosan (Fig. 1), a chitin derivative, after cellulose the most abundant biopolymer on Earth. These polysaccharides contain amino groups which interact with the cell surface of pathogen microorganisms and in this way destroy them by several possible mechanisms [1]. Chitosan's positive charge, the degree of N-deacetylation, the mean polymerization degree and the nature of chemical modifications are the properties which strongly influence its antimicrobial effectiveness [2-4].

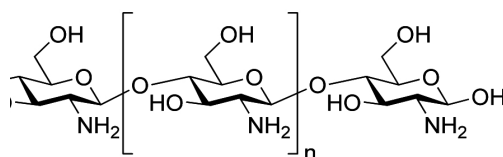


Fig. 1: Schematic presentation of chitosan

Chitosan has been approved as a food ingredient from FDA recently; therefore, the use of chitosan for new product development as well as natural antimicrobial agents would become more and more popular. Chitosan found several applications like coating for fibres in order to develop medical products, for development of biofilms on PET material, etc.

However, for all of these applications it is extremely important to establish the appropriate methodology for characterisation of material specific functionality. This means that it is essential to choose the appropriate methods for physico-chemical characterization of functionalised surfaces.

Amongst them standard non-destructive methods are interesting for the determination of chemical composition of material surfaces. Those methods are XPS (X-Ray Photoelectron Spectroscopy), infrared spectroscopy (FT-IR, ATR-IR) and Raman spectroscopy. FT-IR and Raman spectroscopic methods were mostly used for the characterization of biopolymers structure; such as for polysaccharides and proteins for medical application. It has been shown that longer that are macromolecules of biopolymers, the poorer is their conformation [5]. The result of solid material (such as cellulose or PET) functionalization by use of polysaccharides and proteins are new functional

groups attached to material surfaces. Our previous researches show that when ATR-FTIR is used for the determination of different typical functional groups after fibre functionalization processes, several problems appear regarding their detection as well as repeatability for signals typical for specific functional groups. This may be attributed to non-homogenous polysaccharides /proteins adsorption; to a low content of adsorbate on material surface (below the detection limit), to material structure, irregular preparation of samples for experiment (FT-IR analysis), etc.

Thus, the purpose of this paper was to examine the surfaces of two different fibre-forming (cellulose and PET) materials functionalised by chitosan by using the spectroscopic methods ATR-FTIR and complementary Raman technique. Both techniques are useful for qualitative analysis of fibre functional groups. Until now both techniques have not received enough attention and therefore are examined in details and streamlined for the use of fibre formation polymers which are functionalized by bioactive polysaccharides.

The analysis of functionalized PET plastic film has shown that the chitosan attaches to the underlying material only mechanically and/or by means of physical adsorption; on the other hand, no chitosan was detected on the cellulose fibres. The reasons for the latter were discussed.

Experimental

ATR-FTIR

ATR-FTIR was used to examine the influence of activation procedures onto chitosan adsorption. In this way surface chemical composition of PET foils was studied. The analysis was performed on a PerkinElmer Spectrum GX spectrometer, equipped with a diamond crystal ATR attachment. For all the measurements, only dry samples were used. The depth analysis was approximately 0.75 μm . Spectra were recorded at 2 cm^{-1} spectral resolution within the range (4000 – 650) cm^{-1} , using an average of 16 scans.

Raman spectroscopy

FT-Raman spectra were carried out using Perkin-Elmer spectrometer equipped with Nd:YAG laser source. Spectra were accumulated from 64 scans at a resolution of 4 cm^{-1} . An optical bench alignment was performed before each Raman measurement to ensure that the spectrometer was fine-tuned and the detector signal maximized.

Results and discussion

The cellulose viscose fibres were functionalised by high concentrated 1.5 % of chitosan solution. The spectra are shown in Figure 2.

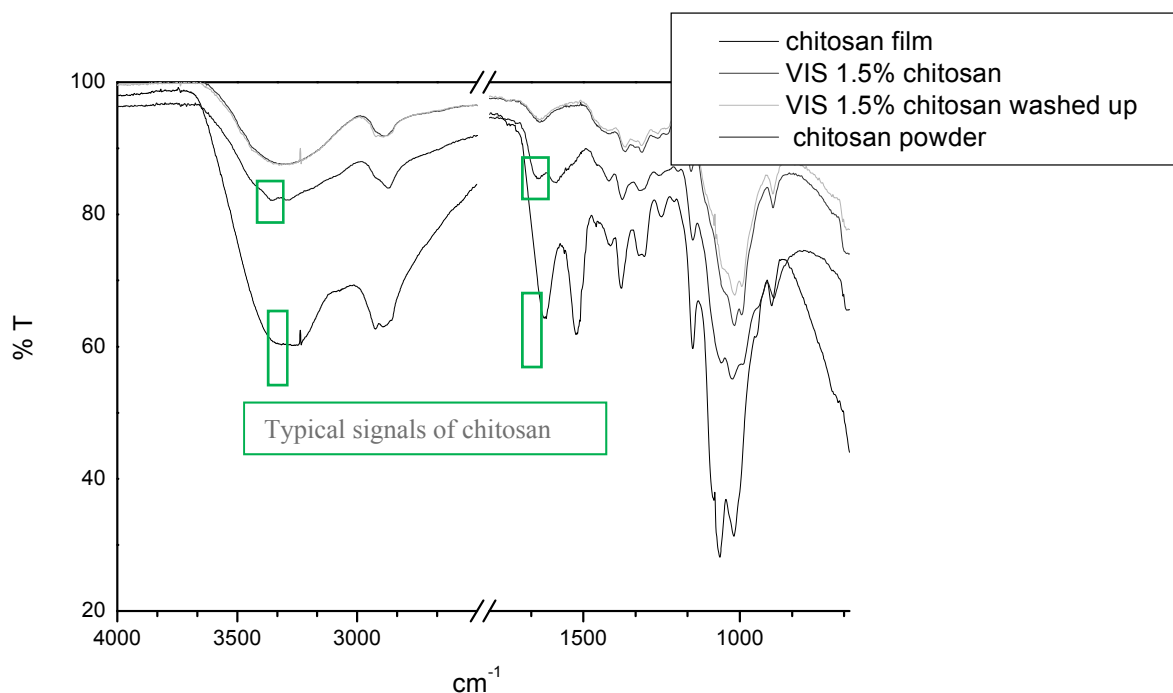


Fig.2: FT-IR ATR spectrum of chitosan powder and chitosan film as references, cellulose viscose fibres coated by 1.5 % chitosan solution and washed until constant conductivity and the same fibres without final washing.

The peaks at 1660 cm^{-1} and 1590 cm^{-1} are characteristic for chitosan and belong to C=O in N-H groups, respectively. These two peaks are clearly seen for pure chitosan in the form of powder as well as for chitosan film structure (created from 1.5 % of chitosan solution). Mentioned peaks were not determined by pure-reference cellulose fibres as was expected due to cellulose structure, but unfortunately neither by viscose cellulose fibres functionalised by chitosan. It has to be mentioned that different chitosan concentrations as an adsorbate for fibres were prepared, fibres were dried at different conditions, ground, prepared by KBr, but although we were not able to

optimise fibres or techniques in order to successfully detect typical peaks for chitosan adsorbed onto fibre surfaces. Complementary Raman technique did not give any of typical chitosan signals for functionalised fiber surfaces (Figure 3).

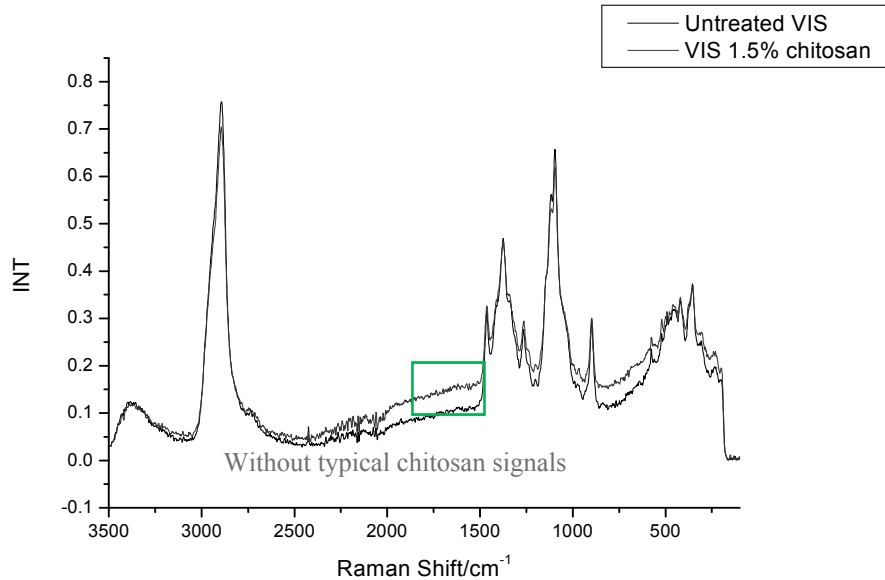


Fig. 3: RAMAN spectrum of untreated cellulose viscose fibres and viscose fibers functionalized with 1.5 % chitosan solution

Analysis of functionalised cellulose viscose fibres by ATR-FTIR demonstrated that there were no detectable signals typical for chitosan. It is speculated that this is due to the covering of hydroxyl groups of original cellulose with amino groups of chitosan. The another reason may be in low chitosan concentration onto fibre surface that may be under the detection limit. However, Raman technique showed the same; it is not possible to detect typical spectra of chitosan on fiber surface.

When PET plastic films functionalised by chitosan were analysed by ATR FT-IR spectroscopy it is shown that chitosan was successfully distributed on their surfaces (Figure 4). This was proved by the presence of NH stretching peak in the area between 3300cm⁻¹ and 3340 cm⁻¹. With appearance of amino peak, the CH wagging peak in the area between 2950 cm⁻¹ and 3010 cm⁻¹ has increased. As ATR-FTIR method detects functional groups down to the depth of 0.75 μm the additional prove for successful impregnation is reduction of -C=O stretching peak in the area from 1630 cm⁻¹ to 1720 cm⁻¹. The thin chitosan film bounded to PET plastic foil was also seen by eyes.

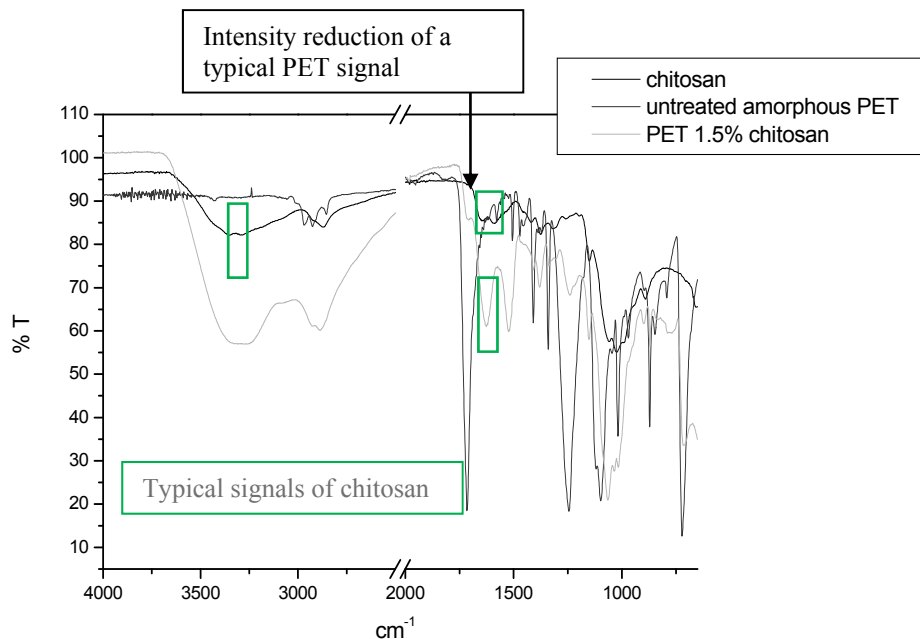


Fig. 4: FT-IR ATR spectrum of chitosan, untreated amorphous PET and PET foils functionalised by 1.5 % of chitosan solutions



Conclusions

It can be concluded that ATR-FTIR and Raman techniques are not suitable for detection of chitosan adsorbed onto viscose cellulose fibre surfaces. Due to the similar chemical structure of chitosan and cellulose typical spectra of both polymers are covered by each other which pointed out that both techniques are not suitable to analyse those kind of samples.

By PET plastic foils both techniques are suitable for analysing the adsorption of chitosan onto PET surface. Typical peaks that belongs to chitosan were detected onto PET plastic film surfaces.

References

1. Hoenich N. Cellulose for Medical Applications: Past, Present, and Future. *Bioresources*. 2006;1(2):270-80.
2. Kumar MNVR. A review of chitin and chitosan applications. *React Funct Polym*. 2000;46(1):1-27.
3. Lim SH, Hudson SM. Synthesis and antimicrobial activity of a water-soluble chitosan derivative with a fiber-reactive group. *Carbohydr Res*. 2004;339(2):313-9.
4. Simoncic B, Tomsic B. Structures of Novel Antimicrobial Agents for Textiles - A Review. *Text Res J*. 2010;80(16):1721-37.
5. Zhbakov RG, Firsov SP, Korolik EV, Petrov PT, Lapkovski M, Tsarenkov VM, Marchewka MK, Ratajczak H.. Vibrational spectra and the structure of medical biopolymers. *Journal of Molecular Structure* 2000;555: 85–96.

AN ANALYSIS OF SINGLE-PASS CONVENTIONAL SPINNING PROCESS

P. Piljek¹, Z. Keran¹ and M. Math¹

¹ University of Zagreb, Faculty of Mechanical Engineering and Naval Architecture,
Ivana Lucica 5, HR-10000 Zagreb, CROATIA

Keywords: Conventional spinning, Metal spinning, Single-pass, Forming force

Abstract. Conventional metal spinning is a complex flexible manufacturing process with high efficiency for small and single series of parts. Spinning also has a possibility of producing parts that could not be deep drawn. In this paper, single-pass conventional spinning process, with straight line roller trace, has been studied. Spinning has been taken as a rotational forming process that is not set out to change the wall thickness. Both, the blank and the formed product have roughly the same thickness. Flat disk has been formed by a spinning operation into a cylindrical shape. The used material was St14 steel. Theoretical and numerical analysis of metal spinning process has been discussed to investigate stressed state as well as forming force components. Finite Element (FE) simulation model was developed with the MSC MARC software. By comparing the forming force components of the experimental samples with the corresponding numerical results good agreements have been observed with the maximum error less than 6%, while analytical error was more significant.

Introduction

Spin forming, often called spinning, is process of metal forming into various seamless, axisymmetric shapes. During process, forming is done by a combination of rotational motion and force. The equipment for spin forming is based on lathe technology with minor modifications. Basic setup requires a blank, mandrel and a tool. Starting workpiece is commonly circular blank of a flat sheet, metal disc, which is rotated at high speeds together with a mandrel. Also, sheet preforms can be used as starting workpiece in order to reduce forming stresses.

During the process a blank is pressed against rotating mandrel with a rigid tool to form a shape of desired component. Tool is moved over mandrel from the centre of disc. Most commonly tools are various types of rollers controlled either manually or hydraulically. Typically, spinning is performed at room temperature. However, elevated temperature spinning is performed in case of components with thick section or alloys with low ductility.

Spinning is used for shapes which are difficult to form economically with other techniques. It can be used to cost-effectively produce single or small amount of components out of expensive materials or large quantities of components out of low cost materials. The range of components include: bases, baskets, basins and bowls; bottoms for tanks, hoppers and kettles; canopies, caps and canisters; housing for blowers, fans, filters and fly-wheels; ladles, nozzles, orifices and tank outlets; pails, pans and pontoons; cones, covers and cups; cylinders and drums; funnels and horns; domes hemispheres and shells; rings, spun tubing and seamless shapes; vents, venturis and fan wheels.

There are two distinct spinning methods, referred as conventional spinning or manual spinning and shear spinning or power spinning. In conventional spinning the resulting spun component will have a diameter smaller than a blank but will maintain a constant thickness, while in shear spinning roller not only bends the sheet against the mandrel, it also applies a downward force during movement resulting with stretching the material over mandrel. By doing so, the diameter of resulting spun component will remain equal, but the thickness of the component walls will be thinner. [1, 2]

This paper is dealing with single-pass conventional spinning process, so thickness of spun component remains constant during process. Furthermore, it gives comparison of results obtain from analytical and numerical approach with experimental data.

Conventional spinning process

Conventional spinning process is done by pressing tool against circular metal disc which is rotated using a lathe spinning machine. There are various types of tools used during process, from numerous types of simpler tools to rollers with different shapes. Conventional spinning is usually carried out with only one roller. However, in cases when a high strength metal is spun, an undesirable single side load is generated. In such cases, two rollers, which are placed diametrically over each other, need to be employed to balance the applied loading. During forming there is no significant change in component thickness, so conventional spinning is essentially a shaping technique.

Metal spinning can be executed with or without mandrel. The sheet preform is usually deformed over a mandrel with predetermined shape, but some simple shapes can be spun without it [3]. In most cases mandrel is a one-piece solid form with external shape same as component internal shape. For more complex parts, such as those with reentrant surfaces, multi-piece mandrel can be used. Because it does not experience much wear during forming, it can be made of wood or plastic. However, for large quantities of components or tight tolerances, metal mandrel is used. As the tool is applied locally on the workpiece, the total forming forces are reduced significantly compared to conventional press forming. This reduces the required load capacity and cost of the forming machine. Also, very simple tool design and usage of same tool for different parts production contributes to low process costs. In addition, spun component usually has a surface of sufficient quality so no additional machining is required and good mechanical characteristic of spun component can be achieved.

Conventional spinning is only economical for low volume production.

Analytical approach

Stress – strain state

Modelling of spinning process is similar to process of deep drawing. Main difference is related to local plastic deformation zone that is created under the roller. For analysing of stressed state, workpiece is divided into several different zones at which different schemes of stresses occur (Figure 1).

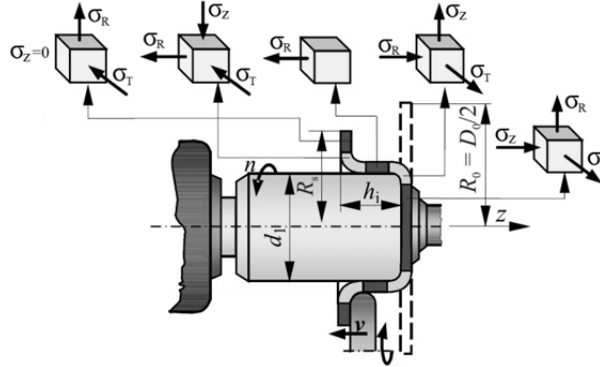


Figure 1: Different schemes of stress state [4]

During spinning process, blank is subjected to a combination of tension and compression. When the roller moves towards the edge of the blank, radial tensile as well as tangential compressive stresses are generated. The tensile stress produces a flow in the direction along the mandrel and causes thinning, which is balanced by the thickening effect due to the compressive stress. As a result of compressive stress, the material can be displaced towards the mandrel while maintaining almost constant thickness. Direction of the material flowing speed during deformation process is the same as the axial speed of pressed roller.

At element wreath flat stress state is assumed due to absence of normal stress ($\sigma_z = 0$). From equilibrium equation and plastic flowing condition we get differential equation [4, 5]

$$d\sigma_R = -\beta \cdot k_{sr} \cdot \frac{d\rho}{\rho} \quad (1)$$

where is:

β – Lode coefficient ($\beta = 1$ to $2/\sqrt{3}$),

k_{sr} – the average value of specific flow stress,

ρ – current coordinate of wreath radius.

Solving the equation for boundary conditions (absence of radial stress at the edge of blank) gives radial stressed component that incites plastic deformation at component wreath [4, 5]

$$\sigma_R = \beta \cdot k_{sr} \cdot \ln \frac{R_s}{\rho} \quad (2)$$

where R_s is current radius of the wreath.

Due to flat stress state at wreath, tangential stress is obtained from plastic flow condition

$$\sigma_T = \beta \cdot k_{sr} \cdot \left(1 - \ln \frac{R_s}{\rho}\right) \quad (3)$$

During conventional spinning process maximum axial stress is generated almost at the beginning of process when the roller-sheet contact is established [2], and it is defined with combination of plastic deformation, bending and friction [4]

$$\sigma_{z,max} = \left(1.1 \cdot k_{sr} \cdot \ln \frac{R_s}{r_1} + k_{sr} \cdot \frac{s}{2\rho_w + s}\right) \cdot e^{\mu\alpha} \quad (4)$$

where is:

r_1 – mandrel radius,

s – blank thickness,

ρ_w – roller roundness,

μ – coefficient of friction,

α – bending angle.

Radial stress component reaches a maximum at the end of process where the stress state is treated as flat because of absence of axial stress ($\sigma_z = 0$). Thereupon, equation for maximum radial stress can be obtain from plastic flow condition [4]

$$\sigma_{R,max} = \beta \cdot k_{sr} . \quad (5)$$

Accordingly simplified plane stress state is taken into account for tangential stress [4]

$$\sigma_{T,max} = \left(\frac{\sigma_z + \sigma_R}{2} \right) = \frac{1}{2} \cdot 1.15 \cdot k_{sr} \quad (6)$$

Tool forces

Tool forces in spinning are conventionally resolved into three mutually perpendicular components: radial (F_R), axial (F_Z) and tangential (F_T), as shown in Figure 2. Kobayashi et al. 1961 [5] calculated the tool force by assuming uniform roller contact pressure. Radial and axial forces are estimated from the projected contact areas. However, these components show weak agreement with the experiments. Due to difficulty in finding the exact size of the three-dimensional contact area, empirical equations given by Jurkovic et al. [4] are used where geometry is defined by three process parameters; thickness, radius of roller and feed ratio.

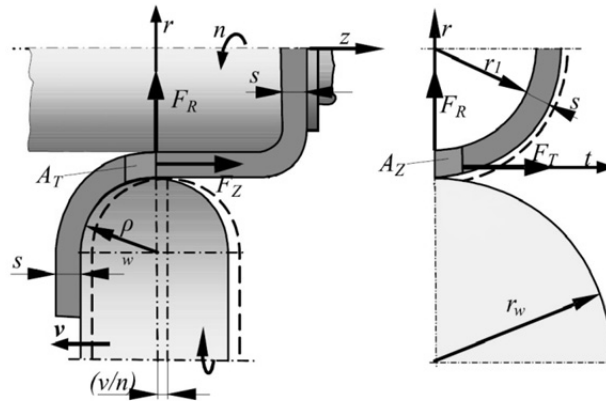


Figure 2: Tool forces in conventional spinning process

The maximum force components are calculated as:

$$\begin{aligned} F_{Z,max} &= A_Z \cdot \sigma_{Z,max} , \\ F_{R,max} &= A_R \cdot \sigma_{R,max} , \\ F_{T,max} &= A_T \cdot \sigma_{T,max} . \end{aligned} \quad (7)$$

Where contact surfaces are given by expressions

$$\begin{aligned} A_Z &= 2 \cdot s \cdot \sqrt{d_w \cdot \left(\frac{v}{n}\right)} , \\ A_R &= 2 \cdot \left(\frac{v}{n}\right) \cdot \sqrt{d_w \cdot \left(\frac{v}{n}\right)} , \\ A_T &= \frac{1}{2} \cdot s \cdot \sqrt{2 \cdot \rho_w \cdot \left(\frac{v}{n}\right)} . \end{aligned} \quad (8)$$

where is:

d_w – roller diameter,

$\frac{v}{n}$ – roller feed ratio.

Results

Parameters used in calculations are extracted from [4] ($R_0 = 50$ mm, $r_1 = 30$ mm, $k_{sr} = 215$ MPa, $\mu = 0.1$, $d_w = 50$ mm, $\rho_w = 5$ mm, $v = 100$ mm/min, $n = 450$ rpm). By analytical analysis of tool forces following results are obtained:

$$F_{Z,max} = 414 \text{ N} ,$$

$$F_{R,max} = 366 \text{ N} ,$$

$$F_{T,max} = 92 \text{ N} .$$

Analytical results are compared to experimental results of one-pass conventional spinning given by Jurkovic et al. [4]. Percentage differences are shown in following table.

Table 1: Analytical and experimental result comparison

	Analytical	Experimental	Δ
$F_{z,max}$	414 N	395 N	4.8 %
$F_{R,max}$	366 N	358 N	2.2 %
$F_{T,max}$	92 N	74 N	24.3 %

Numerical analysis

Recent studies are most commonly focused on shear spinning process, while one-pass conventional spinning have not had that much attention.

MSC Mentat Marc was used to simulate the spinning process. Because of the symmetrical characteristic of component simplified finite element model was created using 2-D element type. Corresponding geometry and dimensions are shown in Figure 3.

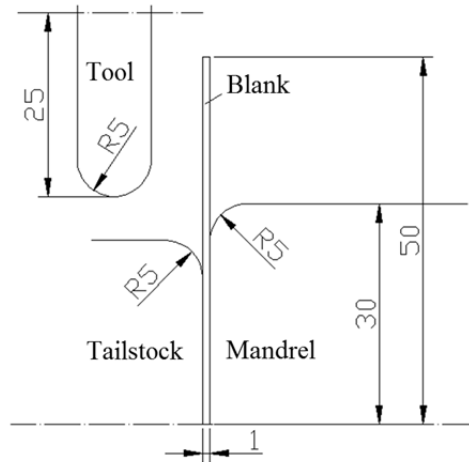


Figure 3: Geometries and dimensions of the model

Parameters used in simulation are given in following table.

Table 2: Initial numerical parameters

s	1 mm	blank thickness
D_0	100 mm	initial blank diameter
d_1	60 mm	mandrel diameter
d_w	50 mm	roller diameter
ρ_w	5 mm	roller roundness
v/n	0.222 mm/rev	roller feed ratio
μ	0.1	coefficient of friction

The flow curve for material St14 and tool feed rate are given with following diagrams.

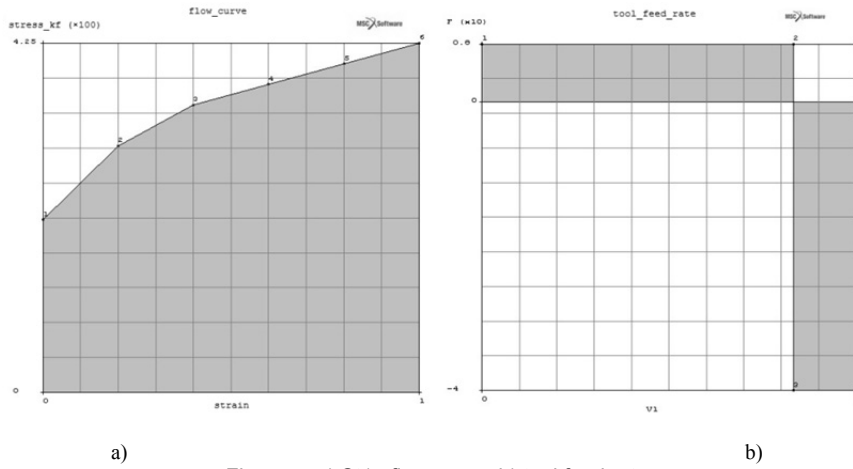


Figure 4: a) St14 flow curve; b) tool feed rate

Differences between numerical and experimental data are around 5.8 %. Distribution of resulting equivalent stress is given in Figure 5.

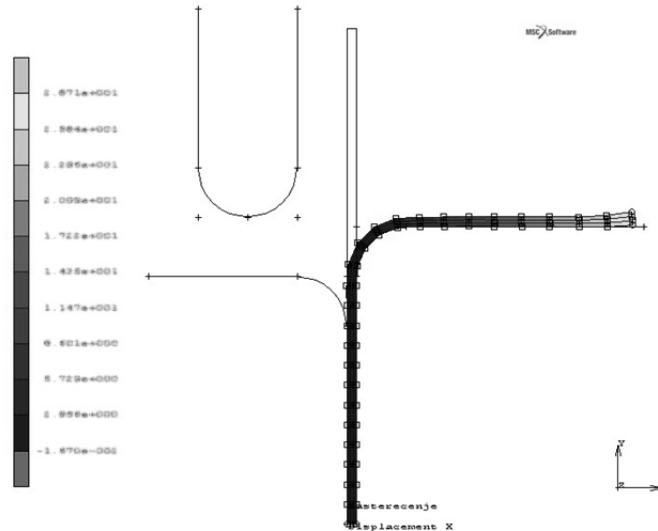


Figure 5: Equivalent Von Mises Stress

Conclusion

For one-pass conventional spinning, significant deviations of tool forces are noticed comparing analytical results with experimental while corresponding numerical analysis shown good agreements. Observed disagreements in analytical approach are consequence of many nonlinear influence factors during process which are impossible to cover with simple analytical model. Therefore, assumptions are used such as uniform contact pressure, which additionally increases the error of the model. Due to assumptions and complicated contact conditions between roller and mandrel, finding the correct coefficient of friction and corresponding contact geometry is quite difficult to accomplish. Further work is required in order to predict tool forces with simple analytical model suitable for direct usage in the spinning industry.

References

- [1] Wong, C. C., Dean, T. A., Lin, J.: A review of spinning, shear forming and flow forming processes, *International Journal of Machine Tools and Manufacture*, 43, 1419-1435, 2003.
- [2] Music, O., Allwood, J. M., Kawai, K.: A review of the mechanics of metal spinning, *Journal of Materials Processing Technology*, 210, 3-23, 2010.
- [3] Kawai, K., Yang, L. N., Kudo, H.: A flexible shear spinning of axi-symmetrical shells with a general-purpose mandrel, *Journal of Materials Processing Technology*, 192-193, 13-17, 2007.
- [4] Jurkovic, M., Jurkovic, Z. & Mahmic, M.: An analysis and modelling of spinning process without wall-thickness reduction, *METABK*, 45, 307-312, 2006.
- [5] Math, M.: Uvod u tehnologiju oblikovanja deformiranjem, *Fakultet strojarstva i brodogradnje, Sveuciliste u Zagrebu, Zagreb*, 2003.
- [6] Kobayashi, S., Hall, I. K., Thomsen, E. G.: A theory of shear spinning of cones, *Journal of Engineering for Industry, ASME (Series B)* 83, 485-495, 1961.



International Conference on Innovative Technologies, IN-TECH 2012,
Rijeka, 26. - 28.09.2012



NUMERICAL MODELING OF PRESSURE VESSEL UNDER CREEP REGIME

D. Pesa¹, and D. Lanc¹

¹ Faculty of Engineering, University of Rijeka,
Vukovarska 58, Rijeka, Croatia

Keywords: Creep, Pressure Vessel, Finite Elements, Numerical Modeling

Abstract: Under special conditions behaviour of some materials is time-dependent and is called viscoplastic behaviour. One of such time effects is creep and is defined as time dependent and permanent deformation when material is subjected to a constant load or stress. Circumstances under which the creep manifests suppose exposition to long period of load at high temperature regime. Creep is an undesirable phenomenon and often the limiting factor in the lifetime of the structure. This paper deals with finite element simulation of creep phenomenon in the pressure vessel. Simulation is carried out for two different kind of materials and for two different creep regime each.

Introduction

Pressure vessels belong to the energy applications which may involve viscoplastic conditions under their multiaxial stress state. The design specifications will dictate a limiting design strain that are of interest for design life. According to the specific and very complex material behaviour under high temperature environment, much time and effort has been expended to describe and predict creep failure.

At elevated temperatures the life of the structure member may be severely limited even for loads less than design load. Namely, at such conditions inelastic strain may be produced in the material that increases with time.[1,2]

Hence, the material is said to creep. This situation will occur in any metal subjected to a sustained load at a temperature slightly above its recrystallization temperature. Service applications, such as pressure vessels which operate under a multiaxial state of stress may be involved in mentioned conditions

However, in design procedure analytical solutions are not efficient while long-time creep tests are very expensive. Because of the complex material behaviour under special environment conditions as well as geometrical modelling in present time according to high computer performances and possibilities of numerical modelling, finite element method is used.

Therefore, the presented paper deals with the finite element modelling of viscoplastic material behaviour. On the basis of this numerical modelling as a very useful technique, the prediction of material behaviour in complex environment conditions can be obtained. The main goal is to determine the lifetime of a pressure vessel made of two different materials at two different temperatures.

Creep modeling

Typical creep curve of strain versus time at constant stress and constant temperature is shown in Fig. 1. [3,4]

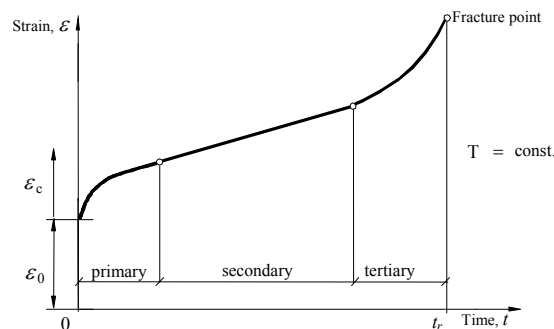


Fig. 1. Typical creep curve at constant stress and constant temperature

Upon application of the load there is an instantaneous deformation ϵ_0 and depending on stress level and temperature may include both elastic and plastic parts. Primary creep occurs first with a characteristic of continuously decreasing creep rate. For secondary creep stage the creep rate is constant. During the tertiary creep, the creep rate increase and this phase finishes with rupture of the structure. Secondary creep phase is of the greatest importance in engineering practise because it is the phase of the longest duration and lifetime of the structures are mostly shorter than this phase.

Creep material behaviour can be modeled according to Eq. (1),

$${}^2\varepsilon_{ij}^c = {}^2\varepsilon_{ij}^c - {}^1\varepsilon_{ij}^c \quad (1)$$

Creep deformation increment can be calculated as in Eq. (2):

$$\Delta\varepsilon_{ij}^c = {}^1k {}^1S_{ij} \quad (2)$$

while ${}^1S_{ij}$ is deviatoric stress tensor in configuration C_1 and ε_{ij}^c denotes creep deformation tensor. Factor k is defined as:

$${}^1k = 1.5 \left(\frac{{}^1\bar{\varepsilon}^c}{{}^1\bar{\sigma}} \right) \Delta t \quad (3)$$

with $\bar{\varepsilon}^c$ and $\bar{\sigma}$ as effective creep strain rate and effective stress. In the case of creep configurations C_1 and C_2 are real time configurations, and time increment Δt represents the real time passed during the element movement from configuration C_1 to configuration C_2 . Effective creep strain rate $\bar{\varepsilon}^c$ from Eq. (3) can be obtained according to Norton power creep law as in Eq (4),

$$\bar{\varepsilon}^c = K \bar{\sigma}^n \quad (4)$$

where K and n are Norton material constants.

Modeling of the pressure vessel

Fig 2. shows the dimensions of the analyzed pressure vessel. The pressure vessel contains compressed gas and should be designed according to the norms HRN M.E2.251, M.E2.252, M.E2.253, M.E2.254, M.E2.256, M.E0.021 [5]. The head wall has a torispherical shape and no additional reinforcements of the head wall are necessary.

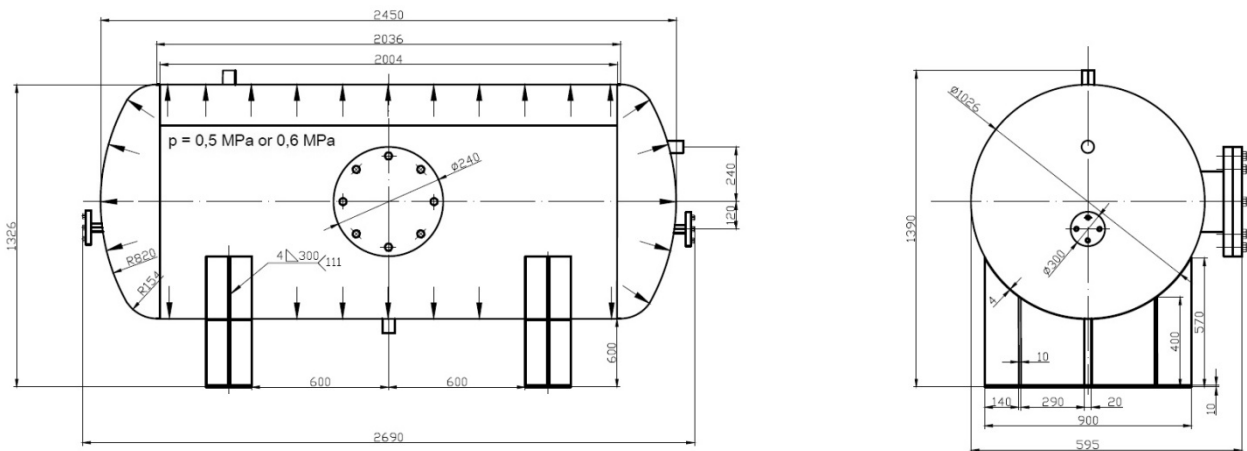


Fig. 2. Dimensions of the pressure vessel

The geometry of the pressure vessel was modeled in Catia V5R19. The model was simplified in the way that unimportant parts like flanges, pipes or supporting legs which don't undergo significant deformation were excluded. The obtained surface geometry was imported into FEMAP with NX Nastran software and discretized by the triangular plate elements. The model was meshed with 19342 elements.

Boundary conditions for the model were radial displacements obtained at relevant positions by global analysis. For further analysis, maximal radial displacement on node 6457 was selected, as shown in Fig. 3. The given boundary condition is that maximal radial displacement on the relevant node 6457 doesn't exceed 1mm after 2500 hours (approximately 100 day) under given operating conditions like pressure and temperature.

The pressure vessels was modeled with two wall thickness ($t = 5\text{ mm}$ and $t = 6\text{ mm}$) and two different pressure each ($p = 0,5\text{ MPa}$ and $p = 0,6\text{ MPa}$). The thickness of the torispheric head is $t = 10\text{ mm}$. Beside that, two different composition carbon are use steels (material A and material B) and for first carbon steel two different temperatures are used. Norton power creep law is adopted with following constants [6]

- 1) material A - carbon steel (0.15 C, 0.50 Mn, 0.23 Si) at 538 °C: $n = 3.05$, $K = 0,12 \cdot 10^{-13} [10\text{ mm}^2/\text{N}]^n \cdot \text{h}^{-1}$;
- 2) material A - carbon steel (0.15 C, 0.50 Mn, 0.23 Si) at 649 °C: $n = 2.85$, $K = 0,16 \cdot 10^{-10} [10\text{ mm}^2/\text{N}]^n \cdot \text{h}^{-1}$;
- 3) material B - carbon steel (0.43 C, 0.68 Mn, 0.20 Si) at 649 °C: $n = 1.70$, $K = 0,12 \cdot 10^{-8} [10\text{ mm}^2/\text{N}]^n \cdot \text{h}^{-1}$.

Analysis were held for three different cases:

- 1) material A at 649 °C with wall thicknesses of $t = 5 \text{ mm}$ and $t = 6 \text{ mm}$ and pressures $p = 0,5 \text{ MPa}$ and $p = 0,6 \text{ MPa}$ each;
- 2) material A and B at 649 °C with wall thickness of $t = 6 \text{ mm}$ and pressure $p = 0,6 \text{ MPa}$;
- 3) material A at 538 °C and 649°C with wall thickness of $t = 6 \text{ mm}$ and pressure $p = 0,6 \text{ MPa}$;

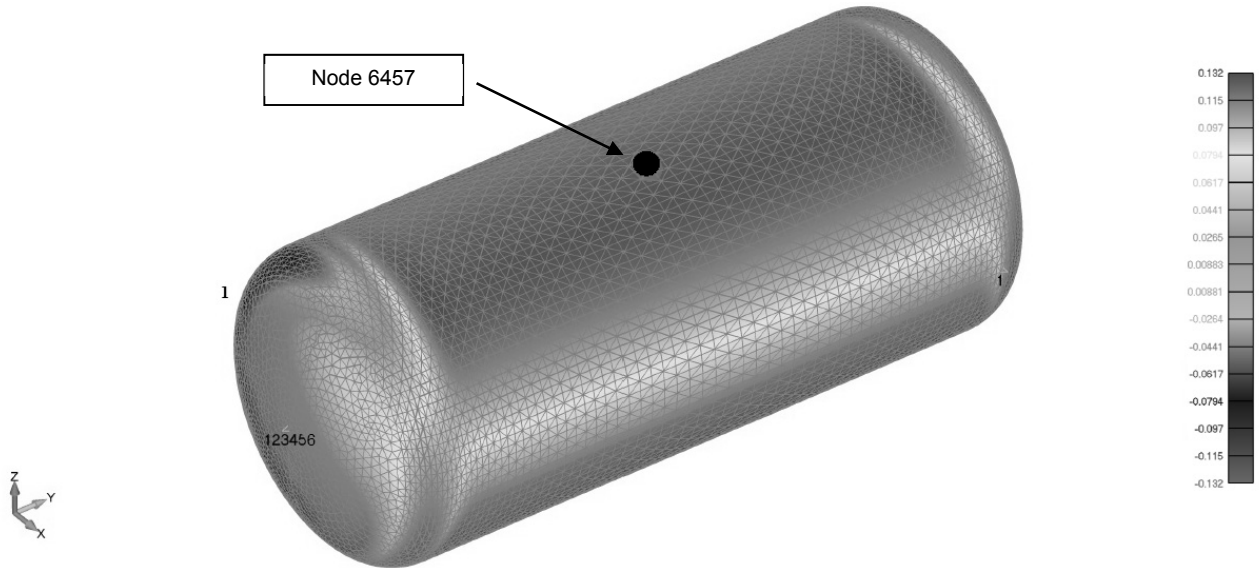


Fig. 3. Finite element model of the pressure vessel

Upon creation of the model, the NX Nastran solver was used for calculations. The analysis of a designed model should determine the minimal allowable wall thickness and maximal allowable operating pressure for safe operating at elevated temperatures.

Results

The first analysis was held for material A at 649 °C with wall thicknesses, $t = 5 \text{ mm}$ and $t = 6 \text{ mm}$ and pressures, $p = 0,5 \text{ MPa}$ and $p = 0,6 \text{ MPa}$ each. The obtained results are given in Fig. 4. The results shows that the allowed maximal displacement of 1 mm will be exceed only for the combination of wall thickness, $t = 5 \text{ mm}$ and pressure $p = 0,6 \text{ MPa}$. This will happen after approximately 1600 hours. All the other cases don't exceed the boundary condition.

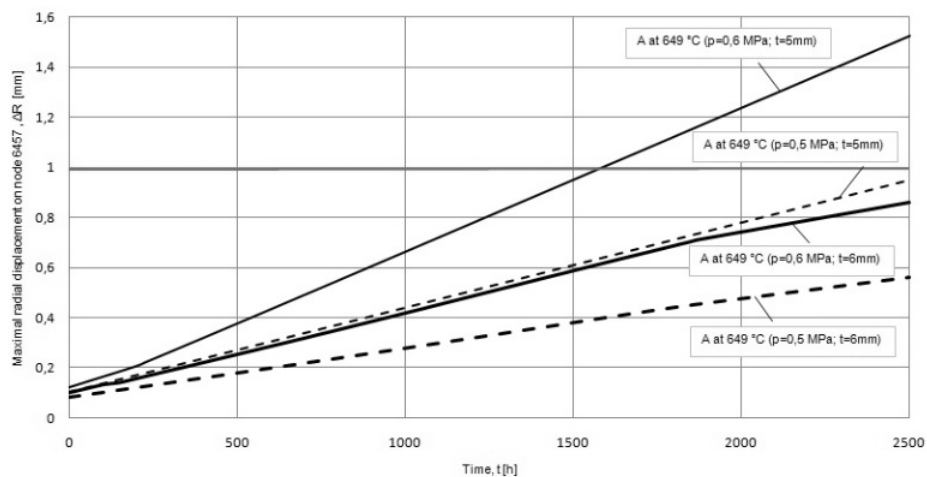


Fig. 4. Creep curves for material A under 4 different operating conditions

The second analysis was held for material A and B at 649 °C with wall thickness, $t = 6 \text{ mm}$ and pressure $p = 0,6 \text{ MPa}$. Fig. 5. (left) shows very similar results for these two carbon steels at the same temperatures. Material B is slightly more resistant to creep and shows smaller displacement after 2500 h. Hence, both materials won't exceed the boundary condition and the maximal radial displacement is smaller than 1 mm after 2500 hours under given operating conditions.

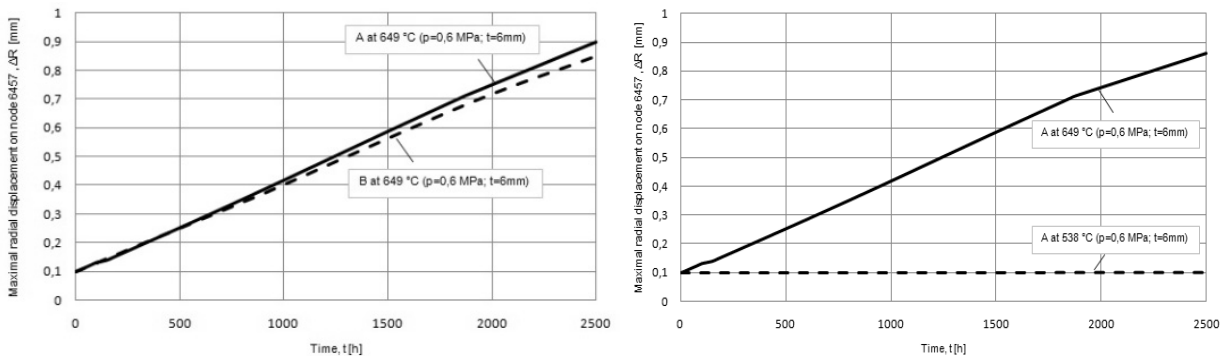


Fig. 5. Creep curves for material A and B at same temperature (left); creep curves for material A at two different temperatures (right)

The third analysis was held for material A at temperatures of 538 °C and 649 °C. The creep curves in Fig. 5. (right) show negligible increase of displacement at temperature of 538 °C. Significant displacements at these temperature occur after 25000 hours. Displacement growth rate is much faster at higher temperatures, which is visible for the same material at 649 °C. Even though, the maximal allowed displacement of 1 mm after 2500 hours is not exceeded.

Conclusion

This paper presents a numerical procedure of significant importance in special design field. In this case, a procedure for numerical analysis of pressure vessels under creep regime was presented. Presented procedures can be easily adopted for the analysis of different pressure vessel geometries or operating parameters.

Many conclusions can be obtained from the given results. For example, relatively small changes in temperature can significantly change creep resistance. Furthermore, every single material (in this case carbon steel) acts different under creep regime. This is the reasons why various experiments are held to determine creep law parameters like Norton power law parameters presented in this paper. The measured parameters enables an incorporation of material properties with creep power laws in a numerical model and a precise prediction of structures lifetime under creep regime.

Acknowledgment

The research presented in this paper was made possible by the financial support of the Ministry of Science, Education and Sports of the Republic of Croatia, under the project No.069-0691736-1737 and No.069-0691736-1731, and also by the grant of "Zaklada Sveucilista u Rijeci".

References

- [1] N.M. Beljajev: *Soprotivljenje materijalov*, (Fitzmatgiz, Moscow, 1959).
- [2] J. Brnić., D. Lanc., G. Turkalj, M. Čanađija.: Viscoplastic analysis of energetic equipment members using finite element method, *Zbornik radova 5. međunarodnog simpozija Dijagnostika električnih strojeva, transformatora i uređaja & Kvaliteta električne energije EEDEEQ 2000*, Rovinj, 2.-3. listopada 2000., pp. 3-6.
- [3] W. N. Findley, J. S. Lai, K. Onaran: *Creep and Relaxation of Nonlinear Viscoelastic Materials*, (Dover Publications, New York, 1989).
- [4] R. K. Penny, D. L. Marriott: *Design for Creep*, (Chapman & Hall, London, 1995).
- [5] Norme/Norms: HRN (JUS) M.E2.250-256 & HRN(JUS) M.E0.021, Hrvatski zavod za norme, Zagreb.
- [6] J. Brnić: *Elastomechanics and Plastomechanics*, (Školska knjiga, Zagreb, 1996).

FEM SIMULATION OF STRUCTURAL BEHAVIOUR OF LAMINATED COMPOSITE PLATE

I. Sterpin¹, and D. Lanc²

¹ TVD consulting, Žegoti bb, 51215 Kastav, Croatia

² Department of Engineering Mechanics, Vukovarska 58, 51000 Rijeka, Croatia

Keywords: Composite plate, FEM simulation

Abstract. This paper present finite element simulation of laminated composite plate under extensional loading conditions. Simulation is carried out using composite plate finite element. The structural model includes extensional-bending coupling and the effect of torsional-bending coupling. In the numerical analysis a square composite plate is assumed to experience an extensional loading and different ply orientation. The obtained results for deformed shapes are mutually compared.

Introduction

Designers have more freedom when they using composite material than other regular materials, because with composites can easily satisfy they mandatory assignments, like using the right fiber or flakes and match them with a choice of different ceramics, resins or metals. The importance of fibre reinforced composite related products cannot be denied in today's world. Their high strength and stiffness to weight ratios results in weight saving, so they can replace the traditional materials in many industries such as automotive, aerospace, marine and architectural structures [1,2]. The structural behaviours of fibre composite laminates varies with considered combination of laminate parameters such as sequence of lamina angels, number of layers, etc.

Macromechanics analysis of laminate properties

It is always essential to have a good understanding of the basic equations ruling the laminate performance. The basic laminate equations are presented in the following items. Stress-strain relationships for composites are defined below:

$$\sigma_{ij} = Q_{ij} \cdot \varepsilon_{ij} \quad (1)$$

where Q_{ij} is the lamina stiffness. The stiffness matrix for plane stress is called reduced stiffness matrix, where, $ij=1,2$ and 6:

$$[Q] = \begin{bmatrix} Q_{11} & Q_{12} & Q_{16} \\ Q_{21} & Q_{22} & Q_{26} \\ Q_{16} & Q_{26} & Q_{66} \end{bmatrix} = \begin{bmatrix} \frac{E}{1-\nu} & \frac{\nu_{12}E_{22}}{1-\nu_{12}\nu_{21}} & 0 \\ \frac{\nu_{12}E_{11}}{1-\nu_{12}\nu_{21}} & \frac{E_{22}}{1-\nu_{12}\nu_{21}} & 0 \\ 0 & 0 & G_{12} \end{bmatrix} \quad (2)$$

$Q_{16} = Q_{61} = Q_{26} = Q_{62} = 0$, for pricipal fiber directions.

Lamina Stress-Strain relationships

A laminate is composed of unidirectionally reinforced lamina oriented in various directions. The elastic stress-strain relations of the lamina are expressed in matrix form. With x_1 in the fiber direction, x_2 transverse to the fibers in the plane of the lamina, and x_3 normal to the plane of the lamina, these material properties define the lamina properties [3, 4]:

$$\begin{aligned} E_1 = E_L^* & & \nu_{12} = \nu_L^* \\ E_1 = E_3 & = E_T^* & \nu_{23} = \nu_T^* \\ G_{12} = G_L^* & & G_{23} = G_T^* \end{aligned} \quad (3)$$

Where E represents Young's modulus of elasticity, ν is Poisson's ratio, G is shear modulus, L is longitudinal, T is transverse, and $*$ represents the effective properties. The lamina, at this point, are treated as homogeneous, effective, transversely isotropic materials, and the strains aren't written with overbars.

Taking into account symmetry relations:

$$\frac{\nu_{21}}{E_2} = \frac{\nu_{12}}{E_1} = \frac{\nu_{31}}{E_3} = \frac{\nu_{13}}{E_1} = \frac{\nu_{23}}{E_2} = \frac{\nu_{32}}{E_3} \quad (4)$$

follows:

$$\begin{Bmatrix} \varepsilon_{11} \\ \varepsilon_{22} \\ \varepsilon_{33} \\ 2\varepsilon_{23} \\ 2\varepsilon_{13} \\ 2\varepsilon_{12} \end{Bmatrix} = \begin{bmatrix} \frac{1}{E_1} & \frac{-\nu_{12}}{E_1} & \frac{-\nu_{13}}{E_1} & 0 & 0 & 0 \\ \frac{-\nu_{12}}{E_1} & \frac{1}{E_2} & \frac{-\nu_{23}}{E_2} & 0 & 0 & 0 \\ \frac{-\nu_{13}}{E_1} & \frac{-\nu_{23}}{E_2} & \frac{1}{E_3} & 0 & 0 & 0 \\ 0 & 0 & 0 & \frac{1}{G_{23}} & 0 & 0 \\ 0 & 0 & 0 & 0 & \frac{1}{G_{12}} & 0 \\ 0 & 0 & 0 & 0 & 0 & \frac{1}{G_{12}} \end{bmatrix} \begin{Bmatrix} \sigma_{11} \\ \sigma_{22} \\ \sigma_{33} \\ \sigma_{23} \\ \sigma_{13} \\ \sigma_{12} \end{Bmatrix} \quad (5)$$

It is best in the analysis of laminates to use engineering shear strains rather than tensor shear strains. For plane stress state of lamina it is: $\sigma_{13} = \sigma_{23} = \sigma_{33} = 0$ so Eq 5. reduces to:

$$\begin{Bmatrix} \varepsilon_{11} \\ \varepsilon_{22} \\ 2\varepsilon_{12} \end{Bmatrix} = \begin{bmatrix} \frac{1}{E_1} & \frac{-\nu_{12}}{E_1} & 0 \\ \frac{-\nu_{12}}{E_1} & \frac{1}{E_2} & 0 \\ 0 & 0 & \frac{1}{G_{12}} \end{bmatrix} \begin{Bmatrix} \sigma_{11} \\ \sigma_{22} \\ \sigma_{12} \end{Bmatrix} \quad (6)$$

and thus the state of stress and strain is determined.

The reduced stiffness and compliance matrices relate stresses and strains in the principal material directions of the material. To define the material response in directions other than these material coordinates, transformation relations must be developed for the material stiffnesses. In Fig. 1, two sets of coordinate systems are shown. The 1-2 coordinate system corresponds to the principal material directions for a lamina, while the x-y coordinates are arbitrary and are related to the 1-2 coordinates through a rotation about the axis out of the plane of the figure. The angle, θ , is defined as the rotation from the arbitrary x-y system to the material 1-2 system (θ is positive for a counterclockwise rotation)

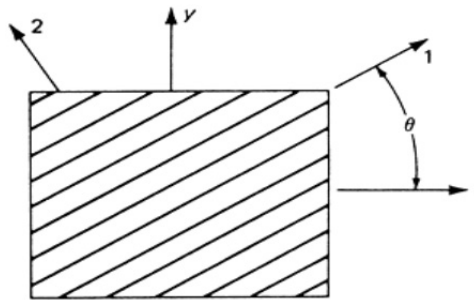


Fig. 1 Coordinate systems; 1, 2, principal material coordinates; x, y, laminate or arbitrary coordinates

The transformation of stresses from the 1-2 system to the x-y system follows the rules for transformation of tensor components. Thus:

$$\begin{Bmatrix} \sigma_{xx} \\ \sigma_{yy} \\ \sigma_{xy} \end{Bmatrix} = \begin{bmatrix} m^2 & n^2 & -2mn \\ n^2 & m^2 & 2mn \\ mn & -mn & m^2 - n^2 \end{bmatrix} \begin{Bmatrix} \sigma_{11} \\ \sigma_{22} \\ \sigma_{12} \end{Bmatrix} \quad (7)$$

where $m = \cos \theta$ and $n = \sin \theta$. In these relations, the subscripts x and y are used to refer to the laminate coordinate system.

Stress and moment resultants

Usually we use stress and moment resultants in plate theory, to develop a general load, strain, curvature relationship. Fig. 2 show plate forces N and moments M .

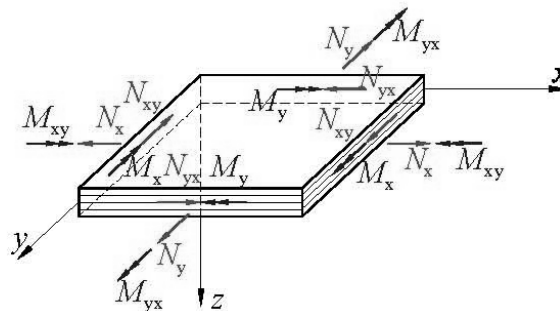


Fig. 2 Plate forces and moments

Matrix form relation that explains plate behaviour is:

$$\begin{Bmatrix} N_x \\ N_y \\ N_{xy} \\ M_x \\ M_y \\ M_{xy} \end{Bmatrix} = \begin{bmatrix} A_{11} & A_{12} & A_{16} & B_{11} & B_{12} & B_{16} \\ A_{21} & A_{22} & A_{26} & B_{21} & B_{22} & B_{26} \\ A_{61} & A_{62} & A_{66} & B_{61} & B_{62} & B_{66} \\ B_{11} & B_{12} & B_{16} & D_{11} & D_{12} & D_{16} \\ B_{21} & B_{22} & B_{26} & D_{21} & D_{22} & D_{26} \\ B_{61} & B_{62} & B_{66} & D_{61} & D_{62} & D_{66} \end{bmatrix} \begin{Bmatrix} \varepsilon_x \\ \varepsilon_y \\ \varepsilon_{xy} \\ \kappa_x \\ \kappa_y \\ \kappa_{xy} \end{Bmatrix} \quad (8)$$

A, B and D terms make up the laminate stiffness matrix, ε is the mid-plane strains and κ is curvatures. The terms of the stiffness matrix are:

$$A_{ij} = \sum_{i=1}^N (\bar{Q}_{ij}) (z_i - z_{(i-1)}); \quad B_{ij} = \frac{1}{2} \sum_{i=1}^N (\bar{Q}_{ij}) (z_i^2 - z_{(i-1)}^2); \quad D_{ij} = \frac{1}{3} \sum_{i=1}^N (\bar{Q}_{ij}) (z_i^3 - z_{(i-1)}^3) \quad (9)$$

so called: *A* - extensional stiffness, *B* - coupling stiffness and *D* – bending stiffness [3, 5].

In expressions above $\bar{Q}_{ij} = Q_{ij}$ rotated into material coordinates from principal coordinate directions.

The differences in *z* represent individual ply thicknesses, as seen in Fig. 3.

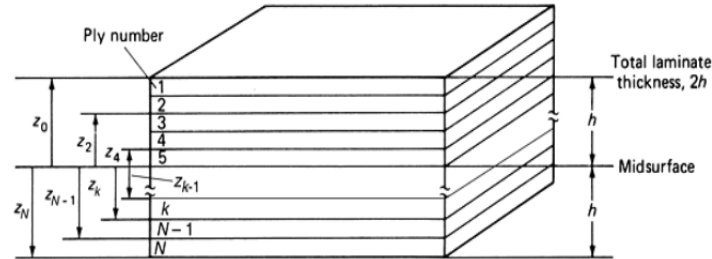


Fig. 3 Laminate construction

K is the total number of plies, z_i is defined in fig.1 and superscript *i* denotes a property of the *i*-th ply. $z_i - z_{(i-1)}$ is equal to the ply thickness. Coupling stiffness matrix *B* relate bending strains with normal stress, twisting strains to normal stresses and also shear strains to bending stresses [2, 6]. If the laminate is symmetric, then the B_{ij} terms will be the same for each mirrored ply above and below the midplane, with the exception of sign of the $(h_k + h_{k-1})/2$ term being negative if it is below the midplane (-*z*) and positive if it is above the midplane (+*z*). Thus, when summed, the result will be zero for all B_{ij} .

Example of analysis of laminate plate

In this section is showed how laminate plate is behave upon extensional loading over the plate edge. Three diferent stacking sequences of ply orientations are considered $[0/90]_s$, $[0/90/0/90]$ and $[45/0/45/0]$. Laminate plates are from carbon/epoxy material with material moduli: $E_1 = 1.55 \times 10^{11} \text{ Pa}$, $E_2 = 1.21 \times 10^{10} \text{ Pa}$, $\nu_{12} = 0.248$, $G_{12} = 4.4 \times 10^9$. Dimensions are 1000 x 1000 mm with overall thickness of 0.5mm. Material is observed as orthotropic and during analysis is used 2d orthotropic elements. Due to the simetry only one half of laminate is modeled. There is no restrains except in the middle, to prevent displacement of laminate plate as a rigid body during analysis.

Figures below show the plate deformed shapes for some laminate cases.

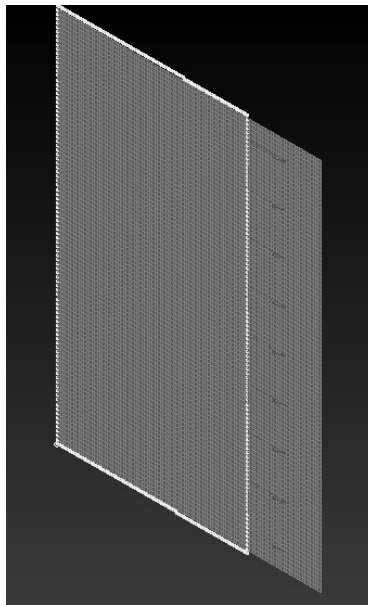


Fig. 4 Deformed shape for $[0/90]_s$ laminate plate

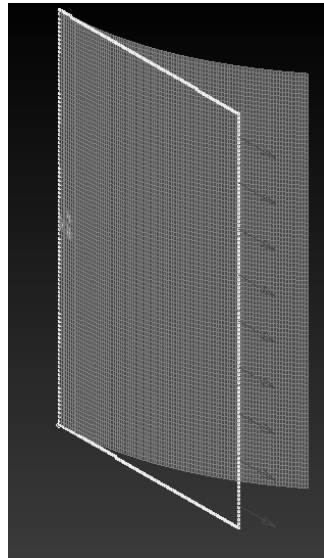


Fig 5. Deformed shape for [0/90/0/90] laminate plate

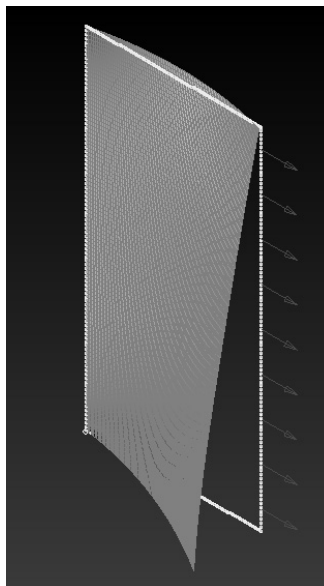


Fig 6. Deformed shape for [45/0/45/0] laminate plate

Conclusion

The paper presents the influence of laminate layer distribution on the deformation of the laminate plate exposed to extensional load. Deformations obtained for the different orientation of laminate layers were compared with the panel deformations of isotropic material. From the previous figures is clearly seen an deformed shape of laminate plate during activity of different loading. Through the curvatures of deformed edges of laminated plates for some cases of ply orientation it is clearly discernible extensional-bending coupling as well as shear-bending coupling as it was expected by laminate theory exposed in the previous section. Such a often unwanted deformation like that can be avoid by proper arrangement of layer orientation as shown in the case of symmetric laminate.

Acknowledgment

The research presented in this paper was made possible by the financial support of the Ministry of Science, Education and Sports of the Republic of Croatia, under the project No.069-0691736-1737 and No.069-0691736-1731.

References

- [1] M.M. Kaminiski: *Computational Mechanics of Composite Materials*, (Springer, London, 2002).
- [2] R. M. Jones: *Mechanics of composite materials*, (Taylor & Francis, New York, 1999).
- [3] J.N. Reddy: *Mechanics of laminated composite plates and shells, Theory and Analysis*, (CRC Press, Boca Raton, 1997).
- [4] D. Gay, S.V. Hoa, S. W. Tsai: *Composite materials (design and applications)*, (CRC Press, Boca Raton, 2003).
- [5] V.V. Vasiliev & E.I. Morozov: *Mechanics and Analysis of Composite Materials*, (Elsevier, Kidlington, 2001).
- [6] K. Kaw: *Mechanics of composite materials*, (Taylor & Francis, London, 2006).



OVERVIEW OF SEARCH-BASED OPTIMIZATION ALGORITHMS USED IN SOFTWARE ENGINEERING

G. Mauša¹, T. Galinac Grbac¹, B. Dalbelo Bašić²

¹ Goran Mauša, University of Rijeka, Faculty of Engineering, Vukovarska 58, HR-51000 Rijeka, Croatia

¹ Tihana Galinac Grbac, University of Rijeka, Faculty of Engineering, Vukovarska 58, HR-51000 Rijeka, Croatia

² Bojana Dalbelo Bašić, University of Zagreb, Faculty of Electrical Engineering and Computing, Unska 3, HR-10000 Zagreb, Croatia

Keywords: software engineering, optimization, algorithms

Abstract. Search-based software engineering is a novel and an emerging area of software engineering. It consists of search-based optimization algorithms used in various problem solving applications. Although search-based software engineering is becoming used in almost every area of software engineering, there are still areas that exploit its advantages less often than others. This paper presents how to use the search-based software engineering algorithms and which problem domains can they be used upon. It also explores a potential scope of further research within the area itself.

Introduction

Usage of search-based optimization algorithms in software engineering is an emerging and separate area of software engineering, called the search-based software engineering (SBSE). It is present in all sorts of optimization or multi-objective problems and every study indicates the advantages of solving a problem with such algorithms [1]. Many software engineering problems have too many possible solutions to a problem in their search space for the exhaustive search to finish in reasonable time. Sometimes it is sufficient to find one optimal solution or a "near optimal" solution to a problem [2]. In both cases, search-based optimization algorithms, often referred to as heuristic algorithms, may find its use in efficiently solving a problem or offering an insight into the range of possible solutions.

This paper presents an overview of current research in search-based software engineering and explores the potential scope of further research in the area. The next section describes the heuristic algorithms, along with requirements for their usage, general steps that are common to every algorithm, division of algorithms and the most often used ones. The following section presents a scope of some of the current research in the search-based software engineering area and the final section gives the conclusion.

Heuristic algorithms

Heuristic algorithms are a large group of search-based optimization algorithms. They originate from the desire to speed up the process of exhaustive search, which are too slow when dealing with problems with wide range of possible solutions. The simplest definition which presents the essence of heuristic algorithms is "proceeding by trial and error", found in Oxford Reference Dictionary. Every heuristic algorithm employs some degree of randomness into the optimization procedure and skips a great deal of possible solutions in its search for an optimal one [3].

Requirements

There are two key requirements for using search-based optimization algorithms: search space and fitness function. The search space can be defined as n -dimensional space where an object of optimization can be found, where n represents the number of variable parameters that define the object. The larger the search space is, the greater is the need for search-based optimization algorithm usage. The fitness function is a quantitative measure of the object's quality. It is the basis for comparison of different variations of the object, i.e. the candidate solutions we examine during optimization and it leads the search to an optimal or near optimal solution. The fitness function shows great flexibility, because it is defined according to the problem one is trying to analyze. This is the reason why search-based algorithms are applicable in various problem domains, covering all parts of software product life cycle.

General procedure

There are four general steps common to any heuristic algorithm, presented in figure 1. The initialization is the first phase of each heuristic algorithm and it is the only one that occurs without repeating. Most often, it involves random choice of initial candidate solution. Depending on the algorithm, it may be a single solution or a set of solutions. After initializing the iterative search for an optimal solution, the iterative search procedure may begin. First, the quality of a candidate solution needs to be checked and the fitness function, a key factor of any heuristic algorithm, comes into place. The modification of the candidate solution with the goal to find an optimal one is the second step of iterative search. Usually, the modification phase slightly changes the previously selected candidate solution and looks for neighboring solutions in the search space. Slightly changing the candidate solution means incrementing or decrementing the values of parameters that describe that candidate solution. The decision is the fourth step of the whole process, but the third step of iterative search process and it depends on the algorithm we choose to implement.

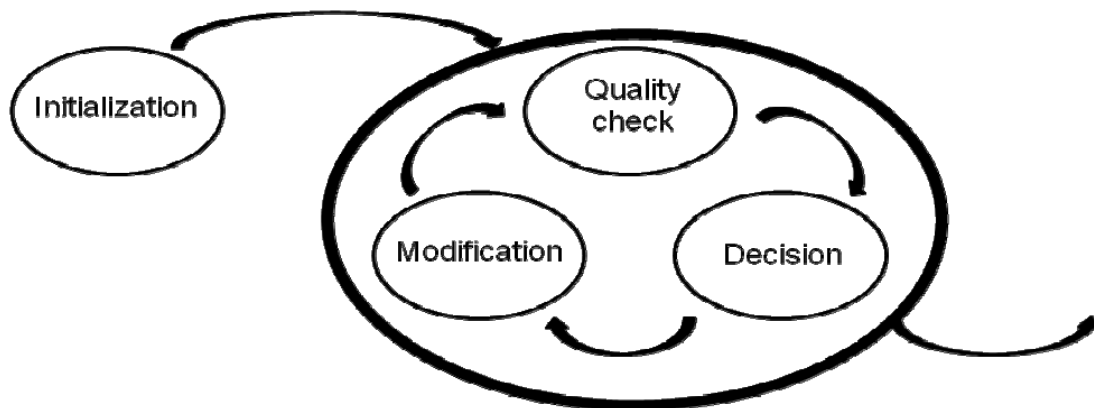


Fig. 1 Heuristic algorithm general steps

There are several reasons for an algorithm to stop the search. If the fitness function presents a well known parameter, the domain experts may be able to define a fitness function threshold that presents a solution that is good enough for their specific task. If the algorithm does not have such a stopping criteria, some algorithms stop after determining they are unable to find a better solution than the one they had already found. Either way, every algorithm must have a maximum number of iterations that prevents the algorithm from turning into an endless loop since the search is mostly random and does not keep track of previously examined solutions.

Most common algorithms

According to some differences in the previously explained general steps, the heuristic algorithms may be divided into following groups:

1. Single-State Methods and Population Methods
2. Local Search Methods and Global Search Methods

The single-state methods examine only one candidate solution at a time, while population methods use a larger set of candidate solution at each step of the search procedure. Using a set of solutions gives additional ways to modify the candidate solutions, often inspired from nature. This can be noticed in the mere names of algorithms like genetic algorithms, ant colony or swarm optimization. The second division refers to the performance of the algorithm. Local search methods look for an optimal solution on a local level, which can trap them in a local optimum. Global search methods, on the other hand, avoid local optimum traps and perform the search on a global level. An obvious question why would anyone use a single state local search method, with such obvious limitations and flaws may arise from the division we presented. The answer to that question is in the ever present trade-off between efficiency and effectiveness.

Heuristic algorithms, as a part of search-based software engineering, found its usage across all the stages of software product life cycle, from requirements to testing. The most common algorithms are genetic algorithms, genetic programming, hill climbing and simulated annealing [4]. Genetic algorithms are a group of population based, global search methods, inspired by nature. The modification phase of these algorithms involves gene mutation and recombination from the fittest parents with the goal to find even fitter offspring. Hill climbing and simulated annealing, on the other hand, are representatives of single state, local search methods. Hill climbing is inspired by climbers will to always go up the hill each step of the way, meaning it will choose a better solution each time there is one in the neighborhood. Simulated annealing found inspiration in metallurgy and unlike hill climbing, it can sometimes choose an inferior solution before next modification phase.

Search-based software engineering usage

SBSE is a widespread group of optimization techniques that found usage in almost every stage of software product lifecycle. However, there are still software engineering areas that exploit its benefits much more often than others, like software testing [5]. Here are some applications of SBSE in most recent studies:

- Solving the next release problem [5]–[7]
- Automatic software repair problem [8]–[13]
- Test data optimization problem [14]–[18]
- Generating higher order mutants [19], [20]
- Other multi-objective problems in software engineering [21], [22]

Next Release Problem

The next release problem is a multi-objective problem which requirements should appear in the next release of a software product. The task of SBSE is to choose a small subset among all possible requirements in order to satisfy as many stake-holders or customers as possible and to minimize the cost at the same time. Solving the next release problem is difficult and often has so many combinations of solutions that it becomes practically impossible to solve manually. Using SBSE does not give a specific answer to that problem but instead gives a range of equally good, near optimal solutions. That provides a valuable and necessary support for the decision maker. Zhang et al. [6] used search-based optimization techniques to automate the search for optimal or near optimal allocations of requirements that balance competing stake holder objectives in next release problem. NSGAII and two-archive algorithm were compared in performance and the two-archive algorithm proved to be the better one. Durillo et al. [5] analyzed which features to include in the next release of product in order to satisfy as many customers as possible with minimal cost using 3 multi-objective metaheuristics. NSGA-II was used as a reference algorithm in the field of multi objective optimization, MOCell because it outperformed NSGA-II in several studies and PAES as one of the simplest techniques. The results showed that NSGA-II finds the highest number of optimal solutions, MOCell finds the widest range of different solutions and PAES was fastest but worst, as expected. Finkelstein et al. [7] made a proposition that each notion of fairness in

next release problem should form an objective in multi-objective, pareto optimal SBSE setting. Comparing the NSGA-II and the two-archive algorithm, the results showed that they performed equally well with random data sets, while NSGA-II performed better with real data set obtained from Motorola.

Automatic Software Repair

Fixing bugs is a difficult and time-consuming manual process and some reports say software maintenance usually consumes about 90% of all costs after delivery of a product. An efficient, fully automated technique for repairing program defects could, therefore, alleviate that heavy burden. The idea of using SBSE in automatic software repair is actually rather simple but efficient. First task is to locate the region of the program relevant to an error. An SBSE algorithm is then used to produce simple changes along the path where the fault lies, trying to eliminate the fault and maintain the functionality of original program at the same time. Weimer et al. [8] used genetic programming for software repair phase in fully automated method for locating and repairing bugs in software. Fast et al. [9] used genetic programming in automated program repairing as well, but their focus was in improving fitness-function which resulted in efficiency improvement of 81%. Forrest et al. [10] combined genetic programming with program analysis methods to repair bugs in the off-the-shelf legacy C programs and managed to repair all of 11 programs they used. Schulte et al. [11] explored the advantages of assembly-level repair using evolutionary computing in automated program repair problem. Having all the advantages of assembly level approach over source code level approach, they obtained nearly as efficient results as at source code level. Nguyen et al. [12] successfully used genetic programming approach to automate repairing program bugs in existing software with average running time from half a second to ten minutes. Weimer et al. [13] also successfully used genetic programming in automatic bug repair in off-the-shelf legacy C programs combining program analysis methods with evolutionary computing. Their approach requires 1428 seconds and 3903 fitness evaluations per constructing a repair on average. All of these promising results indicate SBSE being the proper choice for automated software repair.

Test Data Optimization

Test data generation, regeneration and minimization are three different approaches to test data optimization problem. They tend to identify near optimal test sets in reasonable time using Evolutionary testing, a sub-field of SBSE techniques, often called Search-based Testing. Test data generation begins from scratch, regeneration uses the pre-existing test data as a starting point and test suite minimization tends to identify and remove redundant test cases.

The problem how to test something that reacts in different manner to the same test input over time can be found when dealing with autonomous agents. Nguyen et al. [14] proposed a solution to that problem and used evolutionary optimization to generate demanding test cases for such autonomous agents that produce different output to the same input, due to increasing knowledge for example. NSGA-II algorithm as a fast multi-objective genetic algorithm that in other studies proved to be better in finding widely spread solutions and with better convergence to the optimum compared to other algorithms was used in their study. Harman and McMinn [15] analyzed which type of search is best for structural test data generation problem. They used evolutionary testing as a global search algorithm, hill climbing as a local and a hybrid memetic algorithm for that purpose. Their suspicion proved to be correct and the results showed that hybrid approach, in terms of coverage, is capable of best overall performance. McMinn et al. [16] also compared evolutionary testing as a global search algorithm, hill climbing as a local search and a hybrid memetic algorithm in search-based structural test data generation problem, but with the improvement of irrelevant input variable removal (INVR). The results expectedly showed that all search algorithms are more successful and cover more branches with INVR and that memetic algorithm is the most prolific technique at successfully finding significance with and without INVR.

There are many testing scenarios in which a tester may already have some pre-existing test cases. They could have been created by tester, based on his experience, expertise and domain knowledge, by developer or they may be present from regression testing of previous version of product. In order to exploit the effort and knowledge put together to form this test cases, Yoo and Harman [17] proposed using pre-existing test data as a starting point in search-based test data generation, making it a regeneration process. They used hill climbing without random initialization, but with random-first-ascent and pre-existing test data. The results were promising, indicating the proposed approach can be up to two orders of magnitude more efficient, achieve higher structural coverage and equal component level of mutation score with much lower cost compared to a state-of-the-art search-based testing technique.

Test suite minimization can prove to be very important in strict time limits, often given in regression testing. Regression testing has to guarantee that the recent changes in a program do not interfere with its functionality. Due to ever growing test suite, it is prohibitively expensive to execute the entire test suite. Yoo and Harman [18] analyzed the hybrid algorithm that combines the efficient approximation of the greedy algorithm with the capability of population based genetic algorithm for pareto efficient multi-objective test suite minimization. They found greedy algorithm may provide a good approximation of pareto front in smaller software products, but for larger products, the usage of HNSGA-II is suggested due to more precise test suite minimization.

Higher Order Mutation Generation

It is said that 90% of faults which survived the testing procedure have to be complex ones. In order to reduce their number, we need to learn more about them. Higher order mutants (HOMs) are deliberately faulty programs used in software testing process. The order of mutant reflects the number of injected faults into the original program. Finding higher order mutants that create subtle and complex faults and sometimes practically mask one another helps us locating this hazardous combination of otherwise harmless faults when they exist separately. Such HOMs are more difficult to find with simple test cases and there lies a possible usage of HOMs - to find better test cases.

Jia and Harman [19] compared the performance of 3 algorithms for finding optimal HOMs: greedy algorithm, genetic algorithm and hill climbing algorithm. The results showed that genetic algorithm performed best because it finds most subsuming HOMs, hill climbing always finds the highest fitness HOMs and greedy algorithm finds the highest order HOMs. What makes their findings questionable is the fact that random search found more HOMs than greedy algorithm and hill climbing. Langdon et al. [20] explored the usage of multi-objective pareto optimal approach with Monte Carlo sampling, NSGA-II genetic algorithm and genetic programming to search for higher order mutants which are both harder to kill and more realistic. They found their higher order genetic programming mutation testing approach able to find even such simple faults that in combination mask each other and therefore form complex faults very difficult to detect.

Other Multi-Objective Problems in Software Engineering

Besides next release problem, there are many more problems which involve incomparable and often opposite multiple objectives in software engineering. A well known and highly important and challenging problem in software engineering is the one that requires high degree of cohesion and low degree of coupling for a good module structure. This problem is even more intensified as software evolves and its modular structure tends to degrade. Praditwong et al. [21] compared automated techniques for suggesting software clustering, delimiting boundaries between modules that maximize cohesion and minimize coupling. They used hill climbing as a single-objective

algorithm and two-archive algorithm as a multi-objective with 2 different approaches: the maximizing cluster approach (MCA) and equal-size cluster approach (ECA). The results indicated that ECA is superior to MCA and hill climbing in this task.

Many other multi-objective, but completely different problems in software engineering can be found in software engineering management. Project managers often do not understand the complex optimization techniques and they do not need to, in order to benefit from them. It is important to provide them with tool they can easily give input to and to obtain visually acceptable output that can help them in making important decisions. One such problem was analyzed by Di Penta et al. [22] where they used 3 metaheuristics in staff and task allocation with the objective to minimize the completion time and reduce schedule fragmentation. They compared the performance of NSGA-II, stochastic hill climbing and simulated annealing as most widely used SBSE techniques that appear in 80% publications. The results were compared in single objective optimization approach where simulated annealing was the best algorithm.

Conclusion

Unlike other engineering disciplines where search-based algorithms found application in, software engineering is the only discipline whose artifacts are solely virtual. The mere lack of possible simulations or models which can represent and optimize its artifacts makes SBSE and used fitness function the closest thing to an artifact. This property makes SBSE very attractive and potentially beneficial field. Search-based algorithms are attractive in software engineering also due to the fact that the data in software engineering are often inaccurate, over dispersed and incomplete, making some traditional optimization techniques inappropriate.

Software testing exploited the search-based algorithms more than any other software engineering field. We showed the basic requirements and potential application for these algorithms in other optimization or multi-objective problems from various software engineering areas. Besides making use of obviously beneficial algorithms in other unexplored areas, there is also work to be done with the algorithms themselves. The emerging hybrid algorithms show very promising results and offer a potential scope for future research. To sum up, the potential of using SBSE is vast and still needs to be explored more thoroughly.

References

- [1] M. Harman and A. Mansouri: Search based software engineering: Introduction to the special issue of the IEEE transactions on software engineering, Volume 36(6), p.p. 737–741, 2010.
- [2] S. Luke: Essentials of Metaheuristics (Lulu, 2009), Available for free at <http://cs.gmu.edu/~sean/book/metaheuristics/>
- [3] D. L. Kreher, D. R. Stinson: Combinatorial Algorithms: Generation, Enumeration and Search. (CRC Press LLC, 1999)
- [4] G. Lu, R. Bahsoon, and X. Yao: Applying Elementary Landscape Analysis to Search-Based Software Engineering, SSBSE '10, p.p. 3-8, 2010
- [5] J. J. Durillo, Y. Zhang, E. Alba, M. Harman and A. J. Nebro: A study of the bi-objective next release problem. Empirical Software Engineering, Vol. 16(1), p.p. 29–60, February 2011
- [6] Y. Zhang, M. Harman, A. Finkelstein, and S. A. Mansouri: Comparing the performance of metaheuristics for the analysis of multi-stakeholder tradeoffs in requirements optimization, Information and Software Technology, Vol. 53(7), p.p. 761–773, July 2011
- [7] A. Finkelstein, M. Harman, S. A. Mansouri, J. Ren, and Y. Zhang: A search based approach to fairness analysis in requirement assignments to aid negotiation, mediation and decision making, Requir. Eng., Vol. 14, p.p. 231–245, October 2009
- [8] W. Weimer, T. Vu Nguyen, C. Le Goues, and S. Forrest: Automatically finding patches using genetic programming, IEEE Computer Society, In Proc. of the ICSE '09, p.p. 364–374, 2009.
- [9] E. Fast, C. Le Goues, S. Forrest, and W. Weimer: Designing better fitness functions for automated program repair. In Proc. of 12th annual conference GECCO '10, p.p. 965–972, 2010
- [10] S. Forrest, T. Vu Nguyen, W. Weimer, and C. Le Goues: A genetic programming approach to automated software repair, in Proc. of the 11th Annual conference GECCO '09, p.p. 947–954, 2009
- [11] E. Schulte, S. Forrest, and W. Weimer: Automated program repair through the evolution of assembly code, in Proc. of the IEEE/ACM international conference ASE '10, p.p. 313–316, 2010
- [12] T. Vu Nguyen, W. Weimer, C. Le Goues, and S. Forrest: Using execution paths to evolve software patches, in Proc. of the IEEE International Conference on ICSTW '09, p.p. 152–153, 2009
- [13] W. Weimer, S. Forrest, C. Le Goues, and T. Vu Nguyen: Automatic program repair with evolutionary computation, Commun. ACM, Vol. 53, p.p. 109–116, May 2010
- [14] Cu D. Nguyen, A. Perini, P. Tonella, S. Miles, M. Harman and M. Luck: Evolutionary testing of autonomous software agents, in Proc. of The 8th International Conference AAMAS '09, Vol. 1, , p.p. 521–528, 2009
- [15] M. Harman and P. McMinn: A theoretical and empirical study of search-based testing: Local, global, and hybrid search, IEEE Transactions on Software Engineering, Vol. 36, p.p. 226–247, March 2010
- [16] P. McMinn, M. Harman, K. Lakhota, Y. Hassoun and Joachim Wegener: Input domain reduction through irrelevant variable removal and its effect on local, global and hybrid searchbased structural test data generation, IEEE Transactions on Software Engineering, 2011
- [17] S. Yoo and M. Harman: Test data regeneration: Generating new test data from existing test data. Journal of Software Testing, Verification and Reliability, To appear
- [18] S. Yoo and M. Harman: Using hybrid algorithm for pareto efficient multi-objective test suite minimization, Journal of Systems and Software, Vol. 83, p.p. 689–701, April 2010
- [19] Y. Jia and M. Harman: Higher order mutation testing, Information and Software Technology, Vol. 51, p.p. 1379–1393, October 2009
- [20] W. B. Langdon, M. Harman, and Y. Jia: Efficient multiobjective higher order mutation testing with genetic programming, Journal of Systems and Software, Vol. 83, p.p. 2416–2430, December 2010
- [21] K. Praditwong, M. Harman, and X. Yao: Software module clustering as a multi-objective search problem. IEEE transactions on software engineering, Vol. 37, p.p. 264–282, March 2011
- [22] M. Di Penta, M. Harman, and G. Antoniol: The use of search-based optimization techniques to schedule and staff software projects: an approach and an empirical study, Software: Practice and Experience, Vol. 41, p.p. 495–519, April 2011

THE POTENTIAL OF MANURE UTILIZATION FOR DEVELOPMENT OF SMALL TO MEDIUM SCALE PLANTS FOR BIOGAS PRODUCTION IN THE VOJVODINA REGION

Z. Čepić¹, M. Sremački¹, M. Živančev¹, Z. Đukić¹, D. Ubavin¹ and M. Vojinović Miloradov¹

¹ Trg Dositeja Obradovića 6, Faculty of technical sciences, Department of Environmental engineering and occupational safety and health, University of Novi Sad, Serbia

Keywords: Manure, biogas, anaerobic digestion, mesophilic process

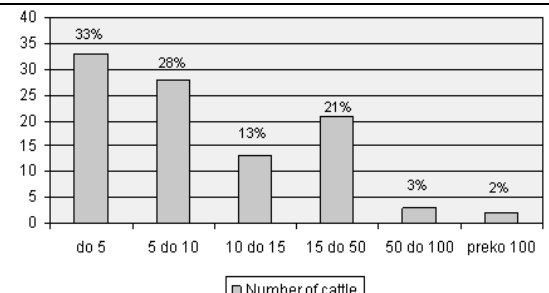
Abstract. Autonomous Province of Vojvodina with typical geological characteristics of a plain and high quality soil is the main agricultural potential of Republic of Serbia. Agricultural sector of farming is one of the interesting segments as an emerging challenge for waste management sector also it is a large emerging resource for biogas production. Although statistically AP Vojvodina contributes in 17% in Republic's animal farming activities it has a real potential for utilization of produced manure as primary resource for production of biogas and reaching energy independence of small to medium animal farms. This paper is representing the research of small to medium scale anaerobic digesters for manure development potential in Vojvodina region with purpose of biogas production. As the previous studies show the greatest potential for biogas production has poultry manure but also has a very low production rate and it will not be considered here. The focus of this paper will be pig and cattle manure as material for biogas production in mesophilic anaerobic digestion process, which in case of farming structure of Vojvodina region represents 87%. The paper will show statistical, technical and engineering, planning and designer data for development of small to medium plant for mesophilic anaerobic digestion of manure in AP Vojvodina.

Introduction

AP Vojvodina has a great potential for agricultural activities, plant and animal farming. Animal farming in Vojvodina region has potential to be one of great producer of primary material for biogas production and co-generation of heat and energy. Livestock farming is the most intensive agricultural production and has multiple significance for both producers and consumers. Accordingly, in almost all projections of agricultural production in AP Vojvodina it is set as a goal to increase the share of livestock production to 60% of total agricultural production, instead of 25-35% which is level today. [1]

According to current situation in region, small to medium farms represent the largest share of total number of farms. Therefore this paper will present the digesters for this category of farms in order to achieve certain level of independence in the supply of electricity and heat. Digesters are also proven as a successful means of disposal and treatment of waste and wastewater.

Table 1. Structure of farms and biogas yield potential in AP Vojvodina [1, 2]

Animal sort	Number		Farm structure (cattle number)	Potential biogas yields [m ³ /y]
Cattle	220 000		To 5 animals	1 341
Pigs	1 289 000	From 5 to 10 animals	1 341 – 2 682	
Goats and sheep	272 000	From 10 to 15 animals	2 682 – 4 023	
Horses	5 000	From 15 to 50 animals	4 023 – 13 410	

Anaerobic digestion

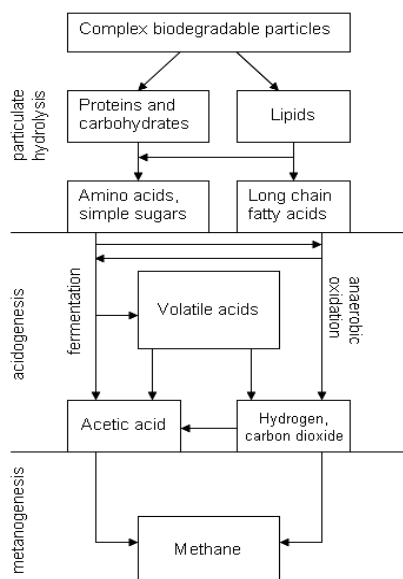
Anaerobic digestion is the natural breakdown of organic materials into biogas and compost. This takes place naturally, or in an anaerobic digester. Anaerobic digestion is a series of processes in which microorganisms break down biodegradable material in the absence of gaseous oxygen. It is widely used to treat wastewater sludge and organic wastes because it provides volume and mass reduction of the input material. Anaerobic digestion is a renewable energy source because the process produces a methane rich biogas suitable for energy production helping replace fossil fuels. [3]

Careful control of the digestion temperature, pH, redox potential and loading rates is crucial to obtain efficient breakdown of the material, disturbances to a digest can lead to process failure. Ensuring that the quality and quantity of input materials to the digesters are maintained and that the process effectively monitored is essential for ensuring that a digester's performance is reliable.

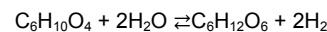
There are 3 different anaerobic digestion processes which differ in temperature range and microorganisms that are performing degradation of organic mass and producing biogas - *psychophilic*, *mesophilic* and *thermophilic* processes. Psychophilic processes take place on temperatures lower than 20°C are not optimal because these processes are studied and developed for extreme climatically conditions. Mesophilic digestion is an anaerobic digestion process which takes place at 20 to 45°C, optimally around 30 to 38 °C, where mesophiles are the primary microorganism present. Mesophilic species outnumber thermophiles, and they are also more tolerant to

changes in environmental conditions than thermophiles. Mesophilic systems are considered to be more stable than thermophilic digestion systems, although the thermophilic process takes a less amount of time. [3]

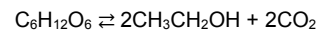
Important characteristics of anaerobic digester design, beside the temperature are *moisture content of feedstock; continuity and scale of process; flow and stirring of feedstock*. *Moisture content of feedstock* - wet or dry process – the difference between what is considered a wet process and a dry process is quite small. Effectively, in wet process the feedstock is pumped and stirred and in dry process it can be stacked. Dry process is less economically demanding than wet process as it has lower heat and water consumption but wet process has lower initial investment. Dry process has higher value of gas production per unit feedstock. Different studies have shown that *continuous process* is more efficient and easier for operation than *batch process*. Continuous process will be regarded as best available technology and recommendation for target group of small and medium farms. Scale of process is regarding the steps of anaerobic process – hydrolysis, acidogenesis, acetogenesis and methanogenesis. All of these metabolic stages can be performed in *single digester* or separately in *multiple digesters*. Multiple digesters can perform in higher efficiency levels than single (higher biogas production) but have significantly higher initial and operational cost. *Vertical reactors* simply take feedstock in a pipe on one side while digester overflows through a pipe on the other. In *horizontal plug-flow systems* a more solid feedstock is used as a 'plug' that flows through a horizontal digester at the rate it is a fed in. Vertical tanks are simple and cheaper to operate, but the feedstock may not residue in the digester for the optimum period of time. Horizontal tanks are more expensive to build and operate, but the feedstock will neither leave the digester too early nor stay in it for an uneconomically long period.



Hydrolysis



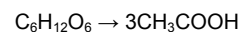
Acidogenesis 1



Acidogenesis 2



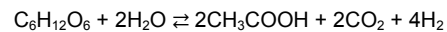
Acidogenesis 3



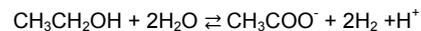
Acetogenesis 1



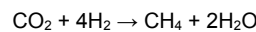
Acetogenesis 2



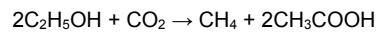
Acetogenesis 3



Methanogenesis 1



Methanogenesis 2



Methanogenesis 3

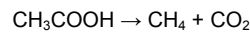


Figure 1: Multi step nature of anaerobic operations and reactions that take place during the process [4]

Potential of biogas production from anaerobic digestion of manure in AP Vojvodina

Official statistical data of cattle farming for AP Vojvodina show the real potential of anaerobic digestion process incorporation for small and medium farms in order to achieve a certain percentage or full energy independence and complete the cycle for certain waste streams on these farms.

Average potential of different type of manure per cubic meter is relatively similar for cattle, pigs, horses, sheep and goats. Cattle, horses, goat and sheep manure has slightly higher potential for biogas yield being dryer and possibly containing straw than pig manure. Average biogas potential is as follows - cattle manure 30 m³/t, pig manure 25m³/t, horse manure 30 m³/t, goat and sheep 28m³/t. [5]

Table 2. Potential of biogas yield and manure production of animal types in AP Vojvodina [6]

Animal sort	Average weight [kg]	Total manure per animal [t/y]	Biogas yields per animal [m ³ /y]	Total mass of manure [t/y]	Biogas yields [m ³ /y]
Cattle	389	8.94	268.2	1 967 628	59 028 840
Pigs	59,2	0.95	23.75	1 224 742.3	30 618 557.5
Goats and sheep	38	0.71	14.2	193 402.5	4 835 062.5
Horses	400	7.59	227.7	37 960	113 880
Total biogas yield potential of AP Vojvodina					95 621 260 m³/y

Table 3: Biogas guideline data [7]

Retention time	40 - 100 days
Biogas energy content	6 kWh/m ³ = 0.6 L diesel fuel
Biogas generation	0.3-0.5 m ³ gas/(m ³ digester volume per day)
1 cow yields	9-15 kg dung/day = 0.4m ³ gas/day
1 pig yields	2-3 kg dung/day = 0.15 m ³ gas/day

Gas requirement for cooking	0.1-0.3 m ³ /person
For 1 lamp	0.1-0.15 m ³ /h
For engines	0.6 m ³ /kWh

A simple 8 - 10 m³ biogas plant produces 1.5-2 m³ and 100 L digested-slurry fertilizer per day on dung from 3-5 head of cattle or 8 - 12 pigs. With these amount of biogas, a 6 - 8 person family can:

- cook 2-3 meals or
- operate one refrigerator all day and two lamps for 3 hours or
- operate a 3 kW motor generator for 1 hour. [7]

Anaerobic digesters for small and medium farms

The small-scale mesophilic bioreactor has a 6m³ volume and requires the equivalent of waste material generated from 4 cows. The temperature of the reactor is 25-40°C. Modern mesophilic bioreactors can produce 0.2-0.4 m³ per m³ of installation. [8] The amount of biogas spent to keep substrate temperature within the limits of 50-55°C (hemophilic bioreactors) did not exceed 25% of produced biogas, even under the worst climatic conditions (average temperature -80C). Manure ration of wet/dry matter is 30:70 or 35:65, respectively.

Each cubic meter (m³) of biogas contains the equivalent of 6 kWh of energy. However, biogas convert to electricity, in a biogas electric generator, it could be get about 2 kWh of useable electricity. The rest turns into heat which can also be used for heating applications. About 2 kWh is enough energy to power a 100 W light bulb for 20 hours or a 2000W hair dryer for 1 hour. [9]

Anaerobic digester design biogas yields and use

Anaerobic digester may have different size depending on number of animals and retention time. It is chosen that number of cattle should be an equivalent, because daily generated manure of cattle is ten times more than pigs. Upper limit for small farms is chosen to be 10 head of cattle; for medium size farms lower limit is 15 and upper limit is 50 head of cattle. The table 4 is presenting required volumes of digesters and projected biogas yields, depend on number of animals, for retention time of 30 days.

Table4: Biogas guideline data [7]

Number of animals	Optimal volume of anaerobic digester [m ³]	Daily biogas yield [m ³]
5 head of cattle and 5 pigs	4.4	4.05
10 head of cattle	7.3	7.35
15 head of cattle	10.9	10.95
50 head of cattle	36.4	36.75

The daily maintenance of biogas plant

For a 5m³ biogas plant to keep a 5m³/day biogas production, 75kg cow dung or 55kg pig dung is needed daily. In the period of normal operation you can increase the concentration of the feeding materials up to 8 ~ 10%. The liquid from the biogas plant can be recycled.

For a small farm (the product is composed of an anaerobic fermentation tank, a gas storage bag, a gas pump, a solar charger, as well as gas pipeline and appliances. It is easy and quick to install, convenient to transport, wide range of fermentation material, high gas production rate (production rate can reach 0.8m³gas/m³).

Design recommendations for small and medium farm AD plants in Serbia

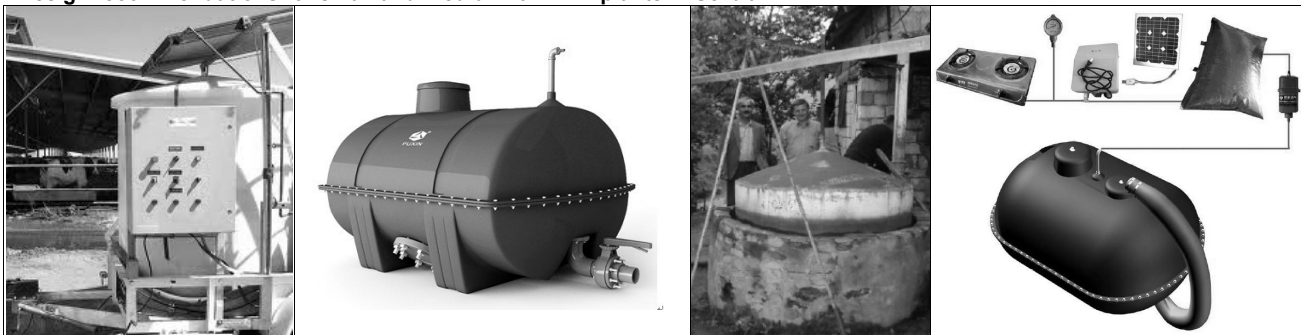
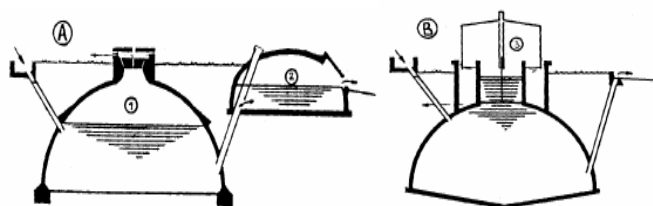


Figure 1. Small-Scale Biogas Reactors of Fixed-Dome (A) and Floating-Dome (B) Types



Source: TACIS, 1997.

Figure 1. Anaerobic digester design, low to high installation costs digester, small and medium scale digesters

Economical evaluation of anaerobic digester design for small and medium farms with BAT recommendations

There has been a great number of studies developed about economic viability of anaerobic digestion of manure. The best solution for the efficient electricity are shown in the table 5.

Table 5: Biogas guideline data [10]

Digester parameters	Small farm		Medium farm	
Number of cattle	5 -10		11 - 50	
Process characteristics (temperature, moisture content...)	Mesophilic		Mesophilic	
	Dry		Wet	
	Single digester		Single digester	
Construction* parameters	Continuous		Continuous	
	Vertical		Vertical	
	Portable (80kg)		Built-in	
	Heat generation		Heat/electricity generation	
	High reliability, low O&M cost		High reliability, low O&M cost – up to 40 years	
	200 – 2000 \$		2000 – 15000 \$	

*Price is varied according to the installed household appliances, heat and/or electricity generators

Conclusion

There are real advantages as well as disadvantages. Taking all advantages and disadvantages into decision making process, there is a justified possibility of installing the anaerobic bioreactor system for small and medium sized farms in region of AP Vojvodina. The difference between viability of systems is that for small farms it is possible and optimal to install a system for heating, while for medium farms it is possible to convert biogas to electricity. The costs of bioreactors of recommended types, is relatively high but has downward trend. Farming has shown to be one of the large emerging source for biogas production.

Taking the fact that these kinds of farms are in rural area, where no sewage system, further research should address the merging of these plants with sewage. Thus the plants would have even more benefits and would solve some more problems.

Acknowledgment

The research within this paper was supported by Ministry of Education and Science, Republic of Serbia (project number III46009).

References

- [1]. Official site of Statistical Office of the Republic of Serbia, Status of animal farming in AP Vojvodina, 24.04.2012. <http://webrzs.stat.gov.rs/WebSite/>
- [2]. Information on the livestock production status and problems in AP Vojvodina, Chamber of commerce and industry of Serbia, QG 731-01 (2010), Novi Sad, Serbia.
- [3]. Drawnel: Increase of biogas production at Käppala WWTP: disintegration methods and laboratory scale biogas measurements, Master of Science Thesis (2008), KTH Industrial Engineering and Management, Stockholm, Sweden.
- [4]. M. Sremački "Use of various analytical tools for characterization of organic matter in context of co-digestion", internship Veolia Water rapport (2008).
- [5]. K. Navickas "Biogas for farming, energy conversion and environment protection", Proc of Bioplin, tehnologija in okolje, Rakičan, Slovenia (2007), pp 25-30.
- [6]. Study: Biomass market development in AP Vojvodina, Provincial center for energetic efficiency, Faculty of technical sciences, University of Novi Sad, (2010).
- [7]. U. Werner, U. Stöhr, N. Hees "Biogas plants in animal husbandry", A Publication of the Deutsches Zentrum für Entwicklungstechnologien _ GATE, a Division of the Deutsche Gesellschaft für Technische Zusammenarbeit (GTZ) GmbH – 1989
- [8]. Study "Biogas production" Georgia
- [9]. http://www.electrigaz.com/faq_en.htm
- [10]. <http://www.ruralcostarica.com/biogas-video.html>

BI-METALLIC COLD BACKWARD EXTRUSION – NUMERICAL SIMULATION WITH EXPERIMENTAL VERIFICATION

M. Plancak¹, D. Movrin¹, Z. Car², D. Vilotić¹, I. Kacmarcik¹, M. Kršulja²

¹ Faculty of Technical Science, University of Novi Sad, Trg Dositeja Obradovica 6, 21000 Novi Sad
Serbia

² Faculty of Engineering, University of Rijeka, Vukovarska 58, 51000 Rijeka
Croatia

Keywords: bi-metallic extrusion, numerical simulation, experiment

Abstract. Bi-metallic extrusion is a metal forming operation where billet is composed of two different metallic materials which are then concurrently extruded into a final workpiece. In this way final component, consisting of two different materials which are metallurgically bonded, is created. Extrusion of bi-metallic workpieces differs in many aspects from the classical single-metal extrusion. Although bi-metallic extrusion enables beneficial utilization of favourable characteristics of both paired materials, this process has not been often applied in the industrial practice so far. This is mainly due to the certain dearth of knowledge and experience in this field. The present study is bound to the backward extrusion of bi-metallic materials. Combination of Al-Cu as a billet composition is explored numerically and experimentally. Material flow as well as mechanical properties of the obtained bi-metallic component have been determined and analysed.

Introduction

Cold extrusion of mono-metal billets is well established technology which makes it possible to manufacture small and middle size components in very efficient way. There are numerous advantages of this technology when compared to other manufacturing methods such as better material utilization, short production time, excellent mechanical properties and surface quality of extruded workpieces.

Further investigation of cold extrusion goes in various directions. One of the significant research fields in this context is development of a new extrusion processes which would enable even wider industrial application of this technology.

Bi-metallic cold extrusion is a modern metal forming operation where an initial billet, consisting of two or more different materials, is extruded and, as a result, multiple material component is produced. In most cases billet consists of two different materials, although combination of two different alloys of the same material is also applicable. Application of bi-metallic extrusion enables beneficial utilization of favourable characteristics of both extruded materials.

During concurrent extrusion of composite billet metallurgical bound between different billets components is created, which omits the need for additional subsequent joining of two materials.

Different geometrical shapes of the bi-metallic workpiece can be produced, but in most cases bi-metallic components are in the form of core-sleeve configuration. So, for instance, sleeve material can be used as a layer because of a favourable anti-corrosions properties and core material can be chosen as a carrier due to lower weight and price. Many other requirements of the product can be fulfilled by proper choice of both materials in bi-metallic extrusion (e.g. thermal expansion, mechanical strength, electric conduction). As one example in [] has been reported that bimetallic copper/aluminium rod is 40-60% lighter and 30-40% cheaper in comparison with Cu rod.

One of the main challenge which has to be solved in bi-metallic extrusion is occurrence of different flow patterns of both applied materials. Softer material flows easier and its velocity field differs from other paired material. This leads to non-homogenous thickness of metal layer or – in extreme case – to the cracks in softer or harder material. In order to produce sound bi-metallic component all significant influential parameters should be chosen in proper way.

Bi-metallic extrusion

Bi-metallic extrusion is applied in most cases in three different geometrical forms: forward extrusion, backward extrusion and tube extrusion. In forward extrusion bi-metallic billet, composed of outer sleeve and inner core, is extruded by the punch through the die-opening and, as a result, bi-metallic rod is produced, figure 1a.

Bi-metallic tubes and tube-like hollow components can be produced by two different extrusion methods: forward tube extrusion by the punch provided with the mandrel (Fig. 1b) [1] and extrusion-piercing in a profiled die using the punch and separate mandrel (Fig. 1c) [2].

In all cases material combination can be twofold, depending on the requirements of the final workpiece: a) hard sleeve material and soft core material, b) soft sleeve material and hard core material.

Process of bi-metallic extrusion has been investigated by a number of authors. In [3] bi-metallic extrusion of tubes by using profile dies and mandrels is elaborated. Theoretical results obtained by slab method are compared with experiment and fair agreement was found. Geometrical configuration of billet and die and its impact on the workpiece tolerance in bi-metallic tube extrusion is studied in [4]. Novel billet design has been proposed which decreases the “out of tolerance” geometry.

Research on backward bi-metallic extrusion has been reported in [4] [5]. Experimental part of the investigation was performed by using hard plastiline / soft plastiline combination. Focus has been placed on the layer thickness homogeneity. Velocity field and theoretical analysis was carried out by Upper Bound method.

Among diverse process parameters which affect the quality of final product, initial billet geometry is one of the most significant. In [6] authors investigated forward extrusion and concluded that not only ratio of core /sleeve radius, but also ratio of the core / sleeve length influences the dimensional stability of the rod longitudinal cross section. They proposed one optimal initial core material length for every concrete extrusion case (reduction in area, die angle, die land, flow stress of sleeve and core materials) which, as a result, gives a correct product. Impact of die geometry in the strength of the bond between two materials in forward extrusion was investigated in [7]. It was

concluded by FE analysis and by experimental research that die angle of 25% results in optimum velocity field and, consequently, highest shear strength of the bond.

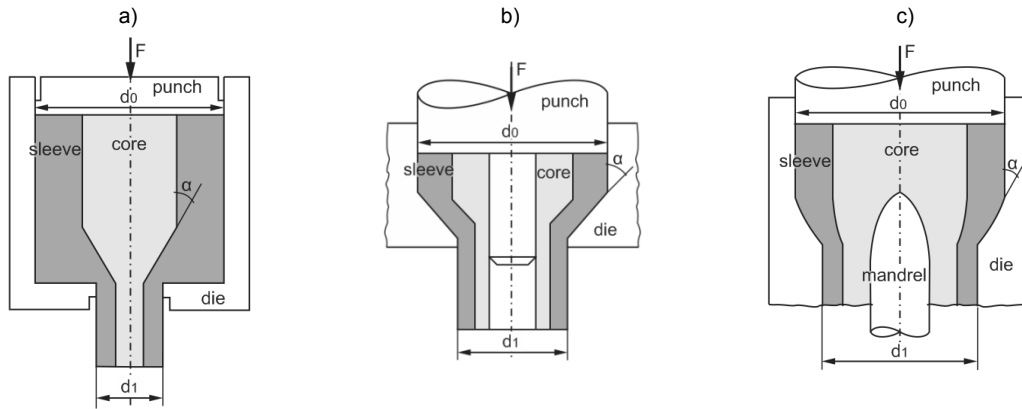


Fig. 1 Different variants of bi-metallic extrusion a.) forward extrusion b. and c.) tube extrusion

In the current paper investigation of bi-metallic backward extrusion process is presented. Billet with the Al/Cu combination has been used. Numerical analysis (FE) and experimental work were performed in order to explore material flow, geometry of the extruded product as well as the required extrusion force.

Experimental investigation

Bi-metallic billets were composed of Al outer sleeve and Cu inner core (Figures 2 and 3.). Dimensions of the composite billet placed in the die are also shown in Fig. 2 Punch (1) has a slightly smaller diameter than Cu-core (18.9 mm compared to 22 mm). Flow curves for both billet materials are obtained in Rastegaev test:

$$\sigma_{Cu} = 362.67 \cdot \varphi^{0.1828} \quad (\text{Cu}) \quad (1)$$

$$\sigma_{Al} = 191 \cdot \varphi^{0.165} \quad (\text{Al}) \quad (2)$$

Before extrusion billet was lubricated by mineral oil.

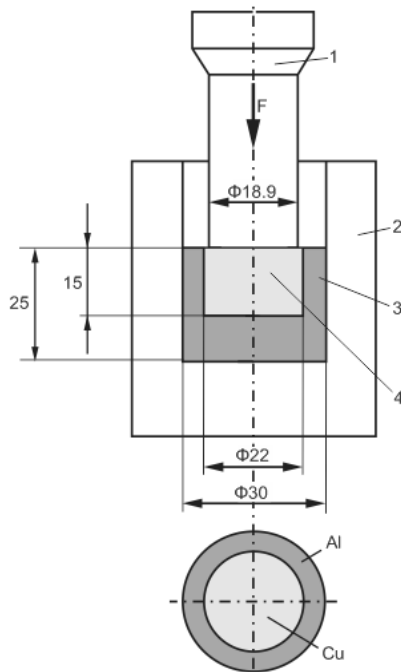


Fig. 2. Configuration of billet and die (1 – punch, 2 – die, 3 – Al, 4 – Cu)

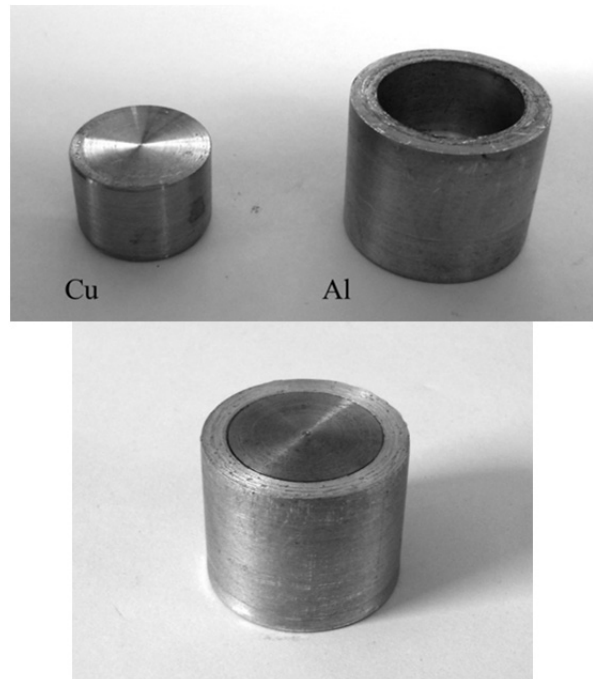


Fig 3. Photograph of separated copper and aluminium parts (above) and composed billet (below)

In order to assemble Cu-core into Al-sleeve in proper way, geometrical overlapping between both parts was made and aluminium was preheated and copper was cooled so that an adequate fit could be achieved. During extrusion force – stroke diagram was recorded. At the end of the operation bi-metallic workpiece was ejected from the die by ejector which is integral part of the press at which extrusion was performed (Sack & Kiesselbach Hydraulic 6.3 MN press).

Photographs of the backward extrusion tooling and extruded workpiece cut through the meridian plane are given in Fig. 4 and 5.

Numerical simulation

Numerical simulations by Finite Elements method was carried out in Simufact Forming 10.0. Due to symmetrical nature of the process axisymmetric 2D simulation was performed. In simulation, identical geometrical data (tool, die and billets dimensions), tool stroke, tool velocity and materials were employed as in the experiment. Hydraulic press with 0.1 tool velocity was used. Material was modelled as an isotropic elasto-plastic body and punch and die were set as rigid bodies without heat conduction. Both Cu and Al parts were divided by 0.25 mm and 0.65 mm element sized mesh retrospectively, with Advanced Front Quad mesher and *quads (10)* element type. Friction factor in all three different interfaces (Cu/Al, Cu/Tool and Al/die) was set to be $m = 0.12$, which corresponds to the friction magnitude when lubrication with mineral oil is applied [8].



Fig. 4. Tooling for bi-metallic backward extrusion

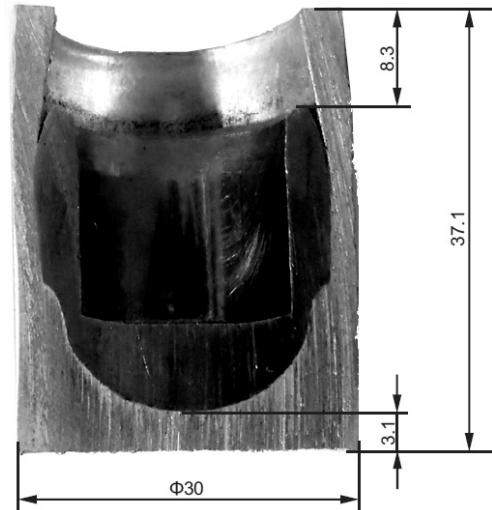


Fig. 5. Meridian cross section of the final experimental workpiece (stroke $s = 15$ mm)

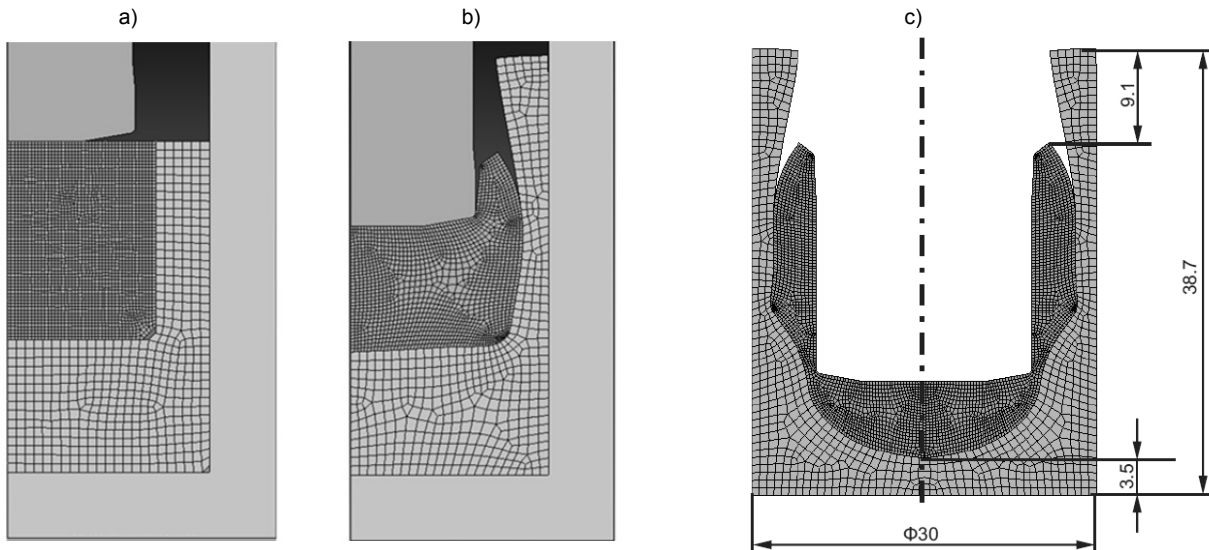


Fig. 6. Numerical simulation: a) start, b) intermediate phase after 6 mm punch stroke and c) end of the process (full cross-section)

Results and concluding remarks

Figure 6a shows initial position in the numerical analysis and division of both billet components into finite elements. Intermediate constellation after 6 mm punch stroke is given in Fig. 6b. As it can be seen copper billet flows sideways and creates a slightly barrel shape. This occurs due to the fact that copper material is significantly stronger than aluminium. In latter phase, this barrelled shape moves upwards and a thin layer is formed on the lower part of the workpiece – Fig 6c. With the progressing punch travel, certain amount of separation between Al and Cu segments takes place in the upper part of the workpiece assembly. Process was terminated after 15 mm punch stroke (Fig. 6c).

By comparing figures 5 and 6c (meridian plane of the workpiece at the end of the process – experiment and numerical simulation), close agreement in the geometrical form of obtained workpiece can be observed. Also, load – stroke diagrams obtained numerically and by experiment show favourable coincidence (Fig. 7). Certain load decline after the punch stroke of ≈ 8 mm can be attributed to the

separation between Al and Cu component. This separation causes decrease of friction amount between Al and Cu materials, which results in load decline.

Future work on current issue will include further optimization of the process in order to obtain sound workpieces, i.e. workpieces with constant layer thickness and with constant bound between two components of the workpiece. In this regard planned investigation would consider different material combinations as well as various geometrical constellations of the bi-metallic assembly.

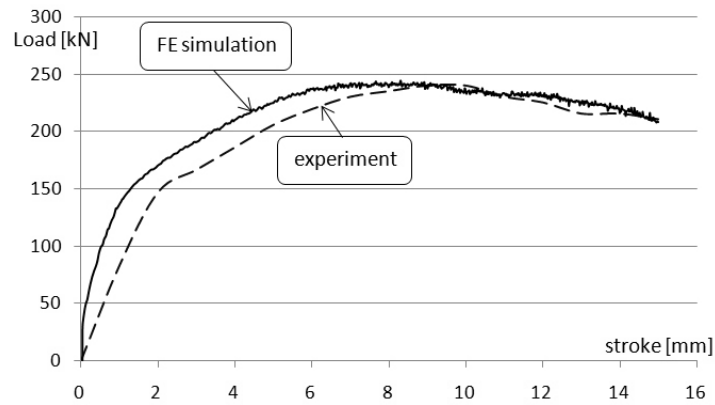


Fig. 7. Load stroke diagrams obtained by experimental investigation and FE simulation

Acknowledgement

This paper is a part of the investigation within the project CEEPUS HR-108. Authors are very grateful for the financial support.

References

- [1] M. E. Epler, W.Z. Misiolek: Novel billet design for co-extrusion of ferrous material tubes, *Materials Science and Engineering*, Volume 429 (2006), p. 43-49.
- [2] N.R. Chitkara, A. Aleem: Axi-symmetric tube extrusion/piercing using die-mandrel combinations: some experiments and a generalized upper bound analysis, *International Journal of Mechanical Sciences*, Volume 43 (2001), p. 1685-1709.
- [3] N. R. Chitkara, A. Aleem: Extrusion of axi-symmetric bi-metallic tubes: some experiments using hollow billets and the application of a generalized slab method of analysis, *International Journal of Mechanical Sciences*, Volume 43 (2001), p. 2857-2882.
- [4] P. Montmitonnet, J. Mstowski: Manufacture of bi-layered plain bearings by bimetallic cold backward extrusion. I – experimental study: simulation with plasticine, *Journal of Mechanical Working Technology*, Volume 8 (1983), p. 327-336.
- [5] P. Montmitonnet, J. Mstowski: Manufacture of bi-layered plain bearings by bimetallic cold backward extrusion. II – mechanical modelling, *Journal of Mechanical Working Technology*, Volume 8 (1983), p. 337-347.
- [6] P. Kazanowski, M.E. Epler, W.Z. Misiolek: Bi-metal rod extrusion – process and product optimization, *Materials Science and Engineering A369* (2004), p. 170-180.
- [7] A. Khosravifard, R. Ebrahimi: Investigation of parameters affecting interface strength in Al/Cu clad bimetal rod extrusion process, *Materials and Design*, Volume 31 (2010), p. 493-499.
- [8] P. Skakun, M. Placak, D. Vilotic, M. Milutinovic, D. Movrin, O. Luzanin: Comparative investigation of different lubricants for bulk metal forming operations, *DEMI 2011*, Banja Luka, 2011.



PROFESSIONAL SOFTWARE FOR HARMONIC ANALYSIS

W. Zhang¹, S. Darie¹

¹ 16870 West Bernardo Drive, Suite 330, San Diego, CA, USA

Keywords: Frequency response, harmonic analysis, industrial power systems, micro smart grid, harmonic filters, power electronic converters, power system harmonics, total harmonic distortion.

Abstract. This paper presents a new professional program developed for harmonic studies: Paladin® DesignBase™ Harmonics from Power Analytics Corporation. The approach, logic, and techniques in system simulation and components modeling are those commonly accepted and well-described in IEEE standards. This paper provides case studies, results, and comparisons based on published IEEE harmonic analysis test systems. The purpose is to validate the program results, validate published results of IEEE harmonic test system studies, provide insight of the variations of the harmonic analysis results, and provide a guideline for harmonics analysis and mitigations techniques.

Introduction

Power quality has become a key-issue in energy supply, and has a new significance in the wholesale market environment. As a commodity, electricity is probably unique in being a product which is manufactured (generated), delivered (transmission, distribution and reticulation) and used (energy utilization) at the same time. By the time the electricity is generated, it will have been delivered and used by the customer, whether it was of good quality or not. Electric power quality broadly refers to maintaining a near sinusoidal waveform of the power distribution bus voltage at rated magnitude and frequency. A full appreciation of the problem of poor quality requires an understanding of the following issues: sources of waveform and magnitude distortion; measurement of waveform and magnitude distortion; effects of waveform and magnitude distortion; solutions to problems caused by waveform and magnitude distortion.

The Paladin DesignBase environment provides a broad range of totally integrated power system solutions, in a robust CAD/CAE system, specifically designed for power system design and simulation. It is a complete commercial power system simulation software package that includes a well- designed harmonic analysis program (Paladin-harmonics). The main focus of commercial software is to provide a tool that is easy to use, in compliance with standards, reliable, efficient and effective. A user can conduct thorough harmonic studies with reasonably less effort and time. The program provides frequency scans at selected buses, harmonic distortion indices at any bus or branch, including transformer k-factor indexes; filter designs, and standard limits checking. The techniques and component models used are configured to those commonly accepted and well described in IEEE standard 399-1997[1].

Power system harmonics are traditionally from non-linear loads, like electric arc furnaces, fluorescent lamps, and wide-spread power electronic controlled motors and loads. Transformers distort voltage and current waveforms to a lesser extent. Renewable energies, such as wind, solar and other distributed generation and energy storage, are being rapidly integrated into our complex power systems and are a significant part of the increasingly wide-spread micro smart grids. These renewable power sources are also harmonic sources, as power electronic devices are applied in converting the power between DC and AC and in control of the power flow, voltage, and frequency.

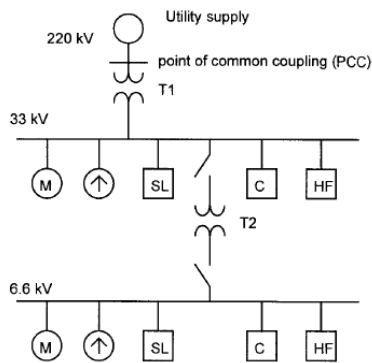
Over the past two decades, mature techniques for power system harmonic analysis have been developed and widely used. Guidelines for the acceptance of harmonic distortion are well-defined through standards such as IEEE std. 519-1992 which is broadly applied by industry and utilities [1]-[6]. Various commercial or non-commercial computer programs are available for assessing harmonic distortions of networks with significant harmonic sources, for detecting harmonic resonance, and for designing and testing harmonic filters.

This paper presents detailed harmonic studies and results for a test system given in [1], and result comparison and discussion for a system given in [3]. The purpose is to provide results, compare the results with the published results of the IEEE test systems, provide insights for harmonic indices and differences of the results, provide a guideline for harmonic analysis and mitigation techniques, and support exchanges of information, ideas and techniques. We believe in the importance of harmonic simulation test systems, and encourage further development and enhancement of harmonic analysis test systems in areas of component models, case studies, harmonic mitigation techniques, new devices such as wind and solar renewable power sources, and better system input data and results.

Test System and the System Data

The test system, as shown in Fig. 1, is from IEEE std. 399-1997 [1]. It is representative of an industrial power system and includes multiple voltage levels, multiple harmonic sources, and power factor correction capacitors. The complete data required for basic harmonic studies are shown in Tables 1-4.

The motor and static loads (M and SL in Fig. 1) are modeled the same as R and X connected in parallel. They are combined into one linear load of 25 MVA at 0.8 lag on the 33 kV bus as shown in Fig. 2 as L-1 load. Similarly, the motor and static load on 6.6 kV bus are combined as L-2 load of 15 MVA at 0.8 lag. The converter on 33 kV bus draws active power of 25 MW as shown in Table 3. From Table 4, we also know that the converter draws 618 amperes at the base frequency, which gives us $618 \times \sqrt{3} \times 33 = 35323$ kVA. The power factor is then $25000/35323 = 0.71$. This fundamental frequency load and the harmonic currents given in Table 4 were entered in the harmonic current source connected at CNV-1 in Fig. 2. The harmonic current source data dialog box is shown in Fig. 3. For the converter connected to the 6.6 kV bus, if the same harmonic content of Table 4 is applied as indicated in [1], the total apparent power drawn from the converter is $618 \times \sqrt{3} \times 6.6 = 7065$ kVA. This obviously cannot deliver 15 MW active power. There must be an error here and we therefore reduced the number to 5 MW. The power factor is then $5000/7065 = 0.71$.



Key:
M—motor load, SL—static load
C—static capacitors, HF—harmonic filters

TABLE 3
LOAD AND CAPACITOR DATA

33 kV bus linear load	25 MVA @ 0.8 lag
33 kV bus converter	25 MW
33 kV bus capacitor	8.4 Mvar
6.6 kV bus linear load	15 MVA @ 0.8 lag
6.6 kV bus converter	15 MW *
6.6 kV bus capacitor	5 Mvar

*this number will be reduced to 5 MW as it doesn't fit

Frequency Scan Studies

Frequency scan is a simple and commonly used technique for harmonic analysis. It is the most effective tool to detect harmonic resonance conditions in a system, and has also been widely used for filter designs. A frequency scan is performed at the 33 kV bus with switch SW-4 open, so the 6.6 kV subsystem is not included in this case. The calculation using Paladin-harmonics is easy; just select 'BUS-33kV' in the drawing and click the 'Frequency Scan' button. The frequency scan dialog box is shown in Fig. 4. The resultant driving point impedance is shown in Fig. 5.

Compare the curve in Fig. 5 to the curve given in [1]; the maximum Z is about $(48.5 - 42.5)/48.5 \times 100 = 12.4\%$ in difference, and the resonant frequency is about $(8.6-8)/8.6 \times 100 = 7\%$ in difference. They do not match exactly and this is one reason that we present our results, and believe our results are more accurate.

A frequency scan is again conducted at the 33 kV bus with switch SW-4 closed, and the resultant driving point impedance is shown in Fig. 6. Note the presence of two resonance points. This is to be expected—typically the number of resonance points is the same as number of capacitors. Comparing this curve to the curve given in [1], the magnitude difference is nearly 20%.

Total Harmonic Distortion Index (THD)

Using Paladin-harmonics, it takes two button clicks to get almost all known harmonics indices for buses and branches. The voltage waveform at the 33 kV bus when SW-4 is open is shown in Fig. 7. The THD is 18.10% which is higher than the 12.23% given in [1]. The THD calculated at the point of common coupling (PCC) or the 220 kV utility supply bus is 2.74% which is more conservative compared to the 1.8% given in [1]. The system operation condition may affect the THD results slightly. The utility short circuit capacity of 4000 MVA is used in the calculation. Also note although the THD at the 33 kV bus is about 18% high, the THD at the PPC is under 3%.

The voltage waveform at the 33 kV bus when SW-4 is closed, CVN-1 is on, but CVN-2 is off is shown in Fig. 8. The THD is 15.44% which is higher than the 9.99% given in [1]. The voltage waveform at the 33 kV bus when SW-4 is closed, CVN-1 is off and CVN-2 is on is shown in Fig. 9. The THD is 4.02 % which is lower than 7.38% given in [1]. This is probably due to the 15 MW converter reduced to 5 MW.

The voltage waveform at the 33 kV bus when SW-4 is closed and both CVN-1 and CVN-2 are on is shown in Fig. 10. The THD is 13.15%. It is interesting to note that the number is lower than the 15.44% which is the THD in the case of CVN-1on and CVN-2 off.

Now leave SW-4 open and turn the capacitor PFC-1 into a single tuned filter at $5^{\circ}0.97 = 4.7^{\text{th}}$ harmonic and assume the filter quality factor is 80. The harmonic voltage at 33 kV bus is shown in Fig. 11. The THD of the bus is 8.67% compared to 18.10% in case of no filter but the capacitor. To further reduce the THD at this location, it will need additional filters installed. The frequency response shown in Fig. 12 shows clearly the impedance drop due to existence of the filter. The filter design dialog box is shown in Fig. 13.

Harmonic Analysis Test System [3], Fig. 14

The test system is a balanced industrial system given in [3] as Test System, Fig. 14. The utility bus ("100:UTIL-69") is at 69 kV and a local plant ("50:GEN-1") operates at 13.8 kV. All the data required for harmonic analysis are given in the reference paper. The obtained bus THD indices are shown in Table 5, in which the second column includes the values given in [3] and the third and fourth columns are the

TABLE 1
UTILITY SUPPLY

Parameter	Value
Supply voltage	220 kV
Short-circuit capacity	4000–10 000 MVA
X/R	20.0

TABLE 2
XFMR DATA

Parameter	T1	T2
Power rating (MVA)	100	30
Voltage rating (kV)	220–33	33–6.6
Impedance (%)	14	10
X/R	10.0	10.0

TABLE 4
HARMONIC CONTENT OF RECTIFIER CURRENT (AC SIDE)

Harmonic number	Frequency (Hz)	Magnitude (A)	Phase (degrees)
1	60	618	0
5	300	124	180
7	420	88	0
11	660	56	180
13	780	47	0
17	1020	36	180
19	1140	33	0

values provided by Paladin-harmonics. Series or parallel RL means the loads were modeled as series or parallel RL circuits. The numbers show that the THD on the harmonic source bus of "49:RECT" is the highest. The THD provided from Paladin-harmonics in both parallel RL and series RL are higher than those given in [3] except for the harmonic source bus. The THD for all buses are higher if the loads are modeled as series RL circuits compared to parallel RL load model.

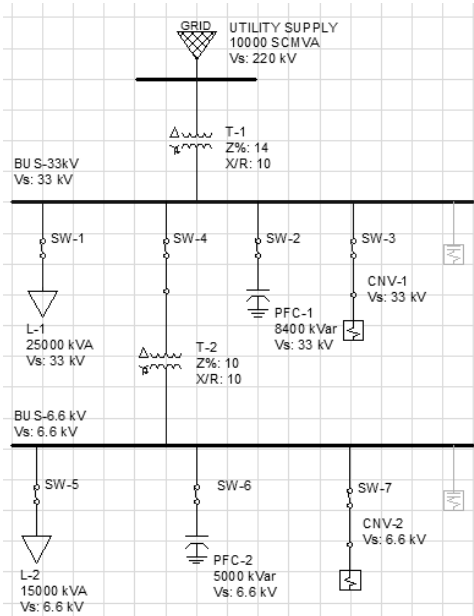


Fig. 2 Paladin DesignBase one-line diagram

Harmonic	Magnitude (%)	Angle (Deg)	Sequence
1	100.00	0.00	Positive
2	5.00	20.06	180.00 Negative
3	7.00	14.24	0.00 Positive
4	11.00	9.06	180.00 Negative
5	13.00	7.61	0.00 Positive
6	17.00	5.83	180.00 Negative
7	19.00	5.34	0.00 Positive
8			
9			
10			
11			
12			
13			
14			
15			
16			
17			

Frequency Scan Options

Starting Frequency: 10 pu, Ending Frequency: 1200 Hz, Step: 0.1 pu

Sequence/Unit Selection: Positive Sequence, Negative Sequence, Zero Sequence, Frequency Unit: pu

Bus Selection: Driving Bus: BUS-33kV

Available Buses: BUS-33kV, BUS-6.6kV, CNV-1, L-1, L-2, PFC-1, PFC-2, T-1 Ph, UTILITY SUPPLY

Selected Buses: BUS-33kV

Fig. 3 and 4: Harmonic Current Source and Frequency Scan

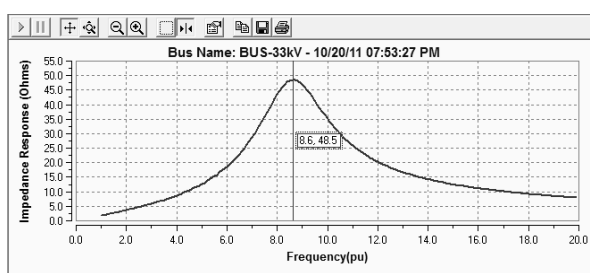


Fig. 5 Driving point impedance at 33 kV bus, SW-4 open

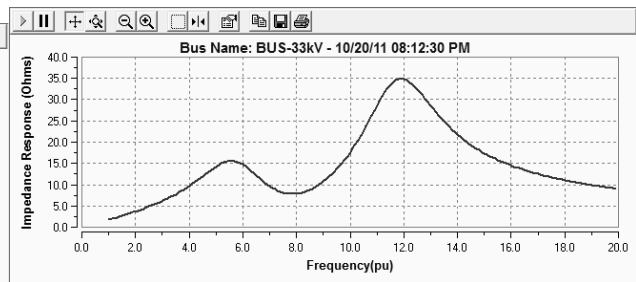


Fig. 6 Driving point impedance at 33 kV bus, SW-4 closed

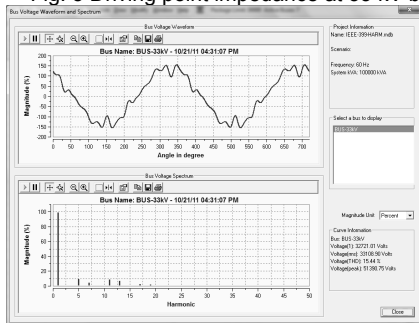


Fig. 7 Harmonic voltage at 33 kV bus, SW-4 opened

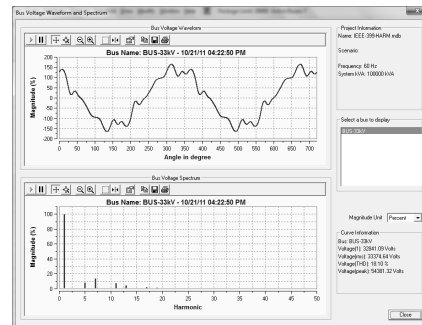


Fig. 8 Harmonic voltage at 33 kV bus with CVN-1, SW-4 closed

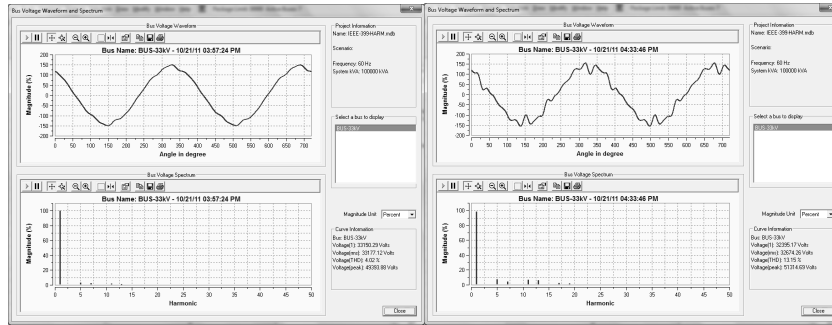


Fig. 9 Harmonic voltage at 33 kV bus with CVN-2; SW-4 closed

Fig. 10 Harmonic voltage at 33 kV bus with both CVN-1 and CVN-2

Conclusions

This paper showed that the input data given in one test system is inaccurate or not clear. We hope this paper encourages further development and enhancement of harmonic analysis test systems and techniques, in areas such as components models, case studies, harmonic mitigation techniques, complete system input data and results, standards and integration of variable renewable energies like solar and wind power sources. Benchmark systems for evaluation and continuous improvements of harmonic simulation techniques and software are crucial and valuable.

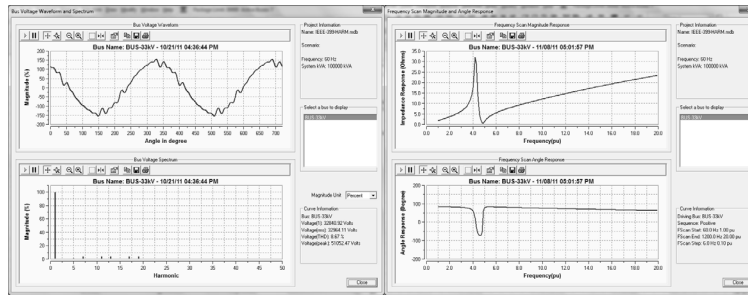


Fig. 11 Harmonic voltage at 33 kV bus with a single tuned filter

Fig. 12 Frequency response at 33 kV bus with a single tuned filter

TABLE 5 THD RESULTS COMPARISON

Bus	THD (%) [3] series RL	THD (%) series RL	THD (%) parallel RL
100:UTIL-69	0.28	0.43	0.31
01:69-1	0.37	0.43	0.31
03:MILL-1	1.93	2.73	1.97
50:GEN1	1.87	2.72	1.96
51:Aux	1.81	2.67	1.94
05:FDR F	1.94	2.73	1.97
49:RECT	8.02	7.21	6.40
39:T3 SEC	1.80	2.62	1.91
26:FDR G	1.93	2.73	1.97
06:FDR H	1.93	2.73	1.97
11:T4 SEC	1.90	2.70	1.96
19:T7 SEC	1.81	2.63	1.92
29:T11 SEC	1.84	2.67	1.94

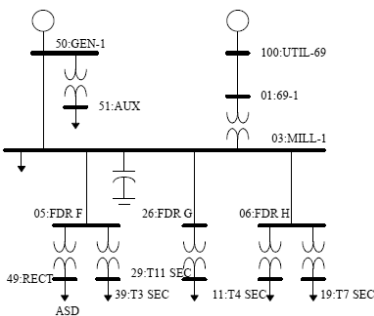


Fig. 13 A balanced industrial system from [3]

Acknowledgements

The authors would like to thank their colleagues in Power Analytics Corporation for their supports in various areas

References

[1] IEEE Standard 399-1997, "IEEE Recommended Practice for Industrial and Commercial Power Systems Analysis".
 [2] IEEE Task Force on Harmonics Modeling and Simulation, "Test systems for harmonics modeling and simulation", *IEEE Trans. Power Del.*, vol. 14, no. 2, pp. 579 - 583, 1999.
 [3] Wilsun Xu, "Status and future directions of power system harmonic analysis", *IEEE Power Engineering Society General Meeting*, Vol.1, pp. 756 - 761, 2004.
 [4] IEEE Standard 519-1992, "IEEE Recommended Practice and Requirements for Harmonics Control in Electrical Power Systems".

FORCE CONTROLLED GRASPING IN A TWO FINGER ROBOTIC HAND

O. B. Lőrinczi¹, P. Aradi² and T. Szalay³

¹ Budapest University of Technology and Economics, Faculty of Mechanical Engineering,
Department of Mechatronics, Optics, and Engineering Informatics
Bertalan Lajos street 4-6, 1111 Budapest, Hungary
(e-mail: lorinczi@mogi.bme.hu)

² Budapest University of Technology and Economics, Faculty of Mechanical Engineering,
Department of Mechatronics, Optics, and Engineering Informatics
Bertalan Lajos street 4-6, 1111 Budapest, Hungary
(e-mail: petra@mogi.bme.hu)

³ Budapest University of Technology and Economics, Faculty of Mechanical Engineering,
Department of Manufacturing Sciences and Technology
Egry József street 1, 1111 Budapest, Hungary
(e-mail: szalay@manuf.bme.hu)

Keywords: biomechanics, robotic hand, force-feedback control

Abstract. One of the most important human senses is the tactile sense – the force or pressure sensing in our hands. Many researches and applications deal with the development of force control in robotics in order to improve the intelligence of robot systems using additional sensing abilities. Within the framework of this development a two finger symmetric robotic hand has been developed. The experimental device is driven by a single DC motor. Both fingers are equipped with strain gauges based force sensors. The controlling hardware has been constructed and manufactured by ourselves that allows easy testing of the different solutions and further development. The control algorithm was programmed in LabVIEW environment. The general goal of this research is the improvement of upper limb prostheses. Force-feedback is necessary, because multi-loop control with visual feedback towards the user and position control with inner feedback loop are not sufficient for the implementation of precise motion. The topic of providing a kind of force feedback available directly for the user is a field in which extremely useful results can be achieved, promising extraordinary change in the usability of prosthetic arms.

Introduction

In this paper, an experimental two-finger gripper mechanism will be described, which is intended to improve the usability of robotic hands in the field of medical applications. The objective of a complex project is the development of a five-finger robotic hand with the most comprehensive control system that is possible to implement. To achieve this goal, the components of the control system have to be analyzed. The components of the control system of a medical purpose robotic hand are shown on Fig 1.

The main parts are as follows:

- Visual feedback to user for position control (commonly used)
- Inner position feedback (commonly used)
- Inner force feedback (less common)
- Force feedback to user (very rare/research phase)

The position feedback is always primary compared to the others; however the information obtained by the haptic sense might have the same importance as the position feedback. In many of the cases, force feedback is not available because of its complementary role and the difficulties of implementation. Typically, special control strategies of the position loop are attempted to substitute the force feedback loop [1,2].

In this study, the potential of the inner force feedback will be inspected. At the Budapest University of Technology and Economics, a force feedback robotic gripper has been developed for the experiments [3]. Using the gripper mechanism equipped with strain gauges, the gripping force can be measured. The acquired data is processed by software, programmed in LabVIEW. Not only the control algorithm that can be implemented, but the mathematical model of the entire gripper mechanism, in order to verify the different control strategies before applying them on the apparatus itself.

First, we verify the proper operation of the gripper mechanism by using a conventional force control with a proportional integrating controller. After that, new control strategies can be developed for additional features. By applying fuzzy control, unexpected situations can be handled in case of extremely fragile or soft materials – or, in possession of the mechanical characteristics of different types of objects – the material, of the handled object can be estimated, just as the proper strategy of grasping; taking advantage of the possibilities of pattern recognition [4] is gaining ground - a step towards cognitive systems.

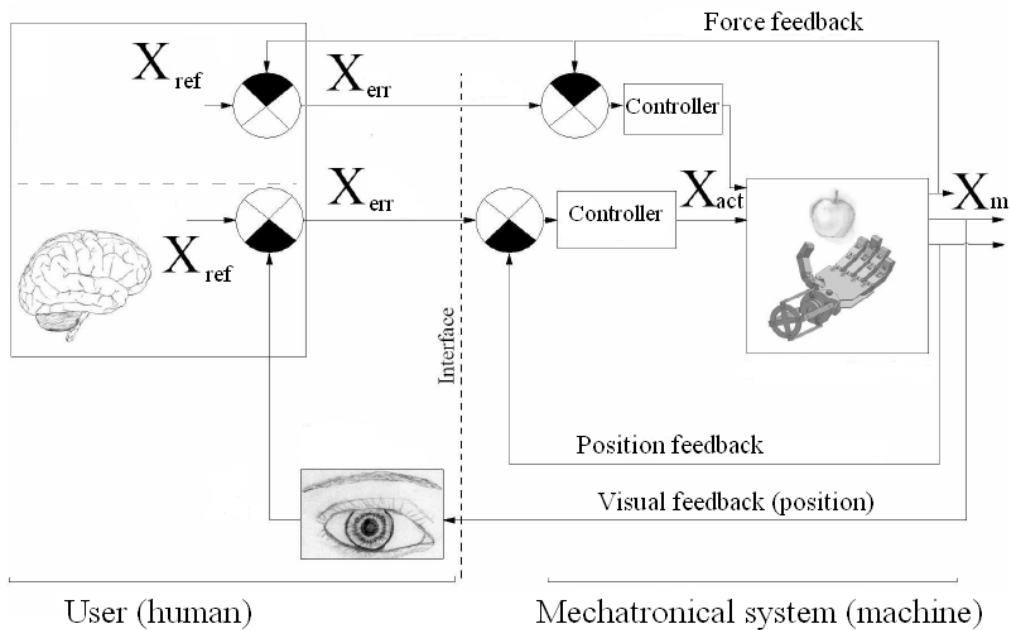


Fig. 1. The control system of an artificial hand

The experimental setup

The main unit of the experimental device is the two-finger gripper mechanism itself (shown on Fig 2). The gripper is driven by a single DC motor; the state variables that can be measured are the gripping force by two strain gauges and the motor rotational speed by a Hall-sensor. An additional unit for the measurement of the position is under development.

Currently, the gripper is able to perform the tasks of the inner force feedback control loop shown on the upper right corner of Figure 1; completed with the measurement of rotational speed and position can expand the possibilities of feasible functions of the experimental device.

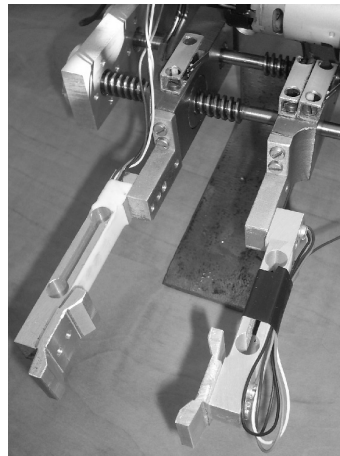


Fig. 2. The construction of the gripper mechanism

The further units shown on Figure 3. are needed to control the gripper. First, a precision instrumental amplifier circuit, and a bidirectional motor controller circuit are necessary in order to create the conditions for measurement and actuation. Since the strain gauges have differential outputs and the voltage range is between $\pm 10\text{mV}$, the instrumental amplifier has to be precise and must be equipped with proper noise filtering (in addition, digital filtering shall be applied after sampling). We use a three-operational-amplifier circuit for the measurement, as it has high reliability yet easy to manufacture.

The inputs for sampling and outputs for actuation are made available by a National Instruments USB-6008 data acquisition I/O unit. With this equipment, the analogue-digital and the digital/analogue conversion and the connectivity with a personal computer are possible also. The software of the control algorithm is running on the PC, what can raise issues about the speed of the control system; since the speed of the I/O unit is 10 kSample/sec, the speed necessary for the software is easily accessible including all signal processing procedures needed.

The software has built-in controlling toolbox, however self-developed control algorithms can be implemented also. The connection with the data acquisition device is pre-constructed; the focus of development can be merely the elaboration of the control strategy for the grasping procedure.

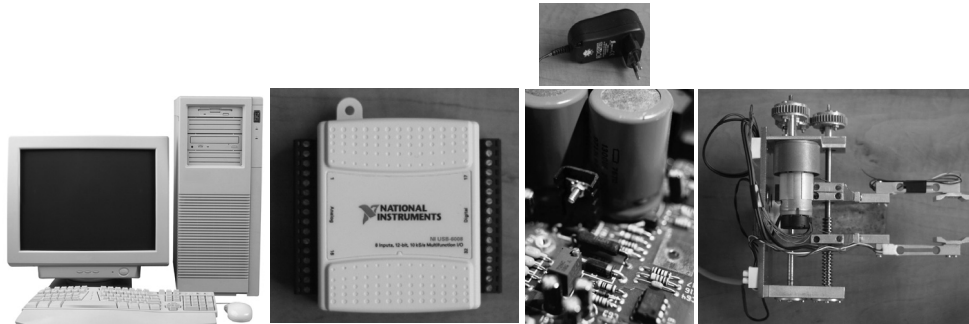


Fig. 3. The experimental setup

Mathematical model and simulation environment

As it was mentioned earlier, the verification of different control strategies is an important phase of the research. The mathematical model can be described in two phases; first, a simple, linearized model has been created, then the non-linear components can be added to the numerical simulation.

From the structure graph, the differential equations of the system can be achieved; after adding the non-linear components, the mathematical model is ready for testing. With this method, a suitable model can be implemented; however the development of a state-space model is planned for more accurate results. The linear part of the mathematical model can be described by the structure graph of each unit (Figure 4.):

- DC motor
- Gear with flexible shafts
- Thread spindle
- Flexible levers

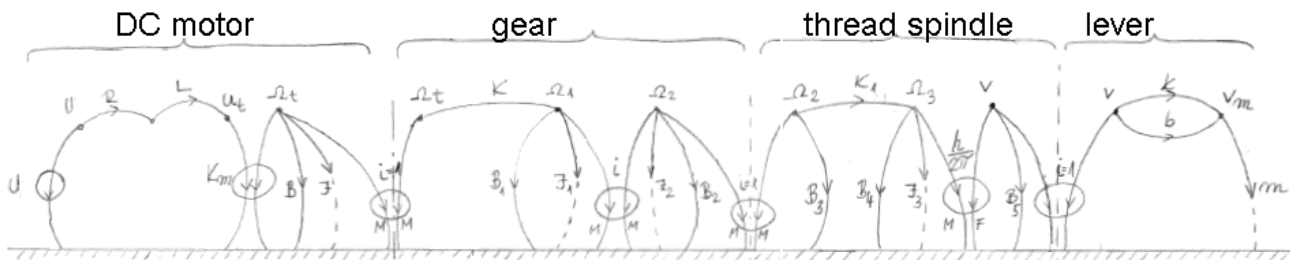


Fig 4. The linearized model

The most conspicuous non-linear behavior is the chuck of the gears. Because of this effect, constant gripping force can be measured however the levers are moving. In this case, the pertinence of the action is cannot be verified without additional information or special control strategy. By increasing the robustness of the control software, the undesired effect of non-linear parts can be avoided, and the system can handle unforeseen events or malfunctions.

One way of giving the software the desired robustness is the application of fuzzy control. Since the appropriate action is influenced by many circumstances, the efficient way for the regulation is the application of numerous if – then type fuzzy rules. By applying the rules, the controller can determine the action suitable for the highest amount of rules. Fuzzy logic control is a well-developed field of science, but it provides infinite approaches in particular tasks just as robotic grippers [5].

The fuzzy control is helpful not only by the means of the feedbacks on the machine side; it can be applied developing a human-machine interface. The EMG signals controlling robotic hands used as prostheses are often processed by neuro-fuzzy algorithms, exactly for the facilitation of controlling by the means of pattern recognition [6].

The most effective tool for the implementation of the numerical simulation and the control algorithms is the National Instruments LabVIEW (Figure 5.); a considerable number of other studies also use it for modeling and simulation tasks regarding robotic grippers and force feedback [7,8]. Built-in control and simulation tools have been used to implement some features and data communication, but self-developed subroutines were necessary for special purposes, e.g. the non-linear behaviour of the gears. Based on the information provided by the simulations, the expected operation of the manufactured gripper mechanism can be estimated without endangering the device.

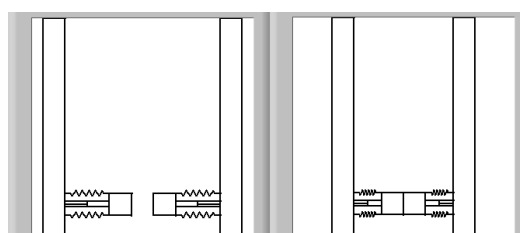


Fig 5. Detail of the software GUI



Conclusion

The paper presented an experiment designed to improve the abilities of gripper mechanisms, particularly in the field of medical applications. Different force-feedback control strategies can be implemented using the experimental setup – furthermore – the algorithms can be verified using the simulation environment implemented in LabVIEW.

The information obtained from the experiments will be utilized in future projects on the way towards the main goal – the development of a fully functional five-finger robotic hand.

Acknowledgements

The work reported in the paper has been developed in the framework of the project „Talent care and cultivation in the scientific workshops of BME" project. This project is supported by the grant TÁMOP-4.2.2.B-10/1-2010-0009.

References

- [1] C. Toledo, L. Leija, R. Muñoz, A. Vera and A. Ramírez: Upper Limb Prostheses for Amputations Above Elbow: A Review, 2009 Pan American Health Care Exchanges – PAHCE. Conference, Workshops, and Exhibits, March 16 - 20, 2009, Mexico City, Mexico, IEEE Catalog Number: CFP0918G, ISBN: 978-1-4244-3669-9, pp. 104-108.
- [2] Tao Geng, Mark Lee, Martin Hülse: Transferring Human Grasping Synergies to a Robot, *Mechatronics*, 21 (2011) pp. 272–284.
- [3] Miklós Gergely Oláh, Clamping force control of a robotic gripper, MSc Thesis, 2011
- [4] Jonathan Becedas, Ismael Payo, and Vicente Feliu: Two-Flexible-Fingers Gripper Force Feedback Control System for Its Application as End Effector on a 6-DOF Manipulator: *IEEE TRANSACTIONS ON ROBOTICS*, VOL. 27, NO. 3, JUNE 2011, pp. 599-615.
- [5] Abidemi Bolu Ajiboye and Richard F. ff. Weir: A Heuristic Fuzzy Logic Approach to EMG Pattern Recognition for Multifunctional Prosthesis Control, *IEEE TRANSACTIONS ON NEURAL SYSTEMS AND REHABILITATION ENGINEERING*, VOL. 13, NO. 3, (SEPTEMBER 2005.) pp. 280-291.
- [6] Francis H. Y. Chan, Yong-Sheng Yang, F. K. Lam, Yuan-Ting Zhang, and Philip A. Parker: Fuzzy EMG Classification for Prosthesis Control, *IEEE TRANSACTIONS ON REHABILITATION ENGINEERING*, VOL. 8, NO. 3, SEPTEMBER 2000, pp. 305-311.
- [7] Giuseppe Carbone, Antonio González: A Numerical Simulation of the Grasp Operation by LARM Hand IV: A Three Finger Robotic Hand, *Elsevier: Robotics and Computer-Integrated Manufacturing* 27 (2011) pp. 450–459.
- [8] Giuseppe Carbone, Stefano Iannone, Marco Ceccarelli: Regulation and Control of LARM Hand III, *Robotics and Computer-Integrated Manufacturing*, 26 (2010) pp. 202–211.

COMPARATIVE ANALYSIS OF THREE MICRO-HOLE MACHINING TECHNOLOGY

V. Csala¹, S. Markos¹ and T. Szalay¹

¹Budapest University of Technology and Economics,
Department of Manufacturing Science and Technology,
1111 Budapest, Egry St. 1. HUNGARY

Keywords: Micro manufacturing, Drilling, EDM, Laser machining

Abstract. The micro machining of holes refer the hole-making in diameter range below millimetre. In the paper three generally used technologies are compared, drilling, laser machining and electrical discharge machining. These technologies were analysed based on experimental measurement of dimensional accuracy, circularity, burr formation and the image of the internal surface. The most important criteria was the quality of the surface, because the main purpose of the examination was to find the most precise process. In addition, calculations were made to determine the costs, considering machining time, tool- and machine costs. In experiments high precision lathe, Nd:YAG laser and electrical discharging machine were used. As final experience the micro drilling resulted the most promising parameters and it was suggested for industrial application.

Introduction

In industrial applications machining micro holes became everyday demand. In medical devices, in vehicle industry and in state of the art technology machining holes below 1 millimeter diameter or below even 100 μm diameter is obvious expectation although there are many challenges and difficulties in these machining technologies. However manufacturing miniature parts or details is not very new, and we knew several technologies that solved this requirement successfully such as laser machining or EDM. The most important difference in today production that nowadays we need to produce high volume of these parts, and we need to keep this ability in our serial production. Fortunately more and more companies provide this technology and the machining of micron measure parts started to develop rapidly [1]

Based on Taniguchi's prognosis machining parts and details in micron range using traditional cutting operations would be available in the beginning of the 21th century [2]. (Figure 1) The curves on the figure show the manufacturing capability of the available technologies from 1940 in the aspect of the achievable accuracy. As Taniguchi defined on the figure the micro machining produce sizes around 100 μm . The most frequently used machining operations and the minimal sizes that can be produced using them summarized in Table 1.

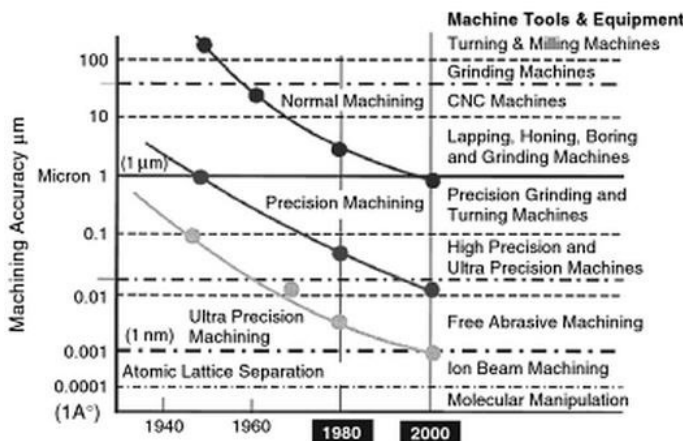


Figure 1 Taniguchi's prognosis modified by Byrne et al. [3]

Machining operation	Achievable size
micro-moulding	500 μm
micro-pressing	50 μm
micro-milling and grinding	25 μm
stereolithography	12 μm
micro-EDM	5 μm
ion-beam machining	0.2 μm

Table 1 Measure limit of the technologies [1]

The motivation that we experimentally compared the most frequently used micro-hole machining operations came from the interest of a company produce medical devices. This company developed medical water jet machining devices for surgery applications. The general structure of the machining device can be seen in Figure 2. In medical devices there are some extreme requirements. The device must be controlled in high precision; the cutting fluid must be bio-compatible and the material of the nozzle also must be bio-compatible. In medical water jet machining mostly saline is used for working fluid and metal or metal alloys for nozzle e.g. alumina, titanium, platinum. In order to provide the necessary speed of the fluid for cutting the nozzle diameter must be between 0.1 – 0.15 mm (Figure 3) [4].

The investigations aimed to choose technology for production of the cutting nozzle of the medical water jet machining device. We have chosen stainless steel test material and we limited our experiments to carry out drilling electrical discharge machining and laser machining trials. Varying the machining parameters we measured the form accuracy, the diameter accuracy, the burr formation, the surface roughness in the hole, the machining time and the cost of the machining. Learning the best parameters in each operation we were able to suggest the technology for the company.

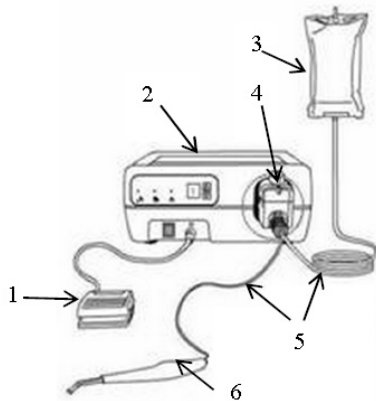


Figure 2 The medical water jet machine

1. pedal (switching on-off the device)
2. motor/generator
3. saline
4. pump piston
5. rubber tubing
6. cutting nozzle

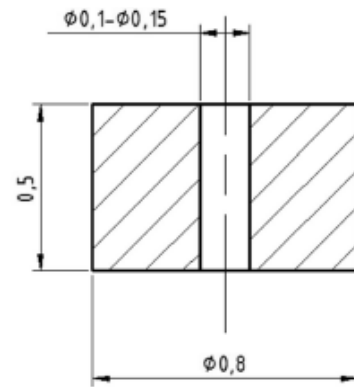


Figure 3 The cutting nozzle

Machining experiments

Micro-drilling

However the drilling operation is a traditional cutting technology and the parameters, the results and the behavior of the process is widely investigated in macro dimension, the micro-drilling has several altering phenomena and we did not conclude the results based on macro experiences. There are many additional influencing parameters such as very high spindle revolution (between $1-12 \times 10^4$ 1/min), the stability of the spindle, the high cutting forces as the consequence of relative big edge radius (see figure 4) [5, 6, 7].

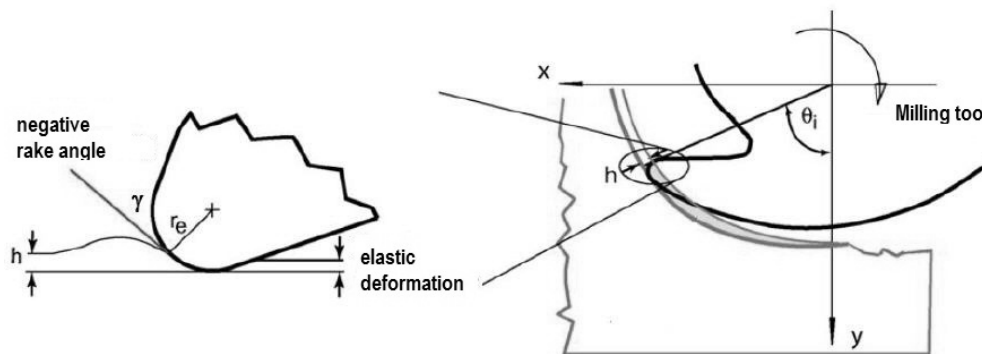


Figure 4 Elastic deformation in micro-drilling as the consequence of the low chip thickness - edge radius ratio

The drilling experiments were carried out in the laboratory of the Department of Manufacturing Science and Technology. The machine tool was an ultraprecision lathe made in the Hungarian company Csepel Machine Tool Works. This machine tool was equipped with an additional high speed spindle maximum 60 000 1/min revolution. Table 2 shows the positioning capability of this machine. Figure 5 shows the machining environment of the micro-drilling experiments

UP 1 lathe (Csepel Ultraturn)	[mm]
axial error of the spindle	0.001
radial error of the spindle	0.001
positioning unit in z direction	0.0001
positioning unit in x direction	0.0001
positioning accuracy	0.001
repeatability	0.001

Table 2 Accuracy of Csepel machine tool



Figure 5 The Csepel Ultraturn machine tool

We bought SECO tools, SD22 center drill and SD26 micro-drill were used. The appropriate tools were chosen after comparing the choice of the main producers based on the price and technology description. We compared the tools of Mitsubishi, Fairtool, Seco and Perfor. Seco was the cheapest with acceptable technology recommendation and the dealer provided the shortest delivery.

Two different stainless steel sheets were used in the experiments, the cutting speed and the feed were varied. The parameters of the experiments are detailed in table 3. Figure 6 shows some of the holes referring to the number in the plan of the experiments.

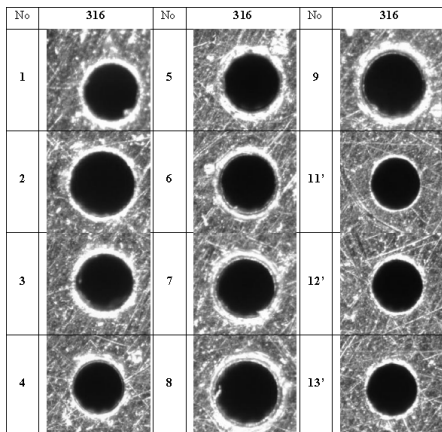


Figure 6 Results of drilling experiments

Plan of experiments					
No.	Diameter [mm]	Cutting speed [m/min]	revolution number [1/min]	feed [mm/rev.]	feed rate [mm/min]
1	0.15	4.712	10000	0.001	10
2	0.15	4.712	10000	0.002	20
3	0.15	4.712	10000	0.003	30
4	0.15	9.425	20000	0.001	20
5	0.15	9.425	20000	0.002	40
6	0.15	9.425	20000	0.003	60
7	0.15	14.137	30000	0.001	30
8	0.15	14.137	30000	0.002	60
9	0.15	14.137	30000	0.003	90

Table 3 Plan of micro-drilling experiments

Laser drilling

The laser drilling experiments were carried out in the laboratory of the Department of Material Science and Engineering. We used the LASAG KLS 246-FC 40 Nd:YAG laser cutting machine that has 15 W average power with maximum 5000 Hz exciting frequency. The minimal focal diameter is 0.03 mm, it is applicable for producing the hole with 0.15 mm diameter. In hole machining application circular trajectory cutting was used. You can see the hole making strategy on figure 7 where the starting of cutting is in the center point (1) then we apply an inner circle for roughing (2) and a second circle is finished the requested diameter (3). The machining environment can be seen on the figure 8.

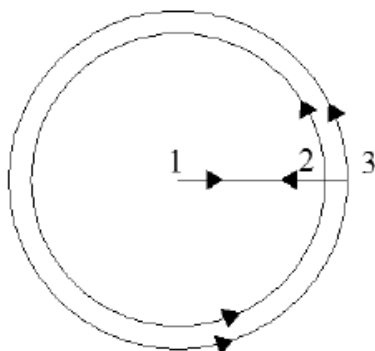


Figure 7 Circular cutting trajectory

During the experiments we varied the pulse time, the frequency the average power, the average energy level and the pressure of the oxygen inlet. Table 4 demonstrates the plan of the laser drilling experiments. As the figure 9 demonstrates the quality of the laser cutting weaker than the micro-drilling operation in the aspect of form and diameter accuracy. There are limited numbers of holes that reach acceptable parameters.

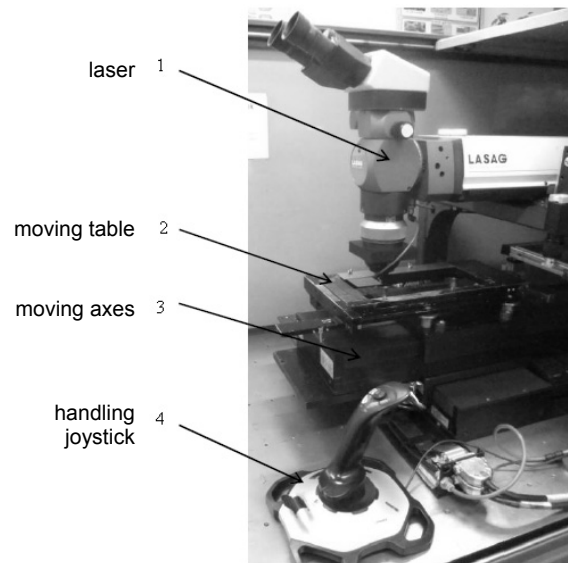


Figure 8 The laser drilling environment

Plan of experiments in laser drilling								
Number of holes	Voltage [v]	Pulse time [ms]	Frequency [Hz]	Cutting speed [m/s]	acceleration [m/s ²]	average power [W]	average energy [mJ]	pressure of oxygen [bar]
1 - 3	350	0.1	500	1	0.5	15	36	4
4 - 6	350	0.1	500	1	0.5	15	36	5
7 - 9	350	0.1	500	1	0.5	15	36	6
10 - 12	350	0.05	900	1	0.5	13-14	15.3	4
13 - 15	350	0.05	900	1	0.5	13-14	15.3	5
16 - 18	350	0.05	900	1	0.5	13-14	15.3	6

Table 4 The plan of the laser drilling experiments

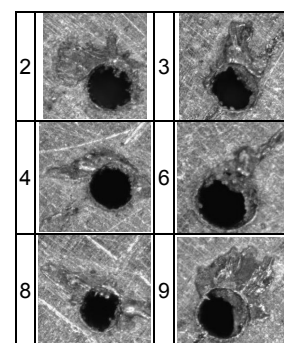


Figure 9 Results of laser drilling

Micro-EDM

The micro electrical discharge machining experiments were carried out in the laboratory of Department of Manufacturing Science and Technology. The machine tool was a Sarix SX100 micro EDM as figure 10 shows. During the hole making pulse time, voltage and frequency were varied. The plan of the micro-EDM experiments can be seen in table 5. The applied parameters were chosen based on previous experiences and state of the arts research literature [7].

Plan of experiment in micro-EDM						
No.	frequency [Hz]	voltage [V]	current [A]	pulse time [ms]	spark-gap [μm]	gain
1	100	80	80	4	72	10
2	100	90	80	4	72	10
3	100	100	80	4	72	10
4	120	80	80	4	72	10
5	120	90	80	4	72	10
6	120	100	80	4	72	10
7	150	80	80	4	72	10
8	150	90	80	4	72	10
9	150	100	80	4	72	10

Table 5 Plan of the micro-EDM experiments

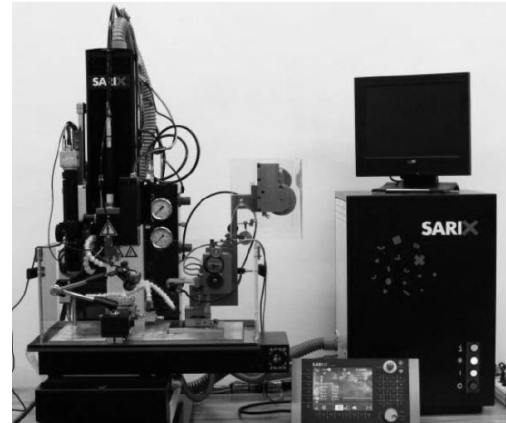


Figure 10 Sarix micro-EDM machine

Figure 11 shows some of the results of these experimental machining. The form accuracy of the holes is comparable with the holes machined by micro-drilling. However in the aspects of cost and machining time this technology is not the most efficient.

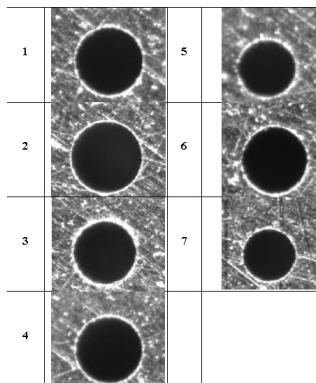


Figure 11 Holes machined by micro-EDM

point of view	micro-drilling	laser drilling	micro-EDM
1	4	1	5
2	5	3	4
3	5	1	3
4	2	1	5
5	4	5	1
6	3	5	1
7	5	5	5
8	5	5	5
9	2	4	4

Table 6 Evaluation of the investigated technologies

Evaluation of the results

The three different technology were investigated considering the aspects of form (1) and diameter (2) accuracy, the surface roughness (3), the burr formation (4), the machining time (5), the machining costs (6), the availability of the technology (7), the possibility in the aspect of medical applications (8) and the accessibility of skilled workers (9). In the table 6 we evaluate these parameters in the scale of 1 to 5, where 5 is the best and 1 is the worst value. The sum of these values gives the overall "goodness" of the particular technology based on our experiments. Using this evaluation we suggest micro drilling for industrial application, the second was micro-EDM and the less applicable may be laser drilling.

Acknowledgement

This research was initiated an industrial demand that aimed to compare the application of hole making technology in micro machining range. The work reported in the paper has been developed in the framework of the project „Talent care and cultivation in the scientific workshops of BME" project. This project is supported by the grant TÁMOP-4.2.2.B-10/1--2010-0009 . This research partly supported by Hungarian Scientific Research Fund, the project number is OTKA 101703. The research results is used in the international bilateral project "Multi-sensors based intelligent tool condition monitoring in mechanical micro-machining", project numer is TÉT_10-1-2011-0233.

References

- [1] John Shanahan (Product Manager of. Makino): Trends in Micro Machining Technologies, EDM Today, (2004)
- [2] Wit Grzesik: Advanced Machining Processes of Metallic Materials, (Elsevier 2008)
- [3] Byrne, Dornfeld, Denkena: Advancing Cutting Technology, CIRP Annals, Manufacturing Technology Vol. 52/2, (2003), pp.483-507
- [4] Vilmos Csala: Application of micro-drilling technology – in Hungarian, (Diploma Thesis, BME 2012)
- [5] Pei Yongchen, Tan Qingchang, Yang Zhaojun. A study of dynamic stresses in micro-drills under high-speed machining. International Journal of Machine Tools & Manufacture. Volume 46, Issue 14 (2006), Pages 1892-1900
- [6] Varga, Gy., Dudas, I.: Modelling of Vibration of Twist Drills when Environmentally Friendly Drilling, International Journal of Mathematical Science, Vol. 6, No. 3-4, (2007), pp.: 319-338, ISSN: 0972-754X



-
- [7] P. Drasnar, J. Kudlacek, V. Kreibich , V. Kracmar, M. Vales: The properties of electrically deposited composite Zn-PTFE coatings, *Modern Machinery Science Journal*, Vol. 4/1 (2011) pp. 248-251
 - [8] K.H Ho, S.T Newman: State of the art electrical discharge machining, *International Journal of Machine Tools and Manufacture*, Volume 43, Issue 13, (2003) , Pages 1287-1300



International Conference on Innovative Technologies, IN-TECH 2012,
Rijeka, 26. - 28.09.2012



THE INFLUENCE OF CHITOSAN'S CHARGE BEHAVIOUR ON ANTIMICROBIAL PROPERTIES

T. Ristić^{1,2}, L. Fras Zemljč², O. Šaupel², and A. Zabret²

¹ Tosama d.o.o., Production of medical supplies, Vir, Šaranovičeva cesta 35, 1230 Domžale, Slovenia

² University of Maribor, Faculty of mechanical engineering, Institute for engineering materials and design, Smetanova 17, 2000 Maribor

Keywords: chitosan, N,N,N-trimethyl chitosan, charge behaviour, antimicrobial activity, medical textiles

Abstract. The influence of chitosans' charge behaviour on antimicrobial activity was investigated. Comparison between medical chitosan (CS), with primary amine groups, and its N,N,N-trimethylated derivative (TMC), chitosan with quaternary ammonium functional groups, was carried out in this study. The products were tested for their potential use as antimicrobial agents. The charge density of chitosan solutions was determined with polyelectrolyte titration at acidic (3.6) and alkaline (7.5) pH and was later related to antimicrobial activities against yeast *Candida albicans*. Both acidic chitosan solutions showed good inhibition of *Candida* strain at all incubation time intervals (up to 7h). TMC sample exhibited high antimicrobial activity at alkaline pH as well, while the CS sample was completely inactive. The results of antimicrobial activity testing have emphasized the importance of charged amine groups for inhibition of microbes.

Introduction

Chitosan is a linear aminopolysaccharide, composed of 2-amino-2-deoxy- β -D-glucan linked with glucosidic linkages [1]. It is obtained by alkaline deacetylation of chitin, which can be found in the exoskeletons of crustaceans, arthropods, and mollusks, as well as the cell-walls of certain fungi [2]. Chitosan has two important structural parameters, the degree of deacetylation (DD) and molecular weight (MW). Its performance within physics and chemistry is determined by the influences of these two parameters on such things as solubility, enrichment ions, the mechanics of the chitosan membrane, flocculation, etc [2]. Advantages such as biocompatibility, biodegradability and non-toxicity make chitosan an interesting biopolymer for many biomedical and pharmaceutical applications [3]. It also exhibit antimicrobial activity against gram-negative and gram-positive, as well as yeast, mould and spores [4, 5]. It is believed that amine groups ($-\text{NH}_2$), present in the chitosan's backbone, are responsible for antimicrobial activity. In acidic solvents, the $-\text{NH}_2$ group of chitosan becomes protonated (NH_3^+) which allows the chitosan to inhibit the growth of microorganisms [6, 7]. Nevertheless, antimicrobial activity is limited to acidic conditions due to its poor solubility above pH 6.5, where chitosan start to lose its cationic nature [8]. While water solubility is an important parameter for chitosan applications as an antimicrobial agent, research has been oriented in preparation of chitosan derivatives soluble in water over a wide pH range [9-13].

N,N,N-trimethyl chitosan (TMC) is a partially quaternized derivative of chitosan obtained by methylation process. Quaternization of the amine groups in the C-2 position creates a permanent positive charge in the chitosan backbone [12], as well as favourable solubility at all pH range. In terms of antibacterial activity TMC has exhibit more pronounced effect against broad spectrum of bacteria than unmodified chitosan [12, 13]. However, in the literature there is still a lack of information regarding its antimycotic activity.

The influence of chitosans' charge behaviour onto antimicrobial activity was investigated. Polyelectrolyte titration was used to establish the amount of amine groups in chitosan (CS) and N,N,N-trimethylated chitosan (TMC) solution at two pHs; i.e. pH 3.6 and pH 7.5. In addition, the antimicrobial activity testing was performed at the same pHs. The growth of microorganisms was monitored by measuring optical density (OD) at 600 nm at different incubation time intervals.

Materials

KiOmedine-CsU[®] medical chitosan (Mw 82000; 77.4 % deacetylated) from vegetal source and N,N,N-trimethyl chitosan (TMC) with 80 % degree of substitution (Mw 90000) were supplied by Kitozyme, Belgium. Lactic acid used for achieving dissolution of chitosan was obtained from Sigma-Aldrich Chemical Co. Ltd. The deionized water was obtained from Millipore Milli-Q water purification system.

Chitosan solution preparation

1 g of chitosan (CS) was suspended in Milli-Q water in order to prepare 0.5 % (w/v) solution. Solution was prepared without heating. Lactic acid (conc.) was added by drops and solution was left stirring overnight. pH of the solution was adjusted to 3.6. In case of the TMC sample, the solutions were prepared without addition of acid, while TMC is water soluble.

Methods

Polyelectrolyte titration

Polyelectrolyte titrations were carried out in an aqueous media at pH =3.6 and pH of 7.5, respectively. 0.1 mL of chitosan solution was pipetted into a titration vessel and a few milliliters of 0.1 mM indicator Toluidine Blue were added. The vessel was then filled up with distilled water to a volume of 40 mL. A Mettler Toledo DL 53 titrator, with a 10 mL burette was used for an incremental addition of polyelectrolyte titrant (PES-Na; c = 10 mM). Incremental additions of 25 μL were added every 3 - 10 seconds. The absorbance was measured as a potential change in mV, using a Mettler Toledo Phototrode DP660, at a wavelength of 660 nm. The concentrations of the protonated amino groups were determined from the equivalent volume of the added PES-Na solution, detected as the steep step in the absorbance vs. the volume V (PES-Na) titration curve, and by estimating the 1:1 binding stoichiometry of the ethylenesulfonate to the amine groups.

Antimicrobial activity

The antimicrobial activity against *Candida albicans* was estimated by turbidity method. Microbial strain was inoculated with liquid nutrient broth (NB) and incubated at 37 °C in laboratory shaker for 24 h and than diluted to give optical density (OD) 0.5 at 600 nm wavelength. It is believed that at these OD values 108 cells per ml are present. The microbial suspension usually absorbs in the wavelength range 600-610 nm. Therefore, higher growth is directly reflected by higher absorption value [15]. When OD value was determined, microbial nutrient broth was further diluted to give final concentration 10⁻³. After dilution, microbial suspension (100µL) was transferred to 96-well microplate and mixed with CS or TMC solution under aseptic conditions to give final volume of 200 µl in each well. Microplate was than incubated for 1, 3, 5, and 7 hours and optical densities were read subsequently.

Results and discussion

Polyelectrolyte titration

In table 1 the amount of protonated amine groups of CS and TMC solutions at acidic (pH=3.6) and alkaline (pH=7.5) conditions are presented. The polyelectrolyte titration results clearly show that the amount of protonated amino groups for both solutions were almost similar at acid pH, and account on average for around 5.5 mmol/g. This can be attributed to complete protonation of chitosans' amino groups in acid medium. On the contrary, in alkaline medium, where the primary amine groups (–NH₂) are fully deprotonated, no charge was detected in CS solution, while the quaternary amine groups of TMC solution accounted for 4 mmol/g of dry sample. Decrease in positive charge is due to primary amine groups' deprotonation at pH 7.5 which is above their pK value (6.3) [14].

Table 1 the amount of determined amino groups (A_i) in CS and TMC solution at pH 3.6 and 7.5

Sample	A _i [mmol/g] pH 3.6	A _i [mmol/g] pH 7.5
CS	5.6	0.0
TMC	5.5	4.0

Antimicrobial activity

Figure 1 and 2 depict antimicrobial activities of CS and TMC solutions at pH 3.6 and 7.5 against *Candida albicans*. Both acidic chitosan solutions showed good inhibition of *Candida* strain at all incubation time intervals (up to 7h). TMC solution exhibited high antimicrobial activity at alkaline pH (7.5) as well, while the CS solution was completely inactive. The results of antimicrobial activity testing are emphasizing the importance of charged amine groups for inhibition of microbes.

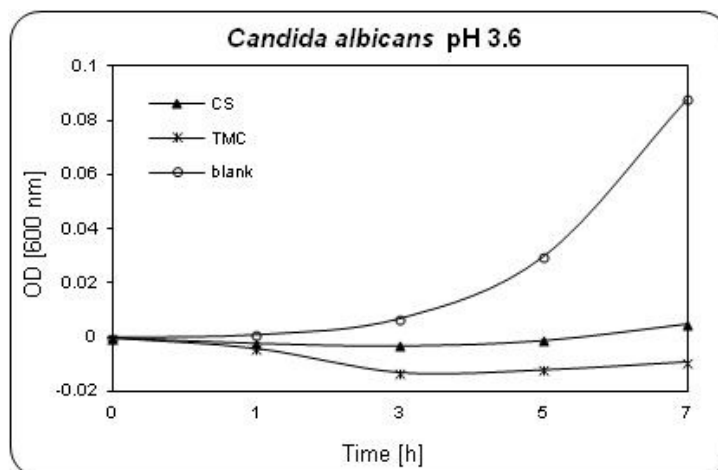


Fig. 1 Antimicrobial activity of CS and TMC solutions against *Candida albicans* at pH 3.6.

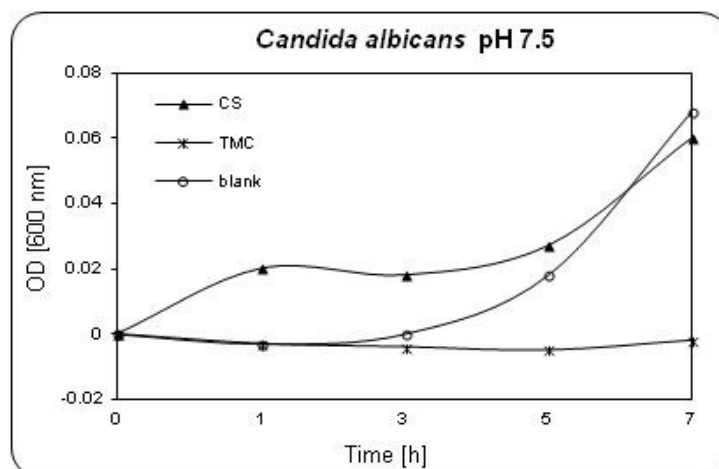


Fig. 2 Antimicrobial activity of CS and TMC solutions against *Candida albicans* at pH 7.5.

Conclusion

The results have confirmed that the chitosan's charge behavior has a great importance on antimicrobial activity. At acidic pH where both chitosan solutions (CS and TMC) were charged with a similar charge density the antimicrobial efficiencies were comparable as well. The main difference between CS and TMC sample was observed at alkaline pH, where TMC was able to inhibit *Candida albicans* effectively and unmodified chitosan (CS) has failed. This has proved that chitosan, unless charged, is not effective.

In case of TMC solution, quaternized trimethyl amino groups have also proven to be responsible for antimicrobial activity. This is in agreement with previously published work [15].

Especially quaternized chitosan (TMC) has a great prospective for medical applications, being particularly attractive as an antimicrobial agent for materials in sanitary use, such as gauze, bandages, tampons, sanitary pads, etc. as it exhibits good antimicrobial activity in wide range of pH scale.

Acknowledgment

Authors would like to thank for financial support. Operation part financed by the European union, European Social Fond.

References

- [1] M.N.V. Ravi Kumar: A review of chitin and chitosan applications, *Reactive & Functional Polymers*, Vol. 46 (2000), p.p. 1–27.
- [2] D. Enescu: Use of Chitosan in Surface Modification of Textile Materials. *Roumanian Biotechnological Letters*, Vol. 13, No. 6 (2008), p.p. 4037–4048.
- [3] Jayakumar, R, Menona, D, Manzoor, K, Nair, SV, Tamura, H. Biomedical applications of chitin and chitosan based nanomaterials—A short review, *Carbohydrate Polymers*, 2010, Vol. 82, 227–232.
- [4] Raafat, D, von Bargaen, K, Haas, A, Sahl, HG. Insights into the Mode of Action of Chitosan as an Antibacterial Compound, *Applied and Environmental Microbiology*, 2008, Vol. 74, No. 12, 3764–3773.
- [5] Kong, M, Chen, XG, Xing, K, Park, HJ. Antimicrobial properties of chitosan and mode of action: A state of the art review, *International Journal of Food Microbiology*, 2010, Vol. 144, 51–63.
- [6] N. Liu, X.G. Chen and H.J. Park: Effect of MW and concentration of chitosan on antibacterial activity of *Escherichia coli*, *Carbohydrate Polymers*, Vol. 64 (2006), p.p. 60–65.
- [7] Y.C. Chung, Y.P. Su, C.C. Chen, G. Jia, H.L. Wang, J.C.G Wu and J.G. Lin: Relationship between antibacterial activity of chitosan and surface characteristics of cell wall, *Acta Pharmacologica Sinica*, Vol. 25, p.p 932–36
- [8] Rabea, El, Badawy, MET, Stevens, CV, Smagghe, G, Steurbaut, W. Chitosan as Antimicrobial Agent: Applications and Mode of Action, *Biomacromolecules*, 2003, Vol. 4, No. 6, 1457–1465.
- [9] Lim, SH, Hudson, SM. Synthesis and antimicrobial activity of a water-soluble chitosan derivative with a fiber-reactive group, *Carbohydrate Research*, 2004, Vol. 339, 313–319.
- [10] Jintapattanakit, A, Mao, S, Kissel, T, Junyaprasert, VB. Physicochemical properties and biocompatibility of N-trimethyl chitosan: Effect of quaternization and dimethylation, *European Journal of Pharmaceutics and Biopharmaceutics*, 2008, Vol. 70, 563–571.
- [11] Rúnarsson, ÖV, Holappa, J, Malainer, C, Steinsson, H, Hjálmsdóttir, M, Nevalainen, T, Másson, M. Antibacterial activity of N-quaternary chitosan derivatives: Synthesis, characterization and structure activity relationship (SAR) investigations, *European Polymer Journal*, 2010, Vol. 46, 1251–1267.
- [12] da Silva, LP, de Britto, D, Regali Selegim, MH, Assis, OBG. In vitro activity of water-soluble quaternary chitosan chloride salt against *E. coli*, *World J Microbiol Biotechnol*, 2010, Vol. 26, 2089–2092.
- [13] Xu, T, Xin, M, Li, M, Huang, H, Zhou, S. Synthesis, characteristic and antibacterial activity of N,N,N-trimethyl chitosan and its carboxymethyl derivatives, *Carbohydrate Polymers*, 2010, Vol. 81, 931–936.
- [14] D. Čakara, L.F. Zemljčić, M. Bračić and K. Stana Kleinschek: Protonation behavior of cotton fabric with irreversibly adsorbed chitosan: a potentiometric titration study, *Carbohydrate Polymers*, Vol. 78, No. 1 (2009), p.p. 36–40.
- [15] T. Ristić, M. Novak, M.K. Kunčić, M. Bračić, A. Zabret, M.Š. Šolinc and L.F. Zemljčić: Shelf-life study of N -trimethyl chitosan antimycotic activity against *Candida albicans*, Egemeditex, Izmir, Turkey, (2012).



PCN2 – CYCLIC LOADING PULSATOR, FOR RESEARCH ON HYDROGEN EMBRITTLEMENT IN SURFACE TREATMENT TECHNOLOGY

K. Vojkovský¹, J. Kudláček¹, M. Pakosta¹ and M. Kršulja²

¹CTU in Prague, Faculty of mechanical engineering, Department of manufacturing technology, Technická 4, 166 07, Prague, Czech Republic

² University of Rijeka, Faculty of Engineering, Vukovarska 58, 51000, Rijeka, Croatia

Keywords: hydrogen, hydrogen embrittlement, testing methods

Abstract. The article deals with the process of hydrogenation and evaluation using an experimental measuring device – Cyclic Loading Pulsator, for destructive testing and identifying the dependencies involved in the effect the hydrogen generated in the processes of surface treatment has on machinery parts.

Introduction

Research on the influence of hydrogen on the properties of steel and subsequent applications of surface treatment is an issue which is currently the subject of much attention. When using contaminated input raw materials there is a risk of hydrogen embrittlement, or it begins to occur in materials that were long considered resistant to this type of degradation.

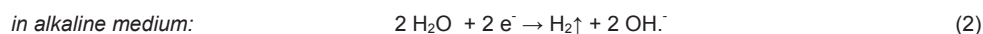
Higher hydrogen content in steels affects their mechanical properties, almost always negatively. It is known that hydrogen reduces ductility, breaking strength and yield strength. Atomic hydrogen dissolved in the steel easily diffuses in the iron grid α even at normal temperatures, and therefore it is easy to saturate the steel by hydrogen and to release it from the steel depending on the external conditions. When exceeding the critical concentration, hydrogen can cause cracking or escape from the material during heat treatment of the material and thus exert a negative effect on the finishes applied to such damaged materials.

Formation of hydrogen

Hydrogen is most frequently formed during pickling in mineral acids, during cathodic electrolytic degreasing, electroplating processes (e.g. zinc plating), also during oxidation (corrosion) of the material, welding and phosphating.

In most cases it involves cathodic reduction. For example, during pickling in mineral acids (HNO_3 , H_2SO_4 , HCl) the relevant anodic step – here the dissolution of metal – takes place at the same place as the formation of hydrogen, [1].

In contrast, during electrolytic degreasing and galvanizing the formation of hydrogen – and dissolution of metal, if any – takes place separately at the anode (1) and (2):



Subsequent reactions take place step by step. Hydroxyl ions discharge separately one by one, water molecules are broken down one after the other. In any case, atomic hydrogen is formed first (3).



Atomic hydrogen necessarily needs to form a bond and is therefore reactive. When it meets another hydrogen atom, they form a bond. In this case we speak about adsorbed (atomic) hydrogen H_{ad} . Adsorbed atomic hydrogen can bind with another of its kind to form a molecule of H_2 , which is eventually released in the form of gas bubbles and no longer poses any threat to the base material. However, adsorbed atomic hydrogen can also diffuse into the material and damage its structure (4).



There is no way to remove hydrogen recombined in hydrogen traps.

Experimental device

The experimental device PCN2 (see Fig. 1) is used for cyclic loading of components that have been exposed to the processes causing hydrogenation. PCN2 consists of three-phase asynchronous electric motor, frequency converter, which allows us to set the acceleration and braking times, to set the engine speed and to program frequency changes in relation to time. Compared to the first version, the new device has been fitted with an electronic circuit and sensors that allow us to stop the device if the tested component gets damaged and to record the time. It also employs an eccentric crank mechanism with a balancing feature, where one rod is placed in the slide housing and a second rod for pre-stressing is mechanically clamped in a clamping cage, [3].

The tested sample, in this case a retaining ring, is placed between the rods and the load is set according to the measuring parameters. The device alternately develops tension and compression at the end of the retaining ring which causes it to open and close. This movement is generated in the mechanical pulsator simulated by the testing device. Intensive simulation of the cyclic stress accelerates the spread of the crack caused by hydrogen present in the material, [2].

Thanks to this device we will be able to get an approximate idea of the number of cycles or the service life of a component that was exposed to the processes involving hydrogenation.

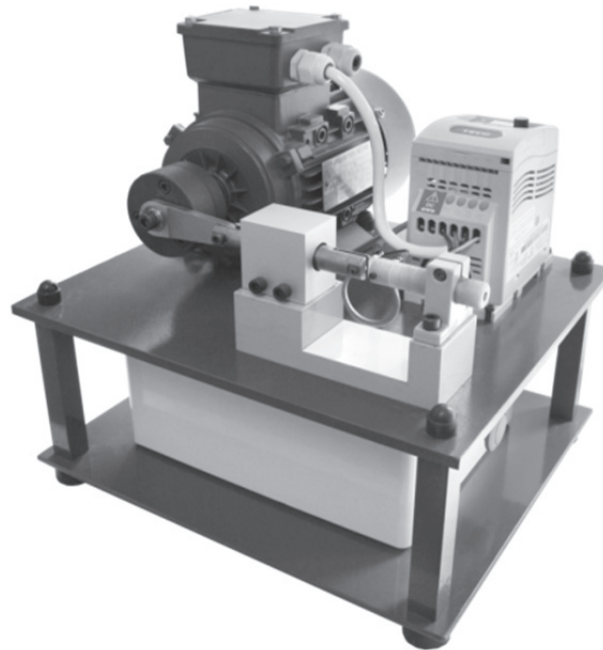


Fig. 1. Experimental device – PCN2

Experimental part

The measurement was carried out using the **DIN 471-AS 35 x 2.5** retaining rings.

Table 1. The chemical composition of the material of the rings in [%]

C	Mn	Si	P	S	Al	Cr	Ni	Mo
0.72	0.64	0.25	0.01	0.001	0.032	0.17	0.042	0.002

The retaining rings were supplied in the raw state without any surface treatment or heat treatment. All samples were degreased ultrasonically using 6 % sodium Pragold 68S, $t_o = 2$ min, $T = 45$ °C and then dried with hot air. In total, 8 sets of measurements were carried out for different types of pre-treatment, 5 pieces for each set. The result of the measurement is the number of cycles calculated based on the time needed to destruct individual rings.

Measurement parameters

The amplitude of opening the retaining ring is 4 mm. The preload of the ring $l_p = 5$ mm, $n_s = 2800$ rev/min⁻¹. The rings were exposed to the pickling solution of **HCl + FeCl₂ + H₂O** (HCl content: 96.0 g/l FeCl₂ content: 119.0 g/l), then they were rinsed in demineralised water $T_o = 23$ °C and dried with hot air $T_s = 20$ s. Then, according to various parameters for individual sets, the rings were exposed to cyclic loading using the experimental device PCN2.

Parameters of individual sets

Set 1: Retaining rings in the raw state exposed to variable loads.

Set 2: Retaining rings exposed to a temperature of 250 °C for 4 hours, let to cool to room temperature on a metal plate and exposed to variable loads.

Set 3: Retaining rings exposed to pickling solution for 2 hours, rinsed in water, dried and with the maximum delay of 10 minutes after pickling exposed to variable loads.

Set 4: Retaining rings exposed to pickling solution for 2 hours, rinsed in water, dried, exposed to a temperature of 200 °C for 1 hour and then exposed to variable loads.

Set 5: Retaining rings exposed to pickling solution for 2 hours, rinsed in water, dried, exposed to a temperature of 250 °C for 4 hour and then exposed to variable loads.

Set 6: Retaining rings exposed to pickling solution for 16 hours, rinsed in water, dried and with the maximum delay of 10 minutes after pickling exposed to variable loads.

Set 7: Retaining rings exposed to pickling solution for 16 hours, rinsed in water, dried, exposed to a temperature of 200 °C for 1 hour and then exposed to variable loads.

Set 8: Retaining rings exposed to pickling solution for 16 hours, rinsed in water, dried, exposed to a temperature of 250 °C for 4 hour and then exposed to variable loads.

Results

Table 2. Values measured by the experimental device of PCN2

Sample No.	Set 1		Set 2		Set 3		Set 4	
	Time	No. of cycles	Time	No. of cycles	Time	No. of cycles	Time	No. of cycles
	t [min.]	N [-]	t [min.]	N [-]	t [min.]	N [-]	t [min.]	N [-]
1	57	79800	45	63000	32	44800	45	63000
2	72	100800	44	61600	38	53200	33	46200
3	66	92400	45	63000	30	42000	23	32200
4	56	78400	47	65800	29	40600	39	54600
5	66	92400	42	58800	33	46200	35	49000
Average value	63.4	88760	44.6	62440	32.4	45360	35	49000

Sample No.	Set 5		Set 6		Set 7		Set 8	
	Time	No. of cycles						
	t [min.]	N [-]						
1	31	43400	29	40600	37	51800	30	42000
2	36	50400	30	42000	34	47600	31	43400
3	37	51800	32	44800	27	37800	27	37800
4	35	49000	31	43400	32	44800	38	53200
5	30	42000	24	33600	36	50400	36	50400
Average value	33.8	47320	29.2	40880	33.2	46480	32.4	45360

Samples after destruction in each set:

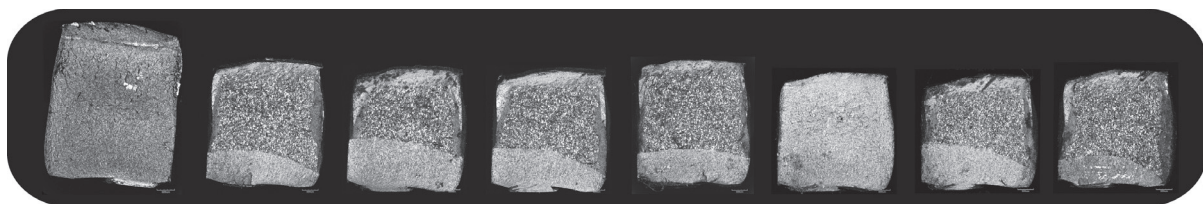


Fig. 2 Details of the retaining rings and fractures recorded by a laser confocal microscope Olympus LEXT OSL 3000 – magnification 120x

Average number of cycles to destruct individual retaining rings

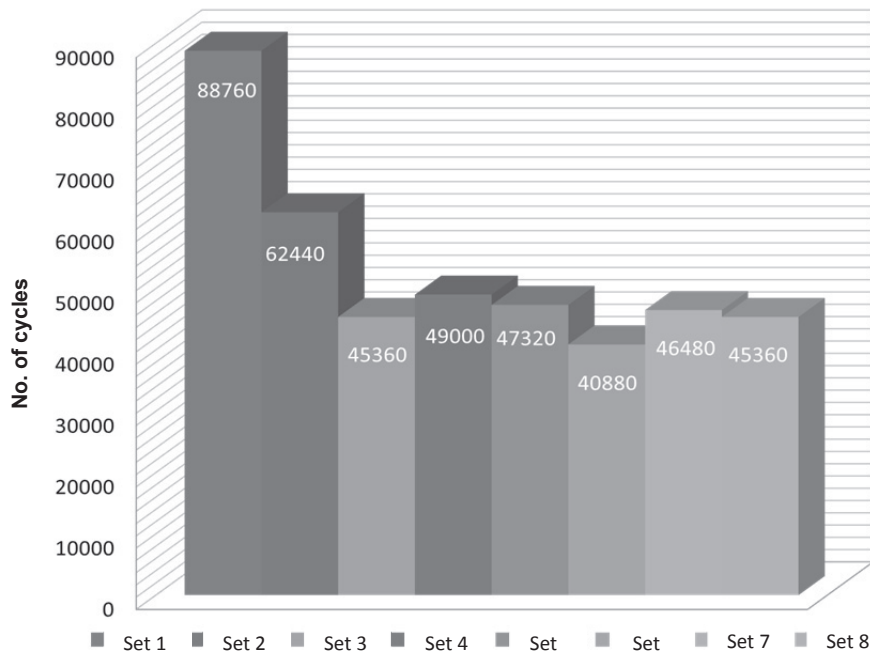


Fig. 2 Chart showing the average number of cycles to destruct individual retaining rings

Conclusion

The results of the measurements (Fig. 2) carried out using the experimental device PCN2 confirm the hypothesis saying which initial conditions of exposure of the material to pre-treatment processes susceptible to hydrogen embrittlement lead to its destruction. When comparing Set 1 and Set 3, we can see that the pickling time of 2 hours shortened the service life of the component by 43.400 cycles compared to Set 1 without pickling. The difference between Set 3 and Set 6 shows the reduction in the number of cycles by 4.480 caused a longer duration of pickling. Set 2, which was exposed to the temperature of 250 °C for 4 hours, shows 26.320 fewer cycles compared to Set 1. Efficient dehydrogenation can be seen in Set 4, where the number of cycles increased by 3,640 compared to Set 3. Longer dehydrogenation of 4 hours at 250 °C in Set 5 and Set 8 shows no difference in the degree of dehydrogenation in comparison with Set 4 and 7, and thus is economically wasteful. The device is currently being used for further detailed experimental tests. The evaluation of fractures in the samples exposed to surface treatments that involve intensive formation of hydrogen and its diffusion into the base metal has also been conducted.

Acknowledgments

The authors would like to acknowledge the support provided by the National CEEPUS Office of Croatia and National CEEPUS Office Czech Republic, which helped the research through mobility in the frame of the CEEPUS II HR 0108 project. Also the authors would like to thank for the support given by the SGS10/259/OHK2/3T/12 project.

References

- [1] VOJKOVSKÝ K.: Vliv vodíku v technologii povrchových úprav, In *Technologické fórum 2010*, Institute of Manufacturing Technology, Faculty of Mechanical Engineering, Czech Technical University in Prague. 5 s., 978-80-01-04586-2
- [2] VOJKOVSKÝ K., VOKŘÁLOVÁ K.: Vliv vodíku na konečnou povrchovou úpravu materiálu. Metodika zkoušek a vyhodnocení vlivu vodíku u aplikací povrchových úprav, In *Technologické fórum 2011*, Institute of Manufacturing Technology, Faculty of Mechanical Engineering, Czech Technical University in Prague. 7 s., 978-80-01-04852-8
- [3] VOJKOVSKÝ K., KUDLACEK J., KREIBICH V., DRASNAR P.: PCN1 - Pulsátor cyklického namáhání na zkoušení materiálu po technologickém zpracování, In: *Progresivní a netradiční technologie povrchových úprav*. Jaroměř: Kudláček Jan, Ing., 2011, s. 97-98. ISBN 978-80-904502-9-5.

INVESTIGATION OF COATINGS FRICTION COEFFICIENT USED IN PRODUCTION OF DEEP DRAWN PACKAGING CANS

M. Kršulja¹, P. Rožkanin², J. Kudláček², L. Pomenić¹ and Zlatan Car¹

¹ University of Rijeka Faculty of Engineering, Vukovarska 58, 51 000 Rijeka, Croatia.

² Czech Technical University in Prague, Faculty of Mechanical Engineering, Technická 4, 166 07 Praha 6, Czech Republic

Keywords: friction, sheet metal, deep drawing, tribology, coating, lacquer

Abstract. In technology of deep drawing of cans the use of lubrication oil has been replaced by coating finishes accordingly to packaged products. Wear of added coating can occur at edges and small radii where the average added coatings due to processing thinning reduces its size. Friction influences deep drawing parameters. If the optimal ratio can be established between coating selection, friction and deformation forces a better control and insight in deep drawing technology is possible. Investigation of friction coefficient for Gold lacquer, Overprint varnish and Alu pigmented lacquer for material TH 550 E2.8/2.8 FS 0.155 mm has been calculated with tribometer TOP 3.

Introduction

Sheet metal forming (SMF) technology uses sheet material that is plastically deformed in two dimensions (the thickness of the sheet is more or less constant) with the possibility of significant elastic recovery or spring back. Each metal forming process has its own characteristic features in terms of tooling and material flow. In Fig. 1 some products of thin sheet that ranges in thickness from 0.15 mm until 0.49 mm metal forming are shown.



Fig. 1 The products made from thin sheet metal forming taps and cans. [1]

Common features of SMF processes are the use of initially flat sheet material cut into an optimized shape (the blank), a punch to transmit the energy needed for the mechanical work, a die that directs the material flow during the process, a blank holder, which controls undesired material flow and wrinkles, and draw beads that are used to restrict material flow. SMF processes are suited for mass production applications and the products are processed, fully automated, in large volumes with the help of industrial presses. Forces that occur in deep drawing range from pneumatic 500 kN to 200.000 kN for Hydraulic presses, for mechanical presses strokes range up to 2000 strokes per minute [2, 3]. In order to control material flow during the deep draw process and surface quality of the formed products adequate lubrication condition need to be obtained. Poor lubrication or coating [4-6] can result fracture that leads to scrap (Fig. 2) due to high friction that limits the desired material flow. One of observed occurrences with low friction forces is pronounced wrinkling and on the other side if friction is too high the material can break. Therefore the friction is a very important parameter of the die construction that needs to be optimized depending on the die construction and forces included in process, and needs to be incorporated in virtual programming of production technology [7].

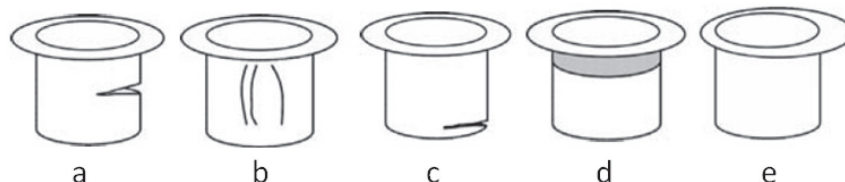


Fig. 2 Poor lubrication influences a) cracks, b) sec. wrinkle/pucker c) crack near bottom d) drawing marks, e) asymmetrical flange [2]

In technology of deep drawing of cans the use of lubrication oil has been replaced by coating finishes (tin layer combined with an organic coating). Coating finish has to have specific properties the capability to provide for adequate flow during the deep draw process and surface quality. Primary function of coating finish in packaging industry is to have adequate durability depending on the pH properties of packaged product. Coating has to resist the temperature of sterilization, transport damages and prevent interaction between product and environment. As the coating is applied before deep drawing process it has to adequately survive the deformation process. In this paper investigation of friction coefficient is conducted for the deep drawing process for material TH 550 E2.8/2.8 FS 0.155 mm that is covered with lacquer and cured for 20 minutes at the temperature of 200 °C. TH 550 is used for shallow deep drawing parts such as taps

and covers of cans, where designation E2.8 defines the tin coating of 2.8 g/m^3 , while the designation FS defines fine stone surface $R_a = 0,25\text{--}0,45 \text{ }\mu\text{m}$, and proof strength R_p of $550 \pm 50 \text{ MPa}$.

Coating

Coating is deposited on the sheet metal plate in accordance to shape and desired layer thickness of selected material, and then cured from 8 to 20 minutes at a temperature of 175°C to 225°C . For sheet metal deep drawing process typical friction factor that is obtained by lubrication is $\mu \approx 0.17$, [3]. This factor was obtained by combination of Gold lacquer Ir and mineral oil Ondina 15. Ondina 15 oil is of high purity and is used in the food and beverage industries. Its manufacturer is familiar company Shell. This oil is tasteless, colourless and odourless because of its extremely high purity it is also used in medicine (medical white oil). Viscosity is $15 \text{ mm}^2/\text{s}$ (at 40°C), the density of 850 kg/m^3 , flash point at 200°C and the solidification point -15°C . The basic purpose are tin sheets and ECCS where requiring high corrosion resistance and extra deep-drawing, which ensures smooth coating based on epoxy phenol. Without the lubrication and coating the hardened steel sliding on tin has the friction coefficient of $\mu = 0.17$ [3], however without the lubrication or coating in current deep drawing process material fractures. Additionally cast iron sliding on tin the friction factor has friction coefficient of $\mu = 0.32$ [4]. This proves that not only the friction factor is important but also the capability of lacquer to contain and regulate material flow. Beside Gold lacquer Alupigmented Lacquer and Overprint varnish were tested and their friction coefficients compared (Table. 1).

Table 1 Lacquer information

Lacquer	Description	Viscosity
Gold lacquer	Color that resembles gold, GL-79-5.	$110 \pm 5 \text{ mm}^2 / \text{s}$ (at 20°C) and the flash point is 37°C
Alupigmented Lacquer [5]	Homogeneous opaque film of silver-grey colour.	$(4,000 \pm 0,015) \text{ mm}$ at $t^\circ = 20,0 \pm 0,5^\circ \text{C}$: in the range of 60-140 sec.
Overprint varnish [6] Miraglaze™ 8909 base E	overprint varnish base, wet-on-wet and wet-on-dry. Varnish with wax and no driers.	10 at 23°C at 25 s^{-1} (Pa.s)

Experimental setup

The friction was determined using a Tribometer TOP 3 (Fig. 3). TOP 3 is an acronym of translation oscillation movement. The settings of the tribological tests are summarized in the Table 2. Friction contact was realized by specimen's pair - tablet and slab which demonstrate a square contact. Friction contact was burdened with a load of 4 kg ($\sim 40 \text{ N}$ force). Slab specimens were made from thin metal plate with special coating (Gold lacquer, Alupigmented Lacquer, Overprint Varnish). Tablet specimens were made from high strength steel 41Cr4. All the specimens were tested for the same time due to comparison of weight losses (Table 3). After 10 minutes it has been found that the main area of coating was removed and maximal test time of 10 min was determined. This time corresponds to a distance of 67 meters. Dynamics of movement was established to a 35 cycles per 1 minute, where 1 cycle = length of $2 \times 0.095 \text{ m} = 0.19 \text{ m}$. All the friction results are enclosed in Table 3 - 5. Weight of tablets and the slabs were measured with an analytical balance Mettler H64 and analytical balance Ohaus explorer pro.

Table 2. The tribological test summarization.

FUNCTIONAL PAIR			TEST SETUP						
Specimen's Marking	Slab	Tablet	Load [N]	Theoretical Pressure [$\text{N} \cdot \text{mm}^{-2}$]	Friction Trajectory [m]	Operation Time [min]	Dynamics [cycles per minute]	Sampling Rate [Hz]	Test Condition
A1	Alupigmented Lacq.	Steel 41Cr4	40	0,13	67	10	35	250	dry friction
A2	Alupigmented Lacq.	Steel 41Cr4	40	0,13	67	10	35	250	dry friction
A3	Alupigmented Lacq.	Steel 41Cr4	40	0,13	67	10	35	250	dry friction
O1	Overprint Varnish	Steel 41Cr4	40	0,13	67	10	35	250	dry friction
O2	Overprint Varnish	Steel 41Cr4	40	0,13	67	10	35	250	dry friction
G1	Gold Lacq.	Steel 41Cr4	40	0,13	67	10	35	250	dry friction
G2	Gold Lacq.	Steel 41Cr4	40	0,13	67	10	35	250	dry friction
G3	Gold Lacq.	Steel 41Cr4	40	0,13	67	10	35	250	dry friction

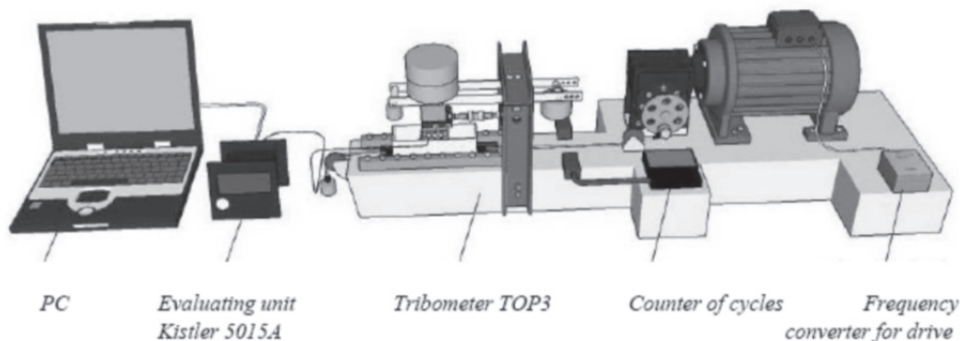


Fig. 3 Tribometer TOP3 with necessary components.

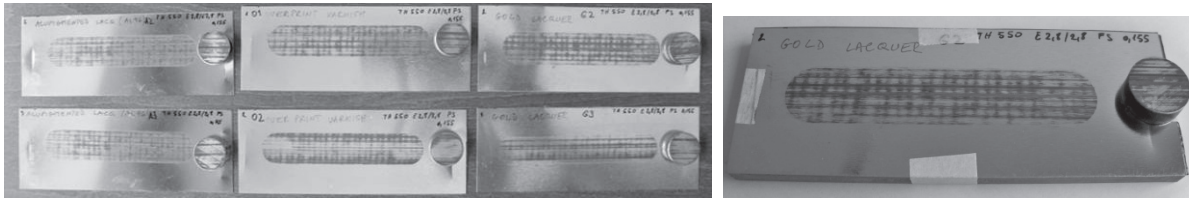


Fig. 4 Test specimens after testing: tablet - $\varnothing 20$ h11 mm, h=8 mm; slab - 135 x 50 x 8 mm

Table 3. Roughness of used tablets

ROUGHNESS OF TABLETS						
No of measurement	1.	2.	3.	4.	5.	Mean
Ra [μm]	0.12	0.12	0.09	0.11	0.10	0.108
Rz [μm]	0.78	0.86	0.61	0.69	0.67	0.722
Rq [μm]	0.15	0.16	0.11	0.14	0.13	0.138

Table 4. Weight losses and mean weight losses (Note: Minus symbol (tablet) means the transfer of coating from slab to the tablet surface.)

WEIGHT LOSSES COMPARISON					MEAN WEIGHT LOSSES		
Marking	Specimen	Weight [g] Before Test	Weight [g] After test	Weight loss [mg]	Coating type	Specimen	Mean Weight loss [mg]
<i>Alupigmented Lacquer</i>					A_{mean}	Slab	2,41
A1	Tablet	18,49231	18,49266	-0,35		Tablet	-0,41
A2	Slab	8,28997	8,28789	2,08	O_{mean}	Slab	2,46
	Tablet	18,53013	18,53071	-0,58		Tablet	-0,51
A3	Slab	8,36417	8,36162	2,55	G_{mean}	Slab	2,35
	Tablet	18,87630	18,87660	-0,30		Tablet	-0,40
<i>Overprint varnish</i>							
O1	Slab	8,37600	8,37306	2,94			
	Tablet	18,50916	18,50977	-0,61			
O2	Slab	8,37664	8,37466	1,98			
	Tablet	18,64923	18,64964	-0,41			
<i>Gold Lacquer</i>							
G1	Slab	8,19132	8,18831	3,01			
	Tablet	18,80400	18,80455	-0,55			
G2	Slab	8,37470	8,37188	2,82			
	Tablet	17,51026	17,51068	-0,42			
G3	Slab	8,41572	8,41449	1,23			
	Tablet	18,86667	18,86690	-0,23			

Table 5. Results of friction coefficients and its time development and mean coefficients on the start/end of tribological test

RESULTS OF FRICTION COEFFICIENTS AND ITS TIME DEVELOPEMENT					RESULTS OF MEAN FRICTION COEFFICIENTS				
Specimen's Marking	Time period for μ calculation				Specimen's Marking	Time period for μ calculation			
	20 - 40 s (after start)		560 - 580 s (before end)			20 - 40 s (after start)		560 - 580 s (before end)	
	μ_s [-]	μ_d [-]	μ_s [-]	μ_d [-]		μ_s [-]	μ_d [-]	μ_s [-]	μ_d [-]
A1	0,4432	0,3992	0,6120	0,5678	A_{mean}	0,4266	0,3655	0,5895	0,5509
A2	0,4080	0,3638	0,5846	0,5654		O_{mean}	0,4370	0,3830	0,5992
A3	0,4286	0,3335	0,5720	0,5195	G_{mean}		0,3682	0,3332	0,6231
O1	0,4365	0,3900	0,6403	0,5615					
O2	0,4374	0,3759	0,5581	0,5124					
G1	0,4635	0,4252	0,6336	0,5931					
G2	0,4194	0,3541	0,6193	0,5690					
G3	0,2216	0,2204	0,6163	0,5564					

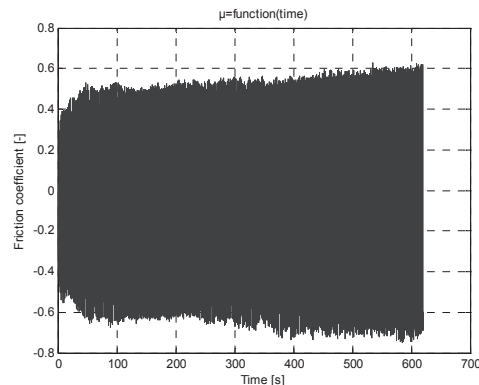


Fig. 5 Example for test A1 Alupigmented Lacquer - results of total test time

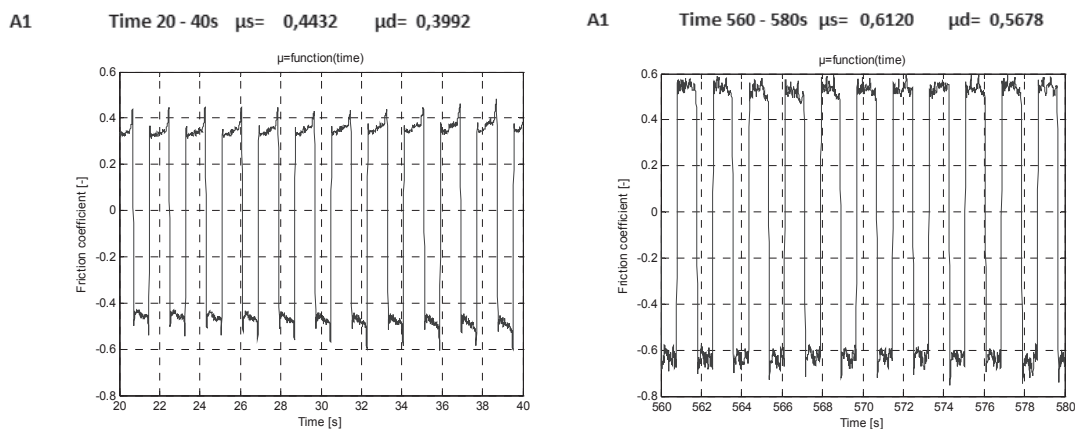


Fig. 6 Example for test A1 Alupigmented Lacquer results from 20 to 40 seconds and a period of 560 to 580 seconds

Conclusion

Tables 3, 4 and 5 show the results of weight losses and the results for friction coefficients for tested materials - Alupigmented Lacquer (A), Overprint varnish (O) and Gold Lacquer (G). The static coefficient of friction is indicated as the μ_s . Dynamic coefficient of friction is indicated as the μ_d . Mean values of all coatings have quite the same range. It can be assumed that the wear of coatings – weight losses will be higher in real process due to higher load exposed on the coating's surfaces. A very important fact is the quickness of deep drawing forming process. It means even the coating will be exposed to higher pressures there will be much less time (trajectory) to wear process. There are two values of friction coefficients in the table 5. First period was taken in time interval from 20 to 40 seconds. The friction coefficient was calculated from the 20 s interval after the tribological test has started. Second period was taken in time interval from 560 to 580 seconds just in the 20 s interval before the test ended. Comparison of friction coefficients in both periods give us information about the coating durability in the time. The most suitable for deep drawing process according the obtained results is the gold lacquer as the friction coefficient for it was the lowest $\mu_s=0.3682$, $\mu_d=0.3332$. In modern processes tin cans [2] are produced without addition of oil, and cans process have shown good formability. Future researches will include Finite element simulation [7] based on obtained friction coefficient for deep draw forming and for incremental metal forming, and higher testing loads for better prediction of real factory conditions.

Acknowledgements

The authors would like to acknowledge the support provided by the National CEEPUS Office of Croatia and National CEEPUS Office Czech Republic, which helped the research through mobility in the frame of the CEEPUS II HR 0108 project.

References

- [1] Private documents MGK-pack, www.mgk-pack.com, 2011.
- [2] Handbook of Lubrication and Tribology, Volume 1, Application and Maintenance, Second edition, International Standard Book Number-13: 978-0-8493-2095-8 (Hardcover) 2006 by Taylor & Francis Group, LLC.
- [3] Branimir Barišić, Analiza pojave Ludersovih traka u procesu izrade proizvoda iz tankostijenog lima, Doctoral thesis, mentor: Prof. Goran Cukor, Rijeka 2005.
- [4] ROYMECH – friction parameters, http://www.roymech.co.uk/Useful_Tables/Tribology/co_of_friect.htm, 2012.
- [5] Khimlex - Varnish-and-lacquer materials for can coating , <http://www.khimlex.ua/en/products/varnish/7.html>, 2012.
- [6] Varnish-and-lacquer materials for can coating, http://www.lawter.com/uploads/pdfs/Lawter_EU_Inks_2012.pdf, 2012
- [7] Božek, P. - Mihok, J. - Barborák, O. - Lahučký, D. - Vaňová, J.: New strategies of virtuality in programming of production technology, In: Annals of DAAAM and Proceedings of DAAAM Symposium. - ISSN 1726-9679. - Vol. 20, No. 1 Annals of DAAAM for 2009 & Proceedings of the 20th international DAAAM symposium "Intelligent manufacturing & automation: Focus on theory, practice and education" 25 - 28th November 2009, Vienna, Austria. - Vienna : DAAAM International Vienna, 2009. - ISBN 978-3-901509-70-4, s. 0403-0404.

AN APPLICATION OF PLANT PATHOGENS, *Phytophthora* spp. BIOLOGICAL CONTROL BY ANTAGONISTIC BACTERIA IN DURIAN FIELD, UTTARADIT PROVINCE, THAILAND

K. Mueangtoom¹

¹ Biology Program, Department of Science, Faculty of Science and Technology, Uttaradit Rajabhat University, Injaimee Road, Mueang, Uttaradit. 53000, THAILAND

Keywords: Durian, Phytophthora, Antagonistic bacteria, Biological control

Abstract. Variation in the morphological characteristics of *Phytophthora* spp. Isolates which were isolated from diseased durian plant parts obtained from Lablæe district, Uttaradit province in the north of Thailand were investigated. Colonies of this pathogen was mostly stellate pattern. Sporangia are ovoid-subpyriform in shape with 35-90 x 22-62 µm in size and the ratio of length and width is 1:1.6 to 1:2.0. Integrated control of this pathogen using the biological control by antagonistic bacteria was used to be an alternative to reduce the use of fungicides in agriculture. In this study, we screened the antagonistic bacteria that can inhibit the growth of *Phytophthora* spp. and found that *Bacillus cereus* showed significant inhibition activity on mycelial growth of *Phytophthora* spp. In dual culture, the fungal mycelium were limited in extension and became swollen and roughly. This may due to antibiotic substances produced by the antagonistic bacteria. The dry cell of *B. cereus* were used to control this pathogen in durian farm using 100 g cell dry weigh / 10 liters water / tree. It was showed 100 % reducing diseases in field trials.

Introduction

Durian (*Durio zibethinus*) is the favorite fruit in many Southeast Asian countries including Thailand, Malaysia, Indonesia and the Philippines. It is a prized tree in many mixed gardens and a valuable orchard crop that commands extraordinarily high prices at local and export markets [1]. The rapid consumer-driven expansion of the durian industry in Thailand has led to the establishment of orchards on increasingly marginal land. This marginal land was badly affected by the devastating floods and the outbreak of Phytophthora that followed killed about 40% of the durian trees [2].

Phytophthora spp. are plant pathogen causing diseases in many species of trees, vegetables and ornamental plants such as durian, citrus, para rubber, pepper, tomato, asparagus and orchid. Nowadays, fungicides are the popular way to prevent and control losses of agricultural products caused by Phytophthora[3]. However, these chemicals remain in nature and affect to ecosystem. To reduce the use of fungicides, the biological control by using antagonistic bacteria is an alternative [4].

In this work, we described the screening and in vitro test of the antagonistic bacteria were described the screening, in vitro and in vivo test against Phytophthora strains which were screened from durian field in Lablæe district, Uttaradit province.

Materials and methods

Phytophthora spp. identification

Durian implants with symptoms of stem rot were collected from several fields in Lablæe district, Uttaradit province, Thailand 2011. Small sections taken from the edge of the stem lesions were placed on PARPH medium after disinfecting then with 10% housekeeping bleach. The semi-selective media (PARPH) had a corn meal agar (CMA) base and included pimarcine (10 mg/l) and quintazone (100 mg/l) for selective inhibition of non-pythiaceous fungi and ampicillin (250 mg/l) and rifampicine (10 mg/l) for bacterial control. Hymexazole (20 mg/l) was used in the medium for partial control of *Pythium* spp [5]. The hyphal tip isolates were kept on slant tubes containing CMA at 4°C.

Phytophthora spp. were grown on V8 agar and potato dextrose agar (PDA), respectively, at 25 °C for determination of morphology under microscope.

Antagonistic bacteria screening

To screen the bacteria, 1 g of soil was dissolved in 10 ml of normal saline and 0.1 ml was spread on Nutrient agar (NA). A single colony of bacteria was isolated and maintained in glycerol stock at -20 °C. The bacterial strains were cultured on NA at 37 °C throughout the experiments. To perform in vitro antagonistic test, the fungi were grown on agar medium at 25°C for 2 days and afterward one-day-old bacterial culture was point inoculated by 2 cm away from peripheral colony. After 2 days, the inhibition zone of fungal growth was measured and the inhibition index was calculated from the ratio of inhibition zone by diameter of bacterial colony. The experiments were performed 3 replicates. The bacterial strains with highest antagonistic activity were identified by morphology and biochemical tests according to the Bergey's Manual of Systematic Bacteriology [6].

Biocontrol effect in vivo

Biocontrol effect of different cell concentrations suspensions of antagonistic bacteria were adjusted to concentrations of 0 g (control treatment), 50 g, 100 g, 150 g and 200 g cell dry weigh in 10 ml distilled water and sprayed to near run-off on durian seeds in the field, using a 1-L sprayer-nozzle bottle. Considering the average surface area of durian seeds, the volume of suspensions applied per seed with this procedure were 1 mL for 10 days.

Germinated seeds were shown in each seed in a field after 1 week. The seedlings were flooded by 20 ml of a small mycelial plug (2×3 mm²) *Phytophthora* spp. spore suspension. After 2 weeks, disease symptoms were scored based upon the following scale: '1' = no sign of disease symptoms; '2' = restricted lesions of approximately 2 mm in diameter or 5 mm in length; '3' = expanding lesions with diameters from 0.2 to 2 cm; '4' = lesions and/or necrosis of several sizes, covering up to 25% of the germinated seed surface; '5' = extended lesions and necrosis over 25% of the germinated seed surface.

Results and Discussions

Phytophthora spp. identification

Phytophthora spp. were isolated from Durian implants with symptoms of stem rot (Table 1). For morphology study, it was found a slightly difference about asexual structure. Sporangia are ovoid, ellipsoid, obpyriform, ovoid-obpyriform, and spherical form in shape with 35 - 90 x 22 - 62 μm in size and the ratio of length and width is 1:1.6 to 1:2.0 (Table 1).

Table 1. *Phytophthora* spp. isolates from Durian implants

Isolate	Implant	Chlamydospores		Sporangia		
		Shape	Avg. Diameter (μm)	Shape	Avg. Length x Breadth (μm)	L:B ratio
L01	Leaf	Globose	30	Ovoid-obpyriform, Spherical, Obpyriform	35-65 x 22-38	1:1.6
L02	Fruit	Globose	39	Ovoid-obpyriform, Ellipsoid, Obpyriform, Spherical	42-85 x 34-62	1:2.0
L03	Branch	Globose	34	Ovoid-obpyriform, Spherical, Obpyriform, Ovoid	45-90 x 25-50	1:1.9

From Table 1 shows All isolates produced globose chlamydospores, which were terminal and intercalary in the mycelium. The average diameter of chlamydospores was 30–39 μm . Based on these morphological characteristics. Several researchers have described the features of *Phytophthora* that distinguish it from other heterothallic species with conspicuous papillate sporangia. The sporangia are variable in shape, depending on isolate, mostly elliptical to ovoid, and prominently papillate. They are variable in size but average 35 to 90 μm in length and 22 to 62 μm in breadth, with length–breadth ratio of 1.6 to 2.0 μm . Many reports have shown that *P. palmivora* produces globose chlamydospores with diameters have been reported to measure 32 to 42 μm [7], averaging 33 μm [8], 36 μm [9] and 36.2 \pm 9.6 μm [10].

Antagonistic bacteria screening

Twenty-one bacteria strains were isolated from Lablæe district. Of these, 3 bacterial strains exhibited antagonistic activity against all 3 strains of *Phytophthora* and strain BL03 was chosen for further study. Only one strain, BL03, showed strong inhibition to the growth of *Phytophthora* spp. (Table 2). In dual culture of BL03 and *Phytophthora* spp., the fungal mycelium observed under light microscope were limited in extension and turned into swollen and roughly and in dual culture of BL07 and *Phytophthora* spp., the fungal mycelium became merely swollen. Based on morphological and biochemical characteristics, BL03 and BL07 were identified as *Bacillus cereus* and *Pseudomonas* sp., respectively.

Table 2 Inhibition index of antagonistic bacteria on *Phytophthora* spp. L01, L02 and L03 isolate.

<i>Phytophthora</i> spp. isolate					
L01		L02		L03	
Bacteria strain	Clear zone (mm)	Bacteria strain	Clear zone (mm)	Bacteria strain	Clear zone (mm)
BL02	12 \pm 0.51	BL03	17 \pm 0.43	BL03	17 \pm 0.55
BL03	21 \pm 0.39	BL07	15 \pm 0.32	BL 04	6 \pm 0.76
BL07	19 \pm 0.55	BL11	12 \pm 0.58		
BL12	22 \pm 0.43				
BL18	7 \pm 0.66				

Many studies have revealed that both *Bacillus* and *Pseudomonas* can be a good candidate for biological control of plant pathogenic fungi. For instance, *Bacillus cereus* UW85 could produce zwittermixin A and antibiotic B which reduced elongation and caused swelling of *P. medicaginis* germ tube [11]. *Bacillus* sp. BC112 could produce chitinase which destroyed cell structure of *Curvularia lutana* [12]. *Pseudomonas aureofaciens* PA147-2 could prevent *Phytophthora* root rot of asparagus caused by *P. megasperma* [13]. *Pseudomonas fluorescens* MM-B16 could generate aerugine and able to inhibit the growth of *Colletotrichum orbiculare* and *Phytophthora capsici* [14]. Therefore, it is possible that *Bacillus cereus* BL03 may produce antibiotic substances that can halt the growth of *Phytophthora*.

Biocontrol effect *in vivo*

The residual biocontrol effects of *Phytophthora* spp. were also investigated under field conditions. After specific time intervals from the moment of application of the antagonist, durian seeds were challenged by the zoospores of the pathogen and disease levels were evaluated (Fig. 1).

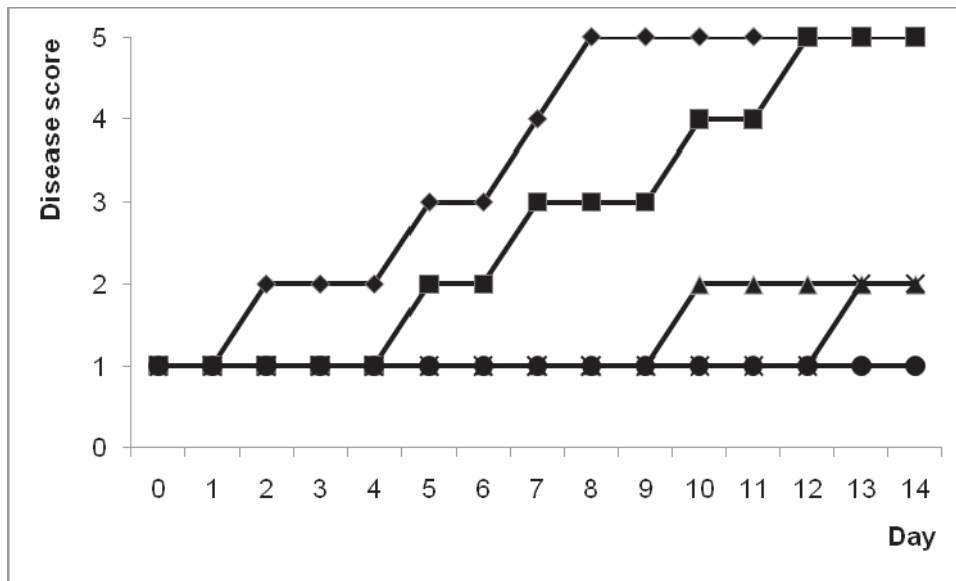


Fig. 1 Residual biocontrol effect of the *B. cereus* BL03 isolate on durian seed challenged by *Phytophthora* spp. with difference cell concentration of 0 (◆), 50 (■), 100 (▲), 150 (X) and 200 (●) g cell / 10 litter / tree

The lowest disease scores occurred with 50 g cell / 10 litters solution during the first 10 days after inoculation with *B. cereus* BL03. Afterwards, disease increased slowly but steadily, reaching severity levels similar to the positive control when seeds were challenged at 14 days of application of *B. cereus* BL03 (Fig.1, Fig. 2). The amount of viable spores of the antagonist remaining on the seed surface was greatly reduced after 10 days, with 100 g cell / 10 litters or higher that could not found diseases until the end of the experiment (Fig. 2).

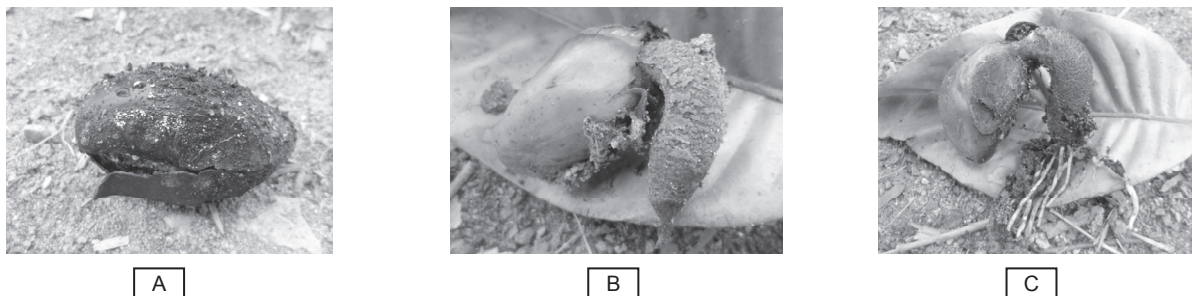


Fig. 2 Challenged durian seed with 0 g cell / 10 litters (A), 50 g cell / 10 litters (B) and 100 g cell / 10 litters (C) of *B. Cereus* BL03 cell suspension after 14 days of *Phytophthora* spp. Inoculation.

The progressive reduction in disease severity by higher inoculums concentrations of the antagonist is not unexpected as high initial inoculum enables full colonization of the seed by the *B. cereus* BL03, thereby improving its biocontrol efficacy. Since the cacao tree presents a complex endophytic [15] and epiphytic microbiota [16], lower initial amounts of the antagonist on the other hand are likely more susceptible to competition effects by other microorganisms. It was suggests that more frequent applications, or higher concentrations of the antagonist may be necessary. Combined application with certain fungicides may be also an alternative that warrants further investigation.

Conclusions

The potential for biological control of diseases has been explored in consideration of the importance of the environment and human health. Moreover, consumers have been more willing to buy chemical-free products with even higher costs. However, chemical application is still the most effective disease management strategy in modern agricultural system. Biological control is a promising alternative to control plant pathogens instead of use of chemicals, therefore much research for biological control agents has been conducted [17]. From this research, *B. cereus* isolates effectively reduced *Phytophthora* root rot on durian. BL03 was the most effective *B. cereus* isolate in biocontrol of *Phytophthora* spp. on durian in naturally field soil. In addition, this isolate produced larger average inhibition zones than other antagonistic bacteria isolates against *Phytophthora* spp. *in vitro* and showed the ability to inhibit *in vitro* growth of durian seed.

The phenomenon can also be exploited in industrial production as sporulation can be induced at the end of cultures [18]. This greatly facilitates post-culture conditioning as bacterial suspensions can be converted to easy to handle powder formulations without the impressive bacterial mortality observed with non-sporulating bacteria [19]. Shelf life of biocontrol based on sporulated bacteria is generally longer and require less storage precaution compared to other products containing living organisms. Bacilli are also relatively easy to produce industrially as they are not particularly exigent regarding nutritional sources. Beside its spore forming ability, *B. subtilis* possess several characteristics that enhance its survival in the rhizosphere and thus



its effectiveness as a biopesticide [20]. This bacterium known to live in aerobic environments can also behave as facultative anaerobe surviving and evolving under low oxygen concentration [21]. This is a real advantage in the rhizosphere as oxygen availability may fluctuate during time and is generally low. Additionally, *Bacillus* strain is a motile bacterium that readily moves towards and on the root surface which facilitates colonization of new ecological niches. Another reason for the high interest in *Bacilli* is the diversity of their modes of action. They can display almost all the mechanisms of biocontrol and bio-stimulation/fertilization mentioned here below and above. Moreover, one strain may often acts through several mechanisms. This enables these bacteria to be effective in many conditions (variety of pathogens, plants, environmental conditions) as one mechanism may act instead of another.

Acknowledgment

This research was financially supported by special research grant 32537 from The office of the higher education commission and The office of national research council of Thailand. The author also thanks Uttaradit Rajabhat University for financial support to IN-TECH 2012 conference.

References

- [1] E. O'Gara, D.I. Guest, L. Vawdrey, P. Langdon and Y. Diczbalis: Phytophthora diseases in durian and durian decline syndrome in Far-North Queensland. In: Drenth, A. and Guest, D.I., (eds.) Diversity and Management of Phytophthora in Southeast Asia. Australian Centre for International Agricultural Research, (Canberra, 2004), pp. 143-152.
- [2] T. Suzui, U. Kueprakon and T. Kamhangridthirong: Phytophthora Disease on some Economic Plants in Thailand. Plant Pathology Div. Dept. of Agr. 113 p. Tsao, P.H. 1974. Phytophthora Disease of Durian, Black Pepper, and Citrus in Thailand. Working Rept. (FAO, 1976). (Mimeographed)
- [3] T. Suzui and U. Kamhangridthirong: *Phytophthora* spp. isolated from some economic plants in Thailand. Tech Bull. Trop. Agr. Res. Cent., Japan. Vol. 12 (1979), pp. 32-41.
- [4] F. Jamali, A. Sharifi-Tehrani, M. Okhovvat, Z. Zakeri and R. Saberi-Riseh: Biological control of chickpea Fusarium wilt by antagonistic bacteria under greenhouse condition. Communication in Agricultural and Applied Biological Sciences. Vol. 69 (2004), pp. 649-651.
- [5] G.M. Waterhouse, F.J. Newhook and D.J. Stamps: Present criteria for classification of Phytophthora, In D.C. Erwin, S. Barnick-Garcia and P.H. Tsao eds. Phytophthora : Its Biology Taxonomy, Ecology, and Pathology. The Amer. Phytopathol. Soc., St. Paul, Minnesota. (1983), pp. 139-147.
- [6] T. Gibson and R.E. Gordon: *Bacillus*, In: Bergey's Manual of Determinative Bacteriology. The Williams and Wilkins Company, Baltimore (1974), pp. 529-555.
- [7] P. Holliday: Fungus diseases of tropical crops. Cambridge, UK, Cambridge University Press (1980), 607 p.
- [8] G.M. Waterhouse: *Phytophthora palmivora* and some related species. In: Gregory, P.H. ed., Phytophthora disease of cacao. London, Longman (1974), pp. 51-70.
- [9] S.F. Ashby: Strains and taxonomy of *Phytophthora palmivora* Butler (*P. faberi* Maubl.). Transactions of the British Mycological Society, Vol. 14 (1929), pp. 18-38.
- [10] G.R.A. Mchau and M.D. Coffey: Isozyme diversity in *Phytophthora palmivora*: evidence for a Southeast Asia centre of origin. Mycological Research, Vol. 98 (1994), pp. 1035-1043.
- [11] L.A. Silo-Suh, B.J. Lethbridge, S.J. Raffel, H. He, J. Clardy, and J. Handelsman: Biological activities of two fungistatic antibiotics produced by *Bacillus cereus* UW85. Appl. Environ. Microbiol. Vol. 60 (1994), pp. 2023-2030.
- [12] S. Basha and K. Ulaganathan: Antagonism of *Bacillus* species (strain BC121) towards *Curvularia lunata*. Curr. Sci. Vol. 82 (2002), pp. 1457-1463.
- [13] S.A.C. Godfrey, M.W. Silby, P.G. Fallon and H.K. Mahanty: Biological control of *Phytophthora megasperma* var. *sojae*, causal agent of Phytophthora rot of asparagus, by *Pseudomonas aureofaciens* PA147-2: a preliminary field trial New Zeal. J. Crop Hort. Sci. Vol. 28(2000), pp. 97-103.
- [14] J.Y. Lee, S.S. Moon and B.K. Hwang: Isolation and antifungal and antiomycete activities of aerugine produced by *Pseudomonas fluorescens* Strain MM-B16, Appl. Environ. Microbiol. Vol. 69 (2003), pp. 2023-2031.
- [15] J. Crozier, S.E. Thomas, M.C. Aime, H.C. Evans, K.A. Holmes: Molecular characterization of fungal endophytic morphospecies isolated from stems and pods of *Theobroma cacao*. Plant Pathology, Vol. 55 (2006), pp. 783-791.
- [16] G.M. Ten Hoopen, R. Rees, P. Aisa, T. Stirrup and U. Krauss: Population dynamics of epiphytic mycoparasites of the genera *Clonostachys* and *Fusarium* for the biocontrol of black pod (*Phytophthora palmivora*) and moniliasis (*Moniliophthora roreri*) on cocoa (*Theobroma cacao*). Mycological Research, Vol. 107(2003), pp. 587-596.
- [17] J. Handelsman and E.V. Stabb: Biocontrol of soilborne plant pathogens. The Plant Cell, Vol. 8(1996), pp. 1855-1869.
- [18] S. Monteiro, J. Clemente, A.O. Henriques, R. Gomes, M. Carrondo and A. Cunha: A procedure for high-yield spore production by *Bacillus subtilis*. Biotechnology Progress, Vol. 21(2005), pp. 1026-1031.
- [19] R. Lolloo, D. Maharai, J. Gørgens, N. Gardiner: A downstream process for production of a viable and stable *Bacillus cereus* aquaculture biological agent. Applied Microbiology and Biotechnology, Vol. 86 (2010), pp. 499-508.
- [20] N. Rosas-Garcia: Biopesticide production from *Bacillus thuringiensis* : an environmentally friendly alternative. Recent Patent in Biotechnology, Vol. 3 (2009), pp. 28-36.
- [21] M. Nakano and M. Hulett: Adaptation of *Bacillus subtilis* to oxygen limitation. Microbiologie, Vol. 157 (1997), pp. 1-7.

LCA AND NEW MATHEMATICAL METHOD FOR THERMIC TREATMENT PROCESSES BY INDUSTRIAL ORGANIC WASTE

V. Mannheim¹, Z. Siménfalvi²

^{1,2} University of Miskolc, Department of Chemical Machinery 3515 Miskolc-Egyetemváros, Hungary

Keywords: LCA, thermic treatment processes, mathematical model

Abstract. In the last few years, several waste energetic utilization/thermic treatment technologies have come to the front and have been declared to be the best available techniques. Priority of the energetic utilization of different types of waste is not unambiguous even today. In fact, it all depends on what type of waste is being treated thermically; therefore it is not the energy content that is the decisive factor. Thus, in case of combustible industrial organic waste, for example, this criterion is obviously of secondary importance, the most important viewpoint is that the least possible harmful material (e.g. end-gas containing unabsorbed chlorine derivatives) should remain at the end of the process. This paper summarises the thermic utilization processes with a comparison between the different technologies, stressing factors affecting their applicability and operational suitability. The research activity can set prognoses and models with LCA analyses and the conscious application of scientific methods, which can offer a prognosis for not tested situations. Despite the fact that chemical industry and the environmental protection are closely interlocked, there is fairly poor national and international professional literature available about the two connected professions. Pyrolysis, plasma-based technologies and gasification can be considered on the basis of three viewpoints: environmental burden, energy efficiency and social-economic viewpoints. While examining the above three viewpoints, it worked out a new mathematical method which besides LCA takes time and probability as well into consideration with the combination of a programming language, and which may mark a new direction for solution and decision even in waste management.

1. Introduction

The persistent organic pollutants (POPs) wastes used oils, waste with content of PCB/PCT and pesticide wastes; take the main place in the group of organic industrial waste and the residues of the POPs waste generated in the processes of the chemical industry. Related to the incipient environmental demands and the reduction of risks, there are two main principles that are practical to follow:

1. Modification of the industrial process with green chemistry methods (primary technology)
2. Working out and optimization for the treatment of POPs waste (secondary technology)

This article would provide new information to the second research trend related to the thermic treatment methods. There are green chemistry methods and some other treatment approaches for decreasing the quantity of the organic industrial waste (the most expedient environmental aids are the usage of low-containing waste processes), but currently thermic treatment processes are the most popular alternatives. In order to choose the best suitable treatment of organic industrial waste, it is indispensable to compare the possible different methods of thermal treatments and prioritise them by environmental, energetic and economic effects. This research can set out alternatives and models with the help of LCA methods, which can extend a prognosis and priority for thermic technologies. The Life Cycle Assessment (LCA) can play an important role in this research. With the application of this method for the thermic processes and technologies, their energetic, economic and environmental efficiency can be determined. With the use of LCAs it can be possible to determine a priority order, not just among each waste processing method but also among thermic utilization processes.

2. Methodology, goal and scope of the research

The first step of this research is to compare the available WtE technologies, which may differ significantly. Nowadays, incineration is the most widely used process, so it is worth comparing with the new thermic technologies. The main advantages are useful end-products, which can be utilised as materials and also energetically. The second step is to set up life cycle assessment models of the WtE technologies. Their advantages and disadvantages are examined in such a multi-component matrix. The LCA software GaBi 5 is the basis for life-cycle impact assessment. The LCA results are analyzed with regard to life-cycle segments and as a functional unit of energy consumption and/or the recoverable energy that can be used [11]. The possible energetic utilisation can be carried out by incineration, cracking (pyrolysis or gasification) and plasma technology, or parallel flow incineration (in equipments). The following sections discuss the most frequently used thermochemical technologies for WtE [3, 12]. These are:

- 1) Incineration: full oxidative combustion;
- 2) Gasification: partial oxidation;
- 3) Pyrolysis: thermal degradation of organic material in the absence of oxygen;
- 4) Plasma-based technology: combination of (plasma-assisted) pyrolysis/gasification of the organic fraction and plasma vitrification of the inorganic fraction of waste feed.

The more advanced thermochemical approaches such as pyrolysis, gasification and plasma-based technologies have been applied to selected smaller scale waste streams, and attempt to control temperatures and pressures of the process. While the application of pyrolysis at low, mid- and high temperature is mainly possible for wastes, gasification is suitable for all burnable materials. In connection with plasma technology, the elimination of dangerous wastes is done by oxidation, and in this method of reduction the goal is to extract raw material. Plasma-based technology is the least-known process. With pyrolysis the emission of heavy metals is lower (due to lack of oxygen), but one of the disadvantages is that the use of pyrooil is accompanied by significant emissions. Besides this, pyrolysis produces a large quantity of pyrocoke with a high concentration of heavy metals in the cinders. Plasma-based technology has a low gas flow, fast

warming and cooling. At the end of the process, with minimal environmental effects, materials of glass and ceramics can be obtained, which can be utilised in the building industry [4, 5, 8].

3. Application of the LCA method with Software GaBi 5

Before new technologies enter the market, however, their environmental superiority over competing options must be asserted based on a life-cycle approach. Life cycle assessment investigates the environmental impacts of systems, processes or products. LCA models the complex interaction between a product and the environment from cradle-to-grave throughout the full life cycle, from the exploration and supply of materials and fuels, to the production and operation of the investigated objects, to their disposal/recycling [11]. The life cycle assessment method is one of the best methods for innovation in the area of enviro-management. The LCA method is usually applied to comparative analysis, when it is possible to choose among the products, processes, services and systems having the same function, but each of them having significantly different environmental effects. The importance of several impact categories can be seen in Table 1. The Economic Input-Output Life Cycle Assessment (EIO-LCA) method estimates the materials and energy resources required for, and the environmental emissions resulting from, activities in our economy. A complete life cycle cost analysis (LCCA) may also include other costs, as well as other accounting/financial elements (such as discount rates, interest rates, depreciation, present value of money, etc.) [2, 6].

Table 1. Impact categories of the CML 2001 method [7]

Impact Categories	Reference
Global Warming Potential (GWP)	kg CO ₂ - Equiv.
Acidification Potential (AP)	kg SO ₂ - Equiv.
Eutrophication Potential (EP)	kg phosphate- Equiv.
Human Toxicity Potential (HTP)	kg DCB- Equiv.
Photochemical Ozone Creation Potential (POCP)	kg ethylene- Equiv.
Ozone Layer Depletion Potential (ODP)	kg R11- Equiv.
Terrestrial Ecotoxicity Potential (TETP)	kg DCB- Equiv.
Marine Ecotoxicity Potential (MAETP)	kg DCB- Equiv.
Freshwater Aquatic Ecotoxicity Potential (FAETP)	kg DCB- Equiv.
Abiotic Depletion (ADP elements)	kg Sb-Equiv.

The GaBi 5 LCA Software that largely encourages the research work came into the market in November 2011 and has several advantages for its former versions. The GaBi 5 Software with databases 2011 establishes Life Cycle Assessment as an essential tool to develop more sustainable products and processes while increasing resource efficiency, reducing material, energy and cost.

4. Complex model for thermic treatments

Application with these viewpoints a complex mathematical model for the thermic treatment processes was carried out, which beside of the parameters examined by LCA method, considers time and probability at the same time. Within the special program system of MATLAB (Matrix Laboratory) based on the background of the pure mathematical statistics (relative frequency- probability), each and every environmental effect would mean the aleatory variable of a thermal treatment process – within an operational process. The main key-questions, test parameters and possible methods of the developed complex model can be the following (see Table 2).

Table 2. Main key-questions, test parameters and possible methods by the complex model [10]

	Load of environment	Energy efficiency	Economic efficiency
Main key-questions	<ul style="list-style-type: none"> - Emissions - Environmental reliability - Treatment of residual materials 	<ul style="list-style-type: none"> - Energetic usefulness 	<ul style="list-style-type: none"> - Extraction and utilization of raw materials - Recirculation in the technology - Costs and cost efficiency - Pay-out period
Test parameters	<ul style="list-style-type: none"> - Input-output balance of material - Emissions in CO₂- Equiv. - Other and toxic emissions 	<ul style="list-style-type: none"> - Input-output balance of energy - Quantity of the energy efficiency - Improving and retarding coefficients for the energy efficiency 	<ul style="list-style-type: none"> - Input-output balance of energy and material - Amount of recovery/utilization - Initial, maintenance and other costs
Possible methods	<ul style="list-style-type: none"> - Material balance equations and technological layout - Sankey diagram - Life Cycle Assessment - EIO-LCA (Economic Input-Output Life Cycle Assessment) 	<ul style="list-style-type: none"> - Energy balance equations and technological layout - Sankey diagram - Life Cycle Assessment (LCA) - EIO-LCA (Economic Input-Output Life Cycle Assessment) 	<ul style="list-style-type: none"> - Material and energy balance equations and technological layouts - Cost analysis - Cost efficiency analysis - Life Cycle Cost (LCC) - Life-Cycle Cost Analysis (LCCA)

In case of the traditional incineration it would also be worth carrying out an examination with a wider spectrum, and besides recoverable energy (and, of course, relief of dumps), attention should be paid to the emission and other alternatives of utilisation [10]. In order to do so, data from manufacturers and system operators are compiled with the help of the GaBi database and complemented with data from different LCA literature.

5. LCA results for thermic treatments

The LCA data represents the conventional incineration (with grate firing), the gasification and the pyrolysis for hazardous waste (with PCBs) in the EU 27 with application of GaBi 5 LCA-software. The inventory data for the system must be mathematically normalized to a functional unit, which has to be set a priori and is not a decision variable. The complex system of LCA method is for 1 kg industrial organic, hazardous waste (with PCBs) with energy recovery by electricity transfer and thermal convection. The allocation is applied and the substitution factor used is 1 to 1. The calorific values are calculated from the elementary composition of hazardous wastes (database GaBi 5 Software). The remaining heat is assumed to be used completely. The emissions to air, the waste transport (truck on road with diesel mix) and the land filling of residues are included in the system. The wastes are transported from production to the thermic treatment technology and the waste disposal in this model (system limit: from production process generated hazardous waste to waste disposal). The applied interpretation method was CML 2011 (November 2010). For the calculation of the mass balance of the process, all input components are split into their composition.

By conventional incineration ($T = 1100\text{ }^{\circ}\text{C}$) the main constituents of syngas are: NO_2 (71,37%), CO_2 (13,38%), SO_2 (11,15%), HCl (3,56%), CH_4 (0,44%), heavy metals and dioxins (0,10%). Dioxins will be not eliminated by syngas cleaning. Due to the contamination with heavy metals, the ash and slag go to landfill for hazardous waste. 1000 kg hazardous waste burnt can be expected, based on its carbon content, to produce 230 kg slag, 45 kg soot and 725 kg syngas. The heat output is used for electricity generation and thermal convection. The complex process will be used 78 kWh of electrical power and 23,5 kWh of thermal energy from natural gas. The input streams to the system are hazardous waste input, thermal energy from natural gas, electricity and water for flue gas cleaning. Output streams leaving the system as solid materials are ash and slag. The emissions to the atmosphere contained in the clean gas come from the flue gas purification. The auxiliary materials used for the flue gas precipitation in the waste incineration plant are lignite, ammonia and lime. According to measurements for Global Warming Potential (GWP) can be determine 5,03 kg CO_2 -Equiv. for the incineration (without syngas treatment). The value of the Ozone Layer Depletion Potential (ODP) is 0,001 kg R11- Equiv. and the Acidification Potential (AP) is 0,259 kg SO_2 -Equiv. Dioxins will be not eliminated by syngas cleaning. By gasification ($T = 1200\text{ }^{\circ}\text{C}$) will be used 50 kWh of electrical power for the complex process. The input streams to the system are hazardous waste input, natural gas (only by start) and electricity. Output streams leaving the system as solid materials are ash and slag. The GWP is 0,989 kg CO_2 -Equiv. for the gasification. The value of ODP is 4,09.10-11 kg R11- Equiv. and the value of AP is 0,18 kg SO_2 -Equiv. By pyrolysis ($T = 500\text{ }^{\circ}\text{C}$) the input streams to the system are hazardous waste input and electricity (70 kWh). Output streams leaving the system are pyrolysis coke, pyrolysis oil and pyrolysis gas. The Global Warming Potential is 15,4 kg CO_2 -Equiv. for the gasification. The value of the Ozone Layer Depletion Potential is 0,0032 kg R11- Equiv. and the Acidification Potential is 0,376 kg SO_2 -Equiv. The investigations show that by pyrolysis the values of Potentials are higher. By plasma-based technology ($T = 3000\text{ }^{\circ}\text{C}$) the Global Warming Potential is 0,836 kg CO_2 -Equiv., the value of the ODP is 4,03.10-8 kg R11- Equiv. and the Acidification Potential is 4,48.10-3 kg SO_2 -Equiv. (see Fig. 1-4).

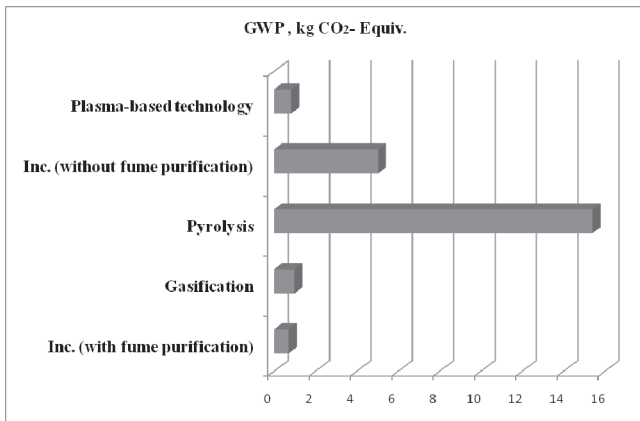


Fig. 1 The Global Warming Potential (GWP) for thermic technologies

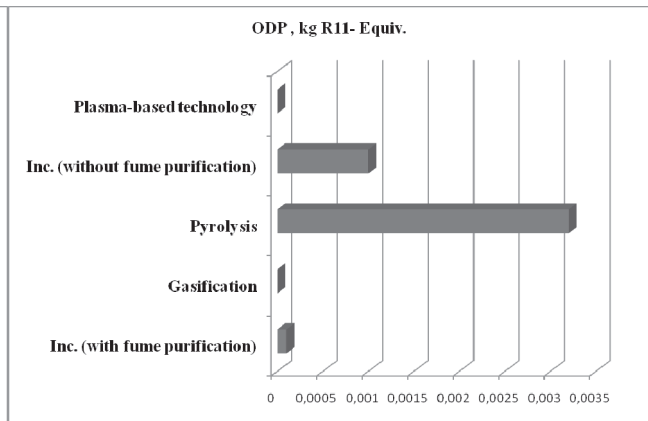


Fig. 2 The Ozone Layer Depletion Potential (ODP) for thermic technologies

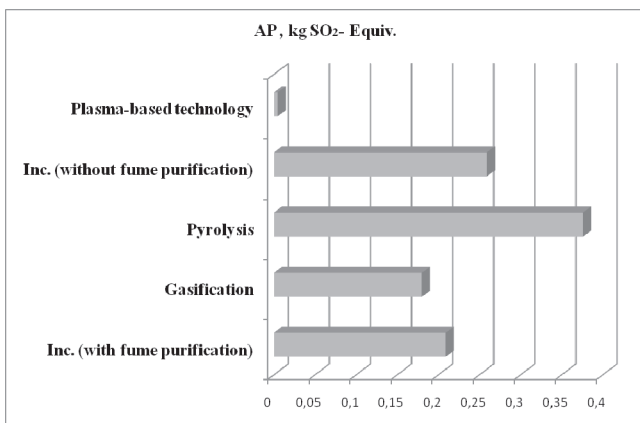


Fig. 3 The Acidification Potential (AP) for thermic technologies

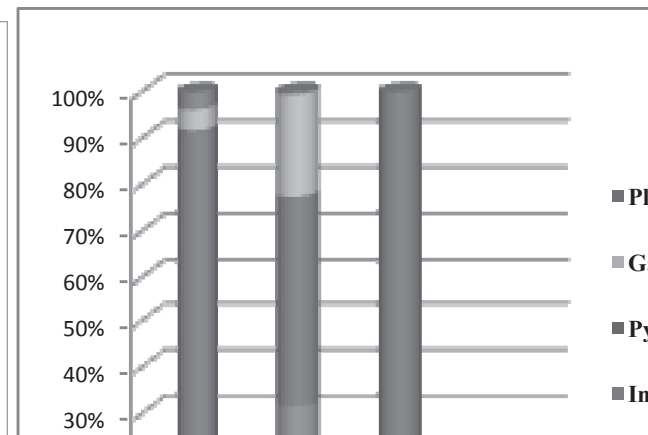


Fig. 4 The values of different Potentials for thermic technologies



6. Summary

This research study can set up prognoses with LCA analyses between thermic treatment processes and their priority. Pyrolysis, incineration, gasification and plasma-based technology can be considered on the basis of viewpoints: environmental burden and energy efficiency. The investigations show that the GWP, the ODP and the AP are very better by the plasma-based technology. According to the load of environment can be determined that the plasma-based technology by 3000 °C is the most enviro-friendly technology.

Acknowledgement

The described work was carried out as part of the TÁMOP-4.2.1.B-10/2/KONV-2010-0001 project in the framework of the New Hungarian Development Plan. The realization of this project is supported by the European Union, co-financed by the European Social Fund.

References

- [1] Bilitevsky, B., Härdtle, G., Marek, K., Weissbach, A., Boeddicker, H., 1994. Waste Management. Verlag Springer, Berlin, Germany.
- [2] Cooper, J.S., Godwin, C., Hall, E.S., 2008. Modeling process and material alternatives in life cycle assessments. *International Journal of Life Cycle Assessment* 13 (2), pp. 115-123.
- [3] Helsen, L., Bosmans, A., 2010. Waste-to-energy through thermochemical processes: matching waste with process. *Proceedings of the International Academic Symposium on Enhanced Landfill Mining, Houthalen-Helchteren, Belgium*, pp. 133-180.
- [4] Hill, T., Downen, S., 2010. Pyrolysis and gasification, Briefing (Draft 2), UK Without Incineration Network (UKWIN). Available electronically at <http://www.ukwin.org.uk>.
- [5] Hogg, R., 2007. Energy from waste by pyrolysis and gasification the experience and performance of an operational plant. *Proceedings of the International Conference on Sustainable Solid Waste Management, Chennai, India*, pp. 385-392.
- [6] Hsu, D.D., 2011. Life cycle assessment of gasoline and diesel produced via fast pyrolysis and hydroprocessing. Technical Report, NREL/TP/-6A20-49341, Colorado. Available electronically at <http://www.osti.gov/bridge>.
- [7] International Organisation for Standardization, ISO 14040:2006, Environmental management-Life cycle assessment-Principles and framework.
- [8] Karagiannidis, A., Malamakis A., 2009. Inventorying the available biomass potential in the region of central Macedonia, Greece. Perspectives for energetic utilization. *Proceedings of the 3rd Conference of Aristotle University's Environmental Council on "Climate change, sustainable development and renewable energy sources"*, Thessaloniki, Greece, pp. 521-529.
- [9] Mannheim, V., 2011. LCA in the waste management, in: Csevár, A. (Ed.), *Hulladékgazdálkodási Tanácsadó*. Verlag Dashöfer, Budapest, Hungary, pp. 187-198.
- [10] Mannheim, V., 2011. Dangerous Factory in the Agriculture. The Pesticide Wastes. The Left overs and the Pesticide Packaging in the Centre. Part 3. *Zöld Ipar Magazin, Professional Journal of the Environmental Protection, the Alternative Energies and The Waste Management* 11, Budapest, pp. 26-28.
- [11] Pehnt, M., 2006. Dynamic life cycle assessment (LCA) of renewable energy technologies. *Renewable Energy* 31, pp. 55-71.
- [12] Young, G.C., 2010. Municipal solid waste to energy conversion processes: Economic, technical, and renewable comparisons. John Wiley & Sons, Inc., New Jersey.

ADVANCED MEASUREMENTS FOR CONTROL AND PROTECTION OF SMART HYDROPOWER SYSTEMS

R. Magureanu¹, S. Ambrosi¹, Cristina Lupu¹

¹ University POLITEHNICA of Bucharest
060042, Spl. Independentei 313, Bucharest, Romania

Keywords: Hydro-Power Systems, Smart Measurements, GPS Synchronization.

Abstract. At world level, over 50% of the electrical energy generated from renewable resources is produced from hydro. In Romania the hydro covers up to 33% from the total national electrical energy demand.

There are three types of hydro electric plants: the first one is using water stored naturally in upstream lakes, the second type are so called Run-of-the-river hydroelectric stations with small or no reservoir capacity, so that practically all the water coming from upstream must be used for generation or allowed to bypass the dam. The third type has also a downstream lake from which the water is pumped back to the upstream one usually during the night when the cost of electricity is low, and then reused for generation when the demand is high.

In order to monitor and control a hydro energy generation system was developed a Wide Area Measurement System (WAMS) based on Phasor Measurement Units (PMU), all data being "time-stamped" with a time tag generated by an atomic clock obtained from the Global Positioning System (GPS), with a precision of +/-400 nanoseconds.

Introduction

Hydro generation of electrical energy represents the less expensive and the most reliable solution of producing electricity. Water energy is an important renewable source and a solution of producing non polluting energy. The hydro turbines can start and stop in a short period of time and consequently the hydro generators can improve the stability of the power grid and control its frequency.

In Romania, about 33% of all electrical energy is produced using hydro generation, both from interior rivers as well as from Danube, with a total installed power of about 7 GW.

Hardware Configuration

In Romania, medium size hydro-generators for interior rivers and in particular on Arges River are of 5MW and 6kV, driven by Kaplan type turbines. In order to transport the electrical energy produced it is stepped up at 20 kV and sent to a local 20/110 kV substation and again to another 110/400kV station which is part of the national system, Fig. 1.

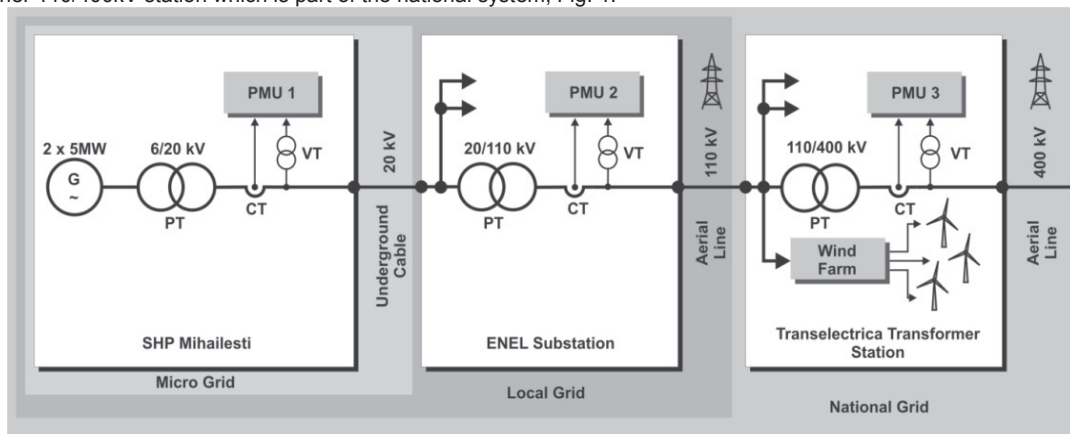


Fig. 1 The way from low-medium to high voltage national grid

A hydropower system can be described mathematically, as any other system in nature by a set of matrix equations:

$$\dot{x} = Ax + Bu + De, \quad (1)$$

where x vector, represent the states, u - vector of the control and e the vector the perturbations. A , B and D are matrixes which are function of the turbines, generators, transformers, transport power lines and their type of control. In order to control such a system is necessary to measure all of states x , or at least part of them and observing the rest, using Lumberger or Kalman observers. Similarly, as not all elements of A , B and D matrixes are known, these parameters have to be estimated.

The measured states in a hydropower system are of different nature:

- Hydraulic: the heads and flows;
- Hydro-mechanic: stator wicket gate position for Francis and the angle of rotor adjustable blades for the Kaplan turbines;

- Electro mechanic: the excitation voltage and current, the rotor position and its speed, the stator voltages and currents.

The selected river for the study was Arges, running from the Center of Romania to the Danube. Upstream there is a 260 MW Hydro plant and along the river there are 19 medium or small hydro plants (SHP). The last small hydro plant, for which advanced measurements were developed, is placed at Mihăilești, close to Bucharest, Fig.2.

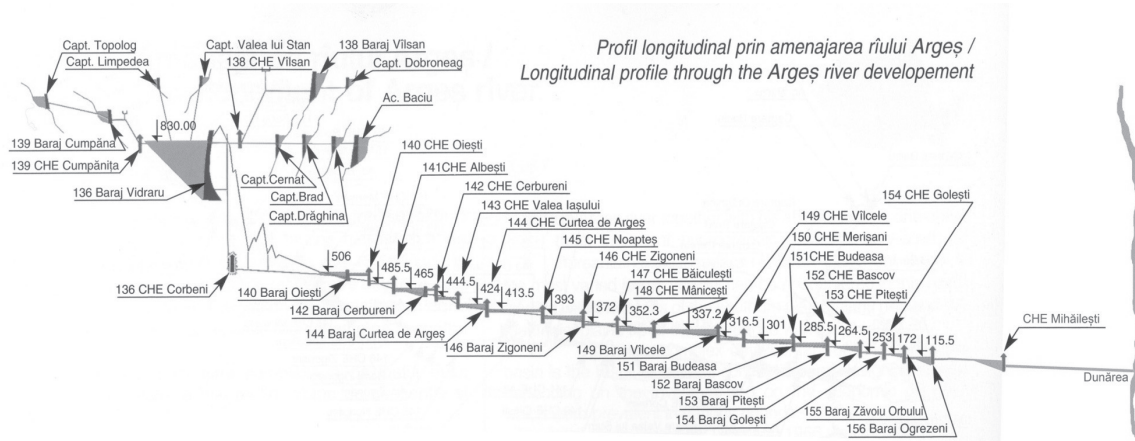


Fig. 2 The Hydro Plants on Arges river

It comprises of two vertical Kaplan Turbines 5MW each coupled to two 6kV synchronous generators. The third turbine is a 375kW Francis horizontal, connected to an asynchronous generator used to guarantee the continuous minimum flow of hydro-plant (see Fig. 3).

The main problem in this setup is to have all the measurements synchronized to a common time source. The best and least expensive solution in this case, is to use the time information provided by Global Positioning System (GPS). By using the time stamp from GPS it would be possible to collect information from different points in power network and be able to analyze it.

As one can see from the Fig. 3, different types of equipment are used to measure the electrical data in different parts of the site.

The 20 kV Line

The measurement of system voltages and currents in the point of common connection (PCC) is done by a Phasor Measurement Unit (PMU) [1] "Model 1133A Power Sentinel™" manufactured by Arbiter Systems. Beside raw data (voltages and currents) the Model 1133A can provide also the absolute phase angle, system frequency, system power, power quality data such as harmonics, K-factor, flicker. All the measurements are time stamped using the time code obtained from an internal GPS receiver. The time code can also be delivered to other equipments via an IRIG-B output signal. The communication between the PMU and the monitoring application can be done using one of the available ports which includes: serial RS-232, serial RS-422 and Ethernet. Of course, in order to obtain the maximum throughput the Ethernet connection is preferable.

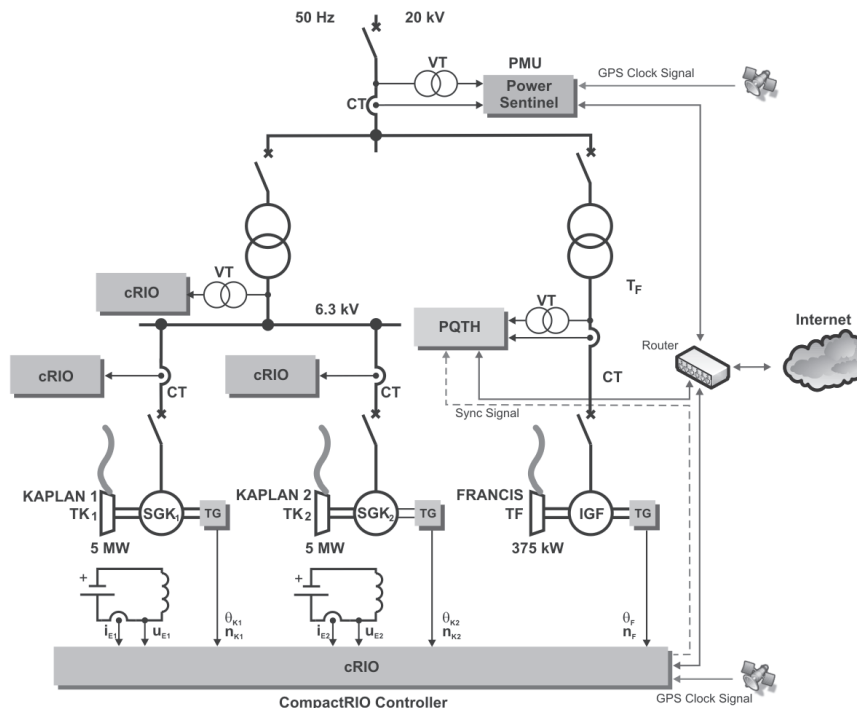


Fig. 3 Monitoring system at Mihăilești Hydro Plant

The Synchronous Generator Groups

The measurements for the two synchronous generators are done by a NI CompactRIO programmable automation controller [2]. The Compact RIO controller was chosen due to its modular design and in our case it includes the following modules:

- A three channels 300 V rms voltage analog input module;
- Two modules for the acquisition of currents up to 5A rms (four channels per module);
- One module for acquisition of analog values in 4-20mA range (eight channels);
- GPS receiver;
- Eight channels digital input module.

The measured values are the 6.3kV line voltages, both synchronous generators currents, excitors voltages and currents. Based on the measured data the rms values are computed, along with voltages and currents phasors, total delivered power, active power, reactive power. All the data is processed locally by an equipment based on a RISC processor and FPGA chip. The data acquisition and calculations for voltages and currents are done at 10ksamples/s and then at a rate of 2 samples per second the RMS values, voltage and current phasors, active and reactive power, power factor, Harmonics and the THD are calculated, recorded and sent to a central server. The waveforms for voltages and currents are re-sampled and sent to the server at a rate of 500 samples/s.

The data can be recorded also locally on internal memory card or to an external hard drive connected to USB port.

Software

To collect, record and display the data from all three equipments a specific software was developed using National Instruments LabView graphical language. As the amount of recorded data is quite huge, and due to the fact that there is a limited bandwidth of internet connection to the site, the software runs on a server installed locally.

In Fig. 4 are presented several screenshots of the software under development showing the data recorded from one synchronous generator.

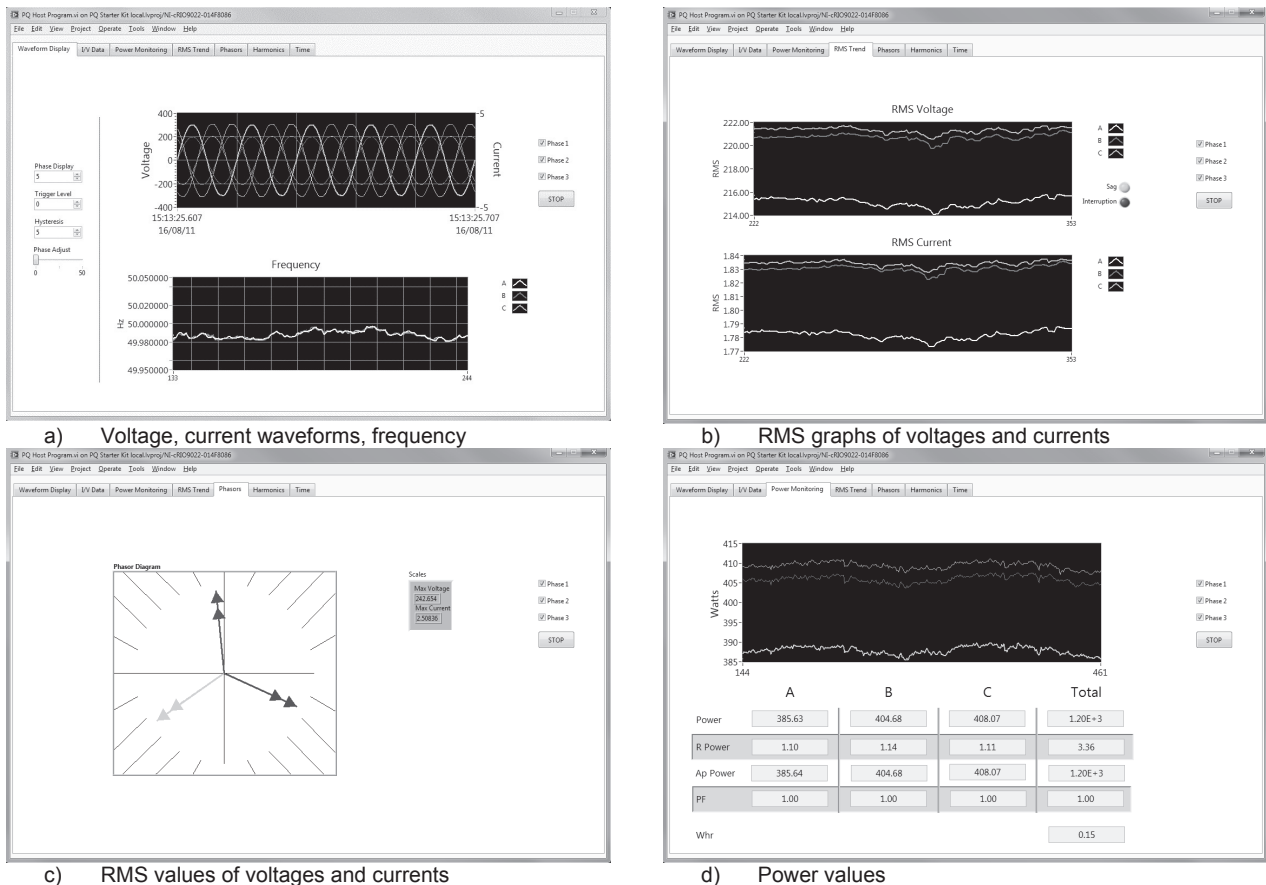
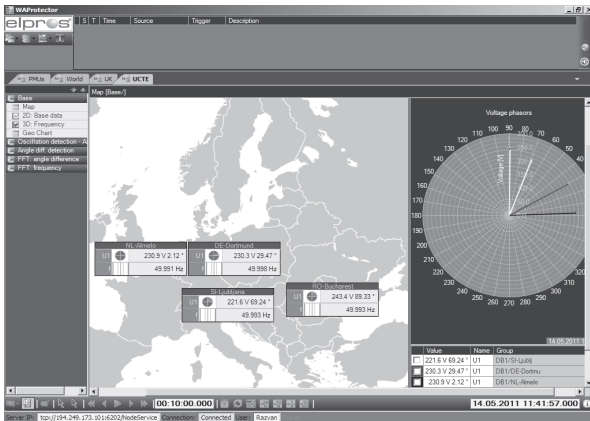
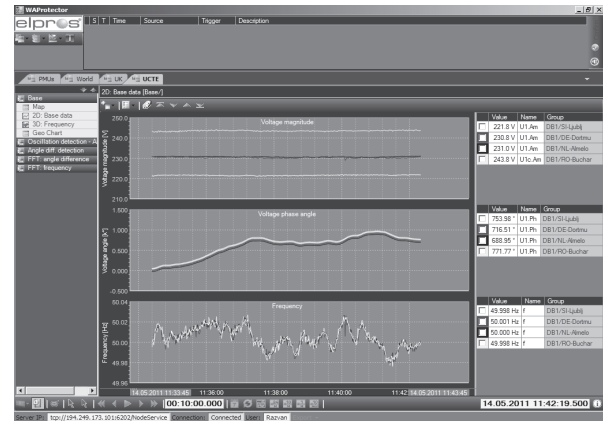


Fig. 4 Monitoring Software Screenshots

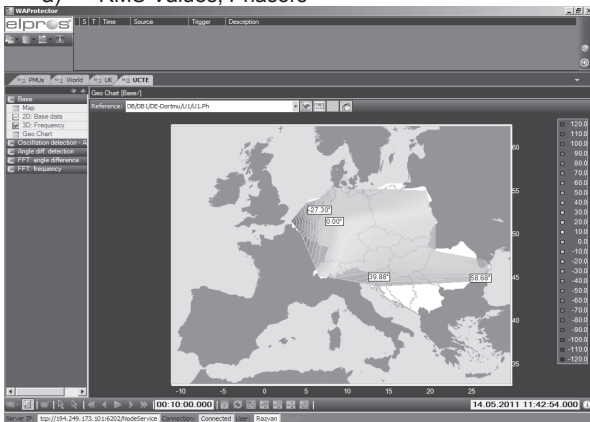
As Romania is part of the European Electric Grid, any change in the system can influence the operation of a hydro plant. As a case study, the data from the Phasor Measurement Unit connected to 20 kV line is also collected by a Wide Area Monitoring System application - WAProtector connected to several PMUs across Europe (Fig. 5).



a) RMS Values, Phasors



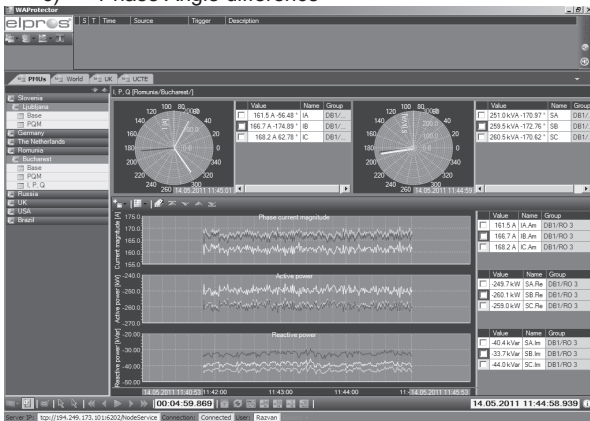
b) Voltages, Phase Angle, Frequency



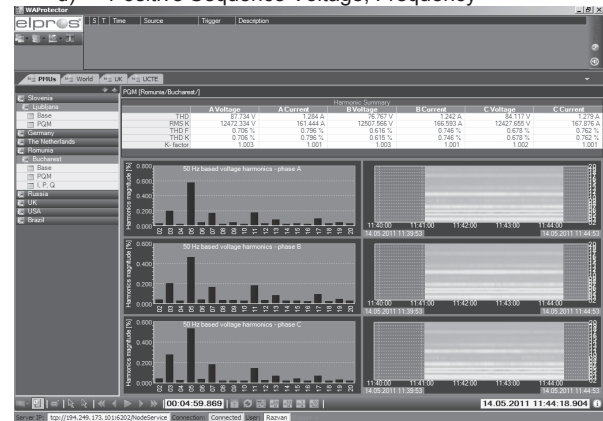
c) Phase Angle difference



d) Positive Sequence Voltage, Frequency



e) Currents, Active Power, Reactive Power



f) Voltage Harmonics

Fig. 5 Monitoring of 20kV line using Phasor Measurement Unit (Arbiter Systems Power Sentinel) in an Academic European Network

Conclusions

The control of a Hydropower System implies the measurement or observation of as many as possible voltages and currents in different points of the grid. The measurements have to be done synchronously using a common time base. The best way in this case is to use the time information obtained from the Global Positioning System. The authors present a solution which includes both: commercial and custom developed products.

Acknowledgment

The present work is a part of the SEE Hydropower project in where the authors are partners.

References

- [1] Model 1133A Power Sentinel™ User Manual, Arbiter Systems Inc
- [2] NI cRIO-9022 Operating Instructions and Specifications, National Instruments Corporation
- [3] Energy Management Modular Smart Power Quality Transducer Type PQT-H, Carlo Gavazzi
- [4] ELPROS WAProtector, www.elpros.si
- [5] Kjølle Arne, *Vannkraftmaskiner*, Fakultet for ingeniørvitenskap og teknologi, 1967, ISBN 82-00-27780-1
- [6] Mihai Cojocar, *Hidroconstructia 2005*, Hindroconstructia SA, ISBN-973-0004208



SEASONAL AND SPATIAL VARIATIONS OF PARTICLE-BOUND POLYCYCLIC AROMATIC HYDROCARBONS IN THE CITY OF NOVI SAD, SERBIA

N. Jovčić¹, J. Radonić², M. Turk Sekulić², M. Vojinović Miloradov², S. Kovačević² and Zoran Čepić²

¹ NIS Gazprom Neft, Narodnog fronta 12, 21000 Novi Sad, Serbia

² Faculty of Technical Science, University of Novi Sad, Trg Dositeja Obradovića 6, 21000 Novi Sad, Serbia

Keywords: Polycyclic Aromatic Hydrocarbons; Ambient Concentrations; Seasonal Variations; Spatial Variations.

Abstract. Concentration levels of twelve particle-bound polycyclic aromatic hydrocarbons (PAHs) were determined in ambient air samples collected at urban, suburban and industrial locations in the city of Novi Sad, Serbia, in order to assess seasonal and spatial variations. The sampling of ambient air has been conducted at five sampling sites. The first site, M1, was located in the Oil Refinery, in proximity of the sewage sludge incinerator. The second location, M2, was positioned in suburban residential area. The third measuring point, M3, was situated near industrial area, with the Oil Refinery, thermal power/heating plant and heavy-traffic road in the vicinity. The fourth site, M4, was located nearby the heavy traffic area, especially busy during the rush hour. The fifth location, M5, was situated at residential district, in the city centre. Sampling campaigns were undertaken during the two 14-day periods: from November 19th to December 2nd 2010 (heating season) and from March 16th to March 29th 2011, using the high volume (HiVol) ambient air samplers. Duration of sampling was 24 h. The content of PAHs associated with suspended particles was analysed using a gas chromatographer coupled with a mass spectrometer (GC/MS). Almost all of the investigated PAHs were found in the suspended particles. The summed concentration of the 12 PAHs ranged from 39.28 to 258.02 ng/m³, with median value 86.71 ng/m³ for the heating season and from 27.81 to 128.32 ng/m³ (median value was 60.525 ng/m³) during the spring. During the winter/heating period, the Σ PAHs concentrations were the highest at the M1 (median value 155.845 ng/m³), while at the M5 the lowest levels were determined (64.52 ng/m³). In March 2011, the content of PAHs was the highest at M2 (median value 79.685 ng/m³), followed by M1 (70.275 ng/m³), M4 (58.31 ng/m³), M3 (50.73 ng/m³) and site M5 (44.005 ng/m³).

Introduction

Polycyclic aromatic hydrocarbons (PAHs) belong to the group of organic compounds containing two or more aromatic rings [1]. PAHs are formed during the processes of incomplete combustion of organic matter exposed to a temperature of 700 °C [2] and they are released, as a complex mixture, primary into the atmosphere. After emission, polycyclic aromatic hydrocarbons distribute between the gas phase and atmospheric particles and even 70%-90% of PAHs are associated with particulate matter at ambient temperature.

In environmental researches, polycyclic aromatic hydrocarbons are of special concern, since some individual PAHs or mixtures of PAHs demonstrate strong mutagenicity, teratogenicity and/or carcinogenicity [3, 4].

PAHs can be emitted from natural and anthropogenic sources. In urban and industrial atmosphere, polycyclic aromatic hydrocarbons are almost entirely anthropogenic in origin [5]. The largest contributors of PAHs in urban and industrial areas are emissions from vehicle exhaust [6] and from industrial processes like primary aluminum production, creosote and wood preservation, waste incineration, cement manufacture, petrochemical and related industries, bitumen and asphalt industries, rubber tire manufacturing, and commercial heat/power production [7].

Among numerous PAHs, United States Environmental Protection Agency (US EPA) has designated 16 of them as priority pollutants: naphthalene (Nap), acenaphthylene (Acy), acenaphthene (Ace), fluorene (Flo), phenanthrene (Phe), anthracene (Ant), fluoranthene (Flu), pyrene (Pyr), benzo(a)anthracene (BaA), chrysene (Chr), benzo(b)fluoranthene (BbF), benzo(k)fluoranthene (BkF), benzo(a)pyrene (BaP), dibenz(ah)anthracene (DahA), benzo(ghi)perylene (BghiP), and indeno(1,2,3-cd)pyrene (IP) [8].

Regarding carcinogenicity, International Agency for Research on Cancer (IARC) has classified PAHs as known human carcinogen (group 1), probable human carcinogen (group 2A), possible human carcinogen (group 2B) and not classifiable as carcinogen to humans (group 3). Naphthalene and acenaphthylene have not been classified by IARC [9]. The IARC classification of polycyclic aromatic hydrocarbons is given in Table 1.

Table 1. IARC classification of polycyclic aromatic hydrocarbons regarding carcinogenicity

PAHs	Class
Nap	-
Acy	-
Ace	3
Flo	3
Phe	3
Ant	3
Flu	3
Pyr	3
BaA	2B
Chr	2B
BbF	2B
BkF	2B
BaP	1
DahA	2A
BghiP	3
IP	2B

Over the past two decades many researches focused on the levels and behavior of ambient air PAHs have been conducted. Despite this, studies on presence of polycyclic aromatic hydrocarbons in ambient air in Serbia are still limited. The objectives of the study were to determine concentration levels of twelve PAHs associated with atmospheric particulate matter at urban, suburban and industrial localities in the city of Novi Sad, Serbia, and, based on the obtained data, to assess seasonal and spatial variations of the pollutants.

Material and Methods

Sampling Locations

140 ambient air samples have been collected at five locations in the city of Novi Sad, Serbia (Fig. 1), during the two seasons. The first site, M1, was located in the Oil Refinery, in proximity of the sewage sludge incinerator. The second location, M2, was positioned in suburban residential area. The third measuring point, M3, was situated near industrial area, with the Oil Refinery, thermal power/heating plant and heavy-traffic road in the vicinity. The fourth site, M4, was located nearby the heavy traffic area, especially busy during the rush hour. The fifth location, M5, was situated at residential district, in the city centre.

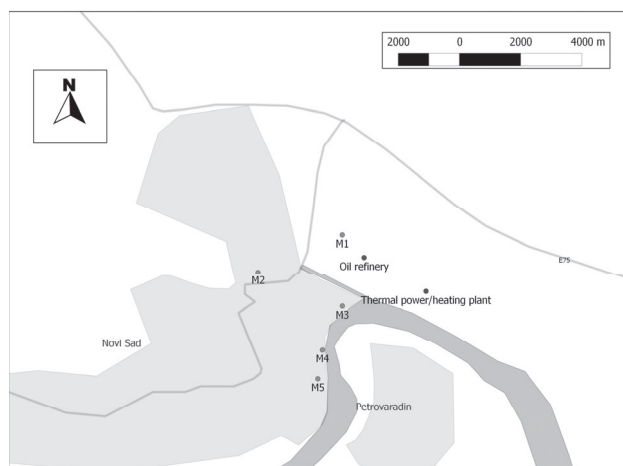


Fig. 1 Sampling locations in the city of Novi Sad

Sampling campaigns were undertaken during the two 14-day periods: from November 19th to December 2nd 2010 (heating season) and from March 16th to March 29th 2011.

Sampling Procedure

Ambient air was sampled using a high volume air sampler TECORA ECHO HiVol with quartz fiber filters (QFFs) which enabled the collection of the suspended particles. Samplers were placed at 4 meters from the ground.

Before usage, QFFs were burned at 400°C for minimum 4h, to minimize the contaminant levels. After returning to ambient temperature, QFFs were wrapped in aluminum foil and stored.

The sampling volume was in the range from 325 to 400 m³ of ambient air in a 24-hour period and 4,804 m³ of air were sampled for 14 days. The amount of sampled air was recorded at the end of each sampling session. After the sampling, quartz fiber filters were wrapped with aluminum foil and transported to the laboratory.

Before analytical procedure, QFF were microwave extracted by 15 ml DCM-acetone mixture for 20 min.

Sample Analysis

Selected polycyclic aromatic hydrocarbons (Acy, Flo, Phe, Ant, Pyr, BaA, Chr, BbF, BkF, BaP, DahA, BghiP) were determined in all samples using a GC-MS instrument (Shimatzu MDGC/GCMS-2010), supplied with an auto sampler and a SPL-2010 capillary column (30 m x 0,25 m x 0,25 µm film), with helium as carrier gas. The samples (1 µl) was injected at 60°C (2 minutes), then at 6°C/min to 280°C, and final temperature was kept for 20 minutes.

Results and Discussion

Almost all of the investigated PAHs were found in the suspended particles. The data on concentration levels of PAHs at five urban/suburban/industrial localities collected during the winter 2010 and spring 2011 are statistically analyzed and presented in Table 2, where the seasonal minimum, maximum, median and average values, along with standard deviation, for every location are given.

Table 2. Minimum (Min), Maximum (Max), Median (Med), Average (Ave) and Standard Deviation (SD) values of the total PAHs concentrations (ng/m³) during the winter/heating period and spring

Season	Sampling Locations	Min	Max	Med	Ave	SD
Heating Season	M1	53.67	237.92	155.845	156.11	64.52
	M2	54.14	258.02	96.545	126.83	68.64
	M3	39.28	248.73	82.235	95.715	53.72
	M4	43.34	239.65	86.71	93.255	46.98
	M5	41.32	147.22	64.52	77.18	33.59
Spring	M1	56.32	128.32	70.275	75.21	22.78
	M2	52.39	96.50	79.685	79.35	14.11
	M3	27.81	73.81	50.73	52.56	14.87
	M4	47.63	101.69	58.31	68.64	20.48
	M5	30.60	61.17	44.005	43.37	9.92

The summed concentration of the 12 PAHs ranged from 39.28 to 258.02 ng/m³, with median value 86.71 ng/m³ for the heating season and from 27.81 to 128.32 ng/m³ (median value was 60.525 ng/m³) during the spring.

During the winter/heating period, the ΣPAHs concentrations were the highest at the M1 (median value 155.845 ng/m³), while at the M5 the lowest levels were determined (64.52 ng/m³). In March 2011, the content of PAHs was the highest at M2 (median value 79.685 ng/m³), followed by M1 (70.275 ng/m³), M4 (58.31 ng/m³), M3 (50.73 ng/m³) and locality M5 (44.005 ng/m³).

Fig. 2 presents seasonal and spatial variations of particle-bound polycyclic aromatic hydrocarbons, classified according to IARC criteria for carcinogen status.

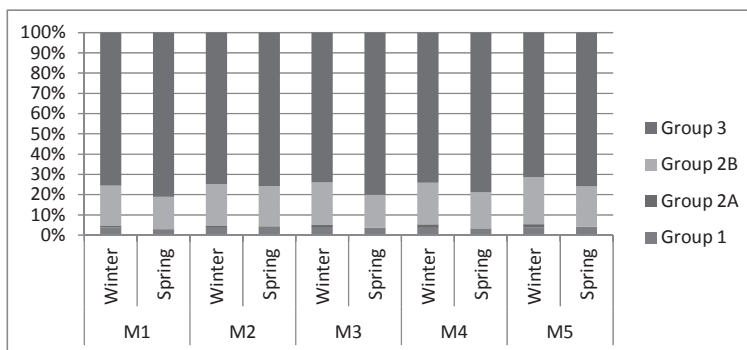


Fig. 2 Seasonal and spatial variations of selected PAHs classified according to IARC criteria for carcinogen status

The fractions of polycyclic aromatic hydrocarbons belonging to the group 1, 2A or 2B during the winter/heating period lied inside the interval 24.40 - 28.70%, while, during the spring, fractions of known, probable and possible human carcinogenic PAHs ranged from 18.90 to 24.18%. At every sampling location in the city of Novi Sad, carcinogenic PAH fraction was higher during the heating season, comparing to values that were detected during the spring.

Conclusion

Polycyclic aromatic hydrocarbons are released, as a complex mixture, primary into the atmosphere, where they distribute between the gas phase and atmospheric particles. Even 70%-90% of PAHs are associated with particulate matter at ambient temperature. Regarding to their strong mutagenicity, teratogenicity and/or carcinogenicity, PAHs are of special concern in environmental researches.

The largest contributors of PAHs in urban and industrial areas are vehicles and industrial activity (aluminum production, creosote and wood preservation, waste incineration, cement manufacture, petrochemical industries, bitumen and asphalt industries, rubber tire manufacturing, and commercial heat/power production).

United States Environmental Protection Agency has designated 16 PAHs as priority pollutants. Regarding carcinogenicity, International Agency for Research on Cancer has classified PAHs as known human carcinogen, probable human carcinogen, possible human carcinogen and not classifiable as carcinogen to humans, while some of them have not been classified.

Although numerous studies have been conducted in order to meet the levels and behavior of atmospheric PAHs, data on presence of polycyclic aromatic hydrocarbons in ambient air in Serbia are still limited.

Selected polycyclic aromatic hydrocarbons (Acy, Flo, Phe, Ant, Pyr, BaA, Chr, BbF, BkF, BaP, DahA, BghiP) were determined in samples of ambient air collected at five locations in the city of Novi Sad, using the high volume sampler. Almost all of the investigated PAHs were found in the suspended particles. The summed concentration of the 12 PAHs ranged from 39.28 to 258.02 ng/m³ for the heating season, and from 27.81 to 128.32 ng/m³ during the spring. During the winter/heating period, the Σ PAHs concentrations were the highest at M1, while at M5 the lowest levels were determined. In spring 2011, the content of PAHs was the highest at M2, followed by M1, M4, M3 and the locality M5. At every sampling location in the city of Novi Sad, carcinogenic PAH fraction was higher during the heating season, comparing to values that were detected during the spring.

The factors that caused higher concentration levels of polycyclic aromatic hydrocarbons during the colder period, most probably, were increased emission of PAHs due to more intense traffic and domestic heating, decreased dispersion of pollutants due to adverse meteorological conditions and, finally, reduced photochemical degradation of PAHs, due to ozone and nitrogen oxides reactions. The lower concentrations during the spring were likely due to easier dispersion of air pollutants, washout effects and, to a lesser extent, photo-degradation of polycyclic aromatic hydrocarbons.

References

- [1] N. Jovčić, J. Radonić, M. Turk Sekulić, M. Vojinović Miloradov and S. Popov: Identifikacija izvora emisije čestične frakcije policikličnih aromatičnih ugljovodonika u neposrednoj blizini industrijske zone Novog Sada. *Hemijska industrija*, DOI: doi:10.2298/HEMIND120113062J (2012), in press
- [2] J. Radonić, M. Vojinović Miloradov, M. Turk Sekulić, J. Kiurski, M. Djogo and D. Milovanović: The octanol-air partition coefficient, K_{OA} , as a predictor of gas-particle partitioning of polycyclic aromatic hydrocarbons and polychlorinated biphenyls at industrial and urban sites. *Journal of the Serbian Chemical Society*, Vol. 76 (2011), No. 3, pp. 447–458.
- [3] J. Radonic, M. Turk Sekulic, M. Vojinovic Miloradov, P. Čupr and J. Klánová: Gas-particle partitioning of persistent organic pollutants in the Western Balkan countries affected by war conflicts. *Environmental Science and Pollution Research*, Vol. 16 (2009), No. 1, pp. 65-72.
- [4] J. Radonić, D. Čulibrk, M. Vojinović Miloradov, B. Kukić and M. Turk Sekulić: Prediction of Gas-Particle Partitioning of Polycyclic Aromatic Hydrocarbons Based on M5' Model Trees. *Thermal Science*, Vol. 15 (2011), No. 1, pp. 105-114.
- [5] J.S. Kreis, G. Welzl, T. Jaensch and A. Kettrup: Occurrence of particle-associated polycyclic aromatic compounds in ambient air of the city of Munich. *Atmospheric Environment*, Vol. 35 (2001), No. 1, pp. S71-S81.
- [6] W.F. Rogge, L.M. Hildemann, M.A. Mazurek, G.R. Cass and B.R.T. Simoneit: Sources of fine organic aerosol: 2. Noncatalyst and catalyst-equipped automobiles and heavy-duty diesel trucks. *Environmental Science and Technology*, Vol. 27 (1993), No. 4, pp. 636–651.
- [7] K. Ravindra, R. Sokhi and R. Grieken: Atmospheric polycyclic aromatic hydrocarbons: Source attribution, emission factors and regulation. *Atmospheric Environment*, Vol. 42 (2008), No. 13, pp. 2895–2921.
- [8] U.S. EPA: *Polynuclear hydrocarbons, Volume 10* (United States Environmental Protection Agency, US-EPA, Washington DC, USA, 1984).
- [9] IARC: *Monographs on the Evaluation of Carcinogenic Risks to Humans, Vol. 92, Some Non-heterocyclic Polycyclic Aromatic Hydrocarbons and Some Related Exposures* (World Health Organization, International Agency for Research on Cancer, Lyon, France, 2010).

RESEARCH OF MOBILE ROBOT BEHAVIOR WITH eMIR

M. Crneković¹, D. Zorc², Z. Kunica³

^{1,2,3} University of Zagreb, Faculty of Mechanical Engineering and Naval Architecture, Ivana Lučića 5, 10002 Zagreb, Croatia

Keywords: mobile robot, environment perception, robot control

Abstract. In this paper a mobile robot for research and education is described. The main reason for building this robot is the possibility to do research in cognitive robotics, goal oriented robot languages and perception of work environment. Robot is equipped with infrared distance sensors and a camera, and complete environment may also be observed using external camera. Robot kinematics model and speed control are integrated in the robot microcontroller, so user sets robot translational and rotational speed only. Controlling the robot is possible from any programming language and operating system that makes this platform very flexible. Robot is equipped with battery and wireless communication which results in bigger autonomy and connection with more powerful computer. The system is able to do fast check of robot control algorithms for single robot behavior or behavior in group of robots. Three robots have been already built, together with test platform 4 x 2 meter in size.

Introduction

Main topic in robot research today is cognitive robotics, and one of the most interesting applications is in mobile robotics. From robot we expect not only the possibility to move but also dealing with its environment. It is favorable for robot to have human perception of environment and moving inside it, so that communication with human may be as simple as possible, and so making the robot easy accessible to people. Until the end of 90's this goal was first tried to reach using an exact mathematical methods (configuration space, potential fields, equidistant paths etc). This approach had multiple drawbacks so researchers start to use tools like neural networks, fuzzy logic etc. This enabled development of goal oriented languages for robot, in contrast to motion control. As the theory was getting more complex, testing by simulation was not sufficient any more. Therefore many researchers started to build mobile robots with various complexity. In time some expensive models prevailed in research labs (like Pioneer), but also a number of smaller and less expensive models appeared on the market. Soon it was clear that for research in cognitive robotics there is no need for expensive robots [1], but the good ideas and adequate knowledge is what is needed [2]. As this research involves the need for constant change, many researchers found out that it is the best to build their own robots. In these way researchers have full insight in robot behavior, but at the expense of more work involved.

One good example is in [3] in which authors have built a complex mobile robot with multiple controllers and sensors with possibility of the robot control through MATLAB. Authors relay mostly on internal robot sensors (ultrasound and infrared distance meters), but the camera, as a powerful source of information, is missing. In [4] eROSI robot is used equipped with camera, accelerometers and wireless communication. The goal was the guidance on docking station, using only vision system, which is by itself important function to obtain robot independence. Paper [5] describes „wheeled mobile robot“ WMR which is in design similar to [3] but oriented towards path following using vision system. Similar system is in [6], describing MiroSot soccer robots. This time vision system is used to control “soccer players” and is located above the playground.

What are common to all those works are relatively simple mobile robot structure and the wish to obtain meaningful robot behavior with a goal to solve relatively abstract jobs.

Basic idea of this research was to build a group of robots capable of dealing with artificial environment. Each robot would have simple task which it needed to execute in an environment not known to it in advance. In the task execution, robot would rely only on its internal sensors, or it would use information from built-in camera. Besides that, for the robot control other camera mounted above work place could be used. Structure of the robot control would be realized using system of independent agents, so that image processing agents would have main role and practically become dominant ones. Robot has a short name eMIR which stands for “educational Mobile Robot Researcher”.

Mechanical system

Three identical robots were built, designated with yellow, blue and red color, Fig. 1. Robot motion is realized using so called differential structure. Basic robot dimensions are given in Fig 2. Low robot height of 110 mm and relatively big drive wheels spacing make robot very stable. The actual robot size of 300 x 250 mm is chosen so that typical netbook computer will fit. Robots are built from plexiglass material, lower plate thickness is 10 mm. It enables easy tool handling, so adding new parts is quick and inexpensive. Upper board is made from the same material, 6 mm thickness, so all components between two boards are protected. Wheels are recessed in the robot body therefore no part of robot can stumble into any obstacle. Robot mass is 3,5 kg and is powered by standard 12 V/2 Ah rechargeable battery. This results in 3 to 4 hour autonomy.

Kinematics model of the mobile robot internal and external coordinate velocities is given with following equations:

$$\begin{aligned}v &= D(\omega_R + \omega_L) / 4 \\ \omega &= D(\omega_R - \omega_L) / 2L\end{aligned}\tag{1}$$

where: v is translational speed and ω rotational speed, ω_R and ω_L are angular speeds of right and left wheel, $D = 80$ mm is wheel diameter and $L = 240$ mm is wheel to wheel distance.

Taking into account maximum motor speed, maximum robot speed is around 0,5 m/s and maximum rotational speed is 240 °/s. Drive wheels are covered with rubber to prevent robot slipping.

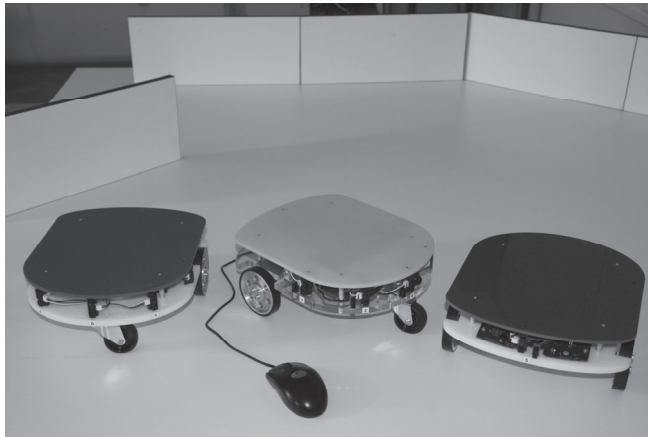


Fig. 1 eMIR mobile robots

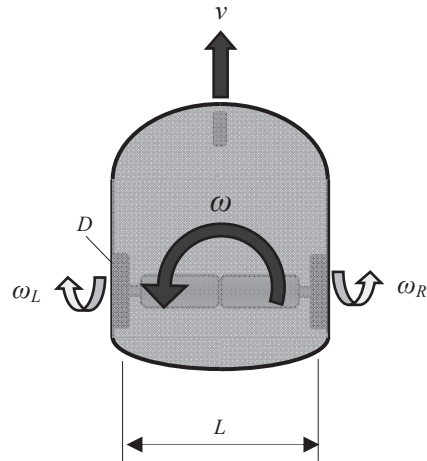


Fig. 2 Robot's basic dimensions and parameters

Energy system

Robot is powered by two DC motors with mechanical gearbox ratio 1:27. Motors type IG-32GM give maximum torque of 0,14 Nm. For motor driving integrated circuit LMD18200 is used (multiwat case) with 3 A current rating. This circuit contains all necessary protection functions, which reduce necessary part count. Motors can work on 24 V but here we use 12 V. This eliminates the need for driver cooling while retaining good driving performance. Maximum output axes rotational speed is 2 s^{-1} while PWM signal frequency is 3,6 kHz. Maximal battery current with all the sensors and camera turned on is 450 mA.

Measurement system

Encoders embedded into motors are used for each wheel speed measurement. Each encoder has two channels with 7 pulse/revolution. Multiplication of encoder pulses and gearbox transfer ratio results in 189 pulse/revolution of gearbox output axle i.e. of the wheel. This gives resolution of $1,9^\circ$ per pulse. If the robot movement is only translation then one pulse measures 1,33 mm. Similar math applied on the robot rotation gives result of 556 encoder pulses for 360° rotation.

Static characteristics of PWM control signal versus free run motor speed is highly linear, Fig. 3. Pulse measurement interval was 260 ms, so that maximum number of pulses is 100. In future projects it is planned to use encoders of somewhat better resolution so that dynamic of speed control will be more favorable.

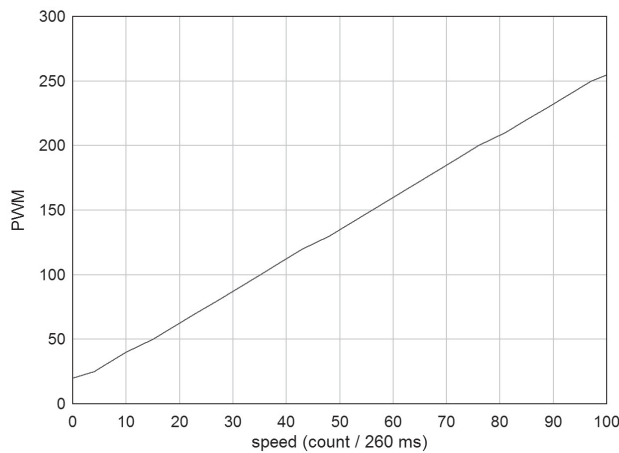


Fig. 3 Static characteristic of DC motor

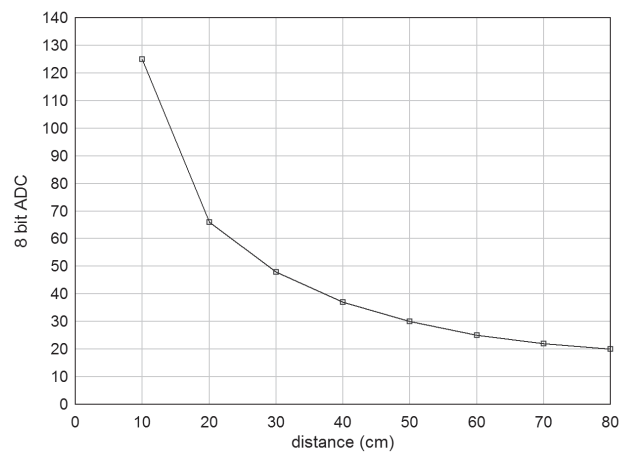


Fig. 4 Characteristic of sensor Sharp GP2Y0A21

During the robot operation battery voltage is measured and used in control algorithm to make decision if the robot should turn off, not to make damage to battery, or alternatively should it go to charging. Charging voltage is also monitored. Robot is equipped with six infrared distance sensors of type GP2Y0A21 with a measuring range 10 to 80 cm. It is well known that those sensors have nonlinear characteristic (Fig. 4) which is internally recalculated to get effective distance in cm. Measuring of each distance channel is done every 10 ms. Measured values pass through the FIR filter after five measurements. Sensor positions on the robot are not equidistant; its placement is shown on Fig. 5. This arrangement of sensors does not give uniform sense of environment, but it is more similar to human perception of the world.

Because distance sensors described do not measure fewer than 10 cm, there are also parallel control distance meters GP2Y0D810Z0F, also produced by Sharp. Their activation means that the obstacle is located between 2 and 10 cm.

Control system

Center of the eMIR robot control system is Atmel microcontroller AT89C51ID2. Having 64 kB of program memory and 1 MHz clock it is quite sufficient for the robot functioning. Functional scheme of the robot control system is given in Fig 6. Wireless communication is carried out by Bluetooth module Sparkfun WRL-00582 having data transfer rate of 57600 bps. As microcontroller does not have A/D

converter, external serial converter ADC LTC1294 is used. The robot power supply is controlled with bistable relay, which can be turned off by program, so robot can shut off by itself. In the development phase there is a need for often change of control program, which is also possible through Bluetooth wireless communication. In fact, parallel to main microcontroller there is also auxiliary controller AT89C4051

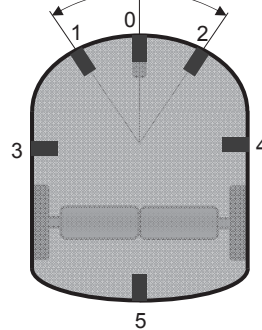


Fig. 5 Placement of infrared distance sensors

for supervision of communication. When it receives certain byte sequence it sets main controller in bootload mode. Eight input/output lines of the main controller remain free in this version and can be used for additional sensors or LCD display. There is also a possibility for audio signals using the built-in horn.

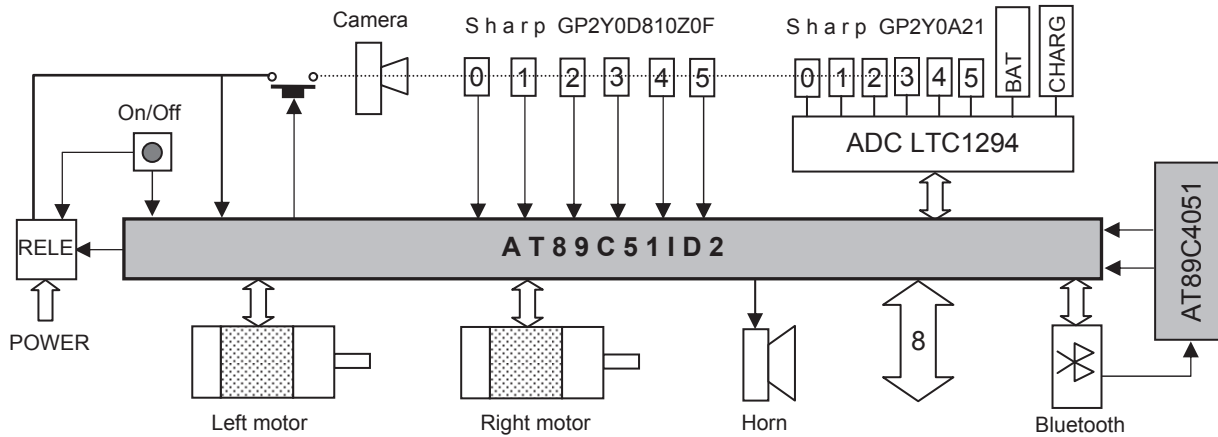


Fig. 6 Functional scheme of control system

The whole control program uses only 3,5 kB of program memory, that is only 5 % of available microcontroller space. Control program provides the following functions:

- supervision of communication and receiving commands
- to control, interpret and execute commands
- to measure motor speed every 260 ms
- to control motor speed every 100 ms using nonlinear PI controller and feedforward
- to read one infrared distance sensor every 10 ms
- to read battery charge state every 100 ms.

The whole robot control algorithm is carried out on personal computer and movement commands are sent to the robot. If the robot is in motion and it does not receive any command during one second, it will stop. If there are no commands in 120 seconds the robot will shut down. Communication between PC and the robot is by data packages in hex system (Table 1) of the following format:

NN aa bb CS /

Table 1. Some eMIR commands

NN	Command	Description
0	# 00 00 00 00 /	Stop the robot and exit from a current task.
1	# 01 vv rr CS /	Move the robot with translation speed vv and rotation speed rr (-100 to +100%).
17	# 11 PP 00 CS /	Define returned information package PP (0, 1 or 2).
19	# 13 tt 00 CS /	Turn on internal horn for time tt tenths of seconds.
255	# FF 00 00 01 /	Turn off the robot.

The byte CS describes so called "check sum" and is used as control of package integrity. If $NN+aa+bb+CS = 0$, command is accepted and executed, if not it is discarded. Data packages from PC to robot are sent 4 to 10 times per second.

If sensors and battery status is requested (PP = 01), this information will be given in the following package:

* 01 aa bb cc dd ee ff gg hh ii CS /

where: 01 – package identifier for the robot sensors
 aa – state of digital infrared sensors
 bb..gg – measurement of distance sensors in cm
 hh – battery voltage
 ii – battery charging voltage
 CS – control sum.

If the robot kinematics is requested (PP = 02), this information will be given in the following package:

* 02 aa bb CS /

where: 02 – package identifier for the robot kinematics
 aa – robot translational velocity v in interval -100 to $+100\%$
 bb – robot rotational velocity ω in interval -100 to $+100\%$
 CS – control sum.

All data are sent in hex system, and robot status is read 3 to 5 time per second. Video image is transferred independently from the robot control system and any system of video transfer can be used.

Control program on computer may be realized in any programming language, operating system or computer type. All what is important to conform given protocol, communication seed and timing defined.

Example

The goal for the robot is to follow wall from its right side and maintain the distance of 20 cm, using constant speed of 20 %, i.e. around 100 mm/s, while maximum rotational speed is set on 10 % i.e. 24 %/s. When front sensor 0 detects an obstacle on distance 15 cm or less, robot should stop. Right wall has two bends on 45°. Fig. 7a shows parameters of movement if guidance is realized using only distance sensors 4, while Fig. 7b shows parameters of movement if guidance is realized using distance sensors 2 and 4. Control program is written in Pascal.

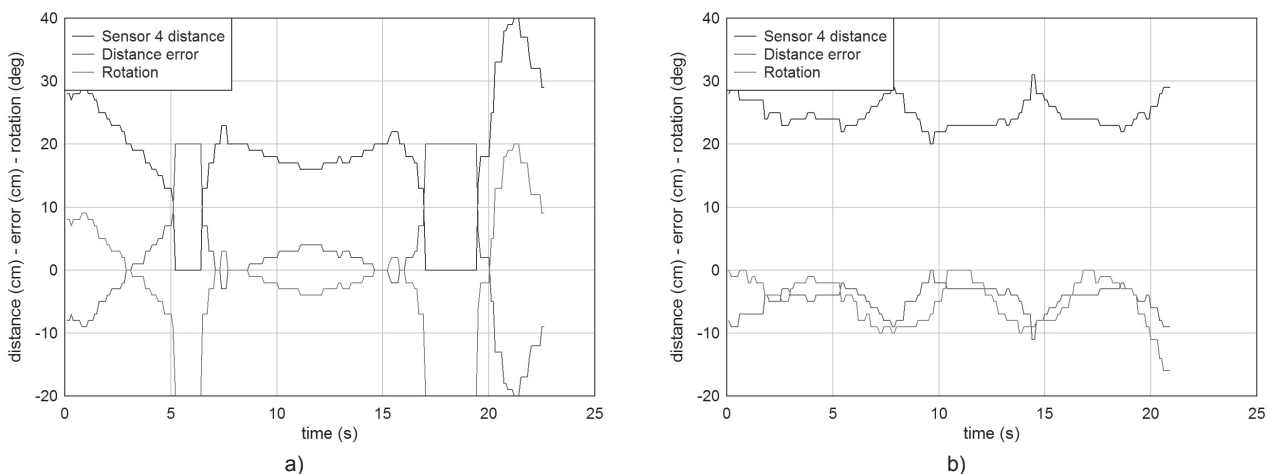


Fig. 7 Wall following: a) by sensor 4, b) by sensors 2 and 4

As it could be expected, guidance using two sensors gives much better result because it can detect distance and needed direction, i.e. it is realized with two state variables. Guidance using one sensor can easily lead to instability.

Conclusion

By realization of the eMIR mobile robots, a good foundation is created for study of mobile robot behavior, single or group. The robots are equipped with internal sensors and camera, so that quantity of information is sufficient for large number of control methods. Because robots can be controlled using any programming language, potential number of users is very large. Additional benefit is external vision system, which is independent from the robot control system.

A preliminary tests show that the robot has very good controllability and reacts fast without oscillation in speed. The robot wheels contact with the surface is so good that there is no slip; therefore commands for the robot relative position and orientation are also possible. Communication over Bluetooth is reliable and works well in real-time.

Further improvement and development will be concentrated in several directions. First, there will be a change in the robot feedback control structure to make the robot start and stop softer. The main development will include the robot guidance by built-in camera which is the main prerequisite for task oriented mobile robot programming language. Parallel with that, task strategies for the robot goal reaching are necessary to be developed. Also, some kind of simple GUI is necessary for testing robot functions and for educational purposes. All of that will be packed in dynamic link library, so it can be used in any programming language.

Acknowledgment

The paper is an outcome of the scientific project "Modelling of mechanical behaviour for assembly, packaging and disassembly", supported by the Ministry of Science, Education and Sports of the Republic of Croatia.

References

- [1] Z. Kunica: Dialectics in Automatic Production, *Proc. of International Scientific Conference "Management of Technology – Step to Sustainable Production 2010"*, Faculty of Mechanical Engineering and Naval Architecture, Zagreb/Rovinj, (2010), pp. 17-18.



-
- [2] Z. Kunica, T. Štampar, S. Bukal, D. Zorc: Braitenberg's Robots in Education and for Research, *Proc. of 1st Regional Conference - Mechatronics in Practice and Education MECH - CONF 2011.*, Subotica, (2011).
 - [3] A. Akšamović, at all: Development of Modular Hierarchical Control Structure for an Autonomous Mobile Robot, *Proc. of International Conference on Electrical Drives and Power Electronics*, Dubrovnik, (2005), E05-53.pdf
 - [4] H. J. Min, A. Drenner, N. Papanikolopoulos: Autonomous Docking for an eROSI Robot Based on a Vision System with Point Clustering, *Proc. of the 2007 Mediterranean Conference on Control & Automation*, Athens, Greece, (2007).
 - [5] J. L. Yang, D. T. Su, Y. S. Shiao, K. Y. Chang: Path-tracking controller design and implementation of a vision-based wheeled mobile robot, *Proc. of the IMechE*, Vol. 223, pp. 847-862.
 - [6] G. Klančar, M. Brezak, D. Matko, I. Petrović: Mobile Robots Tracking using Computer Vision, *Proc. of 13th International Conference on Electrical Drives and Power Electronics*, Dubrovnik, (2005), E05-20.pdf



International Conference on Innovative Technologies, IN-TECH 2012,
Rijeka, 26. - 28.09.2012



EFFECT OF SINTERING ATMOSPHERE ON SURFACE AND HIGH-TEMPERATURE OXIDATION OF PRESSURE-LESS SINTERED MoSi₂-ZrO₂ COMPOSITE

Yiming Yao¹, Erik Ström², Xin-Hai Li³

¹ Department of Materials and Manufacturing Technology, Chalmers University of Technology, Gothenburg, SE-412 96, Sweden

² Sandvik Heating Technology, Hallstahammar, SE-724 27, Sweden

³ Siemens Industrial Turbomachinery AB, Finspong, SE-612 83, Sweden

Keywords: molybdenum disilicide, high temperature application, MoSi₂-ZrO₂ composite, pressure-less sintering, microstructure, oxidation behaviour

Abstract. The effect of sintering atmosphere on high-temperature isothermal oxidation was investigated for molybdenum disilicide composites of MoSi₂+15 vol% ZrO₂ pressure-less sintered in Ar and H₂. XRD and SEM analysis revealed that the outermost surface of as-sintered composite consists of a (Mo, Zr)₅Si₃ layer, and the surface microstructure depended on the sintering gases. Isothermal and thermal cycling oxidation tests were performed at 1400°C for 1000 hours and at 1200°C for 1000 cycles in air, respectively. The as-sintered composites experienced a severe weight loss at initial oxidation, and protective scales were formed after 24 h and 300 h for H₂ and Ar sintered composites, respectively. In contrast, if the as-sintered surface was removed by grinding the material exhibited parabolic response with a low parabolic oxidation rate constant and excellent thermal shock property comparable to monolithic molybdenum disilicide. This work evidenced that the inherent oxidation resistance and self-curing property of MoSi₂+15 vol% ZrO₂ composite, and a strong influence of as-sintered surface microstructure of the composite on high temperature oxidation behaviour.

1. Introduction

Molybdenum silicide based material is a potential candidate for high-temperature components in turbine engine (1400 to 1600°C), due to its high melting point (2030°C), low density (6.25 g/cm³) and good oxidation resistance (up to 1750°C). The major drawbacks that hinder the application are poor room-temperature toughness and degraded strength and creep properties at temperatures over 1200°C. It has been shown that oxide addition or secondary phase reinforcement is an efficient method for strengthening and toughening of the MoSi₂-based composites. Especially, dispersion reinforced molybdenum disilicide composites have been extensively investigated for a wide range of additive materials, including Al₂O₃, ZrO₂, HfO₂, Y₂O₃, SiC, Si₃N₄, TiB₂, ZrB₂, and HfB₂ particles or fibres. ZrO₂ is an attractive toughening additive in terms of its phase transformation toughening mechanism. It has been reported that unstabilized ZrO₂ additives increased room temperature fracture toughness of MoSi₂ by a factor of four without sacrificing the high temperature mechanical properties [1]. It is believed that stress induced dislocations or microcracks in the MoSi₂ matrix can arise from the phase transformation of ZrO₂ occurring above the ductile-brittle transition temperature of MoSi₂, which can localize and shield cracking and crack propagation efficiently in the composite matrix. Good oxidation resistance of MoSi₂-ZrO₂ composites at 1500 and 1600°C were reported based on short term exposures (≤ 100 h) [2]. However, degraded oxidation behaviours were also found in the composite from exposures at relevant temperatures [3]. Obviously, more data from long-time oxidation exposure tests are needed for a careful assessment of this material.

Regarding to manufacturing of MoSi₂-based materials, most of the composites are produced using hot-press (HP) and hot isostatic pressing (HIP) techniques at temperatures around 1500°C. Naturally, high sintering density is expected for the composites by utilizing industrial pressure-less sintering technique. Since reaction with atmosphere occurs primarily near the surface during the pressure-less sintering process, the microstructure and chemistry in the surface region is expected to be different from that in the sintered bulk. The modification is supposed to make strong impact on the oxidation behaviour that is a surface related property. In the present work, fully dense MoSi₂ composites with 15 vol% un-stabilized ZrO₂ were produced with pressure-less sintering in H₂ and Ar atmospheres, respectively. The oxidation resistance of the composite were investigated in long-term isothermal oxidation and thermal cycling oxidation tests. The objective is to investigate the influence of sintering atmosphere on the microstructure and chemistry of the as-sintered surface, and consequently, on the long term oxidation and cycling behaviour of MoSi₂-ZrO₂ composite materials.

2. Experimental

The composites with a composition of MoSi₂- 15 vol.% ZrO₂ were prepared by conventional powder metallurgical process, and pressure-less sintering at 1600 °C for 1 hour in industrial grade H₂ and Ar (denoted as MZ-H and MZ-Ar, respectively). Commercial Kanthal MoSi₂ and DK-1 Zirconium Oxide (DAIICHI KIGENSO KAGAKU KOGYO CO., LTD) were used as raw powders with average size of 2.2 μm and 0.67 μm, respectively. The powder mixture was dispersed by milling in gasoline for 4 hours, and then dried below 100°C. The powder mixture was crushed and sieved through a 400 mesh screen. The green bodies with a density around 60% were prepared by cold isostatic pressing (CIP) under 306 MPa. The sintered density was measured according to ASTM C373, and the relative density (RD) was calculated using theoretical density of d_{MoSi2} = 6.25 g/cm³ and d_{ZrO2} = 5.68 g/cm³. A composite sample with ground/polished surface (denoted as MZ-g) and a MoSi₂ heating element material of Kanthal Super 1700 (KS1700) produced at Sandvik Heating Technology were also investigated as references.

Discontinuous isothermal oxidation was conducted on the composites at 1400°C over 1000 hours in flowing dry air (20 cm³/min), in a horizontally heated Al₂O₃ tube furnace. The testing specimens were supported on a MoSi₂ holder to avoid the reaction with the chamber material. Discontinuous cycling exposures were conducted at 1200°C using air cooling. A heating rate of 20°C/min and cooling rate of

110°C/min were taken between 1200°C and 100°C with holding time of 1 hour for each cycle. Totally, 926 cycles were performed at this temperature. The specimen's mass was carefully measured with an accuracy of 1 µg after exposure for 25, 50, 100, 250, and 1000 hours.

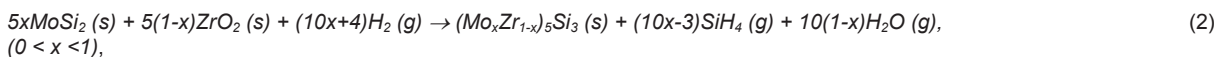
XRD phase analysis was performed using a Bruker D8 Advance X-ray diffractometer (XRD) with Cr-K α radiation. Microanalysis was conducted in a LEO Gemini 1550 field emission gun scanning electron microscope (FEG-SEM) equipped with an Oxford Instruments energy-dispersive X-ray (EDS) microanalyser. Vickers hardness (HV) and indentation fracture toughness (Kc) were measured using a Leitz hardness tester with a Vickers diamond indenter and 10 kg loading. The indentation fracture toughness was calculated using Anstis' equation.

3. Result and discussion

3.1 Microstructure of as-sintered materials

The composites were pressure-less sintered in H₂ or Ar to near full density. The sintered density was 6.00, 6.05 and 6.09 g/cm³ (97.4, 98.2 and K_c = 98.5 % of theoretical density) for MZ-Ar, MZ-g and MZ-H, respectively. The hardness and fracture toughness were HV = 8.94 ± 0.15 GPa and K_c = 3.98 ± 0.67 MPa.m^{1/2} (from a sample with density of d = 6.04 g/cm³). These results are comparable to the previously published data from the same material produced with a hot-pressing technique [4]. XRD analysis showed that the crystalline phases of the bulk material are tetragonal MoSi₂ of C11_b and monoclinic ZrO₂. SEM showed that the ZrO₂ particles with a size range from submicron to 2 µm are homogeneously dispersed in the MoSi₂ matrix. The total amount of other secondary phases, i.e. Mo₅Si₃, SiO₂ and ZrSiO₄ was less than 5 vol% estimated from SEM observations. According to XRD, as-sintered surfaces of MZ-Ar and MZ-H mainly consist of Mo₅Si₃ phase with minor amounts of Al₂O₃ and SiO₂. The existence of Mo₃Si phase cannot be excluded on the as-sintered surface, since the reflections of Mo₃Si are overlapped with those of Mo₅Si₃ phase.

As-sintered surface is characterized as a reactive zone with high content of 5-3 type of silicide with considerable amounts of voids (Fig. 1). The average depth of the reaction zone in MZ-H is above 80 µm. The microstructure can be divided into two parts: outermost layer and subsurface zone (Fig. 1a). The outermost layer of 25 µm consists of 5-3 type silicide. EDS reveals a composition segregation of high Zr alloyed grains with Si:Zr:Mo = 42:15:43 at%, close to (Mo_{0.66}Zr_{0.33})₅Si₃; and low Zr-content grains with Si:Zr:Mo = 37:2:61 at%, close to Mo₅Si₃. Both compositions are within the range of Mo₅Si₃ phases according to the Mo-Si phase diagram. No ZrO₂ particles were detected in the outermost layer in the X-ray maps (Fig. 1a), indicating that ZrO₂ was completely reduced and Zr dissolved in 5-3 phase grains in the top layer. The subsurface below the top layer consisted of large amounts of (Mo, Zr)₅Si₃ fine grains (> 50 vol%) mixed with MoSi₂. The reduction reactions of MoSi₂ and ZrO₂ by H₂ can be described as the reactions:



In present study, x ≈ 0.66 was found in (Mo_xZr_{1-x})₅Si₃ grains, i.e. one third of Mo atoms in Mo₅Si₃ are replaced by Zr. It is considered from reactions (1) and (2) that the reduction of MoSi₂ is enhanced in presence of ZrO₂ in terms of forming highly alloyed (Mo,Zr)₅Si₃ silicide. Voids may result from evaporation of constituents SiH₄ and H₂O. In the subsurface region, the reaction (2) becomes favourable as the partial pressure of H₂ is decreased. Thus, a mixed region of (Mo, Zr)₅Si₃ and MoSi₂ is built up between the reactive outermost surface and un-reacted bulk.

The reaction zone at MZ-Ar surface is much weaker than in the H₂ sintered material (Fig. 1b). The total thickness of reactive zone is about 30 µm. The microstructure consists of a mixture of Mo₅Si₃, (Mo, Zr)₅Si₃ and MoSi₂ silicide grains (Fig. 1b). Although the 5-3 type of silicides was also found in MZ-Ar surface, the reactions are expected to be different between the two sintering gases. In the case of Ar, a low concentration of oxygen could be present in the industrial argon, which can lead to some near-surface oxidation. At temperatures over 700°C, selective oxidation of silicon is allowed, which results in SiO evaporating under low oxygen partial pressure:



Mo₅Si₃ has wider nonstoichiometric range unlike line compound silicides such as MoSi₂ and Mo₃Si, and oxygen diffuses much faster in this phase. The presence and microstructure of 5-3 type silicide at the as-sintered surface plays a significant role on the oxidation behaviour of the composite material.

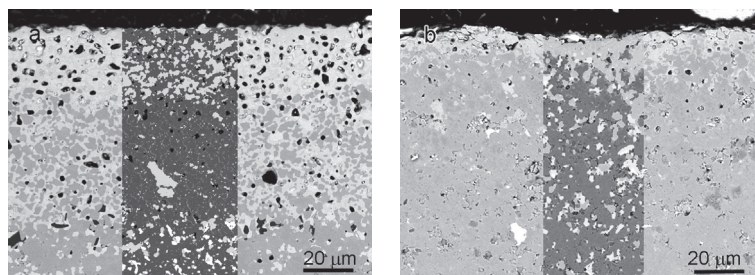


Fig. 1 The microstructure of the as-sintered surfaces of a) MZ-H and b) MZ-Ar, showing a stronger reaction in MZ-H surface than in MZ-Ar surface. In the overlapped X-ray phase maps, blue is MoSi₂, pink is (Mo, Zr)₅Si₃, green is Mo₅Si₃, yellow is ZrO₂.

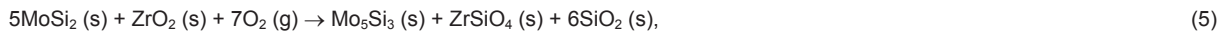
3.2 High temperature oxidation

Fig. 2 shows the appearance of the samples before and after isothermal exposure (Fig. 2a) and a time dependence of weight change at 1400°C for 1000 h in air. KS1700 presents typical parabolic kinetics of MoSi₂ materials with low parabolic rate constant of 4 × 10⁻⁴ mg²cm⁴h⁻¹ after 24 h, indicating that a thin protective silica scale has formed after a few hours of exposure. The ground composite MZ-g displays an excellent oxidation resistance against long-term high-temperature exposure (Fig. 2a), and strong self-healing property. The weight gain rises within 24 hours (Fig. 2b), and then, the curve follows the parabolic kinetic with rate constant of 3.3 × 10⁻³ mg²cm⁴h⁻¹, showing the formation of a thicker scale resulting from ZrO₂ additive. The total weight gain was less than 2 mg/cm² during the whole

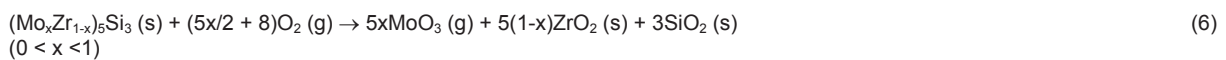
exposure period. The composite material followed the selected oxidation at high temperature and high oxygen pressure. MoSi_2 matrix is oxidized to form Mo_5Si_3 and SiO_2 protective scale according to the reaction:



In the presence of ZrO_2 , the silica from reaction (4) reacts with ZrO_2 to form ZrSiO_4 (zircon), i.e. $\text{SiO}_2 + \text{ZrO}_2 \rightarrow \text{ZrSiO}_4$. In fact, the ZrO_2 additive particles function as a SiO_2 sink, so that more SiO_2 is needed, i.e. more MoSi_2 has to be oxidized from the reaction (4) to form a protective scale compared with in the monolithic silicide. The oxidation of the ground composite MZ-g can be described as:



In contrast, the as-sintered composite samples were covered by white oxidation products after the exposure (Fig 2a). The scale on MZ-H was adhesive, but spalled scale can be visible on the MZ-Ar surface (Fig. 2a). Strong weight loss is displayed at the initial oxidation stage in the weight change curve in both samples (Fig. 3b). The total weight loss is 2.5 and 3.5 mg/cm^2 occurring within 50 h and 350 h for MZ-H and MZ-A, respectively. The weight loss is related to the rapid oxidation of the $(\text{Mo}_x\text{Zr}_{1-x})_5\text{Si}_3$ surface layer to form volatile MoO_3 and zircon:



The oxidation occurring on the as-sintered surface can be described as following. Reaction (6) was predominating and the weight loss continued until the surface $(\text{Mo}_x\text{Zr}_{1-x})_5\text{Si}_3$ phase layer was consumed completely. When a continuous silica layer started to form, reaction (5) took over, and the specific weight increased gradually with exposure time. In the steady oxidation stage, the weight gain presented with a parabolic kinetics, and the oxidation was controlled by oxygen diffusion through the silica scale. The oxidation rates in the steady oxidation stage are close in MZ-H and MZ-Ar (4.7×10^{-3} and $4.6 \times 10^{-3} \text{ mg}^2\text{cm}^{-4}\text{h}^{-1}$) compared to in MZ-g ($3.3 \times 10^{-3} \text{ mg}^2\text{cm}^{-4}\text{h}^{-1}$). According to this hypothesis, MZ-Ar with thinner $(\text{Mo}_x\text{Zr}_{1-x})_5\text{Si}_3$ layer on the as-sintered surface should have had experienced less weight loss resulting from the oxidation. The explanation for the conservation might be found out from the microstructure in the next section.

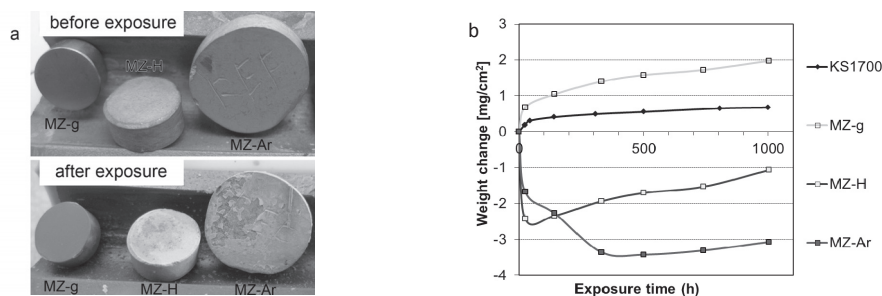


Fig. 3 a) Photos of the materials before and after exposure at 1400°C for 1000 h in air; b) weight change as a function of exposure time at 1400°C.

Fig. 3 shows the photos of samples submitted to cyclic oxidation and the weight change as function of number of cycles from 100 to 1200°C in air. KS-1700 displayed a negligible weight change after 1000 cycles, and the surface was protected by a crack-free glassy silica scale with melting feature. A thin protective scale was formed on MZ-g surface after a slight weight loss during a number of initial cycles. The scale consisted of homogeneously dispersed fine ZrSiO_4 particles ($< 0.5 \mu\text{m}$) in a SiO_2 matrix, and no cracks were observed. ZrSiO_4 particles ($\sim 3 \mu\text{m}$) and micro-cracks were observed in the scale of MZ-Ar after 1000 cycles, which is reflected with larger weight gain shown in Fig. 3b compared to the reference samples.

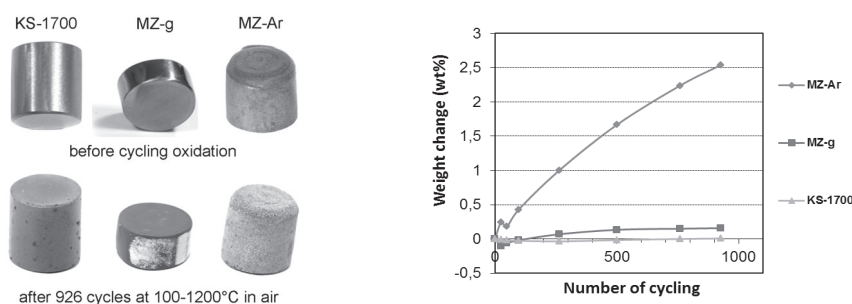


Fig. 3 Samples before and after cycling oxidation (left), and the weight change as a function of thermal cycling oxidation at 1200°C in flowing air (right).

3.3 Microstructure of oxidized materials

XRD analysis reveals that the crystalline phases in the scales are tetragonal ZrSiO_4 and $\alpha\text{-SiO}_2$ for all the studied composite materials after isothermal oxidation at 1400°C. The microstructure is shown in SEM plane-view and cross section images (Fig. 4). A smooth surface of MZ-g comprises glassy scale with embedded fine zircon particles ($1 - 2 \mu\text{m}$). The morphology of MZ-H is similar to that of MZ-g, but area density of zircon particles is much higher than in MZ-g. The zircon particles on MZ-Ar surface are obviously coarsened (up to $5 \mu\text{m}$), and rod-shaped Si-Al-O particles are observed, indicating the diffusion of Al as trace impurity from the bulk. In general, the microstructure of the

oxidized surface consisted of an outermost oxide scale of glassy silica and $ZrSiO_4$ particles; a Mo_5Si_3 layer at interface between the scale and substrate, and sub-scale oxidation zone with high density of Mo_5Si_3 grains and $ZrSiO_4$ particles underneath the Mo_5Si_3 layer (Fig. 4d, e and f). These particles zircon particles are usually core/rim structured with un-reacted ZrO_2 and a thin silica layer was usually found between particles and $MoSi_2$ matrix, indicating an un-equilibrated reaction between ZrO_2 and SiO_2 .

The thicknesses of scale and sub-scale oxidation zone are presented in Table 1. The thickness of MZ-H and MZ-Ar scale is 2 to 3 times of that in MZ-g. In addition, large amounts of zircon particles resulting from the oxidized $(Mo, Zr)_5Si_3$ form networks in the scale layer in MZ-H and MZ-Ar. The network-connected zircon particles and phase boundaries in the scale can provide fast diffusion paths for oxygen towards the matrix. Pores were commonly observed in the scale of MZ-Ar (Fig. 4f) contrasted to that of MZ-H and MZ-g, which might explain the deeper sub-scale oxidation zone related to higher partial pressure of oxygen resulting from poor protection of the scale on MZ-Ar.

Table 1 Oxide thickness and sub-scale oxidation zone depth

	Scale (μm)	Sub-scale oxidation zone (μm)
MZ-g	15 - 25	50 - 100
MZ-H	25 - 60	50 - 60
MZ-Ar	25 - 80	150 - 300

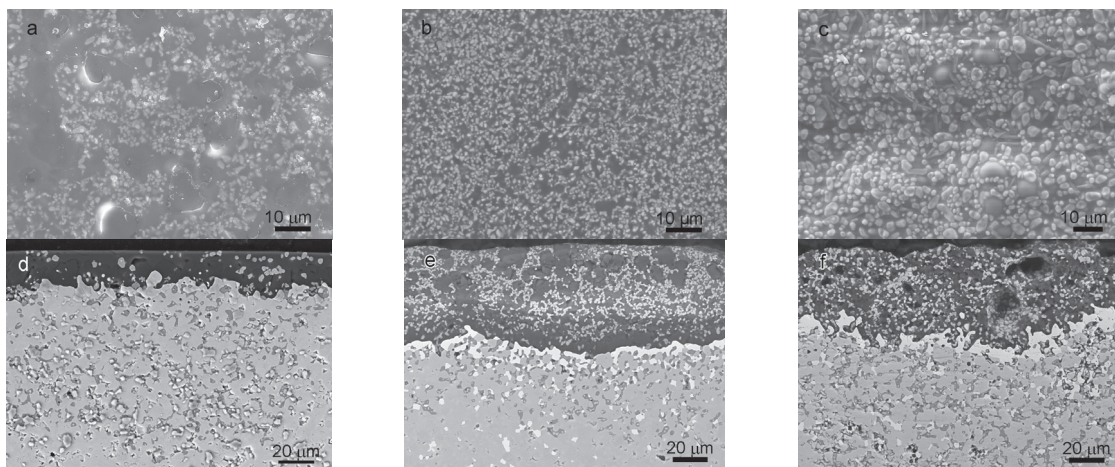


Fig. 4 SEM images of the composites after exposure at 1400°C for 1000 h, a), b) and c) are plane-view images of MZ-g, MZ-H, and MZ-Ar; d), e), and f) are cross-sectional images of MZ-g, MZ-H and MZ-Ar, respectively.

Mo_5Si_3 silicide is known for forming less protective oxide scales than $MoSi_2$ [5]. It is anticipated that the composite will present improved oxidation resistance by means of removing the $(Mo,Zr)_5Si_3$ layer on the as-sintered surface. However, it is not understood why the larger weight loss and longer time taken to parabolic oxidation in MZ-Ar, on which the $(Mo,Zr)_5Si_3$ layer was much thinner than in MZ-H. Regarding the microstructure of the scales, it is inferred that the dense and adhesive oxide scale on MZ-H is formed by the reactive products of reactions (4) and (5) directly from oxidizing $MoSi_2$. In other words, the oxidation reaction (6) producing volatile MoO_3 is completed before the formation of the protective scale begins in MZ-H. In contrast, the reaction (6) seems to be retarded during the formation of the scale on MZ-Ar, which results in a less protective scale with large amounts of pores and a deep sub-scale oxidation region. It is suggested that the microstructure with a pure $(Mo,Zr)_5Si_3$ layer might be preferable to that of dispersed $(Mo,Zr)_5Si_3$ grain in the as-sintered surface. However, the effect of sintered density effect on the oxidation resistance cannot be excluded, since the sintered density of MZ-Ar material was lower than that of MZ-H. It has been reported that the $MoSi_2-ZrO_2$ composite pressure-less sintered in Ar atmosphere presents poor sinterability compared with the material sintered in vacuum or hydrogen [6]. Corresponding microstructure analysis along with kinetic study of isothermal exposure experiment is necessary for further understanding.

4. Conclusion

In this study, excellent oxidation resistance, thermal shock resistance and self-healing properties of pressure-less sintered $MoSi_2-ZrO_2$ composite material were evidenced from a long-term high temperature exposure and cycling oxidation tests. However these properties can be sheltered by great weight loss in the initial oxidation stage resulting from the strong oxidation of $(Mo,Zr)_5Si_3$ silicide presenting on the as-sintered surface. The $(Mo,Zr)_5Si_3$ phase on the outermost surface can be produced by both reduction and oxidation reactions occurring in H_2 and Ar sintering atmospheres. The amount and time period of weight loss are dependent on the microstructure of the $(Mo,Zr)_5Si_3$ layer on the as-sintered sample. Therefore, a surface treatment, for example, grinding or pre-oxidation, is necessary to obtain $MoSi_2-ZrO_2$ composite materials with good oxidation performance in industrial applications.

Acknowledgment

This investigation was financially supported by Swedish National Program KME, Sandvik Materials Technology, and Siemens Industrial Turbomachinery AB. Mr. Niklas Åberg is acknowledged for performing the cyclic oxidation test in Siemens Industrial Turbomachinery AB.

References

- [1] J.J. Petrovic, A.K. Bhattachary, R.E. Honnell, T.E. Mitchell, R.K. Wade, K.J. McClellan, ZrO_2 and ZrO_2-SiC particle reinforced $MoSi_2$ matrix composites, *Mater. Sci. Eng. A*, Vol. 155 (1992), pp. 259-266.



-
- [2] S. Lohfeld, M. Schütze, A. Böhm, V. Güther, R. Rix and R. Scholl, Oxidation behaviour of particle reinforced MoSi₂ composites at temperatures up to 1700°C, Part II: Initial screening of the oxidation behaviour of MoSi₂ composites, *Mater. Corros.*, Vol. 56 (2005), No. 3, pp. 194-158.
- [3] K. Gong, Y. Yao, M. Sundberg, X-H Li, E. Ström, and C. Li, Toughening effect and oxidation behaviour of MoSi₂-ZrO₂ composites, MRS Fall Meeting, *MRS Proc.*, Materials Research Society, Vol. 980 (2006), pp. 339-344.
- [4] Y. Ma, Y. Hao, D. Zhang, N. Yu, Fabrication and fracture analysis of MoSi₂ matrix composites by mechanical alloying, *Trans. Nonferrous Met. Soc. China*, Vol.11 (2001), No.6, pp. 847-851.
- [5] K. Natesan, S.C. Deevi, Oxidation Behavior of molybdenum silicides and their composites, *Intermetallics*, Vol. 8 (2000), pp. 1147-58.
- [6] R. Scholl, T. Jüngling, B. Kieback, Pressureless sintering of MoSi₂ materials, *Mat. Res. Soc. Symp. Proc.*, Material Research Society, Vol 364 (1995), pp 931-935.



International Conference on Innovative Technologies, IN-TECH 2012,
Rijeka, 26. - 28.09.2012



PHISICAL-CHEMICAL PROPERTIES OF POULTRY FEATHER FIBRES

T. Kreže¹, S. Strnad²

^{1,2} University of Maribor, Faculty of Mechanical Engineering,
Institute of Engineering Materials and Design, Slovenia

Keywords: Poultry feather fibres, Mechanical properties, Chemical properties, Water sorption, Microscopy

Abstract. Increased poultry consumption and production has resulted in a concomitant increase in the amount of waste products for disposal by poultry producers. Poultry feathers are waste products for which disposal is difficult and are usually converted to animal feed. Therefore, the right application of poultry feathers will be one of the most important achievements in the field of industrial waste management in the poultry industry in the future. The aim of this research was a thoroughly study of physical-chemical properties of fibres from waste poultry feathers in order to find out in which degree it is comparable to conventional textile fibres. Tensile properties and linear density were determined using Vibrodyn and Vibroscop Apparatus. The extensive microscopic analyses of feathers barbs and rachis were performed using SEM and optical microscopy. The average length of poultry feathers amounted to 1.5-4.5 cm. The linear density of feathers barbs amounted to 26.7 dtex, which is comparable with the values for the medium wool fibres. Tensile properties of poultry feathers rachis ($\sigma = 19$ cN/tex, $\varepsilon = 19.8\%$) are similar to that of wool and lower in the case of feathers barbs ($\sigma = 7.1$ cN/tex, $\varepsilon = 13\%$). Moisture sorption of feather fibres was comparable to most of natural textile fibres, thus it amounted to 10.8 %. Water retention values of feathers, however was by about 17 % lower in comparison to wool fibres. Using potentiometric titration the amount of positive and negative charge per mass (pH 3-11) was determined. The poultry feathers fibres showed typical amphoteric character with the isoelectric point at the pH 5. Maximal amount of positive charge at pH 3 was 222 mmol/kg and the maximal amount of negative charge at pH 9 amounted to 105 mmol/kg.

Introduction

Sustainable development has become widely accepted concept. The concept of zero emissions and zero waste was coined for adaptation of production processes to minimise emissions and waste. During the last three decades, research has been conducted also to improve the agronomic utilization of animal waste, including poultry waste [1]. Poultry industry is globally undergoing strong expansion. In the last 15 years, poultry production increased by about 5 % annually [2]. Feather waste is generated in large amounts as a by-product of commercial poultry processing. It was estimated, that 5 Mt of feathers are produced annually worldwide as a waste stream from the production of chicken meat [3]. Currently feathers are converted into low nutritional value pet food and/or sanitized and land-filled. The costs for such disposal come to the poultry industry, and finally to consumers. Therefore finding the right and wide application of poultry feathers will be one of the most important achievements in the field of industrial waste management and recycling in the poultry industry in the future. Waste poultry feathers can be used as raw material for other processes and products, moreover new products could be developed in such a way that they are biodegradable and therefore much easier to dispose of. Whole feathers and feather fibres barbs have been widely studied for potential biomaterial application due to their inherent properties of thermal and chemical resistance [4]. The presence of hollow honeycomb structures, their low density (0.8 g/cm³ for chicken feathers compared to 1.5 g/cm³ for cellulose fibres and about 1.3 g/cm³ for wool), high flexibility, excellent compressibility and resiliency, ability to dampen sound and warm retention provides them unique properties unlike any other natural or synthetic fibres. Feathers consist of about 90 % of keratin and are as such a large potential source of this protein biopolymer. The structure and properties of poultry feathers barbs make them unique fibres preferable for several applications.

It would be necessary to understand the structure and properties of feather fibres in order to determine their suitability for various applications. The feather is mainly composed of three distinct units or structural levels (Fig.1). The primary level or central shaft of feathers is called the rachis. The primary branches of the rachis or secondary level of the feather are the barbs. The main shaft of a barb is the ramus, and it supports the tertiary branches of the feathers which are called barbules. The barbules are attached to the barbs in a manner similar to the barbs being attached to the rachis. Barbules consist of a series of cells, beginning with the short cells of the base and ending with a series of longer, distal cells called pennulum [5]. The rachis takes place along the entire length of feathers and its length is up to 18 cm. The barbs have lengths anywhere from 1 to 4.5 cm, depending on their location along the length of the rachis. Barbs at the base of the rachis are longer than those at the tip. The tertiary structures the barbules have lengths of about 0.3 to 0.5 mm. Feathers as such can not be processed as the protein fibres wool due to the complex structure of the feathers. The feather rachis is thick and stiff, and therefore not suitable as natural protein fibres. The secondary structures of feathers i.e. the barbs have the structure and properties that make them suitable for use as natural protein fibres. The morphological structure of feather barbs is similar to that of rachis but the physical structure and protein crystals in feather barbs is different than that reported for feather rachis keratin [6].

The aim of this research was to investigate the morphological structure and physical properties of fibres from waste poultry feathers (chicken feathers barbs and rachis) for potential use in development and production of various types of side products of higher added value, such as composite fibreboard insulating panels or functional keratin composite films. In this order tensile properties (tenacity, elongation and modulus) and sorption ability (moisture sorption, water retention value) of chicken feathers barbs and rachis were determined. Using potentiometric titration also the amount of positive and negative charge per mass (pH 3-11) was determined. The extensive microscopic analyses of feathers barbs and rachis were performed using SEM and optical microscopy. The properties of chicken feathers barbs and rachis have been compared with the most common natural protein fibre, wool.

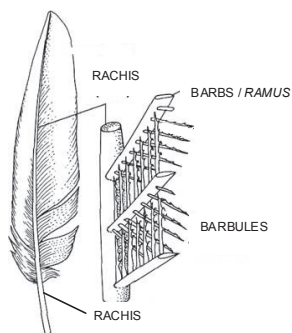


Fig. 1 Structural levels of the feathers; the rachis is the primary, the barbs are the secondary and the barbules are the tertiary structures of the feathers

Materials and Methods

Waste chicken feathers were provided by poultry meat producer Perutnina Ptuj d.d. Feathers have been industrially washed with tap water on the grate. In this manner, major impurities such as blood, secretions, etc. have been removed. Laboratory cleaning procedure was carried out in the washing bath containing water and non-ionic washing agent 1 g/L, at a temperature of 60 °C, for 30 minutes. The bath ratio (mass of feathers/volume of bath) was 1:40. After the washing procedure the fibres were rinsed and dried in a ventilation oven at 40 °C for 72 hours. The extraction of chicken feathers was performed in Soxhlet for 6 h with petroleum ether. Drying procedure was carried out under vacuum for 24 hours.

Morphological structure

Optical microscope *Axiotech 25 HD* (Zeiss) was applied to study the longitudinal features of feathers barbs and scanning Electron Microscope *FESEM Supra VP 35* (Zeiss) was applied for studying the longitudinal and cross-sectional features of feathers barbs and barbules.

Water vapour adsorption

Moisture sorption of feather fibres was determined using *HB43-S Halogen Moisture Analyzer* (Mettler Toledo). Feather fibres were exposed to standard atmosphere 20 ±2 °C, 65% ±2% RH for 24 hours according to standard DIN EN ISO 139:2011 [7].

Water retention power

Water retention power of feather fibres was determined according to standard DIN 53 814 [8]. This method is based on a determination of the quantity of water, which the fibres can absorb and retain under strictly controlled conditions. This property is expressed as a ratio between the mass of water retained in the fibre after soaking (2 hours) and centrifuging (20 min), and the mass of absolute dry sample ($T = 105^{\circ}\text{C}$, $t = 4$ hours).

Swelling of fibres

The swelling of the feather fibres in the aqueous medium was determined on the basis of fibre diameter measurements. Fibre diameter measurements were carried out with microscope *Axiotech 25 HD* (Zeiss) using the image analysis system and supporting software *Kontron KS 300*.

Tensile properties

Measurements of the mechanical properties of the feather fibres (tenacity σ , elongation ε and modulus E) were carried out using the electronically controlled dynamometer CRE VIBRODYN 400 Lenzing Technik Instruments and software package Lenzing Technik Prüf-Software, connected with the measuring instrument VIBROSKOP 400 for the determination of linear density. Measurements were performed on single fibres according to the standard ISO 5079. Measuring conditions: temperature 20 °C, relative humidity 65%, gauge length 20 mm, pre-loading 100 mg, measuring speed 10 mm/min.

Potentiometric titration

The pH potentiometric titration of the grinded poultry feathers ($m = 2.5$ g) suspension was carried out with a two-burette instrument Mettler Toledo T70, in an inert atmosphere (N_2 bubbling). The burettes were filled with 0.1 M HCl and 0.1 M KOH. All solutions were prepared in Milli-Q water with low carbonate content ($< 10^{-5}$ M). This was achieved by boiling and cooling under nitrogen atmosphere. The suspension was titrated in a forth and back manner between the initial pH = 2.6 to the preset pH = 11. The titration experiments were carried out at 0.01 M ionic strength, set to its appropriate value with KCl. The titrant was added dynamically within a preset interval of [0.001 – 0.25] mL. The equilibrium criteria for the timed addition was set to $dE/dt = 0.1/150\text{s}$. Where 150s was the minimum time to reach equilibrium conditions between two additions of the titrant, and the maximum time was set to 7200s. The pH value was measured with a Mettler Toledo DG-117 combined glass electrode. A suspension of non-grinded feathers was titrated under same conditions as the suspension of grinded feathers. A blank HCl-KOH titration was carried out under same conditions as above.

Results and Discussion

Morphological structure of chicken feathers barbs is shown in the Fig. 2. Feather fibres, both the longitudinal views as well as a cross-section, are very different from wool. Longitudinal appearance of wool is characterized by epidermal cells, while feather fibres surface is smooth; however the barbules that are attached to the barbs have a similar function as the epidermal cells of the wool. Both, epidermal cells and barbules provide better adhesion between the fibres. Feather barbs have a specific cross-section, which is completely different than that of wool. In cross-section feathers barbs have honeycomb shaped hollow cells as seen from Fig. 2c. These hollow cells act as air and heat insulators, provide high resistance to compressibility and makes barb to be very light in weight. Only coarser wool fibres

have also a hollow space running lengthwise through the centre (medulla). On the Fig. 3 the longitudinal view of the tertiary structures of the feathers - barbules is presented.

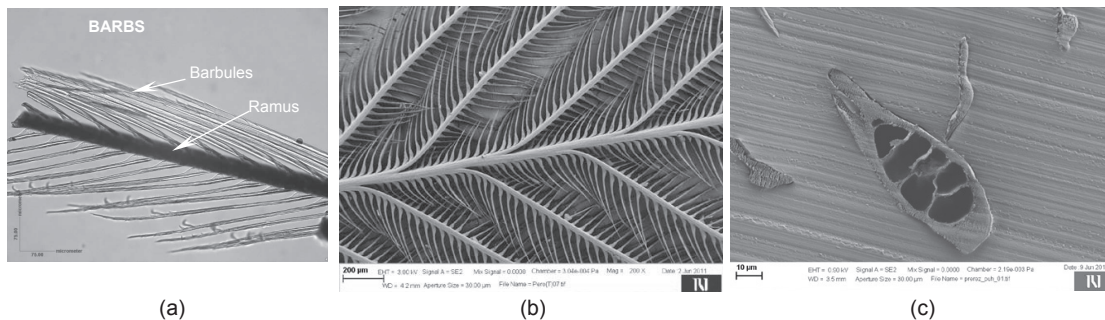


Fig. 2 The chicken feathers barbs and barbules: a) optical microscope at 140X magnification, b) SEM at 200X magnification and c) cross section view of a feathers barb under SEM

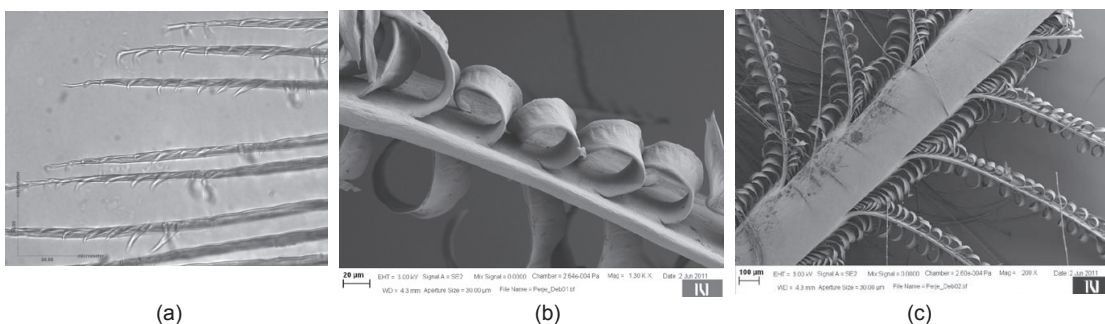


Fig. 3 Longitudinal view of chicken feathers barbules: a) optical microscope at 350X magnification, b) SEM at 1300X magnification; c) feather barbules that are attached to the barbs under SEM at 200X magnification

Sorption properties of feather fibres were comparable to most of natural textile fibres. The moisture regain of chicken feather fibres amounted to 10.9 % (STDEV=2.6 %), which was higher in comparison with cotton fibres ($M_s = 8.5\%$), and comparable to silk ($M_s = 11\%$), and about 25 % lower compared to the most hydrophilic natural fibres, wool ($M_s = 14.5\%$). When considering water retention power the values for cellulose and protein fibres are somewhat higher (WRV for cotton = 45 - 50 %, for silk and wool = 40 - 45 %) when compared to feather fibres (WRV = 37.3 %, STDEV = 4.3 %). Values for fibres other than feathers are taken from the literature **Chyba! Nenalezen zdroj odkazů.** Swelling of feather barbules in aqueous medium was evaluated by fibre diameter measurements using microscopic method. After 24h soaking in MilliQ water, there were no significant changes in fibre diameters of feather barbules, thus the rate of swelling of feather fibres in the transverse direction was 2.3 %, however after 120h the rate of swelling was increased to 23,6 %. Chicken feathers showed relatively high ability to absorb and retain water. The results showed that the hydrophilicity of feather fibres was comparable to natural cellulose and protein fibres.

Tensile properties of chicken feathers rachis and barbs were compared with wool fibres and are presented in the diagram on the Fig. 4. As it could be seen from the diagram the tenacity of feather rachis ($\sigma = 19.04\text{ cN/tex}$), which represent a primary structure of feathers was by about 60 % higher in comparison to feather barbs ($\sigma = 7.1\text{ cN/tex}$), and by about 40 % higher when compared to wool fibres ($\sigma = 10.6\text{ cN/tex}$). Modulus of feather rachis ($E = 175.6\text{ cN/tex}$) was very similar to that of wool ($E = 164.0\text{ cN/tex}$) while modulus of feather barbs ($E = 117.8\text{ cN/tex}$) was by about 30 % lower than that of wool. Feather barbs and feather rachis have lower elongation than that of wool.

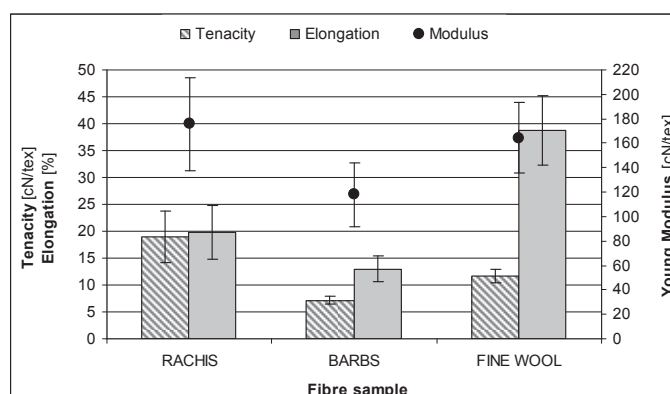


Fig. 4 Tensile properties of chicken feathers rachis and barbs in comparison to wool fibres

The pH potentiometric titrations of poultry feathers were carried out in order to observe their pH dependent charging behaviour. The feathers consist mostly of different types of proteins. Proteins are made up of amino acid chains bound together by peptide bonds between amino and carboxylic groups. Amino acids can get charged positively (amino groups) or negatively (carboxylic groups) due to protonation and deprotonation of their functional groups at certain pH values.

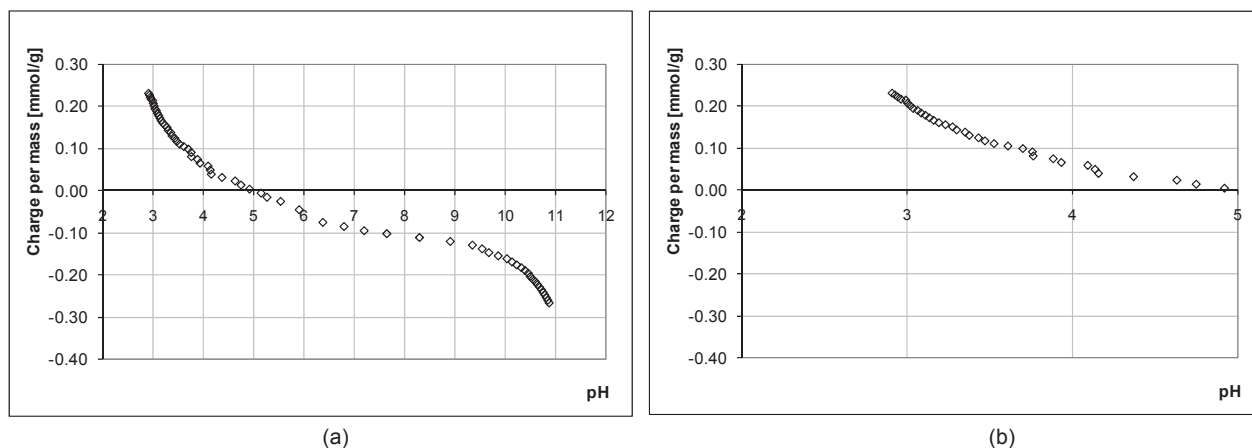


Fig. 5 Charging isotherm of poultry feather suspension (a) and charging isotherm of poultry feathers in the positive region between pH = 3 and pH = 5 (b)

Figure 5a shows the charging behaviour of grinded poultry feathers in the pH region between pH = 3 and pH = 11. Both the positive and the negative nature of the feathers can be observed, with the point of zero charge being around pH = 5. The plateau values of both charges are not defined well. A steep decrease of charge can be observed from pH = 3 to pH = 6. From pH = 6 to pH = 9.5 the decrease of charge is less steep. This part can be considered as the plateau value of negative charges. The plateau of positively charged groups is not so evident. A closer look at the pH region of positive charges, between pH = 3 and pH = 5 (Fig. 5b) shows a small decrease of the curve steepness and a condensation of the charge values around pH = 3. One can determine the positive charge at this point, although it is not evident if the plateau value of the positive charges is near this point. The real amount of positive charges can be therefore higher than the amount calculated from the charging isotherms in Fig. 5a and 5b. The amount of positive charges of feathers calculated from the isotherms is 222 mmol/kg. The amount of negative charge is 105 mmol/kg. The pKa values of the charged species could not be determined, since the proteins in the feathers consist of several amino acids, which exhibit many different pKa values. When the protonation and deprotonation processes of different species are overlapping, then the pKa values are too close to each other for qualitative determination of each species to be possible.

Conclusion

In order to investigate the morphological structure and physical properties of fibres from waste poultry feathers for potential use in development and production of various types of side products of higher added value, tensile properties (tenacity, elongation and modulus) and sorption ability (moisture sorption, water retention value) of chicken feathers barbs and rachis were determined. Using potentiometric titration the amount of positive and negative charge per mass (pH 3-11) was determined. The extensive microscopic analyses of feathers barbs and rachis were performed using SEM and optical microscopy. The properties of chicken feathers barbs and rachis have been compared with the most common natural protein fibre, wool. In cross-section feathers barbs have honeycomb shaped hollow cells, which act as air and heat insulators, provide high resistance to compressibility and makes barb to be very light in weight. The moisture regain of chicken feather fibres amounted to 10.9 %, which was comparable to silk ($M_s = 11\%$), and about 25 % lower in comparison to wool ($M_s = 14.5\%$). Water retention power of feather fibres was by about 20 % lower than that of wool. Swelling of feather barbules in aqueous medium was after 24h soaking in MilliQ water insignificant, however after 120h the rate of swelling was increased to 23.6 %. Chicken feathers showed relatively high ability to absorb and retain water, thus the results showed that their hydrophilicity was comparable to natural cellulose and protein fibres. The tenacity of feather rachis was by about 40 % higher than that of wool, feather rachis however showed by about 50 % lower tenacities in comparison to wool. The modulus of feather rachis was comparable to that of wool; however the elongation was by about 50 % lower. Poultry feathers showed amphoteric charging isotherms with the point of zero charge being around pH = 5. The amount of positive charges of feathers calculated from the potentiometric titrations isotherms was 222 mmol/kg and the amount of negative charges was 105 mmol/kg.

References

- [1] J.M. Kim, W.J. Lim, H.J. Suh: Feather-degrading *Bacillus* species from poultry waste, *Process Biochemistry*, Volume 37, Issues 3, (2001), p. 287-291
- [2] P.M.M. Schrooyen, P.J. Dijkstra, R.C. Oberthür, A. Bantjes, J. Feijen: Partially Carboxymethylated Feather Keratins. 1. Properties in Aqueous Systems, *J. Agric. Food Chem.*, Volume 48, (2000), p.4626-4334
- [3] A. Onifade, N. Al-Sane, A. Al-Musallam, S. Al-Zarban: A review: potentials for biotechnological applications of keratin-degrading microorganisms and their enzymes for nutritional improvement of feathers and other keratins as livestock feed resources, *Bioresour. Technol.*, Volume 66, Number 1, (1998), p. 1-11
- [4] A.J. Poole, J.S. Church and M.G. Huson: Environmentally Sustainable Fibers from Regenerated Protein, *Biomacromolecules*, Volume 10, Issue 1, (2009), p. 1-8
- [5] Richard O. Prum: Development and evolutionary origin of feathers, *Journal of Experimental Zoology*, Volume 285, Issue 4, (1999), p.p 291-306



-
- [6] N. Reddy, Y. Yang: Structure and Properties of Chicken Feather Barbs as Natural Protein Fibers, *J. Polym. Environ.*, 15 (2007), pp. 81–87;
 - [7] DIN EN ISO 139:2011: Textilien - Normalklimate für die Probenvorbereitung und Prüfung (ISO 139:2005 + Amd.1:2011)
 - [8] DIN 53814:1974: Testing of textiles; determination of water retention power of fibres and yarn cuttings. (Prüfung von Textilien; Bestimmung des Wasserrückhaltevermögens von Fasern und Fadenabschnitten.)
 - [9] W.Von Bergen: *Wool Handbook* (Volume 1, Interscience Publishers, John Wiley& Sons New York, 1963)



International Conference on Innovative Technologies, IN-TECH 2012,
Rijeka, 26. - 28.09.2012



CONVERGENCE OF CROATIA AND SLOVAKIA IN THE FIELD OF R&D FOUNDING TO THE EU 27 AVERAGE

E. Spišák¹, E. Spišáková²

¹ Technical university of Košice, Faculty of Mechanical Engineering, Letná 9, 040 01 Košice, Slovakia

² University of Economics in Bratislava, Faculty of Business Economy, Tajovského 13, 041 30 Košice, Slovakia

Keywords: convergence, research, development, Europe 2020, founding of R&D, financial resources

Abstract. Considering the failure of the target of original European Union's strategy called Lisbon Strategy up to the year 2010, it was necessary to develop a new strategy Europe 2020, which extended the time period to achieve the fundamental objectives up to the year 2020. One of the objectives of the strategy is focused on research and development, namely: increasing investment in research and development to 3% of gross domestic product. Therefore, the article is oriented on the trend comparison and the time comparison of research and development in Croatia (as a future Member State of the European Union), and Slovakia. There is analyzed and compared the indicator expressing the share of gross domestic expenditure on research and development on country's gross domestic product. The partial objective in the area of research and development funding is that 2/3 of the financial resources should come from business enterprise sector and 1/3 should be funded by government sector. Therefore the second part of the article deals with the structure of gross domestic expenditure on research and development.

In the last, most important part of the article, we simulate and propose how should grow the expenditure on research and development in Croatia and Slovakia so that these two countries will converge to the EU 27 average and also how they should develop to achieve the target value.

Introduction

Legislation of the Slovak Republic in the area of R&D support is represented by Law 172/2005 about the organization of state support for research and development. According to this law, research is a systematic creative activity taking place in science and technology to societal needs and for development of knowledge. It consists of basic and applied research. Development is a systematic creative activity in the field of science and technology, which uses patterns and knowledge gained through research or based on practical experience in developing new materials, products, equipment, systems, methods and processes, including construction and prototype development [8].

Expenditure on R&D includes total expenses incurred in the organization on R&D activities, i.e. internal expenditure. They consist of capital and current expenditure. The expenses incurred outside the organization include only those, which serve to support internal R&D. The current expenditure includes costs for organization's own activities and their R&D departments and also includes costs for tasks solved by its own organization and work capacity. In addition to its own corporate resources to support R&D activities, they use funds obtained from government sector, from higher educational sector, from private and non-profit organizations and from abroad.

Expenditure on R&D can be measured by [6]:

- Gross domestic expenditure on R&D – GERD – which represents domestic and foreign expenses to conduct R&D within the country over a period of time (with the exception of expenses on R&D that are carried out abroad),
- Gross national expenditure on R&D – GNERD – which includes the country's total expenditure on R&D carried out abroad.

The article will analyze and compare two countries, i.e. Slovakia as a current member state of the EU and Croatia, whose EU membership is already a matter of time.

Convergence or divergence of GERD in Slovakia and Croatia to the EU 27 average

Until recently, the issue of economy competitiveness was dealt with Lisbon Strategy for growth and jobs, whose primary target was, that the EU should become (by the year 2010) most competitive and most dynamic knowledge-based economy in the world, capable of sustainable economic growth in which will be more and better jobs and greater social cohesion [5]. Mentioned document, adopted also by Slovakia, was also focused on improving living standards of citizens of the EU, through the support of R&D funding.

Up to the original Lisbon Strategy, which expired in 2010, has followed a new strategy developed by the European Commission called Europe 2020. As in the Lisbon Strategy, also in Europe 2020, the European Commission identified key objectives to which the fulfilment would occur by 2020 to achieve desired growth and progress in individual Member States, as well as in the European Union.

For the purpose of this article is major the second target about investment into R&D, i.e. GERD, according to which expenditure should grow by 2020 to 3% of GDP¹ (average value for European Union) because the promotion of basic and applied R&D creates a strong presumption for building the knowledge economy, contributes to employment growth, improves quality of life, solves social problems and also contributes to the economic growth of the euro area

From mentioned 3%, at least 2/3 should come from business enterprise sector and 1/3 of funds from government sector. From the EU Member States and also candidate countries, only three countries achieve this target to the year 2010 – Finland 3,87% of GDP, Sweden 3,42% of GDP (decrease of 3,96% of GDP in 2009) and Denmark with a value of 3,06% of GDP. Only these three countries can now compete with the research strength of Japan, South Korea and other developed countries. From the other countries, Germany (2,82% of GDP) and Austria (2,76% of GDP) are approaching to the target. Slovakia and Croatia are in the second half of the scoreboard. In the year

¹ The target value for EU 27 average is 3% of GDP. The target of Slovakia is to increase expenditure on R&D by 2020 to 1% of GDP. Given the fact, that Croatia is not yet Member State of the European Union, target value for this country is not specifically determined.

2010 GERD in Slovakia were only 0,63% of GDP (which is the lowest value of the V4 group) and Croatia 0,73% of GDP. The lowest value of the indicator was recorded in Romania, 0,47% of GDP.

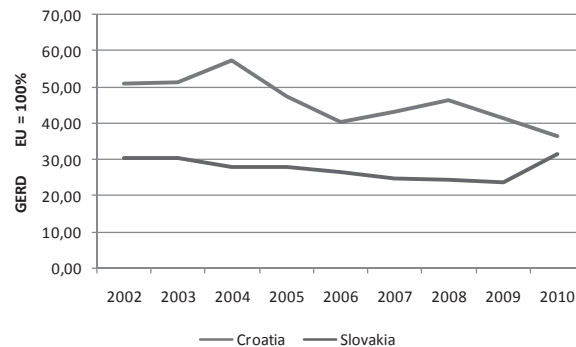


Fig. 1 GERD in Slovakia and Croatia in comparison with EU 27 average (% GDP), EU = 100%
Source: Self elaboration according to the data from Eurostat

Not a very positive trend in funding of R&D can be seen in the EU27, where in recent years, there is a decrease, respectively stagnation. In 2010 GERD was at only 2,00% of GDP. The cause was and always is a number of Member States, especially from a group called catching up countries, which display a lack of activity in this area, and thereby hinder the fulfilment of the target of the Europe 2020.

Despite the fact that GERD in Slovakia have long been not only below the EU average value, but also value of Croatia, their share of GDP in recent years growing slightly. The situation is still very unfavourable, because significant economic growth in the pre-crisis period did not contribute to increase the share of expenditure on R&D in relation to GDP. In 2002, the value of the indicator was 0,57% of GDP, to the year 2009 gradually declining to 0,48% of GDP. The declining value of the monitored indicator caused over the years 2002 - 2009 divergence, not required convergence of Slovakia to the EU 27 average (Fig. 1).

One of the reasons for lagging Slovakia behind the developed countries is that the major Slovak companies are more like "assembling" businesses that don't realize their own engineering. In Slovakia are automobile factories such as Volkswagen Slovakia, Slovakia PSA Peugeot Citroen and KIA Motors Slovakia Ltd. as manufacturing and assembling factories, but where is no realization of its' own research, development and innovation activities. These factories produce cars, respectively components for cars under the strict regulatory requirements and standards from parent companies resident abroad.

Generally, in the current period are innovation in Slovakia realized by business sector based on the use of existing technologies from abroad, not to use the knowledge of their own research. Firms innovate mostly by purchases of machinery and equipment from abroad and they suit them to production process or completely replaced this process by new technologies. Innovation based on the use of their own R&D and results of R&D developed by domestic research institutions are made only in limited extent.

In Croatia we can also say about the divergence of monitored indicator expressing the share of expenditure on R&D on GDP (Fig. 1). The value of the indicator for Croatia is during the entire period greater than the value of this indicator in Slovakia. However, the indicator records fluctuating and ultimately declining trend. In 2002, GERD were 0,96% of GDP, in 2004 increased slightly to 1,05% of GDP. The emergence of financial and economic crisis was reflected in this area negative, because since 2008 was re-recorded a declining trend in the share of GERD in the country's GDP to 0,73% of GDP in 2010.

The structure of GERD in Slovakia and Croatia

GERD comes from three main sources: business enterprise sector, government sector and funds received from abroad and from two secondary sources, i.e. the resources from higher education sector and private non profit sector. In this part of the article we will therefore follow, how both analyzed countries met the intermediate target of Europe 2020, concerning the structure of expenditure on R&D, i.e. 2/3 of resources should come from business enterprise sector and 1/3 from government sector.

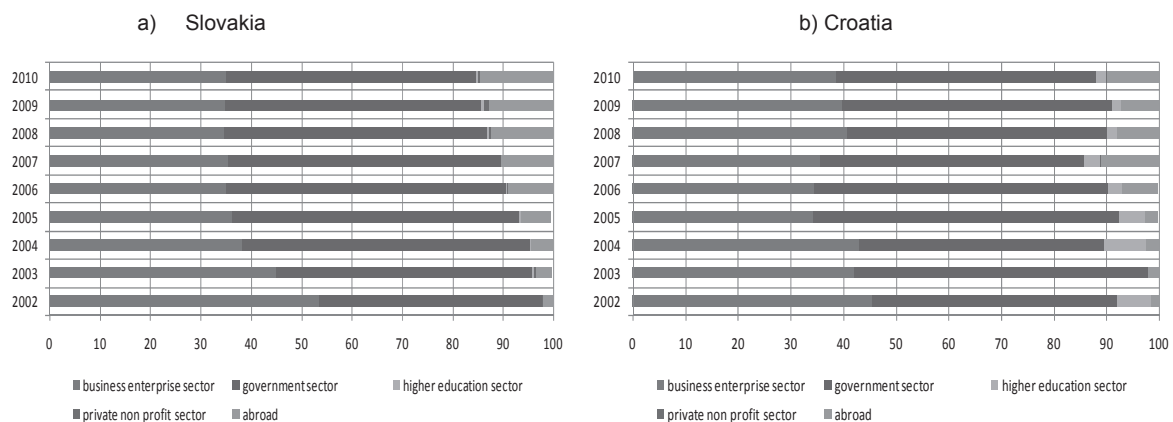


Fig. 2 GERD by source of funds
Source: Self elaboration according to the data from Eurostat

As mentioned earlier, GERD in Slovakia recorded a declining trend. During recent years, the proportion of expenditure on R&D of its own corporate resources (business enterprise sector) in total GERD significantly decreasing, i.e. decrease of 53,6% in 2002 to 35,1% in

2010 (Fig. 2a). On the other hand, government spending and also resources from abroad on R&D in the period increased. Expenditure of private non profit sector and the higher education sector in this period were only a small proportion of total GERD. The structure of expenditure in this area develops in the opposite direction, as it is required by Europe 2020. Business resources were about one third (35,1% of total expenditure in 2010). In most cases Slovak enterprises are unable to compete with foreign companies or enterprises which dispose of new technologies and sufficient equity to finance research, development and thus innovation. Entry of Slovakia to the European Union positively affected the flow of foreign resources into the country to support R&D, which increased from the year 2004 by 10,4%. The share of total abroad expenditure on GERD in 2010 was 14,7%.

Similarly as in Slovakia, also in Croatia the most sources of funding for R&D activities comes from the government sector. The share of government expenditure in total expenditure on R&D varied over the years in the range 46,4% to 58,1%. In 2010, this share was 49,2%. Real business expenditure on R&D in Croatia are not at 2/3 of total expenditure on R&D. Their share of total GERD had cyclical character (Fig. 2b). Resources obtained from abroad are significantly growing. In 2002, their share of total GERD was 1,5% and then rose year on year, until the global crisis, to 10,9% in 2007. In 2010 were R&D activities supported by foreign sources by 9,9% of total GERD.

Expected trends in R&D funding and the convergence to the target of Europe 2020

Engine of any economy in the world in recent years has become research, development and learning that underlie innovative activity of enterprises. Innovation as a key tool for increasing competitiveness have been so understood in the Lisbon Strategy and also in present strategy Europe 2020. Therefore, all advanced economies try to put more emphasis on application of triple helix model, which focuses on cross-linking and co-operation with universities, business and government sectors. The aim of the model is to transfer research results, development and knowledge into practice. Increasing capacity in research, development and innovation across all sectors of the economy, coupled with more efficient use of inputs, will improve the country's competitiveness and support job creation.

The current trend in GERD as well as in Slovakia and Croatia, we can describe by different functions. Monitoring this trend can serve for modelling the expected development of GERD for following years and also for assess the feasibility of achieving the Europe 2020 target by both countries.

If we consider the continuation of trends in the share of expenditure on R&D funding over the past 12 years and we would predict the development of this indicator in subsequent years (for example to the year 2015), we find several points. Conclusions will vary depending on the chosen trend. For Slovakia, we decided to describe the expected development of the indicator by polynomial functions of 2nd range (1) with the highest coefficient of determination ($R^2 = 0,761$). As an example we also state the expected development of indicator described by linear function, according to which the indicator should record in following years even bigger decline than during much of the reporting period.

Although the share of expenditure on R&D on GDP declined in long-term, in recent years it is possible to expect a slight increase (Fig. 3a). This growth should contribute to positive growth of monitored indicator in following years. Polynomial function describing the growth trend of indicator is:

$$y = 0,004x^2 - 0,066x + 0,762 \quad (1)$$

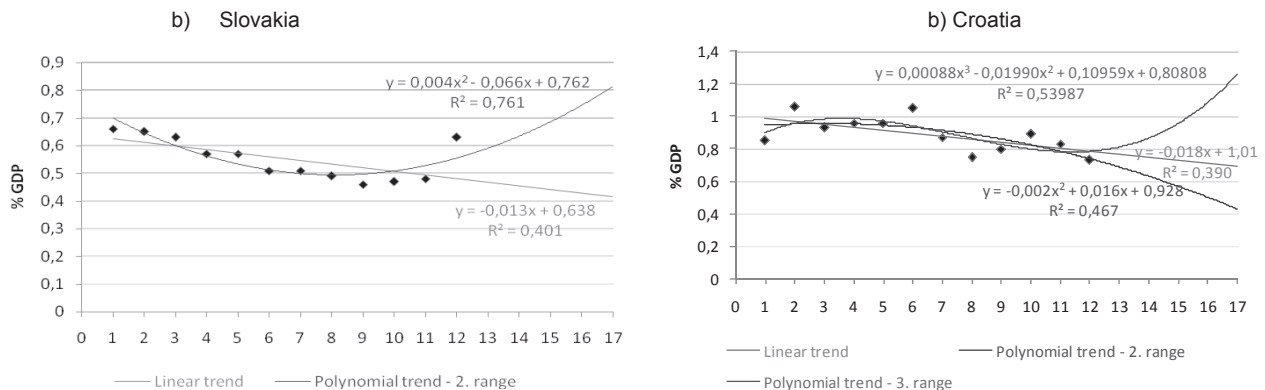


Fig. 3 Simulation of expected development of the expenditure on R&D as a % of GDP
* Years in the graphs ²
Source: Self elaboration

Table 1. Expected development of expenditure on R&D in Slovakia (% of GDP)

Year		2011 (13)	2012 (14)	2013 (15)	2014 (16)	2015 (17)
Expenditure on R&D (% GDP)	Polynomial trend – 2 nd range	0,58	0,62	0,67	0,73	0,80
	Linear trend	0,47	0,46	0,44	0,43	0,42

Source: Self elaboration

2

1999	2000	2001	2002	2003	2004	2005	2006	2007	2008	2009	2010	2011	2012	2013	2014	2015
1	2	3	4	5	6	7	8	9	10	11	12	13	14	15	16	17

According to this model expenditure on R&D in 2015 should reach 0,80% of GDP (Table 1), which can be regarded as a gradual convergence of the indicator to the target value 1% of GDP by 2020. Given past indicator development, we expected this value appears to be real, but it is necessary to take into account the volatility of current period that is significantly negatively affected by the financial and economic crisis, which has grown to a global crisis.

Therefore it is very important to focus on the support not only basic, but mainly applied R&D in Slovakia. The government of the country should take decisive action and increase emphasis on funding this area, also should support the transfer of R&D results into practice. It would be positively reflected in the innovation activity of enterprises, and thus in innovation performance across the country.

After completion of the transport infrastructure, that in recent years has become a priority of the Slovak government and into which flows the greatest amount of funds (for example, from the EU funds³), most of the funds should be directed into research, development and innovation that the country converge to the developed European countries and actually achieve the target of Europe 2020.

Similarly, we can predict the expected development of expenditure on R&D relative to GDP for Croatia. Due to fluctuating development of the monitored indicator, it is very difficult to predict in which direction will indicator developed in following years. Therefore, in this case, we choose a trend with the highest coefficient of determination, i.e. trend described by polynomial function of 3rd range:

$$y = 0,00088 x^3 - 0,019 x^2 + 0,109 x + 0,808 \quad (2)$$

If the expenditure on R&D in relation to the GDP have a growth tendency in following years, their development could be managed by polynomial function of third range (2), according to which the value of indicator in 2015 will reach 1,28% (Table 2). This development would be optimal for Croatia. The worse situation would occur if the trend of expenditure on R&D in relation to GDP managed by polynomial function of second range or by a linear function. In both cases the indicator may decline and then the country would not converge, but diverge from the target of Europe 2020.

Table 2. Expected development of expenditure on R&D in Slovakia (% of GDP)

Year		2011 (13)	2012 (14)	2013 (15)	2014 (16)	2015 (17)
Expenditure on R&D (% GDP)	Polynomial trend – 3th range	0,80	0,88	0,97	1,10	1,28
	Polynomial trend – 2nd range	0,80	0,76	0,72	0,67	0,62
	Linear trend	0,78	0,76	0,74	0,72	0,70

Source: Self elaboration

Conclusion

The level of R&D in the country is affected by the large number of variables, such as the quantity of researchers, the level of technology use, education level of population, amount and level of foreign investment, but also the amount of funds designed to support and develop R&D activities in the country. Expenditure on R&D are essential for transforming the economy to a knowledge-based economy, the use of sophisticated technology, but also to stimulate economic growth. The level of research, development and their financing in Slovakia and Croatia in comparison with most Western European countries is inadequate.

By the modelling of expected development of expenditure on R&D in relation to GDP, we have pointed out possible scenarios for the indicator in the future. About the convergence of indicator to the EU 27 average and therefore to the aim of Europe 2020 we can say, if the trend of future expenditure development on R&D activity will directed in Slovakia by polynomial function of second range (1) and in Croatia by polynomial function of third range (2).

However, also according to the assessments of the European Commission both countries encountered in the area of R&D on several issues, which removal, respectively mitigation will help in convergence of countries to the developed European countries. The most serious problems in the study issue in the Slovakia are according to the European Commission: weak R&D system disables co-operation between academia and industry sectors; underdeveloped system of innovation governance; dual economy and low shares of domestic innovative enterprises limit competitiveness of the country [2].

In order to increase the level of R&D activities in Croatia, will according to the evaluation of the European Commission in following years necessary: to provide access to capital; to increase business R&D expenditures as a means to enhance accessibility of knowledge; to facilitate the protection of intellectual property [1].

Acknowledgment

The article is supported by the project No. 2330263 - Target of Strategy Europe 2020 – Expenditure on Research and Development to 3% of GDP. Reality or Fiction?

References

- [1] EUROPEAN COMMISSION. 2011. INNO-Policy TrendChart – Mini country report / Croatia under Specific Contract for the Integration of INNO Policy Trend Chart with ERAWATCH (2011-2012). 2011a. [cited 15.06.2012]. Available on the Internet: <<http://www.proinno-europe.eu/inno-policy-trendchart/repository/country-specific-trends>>.
- [2] EUROPEAN COMMISSION. 2011. INNO-Policy TrendChart – Mini country report / Slovak Republic under Specific Contract for the Integration of INNO Policy Trend Chart with ERAWATCH (2011-2012). 2011b. [cited 15.06.2012]. Available on the Internet: <<http://www.proinno-europe.eu/inno-policy-trendchart/repository/country-specific-trends>>.
- [3] EUROPEAN COMMISSION. 2010. EURÓPA 2020, Stratégia na zabezpečenie inteligentného, udržateľného a inkluzívneho rastu, Brusel. 2010. 36 s. [cited 29.10.2011]. Available on the Internet: <http://ec.europa.eu/growthandjobs/pdf/complet_sk.pdf>.
- [4] EUROPEAN COMMISSION. 2007. Slovakia, Cohesion Policy 2007 – 2013, 2007. [cited 16.06.2012]. Available on the Internet: <http://ec.europa.eu/regional_policy/atlas2007/fiche/sk_en.pdf>.

³ In the current programming period, i.e. the period 2007 - 2013, are the financial resources from EU funds intended to support the various operational programs of the Slovakia mainly directed to the *Transport* (34,7% of the total budget from EU funds for Slovakia for the period). Then followed the area of *Environment protection and risk prevention* (18,9%), and the area to *Research and technological development, innovation and entrepreneurship* (12,2%) [4].



-
- [5] MINISTERSTVO FINANCIÍ SR. 2005. Stratégia konkurencieschopnosti Slovenska do roku 2010, Národná lisabonská stratégia, 2005. [cited 14.06.2012]. Available on the Internet: <[http://www.rokovania.sk/appl/material.nsf/0/94ECDFE0E61564AC1256FA50033DFB9/\\$FILE/Zdroj.html](http://www.rokovania.sk/appl/material.nsf/0/94ECDFE0E61564AC1256FA50033DFB9/$FILE/Zdroj.html)>
- [6] OECD. 2002. Frascati Manual, Paris, 2002. 423 p. [cited 14.06.2012]. Available on the Internet: <<http://stats.oecd.org/glossary/detail.asp?ID=1162>>
- [7] SPIŠÁKOVÁ, E.: Inovačné aktivity podnikov, možnosti financovania inovácií a ich reálne využitie. Košice: TUKE, 2010. 241 s. ISBN 978-80-553-0587-5
- [8] Zákon č. 172/2005 Z.z. o organizácii štátnej podpory výskumu a vývoja a o doplnení zákona č. 575/2001 Z. z. o organizácii činnosti vlády a organizácii ústrednej štátnej správy v znení neskorších predpisov
- [9] EUROSTAT: <http://epp.eurostat.ec.europa.eu/portal/page/portal/science_technology_innovation/data/database>



International Conference on Innovative Technologies, IN-TECH 2012,
Rijeka, 26. - 28.09.2012



INFLUENCE OF THE CUTTING EDGE RECTIFICATION OF THE CIRCULAR INSERTS FROM CERMET ON THEIR EFFICIENCY

I. Česáková¹, M. Zetek²

^{1,2} University of West Bohemia in Pilsen, Univerzitní 8, 306 14 Pilsen, Czech Republic

Keywords: Cutting edge rectification, surface quality, cermet insert

Abstract. Cutting tool edge modifications are much extended and they are applied on the most of the cutting tools and inserts. The drag finishing and lapping are used for the monolithic cutting tool. The sand blasting, brushing and lapping are used mainly for the cutting inserts. In this area is use in the largest representation the cutting tools from sintered carbide (SC). When the high speed machining (HSC) is used for machining of the hard tool steel workpiece, the SC can not be sufficient. Therefore, very often the cutting ceramic is applicable but their disadvantages are fragility, the thin layers can be limited and higher price. So the article will be deal with possibilities of the HSC machining by the circular cermet inserts. Their main advantages are possibilities of the deposition of the different thin layers and possibilities of their grinding. For maximum reliable and functional are desirable the system substrate-layer considered as a complex. The quality of the deposition influences the inserts surface quality and by the defects on the cutting edge and their microgeometry parameters. It is very important to focus on cutting edge rectification which influences the cutting edge quality and micro geometry. For the experiments the sand blasting and drag finishing for the rectification of the cutting edge were used. The roughness of the inserts surface was different because the different grinding wheels were used like a different rectification methods. So it was very important to monitor the surface process over the all time – after grinding, after modification, after deposition and make correlation between the surface quality and machining. For the surface monitoring the standard roughness and special optical microscope were used. During the tests the cutting inserts quality and tool wear were monitored when machining tool steel EN ISO X210Cr12 with hardness more than 55 HRC.

Introduction

The aims of these experiments was verified whether cermets are be suitable cutting tool material for milling tool steel EN ISO X210Cr12, whether the repetitiveness of their production affect cutting process and what influence have micro-geometry and deposition of thin layers on the cutting process. Cermets were used like round inserts and were grinded from rods. Production of cermet cutting tools is difficult process for reason quality of cutting edge. The next aim was monitored what influence of grinding process with different grinding wheel (different grain size) affect quality of inserts and machining.

This article deal with influences of the cutting edge preparation and deposition of the thin layers on the cermet inserts (CrAlSiN or TiAlSiN) on their quality and cutting tool life.

Experiment

Workpiece

For the experiment the tool steel AISI D3 (EN ISO X210Cr12) with hardness 52HRC was used. These steel is high-chromium ledeburitic alloy steel so it is a hard to machined material. It is caused by the high percentage content of the carbon which causes formation of hard carbide particles and it causes quicker increasing of the tool wear.

Measuring equipment

For the experiments these equipments were used:

- Vertical milling centre MCV 750A – for machining
- MicroCAD Lite GFM and InfiniteFocus G4 Alicona – for measuring of the edge radius. Measuring was made with the cooperation by companies SHM s.r.o. and Hofmeister s.r.o.
- Optical microscope Multichck PC500 - for measuring of the tool wear
- 3-axis dynamometer Kistler – for measuring of cutting forces
- Hommel Etamic T8000 RC, Mahr MarSurf M300 – for measuring of roughness
- TESCAN VEGA TS 5130 – for measuring of the quality of inserts
- The coordinate measuring machine LK G90Cv and screw micrometer – for measuring of insert thickness

Cutting tools

For tests the milling head with two circular cermet inserts TCN 54 with diameter 32 mm was used. The inserts diameter was 12.025 mm. For the grinding the different grinding tools were used which influence inserts roughness. The grinding was made by company HamFinal which is focused for the producing of the cermet cutting tools in the Czech Republic. During the machining only one insert was cut. Tool geometry was negative – axial face angle $\gamma_A = -13^\circ$, radial face angle $\gamma_R = -16^\circ$, geometry of inserts was 0° .

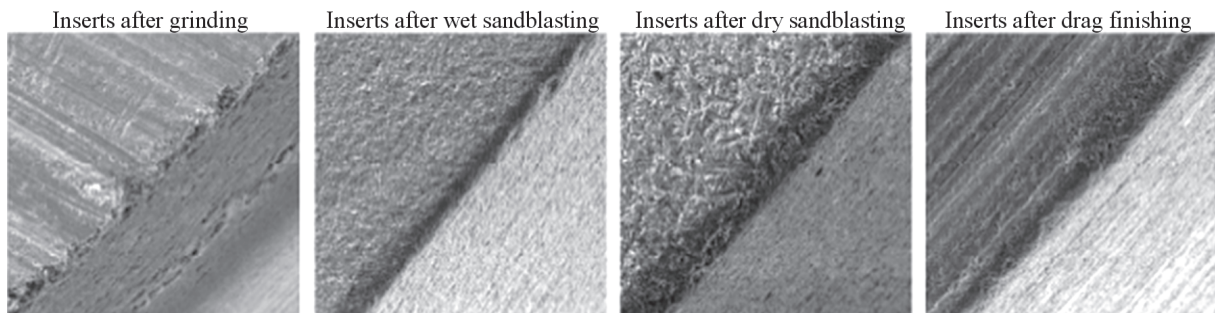
The samples were modified in 4 variations – without modification (after grinding), drag-finishing, dry sandblasting, wet sandblasting and on some of them were deposited thin layers CrAlSiN or TiAlSiN. Different modifications of the edge, which were used, are possible to see in the

Table 1. All of them was made for insert which were grinded with fine grain (roughness of insert – Ra 0,2) and coarse grain (roughness of insert – Ra 0,8).

Table 1. Different modifications of the edge

Number of preparation	Grinding	Drag-finishing	Wet sandblasting	Dry sandblasting	Thin layer CrAlSiN	Thin layer TiAlSiN
1	X	X				
2	X	X			X	
3	X	X				X
4	X		X			
5	X		X		X	
6	X		X			X
7	X			X		
8	X			X	X	
9	X			X		X

In the next picture are showed inserts after different modification of cutting edge. It is possible to see that cutting edge just after grinding wasn't smooth and there were evidenced traces of grinding. Cutting edges after modifications was more quality and the filet was without defections but when was measured radius of cutting edge in most of cases it hadn't the same values. The different was moved about 3-4 μ m. The most different of radius size before and after modification was measured after dry sandblasting. Drag-finishing is typically used for preparation of monolith cutting tools. In these experiments was tested if this preparation is suitable for inserts.



Course of the experiment

When machining with the cermet cutting tools the cutting environment is dry and it eliminate the formation of the heat shock and cracks. Secondly, dry machining causes the decreasing of the costs. Machining was carried out by climb milling in HSC mode.

In the Table 2 there are showed size of radius for all types of preparation. It is interesting that inserts with roughness Ra=0,8 μ m had after modification less value of cutting edge than inserts with roughness Ra=0,2 μ m, when values of cutting edge after grinding were in both cases similar.

Table 2. Size of radius for all types of preparation

Modification of cutting edge	Size of radius [μ m] for inserts Ra=0,2 μ m	Size of radius [μ m] for inserts Ra=0,8 μ m
Grinding	10,2 - 27,7	11,7 - 26,9
Drag-finishing	23,8 - 28,5	22 - 27,4
Wet sandblasting	24,4 - 27,6	18,7 - 21,5
Dry sandblasting	28,3	20,8
Grinding + thin layer CrAlSiN	20,5 - 27,7	16,6 - 18,4
Drag-finishing + thin layer CrAlSiN	26,1 - 26,8	18,6 - 19,2

Wet sandblasting + thin layer CrAlSiN	21,2 - 23,3	18,5 - 21,8
Dry sandblasting + thin layer CrAlSiN	23,8 - 28,4	18,9 - 20
Drag-finishing + thin layer TiAlSiN	20,1 - 24,1	17,9 - 19,7
Wet sandblasting + thin layer TiAlSiN	22,6 - 22,6	20 - 22,2
Dry sandblasting + thin layer TiAlSiN	24,4 - 27,1	21,2 - 22,8

The experiment was divided into three phases:

1st phase of experiment

In this case the inserts from two different production charges were comparing. The tests were focused on influences of these differences on measuring of the tool life. For the tests the inserts without cutting edge modification were used, it's mean the inserts after grinding.

Cutting conditions:

cutting speed - $v_c = 450\text{m/min}$;
feed per tooth - $f_z = 0,05\text{ mm}$;
depth of cut - $a_p = 1\text{ mm}$;
width of cut - $a_e = 1,5\text{ mm}$.

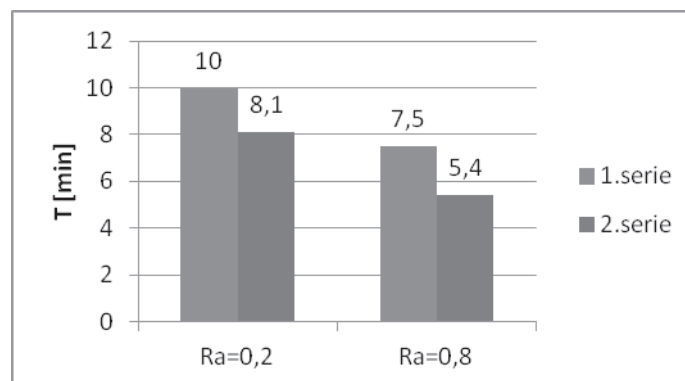


Fig.1 – Influence of two manufacturing series to the tool life ($v_c = 450\text{ m/min}$; $f_z = 0,05\text{ mm}$; $a_p = 1\text{ mm}$; $a_e = 1,5\text{ mm}$)

The figure 1 shows differences in the tool life of cutting tools when inserts from two manufacturing series were used. Main reason is probably different radius of cutting edge. Next influence could have wear of grinding wheel, but this isn't majority part because in both case ($Ra=0,2\mu\text{m}$ and $Ra=0,8\mu\text{m}$) had inserts from second series about 20% less tool life. Samples were monitored by EDM and they weren't seen different between inserts from first and second series. The reason of the lower tool life can be by a different structure of cermets although they have the same commercial mark.

The size of cutting edge radius after grinding:

1st serie - insert with roughness $Ra=0,2\mu\text{m}$ – radius of cutting edge $\rho_r=10,2 - 21,4\ \mu\text{m}$; insert with roughness $Ra=0,8\mu\text{m}$ – radius of cutting edge $\rho_r=11,4 - 19,2\ \mu\text{m}$

2nd serie - insert with roughness $Ra=0,2\mu\text{m}$ – radius of cutting edge $\rho_r=10,2 - 27,7\mu\text{m}$; insert with roughness $Ra=0,8\mu\text{m}$ – radius of cutting edge $\rho_r=11,7 - 26,9\mu\text{m}$

2nd phase of experiment

In this phase was compared influence of all variation inserts on the machining process by cutting conditions:

cutting speed - $v_c = 450\text{m/min}$;
feed per tooth - $f_z = 0,05\text{ mm}$;
depth of cut - $a_p = 1\text{ mm}$;
width of cut - $a_e = 1,5\text{ mm}$.

During the machining was monitored tool life. Tool life for differently prepared inserts shows the figure 2.

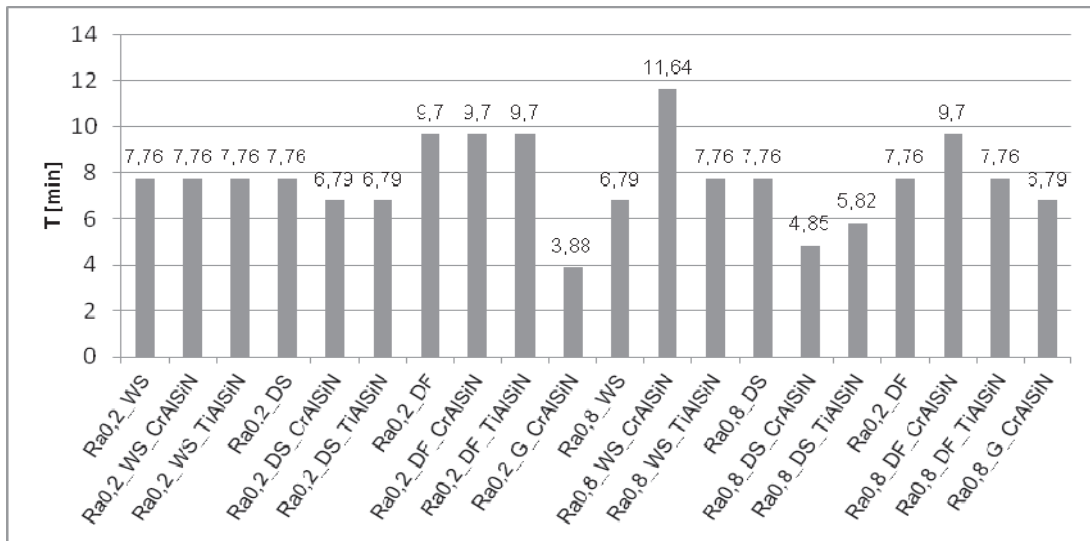


Fig.2 Tool life for differently prepared inserts

3th phase of experiment

Five the best variations from phase 2 were choose. Following picture shows influences radius of cutting edge, roughness of inserts, modification of cutting edge and thin layer on tool life. The graph shows the most useful modifications of cutting edge. Wet sandblasting (WS) with thin layer and drag finishing (DF) in different combinations had the highest tool life.

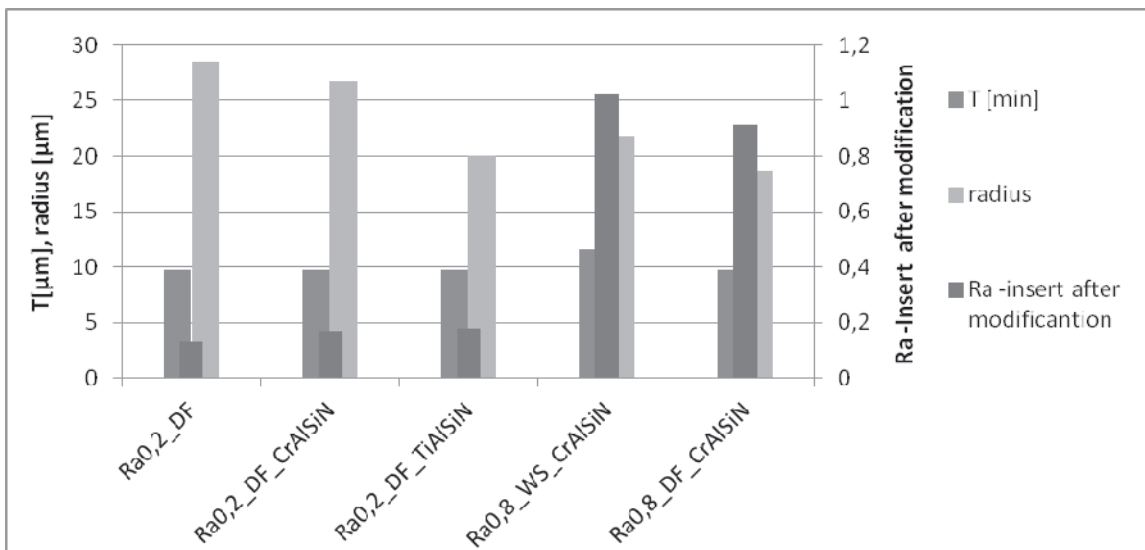


Fig.2 Tool life for differently prepared inserts

Conclusion

The best was preparation by drag finishing in a lot of cases. This modification isn't typically for modification of inserts but these experiments showed that is very useful. In a lot of results are new connections which must be more clarified in the next tests. These tests show that the cermet inserts can be used for the milling of the tool steel and the majority influence on the tool life has preparation method of the cutting edge.

Acknowledgment

This paper is based upon work sponsored by the Student project grant competition no. SGS-2010-083

References

- [1] P. Bůžek Vliv tenkých vrstev a úpravy mikrogeometrie břitu cermetových VBD na frézování zápustkové oceli, diplomová práce, Západočeská univerzita v Plzni 2012, Plzeň 2012.
- [2] J. Sklenička, J. Kutlwašer Modelling and Simulation of Nonhomogenous Yielding, *Journal of Materials Processing Technology*, Volume 186 (2007), Issues 1-3, p. 111-119.

OBSERVATION OF LASER BEAM HARDENED LAYER HARDNESS USING CUTTING FORCE MEASUREMENT

J. Kutlwašer¹, J. Sklenička², E. Samiecová² and M. Zetek²

¹ University of West Bohemia in Pilsen, Faculty of Mechanical Engineering, Department of Machine Design, Univerzitní 8, 306 14, Plzeň, Czech Republic

² University of West Bohemia in Pilsen, Faculty of Mechanical Engineering, Department of Machining Technology, Univerzitní 8, 306 14, Plzeň, Czech Republic

Keywords: laser hardening, measurement, cutting force, piezoelectric dynamometer

Abstract. The paper deals with cutting force measurement that will be used for evaluation of hardness of laser hardened trace. From existing machining technology was chosen drilling. The reasons for this choice are that the feed force during drilling contains the most of workpiece influence and the laser hardened trace size according the best to the drill. Authors want to obtain influence of the hardness on cutting force for regressive analysis of hardness from cutting force at the same cutting conditions. The hardness changes in dependency on parameters of the laser beam and in dependency on the depth from the surface. Laser beam parameters over the traces are known. Method for observing dependency of hardness on depth from surface using cutting forces during drilling is described in the article. This method will be used at the workshop laboratory of Department of Machining Technology for experiments carried on laser hardened layers and should lead to obtaining the quality of laser beam hardening that will be obtained from cutting forces. The preliminary measurement was carried out on workpiece made from tool steel with carbide twist drill coated by thin layer that is designed for machining of materials with difficult machinability. Results from preliminary measurement are discussed in the paper.

Introduction

Nowadays the big accent is putted on methods that don't consume too much time. Consider a need of knowledge of hardness behavior in dependency on a depth from surface of the laser hardened trace, it means to spent pretty much time with cutting off thin layers from the trace and to measure hardness of next layer. This method is very time consumptive and expensive. Authors want to find out if there is a possibility of using cutting force to measure or estimate hardness with adequate accuracy and repeatability. Further authors suppose that this kind of measurement method could be faster and cheaper than often used method described before.

Laser beam hardening

The principle of laser beam hardening is shown in figure 1. Usually it is used for surface hardening of tool steel, especially for shaped dies and moulds. Laser beam hardening has two main advantages. Firstly, it allows to machining all the mould from workpiece that is not hardened. The second advantage of using laser beam hardening is that is not necessary to produce expensive shaped electrodes for induction hardening.

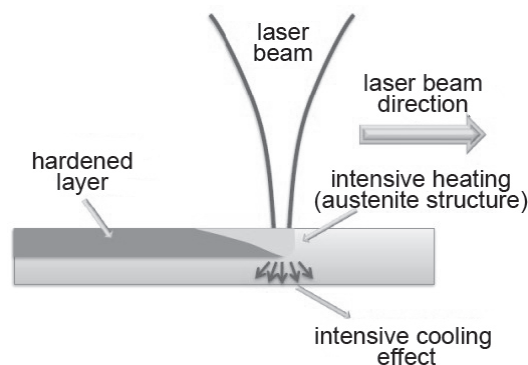


Fig. 1 Principle of laser beam hardening

Method for observing hardness from cutting forces

The method is based on change of cutting force in dependency on change of hardness at the same cutting conditions. First idea for first, we can say preliminary experiments, is to drill 3 mm deep hole, so drill tip is whole in workpiece and cutting edges are all in the cut. The cutting forces are evaluated from this point. Authors decided to use only feed force for evaluation in the preliminary experiment. Spots with known hardness could be obtained from record by time.

Experiment description

Workpiece

Material of workpiece is DIN 90MnCrV8 tool steel. The workpiece dimensions are 170x170x105mm. Eight traces (A to H) were created by laser on the workpiece's surface. Each trace is divided into ten areas (1 to 10). Traces A, B and C were created with constant laser beam power but with variable speed of laser. Other traces were created in opposite way. Figure 2 shows the workpiece gripped in the milling center. Two similar pieces were prepared. One was used for obtaining hardness behavior using "classical" method by cutting up the workpiece in 0.2mm thin layers and measuring hardness in each area of each trace by Wilson & Wolpert WHU-330 portable hardness meter. This was done to the 1.2 mm depth.



Fig. 2 Workpiece

Machine and tool

A monolithic carbide twist drill 5 mm in diameter (figure 3) is chosen for experiments. Three axes MCV 750 A CNC milling machine is machine used for experiments and it is shown in figure 4.



Fig. 3 SH-DRL 8560500 twist drill used for first experiments



Fig. 4 MCV 750A milling machine

Measurement device

The whole measurement chain consists of 9255B KISTLER piezoelectric dynamometer (static) and of 9123C KISTLER rotary piezoelectric dynamometer, connection cables, charge amplifiers, NI DAQ (Data Acquisition) card and a notebook with software prepared in LabVIEW. Amplifiers and notebook with LabVIEW software is shown in picture 5.



Fig. 5 NI Charge amplifiers and measuring notebook

Cutting conditions

Following cutting conditions were chosen for first experiments:
 Cutting speed: $v_c = 12.56 \text{ m}\cdot\text{min}^{-1}$
 Drill revolutions: $n = 800 \text{ rpm}$
 Drilling feed: 0.04 mm per rev.
 Drilling depth: 3 mm

First experiment results

As we can see in figure Fig. 6, the feed force increased remarkably, even if there is not big difference between hardness of first layers (60.7 HRC in area A1 and 61.3 HRC in area C1). That significant difference between feed force values is given by damaged drill tip as the drill reached hardened material that was outside the hardened trace and the workpiece (basic non-hardened) material started to stick on the drill tip and caused a drill tip damage, which is shown in Fig. 7.

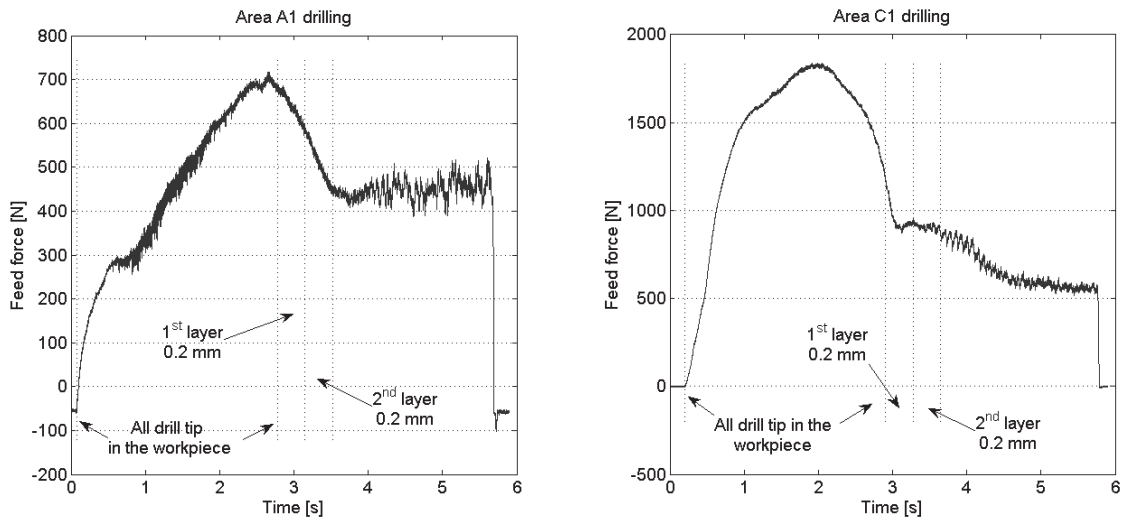


Fig. 6 Comparison of drilling in area A1 and in area C1

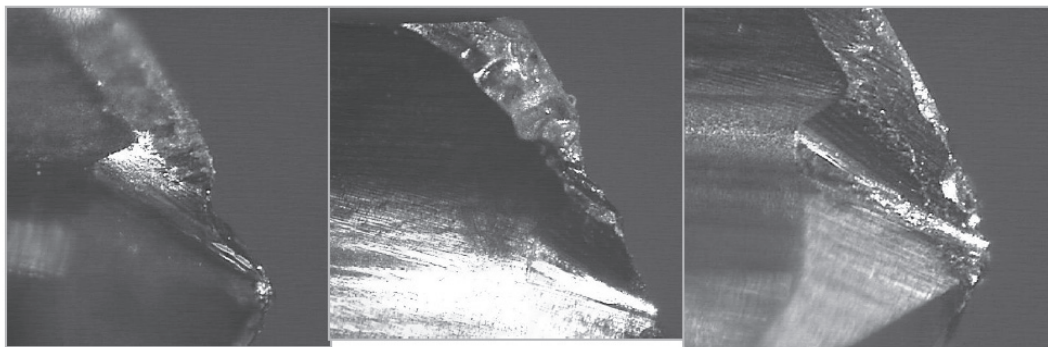


Fig. 7 damaged drill tip

Conclusion

Further experiments will be carried out with drilling deep less than depth of hardening to avoid of drill tip damage caused by sticking of the basic material on it.

As we can see in the following table, there is an increase of feed force, despite decrease of hardness. This is caused by changing width of cut as cutting edge become more and more to the cut. Because of this authors need find out a behavior of feed force in dependency on depth of drill tip from surface at constant cutting conditions and constant hardness. This will be a part of further experiments.

Table 1. Comparison of feed force magnitude and hardness in selected areas

Area	Hardness [HRC]					Magnitude of feed force [N]				
	0.2 mm	0.4 mm	0.6 mm	0.8 mm	1.0 mm	0.2 mm	0.4 mm	0.6 mm	0.8 mm	1.0 mm
A1	60.7	60.0	59.9	58.7	58.7	0	295	350	460	560
D1	62.5	59.3	58.4	48.9	47.4	0	290	390	420	550
G1	59.5	57.5	47.3	28.9	-	0	300	400	570	650

Acknowledgment

This paper is based upon work sponsored by the Student project grant competition no. SGS-2010-083

References

- [1] E. Samiecová, The use of Kistlers dynamometers by the evaluation of the laser-hardened surface layer , diploma thesis, University of West Bohemia in Pilsen, Pilsen, 2012.
- [2] M. Schejbal: *Influence of laser hardening surface layer to cutting forces during milling*, diploma thesis, University of West Bohemia in Pilsen, Pilsen, 2012.

CONDITIONS FOR DEFINING AND A BRIEF OVERVIEW OF THE TECHNICAL SOLUTIONS FOR DESULPHURIZATION FACILITY AND NITROGEN OXIDES EMISSIONS REDUCTION IN POWER PLANT NIKOLA TESLA

B. Nakomčić-Smaragdakis¹, Z. Čepić¹, T. Stajić¹, M. Turk-Sekulić¹, M. Stupavski¹, M. Đogo¹

¹ Faculty of Technical Sciences, Trg Dositeja Obradovića 6, Novi Sad, Serbia

Keywords: power plant, coal fuel, sulphur oxides, nitrogen oxides

Abstract. The combustion process in boilers results in forming flue gasses that are emitted into atmosphere. It is obvious that large energy boilers (fired on coal and liquid fuels) represent the largest percentage of stationary pollution sources. The regulation of gaseous pollutants emissions has the following goals: to provide a better quality of environment in the vicinity of pollution sources on local level and to reduce long distance transboundary transport of gaseous pollutants and thus contribute to the preservation of the environment on global scale. Minimization the emissions from thermal power plants is a modern approach in preserving the environment, and also represent a significant additional cost in electricity generation process. According to the results of existing analysis, it is estimated that the current share of thermal power plants in total sulphur dioxide emissions from stationary sources in Serbia is around 50%, while the share of nitric oxide emissions is around 70%. The power plants Nikola Tesla A and B represents approximately 65% of the total capacity of all power plants fired on coal. An amount of emitted acid oxides in flue gas in the coal-fired power plants depend primarily on fuel characteristics (for sulphur oxides generation), and the combustion method (for nitrogen oxides generation). The conditions and criteria for defining technical solutions for SO₂ and NO_x emission reduction in power plants Nikola Tesla A and B will be discussed in this paper. The paper also provides a brief presentation of technical solutions for desulphurization facility and minimization of nitrogen oxides emissions.

Introduction

Reducing pollutants emissions from thermal power plants is a modern way to preserve the environment, but also represent a significant additional cost in electricity production. According to the results of existing analysis, it is estimated that the actual share of thermal power plants in total sulphur dioxide emissions from stationary sources in Serbia is around 50%, while the nitric oxides have the contribution of around 70%. Thermal power plants Nikola Tesla A and B represents approximately 65% of total capacity of coal fired thermal power plants, which makes a dominant part.[1]

The flue gasses are created during fossil fuel combustion which occurs in large energy boilers (power greater than 300 MWth) and emitted into the atmosphere through flue gas. Flue gas consists of carbon dioxide, nitrogen, oxygen, water vapour, carbon monoxide, nitrogen and sulphur oxides, volatile organic matters and ash particles. The last five substances are considered to be conventional environmental pollutants. In last few years carbon dioxide may also be found in this group because of its indirect contribution to the climate changes which in other segments influence the living world on Earth.

It is clear that power boilers (fired by coal and liquid fuels) make the largest percentage of stationary pollution sources this type. In an era of rapid energy sector development in developed countries, in the 60s of last century, national strategies for pollution levels regulation are based on constructing tall stacks from which flue gases are emitted and the appropriate location selection, through that was possible to decrease the level of pollution in the environment on local level (near-field scale effects).

However, some time after the implementation of this practice (early 70s), the changes in vegetation occurred due to the acid rain in areas where local pollution sources were not present (Scandinavian lakes and their surroundings), and it became clear that the range of gaseous pollutants from stacks is larger scale, and that they subject to long distance pollutant transport (1000 km or more). This way, gaseous pollutants present in flue gas became the cause of environmental degradation on regional and continental level (regional and continental scale effects).[2]

A review of existing sulphur and nitrogen oxides emissions from blocks in power plants Nikola Tesla A and B

The size of acid oxide from coal fired power plants emitted in flue gas depends primarily of the fuel characteristics (sulphur oxides) and its combustion method (nitrogen oxides). Unlike liquid fuels, where it can be assumed that all sulphur is converted to oxides (SO₂ and SO₃) during the combustion, the conversion of coal is different. In fact, the total sulphur contained in coal makes more components that have differently behaviour during combustion process: the largest component of sulphur is pyritic sulphur (found in metal compounds, mostly with iron), and organic sulphur, which represents about around 1/3 of total sulphur, and is located in molecules of organic compounds in fuel, and so called sulphate-sulphur contained in fuel in sulphates (up to 0.1%). During the combustion process, both pyritic and organic sulphur are converted into oxides and make combustible portion of the total sulphur, while sulphate portion do not oxidize but transforms into ash. Depending on the other coal constituents, mainly calcium content and Ca/S ratio, the higher or lower share of formed sulphur oxide will be bound in ashes (which reacts with CaO and transforms into sulphate).

From this aspect, Kolubara coal that was used in power plant in previous period had the following characteristics:

- the total sulphur content from 0,5 – 1%,
- ash content from 12 – 24%,
- CaO content in ash from 3 –7%,

- content of sulphates in the ash from 5 – 8 %,
- a heat capacity from 6500 – 9300 kJ/kg,

Based on these values, it can be concluded that the coal comes with substantial variations in characteristics. A significant percentage of sulphur bind in ashes could not be expected, but a greater portion will be emitted in flue gas.

In addition to mentioned features, the following characteristics of Kolubara lignite are crucial for defining combustor characteristics and combustion parameters: high content of volatiles, low heating value, favourable melting properties of a mineral part of coal and relatively easy flammability.

Unlike sulphur oxides, nitrogen oxides formation is primarily determined by the method of fuel combustion. Since lignite is the fuel with low nitrogen content (about 1%), which partially transform into N₂ and partially oxidize, the formation of NO_x is mainly determined by the combustor conditions. [2]

An overview of possible technical solutions for NO_x emissions reduction

The emission reduction of nitrogen oxides formed during coal combustion can be achieved through:

- Primary measures that include modification of the combustor and combustion parameters in order to reduce possibilities for NO_x development,
- Secondary methods that include an introduction of DENOX plant where NO_x reduction is achieved by its reaction with the active substance – usually with ammonia,
- Application of new combustion technologies - combustion in circulating fluidized bed, gasification etc.

Since the combustion of coal takes place already at relatively low temperatures (lower than for other types of coal and liquid and gaseous fuel), an additional reduction in nitrogen oxides formation can be achieved by reducing the amount of oxygen in the combustor by various methods, such as:

- Fuel combustion outside of stoichiometric conditions (reduction ratio is 25-30%);
- Two stage fuel combustion (reduction ratio is 40-50%);
- Excess air reduction in the combustor (reduction ratio is 10-30%);
- Introduction of cold flue gas recirculation through burner (reduction ratio is 55-60%);
- Use of fine grinding;
- Combination of above mention solutions (reduction ratio is 85-90%).

It is important to emphasize the primary consequences of introducing measures to reduce NO_x formation that due to changed combustion conditions CO content in flue gas increase, as well as an amount of unburned fuel, which results in increased combustion on the grate. This means that the grid should be reconstructed for additional burning at the bottom of the boiler.[3]

NO_x emissions reduction in Thermal Power Plants Nikola Tesla

The production of nitrogen oxides depends on the type of fuel and combustor construction. On the other hand, it can be said that these two factors are highly interdependent, since the type of combustor must be adjusted to fuel characteristics. Thus, the following rules apply for combustion of Kolubara lignite:

- Due to the temperature characteristics of ash, slag drainage in solid form is applied;
- According to the introduction and distribution of heating surfaces P-type boilers are present (blocks A1 and A2) and tower-type boilers (blocks A3-A6 and B1 and B2). Table 1 shows the basic characteristics of boilers in thermal power plant Nikola Tesla.
- Fuel preparation is done by grinding the coal to get coal dust granulation up to 100µm, fluidised bed combustion, with continuous supply of fuel particles in the air stream in the combustor, with continuous drainage of the flue gasses;
- Arrangement of burner for smaller boilers is on the front wall of the combustor, while those with more power (≥ 300 MW) have tangential arrangement (such as those placed in corners of the combustor);
- Jet burners or burners with direct blowing have been applied to the type of burners: the air mixture for these burners is introduced from the mills through multiple parallel channels, and the secondary air is blown in as the upper, lower and core. This way a good mixing can be achieved, which is aided by the fact that the blowing air speed exceeds the speed of the air mixture (more than twice).[2]

Table 1 Basic characteristics of boilers in thermal power plants Nikola Tesla A and B [2]

boiler-block	A1	A2	A3	A4	A5	A6	B1	B2
Manufacturer and boiler type	SES Slovakia	SES Slovakia	SES Slovakia	SES Slovakia	SES Slovakia	Rafaco Poland	Rafaco Poland	Rafaco Poland
Nominal steam production, [t/h]	650	650	920	920	920	920	1880	1880
Boiler shape	P-type	P-type	tower	tower	tower	tower	tower	tower
Water circulation	natural	natural	forced	forced	forced	forced	forced	forced
Method for slag removal	slag is collected and taken by endless belts							
Combustor type	tangential							
Combustor temperature	max. 1100 °C							

Control of NO_x formation in the combustors with given characteristics

Solid fuel combustion process consists of several phases: first is the separation of volatiles and their oxidation, followed by combustion of the rest of the fuel (coke), which requires a certain amount of air. The impact on the amount of formed NO_x is made by reducing the amount of air in the primary combustor zone, thereby reducing the temperature in combustor, which also affects the amount of NO_x reduction occurred.

Supplying the air for an oxidation of the volatiles is carried out by introducing so called "Over-fire-air" in the secondary combustors zone. During this process there is a risk of unburned fuel particles release from the combustion zone, where coal particle size plays an important role and in a manner to get a smaller percentage of unburned fuel (unburned carbon) the finer grinding has to be applied.

Primary measures for NO_x emissions reduction are applied to the boiler plant, i.e. on combustion process. Thus, in above-mentioned types of boilers and arrangement of burners, reduction in NO_x formation is achieved by influencing the combustion of following parameters: temperature in the combustor and residence time of fuel in the zones of temperature peaks. Commercially applied technologies for achieving the effect on these parameters are presented in Table 2. [3]

Table 2 Technologies for NO_x emission reduction applied to boilers with solid slag drainage and tangential and frontal arrangement of burners [3]

Parameter	Available technology	Percentage of emission reduction
1. The reduction of temperature peak	Exhaust gas recirculation Over-fire-air Excess air reduction Low NO _x burners	50-70 %
2. The reduction of residence time in the high temperature zone	Multistage air supply Multistage fuel supply	50-70 %

SO₂ emissions reduction in Thermal Power Plant Nikola Tesla

When it comes to existing thermal power plants, parameters that define the criteria for technical solutions selection, as well as conditions that must be met when choosing any of the solutions can be classified into two main groups:

- Spatial integration and storage of equipment for FGD (flue gas desulphurization),
- The impact of technology on basic FGD technological process.

During the construction of thermal power plants Nikola Tesla A and B there is no space provided for the FGD plant, even the analysis of the existing equipment arrangement in that location can be concluded that condensed schedule of equipment is present in these objects. Any introduction of new equipment in such technological unit may affect the functionality of the existing system and new system for FGD. This also refers to the possibility of maintaining and manipulating the existing equipment and devices, possibilities of disassembling and assembling major parts of the equipment during the overhaul and during the control process while in operation. Taking all these factors into consideration, when choosing limestone-plaster process as a reference, the following must be taken into account:

- Considering an evident need for space rationalization required for the FGD plant, the possibility to implement a joint system for several blocks, in whole or in part should be analyzed. This means that several blocks could share one absorber, or, if this is not convenient, at least some of the auxiliary systems, such as systems for sorbent preparation, suspension deposition, control and management or electricity supply.
- Implemented procedure is built into the area between the electro filter and stack, meaning that practically there is no direct effect on the main components of thermal power plant. However, according to the physical-chemical process of flue gas purification in absorber, it is necessary to carry out previous dust removal: the suppliers of these systems give the guarantee of absorber characteristics if the content of particles in the inlet flue gas max 80 mg/m³. This means that before the introduction of FGD systems, reconstruction of electro filter installation had to be performed on all blocks of power plant A, while for the power plant B can be considered that the efficiency of existing electro filter is satisfactory. In addition, taking into account the total plant capacity for FGD at all locations, the need to significantly expand of the power system is likely to expect. [4,5]

Conclusion

If the conventional flue gas desulphurization would be applied on individual blocks of Power Plant Nikola Tesla A and B, the reference plant would have the following characteristics:

- The procedure of the wet limestone-plaster process, with limestone as the absorbent and plaster as final by-product;
- Absorbers are joint for the blocks of 210MW, and individual for the other blocks in power plant A and B (of 300 and 620 MW);
- Absorber type is DCFS (double-contact flow scrubber);
- Reheating flue gas, after purification, is performed in a regenerative gas-gas heater, so that outlet gas temperature is min. 90°C;
- Water supply is anticipated from wells, or alternatively from Sava River, depending on the total amount of water required;
- Supply of the limestone is performed from a warehouse within the power plant;
- Disposal of thickening plaster suspension is carried out along with the ashes, or is disposed in landfill if its further processing and use to produce plaster is foreseen.

Which method for nitrogen oxides emissions reduction will be implemented in a particular boiler, depends on the projected scope and opportunities for reconstruction of combustor and boiler plant as a whole. The introduction of primary measures for NO_x emissions reduction is typically performed within the overall revitalization of the boiler plant. Thereby the following elements must be taken into account:

- Construction of combustors and predicted interventions,
- Methods for supplying and the distributing air and coal dust,
- Reconstruction existing and introduction of new, special burners that help to reduce NO_x formation (low NO_x burners),
- Required residence time of coal particles in zone of increased O₂ content. [6]

In general, basic steps for regulation of nitrogen oxides emissions in power plant can be defined:

- The replacement of existing burners with new special type of burners is done,
- The conditions for the combustion are provided in several phases: (i) in the first stage combustion is performed in so-called sub-stoichiometric conditions where the burning occurs in mixture of coal dust and air for $\lambda = 0.95$, (ii) in the second phase so-called secondary air is introduced up to $\lambda \approx 1$, where the return of cold flue gases to the combustion chamber can be



made, (iii) in the final stage so-called over-fire-air is introduced - around 15% of air is introduced into the zone above the burners, so that excess air coefficient λ is around 1.15 at the end of the combustors. [1]

Environmental protection is mission and vision of Electric Power Industry of Serbia. After many years in which the available money was invested only in the maintenance of production capacities, environmental protection became priority in the business policy of Electric Power Industry of Serbia. [7]

Acknowledgment

The development of this paper work was supported by Ministry of Education and Science, Republic of Serbia (project number III46009).

References

- [1] Study: Basis for determining the strategy to reduce emissions of SO₂ and NO_x in the Federal Republic of Yugoslavia in the period 1995-2020, the Energoprojekt - ENTEL, April 1996.
- [2] Study: Solving the environmental problems caused by the work of Thermal Power Plants Nikola Tesla A and B, Energoprojekt – ENTEL, 2003.
- [3] EPA: Technical Bulletin – Nitrogen Oxides (NO_x), Why and How They Are Controlled – Office of Air Quality Planning and Standards, EPA 456/F-99-006R, November 1999.
- [4] Mitsubishi Heavy Industries EUROPE, Ltd.: Budgetary Proposal for FGD Nikola Tesla Power Station, Jun 2002.
- [5] Study: System for obtaining, use and disposal of gypsum from the facility for desulphurization of flue gas in CHP Kolubara B, Energoprojekt – ENTEL, 2001.
- [6] World Bank– Low NO_x burners, <http://www.deq.state.or.us/eq/haze/comments/50-USFS.pdf>
- [7] Official site of Electric Power Industry of Serbia, 13.07.2012. <http://www.eps.rs/Eng/Article.aspx?lista=Sitemap&id=10>

MOBILE ROBOT NAVIGATION WITH ANDROID DEVICE USING OPENCV

P. Pászto¹, M. Klůčik¹, L. Chovanec¹, M. Smolák¹ and P. Hubinský¹

¹ Institute of Control and Information Technology, Faculty of Electrical Engineering and Information Technology, Slovak University of Technology, Ilkovičova 3, 812 19 Bratislava, Slovakia

Keywords: mobile robot navigation, OpenCv library, optimization, genetic algorithms, image processing

Abstract. Mobile phones with Android operating system are nowadays equipped with many kinds of sensors which are used to entertain the user. These mobile devices are also equipped with powerful processors. The idea of this work is to use the mobile device's computing power and sensors for an iRobot Create platform navigation. The aim of this article is to discuss the possibility of the usage of one of the most demanding applications in robotics - digital image processing on Android mobile device. An application which uses the mobile device's camera for obstacle detection was designed. The free OpenCV library was used for real time image processing. In order to lower the load of the processor for the image processing, the parameters of algorithms were optimized with the usage of genetic algorithms. The iRobot Create controlled with the mobile phone is able to detect and to avoid obstacles that are recognized with the mobile phone's visual system. The process of obstacles detection is based on the reflected circles recognition from the obstacle which is lighted with four LED diodes. The article is a demonstration that today's mobile phones with Android operating system are usable in robotics and can be used for mobile robots navigation, localization and even communication and can deal with such processor demanding algorithms as image processing algorithms are.

Introduction

Today's mobile devices with Android platforms have a large number of potentially usable sensors in robotics. One of the most powerful sensors is the camera which we want to use to navigate an iRobot Create mobile robot in an unknown environment with obstacles. Image processing algorithms are utilizing CPUs and if the performance of the CPU is not high enough, an optimization of image processing algorithms parameters is needed.

In this article we will describe the process of iRobot Create autonomous navigation with HTC Desire mobile phone. The robot is controlled with the Android device over Bluetooth. Obstacle detection is done by illuminating the obstacles with couple of LED diodes and detecting the reflected circles with the device's visual system. The process of OpenCV installation onto the device and the circle detection algorithm and its optimization will also be described.

Controlling iRobot Create over Bluetooth

iRobot Create is controlled by sending some combination of bytes over Bluetooth to the robot **Chyba! Nenalezen zdroj odkazů..** In the manual **Chyba! Nenalezen zdroj odkazů.** there are described all the possible commands to control the mobile robot. In this section we will deal with communication between the HTC device and the mobile robot over Bluetooth. First of all the devices are needed to be paired.

Following the Android Developers web page **Chyba! Nenalezen zdroj odkazů.** we need to do these steps to establish a communication with the mobile robot: setting up Bluetooth, finding available devices in the local area, connecting devices and transferring data between devices.

Setting up Bluetooth

This step consists of getting the BluetoothAdapter which represents the device's own Bluetooth adapter and enabling the device's Bluetooth adapter. We use a TextView named txtview to list the messages to the user.

Finding available devices

In this case we use the discovery service to find all available devices and then we connect to the mobile robot knowing its name or MAC address. First we need to start the Bluetooth devices discovering process. After it the application must register a BroadcastReceiver for the ACTION_FOUND Intent in order to receive information about each discovered device. If the device's name is the same as the mobile robot's name, we can start a new thread to connect the mobile phone and the robot.

Connecting to iRobot Create

In this new thread we also follow the Android Developers web page and use the connecting as a client connection type. We also need to cancel the discovery process before connecting to the mobile robot. If the connection was successful we can run a new thread to control the mobile robot.

Controlling the iRobot Create

In this thread we need to follow the iRobot Create's manual **Chyba! Nenalezen zdroj odkazů.** to find out, how to set up the mobile robot for working (for example choosing its operating mode, etc.) and also the Android Developers web page to know how to send commands for the mobile robot using an OutputStream. We show an example how to make the mobile robot moving forward. First we need to get the input and the output stream. Then we can make the mobile robot moving forward with a speed of 100 mm/s sending data through the output stream.

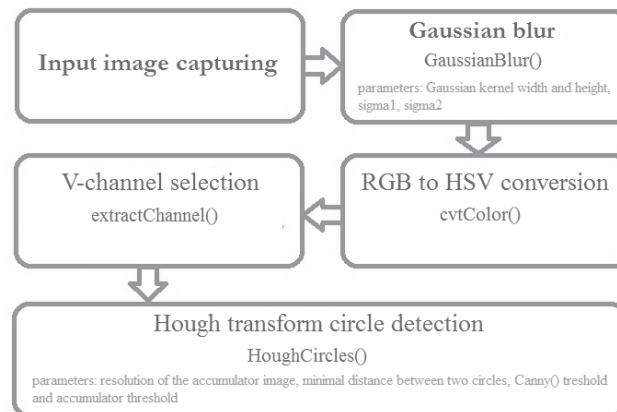


Fig. 3. The algorithm of circle detection

Example of this algorithm recognizing one circle is shown below:

```

capture.retrieve(mImage, Highgui.CV_CAP_ANDROID_COLOR_FRAME_BGR);
Imgproc.GaussianBlur(mImage, mImage, new Size(5,5), 0, 0);
Imgproc.cvtColor(mImage, mImage, Imgproc.COLOR_BGR2HSV);
Core.extractChannel(mImage, mHImage, 2);
Imgproc.HoughCircles(mHImage, mCircles, Imgproc.CV_HOUGH_GRADIENT, 1, 70, 100, 20, 5, 100);
Imgproc.cvtColor(mHImage, mImage, Imgproc.COLOR_GRAY2BGR, 4);
double foundCircles[];
if(mCircles.size().width!=0 && mCircles.size().height!=0){
    foundCircles = mCircles.get(0, 0);
    Core.circle(mImage, new Point(Math.round(foundCircles[0]),Math.round(foundCircles[1])),
        (int)Math.round(foundCircles[2]), new Scalar(255,0,0));
}
  
```

Genetic algorithms as method for visual system optimization

Genetic algorithms were used for optimization of the image processing (or optimization of the reflected circles recognition). Genetic algorithms are universal browsing and optimization method, so it can be used with many advantages for an optimization of image processing **Chyba! Nenalezen zdroj odkazů..** Results that are presented in this paper are simple experiments with usage of genetic algorithms for optimization assigned to circles recognition in obtained image.

Parameters shown on Fig. 3. were optimized with genetic algorithms. These parameters have an important role in circles detection in obtained picture. By solving more complex tasks with increasing numbers of parameters is much more time needed to solve these tasks. By solving tasks with increasing number of variables, can the dimension of searched space increase exponential **Chyba! Nenalezen zdroj odkazů..**

In the optimization process is a crucial found circle. Searched circles can be characterized by the following parameters: radius, position of the center of the circle in the analyzed image. From these parameters can be determined a criterion for searching the circle in a particular image. In the optimization process there were used several variants of images and to each image the correct parameters have been assigned. The following criterion has been determined to investigate the accuracy of the identified circle (this criterion is applied only to one image):

$$f(x, y, r) = (x - x_w)^2 + (y - y_w)^2 + (r - r_w)^2 \quad (1)$$

where:

- x – is x position of identified circle centre
- y – is y position of identified circle centre
- r – is the radius of identified circle
- x_w – is the centre of correct identified circle
- y_w – is the centre of correct identified circle
- r_w – is the radius of correct identified circle/ellipse

In the optimization process the standard configuration of evolution process was used (order of mutation and crossover operations, the elite selection). Configuration of evolution is shown Fig. 4. The Fig. 5. is showing the course of evolution during the development of criterion for each generation. It can be seen that in ten evolution courses the criteria development reliable approaches zero.

The optimized parameters were used in the algorithm for reflected circles detection. The created mobile robot is shown on Fig. 6.

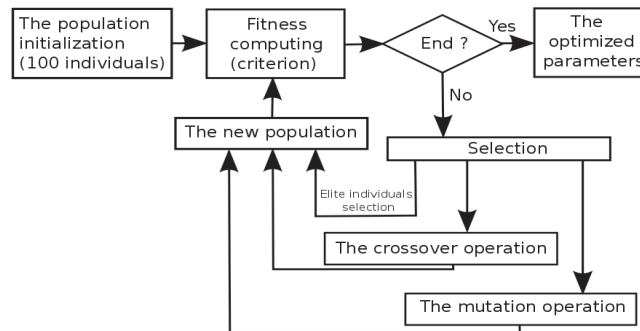


Fig. 4. The used method of genetic algorithms for optimization of image processing

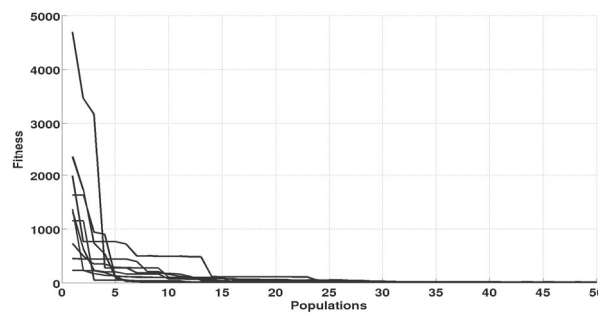


Fig. 5. Evolution of optimization criterion

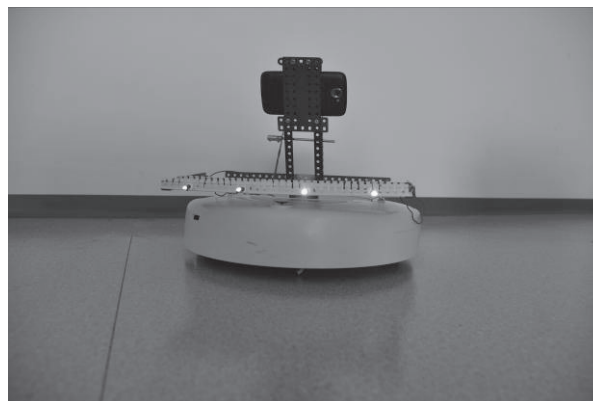


Fig. 6. The mobile robot iRobot Create navigated with Android device

Conclusion

The created mobile robot navigated with Android device HTC Desire is able to move in unknown environment with obstacles, to detect and avoid them and to create a map of the obstacles with their position in the environment. The robot is fully autonomous and can work in real-time. We can see that the Android devices can be used in robotics (and even with visual system algorithms running on them).

The experiments with this mobile robot are published on youtube.com:

<http://www.youtube.com/watch?v=9smNaAXDnJU&feature=plcp>

<http://www.youtube.com/watch?v=qox60a5RRc&feature=plcp>

These experiments are demonstrating the mobile robot's ability of obstacle detection and avoidance, autonomy and real-time working. More information about the mobile robot can be found on www.petesoftware.tk.

Acknowledgment

This work has been supported by VEGA 1/0690/09.

References

- [1] http://www.irobot.com/filelibrary/pdfs/hrd/create/Create%20Manual_Final.pdf
- [2] <http://developer.android.com/guide/topics/wireless/bluetooth.html>
- [3] <http://developer.android.com/guide/topics/wireless/bluetooth.html>
- [4] http://opencv.itseez.com/doc/tutorials/introduction/android_binary_package/android_binary_package.html
- [5] SEKAJ, I.: Evolučné výpočty a ich využitie v praxi. Iris, Bratislava, 2005., ISBN 80-89018-87-4.

EVALUATION AND THE USE OF GPS RECEIVERS FOR SMALL MOBILE ROBOTS IN LOCAL COORDINATE SYSTEM

J. Hanzel¹, M. Klůčik¹, F. Duchoň¹ and J. Rodina¹

¹ Institute of Control and Information Technology, Faculty of Electrical Engineering and Information Technology, Slovak University of Technology, Ilkovičova 3, 812 19 Bratislava, Slovakia

Keywords: autonomous mobile robot navigation, GNSS, GPS receiver, WGS 84, Leica GPS1200,

Abstract. This article deals with a problem of the autonomous robot navigation in the unstructured outdoor environment by using of the GPS data. In order to navigate the robot, the global position data is transformed to the local map in the form of two-dimensional Cartesian coordinate system by proposed procedure. The transformation is based on the mathematical model of the Earth (WGS 84 reference ellipsoid). The aim is to experimentally evaluate a set of GPS receivers applicable as position sensors for small outdoor mobile robots. The evaluation is based on series of measurements executed in different times and places. The measured data is processed by given procedure and acquired positions transformed to the local coordinate system. Consequently the accuracy of the measured positions is statistically evaluated. The evaluation of used GPS receivers is done by comparison with data acquired by precise geodetic GPS system Leica 1200 which is used as reference GPS system. Obtained results of data analysis are used for determination of appropriate solutions for mobile robot sensory system.

Introduction

Autonomous mobile robot is an object capable of motion, observation of its environment and decision making. Control system of the robot has to be able to acquire and to maintain a model of the working environment, to localize the robot in the environment, to plan a target and means of its achievement. Robots internal representation of the working environment from its perspective is considered as the map of the environment. Navigation of a mobile robot in an unknown and uncertain environment requires knowledge of the robot's position. Robot has to be able to determine its own position in the map, what means to solve the localization problem. There are many localization methods in a mobile robotics. Generally they can be divided in absolute localization methods and relative localization methods. The relative methods are referenced to objects in vicinity of the robot and mostly express displacement between two robot positions. Absolute methods use global reference frame, which defines global coordinate system. The approach, which makes use of Global Navigation Satellite System systems – GNSS is an example of absolute method suitable for mobile robot localization in outdoor environment.

Global Navigation Satellite Systems

GNSSs are satellite systems for measuring position and time on Earth. In principle, they are not affected by meteorological conditions. The position is measured using triangulation and trilateration methods and it is given by intersection point of spherical surfaces which radius is equal the distance between a satellite and a measured position. From a geometrical point of view, three coordinates (latitude, longitude and sea level) can be calculated using three satellites. Moreover, the fourth satellite is required to measure time. The higher number of satellites is used for calculation of the position, the more precise the estimate of position should be.

GNSS systems that are currently available are Navstar GPS (GPS) and Glonass. The most commonly used system is GPS and it comprises from a cosmic, control and a user segments which includes GPS receivers. These GPS receivers can be used as an absolute localization system for the mobile robot. However, calculating the global position using GPS is somewhat problematic and the position accuracy is affected by many sources of errors. The most significant are: *satellite geometry* (the position of the satellites in relation to each other and the receiver), *atmospheric effects* (delays of signals passing through individual layers of atmosphere), *multipath effect* (signals bounce off solid objects), *relativistic effects* and other errors.

Due to negative impact of these errors of position measurement, multiple hardware and software solutions have been proposed. One of them is to use more precise measuring unit, such as: INS-GPS (Inertial Navigation System, positioning precision with up to 1m accuracy) [3], DGPS (Differential GPS, positioning precision up to 5m, even 10cm in case of the best implementations) [8,9], WAAS/EGNOS (Wide Area Augmentation System/Euro Geostationary Navigation Overlay Service, positioning precision up to 3m) and RTK GPS (Real Time Kinematics, positioning precision up to several centimeters) [2,6,7]. Another way to improve the estimate of the position by GPS receiver is to use some mathematical approaches. To improve precision and accuracy of GPS positioning many researchers use filters, such as Kalman filter [1,5,6,10].

World Geodetic System

The GPS data is referred to unified global coordinate system named World Geodetic System 1984 (WGS 84). The WGS 84 geodetic system comprises of a standard coordinate frame for the Earth, a standard spheroidal reference surface (reference ellipsoid), and a gravitational equipotential surface (the geoid) that defines the nominal sea level. It has been in use since 1984 and the last revision took place in 2004. The WGS 84 coordinate system is a right-handed, Earth-fixed orthogonal coordinate system and it is graphically depicted in the Fig. 1.

The coordinate origin of the WGS 84 coordinate system is the Earth's centre of mass. In WGS 84, the meridian of zero longitude is an International Reference Meridian (IRM), which is defined by the International Earth Rotation and Reference Systems Service (IERS). The Z-Axis is defined by the direction of the IERS Reference Pole (IRP). The X-Axis is defined by the intersection of the IERS Reference Meridian (IRM) and the plane passing through the origin and normal to the Z-axis. The Y-Axis completes a right-handed, Earth-Centered Earth-Fixed (ECEF) orthogonal coordinate system, measured in the equator plane, 90° east of the X-axis [4].

Global geodetic applications require clear definition of three different surfaces. The first of these is the Earth's topographic surface which includes the landmass topography as well as the ocean bottom topography. In addition to the topographic surface, a definition for a geometric or mathematical reference surface, the ellipsoid, and an equipotential surface called the geoid is required.

The Earth is not a sphere, but an ellipsoid, slightly flattened at the poles and slightly bulging at the equator, which in mathematics is also called an oblate spheroid. The ellipsoid is used as a surface of reference for the mathematical reduction of geodetic and cartographic data. The World Geodetic System (WGS) represents an ellipsoid of which placement, orientation, and dimensions best fit the Earth's equipotential surface coinciding with the geoid. The system was developed from a worldwide distribution of terrestrial gravity measurements and geodetic satellite observations.

The WGS 84 Reference Ellipsoid is defined by the four defining parameters: semi-major axis ($a = 6378137.0$ m), flattening defined as its reciprocal value ($1/f = 298.257223563$), angular velocity of the Earth ($\omega = 7292115.0 \times 10^{-11}$ rad) and Earth's gravitational constant ($GM = 3986004.418 \times 10^8 \text{ m}^3 / \text{s}^2$) [4]. Mathematically, a reference ellipsoid is an oblate spheroid with two different axes: an equatorial radius (the semi-major axis a), and a polar radius (the semi-minor axis b). The numerical value of the the semi-minor axis for the WGS 84 reference ellipsoid is $b = 6356752.3142$ m [4].

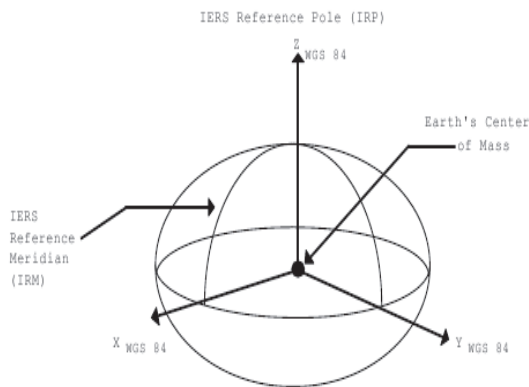


Fig. 1 The WGS 84 coordinate system definition [4]

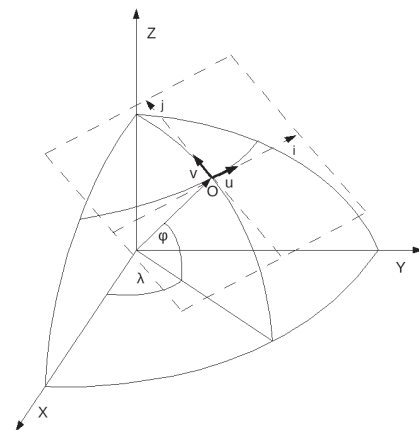


Fig. 2 The WGS 84 coordinate system and the local coordinate system

The position data transformation

For the purpose of the mobile robot navigation in the environment, the control system utilizes a local navigational map. It is simplified two-dimensional model of the environment representation. Accordingly it is necessary to transform the GPS navigational data to the local navigational map. The goal of the transformation process is to calculate position data from the WGS 84 coordinate system to the local coordinate system (LCS) utilized by control system of the mobile robot. The relation between the global WGS coordinate system and local coordinate system is depicted in the Fig. 2.

The local coordinate system has the form of two dimensional Cartesian coordinate system in the Euclidean plane. This plain is defined as the tangent plane to the surface of the reference ellipsoid at the chosen point. This point also serves as the origin of the local coordinate system (Fig. 2). The first step in the transformation of the GPS coordinate, it is necessary to select appropriately the origin O of the local coordinate system according to the given data set. Next it is required to compute the three dimensional geocentric rectangular coordinates (x, y, z) of the origin O of the local system in regard to WGS as defined at Fig. 2. The equations for the co-ordinates calculation are given as follows [4]:

$$x = (N + h) \cos \varphi \cos \lambda, \quad y = (N + h) \cos \varphi \sin \lambda, \quad z = ((b^2 / a^2) N + h) \sin \varphi, \quad (1)$$

where a is semi-major axis and b is the semi-minor axis of the reference ellipsoid, the h denotes the geodetic height (height relative to the ellipsoid) and N denotes the radius of curvature in the prime vertical [4].

After definition of the local coordinate system origin, the second step is to define the equation of the LCS plane in rectangular geocentric coordinates. As the LCS plane is also the tangent plane of the reference ellipsoid, the normal vector of the plane is perpendicular to surface of the ellipsoid in the origin of the local coordinate system O. So the normal vector of the plane can be computed as the gradient of the ellipsoid at the point O. Finally the equation of the LCS plane is given as follows:

$$O_x x / a^2 + O_y y / a^2 + O_z z / b^2 = 1. \quad (2)$$

The third step is to define the right-handed orthonormal Cartesian coordinate system in the LCS plane. So it is necessary in the LCS plane to define two reciprocally perpendicular vectors u, v of the length of 1 (m) at the LCS origin O (Fig. 2). First there are two points defined at the ellipsoid surface with the positions exactly at east and north directions in regard of origin O. By the application of the equations 1 the WGS Cartesian coordinates of these points are calculated. Next the projection of these points to the LCS plane is computed. The vectors defined by projected points and the origin O determinate the directions of the positive half-axes of the coordinate system in the LCS plane. The normalization of these vectors is required in purpose to obtain the orthonormal basis vectors u and v of the LCS in regard to the WGS.

The vectors u and v defines the transition from one coordinate system to another and the local coordinate system is completely defined. Now it is possible to transform measured GPS position coordinates to the local coordinate system. Transformation is performed by the similar procedure as in the case of the calculation of the vectors u and v for the GPS data.

Used GPS receivers

The essential parameters of GPS receivers intended for a small scale outdoor mobile robot are in addition to precision of the measured position dimensions, weight and energy consumption. In the class of small receivers, the energy consumption is sufficiently low, so the weigh and size determined selection of sensors. For the evaluation of appropriate GPS receiver for small outdoor mobile robot, the following GPS receivers were used: Globalsat Technology Corporation GPS Engine Board ET 312 [11], GlobalTop Tech Inc. FGMMOPA6B [12] and Garmin International Inc. GPS 18-5Hz [13]. As the reference GPS system the Leica Geosystems GPS1200 was used [14].

Reference GPS receiver Leica GPS1200

As a reference frame high precision GPS receiver a Leica GX1230+GNSS /ATX1230+GNSS was used. This receiver is able to receive GPS L1, L2 and L5 frequencies, Glonass L1 and L2 frequencies and Galileo E1, E5a, E5b, E5ab and E6 frequencies. Moreover, this receiver is able to perform both code and phase measurements with DGPS or RTK corrections. Because of these facts Leica GX1230+ is able to achieve 0.2 mm positioning precision at phase measurements on L1 and L2 frequencies and 2 cm positioning precision at code measurements on L1 and L2 frequencies.

This receiver has been designed primarily for geodetic measurements. However, its parameters make it suitable for many applications including absolute outdoor mobile robot localization. On the other hand this application is limited with its high prize, weight and energy consumption.

Tested GPS receivers

The GPS receivers ET 312 and FGMMOPA6B with their small size parameters are intended for variable applications where the very small size and weight of the sensor is required. The compact sensor ET 312 is a 20 channel receiver based on SiRF Star III chip working on GPS frequency L1 with active or passive antenna. Its size is 27.9mm x 20mm x 2.9mm and it has 3.3V DC main power input with consumption of 80 mA in continuous mode. It has maximal position accuracy 5m with WAAS enabled and in 2D-RMS mode 10m [11].

The FGMMOPA6B is a patch on top 66 channel GPS receiver based on MediaTek MT3329 chip working on L1 frequency. Its dimensions are 16mm x 16mm x 6mm with dimensions of patch antenna of 15mm x 15mm x 4mm and it has weight of 6g. Its main power input is 3.3 V with consumption of 37 mA. Its 2D-RMS position accuracy is 3m and its maximal accuracy with DGPS is 2.5m [12].

The Garmin GPS 18-5Hz receiver is somewhat bigger receiver of weight 161.6 g of circular shape with 61mm diameter and 19.5mm height. It is a 12 channel receiver with supply input from range of 4.0V to 5.5V and consumption of 65mA at 5.0V. Standard position accuracy is less than 15m and with WAAS support it is less than 3m [13]

All three receivers have serial data output in the form of NMEA 0183 protocol sentences based on WGS84 datum. The ET312 and FGMMOPA6B receivers together with 1EUR coin are shown in Fig. 3 and receiver GPS 18-5Hz is shown in Fig. 4.



Fig. 3 The ET312 (1) and the FGMMOPA6B (2) receivers



Fig. 4 The GPS 18-5Hz receiver

Experimental results

The evaluation of position accuracy of the GPS receivers was based on real data gathered in the series of measurements performed on several places in the outdoor environment. These measurement specifications were chosen with aim to maximally approximate the real conditions during outdoor robot navigation. The experiments were performed at three different places with various satellite visibility conditions. The first experimental position was situated under the wall of the building and thus the sky was greatly shadowed. So the GPS sensors were able to receive the signal only from satellites located in one half of sphere. The second experimental position was situated more far from surround buildings and so it allows receive the signal from much greater space. The third experimental place was located in the middle of large open place, where the maximum number of the satellites can be received. At these places were measured overall five data sets with all four GPS receivers. The experiments number 1 and 3 were performed at first measuring position, the experiments number 2 and 4 at second position and the experiment number 5 was performed at third position. The number of visible GPS satellites was recorded during each experiment in order to check their influence on the accuracy of receivers. Each data set contained unequal but sufficient number of measurements to evaluate the precision of the receiver. The data from reference Leica GPS1200 system were used to define the origin of the local coordinate system. The data from evaluated small scale receivers was then transformed to defined local system and statistically evaluated. The parameters of interest were the mean value of measured position data transformed to local coordinate system and mean Euclidean distance of measured data from origin of local system. The processed experimental data are summarized in Table 1.

Table 1. Experimental results of evaluation of the GPS receivers

Experiment	Number of visible GPS satellites	ET 312		FGMMOPA6B		GPS 18-5Hz	
		(x, y) [m]	d [m]	(x, y) [m]	d [m]	(x, y) [m]	d [m]
1	8	1.99, -0.36	2.02	-0.35, 2.19	2.22	0.44, -0.78	0.90
2	5	-1.44, -0.12	1.45	59.80, 18.25	62.53	-48.68, 12.30	50.21
3	3	-416.94, -189.78	458.11	14.23, 11.03	18.01	58.56, -5.00	58.77
4	8	-4.38, -0.59	4.42	-7.45, -1.52	7.60	15.92, -2.94	16.19
5	7	0.01, -5.04	5.04	19.12, 0.08	19.12	0.04, -1.36	1.36

Conclusion

The aim of the performed experiments was to determine an appropriate GPS receiver for a small scale outdoor mobile robot. The chosen GPS systems had a very small size and weight and the task was to identify their real position accuracy in conditions close to outdoor navigation of mobile robots. However, the determination of the most precise sensor on the basis of acquired data was almost impossible. The values in the Table 1 showed the strong dependency of position correctness on the number of visible satellites. Thus the reliability of the robot localization procedures based on the use of GNSS data might severely fluctuate during the navigation in the environment. The greatest position error had the ET 312 receiver in the experiment with only 3 visible satellites, which is the minimal operable number. On the other hand this receiver had the best results in all remaining experiments. However, there was an interesting result, where most of the measured data was considerably asymmetrically shifted from the real position only along one axis of the local coordinate system. Along the second axis they were located more symmetrically. This property of sensed position data considerably affects the localization of the robot and explanation of this causality needs more experimentation. Even though, the performed experiments revealed interesting properties of the used GPS receivers and opened new ideas for further work.

Acknowledgment

The work has been supported by VEGA grant 1/0690/09. This support is very gratefully acknowledged.

References

- [1] S. Yamaguchi and T. Tanaka, GPS Standard Positioning using Kalman Filter, Proceedings of the *SICE-ICASE International Joint Conference 2006*, Oct. 18-21, 2006 in Bexco, Busan, Korea, pp. 1351-1354.
- [2] Ch. B. Low and D. Wang, GPS-Based Path Following Control for a Car-Like Wheeled Mobile Robot With Skidding and Slipping, *IEEE Transactions on control systems technology*, Vol. 16, No. 2, March 2008, pp. 340-347.
- [3] S. R. un Nabi Jafri, S. M. un Nabi Jafri and S. Z. Shakeel, Intelligent Navigation of Unmanned Land Vehicle by using GPS&One ABS Sensor, Proceedings of the *4th International Conference on Autonomous Robots and Agents*, Feb. 10-12, 2009, Wellington, New Zealand, pp. 273-277.
- [4] NIMA - National Imagery and Mapping Agency, DEPARTMENT OF DEFENSE WORLD GEODETIC SYSTEM 1984, Its Definition and Relationships with Local Geodetic Systems, NIMA TR8350.2, Third Edition, Amendment 2, 2004, http://earth-info.nga.mil/GandG/publications/tr8350.2/tr8350_2.html.
- [5] S. Kwon, K. Yang, S. Park and Y. Ryuh, Robust Mobile Robot Localization with Combined Kalman Filter-Perturbation Estimator, *IEEE/RSJ International Conference on Intelligent Robots and Systems*, Aug. 2005, pp. 4003-4008.
- [6] R. Lenain, B. Thuilot, Ch. Cariou and P. Martinet, Adaptive and predictive non linear control for sliding vehicle guidance (Application to trajectory tracking of farm vehicles relying on a single RTK GPS), Proceedings of *2004 IEEE/RSJ International Conference on Intelligent Robots and Systems*, Sep. 28 - Oct. 2, 2004, Sendai, Japan, pp. 455-460.
- [7] B. Wu, T. Lee, H. Chang, J. Jiang, Ch. Lien, T. Liao and J. Perng, GPS Navigation Based Autonomous Driving System Design for Intelligent Vehicles, Proceedings of the *ISIC/IEEE International Conference on Systems, Man and Cybernetics*, Oct. 7-10, 2007, Montreal, Quebec, pp. 3294-3299.
- [8] K. Ohno, T. Tsubouchi, B. Shigematsu and S. Yuta, Differential GPS and odometry-based outdoor navigation of a mobile robot, *Advanced Robotics*, Vol. 18, No. 6, 2004, pp. 611-635.
- [9] K. Ohno, T. Tsubouchi, B. Shigematsu, S. Maeyama and S. Yuta, Outdoor Navigation of a Mobile Robot between Buildings based on DGPS and Odometry Data Fusion, Proceedings of the *2003 IEEE International Conference on Robotics&Automation*, Sept. 14-19, 2003, Taipei, Taiwan, pp. 1978-1984.
- [10] A. Georgiev and P. K. Allen, Localization Methods for a Mobile Robot in Urban Environments, Open Access at: <http://www.cs.columbia.edu/~allen/PAPERS/tro.final.pdf>
- [11] GlobalSat ET-312 GPS Engine Board, http://www.globalsat.com.tw/products-page.php?menu=2&gs_en_product_id=4&gs_en_product_cnt_id=37
- [12] GlobalTop FGPMOPA6B, <http://www.gtop-tech.com/jsf/moduleproduct.jsf?moid=5a50acc3cd4f20749b345fe86e442ed78a6d204d&suid=d2aafd64c93952bb33c7ee066e322e597947063d&puid=3fd4de25b0dd3bf98c210cb99566759047d54dec>
- [13] Garmin GPS 18-5Hz, www.garmin.com/manuals/425_TechnicalSpecification.pdf
- [14] Leica Geosystems GPS1200, http://www.leica-geosystems.com/common/shared/downloads/inc/downloader.asp%3Fid%3D2620&sa=U&ei=7pE0ULbNEsrJsga_zYDgCA&ved=0CDQQFjAM&usq=AFQjCNH17jH-0lp5y3QKt7LM8_tR_1ue3A



CREATING A WEB-BASED MODEL FOR FINANCIAL PLANNING AND FORECASTING

Aksheta Mehta¹ and Pushkala Muralidharan²

¹ Department of Computer Science, BITS Pilani, Dubai Campus, Dubai International Academic City, Dubai 345055, United Arab Emirates.

² Department of Computer Science, BITS Pilani, Dubai Campus, Dubai International Academic City, Dubai 345055, United Arab Emirates.

Keywords: Financial Planning, Financial Forecasting, Budgeting, Web-based Model.

Abstract. Ever changing economic conditions are driving companies and businesses to become increasingly cautious about the future, creating the need to focus on improving flexibility to dynamically account for the change. This is in turn shifting focus away from budget accuracy, putting companies at risk of falling short of shareholder expectations. Hence giving rise to a need for efficient planning, budgeting, and forecasting for improved agility, accuracy, and corporate performance. This project seeks to comprehend the concepts of financial planning, budgeting and financial forecasting. Furthermore, his project seeks to present a simple web-based model to get rid of the errors and tedium of manual planning and forecasting. Through this model it would be viable for anyone to begin a business or make necessary changes to an already existing business with the least amount of effort.

Introduction

Constantly changing monetary conditions are causing companies and businesses to become progressively cautious about the future, generating the need to emphasize on improving the flexibility to dynamically account for the change. This is in turn shifting focus away from budget exactitude, placing companies at jeopardy of falling short of shareholder expectations. Hence giving rise to a need for efficient planning, budgeting, and forecasting for improved agility, accuracy, and corporate performance.

A *financial plan* is a sequence of steps that are carried out, or objectives that are accomplished, that relate to an individual's or a business's financial undertakings. It evaluates the economics behind the strategy and operations. It is the process of attaining goals and objectives by means of the proper management of finances. The output from a financial plan takes the form of a budget.

Budgeting is the key to financial management. A *budget* is an organizational plan stated in terms of money. It affords a distinct comprehension of the past financial performance to help predict the future financial performance.

Extending former trends and fine-tuning for what is expected is a common approach to preparing a forecast. *Forecasting* is the process of making statements and recommendations about events whose actual outcomes (typically) have not yet been observed. It is a key constituent in determining future procedures, glitches, and opportunities. For the forecast to be as accurate as possible, all the known data must be up to date. In short, a financial forecast is the best guess of the financial outcome of a business, over a period of time.

Many a times the term forecasting is used interchangeably with planning but it must be noted that the two are distinctly different – Forecasting is predicting what the future *will* look like, whereas planning is predicting what the future *should* look like.

Through this project I aim to:

1. To understand the various parameters of financial planning and forecasting and how they are affected by the current market trends and demands.
2. To create a prototype of a web-based model for financial planning and forecasting.

Financial Planning

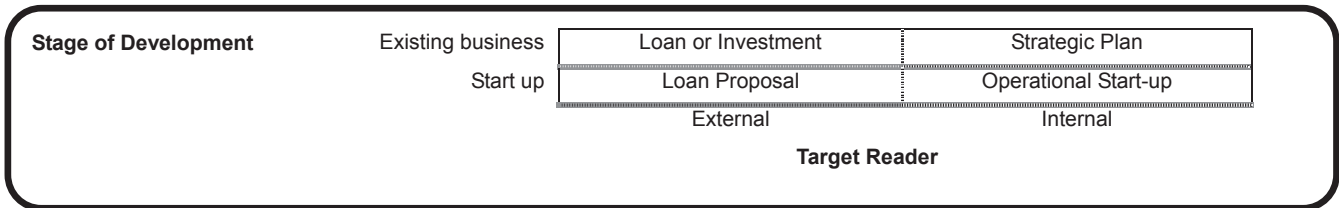
Financial planning is a continuous process of directing and allocating financial resources to meet strategic goals and objectives. It is the task of certifying how a business will manage to attain its strategic targets and destinations. Typically, an organization makes a Financial Plan as soon as the vision and targets have been set. A Financial Plan portrays all of the actions, assets, supplies and materials that are requested to actualize these goals, as well as the timelines included.

Financial planning can moreover be characterized as the course of action by which a business records and conveys its strategic goals in financial terms. A financial planning exercise ordinarily holds point by point plans and budgets, as well as analysis abilities to indicate how the targets are to be grasped.

Business Plan

In business, a financial plan can refer to the three primary financial statements (namely, balance sheet, income statement, and cash flow statement) created within a business plan. It can be interpreted in two ways: by stage of development, and by target reader.

Table 1 Ways of Looking at a business plan



Strategic Planning

Strategic planning is a formal procedure for building targets and goals over the long run. It includes improving a “mission comment” that captures why the organization exists and strategizes how the conglomeration could thrive in the future. Strategic objectives and corresponding goals are developed on the basis of a very exhaustive assessment of the organization and the external environment. Finally, strategic plans are implemented by developing an Operating or Action Plan. This includes a complete set of financial plans or budgets.

Financial Plans (Budgets) ⇒ Operating Plan ⇒ Strategic Plan

Sales Forecast

In order to develop budgets, one must begin with a forecast of what energizes most of the financial activity; like sales. Hence, the first forecast to prepare is the ‘Sales Forecast’. Sales forecasts are generally based on the analysis of old data. An precise sale forecast is critical to the firm’s profitability

Budgeting

The yield from financial planning takes the structure of budgets. The most broadly utilized type of budgets is Pro Forma or Budgeted Financial Statemets. The group for Budgeted Financial Statement is Detail Budgets. Detail Budgets combine sales forecasts, processing forecasts, and different evaluates in backing of the Financial Plan. Collectively, all of these budgets are known as the Master Budget.

Kinds of Budgets

- A survival budget - This is the minimum required in order for the organization or project to survive and do useful work.
- A guaranteed budget - This is based on the income guaranteed at the time the budget is planned.
- An optimal budget. - This covers what you would like to do if you can raise additional money. Once extra money comes in or is promised, it becomes part of your working budget.

Techniques for Budget Calculation

The two main techniques for budgeting are incremental budgeting and zero based budgeting.

- Incremental budgets are budgets in which the figures are based on those of the actual expenditure for the previous year, with a percentage added for an inflationary increase for the New Year.
- In zero based budgets, past figures are not used as the starting point. The budgeting process starts from “scratch” with the proposed activities for the year. Though this technique is extremely tedious it is detailed and accurate.

Budgeted Financial Statements

Based on the detail budgets prepared, the budgets can be finalized in the form of a Budgeted Income Statement. Once a Budgeted Income Statement has been drawn up, a Budgeted Balance Sheet can be chalked up from it. The Budgeted Balance Sheet will provide us with an estimate of how much external financing is required to support our estimated sales.

Cash Budgets

The Cash Budget is a good instance of short-term financial planning. It gauges the inflows and outflows of future cash. They are regularly combined with the Budgeted Balance Sheet. Previous forecasts can be used to aid in the preparation of a Cash Budget.

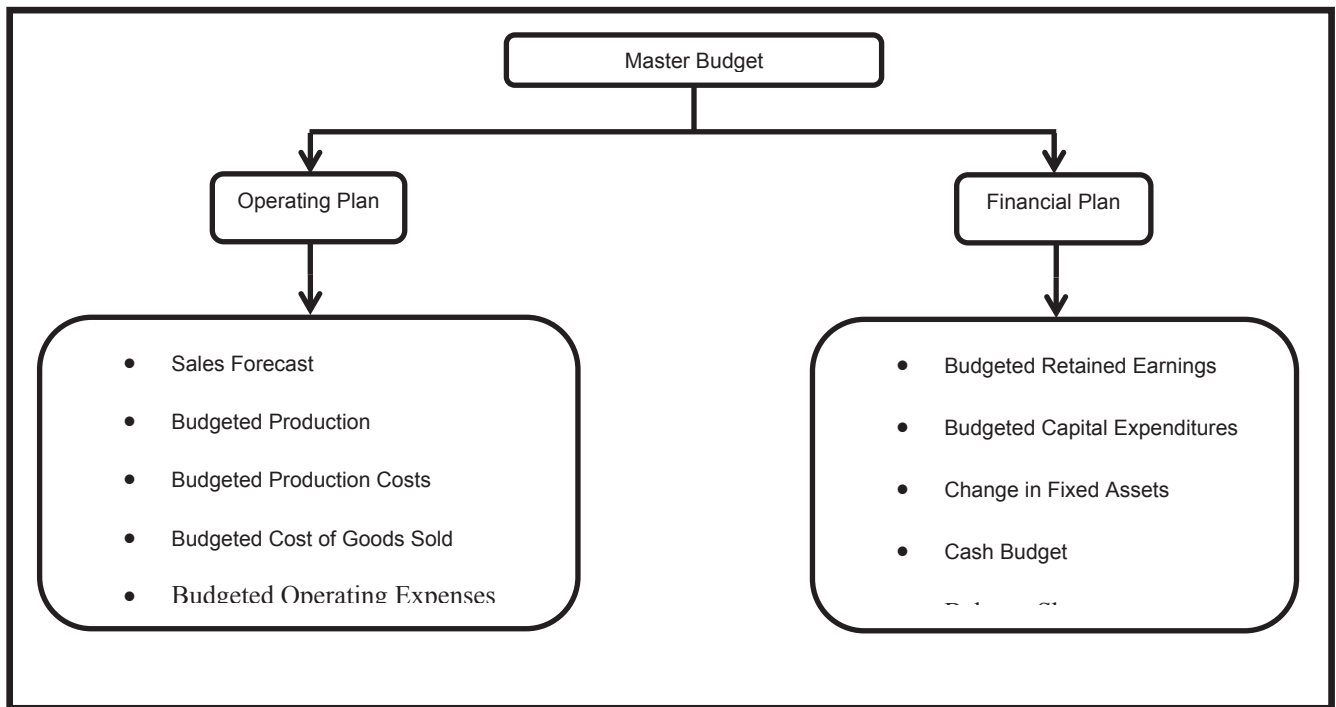


Fig. 1 Budgeting in a Nutshell

Financial Forecasting

Financial Forecasting is a process by which businesses conform to future anticipations dependent upon familiar true appearance bringing about the handling of a redesigned forecast record. This can (but makes a point not to regularly) incorporate acclimations to the budget. Forecasting, re-forecasting, or "rolling-forecasting" can happen numerous times in the midst of a budget period, and can span time from one financial period to the following.

Financial Forecasting is a nexus segment in confirming future operations, situations, and chances. It is a gauge of several key future financial results for a business – imagined income and liabilities. It is the handle of assessing future business exhibition (sales, costs, earnings). Financial forecasts are used to develop the projections of profit and loss statements, balance sheets and, most critically, the cash flow forecast.

Fundamentals of Financial Forecasting

- Forecasting is reliant on past connections and existing authentic data. An alteration in these relationships causes forecasting to become progressively imprecise.
- On the grounds that forecasting might be erroneous owing to lack of certainty, one should regard advancing numerous forecasts under contrasting situations. Each scenario can be assigned a probability and the expected forecast can be arrived at.
- Prolonged planning periods result in erroneous forecasts; in fact, they are directly proportional to each other. To expand reliability in forecasting, a more limited planning period should be recognized. The planning period is subject to how frequently existing plans should be assessed. This relies on stability in deals, business peril, financial conditions, and so forth.
- Forecasting of large inter-related items is more accurate than forecasting a specific itemized amount. When a large group of items are forecast together, errors within the group tend to cancel out. For example, an overall economic forecast will be more accurate than an industry specific forecast.⁷

Techniques of Financial Forecasting

Quantitative or qualitative methods, or a combination of both, can be used to develop forecasts.

- Qualitative method uses the judgment and opinions of knowledgeable people to predict outcomes. This is a more intuitive technique and is typically used when precise data is limited or hard to find. It depends on the following types of information:
 - Judgmental* – Based on "good sense" or a decision made through discerning and evaluating.
 - Consensus* – Based on collective opinion or general accord.
 - Expert* – Based on the advice of an expert.
- Quantitative method applies a set of mathematical rules to a series of past data to predict outcomes. This technique is preferred when sufficient hard data is available. It includes any of the following types of information:
 - Trend Analysis* – Compares historical information to forecast percentage changes.
 - Multiple Regression Analysis* – Uses chosen factors to determine the forecasted percentage change.
 - Time-Series Analysis* – Uses the average percentage change during specific time periods.

Test Scenario

By inputting the documented values to a few of the fields the user can draw up the complete budget using this web-based model. The user is provided with two tables. One which displays the budget without accounting for the *Additional Financing Needed (AFN)* and the

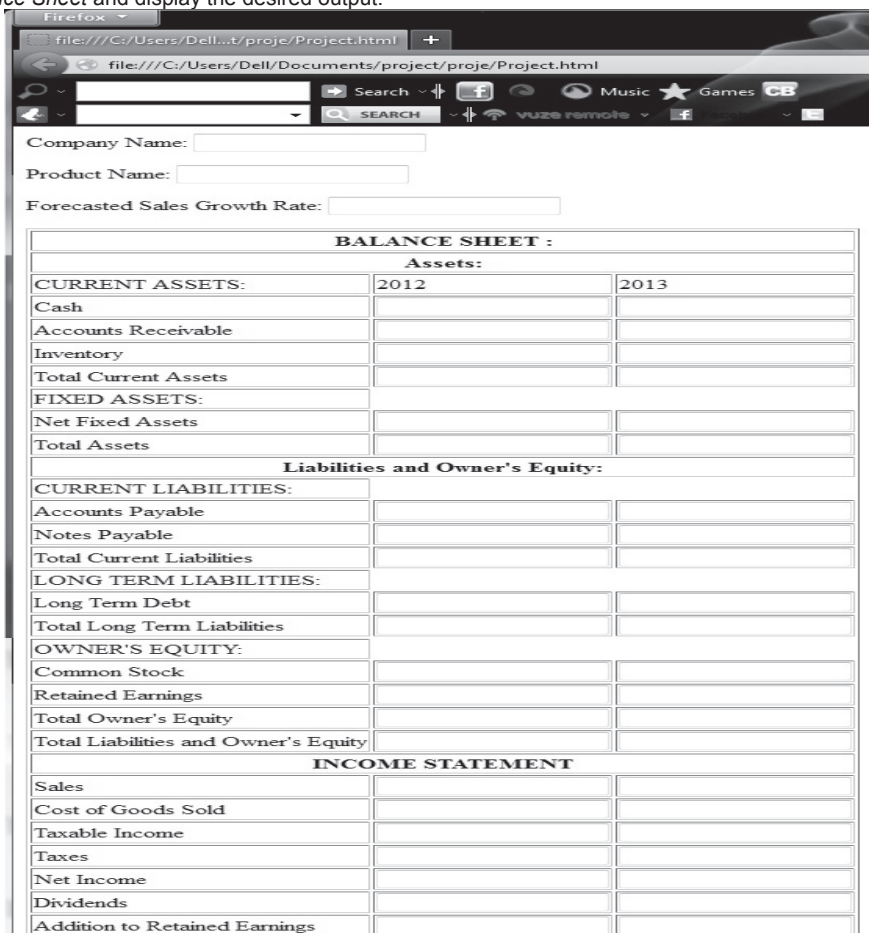
other wherein the AFN is accounted for. The model is even capable of maintaining a database of the company records as required by the user. Based on the records saved it can further predict the *Forecasted Sales Growth* which in helps with the further calculations. However, if no prior records exist for a user then they must enter an approximated amount for the *Forecasted Sales Growth* themselves.

As the user enters the documented values to a few of the required fields the first table begins calculations and displays the tentative or rough Budgeted Balance Sheet, portraying the current year's budget along with a rough forecast for the following year. The output provided by this table is dubbed rough because the calculations that underwent in the creation of this table do not account for the AFN. Based on the outputs and results of the first table the model goes on to calculate the AFN. The AFN calculated is then used by the model to perform further calculations and provide a second table. The second table is the final Budgeted Balanced Sheet, portraying the current year's budget along with the forecast for the following year. The output provided by this table is final as it accounts for any and all discrepancies that appear in the first table, by taking into consideration the AFN.

The fields that must be carefully documented and inputted by the user include:

- Company Name (Only if no record exists for the user)
- Product Name (Only if no record exists for the user)
- Forecasted Sales Growth (Only if no record exists for the user)
- Cash (for the current year)
- Accounts Receivable and Accounts Payable (both for the current year)
- Inventory (for the current year)
- Net Fixed Assets (for the current year)
- Notes Payable (for the current year)
- Long Term Debt (for the current year)
- Common Stock (for the current year)
- Retained Earnings (for the current year)
- Sales (for the current year)
- Cost of Goods Sold (for the current year)
- Taxes (for the current year)
- Dividends (for the current year)

Based on the values entered in the fields listed above the model will calculate the *Rough Budgeted Balance Sheet*, the *AFN* and the *Final Budgeted Balance Sheet* and display the desired output.



Company Name:

Product Name:

Forecasted Sales Growth Rate:

BALANCE SHEET :		
Assets:		
CURRENT ASSETS:	2012	2013
Cash		
Accounts Receivable		
Inventory		
Total Current Assets		
FIXED ASSETS:		
Net Fixed Assets		
Total Assets		
Liabilities and Owner's Equity:		
CURRENT LIABILITIES:		
Accounts Payable		
Notes Payable		
Total Current Liabilities		
LONG TERM LIABILITIES:		
Long Term Debt		
Total Long Term Liabilities		
OWNER'S EQUITY:		
Common Stock		
Retained Earnings		
Total Owner's Equity		
Total Liabilities and Owner's Equity		
INCOME STATEMENT		
Sales		
Cost of Goods Sold		
Taxable Income		
Taxes		
Net Income		
Dividends		
Addition to Retained Earnings		

Fig. 2 Empty First Table



Conclusion

A sound financial plan is the vehicle which plainly states strategic business targets in financial terms. An overall-ready budget shapes the foundation for choice-making throughout the financial year. Nonetheless it is the forecast which permits the business to modify future anticipations on the basis of recent actual performance. No one discipline leads to success, but rather a consolidation of each of the three should be integrated to provide the visibility essential to align strategy with company performance.

References

- [1] Cheng-Few Lee, *Advances in Financial Planning and Forecasting*, Emerald books, JAI Press Inc., 2001, pp.
- [2] Matt H. Evans, *Course 2: Financial Planning and Forecasting*, March, 2000.
- [3] Small Business BC, *Business Planning and Financial Forecasting: A Start-up Guide* [on-line], Available: <http://public-files.prbb.org/intervals/docs/16760815-Business-Planning.pdf>
- [4] Best Practices for Budgeting, Forecasting and Reporting, Available: http://www.adaptiveplanning.com/docs/AP_Best_Practices_Kit_01.pdf
- [5] Cindy Jutras and David Hatch, Aberdeen Group, "Financial Planning, Budgeting and Forecasting in Uncertain Times", January 2009.
- [6] Chapter 12: Financial Planning and Forecasting Financial Statements, Available: http://www.suu.edu/faculty/tufte/10F_F6100/My_Ch12_Show.pdf
- [7] Budgeting, Available: <https://www.civicus.org/new/media/Budgeting.pdf>



International Conference on Innovative Technologies, IN-TECH 2012,
Rijeka, 26. - 28.09.2012



USING ENERGY CONVERSION IN A SOLAR GENERATOR

B. Alsayyed¹

¹ United Arab Emirate University, balsayyed@uaeu.ac.ae

Keywords: solar generator, steam generator, turbine, renewable energy

Abstract. In this paper an innovative solar power generator is designed and implemented. The main idea of this generator is to use a solar collector to heat water and raise it to a certain height, then drop it on a water turbine which is connected to an electric generator. The concept of energy conversion among different types of energy is utilized for the final objective of generating power. Solar power is collected in a form of heat energy to heat water in the solar collector, and then heat is used to raise the water and thus convert the heat energy to potential energy. Potential energy is then converted to mechanical energy that turn the turbine and hence to the generator. This project is at its early stages, however the results are promising.

Introduction

In this paper, the author is investigating a novel idea for a renewable energy system. Despite the name solar generator is very popular in literature; in this paper the idea of the solar generator utilizes a unique energy usage. The main idea is to use the energy conversion from one form to another. A solar collector is utilized to heat water and raise it to a tank at a height. Once the water is raised to a height, it will gain potential energy, which depends on: the temperature and the height. The higher the tank the higher the potential energy. The next step is to drop the water on a turbine that will rotate a generator which will produce power. The uniqueness of the idea is that it combines the steam generator idea and the falls power generation. The water then is redirected to the solar collector, and heated again to repeat the same cycle.

The solar generator does not use solar panels. It eliminates the net CO₂ emission directly. As it does not produce any, neither needs any operation that will result in CO₂ emission.

System configuration

The system main components are shown in figure 1. A solar collector is connected through pipes to a closed tank placed at a height from the collector. The main idea here is to collect the vaporized water resulting from the solar heating in the solar collector and condense it fully or partially in the tank. The collected condensed water is then dropped to the turbine which is placed at the maximum possible height difference in the setup. Hence, the height will control the amount of potential energy the water has. The water will gain kinetic energy as it falls on the turbine. This kinetic energy is a result of the conversion of the potential energy as height is getting lesser. Maximum kinetic energy will occur when the water hits the turbine, and thus rotating. Once the kinetic energy is utilized to turn the turbine, another energy conversion, it will make the turbine rotates. The turbine is connected to an electric generator, which will produce power.

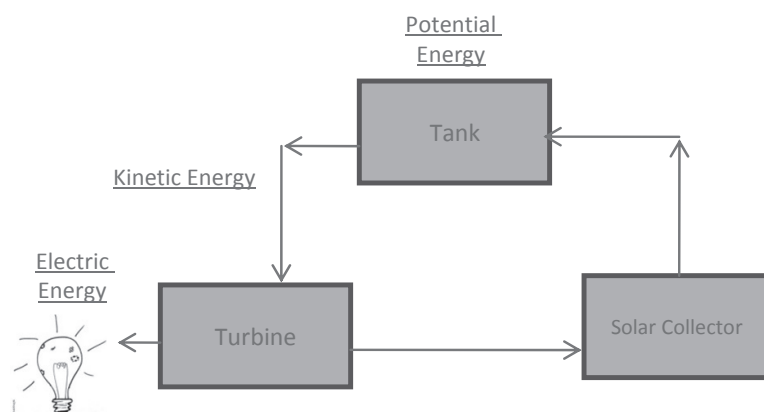


Fig. 1 main components of the system

Implementation and setup

A steel frame is designed to carry the components for the experiment setup. All loads of the components and their center of gravity are identified and the frame was designed to be a stable structure.

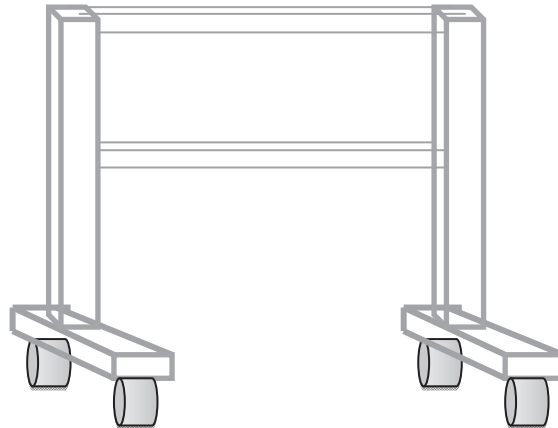


Fig. 2 steel frame

Components for the experiment setup are shown below

- 1- For solar collector a small steam generator has been used to heat water to simulate the solar collector functionality. Figure 3 shows the steam generator.



Fig. 3 steam generator.

- 2- For the tank, a small 10 liter tank has been used. The tank was equipped with a safety valve and a pressure gauge as well as a one-way valve to control the flow of the water. Figure 4 shows the tank.



Figure 4, Tank with its attachments

- 3- Turbine, a small 10 cm. diameter turbine has been used to receive the falling water and rotate. A generator is planned to be coupled with the turbine shaft. Figure 5 shows the turbine used.

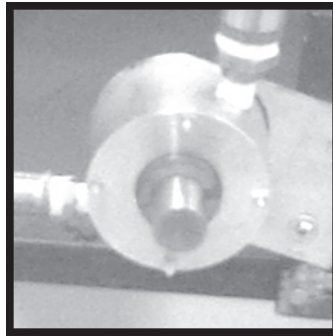


Fig. 5 turbine

The components above are setup on the frame stand such that the tank will be at the highest point and the turbine at the lowest level.

Technical relations:

$$P = \rho \times g \times h \quad (1)$$

For Potential Energy

$$PE = mgh \quad (2)$$

Where:

$$PE = \text{Energy}(J)$$

$$m = \text{mass}(kg)$$

$$g = \text{gravity}(9.8m / s^2)$$

$$h = \text{height} - \text{above} - \text{earth} - \text{surface}(m)$$

For Kinetic Energy

$$KE = \frac{1}{2}mv^2 \quad (3)$$

Where:

$$KE = \text{Energy}(J)$$

$$m = \text{mass}(kg)$$

$$v = \text{velocity}(m/s)$$

Between heater and tank, when water moves from the heater to the tank in the opposite direction of gravity, the heat is converted to potential energy. At temperature 100°C, water density equal 958.3665 kg/m³. Assuming the head of the pipe equal to 3 m, from (1) the pressure equal to 18.8 kpa.

(1) above shows the effect of the head on the potential energy. As we need more potential energy, we need to increase the head. As for practical applications, the turbine and the generator would be placed in the building basement and the tank would be at the building roof.

(3) above shows kinetic energy between the tank and the turbine and how the velocity effect on kinetic energy.

Finding output power from the whole system

To find the output power from the shaft some steps are followed. We must take into consideration that the system is closed system; all the tanks are closed and connected together by pipes.

- Finding volume flow rate, where: $Q = \frac{V_{\text{tank}}}{\text{time}}$ (4)

- Finding velocity: $v = \frac{Q}{A} = \frac{4Q}{\pi D^2}$ (5)

- Finding Reynolds number:
$$\text{Re} = \frac{\rho v D}{\mu} \tag{6}$$

- Finding $\frac{\varepsilon}{D}$: relative roughness. (7)

- Friction factor which is found from the moody chart.
- Finding total friction which is the summation of minor and major losses,

$$\sum F = \frac{4fLv^2}{2D} + \sum k \frac{v^2}{2} \tag{8}$$

- Finding mass flow rate, $m = Q \times \rho$ (9)
- Bernoulli's equation was applied for the system, between the two tanks,

$$\frac{P_2 - P_1}{\rho} + \frac{v_2^2 - v_1^2}{2} + g(z_2 - z_1) = \frac{W_{shaft}}{m} - \sum F \tag{10}$$

- End up with following equation for out power.

Dth following

$$W_{shaft} = m \left[\frac{P_2 - P_1}{\rho} + \frac{v_2^2 - v_1^2}{2} + g(z_2 - z_1) \right] + \sum F \tag{11}$$

Where:

$P = \text{prussure (Pa)}$

$\rho = \text{density (kg / m}^3\text{)}$

$V = \text{flow _ velocity (m / s}^2\text{)}$

$W_{shaft} = \text{net _ shaft _ energy (Watt)}$

Conclusion

This research opens up a potential for developing solar generators with different sizes that would be suitable to be used for household usages. Also, this could be used for use for out of the grid projects during development and for portable usages. Research is still at the very early stages, and next steps include the parameterization of the setup in order to manage the potential power output.

Acknowledgement

The author would like to acknowledge the following students for helping in the setup of the experiment: Hajer Hamdan Abdouli, Naseefa Slayem Al Ameri, Suaad Abdulla Abdulkarim, and Zain Mohammed Abdul Karim.

IDENTIFICATION OF THE DAMAGE IN THE BEAM-LIKE STRUCTURE ON THE BASIS OF TIMOSHENKO BEAM MODEL

S. Shevtsov¹, I. Zhilyaev¹, V. Akopyan², and A. Soloviev²

¹ South Center of Russian Academy, Thekhov str., 41, Rostov on Don, post. code 344006, Russia

² Institute of Mechanics & Applied Mathematics, Stachki str., 200/1, Rostov on Don, post. code 344090, Russia

Keywords: Nondestructive evaluation, Damage identification, Cracked beam, Modal analysis, Timoshenko beam, FEM modelling, Experimental testing

Abstract. The main purpose of the presented article is an investigation of the Timoshenko beam equation sensitivity to the presence of crack in the beam-like structure. We describe the crack in the Timoshenko beam as a cutting in the form as a smoothed delta-function. The solutions of this equation and experimental data on the natural frequencies and vibration modes shape then are used at forming of discrepancy functional that further optimized in order to determine the position and depth of a crack. We compare here the solutions of the cracked Timoshenko beam equation with results of 3D finite element analysis performed on the notched elastic beams and also with experimental data. The advantage of the proposed Timoshenko beam – based approach comparing with the method of two beams connected by a torsion spring, is that the Timoshenko model requires no assumptions about the stiffness of the spring. Moreover, the developed approach allows to model a crack in a non-uniform beams that unallowable in the method of two elastically jointed beams. The advantage of the method as compared with 3D finite element modeling is better performance - the speed of calculation is more than a hundred times higher than for the same accuracy at recovering the natural vibration modes by FEA. Due to these advantages, the Timoshenko beam model can be used in the algorithms for identifying the location and level of damage. Since these algorithms require multiple calculations of the functional, the problem of high-performance computing is essential.

The dependence of the damage identification efficiency on the position of exciting load on the tested structure was revealed. As oscillations stabilization rate depend on the point of applied excitation load, each natural mode should be excited, in their separate locations to avoid a preferential excitation of lower modes and their mixing.

Introduction

The problem of damage identification in the rods and beam-like structures is very important for aircraft, civil and many other applications. The used approaches and damage identification algorithms considered in the surveys [1, 2] are based on dependence of the damage parameters on the modification of the natural modes shape, eigenfrequencies, structural damping parameters, stiffness matrices of the damaged structures. Most sufficient differences between these algorithms are the ways of the objective functional formulation. So, the authors of [2] used the Modal Assurance Criterion (MAC), depended on the natural modes shape modification at presence of damage in a beam structure. Matveev and Bovsunovsky [3] have proposed an approach to the damage identification which uses correlation "eigenfrequency – crack location". Representation of the cracked beam in the form of two perfect beams connected by the elastic spring is used in the works [4-6]. The stiffness parameters of this elastic element were described by Gounaris and Dimarogonas [7] as the local stiffness matrix whereas both perfect beams by the finite element (FE) method. Unfortunately, the way of the local stiffness defining is arbitrary and not strongly determined. Because of sufficient computational cost 3D FE formulation of the cracked structure dynamics is not desirable. Therefore using of analytical representation of the damages in the beam-like structure with relatively small numbers unknown defect's parameters is preferable.

Considering the damage identification as inverse problem one need to conclude that most useful method of the inverse problem resolving include the iterative call of the forward problem solution in order to train the artificial neural network, or in the genetic algorithm, etc. This allows to formulate the main requirements to the model of the damaged structure for the forward problem simulation. These requirements are followed here in the arbitrary order.

1. The computational cost of the model simulation should be minimal.
2. Model of the damaged structure must be dimensionless (universality!).
3. The defect must be fully characterized by as small as possible number of parameters.
4. The output of model must be presented as small as possible number of output variables that can be easily interpreted.
5. These variables must have a minimum cross-correlation.
6. These variables should be properly monitored (preferably by direct measurements) with minimal noise and the influence of environmental factors.
7. At decreasing of degree of damage the model of the damaged structure should be continuously modified to the model of perfect structure.
8. The model simulation results should be less depended on the used numerical simulation method.
9. The model should be stable at small variation of input data.

In this paper we present the way of constructing the cracked Timoshenko beam model (CTBM) and the ability of this model to correctly describe dependencies of the flexural vibration mode shape and some eigenfrequencies on the crack depth and location. We assume here the crack as notch with not interacted coasts that well grounded for the structures loaded by the big static forces and harmonically excited by small amplitude, and also by the established weak dependence of the solution on the notch's width.

The Cracked Timoshenko Beam Model (CTBM)

It is known that generic Timoshenko beam equations correctly takes into account the effects of shear and the section rotation even at quite high frequencies of flexural vibrations

$$\begin{aligned} (EJ\psi_x)_x + kGF(w_x - \psi) &= \rho J \psi_{tt}; \\ [kGF(w_x - \psi)]_x + q &= \rho F w_{tt} \end{aligned} \quad (1)$$

In the above equations E, G, ρ, J, F, L are the Young module, shear module, section moment inertia, section area, and beam length respectively; w, ψ are beam axis deflection and angle of the section rotation; q is distributed load; and k is form-factor equal to 6/5 for rectangular cross section. The boundary conditions for the considered cantilever beam with free load tip are

$$w|_{x=0} = \psi|_{x=0} = \partial \psi / \partial x|_{x=L} = (\partial w / \partial x - \psi)|_{x=L} = 0. \quad (2)$$

Assuming the homogenous cross section of the beam (but this assumption does not limit our next consideration), we exclude the spatial distribution of the section moment inertia and section area

$$J(x) = J_0 \cdot \zeta(x); \quad F(x) = F_0 \cdot \eta(x), \quad (3)$$

where J_0 and F_0 are the section moment inertia and section area along the uncracked part of the beam.

Let the beam cross section has the width b and height h . Then using the known formulas for the rectangular section moment inertia and section area, and relationship between shear and Young modules, Eq. 1 can be rewritten in the form

$$\begin{aligned} (\zeta \psi_x)_x + \frac{6k}{h^2(1+\nu)} \eta (w_x - \psi) &= \frac{\rho}{E} \zeta \psi_{tt}; \\ \frac{k}{2(1+\nu)} [\eta (w_x - \psi)]_x + \frac{q}{bhE} &= \frac{\rho}{E} \eta w_{tt} \end{aligned} \quad (4)$$

At performing of transition to the dimensionless variables according to the rule

$$\xi = x/L \Rightarrow \partial / \partial x = 1/L \cdot \partial / \partial \xi; \quad \tau = t/T \Rightarrow \partial / \partial t = 1/T \cdot \partial / \partial \tau; \quad u = w/L, \quad (5)$$

where dimensionless coordinate ξ , time τ and displacement u expressed trough beam length L and pseudo period T to be defined, system (5) will be transformed to its dimensionless representation

$$\begin{aligned} (\zeta \psi_\xi)_\xi + \frac{6kL^2}{h^2(1+\nu)} \eta (u_\xi - \psi) &= \frac{\rho L^2}{ET^2} \zeta \psi_{\tau\tau}; \\ \frac{k}{2(1+\nu)} [\eta (u_\xi - \psi)]_\xi + \frac{qL}{bhE} &= \frac{\rho L^2}{ET^2} \eta u_{\tau\tau} \end{aligned} \quad (6)$$

In order to simplify the structure of the Eq.6 we define a pseudo period T as

$$T = L \sqrt{\rho/E}. \quad (7)$$

Introducing the dimensionless coefficients

$$A = 6kL^2 / [h^2(1+\nu)]; \quad B = k / (1+\nu) \quad \Phi = qL / (bhE) \quad (8)$$

system (6) can rearranged to the more useful view

$$\begin{aligned} \eta u_{\tau\tau} - B(\eta u_\xi)_\xi + B(\eta \psi)_\xi &= \Phi \\ \zeta \psi_{\tau\tau} - (\zeta \psi_\xi)_\xi - A \eta u_\xi + A \eta \psi &= 0; \end{aligned} \quad (9)$$

If we describe the crack by the delta – like notch with depth $d \in [0;1]$ placed on the dimensionless distance l from the clamped end

$$\delta(\xi) = d \cdot \begin{cases} \cos[\pi(\xi-l)/2\varepsilon], & \xi \in [l-\varepsilon, l+\varepsilon] \\ 0; & \xi \notin [l-\varepsilon, l+\varepsilon] \end{cases}, \quad (10)$$

where variable ε is half width of the notch, the spatial distributions of the beam thick η and section moment inertia ζ are

$$\eta(\xi) = 1 - \delta(\xi); \quad \zeta(\xi) \approx 1 - 3\delta(\xi) \cdot (1 - \delta(\xi))^2 = 1 - 3\delta(\xi) \cdot \eta^2(\xi) \quad (11)$$

As assumed above the notch's coasts not interact, the value of ε practically has no influence on the beam's dynamic behavior, and can chosen from the considerations of numerical stability at model simulation. At performing of harmonical and modal analysis both u and ψ assumed as harmonical oscillations with amplitudes $U(\xi)$, $\Psi(\xi)$, and the boundary value problem for the cantilevered beam is formulated in the form

$$\begin{aligned}
 & -\eta \bar{\omega}^2 U - B(\eta U_\xi)_\xi + B(\eta \Psi)_\xi = \Phi \\
 & -\zeta \bar{\omega}^2 \Psi - (\zeta \Psi_\xi)_\xi - A \eta U_\xi + A \eta \Psi = 0, \\
 & U|_{\xi=0} = \Psi|_{\xi=0} = \Psi_\xi|_{\xi=1} = (U_\xi - \Psi)_\xi|_{\xi=1} = 0
 \end{aligned}
 \tag{12}$$

From the Eqs. 5, 12 imply the relationship between the dimensionless $\bar{\omega}_i$ and expressed in the natural units ν_i eigenfrequencies

$$\bar{\omega}_i \tau = 2\pi \nu_i t \Rightarrow \nu_i = \frac{\bar{\omega}_i}{2\pi L} \sqrt{E/\rho}
 \tag{13}$$

and also expressions for the dimensionless excitation frequency $\bar{\Omega}$ and period \bar{T} through above introduced pseudo-period T

$$\bar{\Omega} = \omega \cdot T; \quad \bar{T} = 2\pi/\omega \cdot T.
 \tag{14}$$

It is worth to deduce here some concluding remarks about obtained CTBM. From the structure of Eq. 12 one can see that our model satisfy mentioned requirements 1-7, it can be easily numerically solved and therefore can be used for the multiple forward problem solving in the iterative loop. But because of inverse problems are not correct, the questions of the solution uniqueness and numerical stability now opened. We leave the strong investigation of these problems out of framework of the presented paper, limiting by the analysis of the numerical results.

Numerical Implementation

All numerical investigations were performed using Comsol Multiphysics FE soft package working in the Partial Differential Equation (PDE) mode. One dimensional FE mesh consisted of 1000 knots, and near 5000 degree of freedom. For the model testing we used a steel beam with dimensions 4cm*5cm*1m and artificially introduced "cracks" – notches with depth: 0.25; 0.5; 0.75 of thick placed at distance 0.15; 0.22; 0.3; 0.4; 0.6; 0.7; 0.8 from clamping end. Obtained results were compared with those obtained concurrently on the 3D FE model containing near 60000 degree of freedom.

It is important to note incomparable computational performance of the tested method. At calculation of the first 6 natural modes the computation time for 3D FE model is of approximately 30 min, whereas 1D CTBM 0.3...0.6 sec only at absolutely identical crack parameters and calculation accuracy. All investigated conditions and defect's parameters have demonstrated good numerical stability of the CTBM finite element implementation and very weak dependence on the FE meshing.

First five eigenfrequencies computed by the different methods deviate one from other for the perfect beam less 0.6% and up to 7% for the damaged beams with the notch depth 0.75. Any difference of the modes shape was not observed. Some mode shapes depicted on the Fig.1 show that bending natural modes and eignfrequencies are most sensitive to the presence of crack, if the crack is located near the zone of maximum curvature of the beam axis (bending moment). These eigenfrequencies are underlined on the right diagram.

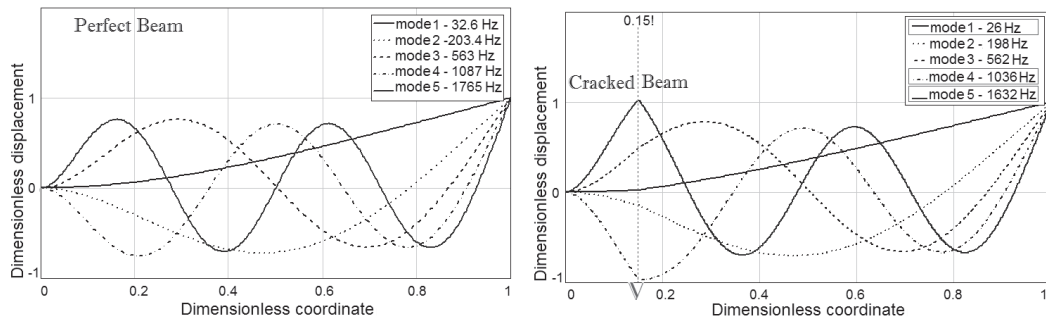


Fig. 1 Comparison of the modes shape for the perfect beam (left) and beam with notch located at $l = 0.15$ (right)

The numerically obtained distribution of the spatial derivative of the cracked beam axis can be accepted as the most informative and reliable criterion allowing to reconstruct the crack depth and location. Some examples are presented on a Fig. 2.

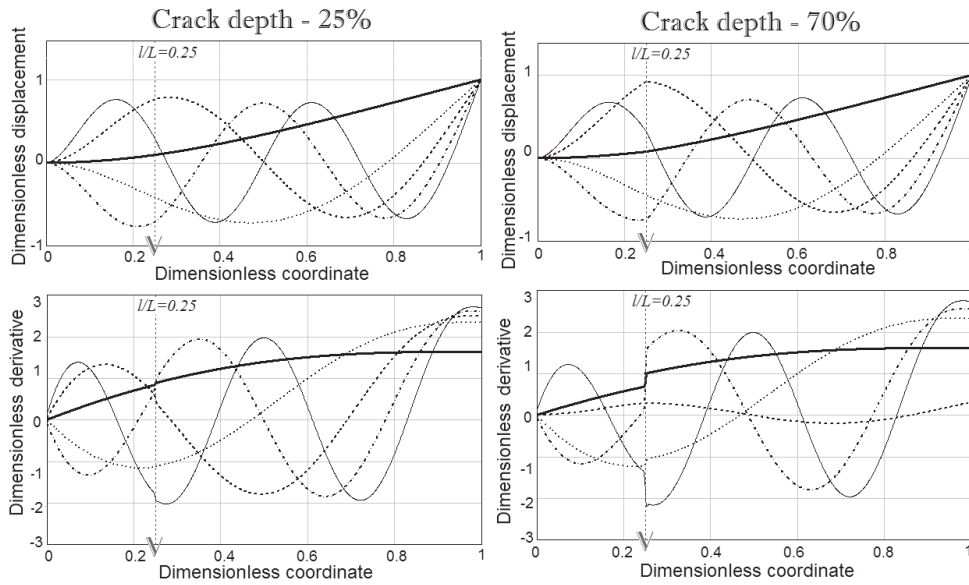


Fig. 2 Dimensionless modes shape and distribution of the spatial derivative of the cracked beam axis

At performing a transient analysis it has been investigated efficiency of the beam excitation and duration of vibration settling time on a desired eigenfrequency depended on the location of the applying force. Thus for successful monitoring of the beam deflection amplitude we need a harmonic load source with possibility of high precision positioning along monitored beam. The similar results have been obtained experimentally.

Some results of numerical frequency response (FRF) analysis of free tip of vibrated damaged beam depicted on the Fig. 3 show dependence of the FRFs peaks shift depended on the degree of damage. This shift also can be used in order to enhance the reliability of the crack parameter reconstruction.

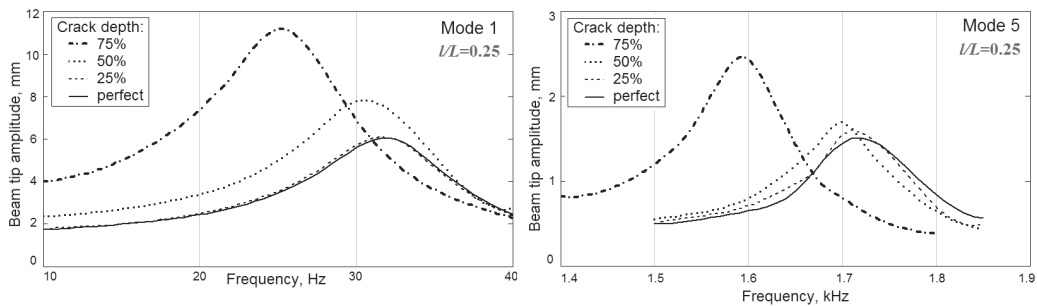


Fig. 3. Peak shift of FRFs of the beam tip vibration amplitude on the 1st (left) and 5th bending modes (right)

Experiment

Spatial distribution and FRF of the beam deflections have been investigated experimentally both for perfect beam samples and samples with several degree of damage. Specimens were manufactured with artificially introduced damages – notches. Experimental setup allows a high precision measuring of the specimens' surface displacement at vibration excited by electromagnet which can be moved along the specimen. All measured information has been digitized and managed in the real time under the computer control.

Some experimentally obtained modes shape for specimens with different degree of damages are presented on the Fig. 4. Experimental points are fitted by the 2nd order splines. From the Figs. 2 and 4 we can conclude that CTBM is less sensitive to the crack depth comparing to high precision experimental data, but CTBM give the right qualitative tendency, and, hence, can be used as the crack presence indicator as well as crack locator.

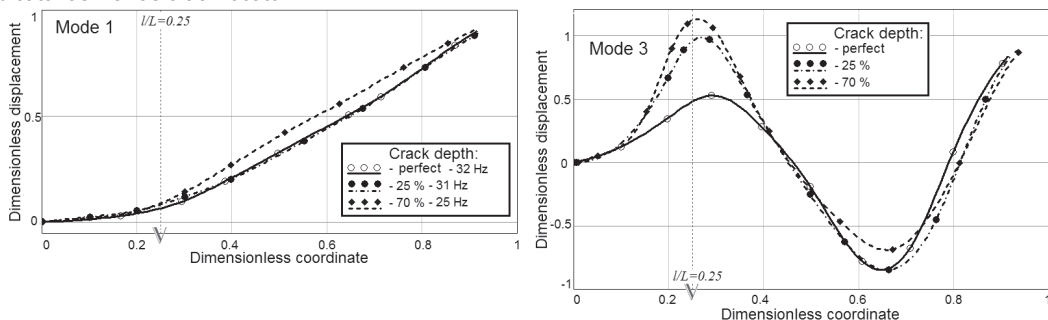


Fig. 4 1st and 3rd natural bending modes shape of specimens with different notches depth



Conclusion

Proposed CTBM is an efficient tool for prediction of the crack location in the arbitrary beams using the measured shift of the FRFs and magnitude of the beam deflection discontinuity at flexural vibration on the first 4...5 eigenfrequencies. As any other approaches, CTBM require the full preliminary information about the FRFs and modes shape of the monitored structure in the frequency range including these 4...5 eigenfrequencies. CTBM provide precision equal to 3D FE models at hundreds time less computational cost. CTBM satisfies all requirements to the models of the forward problem solving and can be successfully used in the neural network and genetic algorithm based method to solving the inverse problem of reconstruction damages in a wide class of beams.

Acknowledgment

This work is partially supported by the Russian Foundation for the Basic Research (Grant 10-08-00093-a).

References

- [1] D.F. Giraldo: *A structural health monitoring framework for civil structures*, (Wash. Univer. Dissert. Depart.of civil engineering. Saint Jouris. – Missouri, 2006).
- [2] Del. Grosso, F. Lanato: A critical review of recent advances in monitoring data analysis and interpretation for civil structures. *Proc. of 4th European Conf. of Struct. Control*. Saint – Petersburg, Vol. 1, (2008), pp. 320-330.
- [3] V.V.Matveev, A.P.Bovsunovsky: Vibration-based diagnostics of fatigue damage of beam-like structures. *J. Sound Vibration*, Vol. 249 (2002), No.1, pp. 23-40.
- [4] M.H.F. Dado, O.A. Shpli: Crack parameter estimation in structures using finite element modeling. *Intern. Journ. Solid and Structures*, Vol.40 (2003), pp. 5389-5406.
- [5] Y. Bamnios, E. Douka and Trochidis: Crack identification in beam structures using mechanical impedance. *J. of Sound and Vibration*, Vol. 256(2) (2003), pp. 287-297.
- [6] G. Gounaris and A.D. Dimarogonas: A finite element of cracked prismatic beam for structural analyses. *Computer and structures*, Vol.28 (1998), pp.309-313.
- [7] S. Orlando, B. Peeters, G. Coppotelli: Improved FRF estimators for MIMO Sine Sweep data, *Proc. of the Conference on Noise and Vibration Engineering ISMA-2008*, Katolieke Universiteit Leuven, Belgium, (2008) pp. 1223-1240.



International Conference on Innovative Technologies, IN-TECH 2012,
Rijeka, 26. - 28.09.2012



ALUMINA CERAMICS BRAZED USING METALLIC ALLOYS

I. Voiculescu¹, V. Geanta², R. Stefanoiu³, H. Binchiciu⁴, D.D. Daisa⁵

¹ University Politehnica of Bucharest, Materials Technology and Welding Department, Splaiul Independentei, 313, Bucharest, 060042, Romania, ioneliav@yahoo.co.uk

² University Politehnica of Bucharest, Materials Science and Engineering Faculty, victorgeanta@yahoo.com

³ University Politehnica of Bucharest, Materials Science and Engineering Faculty radustefanoiu@yahoo.com

⁴ SC SUDOTIM AS SRL, Timisoara, Romania, sudotim_suport@yahoo.com

⁵ SC METAV-CD, Bucharest, Romania, dana_daisa@yahoo.com

Keywords: alumina, brazed, filler metal, metallic glass

Abstract. Alumina ceramics have been brazed by using copper and metallic glass as interlayer materials (brazing agent). The joints were tested for shear strength, and then the fracture surfaces and transversal sections have been analyzed by SEM microscopy. The highest joint strength was 283.43MPa, and was reached for the sample that used a metallic glass interlayer, the bond failed at the ceramic interface. Some joints, however, have shown interfacial defects and debonding at the edges where the values of the residual shear stresses are highest. The results of EDS and SEM analysis have shown the presence of Nb-rich crystals in both glass and metal layers separated by ceramic specimens. The presence of oxygen can also be noted in these areas, thus proving the oxidized state of the surfaces.

1. INTRODUCTION

Nowadays, ceramics have an important part to play in conjunction with other materials. They can add particular functionality or provide added benefit to a component, e.g. as wear surfaces, ultra-hard materials in cutting tools, for corrosion resistance or high temperature protection. As ceramics are now being used in isolation, joining is an increasingly vital technology for the integration of the materials [1]. The use of ceramic components for structural, electrical and electronic applications is rapidly increasing; however most of these applications require joining of ceramics to metals or alloys for multiple functions and reduced costs. Due to the superior properties of ceramic materials at high temperature, it is highly desirable to fabricate metal-ceramic joints, which can withstand higher temperature environments [2, 3, 4]. Most ceramic-metal brazing procedures are carried out in vacuum furnaces, but a simpler approach involves the use of inert atmospheres. For a brazed joint to be successful, it is necessary that the liquid braze metal wets and bonds to the ceramic. More commonly, solid metal interlayers are used which deform or which have expansion coefficient near to the ceramic [5]. When joining dissimilar materials, the thermal expansion mismatch between the materials, their chemical compatibility, and the temperature capabilities of the least refractory member impose processing and joint design constraints [6]. Multilayer Cu/Ni/Cu interlayers that form a thin layer of Cu-rich transient liquid phase have been used to join Al_2O_3 to Al_2O_3 . The Cu/Ni/Cu interlayer finally forms a nickel rich interlayer. However, the joint strength decreased substantially after being exposed to heat treatment in air and argon, although nickel has a high melting point. The presence of oxygen promoted the formation of a spinel at the Al_2O_3 /Nickel interface, which induced cracks in ceramic's surface. To produce strong ceramic/metal interfaces for high temperature applications, it is essential to fabricate metal/ceramic joints which have good oxidation resistance at high temperature [6, 7]. Bond strength is also important for evaluating the properties of the joint. The measurement conditions must provide uniaxially compressive test for ensuring the accurate measurement of tensile and shear bond-strength of ceramic-ceramic and ceramic-metal joining [8].

Bonding strength is not only related to surface-contact angle but also surface roughness. The surface-contact angles of the treated substrates can be reduced compared to that of the as-received substrate. This is probably due to the change of surface chemical composition caused by selective etching of components and surface roughness [9]. Another important variable is the surface finish of the ceramic and filler metal. Prior to brazing, the surfaces of both samples and filler metal must be polished using metallographic sand paper or diamond powder and then ultrasonic cleaned in acetone and alcohol [10]. The higher is the reactivity in a system the higher the work of adhesion. On the other hand, if the stability of the substrate ceramic is higher than that of the reaction product, the work of adhesion of reactive systems mainly depends on the work of adhesion for the metal on the reaction product [11]. Metallic glasses, when used as brazing filler materials [12], devitrify during the heating segment of the brazing cycle. Devitrification is not detrimental to the melting characteristics of the metallic glass. The devitrified metallic glass can be ductile enough to serve as an interlayer in the joint and dissipate residual stresses generated during the cooling cycle. Furthermore, these foils have a significantly smaller amount of surface oxide film, unlike the gas-atomized powders used in filler brazes. These surface oxides prevent fusion of individual particles and result in non-uniform melting [13, 14].

2. EXPERIMENTAL

2.1. Materials

Although Al_2O_3 is a naturally occurring mineral as gibbsite, a number of processing steps must be carried out before it can be used in high-technology ceramic applications. Al_2O_3 based ceramics vary from 80 to 99.8% pure Al_2O_3 , with properties and applications

dependent on the purity. For a 90% Al₂O₃ composition will result in a ceramic suitable for applications requiring toughness and wear resistance, while for corrosion resistance and high-temperature operation, 99.8% Al₂O₃ may be required.

The present paper reports the results of joining alumina pellets using different metallic braze material. The ceramic pellets had a diameter of 15mm and 7mm thick, and were obtained by compacting of 90% Al₂O₃ powder with an organic binder, followed by furnace firing. The average dimension of powder the particles was between 1 and 8 μm, an average pore radius of 3.04 μm, the bulk density of 3.87 ± 0.5g/cm³ and total porosity of 10.80% ± 2%. The surface's roughness, obtained by mechanical polishing using 1200 grit silica carbide paper, was R_z = 3.1μm. The bonding surfaces, both ceramic and metal foil, have been cleaned in acetone and wiped with propylene. In order to diminish the oxidation effects at high temperatures, the surfaces were covered with boric oxide before joining. Copper is often used as material for brazing ceramics due to its plasticity and reduced interfacial stress during solidification. Metallic glasses are stronger, harder, and more ductile than the metals from which they are derived [13, 14]. In the study, as metallic solder, also copper ribbons have been used and a series of experimental strips of Ni₅₉ Cr_{13.5} Zr_{4.3} Fe_{4.2} Nb_{2.9} Si_{15.3} B and Fe_{73.5} Cu₁ Nb₃ Si_{15.5} B, obtained by ultrafast solidification using the following parameters: expulsion nozzle dimensions 0.8x12mm, argon overpressure of 0.25at, and tangential speed of 24m /s.

The average thickness of the metallic glass ribbon was 0.2mm for copper, 0.1mm for nickel based and 0.01mm for ferrous based metallic glass. The microscopically analyze of the metallic solder indicate a crystalline structure and crystallites presence (fig. 1). The dispersive energy X-ray spectrum indicates the main elements of metallic glass ribbon (fig. 2).

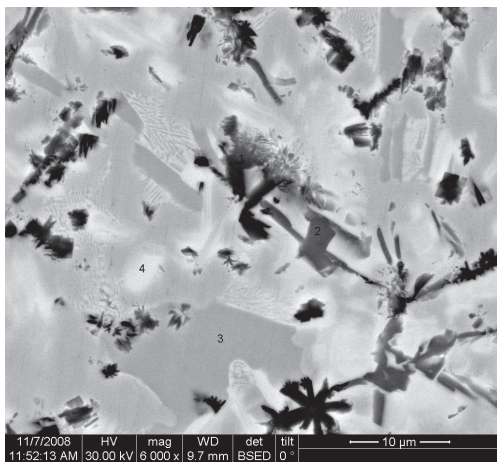


Fig. 1 Microscopically aspect of metallic solders (6000x)

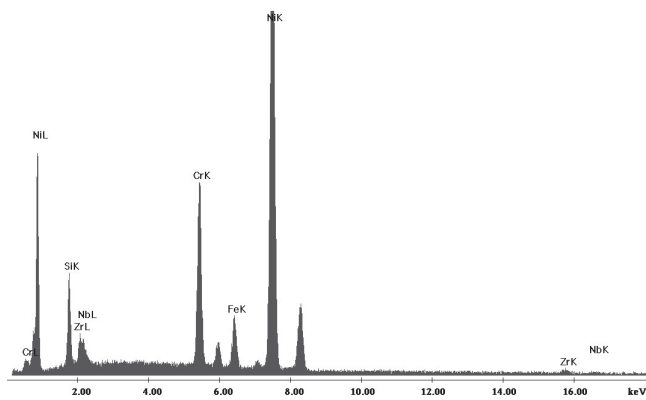


Fig. 2 Dispersive energy X-ray spectrum of nickel based metallic glass ribbon

The existence of crystallization germs in the wide bands justifies the starting of crystallization at lower temperatures than in the thin and completely amorphous strips according to DSC measurement results. The average size of crystallites of rapidly cooled band was calculated using Scherrer method, considering the width of XRD peaks, its value being ~ 16nm. To have a referential value, high purity (99.995% Cu) copper strip was also used for joining in the same brazing conditions.

2.2. Brazing procedure

The brazing process was performed using and an electric resistance furnace. The brazing foil and substrates were arranged in a pill/foil/pill orientation, and the entire assembly was placed into a loading device consisting of two steel plates and four steel bolts, that were hard-chromed. This procedure ensured sufficient contact between the various components of the joint.

In order to establish the optimum domain for the parameters values (lowest temperature and shortest maintaining time) a time–temperature study has been performed, including the thermal gravimetric analysis [12]. The heating cycle employed during the brazing process (fig. 3) was: initial temperature 35°C, final temperature 1100°C, heating speed $v_1=8.27$ °C/min for temperature range of 35 to 750°C, heating speed $v_2=4.14$ °C/min for temperature range of 750 to 950 °C and heating speed $v_3=5.05$ °C/min for temperature range of 950 to 1100 °C, maintained time one hour and cooling speed $V_c= 0.9$ °C/min.

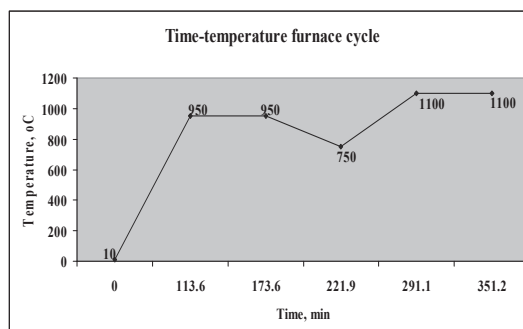


Fig. 3 The working diagrams for brazing

2.3. Joint Strength Measurements

Cylindrical specimens were used to conduct a shear test. A simple device has been used in the shear test and the LLOYD Instruments testing machine, as it can be seen in fig. 4. The normal force applied to the first pallet in the center of the sample was balanced with the shear force at the second pill, so the shear stress can be located at the level of metallic material. To have a correct image of the measured and calculated values, it was considered that the effective solicited surface during the shear test is less than the total area of the ceramic joint. The maximum shear stress at the interface τ_{max} was evaluated using the equation:

$$\tau_{max} = F_{max} / (2\pi dh) \quad (1)$$

where: d is the diameter of the metallic glass ribbon and h is the thickness of the metallic glass ribbon.

The test has been performing using a crosshead speed of 0.1 to 0.2 mm/min. It is important to note that the shear test used was not a standardized test and was used for screening purposes only. After brazing, also the cross sections of the joints and the fracture surfaces were characterized using scanning electron microscopy (SEM) (QUANTA INSPECT F).

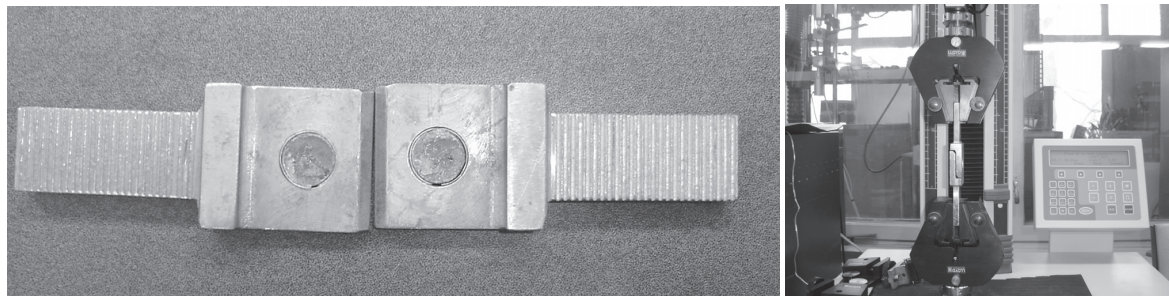


Fig. 4 The shear test device and LLOYD INSTRUMENTS LRX Plus testing machine

3. RESULTS AND DISCUSSIONS

Preliminary wetting studies carried out on the alumina pills indicated that the ferrous based metallic glass and nickel-based metallic glasses wet ceramic surface adequately, the contact angle varying in the range of 19.5° to 20° and 52.6° to 53° ± 0.5°. The experiments demonstrate that successful brazes were produced by using either 100 or 10 μm thick metallic glass strips, for the brazing parameter values of 1100 °C maximum temperature maintaining for 30 minutes. In a real application, thickness will be dictated by the geometry and roughness of the components to be brazed and the ease of incorporating different brazing foil. A scanning electron micrograph of the brazed joints realized at 1100 °C for 30 min holding time, using copper foil, can be seen in Fig 5. The interlayer of the joints mainly contains a continuous matrix phase (dark grey), together with another isolated phase (light grey). As it can be seen in fig. 5, the metal layer located between the two ceramic components is continuously on the length, with different adhesion at the interface with ceramic pills.

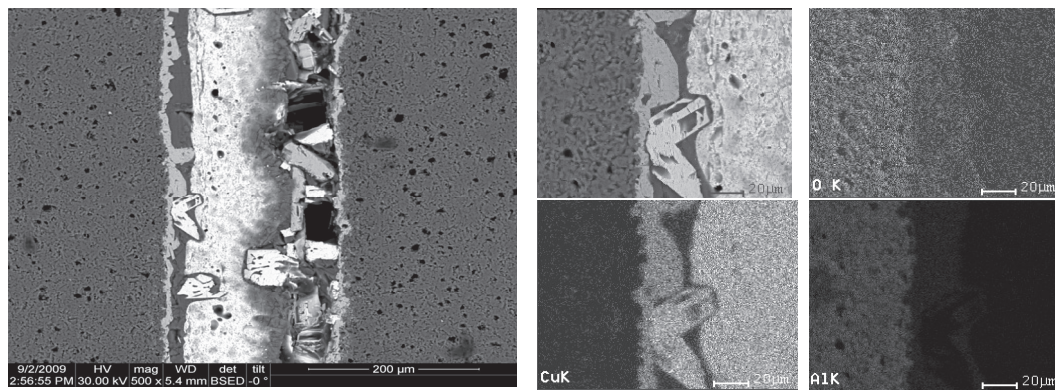


Fig. 5 The joint between two ceramic pellets using as filler metal copper (500x) and Back scatter electron image with wavelength dispersive spectroscopic elemental maps for detected items

The entire surface of the ceramic component is covered with a compact oxide layer. On both sides of the metal area, located in the center section, were found two thin layers with multiple cracks, rich in O, Al, Na, Ca, Si and Mg, and containing small amounts of C, K and Cl (fig. 6).

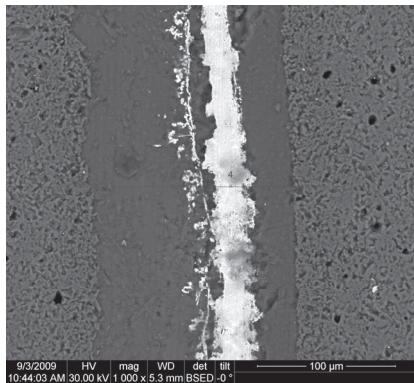


Fig. 6 The joint between two ceramic pellets using as filler metal ferrous based metallic glass, 1000x

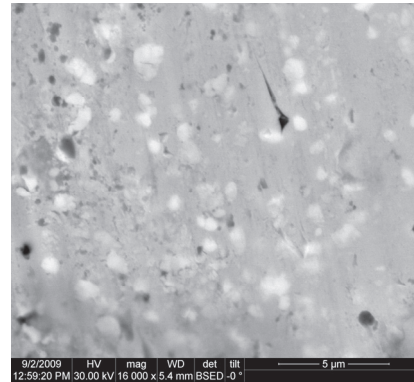
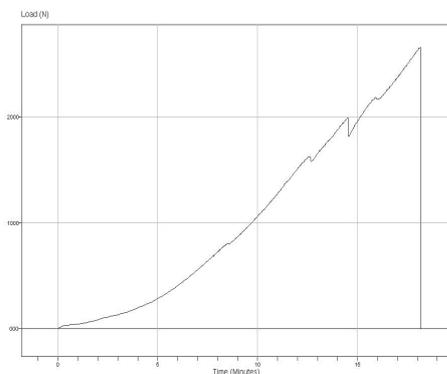


Fig. 7 Back scatter electron image indicating the presence of Nb-rich crystals, 16000x

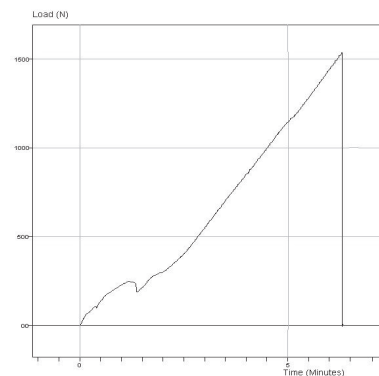
Their appearance suggests a mixture of continuous oxides, interrupted by some compounds rich in Cu and Silicon, with polygonal morphology (probably separated from the liquid directly to solidification). There are visible layers rich in Cu, Al, O, which enters into the pores of the ceramic material.

When metallic glass is used as brazing material, there is a continuous layer and relatively uneven in width at the interface with ceramic components, composed of metal compounds and complex oxides, rich in O, Al, Si, Na and C (fig. 6). From the composition images, it has been identified the presence of both Nb-rich crystals in glass and metal layers located at the interface to ceramic components (fig. 7). In some places, inside these strips, Nb-rich particles are present. Central area has a composition close to that of metallic glass containing Fe, Nb, Cu, Si, B and small amounts of Al, Ca, K. It can be also seen the presence of oxide particles on these surfaces.

The influence of the reactive nature of the braze material on the joint integrity and strength was evaluated using shear tests. A schematic of a shear stress-linear displacement plot obtained in a shear test can be seen in fig. 8. The interfacial shear stress was calculated by balancing the normal force exerted on the alumina pills over the sheared area at the joint interface. The peak stress in the plot corresponds to the peak load at which shear failure occurred in the joint. All of the shear failure occurred in the braze material. The interfacial shear stress values ranged from 199.42 N/mm² (for copper brazes material) to 6942.27 N/mm² (for ferrous based metallic glass brazes material). In all samples was observed that breaking was initiated by the circular cracks. Based on these studies, we can conclude that ferrous based metallic glass can be used successfully to braze alumina to alumina components. The joining process is reactive and results in the formation of intermetallic compounds containing Fe, Nb, Cu, Si and B.



a) $F_{max}=2670N$, testing speed $v=0.2mm/min$



b) $F_{max}=1534N$, testing speed $v=0.1mm/min$

Fig. 9 Schematic breaking shear diagrams: a) ferrous based metallic glass brazing material; b) copper brazing material

4. CONCLUSIONS

Brazing of Al₂O₃ components using metallic glasses as filler metal obtained by ultra-fast solidification can be performed with satisfactory results by using furnace brazing technique. If the brazing material and ceramic surfaces are not properly cleaned and processed (degreasing, etching, polishing) can resulting oxide layers that prevents high resistance to shear. An unwanted effect that appears in the case of brazing is that rapid heating causes cracks in the ceramic material, which may spread in the joining area. In the case of Al₂O₃ components, the combinations of filler materials which provide satisfactory results are Ni₅₉Cr_{13.5}Zr_{4.3}Fe_{4.2}Nb_{2.9}Si_{15.3}B and Fe_{73.5}Cu₁Nb₃Si_{15.5}B.

Shear tests performed on pills type samples assembled with glass metal sheets led to the breaking strength values in the range 5200 – 6942 N/mm². These values are apparently sufficient, but even better values can be obtained using brazing technique in the microwave field with protective atmosphere. Metallographic examination has revealed the appearance of oxide layers at the interface between the ceramic and filler material, containing intermetallic compounds which ensures continuity of connection but does not provide sufficient mechanical strength.

References

- [1] W., Hanson, J., Fernie, Materials World, Vol. 6 No. 9, (1998), pp.524-36;
- [2] L., Junqin, P., Xiao, Journal of Materials Science 36 (2001), pp.1383-1387;



- [3] I., Vida-Simiti, N., Jumate, V., Moldovan, Sintered Materials with Gradual Porous Structure, Conference ASTR, Timisoara, Romania, 2011, pp.245 – 252;
- [4] M., Schwartz, "Ceramic Joining", ASM International, Materials Park, OH (1990), pp.166;
- [5] D. G. Dixon – Ceramic Matrix Composite – Metal Brazed Joints, Journal of Materials Science 30 (1995), pp.1539-1544;
- [6] M.L. Shalz, B.J. Dalgleish, A.P. Tomsia, R.M. Cannon, A.M. Glaeser – Ceramic joining III. Bonding of alumina via Cu/Nb/Cu interlayers, Journal of Materials Science 29(1994), pp.3678-3690;
- [7] R.A. Marks, J.D. Sugar, A.M. Glaeser, Ceramic joining IV. Effects of processing conditions on the properties of alumina joined via Cu/Nb/Cu interlayers, Journal of material science 36 (2001), pp. 5609-5624;
- [8] B., Yiwang, H., Zhang, Y., Zhou, Mat Res Innovat (2002) 6, pp.277-280;
- [9] Z., Sun, D., Pan, J., Wei, C., K., Wong, Ceramics Bonding Using Solder Glass Frit, Journal of ELECTRONIC MATERIALS, Vol. 33, (2004) No. 12, pp.1516-1523;
- [10] Wang Juan, Li Yajian, Huang Wanqun, Materials Science, Vol. 45, No. 1 (2009), pp.125-131;
- [11] Jian Chen, Mingyuan Gu, Fusheng Pan, Metallurgical and Materials Transactions A, VOL. 32A, (2001), pp.2033- 2038;
- [12] Rajendra U. Vaidya, Partha Rangaswamy, Richard G. Castro, John J. Petrovic, and Darryl P. Butt, Use of Metallic Glasses in Molybdenum Disilicide-Stainless Steel Joining, JMEPEG Vol. 9 (3) (2000), pp.280-285;
- [13] A., Mihai, I., Voiculescu, V., Geanta, R., Stefanoiu, H., Binchiciu, D., Daisa, Research project no. 71-118/2007, NANOCERAD, Romanian PNCD I Program, 2007-2010, in Romanian;
- [14] L., Esposito, A., Bellosi, Joining ZrB₂-SiC composites using glass interlayers, JOURNAL OF MATERIALS SCIENCE, 40 (2005), pp. 4445 – 4453.



International Conference on Innovative Technologies, IN-TECH 2012,
Rijeka, 26. - 28.09.2012



EFFECT OF TYPES AND THICKNESS OF LOCAL EVAPORATIVE COOLING PADS INSIDE THE GREENHOUSES IN SUDAN

O. Abdelnaser¹, E. Elmsaad and M.R. Ismail¹

¹ School of Housing Building and Planning, Universiti Sains Malaysia, 11800, Minden, Pulau Penang, Malaysia, E-mail: naser_elamroni@yahoo.co.uk

Keywords: Greenhouses technology, temperature, air velocity, relative humidity, evaporative cooling pads.

Abstract. This study was conducted to evaluate the effect of different types and thickness of evaporative cooling pads on cooling efficiency inside the greenhouses. The tests were carried out at four levels of air velocity through the pad (0.7, 1, 1.5 and 1.75 ms⁻¹), respectively, with three levels of pad thickness (50, 100 and 150 mm), four types of evaporative cooling pads (celdek pads, straw fiber pads, luffa pads and sackcloth pads). The results obtained indicated that there was a significant difference between evaporative cooling pads types and cooling efficiency and highly significant difference between pads thickness and cooling efficiency and significant difference between environmental factors such temperature, relative humidity, air velocity, pressure and water flow rate and cooling efficiency. This study proved that the luffa pads were given high average of saturation efficiency and the study recommended that luffa pads are better than the other evaporative cooling pads.

1. Introduction

A greenhouse is defined as a structure used to protect plants from adverse climatic differences and supplies an environment favorable to plant production. This technique is needed to overcome the high hazards of open field production such as high rainfall, intense solar radiation, weed rivalry, as well as damages caused by diseases, insects, and high temperature and relative humidity [1]. The major purpose of the greenhouse is to raise the yield and quality of vegetable, fruit, flower and aromatic plant production. Moreover, the production can be made continuous throughout the year. The crop production in the greenhouses plays a significant function to supplying adequate food to offset the high import bill of processed and unprocessed horticultural products [2]. A greenhouse consists of several devices to help in controlling plant growth such as temperature, ventilation, and relative humidity, amount of light and carbon dioxide [3]. Evaporative cooling has many practical applications in agriculture. It has become standard for many poultry houses and greenhouses, and is used for swine and dairy cattle. A number of methods are available to protect animals and plants from heat stress due to the high temperature and low relative humidity inside the greenhouse during the summer season by providing optimal growing conditions. Of these methods the evaporative cooling pads system is the most common [4]. Evaporative cooling systems lower air temperature by using mists, sprays or wetted pads. However, introducing water into ventilation air increases relative humidity while lowering the air temperature [4]. Evaporative cooling pad is a reliable method and requires the greatest power consumption. Evaporative cooling systems are based on exchange of sensible heat to latent heat of evaporated water, where water is supplied mechanically. The temperature of air decreased due to evaporation of water in air. Thus, the temperature reduces at the expense of rise in humidity, while the enthalpy of air remains constant in the process. Presently evaporative cooling methods include fan pad, fogging system and roof evaporative cooling [5]. A pad-and-fan cooling system typically consists of axial-flow exhaust fans installed in one side and correctly-sized wetted pads placed along the opposing side. The fans exhaust air from the building and draw in fresh air through the pads. Fan should locate in the side of the building that is downwind of the summertime prevailing winds. To function properly, the fans must be able to develop a slight vacuum inside the building. This requires that the remainder of the building be reasonably airtight [6]. During the hot season the temperature of ambient air inside greenhouses and animal houses increases to over 40 °C causing thermal stress. Thus, there is a need to evaluate the use of locally available cheap materials as cooling pads, particularly in rural agricultural buildings. The need becomes urgent for their off-season production [7]. The evaporative cooling system has been accepted an effective, practical and economically feasible method under hot and arid climatic conditions for many poultry houses and greenhouses [8]. Present the main aim of the research first to determine the effect of type and thickness of local evaporative cooling pads on cooling efficiency inside a greenhouse. Then to investigate the effect of local evaporative cooling pads type and thickness on the environmental parameters (temperature, relative humidity and air velocity and drops pressure) inside a greenhouse, and to assess the optimum water flow rate for the different types and thicknesses of the selected evaporative cooling pads. The steady state will be developed in this research to collecting the data from experimental measurements. The type of experimental data is quantitative data. The experimental work was mainly concerned about effect of types and thickness of evaporative cooling pads (namely: celdek cellulose, straw fiber, sackcloth pads and luffa sponge pads), when used to change environmental conditions inside the greenhouses and also involve measurement of both environmental parameters (temperature and relative humidity and air velocity and drops pressure at different time during the day), with different evaporative cooling pads thickness parameters (50, 100 and 150mm) as well as water flow rates through the pads. The data obtained from the experimental and measurement will be analyzed with use of Statistical Package for the Social Sciences (SPSS).

2. Literature Review

The world situation for agriculture has been changed from abundant to limited resource applications, wide to concentrated farming practices, and random use of chemicals to wise applications, this situation led to the implementation of innovative technologies to face the ever rising demand for food crops in rejoinder to increasing world population. Moreover, the need developing new techniques for off-season production of food crops in response to consumer demands. The increasing demand for non-seasonal fruits, vegetables and other agricultural products needs controlled environments where it is possible to grow them irrespective of the ambient seasonal conditions currently; the greenhouse technology constitutes the most important method for meeting that need [9].

2.1 Scope of Greenhouses Technology

1. Cultivation in problematic zones such as too cold or too hot weathers, damage due to heavy rains, storms, barren and uncultivable lands, waste lands, deserts etc...
2. Greenhouse compounds a round city. Since there is often a larger and sustained demand of vegetables, fruits and ornamental plants throughout the year in big cities, greenhouses could be one of the right choices to meet different demands.
3. Export of agricultural produce – there is a high international demand for horticultural products like cut flowers. Cultivation of export – oriented crops will yield higher foreign substitute to the farmer.
4. Greenhouse for plant promulgation- they are useful for raising seedlings and cuttings, which need controlled environment. Various types of plant materials can be propagated using greenhouse capability.
5. Greenhouse technology for biotechnology – hydroponics or nutrient film technique involves controlled environmental conditions for growing. Also for tissue culture, greenhouse facilities are useful.
6. Cultivation of roses and medicinal plants – greenhouses can support a complimentary environment for production of these crops.
7. Greenhouse for employment generation and raise in income – It can create rural employment, minimize relocation to urban areas, higher returns from small and trivial land holdings and can generate better self-employment activities [1]. Each type of crop that fits greenhouse technology could be grown at home. In fact greenhouse technology can control the environment for wide spread growing of flowers, vegetables, fruits, and medicinal plants [10].

2.2 Greenhouses Constructions and Design

Greenhouses are constructed to preserve the micro - climate preferred by the crops to be grown. They are, in general, considered to be semi-permanent structures and are designed for a service life of 25 years. The structure is supposed to withstand loads due to its own weight, wind, snow and hanging baskets, and should permit maximum light transmission. In any crop production system, measurements of certain parameters are fundamental to the supply of a favorable environment for optimum production. In the case of the greenhouse, instrumentation is an essential part as each activity is governed by appropriate measurement of required parameters [11]. Greenhouses should maintain a controlled environment for plant production with satisfactory sunlight, temperature and humidity. Greenhouses require coverage to maximum light, mostly in the morning hours. Consider the location of existing trees and buildings when choosing your greenhouse site. Water, fuel and electricity make environmental controls possible that are important for positive results [12].

2.3 Greenhouse environmental requirements

Generally, the climatic requirements for plant growth can be summarized as follows [13]:

Plants grown under protected cultivation are those tolerant to average temperatures ranging from 17 to 27°C. Taking into consideration the warming- up effect of solar radiation in the greenhouse, the above temperature range can be probable without any heating arrangement when outside ambient temperature prevails in the range from 12 to 22°C. The absolute maximum temperature for plants should not be higher than 35 to 40°C. The mean daily outside temperature is below 12°C, the greenhouse must be heated, particularly at night. On the other hand when mean daily temperature is above 22°C, especially during summer, artificial cooling is essential. Humidity is expressed as the amount of moisture present in a unit mass or volume of air another commonly used term to express humidity is relative humidity, which is the ratio of the amount of water vapor present in the air to the amount of water vapor required to saturate. In a greenhouse, humidity is affected by the internal microclimate and the external climatic parameters (such as relative humidity, air temperature, air velocity, solar intensity, etc). Humidity affects the leaf area development and stomata conductance of vapor pressure [14]. The most important benefit of greenhouse invention is keeping the environmental conditions under control. One of the most significant environmental factors is the control of greenhouse temperatures. For plants grown in greenhouses, there are a variety of seasonal temperature requirements for each plant. In the controlled production environment, the temperatures necessary by each plant are controlled seasonally. The temperature raise becomes a major problem in greenhouses since glass or plastic cover materials are used in the design, evaluated to walls in other structures which block the penetration of both light and heat [15].

2.4 Evaporative cooling pads

Commercially available cooling pads are expensive, and accordingly, there is an urgent need to evaluate the performance of suitable locally available materials when used as cooling pads, particularly for rural agricultural buildings. In fact, many studies were carried out to evaluate the use of locally available materials as cooling pads, such as: expanded clay, sawdust, vegetable fiber and caol [16], discarded clay bricks, corn- cob and charcoal [17]; ground sponge, stem sponge, jute fiber and charcoal [18]. Moreover, the reported efficiency of some locally available materials was 79% for charcoal, 48% for hazelnut rind and 96% for wood shavings [19]; 89.6 to 92.8% for coir fiber [20]; 47.22% to 85.51% for fine fabric and 63.88 to 86.32% for coarse fabric [8]; 39.9% for palm fiber, 62.1% for jute [21]. Cellulose pads expanded clay and vegetable fiber were recommended as pad materials for evaporative cooling systems [16]. On the other hand, and according to the results of the study by Dzivama et al. [18], stem sponge showed superior pad material qualities compared to ground sponge, jute fiber and charcoal. Gunhan et al. [4] evaluated the suitability of some local materials such as pumice stones, volcanic tuff and greenhouse shading net as cooling pads. They found that volcanic tuff was a good alternative pad material. It gave an evaporative saturation efficiency of 63-81%. [Ahmed et al. (2011) studied sliced wood, straw and celdek cellulose as materials for evaporative cooling pads. Sliced wood pads have more cooling efficiency and crop productivity under greenhouse conditions [22]. From the researches mentioned above, there are no studies about luffa and spen fiber and sackcloth as wetted pad materials. In addition, both that pads materials mentioned above are low cost and easy-to-find in world. Therefore, we consider using those materials as evaporative cooling pad in terms of saturation efficiency and pressure drop across wetted pad. Evaporative cooling systems have many applications, from home and office cooling to animal housing. The principle of evaporative cooling is based on the fact that in order to change water to vapor at the same temperature a substantial amount of heat, known as the latent heat of vaporization, is required. If water at a constant temperature is allowed to evaporate in dry air the only way that this latent heat can be obtained is by taking it from the air. Air will absorb water vapor at a constant wet-bulb temperature. For converting water to water vapor, the necessary latent heat of vaporization is provided by the air. The air dry-bulb temperature, therefore, tends to drop to the wet-bulb temperature, and the degree of cooling is reliant on the efficiency of the air-water mixer [23].

3. Conclusions

Based on the results, the following can be concluded:

For the first objective, the analysis shows that the pad type significantly affects the cooling efficiency. Luffa pads (LPs) had higher saturation efficiencies compared with the straw fiber (SP), celdek (CP), and sackcloth (SaP) pads. Moreover, the current study proves that pad thickness also has a highly significant effect on cooling efficiency. The results show that thicker pads of 150 mm have efficiencies

higher than those of 50 and 100 mm. With regard to the second objective, the results indicate that most environmental factors, particularly temperature and pressure drops, significantly affect the performances of different pad types. Moreover, the current study shows a highly significant relationship between pad thickness and all environmental factors. The pressure drops of airflow significantly increase with the increase in air suction velocity, pad thickness, and water flow rate ($p < 0.01$). Air velocity has a major effect on pressure drop, whereas the water flow rate has a lesser effect. The pressure drops of airflow through the SaP pad were less than 30 Pa under all conditions. For the third objective, pad type, water flow rate, and pad thickness were proven to affect efficiency. The efficiency increased when the pad thickness and water flow rate were increased. Moreover, it was found to be significantly related to other environmental factors, such as temperature and relative humidity. It increased when the pressure drops and air velocity increased. The current study examined the saturation efficiency and pressure drop when a wet LP and SaP, CP, and SP were used in an evaporative cooling system. After a comparison with commercial wet pads, the average saturation efficiency of the wet LP was found to be 73.67%, whereas those of CP, SP, and wet SaP were 70.33%, 71.87%, and 71.21%, respectively. However, the pressure drops of the wet LP and SaP, CP, and SP were significantly different (Table 1). A relationship between pad thickness, cooling efficiency, and environmental parameters was observed. When the pad thickness was increased, the water flow rate, pressure drop, and relative humidity also increased, but temperature and air velocity reduced (Table 2). Moreover, pad thickness and cooling efficiency were also found to be significantly related. All greenhouse parameters significantly affected cooling efficiency. These parameters include temperature, relative humidity, water quantity, pressure drop, and air velocity (Table 3). A significant difference was found between pressure drop, air velocity, and cooling efficiency depending on the different pad types and thicknesses.

Table 1: Descriptive Analysis of the Parameters

Parameters	Types (mean)				Total Mean	SD
	CP	SP	LP	SaP		
Thickness	150	150	150	150	150	41
T in	27.33	24.20	26	28.69	26.55	3.07
RH in	72.06	77.68	73.16	70.34	73.31	6.43
WFR	19.57	16.11	30.41	23.22	22.33	9.87
AV in	1.58	1.65	1.38	2.55	1.77	10.97
Pa	82.71	83.30	92.47	30.98	73.12	45.96
μ	70.33	71.87	73.67	69	71.21	10.93

Table 2: Relationship between evaporative cooling pad types, environmental parameter and cooling efficiency

parameters	types	Tem in	RH in	WFR	A V in	pa	μ
types	1						
Tem in	-.359**	1					
RH in	.110	-.446**	1				
WFR	.287**	-.685**	.589**	1			
AV in	.045	-.078	.092	.176	1		
Pa	.467**	-.239**	.176	.346**	.175	1	
μ	.623**	-.768**	-.002	.763**	.108	.283**	1

Table 3: Relationship between Cooling Pad Thickness, environmental parameter and cooling efficiency

	thickness	Tem in	RH in	WFR	AV in	pa	μ
thickness	1						
Tem in	-.804**	1					
RH in	.577**	-.446**	1				

water	.820**	-.685**	.589**	1			
Air v in	-.242**	-.078	.092	.176	1		
Pa	.305**	-.239**	.176	.346**	.175	1	
μ	.927**	-.768**	.623**	.763**	.108	.283**	1

*Correlation is significant at the 0.01 level (2- tailed)

Acknowledgements

The authors would like to acknowledge the support which is given by TWAS organization and also special thanks go to the Universiti Sains Malaysia, School of Housing Building and Planning, Penang, Malaysia.

References

- [1] A.K., Sharam, V.M., Salokhe: Greenhouse Technology and Application. First edition, (Agrotech Publishing Academy, England, 2006).
- [2] K., Rezuwan: Design and development of tropical greenhouse structures. *Proceedings of 2nd World Engineering Congress* (2002), pp. 22-25. Sarawak, Malaysia.
- [3] J. Badgery-Parker: Agnote DPI/249. Edition 1, (1999) pp. 1–2.
- [4] T., Gunhan, V., Demir, A.K., Yagcioglu: Evaluation of the suitability of some local materials as cooling pads. *Biosystems Engineering*, Volume 96 (2007) p. 369-377.
- [5] A., Ganguly, S., Ghosh: A Review of Ventilation and Cooling Technologies in Agricultural Greenhouse Application. *Iranica Journal of Energy & Environment* 2 (1): 32-46 ISSN 2079-2115 Department of Mechanical Engineering, Bengal Engineering and Science University, Shibpur, Howrah-711103, (West Bengal, India, 2011).
- [6] Bucklin, R. A., Leary, J. D., McConnell, D. B., Wilkerson E. G. (2010). Fan and Pad Greenhouse Evaporative Cooling system, University of Florida, Gainesville FL. Vol.70, No. 1, pp.59-65. U.S.A.
- [7] H.H., Öztürk, A., Başçetinçelik: Greenhouse Ventilation. *Türkiye Ziraat Odaları Birliği Yayınları*. Yayın No. 227, (Ankara, Turkish, 2002).
- [8] C.M., Liao, K.H., Chiu: Wind tunnel modeling the system performance of alternative evaporative cooling pads in Taiwan Region. *Building Environmental*, Volume 37 (2002), p. 177-187.
- [9] M.O., Abdeen: The effect of air pollution and thermal comfort in greenhouses. *ibdigital.epn.edu.ec/bitstream/15000/9377/1/P21*, (2009).
- [10] H.Z., Enoch, Y., Enoch: The history and geography of greenhouses (1999).
- [11] B.V., Elsner, D., Briassoulis, D., Waaijenberg: Review of structural and functional characteristics of greenhouses in European Union countries, Part II: Typical Design requirements. *Journal of agricultural Engineering Research*. (2000) p75:1-16.
- [12] W., John: Greenhouse Heating, Cooling and Ventilation. Biological and Agricultural Engineering. University of Georgia colleges of agricultural and environmental sciences. Family and consumer sciences (2009).
- [13] H., Verlodt: Greenhouses in Cyprus, protected cultivation in the Mediterranean climate. FAO, Rome, Italy (1990).
- [14] O., Jolliet, A., Hortitrans: A model for predicting and optimizing Humidity and Transpiration in greenhouses. *Journal of Agriculture Engineering and Research*, Volume 57 (1994), p.23-37.
- [15] O., Hasan, A., Atilgan, B., Kenan, A., Taner: The efficiency of fan-pad cooling system in greenhouse and building up of internal greenhouse temperature map. *African Journal of Biotechnology* Volume 8 (2009), Issue 20, p. 5436-5444.
- [16] I.F., Tinoco, J.L., Figueiredo, R.C., Santos, J.N., da Silva, T., Yanagi, M., de Paula, N.L., Puglisi, R.B., Vigoderis, M.B., Corderio: Comparison of the Cooling Effect of Different Materials used in Evaporative Pads, (2001) pp 438–442. Campinas, SP, Brazil.
- [17] W., Chunchai: *Application of discarded clay brick and charcoal as cooling pad material for dairy stanchian barn*. Dissertation. Retrieved August 9 (1998), On line at: www.chiangmai.ac.th/abstract/abstract/agi/abstract.
- [18] A.U., Dzivama, U.B., Bindir, F.O., Aboaba: Evaluation of pad materials in construction of active evaporative cooler for stroge of fruits and vegetables in arid environments. *Agricultural Mechanization in Asia, Africa and Latin America*, Volume 30 (1999) Issue (3), p. 51–55.
- [19] M., Dağtekin, G.A., Gürdil, Y., Yıldız, A.N. Uluocak: A research on determination of the efficiency of the different type pad materials of using in evaporative cooling system (fan-pad) in poultry houses. *Proceedings*, (1998) pp 850–857, Tarımsal Mekanizasyon 18, Ulusal Kongresi.
- [20] C.M., Liao, S., Singh, T.S., Wang: Characterizing the performance of alternative evaporative cooling pad media in thermal environmental control applications, *Journal of Environmental Science & Health, Part A –Toxic / Hazardous Substances & Environmental Engineering*, Volume 33 (1998) Issue 7, 1391–1417.
- [21] F. Al-Sulaiman: Evaluation of the performance of local fibers in evaporative cooling. *Energy Conversion Management*, Volume 43 (2002) p. 2267-2273.
- [22] E.M., Ahmed, O., Abaas, M., Ahmed, M.R. Ismail: Performance evaluation of three different types of local evaporative cooling pads in greenhouses in Sudan. *Saudi Journal of Biological Science*, Volume 18 (2011), p. 45-51.
- [23] R.P. Van: *Fruit and vegetable production in warm climates*, (MacMillan, London, 1997), p.486.

INVESTIGATION TO DISTRIBUTION OF ADDITIVES IN OPEN- AND CLOSED-CELL ALUMINUM FOAM

D. Schmidt¹, R. Albrecht¹ and G. Lange¹

¹ Department of Metal Materials and Composites, Gustav-Kirchhoff-Straße 6, 98693 Ilmenau, Germany

Keywords: aluminum foam, fine structure-macro structure-property relationship, additives, lightweight

Abstract. New fields of applications can be developed with the porous structure of cellular materials. In addition to polymer and ceramic foams, especially cellular metallic materials, metal foams, are in our focus of research. Its porous structure allows us to achieve low specific densities. Metal foams can be used as a high energy absorption material particularly for lightweight applications. The production of closed-cell and open-cell metal foams is done by melting or powder metallurgy processes. In practice, primarily aluminum-based foam materials find their application in small series.

The reproducibility of mechanical and functional properties needs a homogeneous pore distribution. The cost-intensive production process of the open-cell metal foams gives a more homogeneous structure than closed-cell metal foams. During the foaming process of powder metallurgy foams, a variety of parameters have an influence on the pore distribution. In addition to the temperature regime, especially the alloy components and additives are important. Above all, the structure-property-relationship of cellular materials is most significant. In this paper, micro- and macro-structures of closed-cell aluminum foams are analyzed and compared as well as the additive distribution in the material (such as titanium from the foaming agent TiH_2).

The goal is to analyze the distribution of the alloy components in the foaming process for a systematic optimization of the manufacturing process in terms of powder composition, powder sizes, compaction ratio, heat treatments and temperature regime.

Introduction

The commercial use of closed-cell metal foams in a large-scale production is currently inhibited mainly by anisotropic and poorly reproducible properties. The influence of various parameters during the manufacturing process is important to the final structure of the material. In addition to material composition, it is primarily the additives that must be considered during the preparation process in a systematic structure investigations. Starting from commercially produced aluminum foams (produced by Alporas method), the influence of the aluminum powder, foaming agent, production of semi-finished goods and foaming parameters with the aim of a more homogenous pore distribution are investigated. In this paper, light microscopic and scanning electron microscopic studies on the distribution of elements in aluminum closed-cell foams, which were generated in different production types, are presented.

Production of cellular metals

Cellular metallic materials can be produced principle in two different ways. In addition to some special forms, melting and powder metallurgy are the main production routes. Figure 1 shows an overview of both production variants with names of conventional products. Next to the kind of production, especially the resulting foam structure is essential for isotropic properties. Compared to closed-cell foams, open-cell materials show an advantage of permeability, for example as a catalyst for liquids and gases. Furthermore open-cell materials exhibit a very homogeneous pore distribution. The resulting structure can be produced by predefined PUR foam according to the principle of lost form. On the other hand, closed-cell metal foams can be produced by melt and powder metallurgy process and offer a great potential as a lightweight material and potential applications as an energy absorbing material [1].

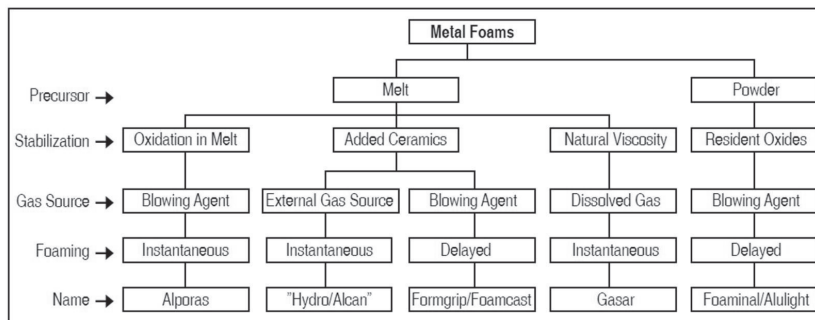


Fig. 1: Overview of the production process of metal foams [3]

The closed-cell foam (Alporas) consists of pure aluminum (Al 99.7) with approximately 1.5 wt% calcium and 1.5 wt% titanium from the foaming agent (TiH_2). Supplying heat during the melting process, the hydrogen from the foaming agent is going to be gaseous and thereby the pores develop. The Alporas foams exhibit a relative density of 0.2 to 0.25 g/cm^3 , an average pore size of 3 - 5 mm and a porosity of 89 - 93% [2, 5].

Attempts of foaming by powder metallurgy

The production of cellular metallic materials with aluminum powder by adding a foaming agent (TiH_2) was developed by the IFAM in Bremen. Larger volumes are produced by using a foaming agent in a melting metallurgical process. For smaller sizes powder is predominantly the basic material for the production of closed-cell foams made by a powder metallurgical process. To ensure isotropic mechanical properties is the main goal. Thus, possibilities of technical application as a large-volume production can be found. Hence a reproducible, in a narrow range of very finely divided pore arrangement is necessary. Many parameters have an influence of the resulting pore structure: The choice of the foaming agent, additives, particle size and distribution of the starting powder, particle size and distribution of the mixture ratio of powder and foaming agent, compaction of the semi-finished product, temperature control and furnace residence time. In initial experiments, aluminum powder was mixed with titanium hydride (TiH_2), compacted with the aid of press tools and foamed in a laboratory furnace. An overview of the used parameters is shown in Table 1.

Tab. 1: Overview of attempts of foaming with different parameter

No.	T [°C]	t [min]	Compression [kN]	Compression [MPa]	TiH ₂ [wt%]
1	800	10	40	127	2
2	800	15	40	127	2
3	900	30	40	27	2
4	850	5	100	318	2
5	850	5	150	477	5
6	850	5	200	637	5
7	850	10	140	446	2
8	850	7	140	446	2
9	850	5	140	446	5

The foaming agent (TiH_2) was made in an inert atmosphere and has a particle sizes smaller than 40 μm (Figure 2, left). A scanning electron microscope image of the semi-finished powder preform (Sample 5: Al-preform with 5 wt% TiH_2 and 150 kN compression) is shown in Figure 2, right (grounded, polished, etched with 5% NaOH for 1 min). The aluminum particles, the TiH_2 particles and the porosity of the sample are identifiable to each other. On the severally regions, needle-shaped structures are recognizable. They are newly formed after the foaming process (Compare with Figure 6).

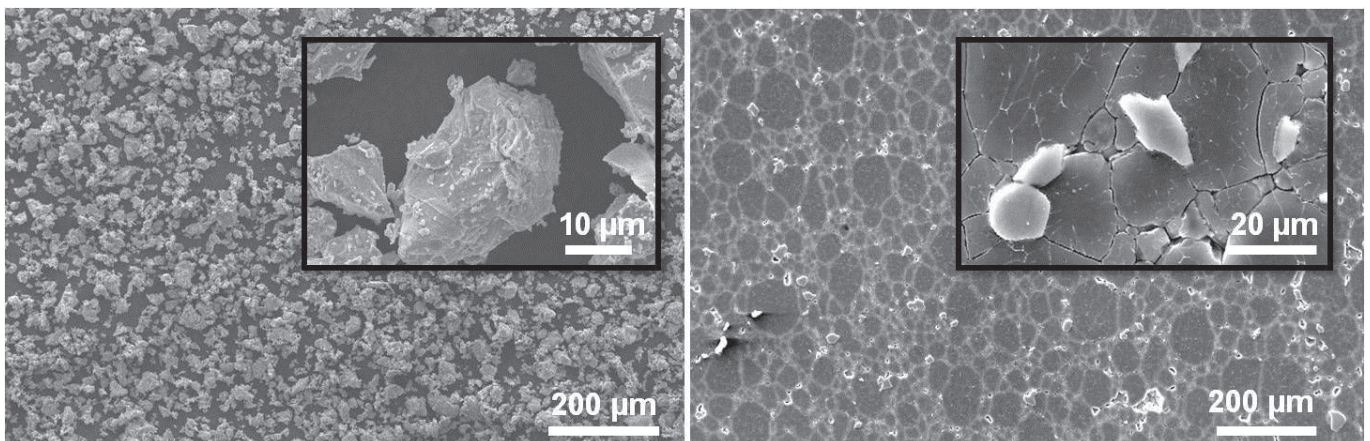


Fig. 2: SEM-investigation of TiH_2 (left), SEM-investigation of a preform of aluminum powder and foaming agent (titanium hydride) – sample polished and etched with NaOH

Structure analysis

The uniform pore distribution is the main challenge during the production of closed-cell metal foams. Figure 3 shows light microscopic pictures of Alporas foam. In addition to an uniform pore size distribution particularly pores with a diameter greater than 6 mm are adversely in terms of mechanical properties. This was demonstrated by static compression tests, plunger with a diameter of 10 mm showed a very large fluctuation in the plateau region in the tension-compression-diagram of metal foams.

Quite clearly is the broad distribution of pore sizes (Figure 3, left). The average pore diameter is in the range between 3 and 5 mm. Mainly, the larger pore diameters are a local weakness in external mechanical stress test. Further the pore walls show of an additional porosity. Figure 3 shows a light microscopic picture of closed-cell walls with the recognizable cell wall porosity, which was etched after

various grinding and polishing steps with NaOH. During the production of Alporas foam the foaming agent TiH_2 is used. TiH_2 decomposes at temperatures above $550\text{ }^\circ\text{C}$ to elemental titanium and hydrogen. Calcium is added to adjust the viscosity of the melt. Element distributions in the aluminum foam were investigated by EDX-examinations in scanning electron microscope. In Figure 4, in addition to scanning electron microscopic pictures of a cell wall, the element distributions of aluminum, calcium and titanium are shown.

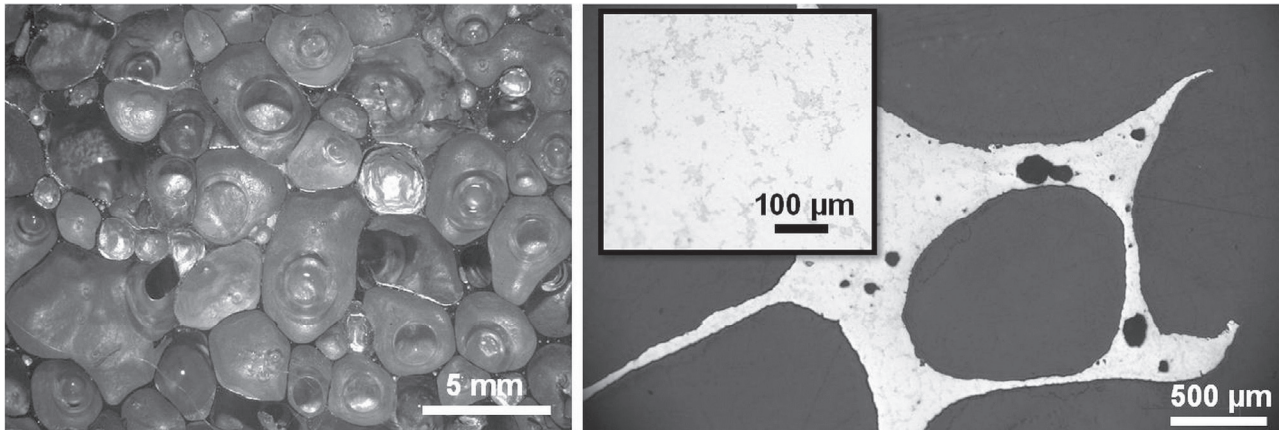


Fig. 3: Light microscopic investigations of Alporas foam (left),
Sample was polished and etched with NaOH (right)

In comparison to the closed-cell aluminum foams (Alporas) in initial experiments samples produced by a powder metallurgical route were produced only with different amounts of the foaming agent. The first goal was to generate a foaming process as a function of powder particle size, the amount of foaming agent, the grade of compaction, temperature and residence time in the furnace (Overview of results: Figure 7).

The influence of different additives (e.g. calcium, different salts) on the oxide layer of the aluminum particles and the viscosity of the melt is under investigation. As in the first series of experiments, the 99.7 Al powder is only added with titanium hydride, especially the titanium distribution is important within the powder compact. After the foaming process, the titanium remains irregular in the aluminum base material to form intermetallic phases of Al-Ti (compare Figure 6, left).

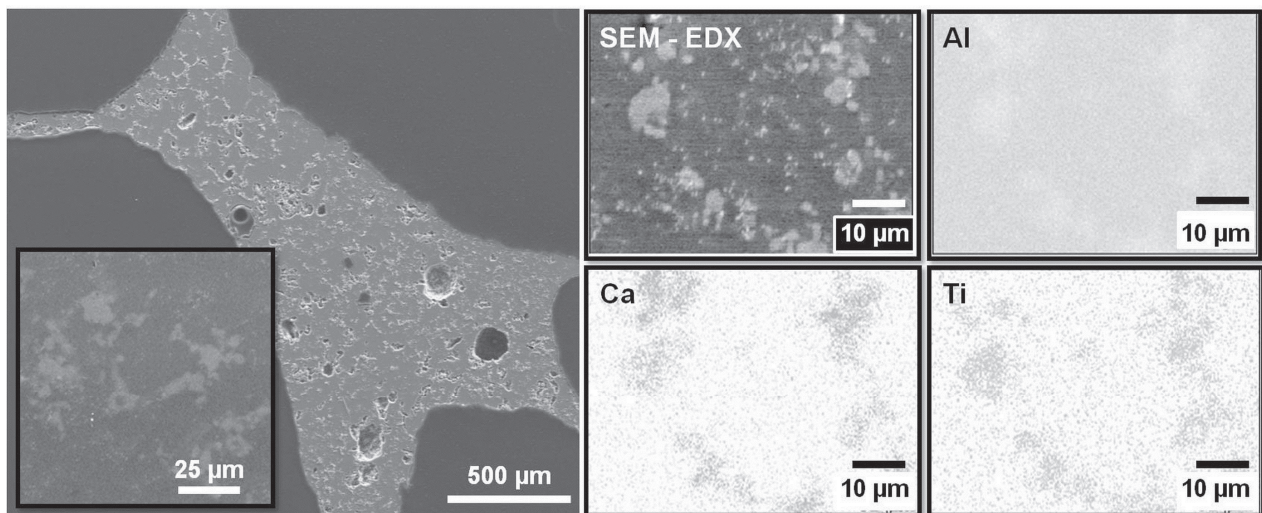


Fig. 4: Scanning electron microscopy analysis of Alporas foam (left) and EDX mapping (right)

Conclusion

Closed-cell aluminum foams offer interesting properties due to their composition. A reproducible production on melting or powder metallurgical routes, which has no defined homogeneous pore distribution, is still a handicap that hinders the application of such devices in series. The influence of different additives and the parameters during the foaming process are primarily the most important indicating devices in terms of mechanical properties. Therefore the relation to the emerging micro structure-macro structure-property relationship is the main item for future metal foam developments. An overview of the main influencing factors is shown in Figure 5.

The pore size distribution referring to the macro structure is the main difference between melting and powder metallurgical produced foams. Variations in the microstructure are results from the starting materials. Aluminum tends to oxidation, especially in regions

near the surface. Alporas foam was produced under an inert atmosphere. In contrast to the powder metallurgical aluminum foam the several particles are clearly visible and limited by needle-shaped structures (Figure 6).

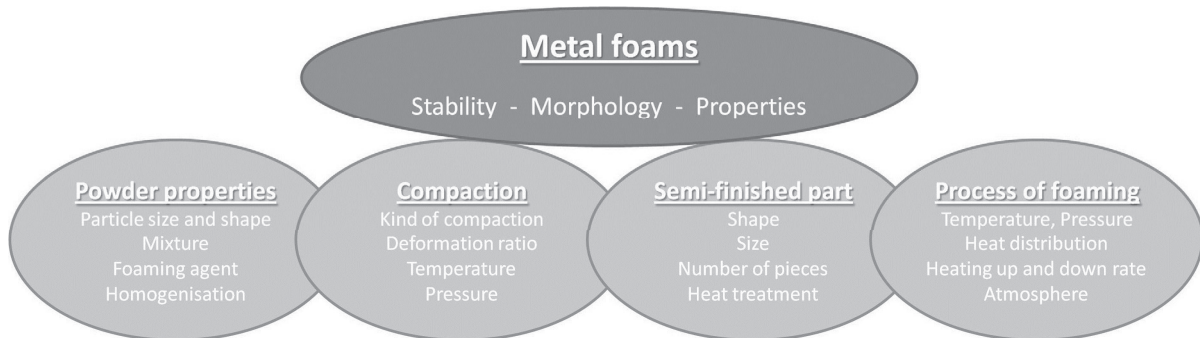


Fig. 5: Influencing foaming factors of powder metallurgical manufactured metal foams [4]

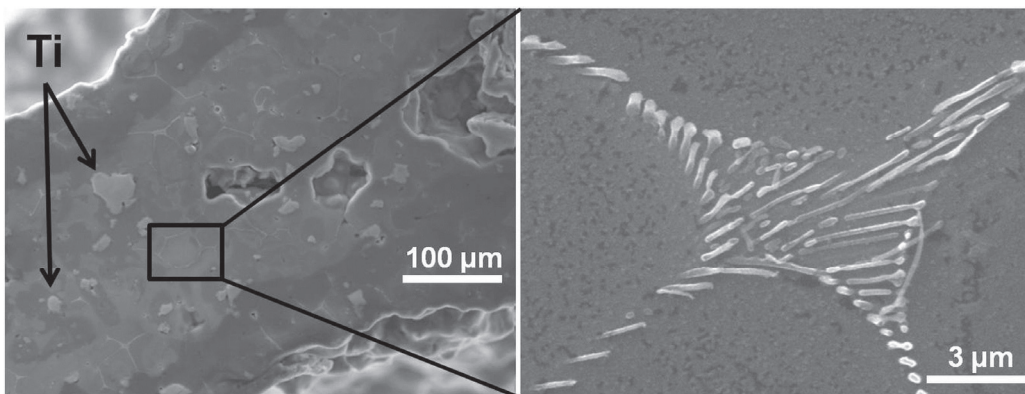


Fig. 6: Scanning electron microscopy analysis of own fabricated Al-foams

The goal-oriented examination of defined parameters will be the subject of further investigations. The results presented in this paper provide a first overview of the influence of content of foaming agent, the grade of compaction, as well as temperature and residence time during the foaming process. The first results are shown in Figure 7.

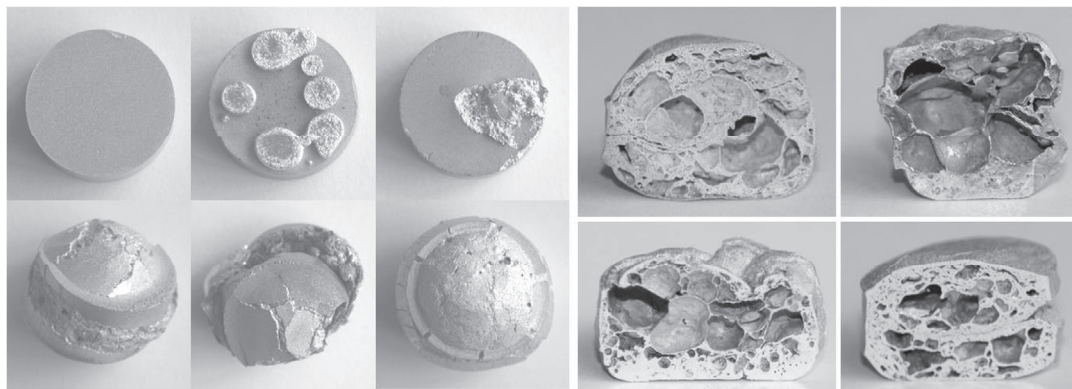


Fig. 7: Overview of self-manufactured aluminum foam samples in relation to Table 1; left: sample 1, 2 and 3 above, and 5, 6 and 9 below, right-hand side: cut through sample 4 and 7 above, respectively 8 and 9 below

References

- [1] Ashby, M. F.; Evans, A. G.; Fleck, N. A.; Gibson, L. J.; Hutchinson, J. W.; Wadley, H. N. G.: Metal Foams: A Design Guide; Woburn, MA; Butterworth-Heinemann; 2000
- [2] Hipke, T.; Lange, G.; Poss, R.: Taschenbuch für Aluminiumschäume; 1. Auflage; Aluminium-Verlag Marketing & Kommunikation GmbH; Dezember 2007; ISBN 978-3-87017-285-5
- [3] Banhart J., Weigand, P.: Powder metallurgical process for the production of metal foams in "Metal Foams", Editors: J. Banhart und H. Eifert, Verlag MIT, Bremen (1998), p. 13-22



-
- [4] Banhart, J.: Manufacturing routes for metallic foams; Journal of Minerals, Metals and Materials Society; Volume 52; Number 12; 2000; p. 22-27
- [5] Lange, G.; Schmidt, D.: Leichtbau mit hybriden Werkstoffsystemen aus Aluminiumschaum und Kunststoff; Tagungsband 32. EFB-Kolloquium 2012 „Produktionssysteme und -methoden für den Leichtbau - Wegbereiter zur E-Mobilität“; 4.02.-15.02.2012; Bad Boll; ISBN 978-3-86776-380-6



International Conference on Innovative Technologies, IN-TECH 2012,
Rijeka, 26. - 28.09.2012



PROBLEM OF FLOW CONTROL OF PRODUCTION MAKE TO ORDER

J. Trojanowska¹ and E. Pająk¹

¹ Poznan University of Technology, Institute of Mechanical Technology, ul. Piotrowo 3, 61-138 Poznan, Poland

Keywords: production flow control, make to order, theory of constraints

Abstract. This article presents an original methodology for production flow control of multiproduction make to order in conditions of limited resources. The presented methodology has been developed based on the assumptions of the theory of constraints, but as support it can be also used lean manufacturing tools. The methodology shows the procedure from point when new production order are put to production department to the moment when it appears on production schedule so as not to cause conflict resources. The presented methodology can be successfully used in small and medium-sized manufacturing companies which offer a wide range of products.

Introduction

Considerations in this section are related to production flow control, so to concern the operating level of function of the enterprise. But it should be noted that the assumptions input to determine the production flow control method must be closely related to the previously developed plan of production, and this in turn results from the manufacturing strategy relate with families of products, also called competitive strategy.

The choice of production strategy for each product family is affected by many factors, such as specific of orders, complexity of products, individual customer requirements. As shown in practice, a company can produce a family of products which adopted different manufacturing strategies. It should be noted that the competitive with one of three factors - time, quality, price - means that the other two are satisfied to the extent acceptable to the customer.

The time competition specially is used for the production or assembly to order and based on implementation of orders in the time required by the customer. The strategy based on time competition is associated with a pull production flow control system consisting of synchronized production purposes, such as lot size, with current customer orders, and not as a push production flow control system, with forecasts of demand.

The price competition is typically for products make to stock. Production is then planned in front and based on the best use of productive resources, thereby rationalization the production costs resulting from a desire to achieve the lowest manufacturing costs.

The quality competition focuses on type of production - engineering to order, but also may relate to products make to order and make to stock, but only in the case of strong brand.

Depending on the type of production adopted different ways of production planning. In the case of production make to stock plans based on the forecast, in the case of engineering or make to order production planning is based on actual reported demand. In the case of assembly to order production planning is a link both ways.

Planning based on forecast demand is burdened with a big mistake because of the difficulty in accurate prediction of the future. However, the implementation of plans prepared for production make to order is not easy. The company must take care of business because the owners, shareholders, so to generate profit. To accomplish this must meet customer requirements, which are constantly changing. This is not always possible to reconcile due to some internal constraints in the enterprise. Fig. 1. illustrates the factors affecting the functioning of the production system.

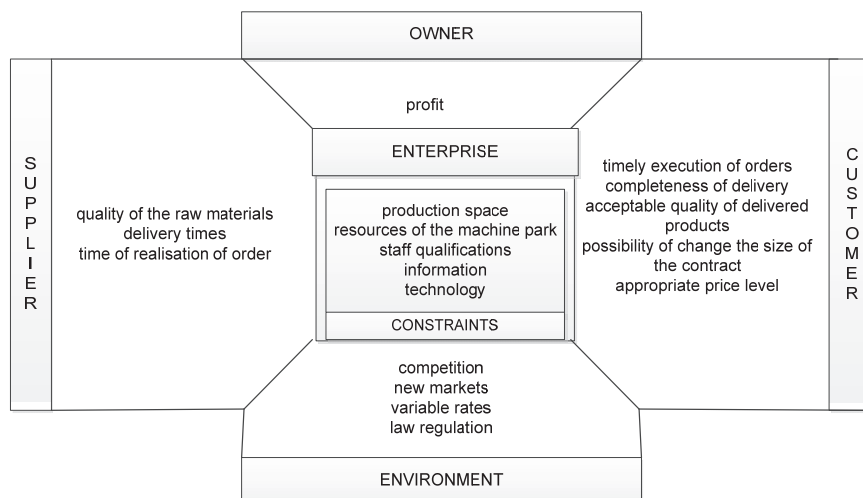


Fig. 1. Factors affecting the functioning of the production system. Source: Own Study

On companies internal constraints consist such elements as inter alia determinants of production space, manufacturing resources, qualifications of employees and others. Setting the company, so customers and suppliers are the source of much variation. Factors

affecting the production plans from suppliers side are: untimely supply, long procurement lead times, poor quality of the raw materials, etc. However, customer requirements which must be considered when planning the production include: product quality, proper price level, an acceptable limit for completion order, complete delivery. Taking into account the factors that affect the feasibility of production orders, please note that the owners or shareholders interested in the profitability of the company, thus obtaining a positive financial result.

As show the results of recent studies [1], conducted on a sample of 192 manufacturing companies from Wielkopolska Region, on the actions taken under the mitigation of the economic crisis last three most frequently occurring response are: to search for a new markets, reduction of production workers and expand the range of products offered. Gaining new clients while diversifying products and reduced employment makes the implementation of production flow control tasks is becoming increasingly difficult due to the dynamically changing environment. On the one hand, this is the need for a profit at a certain level, on the other constantly increasing competition, increasing customer expectations regarding product quality and timeliness of deliveries, etc.

The current market situation and the increasingly common among small and medium-sized manufacturing company strategy of diversification leads to an expansion of its assortment. The wide range of assortment and varied size of the order makes that part of the product range is manufactured in a warehouse, and part of the order. Purchase of raw materials for production is forecasted, which always is erroneous, the greater the longer time horizon of forecasting concerns. A wide and instable assortment causes that it is difficult to predict in advance the appropriate size of potential orders and their likely timing. In addition it is a trend to reduce the average time between the date of receipt of the contract and the date of its execution [2]. Various dates of production orders, insufficient productive resources, problems with timeliness of supply of raw materials cause significant difficulties in planning production, requiring constant adjustments of production plans need to enforce control. Analyzing the situation of manufacturing enterprises should pay attention to certain difficulties that arise in almost every company involved in the manufacture of a wide range of products under different sizes of contracts intermittently flowing. Those include:

- high costs of maintaining stocks of raw materials and storage between operations,
- a long time of flow of material through the production system affects the quality of the finished product
- failure to meet customer orders,
- lack of information online about the current state of realization individual orders,
- plan of production become out of date very fast.

The high variability of conditions both internal and external is a source of serious problem greatly hinders production planning. To manage the manufacturing system of a company the multitude of decision have to be made: setting capacity levels, determination of the production programs, deriving lot sizes, and scheduling jobs on the shop floor [3]. Presented in this paper algorithm is a proprietary solution that could be applied to the planning and production control of multiproduction under limited resources.

Main assumption of TOC

Theory of Constraints (TOC) was published for the first time in 1984 in the book *The Goal: Excellence in Manufacturing* and it was created by a Hebrew PhD physicist Eliyahu Moshe Goldratt. The Theory of Constraints is a new paradigm of running a business. However, the present manuscript will show the theory in relation to problems of productive companies in a financial aspect. Theory of Constraints focuses on system improvement which is define as a series of independent processes. An analogy for a system is chain. Chain means a group of independent links working together toward the overall goal and a weak link is the constraint [4]. TOC assumes that it is possible that there is one cause which has many negative effects. This cause is limiting the system which is divided into external (not depending on a company) and internal. It needs to be pointed out that the constraint connected with company's policy and strategy constitutes even 90%, while the constraints connected with the supplies comprise only 8% [5]. The element of a system which bandwidth determines the efficiency of the whole system is called a bottleneck. Every system has at least one constraint [6]. Finding this element is the basis for improving the production system which, according to TOC, is composed of five steps and is some kind of cycle. The five focusing steps:

- Identify system's constraint: The first step on the way to perfection is finding and accurate pointing to system's supply which limits global efficiency. According to TOC, it is this particular supply where changes should be introduced as improving other elements of a system and improving local efficiency will not lead to improving whole system's efficiency because it is the weakest link which affects global efficiency.
- Decide how to exploit system's constraint: The second step of TOC points one's attention to the fact that the supply identified as system's constraint should be exploited to its maximum. Such exploitation can be achieved thanks to bottleneck's constant work. An increase in bottleneck's exploitation can be also achieved by moving some activities to other less loaded work posts which are technologically adapted to doing these activities [7].
- Subordinate everything else to the above decision: Previous step has made system's constraint work with maximum efficiency so step 3 is to adjust the pace of other elements to constraint's pace of work. Otherwise, if we allow other elements to produce faster and more, we are going to generate expenses. It can increase local efficiency but it will not help in increasing the overall process.
- Elevate system's constraint: Step 2 and 3 are very important in TOC as they contribute to sorting the system. There are still, however, many methods to increase production and improve the system. Step 4 of TOC allows for investments which contribute to increasing the efficiency of the whole system by strengthening the constraint. It can be achieved by increasing the number of annual shifts.
- If in the previous steps a constraint has been broken, go back to step 1, but do not allow inertia to cause system's constraint: Breaking the constraint should be achieved by a constant increase in the efficiency as a result of realising step 4. Then another supply which limits system's prospects should be found. Discussed steps have been shown in figure 2 as a process of constant improvement.

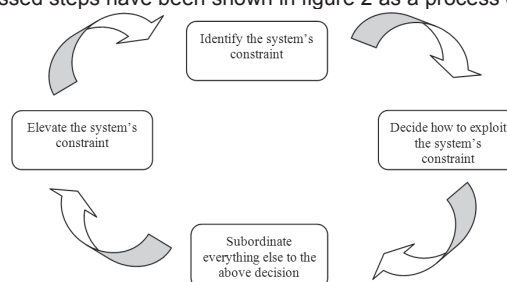


Fig. 2. The process of continuous improvement in TOC. Source: Own Study

Realising the steps, or actually TOC cycle, in appropriate way will make the constraints stop be perceived as something bad. On the contrary, they will become a chance for developing a company. Nevertheless, a bottleneck should not be ignored "There is really no choice in this area. It is us who manage the constraints. Otherwise, the constraints can manage us. Constraints will determine the size of production whether we will acknowledge their existence and manage them or not" [8].

Algorithm of planning and flow control of multiproduction

The algorithm shown in figure 3 presents the subsequent steps in the planning and production control. The procedure according to the steps described in the algorithm should be started when the production department, for example the production manager, will receive the information about a new order from the customer.

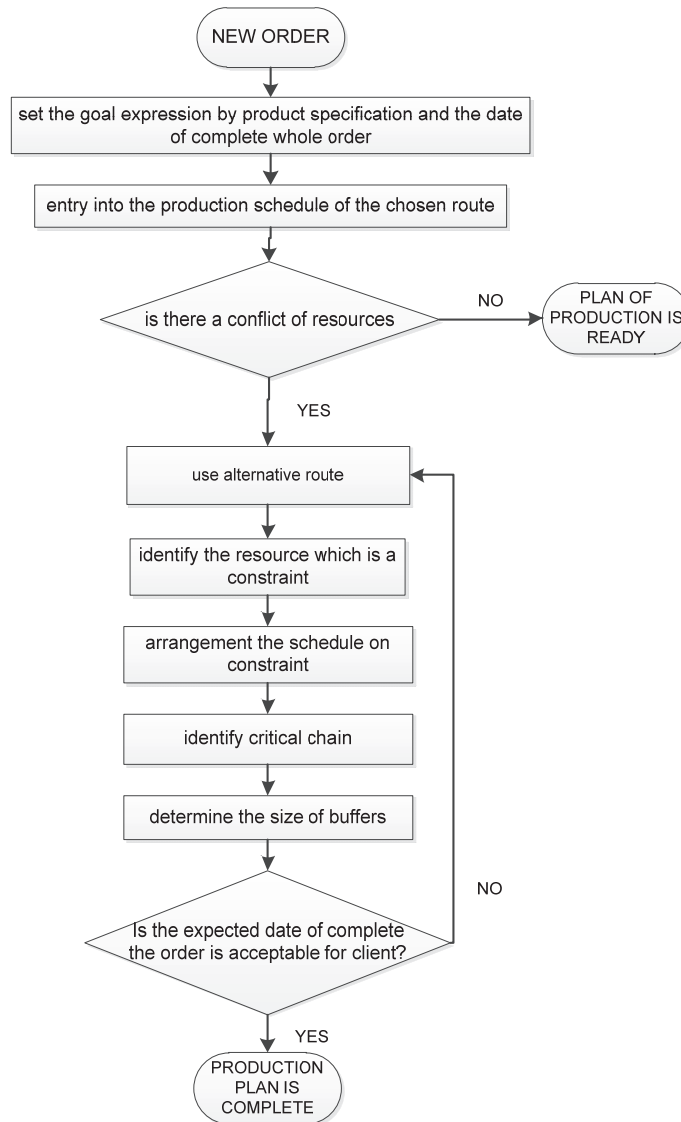


Fig. 3. Algorithm of flow control process of production make to order. Source: Own Study

Describe of methodology

The first step is to clarify the purpose, what is mean:

- definite article; clarify customer requirements, particularly important in the case of production make to order, determine product specifications, this point allow also to determine what are the specification requirements of a resource that must be engaged in the manufacture of that product;
- setting a deadline for order completion, as the deadline for order completion shall be deemed to transfer the entire requested assortment, listed on the production order, to warehouse of finished goods; depending on the type of order processing the deadline for order completion for example may result from a procurement or contract terms which where agreed by the manager of production with an eye to the best use of production resources.

In the first step it is also possible to determine priority order, for example, depending on whether the product is manufactured on the magazine (low priority) or for example a product produced under the auction (high priority).



The next step is to physically enter the current timetable for the production of new orders, the assignment of its implementation to specific resources, according to the most optimal route. To perform this step is necessary to in-depth knowledge of technological operations.

The third step is the identification of resource conflicts, so to check whether the input to the timing of new orders are not charged while the same resources and whether we have such a number of direct production workers, who provide support for all necessary and relevant to the process of manufacturing machines.

The fourth step is to use alternative routes in case of local constraint. If in previous step a collision or a lack of resources is detected. Then to the production schedule should be add an alternative route, or provide alternative resources on which it is possible to implement the order. The choice of alternative route are connection with the product strategy (time, quality or costs). Used route have an impact on the specifics of the contract, once it must be produce as soon as possible, while other in the best quality. It is important to remember the terms of the contract award (the requirements for the timeliness, quality, customer special requests). The implementation of this step is intended to circumvent local constraints. It may happen so that irrespective of the route and so would there be a resource conflict. Then go to the next step - the identification of constraints.

Identification of constraints means indication the resource which caused that production process couldn't make more elements. It could be for example machine or employee. It is easy to indication the constraint by check amount of work in progress before every production position. It is high probably that the position before which there are the biggest work in progress is the system constraint. If making further orders different resources are identified as constraints, then we are dealing with local constraint. However, if the long-term observation is that generally the same resource, the machine or employee is a source of production slowing down, then we are dealing with a global constraint.

Step number five is to arrangement the schedule on constraint. To achieve this step first it is important split the orders on which involves a resource which is define in the previous step as a constraints and those that do not involve this resource. Then the scheduled should be supplement by orders identify in first group, it should be placed in the schedule in the way which caused uninterrupted operation of resource identified as a constraint. Through the implementation of this step is possible to identify the critical chain.

Next step is to determine, based on experience and practice of business, size of buffers. Timing buffer should be shown between successive tasks on the critical chain to secure the implementation of further orders in case of delays on any of the tasks. Timing buffers should also be placed on the paths come to tasks which are on critical chain because in case to delay the execution of these tasks do not influence the disruption that is a resource limitation. It is important to attitude of timing buffers in correct way. By their use brought the expected effects should accept the principle that if task is completed earlier it should be transferred to another position. It can't expect to the end of time determined by the buffer, if the next production position is free.

If date of the order which is read from schedule is not acceptable for the client, given the urgency of such order or award of contract, return to step four, and consider using alternative routes. However, if date of the order is satisfactory, meets the requirements of the customer, the production schedule is ready. It is important to know, that due to the use of timing buffer, the date of execution of order which is read from schedule are very likely to meet deadlines for orders. Proceedings in accordance with the algorithm steps increases the timeliness of execution.

Summary

The presented algorithm is based on assumptions of the theory of constraints, which focuses on system improvement which is define as a series of independent processes and was described in [9]. Presented algorithm was pre-tested in the company which manufactures water and sewerage fittings. The company employs about 90 people, of which nearly 60 are employees which works on production. The orders for the production flow irregularly and are characterized by high volatility. It happens that the client shortly before delivery increases the number of ordered items or even order new range. Machines are set in socket-type way and there are slightly more than the operators. Employees can perform various types of work, but even within one specialty, such as for example powder painters, vary widely in efficiency and scope of work that can be entrusted to them. Algorithm allows for efficient production planning, production manager gave reliable information about the current extent of the order and significantly reduced the work in progress.

In order to facilitate the transmission online information from shop floor to the system it is possible to use the multi-agent system or radio-frequency identification. But these are relatively expensive technology. The company, which was tested the algorithm uses a terminal set in a central location on the shop floor. Data were input using terminal by the operator after each finished lot, which is confirmed by the master production. This allows the production manager to keep control execution of specific tasks.

Very important element is discipline and workers self-control. Good production results are achievable using the appropriate incentive and high culture of the organization.

References

- [1] Koliński A., Trojanowska J., Kolińska K., *Analiza wykorzystania metod i technik zarządzania przedsiębiorstwem produkcyjnym w celu minimalizowania skutków kryzysu gospodarczego – wyniki badań*, Gospodarka Materiałowa, no.8, 2011.
- [2] R. Knosala and others: *Computer support for business management* (in Polish), Polish Economic Publishing House, Warsaw, 2007.
- [3] R. Kolish: *Make-to-order assembly management*, Springer-Verlag Berlin, Heidelberg, 2001.
- [4] J. Trojanowska, E. Pająk: *How to Improve Production Processes by Using Contemporary Methods of the Production Management*, Proceedings of III International Interdisciplinary Technical Conference of Young Scientists, 2010, pp. 575-580.
- [5] M. Woeppel: *The manufacturer's guide to implementing the theory of constraints*, St. Lucie Press, Boca Raton, Florida 2001.
- [6] E. M. Goldratt, J. Cox: *The Goal. Excellence In Manufacturing*, North River Press, New York, 1984.
- [7] J. Liker: *The Toyota Way: Fourteen Management Principles from the World's Greatest Manufacturer*, McGraw-Hill, New York 2004.
- [8] E. Noreen, D. Smith, J. T. Mackey: *The Theory of Constraints and its Implication for Management Accounting*, North River Press, New York, 1995.
- [9] J. Trojanowska, A. Koliński, K. Kolińska: Using of throughout accounting In manufacturing companies – case studies, *Management and Production Engineering Review*, Volume 2, March 2011, pp. 47-54.

RESEARCHES OF THE IMPACT OF INCORRECT DIAGNOSIS CAUSES OF DAMAGE TURBOCHARGER ON THE EFFICIENCY OF THE NEW COMPONENT

M. Idzior¹, J. Merkisz², M. Bajerlein³ and M. Bieliński⁴

¹ Poznan University of Technology, 60-968 Poznań, marek.idzior@put.poznan.pl,
tel. (+48) 61 665-23-50, Poland

² Poznan University of Technology, 60-968 Poznań, jerzy.merkisz@put.poznan.pl,
tel. (+48) 61 665-27-91, Poland

³ Poznan University of Technology, 60-968 Poznań, maciej.bajerlein@put.poznan.pl,
tel. (+48) 61 665-27-91, Poland

³ Poznan University of Technology, 60-968 Poznań, maciej.bielinski@doctorate.put.poznan.pl,
tel. (+48) 61 665-27-91, Poland

Keywords: turbocharger, combustion engine, maintenance, damage

Abstract. This article describe a case of damage caused by non-removal of a turbocharger primary cause of failure. Focused on describing the effects within the turbocharger bearing system. Description supported a detailed photographic documentation using a microscope. Conducted a discussion on the causes of failure.

Introduction

This article is based on research material - broken turbochargers removed from vehicles operating in realistic conditions. The study was conducted at facility involved in the regeneration and repair charging systems for internal combustion engines. Analyzed typical model of Garrett turbocharger used in passenger cars. Observation was carried out using a microscope Motic SMZ-168 equipped with a camera company Motic 2000. Presented the design and principle of operation of the turbocharger and an analysis of the elements of the device damage caused by interference of a foreign body in the compressor rotor.

This publication is limited to the analysis of damage caused by the lack of suitable turbocharger lubricating oil parameters. Omitting the description of the structure and working principle. The engine, which came analyzed turbocharger had already mentioned this component. Damage described in the turbocharger, resulted from the failure to comply with the necessary corrective actions, which is remove the causes of damage - does not identify the contaminated oil. Failing to remove the primary causes of damage results in the new turbocharger is mounted a rapid destruction. This event is commonly noticed in practice.

Description of damage to the turbocharger bearings in place as a result of momentary interruption in the supply of lubricating oil

Turbocharger bearing system is shown in Figure 1. It consists of a set of slide bearings, journal bearings and thrust bearing. Turbocharger bearing system is shown in Figure 1. It consists of a set of bearings, the transverse and longitudinal. Bearing sleeve is made of an alloy of bronze, cooperating with the valve shaft with a chrome steel. Grease is the oil from the bus engine. Disc thrust bearing is also made of an alloy of bronze, cooperating with two pins. Oil is supplied to the bearings through the holes radially arranged next to the circumference of the sleeve (4 per side). The middle hole is used for oil draining and receiving heat from the friction zone. To the thrust bearing oil is fed from the body by a single duct made in the disc. Oil is drained by canals on the surface of the disc. Oil from the transverse and longitudinal bearing gets to the middle area of the body of a turbocharger, which continued for drainage orifices reaches the sump of the engine.

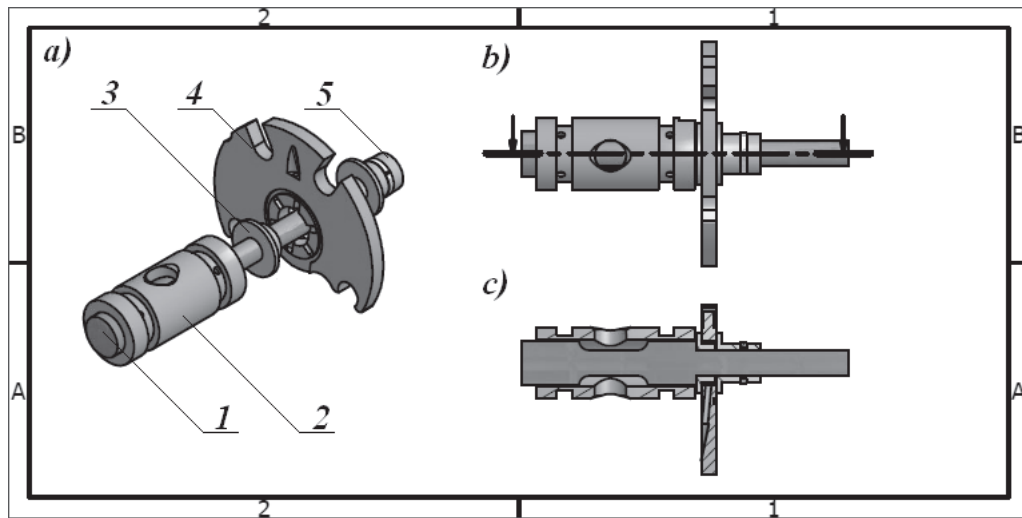


Fig. 1. Construction of a turbocharger bearing system: a) isometric view 1 - shaft, 2 – journal bearing bush, 3, 5 – bearings pin, 4 – journal bearing disc, b) view of submission, c) cross-section view

In the described turbocharger, oil was contaminated by the hard inclusions such as burnt oil in the conduits or the origin of metallic foreign bodies. Impurified oil splashed into the zone of cooperation pairs of friction bearings causes abrasive surface. Abrasion occurs due to implantation in hard-contamination of one of them. This causes furrowed and microcutting contrasurface. This event is compounded by the high speed rotor and an insufficient quantity of oil in areas of friction.

Abrasive wear the disc around thrust bearing shown in Figure 2a. and the new bearing surface in Figure 2b.

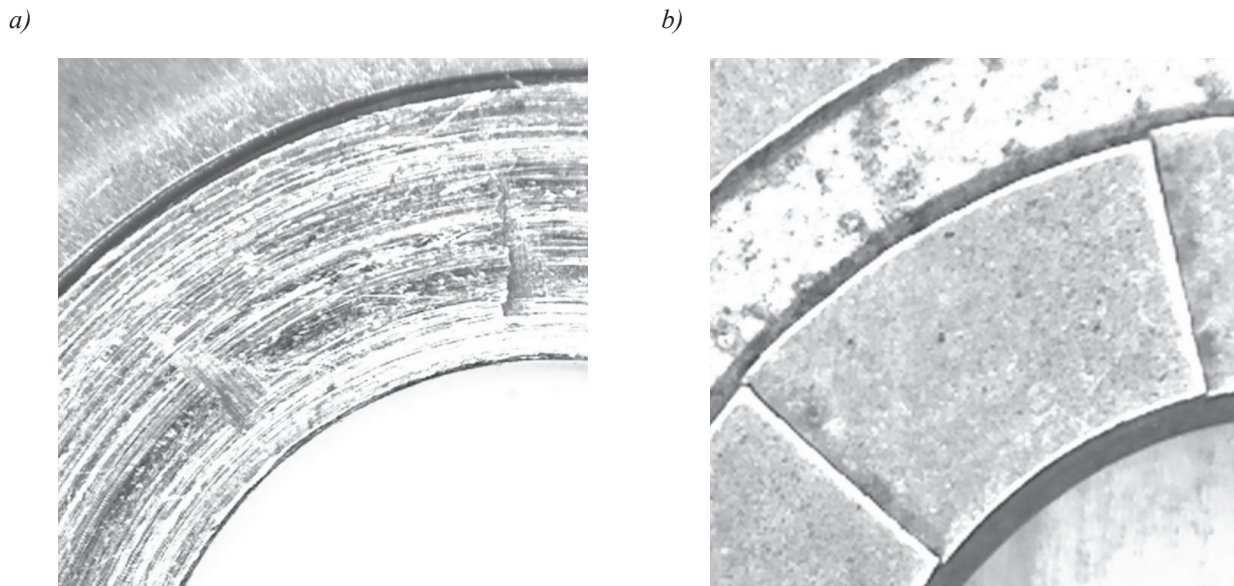


Fig. 2. Thrust bearing disc: a) damaged area, b) new surface (magnification 10 x)

As a result of adverse events, bearing, by modifying geometrical parameters did not attended its function. Distortion of these parameters resulted in the presence of the turbocharger shaft axial clearance, which contributed to increased stress in the sealing rings and, consequently, break the ring on the side of the turbine. Ringless results in a decrease of oil pressure in bearings, and penetration of it into the exhaust system. The pressure drop of oil worsens the conditions in the bearing lubrication, and the ability to create a film of oil. In this case, the liquid friction becomes to mixed friction.

Because of this, and the fact that the contaminated oil, mechanical wear has been cooperating with the pivot shaft bearing section. It was observed deep sulcus and grooves on its surface (Fig. 3).



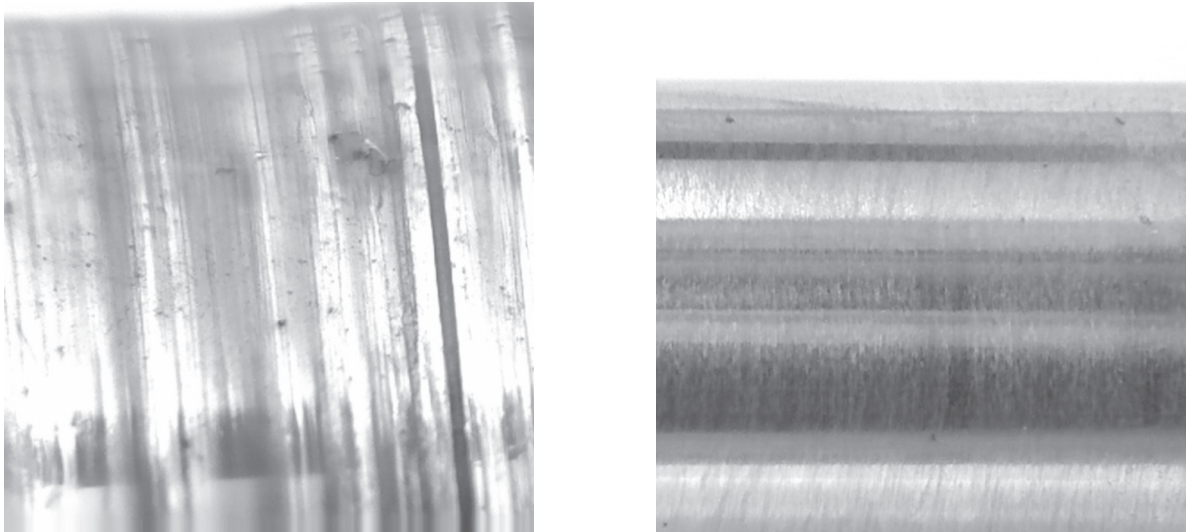
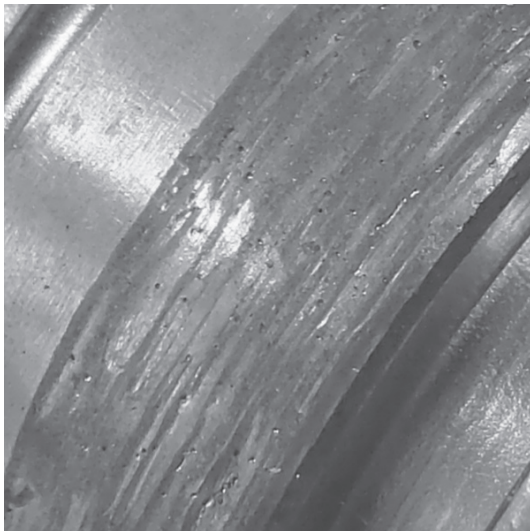


Fig. 3. Turbine shaft: a) lateral sulcus and grooves, b) new shaft surface (magnification 20 x)

Destruction within the journals shaft and bearings components, also affect the emergence of negative vibrations shaft of the turbocharger. Vibrations of small amplitude but high frequency ($f \approx 3\text{kHz}$), the destruction process in these areas increase. The adverse effect of vibration can be observed on the outer surface of the thrust bearing. Because the nominal sleeve remains stationary relative to the body, in this connection, there is a fretting event. Destructive mechanism of this process is the simultaneous influence of adhesion, grafting intensive oxidation.

a)



b)



Fig. 4. Thrust bearing bush: a) outside surface (magnification 20 x), b) new bearing bush (magnification 3 x)

This intense oxidation is caused by increased activity of the surface layer as a result of contact stress and strain [2]. The effect of fretting on the surface of the thrust bearing is shown in Figure 4, which confirms the oscillation compressor - shaft - turbine.

The increasing amplitude of vibration, with unchanged frequency led to an increase in stress in the shaft turbocharger and its bursting. As a result, the team has been destroyed, damaging the rotor blades of the turbine and compressor.

a)

b)

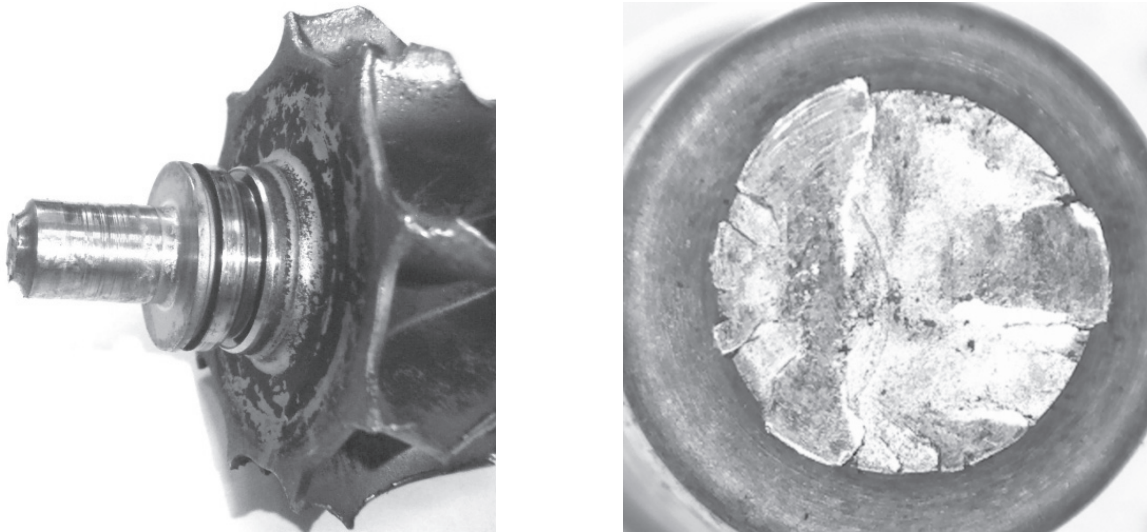


Fig. 5. The broken shaft a) magnification 2 x, b) magnification 10x

Conclusion

This failure analysis shows that during replacement of used turbochargers for a new, should be removed cause of the damage. If this step is neglected or damaged causes diagnosis will be incorrect turbocharger component failure is repeated. In the current case before the next turbocharger replacement would replace the turbo engine oil and filter. In addition, consideration should be given to the patency of the channel inlet and outlet of the turbocharger oil or prophylactically replaced.

References

References are cited in the text just by square brackets [1]. Two or more references at a time may be put in one set of brackets [3, 4]. The references are to be numbered in the order in which they are cited in the text and are to be listed at the end of the contribution under a heading References, see our example below.

- [1] Idzior M, Bieliński M, Borowczyk T.: „Analiza uszkodzeń turbosprężarki Garrett GT 1749V w rzeczywistych warunkach eksploatacji” Szczyrk 2011
- [2] Lawrowski Z.: Tribologia. Tarcie, zużywanie i smarowanie, Wrocław, Oficyna Wydawnicza Politechniki Wrocławskiej 2008
- [3] Materiały zebrane z praktyki rzeczoznawczej autorów
- [4] Turbocharger Technician's Guide, Detroit/Michigan, Detroit Diesel Corporation 1994

THE IMPACT OF MODIFIED PISTON TWO STROKE ENGINE ON TOXIC EMISSIONS DETERMINED ON THE BASIS OF RESEARCH CARRIED ON THE CHASSIS DYNAMOMETER

J. Merkisz¹, M. Bajerlein², M. Dobrzyński³ and Ł. Rymaniak⁴

¹ Poznan University of Technology, Piotrowo st. 3, 60-965 Poznań, Poland, tel. +48 61-665-22-07, e-mail: jerzy.merkisz@put.poznan.pl

² Poznan University of Technology, Piotrowo st. 3, 60-965 Poznań, Poland, tel. +48 61-665-27-91, e-mail: maciej.bajerlein@put.poznan.pl

³ Poznan University of Technology, Piotrowo st. 3, 60-965 Poznań, Poland, tel. +48 61-665-20-22, e-mail: michal.dobrzynski@put.poznan.pl

⁴ Poznan University of Technology, Piotrowo st. 3, 60-965 Poznań, Poland, tel. +48 61-647-58-62, e-mail: Lukasz.m.rymaniak@doctorate.put.poznan.pl

Keywords: city scooter, exhaust emissions, modified piston, two-stroke engine

Abstract. The Institute of Combustion Engines and Transport at Poznan University of Technology conducted exhaust emissions tests on motorized scooters fitted with two-stroke engines. Two vehicles were tested, each fitted with a different type of piston. The first was fitted with a standard piston as recommended by the manufacturer. The other was fitted with a special piston of innovative design allowing the application of fuel with a lower lubricant content. The vehicle was powered by fuels with various gasoline to oil ratios. The tests were conducted on a dedicated chassis dynamometer that allowed the measurement of the power output, speed and acceleration of scooter. The exhaust components such as NO_x, CO, HC, CO₂ were analyzed in terms of their emission level.

Introduction

Today transportation is one of the basic factors influencing the economic development worldwide. In the case of road transportation there are many categories into which vehicles are divided in terms of their design, purpose, conditions of operation etc. Vehicle manufacturers offer an increasing number of hybrid vehicles, electric vehicle and vehicles fueled with alternative fuels [1]. An important category in the discussed group is motorcycles and motorized scooters. Both in city agglomerations and non-urbanized areas they play an important role. Motorcycles allow quick traveling even if the streets are congested or the roads are in poor condition. In the case of motorized scooters another benefit is the possibility of using it without any special driver's license. Coming of normative age suffices.

Research Methodology

Research Object

The objects of the research were two motorized scooters. The difference between them was the design of the piston. A scooter fitted with a standard piston was tested first (manufacturer specifications). The second measurement series was done with a modification of the engine (scooter with a piston of special design was fitted Fig. 1). This piston enables the engine operation on mixtures of lower oil content than the manufacturer specifies. Table 1 presents the basic technical specifications of the vehicles. From the patents description number 10 2005 030 556 „MULTIPART PISTON AND METHOD OF MULTIPART PISTON MANUFACTURING” (patent application PCT/EP2006/005986) it results that the applied piston is a multipart one with at least one upper part and one lower part with the piston wall (sliding part) and at least a part of the piston crown forms the upper part [2]. The other assumption of the discussed design is that the upper part of the piston is made from material other than the one in the lower part. The contact point of the two parts shows a 5 to 60% lower thermal conductivity than the material that the lower part is made of. A lower thermal conductivity of the joint between the lower and the upper part of the piston positively limits the heating up of the lower part of the piston during engine operation. Hence, we can significantly reduce the amount of oil added to the fuel in the case of two stroke engines as compared to a conventional monolithic piston solution [2].

Table 1. Technical specifications of the tested scooters

Type	Two-stroke, spark ignition
Displacement	0,49 cc
Maximum speed with the speed limiter	45 km/h
Maximum speed without the speed limiter	75 km/h
Maximum engine speed	9000 rpm
Engine power output	3,3 kW (4,5 HP)
Engine start-up	Electric/kick-start
Brake front/rear	Disc hydraulic
Tire size front/rear	130 / 60 – 13
Dimensions: length/width/height	1880 / 740 / 200 mm
Weight	92 kg



Fig. 1 A scooter when tested on the chassis dynamometer

The Applied Fuel

The principle of operation of a two-stroke engine consists in realizing of the intake, compression, power and exhaust strokes in a single engine crankshaft revolution. Hence, a full work cycle takes place within two strokes: from bottom dead center (BDC) to top dead center (TDC) and vice versa. The design of the solution requires a use of a mixture of gasoline and oil that will ensure proper operation of the piston assembly.

For the tests the authors used BP 95 gasoline type. It is an unleaded gasoline of the octane number of 95 purchased at one of the BP gas stations. The lubricant used was 2 TAKT TEILSYNTHETISCHES 1052 by LIQUI MOLY GmbH. It is universal semi synthetic oil for two-stroke air-cooled and liquid cooled engines. It can be added to the fuel directly in the tank or through a dispenser fitted in the fuel system. Thanks to its good physical properties the manufacturer recommends its application in a wide range of vehicles and machines such as the likes of motorcycles, gardening tools, rotary snowplows [3].

Chassis Dynamometer

The tests on the scooters were performed on a scooter chassis dynamometer INERTIAL 70 manufactured by SOFT-ENGINE s.r.l. The stand enables the measurement of the instantaneous power output and torque on the wheels of the vehicle, the covered distance, acceleration and speed. During the preparation of the stand the values of ambient temperature, pressure and humidity are entered into the system including the adjustment values. The last parameter is vehicle specific. Large amount of information positively influences the accuracy of the measurement.

Exhaust Emission Equipment

The exhaust emissions (including the toxic ones) were measured with a portable exhaust emission analyzer SEMTCH DS manufactured by SENSORS Inc. The device is one of the most modern measurement systems in the category of PEMS (Portable Emissions Measurement Systems). It measures the exhaust emissions in both gasoline and diesel engines in a wide range of their displacements. Its application enables the measurement of the fuel consumption, mass exhaust gas flow, oxygen content and the content of other exhaust components in the exhaust gases such as: CO, CO₂, NO, NO₂ and THC.

Results and Discussion

In order to carry out the analysis of the motorcycle ecological indexes the exhaust emissions were measured. The vehicle fitted with the standard piston (marked: st) was tested on a mixture of oil and gasoline with the ratio of 1:30. The other scooter, fitted with the modified piston was supplied with the mixture of the ratios of: 1:30, 1:100 and 1:200. Prior to the initiation of each test session in which the ratio of fuel to oil was tested the vehicles operated on the maximum throttle opening characteristics for 10 min. This aimed at burning of the fuel left in the fuel system after the last measurement session and forcing a flow of high intensity through the measurement equipment containing the exhaust gases from the last measurement session. Additionally, prior to the initiation of the first measurements the scooter engines were warmed up through operation at low loads for several minutes.

In each measurement series four tests were carried out lasting 300 s each when the scooters operated at full power. During the testing the emissions of CO₂, CO, NO_x and THC were recorded. Figure 2 presents the average obtained results converted into a unit of distance – in this case 1 km. In order to verify the correctness of the obtained exhaust emission tests results, the authors calculated the fuel consumption based on the carbon balance method [4]. It consisted in determining of the amount of used fuel based on the measured emission of CO₂, CO and HC. The results of the calculations are listed in table 2. For gasoline engines in this method the following formula is used:

$$FC_w = (1154/\rho_{fuel}) * [(0,866*HC) + (0,429*CO) + (0,273*CO_2)] \quad (1)$$

where:

FC – fuel consumption in [dm³/100 km] or [m³/100 km] depending on the fuel type;

HC, CO, CO₂ – measured exhaust emissions [g/km];

ρ_{fuel} – test fuel density in the temperature of 15°C [g/cm³].

While defining the value of the fuel density the influence of the lubricating oil application on this parameter was taken into account.

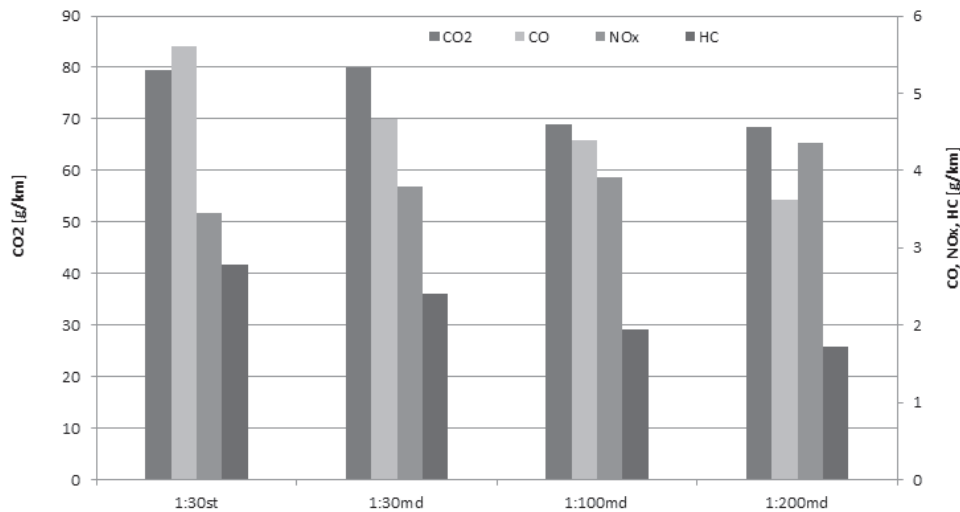


Fig. 2 Exhaust emission of CO₂, CO, NO_x, and HC

Table 2. The fuel consumption calculated with the Carbon Balance method

Cycle	Fuel consumption [dm ³ /100km]
1:30st	4,19
1:30md	4,02
1:100md	3,57
1:200md	3,46

Conclusion

Two-stroke engines are characterized by high exhaust emissions, particularly hydrocarbons. This results from the need to mix the lubricating oil with the fuel so as to prevent engine lockup. Motorized scooters powered with this type of engines are not usually fitted with aftertreatment systems due to limited production costs. Yet, all newly registered motorcycles and motorized scooters in the European Union must meet the appropriate requirements related to their homologation [5, 6]. In terms of environment protection we need to take every effort to make two-stroke vehicle engines as ecological as can be. This can be obtained through the application of special design solutions in the engines that will allow the use of fuel/oil mixtures of lower oil content - for example: modified piston.

The ecological indexes improved significantly for the vehicle powered with fuel containing less lubricating oil than recommended by the manufacturer. We may state that in the case of fuel consumption, a lower content of oil means lower exhaust emissions of the vehicle. An increase in the emission was recorded exclusively for NO_x. This growth confirms the obtainment of the greatest thermal efficiency, which is very advantageous in terms of reduction of the gas mileage and the emission of CO₂. It means that the process of combustion continued in the most efficient way and the lowest losses occurred during the combustion.

The vehicle fitted with the modified piston has lower fuel consumption. The higher the oil gasoline ratio the lower the fuel demand. Based on the obtained data we can conclude that the modernization of the piston improves the overall engine efficiency. In the case of the oil/gasoline mixture 1:100 taking the generated power into account the gas mileage was on a low level of 3,57 dm³/100 km (calculated with the Carbon Balance method). Hence, the generated mechanical work required a supply of the lowest amount of chemical energy. The use of the fuel in this proportion ensured proper lubrication as the growth in the friction losses did not occur. For this mixture durability tests were conducted as well that confirmed proper lubrication. Friction losses could have negatively influenced the power output, but it did not happen. When the mixture of oil/gasoline of 1:200 was applied the lowest gas mileage was obtained that equaled 3,46 dm³/100 km (calculated with the Carbon Balance method). Yet, in this case there is a risk that proper lubrication of all of the piston and the crank assemblies is not ensured.

Presently, the Institute of Combustion Engines and Transport of Poznan University of Technology is conducting tests on vehicles powered by small displacement two-stroke engines. The research presented in the paper constitutes a fragment of the entire series of tests conducted on this type of vehicles. Additionally, the Institute prepares a unique test that will reflect the actual driving conditions for motorized scooters to the greatest possible extent.

References

- [1] J. Merksiz: The automotive market in the time of global economic crisis. *Combustion Engines*, no. 3/2009.
- [2] Patents no. WO 2007/025581 and 10 2005 030 556 „MULTIPART PISTON AND METHOD OF MULTIPART PISTON MANUFACTURING” (patent application PCT/EP2006/005986).
- [3] http://www.liquimoly.pl/features/katalog?page=shop.product_details&flypage=flypage.tpl&product_id=245&category_id=51
- [4] Y. Gao, Checkel M.D., Experimental Measurement of On-Road CO₂ Emission and Fuel Consumption Functions. SAE Technical Paper Series 2007-01-1610.
- [5] Commission Regulation (EC) No. 692/2008 of 18 July 2008 implementing and amending Regulation (EC) No 715/2007 of the European Parliament and of the Council of 20 June 2007 on type approval of motor vehicles with respect to emissions from light passenger and commercial vehicles (Euro 5 and Euro 6) and on access to vehicle repair and maintenance information. OJ L 199/1, 29.7.2008.
- [6] Directive 2002/24/EC OF the European Parliament and of the Council of 18 March 2002 relating to the type-approval of two or three-wheel motor vehicles and repealing Council Directive 92/61/EEC. OJ 124/1, 9.5.2002.



International Conference on Innovative Technologies, IN-TECH 2012,
Rijeka, 26. - 28.09.2012



METHODS OF RESEARCHES AND EVALUATION OF WEAR INJECTORS USED IN MODERN COMPRESSION IGNITION ENGINES

M. Idzior¹, J. Merkisz², M. Bajerlein³ and P. Stobnicki⁴

¹ Poznan University of Technology, 60-968 Poznań, marek.idzior@put.poznan.pl,
tel. (+48) 61 665-23-50, Poland

² Poznan University of Technology, 60-968 Poznań, jerzy.merkisz@put.poznan.pl,
tel. (+48) 61 665-22-07, Poland

³ Poznan University of Technology, 60-968 Poznań, maciej.bajerlein@put.poznan.pl,
tel. (+48) 61 665-27-91, Poland

⁴ Poznan University of Technology, 60-968 Poznań, pawel.stobnicki@doctorate.put.poznan.pl,
tel. (+48) 61 665-20-49, Poland

Keywords: Combustion engine, injector, common rail system

Abstract. The article presents the general characteristics of the CR injection systems currently used in compression ignition engines as well as information on the diagnosis of injectors in these systems. Describes the basic methodology to enable a full assessment of the actual state operated injectors.

Introduction

The arrangement of contributing towards the type Common Rail is applied in internal-combustion engines with the self-ignition for a dozen or so years. This arrangement allowed above all for dividing the injection process from the process of pumping fuel, independence of the injection pressure from the rotation speed of the engine, division of the injected dose of fuel into parts and a lot other. The arrangement belongs to very precise apparatus, for which the electronic control unit will supervise work. In the course of final years four generations of this system occurred. Defects turning up at first years of applying the Common Rail arrangement have most often concerned injectors, pumps of the high pressure and control valves. In workshops they were making the exchange of the entire elements on new (by virtue of creating only a base of defects) what was combined with expensiveness [2,3]. At present a procedure of the diagnosis and evaluations of the technical condition of particular elements of the arrangement were controlled. Also a possibility of performed repairs unfolded (fig. 1).

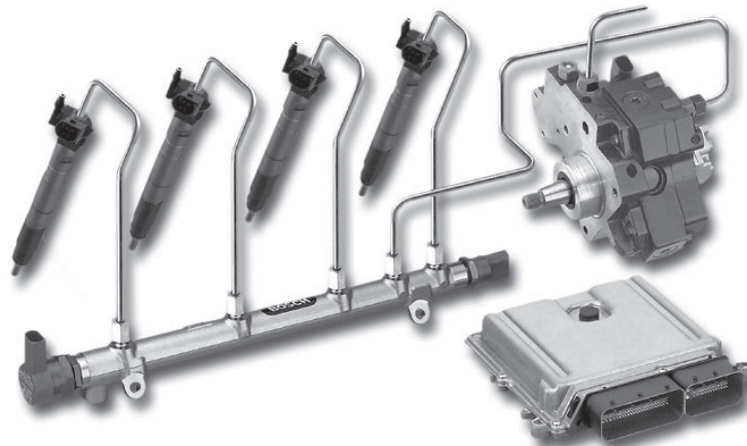


Fig. 1. Basic elements of the injection system Common Rail

Evaluation of the state of injectors

It is possible to describe the state of consuming injectors evaluations of damage based on basic methods, taking into account [1]:

- 1). verification of the work of the injector control signal (on the basis of which it is possible to establish dose levels including the correction),
- 2). flow tests - measurement of the fuel injector hitting the transfer,
- 3). organoleptic or by using an optical microscope recognition of a state of injector elements (such as pairs of precision, as well as corrosion of metal components of the injector and loss of material) - (fig. 2 - 5)
- 4). injector performance testing on special testers (test can be performed both before and after any repair injector) allow to examine the size of such tightness, dosage, hitting the fuel stream to transfer (fig. 6).

Assessment of injector by organoleptic

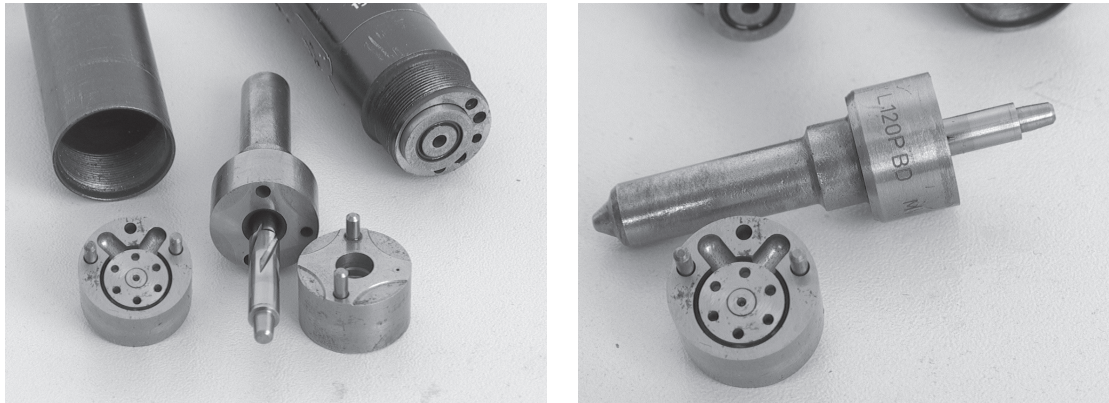


Fig. 2. Use of injector actuators by Bosch

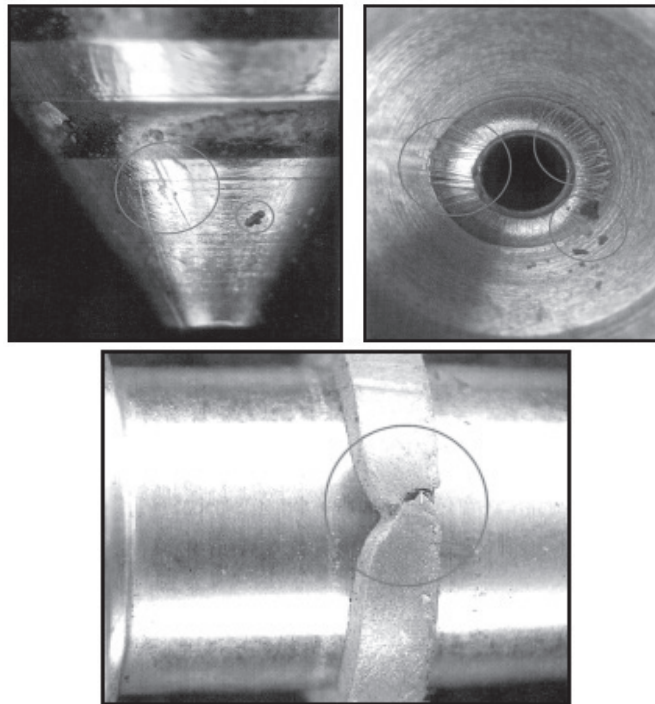


Fig. 3. Scratch the surface of the atomizer and precision pairs crack sealing high-pressure injector



Fig. 4. View of the injector

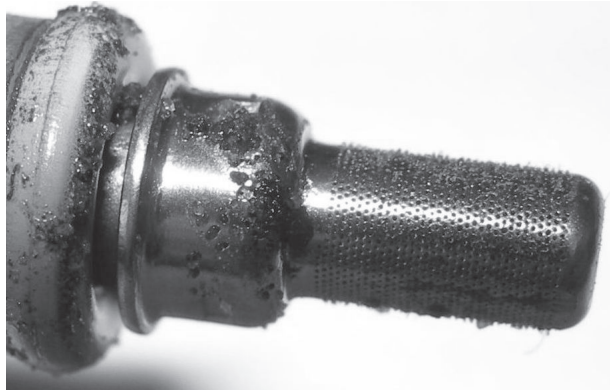


Fig. 5. The filter tank sensor system Common Rail contaminated metal filings

Injector performance testing

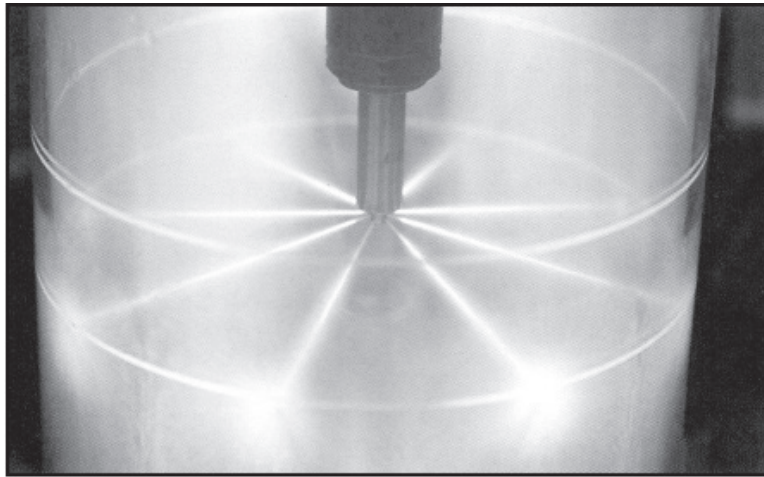


Fig. 6. Observing the shape of the fuel spray jets

Optical research on the process of the spraying of fuel

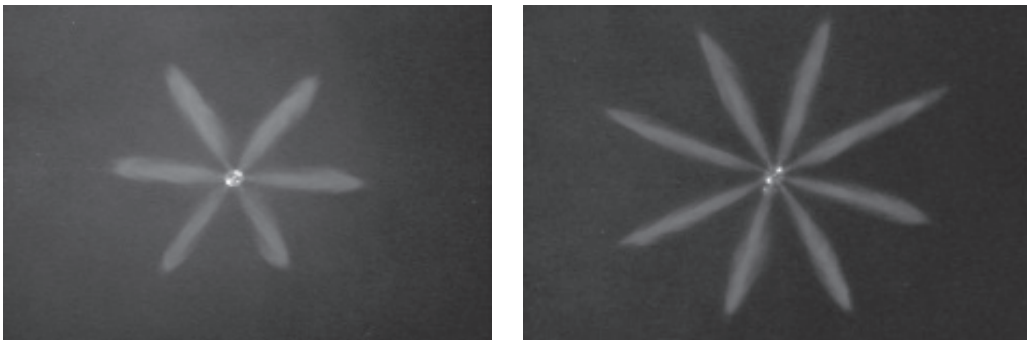


Fig. 7. Due spraying of the stream of fuel

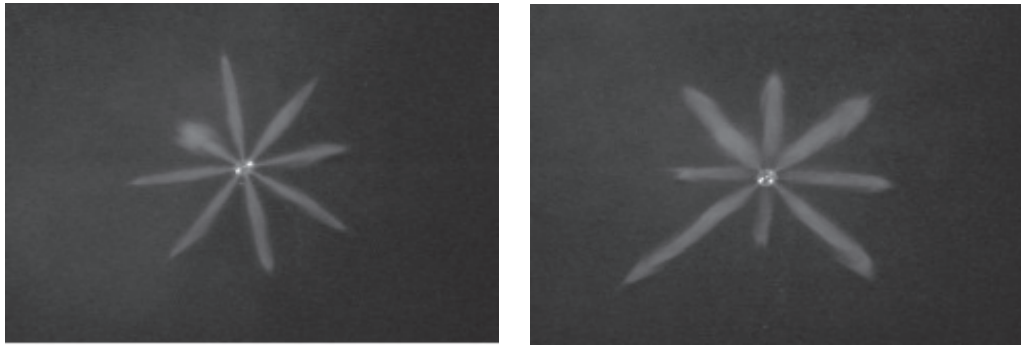


Fig. 8. Improper spraying of the stream of fuel

Conclusion

Presented methods enable the evaluation of the technical condition of described injectors, about unusually complicated and high of advanced structure, into the way relatively panes and getting credible and sufficient information. Implementing improved injection systems, the burn and the reduction in toxic connections constitutes main direction of the development of engines to a purpose fulfilling norms of the exhaust emission. Modern engines about the self-ignition equipped with the Common Rail arrangement should be characterized by a considerable emissions reduction of toxic compounds of the exhaust fumes, as well as a fuel consumption.

References

- [1] GÜNTHER H. The Common Rail Injection Systems. Warszawa WKiŁ. 2010
- [2] KOZAK W. The physic-chemical aspects of Internal Combustion Engines Control. Poznań, WPP 2011
- [3] SERDECKI W. Internal Combustion Tests. Poznań, WPP 1998

THE ANALYSIS OF INFLUENCE OF THE EGR VALVE OPENING DEGREE OF ON THE EMISSION OF TOXIC COMBUSTION ENGINES WITH DIRECT INJECTION

M. Idzior¹, J. Merkisz², M. Bajerlein³ and P. Daszkiewicz⁴

¹ Poznan University of Technology, 60-968 Poznań, marek.idzior@put.poznan.pl, tel. (+48) 61 665-23-50, Poland

² Poznan University of Technology, 60-968 Poznań, jerzy.merkisz@put.poznan.pl, tel. (+48) 61 665-22-07, Poland

³ Poznan University of Technology, 60-968 Poznań, maciej.bajerlein@put.poznan.pl, tel. (+48) 61 665-27-91, Poland

⁴ Poznan University of Technology, 60-968 Poznań, pawel.daszkiewicz@doctorate.put.poznan.pl, tel. (+48) 61 647-58-62, Poland

Keywords: Exhaust gas recirculation, direct injection, compression ignition, internal combustion engine emissions

Abstract. The article presents information on the effects of the EGR valve opening degree of the emission of toxic compounds emitted by the combustion engine. The study was conducted on single engine ignition test bench equipped with a solenoid injector Bosch. In addition, the study used a specially designed and constructed exhaust gas recirculation.

Introduction

The Dynamic carmakers efforts towards producing vehicles that emit minimal amounts of toxic compounds emitted by internal combustion engines generate more and newer systems that can ensure the more effective their reduction. One such system is the system of EGR (Exhaust Gas Recirculation). The principle of gas recirculation system is based on the electronic valve placed in the duct connecting the exhaust manifold of the intake manifold through which part of the exhaust gas emerging from the engine exhaust system again goes to the engine combustion chamber. By using such a solution is possible to reduce environmentally harmful emissions of NOx and reducing HC emissions of unburned hydrocarbons.

To ensure proper operation of exhaust gas recirculation system is necessary to return the correct dosage amount of gas involved in the combustion process. Number of gas, which should take part in the combustion process is dependent on engine load, its speed, engine coolant temperature, air temperature and the portion flowing into the intake manifold. After gathering this information, it opens the EGR valve causing a corresponding flow of exhaust gases. The internal combustion engine ignition back into the combustion chamber can hit up to 50% by volume with reduced exhaust temperature to 450 °C.

The test

Assess the impact of the EGR valve opening degree of the emission of toxic compounds emitted by the combustion engine was based on analysis of the obtained results. Motor fed by an external fuel injection system common rail [2]. The study was conducted on a test bed equipped with a test engine ignition direct injection (Table 1). This is a single-cylinder AVL 5804, equipped with four-valve cylinder head with two overhead camshafts and independent systems to stabilize the temperature of the lubricating oil and cooling liquid [3], [4].

Table 1 The motor parameters AVL 5804 [1].

No.	Size	Unit	AVL 5804
1	i	[-]	1
2	S × D	[mm × mm]	90 × 85
3	Vc	[dm ³]	0,5107
4	nmax	[rpm]	4200
5	ε	[-]	19,9
6	pe	[bar]	12,2
7	Ne max	[kW]	16 at 4000 rpm
8	Mo max	[N·m]	56 at 2000 rpm
9	ge	[g/(kW·h)]	251 at Mo max

Bosch solenoid injector with the symbol 0 445 110 131 000 centrally placed in the head in the axis of the cylinder. The engine was coupled to the brake type prądnicowego. Diagram of the engine along with the test apparatus used is shown in (Fig. 1), while in (Fig. 2) shows the view of the injector, cylinder head and piston engine in question.

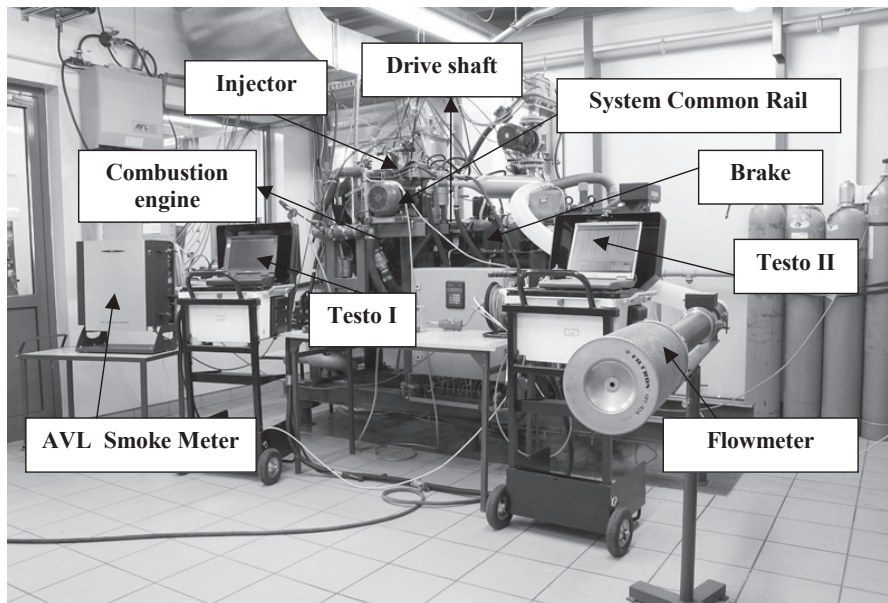


Fig. 1. Schematic of the test.

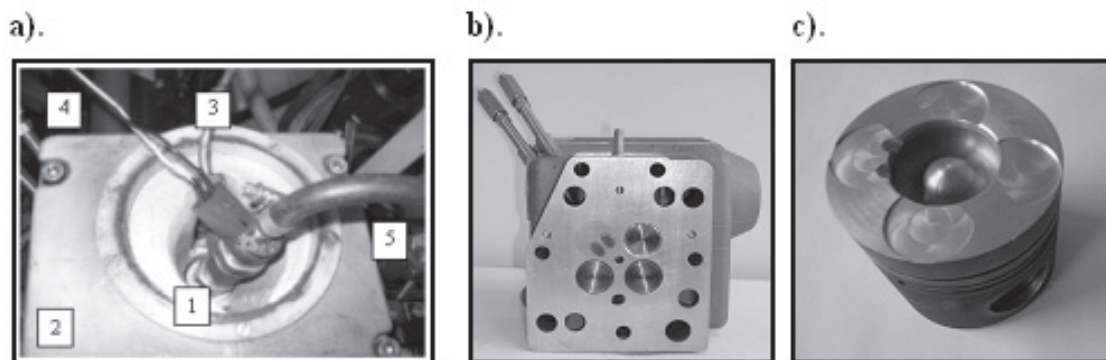


Fig. 2. a). View of the injector solenoid mounted on the head: 1 - injector, 2 - valve cover, 3 - wire injection, 4 - power cords, 5 - fuel overflow line, b). View of the head, c). View AVL research engine piston 5804 [1].

Analysis of test results

Influence of the EGR valve opening degree of the toxic emissions such as NO_x, CO, HC and FSN was performed on a specially designed test stand shown schematically in (Fig. 3). The study was performed for the engine speed $n = 1400$ [r / min], at constant pressure in the tray, level 120 [MPa]. During the tests the engine torque was increased from 0 to 20 [nm], toxic emissions were recorded using specialized measuring equipment (Testo I, II and testo AVL Smoke Meter) for different degrees of opening of the EGR valve.

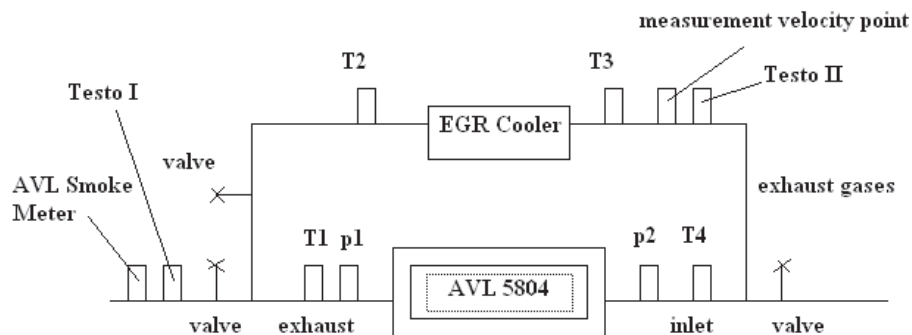


Fig. 3. Diagram of exhaust gas recirculation is used in the study.

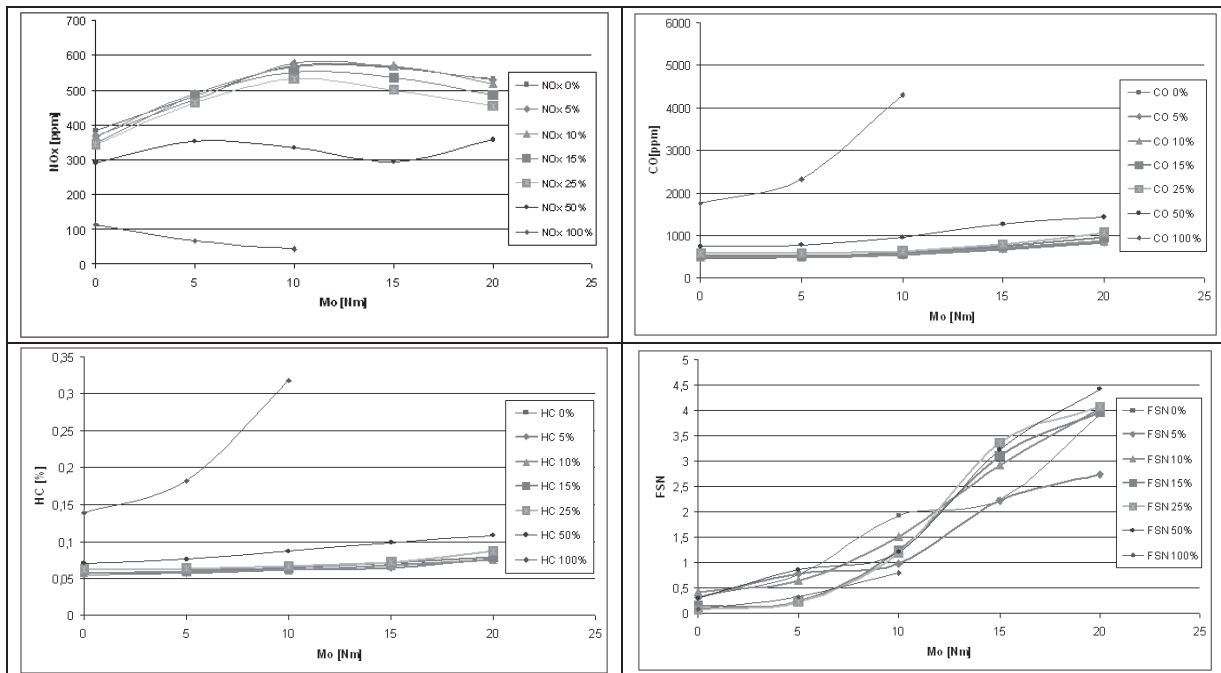


Fig. 4. Influence of the EGR valve opening percentage of the emission of NOx, CO, HC, CO2 and FSN for TESTO I.

In order to assess the impact of the EGR valve opening degree of the emission of toxic compounds analyzed the results of emission tests and opacity obtained during the measurements. The characteristics described above can be concluded that the percentage of EGR valve opening degree has a significant impact on emissions of toxic compounds in question. NOx emissions decreased with increasing percentage EGR valve opening degree, while other compounds such as CO, HC and FSN had a growing trend. It should also be noted that with 100 percent opening of the EGR valve was not possible to measure the full range of torque. The reason for this phenomenon was a global shortage of oxygen, which is too small a value not allowed to conduct research in the whole range of torque. Influence of the EGR valve opening percentage of toxic emissions in the analyzer testo I and AVL Smoke Meter is shown in (Fig. 4).

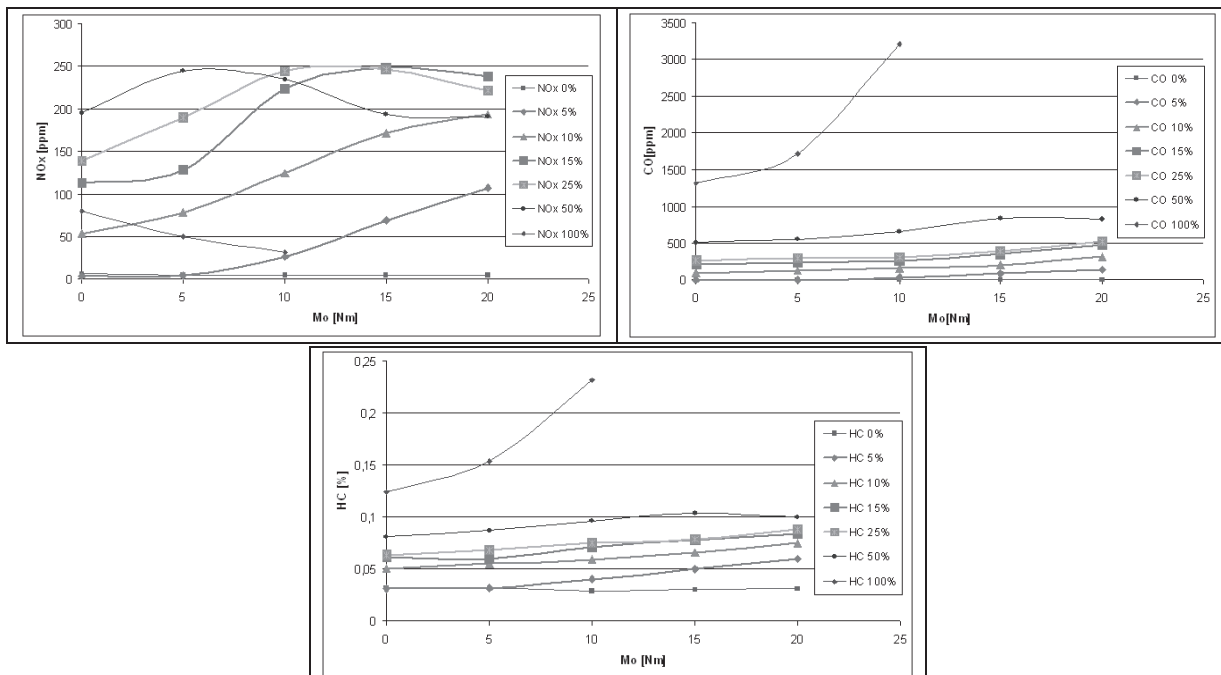


Fig. 5. Influence of the EGR valve opening percentage of the emission of NOx, CO, HC, CO2 and FSN for TESTO II.

Similarly shaped the course of the characteristics of the emission of toxic compounds under consideration for the analyzer Testo II. NOx emissions decreased with increasing percentage EGR valve opening degree, but was at a much lower level than the analyzer Testo I. As regards the emission of CO, HC 100 percent at the opening of the valve was characterized by a sharply rising trend. Also observed



the phenomenon of the global shortage of oxygen, which is too small a value not allowed to study the full range of torque. Influence of the EGR valve opening percentage of toxic emissions in the analyzer Testo II is shown in (Fig. 5).

Conclusion

EGR is used in engines to reduce NO_x emissions by lowering the maximum combustion temperature. This is done by increasing the thermal capacity of the intake charge, for example, by bringing the fresh charge with a number of substances with higher heat capacity than air-fuel mixture. Dilution of the load caused by bringing together a certain amount of exhaust gas with fresh charge results in slower growth of consumption and emissions of HC, CO and FSN due to an increase in the extinction of the flame zone on the walls. The introduction of only the exhaust gas recirculation can reduce NO_x emissions in the engine, but at the expense of an increase in emissions of products of incomplete combustion.

References

- [1] BAJERLEIN M. Analiza wybranych wielkości termodynamicznych procesu spalania w silniku o zapłonie samoczynnym przy zasilaniu olejem napędowym z rozpuszczonymi spalinami. Praca doktorska, Wydział Maszyn Roboczych i Transportu Politechniki Poznańskiej, Poznań 2007.
- [2] GÜNTHER H. Układy wtryskowe Common Rail. Warszawa WKiŁ. 2010.
- [3] KOZAK W. Fizykochemiczne podstawy regulacji i sterowania silników spalinowych. Poznań, WPP 2011.
- [4] SERDECKI W. Badania Silników Spalinowych. Poznań, WPP 1998.

INFLUENCE OF STRAIN RATE ON COLD SHEET METAL FORMING

T. Pepelnjak¹, S. Smoljanič², R. Zakrajšek¹

¹ Forming Laboratory, Faculty of Mechanical Engineering, University of Ljubljana, Aškerčeva 6, SI-1000 Ljubljana, Slovenia

² Faculty of Technical Sciences, University of Novi Sad, Novi Sad, Serbia

Keywords: strain rate, sheet metal forming, deep drawing, room temperature

Abstract. In modern production time necessary for particular forming operation needs to be steady shortened due to the cost reduction. It is known that in warm and hot forming the forming speed and with it combined strain rate has immense role on material flow in bulk and sheet metal operations. The influence of the strain rate on the flow curve is only rarely analyzed at room temperature.

Presented work analyzes the influence of strain rate on flow curve of DC04 material obtained by the uni-axial tensile test. After the evaluation of the flow curves as a function of strain rate the deep drawing of box-shaped test specimen was performed. At different forming speeds the influence of the forming speed on the forming force and onset of necking was analyzed.

Introduction

The effect of strain rate and process temperatures at forming processes and in particular on material formability is known already from the end of previous century. Several researchers have also realized that the influence of strain rate is more emphasized at elevated temperatures above the recrystallization point of the observed material. At the same time the flow curves are in these cases significant lower in comparison to those obtained for the same material at a room temperature. Characteristics of relation among tension and deformation under a high speed load are very important for further numerical calculations of forming processes and crash-test simulations.

Velocity effect of the plastic deformation on flow curve of different materials has been researched during last decades with different testing methods. Additionally, various material reactions can be observed when velocity influence on plastic deformation is studied. Therefore, the understanding of plastic behaviour of various materials and their alloys processed by various forming operations with different stress-strain conditions is of the highest importance.

Review of previous research

In the last century many researchers have analysed forming velocity and with it connected strain rate effect on plastic deformation and flow curves of various materials. Rao and Doraivelu [1] in 1980 made comparison of earlier researches and conclude that different materials can be successfully processed with different speeds having different limits of the highest attainable strain rate. As a highest attainable was declared the strain rate where the material was still deformable without fast tearing. For example, steel and some aluminium alloys can be deformed in strain rate range from $2 \times 10^{-3} \text{ s}^{-1}$ to $3 \times 10 \text{ s}^{-1}$, copper and brass in range from 10^{-3} to 10^{-2} s^{-1} , steel at high temperature from 10 to 10^3 s^{-1} , stainless steel in rate range from 5×10^{-6} to $3 \times 10^{-2} \text{ s}^{-1}$. Bailey, Haas and Shah [2] in 1971 made a research about velocity and temperature effect on flow curve of aluminium alloys. Obtained results have shown that required stress in tension necessary to obtain particular deformation is getting higher with increase of a strain rate at a constant temperature, and getting lower with increase of a temperature at a constant strain rate. Velocity effect of a deformation is getting more pronounced with increasing of temperature. Rao, Prasad and Hawbolt [3] in 1996 made a research on low carbon steel. On the basis of their results it can be concluded that with enhancement of strain rate and reduction of temperature, tensile strength is increasing and entire flow curve of material increase its level. Lee and Yeh [4] in 1997 made some experiments to determine dynamic relation between yield strength and deformation of steel alloy. Obtained results showed that yield strength is magnifying with increasing of strain rate or with decrease of the temperature. Odeshi, Al-ameeri and Bassim [5] in 2005 investigated velocity effect of projectile impact on deformation speed of material and its flow curve. On the basis of experiments they determined that speed of projectile impact has an effect on the strain rate of the observed material. When the speed of projectile impact and also strain rate are higher, the higher is yield strength maximum. Tsao, Wu, Leong and Fang [6] observed flow curve behaviour of commercially pure titanium during the hot tensile deformation. In this case, level of flow curve is again increasing with increasing of strain rate and decreasing with changing of temperature. In order to obtain reliable data of the materials used in automotive industry Kim and Huh [7] have analysed deformability of two steels common used in body-in-white production. They have selected CQ (commercial quality) steel and dual phase ferrite-martensite steel DP590. The common tensile test, used for analysis of the flow curve was not applicable for their research due to the large testing length of 80 or 50 mm. Since the strain rate is calculated from the deformation speed and the length of the specimen as

$$\dot{\varphi} = \frac{d\varphi}{dt} = \frac{v}{l} \quad [\text{s}^{-1}] \quad (1)$$

the total deformed length should be as small as possible. In Eq. 1 the φ represents logarithmic strain, v the deformation speed and l the length of a specimen. For this purpose Kim and Huh have selected miniaturized tensile specimens – Figure 1. Good clamping of the specimen necessary to minimise dynamic responses of the entire testing system was assured by screwing of the specimen into the clamping head. They diminish with such clamping system also the sliding danger which may appear at high testing velocities.

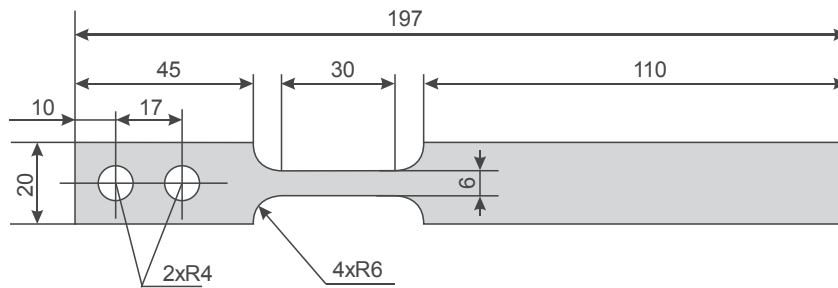


Figure 1: Specimen for testing at high strain rates [7].

The selected steels CQ and DP590 have shown that also at room temperature the flow curves are increasing with the increase of the strain rate. The authors have selected large testing range of the strain rates from 0.001 s^{-1} to 100 s^{-1} with an increment of one decade. The obtained flow curves for the rolling direction (RD) are presented on Figure 2.

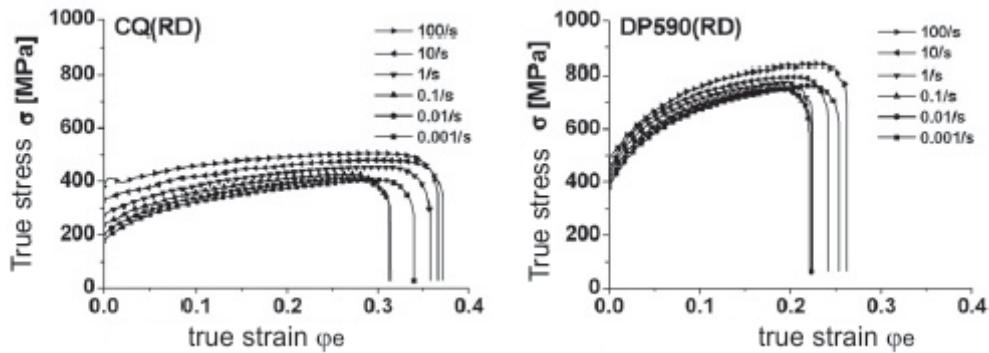


Figure 2: Flow curves of CQ and DP590 steel at various strain rates [7].

For both steels it can be observed that the yield stress and the level of the flow curve increases with the strain rate. Considering the CQ steel, this phenomenon is more emphasized at lower strains up to the $\phi_e=0.1$ while at DP590 steel quality the increase of the flow curve is more emphasized at strains above $\phi_e=0.1$. On the other hand the behaviour regarding the total elongation is similar: it is increased from $0.1-100 \text{ s}^{-1}$ while at quasi-static strain conditions below strain rate of 0.1 s^{-1} the total elongation is smaller and the material rupture at lower equivalent strains. Kim and Huh have analysed also the forming limit diagram under quasi-static loading at strain rate of 0.001 to 0.0018 s^{-1} and at strain rate of $60-120 \text{ s}^{-1}$. For both materials, there is no significant decrease in the forming limit curve (FLC) and only minor difference between the static and dynamic loading. The difference between both strain rates ranges is to observe only at the range between bottom and upper FLC line determining the reliability band of the FLD. The narrowing of this bend is more emphasized in the case of the dual phase steel DP590 – Figure 3.

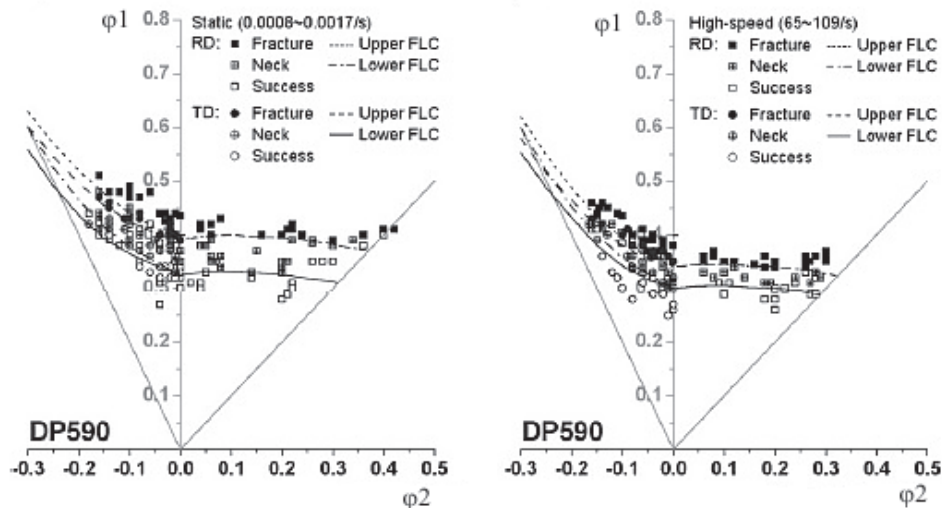


Figure 3: Forming limit curves of DP590 at different strain rates [7].

Jie et. all [8] have analysed the influence of strain rate on aluminium killed steel (AKDQ). They have also selected downscaled specimen with similar dimensions as Kim and Huh, however they have used for experiments the multipurpose Interlaken servo press with 260kN nominal force. They have found out that with the increase of the strain rate the flow curve and yield point of the material are also increased. The forming analyses of magnesium alloy AZ31 done by Lee et. all [9] at elevated temperatures between 250 and 400 °C has shown that the increase of the strain rate also here increase the level of the flow curve but on the other hand the forming limit curve decreases at higher strain rates.

Material properties of DC04

The household appliance industry and some applications of automotive sector use steels of DC quality, mostly suitable for painting after the forming. Since the companies are also in this sector forced to shorten the production times the analyses of the material DC04 on various strain rates were performed. Two speeds of the tensile testing machine were selected resulting in a strain rate of 0.0025 s⁻¹ and 0.02 s⁻¹. In order to improve the accuracy of the measurements of the uni-axial tensile test the standardized 80x20 mm specimens were selected despite lower attainable strain rates. The selection of the forming velocity at testing machine was adapted to the performances of the hydraulic press Litostroj where the deep drawing tests of box-like specimens were performed. The formability of the material was analysed in three directions regarding the rolling direction: longitudinal, transverse and at 45°. The flow curves at both analysed strain rates for all three directions are presented on Figure 4.

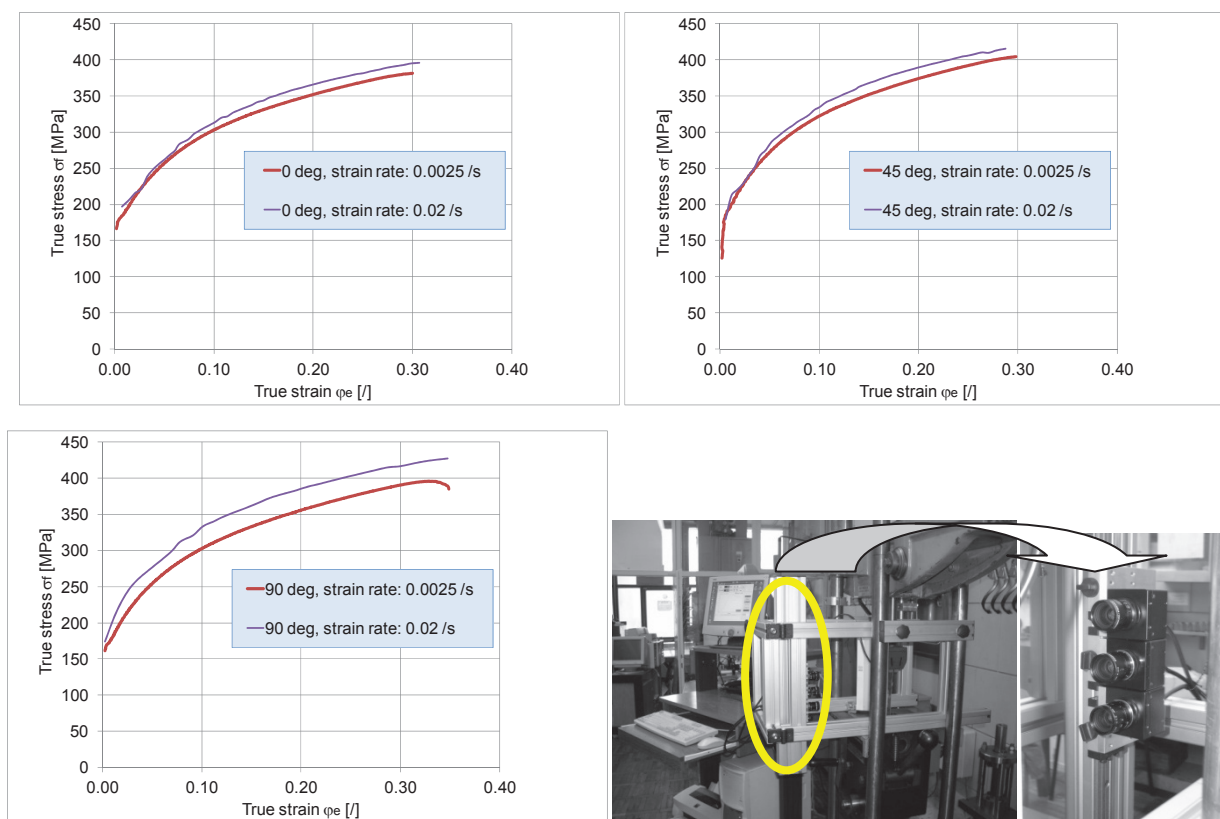


Figure 4: Comparative flow curves for different directions regarding the rolling direction of the sheet metal (top and bottom left) and measurement equipment for acquisition of the tensile test (bottom right).

Differences between the flow curves obtained at both strain rates are clearly visible. The highest increase of the flow curve can be observed perpendicular to the rolling direction where material expresses also the highest elongation at fracture. The material of DC04 quality expresses at observed strain rates only minor decrease of the total elongation at strain rate 10 times higher as the standardised one.

Deep drawing analyses

The forming of a rectangular box has served for comparative determination of necking and tearing limit for analysed material DC04 at two different strain rates. The forming speed was set to quasi-static forming with punch speed of 5 mm/s and at 4-times higher speed of 20 mm/s being the press maximal speed. The blank has dimensions of 165x145mm with 20 mm trimmed corners while the drawn box has dimensions of 70x100 mm with radii of 5, 8, 11 and 15 mm on its circumference, bottom radius of 5 mm and a flange radius of 7 mm – Figure 5. Different drawing depths were selected in order to determine the necking and fracture limit of the drawn box. The onset of necking followed by corner tearing appears at the smallest box corner. Since the flow curves of the DC04 material have shown the sensitivity on the strain rate it was to expect that the forming force should be also higher at higher forming speeds. The acquisition of force versus punch travel diagram did not prove this assumption. The course of the forming force was almost identical for both forming speeds.

Onset of necking appears at punch speed of 4 mm/s at the drawing depth of 25.3 mm while the fracture of the smallest corner appears at drawing depth of 27.7 mm. On the other hand, the necking range of the smallest corner at drawing speed of 20 mm/s is wider having a spread from drawing depth of 27 to 34 mm and the box tearing appears at drawing depths above 34 mm.

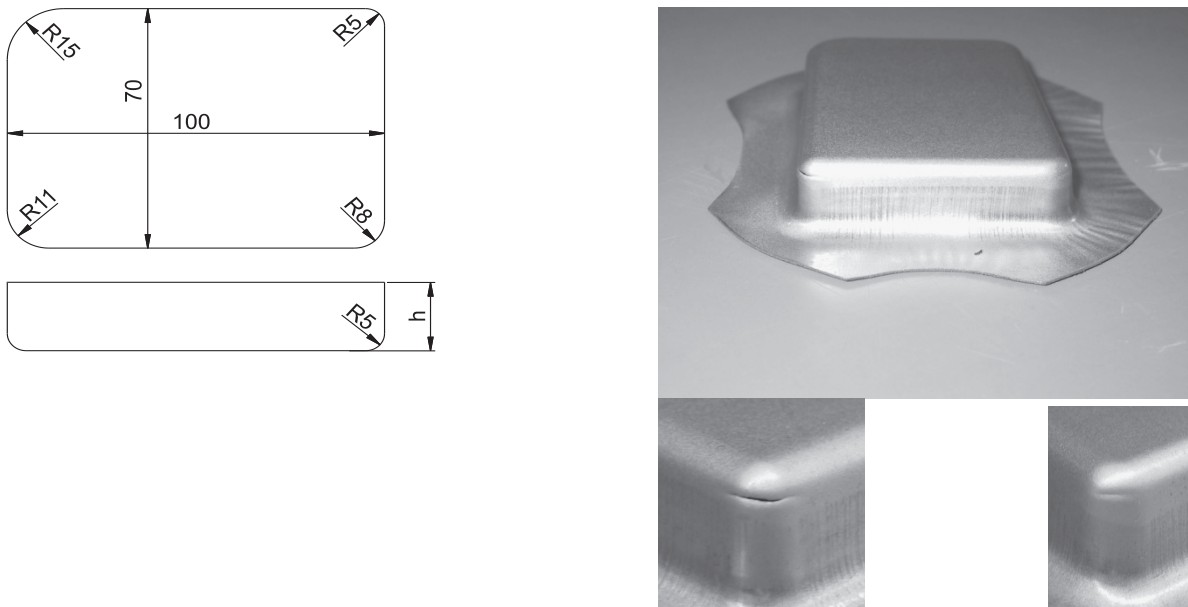


Figure 5: Specimen geometry (left) and specimen formability limit with tearing (bottom left) and necking (bottom right).

Conclusions

The strain rate and temperature have immense influence on flow curves and forming limit diagrams at warm and hot forming. At room temperature the strain rate influence is less emphasised and therefore less known in industrial practice. With drastically decrease of production times in stamping operations the strain rate influence cannot be neglected. Recent works have shown that in some cases also at room temperature the increase of the yield stress and flow curves is observed with increase of the strain rate. The flow curves of DC04 material were analysed at two strain rates: 0.0025 and 0.02 s^{-1} . Flow curves in three main directions according to the rolling direction have shown increase of the flow curve level at a higher strain rate without any decrease of the total elongation at fracture. The deep drawing test on the other hand has shown interesting phenomenon where the localisation on the critical corner of the specimen appear earlier at small forming speed of 4 mm/s as at five times higher forming speed of 20 mm/s . With further research work the FLD need to be determined for both forming speeds and FEM simulations of the deep drawing of the test box need to be performed.

Acknowledgment

This paper is part of research work within the Eureka project E! 5783 - ECO-CAN entitled INNOVATIVE ECO-FRIENDLY PROCESSING OF VOLUMETRIC SHEET METAL COMPONENTS financed by the Slovene Ministry of Education, Science, Culture and Sport. The authors are very grateful for the financial support.

The authors thank the CEEPUS programme for making them possible to be mobile within the network CII-HR-0108.

References

- [1] K.P. Rao, S.M. Doraivelu: Flow curve and deformation of materials at different temperatures and strain rates, *Journal of mechanical working technology*, Vol. 6 (1982), pp. 63-88.
- [2] J.A. Bailey, S.L. Haas, M.K. Shah: Effect of strain rate and temperature on the resistance to torsional deformation of several aluminium alloys, *International Journal of Mechanical Sciences*, Vol. 44 (1972), pp. 735-754.
- [3] K.P. Rao, Y.K.D.V. Prasad, E.B. Hawbolt: Hot deformation studies on a low – carbon steel: Part I – Flow curves and the constitutive relationship, *Journal of materials processing technology*, Vol. 56 (1996), pp. 897-907.
- [4] W. – S. Lee, G. – W. Yeh: The plastic deformation behaviour of AISI 4340 alloy steel subjected to high temperature and high strain rate loading conditions, *Journal of materials processing technology* Vol. 71 (1997), pp. 224-234.
- [5] A.G. Odeshi, S. Al – ameer, M.N. Bassim: Effect of high strain rate on plastic deformation of a low alloy steel subjected to ballistic impact, *Journal of materials processing technology*, Vol. 162-163 (2005), pp. 385-391.
- [6] L.C. Tsao, H.Y. Wu, J.C. Leong, C.J. Fang: Flow stress behaviour commercial pure titanium sheet during warm tensile deformation, *Materials and Design*, Vol. 34 (2012), pp. 179-184.
- [7] S.B. Kim, H. Huh, H.H. Bok, M.B. Moon: Forming limit diagram of auto-body steel sheets for high-speed sheet metal forming, *Journal of Materials Processing Technology*, Vol. 211 (2011), pp. 851–862.
- [8] M. Jie, C.H. Cheng, L.C. Chan, C.L. Chow: Forming limit diagrams of strain-rate-dependent sheet metals, *International Journal of Mechanical Sciences*, Volume 51, Issue 4, April 2009, pp. 269–275.
- [9] Y.S. Lee, Y.N. Kwon, S.H. Kang, S.W. Kim, J.H. Lee: Forming limit of AZ31 alloy sheet and strain rate on warm sheet metal forming, *Journal of Materials Processing Technology*, Vol. 201 (2008), pp. 431–435.

RESEARCH ON THE INFLUENCE OF ALLOYING ELEMENTS ON THE MICROSTRUCTURE AND MICROHARDNESS OF BIOCOMPATIBLE COBALT-CHROMIUM ALLOYS

V. Geanta¹, I. Voiculescu², R. Stefanoiu³, D.D. Daisa⁴, E. Binchiciu⁵,

¹ University Politehnica of Bucharest, Materials Science and Engineering Faculty, victorgeanta@yahoo.com

² University Politehnica of Bucharest, Materials Technology and Welding Department, Splaiul Independentei, 313, Bucharest, 060042, Romania, ioneliav@yahoo.co.uk

³ University Politehnica of Bucharest, Materials Science and Engineering Faculty, radustefanoiu@yahoo.com

⁴ SC METAV-CD, Bucharest, Romania, dana_daisa@yahoo.com

⁵ SC SUDOTIM AS SRL, Timisoara, Romania, sudotim_suport@yahoo.com

Keywords: biomaterials, alloying materials, manufacturing, microhardness, microstructure

Abstract. Biocompatible materials used for the orthopaedic implants must have special properties in terms of mechanical, physical, chemical and biological behaviour to extremely severe requirements. Different degree of alloying with chemical elements of biocompatible materials causes variations of the microhardness and of wear resistance. In the paper, some Co-Cr alloys have been studied, both as cast and prepared for deformed state. The alloying elements that have been introduced into the cobalt metallic matrix, in various proportions, were: Cr, C, Ta, Mo, Ni, N, Fe, W, Ti etc. The samples have been obtained in a vacuum induction furnace (VIM), and then the influence of alloying elements on microhardness and microstructure of biocompatible Co-Cr alloys has been analyzed. Microstructural aspects were analyzed by optical and electronic microscopy and microhardness measurements were performed at the microstructural constituent's level. The microhardness values were in the range 281-340 HV_{0.1}.

1. Introduction

Total replacement of elements of the human skeletal system is a current solution for various destructive diseases or bone injuries and surgery for implantation of orthopedic metallic elements are applied widely. Joints of the hip and / or knee are the most common and suitable for partial or total reconstruction. Also common applications are for immobilization with various devices of different portions of the fractured bone. Currently there are three types of metallic materials used for orthopedic implants: stainless steel, titanium alloys and cobalt-based super alloys, each with advantages and disadvantages.

Unlike dental, facial, head, etc, orthopedic implants are subject to strong demands, especially the cyclic stresses (fatigue). Prosthetic hip, knee, certain segments of the spine implanted application supports over 1,000,000 cycles in a year, for a sedentary person, showing tremendous stamina important to orthopedic implant materials. For orthopedic applications, one of the important indicators of performance materials is the number of "revisions" that a permanent implant is subject before breakage or wear. The world most implantable prostheses break by fatigue, which is the main concern when choosing the material. However, there are very few data on fatigue and wear characteristics of materials used for orthopedic prosthetics.

We now consider hip prostheses designed a full metal solution as the more likely and economical. Between 1988 and 1996, were performed approximately 50,000 implanted metal prostheses, which showed lower wear rates than the one predicted in vitro [1]. Cast cobalt-base alloys for surgical implants were proposed over 70 years ago. Continuous development of hardware technologies, and progress in understanding the Co-Cr system justified the choice of materials for a variety of biomedical applications [2]. In order to increase the mechanical properties, tests are performed alloying and micro-alloying with various elements such as Cr, W, Ta, Mo, Ni, N, Fe, W, Ti, etc.. Cobalt provides unique metal matrix due to allotropic transformation that occurs at a temperature of 4220C, when compact hexagonal phase transformation that occurs in face centered cubic phase. Alloying elements such as Fe, Mn, Ni and C stabilizes CFC phase packing defects and increase energy while elements Cr, Mo, W, Si phase stabilizes h.c. and lowers the energy of these defects. Items in the second category are almost always present in cobalt alloys, due to the effects of decreased reactivity to the environment (for Cr) and hardening (Mo, W).

Possibility of solid solution hardening by alloying, or by precipitation are visible on the equilibrium diagrams of binary systems, or with greater accuracy, in the quasi-binary sections of multi charts. Usually, replacement elements will produce a weak hardening of the matrix. Examples are V, Ta and Nb in titanium alloys, as well as nickel alloys of iron and chromium. This weak hardening is explained by the fact that high levels of soluble elements require replacement atomic radii close to those of the base metal in the matrix lattice as only residual stresses there. By comparison, interstitial atoms such as oxygen in titanium, or carbon in iron, can be made more effective by applying tension in the crystalline matrix network, but even more effective is by precipitation hardening. The semi-coherent and coherent secondary phases are able to produce in the metallic lattice internal tension that involves the enhancing of mechanical properties. By varying the parameters of aging can be obtained precipitate sizes and optimal distribution into lattice to best block the movement of dislocations.

2. Experimental

2.1. Equipment

Producing some categories of special high purity alloys with superior mechanical properties, such as superalloys based on nickel, chromium and cobalt is done with great efficiency in vacuum induction furnace (VIM). Improvements in investment casting alloy technological is strong justification to consider this technology for a variety of biomedical applications. Experiments to obtain biocompatible alloys Class Co-Cr were carried out in the vacuum induction furnace Balzers type HU-40-25-40-04 of the Material Science and Engineering Faculty of the University Politehnica of Bucharest. The main technical characteristics of the furnace vacuum induction used in the experiments are: Power consumption: 48 KVA, voltage: 3x380 V Frequency: 50 Hz Rated power: 40 KW Rated Voltage: 250 V, Power: approx. 0-44 KW.

2.2. Materials

Special quality conditions to obtain biocompatible Co-Cr alloys: purity, melting temperatures limited to max values 1600 C, relatively low carbon content based on which mainly takes place the carbon auto de-oxidation reaction during the vacuum melting process, requires that the experiments maintain rigorous quality materials. It is mandatory necessary that all raw materials and master alloys are metallic materials whose chemical composition (including impurities content) is known. To obtain the experimental charges of class Co-Cr, high purity materials were used, with the following degree of purity for chemical composition: cobalt, chromium, tungsten, tantalum, nickel and molybdenum metals with a purity degree over 99%; extra low steel, MK3 mark, with composition: C = 0.02%, Si = 0.04%, Mn = 0.21%, S = 0.02%, P = 0.015%, Ni = 0.2%, Cr = 0.15%, Mo = 0.07% 0.14% Cu, Al = 0.12%, Fe = ball. %.

2.3. Working procedure

Compositional design of Co-Cr alloys and their processing mode influences the final product characteristics and application. Most of the properties of the cobalt base alloys derived from crystallographic nature of the metal.

Several methods are known for obtaining Co-Cr alloys depending on the materials used, the degree of purity required, the finishing procedure, the required properties etc. Such alloys can be obtained by metal injection molding processes, vacuum arc re-melting, vacuum induction melting, etc. To improve the Co-Cr alloys metallic properties are practiced alloying procedures with various metals: nickel, molybdenum, tungsten, etc and carbon. Some mechanical tests has been applied in order to estimate the characteristics of the new alloys, like wear, micro-hardness, mechanical properties (yield, tensile strength, elongation, fracture toughness, creep resistance, etc.) as well as the corrosion and degradation resistance, immune response [2, 3].

To determine the influence of chemical composition on micro-hardness of the Co-Cr alloys, several samples with different chemical compositions were prepared. Twelve prospects of Co-Cr alloy have been designed, with composition within the average range: Co = 53.2 to 56.2%, Cr = 23.53 to 24.53%, Mo = 6.51 to 8.03 % Ni = 7.90 to 10.7%, W = 0.06 to 0.31%, Ta = 1.09 to 2.08%, C = 0.02 to 0.05% and other minor residual elements present in the alloys.

Program development experiments included several batches of biocompatible cobalt base alloys, coded C1/1,2; C2/1,2; C3/1,2; C4/1,2; C5/1,2; C6/1,2. In preparing these batches we aimed at establishing a stable electrical regime, including heat and pressure adjusting procedure, to ensure proper assimilation of alloying elements in compliance with the range of desired composition (Table 1).

The classic procedure, imposing a vacuum of 10^{-2} bars during the alloying process, allow to obtaining a great variety of Co-Cr alloys, with a good coefficient of efficiency. After alloying and refining the Co-Cr alloys were cast in air chilled metallic molds [4].

3. Results and discussions

3.1. Chemical compositions

Chemical compositions of samples were determined by optical emission spectrometry using a spark SPECTROMAX device in the LISEOFRX laboratory from UPB-SIM and are presented in Table 1. It was observed a good distribution of elements during the alloying.

Table 1. Chemical composition of the Co-Cr biomaterials

Sample code	Chemical composition, %													
	C	Si	Mn	P	S	Cr	Ni	Mo	Fe	W	Ta	Ti	Co	Other
C1/1	0.03	0.32	0.13	0.03	0.01	24.04	10.55	6.66	1.52	0.13	1.41	0.13	55.00	0.04
C1/2	0.02	0.37	0.13	0.04	0.01	23.86	10.68	6.39	1.54	0.11	1.09	0.04	55.70	0.02
C2/1	0.02	0.28	0.14	0.04	0.02	23.63	10.56	7.19	1.48	0.19	1.27	0.49	54.60	0.09
C2/2	0.02	0.39	0.13	0.03	0.01	23.81	10.70	6.81	1.51	0.13	1.09	0.23	55.10	0.04
C3/1	0.03	0.22	0.15	0.04	0.01	23.55	10.26	8.03	1.40	0.31	1.72	1.04	53.20	0.04
C3/2	0.03	0.28	0.14	0.03	0.01	23.67	10.36	7.63	1.44	0.22	1.64	0.72	53.80	0.03
C4/1	0.04	0.34	0.14	0.03	0.02	23.53	10.57	6.49	1.54	0.07	1.83	0.07	55.20	0.13
C4/2	0.04	0.37	0.14	0.04	0.02	23.54	10.61	6.47	1.53	0.06	1.75	0.05	55.30	0.08
C5/1	0.05	0.36	0.14	0.03	0.01	24.53	7.90	6.89	1.49	0.18	1.91	0.13	55.90	0.48
C5/2	0.04	0.42	0.14	0.04	0.01	24.43	7.95	6.86	1.50	0.15	1.81	0.13	56.20	0.32
C6/1	0.04	0.32	0.15	0.04	0.01	23.92	10.18	6.52	1.50	0.11	2.08	0.07	54.10	0.96
C6/2	0.04	0.34	0.15	0.04	0.02	23.98	10.18	6.51	1.50	0.11	2.06	0.07	54.10	0.90

3.2. Preparing of Samples

Samples were prepared and analyzed in the laboratory LAMET of UPB, according to the following procedures:

- Cutting, using a high precision cutting machine IsoMet Buehler 4000;
- Embedding in phenol resin, using an automatic press IPA 40;
- Surface polishing, using a Alpha Beta Vector Buehler Polisher;
- Micro etching, using a special electrolytic reagent prepared with 10g of oxalic acid dissolved in 100 ml distilled water and using a stabilized power source [5]. For electrolytic etching, direct current in electrolysis cell was applied.

3.3. Microhardness Measuring

The determination of the microhardness $HV_{0.1}$ values was performed using a Shimadzu HMV 2T device, with a force of 980.7mN and measurement time of 10 s. Test results of microhardness $HV_{0.1}$ for the lot of 12 samples analyzed are presented in Table 2. Singular values of the microhardness are situated in a limited area of dispersion, which shows good homogeneity of the material. These depend on the method of production, the quality of materials, the equipment and experimental procedure performance.

The range of values for microhardness is measured in the range of 281 ... 340 $HV_{0.1}$, and only because of the influence of alloying elements constituting the alloy. Samples were cooled under the same conditions, air atmosphere, without being subjected to further heat treatment. In order to establish the influence of each alloying element on the microhardness values were analyzed separately the effects of carbon, chrome, nickel, molybdenum, tungsten, tantalum and cobalt contents in Co-Cr analyzed biocompatible metallic alloys (Fig. 1 to 6).

At the same time using optical microscopy was investigated the microstructure of the alloys included in Fig. 7 to 10.

Table 2. Microhardness values $HV_{0.1}$ of Co-Cr alloys

Sample	Mesured values in different areas of the sample, $HV_{0.1}$	Average value
C1/1	321, 316, 329, 324, 335	325
C1/2	269, 276, 290, 304, 290	286
C2/1	291, 295, 293, 302, 282	293
C2/2	287, 299, 290, 303, 306	297
C3/1	306, 298, 302, 312, 321	308
C3/2	275, 303, 278, 274, 274	281
C4/1	317, 311, 311, 307, 281	305
C4/2	271, 286, 273, 304, 296	286
C5/1	344, 356, 329, 335, 336	340
C5/2	305, 313, 335, 312, 311	315
C6/1	290, 301, 299, 288, 293	294
C6/2	320, 335, 318, 330, 301	321

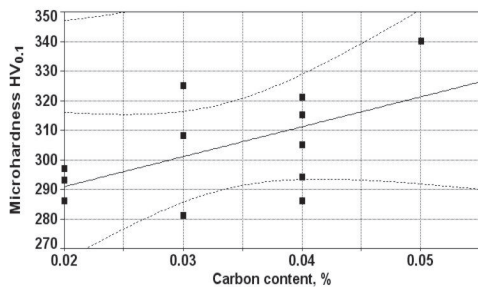


Fig. 1. Influence of carbon content on the microhardness $HV_{0.1}$.

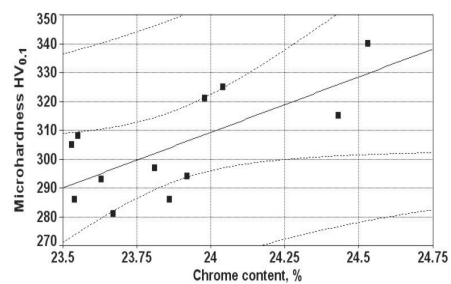


Fig. 2. Influence of chrome content on the microhardness $HV_{0.1}$.

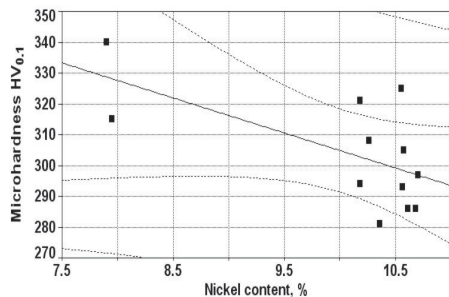


Fig. 3. Influence of nickel content on the microhardness $HV_{0.1}$.

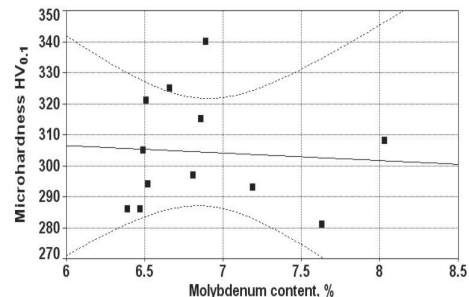


Fig. 4. Influence of molybdenum content on the microhardness $HV_{0.1}$.

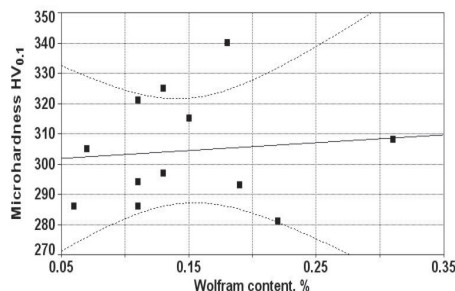


Fig. 5. Influence of tungsten content on the microhardness $HV_{0.1}$.

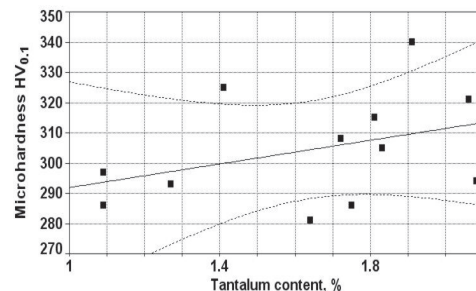


Fig. 6. Influence of tantalum content on the microhardness $HV_{0.1}$.

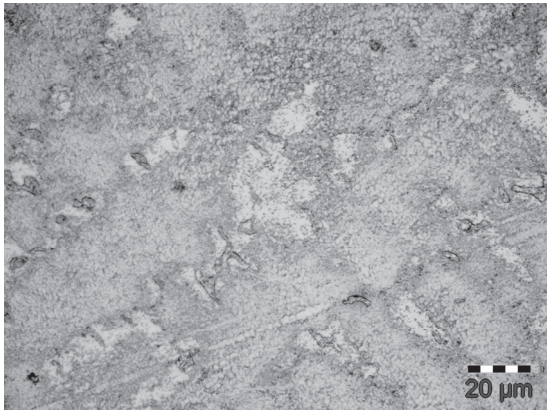


Fig. 7. Sample 6/1. Fine dendritic microstructure and eutectic containing precipitates. 1000x

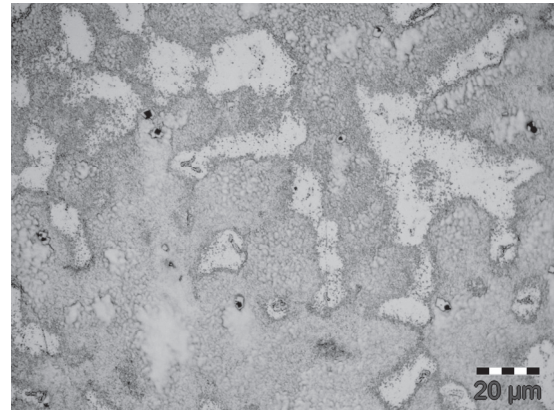


Fig. 8. Sample 2/2. Rough dendritic microstructure and fine eutectic with precipitates. 1000x



Fig. 9. Sample 3/2. The dendritic microstructure is preserved but the eutectic volume is increased. 1000x.

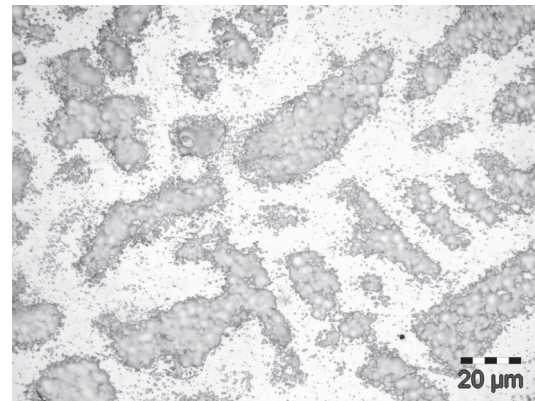


Fig. 10. Sample 5/2. Dendrites and eutectic in close balance distribution. 1000x.

4. Conclusions

During the process of development and refinement of Co-Cr alloys was determined a good distribution of the alloying elements in bath with a maximum efficiency of the product.

In terms of microhardness, increased carbon content, even at very low values, due to its low solubility in cobalt at the working temperature, can strengthen the metal matrix mainly by forming carbides of alloying elements such as Mo, W, Nb. Morphology and arrangement of the carbides into the metallic lattice of the alloy affects deformability and microhardness (Fig. 1) that is an important characteristic for prosthetic components with high resistance to wear. Effect of chromium, the main alloying element in cobalt base alloys, is mainly to increase corrosion resistance and its presence in the cobalt in solid solution hardens to a greater extent than carbon, (Fig 2), effect that is amplified by increased percentage of carbon with which forms carbides, much like the Mo and W. The addition of nickel in metal matrix of Co-Cr-Mo allows the increasing of the deformability, by increasing of the energy of defects packaging that is useful for processing of components in order to create complex configurations (Fig. 3). Elements such as W, Ta, Mo leads to hardening of metallic matrix by forming stable carbides at high temperatures (Fig. 4 to 6).

The microstructure of studied alloys shows classical dendritic morphology, as evidence of casting process. Remarkable is the influence of chemical composition on the eutectic percentage, in relation with the proportion of dendrite formations, rich in Co and Cr, while other alloying elements added in different amounts, lead to formation of precipitates showing different shades in the metallographic images (Fig. 7 to 10).

References

- [1] R. Tandom. *Net-Shaping of Co-Cr-Mo (F-75) via Metal Injection Molding*. Cobalt-base Alloys for Biomedical Applications, ASTM STP 1365, J. A. Disegi, R. L. Kennedy, R. Pilliar, Eds., American Society for Testing and Materials, Fredericksburg, VA, 1999.
- [2] H.J. Breme, J.A. Helsen *Selection of materials*, Metals as Biomaterials, John Wiley & sons, Ltd by Medy-Tech Publications, Storrington, West Sussex RH20 4HH, UK, 1998.
- [3] Alexandrescu E., Roman I., Ioncea A., Vasile E., Geanta V. Daisa D. *Aliaje biocompatibile ale cobaltului destinate implantologiei ortopedice. Influența particularităților microstructurale și microcompoziționale asupra comportării la coroziune electrochimică*. Conference „EXCELLENCE RESEARCH - A Way to ERA”, Braşov, Romania, 24-26 October 2007, Editura Tehnică, ISSN 1843-5904, L.223.
- [4] V. Geanta, R. Stefanoiu. *Ingineria producerii oțelului - Engineering of Steelmaking*. Editura BREN, Bucureşti, 2008, ISBN 978-973-648-746-0, 322p.
- [5] I. Voiculescu, C. Rontescu, L. Dondea. *Metalografia imbinarilor sudate*. Editura Sudura, Timisoara, 2010.
- [6] ASM Handbook. *Metallography and Microstructures*, Vol. 9, Chapt. “Microstructure of Cobalt and Cobalt-base Alloys” and “Metallography of Biomedical Orthopedic Alloys”, Ohio, 2004.

DSP-BASED CONTROL SYSTEM FOR EXCITATION CONTROL OF SYNCHRONOUS GENERATOR

N. Bulic¹, D.Sumina² and Z. Car³

¹ University of Rijeka, Faculty of Engineering
Vukovarska 58, Rijeka, Croatia

² University of Zagreb, Faculty of Electrical Engineering and Computing
Unska 3, Zagreb, Croatia

³ University of Rijeka, Faculty of Engineering
Vukovarska 58, Rijeka, Croatia

Keywords: Digital signal processor, Control system, Generator excitation system

Abstract. The paper presents a digital control system based on the TMS320F2812 digital signal processor. The role of this system is to allow easier and faster development and testing of advanced control structures for synchronous generator connected to the power network. The code development is supported by two software tools where the code can be developed in the C/C++ programming language or in a graphical environment. New generation of digital signal controllers together with the software programming tools offers good platform in area of development complex control algorithms and laboratory testing of new control strategies for synchronous generator excitation control.

Introduction

This paper presents a digital signal processor (DSP) based control system developed for the excitation control of a synchronous generator, which can also be used for the control of any type of the motor or power converter. The digital control system is used in the excitation control system for synchronous generator, in which performances of both the conventional control structure and new control structures can be analyzed.

DSP manufacturers offer a great number of DSP starter kits and evaluation modules to evaluate the functionality of a particular DSP. However, these are general purpose tools and they mostly do not meet the application-specific requirements, so additional hardware is needed to satisfy the required specifications. This is particularly true in the DSP-based excitation control of synchronous generators. DSP manufacturers support the DSP starter kits with powerful debugging tools that allow users to develop their code and analyze the real-time performance of the system. Nevertheless, the proposed control system is developed for a specific application, at the same time being flexible for use in other applications.

Hardware

The proposed system consists of a four-layer printed circuit mainboard including a digital signal processor TMS320F2812 [1-3]. Beside the processor, 512 kB x 16 of supplementary memory, digital and analogue inputs and outputs, PWM outputs, communication modules, a LCD connector and an encoder input are placed on the mainboard. The system includes 24 galvanic isolated digital inputs and 24 galvanic isolated digital outputs. While the system is performing a reset, all outputs are set to an inactive state (blank on reset). Furthermore, the system includes 16 galvanic isolated analogue inputs, two analogue outputs with 12-bit resolution, and 12 PWM outputs. The data exchange between the PC and the control system is carried out by a JTAG (Join Test Action Group) emulator.

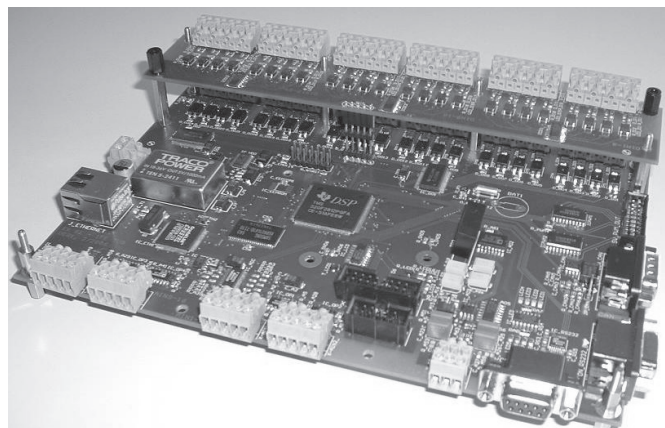


Fig. 1 Mainboard

The mainboard is rack-mounted together with power supplies, a LCD display, a JTAG emulator, current and voltage measurement transformers, a generator excitation current transducer, an AC/DC converter, etc. (Fig. 2(a)).

The laboratory model, whose structure is shown in Fig. 2(b), enables an experimental verification of excitation control algorithms for voltage control and power system stabilization. This laboratory model enables the testing of various algorithms for excitation control as well as the testing of a system in different characteristic operating conditions (step change in active power reference or voltage reference).

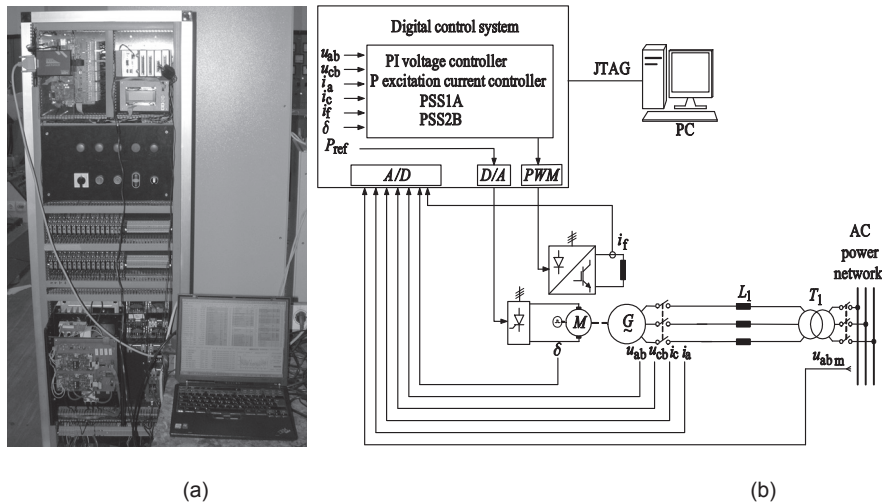


Fig. 2 Laboratory model. (a) rack; (b) structure.

Thyristor converter (100kW) with an output current controller for supplying electrical power to two DC motors as prime movers (one on each generator side) is also included in the laboratory model (Fig. 3(a)), and a salient-pole synchronous machine (83kVA). The synchronous generator is connected to the network through reactance of 0.25 p.u. (Fig. 3(b)). A two-quadrant IGBT AC/DC converter is used as an excitation current source. The rotor speed and position are measured by an optical encoder.

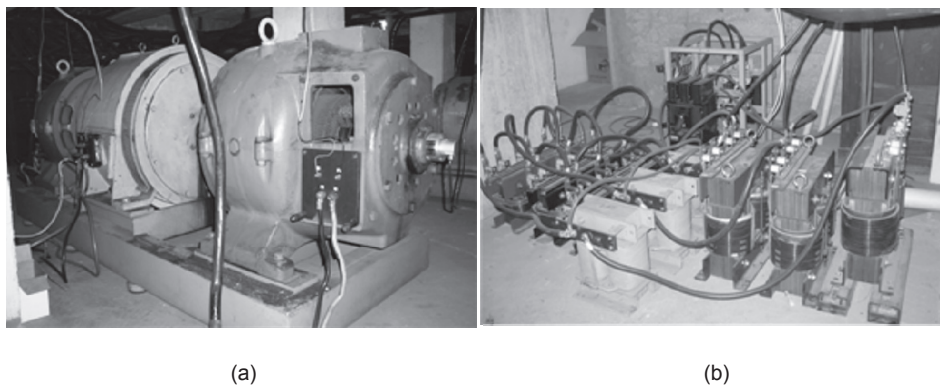


Fig.3 (a) Synchronous generator with DC motors as prime movers; (b) Inductors between synchronous generator and network

AC/DC converter

For supplying the generator excitation current, an AC/DC converter is used. The AC/DC converter includes a three-phase bridge rectifier, a DC link with a detection of DC voltage, a braking resistor, and a DC chopper (Fig. 4). The control electronics monitor the level of voltage within the DC link and when this rises above a limit, the braking resistor is switched into the circuit by the use of an IGBT. When the DC voltage drops to a safe level, the load resistor is switched off. The frequency of the pulse-width modulated signal is 500 Hz.

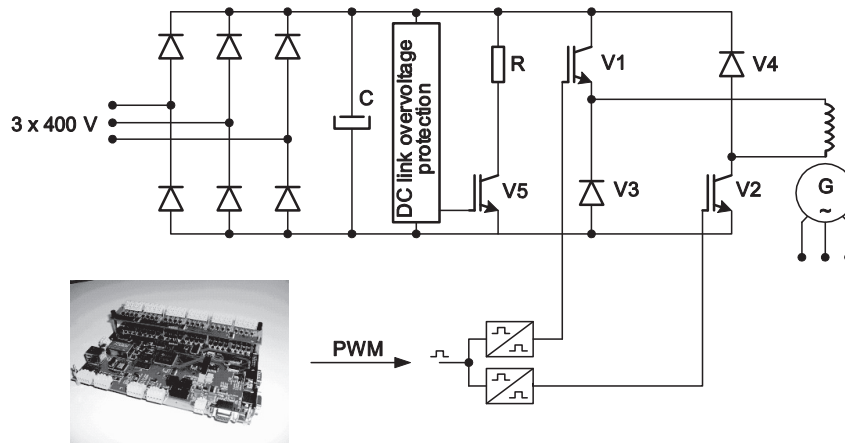


Fig. 4 AC/DC converter for supplying generator excitation current

Software

The implemented operation system is designed in such a way that it has two interrupts and three periodic functions. The highest priority interrupt is linked to analogue inputs and is performed by a frequency of 5 kHz, which is also the analogue signal sampling frequency. The second interrupt has lower priority and is performed by a frequency of 500 Hz which is the frequency of pulse-width modulation. Periodic functions do not have priority and are therefore executed when there are no interrupts.

Depending on the control demands and the functions being performed by individual circuit and software parts, the digital system function units are implemented as follows:

- first level interrupt (5 kHz) – processing of the measured analogue signal, protective functions, analogue output refreshing,
- second level interrupt (500 Hz) – control structure, generating of the PWM signal,
- periodic function (100 Hz) – digital input and output and processing of the function keys,
- periodic function (10 Hz) – communication routines,
- periodic function (1 Hz) – LCD.

For the development of the user code two types of software packages are used: Code Composer Studio12 (CCS) and VisSim13. These tools can be used in the code development for the Texas Instruments TMS320Cx family of processors.

Code Composer Studio

CCS is a software package which includes a source code editor, a debugger, a project manager, a profiler, probe points, and real-time analysis and visualization tools (Fig. 5) [4]. This tool allows code development in the C or C++ programming language, debugging, disassembly, real-time variable modification, and recording. CCS includes the library of predefined functions (PID controllers, PWM and signal generators, mathematical functions), so these functions can be used in the code development process.

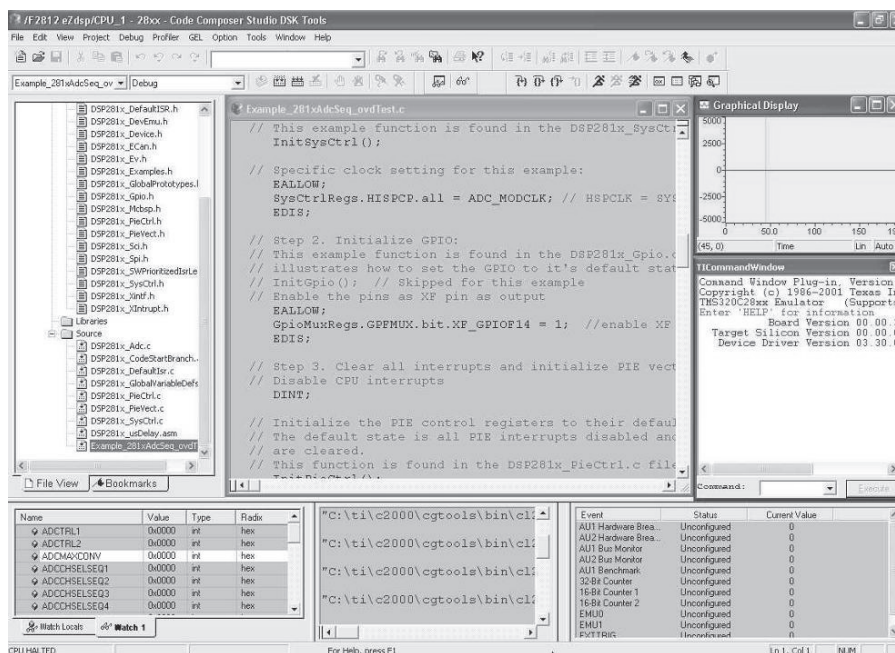


Fig. 5 Code Composer Studio screenshot.

VisSim

Software package VisSim is a software tool for the code development for Texas instruments C2000 DSPs (Fig 6). It is a graphical programming tool with predefined blocks and target specific blocks [5]. When the model of the plant is completed, it can be first simulated in VisSim to verify the algorithm behavior. Furthermore, VisSim allows users to generate a fixed point C code from a structure drawn in VisSim and it includes a Code Composer plug-In. VisSim automatically translates the drawn diagrams into a highly optimized ANSI C code, that can be compiled and run on the target system.

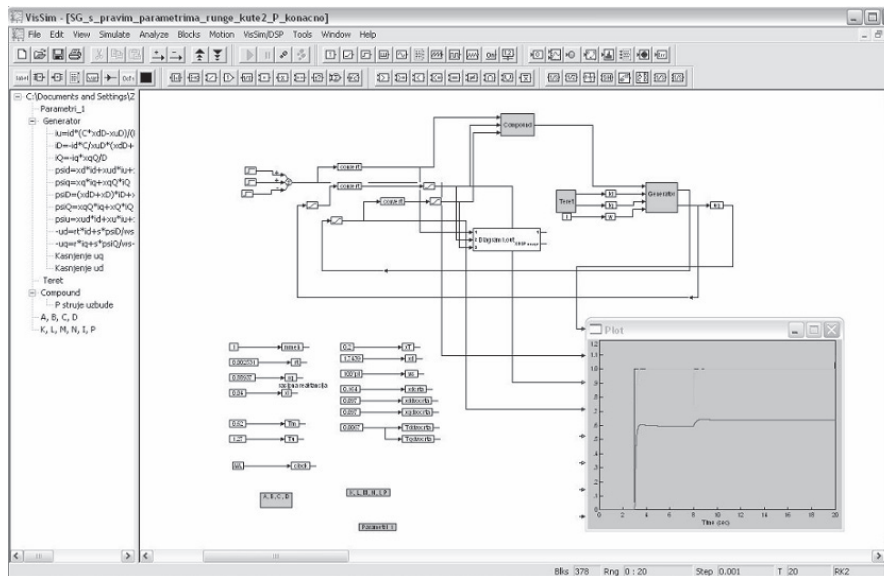


Fig 6. VisSim screenshot.

Conclusion

This paper presents tools used for control of synchronous machines and excitation systems. The presented laboratory model consists of a digital control system based on the DSP TMS320F2812 used for the excitation control of a synchronous generator. Software packages Code Composer Studio and VisSim allow users to develop the code in the C or C++ programming language or in graphical environment. Also, the paper presents organization of the implemented algorithm and functions of digital control system. These hardware and software development tools allow the user to create control functions of the system and easily test the developed algorithms.

References

- [1] Texas Instruments, 'TMS320F2810, TMS320F2811, TMS320F2812: Digital Signal Processors', Data Manual, 2004.
- [2] Texas Instruments, 'TMS320F2812 Analogue-to-Digital Converter (ADC) Peripheral Reference Guide', Literature Number SPRU060, 2002.
- [3] Texas Instruments, 'TMS320F2812 Event Manager (EV) Peripheral Reference Guide', Literature Number SPRU065, 2002.
- [4] Texas Instruments, 'Code Composer Studio v3.0 Getting Started Guide', Literature Number SPRU509E, 2004.
- [5] Visual Solutions Inc, 'VisSim V5.0 users guide', Westford MA, 2002.

NEW TECHNOLOGY FOR VARIABLE PITCH AND VARIABLE SCREW PROFILE WORMS MANUFACTURING

Cs. Gyenge¹, L. Oláh² and Hodis Andrei³

¹ Professor Technical University of Cluj-Napoca, Romania

² PhD – ROTORCRAFT AG, Switzerland

³ PhD stud. Technical University of Cluj-Napoca, Romania

Keywords: Gearing, Precision turning, roller transmission

Abstract. The rolling transmission wheels have variable pitch and variable screw profile surface section. In this paper is presented the screw geometric profile and one new machining technology developed by our team. Machining with high precision turning is a promising solution. The profile manufacturing can only be made on high precision machines, which are available at Direct-Line Ltd.in Budapest, where was realized the experiments.

1. Introduction

It is well-known that the CAD / CAM systems has enabled to develop a lot of new and more complicated products and technologies. A good example in this way can be the rolling-element drive, [1], which create the new relationship of the gears and worm wheels with a near-pure rolling contact. The rolling-element transmission eliminates the disadvantages of conventional engines, advantageous properties of the 21 century power plant be considered [2]. The gears, worm and worm wheel load transmitting surfaces, variable pitch screw profile and changing areas will be. Machining of such surfaces, cutting, 5 axis tool movement is normally possible. The CAD / CAM system has enabled the production of such surfaces, but it is necessary to solve some specific technological and economical problems. In this purpose our team developed and verified new CNC technologies for manufacturing the variable pitch screw section at one Ultra-precision surface machine. The use of high-precision lathe, hard ball screws and nuts are made of hardened cutting process. Periodically repeated, variable pitch and variable surfaces for high precision hard turning screw section, a new technology, according to the results of research and testing, the range of geometric, industrially applicable and will be a competitive solution.

2. The practical utilization domain of variable pitch and section screw

The variable pitch and section screw is one active element of the new type of rolling devices having high precision and long life. In figure 1 there are presented a conceptual schema of related gearbox having 45 ° angle between functional axes.

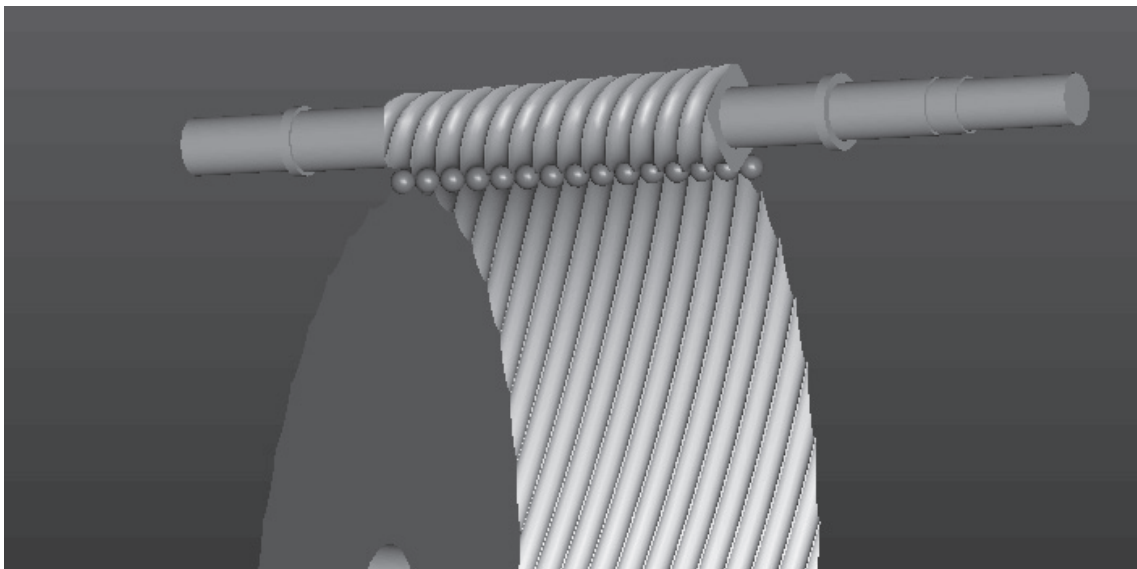


Fig 1.Utilization of the variable pitch and section screw at one special gearbox.

The rolling-element involved in rotation of the wheels and the torque transmitting balls roll along are moving across a spatial curve, which is also called the switching path. To be able to realize one good contact between, without big value of friction and slipping it necessary to have one special variable pitch and section screw.

3. Geometry of new variable pitch and section screw

In order to present we have chosen a particular worm axes used in precision mechanics (Fig. 2). The 3D model was designed with ReEngineer program. In figure 3 we can see the diagram of pitch changing along the axes, in comparison with one constant pitch screw (represented with interruption line)

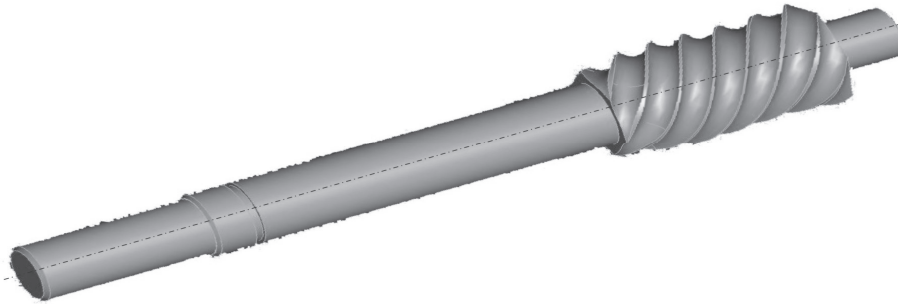


Fig.2. General view of variable pitch and section worm

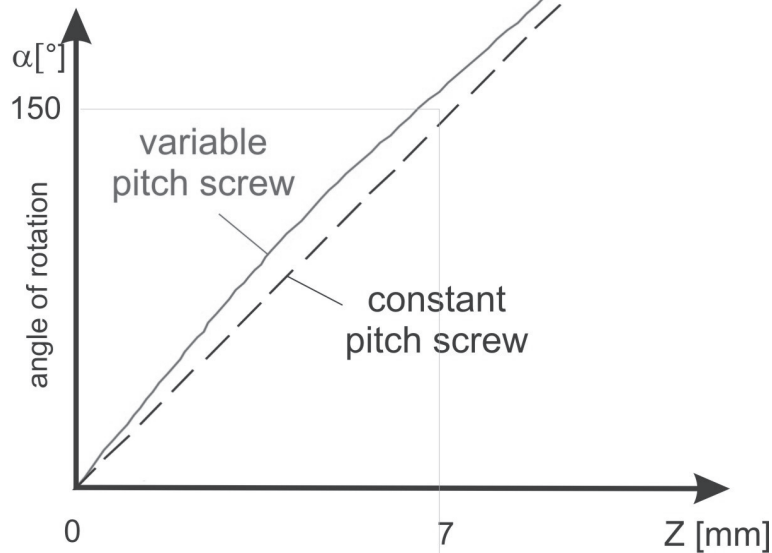


Fig.3. Pitch variation diagram

The normal section of worm is presented in figure 4, from which we can observe the continuing variation of curvature. Ball bearing load capacity is highly influenced by the contact point radius. Along the worm axes the radius $R_{21}, R_{22}, R_{23} \dots R_{2n}$ is in continuing changing. So in every section there are different profile (fig.5.)

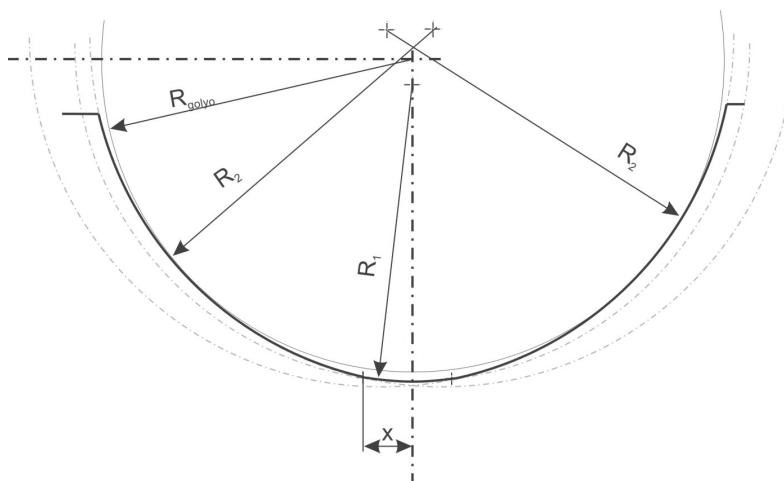


Fig.4. The normal section of analyzed worm

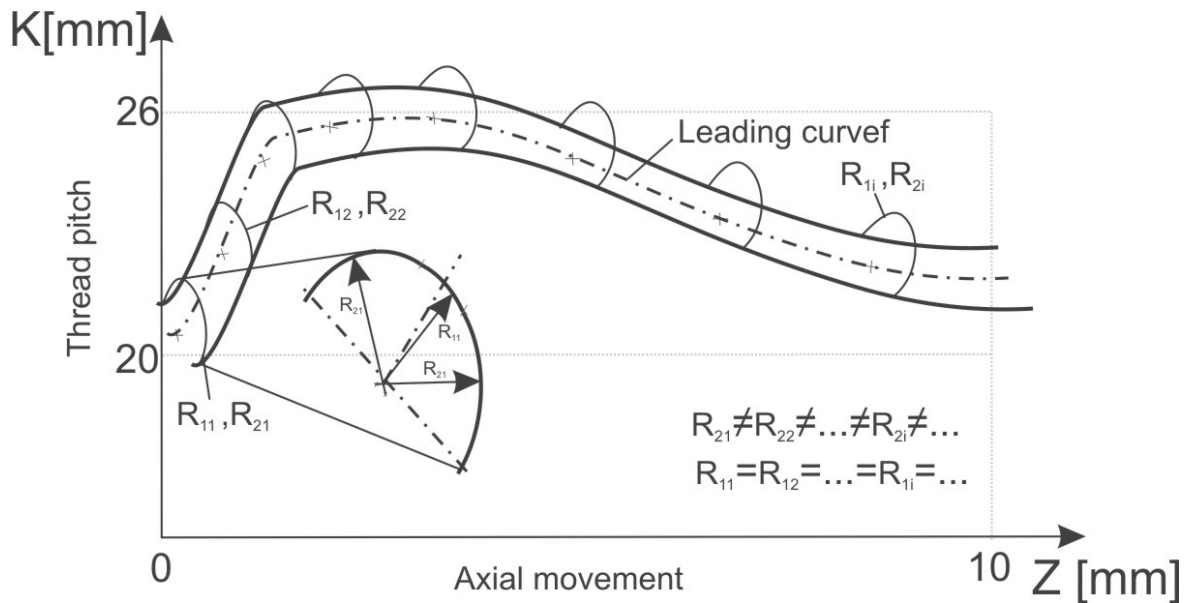


Fig.5. Continuing variation of section along the helical line

4. New technology for manufacturing of variable pitch and section worm

The manufacturing of variable pitch and section worm contain from two different phase: roughing and finishing. In both two phase we programmed screw chains. In the phase of roughing the movement speed of tool is on synchrony with main axes of the machine. Taking in consideration the fact of relative big value of pitch, it is necessary to realize high value for stopping and starting accelerations.

Rough cutting.

At this phase isn't necessary to realize absolute accurate equidistant profile of screw helical flute because the addition for finishing is bigger in comparison with section profile modification. For programming the special machine tool we calculated the X, Y, Z coordinate of succession points. Between the successive points we introduced some short Archimedean helical lines, which will be realized by tool (fig.6). In the figure with interrupted line we represented the profile which will be realized at roughing phase. Using the geometrical data sheet we built one special program which was enabling to realize the necessary helical flute. For these phase we used one CBN tool with $R = 0,4$ mm top radius.

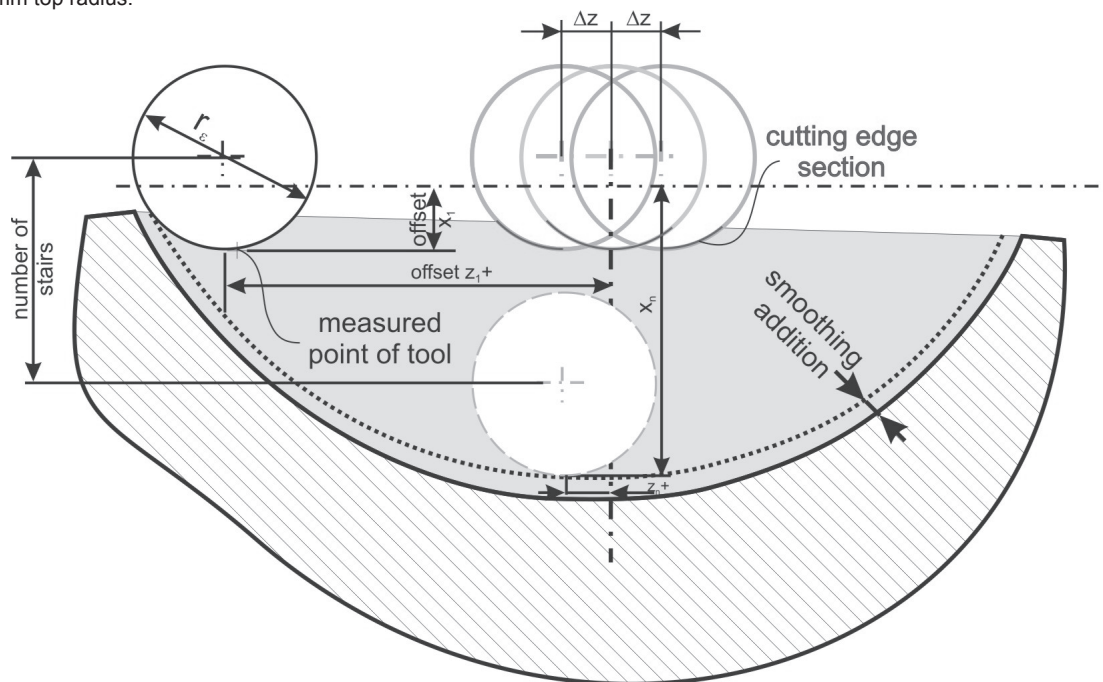


Fig.6. The profile at rough cutting in axial section.



Smooth cutting phase

For finishing we developed one special program enable to realized the variable pitch and section helical surfaces on necessary quality. As against with roughing, here for every crossing was necessary one characteristic orbit for tool. These orbits was established with one special program developed by us. The finishing phase was realized with one CBN tool with $R = 0,8$ mm top radius.

5. Conclusions

The high worm realized by ultra precision touring was compared with some worms realized by milling and the result was that at our technology it s possible to obtain higher quality for rolling balls. The manufacturing time was little bigger but taking in consideration the obtained quality, we appreciate for the following our researches in this field, it is necessary to increase the developed program. At the same time, we conclude that for serial production of drives with rolling bells it is necessary to solve a lot of technological and economical aspects.

References

- [1] Inventor: István Bogár, Roller Transmission Gearing Mechanism Patent publication No.: WO 2007/077470 A1
- [2] Bogár I., Reith J., Mészáros I., Oláh L. M. Technological problems of roller gearing mechanism, Gépészet 2010. Budapest, 2010. Május 25-26
- [3] I. Mészáros, D. Szepesi, Hochpräzisions-Hartdrehen als optimierter Prozess Werkstatt und Betrieb 138 Jahrgang 11.11.2005, pp.58-62
- [4] Mészáros, I. Huijbers, M., Hartgewindedrehen verkürzt die Prozesskette Wekstatt und Betrieb 9/2002 p 33-35
- [5] Mészáros, I. Huijbers, M. Das Hartdrehen bekommt neue Anwendungsfelder Werkstatt und Betrieb 4/2003 p26-28

THE MAIN INVENTORY MANAGEMENT SYSTEMS – THEORY OF INVENTORY, THREE METHODOLOGIES

H. Pechová¹, V. Preclík¹

¹ CTU in Prague, Faculty of mechanical engineering, Department of manufacturing technology, Technicka 4, 166 07, Prague, Czech Republic

Keywords: logistics, methodology, inventory management, inventory theory

Abstract. Logistics is important for functionality of companies. Financial losses are caused by bad logistics. Therefore it is very important to know which problems need to be solved and where to start from. If no problems occur it is very probable that a basic problem exists. Some basics don't function. The question is if a method, which can find poor places in processes and give good strategy for finding it, exists. The other question are the ordering systems, which are an important part of logistics.

Introduction

The article discusses the design of a suitable methodology, which depends on inventory management, inventory theory, transportation and on many other factors. Such a methodology is needed, which shortens the time delays and time losses between individual operations. Delays are minimized and business continuity and supplement of products is ensured. This leads to the fact that companies give their products on time without production errors.

The main inventory management system

dependent demand - it can be inferred from the demand for a commodity or item. For example, demand the production hall, which has certain requirements for warehouse, storage products, the specific amount in order to build the planned number of final products • **appropriate dose planning method** - used in manufacturing enterprises. Assemble the production schedule for finished products and then use the BOM needed to calculate all components. The time advance in this case does not count. • **Equipment Material Requirements Planning MRP 1** - designed to calculate dependent demand in quantity and time. The calculation is based on a fixed production plan, the bill of materials and data on the existing backlog of orders. It is important that the final product was completed when the customer requests it.

Independent demand - occurs randomly and is not related to demand for other types of goods as demand for goods in the shopping center. For an independent inquiry is used: • **statistical method of determining benefits** - a common method for inventory management. Unable to plan future moments ordering (dose according for example Campova formula) • **The method of time-ordering moment** - except for portion size and safety stock into account the time value. It is determined in which time they will have to be submitted orders and contracts to ensure the expected need.



Fig.1 Packaging Machina

Management systems for independent demand

Ordering systems are used for inventory management of individual inventory items with uniform, constant, independent of demand. The tale of demand is defined so that its expected - the planned size does not change with time. It is a stationary demand. In these systems,

the signal of the need to make an order to replenish inventory published in fall layout (signal stock) below a certain amount of the (order level).

Order level inventory (also known as point of order or signal level) is proposed to cover the required reliability of the demand during the expected duration of the interval from the signal of the need to subscribe to receive the delivery to the warehouse. This time period is called cost and denoted by t_p . Order management systems implemented according to the flow of material supplies. These systems do not identify the future moments before ordering, as well as moments or future deliveries to the warehouse. The lengths of the intervals between deliveries vary, depend inter alia on the quantitative and temporal fluctuations of demand from planned.



Fig.2 Automation Robot

Variants of ordering system

Ordering systems give the answer to the question when and how much to order for replenishment. As the moment the signal of the need for order and order size for the two alternatives are available. Combining these two variants are formed four ordering systems, which are called (Bo Q), (Bo, S), (Bk, Q), (Bk, S).

Variants of the time of the signal:

- Signal is issued at the time when the disposition of stock items first order drops below the level called Bo, store layout is compared continuously with ordering levels, ie at each occurrence requirement to be dispensed (each dispensing items - signání assembly can occur per day)

- Store layout is compared with ordering levels, Bk known only periodically at intervals of fixed length t labeled (for example, weekly, biweekly or monthly) - signal generated only periodic reports are more comprehensive

Inventory management systems

Default assumptions - system (Bo Q):

- depletion of course be taken to facilitate the uniform
- size of the replenishment is done in certain doses, the dose is called (Q)
- order processing takes time t_l (delivery time), order must be made before the stock falls to zero, precisely the time t_l
- the amount of inventory, if reached, or exceeded it is necessary to place an order, call the order level (B)
- coverage for variations in delivery times we need to create safety stock (Pz)

Systems "Bo" need for its proper function carefully and keeping records current inventory. They are used to manage inventories, especially for a limited number of significant items of great value annual sales or consumption, as well as expensive or important items for other reasons. The disadvantage of these systems is more labor intensive inventory management. If this is the order quantity, the "Q" are universally applicable. For less frequent demand (requests for larger quantities come with longer distances) are recommended for systems rather "S". They minimize the impact of fluctuations in demand variability on the time interval between orders (and hence supply) for production orders greater regularity of spacing between doses may have a positive impact on the planning and production management, or maintenance and repairs.

Theory of inventory

The role models of inventory management is to determine how many products produce or order to store. At the same time is necessary to provide an economically advantageous relationship between the costs of storage products and losses as a result few stocks.



Inventory management models are designed to reduce total cost of acquisition, storage and use of supplies, including potential losses that may occur if the supply is not needed. The sizes of orders and dates are the end result of the calculations performed.

The essence of the theory of inventory

Exist basic information, which is good know during control inventory systems. And from these shows, when is preferable smaller or larger reserve. Insufficient supply may cause high losses, which are higher than the cost of storage, such as loss of customers or stopping production Regular orders (supply) reduce the cost of resources that are bound in stocks and also reduce storage costs. They increase the cost of the items associated with supply processes as well as shipping costs. The inventory is a certain amount of funds that they are unnecessarily high, thus blocking funds that could be used otherwise. (You still need to count the cost of storage).

Three Methodologies

In the design process of a suitable methodology I compare three methodologies. The first methodology is KLA, the second methodology is VDA 6.3. and the third which I discuss is MMOG. I examine which one would be the best and most effective for the production process.

The 3 methods: 1) Methodology by KLA, 2) VDA 6.3., 3) MMOG

Methodology by KLA - In this method control, production and quality take approximately the same percentage part. The biggest part in this methodology take logistics and support processes. The advantages of this method are that it is logistically detail, and reveals the potential of design activities. The disadvantages are: not too good efficiency and not very good continuity.

Methodology by VDA 6.3. - In methodology VDA 6.3. control, production, quality and logistics approximately the same percentage part. The advantages of this methodology are: the volume of all departments, shows good continuity and another advantage is customer regulations. Disadvantages are that it does not go into depth and do not detect potentials.

Methodology by MMOG - This method includes in addition supporting files. Supporting files plus control, production and quality take approximately the same percentage part. Logistics take approximately fifty percent in this method. The advantages are that it is logistically detail, allows detection of potentials, allows selection efficiency and customer regulations. The disadvantages are the necessity of supporting files and poor continuity.

Logistics audit - methodology

Logistics audit is defined as global diagnostics of production processes. Logistics audit consists of: Objektivit, The auditor's independence, Concealing some business data, Follow-up solutions, Repetition, Control outputs.

The reasons why to study logistics audit are to be able to find problems of logistical character. Nowadays the detection of such logistical problems is very significant and also complex activity. If the provided logistical auditor is capable of designing the project assignment or changing the program according to the audit results, then analysis may be more effective and go more in depth. In the absence of standard logistics, for example ISO 9000 standard of management quality, it is not a problem. Integral logistics is nowadays a field that is spread and highly structured. The methodology allows the logistics so-called „mirror“ for all type of organization and management of material flow.

Content logistics audit

The starting point of logistics audit is the division of the functions of the firm on primary and secondary. The primary functions include PURCHASE-PRODUCTION(or OUTPUT)-SALE. The material flow is implemented based on these functions. The secondary function has its own logistics, quality, skills, technology, information and money.

The design scope of logistics audit

Logistics audit, its scope is dependent on how the organization is large and further the process and product complexity of its activities. For this purpose, a table giving the capacity requirements for an audit, related to the cast discussed the primary functions (Purchasing - Production - Sale), to locate the company's organizational units and the total number of employees. Implementation of logistics audit depends on the precise preparation and good organization. Then followed a lot of interviews and visits to company premises and at the same stage of information materials. Audit results are documented, then submitted for approval and verification of the audited company managers, and finally presented to the senior management of the company.

The outputs of the logistics audit

The set two circuits logistics audit objectives are prepared and documented two main outputs: Report audit of logistics, Materials for making the project (program) changes in logistics. Entering the project (program) changes in logistics includes parts that are usual for

subsequent analysis of additional processes and proposal for implementation of the logistics elements, meet the required logistics functions. Making the proposed changes can be achieved by solving individual tasks to designated experts, organizations, training and workshops, or implementation of other projects (or subprojects) in connection with other functions company-wide management system.

Evaluation of the importance of logistics audit

Only logistics audit solve incurred or expected role in the logistics, company is facing. In addition to observation status, you need to find such paths that lead to positive changes in the company. The issues of what needs to change, audit determines how, by whom, when and for how much change is possible. The audits show that this form of input into the issue of logistics is an effective and important element of logistics consulting services. **Diagnostics - the result of** structure, marking and sorting errors or achieve the highest possible condition based on good design solutions and build the right priorities

Evaluation

The goal is to design such a methodology in logistics, which will be optimal for the concrete manufacturing process. The characteristics of the optimal methodology are minimal delays, high quality, efficiency, and productivity and of course minimum cost. An important feature of logistics process is taking in account a time reserve storage and transportation to the customers. And of course deliver the products with the required quality and within the required term. Fulfilling all these criteria is accomplished by choosing the optimal methodology of the manufacturing process and having a well-coordinated logistic string.



Fig.3 Handling Technique – Forklift

References

- [1] Preclík, V.: Průmyslová logistika, CVUT Praha 2006
- [2] Vokálová, J.: Modelování v řízení 30, CVUT Praha 2004
- [3] Ambrosino, G.; Boero, M.; Nelson, J. D.; Romanazzo, M.: Systéme and Advanced Solutions for eLogistics in the Sustainable City, ENEA 2005 Rome (Italy)

[4] <http://www.dynamicfuture.cz/>

Fotos used from Brno Expo 2011

VIRTUAL MODEL AND PRODUCTION PLANT SIMULATION FOR OPTIMIZATION OF POWDER COATING PROCESS

L. Šikulec¹, D.Hasković¹ and H. Radelja¹

¹ University of Rijeka, Faculty of Engineering, Vukovarska 58, Rijeka, Croatia

Keywords: virtual model, production plant simulation, optimization, powder coating

Abstract. The paper presents proposal of optimization strategies for powder coating facility. The powder coating production line is analyzed and virtual model is created using Plant Simulation software. Model was used for simulation of production process to find weaknesses of the process. Different strategies for improving the process are considered.

Introduction

Because of the growing competition, the pressure to increase the efficiency of production systems has increased significantly. In addition, the number of technical components in a number of products increases, and therefore also growing requirements for installation and logistics processes. These demands could be answered with the help of appropriate tools for product lifecycle management (PLM), which enable re-use of data that are always available to any user who need support and effective cooperation between the various departments. Simulating the complete flow of materials that includes supporting the production, storage and transport activities is recognized as the key to a successful business, and is now widely used in the industry [1-10]. It is possible to achieve a reduction in inventories and an increase of throughput by around 20-60%, and increase the productivity of existing production systems by about 15-20%.

The reason for performing simulation can be to achieve strategic, tactical or operational objectives. To achieve the strategic goal is observed that the factory would be built in the country taking into account the logistics and efficiency of workers, machinery malfunctions, flexibility, storage costs etc. In order to achieve tactical objectives, the simulation is performed for an average time of 1-3 months in order to analyze the need for resources, optimize the sequence of operations and the size of the series. To simulate the operational level, information about the current state of manufacturing equipment and state of the current work should be concluded, in order to ascertain time and to achieve planned production to determine support strategies for disruptions in production.

Coating process

Due to the large share of manual labor in the factory for the powder coating it was not practical to use classical methods of optimization, so method based on the stochastic processes were looked into for optimization, in order to:

- detect and display problems that might otherwise lead to costly and time-consuming corrections,
- providing mathematically calculated performance indicators rather than instinct "experts",
- reduction of investment costs of production without affecting the required amount of production,
- optimizing the performance of existing production system.

Tools used for powder coating process simulation and optimization

Plant Simulation

Is based on the object oriented programming with following features.

- Inheritance: Creating a database with its own facilities that can always be used. Unlike the copy, any changes to the object within the database is transferred to all objects-descendants.
- Polymorphism: Classes can be taught, and the methods can be performed again redefined. This allows for quicker and easier creation of complex models with a clear structure.
- Hierarchy: Complex structures can arise in several logical layers. This allows top-down and bottom-up approach to design.
- Possibility to import data from other systems, such as Access or Oracle databases, Excel spreadsheets ...
- Integration: Plant Simulation is supporting import of data from other PLM programs
- Download of the spatial distribution of other programs (AutoCAD, MicroStation, FactoryCAD ...) directly in the simulation
- Includes tools for detection and detailed analysis of the bottlenecks (Bottleneck Analyzer), a tool for monitoring the material flow (Sankey diagrams) and a tool for detecting oversized resources (Chart Wizard).

Optimization:

Following tools were used for optimization:

- The Experiment Manager automatically generates scripts or evaluating interactions between two input parameters.
- Genetic algorithms are searching in wide range of solutions.
- Neural networks are displayed on the connections between the input and output parameters and can be used for prediction.
- Data Analysis: Detection of interdependence, regression analysis, functions eligibility.

Simulation

Manufacturing is one of the most important areas for application of simulation. Simulations are very important and valuable tools used by engineers to assess the justification of the investment cost in equipment and facilities such as factories, warehouses and distribution centers. A simulation allows predicting the performance of an existing or planned system and is used to compare alternative solutions to a problem. Another important goal of simulation is to determine the performance of production. In simulation plan we used following information's abbot process: Structural data factory layout, Means of production, Transport functions, Transport routes, Areas limitations, Production time data usage, Performance Information, Conveyors capacity, Material flow information's, Availability, Working time, Shifts schedule, Product Data Work Plan and all others organization information's which we have collected in the company.

Powdery Coating

All pieces which will be coated should hang up on conveyer. The entire cycle is composed of the following phases:

- 1) Preliminary stages of cleaning / degreasing
- 2) Drying in an oven
- 3) Application of the powder in the chamber
- 4) Polymerization in the oven
- 5) Cooling



Fig. 1 Powder coating production line

Virtual model

It is necessary to define a model that describes the real manufacturing system for powder coloring work pieces that are used in the company Alpron. It is important to successfully replicate the results that are achieved in the real world, and when that is achieved, apply optimization methods and searching for better and more efficient ways. Each element of the virtual model has a specific function that attempts to replicate the real world. By changing the parameters, it is possible to see how the results change, and whether the changes contribute to the improvement of the process. Based on data collected from documentation and observation of the technological cycle and containing the type of equipment, cycle time, capacity, consumption, length of lines, etc., and the layout of the production facility started the modeling.

The whole process can be divided into fully automated part and on the part of workers who perform. Automated part of the process includes conveyors, washing phase, the phase of drying in the oven and roast or phase polymerization. Jobs hanging work pieces, deflation, causing dust and removing work pieces performed by employees.



Conclusion

When compared with the behavior of the actual production system the simulation model results depend on the quality of the input data and the accuracy of the virtual model. When it comes to assembly processes and transportation systems, their control systems, workers with multiple profiles or qualification, warehouse management, manufacturing processes become very complex. By using object orientation and inheritance, it is possible to optimize multiple parameters of the system taking into account the reduction of supplies, increase efficiency and throughput.

Visualizing the whole model in a 3D environment provides more realistic presentation of the system behavior. In conjunction with the insight in a virtual reality model one can really get a sense of how things will look like and what are the potential weaknesses of the current model before the production system is build, which allows for changes at minimal cost.

Based on the results of analysis of bottlenecks and usability of the system, it can be concluded that the throughput of the system can be increased with fully automated powder coating process by replacement of the workers with machines or robots. This decision depends on the size of the planned series, and the financial, technological and spatial capacity of the company. Greater efficiency can be achieved by accelerating production lines speed from 1 m/min up to maximum of 3 m/min, whilst taking into account the increase in energy consumption and increased system load.

Future research will consider the possibility of reorganizing the weak work places and used to compare the solution of spatial reorganization of production lines and serving more jobs from one worker to the decision process of automating and replacing workers with machines. Also, examine the values of speed production lines in order to find optimal values for different objective functions, higher productivity, and lower costs.

Acknowledgment

The authors would like to acknowledge the support provided by the University of Rijeka Foundation and Alpron d.o.o., Croatia.

References

- [1] Bangsow, Steffen: Manufacturing Simulation with Plant Simulation and SimTalk, Springer-Verlag Berlin Heidelberg, 2010.
- [2] Kršulja, Marko; Cukor, Goran; Car, Zlatan. Simulation of Product Logistic, Investigation of Facility Layout Capabilities, *International Conference on Innovative Technologies IN-TECH*, Prag : Tisk AS, s.r.o., Jaroměř, ISBN: 978-80-904502-6-4, 2011.
- [3] Šikulec, Leon; Radelja, Hrvoje; Kršulja, Marko; Car, Zlatan. Comparison in Production Planning of the Classical Method and RL Advanced Algorithms, *Proceedings of International Conference on Innovative Technologies IN-TECH*, Prag : Tisk AS, s.r.o., Jaroměř, ISBN: 978-80-904502-6-4, 2011.
- [4] Car, Zlatan; Barišić, Branimir; Kršulja, Marko: Simulation and Modelling of Paths Processing Time in a Flexible Manufacturing System. *Výrobné inžinierstvo*. VIII (2009), 3; 40-45.
- [6] Stankovic, I.; Car, Z; Barišić, B.: Comparative Simulation of Heavy Machining Production System, *Engineering Review*, 31-1 (2011), 1-11
- [7] Car, Zlatan; Hatono, Itsuo; Ueda, Kanji: Reconfiguration of Manufacturing Systems Based on Virtual BMS. *CIRP Journal of Manufacturing Systems*. 33 (2004), 1; 15-24.
- [8] Adar A. Kalir, Subhash C. Sarin: A Method For Reducing Inter-Departure Time Variability in Serial Production Lines, *Int. J. Production Economics*, 120 (2009) 340-347.
- [9] Ari-PekkaHameri: Production Flow analysis Cases From Manufacturing and Service Industry, *Int. J. Production Economics*, 129 (2011) 233-241.
- [10] NimaSafaei, RezaTavakkoli-Moghaddam: Integrated Multi-Period Cell Formation and Subcontracting Production Planning in Dynamic Cellular Manufacturing Systems, *Int. J. Production Economics*, 120 (2009) 301-314.
- [11] Internal documents, Alpron d.o.o. , <http://www.alpron.hr/>, 2012.

INVESTIGATION OF SINGLE POINT INCREMENTAL FORMING PROCESS APPLIED ON THIN SHEET METAL

M. Kršulja¹, K. Kuzman², M. Plančak³, M. Math⁴ and Z. Car¹

¹ University of Rijeka Faculty of Engineering, Vukovarska 58, 51 000 Rijeka, Croatia.

² University of Ljubljana Faculty of Mechanical Engineering, Aškarčeva 4, 1000 Ljubljana, Slovenia.

³ University of Novi Sad Faculty of Technical Engineering, Trg Dositeja Obradovića 6, Novi Sad, Serbia.

⁴ Faculty of Mechanical and Naval engineering, Ivana Lučića 5, 10002 Zagreb, p.p. 102, Croatia.

Keywords: SPIF, deep drawing, sheet metal forming, incremental, Solidcam

Abstract. Single incremental metal forming SPIF and deep drawing process are similar technologies and SPIF can be used to build a prototype for additional analysis and later construction. In this paper the selection of parameters needed for SPIF process production with software Solidcam are shown. A consideration to strain hardening has been given. Experiment on a thin sheet metal TH435 CA ST E2.8/2.8 of 0.19 mm thickness has been conducted in order to understand basics of the technology.

Introduction

The Single Point Incremental Forming (SPIF) process is a flexible sheet metal forming method adapted to form various complex shapes using a milling machine, a multi-axis robot or a dedicated machine without the need of specific and costly tools, such as a punch and die, as described by [1]. To increase the quality of the final geometry, it is still possible to use a die that can be manufactured in a cheap material because the applied forces are low. Depending on the length of the tool path and speed of the tool, the forming process can take up to a few hours for large parts. It is, in consequence, adapted to small batch production and rapid prototyping. Furthermore, the SPIF process, is known to shift Forming Limit Diagrams (FLD) to higher formability [2] compared to conventional forming processes. Because SPIF has a high industrial interest, the applicability of this technique on the new material studied must be experimentally verified. The problem of shape inaccuracy which is usually an important limiting factor for SPIF applications, must be solved [3]. The SPIF process can be optimized by experimental trials and errors and/or by a numerical analysis. The numerical approach predicts the forming forces and the final shape according to the tool path. However such information is accurate only if the simulation has been validated by experiments. During the working process the position of the tool is defined by the process kinematics and the force of deformation depends on the tool path. The forming force is controlled by the operator during the whole process. As it can be seen from Fig. 1 a sheet of metal is tightly clamped in a working device and then the spherical tool executes the working process. The tool moves along a predetermined contour in the horizontal plane, after which the tool incrementally descends and starts a new contour in the next horizontal plane, building up the workpiece layer by layer.

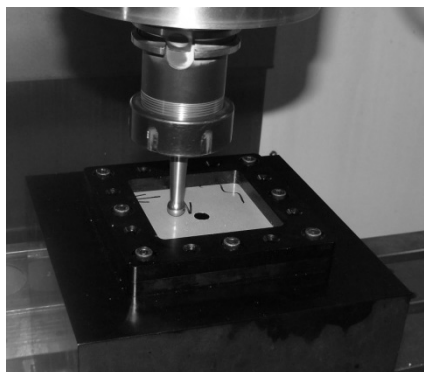


Fig. 1 The experiment in this investigation was conducted on a Hurco VMX 30m milling machine

Thinning of the workpiece is the dominant failure mode in SPIF and is related to the workpiece drawing angle. For a given material and initial thickness, the maximum drawing angle represents the limits of the conventional incremental forming process. In this investigation thin sheet metal TH435 thickness 19 mm was used, the material is used in packaging industry for cans that are made for meat products. The used specimens were coated from both sides with Alupigmented Lacquer homogeneous opaque film of silver-grey color.

Solidcam

Solidcam software 2009 was used to simulate milling parameters needed for deformation process of incremental sheet metal forming. The model was done in Solidworks software and in Solidcam the target, stock, tools and a strategy for tool path was selected.

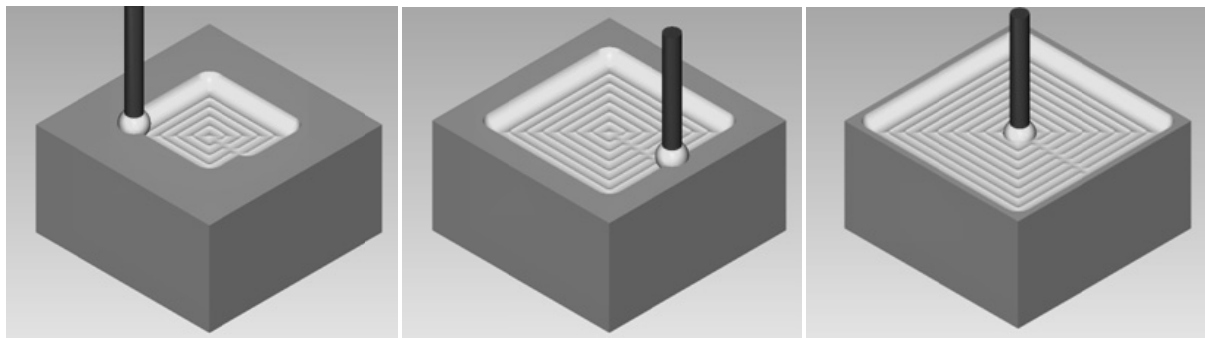


Fig. 2 The programming of layer by layer cutting-deformation

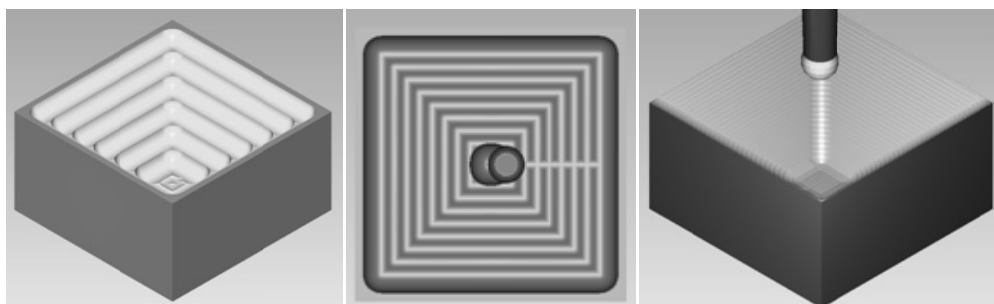


Fig. 3 Final look of solidcam modeling

The programming was done by creating milling condition that would remove layer by layer (Fig. 2 and 3) but instead of cutting deformation is introduced. This manner of programming allows for corrections of the deformation process, however material hardening takes place. Low carbon steel generally exhibits a very linear stress-strain relationship up to a well defined yield point (Fig. 4), [4]. The linear portion of the curve is the elastic region and the slope is the modulus of elasticity or Young's Modulus. After the yield point, the curve typically decreases slightly because of dislocations escaping from Cottrell atmospheres. As deformation continues, the stress increases on account of strain hardening until it reaches the ultimate strength. Therefore it can be said that the work done is conducted on a strain hardening and close to necking area (4 and 5 on the Fig. 34 which makes material brittle and prone to crack occurrence. It is because plastic deformation is accomplished by substantial movement of atomic planes, dislocations which may encounter various obstacles. This movement becomes more complex as number slip systems may be activated during the deformation.

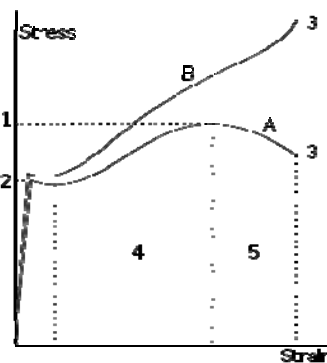


Fig. 4 Strain hardening and the stress strain curve

The most common equations used to describe the hardening behavior of the material flow is (1):

$$(1)$$

where σ – is strength coefficient and n – is strain hardening exponent. The strain-hardening exponent may have values from $n=0$ (perfectly plastic solid) to $n=1$ (elastic solid). For most metals n has values between 0.10 and 0.50. The Power law equation described above is also known as Holloman-Ludwig equation.

Tools

Experimental work has been executed on a CNC milling machine Hurco 30 using specially adapted tooling connected accordingly to tool holder CAT 20. Rod shaped tool (Fig. 5) was used in order to create necessary deformations. This tool has a smooth hemispherical head of diameter $\varnothing 12$ mm and it is clamped into a spindle of the milling machine. Tool used in process was $\varnothing 12$ mm carbide tool of total tool length 120 mm, the tool was selected as lollipop milling tool as it is the most similar to the actual tool used in process. Adequate length

of outside holder is necessary for reduction of possible vibrations the primary impact of workholding on surface finish is vibration. In the worst case vibration will turn into chatter, which is a harmonic effect that will be very visible on the surface finish. Cutting conditions were selected feed $v_x = 1000$ mm/min, spin rate = 3000 rpm feed $Z = 33$ mm/min, Δz was selected as 1 mm (Fig. 5 and 6). The feed z was used in combination with helical path in order to avoid direct pressure on single point while lowering for the assigned Δz .



Fig. 5 Tool used in the proces is similar to lollipop mill and was made of carbide steel

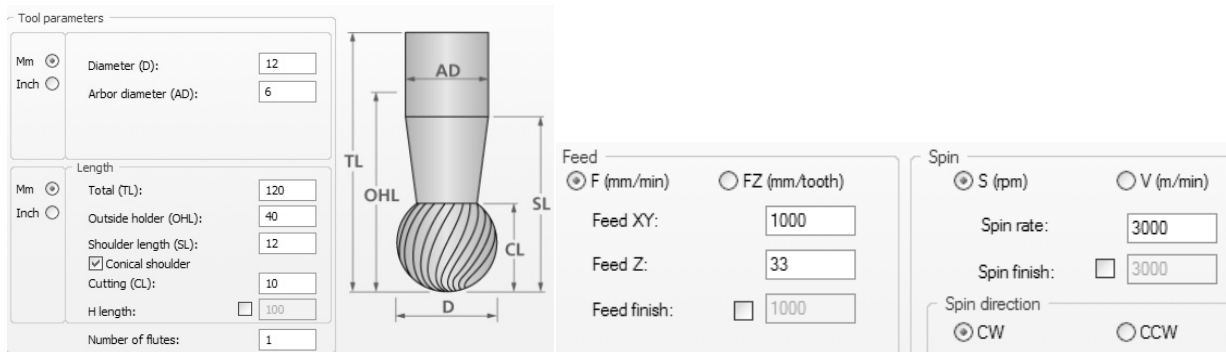


Fig. 6 Cutting conditions

Overlap

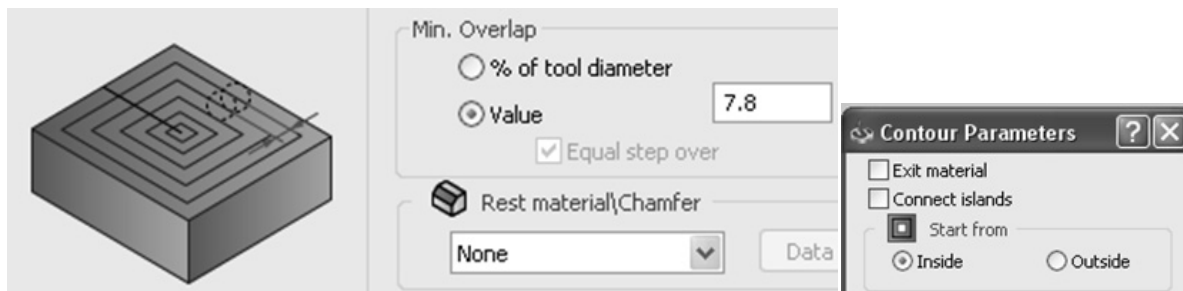


Fig. 7 Scalop or minimum overlap was selected as 0.6 of the tool diameter, center was selected as the starting point

Overlap Fig. 7 determines the distance from the number of passes and distance between each pas in xy direction. Recommendations in literature for minimum milling overlap are 60 % of tool diameter and this distance was used in the investigation. As the tool is in contact with surface with one point and comes to a higher surface contact when it is working edges different strategies can be applied. The thinning can be regulated by careful tool-path generation and modification of overlap by equalizing the stress-strain conditions between each pass.

Experiment

Experiment was conducted with a specimen of 100 x 100 mm and the product dimensions of $\varnothing 60 \times 10$ mm. Material that was used was TH 435 CA ST E2.8/E2.8 with 0.19 mm thickness, [8]. The workholder was made of aluminium and carved from one block to increase stiffness of clamping process and remove possible workholder vibrations. For experiment purposes a round path was selected, a depth the contour parameters for the experiment were selected from program and taken from the center toward the outside. A hole was drilled at the center of specimen after it was clamped in order to increase stability of the deformation process [6, 7]. The wall angle was 90° and it broke at the 10 mm depth.

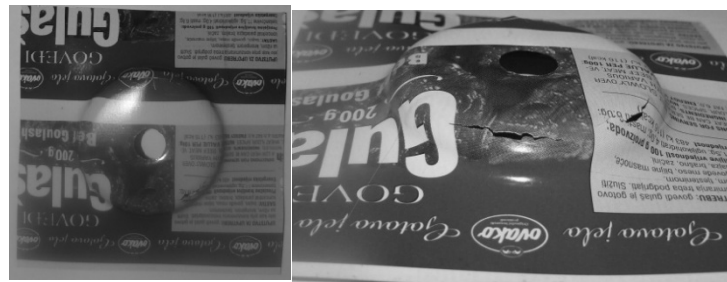


Fig. 8 The tested cone

In the Fig. 7 the tested cone is shown. The crack occurred in two places at the opposite direction this indicates dependency on anisotropy properties as the crack first occurred direction of rolling at the 0° of material Fig. 9. Variations of rotational spin speed from 1000 rpm and 3000 rpm were used and they showed no noticeable difference and also the $\Delta z = 2$ mm and $\Delta Z = 1$ mm, however the material hardened and broke at the steep angle.

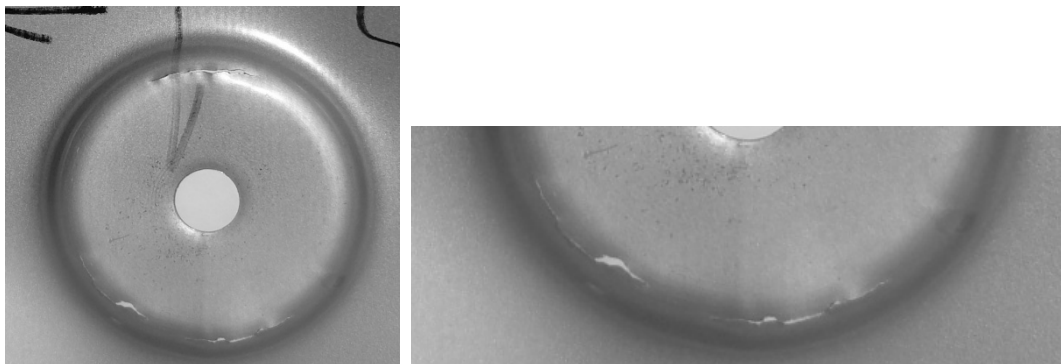


Fig. 9 Crack occurred in the rolling direction 0°

Conclusion

Incremental sheet forming process is a very promising manufacturing process which still requires further optimizations namely in the speed of the process and optimal tool path strategies. Numerous studies have demonstrated the effect of process parameters like advancing speed, forming force, tool depth step in the characteristics of the formed parts. Future research will include Finite element simulation based on different friction factors and possibilities to add to the formability process, with an elastic springback analysis, but also the evolution of strain and thickness distribution. Slip planes will also be investigated as slip depends on many factors including external load and the corresponding value of shear stress produced by it. For obtaining greater formability, the geometry of crystal structure and the orientation of active slip planes with the direction of shearing stresses generated needs to be addressed. Also the speed is very important and it can be achieved by designing faster and multiple clamping systems, and optimizing tool speeds, rotation, feed, feed in the z direction and amount of the lowering Δz .

References

- [1] Allwood, J.M., Shouler, D.R., 2009. Generalised forming limit diagrams showing increased forming limits with non-planar stress states. *International Journal of Plasticity* 25 (7), 1207–1230, doi:10.1016/j.ijplas.2008.11.001.
- [2] Filice, L., Fratini, L., Micari, F., 2002. Analysis of material formability in incremental forming. *CIRP annals—Manufacturing Technology* 51 (1), 199–202.
- [3] Micari, F., Ambrogio, G., Filice, L., 2007. Shape and dimensional accuracy in single point incremental forming: state of the art and future trends. *Journal of Materials Processing Technology* 191, 305–390.
- [4] Stress strain curve, http://en.wikipedia.org/wiki/Stress-strain_curve, 2012.
- [6] Julian M. Allwood, Daniel Braunb, Omer Music, The effect of partially cut-out blanks on geometric accuracy in incremental sheet forming, *Journal of Materials Processing Technology* 210 (2010) 1501–1510.
- [7] Z. Cui, L. Gao, Studies on hole-flanging process using multistage incremental forming, *CIRP Journal of Manufacturing Science and Technology* 2 (2010) 124–128.
- [8] MGK-pack - Pluto - Tinplate spec 2012, Private documents MGK-pack – Pluto, Rijeka 2012.

ANALYSIS OF THE DESIGNING RELATIONSHIP RESULTING FROM USING THE GOLDEN RATIO AND ITS DERIVATIVES IN THE ANCIENT CIVILIZATIONS (ANCIENT EGYPTIAN – GREEK – ISLAMIC)

Dr. Ebtesam Khamees¹

¹Lecture of interior design department, Faculty of Applied Arts, Helwan University, Cairo, Egypt

Keywords: Golden ratio – designing networks – designing relationships – old civilizations – old Egyptian civilization – Greek civilization – Islamic civilization

Abstract. Using the golden ratio in the old civilizations is considered a main direction of any design that has an authentic value and artistic sense. The old civilizations used the golden ratio in many of its architectural and decorative designs and furniture designs by networks that have been a direct application for that ratio. The most important civilizations are the old Egyptian civilization, Greek civilization and Islamic civilization. These three civilizations are considered the most important civilizations that established networks using science in the design, which depended upon that in all of its arts. So, it was important studying the way of using these civilizations for the golden ratio in building its designing networks, trying to conclude the designing relationships resulting from its using in each civilization and extent of success of applying that upon the contemporary designs.

Introduction

The pro-rata principle is the main criterion of design in all of the ancient civilizations starting from the Egyptian civilization that left many of the effects in all fields of arts, architecture, interior design and furniture. All of them are based upon engineering and calculating systems, its basis is pro-rata. They reached to engineering relationships and designing networks that made a civilization that is mother of the ancient civilizations. Do not say about its power of the Greek civilization where the genius Euclides in 300 B.C. several of important engineering and calculating that assisted the designer upon achieving the greatest designs. But the Islamic civilization including tremendous momentum of wonderful heritage in all fields of architecture to interior design and furniture design and terminating with the Islamic ornaments. All of them are based upon calculating and engineering theories based upon using the pro-rata principle. Its most important principle that is the golden ratio is used, in a way created several of marvelous designing relationships that constituted infinite designs that made it one of the most important and most successful ancient civilizations in this field.

Different uses for golden ratio derivatives in the ancient civilizations:

Pro-rata laws are multiplied in the civilizations. All of them participated in one common factor that is all of them are derived from the golden ratio. It is admirable that each of them used the golden ratio itself but in different style resulted in a different group of the designing relationships that distinguished each civilization than the other one where this research seeks to identify these relationships and difference aspects between them. These laws are the following:

First: ancient Egyptian civilization: there are many of laws specialized for pro-rata that depends upon the golden ratio used by the ancient Egyptian including: Small arm - Royal arm - Longitude - division - Netting division.

Second: ancient Greek civilization: the Greek used many of theories specialized for pro-rata that depended upon the golden ratio that based upon several of the designs in different fields of art including:
- Pythagoras' theories in pro-rata (musical ratio theories – Pythagoras fourfold theory) - Euclides theories for proportionality – golden sector ratio (engineering theories).

Third: ancient Islamic civilization: the Muslim artist and designer used several of the previous ratios used by the ancient civilizations but in different style including:
Engineering sequences – ideal ratios – golden ratios – using the square – golden rectangle – fifth root rectangle – golden sector - Pythagoras' quadripartite – proportional Safa brothers system.

The designing relationships resulting from using the design fundamentals in the ancient civilizations:

The designing relationships with authentic and distinguished values for the ancient civilizations are multiplied and differed. For instance, the designing relationships resulting from designing an ancient Egyptian temple façade differs from that is resulting from designing an Egyptian furniture unit too, than that is resulted from designing some of the decorative units in the same civilization. Also, it differs from one civilization to the other. Determining category of these relationships depends upon extent of its domination in the design.

Hence, we should identify the designing relationships for some design that it is: (outcome of using certain designing bases on designing some area leads to manifesting authentic values by themselves where they would have the domination in this design). Using the golden ratio in each of the architectural, interior and decorative design in the three ancient civilizations that have an imprint in the humanity history such as the ancient Egyptian, Greek, Roman and Islamic civilization led to creating several of the successful designing relationships that differed in each civilization according to the design fundamentals distinguished by that civilization in a way led to

difference of the feature in each of these civilizations than the others in spite of proving the factory of using the golden ratio in a way gives for its use the magic imprint for multiplication of successful relationships in each civilization.

For instance, the common, powerful and successful designing relationships in the three major civilizations are (exchange and repetition), sometimes contiguity and overlapping. By the analytical study, we can touch synchronism of existence of these relationships with using pro-rata rules especially the golden ratio in the design and also difference of the design bases supporting that in each civilization than the other one.

Concluding the designing relationships resulting from using the golden ratio in the ancient civilizations:

First: the ancient Egyptian civilization

The following Figure (1) clarifies the horizontal projection for Horus temple in Edffo. The above planning clarifies using the designer for the golden ratio in designing the projection. By analyzing the designing relationships generated from the design, we find that there is rhythmic degradation resulted from using the golden rectangle and also the symmetry around the horizontal pivot. But the Figure (2) is a ledge on the form of Copra decorations over cornice. It was divided with the golden ratio and its derivatives. It was resulted several of the successful designing relationships including overlapping.

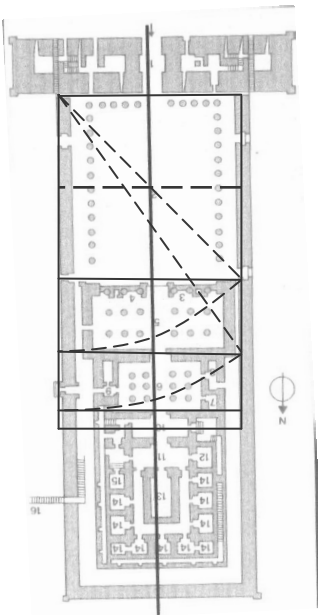


Fig. 1 the horizontal projection orus temple in Edffo.

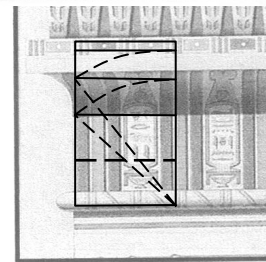
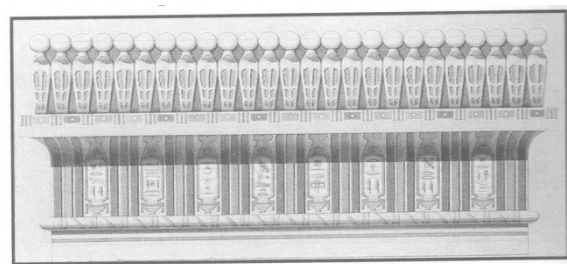


Fig. 2 a ledge of Copra decorations over Egyptian cornice.

But the Figure (3) is for some of the ancient Egyptian furniture pieces. Its design is ratios and measurements specialized for the Ancient Egyptians. It was derived also from the golden ratio. Both designs contained several of the successful designing relationships including contiguity, overlapping, symmetry and repetition.

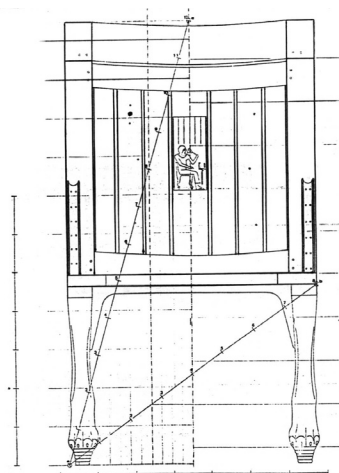


Fig. 3: chairs from the modern state that ratios were used in its design.

Second: ancient Greek civilization:

The following Figure (4) clarifies the front façade for Parthenon temple near Acrohol. It is surrounded by golden rectangle as we see in analysis of the facade. It consists of several of other rectangles. All of that contained several of designing relationships that gave it marvelous authentic values including symmetry and repetition where it seems as if the golden ratio has automatic renewal in each of addition or subtraction process, meaning that if a square is deduced from the golden rectangle, the rectangle will remain also golden. Consequently, it results these marvelous authentic relationships. Also, the horizontal projection for the Greek temple in diagram (4) that holds the same authentic values resulted from using pro-rata in the horizontal division.



Fig. 4: the horizontal projection and the façade specialized for Parthenon temple and analysis of the ratios used in the design

Third: ancient Islamic civilization

But the Islamic civilization invented in using the golden ratio and its derivatives in all of its designs that followed engineering systems and bases specialized for it in the way of its handling for the vocabulary. It was resulted unique variance in the designs and the relationships resulted from that, where special relationships were emerged including collaboration, contiguity, overlapping, repetition and interaction. With each design, many permutations emerge for several of more powerful designs with designing relationships hold marvelous authentic values. We remark that in the following Figures (5, 6).

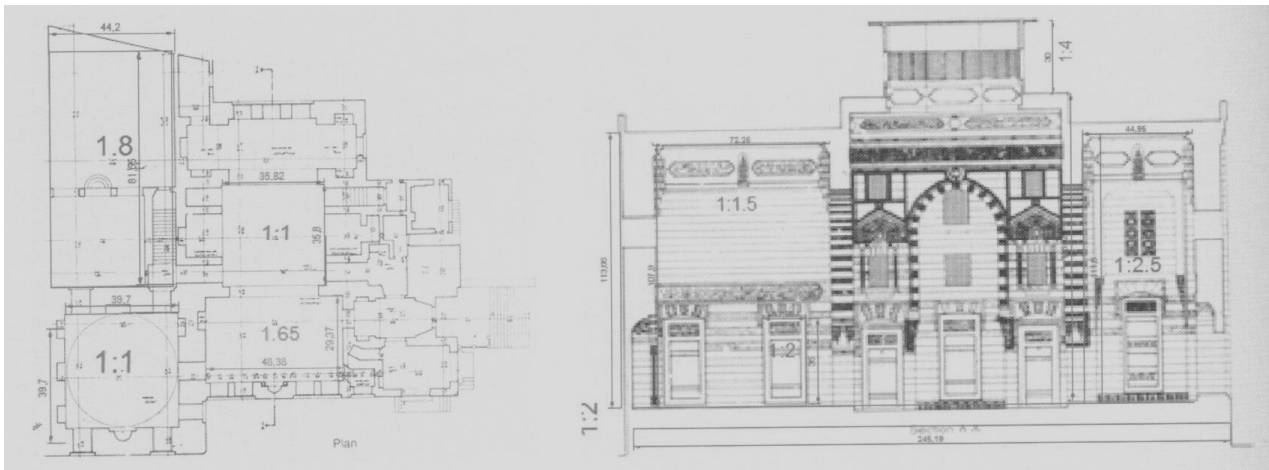


Fig. 5: the vertical and horizontal projections for mosque and school of Sultan Qaitbay and the ratios used in the design.

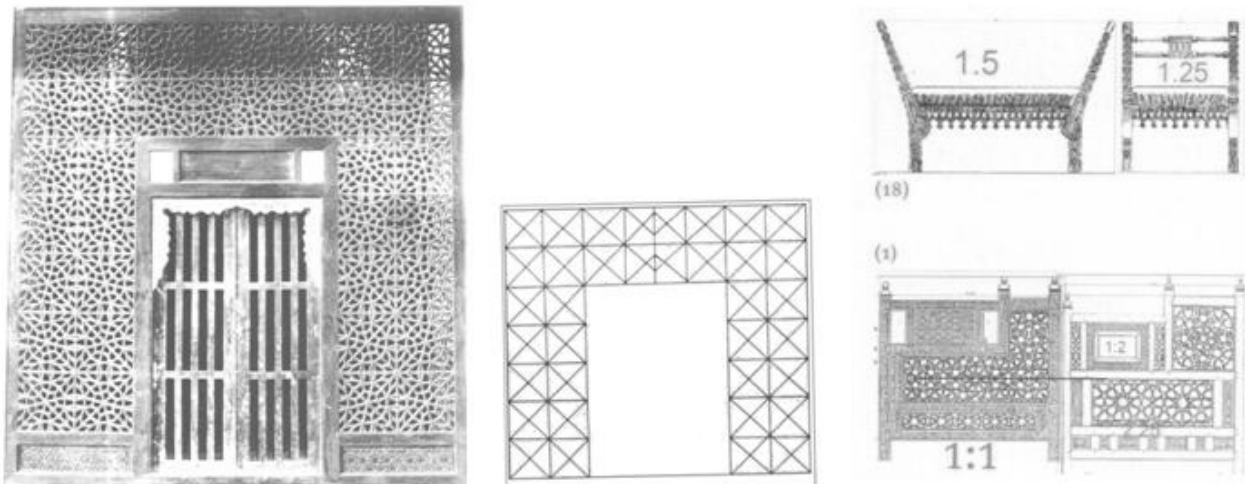


Fig. 6: window of Sultan Barkouk's grave in the Mamluk age, some of the furniture units and analysis of the ratios specialized for its design

Conclusion

As conclusion, using the golden ratio and its derivatives in the ancient civilizations lead to several important results.

Results of the research:

- The three powerful ancient civilizations divided using the golden ratio and its derivatives in its designs.
- Using the engineering ratios created several of different designing relationships that distinguished these designs and gave it eternal authentic values.
- The different designing relationships resulted in uniqueness for each civilization than its equivalents in spite of proving using these ratios in a way proved richness of using it in the designing relationships.

Recommendations of the research:

- The Researcher recommends using the golden ratio and its derivatives as a basis in the contemporary designs in order to achieve the good relationships between the design vocabulary that exceed the authentic value for any design and its distinction than the other.
- Studying the Aesthetic values in the ancient civilizations and benefiting from them in our contemporary designs.

References

- [1] Ahmed Abdel Kareem, Professor Doctor, "rhythmic systems in Islamic art authentications", Atlas House for Publication and Media Production, Giza, Cairo, 2007.
- [2] Amal Abdel Khalek Awad, assistant lecturer, "pro-rata in the Arab heritage as a part of interior design and furniture education system", forum of first national constructive heritage, published research, Jeddah, Kingdom of Saudi Arabia, 2011 , p. 295 - 299.
- [3] Sherine Yousry Kamal El-Zomor, " Pro-rata as a main element of the design elements and extent of its influence upon the interior design in the Islamic style", Master thesis, Faculty of Applied Arts, Helwan University, 2007.
- [4] Sir Fletcher, "A History of architecture on the comparative method".
- [5] Umaima Ibrahim Kasem, "fundamentals of the organic furniture design and its connection with the ancient Egyptian furniture", Doctorate thesis, Faculty of Applied Arts, Helwan University, 1999, p. 211 - 220.
- [6] Wael Mohamed Kamel El-Sayed, "interior design and ancient Egyptian model givens for the tourist establishments in Luxor", Master thesis, Faculty of Applied Arts, Helwan University,2007, p. 77 - 90.

SYNERGISTIC FORMULATION OF CHITOSAN AND CURCUMIN AS A POTENTIAL ANTIMICROBIAL AND ANTIOXIDANT COATING FOR POLYMERS

L. F. Zemljič¹, T. Ristić², M. Bračič¹, J. Volmajer¹

¹ University of Maribor, Faculty of Mechanical Engineering, Institute for Engineering Materials and Design, Smetanova 17, 2000 Maribor

² Tosama d.d., Vir, Šaranovičeva cesta 35, 1230 Domžale, Slovenia

Keywords: chitosan, curcumin, synergistic formulation, functionalization, antimicrobial activity, antioxidant properties

Abstract. The purpose of our work is to develop new synergetic combinations between chitosan and curcumin which will demonstrate antimicrobial and antioxidant characteristics. Diverse synergetic combinations were adsorbed onto the viscous fabric to reach the antimicrobial properties essential for medical textiles. Those synergistic formulations adsorbed onto fibres were compared to the fibres coated only by chitosan and only by curcumin, respectively.

Introduction. Among the various polysaccharide products, amino functional polysaccharides are the most promising as antimicrobial substances useful for many applications [1]. These polysaccharides contain amino groups which interact with the cell surface of pathogen microorganisms and in this way destroy them by several possible mechanisms [1]. One of the most popular amino polysaccharide is chitosan obtained by alkaline deacetylation of chitin. Chitosan's positive charge, the degree of N-deacetylation, the mean polymerization degree and the nature of chemical modifications are the properties which strongly influence its antimicrobial effectiveness [1]. Chitosan has been approved as food ingredient from FDA recently; therefore, the use of chitosan for new product development as well as natural antimicrobial agents would become more popular.

However, in spite of amino polysaccharides excellent antimicrobial activity, most of them show very poor antioxidant activity [2] which is significant when developing innovative biomaterials for medical devices, such as bioactive dressings and wound healing isolation materials, or a bioactive material to be used in e.g. food packaging. For these applications it is essential to provide, besides antimicrobial inhibition, a reduction in those reactive oxygen species that are strongly implicated in the pathogenesis of e.g. wounds, causing injury with bio-molecules such as lipids, proteins and nucleic acids, as well as depleting the human skin, and/or e.g. retard the degradation reactions of fats and pigments in food products [3]. Thus, it is very much appreciated to increase antioxidant activity of bioactive polymers mentioned with the natural compounds with proven high antioxidant capacity, such as plant phenolics. The antimicrobial and antioxidant activity depended on the concentration and chemical nature of the phenolic compounds in the extracts.

The aim of our paper was to prepare synergistic formulation of chitosan (Figure 1) and curcumin (Figure 2), a natural plant phenolic, in order to obtain a wide spectrum antimicrobial as well as antioxidant agent that may be applied onto polymers as a bioactive film.

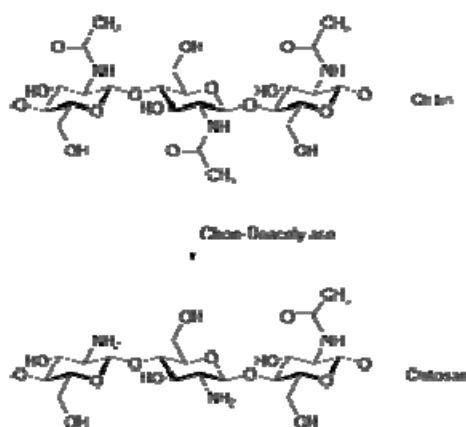


Fig.1: Deacetylation of chitin into chitosan [4]



Fig. 2: Curcumin in powder [5]

Our paper presents the development of curcumin-chitosan formulations and their applications onto fibre-oriented polymers (cellulose fibres). Cellulose fibres were characterised toward formulation adsorption onto cellulose. Finally, antimicrobial and antioxidant (not shown here) properties of functionalised cellulose material were examined.

Experimental

Materials

The samples preparation and notations are listed in the Table 1.

Table 1: Sample notations

Sample	Description of samples
A	Alkaline washed viscose fabric
B	A, functionalised by acidic solution of chitosan (w/w=0,5 %).
C	A, functionalised by curcumin in ethanol solution (w/w=0,5 %)
D	A, functionalised first by chitosan solution (w/w=0,5 %), and after drying of sample, with curcumin in ethanol (w/w=0,5 %).
E	A, functionalised by chitosan (w/w=0,5 %) and curcumin (w/w=0,5 %) in water solution in the ratio 1:1.

Methods

Kjeldahl Analysis

About 1.5 g of the sample was digested with H_2SO_4 and a catalyst containing 2.8% TiO_2 , 3.0% $CuSO_4 \cdot 5H_2O$, and 94.2% K_2SO_4 . The residue was treated with NaOH to liberate NH_3 , which was subsequently absorbed in boric acid and titrated with HCl. All samples were analyzed at least in triplicate to ensure reproducibility and to exclude statistical errors.

Antimicrobial Test

The antimicrobial properties of the treated fabrics were evaluated by ASTM E2149-01,22 which is a quantitative antimicrobial test method performed under dynamic contact conditions. Gram-positive and Gram-negative bacteria were used as test organisms. The incubated test culture in a nutrient broth was diluted using a sterilized 0.3 mM phosphate buffer (KH_2PO_4 ; pH 6.8) to give a final concentration of 1.5-3.0 $\times 10^5$ colony forming units (CFU)/mL. This solution was used as a working bacterial dilution. Each fabric (0.5-2 g) was cut into small pieces (1×1 cm) and transferred to a 250 mL Erlenmeyer flask containing 50 mL of the working bacterial dilution. All flasks were capped loosely, placed on the incubator, and shaken for 1 h at 37 °C and 120 rpm using a Wrist Action incubator shaker. After a series of dilutions using the buffer solutions, 1 mL of the diluted solution was plated in nutrient agar. The inoculated plates were incubated at 37 °C for 24 h, and the surviving cells were counted. The average values of the duplicates were converted to CFU/mL in the flasks by multiplying with the dilution factor. The antimicrobial activity was expressed as R) % reduction of the organism after contact with the test specimen compared to the number of microorganisms cells surviving after contact with the control.

Results and discussion

Table 2 shows the amount of total nitrogen present in the fabrics (v mmol/kg).

Table 2: Total N (mmol(kg) present in the fabrics

Sample	Ni (mg/L)	Ni (mmol/kg)
A	0,263	4,70
B	4,03	71,69
C	0,349	6,23
D	0,701	12,52
E	4,76	85

In the case of the reference sample obviously certain impurities were presented as a result of the fibers/fabric production and treatments. Nitrogen which was detected in the curcumin is also the consequence of different impurities which often appear in commercial products. Despite the small presence of nitrogen impurities present in the fabric samples as well as in curcumin the highest nitrogen content was expected in the case of samples treated with solution of chitosan or chitosan in combination with the curcumin. The highest nitrogen content shows the sample E (fabric, functionalized with aqueous solution of chitosan and curcumin, respectively). If compared to the reference sample of viscose-chitosan (sample B) it contains for 18 % more nitrogen which means that the chitosan in combination with curcumin is bounded in a higher extent onto the fabric surface as chitosan alone. Sample D which was treated within two stages first, with the water solution of chitosan and, second with the ethanol solution of curcumin shows a very low concentration of nitrogen which is only a 12.52 mmol/kg. This is probably result of a chitosan leaching from the surface of the fabric when applied the second functional layer; i.e. fabric treatment with the ethanol solution of curcumin.

The results of the reduction of pathogenic bacteria are given in Table 3.

Table 3: Reduction of various pathogenic bacteria

Sample	Staphylococcus Aureus	Escherichia Coli	Streptococcus Agalactiae
A	95%	48%	20%
B	97 %	94%	6%
C	82 %	11 %	24 %
D	94 %	92%	No reduction
E	98 %	98 %	No reduction



As a reference alkaline washed viscose fabric was used (sample A) which unexpectedly showed anti-microbial activity on the bacterium *Staphylococcus aureus*. The most likely explanation for this result is unsuitable surface of the fabric for the growth and reproduction of bacteria since the reduction to these bacteria is seen with all other samples [6]. It is clearly seen that when fabrics were functionalised with combination of both polymers (sample D and sample E) an antimicrobial character was similar or slightly improved in comparison with fabrics coated by chitosan only. The most important fact is that beside antimicrobial properties also antioxidant properties were introduced to those fabrics coated by chitosan-curcumin formulations (sample D and E). Fibres coated only by chitosan did not express any antioxidant activity. Those results will be in detailed presented in subsequent paper (Fras et al., *Textile research Journal*).

Conclusions

It is concluded that the antimicrobial properties of fabrics functionalized with the formulation of chitosan-curcumin depend on the nitrogen content which indicates the quantity of amino groups which are responsible for the antimicrobial character of chitosan. Curcumin as adsorbent for textiles in combination with chitosan represents an added value because of its anti-oxidative properties, whilst slightly improve an existing antimicrobial performance of chitosan.

References

- [1] M.N.V. Ravi Kumar: A review of chitin and chitosan applications, *Reactive & Functional Polymers*, Volume 46 (2000), p. 1-27.
- [2] R. Ahvenainen: *Novel food packaging techniques* (Woodhead Publishing in food science and technology, Boca Raton; Cambridge, 2003)
- [3] L. Fras Zemljič, V. Kokol, D. Čakara: Antimicrobial and antioxidant properties of chitosan-based viscose fibres enzymatically functionalized with flavonoids, *Tex. res. j.*, Volume 81 (2011), p.1532-1540
- [4] <http://iopscience.iop.org/2043-6262/2/4/045004/fulltext/>
- [5] http://zdravozivljenje.eu/sl/Zelisca_in_Zacimbe/Antioksidativni_in_protivnetni_ucinki_KURKUME/
- [6] A. Gericke, J., Van der Pol: A comparative study of regenerated bamboo, cotton and viscose rayon fabrics. Part 2: Antimicrobial properties, *Journal of Family Ecology and Consumer Sciences*; Volume 39 (2011), p. 10-18.

ICE JET MACHINING: PRESENTATION OF THE PROTOTYPE DEVELOPMENT

M. Jerman¹, A. Lebar¹, H. Orbanic¹, M. Junkar¹ and A. Suárez²

¹ University of Ljubljana, Faculty of Mechanical Engineering, Laboratory for Alternative Technologies, Slovenia

² Tecnalia, Manufacturing Engineering Department, Spain

Keywords: AWJ, sub cooled water, ice particles, cryogenic gas, ice jet

Abstract. During the last few years different research groups have been developing systems for transformation of abrasive water jet into ice jet, where the use of mineral abrasive is being replaced with ice particles. This can be achieved in several different ways. In this paper we present the results from the combined research work between University of Ljubljana (SI) and Tecnalia (ES), which has been done on developing the prototypes for generation of the Ice Jet (IJ) technology. More specifically the development of the prototype which generates the ice particles inside the mixing chamber of the cutting head by partial transformation of the high speed water jet into ice particles. This is accomplished by injection of the cryogenic gas into the mixing chamber. The prototype uses the high pressure water that is being precooled below its freezing point prior entering the cutting head.

Introduction

Abrasive water jet (AWJ) machining process uses a high speed water jet for acceleration of very hard abrasive grains thus enabling the removal of work piece material. The high speed water jet is generated by pushing the water under high pressure, up to 600MPa, through the water nozzle of a small diameter (0,08 mm-0,4mm) where the potential energy is transformed to kinetic energy, achieving supersonic speeds of the formed water jet. The process is universal as it is possible to machine almost any kind of material regardless of its composition, structure, hardness or other physical properties. This makes it possible to machine different new materials which cannot be machined by traditional machining processes. AWJ machining technology has received considerable attention from several domains of production industry due to this competitive advantage. The process is depicted on Fig.1 a).

Many industrial processes and specifically the AWJ machining, produce waste that is in the form of sludge in which waste material is mixed with water. The quantity of abrasive material produced in the waste is huge in the comparison to the quantity of residuals of workpiece material. Handling of this sludge is usually not critical since abrasive material is non-toxic, but in some applications the workpiece residuals can be harmful to the environment.

One of possible solutions is to substitute abrasive particles in AWJ with ice crystals and thus get rid of the majority of material in the waste sludge. Injection of ice particles into the high speed water jet can be divided into two basic principles: (1) injection of super cooled ice particles that are prepared in advance and (2) generation of ice particles in-situ during the cutting process itself by transformation or freezing of the water jet which can be further divided into two methods, the freezing by injection of the liquefied gas (e.g. liquefied nitrogen) into the mixing chamber, depicted on Fig.1b), and the transformation by sub cooling of the water under high pressure before the water nozzle. The idea of Ice Jet was already tested as several authors reported [1-4] but several issues are left to be solved.

Previous experiments from the research done by Geskin et al.[1], Truchot et al. [2], demonstrated the effectiveness of the use of ice particles as a substitute for abrasives. The principal shortcoming of WJ is the low efficiency of the energy transfer between the jet and the work piece. The energy efficiency of AWJ is still low although acceptable.

In his thesis, Shiskin [3] investigated the application of ice powder for material processing. Among other the study involved investigation of water freezing and formation of water, ice and air jet stream for cutting and cleaning purposes.

In his research Wang et al. [5] measured the dynamic characteristics of an ultra-high pressure fine jet using the high speed camera as well as the properties of droplets using the Phase Doppler Anemometry (PDA). He discovered that at the pressure of 200 MPa and an water orifice with diameter of 0,25 mm, the diameters of water droplets at the distance of 90 mm from the orifice range from 75 μ m at the middle of the jet and 200 μ m at the edge of the jet. This size is appropriate as the granulation of the most frequently used mineral abrasive of mesh #80 has in average the same size. This means that the bigger the droplet, the smaller the velocity of the droplet. We are counting on freezing the slower and bigger droplets as they will spend more time in the mixing chamber and therefore be in the contact with cooling media longer. Also the bigger droplets are at the edge of the jet and are therefore better exposed to the cooling media.

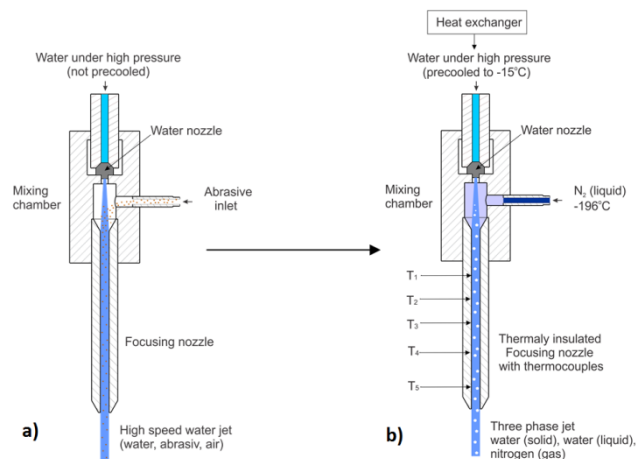


Fig.1 a) Schematic depiction of abrasive water jet (AWJ) and b) transformation to ice jet (IJ).

Development of the Prototype

As mentioned the ice particles in the prototype are being generated inside of the cutting head of the AWJ machine, during the machining process. For this purpose the efforts have been focused on discovering the most efficient way to remove the energy in the form of heat from the water. The method used is based upon the extreme high enthalpy of evaporation of the cryogenic liquefied gases such as liquefied carbon dioxide (-78,5°C) and liquefied nitrogen (-195,9°C). These enable a massive heat transfer from water to gas and a subsequent phase transformation in the mixing chamber and the focusing nozzle. Method is depicted on Fig. 2. Ice particles are then accelerated by the high speed water jet. This approach was already studied by another research group [3, 4], which obtained some promising cutting results in cutting aluminum work piece. The properties of the generated ice particles greatly depend on the temperature. The lower it is, the better the mechanical properties such as hardness [6]. In the previous research [7], we have measured the water jet temperatures at different pressure conditions using different cutting head configurations. From this work we have measured that the temperatures inside the cutting head at 200 MPa are around 60°C. Most of the temperature buildup occurs on the water nozzle. This means that we have to remove a lot of heat from the high speed water jet before the water phase transformation to ice phase even takes place. Since the speed of the water jet is very high, around 600 m/s at 200MPa, the time it takes for the water to go through the cutting head is very short, on the scale of 10⁻⁴ s. This creates difficult conditions for generation of ice particles inside of the cutting head.

We have addressed this problem by installing the heat exchanger for the high pressure water before the cutting head. This can be done because of the property of water which at the pressure of 200 MPa can be sub-cooled to -20°C and still remain in its liquid form [8]. In this way the temperature of water entering the mixing chamber has been reduced by at least 40°C. In order to maintain the cooled down water at the low temperatures as it flows from the heat exchanger unit to the cutting head, the whole system from the heat exchanger on had to be thermally insulated in order to prevent heat exchange with the environment.

When liquefied nitrogen [LN] comes into contact with the warm water jet it evaporates and by that removes the heat from the water, freezing it in the process. As the nitrogen evaporates however it increases in volume around 680 times. This creates a gas pocket inside the mixing chamber and prevents the liquid phase to flow inside. In this way the cooling capacity of the system is greatly reduced as the gas phase, while still very cold has greatly inferior cooling capabilities than the liquid phase. To assure the constant flow of the liquid phase we have created the gas release vent in the mixing chamber. In this way the excess gas phase can leave the mixing chamber through the vent and the liquid phase can flow continuously.

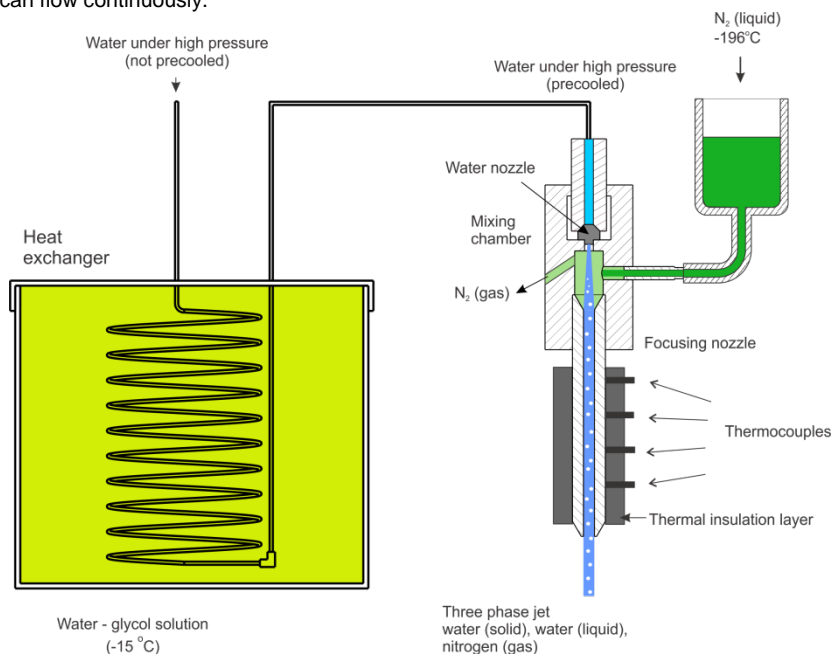


Fig.2 Schematic depiction of the Ice Jet Prototype 2. Sub-cooling the water under high pressure and injection of the liquid nitrogen.

Experimental setup

The built prototype is depicted on Fig.2. The main part of the prototype that was built was the heat exchanger unit which is composed of the cooling unit with the glycol heat exchanger, of the glycol-water solution tank and of the high pressure pipes bent into a spiral. The cooling compressor (refrigerator unit) uses the internal heat exchanger to cool down the glycol water solution inside of the tank to the temperatures down to -20°C . It was costume build for this purpose and has the cooling power of around 7 kW. The power was calculated to successfully cool down the high pressure water from 20°C to at least -15°C . The glycol-water solution tank has a volume of 200 l and is also used as a heat storage tank because of its volume. The mixture of glycol and water is set to 50-50% and it can be cooled to around -40°C without freezing. The whole tank is thermally insulated using a 20 mm layer of armafex foam. Both the cooling compressor and the glycol-water solution tank are positioned on a costume build cart for mobility of the system. The $\frac{1}{4}$ " high pressure tubes of a length of 12 m bent into a spiral are submerged into the tank and this forms a second, high pressure, heat exchanger unit.

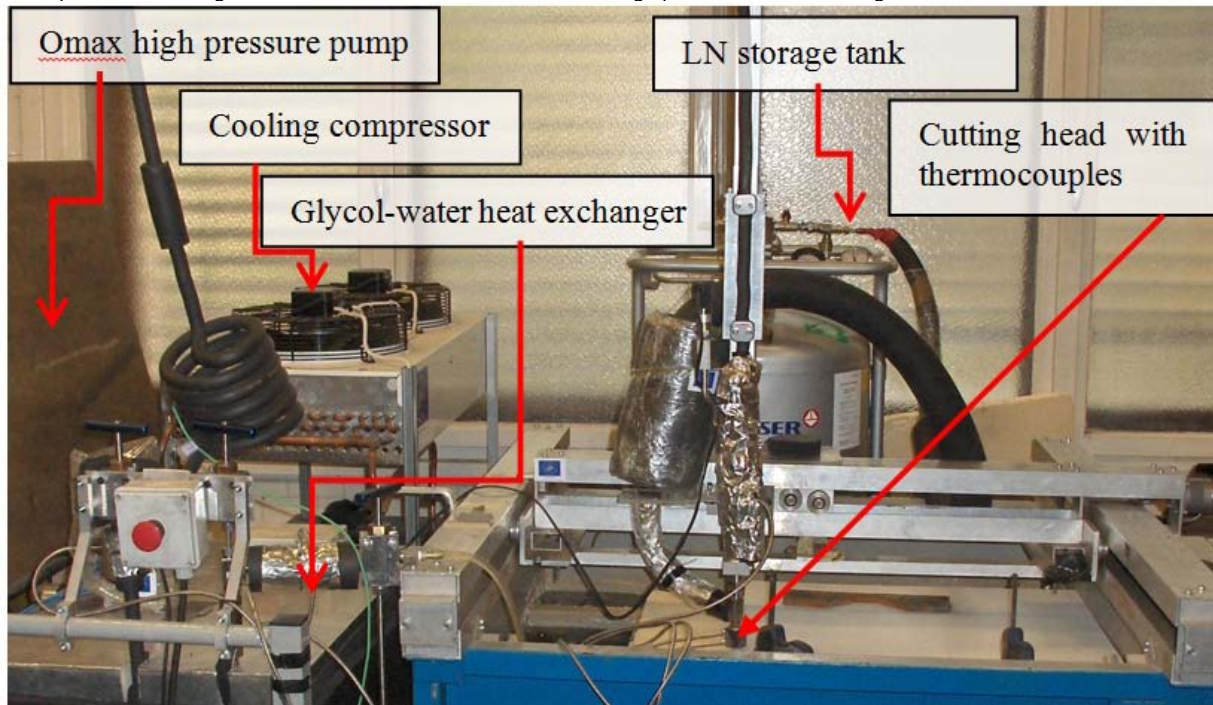


Fig.3 The prototype experimental site.

To cool down the glycol-water solution, the water in the submerged high pressure pipes needs to be under high pressure otherwise it would freeze. For this reason the high pressure water pipe system is divided into two lines. A direct line for warm (not precooled) water and a bypass line that goes through the heat exchanger, also called the cold line. To maintain the water inside the cold line under the pressure, the system of two manual valves and a check valve are used. After the exit from the cold line the whole high pressure pipe system has been insulated using the armafex foam to prevent the heat exchange between the surrounding air. The cold water then enters the cutting head and gets heated up inside the water nozzle as the transformation from the potential to kinetic energy takes place. The LN is then injected inside the mixing chamber at atmospheric pressure as can be seen on Fig.2. Inside the mixing chamber the jet creates under pressure which sucks the LN inside. The amount of LN used can be controlled using different size inlet nozzles. As the LN comes in contact with water it starts evaporating and the excess gas phase leaves the cutting head through the gas release vent. Without this vent the cooling process is very low. The whole system is equipped with thermocouple temperature sensor to monitor and control the process.

Results and conclusions

The developed prototype has so far been tested only in terms of temperature measurements and jet stability observations. Already in our first attempts it became obvious that the stability of the process in terms of temperatures and jet coherence will be difficult. The amount of LN used is very important as too little will result in insufficient cooling of the jet while too much will cause the jet to break up as the liquid phase will transform into gas inside of the jet. The process also needs a control system to defrost the possible ice clogs in the inlet nozzle or outlet vent in order to become useful for continuous use. There is also the issue of starting and stopping of the machine as the water inside of the cutting head tends to freeze when the process is interrupted for a short time. So the heating system will also be needed. We have so far measured temperatures below -30°C inside of the cutting head, which is promising. Until now the main objective was to insure repeatability of the process which has now been established to the point where we will continue with some smaller modifications to optimize the injection of LN and begin with the cutting tests of different materials.

Acknowledgment

This work is partially supported from the Slovenian Ministry of Higher Education, Science and Technology with the program Innovative production systems (P2-0248). ICE JET project is a project supported by the European Commission LIFE+. The program is being carried out in Spain and Slovenia from 2010 to 2012. The European Commission contributes with 763.962 € of a total budget of 1.614.125 €.



References

- [1] E. Geskin, L. Tismenetskiy, F. Li, "Development of Ice Jet Machining Technology", NJIT, 8th American Water Jet Conference, 1995, pp. 671-680.
- [2] P. Truchot, P. Mellinger, and R. Duchamp, "Development of a Cryogenic water jet technique for biomaterial processing applications", 6th American Water Jet Conference, August 17-19, Houston, Texas, WJTA, Omnipress: paper 3-G, 1991, p.473-480.
- [3] D. V. Shishkin, "Development of Icejet machining technology", NJIT, Thesis, 1999.
- [4] F-W. Bach, T. Hassel, C. Biskup, N. Hinte, A. Schenk, F. Pude, "In-process generation of water ice particles for cutting and cleaning purposes", in: Proc. 20th International conference on Water Jetting, BHR Group, Graz, Austria, 2010, p. 275-283.
- [5] Y. L. Wang, M. G. Yang, B. Gao, C. Kang, B. Chen, "Measurement of ultra-high pressure water jet", in: Proc. 20th International conference on Water Jetting, BHR Group, Graz, Austria, 2010, p. 317-328.
- [6] D. K. Shanmugam: Development of Ice Particle Production System for Ice Jet Process, 2005, Ph.D thesis.
- [7] M. Jerman, H. Orbanic, I. Etxeberria, A. Suarez, M. Junkar and A. Lebar, "Measuring the Water Temperature Changes Throughout the Abrasive Water Jet Cutting System" in 2011 American WJTA-IMCA Conference and Expo, September 19-21, 2011 Huston, Texas, Paper C4.
- [8] Hoops, P. :Ice Physics, Oxford, England, Clarendon Press, 1974.

CFD INVESTIGATION OF THE TURBULENT FLOW IN A ONE-STAGE RADIAL-FLOW BLOWER AGGREGATE

L. Kalmár¹, G. Janiga² and L. Soltész³

¹ University of Miskolc, Department of Fluid and Heat Engineering, H-3515 Miskolc-Egyetemváros, +36-30-2787917, aramka@uni-miskolc.hu, Hungary

² University of Magdeburg "Otto von Guericke" (ISUT/LSS), janiga@ovgu.de, Germany

³ Elektrolux Lehel Ltd. Floor Care Factory, laszlo.soltesz@electrolux.hu, Hungary

Keywords: radial-flow blower-aggregate, CFD simulation unsteady turbulent flow

Abstract. This paper deals with the CFD investigation of the turbulent flow in one-stage radial flow blower-aggregate indicated by **BA1**. The main aim of this numerical investigation is to determine the relevant operating characteristics of the blower-aggregate and to determine detailed information about the flow characteristics inside it. The distributions of these flow characteristics in the blower-aggregate determined by commercial code ANSYS-FLUENT are available to judge whether the elements of the blower-aggregate are working properly, or not. The CFD investigations mentioned above were carried out for the blower aggregate **BA1** and the results are shown in this paper and are compared with the calculated results for the blower aggregate **BA0**.

Introduction

The investigated blower aggregate is demonstrated in Fig. 1 in a disassembled state showing the main parts of the blower.

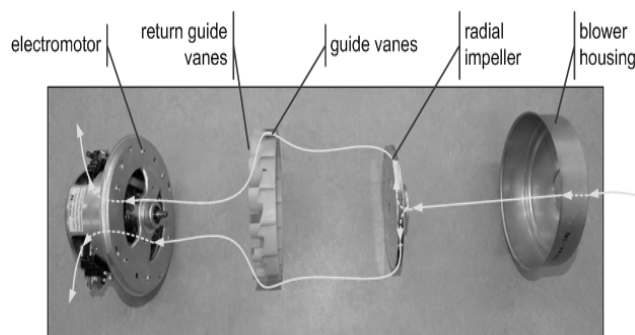


Fig. 1 The main parts of the investigated blower aggregate

The first step of our numerical investigation was to create the complete computational domain of the blower-aggregate. It has been produced using the commercial pre-processing tool of ANSYS-GAMBIT. The complete three-dimensional computational domain of the blower aggregate is illustrated in Fig. 2 with two different views. Here, a slightly simplified inlet and outlet parts can be observed compared to the Fig. 1. In order to produce a relatively homogenous velocity distribution along the inlet cross-section during the numerical simulation, the inlet cross section has been extruded producing a short cylindrical pipe section. At the outlet section of the blower two short cylindrical pipe sections were connected with the similar shape of the cross-section, which can be seen in the wall between the blower and electromotor (see Figs. 1 and 2).

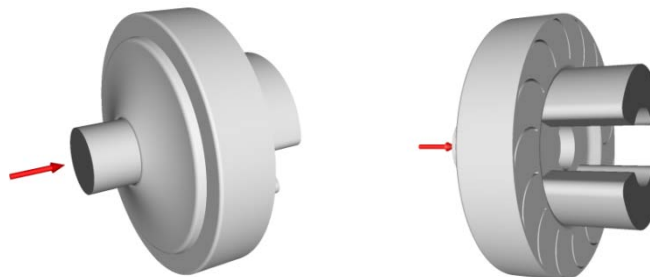


Fig. 2 The produced three-dimensional computational domain of the blower aggregate

The outer parts of the computational domain – including the inlet and outlet parts as well as the house of the blower aggregate – are exemplified in Fig. 2. The inner parts of this domain, the stationary guide vanes (indicated by **BA1**) and the rotating impeller vanes are represented in Fig. 3 and Fig. 4, respectively. The air flows into the blower throughout the inlet section and arrives to the impeller, then flows across it which increases the total energy of the air. After the air arrives the guide vanes at the impeller side then it flows into the guide vanes on the back side. Finally the air flows through the pressured side of the blower and leaves the blower throughout the outlet sections.



Fig. 3 Photo of the impeller and guide vanes of **BA1**



Fig. 4 The three-dimensional model of the impeller

The main aim of this numerical investigation is to determine the relevant operating characteristics of the blower relying on computational fluid dynamics (CFD).

Computational details

The numerical simulation with a rotating part requires that the computational domain has to be divided into sub domains, as shown in Fig. 5. Two principal sub-domains have to be introduced: the rotational sub-domain (named **ROTOR**) is the sub-domain with the blower impeller and the stationary sub-domains (named **STATOR**) which are bounded by the walls of the blower, the guide vanes and return guide vanes.

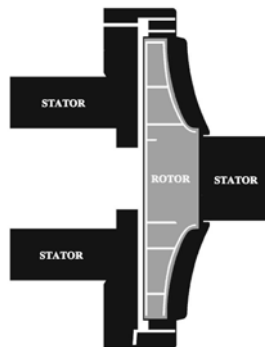


Fig.5 Partitioning of the total computational domain

The numerical computations rely on the finite volume methods and are performed in the commercial solver ANSYS Fluent [1]. The corresponding unstructured finite volume mesh has been created in the commercial pre-processor tool ANSYS Gambit emphasizing the importance of the mesh quality. One of the characteristic mesh quality parameter is the equi-angle skewness of the mesh elements (shown in Table 1). The complete computational grid involves 11.27 million cells with the maximum skewness parameter of 0.87, which proves that the mesh quality is acceptable for the numerical computations.

Table 1. Skewness parameters of the computational grid for total computational domain

From value	To value	Count in range	% of total count
0	0.1	5 578 911	49.52
0.1	0.2	2 435 866	21.62
0.2	0.3	1 288 784	11.44
0.3	0.4	1 162 310	10.32
0.4	0.5	601 143	5.34
0.5	0.6	144 875	1.29
0.6	0.7	49 394	0.44
0.7	0.8	4 076	0.04
0.8	0.9	813	0.01
0.9	1	0	0.00
		11 266 172	100

The part of the unstructured mesh using hexahedral elements is exemplified in Fig. 6.



Fig. 6. The surface mesh of the blower impeller

Computational results

The “density based implicit Gauss-Seidel” [1] numerical procedure has been applied in the unsteady numerical flow computations. According to the relative high velocities in the blower the flow has been considered as compressible, therefore, the perfect-gas law with the $k-\omega$ SST turbulence model have been applied in the unsteady simulations.

The configuration of the blower aggregates **BA1** has newly designed stationary guide vanes and the stationary return guide vanes with new blade geometries, otherwise, the other parts correspond to the previously investigated configuration **BA0** [2].

The computational results obtained by ANSYS Fluent are represented in figures and diagrams. Figs. 8 and 9 show the streamlines of the velocity fields, while the Figs. 10 and 11 below give information about the variations of average absolute pressure and the mass-flow rate (concerning to the denoted 16 different cross-sections of the total flow-domain shown in Fig. 7) in the direction of the main flow inside the aggregate.

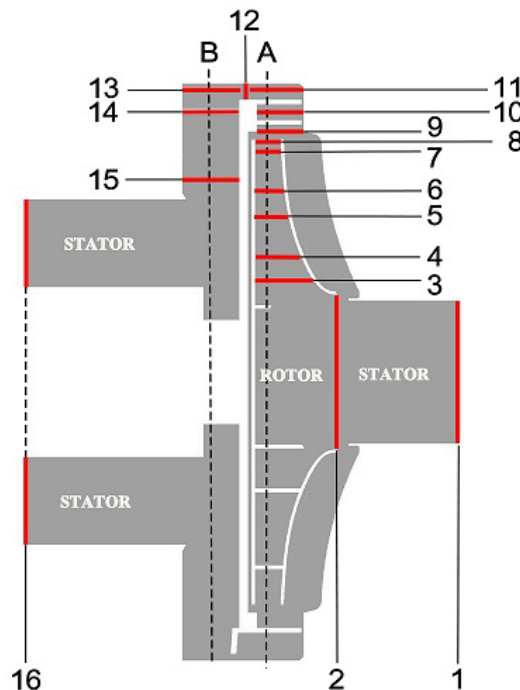


Fig. 7 Partitioning of the computational domain

In Fig. 8 the streamlines of the relative (inside the impeller) and the absolute (inside the guide vanes) velocity fields are shown along the plane **A**. Fig. 9 shows the streamlines of the velocity (inside the return guide vanes and the pressured side of the blower) along the plane **B**.

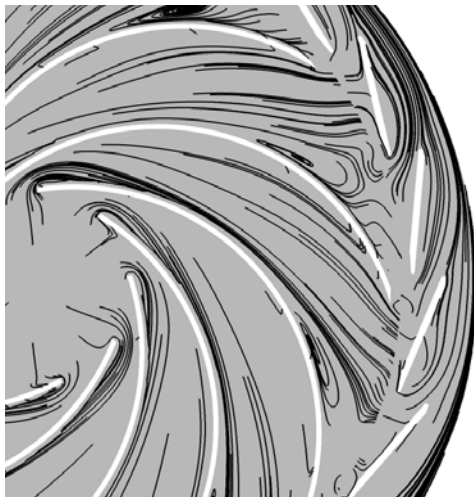


Fig. 8 Streamlines in the plane **A**

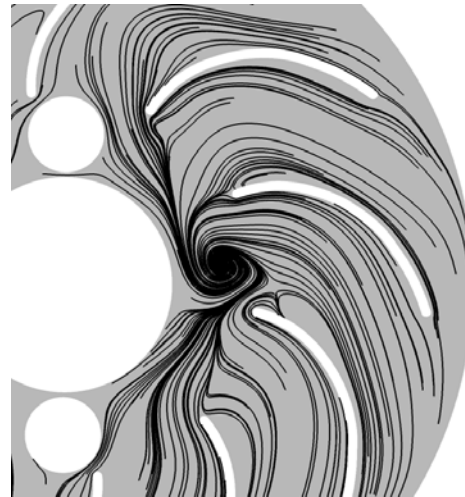


Fig. 9 Streamlines in the plane **B**

Figs. 8 and 9 give insight into the local structures of the flow using streamlines along the two planes indicated by **A** and **B**. Finally three different operating points of the blower were numerically investigated by ANSYS-FLUENT [1]. One of the initial parameters of our calculation was the mass-flow rate at the inlet. The pressure difference between the outlet and inlet sections of the blower has been derived from the computations.

Figs. 10 and 11 show the variations of the averaged flow parameters. They are determined by the surface integral of the physical fields in the blower aggregates indicated by **BA0** and **BA1**. All the presented results are obtained for operation state *II* of the blower aggregate at the mass flow rate $\dot{m}_i = 0.033$ kg/s. Knowing the variations of these averaged parameters is very important, if we want to get useful information about the overall operational characteristics of the blower.

Sixteen different cross-sections are illustrated in Fig. 7. The obtained values of the average absolute pressure for the indicated 16 sections and the variations of this characteristic flow variable are shown in Fig. 10. The values of the average mass flow rate concerning these cross sections are also computed and shown in Fig. 11.

The variations of the absolute pressure for **BA1** and **BA0** is shown in Fig. 10 between sections 2 and 8 (inside the impeller). The absolute pressure energy is increasing in a very similar way through the impeller. Between sections 8 and 10 the increasing in the cross sectional areas also are shown a small changing of the absolute pressure. In Fig. 11 for both blower-aggregates the average mass flow rates between sections 2 and 8 the relatively large increase can be observed. The increase of the mass flow rates is caused by leakage.

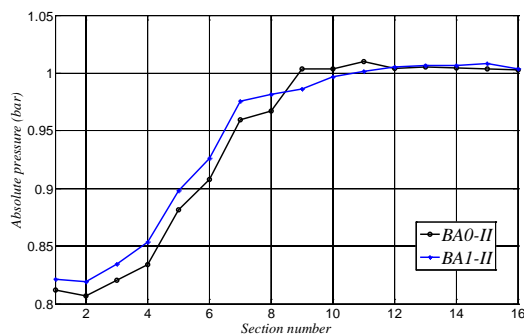


Fig. 10 Variation of the average absolute pressure

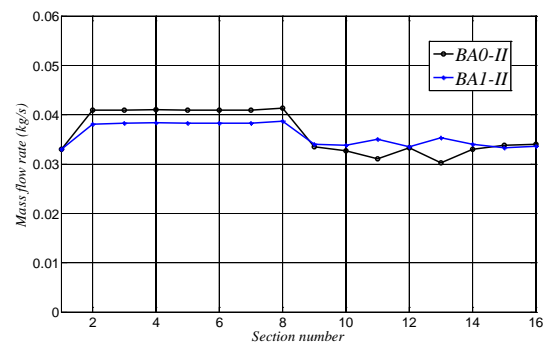


Fig. 11 Variation of the average mass flow rate

Conclusion

By comparing the distributions of the average absolute pressure and the mass flow rate concerning to operating point *II* of the blower aggregates **AB0** and **AB1** some small differences can be noticed. In Fig. 10 between sections 2 and 8 (inside the impeller) the variations of the absolute pressure are shown very similar energy increase through the impeller. Between sections 8 and 10 the increase in cross sectional area also causes a small increase in the absolute pressure. In Fig. 11 between sections 2 and 8 the relatively large increase caused by leakage.

Acknowledgment

The described work was carried out as part of the TÁMOP-4.2.1.B-10/2/KONV-2010-0001 project in the framework of the New Hungarian Development Plan. The realization of this project is supported by the European Union, co-financed by the European Social Fund. The permission to publish this work is warmly acknowledged to Electrolux Lehel Ltd.

References

- [1] Fluent Inc. FLUENT 6.3 User's Guide, Lebanon, New Hampshire, (2006).
- [2] L., Kalmár, G., Janiga, G., Kristóf, B., Fodor, L., Soltész, Z., Varga : Numerical simulation of the flow in one-stage radial-flow blower aggregate, Proceeding of MicroCAD International Computer Science Conference, Miskolc, (2011), pp. 39-44.